

This Page Is Inserted by IFW Operations
and is not a part of the Official Record

BEST AVAILABLE IMAGES

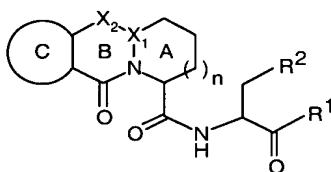
Defective images within this document are accurate representations of the original documents submitted by the applicant.

Defects in the images may include (but are not limited to):

- BLACK BORDERS
- TEXT CUT OFF AT TOP, BOTTOM OR SIDES
- FADED TEXT
- ILLEGIBLE TEXT
- SKEWED/SLANTED IMAGES
- COLORED PHOTOS
- BLACK OR VERY BLACK AND WHITE DARK PHOTOS
- GRAY SCALE DOCUMENTS

IMAGES ARE BEST AVAILABLE COPY.

**As rescanning documents *will not* correct images,
please do not report the images to the
Image Problem Mailbox.**



| Example | R ¹ | R ² | Ring C | n | X ₁ | X ₂ |
|---------|-------------------|-------------------|----------|---|----------------|----------------|
| 1 | CH ₂ F | CO ₂ H | Benzo | 0 | C | N |
| 2 | CH ₂ F | CO ₂ H | Benzo | 1 | C | N |
| 3 | CH ₂ F | CO ₂ H | Benzo | 0 | C | C-H |
| 4 | CH ₂ F | CO ₂ H | Benzo | 1 | C | C-H |
| 5 | CH ₂ F | CO ₂ H | Benzo | 1 | N | C=O |
| 6 | CH ₂ F | CO ₂ H | Pyrazino | 1 | N | C=O |

REMARKS

Applicants have amended the claims in response to the restriction requirement and the Office Action.

Applicants have amended the definition of R² in claims 1-4 to be directed to compounds elected in response to the Examiner's restriction requirement (see below).

Applicants have amended claim 1 to delete the term "derivative" and recite the term "salt." Support for this amendment may be found throughout the specification as originally filed (see page 22, line 12 to page 23, line 2; page 23, lines 12-15; and page 23 lines 27-30).

Applicants have amended claim 1 to clarify that the isosteres are of carboxylic acids. Support for this amendment may be found throughout the specification as originally filed (see page 12, lines 11-18).

Applicants have amended claim 1 to recite certain types of C-rings (i.e., those that do not have a NH group adjacent to the carbonyl of ring B). As amended Ring C may not have a -N(H)- moiety at a certain position in the ring. Support for this amendment may be found throughout the specification as originally filed (page 15, line 10 to the end of page 16, disclosing compounds having this structural feature).

Applicants have amended claim 5 to recite the compounds of Table 2. Support for this amendment may be found throughout the specification as originally filed (see page 17, lines 1-5).

Applicants have submitted herewith an Appendix of Amendments indicating the amendments to the claims. In the Appendix, bracketing indicates deletions and underlining indicates insertions.

None of these amendments adds new matter.

The Restriction Requirement

Applicants note that the Examiner has considered their July 29, 2002 traversal of the restriction requirement but deemed it not persuasive. Accordingly, the Examiner has examined claims

1-13 to the extent that they embrace the elected subject matter. Applicants have therefore amended the claims to be directed to this subject matter.

The Rejections

35 U.S.C. § 112, Second Paragraph

Claims 1-13 stand rejected under 35 U.S.C. § 112, second paragraph as being indefinite for failing to "particularly point out and distinctly claim the subject matter which applicant regards as the invention." Applicants traverse each of the Examiner's specific contentions below.

1. The Examiner contends that the term "derivative" renders claim 1 indefinite. Applicants have amended claim 1 to delete the term "derivative" thus obviating this contention.

2. The Examiner contends that the term "isostere" in claim 1 is vague and unclear. According to the Examiner it is unclear whether the isosteres are of only the carboxylic acid group. And the Examiner contends that "an enablement issue" would arise if claim 1 encompasses isosteres of amides and esters. Applicants have amended claim 1 to clarify that the isosteres are of the carboxylic acid groups only, thus obviating this contention.

3. The Examiner contends that the term "feature" in claim 2 is unclear and should be replaced with "group".

Applicants have amended claim 2 as suggested by the Examiner thus obviating this contention.

4. The Examiner contends that claim 5 is objectionable for referring to a Table. Applicants have amended claim 5 to recite the compounds in the Table thus obviating this contention.

35 U.S.C. § 112, First Paragraph

Claims 7-10 and 13 stand rejected under 35 U.S.C., first paragraph as lacking enablement.

Claims 7-10 and 13 are fully enabled by the evidence of record for the following reasons.

The *in vitro* assays provided at pages 49-54 of the specification are useful for determining that the compounds of the present invention are inhibitors of caspases. Applicants will show below that inhibition of caspases have been linked to therapeutic benefits in the claimed diseases.

Applicants disagree that it is incredible that applicants' compounds could be used to treat all the recited diseases. As set forth in applicants' specification, caspase inhibition had been linked to the treatment of the claimed diseases at the time of applicants' filing date (see, e.g., specification at page 4, line 19 to page 5, line 4). These links continue to be confirmed. Thus, even if the disease are varied, they have in common a link to caspases.

For example, early work established that IL-1 β , a cytokine released from stimulated monocytic cells, is an early and primary player in activating inflammation pathways associated with immune disorders and disease (see, e.g., specification page 2, lines 9-18; D. K. Miller et al.¹; and Geiger et al.²). Therefore, it has been established that caspase-1 (also known as ICE) inhibitors are therapeutically useful because they block the formation of active IL-1 β . Importantly, this usefulness has been demonstrated *in vivo*.

Ku reports that administration of an ICE (caspase-1) inhibitor is effective at reducing IL-1 β levels *in vivo*, and in reducing and alleviating inflammatory-associated symptoms and disease states.³ In particular, Ku shows that an ICE inhibitor that reduces IL-1 β levels *in vivo* can have profound effects on inflammation as demonstrated in a mouse with collagen- or LPS-induced arthritis, an accepted animal model for rheumatoid arthritis in humans. In fact, the data clearly show that treatment with the ICE inhibitor is more effective on the induced

¹ Miller, D. K. et al., "The IL-1 β Converting Enzyme as a Therapeutic Target," Annals N.Y. Acad. Sci., 696, pp. 133-148 (1993) (Exhibit 1).

² Geiger, T. et al., "Neutralization of Interleukin-1 β Activity *in vivo* with a Monoclonal Antibody Alleviates Collagen-induced Arthritis in DBA/1 Mice and Prevents the Associated Acute-phase Response," Clin. Exper. Rheumatol., 11, pp. 515-22 (1993) (Exhibit 2).

³ Ku, G. et al., "IL-1 β Converting Enzyme Inhibition Blocks Progression of Type II Collagen-Induced Arthritis in Mice," Cytokine, 8, pp. 377-386 (1996) (Exhibit 3).

inflammation than treatment with steroidal anti-inflammatory agents used to treat human inflammation. Importantly, the level of ICE inhibition demonstrated by applicants' compounds (see, e.g., specification pages 49-54) would also be expected to be therapeutically useful.

Similarly, B. E. Miller reports that parenteral administration of an ICE inhibitor selectively inhibits mature IL-1 β production *in vivo*.⁴

D. K. Miller reports that mature IL-1 β release in human peripheral blood monocytes was inhibited in a dose-responsive fashion from cells pre-treated with an ICE inhibitor, but not in cells pre-treated with a control.

These studies demonstrate a correlation between *in vitro* and *in vivo* data. Thus, applicants' *in vitro* data are sufficient to support the claimed methods directed to treating various diseases by inhibiting interleukin-1 β *in vivo*.

Applicants discuss further the correlation between caspases, IL-1, apoptosis, and the claimed diseases in more detail below.

As established throughout applicants' specification as filed, the diseases recited in applicants' claims are associated with caspases. These diseases are IL-1- (inflammatory or

⁴ Miller, B. E. et al., "Inhibition of Mature IL-1 β Production in Murine Macrophages and a Murine Model of Inflammation by WIN 67694, an Inhibitor of IL-1 β Converting Enzyme," J. Immunol., 154, pp. 1331-38 (1995) (Exhibit 4).

immunoregulatory) or apoptosis-mediated (see, page 3, lines 6-28). The links between IL-1, apoptosis and caspases have been established (see, page 1, line 31 to page 4, line 4).

Furthermore, the art in the field confirms the link between caspases and applicants' recited diseases. Applicants will demonstrate that a link exists between, each of the claimed disease. Therefore, applicants are entitled to claims directed to the treatment of the various diseases recited in claims 7-10 and 13.

Specifically, Bani has confirmed a correlation between IL-1 β levels and tumor metastases.⁵ As discussed in Bani, "treatment of mice with IL-1 β can increase the number of artificial or spontaneous metastases and ... this effect is not limited to a single tumor type or to a specific organ" (Bani, p. 119). Metastasis formation was shown in several different tumor lines (Bani, p. 120). Thus, a skilled practitioner would expect that inhibition of IL-1 would decrease metastasis formation in a wide variety of tumors. This data demonstrates a correlation between a decrease in IL-1 β levels and the treatment of tumors.

Dewhirst supports a correlation between bone disease and IL-1 β .⁶ As discussed in Dewhirst, osteoclast-activating

⁵ Bani, M.R., "Effect of Interleukin-1-beta on Metastasis Formation in Different Tumor Systems," J. Natl. Cancer Inst. 83, pp. 119-123 (1991) (Exhibit 5).

⁶ Dewhirst, F.E. et al., "Purification and Partial Sequence of Human Osteoclast-activating Factor: Identity with Interleukin-1 β ," J. Immunol., 135, pp. 2562-2568 (1985) (Exhibit 6).

Factor ("OAF") stimulates bone resorption (Dewhirst, p. 2562). Dewhirst presents a dose-response curve showing a correlation between dose of OAF and bone resorption in cultured fetal rat long bones (Dewhirst, p. 2566). Furthermore, as stated in Dewhirst, "[a] correlation between OAF production by bone marrow cells and the extent of bone disease and myeloma cell mass has been demonstrated" (Dewhirst, p. 2562). Importantly, Dewhirst has shown that OAF is identical to IL-1 β (Dewhirst, p. 2562). Thus, Dewhirst supports a correlation between a decrease in IL-1 β levels and the treatment of bone disease.

A correlation between sepsis and septic shock and IL-1 has been established by Ohlsson.⁷ Ohlsson showed that eight of ten rabbits treated with *Escherichia coli* endotoxin died within 48 hours (Ohlsson, p. 550). In contrast, nine of ten rabbits treated with *Escherichia coli* endotoxin and IL-1ra "survived seven days and appeared to make a full recovery" (Ohlsson, p. 550). This study demonstrates that reduction of IL-1 levels is a viable treatment for sepsis and septic shock.

Humans with sepsis have responded favorably to IL-1ra treatment in a clinical trial reported by Boermeester.⁸

⁷ Ohlsson, K. et al., "Interleukin-1 Receptor Antagonist Reduces Mortality from Endotoxic Shock," Nature, 348, pp. 550-552 (1990) (Exhibit 7).

⁸ Boermeester, M.A. et al., "Interleukin-1 Blockade Attenuates Mediator Release and Dysregulation of the Hemostatic Mechanism During Human Sepsis," Arch. Surg., 130, pp. 739-748 (1995) (Exhibit 8).

Boermeester treated 26 patients who were suffering from sepsis syndrome with intravenous IL-1ra (Boermeester, p. 739). The patients were evaluated after 72 hours (Boermeester, p. 740). The patients that had been treated with IL-1ra had reduced levels of several inflammatory mediators (Boermeester, p. 742). Boermeester also discusses a study that demonstrated improved survival in a primate septic shock model (Boermeester, p. 739). Thus, a correlation between reduction in IL-1 levels and the treatment of sepsis and septic shock has been demonstrated.

As discussed above, Ku has also reported a correlation between IL-1 inhibition and treating inflammation and rheumatoid arthritis based on a mouse model of rheumatoid arthritis.

ICE (caspase-1) inhibitors have been shown to be effective at reducing the severity and mortality of induced pancreatitis in rats.⁹ Norman demonstrated, in a rat model of pancreatitis, that animals treated with the ICE inhibitor VE-13045, a novel, irreversible peptidyl ICE inhibitor, have a mortality rate of 22% as compared to a mortality rate of 68% for untreated animals (Norman, p. 116). Moreover, animals receiving the ICE inhibitor exhibited significantly less severe pancreatitis (Norman, p. 116). Norman concludes that "[t]he current series of experiments demonstrates the efficacy of VE-

⁹ Norman, J. et al., "Severity and Mortality of Experimental Pancreatitis are Dependent on Interleukin-1 Converting Enzyme (ICE)," J. Interferon Cytokine Res., 17, pp. 113-118 (1997) (Exhibit 9).

13045 in antagonizing ICE *in vivo* and confirms the importance of ICE in the processing and secretion of IL-1" (Norman, p. 117). Norman's study further demonstrates the profound detrimental effect of IL-1 β during acute pancreatitis and therapeutic applications of ICE blocked in this disease.

Estrov has linked suppression of IL-1 β production with suppression of proliferation of acute myelogenous leukemia cells.¹⁰ Estrov isolated and treated the cells with a small-molecule inhibitor of ICE (Estrov, p. 387). Proliferation of the inhibitor-treated cells was significantly suppressed, in contrast to control-treated cells. Estrov showed similar results with an IL-1-responsive AML cell line (Estrov, p. 387).

McCarthy has demonstrated that IL-1 plays a role in graft-versus-host disease (GVHD).¹¹ McCarthy teaches that the *in vivo* administration of human IL-1ra "reduce[d] the immunosuppression and mortality of GVHD" in mice that had received a graft of hematopoietic stem cells (McCarthy, p. 1915). McCarthy thereby establishes a link between IL-1 and GVHD and between IL-1 and autoimmune disease.

¹⁰ Estrov, Z. & Talpaz, M., "Role of Interleukin- β Converting Enzyme (ICE) in Acute Myelogenous Leukemia Cell Proliferation and Programmed Cell Death," Leukemia & Lymphoma, 24, pp. 379-391 (1997) (Exhibit 10).

¹¹ McCarthy, P.L., "Inhibition of Interleukin-1 by an Interleukin-1 Receptor Antagonist Prevents Graft-Versus Host Disease," Blood, 78, pp. 1915-1918 (1991) (Exhibit 11).

Lan has treated another autoimmune disease, glomerulonephritis, with IL-1ra.¹² Lan evaluated the effect of IL-1ra treatment on the progression of established rat accelerated anti-GBM disease, a severe model of glomerulonephritis (Lan, p. 1307). Lan determined that IL-1ra treatment over days 7 to 21 halted the progression of established disease (Lan, p. 1308). Lan concluded that IL-1 plays a key role in the progressive/chronic phase of renal injury in experimental crescentic glomerulonephritis, an autoimmune disease (Lan, p. 1303). Lan thereby establishes a link between IL-1 and autoimmune disease, and confirms the usefulness of ICE (caspase-1) inhibitors in the treatment of autoimmune diseases.

As discussed above, ICE (caspase-1) has been linked to the regulation of apoptosis in neurodegenerative diseases (see, specification page 3, line 12 to page 4, line 4). ICE is, therefore, a useful target for diseases associated with apoptotic pathways.

Specifically, *in vivo* inhibitory effects of ICE have been demonstrated via an apoptotic pathway. Endres has shown an ICE inhibitor (z-VAD.FMK) to exhibit neuroprotective effects in a mouse model of mild ischemia.¹³ Endres demonstrated that mice

¹² Lan, H.Y., "Interleukin-1 Receptor Antagonist Halts the Progression of Established Crescentic Glomerulonephritis in the Rat," Kidney Internat., 47, pp. 1303-1309 (1995) (Exhibit 12).

¹³ Endres, M. et al., "Attenuation of Delayed Neuronal Death After Mild Focal Ischemia in Mice by Inhibition of the Caspase

treated with 120 ng of z-VAD.FMK 6 hours after reperfusion decreased infarct size and neurologic deficits at 72 hours, and sustained these protective effects for at least 7 days (Endres, p. 242). Thus, Endres supports a correlation between ICE inhibitors and the treatment of stroke and other CNS injuries (Endres, p. 246).

Rouquet has also shown an ICE inhibitor to be effective in reducing *in vivo* liver apoptosis in mice.¹⁴ This type of apoptosis is found in viral and inflammatory liver diseases (Rouquet, p. 1192). Rouquet concludes that "in vivo inhibition of ICE-dependent apoptosis ... represents an attractive approach for treating liver injuries, including ... those caused by inflammatory, viral and autoimmune diseases" (Rouquet, p. 1194).

Yaoita also supports the attenuation of apoptotic effects by administration of an ICE inhibitor.¹⁵ Yaoita assessed the administration of the ICE-like inhibitor ZVAD-fmk in a rat model for myocardial reperfusion injury, and showed that ZVAD-fmk was effective in reducing myocardial reperfusion injury, which

Family," J. Cereb. Blood Flow and Metab., 18, pp. 238-247 (1998) (Exhibit 13).

¹⁴ Rouquet, N. et al., "ICE Inhibitor YVADcmk is a Potent Therapeutic Agent Against *In Vivo* Liver Apoptosis," Curr. Biol., 6, pp. 1192-1195 (1996) (Exhibit 14).

¹⁵ Yaoita, H. et al., "Attenuation of Ischemia/Reperfusion Injury in Rats by a Caspase Inhibitor," Circulation, 97, pp. 276-281 (1998) (Exhibit 15).

could be at least partially attributed to the attenuation of cardiomyocyte apoptosis (Yaoita, p. 279).

In addition to its role in the regulation of IL-1, apoptosis, and diseases related thereto, ICE (caspase-1) has been linked to the conversion of pro-IGIF to the pro-inflammatory cytokine IGIF, also known as IL-18, and to IFN- γ production *in vivo* (see, specification page 3, lines 9-13). IFN- γ has been shown to contribute to the pathology associated with a variety of inflammatory, infectious and autoimmune disorders and diseases. ICE is, therefore, also a useful target for IL-18-based therapeutic strategies because of its role in producing active IL-18.

ICE (caspase-1) activity has also been linked to intestinal inflammation, including colitis, inflammatory bowel disease, and Crohn's disease. Specifically, Siegmund discusses the role of ICE in the processing of IL-18.¹⁶ Siegmund showed that blockade of the inflammatory cytokine IL-18 in a mouse model of DSS-induced colitis significantly decreased histological signs of inflammation (Siegmund, p. 5).

A study on human myocardial tissue indicated that IL-1 β and IL-18 are present in the heart after ischemia.¹⁷ Pomerantz

¹⁶ Siegmund, B., "Interleukin-1 β Converting Enzyme (Caspase-1) in Intestinal Inflammation," Biochem. Pharmacol., 64, pp. 1-8 (2002) (Exhibit 16).

¹⁷ Pomerantz, B.J. et al., "Inhibition of Caspase 1 Reduces Human Myocardial Ischemic Dysfunction via Inhibition of IL-18 and IL-

has shown that administration of an ICE inhibitor before the onset of ischemia resulted in the attenuation of ischemia-induced myocardial dysfunction (Pomerantz, p. 2874). Pomerantz therefore supports a correlation between ICE and IL-18 inhibition and the treatment of degenerative diseases such as myocardial ischemia.

Vidal-Vanaclocha has investigated the role of IL-18 in mouse B16M cell adhesion to hepatic sinusoidal endothelium ("HSE") in a model of cancer cell adhesion.¹⁸ Importantly, administration of recombinant IL-18BP, an naturally occurring inhibitor of IL-18, completely reduced the adhesiveness of HSE for melanoma cells, indicating a strategic role for IL-18 in liver metastasis (Vidal-Vanaclocha, p. 738). Vidal-Vanaclocha thus supports a correlation between ICE and IL-18 inhibition and the treatment of cancer metastases.

Chen has reported that inhibition of caspases has efficacy in a mouse model Huntington's disease.¹⁹ Administration of either a broad caspase inhibitor or a combination of a caspase-1 inhibitor and a caspase-3 inhibitor, resulted in extended survival relative to the control group (Chen, p. 800).

1 β ," Proc. Natl. Acad. Sci., 98, pp. 2871-2876 (2001) (Exhibit 17).

¹⁸ Vidal-Vanaclocha, F. et al., "IL-18 Regulates IL-1 β -dependent Hepatic Melanoma Metastasis via Vascular Cell Adhesion Molecule-1," Proc. Natl. Acad. Sci., 97, pp. 734-739 (2000) (Exhibit 18).

¹⁹ Chen, M. et al., "Minocycline Inhibits Caspase-1 and Caspase-3 Expression and Delays Mortality in a Transgenic Mouse Model of Huntington Disease," Nature Med., 6, pp. 797-801 (2000) (Exhibit 19).

Chen concludes that "an effective therapeutic intervention in HD will likely require inhibition of at least both of these caspases" (Chen, p. 800). Importantly, applicants have demonstrated that their compounds inhibit both caspase-1 and caspase-3 (see specification as originally filed at p. 49, line 25 to page 50, line 3).

Grierson has linked caspase inhibition and Kennedy's disease in a whole cell model.²⁰ The caspase inhibitor VAD-fmk increased cell survival in a model of Kennedy's disease (Grierson, p. 19). Caspase activity has been linked to Kennedy's disease through cleavage of the androgen receptor.²¹ These documents support a correlation between caspase inhibition and Kennedy's disease.

A link has also been established between epilepsy and caspases.²² Kondratyev demonstrated that a "caspase-3 inhibitor ... significantly reduces vulnerability to the neuronal cell death that occurs" in an epilepsy model (Kondratyev, p. 222). Rats treated with the inhibitor before and again after a seizure had

²⁰ Grierson, A.J. et al., "Androgen Induced Cell Death in SHSY5Y Neuroblastoma Cells Expression Wild-type and Spinal Bulbar Muscular Atrophy Mutant Androgen Receptors'" Biochim. Biophys. Acta, 1536, pp. 13-20 (2001) (Exhibit 20).

²¹ Ellerby, L.M. et al., "Kennedy's Disease: Caspase Cleavage of the Androgen Receptor Is a Crucial Event in Cytotoxicity," J. Neurochem., 72, pp. 185-195 (1999) (Exhibit 21).

²² Kondratyev, A. & Gale, K., "Intracerebral Injection of Caspase-3 Inhibitor Prevents Neuronal Apoptosis After Kainic Acid-evoked Status Epilepticus," Mol. Brain Res., 75, pp. 216-224 (2000) (Exhibit 22).

"markedly" less apoptosis in the rhinal cortex and hippocampus compared to control animals (Kondratyev, p. 217 & 223). Other studies support this link.²³ For example, in a rat model of epilepsy, caspase inhibition also "significantly improved neuron survival ... following seizures" (Henshall, p. 1220, 1222).

Prion disease has been linked to caspase-3.²⁴ A hallmark of prion disease is the presence of prion protein "PrP" and neurodegeneration. Caspase-3 induction was shown to occur "significantly prior to" PrP deposition and the onset of clinical symptoms (Jamieson, p. 3569). Caspase-3 activation has also been shown in a human form of prion disease, Creutzfeldt-Jakob disease (CJD).²⁵ Puig demonstrated "selective activation of caspase-3 in association with increased cellular vulnerability in CJD" (Puig, p.1, abstract). These studies confirm a link between caspases and prion disease.

Li has linked caspase inhibition and spinal cord injury treatment.²⁶ Administration of a broad caspase inhibitor to mice

²³ Henshall, D.C et al., "Involvement of Caspase-3-like Protease in the Mechanism of Cell Death Following Focally Evoked Limbic Seizures," J. Neurochem., 74, pp. 1215-1223 (2000) (Exhibit 23).

²⁴ Jamieson, E. et al., "Activation of Fas and Caspase 3 Precedes PrP Accumulation in 87V Scrapie," Neurochem., 12, pp. 3567-3572 (2001) (Exhibit 24).

²⁵ Puig B. & Ferrer, I., "Cell Death Signaling in the Cerebellum in Creutzfeldt-Jakob Disease," Acta Neuropathol. (Berl.), 102, pp. 207-215 (2001) (Exhibit 25).

²⁶ Li, M. et al., "Functional Role and Therapeutic Implications of Neuronal Caspase-1 and -3 in a Mouse Model of Traumatic Spinal Cord Injury," Neurosci., 99, pp. 333-342 (2000) (Exhibit 26).

having spinal cord injuries "reduced post-traumatic lesion size and improved neurological recovery" (Li, p. 339). The observations included that IL-1 β levels after spinal cord injury, were 17-fold higher in injured mice than in control mice. However, treatment of the injured mice with a caspase inhibitor, led to a 52.3% reduction in IL-1 β levels (Li, p. 335, and Table 2, p. 337). According to Li, this study showed that "following acute surgical decompression and stabilization, local delivery of caspase inhibitors can be one of the components of an SCI treatment protocol in humans" (Li, p. 341).

Li's expectation that these results are applicable to humans is well grounded. Both apoptosis and activation of caspase-3 has been found in humans having spinal cord injuries.²⁷ According to Emery, "apoptotic cell death is observed from 3 hours to 8 weeks after traumatic human [spinal cord injuries]" (Emery, p. 918).

Activation of caspase-3 has been shown in humans suffering from traumatic brain injury.²⁸ Furthermore, caspase inhibition has been shown to be effective at treating traumatic

²⁷ Emery, E. et al., "Apoptosis After Traumatic Human Spinal Cord Injury," J. Neurosurg., 89, pp. 911-920 (2000) (Exhibit 27).

²⁸ Haerter, L. et al., "Caspase-3 Activity is Present in Cerebrospinal Fluid from Patients with Traumatic Brain Injury," J. Neuroimmunol., 121, pp. 76-78 (2001) (Exhibit 28).

brain injury in an animal model.²⁹ In particular, administration of a broad caspase inhibitor "improved motor and cognitive neurological dysfunction after [traumatic brain injury]" in rats (Knoblach, p. 1168). The injured animals performed better than control animals in several tests (Knoblach, p. 1161). These studies confirm the relationship between caspases and traumatic brain injury and demonstrate the efficacy of treating traumatic brain injury with caspase inhibitors.

Caspase inhibition has been linked to treatment of amyotrophic lateral sclerosis (ALS).³⁰ A broad caspase inhibitor demonstrated "inhibition of disease progression and extended survival in a transgenic mouse model of ALS (Li II, p. 338). Elevated caspase levels, particularly ICE levels, have been found in human ALS patients.³¹ Ethical considerations may have limited this study. Nevertheless, it indicates that the same disease state exists in human ALS patients as exists in animal models of ALS. It would, therefore, be believable to a skilled

²⁹ Knoblach, S.M. et al., "Multiple Caspases are Activated after Traumatic Brain Injury: Evidence for Involvement in Functional Outcome," J. Neurotrauma, 19, pp. 1155-1170 (2002) (Exhibit 29).

³⁰ Li, M. et al., "Functional Role of Caspase-1 and Caspase-3 in an ALS Transgenic Mouse Model," Science, 288, pp. 335-339 (2000) (Exhibit 30; "Li II").

³¹ Ilzecka, J. et al., "Interleukin-1 β Converting Enzyme/Caspase-1 (ICE/Caspase-1) and Soluble APO-1/Fas/CD 95 Receptor in Amyotrophic Lateral Sclerosis Patients," Acta Neurolog. Scand., 103, pp. 255-258 (2001) (Exhibit 31).

practitioner that caspase inhibition would be useful in methods for treating ALS.

Caspases have also been linked to Alzheimer's disease. Allen linked caspase inhibition to protection against β -amyloid peptide induced apoptosis.³² β -amyloid peptide is associated with neurodegeneration in Alzheimer's disease. Caspases have been shown to be activated in human Alzheimer's disease brains.³³ Importantly, other studies are confirming the link between caspases and Alzheimer's disease.³⁴ According to Su, "caspase-3 inhibition may be a viable therapeutic target for slowing the progression of AD" (Su, p. 356).

Caspase inhibition has been linked to the treatment of multiple sclerosis.³⁵ In a mice model (experimental autoimmune encephalomyelitis), a caspase-1 (ICE) inhibitor reduced encephalomyelitis at some phases of the disease course.³⁶

³² Allen, J.W. et al., "Multiple Caspases are Involved in β -Amyloid-Induced Neuronal Apoptosis," J. Neurosci. Res., 65, pp. 45-53 (2001) (Exhibit 32).

³³ Rohn, T.T. et al., "Caspase-9 Activation and Caspase Cleavage of tau in the Alzheimer's Disease Brain," Neurobio. Dis., 11, pp. 341-354 (2002) (Exhibit 33).

³⁴ Su, J.H. et al., "Activated Caspase-3 Expression in Alzheimer's and Aged Control Brain: Correlation with Alzheimer Pathology," Brain Res., 898, pp. 350-357 (2001) (Exhibit 34).

³⁵ Ahmed, Z. et al., "A Role for Caspase-1 and -3 in the Pathology of Experimental Allergic Encephalomyelitis," Am. J. Path., 161, pp. 1577-1586 (2002) (Exhibit 35).

³⁶ Furlan, R. et al., "Caspase-1 Regulates the Inflammatory Process Leading to Autoimmune Demyelination," J. Immunol., 163, pp. 2403-2409 (1999) (Exhibit 36).

Caspase-1 levels have been shown to be elevated in the brains of humans that had multiple sclerosis.³⁷ Furthermore, in a human cell line that is relevant to multiple sclerosis, a caspase inhibitor "was able to block the cytotoxic effects of TNF- α /IL-1 β in a dose-dependent manner" (Ming, p. 17).

Caspases have been linked to Parkinson's disease. A protein caspase inhibitor (p35) has been shown to reduce the effects of Parkinson's disease in a mouse model.³⁸ Caspase levels have been positively correlated in the brains of humans who had Parkinson's disease.³⁹

Caspases have been linked to atherosclerosis. Increased apoptosis is thought to be correlated with plaque complications in atherosclerosis, such as rupture.⁴⁰ Jacob demonstrated that caspase-3 is elevated in human plaques, which

³⁷ Ming, X. et al., "Caspase-1 Expression in Multiple Sclerosis Plaques and Cultured Glial Cells," J. Neurol. Sci., 197, pp. 9-18 (2002) (Exhibit 37).

³⁸ Viswanath, V. et al., "Caspase-9 Activation Results in Downstream Caspase-8 Activation and Bid Cleavage in 1-Methyl-4-Phenyl-1,2,3,6-Tetrahydropyridine-induced Parkinson's Disease," J. Neurosci., 21, pp. 9519-9528 (2001) (Exhibit 38).

³⁹ Hartmann, A. et al., "Caspase-3: A Vulnerability Factor and Final Effector in Apoptotic Death of Dopaminergic Neurons in Parkinson's Disease," PNAS, 97, pp. 2875-2800 (2000) (Exhibit 39).

⁴⁰ Jacob, T. et al., "Differential Proteolytic Activity and Induction of Apoptosis in Fibrous Versus Atheromatous Plaques in Carotid Atherosclerotic Disease," J. Vasc. Surg., 33, pp. 614-620 (2001) (Exhibit 40).

corroborates earlier work on "carotid artery plaques" (Jacob, p. 618).

Cell death has been linked to various types of graft rejection, including in coronary artery bypass grafts.⁴¹ In human tissue, caspase-3 was "expressed in all areas of the grafts" (Wang, p. 323).

Caspases have been linked to heart disease. A caspase-3 inhibitor has been shown to reduce myocardial stunning in a "working-heart rat model" (Ruetten, p. 2069).⁴² Caspase-3 has also been linked to heart disease in humans.⁴³

Caspases have also been linked to heart failure. Specifically, caspases have been shown to be elevated in patients undergoing heart failure.⁴⁴ Furthermore, the protein caspase

⁴¹ Wang, A.Y. et al., "Expression of Apoptosis-related Proteins and Structural Features of Cell Death in Explanted Aortocoronary Saphenous Vein Bypass Grafts," Cardiovasc. Surg., 9, pp. 319-328 (2001) (Exhibit 41).

⁴² Ruetten, H. et al., "Inhibition of Caspase-3 Improves Contractile Recovery of Stunned Myocardium, Independent of Apoptosis-inhibitory Effects," J. Am. Coll. Cardiology, 38, pp. 2063-2070 (2001) (Exhibit 42).

⁴³ Mallat, Z. et al., "Evidence of Apoptosis in Arrhythmogenic Right Ventricular Dysplasia," N. Eng. J. Med., 335, pp. 1190-1196 (1996) (Exhibit 43).

⁴⁴ Birks, E. et al., "Quantitative Myocardial Cytokine Expression and Activation of the Apoptotic Pathway in Patients Who Require Left Ventricular Assist Devices," Circul., 104 (suppl. I), pp. I233-I240 (2001) (Exhibit 44).

inhibitor p35 had "a positive impact on contractility" in a rabbit model of heart failure (Laugwitz, p. 2061).⁴⁵

Similarly, caspases have been linked to myocardial infarction. Administration of a caspase inhibitor reduced ischemia in a rat model.⁴⁶ Elevated levels of capase-3 and apoptosis have been observed in human heart tissue after acute myocardial infarction.⁴⁷ According to Baldi, these results in combination with "experimental models" shows that "anti-apoptotic therapy (i.e. treatment with ... a broad caspase inhibitor) reduced infarct size ... thus opening new avenues in the diagnosis and treatment of ischemic heart disease (Baldi, p. 173).

Sansonetti-1 demonstrates a critical role for IL-1 in the pathogenesis of shigellosis.⁴⁸ In an *in vivo* rabbit model of experimental shigellosis, treatment with soluble IL-1 receptor antagonist decreased inflammation, destruction and bacterial invasion of their tissues. Sansonetti-2 similarly confirms that

⁴⁵ Laugwitz, Karl-Ludwig et al., "Blocking Caspase-Activated Apoptosis Improves Contractility in Failing Myocardium," Human Gene Therapy, 12, pp. 2051-2063 (2001) (Exhibit 45).

⁴⁶ Yaoita, H. et al., "Attenuation of Ischemia/Reperfusion Injury in Rats by a Caspase Inhibitor," Circulation, 97, pp. 276-281 (1998) (Exhibit 46).

⁴⁷ Baldi, A. et al., "Apoptosis and Post-infarction Left Ventricular Remodeling," J. Mol. Cell. Cardiol., 34, pp. 165-174 (2002) (Exhibit 47).

⁴⁸ Sansonetti, P.J. et al., "Role of Interleukin-1 in the Pathogenesis of Experimental Shigellosis," J. Clin. Invest., 96, pp. 884-892 (1995) (Exhibit 48).

caspase-1 is essential for shigella-induced inflammation in mice.⁴⁹

Arndt confirmed a correlation between ICE, IL-18, and IL-1 β and acute lung injury using a murine model of hemorrhage or endotoxemia.⁵⁰ The studies implicate ICE and IL-18 in the modulation of the development of acute lung injury after endotoxemia (Arndt, p. 708).

Bataille confirmed a critical role for IL-1 β and IL-6 as osteoclast-activating factors responsible for the pathogenesis of bone lesions associated with multiple myeloma.⁵¹

Apoptosis, inflammatory cytokines, such as IL-1, and/or caspases have been linked to other diseases as follows. Hoek demonstrates a link between caspases and excess dietary alcohol intake disease.⁵² Feltkamp has linked apoptosis and uveitis.⁵³

⁴⁹ Sansonetti, P.J. et al., "Caspase-1 Activation of IL-1 β and IL-18 are Essential for *Shigella flexneri*-Induced Inflammation," Immunity, 12, pp. 581-590 (2000) (Exhibit 49).

⁵⁰ Arndt P.G., et al., "Expression of Interleukin-18 in the Lung After Endotoxemia or Hemorrhage-induced Acute Lung Injury," A.J. Respir. Cell Mol. Biol., 22, pp. 708-713 (2000) (Exhibit 50).

⁵¹ Bataille R., et al., "The Critical Role of Interleukin-6, Interleukin-1 β -Dependent and Macrophage Colony-stimulating Factor in the Pathogenesis of Bone Lesions in Multiple Myeloma," Int. J. Clin. Lab. Res., 21, pp. 283-287 (1992) (Exhibit 51).

⁵² Hoek, J.B. & Pastorino, J.G., "Excess Dietary Alcohol Intake Disease," Alcohol, 27, pp. 63-68-590 (2002) (Exhibit 52, abstract only).

⁵³ Feltkamp, T.E. & Ringrose, J.H., "Acute Anterior Uveitis and Spondyloarthropathies," Curr. Opin. Rheumatol., 10, pp. 314-318 (1998) (Exhibit 53, abstract only).

Rodriguez-Ramos has linked caspases and inflammatory peritonitis.⁵⁴ Ravage has linked inflammatory cytokines and burns.⁵⁵ Ehrmann⁵⁶ and Bantel⁵⁷ have linked caspases and hepatitis. Konishi has linked caspases and atopic dermatitis.⁵⁸ Akasaka has linked caspases and scarring.⁵⁹ Boudard has linked caspases and myelodysplastic syndrome.⁶⁰ Mongan has linked caspases and haemorrhagic shock.⁶¹ Zhao⁶² and James⁶³ have linked

⁵⁴ Rodriguez-Ramos, C., et al., "Expression of Proinflammatory Cytokines and their Inhibitors During the Course of Spontaneous Bacterial Peritonitis," Dig. Dis. Sci., 46, pp. 1668-1676 (2001) (Exhibit 54, abstract only).

⁵⁵ Ravage, Z.B., "Mediators of Microvascular Injury in Dermal Burn Wounds," Inflammation, 22, pp. 619-29 (1998) (Exhibit 55, abstract only).

⁵⁶ Ehrmann, J. Jr. et al., "Apoptosis-related Proteins, BCL-2, BAX, FAS, FAS-L and PCNA in Liver Biopsies of Patients with Chronic Hepatitis B Virus Infection," Pathol. Oncol. Res., 6, pp. 130-135 (2000) (Exhibit 56, abstract only).

⁵⁷ Bantel, H. et al., "Caspase Activation Correlates With the Degree of Inflammatory Liver Injury in Chronic Hepatitis C Virus Infection," Hepatology, 34, pp. 758-67 (2001) (Exhibit 57, abstract only).

⁵⁸ Konishi, H. et al., "IL-18 Contributes to the Spontaneous Development of Atopic Dermatitis-like Inflammatory Skin Lesion Independently of IgE/stat6 under Specific Pathogen-free Conditions," Proc. Natl. Acad. Sci. U.S.A. 20, pp. 11340-11345 (2002) (Exhibit 58, abstract only).

⁵⁹ Akasaka, Y., et al., "Enhanced Expression of Caspase-3 in Hypertrophic Scars and Keloid: Induction of Caspase-3 and Apoptosis in Keloid Fibroblasts in vitro," Lab. Invest., 80, pp. 345-357 (2000) (Exhibit 59, abstract only).

⁶⁰ Boudard, D. et al., "Expression and Activity of Caspases 1 and 3 in Myelodysplastic Syndromes," Leukemia, 14, pp. 2045-2051 (2000) (Exhibit 60, abstract only).

caspases to HIV-related encephalitis. Zhang has linked caspases and ageing.⁶⁴ Tsuda⁶⁵ and Sawaya⁶⁶ have linked caspases and alopecia and hair loss, respectively. Hauser has linked caspases and renal disease.⁶⁷ Yang has linked caspases and kidney disease.⁶⁸ Ashktorab has linked caspases and H. pylori-associated ulcer disease.⁶⁹ Perskvist has linked caspases and

⁶¹ Mongan, P.D., "Pyruvate Improves Redox Status and Decreases Indicators of Hepatic Apoptosis During Hemorrhagic Shock in Swine," Am. J. Physiol. Heart Circ. Physiol. 283, pp. H1634-644 (2002) (Exhibit 61, abstract only).

⁶² Zhao, M.L., et al., "Expression of Inducible Nitric Oxide Synthase, Interleukin-1 and Caspase-1 in HIV-1 Encephalitis," J. Neuroimmunol., 115, pp. 182-91 (2001) (Exhibit 62, abstract only).

⁶³ James, H.J. et al., "Expression of caspase-3 in brains from paediatric patients with HIV-1 encephalitis," Neuropathol. Appl. Neurobiol. 25, pp. 380-386 (1999) (Exhibit 63, abstract only).

⁶⁴ Zhang, Y. et al., "Age-associated Increases in the Activity of Multiple Caspases in Fisher 344 Rat Organs," Exp. Gerontol., 37, pp. 777-89 (2002) (Exhibit 64, abstract only).

⁶⁵ Tsuda, T. et al., "Inhibitory Effect of M50054, a Novel Inhibitor of Apoptosis, on Anti-Fas-antibody-induced Hepatitis and Chemotherapy-induced Alopecia," Eur. J. Pharmacol. 433, pp. 37-45 (2001) (Exhibit 65, abstract only).

⁶⁶ Sawaya, M.E. et al., "Effects of Finasteride on Apoptosis and Regulation of the Human Hair Cycle," J. Cutan. Med. Surg., 6, pp. 1-9 (2002) (Exhibit 66, abstract only).

⁶⁷ Hauser, P. & Oberbauer, R., "Tubular Apoptosis in the Pathophysiology of Renal Disease," Wien Klin. Wochenschr. 114, pp. 671-677 (2002) (Exhibit 67, abstract only).

⁶⁸ Yang, B. et al., "Caspase-3 and Apoptosis in Experimental Chronic Renal Scarring," Kidney Int., 60, pp. 1765-1776 (2001) (Exhibit 68, abstract only).

⁶⁹ Ashktorab, H., et al., "In vivo and in vitro Activation of Caspase-8 and -3 Associated with Helicobacter pylori Infection,"

tuberculosis.⁷⁰ Koedel⁷¹ and Braun⁷² have linked caspases to meningitis.

Thus, a link between caspase inhibition and the diseases recited in claims 7-10 and 13 has been established. Applicants have shown that caspase activation is associated with diseases and that caspase inhibition is associated with alleviation of diseases. In view of the teachings of applicants' specification and the knowledge in the art, the skilled artisan would be able to practice the claimed methods without undue experimentation and would expect the claimed methods to work.

For all of these reasons, applicants request that the Examiner withdraw these section 112, first paragraph rejections.

Microbes Infect., 4, pp. 713-22 (2002) (Exhibit 69, abstract only).

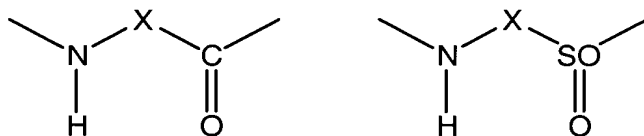
⁷⁰ Perskvist, N., et al., "Mycobacterium tuberculosis Promotes Apoptosis in Human Neutrophils by Activating Caspase-3 and Altering Expression of Bax/Bcl-xL via an Oxygen-dependent Pathway," J. Immunol., 168, pp. 6358-65 (2002) (Exhibit 70, abstract only).

⁷¹ Koedel, U., et al., "Evidence from Pharmacologic Caspase Inhibition and Caspase-1-deficient Mice," Ann. Neurol., 51, pp. 319-329 (2002) (Exhibit 71, abstract only).

⁷² Braun, J.S., et al., "Neuroprotection by a Caspase Inhibitor in Acute Bacterial Meningitis," Nat. Med., 5, pp. 298-302 (2002) (Exhibit 72, abstract only).

Claims 1-10 and 13 stand rejected as being obvious in view of Bemis et al. WO 95/35308. The Examiner contends that Bemis teaches several ICE inhibitors that include compounds in applicants' claims. Applicants traverse.

The Bemis' compounds have certain hydrogen bonding moieties that are absent from applicants' claimed compounds. According to Bemis, the hydrogen bonding moieties are an essential part of the ICE inhibitors (see page 14, lines 2-14; page 18, lines 21-30; page 25, lines 17-25)). Bemis depicts these moieties as either one of the following structures:



As noted by the Examiner, Bemis discloses pyrimidone compounds. Importantly, each of these pyrimidone compounds have the required hydrogen bonding moieties. Furthermore, all of the R_1 groups in Bemis noted by the Examiner call for these hydrogen bonding moieties (in formula α at page 26). For example, when R_1 is (t), one hydrogen bonding moiety is on the 5-membered ring and the other hydrogen bonding moiety is on the 6-membered ring.

In contrast, applicants' claimed compounds do not have these hydrogen bonding moieties. As amended claim 1 excludes a

-N(H)- group from ring C at the position beta to the indicated ring-B carbonyl. None of the rings exemplified in applicants' description have a hydrogen bonding moiety that would correspond to the hydrogen bonding moiety on, for example, the 5-membered ring in those Bemis compounds wherein R₁ is (t).

For all of the above reasons, applicants request that the Examiner withdraw these § 103 rejections.

Conclusion

In view of the above, applicants request that the Examiner enter the above amendments, consider the foregoing remarks, and allow the pending claims to issue.

Respectfully submitted,



Lisa A. Dixon (Reg. No. 40,995)
Attorney for Applicants

VERTEX PHARMACEUTICALS INCORPORATED
130 Waverly Street
Cambridge, Massachusetts 02139
Telephone: (617) 444-6396
Facsimile: (617) 444-6483

— — —

-



R^1 is hydrogen, CHN_2 , R, or $-CH_2Y$;

R is an aliphatic group, an aryl group, an aralkyl group, a heterocyclic group, or a heterocyclylalkyl group;

Y is an electronegative leaving group.

R is an aliphatic group, an aryl group, an aralkyl group, a heterocyclic group, or a heterocyclylalkyl group;

Y is an electronegative leaving group;

Y is an electronegative leaving group;

R² is CO₂H, CH₂CO₂H, or esters, amides or isosteres of CO₂H or
CH₂CO₂H thereof;

R^2 is CO_2H , CH_2CO_2H , or esters, amides or isosteres of CO_2H or CH_2CO_2H , thereof;

X_2-X_1 is $N(R^3)-C(R^3)[, C(R^3)_2-C(R^3), C(R^3)_2-N,]$ or $N=C[, C(R^3)=N,$
 $C(R^3)=C, C(=O)-N, \text{ or } C(=O)-C(R^3)]$;

each R³ is independently selected from hydrogen or C₁₋₆ aliphatic,
Ring C is a fused aryl ring, provided that the fused aryl ring

Ring C is a fused aryl ring, provided that the fused aryl ring does not have an -N(H)- group at the position adjacent to the

n is 0, 1 or 2; and

each methylene carbon in Ring A is optionally and independently substituted by =O, or by one or more halogen, C₁₋₄ alkyl, or C₁₋₄ alkoxy.

2. (Amended) The compound of claim 1 having one or more of the following [features] groups:

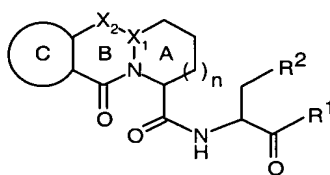
- (f) R¹ is -CH₂Y wherein Y is a halogen, OR, SR, or -OC=O(R), wherein R is an aryl group or heterocyclic group;
- (g) R² is CO₂H or esters, amides or isosteres of CO₂H thereof;
- (h) X₂-X₁ is N=C[, C(R³)=C, or C(=O)-N];
- (i) Ring C is a fused five or six-membered aromatic ring having zero to two heteroatoms; and
- (j) n is 0 or 1.

3. (Amended) The compound of claim 2 wherein:

- (f) R¹ is -CH₂Y wherein Y is a halogen, OR, SR, or -OC=O(R), wherein R is an aryl group or heterocyclic group;
- (g) R² is CO₂H or esters, amides or isosteres of CO₂H thereof;
- (h) X₂-X₁ is N=C[, C(R³)=C, or C(=O)-N];
- (i) Ring C is a fused five or six-membered aromatic ring having zero to two heteroatoms; and
- (j) n is 0 or 1.

4. (Amended) The compound of claim 3 wherein R^1 is $-CH_2Y$ wherein Y is F; R^2 is CO_2H or an ester or amide thereof; X_2-X_1 is $N=C[$, $CH=C$, or $C(=O)-N]$; Ring C is benzene ring; and n is 0 or 1.

5. (Amended) The compound of claim 1, said compound selected from the compounds: [listed in Table 2.]



| Example | R^1 | R^2 | Ring C | n | X_1 | X_2 |
|---------|---------|---------|----------|---|-------|-------|
| 1 | CH_2F | CO_2H | Benzo | 0 | C | N |
| 2 | CH_2F | CO_2H | Benzo | 1 | C | N |
| 3 | CH_2F | CO_2H | Benzo | 0 | C | C-H |
| 4 | CH_2F | CO_2H | Benzo | 1 | C | C-H |
| 5 | CH_2F | CO_2H | Benzo | 1 | N | C=O |
| 6 | CH_2F | CO_2H | Pyrazino | 1 | N | C=O |

Miller, OK

ANNALS OF THE NEW YORK ACADEMY OF SCIENCES
Volume 696

FILE COPY ICEPC

**IMMUNOSUPPRESSIVE AND
ANTIINFLAMMATORY DRUGS**

Edited by Anthony C. Allison, Kevin J. Lafferty, and Hans Fliri



*The New York Academy of Sciences
New York, New York
1993*

of deoxyspergualin on lymphocytes and
48: 1048-1052.

INGH & S. L. KELLEY. 1993. Mechanism
suppressive drug. Ann. N.Y. Acad. Sci.

ITZ. 1987. 15-Deoxyspergualin (a new
liferation. Transplant. Proc. 19: 4239-

II. FUJII, J. E. TALMADGE, T. TAKEUCHI.
ssant, markedly inhibits human mixed
activity in vitro. Int. J. Immunophar-

II. 1989. Serum effect on cellular uptake
and their metabolites by L5178Y cells.

AGI & H. UMEZAWA. 1987. Immunosup-
fect on the antibody responses. Immu-

ABE & T. TAKEUCHI. 1992. Myelopro-
splenic colony-forming cell injury and
Cancer Res. 83: 789-793.

deoxyspergualin on the expression of
pre-B cell line. Ann. N.Y. Acad. Sci.

põnsive variants of the mouse B cell
1. Som. Cell Genet. 9: 699-720.

pa immunoglobulin enhancer-binding
1. Cell 47: 921-928.

PPER & C. WALSH. Quantitation of the
ergualin and analogs with Hsp70 and

II. H. I. SCHER, L. A. SPRANCMANIS, C.
ING. 1991. Clinical pharmacology of
r. Cancer Res. 51: 3096-3101.

N. M. GREEN. 1991. A hypothetical
used on the peptide binding domain of

ON, H. Z. NELLY, V. A. RUFF, R. A.
component of the steroid receptor
homology to FKBP-12 and FKBP-13.

S. L. SCHREIBER. 1992. Association of
ticoid receptor complex. Science 256:

immunophilins and their immunosup-

GIBSON, J. GREENE, J. LEDBETTER, C.
tion in vivo by a soluble form of the
192.

The IL-1 β Converting Enzyme as a Therapeutic Target

DOUGLAS K. MILLER,^a JIMMY R. CALAYCAY,^b
KEVIN T. CHAPMAN,^c ANDREW D. HOWARD,^a
MATTHEW J. KOSTURA,^d SUSAN M. MOLINEAUX,^e
AND NANCY A. THORNBERRY^f

^aDepartment of Biochemical and Molecular Pathology

^bDepartment of Analytical Biochemistry

^cDepartment of Medicinal Chemical Research

^dDepartment of Cellular and Molecular Pharmacology

^eDepartment of Molecular Immunology

^fDepartment of Biochemistry

Merck Research Laboratories

Post Office Box 2000

Rahway, New Jersey 07065-0900

INTRODUCTION

Interleukin-1 β (IL-1 β) and interleukin-1 α (IL-1 α) are proinflammatory cytokines that promote leukocyte infiltration, prostaglandin synthesis, joint swelling, and tissue destruction.¹⁻⁸ IL-1 α and IL-1 β are members of a family of cytokines that also includes the IL-1 receptor antagonist protein (IL-1RA; see FIGURE 1), all of which are synthesized most prominently by monocytic cells. In contrast to the agonist activity of IL-1 α and IL-1 β ,⁹ IL-1RA is a strict antagonist on IL-1 receptors. It is synthesized on membrane-bound polysomes and exported via the classical endoplasmic reticulum (ER)/Golgi route where it becomes glycosylated. IL-1 α and IL-1 β , on the other hand, both lack leader sequences and are found in cytoplasm.¹⁰⁻¹⁴ IL-1 β is released from cells following stimulation, and it is the major agonist form of IL-1 found in biological fluids during diseased states.^{15,16} In contrast, IL-1 α remains largely intracellular in spite of its synthesis at significant levels.^{13,17} IL-1RA is also released from stimulated cells, but its appearance in blood is delayed relative to that of IL-1 β . Because IL-1RA is produced at about 100-fold higher concentrations than IL-1 β , it may serve to decrease IL-1 β activity.¹⁸

The importance of IL-1 as a target for antiinflammatory therapy is shown by the efficacy of IL-1RA, soluble IL-1R, and antiIL-1 receptor monoclonal antibodies in several animal models of human disease.¹⁹⁻²³ For example, PMN infiltration, swelling, and tissue necrosis were reduced in a rabbit model of inflammatory bowel disease by IL-1RA. Mortality was drastically reduced in murine graft vs host disease with the use of IL-1RA. Truncated soluble IL-1 receptors showed efficacy in reducing the swelling in cat adjuvant arthritis and blocking allograft rejection in mice.²⁴ Monoclonals against the IL-1 receptor have also been shown to block PMN extravasation and acute phase protein synthesis in mice.²⁵

The importance of IL-1 β as the primary form of IL-1 responsible *in vivo* has been confirmed recently by the discovery of pox virus proteins that are specific for IL-1 β . A pox virus protein, similar in structure to soluble type II IL-1 receptors, bound only IL-1 β and not IL-1 α . Production of this protein by the virus reduced the cell-

| | IL-1 α | IL-1 β | IL-1RA |
|---|---------------------|--|------------------------|
| Major Cell Source | Macrophage | Macrophage | Macrophage |
| Biosynthesis | 31 KDa Cytoplasm | 31 KDa Cytoplasm | 18-22 KDa Golgi-CHO |
| Proteolytic Processing for Activation | — | + (17.5 KDa) Asp ¹¹⁶ -Ala ¹¹⁷ | — |
| Receptor Active Form | 31 KDa Agonist | 17.5 KDa Agonist | 22 KDa Antagonist |
| Secreted <i>in vitro</i> | — | + | + |
| Presence in Disease States (CSF, Synovial Fluid) | + | +++ | ++++ |

FIGURE 1. Characteristics of the IL-1 family of molecules binding to IL-1 receptors.

mediated immune response induced by the infection, suggesting that the host response was primarily IL-1 β mediated.^{26,27}

ROLE OF ICE IN IL-1 ACTIVATION

While both IL-1 β and IL-1 α are synthesized as 31-kDa forms, only IL-1 α is active on IL-1 receptors without further processing; IL-1 β must first be processed from its inactive 31-kDa cytoplasmic precursor form (pIL-1 β) to an active 17.5-kDa mature form (mIL-1 β).^{9,17,28} A unique cytoplasmic enzyme thus far found only in monocytic cells has been identified, termed IL-1 β converting enzyme (ICE).²⁹⁻³⁴ ICE cleaves the Asp¹¹⁶-Ala¹¹⁷ bond of pIL-1 β to generate the mIL-1 β (see FIGURE 2). It also cleaves pIL-1 β at a secondary cleavage site Asp²⁷-Gly²⁸ to form small amounts of a 28-kDa fragment which can be further processed to the 17.5-kDa form. In contrast, ICE does not appear to cleave other proteins containing Asp-X linkages.³⁰ ICE is essential for the generation of mIL-1 β : cells lacking ICE activity even when transfected with pIL-1 β do not form active mIL-1 β .^{35,36} Another protein, crmA, synthesized by pox viruses provides additional support for the intracellular role of ICE in mIL-1 β formation: this serpin inhibits the processing of pIL-1 β by ICE.³⁷ No enzyme has been found to specifically process IL-1 α , although calpain has been shown to cleave IL-1 α .³⁸ Because IL-1 α remains largely cell associated and is not normally secreted, its appearance on the outside of cells may be associated with cell death.^{13,39} The presence of a processed extracellular active 17-KDa form of IL-1 α may result from cleavage by other proteases ("bystander proteases") at, for example, the Phe¹¹⁸-Leu¹¹⁹ bond⁴⁰ (see also Reference 41).

No mIL-1 β is found inside cells, and little pIL-1 β is found outside cells in the absence of cell damage. Pulse-chase analysis indicates that there is a precursor-product relationship between intracellular pIL-1 β and secreted mIL-1 β .^{13,42} Thus, the cleavage of pIL-1 β must be closely associated with the secretion of mIL-1 β . The unusual mechanism of synthesis, posttranslational modification, and cellular export of IL-1 β presents a number of potential sites for therapeutic interdiction. Because of the substrate specificity of ICE, development of an inhibitor for ICE represents a unique opportunity to develop a small molecule inhibitor of mIL-1 β formation.

CHARACTERIZATION OF ICE ENZYMATIC ACTIVITY

To determine the minimum recognition sequence of ICE, a 14-amino-acid peptide spanning the Asp-Ala cleavage site of pIL-1 β , NEAYVHDAPVRLN, as well as series of amino-terminal or carboxy-terminal truncations were prepared. These peptides were used as substrates for ICE, and their relative activity (V_{max}/K_m) was compared³⁴ (FIGURE 3, top). The results indicated that residues beyond P1' were not required, and at P1' only a methylanine substituent was necessary. At least four residues to the left of the cleavage site were necessary for activity; no cleavage activity was observed when the Tyr was removed.

Using a pentapeptide to further characterize the relative activity of individual amino acids in the sequence, it was determined that Ac-Tyr-Val-Ala-Asp-Gly was recognized best by ICE (FIGURE 3, bottom). Asp is absolutely required at the P1 position; glutamate at this position is cleaved only slightly. Small aliphatic residues (Gly and Ala) are preferred in P1'. Substitutions in P2 are well tolerated, Val is preferred in P3, and hydrophobic residues are preferred in P4. To facilitate rapid, sensitive measurement of ICE, a fluorometric assay utilizing Ac-Tyr-Val-Ala-Asp-amino-4-methylcoumarin (AcYVAD-AMC) as a substrate was subsequently employed.³⁴

ICE was found to be a thiol protease based upon its inhibition by a number of thiol selective reagents such as *N*-ethyl maleimide and iodoacetic acid (TABLE 1). It was not inhibited by inhibitors of serine or aspartyl proteases such as PMSF, leupeptin, or pepstatin. While ICE activity was not inhibited by EDTA, addition of *o*-phenanthroline resulted in inhibition after a prolonged incubation, suggesting that ICE might be a metalloprotease. This inhibition was reversed by high (10 mM) but not low (0.1 mM) DTT. The addition of copper increased the rate of inhibition, and

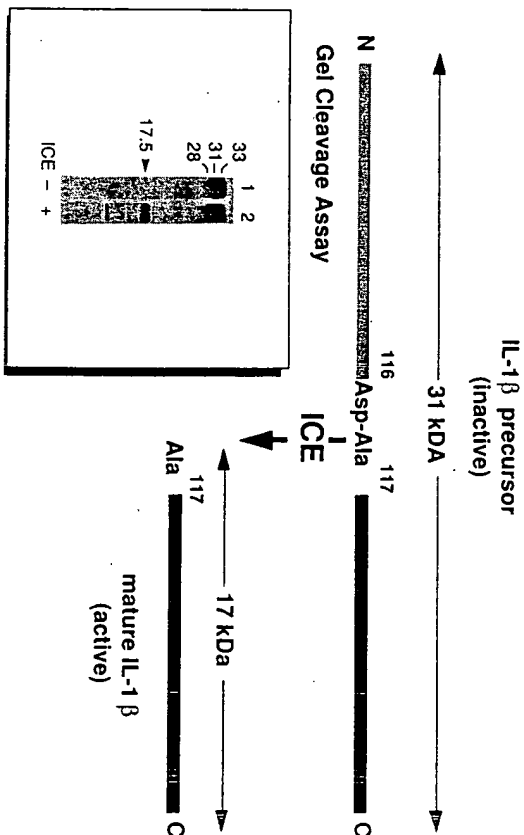


FIGURE 2. Cleavage of the IL-1 β precursor by ICE to generate mIL-1 β . Inset, autoradiograph of an SDS-PAGE gel of 31-kDa Asp³⁵-Met *in vitro* translated pIL-1 β cleaved by ICE to 17.5-kDa mIL-1 β .³⁰

the simultaneous addition of EDTA prevented any inhibition. These results suggested that the *o*-phenanthroline inhibition of ICE occurred by a metal-catalyzed oxidation of a labile thiol.³⁴

Definitive evidence that ICE was a cysteine protease came from potent inhibition by a peptide diazomethylketone (L-707,509) and a peptide aldehyde³⁴ (L-709,049; Figure 4). Addition of 250 nM of a peptide diazomethylketone resulted in time-dependent and complete inhibition of ICE activity, but this was prevented by saturating levels of the AcYVAD-AMC substrate ($70 \times K_m$; $K_m = 14 \mu\text{M}$). Addition of a high concentration of the substrate after inhibition had occurred did not relieve the inhibition, indicating that the inhibition was irreversible. The peptide aldehyde

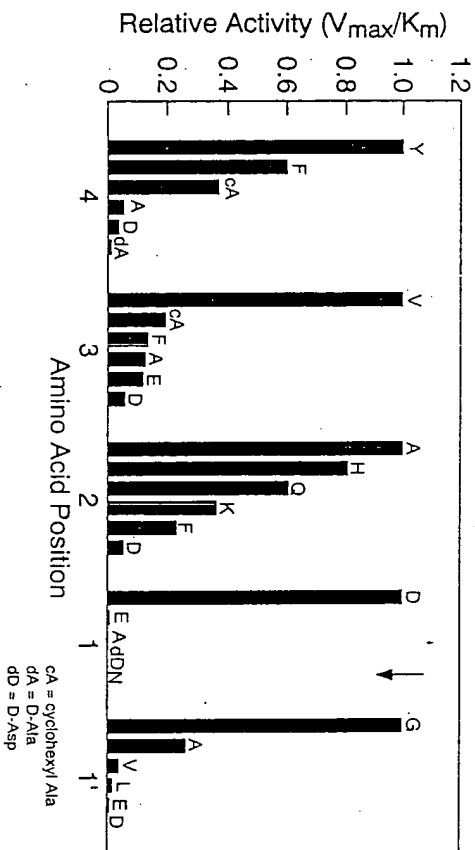
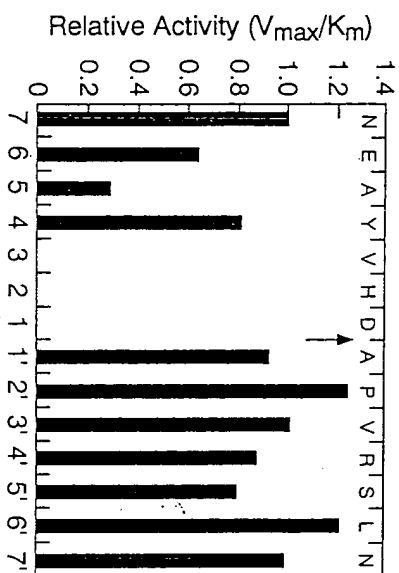


FIGURE 3. Effect of truncation and amino acid substitution on ICE activity. Substrates and products were separated by RP-HPLC and quantitated. Top, ICE activity (V_{max}/K_m) of either N- or C-terminally truncated peptides of the 14-mer pIL-1 β spanning peptide NEAYVH-DAPVRLN; activity was expressed relative to that of the 14-mer defined as 1.0. Bottom, ICE activity of a pentapeptide with the indicated amino acid substitutions; activity was expressed relative to Ac-YVADG defined as 1.0.

TABLE 1. Inhibition of YVAD-AMC Cleavage by Inhibitors of Various Classes of Proteases^a

| Class | Reagent | Inhibition |
|-------------------|---|-------------|
| Serine | PMSF (1 mM) | 0 \pm 2 |
| | DFP (1 mM) | 6 \pm 8 |
| | leupeptin (1 mM) | 1 \pm 2 |
| | pepsatin (0.1 mM) | 0 \pm 2 |
| Aspartyl Thiol | NEM (1 mM) | 99 \pm 1 |
| | iodoacetate (1 mM) | 99 \pm 5 |
| | E-64 (1 mM) | 0 \pm 1 |
| | EDTA (10 mM) | 13 \pm 10 |
| Metallo | OPAb ^b (1 mM) $t_{1/2} = 60$ min) | 98 \pm 3 |
| | OPA (1 mM) + 10 μM Cu ²⁺ ($t_{1/2} = 1$ min) | 99 \pm 3 |
| | OPA + EDTA | 10 \pm 10 |
| | OPA + 10 mM DTT | 10 \pm 10 |
| | OPA + 0.1 mM DTT | 98 \pm 3 |

^a Assays were done at the indicated concentration of inhibitors and expressed as a percentage of uninhibited activity. Inhibitors included phenylmethylsulfonylfluoride (PMSF), diisopropyl fluorophosphate (DFP), *N*-ethyl maleimide (NEM), and 1,10 (*ortho*)-phenanthroline (OHPA).
^b O-Phenanthroline inhibits ICE via metal catalyzed oxidation.

L-709,049 was also a competitive inhibitor of ICE activity, but saturating levels of substrate added after inhibition had occurred could reverse the inhibition. A competitive substrate peptide hydroxylamine (L-700,018) could also inhibit ICE cleavage, as shown here using *in vitro* translated ³⁵S-Met-labeled pIL-1 β (Figure 5). ICE was not inhibited by a specific elastase inhibitor (L-680,833).⁵¹

PURIFICATION AND STRUCTURE OF ACTIVE ICE

Active ICE was purified to homogeneity by conventional ion exchange and reverse phase high-performance liquid chromatography (RP-HPLC) techniques⁴¹ as well as with an inhibitor affinity column.³⁴ Because the P2 position in ICE substrates was relatively insensitive to substitution (Figure 3), a reversible peptide aldehyde inhibitor was prepared with Lys in place of Ala in P2. The Ac-YVAD-CHO was coupled via a spacer arm to Sepharose 4B (Figure 6) to generate a specific affinity matrix. Crude dialyzed THP-1 cytosol or a partially purified DEAE pool of that cytosol was allowed to bind to the column and extensively washed. ICE was specifically eluted with 100 μM L-709,049, and found to contain by sodium dodecyl sulfate-polyacrylamide gel electrophoresis (SDS-PAGE) two tightly associated proteins at 20 and 10 kDa (termed p20 and p10 respectively) in a 1:1 ratio (Figure 6). To recover active ICE, the L-709,049 bound ICE was first incubated with oxidized glutathione (to form a stable, inactive enzyme-glutathione conjugate) and hydroxylamine (to destroy the aldehyde inhibitor). Secondly, after desalting, DTT was added to remove the glutathione and generate the active enzyme.

Because the Cys active site thiol is more than 10-fold more reactive than ordinary thiols, the Cys could be readily labeled with ¹⁴C-iodoacetate. Since the alkylation was competitive with substrate, saturating levels of substrate could prevent the labeling. As shown in Figure 7A, ICE inhibition could be almost totally achieved with 100

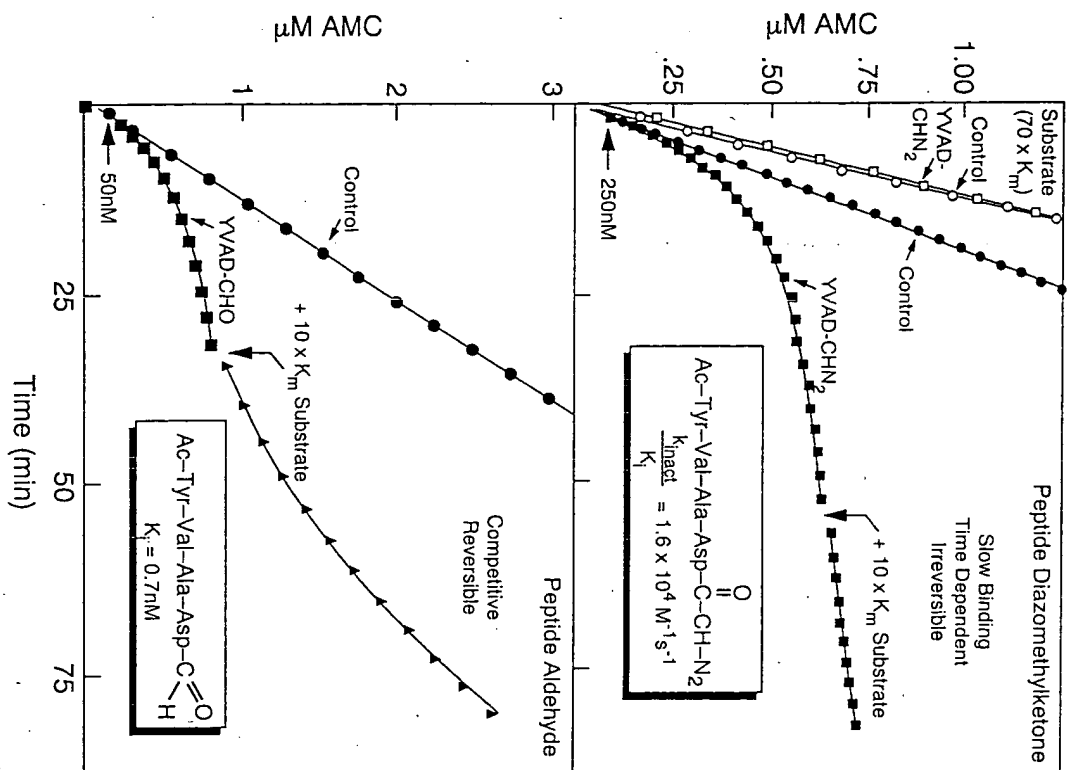


FIGURE 4. Inhibition of ICE by the thiol protease inhibitors Ac-VVAD-diazomethylketone (L-707,509, top) and aldehyde (L-709,049, bottom) using Ac-VVAD-AMC at its K_m (14 μM). (Taken from Thornberry *et al.*,³⁴ with permission.)

μM iodoacetic acid at 40 min. Under these conditions in the absence of substrate, the p20 protein was selectively labeled (FIGURE 7B). With saturating amounts of substrate where no enzyme inhibition was observed, no p20 labeling occurred. Isolation of the p20 followed by tryptic cleavage and C₈ RP-HPLC separation of the resultant peptides led to the identification of a single labeled peptide (FIGURE 7C) which had the sequence Val-Ile-Ile-Gln-Ala-(¹⁴C)Cys.

After obtaining sequence of tryptic and Asp-N peptides of the p20 and p10

proteins, degenerate oligonucleotides were used to PCR ICE cDNA fragments. These were used to screen a THP.1 monocytic cell cDNA library for full-length cDNA clones. All clones cross-hybridized with probes to both p20 and p10, indicating that both ICE proteins were encoded on a single mRNA. The resultant open reading frame encoded a 45-kDa protein (p45; FIGURE 8) which contained a 13-kDa polypeptide N-terminal to the p20 and a 2-kDa peptide separating the p20 from the p10 which were not found on the isolated active enzyme (FIGURE 9). No sequence homology to other Cys proteases or other proteins in the protein databank was observed.³⁴ The human cDNA was used to clone out the mouse^{44,45} and rat⁴⁶ forms of the enzyme (FIGURE 8). All three proteins contained the active site Cys with considerable stretches of amino acid identity particularly in the p10 region where there was 81% amino acid identity between the mouse and human proteins. Identity was less in the p20 region (62%) and still less in the pro domain (53%).⁴⁴ An alternatively cleaved, 1.6-kDa higher molecular weight form of the p20, termed p22, was in some cases purified along with the p20 protein (FIGURE 9).⁴³ All four cleavage sites generating the p20, p22, and p10 proteins followed Asp residues, perhaps indicating autoproteolysis of the p45.³⁴

The p45 form of ICE is the major form of ICE found in monocytic cells as determined by immunoblots with antibodies generated to affinity purified human ICE. Extracts of p45 have, however, no detectable pIL-1 β cleavage activity. Only after dialysis or short incubations at 30°C, when p45 is cleaved to the p20/p10 form of the enzyme, is significant pIL-1 β cleavage activity seen.⁴⁷ Both p20 and p10 are necessary for ICE activity; ion exchange column fractions of cytoplasmic extracts containing p20 in the absence of p10 contain no ICE activity.⁴³

Expression in COS-7 cells of the p45 ICE protein resulted in generation of pIL-1 β cleavage activity that could be inhibited by the peptide aldehyde inhibitor L-709,049 (FIGURE 10). An ¹¹⁶Asp to Ala mutant of pIL-1 β was not a substrate for

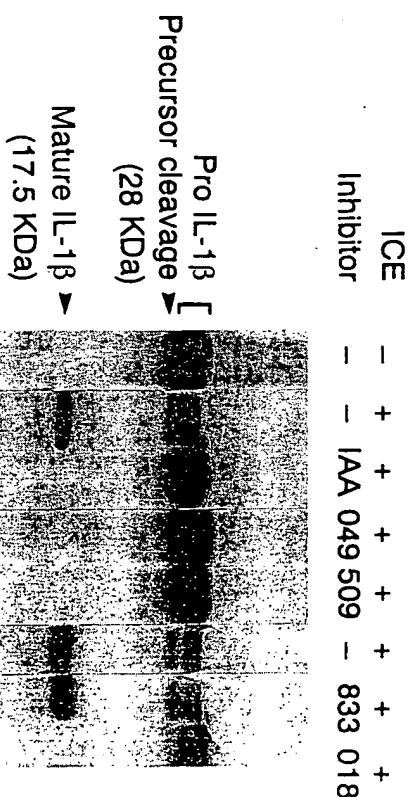


FIGURE 5. Inhibition of ICE cleavage of ³⁵S-Met-labeled pIL-1 β by various inhibitors: IAA, iodoacetic acid, 5 mM; 049, L-709,049, Ac-VVAD-CHO, 0.5 μM ; 509, L-707,509, Ac-VVAD-CN₂, 10 μM ; 833, L-680,833, 5 μM ; 018, L-700,018, Ac-VVAD-NH₂OH, 0.5 mM.

the recombinant ICE.³⁴ Expression of human p45 in *Escherichia coli* or *baculovirus* systems, followed by purification on the peptide aldehyde affinity column resulted in the purification of both p20 and p10 in 1:1 ratios.⁴⁸ Presumably the N-terminal domain of the p45 is necessary for proper folding of the p20 and p10 proteins;

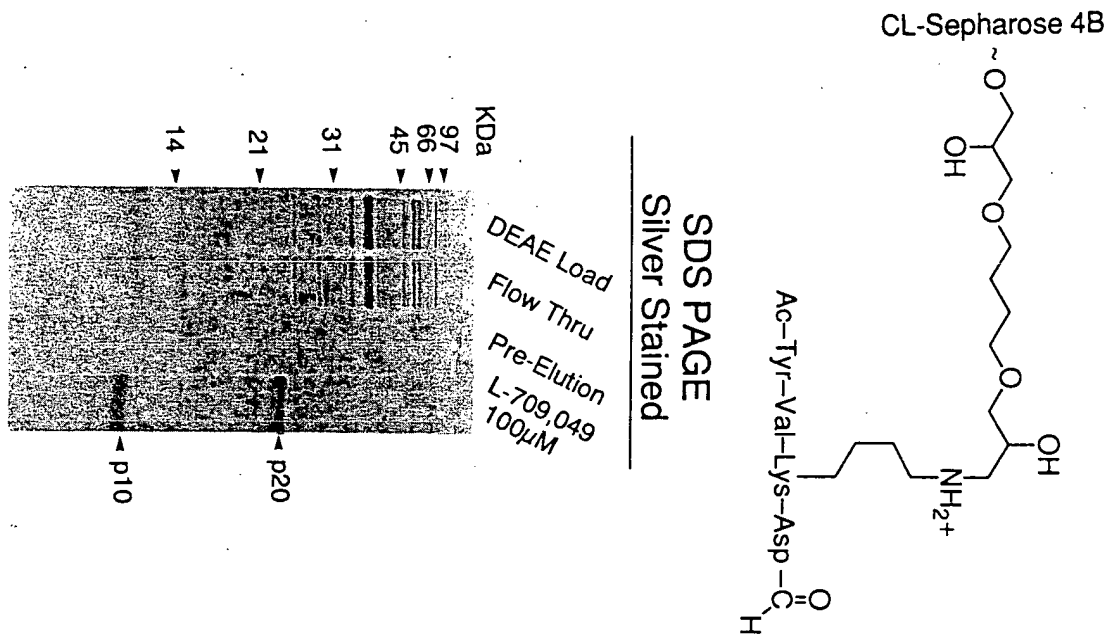


FIGURE 6. Affinity purification of ICE. Top: A peptide aldehyde affinity matrix was prepared by coupling AcYVKD-CHO to Sepharose 4B as shown.³⁴ Bottom: Silver-stained SDS-PAGE of fractions from an affinity column purification beginning with a partially purified DEAE fraction of ICE.⁴³ The load, the flowthrough fraction, a column fraction after extensive washing, and the proteins eluted by 100 μ M L-709,049 are shown.

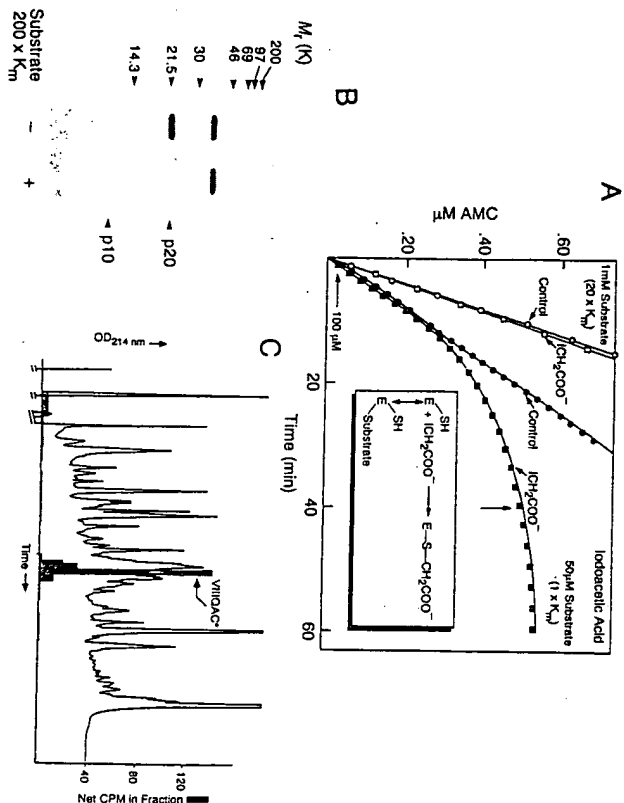


FIGURE 7. Inhibition of ICE by 14 C-iodoacetic acid and its labeling of the active site Cys. A: Kinetic analysis of iodoacetic acid inhibition of ICE using 100 μ M iodoacetic acid and its competition by saturating substrate. B: Under conditions of 99% inhibition of ICE (40 min), the p20 protein found in a partially purified sulfolipyl-HPPLC fraction of active⁴³ THP.1 ICE was labeled and identified following SDS-PAGE and autoradiography.³⁴ C: C α -RP-HPPLC chromatography of the tryptic peptides of the p20 labeled with 14 C-iodoacetic acid (the p20 was purified by C α -RP-HPPLC prior to trypsin cleavage). Only one peptide was labeled, and sequencing of this peptide revealed that the active site Cys was found in a sequence VIIHQAC.⁴³

coexpression of isolated p20 and p10 together in *E. coli* did not produce any active enzyme.⁴⁸ The activity of the recombinant enzyme was comparable to that of the native THP.1 enzyme; the ICE inhibitor affinity column yielded similar amounts of isolated enzyme for the same amount of activity units applied. Occasionally a processed form of p10, termed p7, presumably also formed by autocatalysis, could be copurified on the affinity column.⁴⁸ This form could also be generated in small amounts in highly purified fractions of THP.1 ICE where it contained substantially less activity.⁴³

EFFECT OF INHIBITION OF ICE ON IL-1 β SECRETION FROM MONOCYTES

To determine the effect of ICE inhibitors on mL-1 β production in human monocytes, 35 S-Met labeled heparinized blood was stimulated with heat-killed *Staphylococcus aureus* which has been shown to promote both rapid synthesis of pIL-1 β as well as rapid release extracellularly of mL-1 β .⁴⁹ When this stimulation was performed on cells preincubated with the peptide aldehyde inhibitor L-709,049, mL-1 β release was inhibited in a dose-responsive fashion with an IC₅₀ of about 2

μM (Figure 11). In contrast, the addition of a control peptide aldehyde with a D-Ala residue in the P3 position ($K_i = 1.5 \mu\text{M}$ vs. $K_i = 0.8 \text{ nM}$ for L-709,049) resulted in little observable inhibition of mL-1 β release.³⁴ The specificity of this inhibition for IL-1 β release was shown by the lack of inhibition of TNF α , IL-6, or IL-8 release by the same cells (Figure 12).

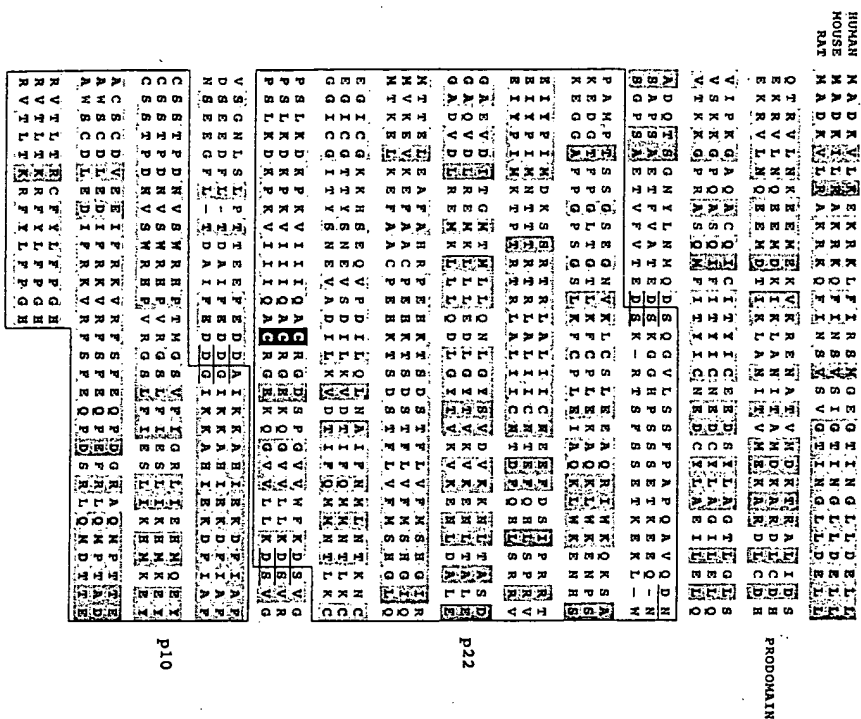


FIGURE 8. The amino acid sequence of human, mouse, and rat ICE. ICE was cloned as described.^{34,44,46} and the aligned open reading frame is shown. Shaded areas indicate amino acids of identity or close similarity. The boxed in regions correspond to the sequence contained within the p22 and p10 proteins. The active site Cys is shown in black. Sites of cleavage to form the individual p22, p20, and p10 proteins are underlined.

DISCUSSION

We have succeeded in purifying, characterizing, and expressing ICE, a unique Cys protease from monocytic cells that cleaves pIL-1 β at the Asp¹¹⁶-Ala¹¹⁷ bond. That ICE is a cysteine protease is shown by its sensitivity to known nonspecific thiol

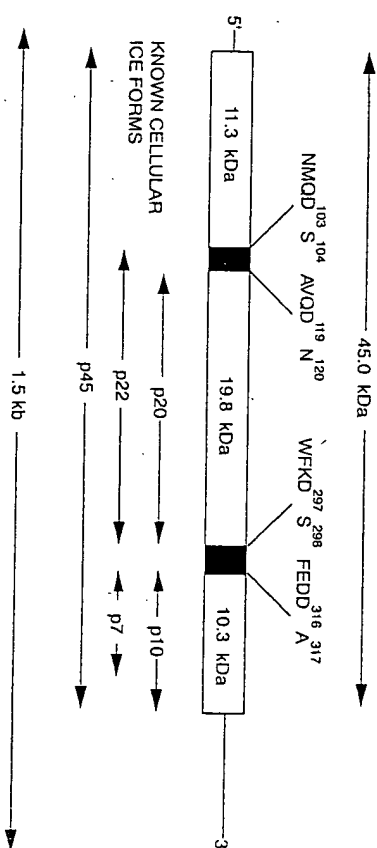
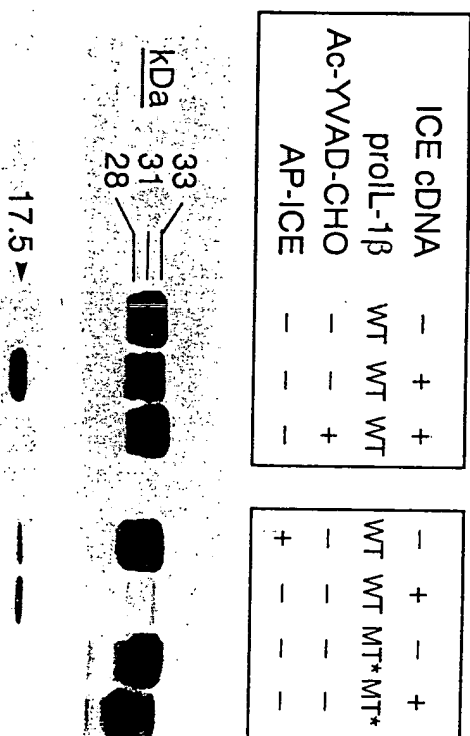


FIGURE 9. Structural organization of the human ICE precursor protein (p45) and the sites of cleavage found in ICE forms identified in THP-1 cells and recombinant expression systems, including p22, p20, p10, and p7, a truncated form of p10.

alkylating agents such as NEM and iodoacetic acid, and its insensitivity to Ser, Asp, or metalloprotease inhibitors. More definitively, such specific agents as tetrapeptide aldehydes or diazomethylketones inhibit ICE, while, in contrast, a truncated carboxybenzoyl aspartyl diazomethylketone is 10,000-fold less potent as an ICE inhibitor.³⁴ Furthermore, the replacement of the active site Cys with Ala totally eliminates any ICE activity.⁵⁰ The minimum recognition sequence for ICE is a relatively small



* Asp¹¹⁶ → Ala¹¹⁶

FIGURE 10. Functional expression of active recombinant ICE expressed in COS-7 cells. Extracts of cells transfected with human p45 ICE were incubated with ³⁵S-Met-labeled wild-type pIL-1 β (WT) or a Ala¹¹⁶ mutant of IL-1 β (MT) in the presence or absence of affinity purified ICE (taken from Reference 34 with permission). The resultant samples were separated by SDS-PAGE and visualized by autoradiography.

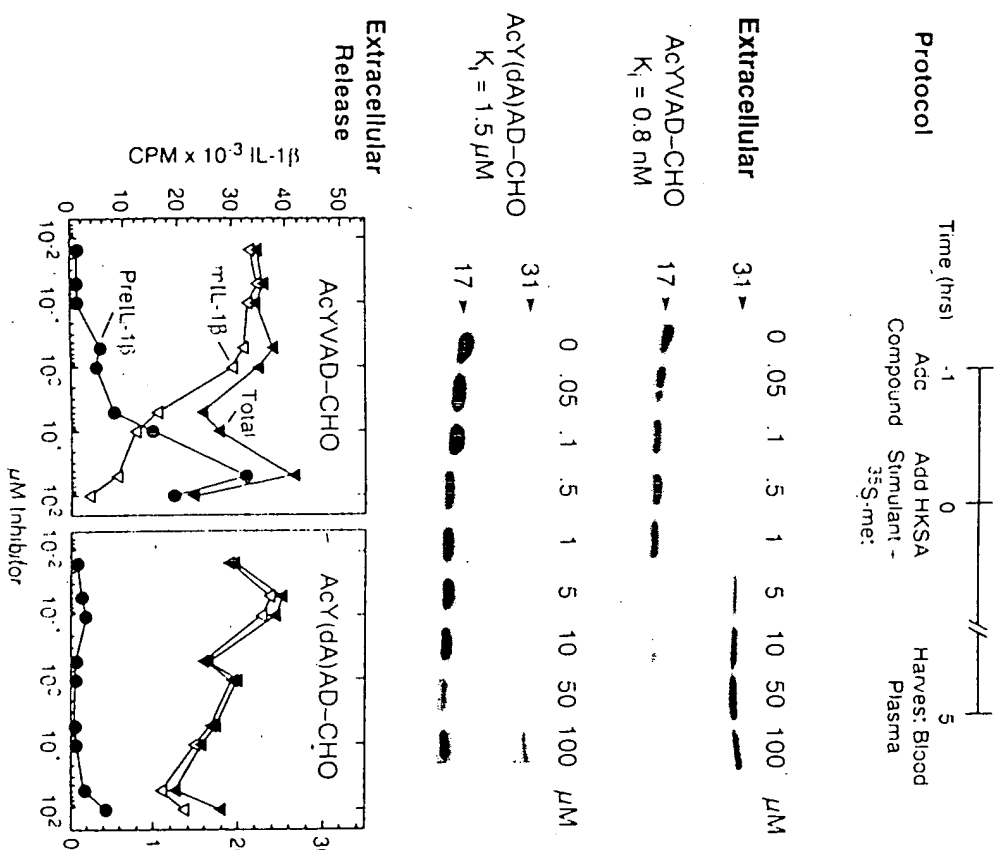


FIGURE 11. Inhibition of mIL-1 β release from human peripheral blood monocytes by a peptide aldehyde inhibitor (AcYVAD-CHO) or a relatively inactive D-Ala control peptide (AcYdaAD-CHO). ^{35}S -Met-labeled heparinized blood was preincubated with indicated concentrations of the inhibitor for 1 h, followed by a 5-h incubation with heat-killed *Staphylococcus aureus*. The plasma was removed and immunoprecipitated with antiIL-1 β antiserum, and the immunoprecipitates were separated by SDS-PAGE and subjected to autoradiography. Radioimaging of the individual bands is shown at the bottom (Taken from Reference 34 with permission).

tetrapeptide characterized most prominently by the absolute necessity for an Asp in P1 and secondarily by the need for a relatively large hydrophobic group in P4. ICE bears no homology to other known Cys or Ser proteases; the original observation of active site sequence similarity to Ser proteases³⁴ was not borne out when the mouse and rat sequences were obtained⁴⁴⁻⁴⁶ in that the Ser289 was replaced by a Lys.

ICE itself appears to require processing before it can become active. While it is synthesized as a 45-kDa protein and is the predominant cellular form seen in monocytic cells, it has no detectable pIL-1 β cleavage activity until removal of a precursor domain of about 13 kDa and a 2-kDa intervening piece between the p20 and p10 proteins. Exactly how and where this processing occurs is not known, but all of the cleavage sites are preceded by Asp residues. Because purified ICE can cleave the p45 precursor, it is possible that this processing is autocatalytic.³⁴

Whereas active ICE is a complex of freely dissociable inactive monomers,³⁴ there is no evidence that the p20 and p10 polypeptides themselves are freely dissociable from one another. Simultaneous expression of both p10 and p20 in *E. coli* does not generate active ICE.⁴⁸ Furthermore, purification by ion exchange columns of active ICE from THP-1 cytoplasmic extracts has shown no evidence for p10 separate from p20.⁴³ What is seen is that p10 is susceptible to proteolysis, and that p20 is found associated not only with intact p10, but also with a lower molecular weight C-terminally cleaved form of p10 (p7) forming an ICE complex with reduced activity. p20 can also be found with all of the p10 removed, in which case no ICE activity is seen.⁴³ Thus, the p10 part of ICE is clearly needed for ICE activity. Not surprisingly, it is the most conserved portion of ICE (Figure 8).

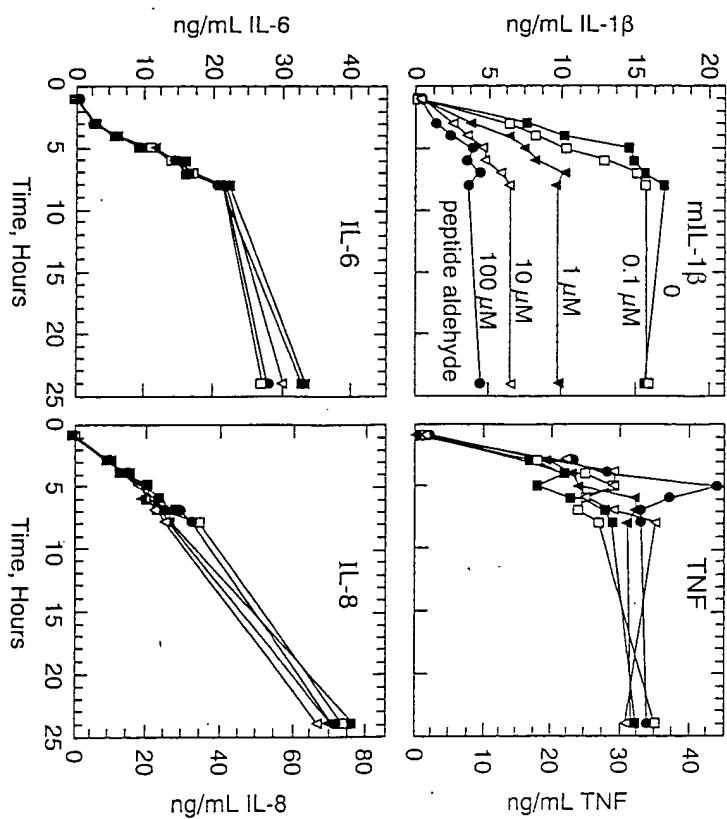


FIGURE 12. Effect of a specific ICE inhibitor on release of cytokines from *S. aureus*-stimulated human peripheral blood monocytes. Various concentrations of the peptide aldehyde inhibitor (AcYVAD-CHO) were preincubated with cells as described in Figure 13, and the supernatants were analyzed by ELISA for IL-1 β , TNF α , IL-6, or IL-8 release.

We have shown that specific inhibitors of ICE can be synthesized; the peptide aldehyde inhibitor affinity column will purify active ICE from THP-1 cytosol in a single step. Furthermore, this inhibitor can inhibit release of mL-1 β from activated monocytes without preventing the release of TNF α , IL-6, or IL-8. Even though inhibition of ICE inhibits cellular pIL-1 β processing, pIL-1 β secretion from the monocyte cell is unaffected (see Figure 13); that is, secretion occurs independently of processing. A critical issue, then, in the development of a therapeutic ICE inhibitor is whether or not pIL-1 β might be processed by "bystander proteases" at sites of inflammation to yield an active product with activity similar to mL-1 β . Secondly, there is the question of whether other cytokines such as TNF α or IL-1 α released from damaged cells might be sufficient to maintain the inflammatory response.

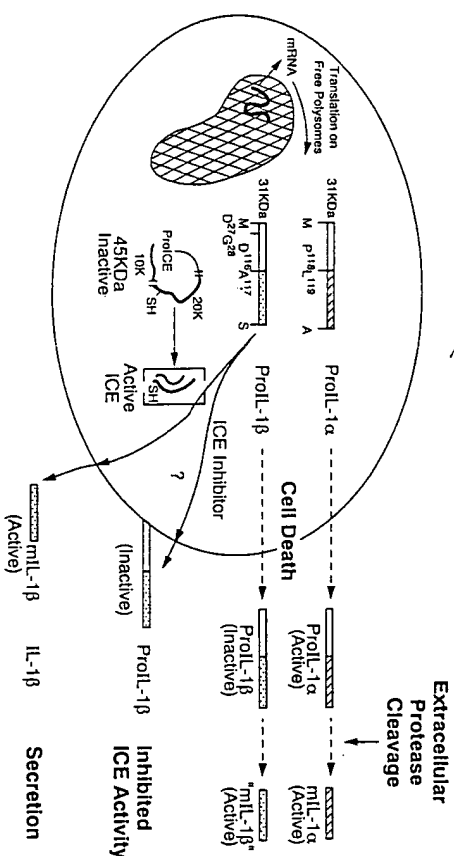


FIGURE 13. Schema of IL-1 processing and secretion. IL-1 α and IL-1 β are synthesized as 31-kDa cytoplasmic precursor proteins. The precursors are ordinarily not released from cells except following cell damage or death, at which time they could be potentially cleaved by other proteases. The 31-kDa IL-1 β is normally processed to the 17.5-kDa mL-1 β by an active form of ICE that is itself activated from a 45-kDa precursor. Cleavage of pIL-1 β occurs independently of mL-1 β secretion, since inhibition of ICE cleavage results in extracellular accumulation of pIL-1 β .

ACKNOWLEDGMENTS

We thank Drs. John Schmidt and Michael Tocci for their support and critical comments concerning these studies.

REFERENCES

- SCHMIDT, J. A. & M. J. TOCCI. 1990. In The Handbook of Experimental Pharmacology 1. Peptide Growth Factors and Their Receptors. M. Sporn & A. Roberts, Eds. 95: 473-521. Springer Verlag, Berlin, Germany.
- DINARELLO, C. A. 1988. FASEB J. 2: 108-115.

MILLER *et al.*: IL-1 β CONVERTING ENZYME

- PETTIPHER, E. R., G. A. HIGGS, & B. HENDERSON. 1986. Proc. Natl. Acad. Sci. USA 83: 8749-8753.
- STIMPSON, S. A., F. G. DALLDORF, I. G. OTTERNESS & J. H. SCHWAR. 1988. J. Immunol. 140: 2964-2969.
- HOM, J. T., A. M. BENDALE & D. G. CARLSON. 1988. J. Immunol. 141: 834-841.
- EASTGATE, J. A., N. C. WOOD, F. S. DI GIOVINI, J. A. SYMONS, F. M. GRIMMONT & G. W. DUFF. 1988. Lancet ii: 706-709.
- WADA, H., S. TAMAKI, M. TANIGAWA, M. TAKAGI, Y. MORI, A. DEGUCHI, N. KATAYAMA, T. YAMAMOTO, K. DEGUCHI & S. SHIRAKAWA. 1991. Thromb. Haemostasis 65: 364-368.
- STARNES, J. 1991. Semin. Hematol. 28: 34-41.
- MOSLEY, B., D. L. URDAL, K. S. PRICKETT, A. LARSEN, D. COSMAN, P. J. CONLON, S. GULLS & S. K. DOWER. 1987. J. Biol. Chem. 262: 2941-2944.
- GIRI, J. G., P. T. LOMEDICO & S. B. MIZEL. 1985. J. Immunol. 140: 343-349.
- AURON, P. E., S. J. WARNER, A. C. WEBB, J. G. CANNON, H. A. BERNHEIM, K. J. MCADAM, L. J. ROSENWASSER, G. LOPRESTE, S. F. MUCCI & C. A. DINARELLO. 1987. J. Immunol. 138: 1447-1456.
- SINGER, I. I., S. SCOTT, G. L. HALL, G. LIMUCCO, J. CHIN & J. A. SCHMIDT. 1988. J. Exp. Med. 167: 389-407.
- HAZUDA, D. J., J. C. LEE & P. R. YOUNG. 1988. J. Biol. Chem. 263: 8473-8479.
- HAZUDA, D., R. L. WEBB, P. SIMON & P. YOUNG. 1989. J. Biol. Chem. 264: 1689-1693.
- GRASSI, J., C. J. ROBERGE, Y. FROBERT, P. PRADELLES & P. E. POUBELLE. 1991. Immunol. Rev. 119: 125-145.
- AOTSUKA, S., K. KAKAMURA, T. NAKANO, M. KAWAKAMI, M. GOTO, M. OKAWA-TAKATSUJI, M. KINOSHITA & R. YOKOHARI. 1991. Ann. Rheumat. Dis. 50: 27-31.
- LONNEMANN, G., S. ENDRES, J. W. M. VAN DER MEER, J. G. CANNON, K. M. KOCH & C. A. DINARELLO. 1989. Eur. J. Immunol. 19: 1531-1536.
- GRANOWITZ, E. V., A. A. SANTOS, D. D. POUTSIKA, J. G. CANNON, D. W. WILMORE, S. M. WOLFF & C. A. DINARELLO. 1991. Lancet 338: 1423-1424.
- AREND, W. P. 1990. Prog. Growth Factor Res. 2: 193-205.
- DINARELLO, C. S. & R. C. THOMPSON. 1991. Immunol. Today 12: 404-410.
- DINARELLO, C. A. 1992. Semin. Immunol. 4: 133-145.
- OHSSON, K., P. BJORK, M. BERGENFELDT, R. HAGEMAN & R. C. THOMPSON. 1990. Nature 348: 550-552.
- SMITH, R. J., J. E. CHIN, L. M. SAM & J. M. JUSTEN. 1991. Arthritis Rheumatism 34: 78-83.
- FANSTLOW, W. 1990. Science 248: 739-742.
- MCINTYRE, K. W., G. J. STEPHAN, K. D. KOLINSKY, W. R. BENJAMIN, J. M. PLOCHINSKI, K. L. KAFFKA, C. A. CAMPBELL, R. A. CHIZZONITE & P. L. KILIAN. 1991. J. Exp. Med. 173: 931-939.
- SPRIGGS, M. K., D. E. HURBY, C. R. MALISZEWSKI, D. J. PICKUP, J. E. SIMS, R. M. L. BULLER, & J. VANSLYKE. 1992. Cell 71: 145-152.
- ALCAMI, A. & G. L. SMITH. 1992. Cell 71: 153-167.
- LIMUCCO, G., S. GALUSKA, J. CHIN, P. CAMERON, J. BOGER & J. A. SCHMIDT. 1986. Proc. Natl. Acad. Sci. USA 83: 3972-3976.
- KOSTURA, M. J., M. J. TOCCI, G. LIMUCCO, J. CHIN, P. CAMERON, A. G. HILLMAN, N. A. CHARTRAIN & J. A. SCHMIDT. 1989. Proc. Natl. Acad. Sci. USA 86: 5227-5231.
- HOWARD, A. D., M. J. KOSTURA, N. THORNBERRY, G. J. F. DING, G. LIMUCCO, J. WEIDNER, J. P. SALLEY, K. A. HOGGUE, D. D. CHAPLIN, R. A. MUMFORD, J. A. SCHMIDT & M. J. TOCCI. 1991. J. Immunol. 147: 2964-2969.
- BLACK, R. A., S. R. KRONHEIM, M. CANTRELL, M. C. DEBILLY, C. J. MARCI, K. S. PRICKETT, J. WIGNALL, P. J. CONLON, D. COSMAN, T. P. HOPP, *et al.* 1988. J. Biol. Chem. 263: 9437-9442.
- BLACK, R. A., S. R. KRONHEIM & P. R. SLEATH. 1989. Fels. Lett. 247: 386-390.
- SLEATH, P. R., R. C. HENDRICKSON, S. R. KRONHEIM, C. J. MARCI & R. A. BLACK. 1990. J. Biol. Chem. 265: 14526-14528.
- THORNBERRY, N. A., H. G. BULL, J. R. CALAYCAY, K. T. CHAIKMAN, A. D. HOWARD, M. J. KOSTURA, D. K. MILLER, S. M. MOULINEAUX, J. R. WEIDNER, J. ADINIS, K. O. ELLISTON, J. M. AVILA, R. J. CASANO, J. CHIN, G. J. F. DING, L. A. EGGER, E. P. GARFNEY, G.

- LIMJUCO, O. C. PALLYHA, S. M. RAJU, A. M. ROLANDO, J. P. SALLEY, T. T. YAMIN, T. D. LEE, J. E. SHIVELY, M. MACCOSS, R. A. MUMFORD, J. A. SCHMIDT & M. J. TOCCI. 1992. *Nature* 356: 768-774.
35. YOUNG, P. R., D. J. HAZUDA & P. L. SIMON. 1988. *J. Cell Biol.* 107: 447-456.
 36. FUHLBRIGGE, R. C., S. M. FINE, E. R. UNANUE & D. D. CHAPLIN. 1988. *Proc. Natl. Acad. Sci. USA* 85: 5649-5653.
 37. RAY, C. A., R. A. BLACK, S. R. KRONHEIM, T. A. GREENSTREET, P. R. SLEATH, G. S. SALVESEN & D. J. PICKUP. 1992. *Cell* 69: 597-604.
 38. KOBAYASHI, Y., K. YAMAMOTO, T. SAIDO, H. KAWASAKI, J. J. OPPENHEIM & K. MATSUSHIMA. 1990. *Proc. Natl. Acad. Sci. USA* 87: 5548.
 39. HOGQUIST, K. A., E. R. UNANUE & D. D. CHAPLIN. 1991. *Proc. Natl. Acad. Sci. USA* 88: 8485-8489.
 40. CAMERON, P. M., G. A. LIMJUCO, J. CHIN, L. SILBERSTEIN & J. A. SCHMIDT. 1986. *J. Exp. Med.* 164: 237-250.
 41. DINARELLO, C. A. 1991. *Blood* 77: 1627-1652.
 42. DIGIOVINE, F. S., J. A. SYMONS & G. W. DUFF. 1991. *Immunol. Lett.* 29: 211-218.
 43. MILLER, D. K., J. M. AYALA, L. A. EGGER, S. M. RAJU, T.-T. YAMIN, G. J.-F. DING, E. P. GAFFNEY, A. D. HOWARD, O. C. PALLYHA, A. M. ROLANDO, J. P. SALLEY, N. A. THORNBERRY, J. R. WEIDNER, J. H. WILLIAMS, K. T. CHAPMAN, J. JACKSON, M. J. KOSTURA, G. LIMJUCO, S. M. MOLINEAUX, R. A. MUMFORD & J. R. CALAYCAY. 1993. *J. Biol. Chem.* 268: 18062-18069.
 44. MOLINEAUX, S. M., F. J. CASANO, A. M. ROLANDO, E. P. PETERSON, G. LIMJUCO, J. CHIN, P. R. GRIFFIN, J. R. CALAYCAY, G. J.-F. DING, T.-T. YAMIN, O. C. PALLYHA, S. LUELL, D. FLETCHER, D. K. MILLER, A. D. HOWARD, N. A. THORNBERRY & M. J. KOSTURA. 1993. *Proc. Natl. Acad. Sci. USA* 90: 1809-1813.
 45. NETT, M., D. CERRETTI, R. BLACK & D. CHAPLIN. 1992. *FASEB J.* 6: A2056.
 46. SHIVERS, B. D., D. A. GIEGEL & K. M. KEANE. 1993. *J. Cell. Biochem.* 17B: 119.
 47. MILLER, D. K., J. M. AYALA, E. BAYNE, K. CHAPMAN, J. CHIN, S. DONATELLI, L. A. EGGER, A. HOWARD, M. KOSTURA, S. M. MOLINEAUX, A. M. ROLANDO & T. T. YAMIN. 1993. *FASEB J.* 7: A267.
 48. HOWARD, A. D., O. C. PALLYHA, G. J.-F. DING, E. P. PETERSON, J. C. CALAYCAY, P. R. GRIFFIN, R. A. MUMFORD, A. B. LENNY, D. K. ROBINSON, S. WANG, M. SILBERKLANG, C. LEE, W. SUN, J. M. AYALA, L. A. EGGER, D. K. MILLER, S. M. RAJU, T. T. YAMIN, J. JACKSON, K. T. CHAPMAN, J. A. SCHMIDT, M. J. TOCCI & N. A. THORNBERRY. 1993. *J. Cell. Biochem.* 17B: 146.
 49. SCHINDLER, R., B. D. CLARK & A. A. DINARELLO. 1990. *J. Biol. Chem.* 265: 10232-10237.
 50. HOWARD, A. D., G. J.-F. DING, A. M. ROLANDO, O. C. PALLYHA, E. P. PETERSON, F. J. CASANO, E. K. BAYNE, S. DONATELLI, J. M. AYALA, L. A. EGGER, D. K. MILLER, S. M. RAJU, T. T. YAMIN, J. JACKSON, K. T. CHAPMAN, N. A. THORNBERRY, J. A. SCHMIDT, M. J. TOCCI & S. M. MOLINEAUX. 1993. *J. Cell. Biochem.* 17B: 113.
 51. KNIGHT, W. B., B. G. GREEN, P. GALE, R. CHABIN, A. MAYCOCK, W. M. WESTLER, H. WESTON, C. DORN, P. FINKE, W. HAGMANN, J. HALE, J. LIESCH, M. NAVIA, S. SHAH, D. UNDERWOOD & J. B. DOHERTY. *Biochemistry* 31: 8160-8170.

Bicyclic In of Cytokin

J. C. LEE,^a
D. DUNN
J. R. WHITE,

^aDe
^bDepartment of
^cI
^dD
Sm

Ki

The network of immu
cell types and mediators a
(collectively termed lymph
and function of a variety
of these molecules have
these proteins through re
important pathways oper
kins and colony stimulat
each comprised of a mu
properties. Understandi
vided new and importan
inflammation. The study
and the resulting infla
strategies for the develo
variety of autoimmune a
Interleukin-1 (IL-1)
proinflammatory cytokin
been suggested to play
diseases, such as rheum

Strategies f

Studies of the biosy
least three strategies t
pharmacological interv
receptor antagonism, l

Neutralization of interleukin-1 β activity *in vivo* with a monoclonal antibody alleviates collagen-induced arthritis in DBA/1 mice and prevents the associated acute-phase response

T. GEIGER, H. TOWBIN, A. COSENTI-VARGAS, O. ZINGEL, J. ARNOLD, C. RORDORF, M. GLATT, K. VOSBECK
Research Department, Pharmaceuticals Division, Ciba-Geigy Ltd., CH-4002 Basel, Switzerland

ABSTRACT. Interleukin-1 (IL-1) has been implicated in the development and progression of a variety of acute and chronic inflammatory diseases. Due to its pro-inflammatory and tissue-degrading activities, IL-1 is regarded as a major mediator of chronic inflammatory joint diseases, including rheumatoid arthritis in man, adjuvant arthritis in rats and collagen-induced arthritis in mice. However, conclusive experimental evidence for the crucial role of IL-1 in the development of joint destruction has not been presented as yet. In the present study, we investigated the effect of a neutralizing monoclonal mouse antibody against mouse IL-1 β (IgG1 isotype) on the development and progression of collagen-induced arthritis in DBA/1 mice. The antibody was injected intraperitoneally 3 times a week, either from day 3 or from day 21 after primary immunization, to day 60.

In the positive control group an arthritis incidence of 80% was observed after 60 days. The injection of a control antibody of the same isotype did not influence the incidence of arthritis, whereas injection of anti-IL-1 β from day 21 reduced the arthritis incidence to about 30%. Injection of anti-IL-1 β starting at day 3 totally prevented both the development of arthritis and the associated increase of the acute phase protein serum amyloid P (SAP). Anti-collagen antibody titers, which increased significantly after immunization, were not influenced by the injection of anti-IL-1 β antibodies, in spite of the suppressive effect on arthritis development. Joint destruction in the arthritic animals, as measured by X-ray scoring, was significantly influenced towards normalization in the animals treated with anti-IL-1 β antibodies.

Taken together, our results present clear evidence for the involvement of IL-1 β in the development and progression of collagen arthritis in mice.

Key words: collagen-induced arthritis, interleukin-1, monoclonal antibody, rheumatoid arthritis, acute phase response.

Introduction

Type II collagen-induced arthritis in rodents is regarded as one of the best animal models for rheumatoid arthritis and has been reported to have a number of characteristics in common with rheumatoid arthritis in man. Both diseases share the humoral and cellular immunological responses to

type II collagen, although these responses are much more consistent in CIA compared to RA (1-4). In addition, MHC class II linkage (2, 5, 6) and a pronounced acute phase reaction (7-10) are characteristically observed in both diseases and the synovial inflammation of collagen-induced arthritis, as analyzed by histology and immunohistochemistry, is quite similar to the situation in active stages of RA (11, 12).

Address reprint requests to: Thomas Geiger, MD, R-1056, P.30, Ciba-Geigy Ltd., CH-4002 Basel, Switzerland.

Received on May 5, 1993; accepted in revised form on August 17, 1993.

Abbreviations used in this report: CIA: type II collagen-induced arthritis; collagen II: bovine type II collagen; ELISA: enzyme-linked immunosorbent assay; IL-1: interleukin-1; IFN- γ : interferon- γ ; mAb: monoclonal antibody; MTT: thiazolylblue tetrazoliumbromide; SAP: serum amyloid P component; TNF- α : tumor necrosis factor α .

In the development and progression of both CIA and RA the pro-inflammatory activities of various cytokines such as IL-1 α and IL-1 β or TNF- α have been implicated (13-16). At present, it is not clear which member of the IL-1 family of monokines, IL-1 α or IL-1 β , plays the predominant role in the evolution of chronic inflammatory and arthritic diseases. With the availability of neutralizing antibodies to various cytokines in sufficient amounts during the last few years, it became possible to define the role of those cytokines in the pathophysiology of arthritic diseases.

In the present study, we investigated the effect of a neutralizing monoclonal antibody to murine IL-1 β on the development of collagen-induced arthritis in DBA/1 mice. Our aim was to study whether the systemic neutralization of IL-1 β exerted an effect on joint destruction, on the associated acute phase response, and on the humoral response to heterologous collagen.

Materials and methods

Materials. Keyhole limpet hemocyanin (KLH), rabbit anti-mouse SAP and goat anti-mouse IgG, peroxidase-linked, was obtained from Calbiochem (San Diego, USA). Donkey anti-rabbit IgG, horseradish peroxidase-linked antibody, was procured from Amersham Buchler (Buckinghamshire, UK). Recombinant murine IL-1 α was obtained from British Biotechnology (Abingdon, UK).

Male DBA/1 H-29 mice, age 6 to 8 weeks, were used for the experiments.

Preparation and in vitro testing of monoclonal mouse anti-mouse IL-1 β antibodies. Recombinant mouse IL-1 β was expressed in *E. coli* using standard techniques. The hybridoma cell line producing the monoclonal anti-IL-1 β antibody (1400.24.17) was generated by fusing spleen cells of a BALB/c mouse which had been repeatedly immunized with a conjugate of recombinant mouse IL-1 β and KLH using described methods (17). The antibody was purified from ascites fluid by precipitation with ammonium sulfate and ion exchange chromatography. The control antibody 1226.31.3 against levoprotelin was generated identically.

IL-1 activity was determined by proliferation of D10S cells using the MTT protocol (18). Briefly, 2×10^4 cells were cultured in the presence or absence of the test antibody plus recombinant mouse IL-1 β for 45 hours. The final volume was 200 μ l. 100 μ l were removed and replaced with 25 μ l of an MTT (3-[4,5 dimethylthiazol-2-yl]-2,5-diphenyltetrazolium bromide; thiazolylblue) solution (5 mg/ml). After incubation for 2 hours at 37°C, 100 μ l of a solution of 20% (w/v) sodium dodecylsulfate in DMF/water (1:1, ref. 19) were added to dissolve the crystals. The plates were read at 540 nm.

Preparation of fetal bovine collagen type II. A fetal calf was obtained from the slaughterhouse and the articular cartilage was dissected and extracted with a papain solution, essentially as described by Strawich and Nimni (20). All subsequent steps were performed at 4°C.

The viscous residue was further extracted with 0.45 M sodium chloride, followed by 0.5 M acetic acid. Acid soluble collagen II was precipitated with 2.7 M sodium chloride and redissolved in 0.5 M acetic acid. After centrifugation, the clear solution was dialysed against 20 mM sodium phosphate to precipitate type II collagen. Solubilization in acetic acid and precipitation in 2.7 M sodium chloride was repeated, and after resolubilization and extensive dialysis in 50 mM acetic acid, the type II collagen was lyophilized and stored at -80°C. The quality of the collagen II preparation was judged by electrophoresis on 5% polyacrylamide gels and the preparations were found to be essentially pure, except for trace amounts of type I and type IX collagen.

Arthritis induction and animal treatment. One volume of type II collagen, dissolved in 10 mM acetic acid (4 mg/ml), was emulsified in an equal volume of complete Freund's adjuvant (Sigma) by repeated passage through a nearly closed stopcock mounted between two 1 ml syringes. The final emulsion remained stable as a drop on the surface of water for more than 5 minutes. Male DBA/1 mice, 6 to 8 weeks of age, were immunized intradermally with 50 μ l of the collagen emulsion at the base of the tail (100 μ g type II collagen/mouse). The day of primary immunization corresponds to day zero in the figures. Three weeks later (corresponding to day 21), a booster injection of the same composition and amount was given at the contralateral side of the tail base.

All animal manipulations, other than the antibody treatment, were performed under isoflurane anesthesia (Forene®, Abbott, USA). Monoclonal anti-IL-1 β antibodies were diluted in 0.9% pyrogen-free saline and injected three times per week intraperitoneally (100 μ g/mouse per injection). Control animals were injected either with saline alone or with a non-cytokine monoclonal antibody of the same isotype (IgG1, mAb 1226.31.3), directed against an anti-depressant (anti-levoprotelin).

For the clinical scoring, arthritic symptoms were carefully examined three times a week and animals showing any sign of arthritis (swelling, redness of paws or limping) were considered arthritic. Blood was collected under deep anesthesia by orbital bleeding on day 21 and at the end of the experiment on day 60, before final asphyxiation in CO₂. For X-ray analysis, the animals were placed in a ventral position on Kodak X-Omat MA films and exposed with 28 kV, 125 mAs at a distance of 45 cm from the X-ray device (Mammomat, Siemens).

Assessment of X-ray photographs. Eighteen joints per paw were evaluated using a binocular microscope. Arthritis signs were loss of bone walls, loss of metaphyseal bone density or destruction of the joint architecture. Each joint was given a rating of 0 (non-arthritic) or 1 (arthritic). A score of 1 meant that at least one side of the articulation showed a clear loss of the bone wall contour or a clear loss of metaphyseal bone density. The theoretical maximum score was 72 per animal (all joints in all four paws affected). All X-ray photographs were evaluated at least twice in a blinded fashion by one investigator.

Determination of serum amyloid P component (SAP) by ELISA. SAP plasma levels were determined by a solid phase enzyme-linked immunoassay. The ELISA was performed essen-

tially as described by Serban and Rordorf-Adam (21). Briefly, the wells of polystyrene microtiter plates were coated with trinitrophenylated keyhole limpet hemocyanin (TNP-KLH), then incubated with SAP-containing samples. The wells were sequentially incubated with rabbit anti-mouse SAP antiserum and horseradish peroxidase-linked donkey anti-rabbit IgG conjugate. Purified mouse SAP was used as a standard. The ELISA plates were read at 490 nm in a computer-driven ELISA reader (Canberra Packard).

Determination of anti-collagen antibodies. 96-well microtiter plates were coated with type II collagen dissolved in sodium bicarbonate buffer, pH 8.3 (25 μ g/ml). The sera were added at a 1:1000 dilution and bound mouse immunoglobulin was detected with peroxidase labeled goat antimouse IgG antiserum, essentially as described by Gossiau and Barrach (22).

Statistical analysis. Statistical analysis was performed using the InStat computer program (GraphPadTM, San Diego, USA). The data are expressed as the mean \pm SEM. Ten identically treated animals were used per group. The statistical significance between groups was calculated using the non-parametric Mann-Whitney U-test. For paired samples, the Wilcoxon signed-ranks test was used.

Results

Inhibition of D10S cell proliferation with monoclonal anti-IL-1 β antibody

The capacity of the monoclonal anti-IL-1 β antibody 1400.24.17 to inhibit the proliferation of the murine T-cell line D10S was investigated. Figure 1 shows that about 50

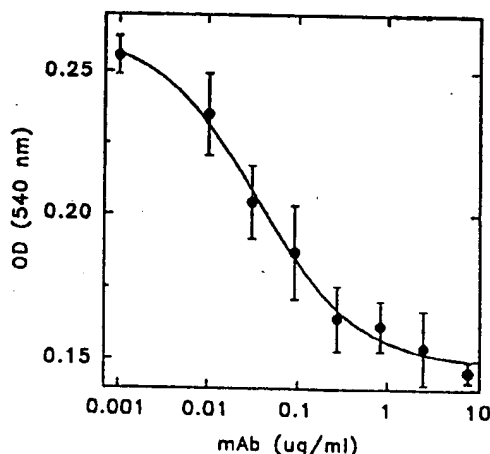


Fig. 1. Inhibition of IL-1-dependent proliferation of D10S cells by mAb 1400.24.17. 2×10^4 D10S cells were cultured in the presence or absence of monoclonal anti-IL-1 β antibody and recombinant mouse IL-1 β (100 pg/ml) for 45 hours. MTT solution was added and after incubation for 2 hrs at 37°C the crystals were dissolved and the plates were read at 540 nm.

ng/ml of monoclonal anti-IL-1 β were required to half-maximally inhibit the proliferation induced by a constant concentration of murine IL-1 β (100 pg/ml). In cultures without the addition of IL-1 β , the antibody had no influence on the proliferation of D10S cells. Furthermore, the antibody did not interfere with the proliferation of D10S cells in response to human IL-1 α (data not shown). Unspecific toxic effects of the antibody on the viability of D10S cells could thus be excluded.

The cross-reactivity of the monoclonal anti-IL-1 β antibody with murine IL-1 α was further investigated. The specificity of the monoclonal antibody 1400.24.17 for IL-1 β was demonstrated by the ability of mouse IL-1 β to efficiently compete with labeled IL-1 β for binding to a limiting amount of antibody (Fig. 2). In contrast to IL-1 β , IL-1 α did not show any inhibition of binding. These results clearly demonstrate that mAb 1400.24.17 is specific for murine IL-1 β , without crossreacting with mouse IL-1 α .

Effect of the monoclonal anti-IL-1 β antibody on the development and progression of collagen-induced arthritis in DBA-1 mice

Taking into account the *in vitro* neutralizing capacity of the antibody 1400.24.17, we injected 100 μ g of monoclonal anti-IL-1 β 3 times per week. Two different treatment schemes were selected, starting antibody treatment either at day 3 after primary immunization or at day 21, a time point where the early immunological reactions were already completed but where the arthritis was not yet manifest.

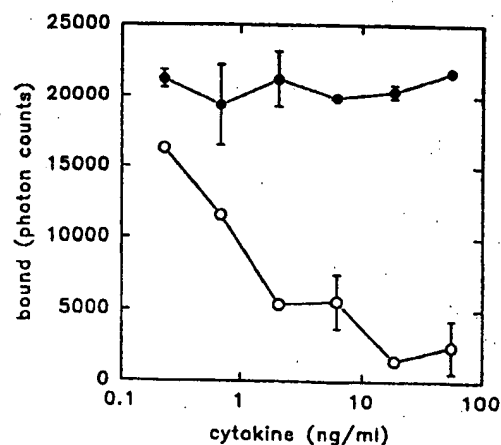


Fig. 2. Inhibition tests with mAb 1400.24.17 and mouse IL-1 α or IL-1 β . The monoclonal antibody 1400.24.17 (1.6 ng/ml) was incubated for 18 hrs at 4°C with varying concentrations of mouse IL-1 α (●) or mouse IL-1 β (○) in the presence of a constant amount of chemiluminescently labeled mouse IL-1 β (1 ng/ml). Separation of bound from non-bound was achieved by incubation with paramagnetic particles carrying anti-mouse IgG immunoglobulins. After washing, the bound fraction was determined in a luminometer.

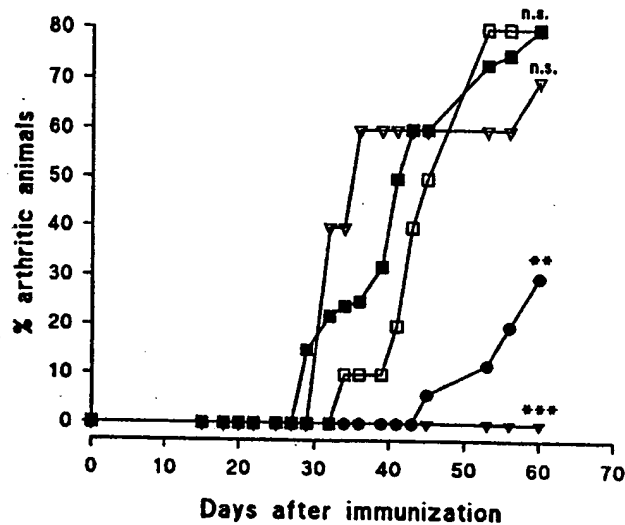


Fig. 3. The effect of anti-IL-1 β antibodies on arthritis incidence: clinical scoring. CIA was induced in DBA/1 mice at day 0 (primary immunization) by an intracutaneous injection of bovine type II collagen in Freund's complete adjuvant. At day 21 the animals received a booster injection. Arthritis development was monitored 3 times a week (swelling, redness of paws, limping). Animals with any positive signs, irrespective of the severity, were regarded as arthritic.

■ untreated control; ▽ saline; □ control antibody; ● anti-IL-1 β (day 21 to end); ▽ anti-IL-1 β (day 3 to end). Statistical analysis was performed using Fisher's test with the following limits: n.s.: $p > 0.05$; ** $p < 0.01$; *** $p < 0.001$.

Figure 3 shows the clinical incidence of arthritis after the selected treatments. Arthritis developed in the untreated animals of the positive control group at day 30 and constantly increased until the end of the experiment at day 60, resulting in 80% arthritic animals. Injections of saline or control antibody did not significantly influence the time course or incidence of arthritis (n.s., $p > 0.05$). In contrast, treatment with anti-IL-1 β antibodies starting at day 21 significantly reduced the arthritis incidence to about 30% ($p < 0.01$). In addition, a clear retardation of arthritis development was observed, with first clinical disease manifestations around day 50. Neutralization of IL-1 β with the monoclonal antibody starting on day 3 after immunization totally prevented the occurrence of arthritis ($p < 0.001$). The animals in the negative control group (not immunized) did not develop any signs of arthritis (data not shown).

Effect of anti-IL-1 β on joint destruction by X-ray scoring

Collagen-induced arthritis in mice results in the destruction of the joint architecture through the loss of cartilage and the demineralization of bone. The pro-inflammatory and catabolic activities of IL-1 have been implicated in these processes.

X-ray scoring of the joints of collagen-arthritis mice

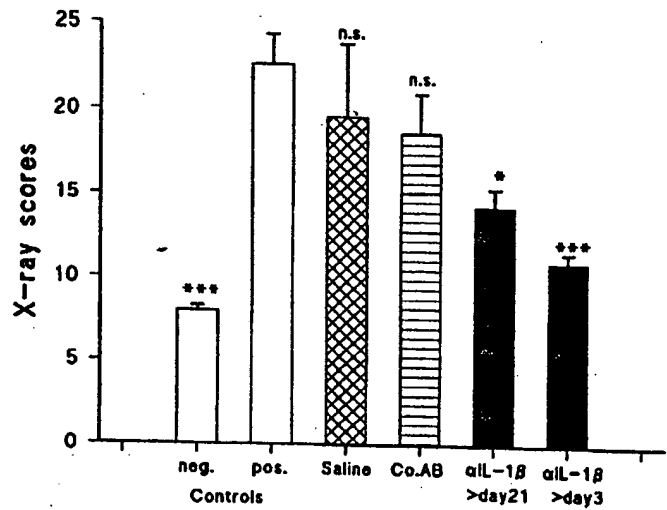


Fig. 4. The effect of anti-IL-1 β antibodies on joint destruction: X-ray scoring. At day 60, the animals were sacrificed and X-ray pictures were taken as described in Materials and methods. The X-rays were evaluated using a binocular microscope in a double-blinded fashion. The theoretical maximal score was 72 (all 18 joints of all paws affected). Results are expressed as means \pm SEM.

Open bars: controls (neg.: no arthritis induced; pos.: arthritic control); cross-hatched bars: saline injections, starting at day 3; horizontally striped bars: control antibody starting at day 3; solid bars: anti-IL-1 β starting at day 21 (left) or day 3 (right). n.s.: not significant; * $p < 0.05$; *** $p < 0.001$ (Mann-Whitney U-test).

was performed at day 60. In Figure 4 it can be seen that established arthritis was associated with an increased number of affected joints. However, the scores in arthritic animals never reached the theoretical maximum of 72, as most of the arthritic animals only had one or two affected paws. Neither the injections of saline, nor the injection of control antibody resulted in a significant effect. In contrast, anti-IL-1 β antibodies, given from day 21 up to the end of the experiment, reduced the joint destruction score significantly. When given from day 3 after immunization, the antibody was even more effective in ameliorating joint destruction ($p < 0.001$), although complete protection of joint destruction was not achieved, as compared to the negative control group.

Effect of anti-IL-1 β on plasma levels of serum amyloid P (SAP)

SAP is one of the major positive acute phase proteins in the mouse and has been shown to increase during the development of arthritis in the CIA model (7, 21, 23).

Figure 5 shows the SAP levels in serum taken at day 21 (open bars) and at day 60 (solid bars). The SAP levels at day 60 were found to be significantly increased in arthritic animals ($240 \pm 103 \mu\text{g/ml}$) but were rather low in non-

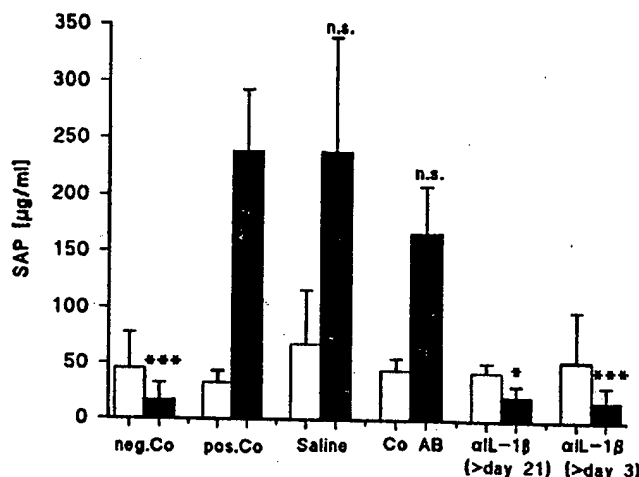


Fig. 5. The effect of anti-IL-1 β antibodies on the acute phase response. Comparison of serum SAP levels at day 21 and day 60. Blood was collected by orbital bleeding at day 21 (open bars) and at day 60 (solid bars) for the determination of SAP. Serum SAP levels were measured by ELISA. The results are expressed as means \pm SEM. n.s.: not significant; * $p < 0.05$; *** $p < 0.001$. The differences in serum SAP between days 21 and 60 for the various treatment groups were statistically analyzed using the Wilcoxon test for paired samples.

arthritic animals (17.2 ± 15 μ g/ml, $p < 0.001$). Neither injections of saline nor injections of control antibody significantly reduced these elevated SAP levels. In contrast, injection of anti-IL-1 β from day 21 or from day 3 onwards reduced the SAP levels (21 ± 9.1 μ g/ml and 18.2 ± 13.8 μ g/ml, respectively). The SAP levels of the latter group (day 3) were not statistically different from the levels of non-arthritic animals ($p = 0.13$, Mann-Whitney U-test).

SAP plasma levels at day 60 were further compared to those at day 21. Figure 5 shows that SAP levels in immunized animals at day 21 were not different from those of the animals in the negative control group, indicating that the acute-phase reaction in the animals is not observed before the development of arthritis. In arthritic animals, a highly significant increase in serum SAP levels was found between days 21 and 60 ($p < 0.01$). A significant increase was also observed in animals that had been treated with saline ($p < 0.01$) or with control antibody ($p < 0.05$). In contrast, mice that had been treated with anti-IL-1 β antibodies starting at day 21 or at day 3 after immunization did not show an increase in serum SAP levels between days 21 and 60. The animals treated with anti-IL-1 β antibodies instead showed a tendency toward decreased SAP levels, comparable to the animals of the negative control group (difference in SAP levels between days 21 and 60 not significant). These results demonstrate that the injection of anti-IL-1 β antibodies totally prevented the arthritis-associated acute-phase response.

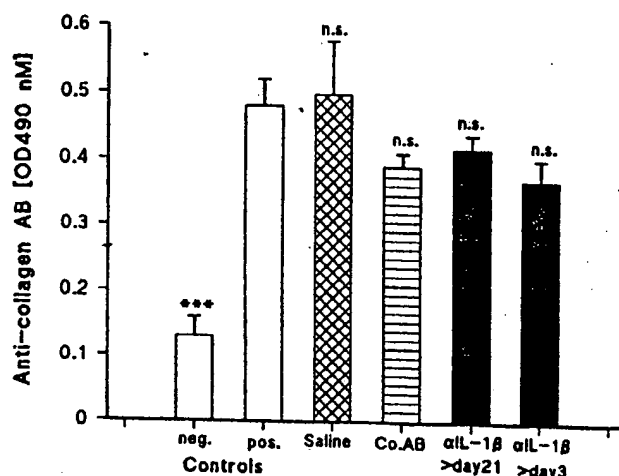


Fig. 6. The effect of anti-IL-1 β antibodies on anti-collagen IgG antibody levels. CIA was induced as specified in the legend to Figure 3. On day 60, blood was collected by orbital bleeding under deep narcosis and the serum was prepared. Anti-collagen antibody titers (IgG) were determined by ELISA.

Results are expressed as means \pm SEM. The symbols and confidence limits are the same as in Figure 4.

Effect of anti-IL-1 β treatment on the humoral response to heterologous type II collagen

In the final set of measurements we investigated the humoral response to heterologous collagen, which has been found to result in high levels of circulating antibodies to type II collagen in CIA, first of the IgM isotype, later in the disease of the IgG isotype (1, 2, 24).

As shown in Figure 6, anti-collagen antibodies (IgG) increased significantly after immunization with type II collagen (day 60 after immunization). The titers of anti-collagen antibodies were not significantly influenced by the injection of either saline or control antibodies. Interestingly, injections of anti-IL-1 β antibodies, starting either at day 21 or at day 3, had no significant effect on anti-collagen antibody titers, in spite of their suppressive effect on the other parameters of arthritis.

Discussion

In the present study we show that the evolution of collagen-induced arthritis in mice is suppressed by treatment of the animals with a neutralizing monoclonal antibody to IL-1 β . The clear suppressive effect of the treatment with this antibody, which is directed only against IL-1 β , was somewhat unexpected. The interleukin-1 family consists of two members, IL-1 α and IL-1 β , which are functionally indistinguishable and possess a wide spectrum of pro-

inflammatory properties, including bone demineralization, cartilage destruction, acute phase protein induction and fever induction (25).

Although IL-1 α and IL-1 β are the products of distinct genes, they bind to the same cell surface receptors and share various biological activities. While IL-1 β is mainly secreted, IL-1 α exists in a membrane-associated form that has been implicated in the antigen-presenting capacities of cells of the monocyte/macrophage lineage (25, 26). Our neutralizing antibody to IL-1 β did not neutralize IL-1 α , but nevertheless resulted in a clear and almost complete suppression of joint destruction in collagen-induced arthritis in mice and completely prevented the associated acute phase response. These results suggest an important role of IL-1 β in the pathophysiological disturbances seen in collagen-induced arthritis, and perhaps also in different chronic inflammatory joint diseases, including rheumatoid arthritis in man.

Evidence for the involvement of cytokines in the development of collagen-induced arthritis has been presented recently, both by the application of recombinant cytokines and by the neutralization of cytokine activity with antibodies. Killar and Dunn (14) described the potentiation of collagen-induced arthritis in mice upon the systemic administration of recombinant IL-1 β and concluded that this effect may be due in part to an augmentation of the immune response to heterologous collagen.

A similar potentiation of disease was described after the systemic application of TNF- α (15) or IL-1 β (16) by osmotic minipumps or by the intra-articular injection of TNF- α or TGF- β (27), although in another report a protective effect of TGF- β was described (28). Suppressive effects on collagen arthritis were reported in studies using antibodies directed against the T-cell receptor $\alpha\beta$ framework (29, 30) and after the subcutaneous application of interferon- γ . The latter treatment was associated with a significant suppression of the serum anti-collagen antibody response (31).

Due to their various pro-inflammatory activities, including the induction of tissue-degrading enzymes in cartilage, IL-1 β and TNF- α have been regarded as major mediators in the connective tissue destruction associated with chronic inflammatory joint diseases (32-34). The administration of neutralizing anti-TNF antibodies prior to disease onset significantly reduced paw swelling and histological severity without reducing the incidence of arthritis or the level of circulating anti-type II collagen IgG (35). Although in that study the levels of monoclonal antibodies administered were comparable to those of our study, we found a clear and almost complete suppressive effect on the incidence of arthritis when anti-IL-1 β antibodies were injected prophylactically. This difference in efficiency might indicate that IL-1 β is a predominant

mediator for the development of arthritis, the neutralization of which is more favourable in terms of the prevention of arthritic disease. Nevertheless, it is not possible to predict which cytokine actually plays the dominant role in the development of arthritic diseases, due to the fact that the neutralization of one cytokine by the injection of antibodies might exert potent negative feedback effects on the entire cytokine system (25).

However, Piguet *et al.* (36) recently reported that the neutralization of TNF by either anti-TNF antibodies or soluble TNF receptors arrested the evolution of collagen arthritis, as shown by histological analysis. This effect was seen when treatment was started 2 weeks after immunization, but was not observed when treatment was started 2 months after induction of the disease. Consistent with our findings, treatment with anti-TNF antibodies did not influence the production of anti-collagen antibodies. These results are in agreement with our observations, in the sense that the potency of neutralizing IL-1 β is most effective when started early after immunization. We entirely agree with the conclusions drawn by Piguet *et al.* (36) that the antagonism of cytokines, when achieved in an early phase, can prevent the long-term evolution of collagen arthritis. It would be interesting to investigate whether the inhibition of IL-1 β , in contrast to TNF- α , still exerts an alleviating effect on arthritis when given therapeutically in established arthritis, instead of prophylactically.

In several studies the role of IL-1 in the evolution of collagen-arthritis was investigated by either injecting IL-1 and monitoring aggravation of experimental arthritis (14, 16, 37), by neutralizing IL-1 with antibodies (38), or by injecting recombinant human IL-1 receptor antagonist, an endogenous inhibitor of IL-1 (39). Most of these studies presented evidence for the important role of IL-1 in the development and progression of arthritic diseases. However, discrimination between the relative contributions of the two IL-1 forms, IL-1 α or IL-1 β , could not be achieved with these approaches.

Nevertheless, in the study by van de Loo *et al.* (38) the authors identified the released IL-1 in synovial tissue to be primarily of the IL-1 α subtype. In that study it was demonstrated that the cartilage proteoglycan loss could be efficiently prevented by a mixture of neutralizing antibodies directed against both IL-1 α and IL-1 β . The finding of primarily IL-1 α in synovial tissue contrasts with our results, inasmuch as we describe in this paper an almost complete protective effect of anti-IL-1 β antibodies in mouse collagen-induced arthritis. One explanation for this discrepancy might be the stimulus used to induce the arthritis, i.e. heterologous collagen in our study and mBSA in the study by van de Loo *et al.* Another explanation might be differences in the specificity and/or affinity of the antibodies used. From our results we conclude that IL-1 β is the mediator

predominantly responsible for the pathophysiological disturbances in collagen arthritis, including joint destruction and the concomitant acute phase reaction, although a secondary effect on IL-1 α expression by negative feedback inhibition was not excluded specifically in our study.

The humoral response to heterologous collagen has been regarded as an absolute prerequisite for the development of arthritis in this animal model. Moreover, the rise in anti-collagen IgG antibodies has been shown to occur concurrently with the development of arthritic disease (40, 44). In addition, passive transfer of arthritis with anti-collagen antibodies has been achieved (41-43). These results were taken as an indication that the response to heterologous collagen is correlated with the evolution of arthritis. However, in this study we clearly show that the suppression of arthritis development by the application of an anti-IL-1 β antibody occurs without an effect on anti-collagen antibody titers. Similar effects, i.e. alleviation of arthritis without suppression of anti-collagen antibody titers, have been described after the injection of anti-TNF antibodies (35, 36). In contrast, injection of anti-IFN- γ antibodies resulted in a significant modulation of collagen-arthritis which was associated with a pronounced suppression of the serum anti-collagen antibody response (31).

In accordance with published data (35, 36), our results suggest that the alleviation of arthritis is not necessarily reflected by a concomitant suppression of the humoral response to heterologous collagen, but can occur without reduction of anti-collagen antibody titers. This finding might be taken as an indication that the antibody response to collagen, although an absolute prerequisite for arthritis to develop, is not correlated to the severity and progression of the disease. In addition, these findings argue for an important role of cell-mediated immune responses in the pathophysiology of arthritic diseases, which are presumably negatively influenced by the inhibition of pro-inflammatory cytokines such as IL-1 β or TNF α .

Taken together, the protective effect of the inhibition of the pro-inflammatory cytokine IL-1 β in this model supports the concept that potent IL-1 and/or cytokine antagonists might supply us with new and hopefully more effective therapeutics for the treatment of rheumatoid arthritis and, perhaps, other autoimmune diseases.

Acknowledgments

We thank Dr. B. Meier, Versuchstierzucht Sisseln, for the breeding of DBA-1 mice and Dr. A. Schmitz and Dr. J. van Oostrum for the expression in *E. coli* and for the purification of mouse IL-1 β . We thank Dr. I. Wiesenberg and Dr. T. Hall for their critical reading of the manuscript and for helpful suggestions. The skillful technical assistance of Mrs. J. Motz is also gratefully acknowledged.

References

1. WOOLEY PH, LUTHRA HS, STUART JM, DAVID CS: Type II collagen-induced arthritis in mice. Major histocompatibility complex linkage and antibody correlates. *J Exp Med* 1981; 154: 688-700.
2. HOLMDAHL R, ANDERSON ME, GOLDSCHMIDT TJ, JANSSON L, KARLSSON M, MALMSTROM V, MO J: Collagen induced arthritis as an experimental model for rheumatoid arthritis. *APMIS* 1989; 97: 575-84.
3. STUART JM, POSTLETHWAITE AE, TOWNES AS, KANG AH: Cell-mediated immunity to collagen and collagen α chains in rheumatoid arthritis and other rheumatic diseases. *Am J Med* 1980; 69: 13-18.
4. MENZEL J, STEFFEN C, KOLARZ G, KOJER M, SMOLEN J: Demonstration of anticollagen antibodies in rheumatoid arthritis synovial fluids by radioimmunoassay. *Arthritis Rheum* 1978; 21: 243-8.
5. WOOLEY PH, DILLON AM, LUTHRA HS, STUART JM, DAVID CS: Genetic control of type II collagen-induced arthritis in mice: Factors influencing disease susceptibility and evidence for multiple MHC-associated gene control. *Transplant Proc* 1983; 15: 180-5.
6. LANCHBURY JS: The HLA association with rheumatoid arthritis. *Clin Exp Rheumatol* 1992; 10: 301-4.
7. BLIVEN ML, WOOLEY PH, PEPYS MB, OTTERNESS IG: Murine type II collagen arthritis: Association of an acute-phase response with clinical course. *Arthritis Rheum* 1986; 29: 1131-8.
8. KINGSLEY G, PITZALIS C, PANAYI GS: Immunogenetic and cellular immune mechanisms in rheumatoid arthritis: Relevance of new therapeutic strategies. *Br J Rheumatol* 1990; 29: 58-64.
9. HARRIS ED: Rheumatoid arthritis. Pathophysiology and implications for therapy. *N Eng J Med* 1990; 322: 1277-89.
10. NAKAMURA T, BOARD PG, MATSUSHITA K, TANAKA H, MATSUYAMA T, MATSUDA T: α 1-acid glycoprotein expression in human leukocytes: Possible correlation between α 1-acid glycoprotein and inflammatory cytokines in rheumatoid arthritis. *Inflammation* 1993; 17: 33-45.
11. CAULFIELD JP, HEIN A, DYNESIUS-TRENTHAM R, TRENTHAM DE: Morphologic demonstration of two stages in the development of type II collagen-induced arthritis. *Lab Invest* 1982; 46: 321-43.
12. HOLMDAHL R, KLARESKOG L, RUBIN K, LARSSON E, WIGZELL H: T-lymphocytes in collagen II-induced arthritis in mice. Characterization of arthritogenic collagen II-specific T-cell lines and clones. *Scand J Immunol* 1985; 22: 295-306.
13. RIDDERSTAD A, ABEDI-VALUGERDI M, MOLLER, E: Cytokines in rheumatoid arthritis. *Annals Med* 1991; 23: 219-23.
14. KILLAR LM, DUNN CJ: Interleukin-1 potentiates the development of collagen-induced arthritis in mice. *Clin Sci* 1989; 76: 535-8.
15. BRAHN E, PEACOCK DJ, BANQUERIGO ML, LIU DY: Effects of tumor necrosis factor alpha on collagen arthritis. *Lymphokine Cytokine Res* 1992; 11: 253-6.
16. HOM JT, BENDELE AM, CARLSON DG: *In vivo* administra-

- tion with IL-1 accelerates the development of collagen-induced arthritis in mice. *J Immunol* 1988; 141: 834-41.
17. GALFFRÉ G, HOWE SC, MILSTEIN C, BUTCHER GW, HOWARD JC: Antibodies to major histocompatibility antigens produced in hybrid lines. *Nature* 1977; 266: 550-1.
 18. ORENCOLE SF, DINARELLO CA: Characterization of a subclone (D10S) of the D10.G4.1 helper T-cell line which proliferates to attomolar concentrations of interleukin-1 in the absence of mitogens. *Cytokine* 1989; 1: 14-22.
 19. HANSEN MB, NIELSEN SE, BERG KJ: Re-examination and further development of a precise and rapid dye method for measuring cell growth/cell kill. *Immunol Methods* 1989; 119: 203-10.
 20. STRAWICH E, NIMNI ME: Properties of a collagen molecule containing three identical components extracted from bovine articular cartilage. *Biochemistry* 1971; 10: 3905-11.
 21. SERBAN D., RORDORF-ADAM C: Quantitation of serum amyloid P component by an enzyme-linked immunoassay. *J Immunol Methods* 1986; 90: 159-64.
 22. GOSSLAU B, BARRACH HJ: Enzyme-linked immunosorbant microassay for quantification of specific antibodies to collagen type I, II, III. *J Immunol Methods* 1979; 29: 71-7.
 23. CACCESE RG, ZIMMERMAN JL, CARLSON RP: Bacterial lipopolysaccharide potentiates type II collagen-induced arthritis in mice. *Med Inflamm* 1992; 1: 273-9.
 24. SEKI N, SUDO Y, MIZUHARA H, ORITO K, IMASAKI A, ONO S, HAMAOKA T, SENOH H, FUJIWARA H: Type II collagen-induced murine arthritis: Induction of arthritis depends on antigen-presenting cell function as well as susceptibility of host to an anticollagen immune response. *J Immunol* 1992; 148: 3093-9.
 25. DINARELLO CA: Interleukin-1 and interleukin-1 antagonism. *Blood* 1991; 77: 1627-52.
 26. OPPENHEIM JJ, KOVACS EJ, MATSUSHIMA K, DURUM SK: There is more than one interleukin-1. *Immunol Today* 1986; 7: 45-56.
 27. COOPER WO, FAVA RA, GATES CA, CREMER MA, TOWNES AS: Acceleration of onset of collagen-induced arthritis by intra-articular injection of tumour necrosis factor or transforming growth factor-beta. *Clin Exp Immunol* 1992; 89: 244-50.
 28. KURUVILLA AP, SHAH R, HOCHWALD GM, LIGGITT GD, PALLADINO MA, THORBECKE GJ: Protective effect of transforming growth factor β 1 on experimental autoimmune diseases in mice. *Proc Natl Acad Sci USA* 1991; 88: 2918-21.
 29. MODER KG, LUTHRA HS, KUBO R, GRIFFITHS M, DAVID CS: Prevention of collagen induced arthritis in mice by treatment with an antibody directed against the T cell receptor $\alpha\beta$ framework. *Autoimmunity* 1992; 11: 219-24.
 30. CHIOCCIA G, BOISSIER MC, FOURNIER C: Therapy against murine collagen-induced arthritis with T cell receptor V_{β} -specific antibodies. *Eur J Immunol* 1991; 21: 2899-905.
 31. NAKAJIMA H, TAKAMORI H, HIYAMA Y, TSUKADA W: The effect of treatment with interferon-gamma on type II collagen-induced arthritis. *Clin Exp Immunol* 1990; 81: 441-5.
 32. DINARELLO CA, WOLFF SM: The role of Interleukin-1 in disease. *New Engl J Med* 1993; 328: 106-13.
 33. SAKLATVALA J: Tumor necrosis factor alpha stimulates resorption and inhibits synthesis of proteoglycan in cartilage. *Nature* 1986; 322: 547-9.
 34. BERTOLINI DR, NEDWIG G, BRINGMAN T, SMITH D, MUNDY GR: Stimulation of bone resorption and inhibition of bone formation *in vitro* by human tumor necrosis factor. *Nature* 1986; 319: 516-20.
 35. WILLIAMS RO, FELDMANN M, MAINI RN: Anti-tumor necrosis factor ameliorates joint disease in murine collagen-induced arthritis. *Proc Natl Acad Sci USA* 1992; 89: 9784-8.
 36. PIGUET PF, GRAU GE, VESIN C, LOETSCHER H, GENTZ R, LESSLAUER W: Evolution of collagen arthritis in mice is arrested by treatment with anti-tumour necrosis factor antibody or a recombinant soluble TNF receptor. *Immunology* 1992; 77: 510-14.
 37. HOM JT, GLISZCZYNSKI VL, COLE HW, BENDELE AM: Interleukin 1 mediated acceleration of type II collagen-induced arthritis: Effects of anti-inflammatory or anti-arthritis drugs. *Agents Actions* 1991; 33: 300-9.
 38. VAN DE LOO FAJ, ARNTZ OJ, OTTERNESS IG, VAN DEN BERG WB: Protection against cartilage proteoglycan synthesis inhibition by anti-interleukin-1 antibodies in experimental arthritis. *J Rheumatol* 1992; 19: 348-56.
 39. SCHWAB JH, ANDERLE SK, BROWN RR, DALLDORF FG, THOMPSON RC: Pro- and anti-inflammatory roles of interleukin-1 in recurrence of bacterial cell wall-induced arthritis in rats. *Infect Immun* 1991; 59: 4436-42.
 40. WATSON WC, TOWNES AS: Genetic susceptibility to murine collagen II autoimmune arthritis. Proposed relationship to the IgG2 autoantibody subclass response, complement C5, major histocompatibility complex (MHC) and non-MHC loci. *J Exp Med* 1985; 162: 1878-83.
 41. STUART JM, CREMER MA, TOWNES AS, KANG AH: Type II collagen-induced arthritis in rats. Passive transfer with serum and evidence that IgG anticollagen-antibodies can cause arthritis. *J Exp Med* 1982; 155: 1-16.
 42. STUART JM, DIXON FJ: Serum transfer of collagen-induced arthritis in mice. *J Exp Med* 1983; 158: 378-92.
 43. TERATO K, HASTY KA, REIFE RA, CREMER MA, KANG AH, STUART JM: Induction of arthritis with monoclonal antibodies to collagen. *J Immunol* 1992; 148: 2103-8.
 44. STUART JM, TOWNES AS, KANG AH: Nature and specificity of the immune response to collagen in type II collagen-induced arthritis in mice. *J Clin Invest* 1982; 69: 673-83.

INTERLEUKIN-1 β CONVERTING ENZYME INHIBITION BLOCKS PROGRESSION OF TYPE II COLLAGEN-INDUCED ARTHRITIS IN MICE

George Ku, Ted Faust, Linda L. Lauffer, David J. Livingston, Matthew W. Harding

To IL-1 β is a principal mediator in the pathogenesis of inflammatory disease. The IL-1 β -converting enzyme (ICE), a novel cysteine protease, is required for processing of the 31 kDa IL-1 β precursor to generate the 17 kDa proinflammatory mature form. We investigated the effect of two irreversible peptidyl ICE inhibitors, VE-13,045 and VE-16,084, on IL-1 production in vitro and in vivo in acute and chronic inflammatory disease models. In vitro, VE-13,045 and VE-16,084 inhibited IL-1 β secretion by LPS-stimulated human adherent mononuclear cells (IC₅₀'s of 0.4 μ M and 2.0 μ M, respectively) and murine splenic monocytes (IC₅₀'s of 10 μ M and 1.3 μ M, respectively). Both VE-13,045 and VE-16,084 also inhibited LPS stimulated IL-1 α secretion, although with reduced potency. In vivo, a single intraperitoneal dose of VE-13,045 (50 mg/kg) administered to mice 60 to 75 minutes after a 40 mg/kg LPS challenge significantly reduced IL-1 β serum levels by 50 to 70%. In the DBA/1J mouse model of Type II collagen-induced arthritis, prophylactic treatment with VE-13,045 (50 and 100 mg/kg/day) significantly delayed the onset of inflammation, with a 60% overall reduction in disease severity. VE-13,045 was more effective than either indomethacin (2 mg/kg/day) or methyl prednisolone (10 mg/kg/day). VE-13,045 was also effective in reducing inflammation and progression of arthritis when administered to mice with established disease. Histological analysis of wrist joints showed a reduction in synovial membrane damage, inflammatory cell infiltration and fibrosis, and cartilage erosion in VE-13,045-treated animals. This is the first demonstration of efficacy for an ICE inhibitor in a chronic disease model and suggests that ICE is an important target for design of anti-inflammatory or disease modifying drugs.

© 1996 Academic Press Limited

IL-1 is a principal mediator in the pathogenesis of several diseases including rheumatoid arthritis, systemic inflammatory response syndrome (SIRS), inflammatory bowel disease, glomerulonephritis and insulin-dependent diabetes mellitus.¹ The proinflammatory activities of IL-1 have been characterized extensively and its importance in the pathogenesis of multiple diseases reflects IL-1 induction of other cytokines, cell adhesion molecules and inflammatory mediators.^{2,3} There are two IL-1 agonists, IL-1 α and IL-1 β , that share minimal sequence identity;^{4,5} however, both IL-1 α and IL-1 β interact with the same cellular receptors and their biological activities are indistinguishable.^{6,7} Several

strategies for blocking IL-1 have been explored, including use of the IL-1 receptor antagonist (IL-1RA) and soluble IL-1 receptors (sIL-1R).^{8,9} Results from animal and initial human studies show that blocking IL-1 activity may have a therapeutic benefit. In animal studies, IL-1RA or sIL-1R treatment reduces the severity of endotoxin induced sepsis,¹⁰⁻¹² prevents allograft rejection,⁹ graft versus host disease¹³ and blocks progression of arthritis in experimental models.¹⁴⁻¹⁶ Initial clinical studies in patients with rheumatoid arthritis suggests that intra-articular or subcutaneous administration of sIL-1R or IL-1RA may reduce joint tenderness and inflammatory symptoms.¹⁷⁻¹⁹ However, in patients with SIRS, IL-1RA treatment has a more limited therapeutic benefit, which may reflect the involvement of TNF- α and other mediators.²⁰

IL-1 β and IL-1 α are each synthesized as 31–33 kDa precursors lacking conventional secretory signal sequences^{4,5} and both cytokines are processed to mature forms by proteases.²¹⁻²⁴ Membrane associated IL-1 α precursor has biological activity,^{25,26} although the IL-1 α precursor may be processed to its mature form by the calcium-dependent protease, calpain.^{21,22} Mature 17 kDa IL-1 β is generated by the IL-1 β converting enzyme

From Vertex Pharmaceuticals Incorporated, 40 Allston Street, Cambridge, MA 01239, USA

Correspondence to: M.W. Harding, email address: Harding-@vpharm.com

Received 31 August 1995; revised and accepted for publication 15 December 1995

© 1996 Academic Press Limited
1043-4666/96/050377+10 \$18.00/0

KEY WORDS: interleukin 1 β /interleukin 1 β converting enzyme/arthritis/inflammation

(ICE), a unique cytoplasmic cysteine protease that is essential for IL-1 β precursor processing and export of mature IL-1 β from monocytes.^{27,28} ICE is composed of two non-identical 20 and 10 kDa subunits which are derived from a 45 kDa proenzyme by autoprocessing.^{27,29} The three-dimensional structure of ICE complexed with prototype inhibitors has been solved and catalytic residues in the active site have been identified.^{30,31}

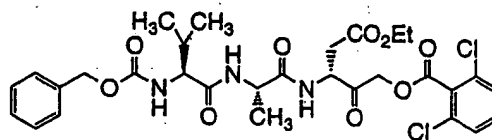
There is considerable interest in ICE as a target for design of novel anti-inflammatory or disease modifying drugs. Studies with prototype ICE inhibitors have demonstrated activity in blocking IL-1 β production by monocytes in vitro and in whole blood assays.²⁷ However, the potential of ICE inhibitors for efficacy in vivo has not been evaluated. We have initiated experiments to investigate the biological function of ICE in vivo, including studies with ICE-deficient mice.³² Here we have utilized two prototype peptidyl ICE inhibitors, VE-13,045 (carbobenzyloxy-Val-Ala-Asp-(O-Et)-CH₂O-dichlorobenzoate), and VE-16,084 (carbobenzyloxy-Val-Ala-Asp-CH₂O-dichlorobenzoate) to evaluate the efficacy of ICE inhibition on IL-1 production in vivo. In a model of SIRS, we measured the effect of ICE inhibition on IL-1 β serum levels in LPS-challenged mice. We chose Type II collagen-induced arthritis (CIA) in the mouse as a model of rheumatoid arthritis (RA). CIA involves MHC class II linkage, humoral and cellular immunological responses to Type II collagen (CII), synovial inflammation, cartilage and bone destruction similar to human RA.³³ Neutralization of IL-1 activity in vivo with anti-IL-1 β and anti-IL-1 α antibodies or IL-1RA blocks disease progression^{34,35} suggesting a pre-dominant role for IL-1 in the pathogenesis of CIA. We examined, therefore, the therapeutic potential of ICE inhibitors in this chronic disease model.

RESULTS

Chemical structure and properties of prototype peptidyl ICE inhibitors

VE-13,045 and VE-16,084 (carbobenzyloxy-Val-Ala-Asp-(O-Et)-CH₂O-dichlorobenzoate and carbobenzyloxy-Val-Ala-Asp-CH₂O-dichlorobenzoate; Figure 1) are potent irreversible ICE inhibitors. In an in vitro enzyme assay, VE-13,045 and VE-16,084 inhibit ICE activity with IC₅₀'s of approximately 1 μ M and 10 nM, respectively. The two compounds differ only by the presence of an ethyl ester side chain in the aspartyl moiety of VE-13,045. In cellular assays in vitro, the ester side chain is probably hydrolysed to the free acid (VE-16,084) by membrane non-specific acid esterase. Differences in potency observed with these compounds

VE-13,045

carbobenzyloxy-Val-Ala-Asp(OEt)-CH₂O-dichlorobenzoate

VE-16,084

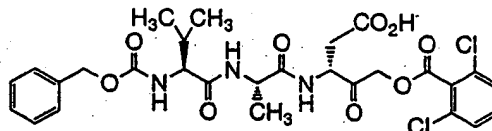
carbobenzyloxy-Val-Ala-Asp-CH₂O-dichlorobenzoate

Figure 1. Chemical structure of prototype peptidyl ICE inhibitors, VE-13,045 and VE-16,084.

in vitro may reflect plasma membrane lipid composition and permeability, enhanced or diminished uptake of the ester or acid forms, rate of ester hydrolysis to the acid, and general stability of the compounds after exposure to cellular proteases. In vivo, the aspartyl ester side chain in VE-13,045 is rapidly hydrolyzed, with a serum half life of about 10 min, yielding VE-16,084 (I.R. Ager and J. M. C. Golec, personal communication) as the bioactive molecule.

Inhibition of ICE activity in vitro blocks secretion of both IL-1 β and IL-1 α

VE-13,045 and VE-16,084 block secretion of IL-1 β (IC₅₀'s of 0.4 μ M and 2.0 μ M, respectively) by LPS stimulated human adherent monocytes (Fig. 2A). Both compounds also block IL-1 β secretion after nigericin treatment³⁶ of murine splenic monocytes stimulated overnight with LPS. Here, VE-16,084 is more potent (IC₅₀ ~1.3 μ M) than VE-13,045 (IC₅₀ ~10 μ M; Fig. 2B). The cellular potency of VE-16,084 for inhibition of IL-1 β secretion by murine splenic monocytes is consistent with results from an independent study with the same compound (WIN 67694) after LPS stimulation of thioglycolate elicited murine peritoneal macrophages.³⁸

Surprisingly, VE-13,045 and VE-16,084 block secretion of IL-1 α by human adherent monocytes (IC₅₀'s of 0.3 μ M and 10 μ M, respectively; Fig. 2A). Both compounds also affect IL-1 α secretion by murine splenic monocytes treated with nigericin, however, VE-13,045 is a less potent inhibitor of murine IL-1 α secretion (IC₅₀ of >20 μ M) than VE-16,084 (IC₅₀ ~10 μ M; Fig. 2B). No inhibition of TNF- α or IL-6 secretion was observed with VE-13,045 or VE-16,084 in these experiments (not shown). Also, VE-13,045 and VE-16,084 did not effect viability of human or mouse mono-

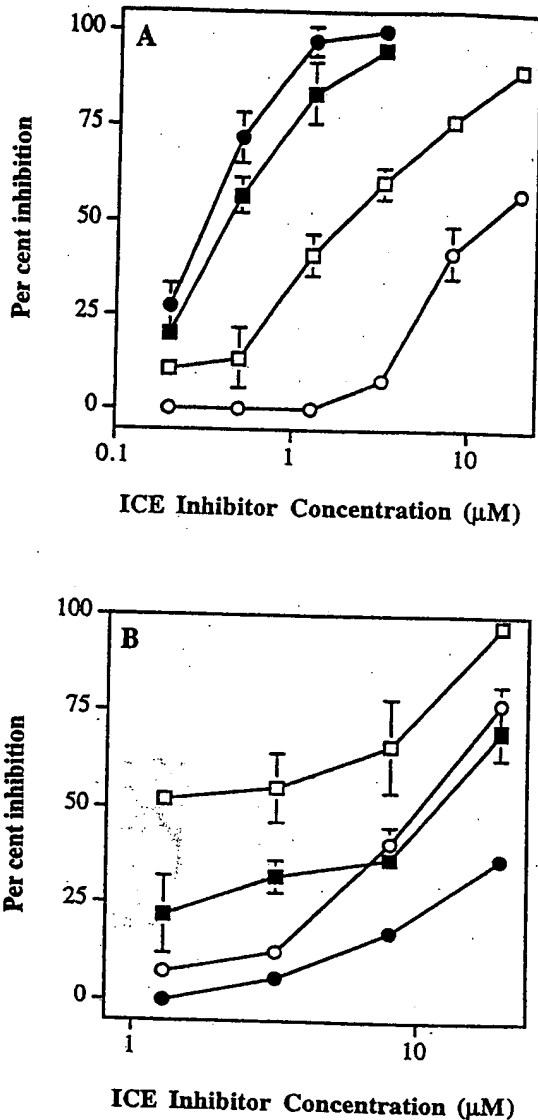


Figure 2. Effect of VE-13,045 and VE-16,084 on IL-1 β and IL-1 α secretion by LPS-stimulated (A) human adherent monocytes and (B) nigericin treated murine splenic monocytes.

Human or murine cells were incubated with LPS (1 μ g/ml and 10 μ g/ml, respectively) for 16–18 h. Murine cells were then washed and incubated with 10 μ M nigericin for an additional 30 min. Cytokine levels in culture supernatants were measured by ELISA. Results are expressed as the % inhibition (mean \pm SEM) by VE-13,045 (closed symbols) or VE-16,084 (open symbols) for IL-1 β (squares) and IL-1 α (circles) secretion compared to LPS-stimulated control cultures. These data are representative of at least four replicate experiments.

cytes in these assays as measured by trypan blue staining or lactate dehydrogenase activity in culture supernatants, and concentrations as high as 40 μ M have no effect on proliferation of THP-1 monocytes (not shown).

VE-13,045 blocks LPS-induced IL-1 β production in vivo

Initial experiments established an LPS dose-response and time course profile of serum cytokines in CD1 mice. After administration of LPS at 40 mg/kg,

TABLE 1. Effect of VE-13,045 administration on IL-1 β serum levels in LPS challenged CD1 mice

| Time of VE-13,045 administration relative to LPS-challenge | Number of determinations | Serum IL-1 β (pg/ml) | Mean % inhibition |
|--|--------------------------|----------------------------|-------------------|
| LPS control | 4 | 490 \pm 164 | |
| Concurrent with LPS | 2 | 460 \pm 35 | 7 |
| +30 min | 2 | 414 \pm 216 | 15 |
| +45 min | 2 | 473 \pm 264 | 4 |
| +60 min | 4 | 214 \pm 153 | 56 |
| | | | $P < 0.01$ |
| +75 min | 2 | 158 \pm 63 | 68 |
| +90 min | 2 | 474 \pm 67 | 4 |
| | | | $P < 0.01$ |

CD1 mice ($n = 6$ –10 per dose group) were challenged with LPS (40 mg/kg in 0.5% CMC-PBS at 20 ml/kg) by intraperitoneal injection. VE-13,045 (50 mg/kg) prepared in olive oil:ethanol:DMSO (90:5:5) was also administered by intraperitoneal injection simultaneously with LPS or at time points after LPS challenge. Mice were bled 7 h after LPS challenge and IL-1 β serum levels were determined by ELISA.

serum IL-1 α and IL-1 β levels begin to increase after 1–2 h and peak at 6–8 h while serum TNF- α or IL-6 reached maximal levels at 1.5–2 h. VE-13,045 was administered before, with or after LPS and serum IL-1 α and IL-1 β levels were measured 7 h after LPS challenge. Significant inhibition of LPS-induced IL-1 β production was observed with a single 50 mg/kg dose of VE-13,045 administered 60–75 min after LPS (Table 1). VE-13,045 administration 30, 60 or 90 min before or simultaneously with LPS failed to reduce IL-1 β levels (data not shown). Some reduction in serum IL-1 α levels was also noted in VE-13,045 treated mice, but this effect was variable. No effect of VE-13,045 was observed on serum levels of TNF- α or IL-6 in LPS-challenged mice (data not shown).

This effect of the timing of VE-13,045 administration on reduction of IL-1 β serum levels is consistent with its pharmacokinetics and the time course of IL-1 β production. In pharmacokinetic studies, a single 20 mg/kg intraperitoneal dose of VE-16,084 in mice resulted in a maximum plasma concentration (C_{max}) of approximately 10–12 μ g/ml within 10–15 min and an estimated terminal elimination half life ($t_{1/2\beta}$) of 15–20 min (I. R. Ager and J. M. C. Golec, unpublished observations). Therefore, a maximum inhibitory effect was observed when plasma drug concentrations coincided with the initial increase in IL-1 β production (between 1–2 h), resulting in maximum reduction in the serum IL-1 β levels measured at the 7 h time point.

Incidence and progression of Type II collagen-induced arthritis

We initially evaluated the incidence, severity and progression of Type II collagen arthritis in DBA/1J mice.

induced by immunization with 100 μ g CII followed by a booster injection of 100 μ g CII 21 days later.^{34,37} We detected a 60% incidence of arthritic disease when following this protocol, with an average severity of level 2 (focal swelling of the wrist) observed within 14 days of the CII booster injection. When the booster injection was increased to 200 μ g CII, we detected a 100% incidence of inflammation and a consistent time course progression of arthritic disease. Erythema (level 1) was first evident 4–5 days after the CII booster injection. Focal carpal (wrist) joint swelling (level 2) occurred within 8–12 days, with progressive swelling of the entire wrist (level 3) by day 16 to 18. Progression of swelling to

the metacarpal/metatarsals (palm region; level 4) was observed in 10–15% of the animals and further progression to the metacarpophalangeal or metatarsal-phalangeal joints (level 5) in only 5% of the animals.

Prophylactic and therapeutic efficacy of VE-13,045 in Type II collagen-induced arthritis

The incidence and progressive pattern of inflammation and arthritic disease observed in the modified Type II collagen arthritis model described above appeared to be suitable for testing the therapeutic potential of ICE inhibitors. Therefore, we evaluated

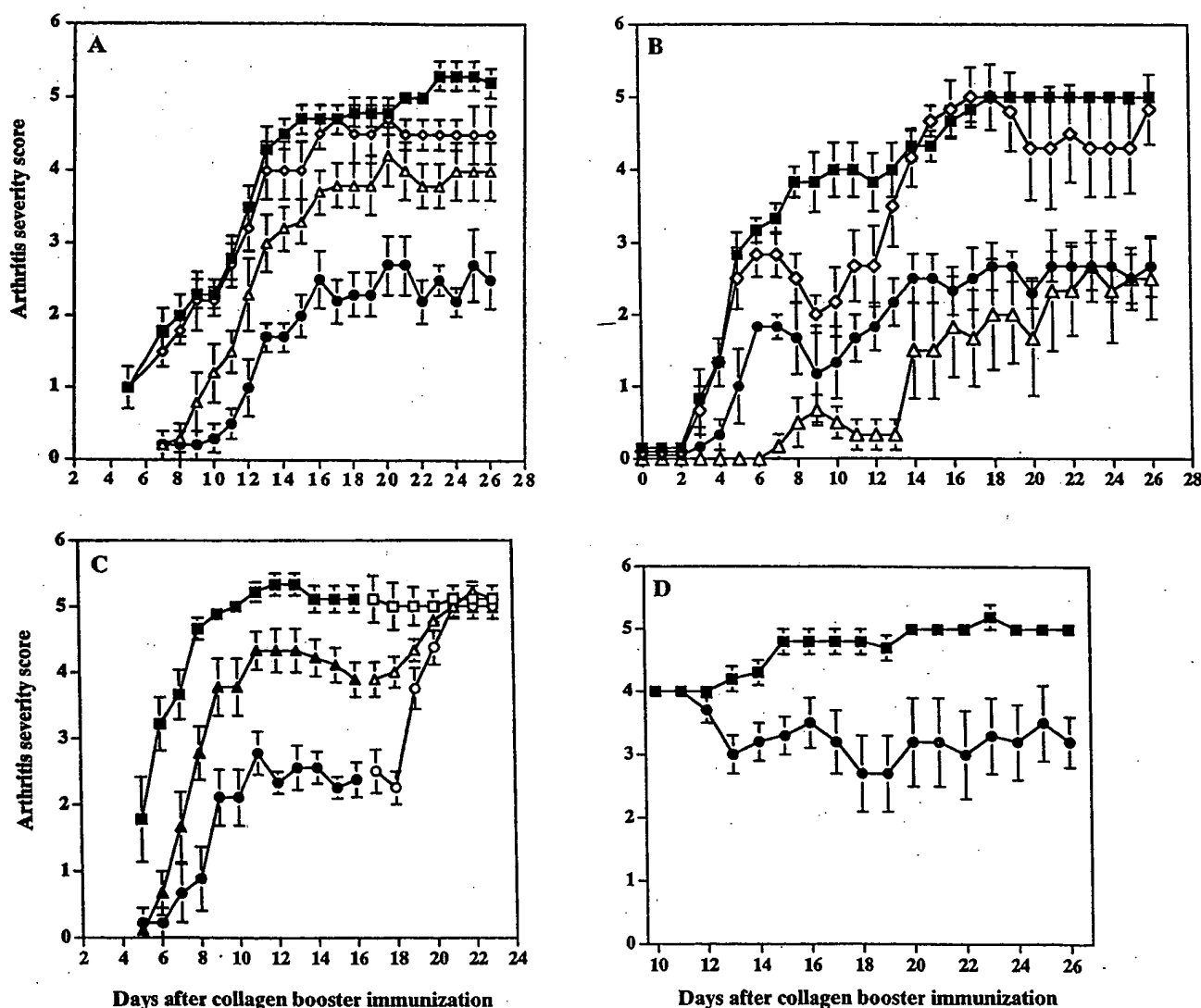


Figure 3. Effect of VE-13,045 on the clinical course of Type II collagen-induced arthritis in DBA/1J mice.

(A) Prophylactic therapy with VE-13,045 (□; 50 mg/kg/d), prednisolone (Δ; 10 mg/kg/d) and indomethacin (◇; 2 mg/kg/d) compared to vehicle-treated mice (■). (B) Prophylactic dose-response study with VE-13,045 at 100 mg/kg/d (Δ), 50 mg/kg/d (□) and 25 mg/kg/d (◇) compared to vehicle-treated mice (■). (C) Prophylactic therapy with VE-13,045 (□) and prednisolone (Δ) followed by treatment termination (open symbols). (D) Clinical course of established CIA in VE-13,045 treated (□) or vehicle-treated (■) mice starting 10 days after the CII booster injection. Mice (6–10 per group) were injected intradermally with 100 μ g of chick CII on day 0, followed by a 200 μ g booster injection on day 21. Front paws were examined daily after the CII booster injection, the status of arthritic disease was scored as described in Methods, a combined score of front paws was determined and expressed as the mean \pm SEM for each treatment group.

VE-13,045 for prophylactic efficacy in comparison to indomethacin and methyl prednisolone. Results in Figure 3A demonstrate superior efficacy of VE-13,045 in reducing the severity of inflammation and progression of arthritic disease. Daily administration of VE-13,045 (50 mg/kg) delayed the onset of inflammation by 6 days with a 60% overall reduction in arthritic disease compared to vehicle-treated animals (significance of $P < 0.01$ for days 10 to 26). In contrast, daily administration of indomethacin (2 mg/kg) failed to prevent the progression of arthritis, whereas methyl prednisolone (10 mg/kg) delayed the onset of inflammation by 4 days, but reduced overall disease severity by only 20% (significance of $P < 0.05$ for days 18–26; Fig. 3A).

Another experiment (Fig. 3B) tested VE-13,045 doses of 25, 50 and 100 mg/kg/day. Treatment with 100 mg/kg delayed onset of inflammatory symptoms by 10 days compared to untreated animals. The progression of disease in this group was slower between days 15 and 20, however, after 22–26 days, the severity of arthritic disease was similar to the 50 mg/kg treatment group, with a combined severity score of approximately 2.5 for both groups. VE-13,045 treatment at 25 mg/kg/day had a transient effect on symptoms (between days 7 to 13), but no overall sustained or consistent effect on progression of arthritic disease.

In another experiment, animals were treated with VE-13,045 (50 mg/kg) or prednisolone (10 mg/kg) for 16 days and then treatment was discontinued. The degree of inflammation in the affected paws increased within 2–3 days and the severity of arthritic disease rapidly progressed to the same level as the vehicle treated group within 4–5 days (Fig. 3C). These results suggest that the efficacy observed may reflect suppression by VE-13,045 of an active IL-1 β dependent inflammatory process. The efficacy of VE-13,045 was next evaluated in animals with established CIA. Daily treatment (50 mg/kg) was initiated in randomized groups of animals with focal swelling of the wrist (level 2) starting 10 days after the CII booster injection. Mice treated with the ICE inhibitor showed a 20% reduction in inflammation beginning 2 days after treatment initiation, with a 40% overall reduction in disease severity that was sustained over the 16 day treatment interval (significance of $P < 0.01$; Fig. 3D). Progression of arthritic disease (from a combined score of 4–5; a 20% increase in severity) was observed in the vehicle-treated group.

Histological evaluation of wrist paw joints from untreated and VE-13,045 treated mice

Wrist paw joints from vehicle-treated and VE-13,045 treated mice were evaluated to assess the extent of synovitis, inflammatory cell infiltration, fibrosis, and cartilage erosion. Figure 4 A–F shows histological

changes in wrist joints from representative mice. Compared to a normal mouse wrist joint (Fig. 4A), invagination of the synovial membrane with infiltration of inflammatory cells and marked cartilage erosion is evident in the wrist joint of a representative vehicle-treated mouse 23 days after the CII booster injection (Fig. 4B). In contrast, prophylactic treatment with VE-13,045 reduced the extent of synovial membrane damage and inflammatory cell infiltration and minimized cartilage erosion (Fig. 4C). In the therapeutic regimen, histological evaluation shows progression of arthritic disease with invagination of the synovial membrane, inflammatory cell infiltration, fibrosis and cartilage erosion in untreated mice (Fig. 4E) compared to the histological extent of joint damage noted in a representative mouse sacrificed 10 days after the CII booster (Fig. 4D). VE-13,045 treatment prevented further progression of inflammatory cell infiltration and joint destruction (Fig. 4F) concurrent with the reduction in inflammatory symptoms observed in these animals (see Fig. 3D).

Treatment with an ICE inhibitor reduces serum amyloid A levels

Sera were obtained from animals in untreated and treated groups at three time points during the clinical course of CIA for determination of serum amyloid A (SAA) levels. Table 2 shows that treatment with indomethacin and prednisolone reduced SAA levels compared to the vehicle-treated group within 5 days of the CII booster injection. VE-13,045 treatment (50 mg/kg/day) also reduced SAA levels suggesting that a generalized reduction in the acute phase inflammatory response is associated with ICE inhibition in CIA. Treatment with each of the three agents reduced SAA to a level comparable to normal mice ($4.5 \pm 0.3 \mu\text{g/ml}$) by Day 26, independent of the clinical status of CIA at that time (Table 2).

TABLE 2. Time course profile of serum amyloid A levels in mice with Type II collagen-induced arthritis

| Treatment group | Time after type II collagen booster | | |
|-----------------|-------------------------------------|-----------------|----------------|
| | Day 5 | Day 12 | Day 26 |
| Vehicle-treated | 39.2 \pm 25 | 21.3 \pm 10.3 | 24.2 \pm 7.6 |
| VE-13,045 | | | |
| 50 mg/kg/d | 20.2 \pm 3 | 11.9 \pm 6 | 4.5 \pm 1.2 |
| Prednisolone | | | |
| 10 mg/kg/d | 9.6 \pm 6 | 8.0 \pm 5.4 | 5.3 \pm 1.8 |
| Indomethacin | | | |
| 2 mg/kg/d | 14.9 \pm 6.4 | 3.4 \pm 0.3 | 3.2 \pm 0.2 |

Mice ($n = 8$ per treatment group) were bled at three time points during the clinical course of CIA and serum amyloid A levels were determined by ELISA. Data are expressed as the mean \pm standard deviation in $\mu\text{g/ml}$. Serum amyloid A levels for normal DBA/1J mice ($n = 6$) were $4.5 \pm 0.3 \mu\text{g/ml}$.

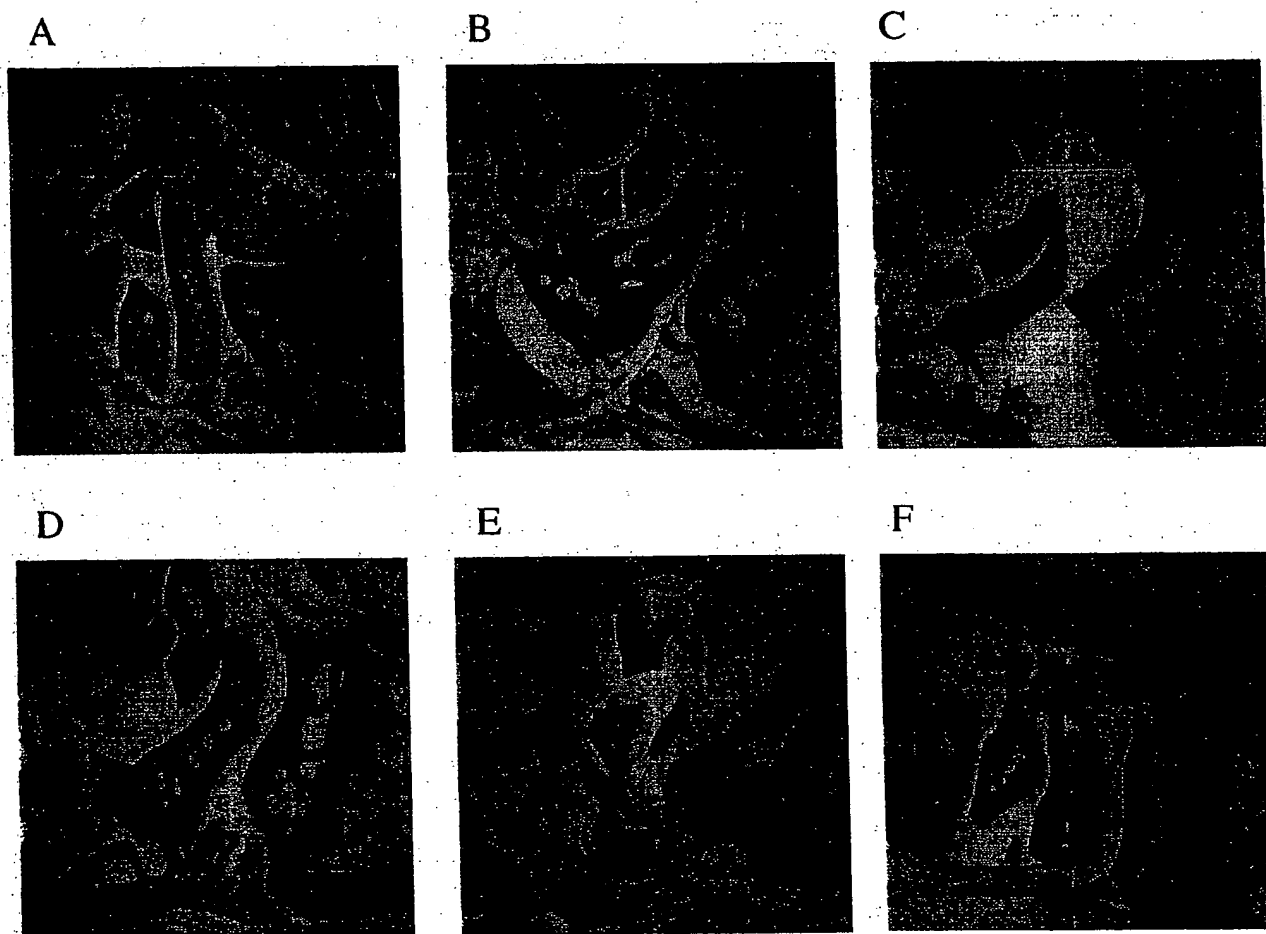


Figure 4. Histological evaluation of front paw wrist joints from representative DBA/1J mice with Type II collagen-induced arthritis.

(A–C) Prophylactic therapy of CIA: comparison of a wrist joint from a normal mouse (A) and a vehicle-treated mouse (B) on day 23 shows invagination of the synovial membrane with fibrosis and inflammatory cell infiltration into the joint space with cartilage erosion compared to a VE-13,045 wrist joint (C) on day 23 with minimal evidence of synovitis or cartilage erosion and no inflammatory cell infiltrate in the joint space. (D–F) Therapy of established CIA: a wrist joint 10 days after the CII booster injection (D) with initial evidence of synovitis and cellular infiltration compared to progression of CIA in an untreated wrist joint (E) on day 26, with extensive synovitis, fibrosis, cellular infiltration and complete erosion of cartilage over the bone growth plate. VE-13,045 treatment (F) prevented further progression of CIA evaluated on day 26 compared to the histologic extent of disease on day 10 (D).

DISCUSSION

We have shown that two irreversible prototype inhibitors of ICE effectively block secretion of both IL-1 β and IL-1 α in vitro and provide the first evidence for efficacy of an ICE inhibitor in a chronic inflammatory disease model. Murine CIA shares several immunological and pathogenetic features of RA in humans³³ and recent studies have identified a prominent role for IL-1, TNF- α and other proinflammatory cytokines and chemokines in the evolution of CIA.^{39–43} Treatment of mice with IL-1RA has been shown to delay the onset and reduce the incidence and severity of CIA,¹⁴ and prophylactic treatment with anti-IL-1 β and anti-IL-1 α antibodies alone or in combination can completely alleviate CIA in mice.^{34,35} Similarly, prophylactic treatment with anti-TNF- α ,⁴⁴ soluble TNF- α receptor⁴⁵ or a TNF- α receptor-Fc fusion protein⁴⁶ may also reduce the incidence and severity of CIA.

In addition to a role in the induction of CIA, localized production of IL-1 β and TNF- α by synoviocytes and infiltrating inflammatory cells contributes to progressive disease and joint destruction. Both cytokines induce tissue degrading matrix metalloproteinases and may suppress chondrocyte proteoglycan synthesis. Administration of IL-1 to mice with antigen⁴⁷ or collagen-induced arthritis⁴⁸ exacerbates the course of disease due to enhanced synovitis, inflammatory cell infiltration, fibrosis, cartilage and bone erosion. Similar results have been observed after intra-articular injection of TNF- α ⁴⁹ and mice expressing a human TNF- α transgene develop a chronic destructive polyarthritis that can be prevented by treatment with anti-TNF- α antibodies.⁵⁰ The multiple roles of IL-1 and TNF- α in arthritic disease⁵¹ and efficacy observed with IL-1RA, anti-IL-1 or TNF- α antibody treatments suggests strategies for potential therapeutic intervention in both the induction and progressive phases of disease.

Results of this study implicate activation of ICE and subsequent processing of IL-1 β in the induction and progression of CIA. Prophylactic treatment with VE-13,045 delayed the onset of inflammatory symptoms, blocked progression of synovitis and infiltration of inflammatory cells and reduced joint destruction in comparison to vehicle-treated animals. Therapeutic treatment with VE-13,045 also blocked progression of inflammation and halted further cellular infiltration and cartilage erosion. ICE inhibition in established disease appears to be more effective than blocking TNF- α since anti-TNF- α treatment is less effective in reversing the course of established disease.^{44,45} The efficacy observed with VE-13,045 in both prophylactic and therapeutic treatment regimens is further evidence of the central role of IL-1 β in CIA and our results also suggest that the CIA model is well suited for pharmacodynamic evaluation of ICE inhibitors.

VE-13,045 is remarkably effective in vivo considering its modest in vitro potency (IC_{50} ~1.3 μ M for VE-16,084), C_{max} (10–12 μ g/ml) and short plasma half life ($t_{1/2\beta}$ ~20 min). The efficacy observed with VE-13,045 may reflect in part the irreversible nature of this inhibitor due to inactivation of ICE molecules in cells at the inflammatory site. Compared to a reversible inhibitor, synthesis of new ICE precursor or processing of active ICE from existing p45 precursor in macrophages, synoviocytes or other IL-1 β producing cells in situ is necessary to overcome the irreversible inhibitor effect. Inflammatory and arthritic symptoms and histological evidence of disease persisted in animals in both the prophylactic and therapeutic treatment groups. Sustained disease may result from less than complete inhibition of ICE activity, which is consistent with the single daily administration of VE-13,045 and its short half life. Alternatively, residual disease may reflect the complexity of the cellular and molecular components involved in the pathogenesis of CIA. In addition to IL-1 and TNF- α , other cytokines (IFN- γ , IL-6, TGF- β) and chemokines (MIP-1 α and MIP-2) may contribute to joint inflammation.^{39–43} Also, local deposition of anti-Type II collagen antibodies, complement activation, generation of C5a, and production of leukotrienes or other mediators may lead to recruitment of cells to the inflammatory site, sustaining an intermediate level of joint inflammation. However, the near complete suppression of CIA with anti-IL-1 antibody treatment^{34,35} suggests that more frequent administration or higher doses of an ICE inhibitor, or the use of more potent compounds with improved pharmacokinetics may further enhance the efficacy of an ICE inhibitor in CIA.

The inhibition of IL-1 α secretion by ICE inhibitors in vitro is consistent with results from studies with ICE-deficient mice. We and others^{32,52} have observed diminished secretion of IL-1 α by LPS-stimulated monocytes

from ICE^{-/-} mice compared to monocytes from ICE^{+/+} mice. Also, ICE^{-/-} mice challenged with 32 mg/kg LPS had diminished serum levels of IL-1 α (52; G. Ku and M. W. Harding, unpublished observations). Inhibition of IL-1 α secretion by ICE inhibitors or in ICE^{-/-} mice suggests a role for ICE in IL-1 α release. Although ICE does not directly process the IL-1 α precursor,²⁶ ICE may interact with or activate calpain^{23,24} or other proteins involved in IL-1 α processing and release. Alternatively, ICE may be part of a molecular assembly or complex involved in the export of IL-1 α through the plasma membrane.

A recent study identified several variants of ICE (ICE- β , ICE- γ , ICE- δ and ICE- ϵ) generated by alternative splicing of ICE mRNA.⁵³ It is possible that ICE, or a splicing variant of ICE, may perform a chaperonin-like function in IL-1 α release, independent of its protease activity. If the effect of VE-13,045 and VE-16,084 observed in this study result from steric hindrance or a conformational change in ICE that alters critical protein-protein interactions, it will be of interest to evaluate other chemical classes of ICE inhibitors for an effect on IL-1 α release. A strategy for blocking the biological actions of IL-1 α may result from further investigating the role of ICE in IL-1 α release.

Improving on the irreversible, peptidyl ICE inhibitors for therapeutic applications will require the design of non-peptidyl compounds. The availability of the high-resolution crystal structure of ICE, as well as structure-activity investigations of peptidyl ICE inhibitors, should lead ultimately to the design of an orally bioavailable compound with improved cellular potency and pharmacokinetic properties. The efficacy of VE-13,045 in CIA suggests that such a compound may be suitable for clinical evaluation in patients with RA, osteoarthritis or other clinical indications where IL-1 β contributes to the progression of inflammatory disease.

MATERIALS AND METHODS

Materials

Lipopolysaccharide (LPS, from *E. coli* serotype 0111:B4, trichloroacetic acid extracted), indomethacin, methyl prednisolone, Freund's complete adjuvant, and carboxymethyl cellulose were purchased from Sigma (St Louis, MO); chick sternum-derived Type II collagen (CII) from Elastin Products (Owensville, MO); and olive oil (extra virgin) from a local store. Male CD1 mice (20–22 grams) and male DBA/1J mice (age 6 weeks) were purchased from Charles River (Wilmington, MA) and Jackson Labs (Bar Harbor, ME), respectively. Mice were given food (Purina rodent chow) and water *ad libitum*. ELISAs for murine IL-1 β (PerSeptive Diagnostics, Cambridge, MA), human IL-1 α and IL-1 β (R & D Systems, Minneapolis, MN), murine IL-1 α (Genzyme,

Cambridge, MA), TNF- α , IL-6 and murine serum amyloid A (Biosource International, Camarillo, CA) were obtained from commercial sources and performed according to the manufacturers' suggested protocols. VE-13,045 and VE-16,084 were provided by Dr J. M. C. Golec (Hoechst-Roussel, Swindon, UK). Stock solutions were prepared in DMSO and stored at -20°C .

Induction of IL-1 β and IL-1 α in vitro

Buffy coat cells were obtained from blood donors and peripheral blood mononuclear cells (PBMC) were isolated by centrifugation in LeukoPrep tubes (Becton-Dickinson, Lincoln Park, NJ). PBMC were added (3×10^6 /well) to 24-well Corning tissue culture plates and after 1 h incubation at 37°C , non-adherent cells were removed by gentle washing. Adherent mononuclear cells were stimulated with LPS (1 $\mu\text{g}/\text{ml}$) with or without ICE inhibitors (0.2–20 μM VE-13,045 or VE-16,084) in 2 ml RPMI-1640-10% FBS. After 16–18 h incubation at 37°C , IL-1 β and IL-1 α were quantitated in culture supernatants by ELISA. For isolation of murine adherent mononuclear cells, spleens were excised from DBA/1J mice, single cell suspensions were prepared and added to 12-well tissue culture plates (1×10^7 /well), adherent mononuclear cells were isolated and stimulated with LPS (10 $\mu\text{g}/\text{ml}$), with or without ICE inhibitors in 0.5 ml RPMI-1640-10% FBS. After 16–18 h, supernatants were harvested, cells were washed once, incubated for 30 min with 10 μM nigericin³⁶ in 0.5 ml RPMI-1640-10% FBS containing the ICE inhibitors (at the same concentrations as in the overnight cultures), and supernatants were harvested again for quantitation of IL-1 β and IL-1 α . Viability of monocytes before or after nigericin stimulation was $>98\%$ as measured by trypan blue staining or lactate dehydrogenase activity in culture supernatants, indicating that minimal cytolysis had occurred during the experiments.

Acute induction of IL-1 α and IL-1 β production in vivo

LPS mixed with 0.5% carboxymethyl cellulose in PBS, pH 7.4, was administered by intraperitoneal injection (40 mg/kg LPS) in a dose volume of 20 ml/kg. VE-13,045 stock solutions in DMSO were then dissolved in olive oil:ethanol:DMSO (final concentration 90:5:5; v/v/v) and administered by intraperitoneal injection at 50 mg/kg in a dose volume of 5 ml/kg. VE-13,045 or the vehicle [olive oil:ethanol:DMSO (90:5:5, v/v/v)] alone was administered to mice simultaneous with LPS, or at various time points before or after LPS. Mice were euthanized 7 h after LPS challenge for blood collection. Serum IL-1 β was measured with an ELISA specific for mature IL-1 β . Specificity was determined by testing the reactivity of purified recombinant murine pro-IL-1 β in the ELISA. At concentrations of 20 pg/ml and 10 ng/ml, respectively, mature and precursor IL-1 β were recognized equally, indicating a cross-reactivity of 0.2% (data not shown). Serum IL-1 α was measured with an ELISA that detects both the precursor and mature forms. Statistical significance between groups was determined by Student's *t*-tests.

Type II collagen-induced arthritis

Type II collagen-induced arthritis was established in male DBA/1J mice as described by Wooley.³⁷ Briefly, chick sternum Type II collagen (4 mg/ml in 10 mM acetic acid) was emulsified with an equal volume of Freund's complete adjuvant (FCA) by repeated passages (400) between two 10-ml glass syringes connected with a gauge 16 double-hub needle. Mice were immunized by intradermal injection (50 μl ; 100 μg CII per mouse) of the collagen emulsion at the base of the tail on day 0 and again with 50 μl or 100 μl (200 μg CII) of a freshly prepared collagen emulsion 21 days later at the contra-lateral side of the tail base. VE-13,045 was prepared as described above (90:5:5 olive oil:ethanol:DMSO) and administered daily (25, 50 or 100 mg/kg) by intraperitoneal injection. Both indomethacin (2 mg/kg) and methylprednisolone (10 mg/kg) were prepared in PBS and administered daily by oral gavage. For the prophylactic regimen, drug treatments were initiated within 2 h of the CII booster immunization. For the therapeutic regimen, mice with a similar degree of inflammation were selected (10 days following the CII booster) and randomized for treatment with VE-13,045 or the vehicle alone.

Scoring of arthritic symptoms

Front paws (ventral surface) were examined daily after the CII booster injection and scored (Arthritis Index) for severity of inflammation and arthritic disease as follows: Level 1 - erythema; Level 2 - focal carpal (wrist) joint swelling; Level 3 - swelling of the entire wrist; Level 4 - spread of swelling to the metacarpal/metatarsal (palm) region; Level 5 - swelling affecting the metacarpophalangeal or the metatarsophalangeal joints. The score of both front paws was combined and the mean \pm SEM determined for each treatment group. Rear paws were not scored in this study. The statistical significance between groups was determined by Mann-Whitney nonparametric analysis.

Histological examination of inflamed paws

Untreated animals with arthritic disease at each severity level were sacrificed and paws were removed for histological evaluation. Animals in prophylactic regimens were sacrificed at the end of the treatment period. For the therapeutic regimen, animals exhibiting comparable levels of inflammation were sacrificed on day 10 and front paws were processed for histological evaluation as a reference. The remainder of the animals were sacrificed at the end of the treatment period. Paws were fixed with 10% formalin in PBS for 48 h at 25°C , then de-calcified in 10% formic acid in water for 24 h at 25°C . The tissues were embedded in paraffin, sagittal sections were prepared, and stained with Giemsa.

Acknowledgements

We thank M. Grim, S. D. Jones and J. M. C. Golec for synthesis and provision of VE-13,045 and VE-16,084, Y. P. C. Luong and S. A. Raybuck for enzymatic evaluation of ICE inhibition by these compounds, I. R. Ager and J. M. C. Golec for pharmacokinetic data, and

U. Germann and V. Sato for critical review of the manuscript.

REFERENCES

1. Dinarello CA, Wolff SM (1993) The role of interleukin-1 in disease. *N Eng J Med* 328:106-113.
2. Dinarello CA (1989) Interleukin-1 and its biologically related cytokines. *Adv Immunol* 44:153-205.
3. Dinarello CA (1994) The interleukin-1 family: 10 years of discovery. *FASEB J* 8:1314-1325.
4. March CJ, Mosley B, Larsen A, Cerretti DP, Braedt G, Price V, Gillis S, Henney CS, Kronheim SR, Grabstein K, Colulun PJ, Hopp TP, Cosman D (1985) Cloning, sequence and expression of two distinct human interleukin-1 complementary DNAs. *Nature* 315:641-645.
5. Gray PW, Glaister D, Chen E, Goeddel DV, Pennica D (1986) Two interleukin-1 genes in the mouse: cloning and expression of the cDNA for murine interleukin-1 β . *J Immunol* 137:3644-3648.
6. Dower SK, Kronheim SR, Hopp TP, Cantrell M, Deeley M, Gillis S, Henney CS, Urdal DL (1986) The cell surface receptors for IL-1 are identical. *Nature* 324:266-268.
7. Sims JE, Gayle MA, Slack JL, Alderson MR, Bird TA, Giri JG, Colotta F, Re F, Mantovani A, Shanebeck K, Grabstein KH, Dower SK (1993) Interleukin-1 signaling occurs exclusively via the type I receptor. *Proc Natl Acad Sci USA* 90:6155-6159.
8. Arend WA (1993) Interleukin-1 receptor antagonist. *Adv Immunol* 54:167-227.
9. Fanslow WC, Sims JE, Sassenfeld H, Morrissey PJ, Gillis S, Dower SK, Widmer MB (1990) Regulation of alloreactivity *in vivo* by a soluble form of the interleukin-1 receptor. *Science* 248:739-742.
10. Ohlsson K, Bjork P, Bergenfeldt M, Hageman R, Thompson RC (1990) Interleukin-1 receptor antagonist reduces mortality from endotoxin shock. *Nature* 348:550-552.
11. Alexander HR, Doherty GM, Buresh CM, Venzon DJ, Norton JA (1991) A recombinant human receptor antagonist for interleukin-1 improves survival after lethal endotoxemia in mice. *J Exp Med* 173:1029-1032.
12. Wakabayashi G, Gelfand JA, Burke JF, Thompson RC, Dinarello CA (1991) A specific receptor antagonist for interleukin-1 prevents *Escherichia coli* induced shock. *FASEB J* 5:338-343.
13. McCarthy PL, Abhyankar S, Neben S, *et al.* (1991) Inhibition of interleukin-1 by Interleukin-1 receptor antagonist presents graft vs host disease. *Blood* 78:1915-1918.
14. Wooley PH, Whalen JD, Chapman DL, Berger AE, Richard KA, Aspar DG, Staite ND (1993) The effect of an interleukin-1 receptor antagonist protein on Type II collagen-induced arthritis and antigen-induced in mice. *Arthritis Rheum* 36:1305-1314.
15. Schwab JH, Anderle SK, Brown RR, Dalldorf FG, Thompson RC (1991) Pro- and anti-inflammatory roles of interleukin-1 in recurrence of bacterial cell wall-induced arthritis in rats. *Infect Immun* 59:4436-4442.
16. Lewthwaite J, Blake SM, Hardingham TE, Warden PJ, Henderson B (1994) The effect of recombinant human interleukin-1 receptor antagonist on the induction phase of antigen induced arthritis in the rabbit. *J Rheumatol* 21:467-472.
17. Dreylow B, Capezio J, Lovis R, Jacobs C, Landay A, Pope RM (1993) Phase I study of recombinant human interleukin-1 receptor administered intra-articularly in active rheumatoid arthritis. *Arthritis Rheum* 36 (Suppl 9):S39.
18. Lebsack ME, Paul CC, Bloedow DC, Burch FX, Sack MA, Chase W, Catalano MA (1991) Subcutaneous IL-1 receptor antagonist in patients with rheumatoid arthritis. *Arthritis Rheum* 36 (Suppl 9):S45.
19. Lebsack ME, Paul CC, Martindale JJ, Catalano MA (1993) A dose and regimen ranging study of IL-1 receptor antagonist in patients with rheumatoid arthritis. *Arthritis Rheum* 36 (Suppl 9):S39.
20. Dinarello CA, Gelfand JA, Wolff SM (1993) Anticytokine strategies in the treatment of the systemic inflammatory response syndrome. *JAMA* 269:1829-1835.
21. Carruth LM, Derczuk S, Mizel SB (1991) Involvement of a calpain-like protease in the processing of the murine interleukin-1 α precursor. *J Biol Chem* 266:12162-12167.
22. Kobayashi Y, Yamamoto K, Saido T, Kawasaki H, Oppenheim JJ, Matsushima K (1990) Identification of calcium activated neutral protease as a processing enzyme of human interleukin-1 α . *Proc Natl Acad Sci USA* 87:5548-5552.
23. Black RA, Kronheim SR, Sleath PR (1989) Activation of interleukin-1 β by a co-induced protease. *FEBS Lett* 247:386-390.
24. Kostura MJ, Tocci MJ, Limjuco G, Chin J, Vamerson P, Hillman AG, Chartrain NA, Schmidt JA (1989) Identification of a monocyte specific pre-interleukin 1 β convertase activity. *Proc Natl Acad Sci USA* 86:5227-5231.
25. Kurt-Jones EA, Beller DI, Mizel SM, Unanue ER (1985) Identification of a membrane-associated interleukin-1 macrophages. *Proc Natl Acad Sci USA* 82:1204-1208.
26. Fuhlbrigge RC, Fine SM, Unanue ER, Chaplin DD (1988) Expression of membrane interleukin-1 fibroblasts transfected with murine pro-interleukin-1 α cDNA. *Proc Natl Acad Sci USA* 85:5649-5653.
27. Thornberry NA, Bull HG, Calaycay JR, Chapman KT, Howard AD, Kostura MJ, Miller DK, Molineaux SM, Weidner JR, Aunins J, Elliston KO, Ayala JM, Casano FJ, Chin J, Ding GJ-F, Egger LA, Gaffney EP, Limjuco G, Palyha OC, Raju SM, Rolando AM, Salley JP, Yamin T-T, Lee TD, Shively JE, MacCross M, Mumford RA, Schmidt JA, Tocci MJ (1992) A novel heterodimeric cysteine protease required for interleukin-1 β processing in monocytes. *Nature* 356:768-774.
28. Ceretti DP, Kozlosky CJ, Mosley B, Nelson N, Van Ness K, Greenstreet TA, March CJ, Kronheim SR, Druck T, Cannizzaro LA, Huebner K, Black RA (1992) Molecular cloning of the IL-1 β converting enzyme. *Science* 256:97-100.
29. Ayala JM, Yamin T-T, Egger LA, Chin J, Kostura MJ, Miller DK (1994) IL-1 β converting enzyme is present in monocytic cells as an inactive 45-kDa precursor. *J Immunol* 153:2592-2599.
30. Wilson KP, Black JF, Thomson JA, Kim EE, Griffith JP, Navia MA, Murcko MA, Chambers SP, Aldape RA, Raybuck SA, Livingston DJ (1994) Structure and mechanism of interleukin-1 β converting enzyme. *Nature* 370:270-275.
31. Walker NPC, Talanian RV, Brady KD, Lang LC, Bump NJ, Ferenz CR, Franklin S, Ghayur T, Hackett MC, Hammill LD, Herzog L, Hugunin M, Houy W, Mankovich JA, McGuinness L, Orlewicz E, Paskind M, Pratt CA, Reis P, Summani A, Terranova M, Welch JP, Xiong L, Moller A, Tracey DE, Kamen R, Wong WW (1994) Crystal structure of the cysteine protease interleukin-1 β converting enzyme: A (p20/p10) $_2$ homodimer. *Cell* 78:343-352.
32. Kuida K, Lippke JA, Ku G, Harding MW, Livingston DJ, Su MS-S, Flavell RA (1995) Altered cytokine export and apoptosis in mice deficient in interleukin-1 β converting enzyme. *Science* 267:2000-2003.
33. Homdahl R, Andersson M, Goldschmidt TJ, Gustafsson K, Jansson L, Mo JA (1990) Type II collagen auto-immunity in animals and provocations leading to arthritis. *Immunol Rev* 118:193-232.
34. Van den Berg WB, Joosten LAB, Helsen M, van de Loo FAS (1994) Amelioration of established murine collagen induced arthritis with anti-IL-1 treatment. *Clin Exp Immunol* 95:237-243.
35. Geiger T, Towbin H, Cosenti-Vargas A, Zingle O, Arnold J, Rordorf C, Glatt M, Vosbeck K (1993) Neutralization of interleukin-1 β activity *in vivo* with a monoclonal antibody alleviates collagen-induced arthritis in DBA/1 mice and prevents the associated acute-phase response. *Clin Exp Rheum* 11:515-522.
36. Perregaux D, Barberia J, Lanzetti AJ, Geoghegan KF, Carty TJ, Gabel CA (1992) IL-2 β maturation: evidence that mature cytokine formation can be induced specifically by nigericin. *J Immunol* 149:1294-1303.

37. Wooley PH (1988) Collagen arthritis in the mouse. *Methods Enzymol* 162:361-373.
38. Miller BE, Krasney PA, Gauvin DM, Holbrook KB, Kounz DJ, Abruzzese RV, Miller RE, Pagani KA, Dolle RE, Ator MA, Gilman SC (1995) Inhibition of mature IL-1 β production in murine macrophages and a murine model of inflammation by WIN 67694, an inhibitor of IL-1 β converting enzyme. *J Immunol* 154:1331-1338.
39. Thorbecke GJ, Shah R, Leu CH, Kuruvilla AP, Hardis AM, Palladino MA (1992) Involvement of endogenous tumor necrosis factor alpha and transforming growth factor beta during induction of collagen type II arthritis in mice. *Proc Natl Acad Sci USA* 89:7375-7379.
40. Takai YN, Seki N, Senoh H, Yokota T, Lee F, Hamaoka T, Fujiwara H (1989) Enhanced production of interleukin-6 in mice with type II collagen-induced arthritis. *Arthritis Rheum* 32:594-600.
41. Mauritz NJ, Holmdahl R, Jonsson R, Van der Meide PH, Scheynius A, Klareskog L (1988) Treatment with gamma-interferon triggers the onset of collagen arthritis in mice. *Arthritis Rheum* 31:1297-1304.
42. Cooper SM, Sriram S, Ranges GE (1988) Suppression of murine collagen induced arthritis with monoclonal anti-Ia antibodies and augmentation with IFN-gamma. *J Immunol* 141:1958-1962.
43. Kasama T, Strieter RM, Lukacs NW, Lincoln PM, Burdick MD, Kunkel SL (1995) Interleukin-10 expression and chemokine regulation during the evolution of murine type II collagen-induced arthritis. *J Clin Invest* 95:2868-2876.
44. Williams RO, Feldmann M, Maini RN (1992) Anti-tumor necrosis factor ameliorates joint disease in murine collagen-induced arthritis. *Proc Natl Acad Sci USA* 89:9784-9788.
45. Piguet PF, Grau GE, Vesin C, Wetscher H, Gentz R, Lesslauer W (1992) Evolution of collagen arthritis in mice is arrested by treatment with anti-tumor necrosis factor (TNF) antibody or a recombinant soluble TNF receptor. *Immunol* 77:510-514.
46. Wooley PH, Dutcher J, Widmer MB, Gillis S (1993) Influence of a recombinant human soluble tumour necrosis factor receptor Fc fusion protein on type II collagen-induced arthritis in mice. *J Immunol* 151:6602-6607.
47. Staite ND, Richard KA, Aspar DG, Franz KA, Galinet LA, Dunn CJ (1990) Induction of an acute erosive monarticular arthritis in mice by interleukin-1 and methylated bovine serum albumin. *Arthritis Rheum* 33:253-260.
48. Hom JT, Gliszczyński VL, Cole HW, Bendele AM (1991) Interleukin-1 mediated acceleration of type II collagen-induced arthritis: Effects of anti-inflammatory or anti-arthritis drugs. *Agents Actions* 33:300-309.
49. Cooper WO, Fava RA, Gates CA, Cramer MA, Townes AS (1992) Acceleration of onset of collagen-induced arthritis by intra-articular injection of tumor necrosis factor or transforming growth factor-beta. *Clin Exp Immunol* 89:244-250.
50. Keffer J, Probert L, Czaizlis H, Georgopoulos S, Kaslaris E, Kioussis D, Kollias G (1991) Transgenic mice expressing human tumor necrosis factor: a predictive genetic model of arthritis. *EMBO J* 10:4025-4031.
51. Arend WP, Dayer JM (1995) Inhibition of the production and effects of interleukin-1 and tumor necrosis factor α in rheumatoid arthritis. *Arthritis Rheum* 38:151-160.
52. Li P, Allen H, Banerjee S, Franklin S, Herzog L, Johnston C, McDowell J, Paskind M, Rodman L, Salfeld J, Towne E, Tracey D, Wardwell S, Wei F-Y, Wong W, Kamen R, Seshardi T (1995) Mice deficient in IL-1 β converting enzyme are defective in production of mature IL-1 β and resistant to endotoxic shock. *Cell* 80:401-411.
53. Alacerri ES, Fernandes-Alnmeri T, Litwack G (1995) Cloning and expression of four novel isoforms of human interleukin-1 β converting enzyme with different apoptotic activities. *J Biol Chem* 270:4312-4316.

Inhibition of Mature IL-1 β Production in Murine Macrophages and a Murine Model of Inflammation by WIN 67694, an Inhibitor of IL-1 β Converting Enzyme¹

Bruce E. Miller,^{2*} Philip A. Krasney,* Donna M. Gauvin,* Kim B. Holbrook,* David J. Koonz,* Ronald V. Abruzzese,* Robert E. Miller,[†] Karen A. Pagani,[‡] Roland E. Dolle,[§] Mark A. Ator,[†] and Steven C. Gilman*

Departments of *Inflammation Pharmacology, [§]Medicinal Chemistry, [†]Immunobiology, and [‡]Biochemistry, Sterling Winthrop Pharmaceuticals Research Division, Collegeville, PA 19426

The proinflammatory cytokine IL-1 β is synthesized by activated monocytes and macrophages as a 31-kDa, biologically inactive precursor that is proteolytically processed to the biologically active 17-kDa mature molecule by the IL-1 β converting enzyme (ICE). WIN 67694, Z-Val-Ala-Asp-CH₂O(CO)[2,6-(Cl₂)Ph], is a potent, selective inhibitor of human ICE. In activated murine peritoneal macrophages, WIN 67694 inhibited the release of mature IL-1 β with an IC₅₀ of 1.8 μ M without any effect on the release of IL-1 α , IL-6, or TNF- α . The effect was specific to mature IL-1 β release; the ICE inhibitor did not effect IL-1 β RNA levels or precursor protein synthesis. In vivo, WIN 67694 was also able to inhibit selectively the release of IL-1 β in a dose-dependent manner in a subcutaneous tissue chamber implant model of inflammation. IL-1 β levels in tissue chamber fluid were inhibited 35 and 55% at 10 and 100 mg/kg, respectively. IL-1 α , IL-6, and TNF- α levels were not affected. The ability to selectively inhibit mature IL-1 β release in vivo with ICE inhibitors will allow for detailed studies of the role of IL-1 β and ICE in inflammatory diseases. *The Journal of Immunology*, 1995, 154: 1331–1338.

The proinflammatory cytokine IL-1 β is thought to play a key role in several chronic inflammatory diseases, including rheumatoid arthritis and inflammatory bowel disease (1, 2). IL-1 β is synthesized in activated monocytes and macrophages as a 31-kDa biologically inactive precursor molecule that is proteolytically processed to produce a biologically active 17-kDa carboxy terminal polypeptide (3, 4). This cleavage is mediated by the IL-1 β converting enzyme, or ICE³, a novel

cysteine protease (5, 6). The importance of ICE in the production of biologically active IL-1 β is demonstrated by the ability of ICE inhibitors to inhibit the production of mature IL-1 β from activated monocytes and macrophages (6, 7).

Both human and murine forms of ICE have recently been cloned and sequenced (6, 8–10). The two enzymes are highly conserved and exhibit absolute identity at the active site thiol and adjacent residues. The conservation between human and murine ICE suggests that murine models should be appropriate for studying the biologic and pharmacologic consequences of ICE inhibition. Indeed, we show in this study, as has been shown in other studies (11), that human ICE inhibitors retain a high degree of potency in the murine system.

To explore further the biologic and pharmacologic effects of ICE inhibitors, we have characterized the effect of a potent, selective, and irreversible inhibitor of ICE on the production of mature IL-1 β from murine peritoneal macrophages in vitro and in inflammatory exudates in vivo. We demonstrate that selective inhibition of mature IL-1 β generation is achievable in vivo, thereby creating new avenues into studies of the roles of ICE and mature IL-1 β in animal models.

Received for publication July 11, 1994. Accepted for publication October 28, 1994.

The costs of publication of this article were defrayed in part by the payment of page charges. This article must therefore be hereby marked advertisement in accordance with 18 U.S.C. Section 1734 solely to indicate this fact.

¹ All research involving animals described in this publication was performed in accordance with Sterling Winthrop Pharmaceuticals Research Division's (SWPRD) Policy on Animal Use and with all national and federal legislation. All SWPRD animal facilities are accredited by the American Association for Accreditation of Laboratory Animal Care (AAALAC).

² Address correspondence and reprint requests to Dr. Bruce E. Miller, Rhone-Poulenc Rorer Central Research, Department of Inflammation, 500 Arcola Road, Collegeville, PA 19426.

³ Abbreviations used in this paper: ICE, IL-1 β converting enzyme; FBS, fetal bovine serum; TBS, Tris-buffered saline (150 mM NaCl, 20 mM Tris, pH 7.5).

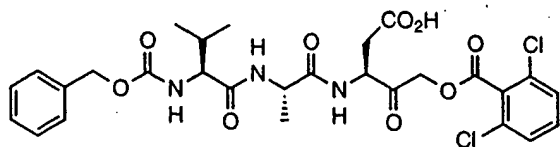


FIGURE 1. Structure of WIN 67694.

Materials and Methods

Materials

RPMI 1640 was obtained from Mediatech, Inc. (Herndon, VA). Heat-inactivated and dialyzed fetal bovine serum (FBS) were obtained from HyClone Laboratories (Logan, UT). Tran³⁵S-label ([³⁵S]methionine/[³⁵S]-cysteine) and [³²P]UTP were obtained from ICN Radiochemicals (Irvine, CA). ELISA kits for murine IL-1 α and TNF- α were purchased from Genzyme Corporation (Boston, MA). WIN 67694, Z-Val-Ala-Asp-CH₂O(CO)[2,6-(Cl₂)Ph] (Fig. 1), was synthesized as recently described (12). This compound has a second-order rate constant of 432,000 M⁻¹ s⁻¹ against human ICE and inhibits IL-1 β secretion from human monocytes with an IC₅₀ of 0.5 μ M (7, 12).

Peritoneal macrophage isolation and activation by LPS

Female, BALB/c mice 8 to 10 wk old (Taconic, Germantown, NY), were injected with 1 ml of 3% Brewer's thioglycolate, and peritoneal exudate cells were isolated 4 to 5 days later by peritoneal lavage with calcium/magnesium-free PBS containing 0.1% glucose. Cells were washed and resuspended in RPMI 1640/25 mM HEPES/5% heat-inactivated FBS at 1.25×10^6 cells/ml. Macrophages were purified by plating 2.5×10^6 cells/well in 6-well plates (Corning, Corning, NY). Cells were allowed to adhere for 2 h, then nonadherent cells were removed by washing. Adherent cells were stimulated with 1 μ g/ml LPS (*Salmonella minnesota* Re595, Calbiochem, La Jolla, CA) for 2 h. To stimulate the release of mature IL-1 β , cells were washed and subsequently incubated for 30 min with 40 μ M nigericin (Sigma Chemical Co., St. Louis, MO) (13). After incubation with nigericin, culture media was collected and centrifuged at 4000 \times g for 10 min. The supernatants were then analyzed for cytokine levels by ELISA.

Pulse-labeling assay for IL-1 β synthesis and secretion

Adherent macrophages were isolated as described above and stimulated with 1 μ g/ml LPS for 90 min. The cells were then washed and incubated for 15 min with cysteine/methionine-free RPMI 1640 containing 1% dialyzed FBS and 1 μ g/ml LPS, and then 100 μ Ci/ml of Tran³⁵S-label was added. The cells were then incubated for an additional 60 min. For determination of IL-1 β synthesis, the media was removed immediately after the labeling step, and cells were lysed by addition of RIPA buffer containing protease inhibitors (14). For measurement of secretion of mature IL-1 β , the labeled cells were incubated with 40 μ M nigericin for 30 min before the collection of media. Lysates and media samples were cleared by centrifugation at 12,000 \times g for 10 min. An aliquot of the lysate was immunoprecipitated with goat anti-murine IL-1 β IgG (R&D Systems, Minneapolis, MN). Put briefly, samples were preabsorbed by rotating for 30 min at 4°C with 50 μ l of a 50% slurry of protein G-Sepharose, centrifuged at 12,000 \times g, and the supernatants transferred to new tubes. After the addition of goat anti-murine IL-1 β IgG (15 μ g/ml) (R&D Systems), samples were rotated overnight at 4°C. Fifty microliters of protein G-Sepharose was then added, and samples were rotated for 1 h at 4°C. The immunoprecipitates were washed three times with RIPA buffer and resuspended in SDS-PAGE sample buffer containing 6% mercaptoethanol (15). After heating at 95°C for 3 min, samples were fractionated by electrophoresis on 15% SDS polyacrylamide gels. Gels were treated with Amplify (Amersham, Arlington Heights, IL), dried, and placed on film (Kodak XAR-5) overnight. Bands corresponding to IL-1 β were quantitated by laser densitometry.

mRNA isolation and Northern analysis

Thioglycolate-elicited peritoneal macrophages (1×10^7) were incubated in RPMI 1640/5%, FBS/25 mM HEPES with 1 μ g/ml LPS for 3.5 h.

Total cellular RNA was prepared as described (16). Five micrograms each RNA sample was size-fractionated on a 1.0% agarose/2.2 M formaldehyde gel and transferred to a nylon membrane (Hybond N, Amersham) according to standard protocols (17). Blots were probed with murine IL-1 β and rat cyclophilin cRNAs as described previously (18). Put briefly, blots were prehybridized for 2 h at 57°C in a 50% formamide, 50 μ g/ml heparin buffer, hybridized for 16 h at 57°C in the same buffer, and washed twice at 65°C in 0.2X SSC/0.2% SDS. Autoradiography was conducted at -70°C using Kodak XAR film and Fisher Lightening Plus intensifying screens. Bands were quantitated by laser densitometry. The ³²P-labeled murine IL-1 β cRNA probe was synthesized by in vitro transcription of a full-length murine IL-1 β cDNA in pSG-BSmIL-1 β (+) (kind gift of Dr. David Chaplin; 19). The ³²P-labeled cyclophilin cRNA probe was synthesized by in vitro transcription of a cDNA representing nucleotides 42 to 520 of the rat cyclophilin mRNA (20). The cyclophilin cDNA was generated by reverse transcriptase-PCR using rat whole knee joint RNA as a template and was ligated into pCRII (Invitrogen, San Diego, CA) for in vitro transcription.

Synthesis of ³⁵S-labeled precursor IL-1 β

³⁵S-labeled murine proIL-1 β was generated by in vitro transcription and translation of pSG5 mIL-1 β using a TnT kit (Promega, Madison, WI). pSG5 mIL-1 β contains a full-length murine proIL-1 β cDNA (19) and was constructed by inserting the 1.4-kb IL-1 β EcoRI cDNA fragment of pSG-BSmIL-1 β (+) into pSG5 (Stratagene, La Jolla, CA).

ICE activity in cell lysates

Macrophage lysates were prepared by four freeze-thaw cycles. The lysates were centrifuged at 16,000 \times g for 20 min, and ICE activity was measured in the supernatants. An 18- μ l aliquot of the cell lysate added to tubes containing 1 μ l of [³⁵S]methionine-labeled murine precursor IL-1 β and 11 μ l of assay buffer (30% glycerol, 30 mM Tris, pH 8.0). Tubes were incubated for 60 min at 30°C. The reactions were stopped by the addition of 15 μ l of 4 \times SDS sample buffer containing 25% 2-ME. Aliquots were fractionated on 15% SDS polyacrylamide gels as described above.

Murine IL-1 β ELISA

ELISA plates (Costar high binding plates) were coated with a hamster mAb to murine IL-1 β (Genzyme) (5 μ g/ml) in PBS overnight at 4°C, washed, and blocked with 3% BSA in Tris-buffered saline (TBS) for 1 h. Aliquots (100 μ l) of diluted samples were added and incubated for 2 h at room temperature. The plates were washed five times and incubated for 1 h at room temperature with 10 μ g/ml of goat anti-murine IL-1 β IgG (R&D Systems). After five washes, the plates were incubated for 1 h at room temperature with a 1:2000 dilution of an alkaline phosphatase-conjugated mouse anti-goat IgG. After four washes, the plates were incubated with substrate solution (1 mg/ml p-nitrophenylphosphate in alkaline buffer, Sigma Chemical Co.). Color development was quantitated by reading the OD₄₀₅ on a plate spectrophotometer (Molecular Devices Corporation, Menlo Park, CA).

Specificity of murine IL-1 β ELISA

To determine which forms of IL-1 β were detected by the ELISA assay, a sample containing ³⁵S-labeled precursor and mature IL-1 β derived by combining samples of secreted material (mature IL-1 β) and cell lysates (precursor IL-1 β) was incubated in wells coated with the hamster mAb to murine IL-1 β . After a 1 h incubation, unbound material was removed by washing, and the bound material was solubilized by adding 100 μ l of SDS-sample buffer and incubating for 30 min at room temperature. Bound material was fractionated by SDS-PAGE followed by fluorophorylation as described above. Under the conditions of the ELISA assay, only mature IL-1 β was bound to the plates, and no binding of precursor IL-1 β was observed (data not shown). The ELISA was able to detect mature IL-1 β over the range 10 to 10,000 pg/ml and did not detect murine IL-1 α , IL-2, IL-4, IL-6, IL-10, TNF- α , or IFN- γ at concentrations up to 100 ng/ml.

FIGURE 2. Pulse-chase analysis of IL-1 β secretion from murine peritoneal macrophages. Adherent macrophages were stimulated with 1 μ g/ml LPS and labeled with Tran³⁵S-label for 60 min followed by incubation with 40 μ M nigericin for 30 min. IL-1 β was immunoprecipitated from the media and analyzed by SDS-PAGE. WIN 67694 was added to the cells after the adherence step and was present for the remainder of the experiment.

31kDa →
28kDa →

17kDa →

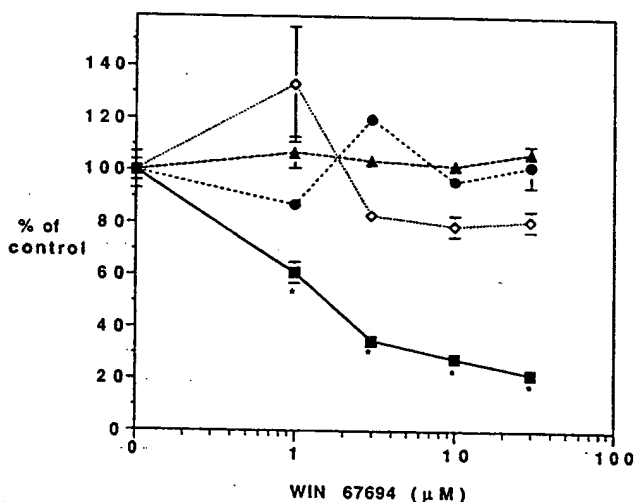
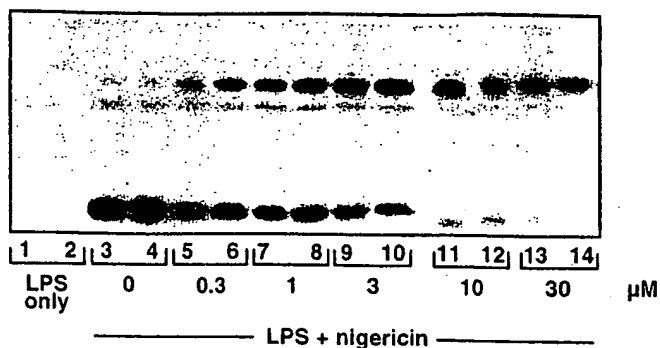


FIGURE 3. Effect of WIN 67694 on cytokine release by LPS-stimulated peritoneal macrophages. Adherent macrophages were stimulated with 1 μ g/ml LPS for 2.5 h followed by 40 μ M nigericin for 30 min. Cytokine levels were measured by ELISA in the culture media. ■, IL-1 β ; ◇, IL-1 α ; ●, IL-6; ▲, TNF- α . Results are means \pm SEM. * p < 0.05 compared with control value.

Murine IL-6 ELISA

Procedures were identical to that described above for the IL-1 β ELISA except for the following: 1) plates were coated with a rat mAb to murine IL-6 (Upstate Biotechnology, Inc., Lake Placid, NY) (1 μ g/ml in PBS) and 2) after the sample incubation step, plates were incubated with 2 μ g/ml of goat anti-murine IL-6.

Cytokine production in vivo

To study IL-1 β production in vivo, we employed a model recently described by Dawson et al. (21). Cylindrical Teflon chambers, 20 mm \times 10 mm, (kindly provided by Dr. Klaus Vosbeck, Ciba-Geigy, Basle) were implanted subcutaneously into the backs of female BALB/c mice under isoflurane anesthesia. After chamber implantation, the mice were allowed to recover for 14 days. An inflammatory response was initiated in the chamber by the injection of a suspension of 1% zymosan A (Sigma Chemical Co.) in pyrogen-free saline (Baxter, Deerfield, IL) through one of the chamber's access holes. Six h after zymosan administration, an aliquot of the chamber fluid was collected by inserting a 20-gauge needle into the chamber and aspirating the fluid. The fluid was centrifuged at 1000 \times g for 10 min to remove free cells, and the supernatant was stored at -20°C for ELISA analysis. For experiments in which the inhibition of IL-1 β production by WIN 67694 was examined, the compound was prepared in polyethylene glycol-400/water (80%/20%, v/v) at 10 or 20

mg/ml and administered by intraperitoneal injection at 1, 3, and 5 h after zymosan injection.

WIN 67694 quantitation in plasma and tissue chamber fluid

WIN 67694 was quantified in the plasma and tissue chamber fluid samples by an in vitro fluorogenic ICE bioassay. The samples were initially diluted in assay buffer (0.01 M HEPES (pH 7.5), 25% glycerol) to solutions containing 6% plasma or tissue chamber fluid. Subsequent dilutions were prepared using 6% normal plasma or tissue chamber fluid in assay buffer. A standard curve of WIN 67694 was prepared in assay buffer containing either 6% normal plasma or tissue chamber fluid. The samples and standards were preincubated with human recombinant ICE for 15 min at 37°C, and the enzyme reactions were initiated with substrate, Suc-Tyr-Val-Ala-Asp-7-amido-4-methylcoumarin (Bachem). The final reaction mixtures, which contained 0.01 M HEPES (pH 7.5), 25% glycerol, 1 mM DTT, 2% plasma or tissue chamber fluid, and 15 μ M ($1 \times K_m$) substrate, were incubated for 30 min at 37°C. The reactions were terminated using 0.1N HCl and were neutralized with an equal volume of 1 M Tris (pH 10.5). Fluorescence was read at an excitation wavelength of 355 nm and an emission wavelength of 460 nm using a Fluoroskan II plate reading fluorimeter (LabSystems, Marlboro, MA). The data were fit using the four-parameter IC₅₀ equation, and the results from the standard curve were used to calculate concentrations for unknowns that fell between 20 and 80% of control. Known concentrations of WIN 67694 also were run in the bioassay, and the concentrations calculated from the standard curve fell within 20% of the expected values.

Results

IL-1 β secretion from peritoneal macrophages

Immunoprecipitation of culture media from LPS-stimulated macrophages labeled with Tran³⁵S-label indicated that cells stimulated with only LPS released no detectable IL-1 β (Fig. 2, lanes 1 and 2). This result is similar to that recently reported by other investigators (13, 22, 23). In contrast, treatment of LPS-stimulated macrophages with nigericin resulted in secretion of a large amount of predominantly mature IL-1 β (Fig. 2, lanes 3 and 4). Mature IL-1 β accounted for greater than 95% of the total IL-1 β detected extracellularly. The induction of mature IL-1 β release in response to nigericin is similar to that reported by Perregaux et al. (13). The effect of this K⁺/H⁺ ionophore (24) cannot be explained simply by cell lysis because it has been shown that nonspecific lytic agents cause release of large amounts of only precursor IL-1 β (13, 23), and high extracellular levels of K⁺ present during nigericin treatment can block both the nigericin-induced release of mature IL-1 β and the nigericin-induced increase in ICE

FIGURE 4. Synthesis of precursor IL-1 β by murine peritoneal macrophages. Adherent peritoneal macrophages were stimulated with 1 μ g/ml LPS for 90 min and labeled with Tran-³⁵S-label for 60 min. Cells were lysed by addition of RIPA buffer containing protease inhibitors. Precursor IL-1 β was isolated from cell lysates by immunoprecipitation and analyzed by SDS-PAGE and laser densitometry.

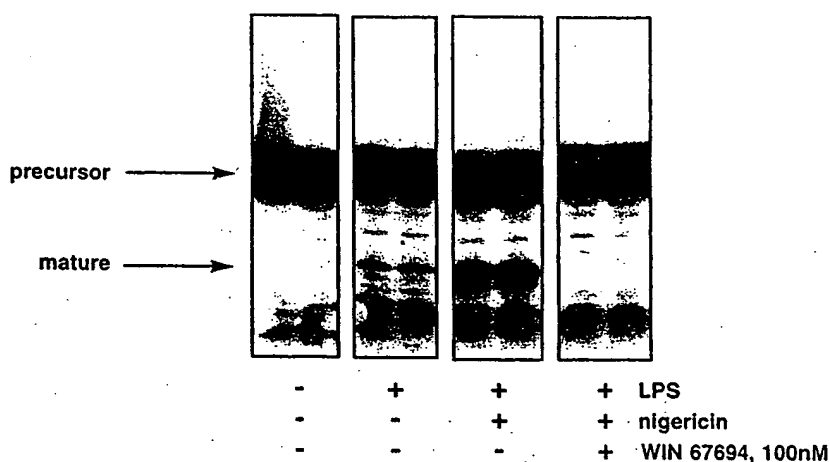
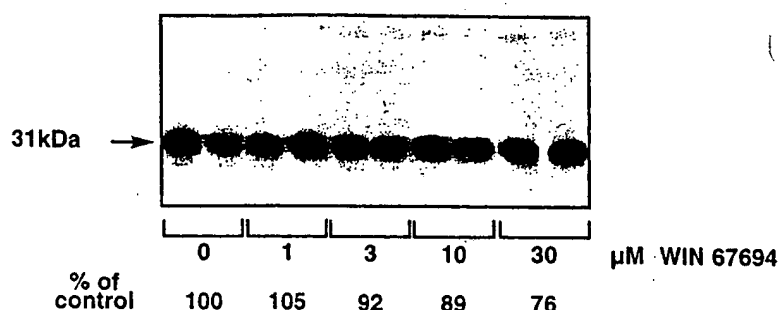


FIGURE 5. ICE activity in murine peritoneal macrophage cell lysates. Cell lysates were prepared and ICE activity was measured as described in *Materials and Methods*.

activity in cell lysates (B. E. Miller, D. M. Gauvin, K. B. Holbrook, manuscript in preparation). A small amount of full-length precursor IL-1 β was also detected in the extracellular media of nigericin-treated cells as was a minor amount of a 28-kDa processed IL-1 β product that is produced as a result of cleavage by ICE at the Asp²⁷-Gly²⁸ bond, a secondary cleavage site (3, 5, 25). Release of mature IL-1 β was inhibited in a dose-dependent manner by the ICE inhibitor WIN 67694 with an IC₅₀ of 1.8 μ M (Fig. 2). The inhibition of mature IL-1 β release was associated with increased release of precursor IL-1 β . This result is similar to the that in the studies with human monocytes reported by Thornberry et al. (6) and Uhl et al. (7). ELISA measurements confirmed the inhibition of mature IL-1 β release seen with the pulse-chase assay and showed that WIN 67694 treatment did not affect the release of IL-1 α , IL-6, and TNF- α , demonstrating the specificity of WIN 67694 action on the production of mature IL-1 β (Fig. 3).

IL-1 β mRNA expression and precursor synthesis

To determine if WIN 67694 affected the induction of IL-1 β mRNA expression during LPS activation, macrophages were incubated with LPS in the presence or absence of 30 μ M WIN 67694. Treatment with WIN 67694 during the activation period had no effect on the level of IL-1 β mRNA as measured by Northern analysis (data not shown). To determine if WIN 67694 affected precursor IL-1 β synthesis, LPS-stimulated macrophages were pulse-

labeled with Tran-³⁵S-label, and synthesis of IL-1 β was measured by quantitating the amount of immunoprecipitated precursor IL-1 β in the cell lysates. WIN 67694 at concentrations up to 10 μ M had no effect on IL-1 β synthesis (Fig. 4). At 30 μ M, a 24% reduction in precursor IL-1 β synthesis was observed.

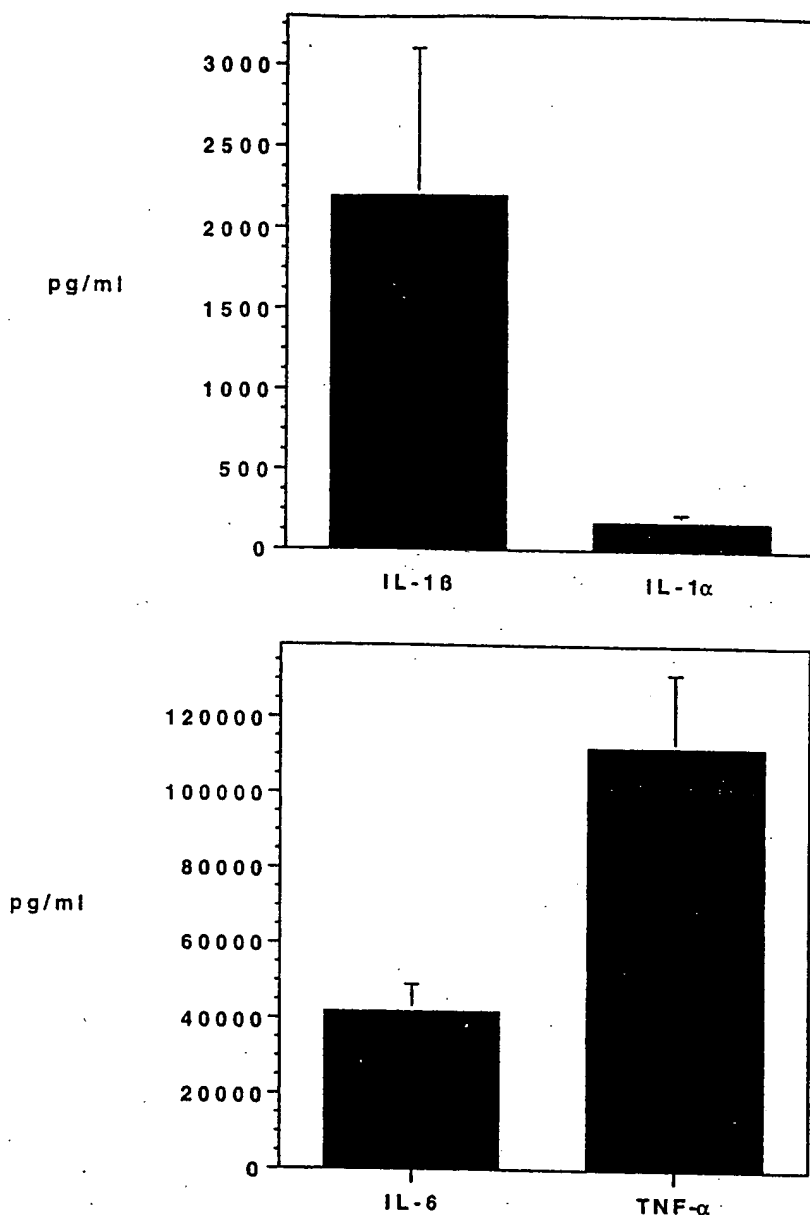
IL-1 β converting enzyme activity

ICE activity in cell lysates was determined by assessing the conversion of exogenous, radiolabeled precursor IL-1 β to mature IL-1 β . Unstimulated macrophages contained a low level of enzyme activity (Fig. 5). However, stimulation of cells with LPS alone for 2.5 h resulted in increased enzyme activity. Treatment with nigericin after LPS stimulation (the same regimen used to induce the release of mature IL-1 β) resulted in a large increase in ICE activity compared with that in unstimulated cells or cells treated with LPS alone. The ICE activity in macrophage lysates was inhibited by WIN 67694.

IL-1 β secretion in vivo

As reported recently by Dawson et al. (21), the subcutaneous implantation of small, plastic chambers into mice provides a readily accessible compartment for assessing cytokine secretion in vivo. Injection of zymosan into the chambers was reported to cause the production of large amounts of IL-1 β and IL-6 (21). In our study, we saw

FIGURE 6. Cytokine levels in tissue chamber fluid. Subcutaneously implanted tissue chambers were injected with 500 μ l of a 1% suspension of zymosan A in saline and tissue chamber fluid collected 6 h later. Cytokine levels were measured by specific ELISAs. Values are means \pm SEM.



similar results along with high levels of both IL-1 α and TNF- α (Fig. 6). Thus, this model may be useful for looking at the effects of anti-inflammatory agents on the production of a number of cytokines in vivo. To determine if IL-1 β release could be inhibited in vivo, tissue chambers were injected with zymosan, followed by i.p. administration of WIN 67694 at 1, 3, and 5 h after zymosan administration. Preliminary experiments had determined that, because of rapid clearance of this compound in the mouse, this dosing regimen was necessary to maintain efficacious concentrations in plasma and tissue chamber fluid (B. E. Miller, D. M. Gauvin, K. G. Holbrook, unpublished observations). The half-life of WIN 67694 in plasma and tissue chamber fluid was 40

min and 150 min, respectively. WIN 67694 treatment resulted in a dose-dependent reduction in IL-1 β levels in tissue chamber fluid (Fig. 7). IL-1 β levels were reduced 35 and 55% below control levels at 10 mg/kg and 100 mg/kg, respectively. Levels of IL-1 α , IL-6, and TNF- α were not significantly affected by treatment with WIN 67694, thus demonstrating that an ICE inhibitor is able to selectively block the release of IL-1 β in vivo. The concentration of WIN 67694 in plasma and tissue chamber fluid is shown in (Table 1). The percent reduction in IL-1 β levels observed after in vivo treatment with WIN 67694 (35 and 55% inhibition at tissue chamber levels of 0.6 and 8.2 μ M, respectively) is consistent with what would be predicted based on the in vitro dose

FIGURE 7. Effect of WIN 67694 on cytokine levels in tissue chamber fluid. Subcutaneously implanted tissue chambers were injected with 500 μ l of a 1% suspension of zymosan A in saline. WIN 67694 was prepared as a solution in PEG-400/water and administered by i.p. injection 1, 3, and 5 h after zymosan. Tissue chamber fluid was collected 6 h after zymosan. Cytokine levels were measured by specific ELISA. ■, IL-1 β ; ●, IL-1 α ; ◆, IL-6; ▲, TNF- α . Values are mean \pm SEM. * p < 0.05 compared with control. The dashed lines indicate 100 and 50% of the control values. The experiment was repeated two times with similar results.

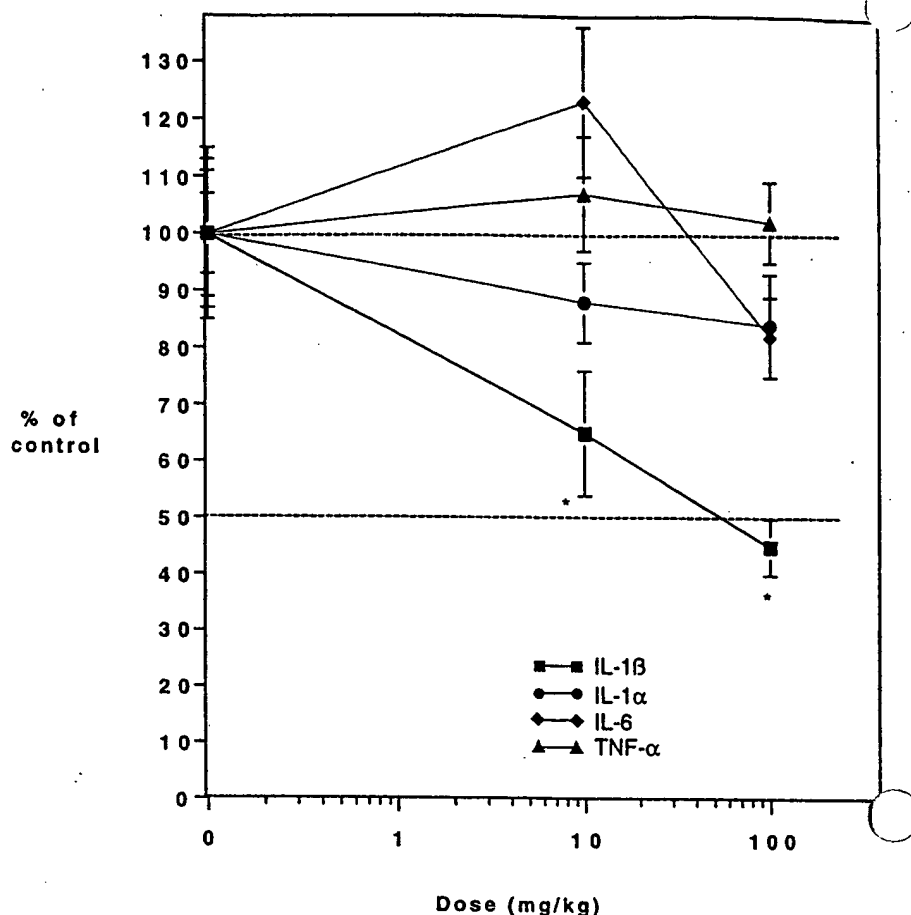


Table 1. WIN 67694 concentrations in plasma and tissue chamber fluid after i.p. administration

| Dose (mg/kg) | Concentration (ng/ml) ^a | |
|--------------|------------------------------------|----------------------------|
| | Plasma | Tissue chamber fluid |
| 10 | 1,118 \pm 164 (1.8) | 348 \pm 72 (0.6) |
| 100 | 90,799 \pm 4,952 (146) | 5,117 \pm 1,058 (8.2) |

^a Values are means \pm SEM. Concentration in μ M is shown in parentheses.

response for inhibition of IL-1 β secretion from peritoneal macrophages in which inhibition at 1 μ M was approximately 35% and inhibition at 10 μ M was approximately 75%.

Discussion

Several studies have demonstrated that peptide-based inhibitors of human ICE can selectively block release of IL-1 β from human peripheral blood monocytes without effect on the release of other cytokines. In this study, we have shown that an ICE inhibitor is able to selectively

block the release of IL-1 β from activated murine macrophages. More importantly, we have shown that mature IL-1 β production in vivo can be inhibited by parenteral administration of an ICE inhibitor. To our knowledge, this is the first demonstration that an ICE inhibitor can selectively inhibit mature IL-1 β production in vivo.

Although the precise role of IL-1 β in disease pathogenesis is still unclear, several lines of evidence implicate IL-1 β as a contributory or causative factor in the pathogenesis of rheumatoid arthritis and several other inflammatory diseases. IL-1 β levels have been shown to correlate with disease activity in synovial fluid from rheumatoid arthritis patients (26–28). Several recent studies (29, 30) with animal models of arthritis have shown that Abs to IL-1 reduce both clinical indicators of disease and the histologic evidence of joint damage. Although a more pronounced effect was seen with Abs to both IL-1 α and IL-1 β , Abs to IL-1 α alone were ineffective whereas Abs to IL-1 β resulted in a significant reduction in disease parameters. In addition, inhibition of IL-1 activity with the IL-1 receptor antagonist has been shown to block several events important in arthritic disease, including IL-1-induced metalloproteinase induction in chondrocytes and synovial lining cells and cartilage matrix degradation in explant cultures (31–33).

No studies on the function of ICE in vivo or its role in inflammatory diseases have yet been reported. Precursor IL-1 β can be released as a consequence of cell lysis or damage and can be processed to biologically active peptides in vitro by extracellular enzymes (e.g., elastase, cathepsin G, and stromelysin) commonly found at sites of an inflammatory response (34). The extent to which this actually occurs in vivo is unknown. However, the importance of ICE in generating an inflammatory response is strongly suggested by the recent results of Ray et al. (35). These investigators showed that the cowpox virus encodes for a 38-kDa ICE inhibitor. Lesions produced in response to infection by wild-type virus contained few inflammatory cells, whereas lesions produced by a mutant virus that lacked the 38-kDa ICE inhibitor were characterized by a large influx of inflammatory cells. These observations provide evidence supportive of a role for ICE in the generation of an inflammatory response in vivo. The potential advantages and disadvantages of ICE as a therapeutic target have been discussed in a recent review (36).

In summary, we have demonstrated that an ICE inhibitor is able to selectively inhibit the production of mature IL-1 β both in vitro and in vivo. The development of potent and selective inhibitors of ICE that, as reported in this study, are active in vivo will permit detailed studies of the role of this enzyme and IL-1 β in inflammatory disease.

References

- Dinarello, C. A. 1991. Interleukin-1 and interleukin-1 antagonism. *Blood* 77:1627.
- Dinarello, C. A. 1993. Modalities for reducing interleukin 1 activity in disease. *Trends Pharmacol. Sci.* 14:155.
- Black, R. A., S. R. Kronheim, and P. R. Sleath. 1989. Activation of interleukin-1 β by a co-induced protease. *FEBS Lett.* 247:386.
- Hazuda, D. J., J. C. Lee, and P. R. Young. 1988. The kinetics of interleukin 1 secretion from activated monocytes. *J. Biol. Chem.* 263:8473.
- Kostura, M. J., M. J. Tocci, G. Limjuco, J. Chin, P. Cameron, A. G. Hillman, N. A. Chartrain, and J. A. Schmidt. 1989. Identification of a monocyte specific pre-interleukin 1 β convertase activity. *Proc. Natl. Acad. Sci. USA* 86:5227.
- Thornberry, N. A., H. G. Bull, J. R. Calaycay, K. T. Chapman, A. D. Howard, M. J. Kostura, D. K. Miller, S. M. Molineaux, J. R. Weidner, J. Aunins, K. O. Elliston, J. M. Ajaya, F. J. Casano, J. Chin, G. J. F. Ding, L. A. Egger, E. P. Gaffney, G. Limjuco, O. C. Palyha, S. M. Raju, A. M. Rolando, J. P. Salley, T. T. Yaman, T. D. Lee, J. E. Shively, M. MacCross, R. A. Mumford, J. A. Schmidt, and M. J. Tocci. 1992. A novel heterodimeric cysteine protease is required for interleukin-1 β processing in monocytes. *Nature* 356:768.
- Uhl, J., L. Brophy, J. Stevenson, R. Dolle, C. Helaszek, R. Miller, and M. Ator. 1993. Secretion of human monocyte mature IL-1 β : optimization of culture conditions and inhibition by ICE inhibitors. *Mol. Biol. Cell* 4(S):341a.
- Ceretti, D. P., C. J. Kozlosky, B. Mosley, N. Nelson, K. Van Ness, T. A. Greenstreet, C. J. March, S. R. Kronheim, T. Druck, L. A. Cannizzaro, K. Huebner, and R. A. Black. 1992. Molecular cloning of the interleukin-1 β converting enzyme. *Science* 256:97.
- Nett, M. A., D. P. Cerretti, D. R. Berson, J. Seavitt, D. J. Gilbert, N. A. Jenkins, N. G. Copeland, R. A. Black, and D. D. Chaplin. 1992. Molecular cloning of the murine IL-1 β converting enzyme cDNA. *J. Immunol.* 149:3254.
- Molineaux, S. A., F. J. Casano, A. M. Rolando, E. P. Peterson, G. Limjuco, J. Chin, P. R. Griffin, J. R. Calaycay, G. J. F. Ding, T. T. Yamin, O. C. Palyha, S. Luell, D. Fletcher, D. K. Miller, A. D. Howard, N. A. Thornberry, and M. J. Kostura. 1993. Interleukin 1 β (IL-1 β) processing in murine macrophages requires a structurally conserved homologue of human IL-1 β converting enzyme. *Proc. Natl. Acad. Sci. USA* 90:1809.
- Casano, F. J., S. M. Molineaux, A. M. Chapman, A. D. Howard, E. P. Gaffney, N. A. Thornberry, K. T. Chapman, J. Chin, G. Limjuco, S. Luell, D. S. Fletcher, and M. J. Kostura. 1992. Isolation, characterization and cloning of murine interleukin-1 converting enzyme. Presented at the Inflammation Research Association Meeting, Sept. 20-24, 1992, Abstract No. W20.
- Dolle, R. E., D. Hoyer, C. V. C. Prasad, S. J. Schmidt, C. T. Helaszek, R. E. Miller, and M. A. Ator. 1994. P₁ aspartate-based peptide α -((2, 6-dichlorobenzoyl)oxy)methyl ketones as potent time-dependent inhibitors of interleukin-1 β -converting enzyme. *J. Med. Chem.* 37:563.
- Perregaux, D., J. Barberia, A. J. Lanzetti, K. F. Geoghegan, T. J. Carty, and C. A. Gabel. 1992. IL-1 β maturation: evidence that mature cytokine formation can be induced specifically by nigericin. *J. Immunol.* 149:1294.
- Young, P. R., D. J. Hazuda, and P. L. Simon. 1988. Human interleukin 1 β is not secreted from hamster fibroblasts when expressed constitutively from a transfected cDNA. *J. Cell Biol.* 107:447.
- Laemmli, U. K. 1970. Cleavage of structural proteins during the assembly of the head of bacteriophage T4. *Nature* 227:680.
- Chomczynski, P., and N. Sacchi. 1987. Single-step method of RNA extraction by acid guanidinium isothiocyanate-phenol-chloroform extraction. *Anal. Biochem.* 162:156.
- Sambrook, J., E. F. Fritsch, and T. Maniatis. 1989. *Molecular Cloning: A Laboratory Manual*. Cold Spring Harbor Laboratory Press, Cold Spring Harbor, NY.
- Krasney, P. A., C. Carr, and D. R. Cavener. 1990. Evolution of the glucose dehydrogenase gene in *Drosophila*. *Mol. Biol. Evol.* 7:155.
- Gray, P. W., D. Glaister, E. Chen, D. Goeddel, and D. Pennica. 1986. Two interleukin 1 genes in the mouse: cloning and expression of the cDNA for interleukin 1 β . *J. Immunol.* 137:3644.
- Danielson, P. E., S. Forss-Petter, M. A. Brow, L. Calvetta, J. Douglas, R. J. Milner, and J. G. Sutcliffe. 1988. p1B15: A cDNA clone of the rat mRNA encoding cyclophilin. *DNA* 7:261.
- Dawson, J., C. Rordorf-Adam, T. Geiger, H. Towbin, S. Kunz, H. Nguyen, O. Zingel, D. Chaplin, and K. Vosbeck. 1993. Interleukin-1 (IL-1) production in a mouse tissue chamber model of inflammation. I. Development and initial characterization of the model. *Agents Actions* 38:247.
- Hogquist, K. A., E. R. Unanue, and D. D. Chaplin. 1991. Release of IL-1 from mononuclear phagocytes. *J. Immunol.* 147:2181.
- Hogquist, K. A., M. A. Nett, E. R. Unanue, and D. D. Chaplin. 1991. Interleukin 1 is processed and released during apoptosis. *Proc. Natl. Acad. Sci. USA* 88:8485.
- Pressman, B. C. 1976. Biological applications of ionophores. *Annu. Rev. Biochem.* 45:501.
- Howard, A. D., M. J. Kostura, N. Thornberry, G. J. F. Ding, G. Limjuco, J. Weidner, J. P. Salley, K. A. Hogquist, D. D. Chaplin, R. A. Mumford, J. A. Schmidt, and M. J. Tocci. 1991. IL-1-converting enzyme requires aspartic acid residues for processing of the IL-1 β precursor at two distinct sites and does not cleave 31-kDa IL-1 α . *J. Immunol.* 147:2964.
- Eastgate, J. A., N. C. Wood, F. S. DiGiovine, J. A. Symons, F. M. Grinlinton, and G. W. Duff. 1988. Correlation of plasma interleukin 1 levels with disease activity in rheumatoid arthritis. *Lancet* ii:708.
- Westacott, C., A. Swan, P. Dieppe, J. Whicher, I. Barnes, D. Thompson. 1991. Cytokines in rheumatoid arthritis. *Ann. Rheum. Dis.* 50:405 (letter).
- Kahle, P., J. Saal, and G. Pawelec. 1991. Cytokines in rheumatoid arthritis. *Ann. Rheum. Dis.* 50:405 (letter).
- Van de Loo, F. A. J., O. J. Arntz, I. G. Otterness, and W. B. van den Berg. 1992. Protection against cartilage proteoglycan synthesis inhibition by antiinterleukin 1 antibodies in experimental arthritis. *J. Rheumatol.* 19:348.

30. Van den Berg, W. B., L. A. B. Joosten, M. Helsen, and F. A. J. van de Loo. 1994. Amelioration of established murine collagen-induced arthritis with anti-IL-1 treatment. *Clin. Exp. Immunol.* 95:237.
31. Henderson, B., R. C. Thompson, T. Hardingham, and J. Lewthwaite. 1991. Inhibition of interleukin-1-induced synovitis and articular cartilage proteoglycan loss in the rabbit knee by recombinant human interleukin-1 receptor antagonist. *Cytokine* 3:246.
32. Smith, R. J., J. E. Chin, L. M. Sam, and J. M. Justen. 1991. Biologic effects of an interleukin-1 receptor antagonist protein on interleukin-1-stimulated cartilage erosion and chondrocyte responsiveness. *Arthritis Rheum.* 34:78.
33. Arend, W. P., H. G. Welgus, R. C. Thompson, and S. P. Eisenberg. 1990. Biological properties of recombinant human monocyte-derived interleukin 1 receptor antagonist. *J. Clin. Invest.* 85:1694.
34. Hazuda, D. J., J. Strickler, F. Kueppers, P. L. Simon, and P. R. Young. 1990. Processing of precursor interleukin-1 β and inflammatory disease. *J. Biol. Chem.* 265:6318.
35. Ray, C. A., R. A. Black, S. R. Kronheim, T. A. Greenstreet, P. R. Sleath, G. S. Salvesen, and D. J. Pickup. 1992. Viral inhibition of inflammation: cowpox virus encodes and inhibitor of the interleukin-1 β converting enzyme. *Cell* 69:597.
36. Miller, D. K., J. R. Calaycay, K. T. Chapman, A. D. Howard, M. J. Kostura, S. M. Molineaux, and N. A. Thornberry. 1993. The IL-1 β converting enzyme as a therapeutic target. *Ann. N.Y. Acad. Sci.* 696:133.

discussed a variety of electrically dependent processes that can contribute to *in vivo* electrically induced tumor regression, including ionization of tumor tissue, ionic transport, tissue dehydration, and the accumulation of leukocytes around the tumor. However, the results shown for the *in vitro* condition (Fig 1) indicate that the suppression of EL4 cell proliferation is due primarily to electrical stimulation with low-level direct current. Also, although the small electrical field intensities produced by the applied voltage levels (<50 V/cm) can affect transmembrane potentials and catalytic activity of membrane-associated enzymes (13), significant increases in cell permeability through electroporation do not account for the suppression of cell proliferation. Normally, electrical field intensity levels approaching 1000 V/cm are required to induce electroporation or to significantly increase cell permeability (14).

The chemical reaction products (dendritic growths) observed with some of the platinum electrodes were very sparse and isolated. These growths normally appeared at the bottom of the electrode. Any significant dendritic growth activity appears to require current levels in excess of the applied low-level currents. Therefore, any chemical activity associated with the platinum electrodes would appear to have had minimal impact on the results. If electrode degradation were significant, one would expect the impact to have suppressive effects. However, the results demonstrate both suppression and stimulation of cell proliferation.

The data shown in Fig 1 further indicate that *in vitro* cell proliferation may be controlled by low-level direct-current stimulation for certain malignant eukaryotic cells. Additional experiments have shown that cell proliferation characteristics can be modulated by changes in cell concentration (data not shown). It may be postulated that there exist multiple windows of enhancement and suppression of cell proliferation that are characteristic for different eukaryotic cell types.

References

- (1) INGVAR S: Reaction of cells to the galvanic current in tissue cultures. *Proc Soc Exp Biol Med* 17:198-199, 1919/1920
- (2) HUZELLA T: Electrical phenomena in tissue cultures in relation to organization. *Arch Exp Zellforsch* 15:250-254, 1934
- (3) ROFFO AE JR: Relation entre les ondes électriques et la multiplication cellulaire dans les

- EXHIBIT**

5
- cultures 42:466-467
 - (4) INGVAR S: Reaction of cells to the galvanic current in tissue cultures. *Proc Soc Exp Biol Med* 17:198-199, 1919/1920
 - (5) GEDDES LA: The beginnings of electro-medicine. *IEEE Eng Med Biol* 3:8-23, 1984
 - (6) PETREQUIN JE: Traitement de certains aneu-rismes. *Bull Gen de Therap* Oct:1-9, 1849
 - (7) NORDENSTROM BEW: Fleischner lecture. Bio-kinetic impacts on structure and imaging of the lung: The concept of biologically closed electric circuits. *AJR Am J Roentgenol* 145:447-467, 1985
 - (8) NORDENSTROM BEW: Biologically Closed Elec-tric Circuits. Stockholm: Medical Publications, 1983, pp 281-317
 - (9) NORDENSTROM BEW: Electrochemical treat-ment of cancer. I. Variable response to anodic and cathodic fields. *Am J Clin Oncol* 12:530-536, 1989
 - (10) BABB MI, DYMOND AM: Electrode Implan-tation in the Human Body, Los Angeles: Brain Information Service/Brain Research Institute, UCLA, 1974
 - (11) GREATBATCH W: The Electrode Interface Be-tween Man and a Prosthetic Stimulator. *IEEE Convention Record*, part 9, March 20-23, 1967. New York: IEEE, 1967, pp 109-117
 - (12) DYMOND AM: Characteristics of the metal-tissue interface of stimulation electrodes. *IEEE Trans Biomed Eng* 23:274-280, 1976
 - (13) WEAVER JC, ASTUMIAN RD: The response of living cells to very weak electric fields: The thermal noise limit [published erratum appears in *Science* 247:1019, 1990]. *Science* 247:459-462, 1990
 - (14) POTTER H: Electroporation in biology: Methods, applications, and instrumentation. *Anal Biochem* 174:361-373, 1988

Effect of Interleukin-1-beta on Metastasis Formation in Different Tumor Systems

M. R. Bani, A. Garofalo,
E. Scanziani, R. Giavazzi*

Experiments were done to determine the effect of interleukin-1-beta (IL-1 β) on metastasis formation in different tumor systems. Intravenous administration of 1 μ g of human recombinant IL-1 β given 1 hour before tumor cell injection augmented lung colony formation (experimental metastases) by the human A375 melanoma variants, the human HT-29M colon carcinoma, the SN12-K1 renal carcinoma in nude mice, the murine B16 melanoma variants, and the murine UV-2237M fibrosarcoma in syngeneic recipients. The same treat-ment did not induce lung colony forma-

tion by a human rectal carcinoma (HCC-P2988) or by a murine reticulum cell sarcoma (M5076), both of which are not metastatic to the lung. Spontaneous metastases were studied in C57BL/6 mice bearing the B16-BL6 melanoma (metastatic to the lung) in their footpad and the M5076 reticulum cell sarcoma (metastatic to the liver) subcutaneously. Daily intraperitoneal treatment with 1 μ g of IL-1 β increased lung and liver metastases. These findings indicate that treatment of mice with IL-1 β can increase the number of artificial or spon-taneous metastases and that this effect is not limited to a single tumor type or to a specific organ. [*J Natl Cancer Inst* 83:119-123, 1991]

During metastasis, extravasation of tumor cells is a complex event that involves the arrest, invasion, and move-ment of tumor cells at the venous or capillary bed of the target organ (1). It is generally proposed that tumor cells pref-erentially attach to the extracellular matrix components of the underlying vascular endothelial cells, and specific recognition mechanisms have been de-scribed (2,3). However, the arrest on microvascular endothelial cells repre-sents the first barrier to the transit of malignant tumor cells. Different adhe-sion mechanisms have been described for the attachment of tumor cells to endothelial cells, and their selective adhe-sion to organ-derived endothelial cells has been reported (4-6).

Recent studies have shown that in-flammatory immunomediators, such as interleukin-1 (IL-1), tumor necrosis fac-tor- α (TNF- α), and interferon gamma, can activate specific adhesive mecha-

FILE COPY

Received July 27, 1990; revised October 11, 1990; accepted October 24, 1990.

Supported by a grant from the Italian Association for Cancer Research, Milan, Italy.

M. R. Bani, A. Garofalo, R. Giavazzi, Mario Negri Institute for Pharmacological Research, Bergamo, Italy.

E. Scanziani, Istituto di Anatomia Patologica Veterinaria e Patologia Aviare, Università degli Studi, Milano, Italy.

We thank Drs I. J. Fidler and S. Naito for providing us with some of the tumor cell lines, Drs E. Dejana and A. Mantovani for helpful discussions, Mrs J. D. Baggott for style editing, and Mrs C. Signorelli for typing the manuscript.

*Correspondence to: Raffaella Giavazzi, PhD, Mario Negri Institute for Pharmacological Research, Via Gavazzoni 11, 24100 Bergamo, Italy.

nisms on endothelial cells, mediating their interaction with circulating cells (7-10). Similarly, our group (11) and others (12-14) have shown that human umbilical endothelial cells activated by IL-1 and TNF- α showed increased adhesiveness for different human tumor cells. We (15) also found that the injection of IL-1 and TNF- α increased the number of lung tumor colonies formed by a human melanoma in nude mice. In the light of those results, which involved an experimental metastasis system, we have evaluated whether interleukin-1-beta (IL-1 β) (a) interferes with the metastatic ability of different tumor systems, (b) changes the metastatic potential of tumor cells, (c) augments metastases in organs other than the lung, and (d) plays a role in the formation of spontaneous metastases in animals bearing a primary tumor.

Materials and Methods

Animals

Male NCr nu/nu mice were obtained from the National Cancer Institute (NCI-Frederick Cancer Research and Development Center, Frederick, Md) and housed in a laminar flow cabinet. Pathogen-free C57BL/6 and C3H/HeN female mice were obtained from Charles River CD (Calco, Italy). Mice were used when 6 to 8 weeks old. The mice received

proper care and maintenance in accordance with institutional guidelines. For metastasis experiments, human tumors were injected into nude mice, the murine B16 melanoma variants and M5076 reticulum cell sarcoma into C57BL/6 mice, and the murine UV-2237M fibrosarcoma into C3H/HeN mice.

Tumor Lines

Human cell lines used were A375 melanoma, which is metastatic to the lung, and its highly metastatic variant, A375M (16); HT-29M colon carcinoma, which is metastatic to the lung (16); SN12-K1 renal carcinoma, which is metastatic to the lung (17); and HCC-P2988 rectal carcinoma, which is tumorigenic but not metastatic (18). Murine cell lines used were B16-F1 melanoma, which is poorly metastatic to the lung, and its highly metastatic variant, B16-BL6 (19); fibrosarcoma UV-2237M, which is metastatic to the lung (20); and M5076 reticulum cell sarcoma, which is highly metastatic to the liver (21). Cell lines were cultured as described in the respective references. The cultured tumor cells used were examined and found free of *Mycoplasma*. For injection, tumor cells were harvested by brief exposure to 0.25% trypsin-0.02% edetic acid (EDTA), washed twice, and resuspended as single-cell suspensions in Ca²⁺- and Mg²⁺-free Hanks' balanced

salt solution (HBSS) at the concentration indicated in the "Results" section. M5076 cells, which grow as a lightly attached monolayer, were harvested by tapping the flask, washed, and resuspended in HBSS.

Interleukin-1- β

Highly purified human recombinant IL-1 β (mature peptide 117-269, in a coliphage specific activity 10⁷ U/mg) was obtained from Sclavo, Siena, Italy, and DeBi Division, Cassina De Pecchi, Italy. Lyophilized IL-1 β was reconstituted in a pyrogen-free, sterile phosphate-buffered saline solution, sterilized by microfiltration in a filter of 0.2- μ m pore size, and stored frozen in 10- μ g aliquots. Working concentrations of IL-1 β were diluted in a volume of 0.2 mL in 0.9% NaCl before injection as indicated in the "Results" section. Control mice received vehicle alone.

Experimental Metastasis Assay

Single-cell suspensions in 0.2 mL of HBSS at the concentrations indicated in the "Results" section were injected intravenously (IV) into the lateral tail vein of mice. Autopsies were performed 8 weeks later for all of the human tumors (with the exception of 12 weeks later for the human HCC-P2988 rectal carcinoma) and 3 weeks later for the murine tumors.

Table 1. Formation of tumor colonies in lungs of mice given an injection of IL-1 β

| Tumor line | No. of cells, $\times 10^4$ | Vehicle | | IL-1 β * | |
|------------------------------|-----------------------------|--|--------------------------------|--|--------------------------------|
| | | No. of mice with lung colonies/total No. of mice | Median No. of colonies (range) | No. of mice with lung colonies/total No. of mice | Median No. of colonies (range) |
| Human | | | | | |
| A375 melanoma | 50 | 6/8 | 1.5 (0-5) | 8/8 | 15† (5-28) |
| A375M melanoma | 50 | 7/8 | 11.5 (0-40) | 8/8 | 57.5† (45-207) |
| HT-29M colon carcinoma | 100 | 5/7 | 1 (0-10) | 7/8 | 7‡ (0-32) |
| SN12-K1 renal carcinoma | 100 | 5/7 | 1 (0-6) | 8/8 | 38† (9 to >100) |
| HCC-P2988 rectal carcinoma | 100 | 0/8§ | — | 0/8§ | — |
| Murine | | | | | |
| B16-F1 melanoma | 5 | 6/8 | 2 (0-6) | 8/8 | 15† (2-38) |
| B16-BL6 melanoma | 2 | 7/8 | 10.5 (0-33) | 8/8 | 87.5 (10-128) |
| UV-2237M fibrosarcoma | 5 | 6/8 | 30 (0-84) | 8/8 | 105† (44-156) |
| M5076 reticulum cell sarcoma | 5 | 0/8§ | — | 1/8§ | — |

*Mice were given IL-1 β 1 hour before the IV injection of tumor cells and were autopsied at the time detailed in the "Materials and Methods" section. Results are representative of at least two different experiments.

† $P \leq .001$ compared with controls.

‡ $P < .01$ compared with controls.

§Presence of tumor was analyzed by histologic examination.

|| $P < .005$ compared with controls.

Table 2. Spontaneous metastases in mice bearing B16-BL6 melanoma and treated with IL-1 β

| Treatment* | No. of lung metastases per mouse | Median No. of lung metastases (range) |
|---------------|------------------------------------|---------------------------------------|
| Vehicle alone | 0, 1, 2, 10, 28, 35, 38, 40, 43 | 28 (0-43) |
| IL-1 β | 15, 17, 20, 32, 76, 124, 216, >300 | 54† (15 to >300) |

*Mice bearing a growing tumor in their footpad were treated daily IP with IL-1 β (1 μ g per mouse) before excision of the primary tumor. Autopsies were performed 3 weeks later. Results are representative of two independent experiments.

† $P = .05$.

Lungs were fixed in Bouin's solution, and the number of tumor colonies was counted under a dissecting microscope. Lungs that presented no visible tumor colonies were processed for histologic examination.

Spontaneous Metastasis Assay

Two slightly different assays were used to study spontaneous metastases. For the B16-BL6 melanoma, C57BL/6 mice were given a 0.05-mL inoculum containing 2×10^5 cells in the hind footpad and treated with IL-1 β for 6 days, starting from when they had palpable tumors. At the end of the treatment, the mice were anesthetized with ether, and legs bearing tumors were amputated. The animals were autopsied 3 weeks later. For the M5076 reticulum cell sarcoma, C57BL/6 mice received a subcutaneous (SC) injection of 2×10^5 cells in a 0.1-mL inoculum. IL-1 β treatment started when mice had tumors of about 5 mm in size. Treatment was continued for 10 days until the mice were autopsied.

In both protocols, IL-1 β was given intraperitoneally (IP) daily at a concentration of 1 μ g per mouse. During IL-1 β treatment, growth of the primary tumor was measured every other day with calipers, and tumor weight was estimated by the formula (length \times width²)/2. Results are representative of two or three independent experiments.

Histologic Analysis

For microscopic studies, lungs were fixed in 10% buffered Formalin, and routine paraffin sections were cut at 5 μ m and stained with hematoxylin-eosin. Two to five isolated sections from each lung were examined to determine the incidence of micrometastases.

Statistical Analysis

Differences in the numbers of metastases were analyzed by use of the Mann-Whitney U test.

Results

Effect of IL-1 β on Experimental Lung Metastases

One microgram of human recombinant IL-1 β given IV to nude mice 1 hour before injection of tumor cells significantly increased the number of lung colonies formed by the human melanomas A375 (poorly metastatic variant) and A375M (highly metastatic variant), the human colon carcinoma HT-29M, and the human renal carcinoma SN12-K1 (Table 1). In contrast, this treatment did not induce the formation of experimental metastases by the human rectal carcinoma HCC-P2988, a nonmetastatic tumor line (Table 1). Under the same experimental conditions, IL-1 β increased the number of lung colonies

formed by the murine B16-F1 (poorly metastatic variant) and B16-BL6 (highly metastatic variant) melanomas and by the UV-2237M fibrosarcoma in syngeneic mice (Table 1). The same treatment did not induce lung colony formation by the murine reticulum cell sarcoma M5076, which selectively metastasizes to the liver and is almost nonmetastatic to the lung (Table 1). In the same experiment, the number of liver colonies after IV injection of M5076 cells was increased in mice receiving IL-1 β (median number of liver colonies = >100 in all mice) compared with that in mice receiving vehicle alone (median number of liver colonies, 65; range, 32 to >100).

Effect of IL-1 β on Spontaneous Metastases

Injection of tumor cell suspension into the tail vein is an accepted experimental model of events related to the arrest and extravasation of tumor cells during metastasis. The effect of IL-1 β on spontaneous metastases was studied in the murine B16-BL6 melanoma and the murine M5076 reticulum cell sarcoma; the former tumor line spontaneously metastasizes to the lung, and the latter tumor line spontaneously metastasizes to the liver. Table 2 shows that treatment with IL-1 β of mice bearing the B16-BL6 melanoma in their footpad increased the number of spontaneous metastases to the lung (median number of lung metastases, 54; range, 15 to >300) compared with the number seen in mice receiving vehicle alone (median number of lung metastases, 28; range, 0 to 43). The growth of the B16-BL6 primary tumor was not directly affected, as shown by the weight of the tumor in the footpad, which was the same in the two groups (data not shown). Treatment of mice bearing the M5076 tumor SC with IL-1 β slightly retarded tumor growth, resulting in a lower tumor weight (mean weight \pm SD, 1.2 \pm 0.8 g) than in control mice (mean weight \pm SD, 1.4 \pm 0.8 g). Autopsy revealed that the tumor burden to the liver was significantly increased in IL-1 β -treated mice (median number of liver foci, 144; range, 11 to >300) compared with that in vehicle-treated mice (median number of liver foci, 72; range, 4 to 124) (Table 3).

Histologic analysis of the lungs of mice bearing the M5076 reticulum cell sarcoma showed tumor cells in the blood vessels, mainly veins and venules. Tumor cells, characterized by a high degree of

Table 3. Spontaneous metastases in mice bearing M5076 reticulum cell sarcoma and treated with IL-1 β

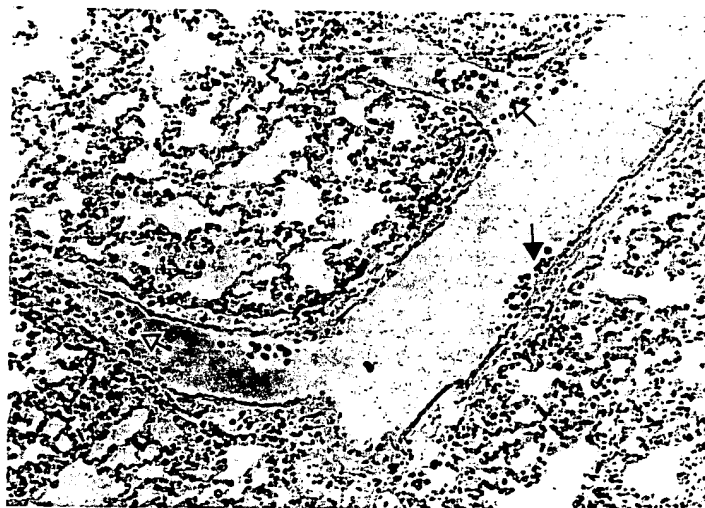
| Treatment* | No. of mice with liver metastases/total No. of mice | Median No. of liver metastases (range) | No. of mice with tumor cells in lung/total No. of mice† |
|---------------|---|--|---|
| Vehicle alone | 11/11 | 72 (4-124) | 2/11 |
| IL-1 β | 10/10 | 144 (11 to >300)‡ | 7/10 |

*Mice bearing an SC tumor were given a daily IP injection of 1 μ g of IL-1 β until they were autopsied. Results are representative of three independent experiments.

†Histologic examination showed tumor cells attached to the vessel wall in the vascular lumen.

‡ $P < .05$.

Fig 1. Photomicrograph of the lung of a mouse bearing the M5076 reticulum cell sarcoma SC and treated with IL-1 β . Presence of neoplastic epithelial cells free in a vein (open arrow) or adhering to the endothelium (solid arrow). (Hematoxylin-eosin, original magnification $\times 150$).



pleomorphism, were seen free in the vascular lumen; in some cases, single or small groups of tumor cells were attached to the vascular endothelium (Fig 1). A higher proportion of lungs showed tumor cell dissemination in the blood vessels in IL-1 β -treated mice (75%) compared with vehicle-treated mice (20%) (Table 3). Tumor cells in the blood vessels were associated with a higher frequency of tumor cells attached to the vascular wall.

Discussion

We have shown previously that IL-1 increased the number of lung colonies formed by a human melanoma in nude mice (15). Here we show that IL-1 β treatment increased the numbers of metastases from tumors of different origin, histologic type, and metastatic potential. The increase in lung colonies induced by IL-1 β was observed with human tumors in nude mice and with murine tumors in syngeneic recipients, suggesting that the results were independent of the T-lymphocyte-deficient immune status of the nude mouse. IL-1 β does not affect the relative metastatic potential of the tumor lines because the difference in metastatic potential was maintained between variants (B16-F1 and B16-BL6; A375 and A375M). Moreover, IL-1 β does not induce lung colony formation by tumor lines that are not metastatic, as was evident for the human HCC-P2988 rectal carcinoma that is highly tumorigenic in nude mice but never produced tumor colonies after IV injection. Similarly, the murine M5076

reticulum cell sarcoma that rarely produces lung metastases did not form macroscopic lung colonies in mice treated with IL-1 β . However, in the same model, IL-1 β increased the number of tumor foci in the liver, an organ to which the M5076 tumor has a propensity to metastasize (21).

The selective tumor colonization of certain organs has been described (22). Several reasons have been given to explain metastasis formation to a specific site, including the arrest of tumor cells at the vascular level, mediated by specific mechanisms (1,23). Here we found an increase in lung and liver metastases depending on the metastatic nature of the tumor cells. This result suggests that IL-1 β does not affect the organ tropism of the metastatic cells and that a similar mechanism(s) might be responsible for the increase in metastases to the lung and liver induced by IL-1 β . These findings are supported by analysis of the distribution and arrest of IV injected radiolabeled tumor cells in the organs of mice pretreated with IL-1 β . At 4 hours after injection with B16-BL6 or M5076 tumor cells, we found an increased retention of radioactivity in the lungs of mice given IL-1 β . However, while the higher retention of radiolabeled B16-BL6 cells lasted more than 24 hours after tumor cell injection and was associated with an increase in lung colonies, the retention of M5076 tumor cells dropped drastically at 24 hours, and the animals had no macroscopic lung colonies at autopsy (data not shown). Similarly, we have shown previously that augmentation of lung colonies by human A375M

melanoma cells in nude mice receiving IL-1 β was associated with a higher retention of radiolabeled tumor cells in the lung (15).

Despite the poor lung-colonizing ability of the M5076 tumor, viable tumor cells have been reported in the lungs of mice with SC primary tumors (24). Interestingly, mice bearing the M5076 tumor and treated with IL-1 β showed increased dissemination of tumor cells to the lung; tumor cells were in the vascular lumen and attached to the vessel walls but did not infiltrate into the lung parenchyma or develop into visible lung metastases (Fig 1). Tumor cells in the lung may be a consequence of tumor cell dissemination from hepatic metastases, although we found a direct correlation between tumor burden in the liver and in the lung for only a few mice. Taken together, these findings support the hypothesis that IL-1 β interferes with the arrest of tumor cells in the secondary organs, but not with the intrinsic capacity of the cells to complete the metastatic process. We have shown already that IL-1 β does not affect colony formation when given 24 hours after the IV injection of tumor cells (15), a time at which the tumor cells presumably have become implanted in the secondary organ.

The entry of hematogenous metastatic cells into organs by way of the microvasculature can be compared to the passage of blood leukocytes into tissues. Endothelial cells are induced by cytokines to express surface antigens that mediate leukocyte adhesion (25-27). Similarly, tumor cells must adhere to and invade through endothelial cells during blood-borne dissemination. Specific adhesion molecules expressed on the endothelial cell surface are suggested to regulate adhesion of malignant tumor cells and to play a role in preferential tissue localization (4,5,23,28). Recently, it has been shown that activation of endothelial cells by cytokines increases tumor cell adhesion (11-14). Inducible endothelial cell-surface molecules that regulate the adhesion of leukocytes may mediate tumor cell adhesion to activated endothelial cells (14). We found that tumor cells shown previously to attach to activated endothelial cells (11) can be induced to form more lung colonies by the injection of IL-1 β . Whether the augmentation of metastases in mice given IL-1 β can be explained by a specific adhesive interaction with vascular endothelium remains

to be clarified. Undoubtedly IL-1 induces a cascade of biologic changes in endothelial cell properties that, in turn, could influence the intravascular transit of tumor cells (8,9,29). Our preliminary studies have shown that the effect of IL-1 β on metastasis formation is not due to a gross vascular injury and that treating mice with anti-inflammatory or anticoagulant agents did not prevent the IL-1 β -induced increase in lung colonies (15). Additional studies are under way to define the role of IL-1 β -inducible endothelial cell effects on the metastatic process.

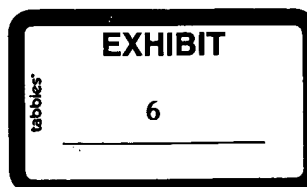
The direct or indirect antitumor effect of IL-1 is controversial (30-32). The antitumor effects of IL-1 on a series of transplanted solid tumors have been reported, together with the antimetastatic activity of IL-1, although it is not clear whether the antimetastatic activity described in those studies was the consequence of a response of the primary tumor (30,32). In another study (31), however, insignificant therapeutic activity was described for IL-1 against artificial and spontaneous metastases. Here we found that, although the M5076 growing SC was slightly responsive to IL-1 β treatment and the B16-BL6 was unresponsive (data not shown), IL-1 β increased the number of metastases formed by both tumor types. These discrepancies with the above studies are most likely due to the different tumor models used and to differences in schedules and doses of IL-1. IL-1 β was given to animals bearing a growing primary tumor (during the tumor cell dissemination phase). The fact that we found an increase in metastases induced by IL-1 β given before amputation of the tumor-bearing limb (eg, results obtained with the B16-BL6 melanoma) agrees with the theory that IL-1 affects the process of tumor cell dissemination rather than the growth of metastases in the secondary organ. Using a similar metastatic model, Castelli et al (31) found no effect on metastasis formation when IL-1 was given after amputation of the tumor-bearing limb (ie, after tumor cells had become implanted in the secondary organ).

In a patient with cancer, the host cell production of IL-1 or other cytokines (eg, during a concurrent inflammatory status) or the production of IL-1 from tumor cells themselves (33-35) might be an event that favors tumor cell dissemination. The results presented here dem-

onstrate that IL-1 β affects the metastatic behavior of tumors of different origin and with different metastatic characteristics.

References

- (1) WEISS L, ORR FW, HONN KV: Interactions between cancer cells and the microvasculature: A rate-regulator for metastasis. *Clin Exp Metastasis* 7:127-167, 1989
- (2) KRAMER RH, GONZALEZ R, NICOLSON GL: Metastatic tumor cells adhere preferentially to the extracellular matrix underlying vascular endothelial cells. *Int J Cancer* 26:639-645, 1980
- (3) LIOTTA LA: Tumor invasion and metastases - role of the extracellular matrix: Rhoads Memorial Award lecture. *Cancer Res* 46:1-7, 1986
- (4) AUERBACH R, LU WC, PARDON E, ET AL: Specificity of adhesion between murine tumor cells and capillary endothelium: An in vitro correlate of preferential metastasis in vivo. *Cancer Res* 47:1492-1496, 1987
- (5) BELLONI PN, TRESSLER RJ: Microvascular endothelial cell heterogeneity: Interactions with leukocytes and tumor cells. *Cancer Metastasis Rev* 8:353-389, 1989
- (6) SHER BT, BARGATZE R, HOLZMANN B, ET AL: Homing receptors and metastasis. *Adv Cancer Res* 51:361-390, 1988
- (7) BUTCHER EC: Warner-Lambert/Parke-Davis Award lecture. Cellular and molecular mechanisms that direct leukocyte traffic. *Am J Pathol* 136:3-11, 1990
- (8) COTRAN RS: American Association of Pathologists president's address. New roles for the endothelium in inflammation and immunity. *Am J Pathol* 129:407-413, 1987
- (9) MANTOVANI A, DEJANA E: Cytokines as communication signals between leukocytes and endothelial cells. *Immunol Today* 10:370-375, 1989
- (10) STOOLMAN LM: Adhesion molecules controlling lymphocyte migration. *Cell* 56:907-910, 1989
- (11) DEJANA E, BERTOCCHI F, BORTOLAMI MC, ET AL: Interleukin-1 promotes tumor cell adhesion to cultured human endothelial cells. *J Clin Invest* 82:1466-1470, 1988
- (12) LAURI D, BERTOMEU M-C, ORR FW, ET AL: Interleukin-1 increases tumor cell adhesion to endothelial cells through an RGD dependent mechanism: In vitro and in vivo studies. *Clin Exp Metastasis* 8:27-32, 1990
- (13) RICE GE, GIMBRONE MA JR, BEVILACQUA MP: Tumor cell-endothelial interactions. Increased adhesion of human melanoma cells to activated vascular endothelium. *Am J Pathol* 133:204-210, 1988
- (14) RICE GE, BEVILACQUA MP: An inducible endothelial cell surface glycoprotein mediates melanoma adhesion. *Science* 246:1303-1306, 1989
- (15) GIAVAZZI R, GAROFALO A, BANI MR, ET AL: Interleukin-1-induced augmentation of experimental metastases from a human melanoma in nude mice. *Cancer Res* 50:4771-4775, 1990
- (16) KOZLOWSKI JM, FIDLER IJ, CAMPBELL D, ET AL: Metastatic behavior of human tumor cell lines grown in the nude mouse. *Cancer Res* 44:3522-3529, 1984
- (17) NAITO S, VON ESCHENBACH AC, GIAVAZZI R, ET AL: Growth and metastasis of tumor cells isolated from a human renal cell carcinoma implanted into different organs of nude mice. *Cancer Res* 46:4109-4115, 1986
- (18) GIAVAZZI R, GAROFALO A, DAMIA G, ET AL: Response to flavone acetic acid (NSC 347512) of primary and metastatic human colorectal carcinoma xenografts. *Br J Cancer* 57:277-280, 1988
- (19) TALMADGE JE, FIDLER IJ: Cancer metastasis is selective or random depending on the parent tumour population. *Nature* 297:593-594, 1982
- (20) GIAVAZZI R, MILLER L, HART IR: Metastatic behavior of an Adriamycin-resistant murine tumor. *Cancer Res* 43:5081-5086, 1983
- (21) HART IR, TALMADGE JE, FIDLER IJ: Metastatic behavior of a murine reticulum cell sarcoma exhibiting organ-specific growth. *Cancer Res* 41:1281-1287, 1981
- (22) SUGARBAKER EV: Patterns of metastasis in human malignancies. *Cancer Biol Rev* 2:235-278, 1979
- (23) NICOLSON GL: Organ specificity of tumor metastasis: Role of preferential adhesion, invasion and growth of malignant cells at specific secondary sites. *Cancer Metastasis Rev* 7:143-188, 1988
- (24) TALMADGE JE, HART IR: Morphologic studies on a murine reticulum cell sarcoma (histiocytic sarcoma) of histiocytic origin and its metastases. *Vet Pathol* 20:342-352, 1983
- (25) BEVILACQUA MP, STENGELIN S, GIMBRONE MA JR, ET AL: Endothelial leukocyte adhesion molecule 1: An inducible receptor for neutrophils related to complement regulatory proteins and lectins. *Science* 243:1160-1165, 1989
- (26) DUSTIN ML, ROTHLEIN R, BHAN AK, ET AL: Induction by IL-1 and interferon-gamma: Tissue distribution, biochemistry, and function of a natural adherence molecule (ICAM-1). *J Immunol* 137:245-254, 1986
- (27) OSBORN L, HESSON C, TIZARD R, ET AL: Direct expression cloning of vascular cell adhesion molecule 1, a cytokine-induced endothelial protein that binds to lymphocytes. *Cell* 59:1203-1211, 1989
- (28) BARBERA-GUILLEM E, ALONSO-VARONA A, VIDAL-VANACLOCHA F: Selective implantation and growth in rats and mice of experimental liver metastasis in acinar zone one. *Cancer Res* 49:4003-4010, 1989
- (29) DINARELLO CA: Interleukin-1 and its biologically related cytokines. *Adv Immunol* 44:153-205, 1989
- (30) BELARDELLI F, CIOLLI V, TESTA U, ET AL: Antitumor effects of interleukin-2 and interleukin-1 in mice transplanted with different syngeneic tumors. *Int J Cancer* 44:1108-1116, 1989
- (31) CASTELLI MP, BLACK PL, SCHNEIDER M, ET AL: Protective, restorative, and therapeutic properties of recombinant human IL-1 in rodent models. *J Immunol* 140:3830-3837, 1988
- (32) NAKAMURA S, NAKATA K, KASHIMOTO S, ET AL: Antitumor effect of recombinant human interleukin 1 alpha against murine syngeneic tumors. *Jpn J Cancer Res* 77:767-773, 1986
- (33) BENNICELLI JL, ELIAS J, KERN J, ET AL: Production of interleukin 1 activity by cultured human melanoma cells. *Cancer Res* 49:930-935, 1989
- (34) FONTANA A, HENGARTNER H, DE TRIBOLET N, ET AL: Glioblastoma cells release interleukin 1 and factors inhibiting interleukin 2-mediated effects. *J Immunol* 132:1837-1844, 1984
- (35) KOCK A, SCHWARZ T, URBANSKI A, ET AL: Expression and release of interleukin-1 by different human melanoma cell lines. *J Natl Cancer Inst* 81:36-42, 1989



PURIFICATION AND PARTIAL SEQUENCE OF HUMAN OSTEOCLAST-ACTIVATING FACTOR: IDENTITY WITH INTERLEUKIN 1β ¹

FLOYD E. DEWHIRST,^{2*} PHILIP P. STASHENKO,[†] JOHN E. MOLE,[‡] AND
TAMOTSU TSURUMACHI[§]

From the Departments of *Pharmacology and †Immunology, Forsyth Dental Center, Boston, MA; the ‡Department of Biochemistry, University of Massachusetts Medical Center, Worcester, MA; and the §Department of Endodontics, Nihon University School of Dentistry, Tokyo, 101, Japan

The lymphokine osteoclast-activating factor (OAF) was purified to homogeneity. OAF was produced by human peripheral blood mononuclear cells stimulated with concanavalin A and phorbol myristate acetate under serum-free culture conditions. OAF was purified by sequential gel filtration, ion-exchange, and reverse-phase HPLC by following bone resorptive activity. Homogeneity was indicated by the criteria of a single 17,800-dalton band on silver-stained polyacrylamide gels, a single pI 6.8 band on isoelectric focusing, and a single amino-terminal sequence. Purified OAF stimulated half-maximal release of calcium from fetal rat long bones at a concentration of approximately 0.66 ng/ml. The amino-terminal sequence of OAF was determined and found to be identical to that of interleukin 1β . Homogeneous OAF possessed an activity of 8.2×10^6 U/mg in the thymocyte proliferation assay. Because the m.w., isoelectric point, amino-terminal sequence, and specific activity in the thymocyte proliferation assay are the same for homogeneous OAF and interleukin 1β , we conclude that they are the same molecule, and that interleukin 1β is the major protein with OAF activity produced by lectin-stimulated peripheral blood mononuclear cells.

Osteoclast-activating factor (OAF),³ a lymphokine that stimulates bone resorption, was originally identified in the culture supernatants of mitogen- or dental plaque extract-stimulated human peripheral blood leukocytes (1). The cellular source of OAF has been controversial. It has been reported that OAF is produced by lymphocytes in a process dependent on macrophage synergy (2, 3), and that isolated monocytes can produce a bone resorptive factor (4). Conflicting data exist with respect to the production of OAF by T lymphocytes (5, 6) and B lympho-

cytes (6, 7). OAF-like bone resorbing activity has also been detected in culture fluids from neoplastic myeloma and lymphoma cell lines (8) and in short-term cultures of bone marrow from patients with myeloma (9). A correlation between OAF production by bone marrow cells and the extent of bone disease and myeloma cell mass has been demonstrated (10, 11). In periodontal disease, both T and B lymphocytes are present in inflammatory cell infiltrates adjacent to sites of bone loss (12), and bone resorbing activity in the putative m.w. range of OAF has been detected in tissue extracts from sites of periodontal destruction (13).

Partial purification of protein(s) with OAF activity has been reported (14–17). However, there are significant differences in reported m.w. and chromatographic properties, and no subsequent publications containing sequence data or definitive biochemical characterization have appeared from these laboratories.

The present report describes methods for the production and purification of microgram quantities of homogeneous OAF. Biologic and biochemical characterization of homogeneous OAF demonstrate its identity with interleukin 1β (IL 1β).

MATERIALS AND METHODS

OAF production. Peripheral blood mononuclear cells (PBMC), obtained as a by-product of plateletpheresis, were separated from granulocytes and erythrocytes by density gradient centrifugation on Ficoll-Hypaque (18). The separated PBMC typically consisted of 80% lymphocytes and 20% monocytes. Cells from one to three donors were washed twice in Eagle's minimum essential medium containing 5% newborn calf serum and 1% 100× penicillin-streptomycin mixture. Cells were washed a third time in final culture medium (FCM) supplemented with 1.0% heat-inactivated, pooled newborn calf serum. FCM consisted of RPMI 1640 with 50 µg/ml gentamicin, 4 mM L-glutamine, 1% 100× Na pyruvate, 1% 100× nonessential amino acids, and 12.5 mM HEPES buffer at pH 7.4. After the final wash, the cells were mixed (two- to three-way mixed lymphocyte cultures) and resuspended in FCM with 1.0% newborn calf serum, 5 µg/ml concanavalin A (Con A), and 25 ng/ml phorbol myristate acetate (PMA), at a final concentration of 3×10^6 cells/ml. Cells were cultured in T-75 plastic culture flasks (Falcon), and cultures were maintained in a 5% CO₂/95% air incubator at 37°C and 95% humidity. After a 16-hr induction phase in serum-containing medium, the adherent cells were rinsed three times with FCM, and the nonadherent cells were washed by centrifugation and replated in the original culture flask in FCM containing 3 µg/ml Con A and 5 ng/ml PMA. After 24 hr culture, the conditioned medium was collected and the cells were cultured for an additional 24 hr for a second collection. The conditioned media were clarified by centrifugation and stored frozen at -70°C.

OAF assay. OAF activity was originally defined as the ability to stimulate release of ⁴⁵Ca from bones in organ culture (1). In the present studies, one unit of OAF activity was defined as the reciprocal titer that stimulated half-maximal bone resorption in fetal rat

Received for publication April 29, 1985.

Accepted for publication July 10, 1985.

The costs of publication of this article were defrayed in part by the payment of page charges. This article must therefore be hereby marked advertisement in accordance with 18 U.S.C. Section 1734 solely to indicate this fact.

¹ This work was supported in part by the Lucile Horton Howe and Mitchell B. Howe Foundation and by National Institutes of Health Grant DE 04881.

² Address all correspondence and reprint requests to Dr. Floyd E. Dewhirst, Forsyth Dental Center, 140 Fenway, Boston, MA 02115.

³ Abbreviations used in this paper: FCM, final culture medium; PMSF, phenylmethylsulfonyl fluoride; LT, lymphotoxin; OAF, osteoclast-activating factor; PBMC, peripheral blood mononuclear cell; PMA, phorbol myristate acetate; RP-HPLC, reverse-phase high-performance liquid chromatography; TNF, tumor necrosis factor.

long-bone organ culture. Samples that contained high activity and no toxic components were diluted at least 1/200 with BGJ_b medium (GIBCO) and tested at twofold serial dilutions. Samples that had low activity, or contained inhibitory components, were concentrated, equilibrated with BGJ_b over an Amicon YM-10 membrane, and tested at twofold serial dilutions. Fetal rat long-bone tissue culture was performed as described (19, 20). Briefly, fetal bones were labeled with ⁴⁵Ca by injecting the mother with 200 μ Ci ⁴⁵Ca (New England Nuclear) on the 18th day of gestation. Radii and ulnae bone shafts were obtained from 19-day fetuses by microdissection. The shafts were first cultured in 0.5 ml BGJ_b medium (GIBCO) containing 1.0 mg/ml bovine serum albumin (Armour) for 1 day to reduce exchangeable ⁴⁵Ca. One bone from a pair (right and left radii or right and left ulnae from a single fetus) was then transferred into medium with OAF (treatment), and the contralateral bone was placed into identical medium without OAF (control). A typical test group consisted of five pairs of bones. Bones were cultured for 5 days in a 95% air/5% CO₂ incubator at 37°C and 95% humidity with one change of media at 2 days. The percentage of ⁴⁵Ca released from a bone into the medium during the 5-day culture was determined by measuring the radioactivity in medium 1, medium 2, and the trichloroacetic acid-solubilized bone by using a liquid scintillation counter. Stimulated resorption was expressed as the paired difference between treatment and control bone percentages of ⁴⁵Ca released during the 5-day culture. For each test group of five bone pairs, a mean, standard error, and *t* were determined. Significance was determined for the paired mean difference differing from zero by a two-tailed Student *t*-test. Dead bone ⁴⁵Ca release in this system was approximately 10%. BGJ_b control ⁴⁵Ca release was between 13 and 18%, and maximum parathyroid hormone ⁴⁵Ca release was 70 to 90%. Because "stimulated" release is expressed as the mean difference between paired BGJ_b control bones (C%) and treated bones (T%), the T%-C% for an inactive treatment is zero, and a maximum parathyroid hormone response is approximately 55 to 75%. Each bone was labeled with approximately 20,000 cpm ⁴⁵Ca.

Polyacrylamide gel electrophoresis. Sodium dodecyl sulfate-polyacrylamide gel electrophoresis (SDS-PAGE) was performed as described by Laemmli (21), using 20-lane, 160 x 140 x 0.75-mm gels with 15% T, 3% C. Proteins were visualized by silver staining (kit from Bio-Rad). The following proteins were used as m.w. standards: BSA, 66 kilodaltons (kD); ovalbumin, 45 kD; carbonic anhydrase, 29 kD; soybean trypsin inhibitor, 20.1 kD; β -lactoglobulin, 18.4 kD; superoxide dismutase, 15.6 kD; and cytochrome c, 12.4 kD. The m.w. of OAF was estimated from a plot of *R_f* vs log(m.w.).

Isoelectric focusing. Analytical isoelectric focusing was performed on an LKB Multiphor flat-bed electrophoresis apparatus by using an 0.5-mm-thick, 5% acrylamide gel. A pH 3 to 10 gradient was generated with the use of LKB Ampholines. The gel was pre-focused for 1 hr at 6 W constant power, and then samples, 7 μ l, were applied to filter paper strips and the proteins were focused for an additional 1.5 hr. The gel was fixed in 30% methanol, 10% TCA, 3.5% sulfosalicylic acid for 1 hr and then fixed overnight in 30% methanol, 12% TCA. The proteins were visualized by silver staining (Bio-Rad).

OAF purification. All purification procedures were performed at 5°C. Two liters of conditioned medium were clarified by centrifugation. The medium was passed through a 50-ml column of DEAE Bio-Gel A (Bio-Rad), equilibrated with PBS, to remove contaminating negatively charged macromolecules. The medium was then concentrated 1000-fold on an Amicon YM-10 membrane and clarified by centrifugation.

Gel filtration chromatography. Two milliliters of concentrated conditioned medium were applied to a 1.6 x 95-cm Bio-Gel P-60 (Bio-Rad) column equilibrated with PBS. Elution with PBS was performed at a flow rate of 7 ml/hr, and fractions of 1.5 ml were collected. Fractions expected to possess OAF activity based on their elution position in previous calibration experiments were pooled and stored frozen at -70°C. The column was calibrated with the following proteins: thyroglobulin, 669 kD; ovalbumin, 45 kD; carbonic anhydrase, 29 kD; soybean trypsin inhibitor, 20.1 kD; and cytochrome c, 12.4 kD. The m.w. of OAF was estimated from a plot of *K_{av}* vs log(m.w.).

CM/DEAE ion-exchange chromatography. Active fractions from three to five Bio-Gel P-60 runs were pooled and concentrated to 1 ml on an Amicon YM-5 membrane and equilibrated with 100 mM Tris-glycine buffer, pH 8.2. The sample was applied to a 1 x 3-cm CM Bio-Gel A column connected in tandem to a 1 x 10-cm DEAE Trisacryl M column (LKB), both previously equilibrated with Tris-glycine buffer. The tandem columns were eluted with 4.5 ml of Tris-glycine buffer, which was sufficient to carry proteins not retained by the CM column onto the DEAE column. The columns were disconnected, and OAF was eluted from the DEAE column with a 300 ml gradient of 0 to 200 mM sodium acetate in Tris-glycine buffer. Chromatog-

raphy was performed at a flow rate of 15 ml/hr, and fractions of 1.5 ml were collected. Samples from every other fraction were taken for analysis by SDS-PAGE and for OAF assay.

Reverse-phase high-performance liquid chromatography (RP-HPLC). HPLC was performed on a Waters chromatographic system with a 3.9 x 30-cm μ Bondapak C₁₈ column. Elution was monitored by using a Hewlett-Packard 1040A Diode Array UV detector. Absorption at 200, 210, 220, 240, 258, 278, and 290 nm was continuously recorded, and flash spectra from 190 to 400 nm were recorded for the base line, upslope, apex, and downslope of each peak. Solvent A was 0.1% TFA in water and Solvent B was 80% acetonitrile in A. The column was equilibrated with 20% B. OAF-containing fractions from DEAE chromatography were pooled, concentrated, and injected onto the column. OAF was eluted with a two-slope gradient: 20 to 40% B in 5 min followed by 40 to 60% B in 60 min. Peak fractions were collected manually. Samples were removed for SDS-PAGE and OAF assay. The samples for bone assay were blown to dryness under a stream of nitrogen and redissolved in BGJ_b medium.

Hydroxyapatite chromatography. OAF-containing fractions from DEAE chromatography were pooled and applied to a 1 x 5-cm column of Ultrogel HA (LKB) previously equilibrated with Tris-glycine buffer. OAF was eluted with a 60-ml gradient of 0 to 75 mM sodium phosphate in Tris-glycine buffer. Fractions of 1.5 ml were collected. Samples of every fraction were taken for analysis by SDS-PAGE and for OAF assay.

Lectin-agarose adsorption. Lectin-agarose gels were obtained from Vector Laboratories. One-milliliter micro-columns were poured and equilibrated in buffers specifically recommended for maximum binding of carbohydrate to each lectin (Vector data sheet). One-milliliter samples of partially purified OAF (obtained after Bio-Gel P-60 chromatography) were equilibrated on Amicon YM-10 membranes with the appropriate buffers for each column, and then applied to columns. The columns were washed with 5 ml starting buffer to obtain filtrate fractions and were eluted with 10 ml buffer containing specific carbohydrates to obtain any bound material.

Stability studies. For chemical stability studies, agents to be tested were added to 1 ml of partially purified OAF (obtained after Bio-Gel P-60 chromatography) at the following final concentrations: 10 mM dithiothreitol, 10 mM sodium dithionite, 1 mM potassium ferricyanide, 0.5 mM cysteine, 10 mM phenylglyoxal, and 10 mM phenylmethylsulfonyl fluoride (PMSF). After 24 hr at 5°C, samples were washed into bone tissue culture media on an Amicon YM-10 membrane.

For physical studies, 50 μ l of highly purified OAF (obtained after DEAE chromatography) were heated to 60°C for 10 or 30 min, lyophilized for 24 hr, and reconstituted with distilled water, or they were frozen at -70°C for 24 hr. The samples were then added to 10 ml of bone tissue culture media and assayed.

NH₂-terminal sequence analysis. Analysis was performed by sequential Edman degradation in the presence of 1.5 mg polybrene on an Applied Biosystems Incorporated gas phase micro sequencer. The phenylthiohydantoin amino acids were separated by HPLC by using a 6 u Zorbax C₁₈ column at 46°C in 10 mM sodium phosphate, 0.025% triethylamine buffer, pH 4.95. All data were quantified by using a Hewlett-Packard 3390A integrator and phenylthiohydantoin norleucine as an internal standard.

Thymocyte proliferation assay. IL 1 bioactivity was determined by its capacity to stimulate thymocyte proliferation in the presence of phytohemagglutinin, as described (22).

RESULTS

Production of conditioned medium. Processing one to three leukopacks typically yielded 2.5 to 7.5 x 10⁸ PBMC for the production of 1.7 to 5 liters of conditioned medium. Conditioned media from the first and second collection periods typically contained 10 to 20 U/ml of OAF activity and approximately 20 μ g/ml protein. The protein content, activity and recovery for each step in OAF purification are presented in Table I.

Purification of human OAF. Passage of conditioned medium through a small DEAE column adsorbed material that prevented concentration above 200-fold on a YM-10 membrane. Protein that precipitated during concentration on the YM-10 membrane was removed by centrifugation. Despite removal of substantial protein during this adsorption/concentration step, there was little loss of OAF activity (Table I).

TABLE I
OAF purification^a

| Stage | Total Protein | Total Activity | Specific Activity | Recovery |
|------------------------|---------------|----------------|-------------------|----------|
| Conditioned medium | 126,000 | 72,000 | 0.6 | 100.0 |
| Adsorbed/concentrated | 22,200 | 64,600 | 2.9 | 89.7 |
| Bio-Gel P-60 | 2,040 | 58,800 | 29 | 81.7 |
| CM/DEAE chromatography | 49 | 43,200 | 881 | 60.0 |
| RP-HPLC | 15 | 22,800 | 1,520 | 31.7 |

^a Purification from 6 liters of conditioned medium. Protein concentrations were determined by measuring optical density and by colorimetric assay. Bone resorption unit of activity equaled amount needed to stimulate half-maximal release of ⁴⁵Ca from fetal rat long bones in 5-day organ culture.

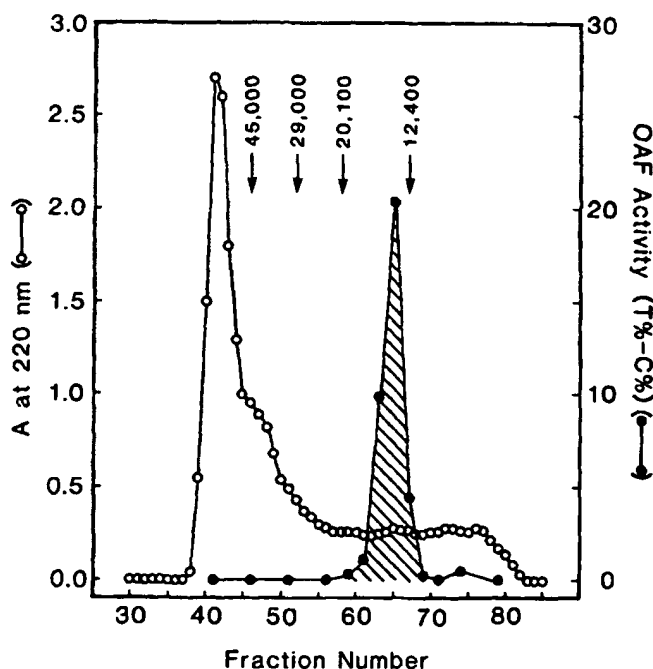


Figure 1. Bio-Gel P-60 chromatography of OAF. OAF-containing conditioned medium was concentrated 1000x and applied to a 1.6 x 95-cm column, equilibrated with PBS. Eluted protein was detected by absorbance at 220 nm. OAF activity was determined by bone organ culture. The elution position of calibration standards is shown with arrows.

The concentrated conditioned medium was applied to a precalibrated Bio-Gel P-60 column. The optical density and activity profiles of a typical chromatographic run are shown in Figure 1. OAF activity was found to elute in a peak at about 13.8 kD. All other fractions lacked activity. Bio-Gel P-60 chromatography resulted in a 10-fold reduction in protein with good recovery of activity (Table I). In some chromatographic runs, recovery at this step was greater than 100%, possibly indicating removal of an inhibitor.

The active fractions from three to five Bio-Gel P-60 chromatographies were pooled, concentrated, and applied to tandem CM and DEAE columns. The optical density and activity profiles for elution of a typical DEAE column are known in Figure 2. OAF activity eluted as a sharp peak at about 15 to 17 mM sodium acetate. The OAF peak represented approximately 1/40 the total protein recovered from the DEAE and CM pre-column (Table I).

Active fractions from DEAE chromatography were pooled, concentrated, and applied to a C₁₈ μBondapak reverse-phase column. The optical density and activity profiles of the RP-HPLC are shown in Figure 3. Peaks A through C had no OAF activity, whereas peak D had a

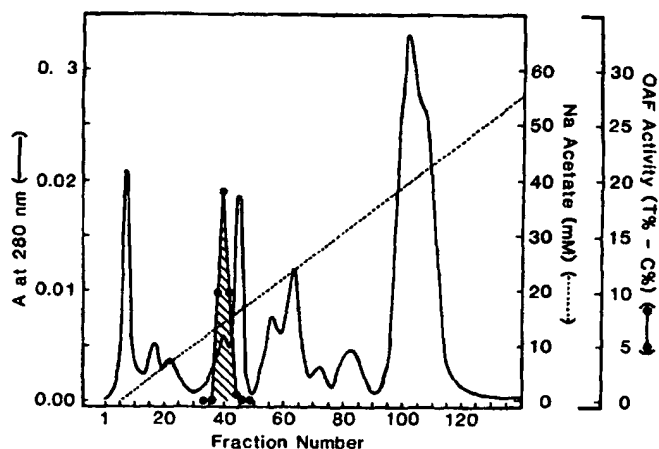


Figure 2. DEAE Trisacryl M chromatography of OAF. Active fractions from Bio-Gel P-60 chromatography were pooled, concentrated, and equilibrated with Tris-glycine buffer. The concentrate was passed through a small CM column onto the DEAE column, and eluted with a 0 to 200 mM Na acetate gradient. Protein concentration was monitored by absorbance at 280 nm. Na acetate concentration was determined from conductance of column effluent. OAF activity was determined by bone organ culture.

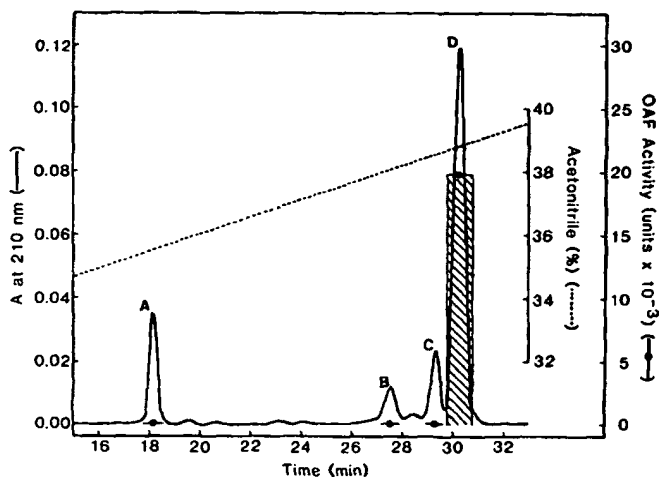


Figure 3. RP-HPLC of OAF. OAF was eluted from a C₁₈ reverse-phase column with an acetonitrile gradient in 0.1% TFA/water. Protein concentration was monitored by absorbance at 210 nm. The major protein peaks are labeled A through D and were tested for OAF activity in bone organ culture.

total of 22,800 U, representing 53% recovery of applied activity (Table I). Figure 4A shows the silver-stained SDS-PAGE of fractions from the DEAE chromatography that were pooled for the RP-HPLC shown in Figure 3. Fractions 44 through 50 contained OAF activity, with the highest activity in fractions 46 through 48. The pooled DEAE sample contained four major proteins of 11.4, 15.3, 16.4, and 17.8 kD. Figure 4B shows the silver staining SDS-PAGE of peak fractions from the reverse-phase column. Fraction D, which contained all of the OAF activity, contained only the 17.8-kD protein. The three lower m.w. contaminating proteins were found in fractions A through C. Approximately 150 ng of protein from fraction D were applied to gel lane D. By the silver-staining method, 1 ng of protein, representing 0.7% contamination, could have been visualized if it had been present.

UV spectra were obtained on the upslope, apex, and downslope for each of the RP-HPLC fractions. The spectra taken at the apices of peaks A through D were clearly

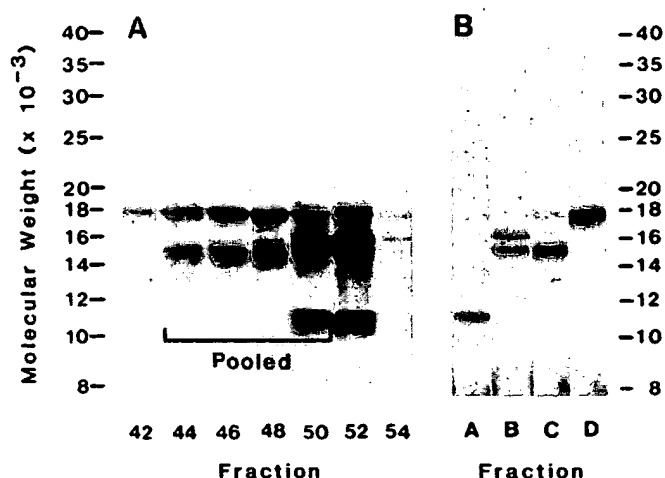


Figure 4. SDS-PAGE of OAF column fractions. PAGE was performed by the method of Laemmli and protein visualized by silver staining. The m.w. scale was determined from the migration of eight protein standards. A. Staining pattern of fractions from a DEAE chromatography near the peak of OAF activity. Fractions 44 through 50 contained OAF activity and were pooled for the RP-HPLC shown in Figure 3. B. Staining pattern of the four major protein peaks obtained from RP-HPLC in Figure 3. One hundred fifty nanograms of protein were applied to lane D as determined by OD₂₁₀ absorption. The sensitivity of the silver staining method was about 1 ng for protein standards.

TABLE II
The passage of OAF through lectin-agarose columns

| Treatment | Carbohydrate Specificity | Activity Filtrate ^a | Activity Eluate ^b |
|--------------------------------------|---|--------------------------------|------------------------------|
| ConA | α -D-mannosyl- α -D-glucosyl- | 72 | 1 |
| Peanut agglutinin | β -D-gal-(1-3)-D-galNAc β -D-galactosyl- | 67 | 0 |
| <i>Ricinus communis</i> agglutinin I | D-galactosyl- | 117 | 9 |
| Soybean agglutinin | N-acetylgalactosaminyl- | 63 | 1 |
| <i>Ulex europaeus</i> agglutinin I | L-fucosyl- | 80 | 1 |
| Wheat germ agglutinin | (β -N-acetylglucosaminyl)- _n sialic acid | 86 | 3 |

^a Percent of applied activity in breakthrough volume and 5 ml wash.

^b Percent of applied activity eluted with 10 ml of specific carbohydrate buffer.

different in their absorption in the 215 to 235 nm range, presumably due to differing tryptophan, tyrosine, and phenylalanine content of the proteins. The three spectra taken at the upslope, apex, and downslope of peak D were superimposable. Superimposition of UV spectra across a peak is an indication of homogeneity.

In a second approach, OAF activity was again identified with the 17.8-kD protein by hydroxyapatite chromatography. Active fractions from DEAE chromatography were pooled and applied to an HA column and eluted with a phosphate gradient. Silver-stained SDS-PAGE of the pooled DEAE fractions (data not shown) demonstrated that the applied sample contained three major proteins of 11.4, 15.3, and 17.8 kD. The three proteins were clearly separated from one another, and OAF activity eluted coincident with the 17.8-kD protein at 18 mM phosphate.

OAF characterization. OAF passed freely through six lectin-agarose columns of widely different carbohydrate specificities, as shown in Table II, indicating its lack of significant glycosylation.

The effect of several agents and treatments on OAF activity is shown in Table III. OAF was stable in the presence of potassium ferricyanide and cysteine, mild

TABLE III
Stability of OAF

| Treatment | Activity ^a | Activity (% Control) |
|--------------------------------------|----------------------------------|----------------------|
| Oxidizing and reducing agents | | |
| Experiment 1 | | |
| OAF control | 15.0 \pm 1.8 (12) | 100 |
| Cystine | 20.7 \pm 4.8 (12) | 138 |
| Potassium ferricyanide | 22.7 \pm 3.9 (12) | 151 |
| Dithiothreitol | 12.1 \pm 3.1 (12) | 83 |
| Sodium dithionite | 12.9 \pm 2.6 (12) | 86 |
| Experiment 2 | | |
| OAF control | 20.5 \pm 3.6 (10) | 100 |
| Potassium ferricyanide | 20.0 \pm 2.7 (10) | 98 |
| Sodium dithionite | 19.1 \pm 2.1 (10) | 93 |
| Protein-reactive agents | | |
| Experiment 1 | | |
| OAF control | 20.5 \pm 3.6 (10) | 100 |
| PMSF | 21.4 \pm 2.9 (10) | 103 |
| Experiment 2 | | |
| OAF control | 38.8 \pm 4.7 (5) | 100 |
| Phenylglyoxal | 3.6 \pm 2.0 (5) ^b | 9 |
| Physical treatments | | |
| Experiment 1 | | |
| OAF control | 39.1 \pm 4.7 (9) | 100 |
| Heat to 60°C, 10 min | -1.2 \pm 3.4 (10) ^b | -3 |
| Freeze -70°C, 24 hr | 25.0 \pm 5.8 (9) | 64 |
| Experiment 2 | | |
| OAF control | 20.5 \pm 3.6 (10) | 100 |
| Lyophilize 24 hr | 23.2 \pm 2.9 (10) | 113 |

^a Values are mean paired T%-C% \pm SE (number of bone pairs) stimulated resorption for 5 days of culture. Maximum parathyroid hormone stimulated release, T%-C%, is 55%-75%.

^b Significantly different from OAF control by two-tailed Student's *t*-test at *p* < 0.01.

| | | | | | | | | | | | | | | | |
|--------------|-----|-----|-----|-----|-----|-----|-------|-----|-----|-------|-------|-------|-----|-----|-------|
| OAF | Ala | Pro | Val | Arg | Ser | Leu | Asn | X | Thr | Leu | Arg | Asp | Ser | Gln | Gln |
| IL 1 β | Ala | Pro | Val | Arg | Ser | Leu | Asn | Cys | Thr | Leu | Arg | Asp | Ser | Gln | Gln |
| | 1 | | | | 5 | | | | | 10 | | | | | 15 |
| OAF | Lys | Ser | Leu | Val | Met | Ser | Gly | Pro | Tyr | Glu | Leu | Lys | Ala | Leu | (His) |
| IL 1 β | Lys | Ser | Leu | Val | Met | Ser | Gly | Pro | Tyr | Glu | Leu | Lys | Ala | Leu | His |
| | 16 | | | | 20 | | | | | 25 | | | | | 30 |
| OAF | Leu | Gln | Gly | Gln | Asp | Met | (Glu) | Gln | Gln | (Val) | (Val) | (Phe) | | | |
| IL 1 β | Leu | Gln | Gly | Gln | Asp | Met | Glu | Gln | Gln | Val | Val | Phe | | | |
| | 31 | | | | 35 | | | | | 40 | | 42 | | | |

Figure 5. NH₂-terminal sequence of OAF. The NH₂-terminal sequence of homogeneous OAF was determined by sequential Edmond degradation on a gas phase micro sequencer. The IL 1 β sequence is from March et al. (24). Amino acids that were identified but present in low yields are shown in parentheses. Cycles in which no amino acid could be identified are shown as an X.

oxidizing agents; sodium dithionite and dithiothreitol, mild reducing agents; and PMSF, a serine protease inhibitor. OAF was inactivated by exposure to phenylglyoxal, an arginine modifying agent. Purified OAF could be frozen and thawed or lyophilized with little loss of activity. OAF activity was lost upon heating to 60°C for 10 min.

A single pI 6.8 silver-stained band was seen for OAF, between human carbonic anhydrase (pI 6.5) and equine myoglobin (pI 7.00) standards, upon isoelectric focusing.

NH₂-terminal sequence analysis. The NH₂-terminal sequence of OAF is shown in Figure 5, as is that for IL 1. Sequence analysis was performed on 730 pmol of native OAF. The initial yield at Ala 1 was 128 pmol, and the repetitive yield between Leu-6 and Leu-10 was 91%. A single amino acid was identified at each step until phase differences appeared in the later cycles. Arginine could not be clearly identified, as it eluted coincident with a background peak in the base line. Cysteine is not easily detected in this system unless the protein is reductively methylated. The lack of identifiable amino acids at OAF positions 4, 8, and 11 is consistent with the presence of Arg and Cys residues at these positions. Amino acids identified, but at low yields, are shown in parentheses.

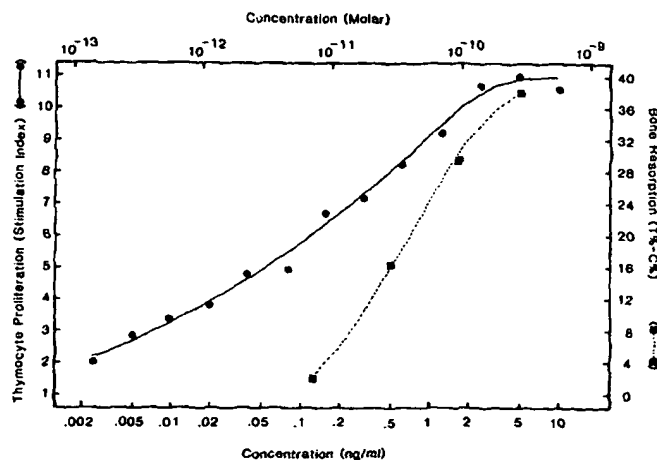


Figure 6. Activity of OAF in bone resorptive and thymocyte proliferation assays. The nanogram concentration of OAF was determined by amino acid analysis, and the molar concentration was based upon a m.w. of 17,377. Bone resorption was determined as release of ^{45}Ca from fetal rat long bones in 5-day culture. Thymocyte proliferation was determined by [^3H]thymidine incorporation in mouse spleen cells co-stimulated with phytohemagglutinin.

The IL 1 sequence is that predicted from cDNA and protein sequencing (22, 23). Ala 1 occurs at position 117 of the IL 1 precursor molecule (22, 23). For each position that an amino acid was identified for OAF, it is identical to that for IL 1.

Biologic activities of OAF. The dose-response curves for OAF in the bone resorption assay and in the thymocyte proliferation assay are shown in Figure 6. The concentration of OAF was estimated by amino acid analysis, and molarity was calculated based upon a m.w. of 17,377. The concentration of OAF for stimulation of half-maximal bone resorption is 0.66 ng/ml, and 0.12 ng/ml for thymocyte proliferation.

DISCUSSION

In the present studies, we have purified OAF from the culture supernatant of Con A- and PMA-stimulated human PBMC (80% lymphocytes and 20% monocytes) by following recovery of bone resorption activity. The isolated protein was found to be homogeneous by the following criteria: a single 17.8-kD band on silver-stained SDS-PAGE gels; a single silver-stained band at pI 6.8 on analytical isoelectric focusing; superimposable UV spectra taken at the upslope, apex, and downslope of the RP-HPLC OAF peak; and an unambiguous N-terminal sequence. Homogeneous OAF appears to be identical to the pI 6.8 species of IL 1 based upon comparison of their N-terminal sequences, amino acid composition, m.w., isoelectric points, inactivation by heating and exposure to phenylglyoxyl, and specific activities in the thymocyte proliferation assay. Each of the 41 amino acids that were positively identified in the N-terminal sequence of OAF was identical to that for the pI 6.8 species of IL 1 (23), recently termed IL 1 β (24). Our results provide two estimates of m.w. for OAF: 13.8 kD from gel filtration and 17.8 kD from discontinuous SDS-PAGE. These agree with values of 13 kD from size exclusion HPLC (25) and 15 to 17.5 kD from gradient SDS-PAGE (25, 26) obtained for IL 1. The m.w. predicted from the cDNA sequence of IL 1 β is 17,377 (23, 24). The isoelectric point for OAF and IL 1 β (25) is 6.8. OAF and IL 1 activities are destroyed by

heating (27) and by exposure to the arginine modifying agent phenylglyoxyl (28). The stability of OAF in the presence of the reducing agents dithiothreitol and sodium dithionite and the serine protease inhibitor PMSF is consistent with the stability of IL 1 in the presence of the reducing agent β -mercaptoethanol and PMSF (29). The passage of OAF thru lectin columns is consistent with the lack of glycosylation found for IL 1 β (26). The specific activity of homogeneous OAF in the thymocyte proliferation assay was 8.2×10^6 U/mg, which compares closely with 7.6×10^6 U/mg reported for homogeneous IL 1 β (25). Finally, IL 1 has been shown to stimulate bone resorption *in vitro* (30, 31). The concentration for half-maximal stimulation of bone resorption for pig IL 1 (31) is identical to that reported for homogeneous OAF. We conclude from these studies that the activity previously described as "OAF" is largely if not solely attributable to IL 1 β , and that "OAF" may not exist as a separate molecular entity.

In designing our protocols, the previously described conditions for the production and initial purification of OAF were deliberately mimicked in order to facilitate isolation of the molecule originally described by Horton et al. (1, 17), and Luben et al. (14). In fact, the OAF/IL 1 β we have purified appears to be identical to the previously partially characterized OAF on the basis of its m.w. on gel filtration chromatography (12 to 18 kD), a steep dose-response curve for bone resorption in the fetal rat long-bone assay, heat lability, and passage through DEAE and CM ion-exchange columns at neutral pH and ionic strength in excess of 50 mM (14, 17).

Purification of OAF in the present studies was significantly aided by modifying the conditions previously used for ion-exchange chromatography in which OAF was not retained on DEAE or CM gels (14, 17). We found that OAF could be retained on DEAE gels by using a Tris-glycine buffer with a higher pH and a lower effective ionic strength. The combined CM adsorption-DEAE ion-exchange step was central to the purification protocol, as it yielded a 30-fold purification.

Biochemical characterizations of OAF by other investigators indicated that the 13 to 25 kD moiety could be converted to a smaller species termed "little OAF" (3.5 kD) by dissociation in 1 M NaCl or 2 M urea (15), although no further biochemical characterization of "little OAF" was subsequently reported. Similarly, the report of the disassociation of OAF into a 9-kD species (16) was not followed by additional biochemical characterization. In our purification procedures, no evidence for bone resorbing activity in the low m.w. range was obtained, nor was the 17.8-kD molecule we isolated dissociated into lower m.w. species on SDS-PAGE under reducing conditions. Moreover, no additional peaks of bone resorbing activity were observed at any other chromatographic step, indicating recovery of the major molecular species with OAF activity. This conclusion is also supported by the high recovery of total OAF activity at each step in the purification.

We cannot at this time, however, rule out the presence of additional minor mediators of bone resorption in stimulated PBMC culture supernatants. Factors with less than 10 to 20% of the activity of IL 1 β may have been present but were missed by our assay procedure. To determine the peak of OAF activity in chromatographic fractions, they were tested at dilutions such that the most

active fraction gave a three-fourths-maximal bone resorptive response. Fractions with less than 10% of the activity of the major fraction would therefore be at the bottom of the assay dose-response curve and would not have had detectable activity.

In addition to IL 1 β , other lymphocyte and monocyte-derived cytokines that could stimulate bone resorption might reasonably be expected to have been present in our starting PBMC conditioned medium. IL 1 α and IL 1 β are reported to have the same biologic activities in several systems (24, 32). However, only one-tenth as much IL 1 α is produced as IL 1 β by stimulated macrophages (24). Therefore, IL 1 α may have been responsible for about 10% of the OAF activity in our PBMC conditioned medium. The lymphocyte product lymphotoxin (LT) and the monocyte product tumor necrosis factor (TNF) have recently been shown to stimulate bone resorption (33, 34). These factors were reported to stimulate half-maximal bone resorption at about 10^{-6} M, which is about 100 times less potent than IL 1 β . Therefore, if equal amounts of IL 1 β , LT, and TNF were produced in lectin-stimulated PBMC cultures, LT and TNF would account for only about 2% of the total OAF activity. Transforming growth factors α and β (35, 36) have also been reported to stimulate bone resorption in vitro, although their presence in lymphocyte/monocyte culture supernatants is unlikely, given their cell sources. The growth factors are also significantly less potent than IL 1 β , having half-maximal activities at approximately 10^{-8} M. The possibility that LT, TNC, or other as yet unidentified factors with OAF activity could act synergistically with IL 1 to resorb bone at concentrations in the range of that observed for homogeneous IL 1 β must still be entertained.

Data that indicate that OAF is a T lymphocyte product (5, 6) appear to be contradictory to the present findings, which strongly support a macrophage/monocyte origin for the majority of OAF activity (4). However, the well-established requirement for macrophage synergy for OAF production (2, 3) suggests a "circular" pathway of stimulation in which monocytes initially facilitate T cell activation, which in turn stimulate monocytes by production of interferon- γ , which further activates monocytes to produce IL 1 (22). Alternatively, activated T cells may in fact elaborate lymphokines such as LT or other factors with OAF activity, which synergize with IL 1 to stimulate bone resorption at sub-nanomolar concentrations. The evaluation of the potential contribution of other mediators with OAF activity to total bone resorbing activity should be facilitated by the availability of antibodies specific for IL 1 α , IL-1 β , LT, and TNF.

Acknowledgments. We thank Drs. Donald Hay and Shelby Kashket for helpful discussions, and Drs. Donald Hay and Edward Moreno for the use of their HPLC instrument. We thank Joanne M. Ago, Susan M. Dearborn, William J. Peros, and Monique L. Blron for their excellent technical assistance. We thank Jan Schafer for her assistance in the preparation of this manuscript.

REFERENCES

- Horton, J. E., L. G. Raisz, H. A. Simmons, J. J. Oppenheim, and S. E. Mergenhagen. 1972. Bone resorbing activity in supernatant fluid from cultured human peripheral blood leukocytes. *Science* 177:793.
- Horton, J. E., J. J. Oppenheim, S. E. Mergenhagen, and L. G. Raisz. 1974. Macrophage-lymphocyte synergy in the production of osteoclast activating factor. *J. Immunol.* 113:1278.
- Yoneda, T., and G. R. Mundy. 1979. Monocytes regulate OAF production by releasing prostaglandins. *J. Exp. Med.* 150:338.
- Rutherford, B., and C. L. Trummel. 1983. Monocyte-mediated bone resorption involves release of nondialyzable substances in addition to prostaglandin. *J. Reticuloendothel. Soc.* 33:175.
- Dewhirst, F. E., Y. P. Zan, L. M. Resmini, and P. Stashenko. 1983. OAF production by human T lymphocyte subsets. *J. Dent. Res.* 62:213.
- Horwitz, M., A. Vignery, R. K. Gershon, and R. Baron. 1984. Thymus-derived lymphocytes and their interactions with macrophages are required for the production of osteoclast-activating factor in the mouse. *Proc. Natl. Acad. Sci. USA* 81:2181.
- Chen, P., C. Trummel, J. Horton, J. J. Baker, and J. J. Oppenheim. 1976. Production of osteoclast-activating factor by normal human peripheral blood rosetting and nonrosetting lymphocytes. *Eur. J. Immunol.* 6:732.
- Mundy, G. R., R. A. Luben, L. G. Raisz, J. J. Oppenheim, and D. N. Buell. 1974. Bone-resorbing activity in supernatants from lymphoid cell lines. *N. Engl. J. Med.* 290:867.
- Mundy, G. R., L. G. Raisz, R. A. Cooper, G. P. Schechter, and S. E. Salmon. 1974. Evidence for the secretion of an osteoclast stimulating factor in myeloma. *N. Engl. J. Med.* 291:1041.
- Durie, B. G. M., S. E. Salmon, and G. R. Mundy. 1977. Multiple myeloma: clinical staging and role of osteoclast activating factor in localized bone loss. In *Mechanisms of Localized Bone Loss*. J. E. Horton, T. M. Tarpley, and W. F. Davis, Eds. Information Retrieval Inc. Washington D.C. P. 319.
- Durie, B. G. M., S. E. Salmon, and G. R. Mundy. 1981. Relation of osteoclast activating factor production to extent of bone disease in multiple myeloma. *Br. J. Haematol.* 47:21.
- Mackler, B. F., K. B. Frostad, P. B. Robertson, and B. M. Levy. 1977. Immunoglobulin bearing lymphocytes and plasma cells in human periodontal disease. *J. Periodont. Res.* 12:37.
- Offenbacher, S., T. A. Binder, F. E. Dewhirst, and J. M. Goodson. 1981. Bone resorptive activity of human periodontal tissues. *J. Dent. Res.* 60:499.
- Luben, R. A., G. R. Mundy, C. L. Trummel, and L. G. Raisz. 1974. Partial purification of osteoclast-activating factor from phytohemagglutinin-stimulated human leukocytes. *J. Clin. Invest.* 53:1473.
- Mundy, G. R., and L. G. Raisz. 1977. Big and little forms of osteoclast activating factor. *J. Clin. Invest.* 60:122.
- Luben, R. A. 1978. Purification of a lymphokine: osteoclast activating factor from human tonsil lymphocytes. *Biochem. Biophys. Res. Commun.* 84:15.
- Horton, J. E., W. J. Koopman, J. J. Farr, J. Fuller-Bonar, and S. E. Mergenhagen. 1979. Partial purification of a bone resorbing factor elaborated from human allogeneic cultures. *Cell. Immunol.* 43:1.
- Böyum, A. 1968. Separation of leukocytes from blood and bone marrow. *Scand. J. Clin. Lab. Invest.* 21(Suppl. 97):77.
- Dewhirst, F. E. 1982. N-acetyl muramyl dipeptide stimulation of bone resorption in tissue culture. *Infect. Immun.* 35:133.
- Dewhirst, F. E. 1984. 6-Keto-prostaglandin E₁ stimulated bone resorption in organ culture. *Calcif. Tissue Int.* 36:380.
- Laemmli, U. K. 1970. Cleavage of structural proteins during the assembly of the head of bacteriophage T4. *Nature* 227:680.
- Mizel, S. B., J. J. Oppenheim, and D. L. Rosenstreich. 1978. Characterization of lymphocyte activating factor (LAF) produced by the macrophage cell line P388D1. I. Enhancement of LAF production by activated T lymphocytes. *J. Immunol.* 120:1497.
- Auron, P. E., A. C. Webb, L. J. Rosenwasser, S. F. Mucci, A. Rich, S. M. Wolff, and C. A. Dinarello. 1984. Nucleotide sequence of human monocyte interleukin 1 precursor cDNA. *Proc. Natl. Acad. Sci. USA* 81:7907.
- March, C. J., B. Mosley, A. Larsen, D. P. Cerretti, G. Braedt, V. Price, S. Gillis, C. S. Henney, S. R. Kronheim, K. Grabstein, P. J. Conlon, T. P. Hopp, and D. Cosman. 1985. Cloning, sequence and expression of two distinct human interleukin-1 complementary DNAs. *Nature* 315:641.
- Schmidt, J. A. 1984. Purification and partial biochemical characterization of normal human interleukin 1. *J. Exp. Med.* 160:772.
- Kronheim, S. R., C. J. March, S. K. Erb, P. J. Conlon, D. Y. Mochizuki, and T. P. Hopp. Human interleukin 1: purification to homogeneity. *J. Exp. Med.* 161:490.
- Simon, P. L., and W. F. Willoughby. 1981. The role of subcellular factors in pulmonary immune function: physicochemical characterization of two distinct species of lymphocyte-activating factor produced by rabbit alveolar macrophages. *J. Immunol.* 126:1534.
- Mizel, S. B., J. M. Dayer, S. M. Krane, and S. E. Mergenhagen. 1981. Stimulation of rheumatoid synovial cell collagenase and prostaglandin production by partially purified lymphocyte-activating factor (interleukin 1). *Proc. Natl. Acad. Sci. USA* 78:2474.
- Dinarello, C. A., K. Bendtzen, and S. M. Wolff. 1982. Studies on the active site of human leukocytic pyrogen. *Inflammation* 6:63.
- Gowen, M., D. D. Wood, E. J. Ihrie, M. K. B. McGuire, and R. G. G. Russell. 1983. An interleukin 1 like factor stimulates bone resorption in vitro. *Nature* 306:378.
- Heath, J. K., J. Saklatvala, M. C. Meikle, S. J. Atkinson, and J. J.

- Reynolds. 1985. Pig interleukin 1 (catabolin) is a potent stimulator of bone resorption in vitro. *Calcif. Tissue Int.* 37:95.
32. Wood, D. D., E. K. Bayne, M. B. Goldring, M. Gowen, D. Hamerman, J. L. Humes, E. J. Ihrie, P. E. Lipsky, and M.-J. Staruch. 1985. The four biochemically distinct species of human interleukin 1 all exhibit similar biologic activities. *J. Immunol.* 134:895.
33. Bertolini, D. R., G. Nedwin, T. Bringman, and G. R. Mundy. 1985. Evidence that recombinant human lymphotoxin possesses OAF activity. *Proceedings of the Seventh Annual Meeting of the American Society for Bone and Mineral Research.* Abstract 69.
34. Gowen, M., G. Nedwin, and G. R. Mundy. 1985. Preferential inhibition of cytokine-stimulated bone resorption by recombinant interferon gamma. *Proceedings of the Seventh Annual Meeting of the American Society for Bone and Mineral Research.* Abstract 67.
35. Ibbotson, K. J., J. Harrod, M. Gowen, S. D'Souza, M. Winkler, G. Carpenter, R. Derynck, and G. R. Mundy. 1985. Effects of human transforming growth factor (TGF) alpha on bone resorption and formation in vitro. *Proceedings of the Seventh Annual Meeting of the American Society for Bone and Mineral Research.* Abstract 64.
36. D'Souza, S. M., K. J. Ibbotson, D. R. Twardzik, B. R. MacDonald, G. J. Todaro, and G. R. Mundy. 1985. Transforming growth factor beta (TGF-beta) resorbs bone and is produced by osteoblast-like bone cells. *Proceedings of the Seventh Annual Meeting of the American Society for Bone and Mineral Research.* Abstract 65.

anti-fasciclin I or anti-HRP. By contrast, unirradiated embryos injected with dye-labelled antibodies, or embryos injected with unlabelled antibodies, regardless of laser irradiation, showed low defasciculation rates. No effect was seen with laser irradiation of embryos injected with labelled BSA, which presents the dye on a nonspecific protein that does not bind membranes. Similarly, there was no effect when labelled hexaalanine was used; this is a hydrophobic peptide that binds to membranes, but not specifically to proteins, thereby acting as a control for nonspecific damage to the membrane by CALI. Thus, it is insufficient to have the dye present on the cell surface to cause defasciculation; the dye must be linked to a specific protein. CALI-treated embryos also had high defasciculation rates on a per-individual basis. Figure 3b compares the percentage of defasciculated trajectories per animal in laser-treated anti-HRP (open bars) versus laser-treated Malachite green/anti-HRP-injected embryos (filled bars). Malachite green/anti-fasciclin I laser-treated embryos showed a similar distribution to that seen using Malachite green/anti-HRP.

Over 80% of injected embryos survive CALI. The treated limb buds show normal segmentation and growth, with the overall length of the T11 axons unaffected (Table 1). The growth cones also appear normal; even defasciculated neurons contact guidepost cells, cross leg segment boundaries and show typical filopodial spread¹². New neurons, such as the femoral chordotonal organ and subgenual organ¹³, are able to differentiate after CALI. CALI does not influence the differentiation of guidepost cells ($n = 202$ limb buds from a single experiment). As CALI causes defasciculation without affecting other phenomena, T11 elongation and guidance are not dependent on fasciculation.

Is fasciclin I solely responsible for the axon adhesion observed in these experiments? Elkins *et al.*¹⁴ have shown that *Drosophila* null mutations of fasciclin I have minor effects on the CNS, but that double mutants of fasciclin I and the Abelson tyrosine kinase gene show significant disruption in axonal organization. As CALI can indirectly inactivate a small complex *in vitro* (data not shown), it is possible that a protein closely bound to fasciclin I is also inactivated. Alternatively, regulatory mechanisms may compensate for the loss of fasciclin I in null mutations. This may not occur during the acute inactivation resulting from CALI.

Cell adhesion has been difficult to demonstrate *in situ* during neuronal development because of the paucity of effective inhibiting probes, and the difficulty of controlling their action over a specific time interval. We have employed a novel technique to demonstrate the role of a specific molecule in mediating axon adhesion by converting a binding reagent into an inhibitor. We suggest that CALI could be generally applied in the functional inactivation of other proteins. □

Received 4 July; accepted 4 October 1990.

- Jessell, T. M. *Neuron* **1**, 3-13 (1988).
- Jay, D. G. *Proc. natn. Acad. Sci. U.S.A.* **85**, 5454-5458 (1988).
- Bastiani, M. J., Harrelson, A. L., Snow, P. M. & Goodman, C. S. *Cell* **48**, 745-755 (1987).
- Patel, N. H., Snow, P. M. & Goodman, C. S. *Cell* **48**, 975-988 (1988).
- Zinn, K., McAllister, L. & Goodman, C. S. *Cell* **53**, 577-587 (1988).
- Elkins, T., Hortsch, M., Biebler, A., Snow, P. & Goodman, C. S. *J. Cell Biol.* **110**, 1825-1832 (1990).
- Bate, C. M. *Nature* **260**, 54-55 (1976).
- Keshishian, H. & Bentley, D. *J. Neurosci.* **9**, 89-102 (1983).
- Condic, M. L. & Bentley, D. *J. Neurosci.* **9**, 2678-2686 (1989).
- Jan, L. Y. & Jan, Y. N. *Proc. natn. Acad. Sci. U.S.A.* **79**, 2700-2704 (1982).
- Snow, P. M., Patel, N. H., Harrelson, A. L. & Goodman, C. S. *J. Neurosci.* **7**, 4137-4144 (1987).
- Caudy, M. & Bentley, D. *J. Neurosci.* **6**, 1781-1795 (1986).
- Keshishian, H. & Bentley, D. *J. Neurosci.* **9**, 103-115 (1983).
- Elkins, T. *et al. Cell* **60**, 565-575 (1990).
- Petrey, D., Buster, D., Donato, K. K. & Anderson, H. *Dev. Growth Differ.* **31**, 299-305 (1989).
- Katz, F., Moats, W. & Jan, Y. N. *EMBO J.* **7**, 3471-3477 (1988).
- Johansen, J., Halpern, M. E. & Keshishian, H. *J. Neurosci.* **9**, 4318-4332 (1989).

ACKNOWLEDGEMENTS. We thank D. Bentley, C. Goodman, W. Gilbert and R. Wyman for comments on the manuscript. A. Harrelson and C. Goodman for the anti-fasciclin I monoclonal, and the MIT Laser Research Center for use of facilities. Supported by the Lucille P. Markey Charitable Trust, the Whitaker Foundation, and Hoffmann La Roche (D.J.), and by the NIH and the March of Dimes Birth Defects Foundation (H.K.).

Interleukin-1 receptor antagonist reduces mortality from endotoxin shock

Kjell Ohlsson*, Peter Björk*, Magnus Bergenfeldt*, Robert Hageman† & Robert C. Thompson†

* Department of Surgical Pathophysiology, University of Lund, Malmö General Hospital, S21401, Malmö, Sweden

† Synergen, Inc., 1885 33rd Street, Boulder, Colorado 80301, USA

ABOUT five out of 1,000 patients admitted to hospital develop bacterial sepsis leading to shock¹, the mortality rate for which is high despite antibiotic therapy². The infection results in hypotension and poor tissue perfusion, and eventually leads to the failure of several organ systems. Bacterial endotoxin is thought to be the direct cause of shock in Gram-negative sepsis, because it can cause shock in animals³, and antibodies against endotoxin prevent Gram-negative shock in animals⁴ and in humans⁵⁻⁷. But, the symptoms of septic shock are the result of the actions of host cytokines induced by the endotoxin. The cytokine interleukin-1 has been implicated as an important mediator of septic shock because it can induce tachycardia and hypotension and act synergistically with tumour necrosis factor to cause tissue damage⁸ and death⁹. We now report that a specific interleukin-1 receptor antagonist reduces the lethality of endotoxin-induced shock in rabbits, indicating that interleukin-1 does indeed play an important part in endotoxin shock.

A recombinant human interleukin-1 (IL-1) receptor antagonist (IL-1ra)^{10,11} that blocks the effects of IL-1 *in vitro* has provided a tool for determining the role of IL-1 in animal models of septic shock. The hypotension and leukopenia that follow a single intravenous injection of recombinant human interleukin-1 β (IL-1 β , 15 μ g kg⁻¹) into anaesthetized rabbits⁸ were blocked in a dose-dependent way by the injection of IL-1ra shortly before IL-1 (Fig. 1a, b). The leukocytosis that occurs at later times in conscious rabbits injected with IL-1 β was also blocked (Fig. 1c). These results indicate that IL-1ra should block the effects of endotoxin shock mediated by IL-1 in rabbits.

Because death is a common outcome of septic shock in humans, we tested the effects of IL-1ra in a model of endotoxin shock in rabbits, for which the mortality rate is similarly high. Intravenous injection of *Escherichia coli* endotoxin (0.5 mg kg⁻¹) into rabbits killed eight of ten animals within 48 hours (Fig. 2). Within the first few hours after the injection the animals' fur became ruffled and they became essentially immobile. The animals' breathing became strained and harsh noises could be heard issuing from their lungs. At autopsy, the lungs showed striking pathological changes. On gross examination they were heavy with a liver-like appearance. Light microscopy revealed that the fine alveolar architecture was disrupted, showing oedematous alveolar walls and a massive accumulation of protein and of red and white blood cells (Fig. 3a).

By contrast, nine of ten rabbits receiving a total of 100 mg kg⁻¹ IL-1ra and the endotoxin survived the observation period of 7 days and appeared to make a full recovery (for dosage, see Fig. 2). These animals moved about the cage, and their fur and breathing appeared to be normal, although the animals were less lively than untreated controls. Rabbits of another group treated in the same way were killed after 24 hours so that their lungs could be examined. On gross examination, small areas of surface bleeding but no gross hepatization was seen, and on microscopic examination, there was no evidence of the massive transudation and cellular infiltration seen in the group treated with endotoxin alone (Fig. 3b). The beneficial effects of IL-1ra are dose-dependent. A group of 10 rabbits treated with 30 mg kg⁻¹ IL-1ra had an intermediate level of mortality, and

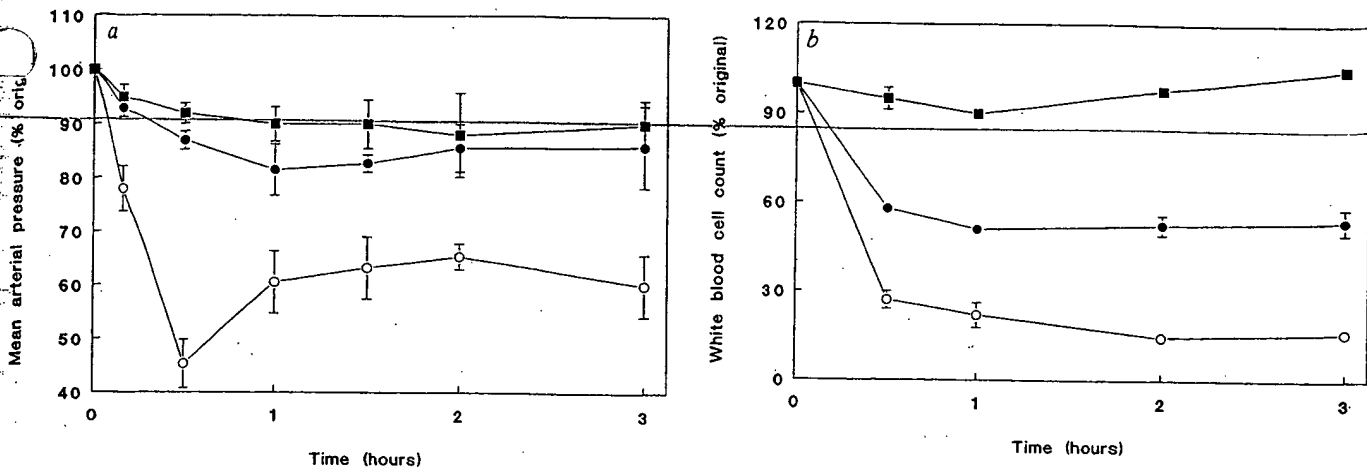


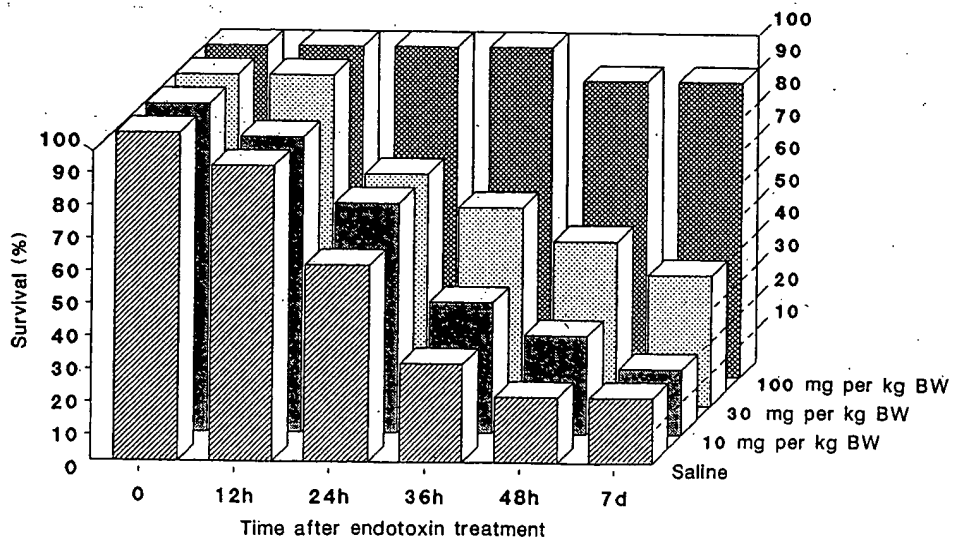
FIG. 1 Effect of IL-1ra on IL-1 β -induced changes in mean arterial pressure and white blood cell count in anaesthetized and conscious rabbits, which are as sensitive to endotoxin and IL-1 as humans⁹. Rabbits (blue chinchilla, 2.5 kg; BomMice, Bomholtgaard Breeding and Research Center Ltd, Bomholtvej 10, DK-8680, Ry, Denmark) were anaesthetized with a single injection of 4 mg kg⁻¹ xylazine and 10 mg kg⁻¹ ketamine. Catheters (PE 50) were placed in the left carotid artery and the superior caval vein to allow for the continuous recording of the arterial and central venous pressure. IL-1 β and IL-1ra (both prepared from *E. coli* and containing <0.5 U endotoxin per mg protein) were injected into the central venous catheter as a bolus over 1 min. During the observation period, blood was withdrawn from the carotid artery catheter for white blood cell count (originally close to 7×10^9 L⁻¹) and platelet counts, and directly into EDTA for plasma samples. Blood samples removed from the catheters were replaced with the same volume of saline (~5 ml over 3 h). The total volume of saline administered was 1 ml per kg body weight per hour. In one series of IL-1/IL-1ra experiments the animals were allowed to wake up after the catheters were in place. The catheters were secured in the neck to allow repeated measurements of blood pressure and also sampling of blood. Rabbits received either 15 μg kg⁻¹ IL-1 β (○), 15 μg kg⁻¹ IL-1 β and 1 mg kg⁻¹ IL-1ra (●), or 15 μg kg⁻¹ IL-1 β and 4 mg kg⁻¹ IL-1ra (■). Rabbits injected with saline or with 4 mg kg⁻¹ IL-1ra remained haemodynamically stable and showed no significant change in the number of white blood cells throughout the observation period (data not shown).

animals given 10 mg kg⁻¹ IL-1ra had the same level of mortality as untreated animals (Fig. 2).

Large doses of IL-1ra were required to block the action of IL-1 in the IL-1- and the endotoxin-induced diseases, despite the fact that IL-1ra and IL-1 are expected to have similar affinities for the IL-1 receptor on the basis of experiments with

mouse cells¹⁰. In part this high dose indicates that more than 50% of IL-1 binding needs to be blocked for 50% of the biological effects of IL-1 to be blocked. Similar effects occur with cells in culture¹². But the high doses needed are also a consequence of the rapid equilibration and clearance of IL-1ra after intravenous injection. In the group of animals receiving a total of 100 mg

FIG. 2 The effect of IL-1ra on the survival rate in endotoxin-induced shock in rabbits. IL-1ra was injected in equal doses just before the injection of endotoxin (*E. coli* 026, B26; Sigma) and every 2 h thereafter for 24 h. The rabbits were not anaesthetized but were under constant observation for 48 h and were then observed during the day-time for up to 7 days. The animals had access to water and food. Injections and blood sampling were made through the ear veins. BW, body weight; d, days.



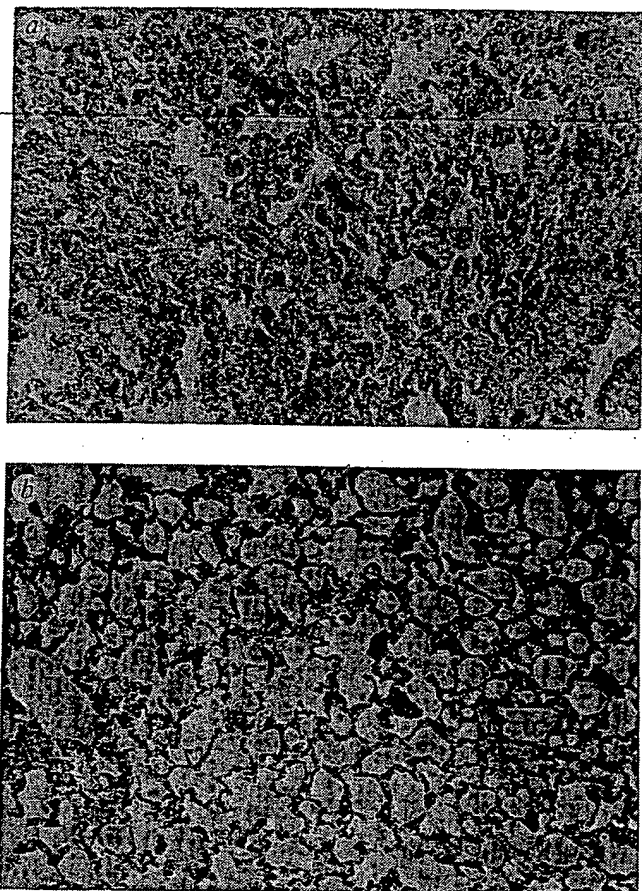


FIG. 3 Microscopic appearance (magnification, 160 \times) of a rabbit lung removed: a, immediately after death at 26 h from an animal receiving endotoxin and no IL-1ra; and b, 24 h after identical injection of endotoxin from an animal receiving 100 mg rhIL-1ra per kg body weight over the first 24 h. Rabbits were killed with pentobarbital. The tissue specimens were fixed in buffered (pH 7.4) 10% formalin, dehydrated and embedded in paraffin. The tissue samples were analysed with light microscopy with haematoxylin-eosin staining.

IL-1ra per kg body weight, the level of IL-1ra in plasma, as measured by a single radial immunodiffusion assay¹³, varied from between 150 $\mu\text{g ml}^{-1}$ 5 minutes after each 7.7-mg kg^{-1} dose, and 20 $\mu\text{g ml}^{-1}$ 2 hours later. These results imply that the quantity of IL-1ra needed to prevent mortality would be considerably reduced if the circulation of the protein could be prolonged.

To determine the time during which IL-1 acts a pathological agent in endotoxin shock we investigated the effects on mortality of delaying the treatment with IL-1ra. When the standard treatment with IL-1ra was delayed for 1 or 2 hours after the endotoxin injection, seven of the eight animals in each group survived the 7-day period whereas three of the four animals in a group not treated with IL-1ra died within 48 hours. These results indicate that IL-1 toxicity can be reversed at least 2 hours after injecting endotoxin. Because IL-1 seems to be a late-acting agent in endotoxin shock, IL-1ra could have therapeutic as well as prophylactic properties in septic shock. This is especially important clinically, where the disease, as measured by hypotension, can be in progress before intervention can be initiated. Experiments are in progress to determine the latest time after administration of endotoxin at which the disease can be prevented.

In light of earlier results implicating tumour necrosis factor as a mediator in endotoxin shock¹⁴⁻¹⁷, the demonstration that IL-1 is also an important mediator shows that the disease probably results from several cytokines acting with additive or syner-

gistic effects. This conclusion is in accordance with IL-1 greatly potentiating the shock action of tumour necrosis factor in mice and rabbits^{8,9}. Other cytokines may also contribute to the pathology of endotoxin shock. But on the basis of the current results we conclude that IL-1 plays an important part in experimental endotoxin shock in animals. It will be worthwhile investigating whether IL-1ra is of practical therapeutic benefit in human septic shock. \square

Received 6 July; accepted 23 October 1990.

1. Lode, H. *Arzneimitteltherapie* **1**, 82-89 (1983).
2. Kreger, B. E., Crave, D. E. & McCabe, W. R., *Am. J. Med.* **68**, 343-355 (1980).
3. Guenter, C. A., Florica, V. & Hinshaw, B. J. *J. appl. Physiol.* **26**, 780-786 (1969).
4. Ziegler, E. J., Douglas, H., Sherman, J. E., Davis, C. E. & Braude, A. I. *J. Immun.* **111**, 433-438 (1973).
5. Ziegler, E. J. *et al. New Engl. J. Med.* **307**, 1255-1230 (1982).
6. Ziegler, E., Sprung, C., Straube, R. & Sadoff, J. *Clin. Res.* **38**, 304A (1990).
7. Gorelick, K. J., Schein, R. M. H., MacIntyre, N. R., Emmanuel, G. R. *Crit. Care Med.* **18**, S253 (1990).
8. Okusawa, S., Gelfand, J. A., Ikejima, T., Connolly, R. J. & Dinarello, C. A. *J. clin. Invest.* **81**, 1162-1172 (1988).
9. Everaerd, B., Brouckaert, P., Shaw, A. & Fiers, W. *Biochem. biophys. Res. Commun.* **163**, 378-385 (1989).
10. Hannum, C. H. *et al. Nature* **343**, 336-340 (1990).
11. Eisenberg, S. P. *et al. Nature* **343**, 341-346 (1990).
12. Arend, W. P., Welgus, H. G., Thompson, R. C. & Eisenberg, S. P. *J. clin. Invest.* **85**, 1694-1697 (1990).
13. Mancini, G., Carbonara, A. O. & Heremans, J. *Immunochemistry* **2**, 235-254 (1965).
14. Michie, H. R. *et al. New Engl. J. Med.* **318**, 1481-1486 (1988).
15. Tracey, K. J. *et al. Science* **234**, 470-474 (1986).
16. Tracey, K. J. *et al. Nature* **330**, 662-664 (1987).
17. Beutler, B., Milsark, I. & Cerami, A. *Science* **229**, 869-871 (1985).

ACKNOWLEDGEMENTS. This research was supported by the Swedish MRC and the Medical Faculty, University of Lund, Sweden. This study was approved by the Ethics Committee for Animal Experiments at the University of Lund. We thank L. McGee for help in preparing the manuscript.

Phage antibodies: filamentous phage displaying antibody variable domains

John McCafferty[†], Andrew D. Griffiths^{*}, Greg Winter^{*‡} & David J. Chiswell[†]

^{*} MRC Laboratory of Molecular Biology, Hills Road, Cambridge CB2 2QH, UK

[†] Cambridge Antibody Technology Ltd, Daly Research Laboratories, Babraham Hall, Cambridge, CB2 4AT, UK

NEW ways of making antibodies have recently been demonstrated using gene technology. Immunoglobulin variable (V) genes are amplified from hybridomas or B cells using the polymerase chain reaction, and cloned into expression vectors. Soluble antibody fragments secreted from bacteria are then screened for binding activities (see ref. 1 for review). Screening of V genes would, however, be revolutionized if they could be expressed on the surface of bacteriophage. Phage carrying V genes that encode binding activities could then be selected directly with antigen. Here we show that complete antibody V domains can be displayed on the surface of fd bacteriophage, that the phage bind specifically to antigen and that rare phage (one in a million) can be isolated after affinity chromatography.

The heavy (VH) and light (VL) chain variable (V) domains of the anti-lysozyme antibody D1.3 (ref. 2) associate tightly as an Fv fragment and bind to antigen with a similar affinity to that of the parent antibody³. To allow expression of both domains on the same polypeptide, they were joined by a flexible linker (Gly₄-Ser)₃ (ref. 4), and the single-chain Fv fragment (scFv) cloned into an fd phage vector (fdCAT1) at the N-terminal region of the gene III protein (Fig. 1). The gene III protein is normally expressed at the tip of fd phage (about four copies per virion), is responsible for attachment of phage to the

[‡] To whom correspondence should be addressed.

Interleukin-1 Blockade Attenuates Mediator Release and Dysregulation of the Hemostatic Mechanism During Human Sepsis

Marja A. Boermeester, MD; Paul A. M. van Leeuwen, MD, PhD; Susette M. Coyle, RN; Gert Jan Wolbink, MD; C. Erik Hack, MD, PhD; Stephen F. Lowry, MD

Objective: To define the influence of interleukin-1 activity on coagulation and fibrinolytic system activation and the release of proinflammatory mediators in the early human response to severe infection.

Study Design: All patients with severe sepsis syndrome who were enrolled from two surgical centers that were participating in a randomized, double-blind, placebo controlled, multicenter, multinational trial of recombinant human interleukin-1 receptor antagonist in the treatment of sepsis syndrome.

Population: Twenty-six patients with sepsis syndrome received an intravenous loading dose of recombinant human interleukin-1 receptor antagonist (100 mg) or placebo followed by a continuous 72-hour infusion of recombinant human interleukin-1 receptor antagonist (1.0 [n=9] or 2.0 [n=8] mg/kg per hour) or placebo (n=9).

Outcome Measure: Responses up to 72 hours after initiation of treatment.

Results: Plasma levels of the anaphylatoxin C3a and

thrombin-antithrombin III complexes were reduced in the high-dose recombinant human interleukin-1 receptor antagonist treatment group after 72 hours ($P<.05$). Similarly, parameters of fibrinolysis, tissue-type plasminogen activator, and plasminogen activator inhibitor type 1 but not plasmin- α_2 -antiplasmin complexes, were also significantly reduced ($P<.05$) after 72 hours of treatment with a high dose of recombinant human interleukin-1 receptor antagonist. Neutrophil elastase- α_1 -antitrypsin complexes and phospholipase A_2 levels were also significantly reduced in the high-dose recombinant human interleukin-1 receptor antagonist treatment group after 72 hours.

Conclusions: The results confirm that activation of the coagulation and fibrinolytic systems and release of soluble inflammatory mediators are consistently observed in patients with severe sepsis syndrome. Interleukin-1 activity contributes to activation of these processes as documented by the reduction in surrogate activation markers during recombinant human interleukin-1 receptor antagonist treatment.

(Arch Surg. 1995;130:739-748)

From the Departments of Surgery (Drs Boermeester and van Leeuwen) and Internal Medicine (Dr Hack), Free University Hospital, Amsterdam; Central Laboratory of the Netherlands, Red Cross Blood Transfusion Services (Drs Wolbink and Hack); and the Laboratory for Experimental and Clinical Immunology, the University of Amsterdam (Drs Wolbink and Hack); and the Laboratory of Surgical Metabolism, Department of Surgery, Cornell University Medical College, New York, NY (Ms Coyle and Dr Lowry).

SEPSIS SYNDROME, characterized by hypotension, vascular collapse, and multiple organ failure, is a significant cause of morbidity and mortality in hospitalized patients and continues to be an important health care problem. It is generally accepted that this syndrome is caused by an excessive release and activation of endogenous inflammatory mediators in response to the infecting microorganisms. Cytokines, particularly interleukin-1 (IL-1) and tumor necrosis factor α (TNF- α), have been implicated as important mediators in the initiation of this inflammatory host response.¹ In accordance herewith, levels of TNF- α and IL-1 β are elevated during experimental endotoxemia^{2,3} as well as during septic shock in baboons⁴ and humans.^{3,5} The intravenous administration of tumor necrosis factor in

animals results in shock, multiple organ failure, and death,^{6,7} whereas infusion of recombinant interleukin-1 in rabbits^{8,9} and primates¹⁰ induces similar cardiovascular effects. Moreover, TNF and IL-1 may synergize in inducing hypotension, tissue injury, and death,^{8,11} as well as in triggering the release of IL-6^{12,13} and presumably IL-8.¹⁴⁻¹⁶ Their overlapping biological effects may be due, at least in part, to stimulation of the production of TNF by IL-1 and vice versa,^{17,18} a situation that very likely occurs in septic shock.¹²

A number of in vitro and in vivo studies have suggested that TNF and IL-1

See Methods in next page

METHODS

PATIENTS

Twenty-six patients were entered in this study. The selection of patients is outlined below. The patients were part of a larger multicenter phase III randomized, double-blind, placebo-controlled study to evaluate the efficacy of interleukin-1 receptor antagonist in reducing 28-day all-cause mortality rate in patients with severe infection. In the present study, all patients from the Free University Hospital (Amsterdam, the Netherlands) and the New York (NY) Hospital who were included in the larger multicenter trial entered this substudy. All patients gave written informed consent, and the protocols were approved by the institutional review boards of each participating hospital.

Patients were randomized, as described previously,³⁰ to one of the following treatment groups: interleukin-1 receptor antagonist, 1.0 mg/kg per hour (n=9); interleukin-1 receptor antagonist, 2.0 mg/kg per hour (n=8); or placebo (vehicle; n=9). These groups are designated below as the low-dose, the high-dose, and the placebo groups, respectively. The treatment regimen in both interleukin-1 receptor antagonist treatment groups was initiated with a 1-minute intravenous bolus of 100 mg of interleukin-1 receptor antagonist in 10 mL of 0.9% sodium chloride solution or an equivalent volume of vehicle in 10 mL of 0.9% sodium chloride solution in the placebo group. Thereafter, interleukin-1 receptor antagonist was administered by continuous intravenous infusion for 72 hours in 0.9% sodium chloride solution infusion bags at an infusion rate of 12 mL per hour. All patients received standard intensive care support, including intravenous administration of fluids, cardiovascular and respiratory support, and administration of appropriate antimicrobial agents, and they could undergo surgery when indicated. All patients started with the assigned treatment within 24 hours after the diagnosis of sepsis syndrome was made. Prior to the start of the interleukin-1 receptor antagonist or placebo infusion, data were collected for calculation of the Acute Physiology and Chronic Health Evaluation (APACHE III) score according to the methods of Knaus et al³¹ to demonstrate that severity of illness was similar among treatment groups.

SELECTION OF PATIENTS

Inclusion criteria of the multicenter trial were as follows: (1) clinical evidence to support a presumptive diagnosis of sepsis syndrome of a presumed infectious origin; (2) fever or hypothermia (core temperature greater than or equal to 38°C or less than or equal to 36°C); (3) tachycardia (≥ 90 beats per minute); (4) tachypnea (≥ 20 breaths per minute) or requirement of mechanical ventilation; and (5) either hypotension (systolic blood pressure of 90 mm Hg or less, mean arterial pressure of 70 mm Hg or less, a decrease in systolic blood pressure of 40 mm Hg or greater, the need for vasopressors [except dopamine administered at a dose

age of less than 5.0 $\mu\text{g/kg}$ per minute] to stabilize blood pressure in the presence of adequate fluid resuscitation), or any two or more of the following signs of organ dysfunction and/or inadequate perfusion: (a) acute deterioration in mental status (in the absence of sedative hypnotic drugs or other therapeutic agents with central nervous system depressant effects); (b) arterial hypoxemia (PaO_2 of 75 mm Hg or less or a PaO_2 -fraction of inspired oxygen ratio of 250 or less); (c) metabolic acidosis ($\text{pH} \leq 7.30$ or base deficit of 5.0 mEq/L or greater) or increased plasma lactic acid concentration; (d) oliguria (urine output of 0.5 mL/kg per hour or less); (e) coagulation abnormalities (prothrombin time or partial thromboplastin time of greater than or equal to 1.2 times the upper limit of normal); (f) thrombocytopenia ($\leq 100 \times 10^9/\text{L}$ or a decrease of 50% or more); (g) cardiac index greater than 4.0 L/min per square meter with systemic vascular resistance less than 800 dynes-sec- cm^2 in the presence of adequate fluid resuscitation. All criteria had to have been met in 24 hours or less prior to treatment.

Patients meeting any of the following criteria were not eligible to participate: age of 18 years or younger; pregnancy; weight greater than 100 kg; evidence of nonseptic cardiogenic shock or a source of uncontrollable severe blood loss; severe, preexisting, parenchymal liver disease with clinically significant portal hypertension; anuria (≤ 50 mL of urine output per day); experiencing rejection of solid organ or bone marrow transplantation; current immunocompromised condition (including but not limited to corticosteroid administration [≥ 1.0 mg/kg per day of prednisone or equivalent], chemotherapy, or radiation) or a disease sufficiently advanced to suppress resistance to infection (including but not limited to leukemia, lymphoma, acquired immunodeficiency syndrome, and known human immunodeficiency virus seropositivity); full-thickness thermal or chemical burn involving 30% or more of total body surface area; receipt of an investigational new drug within the previous 30 days; non-resuscitation agreement; or presence of an irreversible, rapidly fatal underlying disease or injury.

DRUGS

Human recombinant interleukin-1 receptor antagonist (Anakinra, Synergen Inc, Boulder, Colo) was provided in a sterile solution (vehicle) of pH 6.5 that contained sodium chloride, trisodium citrate, disodium citrate, citric acid, edetate disodium, polysorbate 80, and sterile water. As a placebo, the vehicle was used.

BLOOD COLLECTION

For the present study, blood samples were only taken during the time that treatment with interleukin-1 receptor antagonist or placebo was given (72 hours). Thus, although patients were followed up for 28 days, the evaluation period for the present study was considered to be 72 hours. Blood samples were obtained through the patient's arte-

extert their influence during sepsis via the induction of other mediators such as IL-6 and IL-8, arachidonic acid metabolites, and platelet activating factor. These proinflammatory cytokines also induce activation of coagulation and fibrinolysis pathways and induce activation of neutrophils.^{8,12-16,19-25} It has yet to be determined to what

extent TNF- α and IL-1 contribute to the pathogenesis of the sepsis syndrome in humans, either directly or via induction of other inflammatory mediator species.

Recently, a recombinant human antagonist of IL-1 receptors became available for use in clinical studies.^{26,27} This interleukin-1 receptor antagonist binds to

rial line and were collected in 10-mL siliconized tubes that contained 3.8% wt/vol sodium citrate or 150 U of heparin sodium. The blood samples were taken shortly before and at 4, 12, 24, 48, and 72 hours after the start of the treatment regimen. After collection, they were immediately stored in ice to prevent activation of the complement system. Plasma was obtained by centrifugation of blood for 15 minutes at 1300g. All plasma samples were stored in aliquots at -70°C until tested.

ASSAYS

Plasma TNF- α and IL-1 β levels were measured by standard enzyme-linked immunosorbent assay (ELISA) techniques, as reported elsewhere.^{32,33} The sensitivity of these assays is 34 and 8 pg/mL, respectively.

The concentration of IL-6 in plasma was quantified with an ELISA modified from that described in detail before.³⁴ Briefly, purified monoclonal anti-interleukin-6 antibody (mAb CLB-IL6/16) was used as a capture antibody, and biotinylated sheep antibodies in combination with streptavidin-polymerized horseradish peroxidase conjugate (CLB Department of Immune Reagents, Amsterdam) were used to detect bound IL-6. Results were expressed as picograms per milliliter by reference to a standard consisting of recombinant human IL-6.³⁵ The lower detection limit of this assay was 5 pg of IL-6 per milliliter of plasma.

Interleukin-8 was measured with a sandwich ELISA modified from that described previously³⁶: monoclonal anti-interleukin-8 antibody (mAb CLB-IL8/1) and biotinylated affinity-purified sheep anti-interleukin-8 antibodies were used as capture and detecting antibodies, respectively. Polymerized horseradish peroxidase conjugated to streptavidin was used to quantify bound biotinylated antibodies. Results were compared with those obtained with dilutions of recombinant human IL-8 and expressed as picograms per milliliter. The lower detection limit of this assay was 5 pg/mL.

The anaphylatoxin C3a in plasma was measured by a radioimmunoassay as previously described.³⁷

Thrombin-antithrombin III (TAT) complex levels were determined with a novel ELISA. In this assay, monoclonal antibody TR3 against human thrombin and prothrombin was used to catch TAT complexes from samples to be tested. Bound complexes were detected using biotinylated monoclonal antibody ATIII-0 (CLB Department of Immune Reagents) in combination with streptavidin-polymerized horseradish peroxidase. Results of this ELISA were expressed as nanograms per milliliter by reference to a standard consisting of pooled human serum. (The amount of TAT complexes in this in-house standard was assessed using a commercial ELISA for TAT complexes [Behringwerke AG, Marburg, Germany]). The lower limit of detection of this assay was 1 to 2 ng of TAT complexes per milliliter. Normal values (ie, obtained from a panel of normal donors) were less than 4 ng/mL. Comparison of levels in plasma samples from patients with varying levels of TAT com-

plexes (from normal to greater than 1000 ng/mL) obtained with this novel assay for TAT complexes with those measured by a commercial assay (Behringwerke) yielded an excellent correlation ($r=.99$, $n=23$).

Tissue-type plasminogen activator (t-PA) concentrations in plasma were measured with a previously described sandwich ELISA,³⁸ and plasmin- α_2 -antiplasmin (PAP) complex levels were measured with a previously described radioimmunoassay.³⁹

Plasminogen activator inhibitor type 1 (PAI-1) levels were assessed with an ELISA that had been modified from a sandwich-type radioimmunoassay as described in detail before.⁴⁰ In short, monoclonal anti-PAI-1 antibody (mAb CLB-2C8) was used as the coating antibody and biotinylated polyclonal rabbit anti-PAI-1 antibodies as the conjugate. Results were expressed as nanograms per milliliter by reference to a standard curve of human PAI-1. This assay had a lower detection limit of 5 ng/mL.

Neutrophil elastase- α_1 -antitrypsin complexes were determined with a radioimmunoassay as described in detail before.⁴¹

Phospholipase A₂ concentrations in plasma were determined with an ELISA that had been modified from that of Smith et al.⁴² Monoclonal antibodies against human secretory PLA₂ type II (sPLA₂) were used as the coating and catching antibodies. Results were compared with those obtained with cultured medium from Hep G2 cells stimulated with human interleukin-6.⁴⁰ The amount of PLA₂ in this cultured medium was assessed by comparison with purified recombinant human sPLA₂. The lower limit of detection in this assay was 1 ng/mL; the mean \pm SEM normal value as assessed in 19 healthy volunteers was 20 ± 7 ng/mL (range, 9 to 30 ng/mL).

All of the above assays exhibited interassay variation coefficients of less than 15%, as was estimated from the variation of dose-response curves obtained on at least 3 different days over a 3-month period. To minimize interassay variation, all samples were tested within one assay procedure.

STATISTICAL METHODS

The data are expressed as means \pm SEMs. Factorial analysis of variance (ANOVA) was used for comparison of APACHE III scores and demographic data between groups. An ANOVA for repeated measures was used to assess significant changes in variables in the course of the observation period. The nonparametric Mann-Whitney *U* test was used to determine the significance of the differences between groups. The Wilcoxon rank sum test was used to assess the differences within groups between baseline levels and those at subsequent time points. For all tests, a two-tailed *P* value less than .05 was considered statistically significant. The analysis was performed using a commercial statistical package (Stat-View, Abacus Concepts Inc, Berkeley, Calif) on a Macintosh computer (Apple Computer Inc, Cupertino, Calif).

both types of IL-1 receptors with the same affinity as IL-1 but does not induce signal transduction. Interleukin-1 receptor antagonist has been useful in evaluating the influence of IL-1 on secondary mediator systems and physiologic measures of experimental sepsis. In a primate model of lethal septic shock, administration of interleukin-1 re-

ceptor antagonist improved survival and hemodynamic performance and reduced IL-6 levels without affecting circulating TNF concentrations.²⁸ Moreover, administration of interleukin-1 receptor antagonist abrogated aggregation of neutrophils and lung injury in endotoxin-induced⁹ and *Escherichia coli*-induced shock²⁹ in rabbits.

In the present study, we tested the hypothesis that IL-1 may contribute to the activation of other mediator systems such as the complement, coagulation, and fibrinolytic cascades in human sepsis. We also sought to evaluate the role of IL-1 on neutrophil activation and the release of both arachidonic acid metabolites, IL-6 and IL-8. For this purpose, we prospectively analyzed the course of the plasma levels of these mediators during selective inhibition of IL-1 in patients with sepsis syndrome who were enrolled in a phase III study to evaluate the efficacy and safety of interleukin-1 receptor antagonist. The clinical results of this trial have been reported previously.³⁰ Our results indicate that clinical administration over a period of 72 hours of a large molar excess of interleukin-1 receptor antagonist relative to interleukin-1 that is sufficient to block nearly all the IL-1 receptors attenuated activation of the complement, coagulation, and fibrinolytic systems. Furthermore, such intervention reduced the levels of IL-6, neutrophil elastase, and phospholipase A₂ (PLA₂) in patients with sepsis, suggesting that IL-1 activity contributes to the appearance of these inflammatory mediators during human infection.

RESULTS

PATIENTS

The three patient groups accrued from these two institutions were balanced for APACHE III scores at study entry (Table 1) ($P=.86$). In addition, when the groups were compared for distribution of age and gender, no significant differences were observed. The diagnoses on admission to the intensive care units (all patients undergoing

surgery) were the following: intra-abdominal infection ($n=6$); bowel infarction ($n=3$); pancreatitis ($n=3$); pneumonia ($n=3$); gastrointestinal tract perforation and peritonitis ($n=2$); multiple trauma, including intra-abdominal lesions ($n=2$); gastrointestinal tract bleeding ($n=2$); abdominal aortic aneurysm, ruptured or infected ($n=2$); leg amputation ($n=1$); necrotizing fascitis and cellulitis ($n=1$); pelvic abscess ($n=1$); cholangitis ($n=1$); systemic infection of unknown origin ($n=1$); and line sepsis ($n=1$). The three treatment regimens were randomly distributed within the more frequent disease categories.

PLASMA LEVELS OF TNF- α AND IL-1 β

Plasma levels of TNF- α were undetectable except in a few patients who had detectable TNF- α concentrations at only one time point. Similarly, IL-1 β was only randomly detected in the plasma among treatment groups, and such levels were near the detection limit of this assay. Because of the low incidence of detectable TNF- α and IL-1 β levels, neither calculations of means nor statistical analysis of the above data was performed.

EFFECT OF IL-1 RECEPTOR BLOCKADE ON PLASMA LEVELS OF IL-6 AND IL-8

The baseline levels ($t=0$ hours) of IL-6 (Table 2) were not statistically significantly different between groups ($P=.6$). In the placebo group, IL-6 levels remained unchanged during the observation period, whereas administration of interleukin-1 receptor antagonist at either 1.0 or 2.0 mg/kg per hour resulted in a progressive decrease of IL-6 plasma levels over 72 hours. Interleukin-6 levels in the low-dose and high-dose groups were below the levels of the placebo group from $t=24$ hours and $t=48$ hours onward, respectively (data not shown), and remained lower until the end of the treatment period (Table 2). Differences between the groups were not statistically significant at any time point. When the course of IL-6 within each group was considered, both interleukin-1 receptor antagonist treatment groups but not the placebo group showed a significant decrease from $t=4$ hours onward compared with their respective baseline values. In the high-dose group, this decrease was highly significant at $t=4$ hours, $t=12$ hours, and $t=24$ hours (Table 3).

Baseline levels of IL-8 were higher in the high-dose group than those of the low-dose and placebo groups, although this difference did not reach statistical signifi-

Table 1. APACHE III Scores at Study Entry and Demographic Data

| Treatment Group | APACHE III Score [†] | Age, y | Gender |
|-----------------|-------------------------------|----------------|---------|
| Placebo | 78.9 \pm 3.0 | 63.5 \pm 3.3 | 6 M/3 F |
| Low-dose | 77.2 \pm 5.9 | 59.4 \pm 2.6 | 5 M/1 F |
| High-dose | 72.1 \pm 4.3 | 57.3 \pm 7.3 | 5 M/3 F |

*No significant differences were observed between groups, as determined by analysis of variance. APACHE III indicates Acute Physiology and Chronic Health Evaluation. Values are means \pm SEMs.

†Low-dose group was administered interleukin-1 receptor antagonist at a rate of 1 mg/kg per hour; high-dose group, 2 mg/kg per hour.

‡According to the methods of Knaus et al.³¹

Table 2. IL-1 Receptor Blockade and Plasma Levels of IL-6 and IL-8

| Treatment Group | IL-6, pg/mL | | IL-8, ng/mL | |
|-----------------|---------------|---------------|----------------|---------------|
| | $t=0$ | $t=72$ | $t=0$ | $t=72$ |
| Placebo | 245 \pm 67 | 276 \pm 149 | 123 \pm 216 | 110 \pm 361 |
| Low-dose | 191 \pm 146 | 41 \pm 29 | 113 \pm 577 | 117 \pm 46 |
| High-dose | 183 \pm 368 | 68 \pm 374 | 394 \pm 4504 | 166 \pm 86 |

*Values are mean \pm SEM plasma concentrations of interleukin-6 (IL-6) and IL-8 at study entry ($t=0$) and after a 72-hour infusion period ($t=72$). No significant differences were observed between groups.

†Low-dose group was administered interleukin-1 receptor antagonist at a rate of 1 mg/kg per hour; high-dose group, 2 mg/kg per hour.

‡Significant difference ($P<.05$) within group between $t=0$ and $t=72$.

Table 3. Differences (P Values) Within Groups between Baseline Levels (t=0) and Those of Subsequent Time Points*

| | t=0 | t=12h | t=24h | t=48h | t=72h |
|------------------------|-------|-------|-------|-------|-------|
| Placebo Group | | | | | |
| IL-8 | | | | | |
| IL-6 | | | | | |
| C3a | | | | | |
| ELAST- α_1 -AT | | | | | |
| PAP | | <.05† | | <.05† | <.01† |
| TAT | | | | | |
| t-PA | | | | | |
| PAI-1 | | | | | |
| sPLA ₂ | | | | | |
| Low-Dose Group | | | | | |
| IL-8 | <.05† | <.05† | <.05† | <.05† | |
| IL-6 | | | | | |
| C3a | | | | | |
| ELAST- α_1 -AT | | | | | |
| PAP | | <.05† | | | |
| TAT | | <.05† | <.05† | | <.05† |
| t-PA | | | | | |
| PAI-1 | | | | | |
| sPLA ₂ | | | | <.01† | <.05† |
| High-Dose Group | | | | | |
| IL-8 | <.01† | <.01† | <.01† | <.05† | <.05† |
| IL-6 | <.05† | | <.05† | | |
| C3a | | | <.05† | | <.05† |
| ELAST- α_1 -AT | | | | | <.05† |
| PAP | | | | | |
| TAT | <.01† | <.01† | <.01† | <.05† | <.05† |
| t-PA | | | <.05† | <.05† | <.05† |
| PAI-1 | | <.01† | <.05† | <.05† | <.05† |
| sPLA ₂ | | <.05† | <.05† | <.05† | <.05† |

* Baseline levels (t=0) are the values before the start of the infusion. Differences within groups were determined using the Wilcoxon rank sum test. The low-dose group was administered interleukin-1 receptor antagonist at a rate of 1 mg/kg per hour; high-dose group, 2 mg/kg per hour. IL indicates interleukin; ELAST- α_1 -AT, neutrophil elastase- α_1 -antitrypsin; PAP, plasmin- α_2 -antiplasmin; TAT, thrombin-antithrombin III; t-PA, tissue-type plasminogen activator; PAI-1, plasminogen activator inhibitor type 1; sPLA₂, secretory phospholipase A₂; and ellipses, not significant.
† Significantly increased.
‡ Significantly decreased.

cance (high dose vs placebo, $P=.6$; high dose vs low dose, $P=.3$) (Table 2). Interleukin-8 levels in both interleukin-1 receptor antagonist treatment groups were below those of the placebo group from t=48 hours onward and remained at these levels until the end of the treatment period (Table 2). However, there was no statistically significant difference between the interleukin-1 receptor antagonist treatment groups and the placebo group at any time point. In the placebo group, a modest decline in IL-8 level was observed at 12 to 24 hours, after which, values returned to baseline levels (data not shown). Compared with the placebo group, the decline in the low-dose group was protracted for at least 48 hours, but this difference did not reach statistical significance (Table 3). In contrast, a significant decrease in IL-8 levels compared with baseline values was found in the high-dose group at t=4 hours and t=24 hours (Table 3).

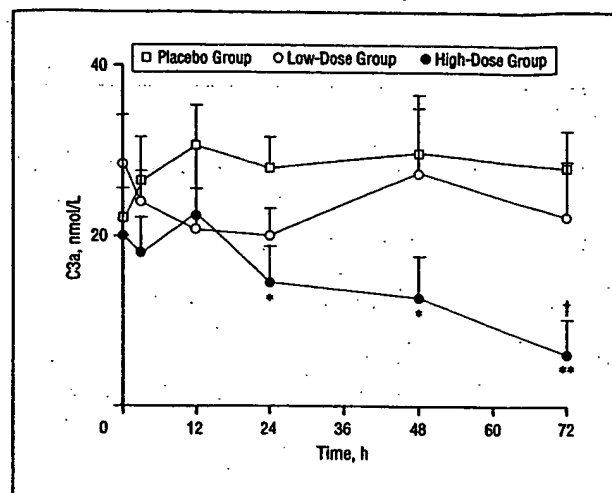


Figure 1. Interleukin-1 receptor blockade and complement activation: mean \pm SEM plasma concentrations of C3a during a 72-hour infusion period in placebo and low-dose (1 mg/kg per hour) and high-dose (2 mg/kg per hour) interleukin-1 receptor antagonist groups. Significant differences between the placebo group and the high-dose interleukin-1 receptor antagonist group are indicated by an asterisk ($P<.05$) or double asterisks ($P<.01$), and those between low-dose and high-dose interleukin-1 receptor antagonist groups are indicated by a dagger ($P<.05$) (Mann-Whitney U test).

EFFECT OF IL-1 RECEPTOR BLOCKADE ON COMPLEMENT ACTIVATION

Plasma levels of C3a were assessed to estimate the extent of complement activation in the treatment groups. Baseline levels of the placebo, low-dose, and high-dose groups were comparable (22.0 ± 3.6 , 28.1 ± 5.0 , and 22.9 ± 5.5 nmol/L, respectively). In the placebo group, a modest increase in circulating C3a levels was observed during the 72-hour period after the infusion had started (Figure 1). This increase was significant compared with baseline values at t=12 hours ($P<.05$; Table 3). In the low-dose group, levels of C3a gradually declined and tended to be less than those in the placebo group from t=4 hours onward. However, neither this difference nor the decrease compared with baseline values was statistically significant. In contrast, the C3a levels in the high-dose group declined over time, achieving a significant difference compared with baseline values at t=24 hours and t=72 hours (Table 3). Compared with the placebo group, levels of C3a were significantly lower in the high-dose group at t=24 hours, t=48 hours, t=72 hours ($P<.05$, $P<.05$, and $P<.01$, respectively; Figure 1). At t=72 hours, the high-dose group showed a significant decrease compared with the low-dose group ($P<.05$), which suggests a dose-dependent effect of interleukin-1 receptor antagonist on diminishing circulating C3a levels.

IL-1 RECEPTOR BLOCKADE AND THE COAGULATION SYSTEM

Levels of plasma TAT were measured to assess the activation of the coagulation system. Baseline values were only moderately elevated in the placebo and low-dose groups, whereas a higher baseline value was observed in the high-dose group. At t=0 hours, three of eight patients in the high-dose group demonstrated higher lev-

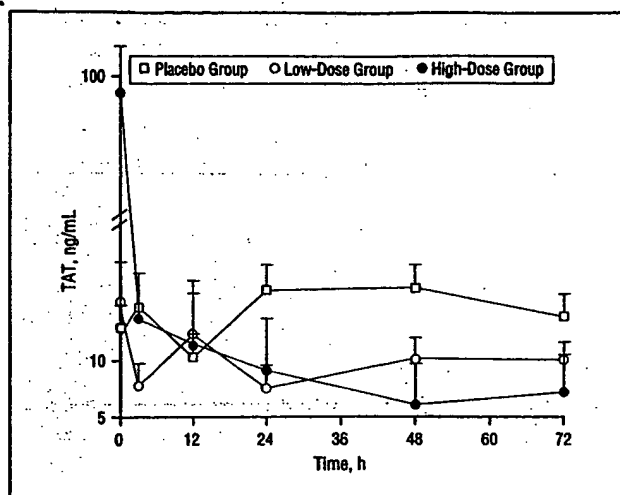


Figure 2. Interleukin-1 receptor blockade and the coagulation system: mean \pm SEM plasma concentrations of thrombin-antithrombin III (TAT) complexes during a 72-hour infusion period in placebo and low-dose (1 mg/kg per hour) and high-dose (2 mg/kg per hour) Interleukin-1 receptor antagonist groups.

els of TAT complexes when compared with patients in both other groups (**Figure 2**). However, the differences between baseline levels of the groups were not statistically significant, nor were the differences at subsequent time points. In the high-dose group, a highly significant decline from baseline values was noted at $t=4$ hours and thereafter (Table 3), reaching TAT levels below those measured in the placebo group 48 hours after start of the infusion (Figure 2).

IL-1 RECEPTOR BLOCKADE AND THE FIBRINOLYTIC SYSTEM

Plasma levels of t-PA and its main inhibitor, PAI-1, and PAP complexes were measured to assess the effect of IL-1 receptor blockade on fibrinolytic system activation (**Figure 3**). Baseline levels of t-PA and PAP complexes in all three patient groups were comparable (Figure 3, top and bottom). In the placebo group, levels of t-PA did not change during the observation period but were only moderately elevated. Following infusion with interleukin-1 receptor antagonist, a gradual decline of t-PA levels was noted in the low-dose group, whereas the high-dose group showed a rapid decline that reached the detection limit of the assay within $t=48$ hours (Table 3 and Figure 3, top).

Activation of fibrinolysis was observed in the placebo group, and PAP complex levels increased during the observation period (Figure 3, bottom). These levels were significantly increased above baseline values at $t=12$ hours, $t=48$ hours, and $t=72$ hours ($P<.05$, $P<.05$, and $P<.01$, respectively) (Table 3). Although an initial increase in PAP complex levels also was observed in both interleukin-1 receptor antagonist treatment groups, this increase did not continue during the 72-hour observation period, as was noted in the placebo group (Figure 3, bottom). However, no significant differences were noted at any time point between groups.

All three study groups demonstrated a decline in PAI-1 levels during the observation period (Figure 3, cen-

ter). In the placebo and low-dose groups, levels of PAI-1 gradually decreased from baseline values but never reached a statistically significant difference from baseline. In contrast, the high-dose group demonstrated a significant decline in PAI-1 levels that was noted within 24 hours and onward (Table 3). This decline coincided with that of the t-PA levels in this group. In the placebo group, levels of PAI-1 tended to decrease, whereas t-PA levels remained unchanged.

For all measured parameters of fibrinolysis, the levels tended to be lower in the high-dose interleukin-1 receptor antagonist group than in the low-dose group, which suggests a dose-dependent effect of interleukin-1 receptor antagonist on the reduction of fibrinolytic system activation.

EFFECT OF IL-1 RECEPTOR BLOCKADE ON NEUTROPHIL ACTIVATION

Neutrophil elastase- α_1 -antitrypsin complexes were also measured to assess neutrophil activation in these patients. Levels of neutrophil elastase- α_1 -antitrypsin gradually declined in both interleukin-1 receptor antagonist treatment groups, notably within 24 hours after the onset of the infusion. In the high-dose group, a significant decrease in neutrophil elastase- α_1 -antitrypsin levels was observed at $t=72$ hours compared with baseline values ($P<.05$) (Table 3). By contrast, the levels of neutrophil elastase and antitrypsin remained unchanged in the placebo group (**Figure 4**).

IL-1 RECEPTOR BLOCKADE AND PLASMA LEVELS OF PLA₂

The activity of phospholipase A₂ is suggested to be the rate-limiting step in the biosynthesis of arachidonic acid metabolites.⁴³ Therefore, levels of sPLA₂ were measured to estimate the in vivo effect of IL-1 receptor blockade on the formation of proinflammatory lipid mediators. Baseline levels of sPLA₂ were comparable between all three groups (**Figure 5**). The levels of sPLA₂ remained unchanged during the 72-hour observation period in the placebo group, whereas those in the low-dose and high-dose groups declined significantly from baseline values from 24 hours onward (Table 3). In the high-dose group, the levels were significantly lower at two time points ($P<.05$) when compared with those in the placebo group (Figure 5).

COMMENT

The cytokines TNF- α and IL-1 are presumed to initiate many aspects of the systemic inflammatory response via activation of various mediator systems. However, the relative contribution of TNF- α and IL-1 to this host response remains unclear. The relative role of IL-1 as a proximal signal in this process was investigated by serially evaluating plasma levels of purported IL-1-inducible inflammatory mediators in patients with sepsis syndrome during infusion of a low or high dose of interleukin-1 receptor antagonist. During such interleukin-1 receptor

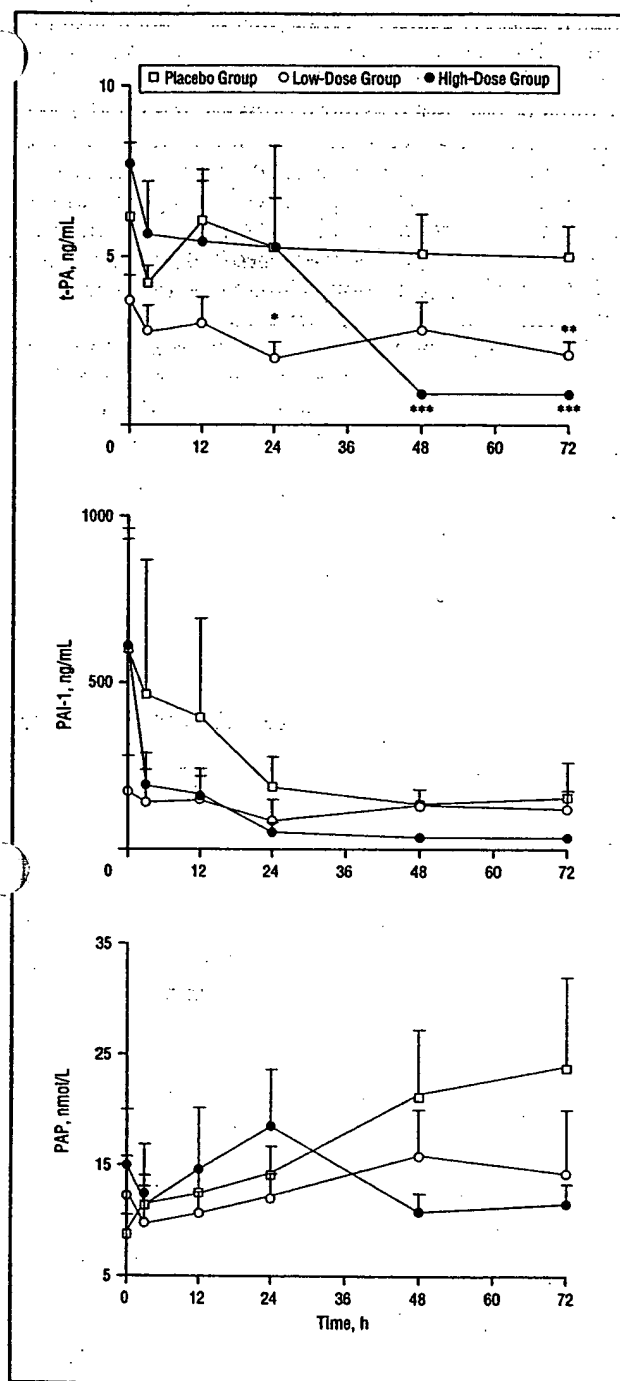


Figure 3. Interleukin-1 receptor blockade and the fibrinolytic system: mean \pm SEM plasma concentrations of tissue-type plasminogen activator (t-PA) (top), plasminogen activator inhibitor type 1 (PAI-1) (center), and plasmin- α_2 -antiplasmin (PAP) (bottom) complexes during a 72-hour infusion period in placebo and low-dose (1 mg/kg per hour) and high-dose (2 mg/kg per hour) interleukin-1 receptor antagonist groups. Significant differences between placebo and respective interleukin-1 receptor antagonist treatment groups are indicated by an asterisk ($P < .05$), double asterisks ($P < .005$), and triple asterisks ($P < .001$) (Mann-Whitney U test).

Antagonist treatment, levels of IL-6 and, to a lesser extent, IL-8 were significantly reduced compared with levels prior to intervention. The levels of such secondary mediators in the placebo group remained unchanged. It was similarly observed that measures of the complement, coagulation, and fibrinolytic system activation also

declined in interleukin-1 receptor antagonist-treated patients without a comparable reduction in the placebo group. Finally, levels of neutrophil elastase and soluble PLA₂ also decreased during the 72-hour treatment period, particularly in the high-dose interleukin-1 receptor antagonist treatment group.

Although a limited number of patients were studied, the levels of inflammatory mediators of the three patient groups were comparable at the time of study entry. Although the mean baseline levels in the high-dose group were higher than those in the low-dose or placebo groups for six of nine measured variables, further comparison of initial APACHE III scores as well as demographic data revealed an equal distribution of these variables among the three study groups.

Changes in secondary mediator levels over time were most prominent in the high-dose interleukin-1 receptor antagonist group. For those parameters in which a reduction in secondary molecules was noted, this generally occurred to a greater extent in the high-dose interleukin-1 receptor antagonist group, further suggesting a dose-dependent influence of interleukin-1 receptor antagonist treatment. This trend was further supported by the course of changes in inflammatory mediator levels following completion of the 72-hour interleukin-1 receptor antagonist treatment period. Plasma samples were also obtained 24 hours after the planned discontinuation of interleukin-1 receptor antagonist infusion in 16 patients. At this time point, several levels of inflammatory mediators increased in patients treated just prior with interleukin-1 receptor antagonist: IL-6 (five of nine patients), IL-8 (four of 10), C3a (five of nine), TAT (three of 10), and PAP (four of 10). This occurred despite the fact that a progressive decrease in the levels of these variables had been observed in all these patients in the preceding 48 to 72 hours. By contrast, none of the patients in the placebo group ($n=5$) sampled at this time point demonstrated change in measured variables (data not shown).

The detection of circulating IL-1 β in patients with sepsis has been noted in up to 37% of patients with sepsis,^{35,44-46} and such results may be influenced by the assay methods.⁴⁷ A very low incidence of detectable IL-1 β was observed in our study. This may be because we collected the initial blood sample just prior to the start of treatment (12 to 24 hours after admission to the intensive care unit). This may also explain why TNF- α was also seldom detected. In patients with sepsis, TNF- α is rapidly eliminated from the circulatory system.⁴⁶ The current study underscores the concept that a lack of detection of IL-1 β in the plasma may not reflect activity at the tissue level.

Numerous studies have implicated a key role for IL-1 in the activation and release of various inflammatory mediators, either directly or via the induction of IL-6 and other cytokines.^{13,16,17,48} In accord with the stimulating effect of exogenous interleukin-1 α on the release of IL-6 observed in nonhuman primates,¹⁰ IL-1 receptor blockade attenuated circulating levels of IL-6 during human sepsis. In addition, plasma IL-6 responses to lethal *E coli* shock are significantly diminished by interleukin-1 receptor antagonist treatment in baboons.²⁸ Earlier phase

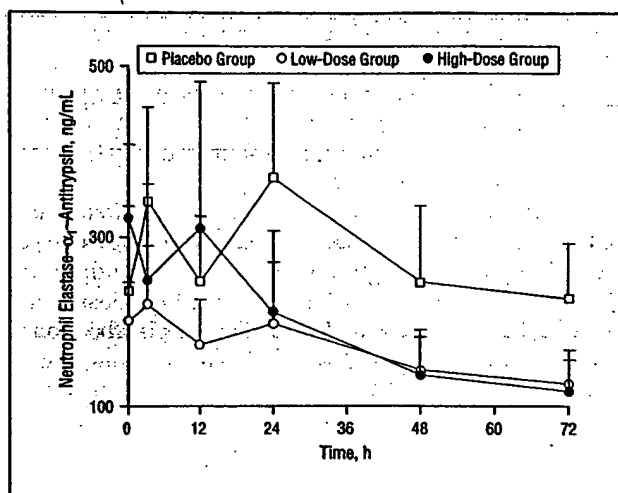


Figure 4. Interleukin-1 receptor blockade and neutrophil activation: mean \pm SEM plasma concentrations of neutrophil elastase- α_1 -antitrypsin complexes during a 72-hour infusion period in placebo and low-dose (1 mg/kg per hour) and high-dose (2 mg/kg per hour) interleukin-1 receptor antagonist groups.

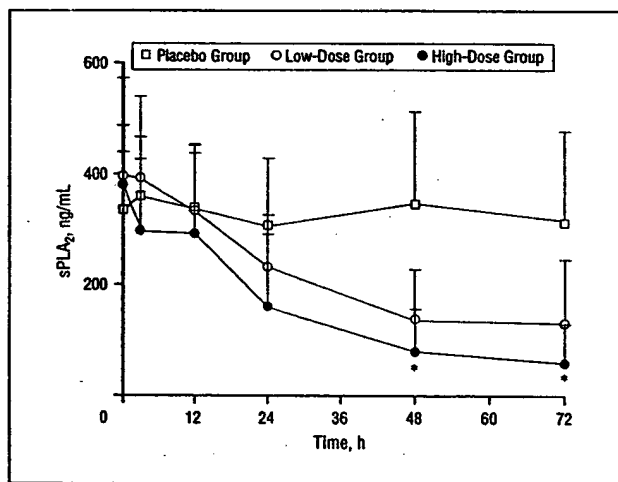


Figure 5. Interleukin-1 receptor blockade and phospholipase A_2 : mean \pm SEM plasma concentrations of secretory phospholipase A_2 (sPLA₂) during a 72-hour infusion period in placebo and low-dose (1 mg/kg per hour) and high-dose (2 mg/kg per hour) interleukin-1 receptor antagonist groups. Significant differences between the placebo and high-dose interleukin-1 receptor antagonist treatment groups are indicated by an asterisk ($P < .05$) (Mann-Whitney U test).

II results also demonstrated a dose-proportional reduction of IL-6 levels during interleukin-1 receptor antagonist treatment.⁴⁹ This effect may well be of clinical importance because increased IL-6 levels have been found to predict a fatal outcome in patients with sepsis syndrome.^{44,50,51} To what extent this reduction in IL-6 levels exerts a direct influence on other mediator systems remains to be determined.

Neutrophil activation and migration⁵² is influenced by IL-8, and levels of this cytokine increase during intravenous administration of interleukin-1 α in primates¹⁴ and are also elevated during human sepsis.³⁶ In accordance with the lack of significant reduction in IL-8 levels during interleukin-1 receptor antagonist treatment in the present study, Fischer et al²⁸ observed no effect of IL-1 receptor blockade on circulating levels of IL-8 in baboons with sep-

sis. No data are available on the role of IL-1 in the induction of IL-8 in patients with clinical sepsis, and our data provide no evidence to suggest a significant role for IL-1 in the appearance of IL-8 during sepsis. Interestingly, however, interleukin-1 receptor antagonist treatment did produce a decrease in levels of circulating neutrophil elastase (complexed to α_1 -antitrypsin), which suggests diminished activation and degranulation of neutrophils. In agreement herewith, in rabbits challenged with endotoxin or *E coli*, neutrophil aggregation in lung tissue was reduced by interleukin-1 receptor antagonist treatment.^{9,29} In vitro studies have shown that interleukin-1 receptor antagonist can bind to type II IL-1 receptors on human neutrophils,⁵³ whereas the ex vivo experiments of Fasano et al²⁵ have demonstrated an increased expression of IL-1 receptors in patients with sepsis syndrome.²⁵ Thus, our results suggest that IL-1 is involved in neutrophil activation in patients with sepsis syndrome.

Complement activation during severe infection is generally considered to result from a direct interaction of complement proteins with bacteria. A complement activation mechanism induced by IL-1 has yet to be described. However, evidence for the existence of a cytokine-inducible pathway has been provided by evaluation of the complement system in patients with cancer who received immunotherapy with recombinant interleukin-2. In these patients, administration of recombinant interleukin-2 yielded a dose-dependent increase in plasma levels of C3a, indicating activation of the complement system.⁵⁴ This complement activation was presumed to be an indirect effect of recombinant interleukin-2 administration, probably via the induction of other cytokines, because in vitro recombinant interleukin-2 did not activate the complement system.⁵⁴ De Boer et al⁵⁵ found a biphasic activation pattern of complement activation in baboons challenged with live *E coli*, the second phase starting 4 to 6 hours after the challenge, at which time the infused microorganisms had been cleared from the circulatory system. In the present study, we observed a dose-dependent reduction in circulating C3a levels during interleukin-1 receptor antagonist infusion, which suggests that an endogenous activation mechanism of complement by IL-1 may occur in patients with severe infection. As neutrophilic proteinases are able to cleave complement factors,⁵⁶ the effect of IL-1 on the activation and degranulation of neutrophils may be significant in this respect. It is noteworthy that activation of the complement system, as reflected by elevated plasma levels of C3a and C4a, correlates with a fatal outcome in patients with sepsis.⁵⁷ Thus, reduction of complement activation via inhibition of IL-1 may be of clinical importance.

Disseminated intravascular coagulation is a major complication of sepsis and results from disturbances of the hemostatic balance of the vascular endothelium. Following endothelial damage, the coagulation system in plasma is activated. This system consists of two cascades, ie, the extrinsic or tissue factor pathway and the intrinsic pathway or contact system of coagulation. Activation of the coagulation system via either route can be quantified by assessment of plasma levels of thrombin complexed to its specific inhibitor, antithrombin III (TAT complexes). This coagulative response is accompanied by a biphasic change

in the fibrinolytic system involving initial stimulation and subsequent inhibition of plasminogen activation^{58,59} as measured by plasma levels of plasminogen complexed to its inhibitor, α_2 -antiplasmin (PAP complexes). In both experimental endotoxemia and septic shock, activation of fibrinolysis is evident by an early increase in t-PA activity followed by a decline that is coincident with the appearance of the main inhibitor of t-PA (PAI-1).^{59,60} A similar pattern has been demonstrated following a TNF challenge in healthy volunteers: the coagulative response is favored as the fibrinolytic response is inhibited after its initial increase.^{20,21} Interleukin-1 receptor blockade markedly attenuated activation of coagulation in our patients, as was evident from the course of TAT complexes. These results are in agreement with in vitro data demonstrating that IL-1 enhances tissue factor expression on human endothelial cells,⁶¹ thereby inducing activation of the extrinsic pathway of coagulation. Furthermore, cultured endothelial cells release PAI-1 in response to TNF and IL-1.^{23,62}

The increase of PAI-1 levels in human sepsis is further documented by our data, which also suggest that IL-1 also stimulates activation of the fibrinolytic system by inducing the release of t-PA and the activation of plasminogen. Conversely, both TNF and IL-1 diminish the secretion of t-PA by cultured human endothelial cells.^{23,62} Thus, the in vivo behavior of TNF in human volunteers as well as our data illustrate a discrepancy between in vitro results and the in vivo situation. Alternatively, thrombin potentially induces the release of t-PA and PAI-1.⁶³ As interleukin-1 receptor antagonist treatment induced decreased circulating TAT complex levels, the decreased release of t-PA and its inhibitor also may have been due to a diminished thrombin formation following interleukin-1 receptor antagonist infusion.

Arachidonic acid derivatives (eicosanoids), such as thromboxane A₂, leukotrienes, and prostaglandins, have potent effects on platelets and neutrophils as well as alter vascular permeability and tissue blood flow.⁶⁴ The release of arachidonic acid from membrane phospholipids is ascribed largely to the hydrolytic action of PLA₂.⁴³ Moreover, PLA₂ is a key regulatory enzyme for the production of platelet activating factor, which has also been implicated as an important mediator of sepsis and septic shock.^{19,65} Elevated levels of secretory PLA₂ correlate to hypotension and pulmonary changes (adult respiratory distress syndrome) in patients with sepsis.^{66,67} In vitro studies have demonstrated that TNF, IL-1, and IL-6 may induce secretion of PLA₂ by various cell types, such as hepatoma cells.⁶⁸ Redl et al⁶⁹ recently confirmed the role of TNF as a mediator of PLA₂ in baboons with sepsis. Our data further extend the in vivo role of cytokines toward the release of PLA₂ by demonstrating that IL-1 receptor blockade induced a dose-dependent decrease of PLA₂ levels.

Our results lead us to conclude that the activation and/or release of inflammatory mediators during severe infection is at least partly attributable to IL-1 activity. The current results further substantiate a pivotal role for this cytokine in the pathogenesis of a generalized host inflammatory response. The attenuation of coagulation, fibrinolytic and complement activation variables, levels of secretory PLA₂, and, to a lesser extent, neutrophil elastase during interleukin-1 receptor antagonist treatment are consistent with the increase

in survival time in patients with disseminated intravascular coagulation or adult respiratory distress syndrome present at study entry, as observed in a previously reported multicenter phase III trial²⁰ in which these patients were accrued. Although this trial did not achieve a statistically significant reduction in the all-cause 28-day mortality rate in interleukin-1 receptor antagonist-treated patients, the current data demonstrate that interleukin-1 receptor antagonist treatment diminishes the appearance of several inflammatory variables and the alterations of coagulation and/or fibrinolysis pathways. These observations lend further support to the concept that IL-1 activity is of importance in the pathogenesis of the more severe manifestations of the systemic inflammatory response syndrome.

Accepted for publication April 2, 1995.

This research was supported in part by grant RO1 GM-34695 from the US Public Health Service, Bethesda, Md.

The human sPLA₂ was donated by F. B. Taylor, Jr, Oklahoma Medical Research Foundation, Oklahoma City. Purified recombinant human sPLA₂ was donated by C. Schalkwijk, Center for Biomembranes and Lipid Enzymology, University of Utrecht (the Netherlands).

We wish to thank Alexander J. P. Houdijk, MD, Anke M. Eerenberg, and Robert I. C. Wesdorp, MD, PhD, for their contribution to the completion of this study. We also wish to thank Charlotte C. Ferwerda for her assistance in the collection of blood samples from patients at the Free University Hospital and Lynn Wood-Keogh for her editorial assistance in the completion of this manuscript.

Stephen F. Lowry, MD, a member of the Editorial Board of the ARCHIVES, received a BA degree magna cum laude from Ohio Wesleyan University, Delaware, Ohio, and an MD degree from the University of Michigan, Ann Arbor. He holds membership in Phi Beta Kappa and Alpha Omega Alpha Honor Medical Society. Dr Lowry is presently professor of surgery at the Cornell University Medical Center.

Reprints not available.

REFERENCES

1. Fong Y, Moldawer LL, Shires GT, Lowry SF. The biologic characteristics of cytokines and their implication in surgical injury. *Surg Gynecol Obstet.* 1990; 170:363-378.
2. Michie HR, Manogue KR, Spriggs DR, et al. Detection of circulating tumor necrosis factor after endotoxin administration. *N Engl J Med.* 1988;318:1481-1486.
3. Cannon JG, Tompkins RG, Gelfand JA, et al. Circulating interleukin-1 and tumor necrosis factor in septic shock and experimental endotoxin fever. *J Infect Dis.* 1990;161:79-84.
4. Fong Y, Lowry SF. Tumor necrosis factor in the pathophysiology of infection and sepsis. *Clin Immunol Immunopathol.* 1990;55:157-170.
5. Calandra T, Baumgartner J, Grau GE, et al. Prognostic values of tumor necrosis factor/cachectin, interleukin-1, interferon- α , and interferon- γ in the serum of patients with septic shock. *J Infect Dis.* 1990;161:982-987.
6. Tracey KJ, Beutler B, Lowry SF, et al. Shock and tissue injury induced by recombinant human cachectin. *Science.* 1986;234:470-474.
7. Tracey KJ, Lowry SF, Fahey III TJ, et al. Cachectin/tumor necrosis factor induces lethal shock and stress hormone responses in the dog. *Surg Gynecol Obstet.* 1987;164:415-422.
8. Okusawa S, Gelfand JA, Ikejima T, Connolly RJ, Dinarello CA. Interleukin 1 induces a shock-like state in rabbits: synergism with tumor necrosis factor and the effect of cyclooxygenase inhibition. *J Clin Invest.* 1988;81:1162-1172.
9. Ohlsson K, Bjork P, Bergenfeldt M, Hageman R, Thompson RC. Interleukin-1 receptor antagonist reduces mortality from endotoxin shock. *Nature.* 1990; 348:550-552.
10. Fischer E, Marano MA, Barber AE, et al. Comparison between effects of interleukin-1 α administration and sublethal endotoxemia in primates. *Am J Physiol.*

- 1991;261:R442-R452.
11. Waage A, Espevik T. Interleukin-1 potentiates the lethal effect of tumor necrosis factor alpha/cachectin in mice. *J Exp Med.* 1988;167:1987-1992.
12. Fong Y, Tracey KJ, Moldawer LL, et al. Antibodies to cachectin/tumor necrosis factor reduce interleukin 1 β and interleukin 6 appearance during lethal bacteremia. *J Exp Med.* 1989;170:1627-1633.
13. Gershengwald JE, Fong Y, Fahey III TJ, et al. Interleukin 1 receptor blockade attenuates the host inflammatory response. *Proc Natl Acad Sci U S A.* 1990; 87:4966-4970.
14. Van Zee KJ, DeForge LE, Fisher E, et al. IL-8 in septic shock, endotoxemia, and after IL-1 administration. *J Immunol.* 1991;146:3478-3482.
15. Redl H, Schlag G, Bahrami U, Schade M, Ceska M, Stütz P. Plasma neutrophil-activating peptide-1/interleukin-8 and neutrophil elastase in a primate bacteremia model. *J Infect Dis.* 1991;164:383-388.
16. Dinarello CA. Interleukin-1 and interleukin-1 antagonism. *Blood.* 1991;77:1627-1652.
17. Ikejima T, Okusawa S, Ghezzi P, van der Meer JWM, Dinarello CA. Interleukin-1 induces tumor necrosis factor in human peripheral blood mononuclear cells in vitro and a circulating TNF-like activity in rabbits. *J Infect Dis.* 1990; 162:215-223.
18. Dinarello CA, Cannon JG, Wolff SM, et al. Tumor necrosis factor (cachectin) is an endogenous pyrogen and induces production of interleukin 1. *J Exp Med.* 1986;163:1433-1450.
19. Fletcher JR, Di Simone AG, Earnest MA. Platelet activating factor receptor antagonist improves survival and attenuates elcosanoid release in severe endotoxemia. *Ann Surg.* 1990;211:312-316.
20. Van der Poll T, Büller HR, ten Cate H, et al. Activation of coagulation after administration of tumor necrosis factor to normal subjects. *N Engl J Med.* 1990;322:1622-1627.
21. Van der Poll T, Levi M, Büller HR, et al. Fibrinolytic response to tumor necrosis factor 26 in healthy subjects. *J Exp Med.* 1991;174:729-732.
22. Nawroth PP, Handley DA, Esmon CT, Stern DM. Interleukin-1 induces endothelial cell procoagulant while suppressing cell surface anticoagulant activity. *Proc Natl Acad Sci U S A.* 1986;83:3460-3464.
23. Emeis JJ, Koolstra T. Interleukin-1 and lipopolysaccharide induce an inhibitor of tissue-type plasminogen activator in vivo and in cultured endothelial cells. *J Exp Med.* 1986;163:1260-1266.
24. Van der Poll T, van Deventer SJH, Hack CE, et al. Effects on leukocytes after injection of tumor necrosis factor into healthy humans. *Blood.* 1992;79:693-698.
25. Fasano MB, Cousart S, Neal S, McCall CE. Increased expression of the interleukin 1 receptor on blood neutrophils of humans with the sepsis syndrome. *J Clin Invest.* 1991;88:1452-1459.
26. Arend WP, Joslin FG, Thompson RC, Hannum CH. An IL-1 inhibitor from human monocytes: production and characterization of biologic properties. *J Immunol.* 1989;143:1851-1858.
27. Eisenberg SP, Evans RJ, Arend WP, et al. Primary structure and functional expression from complementary DNA of a human interleukin-1 receptor antagonist. *Nature.* 1990;343:341-346.
28. Fischer E, Marano MA, Van Zee, et al. Interleukin-1 receptor blockade improves survival and hemodynamic performance in *Escherichia coli* septic shock, but fails to alter host response to sublethal endotoxemia. *J Clin Invest.* 1992; 89:1551-1557.
29. Wakabayashi G, Gelfand JA, Burke JF, Thompson RC, Dinarello CA. A specific receptor antagonist for interleukin 1 prevents *Escherichia coli*-induced shock in rabbits. *FASEB J.* 1991;5:338-343.
30. Fisher CJ Jr, Dhainaut JA, Opal SM, et al. An evaluation of recombinant human interleukin-1 receptor antagonist in the treatment of patients with sepsis syndrome: results from a randomized, double-blind, placebo-controlled trial. *JAMA.* 1994;271:1836-1843.
31. Knaus WA, Wagner DP, Draper EA, et al. The APACHE III Prognostic System: risk prediction of hospital mortality for critically ill hospitalized adults. *Chest.* 1991;100:1619-1636.
32. Kenney JS, Masada MP, Engul EM, Delustro BM, Mulkins MA, Allison AC. Monoclonal antibodies to human recombinant interleukin 1 (IL-1) beta: quantitation of IL-1 beta and inhibition of biological activity. *J Immunol.* 1987;138:4236-4240.
33. Hesse DG, Tracey KJ, Fong Y, et al. Cytokine appearance in human endotoxemia and primate bacteremia. *Surg Gynecol Obstet.* 1988;166:147-153.
34. Helle M, Boelje L, de Groot ER, de Vos A, Aarden LA. Sensitive ELISA for interleukin-6: detection of IL-6 in biological fluids, synovial fluids and sera. *J Immunol Methods.* 1991;38:47-56.
35. Brakenhoff JPJ, de Groot ER, Evers RF, Pannekoek H, Aarden LA. Molecular cloning and expression of hybridoma growth factor in *Escherichia coli*. *J Immunol.* 1987;39:4116-4121.
36. Hack CE, Hart M, Strack van Schijndel RJM, et al. Interleukin-8 in sepsis: relation to shock and inflammatory mediators. *Infect Immun.* 1992;60:2835-2842.
37. Hack CE, Paardekooper J, Eerenberg AJM, et al. A modified competitive inhibition radioimmunoassay for the detection of C3a: use of 125I-C3 instead of 125I-C3a. *J Immunol Methods.* 1988;108:77-84.
38. Van Zonneveld AJ, Veerman H, Brakenhoff JPJ, Aarden LA, Cajot JF, Pannekoek H. Mapping of epitopes on human tissue-type plasminogen activator with recombinant deletion mutant proteins. *Thromb Haemost.* 1987;57:82-86.
39. Levi M, de Boer JP, Roem D, ten Cate JW, Hack CE. Plasminogen activation in vivo upon intravenous infusion of DDAVP: quantitative assessment of plasmin- α_2 -antiplasmin complex with a novel monoclonal antibody based radioimmunoassay. *Thromb Haemost.* 1992;67:111-116.
40. De Boer JP, Abbink JJ, Brouwer MC, et al. PAI-1 synthesis in the human hepatoma cell line Hep G2 is increased by cytokines: evidence that the liver contributes to acute phase behavior of PAI-1. *Thromb Haemost.* 1991;65:181-185.
41. Nuijens JH, Abbink JJ, Wachtvogel YT, et al. Plasma elastase- α_1 -antitrypsin and lactoferrin in sepsis: evidence for neutrophils as mediators in fatal sepsis. *J Lab Clin Med.* 1992;119:159-168.
42. Smith GM, Ward RL, McGuigan L, Rajkovic IA, Scott KF. Measurement of human phospholipase A₂ in arthritis plasma using a newly developed sandwich ELISA. *Br J Rheumatol.* 1992;31:175-178.
43. Irvine RF. How is the level of free arachidonic acid controlled in mammalian cells? *Biochem J.* 1982;204:3-16.
44. Casey LC, Balk RA, Bone RC. Plasma cytokine and endotoxin levels correlate with survival in patients with the sepsis syndrome. *Ann Intern Med.* 1993;119:771-778.
45. Girardin E, Grau GE, Dayer JM, Roux-Lombard P, the J5 Study Group, Lambert PH. Tumor necrosis factor and interleukin-1 in the serum of children with severe infectious purpura. *N Engl J Med.* 1988;319:397-400.
46. Waage A, Brandtzaeg P, Halstensen A, Kierulf P, Espevik T. The complex pattern of cytokines in serum from patients with meningococcal septic shock. *J Exp Med.* 1989;169:333-338.
47. Dinarello CA, Cannon JG. Cytokine measurements in septic shock. *Ann Intern Med.* 1993;119:853-854.
48. Granowitz EV, Clark BD, Vannier E, Callahan MV, Dinarello CA. Effect of interleukin-1 (IL-1) blockade on cytokine synthesis, I: IL-1 receptor antagonist inhibits IL-1-induced cytokine synthesis and blocks the binding of IL-1 to its type II receptor on human monocytes. *Blood.* 1992;79:2356-2363.
49. Fisher CJ Jr, Slotman GJ, Opal SM, et al. Initial evaluation of human recombinant interleukin-1 receptor antagonist in the treatment of sepsis syndrome: a randomized, open-label, placebo-controlled trial. *Crit Care Med.* 1994;22:12-21.
50. Hack CE, de Groot ER, Felt-Bersma RJF, et al. Increased plasma levels of interleukin-6 in sepsis. *Blood.* 1989;74:1704-1710.
51. Fisher CJ Jr, Opal SM, Dhainaut JF, et al. Influence of an anti-tumor necrosis factor monoclonal antibody on cytokine levels in patients with sepsis. *Crit Care Med.* 1993;21:318-327.
52. Hechtman DH, Cybulsky MI, Fuchs HJ, Baker JB, Gimbrone MA. Intravascular IL-8: inhibitor of polymorphonuclear leukocyte accumulation at sites of acute inflammation. *J Immunol.* 1991;147:883-892.
53. Dripps DJ, Verderber E, Ng RK, Thompson RC, Eisenberg SP. Interleukin-1 receptor antagonist binds to the type II interleukin-1 receptor on B cells and neutrophils. *J Biol Chem.* 1991;266:20311-20315.
54. Thijs LG, Hack CE, Strack van Schijndel RJM, et al. Activation of the complement system during immunotherapy with recombinant IL-2: relation to the development of side effects. *J Immunol.* 1990;144:2419-2424.
55. De Boer JP, Creasey AA, Chang A, et al. Activation of the complement system in baboons challenged with live *E coli*: correlation with mortality and evidence for a biphasic activation pattern. *Infect Immun.* 1993;61:4293-4301.
56. Perez HD, Ohtani O, Banda D, Ong R, Fukuyama K, Goldstein IM. Generation of biologically active complement (C5)-derived peptides by cathepsin H. *J Immunol.* 1983;131:397-402.
57. Hack CE, Nuijens JH, Felt-Bersma RJF, et al. Elevated plasma levels of the anaphylatoxins C3a and C4a are associated with a fatal outcome in sepsis. *Am J Med.* 1989;86:20-26.
58. Brandtzaeg P, Joo GB, Brusletto B, Kierulf P. Plasminogen activator inhibitor 1 and 2, α_2 -antiplasmin, plasminogen, and endotoxin levels in systemic meningococcal disease. *Thromb Res.* 1990;57:271-278.
59. De Boer JP, Creasey AA, Chang A, et al. Activation patterns of coagulation and fibrinolysis in baboons following infusion with lethal or sublethal dose of *Escherichia coli*. *Circ Shock.* 1991;39:59-67.
60. Van Deventer SJH, Büller HR, ten Cate JW, Aarden LA, Hack CE, Sturk A. Experimental endotoxemia in humans: analysis of cytokine release and coagulation, fibrinolytic, and complement pathway. *Blood.* 1990;76:2520-2526.
61. Bevilacqua MP, Pober JS, Majumdar GR, Cotran RS, Gimbrone MA Jr. Interleukin-1 (IL-1) induces biosynthesis and cell surface expression of procoagulant activity in human vascular endothelial cells. *J Exp Med.* 1984;160:618-623.
62. Schieff RR, Bevilacqua MP, Sawdey M, Gimbrone MA Jr, Loskutoff DJ. Cytokine activation of vascular endothelium: effects on tissue-type plasminogen activator and type I plasminogen activator inhibitor. *J Biol Chem.* 1988;263:5797-5803.
63. Gelehrter TD, Szyner-Laszuk R. Thrombin induction of plasminogen activator-inhibitor in cultured human endothelial cells. *J Clin Invest.* 1986;77:165-169.
64. Bone RC. Phospholipids and their inhibitors: a critical evaluation of their role in the treatment of sepsis. *Crit Care Med.* 1992;20:884-890.
65. Anderson BO, Bensard DD, Harken AH. The role of platelet-activating factor and its antagonists in shock, sepsis, and multiple organ failure. *Surg Gynecol Obstet.* 1991;172:415-424.
66. Vadas P. Elevated plasma phospholipase A₂ levels: correlation with the hemodynamic and pulmonary changes in gram-negative septic shock. *J Lab Clin Med.* 1984;104:873-881.
67. Vadas P, Pruzanski W, Stefanski E, et al. Pathogenesis of hypotension in septic shock: correlation of circulating phospholipase A₂ levels with circulatory collapse. *Crit Care Med.* 1988;16:1-7.
68. Crowl RM, Stoller TJ, Conroy RR, Stoner CR. Induction of phospholipase A₂ gene expression in human hepatoma cells by mediators of the acute phase response. *J Biol Chem.* 1991;266:2647-2651.
69. Redl H, Schlag G, Schleiber A, Davies J. Tumor necrosis factor is a mediator of phospholipase release during bacteremia in baboons. *Am J Physiol.* 1993; 264:H2119-H2123.

Severity and Mortality of Experimental Pancreatitis Are Dependent on Interleukin-1 Converting Enzyme (ICE)

NORMAN

JUN YANG,¹ GREGORY FINK,¹ GAY CARTER,¹ GEORGE KU,²
WOODY DENHAM,¹ and DAVID LIVINGSTON²

ABSTRACT

Interleukin-1 β (IL-1 β) is produced in large amounts during acute pancreatitis and is believed to play a role in disease progression. Because secretion of IL-1 β is dependent on intracellular processing of pro-IL-1 β by IL-1 converting enzyme (ICE), we aimed to determine the efficacy of a novel ICE inactivator (VE-13045) in inhibiting secretion of active IL-1 β *in vivo* and if the loss of ICE activity would affect the severity and mortality of experimental pancreatitis. Severe hemorrhagic pancreatitis was induced in adult rats by infusion of bile acid into the pancreatic duct. Animals were randomized to receive VE-13045 or vehicle before induction of pancreatitis. To confirm our findings and to ensure that the results were not model dependent, a second series of experiments was conducted using mice possessing a homozygous knockout of the ICE gene in which lethal pancreatitis was induced by feeding a choline-deficient, ethionine-supplemented diet. The severity of pancreatitis was assessed for both experiments by standard surrogate markers, blind histologic grading, and serum IL-1 β and tumor necrosis factor- α (TNF- α) levels. Pancreatic IL-1 β mRNA induction was assessed by differential RT-PCR. Acute pancreatitis was associated with a 120-fold increase in IL-1 β mRNA, which was not affected by ICE inhibition or gene deletion. Cytokine processing and secretion were affected, as evidenced by decreased serum levels of IL-1 β and TNF- α ($p < 0.001$) in all animals with an inactive ICE enzyme. This lack of cytokine production increased survival from 32% to 78% following bile salt pancreatitis ($p < 0.01$) and from 24% to 80% following diet-induced pancreatitis ($p < 0.005$). Both ICE-defective groups demonstrated decreased pancreatic necrosis, edema, inflammation, wet weight (all $p < 0.05$), and amylase and lipase ($p < 0.01$). *In vivo* blockade or genetic deletion of ICE inhibits pancreatitis-induced secretion of proinflammatory cytokines without altering IL-1 mRNA production and is associated with decreased pancreatitis severity and dramatic survival benefits.

INTRODUCTION

THE CYTOKINE INTERLEUKIN-1 β (IL-1 β) plays a pivotal role in acute inflammatory conditions and recently has been implicated in the pathogenesis of acute pancreatitis, a noninfectious inflammatory condition of the pancreas.⁽¹⁻³⁾ Concomitant with the elevation of pancreatic enzymes, IL-1 β can be found in the serum of humans or experimental animals, with serum cytokine levels peaking concomitant with the severity of pancreatic inflammation.⁽⁴⁻⁷⁾ Several studies have demonstrated the production of large amounts of IL-1 β mRNA in the pancreatic parenchyma within hours of the induction of pancreatitis.^(8,9) Soon afterward, IL-1 β gene expression is upregulated in specific distant tissues, such as the liver and lung⁽⁸⁻¹⁰⁾—organs that

characteristically account for the vast majority of pancreatitis-associated morbidity and mortality.^(1,2)

Evidence for the importance of this cytokine in the pathogenesis of pancreatitis has been observed in studies that antagonized circulating IL-1 α and IL-1 β by administration of a recombinant IL-1 receptor antagonist (IL-1Ra). Prophylactic or therapeutic IL-1 blockade was shown to decrease pancreatic destruction and improve survival.⁽¹¹⁻¹³⁾ Furthermore, when acute pancreatitis is induced in animals possessing a homozygous deletion of the IL-1 type 1 receptor (p80), maximal inflammation and pancreatic destruction could not be instilled.⁽¹⁴⁾

IL-1 β is known to be produced as an inactive 31 kDa precursor that undergoes posttranscriptional modification before being secreted.^(3,15-17) This processing is dependent on the cys-

¹Department of Surgery, University of South Florida, Tampa, Florida.

²Vertex Pharmaceuticals Inc., Cambridge, Massachusetts.

teine protease IL-1 converting enzyme (ICE), which cleaves IL-1 β into its active 17 kDa form. Several irreversible peptidyl inactivators of ICE have been reported recently.^(18,19) VE-13045 is one such novel compound that irreversibly and systemically inhibits (inactivates) ICE *in vivo* when administered in the peritoneal cavity. This compound has been shown to decrease lipopolysaccharide (LPS)-induced IL-1 α and IL-1 β secretion and to block the progression of chronic collagen-induced polyarthritis in mice.⁽¹⁹⁾ This compound is not active in these models when administered orally.

The current study was designed to further delineate the importance of IL-1 in the development of pancreatitis and to investigate the mechanism by which it is produced in the course of this disease. Additionally, the *in vivo* efficacy of the ICE inhibitor VE-13045 in decreasing pancreatitis-associated cytokine release and its effects on the severity and mortality of severe lethal pancreatitis were assessed.

MATERIALS AND METHODS

Animal models

Animal studies were performed at an AAALAC-accredited facility in accordance with the Department of Laboratory Animal Medicine at the University of South Florida. Severe lethal pancreatitis was induced by one of two well-described models.

In the first method, acute hemorrhagic necrotizing pancreatitis was induced by the retrograde infusion of bile acid into the pancreatic duct of rats.⁽¹³⁾ Briefly, adult male Sprague-Dawley rats ($n = 24$) (250–300 g) were fasted for 24 h and then anesthetized with sodium pentobarbital (50 mg/kg). The duodenum was exposed through an upper midline incision using aseptic technique. The pancreatic duct was cannulated under 10 \times magnification with PE-10 tubing transduodenally and tied into place around the proximal biliopancreatic duct. A non-crushing clamp was placed across the hepatoduodenal ligament to prevent the injectate from ascending into the biliary tree and liver. Glycodeoxycholic acid (1 mg/kg of 4% solution in phosphate-buffered saline, PBS) (Sigma, St Louis, MO) was injected into the bile duct over 10 min at a pressure never exceeding 10 cm H₂O using a Harvard pump with an inline pressure transducer. Following the injection, the catheter and clamp were removed, and the abdomen was closed in layers. Sham animals ($n = 8$) underwent identical surgical procedures and duct cannulation without bile acid injection.

Inhibition of the ICE enzyme during bile acid pancreatitis was established by the i.p. administration of VE-13045 (15 mg/kg) (Vertex Pharmaceuticals, Cambridge, MA), a recently described irreversible inhibitor of ICE.^(18,19) The antagonist or vehicle was administered to random animals 2 h before and 8 h after pancreatitis induction. The compound was formulated for i.p. administration in olive oil:ethanol:DMSO (90:5:5, v/v/v) as described in Ku et al.⁽¹⁹⁾ The rest of the animals received i.p. injections of vehicle (sterile olive oil) on the same schedule.

The second series of experiments used a model of acute hemorrhagic, necrotizing pancreatitis, which was induced in young female mice (15.4 \pm 0.7 g) by feeding of a choline-deficient,

ethionine-supplemented (CDE) diet (Harlan Teklad, Madison, WI) for 72 h.⁽¹²⁾ Animals were fasted overnight before beginning the diet and were allowed water *ad libitum*. Feeding trays were changed every 6 h to ensure sanitary conditions. Regular chow replaced the experimental diet after 72 h.

Rather than pharmacologic inhibition of ICE, as in the first series of experiments, transgenic C57BL/6 mice possessing a homozygous deletion of the ICE gene ($n = 60$) were used in the CDE model of pancreatitis. Wild-type C57BL/6 animals served as controls ($n = 60$). Transgenic mice with a disrupted ICE gene were provided as a breeding pair as a generous gift from Vertex Pharmaceuticals and the Howard Hughes Medical Institute and were bred in the transgenic facility at the University of South Florida under strict isolation and in compliance with all AAALAC guidelines for the breeding of transgenic animals. Knockout animals used in these experiments have been shown to be homozygous (–/–) for the knockout event by reverse transcription polymerase chain reaction (RT-PCR) of genomic DNA using primers⁽¹⁸⁾ and methods previously described by our laboratory.^(9,14) These animals have been well described and have been shown to lack IL-1 production in *in vitro* experiments.⁽¹⁸⁾ The ICE gene disruption does not affect development, growth rate, or fertility of the animals and does not produce overt effects on the immune system.⁽¹⁸⁾

Pancreatitis severity

The severity of pancreatitis was verified in all animals by blind histologic grading of fixed pancreatic sections (necrosis, vacuolization, edema, and inflammation) as described by our laboratory previously.^(11,12) Severity was also assessed by comparisons of serum amylase, lipase, blood urea nitrogen (BUN), creatinine, and calcium, which were determined on an automated Kodak Ectachem 700 analyzer (Kodak, Rochester, NY). All rats had measurements of ascites volume and pancreatic weight/body weight ratios calculated. The CDE model in the mouse does not allow for these measurements.^(11,12)

Tissue preparation

Following pentobarbital anesthesia (50 mg/kg i.p.), a minimum of 6 surviving animals from each experimental group were killed during maximal pancreatitis (rats at 24 h, mice at 72 h) by exsanguination via cardiocentesis. These time points are well established for both models of pancreatitis to coincide with maximal pancreatic inflammation and cytokine production.^(9–14) Intracardiac injection of sterile PBS was used to purge the circulatory system, and then the pancreas was immediately excised and divided for light microscopy and RNA determination. Total RNA was isolated by guanidium thiocyanate/acid phenol extraction as previously described.⁽²⁰⁾ The integrity of isolated RNA was verified by equimolar 18S and 28S ribosomal RNA bands following denaturing electrophoresis.

Measurement of tissue cytokine mRNA by quantitative differential RT-PCR

Total cellular RNA was primed using oligo (dt)_{12–15} (Gibco, Gaithersburg, MD) and then reverse transcribed utilizing SuperScript II reverse transcriptase (Gibco). The prepared cDNA was subjected to differential PCR with rat-specific and

murine-specific primers for IL-1 β and β -actin obtained from Stratagene (La Jolla, CA). The sequence for IL-1 β was (rat sense = 5'-CAGGATGAGGACATGAGCAC-C3', and antisense = 5'-CTCTGCAGACTCAAACCTCCA-C3'; murine sense = 5'-CAGGATGAGATGAGCACC-3' and antisense 5'-CTCTGCAGACTCAAACCTCCAC-3'). The sequence for β -actin was (rat sense = 5'-GTGGGCCGCTCTAGGCACCA-3', and antisense 5'-CGGTTGGCCTTAGGGTTCAGGGGGG-3'; and murine sense 5'-GTGGGCCGCTCTAGGCACCA-3' and antisense 5'-CGGTTGGCCTTAGGGTTCAGGGGGG-3'). The IL-1 β cDNA products were coamplified with β -actin for 30 cycles using a UNO-Thermoblock (Biometa, Tampa, FL). The reaction products were subsequently visualized by electrophoresis in 2.5% Metaphor agarose (FMC Bioproducts, Rockland, ME) containing ethidium bromide. Ultraviolet illumination was used to visualize the DNA bands, and the gels were photographed digitally and stored on computer disc. Band intensity was determined by optical density with individual cytokine/ β -actin cDNA ratios compared using Sigma Scan software (Jandel Scientific, San Rafael, CA). All primers are known to span at least one intron. The internal standard (β -actin) has been shown previously by our laboratory to be linear and unaffected by the progression of pancreatitis throughout the time course of the experimental models used.^(8,9,20) Additionally, β -actin maintains a linear relationship with IL-1 β from 20 through 40 amplification cycles.^(9,20) Restriction digestion of the resulting cDNA products via PstI yielded the anticipated 340 and 103 bp fragments (rat IL-1 β and β -actin, respectively) and 17 and 245 bp fragments (murine IL-1 β and β -actin, respectively) (data not shown).

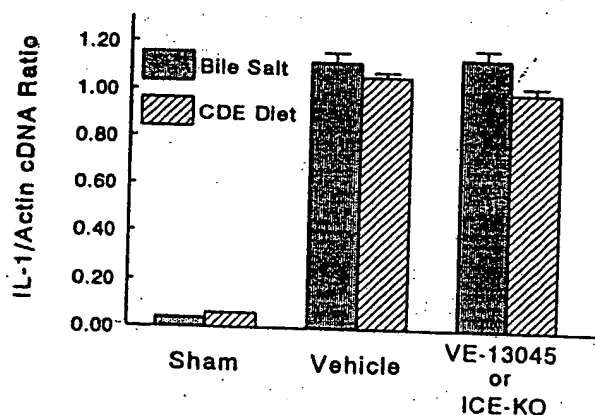


FIG. 1. Intrapancreatic IL-1 β gene induction during severe acute pancreatitis. Two models of pancreatitis are shown. Rats underwent bile salt infusion of the pancreatic duct to produce severe hemorrhagic pancreatitis. Mice were fed a choline-deficient, ethionine-supplemented (CDE) diet to produce severe necrotizing pancreatitis. The cDNA ratios of IL-1 β and the internal standard β -actin are compared after co-amplification via differential RT-PCR for 30 cycles. Sham animals do not develop pancreatitis and show very low constitutive expression of IL-1 β mRNA within pancreatic tissues. The induction of bile salt or CDE diet pancreatitis increases IL-1 β mRNA approximately 120-fold ($p < 0.001$), which is not affected by inactivation of ICE by VE-13045 in rats with bile salt pancreatitis or genetic deletion of the ICE gene in mice with CDE diet-induced pancreatitis.

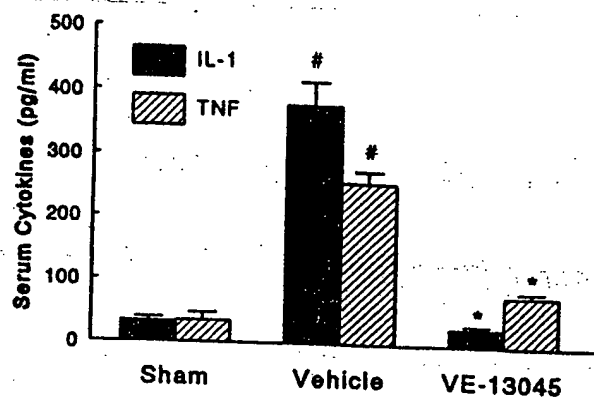


FIG. 2. Serum IL-1 β and TNF- α during bile salt-induced acute pancreatitis. Serum was obtained at 24 h after induction of pancreatitis when pancreatic inflammation and cytokine production are known to be at their peak. Severe pancreatitis is associated with significant elevations in serum IL-1 β and TNF- α ($p < 0.001$ vs. sham, denoted by #). Inhibition of ICE by VE-13045 eliminates the rise in serum IL-1 β while significantly attenuating the rise in TNF- α (both $p < 0.005$ vs. vehicle, denoted by *).

Serum cytokine determination

Serum cytokines were assessed during maximal pancreatitis via murine-specific or rat-specific ELISA as per the manufacturer's direction (Genzyme, Boston, MA). All samples were measured in triplicate by a single investigator (G.K.), who was blinded to treatment group.

Statistical analysis

Results are expressed as means \pm SEM. Statistical analysis was performed using the StatS 3 statistical program (Spreadware, Palm Desert, CA) applying the unpaired two-tailed Student's *t*-test, with significance being assigned to *p* values < 0.05 unless stated otherwise.

RESULTS

Cytokine production

There was little or no constitutive expression of IL-1 β mRNA in the pancreas, although the progression of severe pancreatitis was associated with a near 120-fold increase in the IL-1 β / β -actin mRNA ratio ($p < 0.001$ vs. baseline) (Fig. 1). Administration of the ICE inhibitor VE-13045 had no discernable effect on this upregulation in any of the animals examined ($p = \text{NS}$ compared with sham). Similarly, those animals expressing a homozygous deletion of the ICE gene demonstrated nearly identical upregulation of IL-1 β mRNA in response to the CDE-induced pancreatitis, as did the wild-type animals. Genetic deletion or pharmacologic inactivation of ICE, therefore, had no effect on IL-1 β mRNA induction during pancreatitis.

Both IL-1 and tumor necrosis factor (TNF) protein were absent or present in very low concentrations in the serum of normal animals. Acute pancreatitis was associated with a marked elevation of both these cytokines, which was attenuated signif-

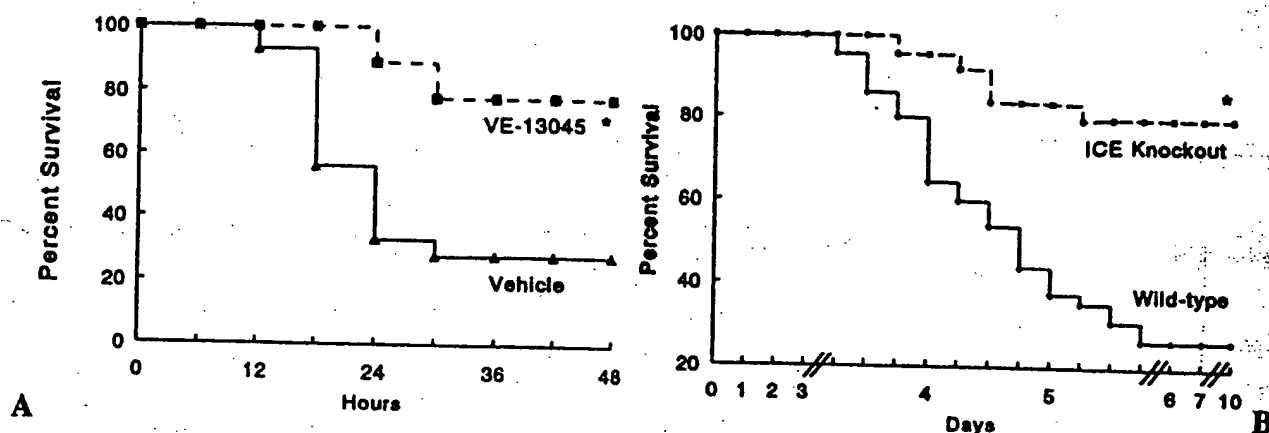


FIG. 3. The effect of ICE inactivation on the mortality of severe pancreatitis. Bile acid-induced pancreatitis ($n = 12/\text{group}$) had a mortality rate of 68%, which was decreased to 22% in those animals receiving the ICE inhibitor VE-13045 (A) ($p < 0.01$, denoted by *). The CDE diet-induced model of pancreatitis ($n = 60/\text{group}$) had a mortality rate of 73% in wild-type animals, which was decreased to 20% in those animals possessing a homozygous deletion of the ICE gene (B) ($p < 0.005$, denoted by *).

icantly in those animals that received the ICE antagonist (both $p < 0.01$) (Fig. 2).

Mortality

Retrograde infusion of bile acid into the pancreatic duct produced a severe hemorrhagic, necrotizing pancreatitis with a mortality rate of 68%. Inhibition of ICE activity via administration of VE-13045 attenuated the mortality rate to 22% (Fig. 3A) ($p < 0.01$). Similarly, the CDE diet produced a severe necrotizing pancreatitis with a 10-day mortality rate of 73% in normal wild-type mice. Genetic deletion of the ICE gene was associated with only a 20% mortality (Fig. 3B) ($p < 0.005$ vs. wild-type).

Pancreatitis severity

All experimental animals developed pancreatitis. Bile salt-induced pancreatitis was associated with the development of marked pancreatic edema and free ascitic fluid. Those animals receiving the ICE inhibitor showed a significant reduction in pancreatic wet weight ($p < 0.05$) but not ascitic volume ($p = 0.47$) (Fig. 4). Serum amylase, lipase, and BUN were also significantly attenuated with ICE inhibition/deletion (all $p < 0.05$), whereas serum calcium and creatinine were not affected (Table 1). Histologic scoring of pancreatic tissues in animals deficient in the ICE gene, as well as those receiving VE-13045, demonstrated reduced edema, necrosis, and inflammatory cell infiltrate (all $p < 0.05$) but not vacuolization (Table 2).

DISCUSSION

Although several serine proteases are capable of processing the IL-1 β precursor to one of several bioactive forms, ICE is the only known protease that generates the mature 17 kDa cytokine with its typical Ala¹¹⁸ amino-terminus.^(3,16-18) The importance of this processing enzyme in regulation of cytokine release has been studied recently *in vitro* using monocytes isolated from mice possessing a homozygous deletion of the ICE gene.⁽¹⁸⁾ These investigators demonstrated that ICE was criti-

cal to the cellular export of mature, bioactive IL-1 β . Moreover, the inability of monocytes to process IL-1 β resulted in substantial reductions in IL-1 α , TNF- α , and IL-6 production, demonstrating further the importance of IL-1 β to the cytokine cascade in general.

There were two experimental strategies available to ascertain the role of ICE in models of pancreatitis. First, we used an irreversible inhibitor of endogenous ICE to prevent its enzymatic activity. The compound we chose for this purpose (VE-13045) is an esterified form of a highly efficient inactivator of ICE (k_{inact} of $1 \times 10^6 \text{ M}^{-1} \text{ s}^{-1}$). The esterified form of this compound is a more potent cellular inhibitor of ICE and is biologically active in suppression IL-1 β secretion *in vivo*.⁽¹⁹⁾ Although the compound is cleared rapidly from the systemic circulation, its ability to irreversibly inactivate the enzyme *in*

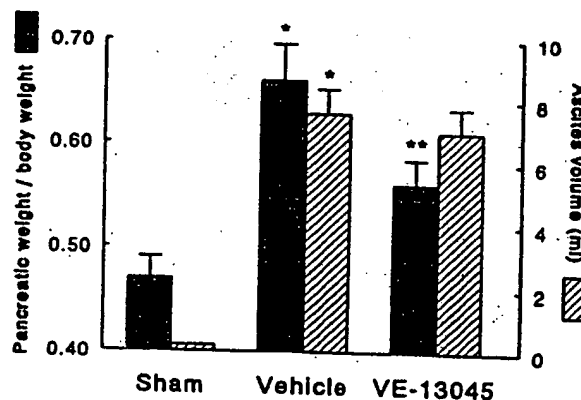


FIG. 4. The effect of ICE inactivation on pancreatic weight and ascites volume in rats with severe pancreatitis induced by bile reflux into the pancreatic duct. The pancreatic weight/body weight ratio increased significantly in vehicle control rats, which developed bile salt pancreatitis ($p < 0.05$ vs. sham, denoted by *). Inactivation of ICE by VE-13045 attenuated this rise by nearly 50% ($p < 0.05$ vs. vehicle, denoted by **). These same animals also developed massive free ascites (vehicle control $p < 0.01$ vs. sham, denoted by *), which was not affected by VE-13045 administration ($p = 0.47$ vs. vehicle control).

TABLE 1. SEVERITY OF PANCREATITIS

| | Bile acid pancreatitis | | | CDE diet pancreatitis | | |
|-------------------------------|------------------------|--------------|----------------|-----------------------|-------------|---------------|
| | Sham | Vehicle | VE-13045 | Baseline | Wild-type | Knockout |
| Serum amylase (IU, thousands) | 0.96 ± 0.7* | 7.32 ± 0.58* | 6.10 ± 0.35*** | 0.54 ± 0.03 | 28.3 ± 2.6* | 15.4 ± 1.2*** |
| Serum lipase (IU, thousands) | 0.08 ± 0.01 | 3.76 ± 0.7* | 1.46 ± 0.2*** | 0.38 ± 0.04 | 18.2 ± 1.7* | 11.9 ± 0.8*** |
| BUN (mg/dl) | 14.1 ± 1 | 91 ± 7* | 74 ± 5*** | 15.3 ± 1 | 46 ± 5.1* | 39 ± 3.2* |
| Calcium (mg/dl) | 9.6 ± 0.3 | 7.7 ± 0.4* | 8.7 ± 0.5* | 9.4 ± 0.2 | 9.2 ± 0.5 | 9.2 ± 0.6 |
| Creatinine (mg/dl) | 0.4 ± .01 | 1.4 ± .02* | 1.3 ± 0.01* | 0.6 ± 0.01 | 1.2 ± .08* | 1.1 ± .03* |

*Values are mean ± SEM.

*Significance from sham or baseline values ($p < 0.01$).**Significance from vehicle or wild type ($p < 0.05$).

vivo when delivered i.p. made it suitable as a probe for the role of ICE in a rapid, acute model of pancreatitis. Use of an exogenous ICE inhibitor allowed us to precisely time the dosing of the compound with respect to disease stimulus.

Our second strategy involved using a transgenic mouse with a disrupted ICE gene. Although the transgenic mice we used show near total suppression in LPS-induced secretion of IL-1 α and IL-1 β and partial suppression of serum TNF- α and IL-6, they present an alternative to the use of an ICE inactivator that potentially inactivates other cysteine protease homologs of ICE. Use of the knockout mouse, therefore, is the most precise method available for studying the effects of deleting the activity of a single enzyme *in vivo*.

The two models of pancreatitis used in the current study are known to be associated with systemic cytokine production that is independent of endotoxin.^(10,21-25) The dramatic rise in IL-1 β mRNA within the pancreas and lung has been demonstrated previously and closely mimics pancreatitis progression.^(8,10) The current series of experiments demonstrates the efficacy of VE-13045 in antagonizing ICE *in vivo* and confirms the importance of ICE in the processing and secretion of IL-1 as well as affecting total TNF production *in vivo*. The animals with pharmacologic blockade of ICE had cytokine production attenuated to an equivalent degree as the knockout animals, sug-

gesting complete enzyme inactivity. Although the process by which IL-1 β is prevented from entering the serum is fairly well characterized, the mechanism by which TNF secretion is attenuated is not known, as it is not a direct substrate of ICE. This decrease in circulating TNF has been demonstrated also in animals pretreated with IL-1Ra before pancreatitis induction⁽¹¹⁻¹³⁾ and is likely due to an overall decrease in the associated systemic inflammatory response and attenuated pancreatitis severity.

The importance of uninhibited production of IL-1 β to the overall progression of acute pancreatitis is apparent in these experiments. By preventing the development of the typical cytokine cascade, nearly every measure of pancreatic damage was diminished. Previous experiments in a nonlethal pancreatitis model demonstrated that an active IL-1 receptor is required for the development of maximal necrosis and pancreatic edema.⁽¹⁴⁾ These findings were confirmed in the two lethal models used in this study, but additional benefits were seen, including decreased pancreatic inflammation and less severe changes in serum BUN. It is possible that some of the decrease in pancreatic damage may be attributed to inhibition of ICE-mediated apoptosis, but little can be said about what effect this mechanism has on the other parameters of pancreatitis, as little is known about the role of apoptosis in the development of pan-

TABLE 2. HISTOLOGIC GRADING OF PANCREATITIS^a

| | Bile acid pancreatitis | | | CDE diet pancreatitis | | |
|---------------|------------------------|--------------------------|--------------|-----------------------|------------|--------------|
| | Sham | Vehicle | VE-13045 | Baseline | Wild-type | Knockout |
| Edema | 0 | 3.3 ± 0.2 ^{b,*} | 0.9 ± 0.1*** | 0 | 3.1 ± 0.2* | 2.6 ± 0.2* |
| Necrosis | 0 | 3.2 ± 0.1* | 0.6 ± 0.1*** | 0 | 3.8 ± 0.1* | 3.0 ± 0.1*** |
| Inflammation | 0 | 3.1 ± 0.1* | 0.7 ± 0.1*** | 0 | 3.6 ± 0.1* | 2.7 ± 0.2*** |
| Vacuolization | 0 | 2.8 ± 0.2* | 2.6 ± 0.1* | 0 | 2.4 ± 0.2* | 2.5 ± 0.1* |

^aHistologic sections were graded in a blinded fashion. Normal tissues were assigned a value of 0, and maximal severity for parameter was assigned a value of 4.

^bValues are mean ± SEM for 10 fields from each pancreatic specimen from all animals.

*Significance from sham or baseline values ($p < 0.01$).

**Significance from vehicle or wild type ($p < 0.05$).

creatitis. Combined with the dramatic survival benefit attributed to ICE inhibition, these studies demonstrate the profound detrimental effect of IL-1 β during acute pancreatitis and suggest that ICE blockade has potential therapeutic applications in this disease.

ACKNOWLEDGMENT

This work was supported by a Veterans Administration Merit Review Grant to J.N.

REFERENCES

- GLASBRENNER, B., and ADLER, G. (1993). Pathophysiology of acute pancreatitis. *Hepatogastroenterology* 40, 517-521.
- STEINBERG, W., and TENNER, S. (1994). Acute pancreatitis. *N. Engl. J. Med.* 330, 1198-1220.
- DINARELLO, C.A. (1996). Biologic basis for interleukin-1 in disease. *Blood* 87, 2095-2147.
- NORMAN, J., FRANZ, M., RIKER, A., and GOWER, R. (1994). Rapid elevation of pro-inflammatory cytokines during acute pancreatitis and their origination within the pancreas. *Surg. Forum* 45, 148-160.
- McKAY, C., GALLAGHER, G., BAXTER, J.N., and IMRIE, C.W. (1994). Systemic complications in acute pancreatitis are associated with increased monocyte cytokine release. *Gut* 35, A575.
- HEATH, D.L., CRUICKSHANK, D.H., GUDGEON, M., JEHANLI, A., SHENKIN, A., and IMRIE, C.W. (1993). Role of interleukin-6 in mediating the acute phase protein response and potential as an early means of severity assessment in acute pancreatitis. *Pancreas* 66, 41-45.
- GROSS, V., LESER, H.G., HEINISCH, A., and SCHOLMERICH, J. (1993). Inflammatory mediators and cytokines—New aspects of the pathophysiology and assessment of severity of acute pancreatitis. *Hepatogastroenterology* 40, 522-530.
- FINK, G., and NORMAN, J. (1997). Specific changes in the pancreatic expression of the interleukin-1 family of genes during experimental acute pancreatitis. *Cytokine* (in press).
- NORMAN, J., FINK, G., CARTER, G., DAVISON, B., GLACCUM, M., and FRANZ, M. (1996). Active interleukin-1 receptor required for maximal progression of acute pancreatitis. *Ann. Surg.* 223, 163-169.
- NORMAN, J., FINK, G., CARTER, G., SEXTON, C., and FRANZ, M. (1995). The induction of multi-organ cytokine gene expression by acute pancreatitis. *Gastroenterology* 108, 306A.
- NORMAN, J., MESSINA, J., FRANZ, M., FABRI, P.J., ROSE-MURGY, A.S., and GOWER, W.R. (1995). Interleukin-1 receptor antagonist decreases severity of experimental acute pancreatitis. *Surgery* 117, 648-655.
- NORMAN, J., FRANZ, M., FINK, G., MESSINA, J., GOWER, W.R., and CAREY, L.C. (1995). Decreased mortality of severe acute pancreatitis following proximal cytokine blockade. *Ann. Surg.* 221, 453-460.
- TANAKA, N., MURATA, A., UDA, K., TODA, H., KATO, T., HAYASHIDA, H., MATSUURA, N., and MORI, T. (1995). Interleukin-1 receptor antagonist modifies the changes in vital organs induced by acute necrotizing pancreatitis in a rat experimental model. *Crit. Care Med.* 23, 901-908.
- NORMAN, J., FINK, G., FRANZ, M., GUFFEY, J., CARTER, G., DAVISON, B., SEXTON, C., and GLACCUM, M. (1996). Active interleukin-1 receptor required for maximal progression of acute pancreatitis. *Ann. Surg.* 223, 163-169.
- THORNBERRY, N., BULL, H., CALAYCAY, J., CHAPMAN, K., HOWARD, A., KOSTURA, M., MILLER, K., MOLINEAUX, S., WEIDNER, J., AUNINS, J., ELLISOTON, K., AYALA, J., CASANO, F., CHIN, J., DING, G., EDGGER, L., GAFFNEY, E., LIMJUCO, G., PALYHA, O., RAJU, S., ROLANDO, A., SALLEY, J., YAMIN, T., LEE, T., SHIVELY, J., MACCROSS, M., MUMFORD, R., SCHMIDT, J., and TOCCI, M. (1992). A novel heterodimeric cysteine protease required for interleukin-1 β processing in monocytes. *Nature* 356, 768-774.
- WILSON, K., BLACK, J., THOMSON, J., KIM, E., GRIFFITH, J., NAVIA, M., MUREKO, M., CHANBERS, S., ALDAPE, R., RAYBUCK, S., and LIVINGSTON, D. (1994). Structure and mechanism of interleukin-1 converting enzyme. *Nature* 370, 270-275.
- CERETTI, D., KOZLOSKY, C., MOSLEY, B., NELSON, N., VAN NEST, K., GREENSTREET, T., MARCH, C., KRONHEIM, S., DRUCK, T., CANNIZZARO, L., HUEBNER, K., and BLACK, R. (1992). Molecular cloning of the IL-1 β converting enzyme. *Science* 256, 97-100.
- KUIDA, K., LIPPKE, J., KU, G., HARDING, M., LIVINGSTON, D., SU, M., and FLAVELL, R. (1995). Altered cytokine export and apoptosis in mice deficient in interleukin-1 converting enzyme. *Science* 267, 2000-2003.
- KU, G., FAUST, T., LAUFFER, L., LIVINGSTON, D., and HARDING, M. (1996). Interleukin-1 β converting enzyme inhibition blocks progression of type II collagen-induced arthritis in mice. *Cytokine* 8, 377-386.
- CHOMCZYNSKI, P., and SACCHI, N. (1987). Single step method of RNA isolation by acid guanidinium thiocyanate-phenol-chloroform extraction. *Anal. Biochem.* 162, 156-159.
- NORMAN, J., and FINK, G. (1995). Acute pancreatitis induces intrapancreatic tumor necrosis factor- α gene expression. *Arch. Surg.* 130, 966-970.
- HUGHES, C., GABER, L., KOTB, M., MAHEY EL-DIN, A., PABST, M., and GABER, A.O. (1995). Induction of acute pancreatitis in germ-free rats: Evidence of a primary role for tumor necrosis factor- α . *Surgery* 117, 201-205.
- GREWAL, H.P., KOTB, M., OHMAN, M., SALEM, A., GABER, L., and GABER, O.A. (1994). Induction of tumor necrosis factor in severe acute pancreatitis and its subsequent reduction after hepatic passage. *Surgery* 115, 213-221.
- FINK, G., and NORMAN, J. (1996). Intrapaneatic interleukin-1 gene expression by specific leukocyte populations during acute pancreatitis. *J. Surg. Res.* 63, 369-373.
- VAN LAETHEM, J.L., MARCHANT, A., DELVAUX, A., GOLDMAN, M., and DEVIÈRE, J. (1995). Interleukin 10 prevents necrosis in murine experimental pancreatitis. *Gastroenterology* 108, 1917-1922.

Address reprint requests to:

James Norman, M.D.

Department of Surgery, 112

University of South Florida

13000 Bruce B Downs Boulevard

Tampa, FL 33612

Received 8 August 1996/Accepted 4 November 1996

Role of Interleukin-1 β Converting Enzyme (ICE) in Acute Myelogenous Leukemia Cell Proliferation and Programmed Cell Death

ZEEV ESTROV* and MOSHE TALPAZ

Department of Bioimmunotherapy, The University of Texas, M. D. Anderson Cancer Center, Box 302,
1515 Holcombe, Boulevard, Houston, TX 77030, U.S.A.

(In final form 20 May 1996)

The proinflammatory cytokine interleukin (IL)-1 has been shown to play a pivotal role in stimulating acute myelogenous leukemia (AML) cell proliferation. The gene for its prominent IL-1 β form produces a 31-kDa precursor protein (pro-IL-1 β) that is biologically inactive unless cleaved to its mature form by a cytoplasmic cysteine protease termed IL-1 β converting enzyme (ICE). Although ICE was first thought to be a unique enzyme with a single biologic activity, several investigators have demonstrated that ICE shares sequence homology with the protein product of *ced-3*, the gene for cell death of the nematode *Caenorhabditis elegans*, and induces apoptosis in different experimental models. It was therefore hypothesized that ICE may either augment the production of mature IL-1 β and stimulate the proliferation of cells, in which IL-1 β acts as an autocrine growth factor, or induce apoptosis. Recent data indicate that ICE is a member of an increasingly recognized family of cysteine proteases. Unlike ICE, the other members of this family do not cleave pro-IL-1 β but are effective inducers of apoptotic cell death, whereas ICE acts primarily as an IL-1 β converting enzyme. Because IL-1 β serves as either an autocrine or paracrine growth factor in AML, we recently investigated the effect of ICE inhibition on AML colony growth and found that ICE inhibition reduced the production of mature IL-1 β and suppressed AML progenitor proliferation. Our data suggest that ICE does not function as an apoptosis gene in AML but rather increases mature IL-1 β production and AML cell proliferation. It is possible, therefore, that ICE inhibitors may be beneficial in AML therapy.

Keywords: Interleukin-1, interleukin-1 β converting enzyme, acute myelogenous leukemia

INTRODUCTION

Acute myelogenous leukemia (AML) progenitors, require the addition of specific cytokines to stimulate their proliferation in tissue culture.^[1] Among the var-

ious cytokines that have been implemented in stimulating the *in vitro* growth of leukemic cells, interleukin (IL)-1 plays a unique role. Bone marrow cells from most AML patients produce IL-1 β , which stimulates leukemia cell proliferation through autocrine

*Corresponding author. Tel.: (713) 794-1675. Fax: (713) 745-2374.

and paracrine mechanisms.^[2,3] IL-1 induces the production of several cytokines such as granulocyte-macrophage colony-stimulating factor (GM-CSF), granulocyte CSF (G-CSF), macrophage CSF (M-CSF), IL-2, IL-3, IL-6, IL-7, IL-8, and tumor necrosis factor (TNF)- α from the leukemic blasts and a variety of cells including accessory cells^[3-6], endothelial cells,^[7-10] and bone marrow stroma.¹¹ In addition, IL-1 upregulates cell-surface receptor expression of several cytokines, synergizes with several growth factors in stimulating progenitor proliferation,^[12-16] and prolongs survival of progenitor cells.^[17] Clinical data also implicate IL-1 in stimulating AML cells. Raza *et al.* found that the presence of IL-1 β gene activity is associated with a poor long-term prognosis in patients with AML,^[18] suggesting that mechanisms similar to those observed in various *in vitro* studies may be operative *in vivo*.

Based on these data, we and others have hypothesized that inhibition of IL-1 activity may suppress leukemia cell-proliferation. Various strategies for inhibiting IL-1 have been explored over the past several years. Subsequent *in vitro* studies have shown that suppression of IL-1 production or interruption of its interaction with its corresponding cellular receptors may suppress the growth of leukemia cells (reviewed in^[19]). As a result, the antileukemic properties of IL-1 receptor antagonist (IL-1RA), IL-4, and suramin are being investigated in clinical trials. Because IL-1 β is the prominent form of IL-1 and because the amount of IL-1 β mRNA found in activated cells is usually 10- to 50-fold greater than that of the IL-1 α form,^[15] several investigators have attempted to identify means for specific inhibition of IL-1 β .^[20]

IL-1 β AND IL-1 β CONVERTING ENZYME (ICE)

The IL-1 family includes IL-1 α , IL-1 β , and IL-1RA.^[15,21] Although found predominantly in monocytes, these cytokines are also produced by a variety of normal and neoplastic cells.^[15,19] IL-1 α and IL-1 β are proinflammatory cytokines. They share 26 amino acid homology, bind to the same receptors, and share a

wide spectrum of biological activities.^[19,22] Nevertheless, IL-1 α and IL-1 β are not interchangeable. Recent data describing an IL-1 β -deficient mouse model indicate that although IL-1 β -deficient mice develop normally, they exhibit an impaired acute-phase inflammatory response and are completely resistant to fever development and anorexia, suggesting that at least some of IL-1 β 's activities cannot be replaced by either IL-1 α or any other cytokine.^[23]

The protein products of the *IL-1 α* and *IL-1 β* genes are 31-kDa precursor forms. Precursor (pro)-IL-1 α is biologically active and binds to IL-1 receptors without further processing.^[24-26] Most pro-IL-1 α remains in the cellular cytosol, where it is phosphorylated at serine 90 and may function as an autocrine messenger.^[27,28] The extracellular 17.5-kDa form of IL-1 α results from cleavage of pro-IL-1 α by different proteases^[15,29-31] at the Phe-Leu^[119] bond. No enzyme has been found to specifically process IL-1 α . In contrast, IL-1 β must first be processed from its inactive cytoplasmic precursor to an active 17.5-kDa mature form.^[24-26] Pro-IL-1 β is cleaved by a unique cytoplasmic cysteine protease termed IL-1 β converting enzyme (ICE)^[32-38] after association with the plasma membrane during the cytokine's secretion^[39] (Fig. 1). ICE cleaves the Asp^[116]-Ala^[117] bond of pro-IL-1 β to generate the mature IL-1 β form and at a secondary cleavage site of Asp^[27]-Gly^[28] to form small amounts of a 28-kDa fragment which can be further processed to the active 17.5-kDa form. Thus far no other protein containing Asp-X linkages has been found to be cleaved by ICE.^[33] ICE is thought to be essential for production of IL-1 β , because cells lacking ICE activity do not form mature IL-1 β even when transfected with pro-IL-1 β .

ICE must be processed before it becomes active.^[37,38] Active ICE is composed of two subunits, p10 and p20, whose crystal structures have been determined;^[40,41] both require oligomerization^[42] for catalytic activity.^[37,38,42,43] The mature p10/p20 form of ICE is derived from a 45-kDa proenzyme (pro-ICE) by autocatalysis.^[37,44] (Fig. 1). The active enzyme is present in various cells at low quantities. It was detectable only by electron microscopy and was shown to be associated with the plasma membrane.^[43] The secretion of mature IL-1 β does not involve the

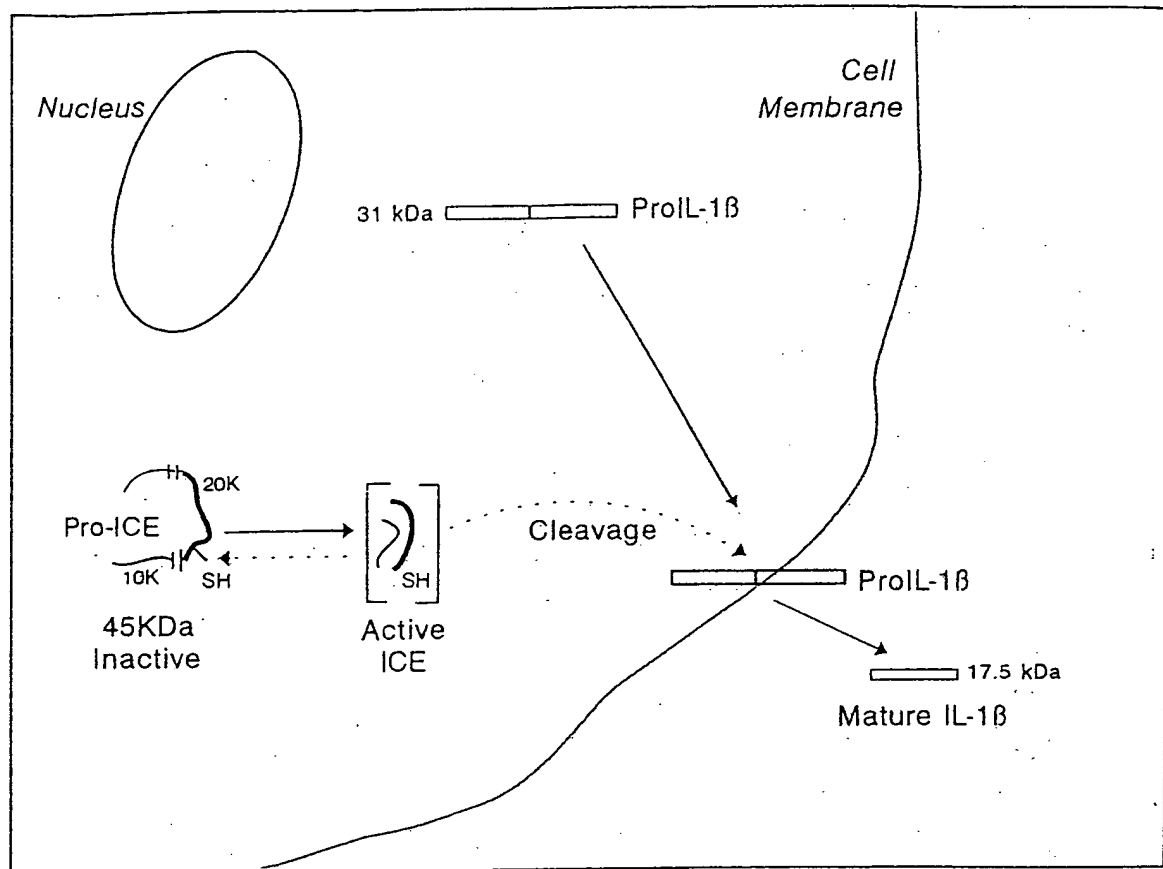


FIGURE 1 Processing of IL-1 β . The protein product of the *IL-1 β* gene is a 31-kDa protein termed pro-IL-1 β . Inactive (pro)-IL-1 β is cleaved by ICE. To become active, ICE has to be cleaved from its 45-kDa inactive proenzyme (pro-ICE) into 10k and 20k biologically active forms by autocatalysis. The cleavage of pro-IL-1 β takes place at the cellular membrane. Only the mature form of IL-1 β is found extracellularly.

Golgi apparatus or endoplasmic reticulum,^[45-47] and its cleavage and secretion are associated with the cell membrane.^[26,48]

ICE AND PROGRAMMED CELL DEATH

Initially, ICE was thought to be a unique cysteine protease with a single specific biologic activity.^[37,38] However, subsequent studies have indicated that ICE may possess additional properties unrelated to pro-IL-1 β cleavage. Yuan *et al.*^[49] found that the CED-3 protein, which induces apoptosis in the nematode *Caenorhabditis elegans* embryonic cells, and ICE share 28% of their amino acids and that ICE is identical

to CED-3 in a 5-amino-acid stretch thought to be the site responsible for ICE's protease activity. They also demonstrated that overexpression of *ICE* induced programmed cell death in Rat-1 fibroblasts^[50] and that the ICE-induced apoptosis could be blocked by the *C. elegans* "anti-death" gene *ced-9*; the human anti-apoptosis gene *Bcl-2*; and *crmA*, the cowpox virus gene whose protein product inhibits ICE's protein-splitting activity.^[51,52] Furthermore, Yuan's group has also shown that microinjection of the *crmA* gene into chicken dorsal root ganglion cells prevented cell death induced by deprivation of nerve growth factor.^[53] suggesting that *ICE* may also be a human cell-suicide gene.

Subsequent studies by other investigators have implicated ICE in several cell-death mechanisms.

Boudreau *et al.*^[54] reported that ICE plays an important role in the extracellular matrix-regulated apoptosis of mammary epithelial cells. Laboratory data suggested that ICE might also be associated with the Fas/APO-1 apoptotic pathway. Fas/APO-1 is a transmembrane 48-kDa glycoprotein that is structurally homologous to TNF- α and nerve growth factor, which is one of the major regulators of apoptosis.^[55] Tewari and Dixit have shown that expression of *crmA* in various cell lines inhibits Fas-induced apoptosis,^[56] and Enarl *et al.* found that both *crmA* and the specific ICE inhibitor tetrapeptide (acetyl-Tyr-Val-Ala-Asp-chloromethylketone) inhibited cytotoxicity induced by anti-Fas antibodies in rat fibroblasts.^[57] Whereas overexpression of ICE potentiated Fas/APO-1-mediated apoptotic cell death, inhibition of ICE activity, by *crmA* or by an antisense ICE construct, suppressed Fas/APO-1- and TNF-mediated apoptosis.^[56,58] Another apoptotic pathway involving ICE was identified by Tamura *et al.*^[59] who demonstrated that ectopic expression of the transcription factor interferon regulatory factor (IRF)-1 results in activation of the endogenous gene for ICE and enhancement of radiation-induced apoptosis.

The *C. elegans ced-9* gene protects cells from undergoing programmed cell death, an effect opposite to that of the *ced-3* gene.^[60] The *ced-9* gene encodes a 280-amino-acid protein with sequence and structural similarities to Bcl-2.^[61] The *Bcl-2* gene was cloned from the breakpoint of the chromosomal translocation t(14;18)(q32.1;q21) characteristic of follicular B-cell lymphoma.^[62-64] Bcl-2 is a member of an ever-expanding family whose members may interact to promote or inhibit programmed cell death (reviewed

in^[65]). The functional resemblance between the *C. elegans ced-9* gene and the mammalian *Bcl-2* proto-oncogene link the Bcl-2 family members that promote cell death (such as Bax) to ICE.^[60,61,65-67] Furthermore, these similarities suggest that the molecular mechanism of programmed cell death has been conserved from nematodes (*ced-3* and *ced-9*) to mammals (*ICE* and *Bcl-2*).

THE ICE FAMILY

Over the last 2 years, several investigators have established that ICE is the first member of a new family of cysteine proteases involved in the induction of programmed cell death (Table I). Kumar *et al.*^[71] identified a set of 11 mouse genes, named *Nedd1* through *Nedd10*, of which *Nedd2* encodes a protein that is similar to ICE (29% identity). They showed that overexpression of *Nedd2* in cultured fibroblasts and neuroblastoma cells resulted in cell death by apoptosis and that this effect could be suppressed by expression of the human *Bcl-2* gene, suggesting that *Nedd2* is functionally similar to the *ced-3* gene in *C. elegans*. Using a mouse *Nedd2* probe, Wang *et al.*^[70] isolated and characterized a *ced-3*-related gene termed *Ich-1*. *Ich-1* mRNA was found to splice into two different forms. One form encodes the protein ICH-1_L, which contains amino acid sequences homologous to both the p20 and p10 subunits of ICE; the second form encodes ICH-1_S, a 312-amino-acid truncated version of the ICH-1_L protein. Whereas overexpression of *Ich-1* induces programmed cell death, overexpression of *Ich-1*_S suppresses rat-1 cell death induced by serum deprivation.^[70]

TABLE I The ICE Family

| Protein | Species | Cleaves IL-1 β | References |
|---------------------------------|-------------------|----------------------|-------------|
| ICE | Human | Yes | 49,50,68,69 |
| CED-3 | <i>C. elegans</i> | ? | 49 |
| Nedd2/ICH-1 | Murine/human | ? | 69-71 |
| prICE/CPP32/Yama | Human | No | 68, 72-78 |
| ICE _{rel} -II/TX/ICH-2 | Human | No | 69, 79-81 |
| ICE _{rel} -III | Human | No | 79 |
| Mch2 | Human | ? | 82 |
| Mch3/ICE-LAP3 | Human | ? | 83-85 |

Other investigators have isolated, characterized, and cloned additional ICE-related proteases. Lazebnik *et al.*^[68] discovered a novel human protease resembling ICE (prICE) and Wang *et al.*^[86] described its hamster homolog. Both Nicholson *et al.*^[73] and Tewari *et al.*^[78] have identified prICE as the ICE relative CPP32- β (also termed Yama^[78]), a cysteine protease that shares even closer homology with CED-3 than does ICE.^[74] CPP32 is a 32-kDa putative cysteine protease that, like ICE, is synthesized as an inactive proenzyme that requires proteolytic activation. Its transcript is highly expressed in most abundant cell lines of lymphatic origin. Similar to ICE, its overexpression in this case in Sf9 insect cells results in apoptosis.^[87] A CPP32-derived enzyme, apopain, is composed of two biologically active 17k and 12k subunits.^[73] The active form of CPP32 (apopain) is identical to prICE.^[73]

Two novel members of the ICE family of proteases, designated ICE_{rel}-II and ICE_{rel}-III, have been recently cloned from human monocytic cells.^[79] Both had a 52% sequence homology to ICE and both contain the pentapeptide sequence of the catalytic cysteine residue. Although both ICE_{rel}-II and ICE_{rel}-III effectively induced apoptosis in fibroblasts, they lack the capability to cleave pro-IL-1 β . ICE_{rel}-II is identical^[88] to the ICE homologues TX and ICH-2 that have been described by Faucheu *et al.*^[80] and Kamen *et al.*^[81] respectively.

Using a polymerase chain reaction (PCR) approach, Fernandes-Alemni *et al.*^[82,83] cloned two novel ICE-like apoptosis genes from human Jurkat T-lymphocytes. The new genes are termed *Mch2* and *Mch3*. *Mch2* encodes a 34-kDa protein that is highly homologous to CPP32 and other members of the *Ced-3*/ICE family. Of the two *Mch2* transcripts (*Mch2* α , 1.7kb and *Mch2* β , 1.4kb), *Mch2* α possesses protease activity. It can cleave PARP *in vitro*, and its overexpression in Sf9 insect cells induces apoptosis.^[82] The *Mch3* gene encodes two *Mch3* proteins: an active *Mch3* α , a cysteine protease with extensive homology to CPP32, and an inactive *Mch3* β variant. *Mch3* α forms an active heterodimer complex with CPP32 and *Mch3* β may act as its inhibitor.^[83] ICE-LAP3, first described as a novel ICE-related protease whose overexpression induced apoptosis in the breast cancer cell line MCF-7,^[84] was later found to be identical to *Mch3*.^[85]

MECHANISMS OF ACTION OF ICE-RELATED PROTEASES

Upon activation, cytotoxic T lymphocytes can exocytose granules whose content is released into the extracellular space between the target cell and the effector. One of the released molecules, perforin (cytolysin), is a pore-forming protein whose sequence and function are similar to those of the lytic complement proteins. In the presence of Ca²⁺ ions, perforin binds to the lipid bilayer of the target cell plasma membrane, and 12 to 18 perforin monomers form transmembrane pores and facilitate the entry of the cytotoxic granzymes into the target cells^[89] (Fig. 2). Granzymes are serine proteases released upon T-cell activation. Granzymes enter the target cell through pores generated by perforin and induce apoptotic cell death through a mechanism that is not fully understood^[90-92] (Fig. 2). Both perforin and granzyme B were found in CD34+ peripheral blood cells mobilized by chemotherapy and G-CSF.^[93] Interestingly, granzyme A, but not granzyme B, was shown to cleave pro-IL-1 β at Arg^[120], four amino acids downstream of the authentic processing site, Asp^[116,94] Darmon *et al.*^[72] have recently shown that granzyme B cleaves and activates the proenzyme CPP32, thus generating CPP32/apopain, the active form that induces programmed cell death (Fig. 3).

The mechanism by which CPP32/apopain induces apoptosis has been recently unfolded. CPP32/apopain cleaves the nuclear enzyme poly ADP-ribose polymerase (PARP), an enzyme involved in DNA repair, chromatin stability, and supervision of genome integrity.^[75,76] Cleavage of PARP was found to be associated with apoptosis in a variety of cell types.^[78] Other ICE family members such as CED-3,^[95] Need2/ICH-1,^[69-71] ICE_{rel}-II/TX/ICH-2,^[69,79-81] *Mch2*,^[82] and *Mch3*/ICE-LAP-3^[83-85] also cleave PARP. However, unlike CPP32, the mechanisms responsible for activation of most of the cysteine proteases resulting in activation of PARP and of apoptotic cell death are not fully understood (Fig. 3). ICE does not cleave PARP^[68] unless present at a very high concentration (50- to 100- fold higher than the concentration needed to process IL-1 β).^[69]

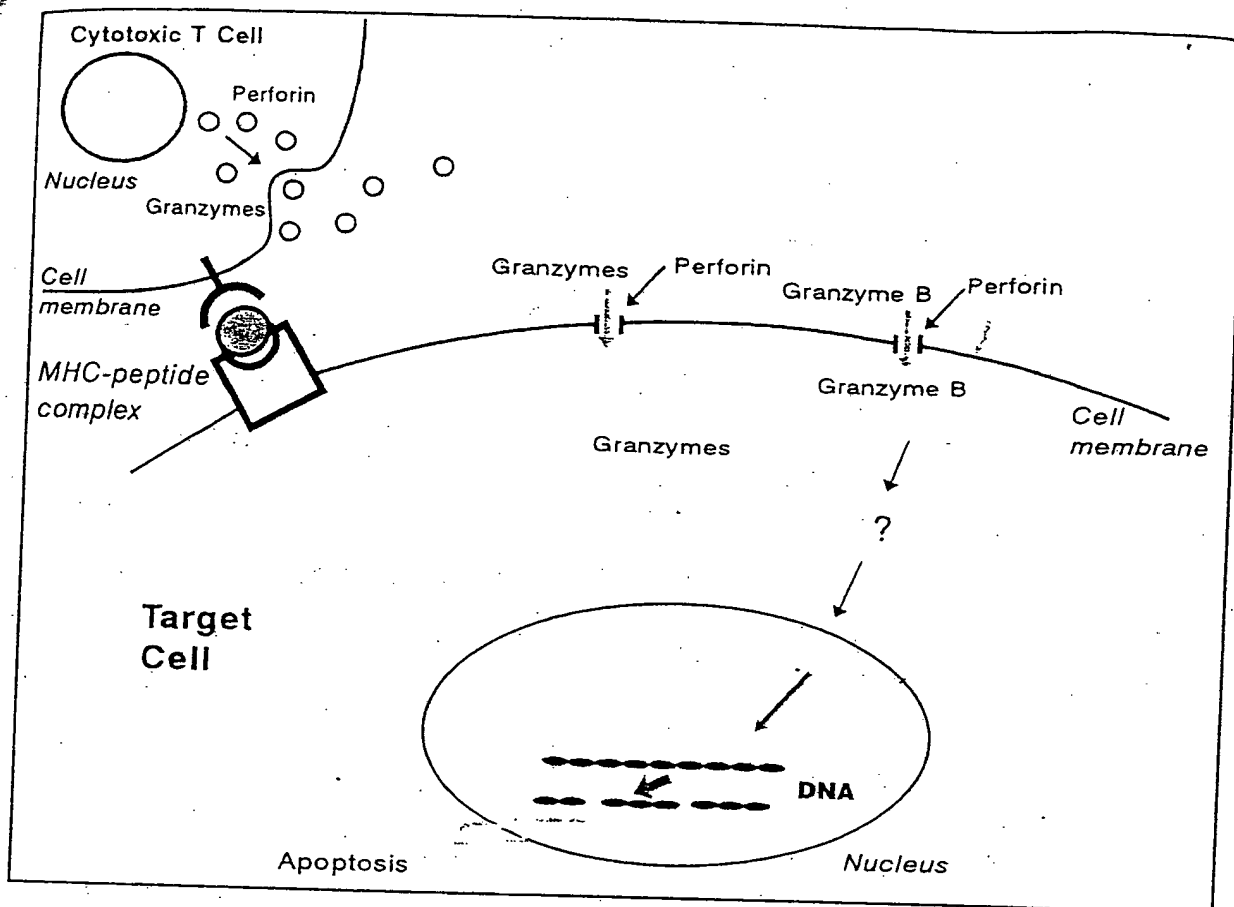


FIGURE 2 Induction of apoptotic cell death by granzymes. The cytolytic T-cell receptor recognizes the MHC-peptide complex of a target cell. The activated T lymphocyte produces perforin and granzymes, and those are exocytosed. Perforin forms pores in the target cell membrane to allow the entrance of granzymes. The granzymes can cause DNA fragmentation and apoptotic cell death.

It has been postulated^[72] that PARP is probably not the sole substrate of CPP32, because PARP-knockout mice develop normally.^[96] Additional substances triggered by ICE-related cysteine proteases, which are also critical to the induction of apoptosis, will probably be found. A number of cellular proteins, such as lamins, are degraded during apoptosis. Like PARP, cellular lamins are cleaved into discrete fragments in cells undergoing programmed cell death and may have a role in the apoptosis cascade. While studying this event, Lazebnik *et al.*^[97] identified an ICE-like protease whose activation is probably a crucial event in the terminal phase of apoptosis. As yet, this protein has not been cloned, and it remains to be seen if it represents an already known member of the ICE family.

Another signaling mechanism employed in the induction of apoptosis is the sphingomyelin pathway. Intensive investigation in the past decade have established the role of membrane glycolipids in transmembrane signal transduction. Recent evidence suggests that TNF- α , Fas/APO-1 ligand, and ionizing radiation utilize the sphingomyelin-ceramide pathway in triggering apoptosis [reviewed in^[98,99]]. Sphingomyelin (*N*-acylsphingosin-1-phosphocholine) is a phospholipid preferentially concentrated in the outer leaflet of the plasma membrane of most mammalian cells. Extracellular agents such as TNF- α or Fas ligand activate sphingomyelinase to generate ceramide and phosphocholine (Fig. 4). Ceramide serves as a second messenger of the sphingomyelin pathway, initiating

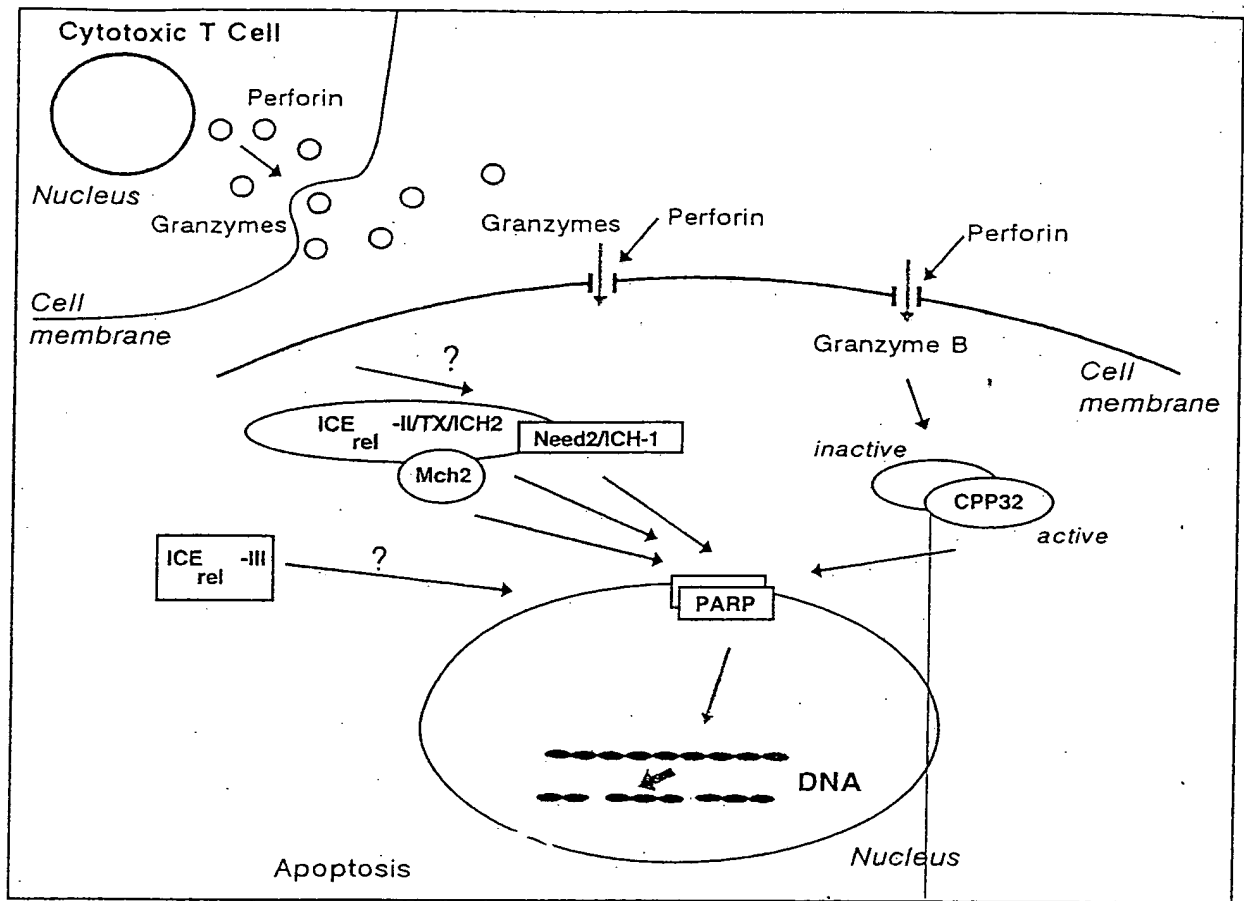


FIGURE 3 Induction of apoptosis by ICE-related cysteine proteases. Activated T lymphocytes excrete both granzymes and perforin. Granzyme B enters the target cell through pores generated by perforin and cleaves and activates CPP32/Yama. The activated CPP32 (CPP32/apopain) cleaves PARP in a process that ends in DNA fragmentation and apoptotic cell death. ICE_{rel}-II/TX/ICH2, Need2/ICH-1, and Mch3 also cleave PARP; however, the mechanisms inducing these activities are still unknown. ICE_{rel}-III induces apoptosis through a mechanism that is yet undefined.

signaling for several biological agents. In particular, ceramide is a potent inducer of apoptosis. The interaction between either Fas/APO-1 or TNF receptor-1 (TNFR-1) and their corresponding natural ligands or agonist antibodies results in both upregulation of ceramide production and activation of CPP32/apopain and Mch3/ICE-LAP3^[84,100] and results in apoptotic cell death.^[56,98,99] Either suppression of ceramide production^[98] or inhibition of CPP32 and Mch3/ICE-LAP3 by the provirus gene product crmA^[56] blocks the Fas/APO-1- and TNFR-1-induced cell death. The apoptotic effects of CPP32 and Mch3/ICE-LAP3 involve interaction between both molecules^[83] and are

associated with cleavage of PARP. Whether this downstream effect is triggered by the sphingomyelin-ceramide pathway remains to be seen (Fig. 4).

Although ICE has been shown to induce programmed cell death, there are at least two indications that other ICE-family proteases that do not possess pro-IL-1 β cleavage activity are physiologic inducers of apoptosis. First, both macrophage and thymocyte apoptosis occur normally in ICE-deficient mice^[101,102] despite major defects in their ICE-dependent generation of mature IL-1 β . Second, *in vitro* models of apoptosis, in which isolated nuclei undergo fragmentation typical of apoptotic cells, implicated CPP32, a pro-

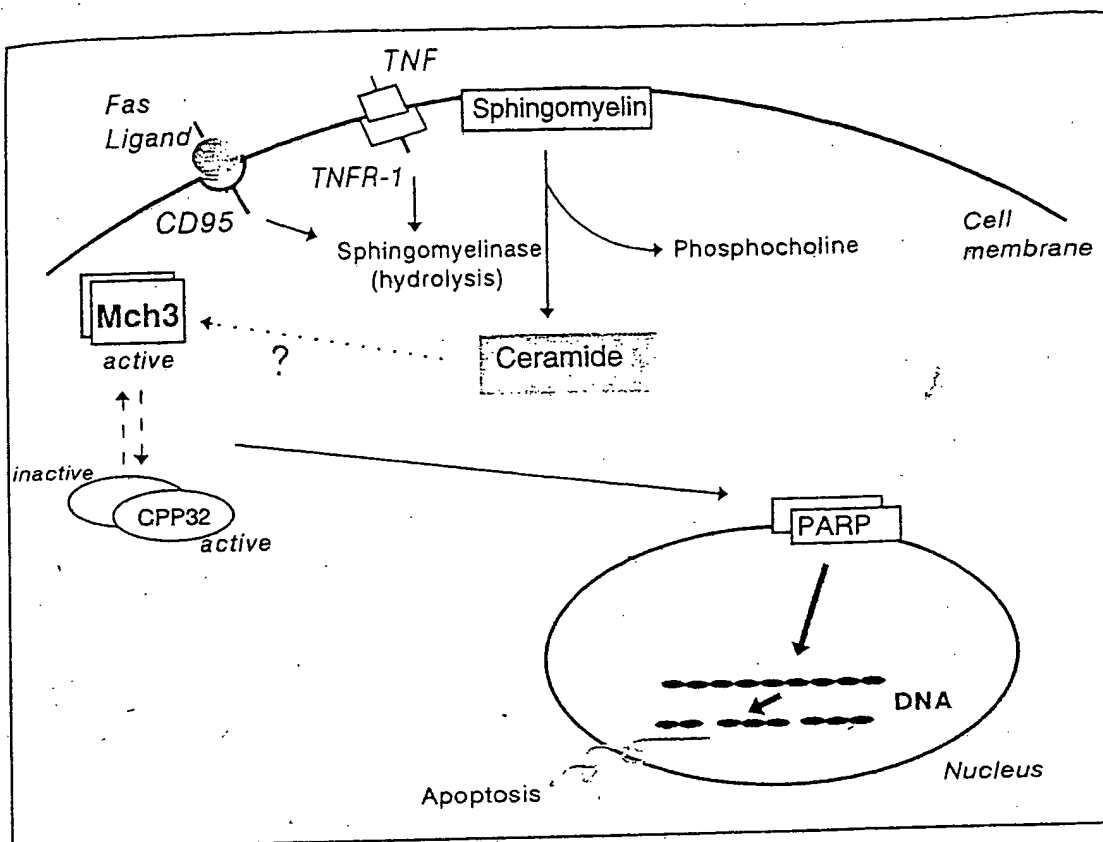


FIGURE 4 Role of the sphingomyelin pathway in the induction of apoptosis. Upon binding to their corresponding ligands, either Fas/APO-1 (CD95) or TNF receptor-1 (TNFR-1) activate the enzyme sphingomyelinase. This hydrolytic process results in the formation of phosphocholine and ceramide. Ceramide induces apoptosis probably through activation of either Mch3/ICE-LAP3, CPP32, or both. The interaction between these two cysteine proteases results in cleavage of PARP, DNA degradation and apoptotic cell death.

tease with a different proteolytic specificity from ICE.^[68] The central role of CPP32/apopain and other ICE family members in cleavage of PARP (but not of pro-IL-1 β) in mammalian cells suggests that ICE is committed mainly to pro-IL-1 β cleavage, whereas apoptosis is induced by other members of its family. Thus proteases with a great degree of sequence homology may exhibit disparate biological activities.

ICE INHIBITION

The cowpox virus serpin, CrmA, is a natural macromolecular inhibitor of ICE.^[51,103] This 31-kDa protein plays an important role in the host inflammatory response to infection by inhibiting the biosynthesis of

biologically active IL-1 β .^[51] CrmA is the only known member of the serpin superfamily to inhibit a cysteine protease rather than a serine protease. It inhibits ICE and other members of this protease family, which require Asp in the p-binding pocket for catalysis,^[44] thus negating their apoptotic effects.^[53]

CrmA is not the only viral product affecting programmed cell death. Some viruses produce suppressors of cell death, presumably to increase virus replication. For example, the baculovirus gene *p35*, inhibits virus-induced apoptosis in insect cells,^[104,105] and the *p35* protein is a substrate for and inhibitor of the *C. elegans* cell death protease CED-3 and of the CED-3-like vertebrate cysteine protease, indicating that *p35* may prevent programmed cell death by acting as a competitive inhibitor of cysteine proteases.^[95]

Several cysteine protease inhibitors, both reversible and irreversible, have been employed in laboratory studies in recent years (reviewed in^[106]). The strategies used to develop these molecules were applied to the development of ICE inhibitors. The most potent and selective inhibitors^[107,108] contain the tetrapeptide sequence Ac-Tyr-Val-Ala-Asp, which is consistent with the substrate specificity of the enzyme (reviewed in^[44]). Whether inhibitors of ICE also inhibit other members of the ICE family has not yet been established.

CLINICAL RELEVANCE OF ICE AND ICE-RELATED PROTEASES IN AML

Whereas activation of the ICE-related cysteine proteases appears to be a novel though nonspecific option for antineoplastic therapy, suppression of ICE activity may provide a specific antileukemic therapeutic approach. Since endogenously produced IL-1 β provides AML progenitors with a growth advantage,^[20,109,110] inhibition of ICE may reduce production of the biologically active IL-1 β , thus suppressing AML cell proliferation.

In a recent study,^[111] we used the ICE inhibitor boc-aspartyl (benzyl) chloromethylketone (BACMK^[52,112]) to test the latter hypothesis. BACMK is a small mole-

cule designed to penetrate cells and bind covalently to the active site of ICE. It disrupts the interaction of ICE with pro-IL-1 β and prevents its cleavage into the biologically active IL-1 β .^[112]

We found that BACMK suppresses the proliferation of both an IL-1-responsive AML cell line (OCI/AML3) and AML progenitors obtained from the bone marrow of 16 AML patients in a dose-dependent fashion. The inhibitory effect was reversed by IL-1 β (Fig. 5), and Z-phe-chloromethyl-ketone, a similar compound designed to inhibit chymotrypsin-like proteases, did not affect cellular growth, thus proving its specificity. BACMK suppressed the production of the biologically active form of IL-1 β by both OCI/AML3 and fresh AML cells, suggesting that its inhibitory effect is mediated through prevention of mature IL-1 β production. In contrast, BACMK did not affect the growth of IL-1-unresponsive AML cell lines or of normal marrow hematopoietic progenitors. Other investigators attained similar results using antisense oligomers for ICE.^[113] In summary, these data indicate that suppressing ICE activity specifically inhibits AML progenitor proliferation, suggesting that ICE inhibitors may provide therapeutic benefits in AML.

Induction of apoptosis in leukemic cells *via* specific stimulation of ICE-related proteases in an appealing

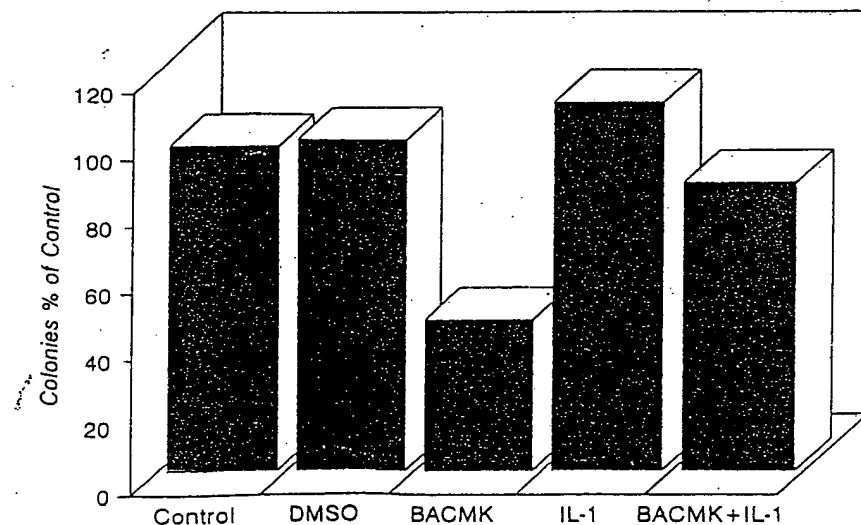


FIGURE 5 Effect of the ICE inhibitor BACMK on AML colony-forming cell proliferation. The means of colony numbers from triplicate cultures of five AML patients are depicted as percentage of control. BACMK was used at 4.0 μ M and IL-1 β at 100 ng/mL.

possibility, although it is probably not practical. Thus, whether suppression of IL-1 β production by ICE inhibitors or induction of apoptosis by activation of ICE-related proteases has clinical significance, remains to be determined.

Acknowledgement

Supported in part by National Cancer Institute Grant No. CA 55164

References

- [1] Clark, S. C. and Kamen, R. (1987). The human hematopoietic colony-stimulating factors. *Science*, 236, 1229-1237.
- [2] Estrov, Z., Kurzrock, R., Estey, E., Wetzler, M., Ferrajoli, A., Harris, D., Blake, M., Gutterman, J. U. and Talpaz, M. (1992). Inhibition of acute myelogenous leukemia blast proliferation by IL-1 receptor antagonist and soluble IL-1 receptors. *Blood*, 79, 1938-1945.
- [3] Hoang, T., Hamman, A., Goncalves, O., Letendre, F., Mathieu, M., Wong, G. G. and Clark, C. S. (1988). Interleukin-1 enhances growth factor-dependent proliferation of the clonogenic cells in acute myeloblastic leukemia and of normal human primitive hematopoietic precursors. *J. Exp. Med.*, 168, 463-474.
- [4] Zucali, J. R., Broxmeyer, H. E., Dinarello, C. A., Gross, M. A. and Weiner, R. S. (1987). Regulation of early human hematopoietic (BFU-E and CFU-GEMM) progenitor cells in vitro by interleukin-1 induced fibroblast medium. *Blood*, 69, 3-37.
- [5] Carter, A., Silvian-Draxler, I. and Tatarsky, I. (1992). Effect in interleukin-1, tumor necrosis factor- α and interferon- α on the blast cells of acute myeloblastic leukemia. *Am. J. Hematol.*, 40, 245-251.
- [6] Oster, W., Cicco, N. A., Klein, H., Hirano, T., Kishimoto, T., Lindmann, A., Mertelsmann, R. H. and Herman, F. (1989). Participation of the cytokines interleukin-6, tumor necrosis factor- α , and interleukin-1 β secreted by acute myelogenous leukemia blasts in autocrine and paracrine leukemia growth control. *J. Clin. Invest.*, 84, 454-457.
- [7] Bagby, G. C. Jr., Dinarello, C. A., Wallace, P., Wagner, C., Hefeneider, S. and McCall, E. (1986). Interleukin-1 stimulates GM-CSF release by vascular endothelial cells. *J. Clin. Invest.*, 78, 1316-1323.
- [8] Herrmann, F., Oster, W., Meuer, S. C., Lindemann, A. and Mertelsmann, R. H. (1988). Interleukin-1 stimulates T lymphocytes to produce granulocyte-monocyte colony-stimulating factor. *J. Clin. Invest.*, 81, 1415-1418.
- [9] Zucali, J. R., Dinarello, C. A., Oblon, D. J., Gross, M. A., Anderson, L. and Weiner, R. S. (1986). Interleukin-1 stimulates fibroblasts to produce granulocyte-macrophage colony-stimulating activity and prostaglandin E. *J. Clin. Invest.*, 77, 857-863.
- [10] Griffin, J. D., Rambaldi, A., Vellenga, E., Young, D., Ostapovicz, D. and Cannistra, S. A. (1987). Secretion of interleukin-1 by acute myeloblastic leukemia cells in vitro induces endothelial cells to secrete colony-stimulating factors. *Blood*, 70, 1218-1221.
- [11] Rennick, D. G., Yang, L., Gemmell, L. and Lee, F. (1987). Control of hemopoiesis by a bone marrow stromal cell clone. Lipopolysaccharide and interleukin-1 inducible production of colony-stimulating factors. *Blood*, 69, 682-691.
- [12] Bartelmez, S. H., Bardley, T. R., Bertonecello, L., Mochizuki, D. Y., Tushinski, R. J., Stanley, E. R., Hapel, A. J., Young, I. G., Kriegler, A. B. and Hodgson, G. S. (1987). Interleukin-1 plus interleukin-3 plus colony-stimulating factor-1 are essential for clonal proliferation of primitive myeloid bone marrow cells. *Exp. Hematol.*, 17, 240-254.
- [13] Stanley, E. R., Bartocci, A., Parükin, D., Rosendaal, M. and Bradley, T. R. (1986). Regulation of very primitive, multipotent, hemopoietic cells by hemopoietin-1. *Cell*, 45, 667-674.
- [14] Zsebo, K. M., Wypych, J., Yushenkov, V. N., Lu, H., Hunt, P., Dukes, P. P. and Langley, K. E. (1988). Effects of hematopoietin-1 and interleukin-1 activities on early hematopoietic cells of the bone marrow. *Blood*, 71, 962-968.
- [15] Dinarello, C. A. (1991). Interleukin-1 and interleukin-1 antagonism. *Blood*, 77, 1627-1652.
- [16] di Giovine, F. S. and Duff, G. W. (1990). Interleukin-1: The first interleukin. *Immunol. Today*, 11, 13-20.
- [17] Sachs, L. and Lotem, J. (1993). Control of programmed cell death in normal and leukemic cells: New implications for therapy. *Blood*, 82, 15-21.
- [18] Raza, A., Preisler, H. D., Li, Y. Q., Larson, R. A., Goldberg, J., Browman, G., Bennet, J., Grunwald, H., Vogler, R. and Kukla, C. (1993). Biological characteristics of newly diagnosed poor prognosis acute myelogenous leukemia. *Am. J. Hematol.*, 42, 359-366.
- [19] Estrov, Z., Kurzrock, R. and Talpaz, M. (1995). Cytokines and their antagonists in myeloid disorders. *Semin. Hematol.*, 32, 220-231.
- [20] Estrov, Z., Kurzrock, R., Talpaz, M. (1993). Role of interleukin-1 inhibitory molecules in therapy of acute and chronic myelogenous leukemia. *Leuk. Lymphoma*, 10, 407-418.
- [21] Arend, W. P. (1993). Interleukin-1 receptor antagonist. *Adv. Immunol.*, 54, 167-227.
- [22] Dower, S. K., Wignall, J. M., Schooley, K., McMahan, C. J., Jackson, J. L., Prickett, K. S., Lupton, S., Cosman, D. and Sims, J. E. (1989). Retention of ligand binding activity by the extracellular domain of the IL-1 receptor. *J. Immunol.*, 142, 4314-4320.
- [23] Zheng, H., Fletcher, D., Kozak, W., Jiang, M., Hoffman, K. J., Conn, C. A., Soszynski, D., Grabiec, C., Trumbauer, M. E., Shaw, A., Kostura, M. J., Stevens, K., Rosen, H., North, R. J., Chen, H. Y., Tocci, M. J., Kluger, M. J. and Van der Ploeg, L. H. T. (1995). Resistance to fever induction and impaired acute-phase reaction in interleukin-1 beta-deficient mice. *Immunity*, 3, 9-19.
- [24] Mosley, B., Urdal, D. L., Prickett, K. S., Larsen, A., Cosman, D., Conlon, P. J., Gillis, S., Dower, S. K. (1987). The interleukin-1 receptor binds the human interleukin-1 alpha precursor but not the interleukin-1 beta precursor. *J. Biol. Chem.*, 262, 2941-2944.
- [25] Lönemann, G., Endres, S., Van der Meer, J. W. M., Cannon, J. G., Ghorbani, R., Dempsey, R. A., Sisson, S. D., Wolff, S. M. and Dinarello, C. A. (1989). In vitro production of IL 1 β , IL 1 α , TNF and IL2 in healthy subjects: distribution, effect of cyclooxygenase inhibition and evidence of independent gene regulation. *Eur. J. Immunol.*, 19, 2327-2333.
- [26] Limjoco, G., Galuska, S., Chin, J., Cameron, P., Boger, J., Schmidt, F. A. (1986). Antibodies of predetermined specificity to the major charged species of human interleukin 1. *Proc. Natl. Acad. Sci. USA*, 83, 3972-3976.

- [27] Beuscher, H. U., Nickells, M. W. and Colter, H. R. (1988). The precursor of interleukin-1 alpha is phosphorylated at residue serine 90. *J. Biol. Chem.*, 263, 4023-4028.
- [28] Kobayashi, Y., Appella, E., Yamada, M., Copeland, T. D., Oppenheim, J. J. and Matsushima, K. (1988). Phosphorylation of intracellular precursors of human IL-1. *J. Immunol.*, 140, 2279-2287.
- [29] Schmidt, J. A. and Tocci, M. J. (1990). In: *The Handbook of Experimental Pharmacology I. Peptide Growth Factors and Their Receptors*, edited by M. Sporn and A. Roberts, pp. 473-521, Berlin, Germany: Springer-Verlag.
- [30] Kobayashi, Y., Yamamoto, Y. K., Saido, T., Kawasaki, H., Oppenheim, J. J., Matsushima, K. (1990). Identification of calcium-activated neutral protease as a processing enzyme of human interleukin 1 alpha. *Proc. Natl. Acad. Sci. USA*, 87, 5548-5552.
- [31] Camron, P. M., Limjoco, G. A., Chin, J., Silverstein, L. and Schmidt, J. A. (1986). Purification to homogeneity and amino acid sequence analysis of two anionic species of human interleukin 1. *J. Exp. Med.*, 164, 237-250.
- [32] Kostura, M. J., Tocci, M. J., Limjoco, G., Chin, J., Comeron, P., Hillman, A. G., Chartrain, N. A. and Schmidt, J. A. (1989). Identification of a monocyte specific pre-interleukin 1 beta convertase activity. *Proc. Natl. Acad. Sci. USA*, 86, 5227-5231.
- [33] Howard, A. D., Kostura, M. J., Thornberry, N., Ding, G. J. F., Limjoco, G., Weidner, J., Salley, J. P., Hogouist, K. A., Chaplin, D. D., Mumford, R. A., Schmidt, J. A. and Tocci, M. J. (1991). IL-1 converting enzyme requires aspartic acid residues for processing of the IL-1 beta precursor at two distinct sites and does not cleave 31-kDa IL-1 alpha. *J. Immunol.*, 147, 2964-2969.
- [34] Black, R. A., Kronheim, S. R., Cantrell, M., Defley, M. C., March, C. J., Pickett, K. S., Wignall, J., Conlon, P. J., Cosman, D., Hopp, T. P. and Mochizuki, D. Y. (1988). Generation of biologically active interleukin-1 beta by proteolytic cleavage of the inactive precursor. *J. Biol. Chem.*, 263, 9437-9442.
- [35] Black, R. A., Kronheim, S. R. and Sleath, P. R. (1989). Activation of interleukin-1 beta by a co-induced protease. *FEBS Lett.*, 247, 386-390.
- [36] Sleath, P. R., Hendrickson, R. C., Kronheim, S. R., March, C. J. and Black, R. A. (1990). Substrate specificity of the protease that processes human interleukin-1 beta. *J. Biol. Chem.*, 265, 14526-14528.
- [37] Thornberry, N. A., Bull, H. G., Calaycay, J. R., Chapman, K. T., Howard, A. D., Kostura, M. J., Miller, D. K., Molineaux, S. M., Weidner, J. R., Aunins, J., Elliston, K. O., Ayala, J. M., Casano, R. J., Chin, J., Ding, G. J. F., Egger, L. A., Gaffney, D. P., Limjoco, G., Palyha, O. C., Raju, S. M., Rolando, A. M., Salley, J. P., Yamin, T. T., Lee, T. D., Shively, J. E., MacCoss, M., Mumford, R. A., Schmidt, J. A. and Tocci, M. J. (1992). A novel heterodimeric cysteine protease is required for interleukin-1 beta processing in monocytes. *Nature*, 356, 768-774.
- [38] Cerretti, D. G., Koslosky, C. J., Mosley, B., Nelson, N., Van Ness, K., Greenstreet, T. A., March, C. J., Kronheim, S. R., Druck, T., Cannizzaro, L. A., Huebner, K. and Black, R. A. (1992). Molecular cloning of the interleukin-1 beta converting enzyme. *Science*, 256, 97-100.
- [39] Singer, I. I., Scott, S., Chin, J., Bayne, E. K., Limjoco, G., Weidner, J., Miller, D. K., Chapman, K. and Kostura, M. J. (1995). The interleukin-1 beta-converting enzyme (ICE) is localized on the external cell surface membranes and in the cytoplasmic ground substance of human monocytes by immuno-electron microscopy. *J. Exp. Med.*, 182, 1447-1459.
- [40] Walker, N. P. C., Talanian, R. V., Brady, K. D., Dang, L. C., Bump, N. J., Ferenz, C. R., Franklin, S., Ghayur, T., Hackett, M. C., Hammill, L. C., Herzog, L., Hugunin, M., Houy, W., Markovich, J. A., McGuinness, L., Orlewicz, E., Paskind, M., Pratt, C. A., Reis, P., Summani, A., Terranova, M., Welch, J. P., Xiong, L., Moller, A., Tracey, D. E., Kamen, R. and Wong, W. W. (1994). Crystal structure of the cysteine protease interleukin-1 beta converting enzyme: A (p20/p10)₂ homodimer. *Cell*, 78, 343-352.
- [41] Wilson, K. P., Black, J. F., Thomson, J. A., Kim, E. E., Griffith, J. P., Navia, M. A., Murcko, M. A., Chambers, S. P., Aldape, R. A., Raybuck, S. A. and Livingston, D. J. (1994). Structure and mechanism of interleukin-1 beta converting enzyme. *Nature*, 370, 270-275.
- [42] Gu, Y., Wu, J., Faucheu, C., Lallanne, J. L., Diu, A., Livingston, D. J. and Su, M. S. (1995). Interleukin-1 beta converting enzyme requires oligomerization for activity of processed forms in vivo. *EMBO J.*, 14, 1923-1931.
- [43] Miller, D. K., Ayala, J. M., Egger, L. A., Raju, S. M., Yamin, T. T., Ding, G. J. P., Gaffney, E. P., Howard, A. D., Palyha, O. C., Rolando, A. M., Salley, J. P., Thornberry, N. A., Weidner, J. R., Williams, J. H., Chapman, K. T., Jackson, J., Kostura, M. J., Limjoco, G., Molineaux, S. M., Mumford, R. A. and Calaycay, J. R. (1993). Purification and characterization of active human interleukin-1 beta converting enzyme from THP-1 monocytic cells. *J. Biol. Chem.*, 268, 18062-18069.
- [44] Thornberry, N. A. and Molineaux, S. M. (1995). Interleukin-1 beta converting enzyme: A novel cysteine protease required for IL-1 beta production and implicated in programmed cell death. *Protein Science*, 4, 3-12.
- [45] March, C. J., Mosle, B., Larsen, A., Cerretti, P., Braedt, G., Price, V., Gillis, S., Henney, C. S., Kronheim, S. R., Grabstein, K., Conlon, P. J., Hopp, T. P. and Cosman, D. (1985). Cloning sequence and expression of two distinct human interleukin-1 complementary DNAs. *Nature*, 315, 641-647.
- [46] Singer, I. I., Scott, S., Hall, G. L., Limjoco, G., Chin, J. and Schmidt, J. A. (1988). Interleukin 1 beta is localized in the cytoplasmic ground substance but is largely absent from the golgi apparatus and plasma membranes of stimulated human monocytes. *J. Exp. Med.*, 167, 389-407.
- [47] Rubartelli, A., Cozzolino, F., Talio, M. and Sitia, R. (1990). A novel secretory pathway for interleukin-1 beta, a protein lacking a signal sequence. *EMBO J.*, 9, 1503-1510.
- [48] Hazuda, D. J., Lee, J. C., Young, P. R. (1988). The kinetics of interleukin 1 secretion from activated monocytes. *J. Biol. Chem.*, 263, 8473-8479.
- [49] Yuan, J., Shaham, S., Ledoux, S., Ellis, H. M. and Horvitz, H. R. (1993). The *C. elegans* cell death gene *ced-3* encodes a protein similar to mammalian interleukin-1 beta converting enzyme. *Cell*, 75, 641-652.
- [50] Miura, M., Zhu, H., Rotello, R., Hartwig, E. A., Yuan, J. (1993). Induction of apoptosis in fibroblasts by IL-1 beta-converting enzyme, a mammalian homolog of *C. elegans* cell death gene *ced-3*. *Cell*, 75, 653-660.
- [51] Ray, C. A., Black, R. A., Kronheim, S. R., Greenstreet, T. A., Sleath, P. R., Salvesen, G. S., Pickup, D. J. (1992). Viral inhibition of inflammation: Cowpox virus encodes an inhibitor of the interleukin-1 beta converting enzyme. *Cell*, 69, 597-604.
- [52] Palumbo, G. J., Pickup, D. J., Fredrickson, T. N., McIntyre, L. J. and Buller, M. L. (1989). Inhibition of an inflammatory response is mediated by a 38-kDa protein of cowpox. *Virology*, 172, 262-273.

- [53] Gagliardini, V., Fernandez, P.-A., Lee, R. K. K., Drexler, H. C. A., Rotello, R. J., Fishman, M. C., Yuan, J. (1994). Prevention of vertebrate neuronal death by the *crmA* gene. *Science*, 263, 826-828.
- [54] Boudreau, N., Simpson, C. J., Werb, Z. and Bissell, M. J. (1995). Suppression of ICE and apoptosis in mammary epithelial cells by extracellular matrix. *Science*, 267, 891-893.
- [55] Nagata, S. and Suda, T. (1995). Fas and Fas ligand: *lpr* and *gld* mutations. *Immunol. Today*, 16, 39-43.
- [56] Tewari, M. and Dixit, V. (1995). Fas- and tumor necrosis factor-induced apoptosis is inhibited by the Poxvirus *crmA* gene product. *J. Biol. Chem.*, 270, 3255-3260.
- [57] Enarl, M., Hug, H. and Nagata, S. (1995). Involvement of an ICE-like protease in Fas-mediated apoptosis. *Nature*, 375, 78-81.
- [58] Los, M., Van de Craen, M., Penning, L. C., Schenk, H., Westendorp, M., Baeuerle, P. A., Droge, W., Krammer, P. H., Flers, W. and Schulze-Osthoff, K. (1995). Requirement of an ICE/CED-3 protease for Fas/APO-1-mediated apoptosis. *Nature*, 375, 81-83.
- [59] Tamura, T., Ishikawa, M., Lamphier, M. S., Tanaka, N., Oishi, I., Alzawa, S., Matsuyama, T., Mak, T. W., Taki, S. and Taniguchi, T. (1995). An IRF-1-dependent pathway of DNA damage-induced apoptosis in mitogen-activated T lymphocytes. *Nature*, 376, 596-599.
- [60] Hengartner, M. O., Ellis, R. E. and Horvitz, H. R. (1992). *Caenorhabditis elegans* gene *ced-9* protects cells from programmed cell death. *Nature*, 356, 494-499.
- [61] Hengartner, M. O., Horvitz, H. R. (1994). *C. elegans* cell survival gene *ced-9* encodes a functional homolog of the mammalian proto-oncogene *bcl-2*. *Cell*, 76, 665-676.
- [62] Tsujimoto, Y., Cossman, J., Jaffe, E. and Croce, C. M. (1985). The t(14;18) chromosome translocation involved in B-cell neoplasms result from mistakes in VDJ joining. *Science*, 228, 1440-1443.
- [63] Bakhshi, A., Jensen, J. P., Goldman, P., Wright, J. J., McBride, O. W., Einstein, A. L. and Korsmeyer, S. J. (1985). Cloning the chromosomal breakpoint of t(14;18) human lymphomas: clustering around J_H on chromosome 14 and near a transcriptional unit of 18. *Cell*, 41, 899-906.
- [64] Cleary, M. L., Smith, S. D. and Sklar, J. (1986). Cloning and structural analysis of cDNAs for *bcl-2* and hybrid *bcl-2*/immunoglobulin transcript resulting from the t(14;18) translocation. *Cell* 47, 19-28.
- [65] Korsmeyer, S. J. (1995). Regulators of cell death. *Trends Genet.* 11, 101-105.
- [66] Hengartner, M. O. and Horvitz, H. R. (1994). Activation of *C. elegans* cell death protein CED-9 by an amino-acid substitution in a domain conserved in Bcl-2. *Nature*, 369, 318-320.
- [67] Vaux, D. L., Weissman, I. L. and Kim, S. K. (1992). Prevention of programmed cell death in *Caenorhabditis elegans* by human *bcl-2*. *Science*, 258, 1955-1957.
- [68] Lazebnik, Y. A., Kaufmann, S. H., Desnoyers, S., Poirier, G. G. and Earnshaw, W. (1994). Cleavage of poly (ADP-ribose) polymerase by a proteinase with properties like ICE. *Nature*, 371, 346-347.
- [69] Gu, Y., Sarnecki, C., Aladape, R. A., Livingston, D. J. and Su, M. S. (1995). Cleavage of poly(ADP-ribose) polymerase by interleukin-1 β converting enzyme and its homologs TX and Nedd-2. *J. Biol. Chem.*, 270, 18715-18718.
- [70] Wang, L., Miura, M., Bergerson, L., Zhu, H. and Yuan, J. (1994). Ich-1, an Ice/ced-related gene, encodes both positive and negative regulators of programmed cell death. *Cell*, 78, 739-750.
- [71] Kumar, S., Kinoshita, M., Noda, M., Copeland, N. G. and Jenkins, N. A. (1994). Induction of apoptosis by the mouse Nedd2 gene, which encodes a protein similar to the product of the *Caenorhabditis elegans* cell death gene *ced-3* and the mammalian II-1 β -converting enzyme. *Genes Dev.*, 8, 1613-1626.
- [72] Darmon, A. J., Nicholson, D. W. and Bleackley, R. C. (1995). Activation of the apoptotic protease CPP32 by cytotoxic T-cell-derived granzyme B. *Nature*, 377, 446-448.
- [73] Nicholson, D. W., Ali, A., Thornberry, N. A., Vaillancourt, J. P., King, C. K., Gallant, M., Gareau, Y., Griffin, P. R., Labelle, M., Lazebnik, Y. A., Munday, N. A., Raju, S. M., Smulson, M. E., Yamin, T. T., Yu, V. L. and Miller, D. K. (1995). Identification and inhibition of the ICE/CED-3 protease necessary for mammalian apoptosis. *Nature*, 375, 37-43.
- [74] Fernandes-Alnemri, T., Litwack, G. and Alnemri, E. S. (1994). CPP32, a novel human apoptotic protein with homology to *Caenorhabditis elegans* cell death protein Ced-3 and mammalian interleukin-1 β -converting enzyme. *J. Biol. Chem.*, 269, 30761-30764.
- [75] Smulson, M., Istock, N., Ding, R. and Cherney, B. (1994). Deletion mutants of poly(ADP-ribose) polymerase support a model of cyclic association and dissociation of enzyme from DNA ends during DNA repair. *Biochemistry*, 33, 6186-6191.
- [76] Ding, R. and Smulson, M. (1994). Depletion of nuclear poly(ADP-ribose) polymerase by antisense RNA expression: influences on genomic stability, chromatin organization, and carcinogen cytotoxicity. *Cancer Res.*, 54, 4627-4634.
- [77] Kaufmann, S. H., Desnoyers, S., Ottaviano, Y., Davidson, N. E. and Poirier, G. G. (1993). Specific proteolytic cleavage of poly(ADP-ribose) polymerase: An early marker of chemotherapy-induced apoptosis. *Cancer Res.*, 53, 3976-3985.
- [78] Tewari, M., Quan, L. T., O'Rourke, K., Desnoyers, S., Zeng, Z., Beidler, D. R., Poirier, G. G., Salvesen, G. S. and Dixit, V. M. (1995). Yama/CPP32 beta, a mammalian homolog of CED-3, is a CrmA-inhibitable protease that cleaves the death substrate poly(ADP-ribose) polymerase. *Cell*, 81, 801-809.
- [79] Munday, N. A., Vaillancourt, J. P., Ali, A., Casano, F. J., Miller, D. K., Molineaux, S. M., Yamin, T.-T., Yu, V. L. and Nicholson, D. W. (1995). Molecular cloning and pro-apoptotic activity of ICE_{rel}II and ICE_{rel}III, Members of the ICE/CED-3 family of cysteine proteases. *J. Biol. Chem.*, 270, 15870-15876.
- [80] Faucheu, C., Diu, A., Chan, A. W., Blanchet, A. M., Missec, C., Here, F., Collard-Dutilleul, V., Gu, Y., Aldape, R. V., Lippke, J. A., Rocher, C., Su, M. S., Livingston, D. J., Hercend, T. and Lalanne, J. L. (1995). A novel human proteinase similar to the interleukin-1 β converting enzyme induces apoptosis in transfected cells. *EMBO J.*, 14, 1914-1922.
- [81] Kamens, J., Paskind, M., Hugunin, M., Talanian, R. V., Allen, H., Banach, D., Bump, N., Hackett, M., Johnston, C. G., Li, P., Mankovich, J. A., Terranova, M. and Ghayur, T. (1995). Identification and characterization of ICH-2, a novel member of the interleukin-1 beta-converting enzyme family of cysteine proteases. *J. Biol. Chem.*, 270, 15250-15256.
- [82] Fernandes-Alnemri, T., Litwack, G. and Alnemri, E. S. (1995). Mch2, a new member of the apoptotic Ced-3/Ice Cysteine protease gene family. *Cancer Res.*, 55, 2737-2742.
- [83] Fernandes-Alnemri, T., Takahashi, A., Armstrong, R., Krebs, J., Fritz, L., Tomaselli, K. J., Wang, L., Yu, Z., Croce, C. M., Salvesen, G., Earnshaw, W. C., Litwack, G. and Alnemri, E.

- S. (1995). Mch3, a novel human apoptosis protease highly related to CPP32. *Cancer Res.*, 55, 6045-6052.
- [84] Duan, H., Chinnaiyan, A. M., Hudson, P. L., Wing, J. P., He, W.-W. and Dixit, V. M. (1996). ICE-LAP3, a novel mammalian homologue of the *Caenorhabditis elegans* cell death protein ced-3 is activated during Fas- and tumor necrosis factor-induced apoptosis. *J. Biol. Chem.*, 271, 1621-1625.
- [85] Chinnaiyan, A. M., Orth, K., O'Rourke, K., Duan, H., Poirer, G. G. and Dixit, V. M. Molecular ordering of the cell death pathway: Bcl-2 and Bcl-x_L function upstream of the CED-3-like apoptotic proteases. *J. Biol. Chem.*, (in press).
- [86] Wang, X., Pai, J. T., Wiedenfeld, E. A., Medina, J. C. and Slaughter, C. A. (1995). Purification of an interleukin-1 beta converting enzyme-related cysteine protease that cleaves sterol regulatory element-binding proteins between the leucine zipper and transmembrane domains. *J. Biol. Chem.*, 270, 18044-18050.
- [87] Fernandes-Alnemri, T., Litwack, G. and Alnemri, E. S. (1994). CPP32, a novel human apoptotic protein with homology to *Caenorhabditis elegans* cell death protein Ced-3 and mammalian interleukin-1 β -converting enzyme. *J. Biol. Chem.*, 269, 30761-30764.
- [88] Kumar, S. and Harvey, N. L. (1995). Role of multiple cellular proteases in the execution of programmed cell death. *FEBS Lett.*, 375, 169-173.
- [89] Young, J. O.-E. (1989). Killing of target cells by lymphocytes: a mechanistic view. *Physiol. Rev.*, 69, 250-314.
- [90] Berke, G. (1995). The CTL's kiss of death. *Cell*, 81, 9-12.
- [91] Jenne, D. E. and Tschopp, J. (1988) Granzymes: A family of serine proteases in granules of cytolytic T lymphocytes. *Curr. Top. Microbiol. Immunol.*, 140, 33-47.
- [92] Smyth, M. J. and Trapani, J. A. (1995). Granzymes: exogenous proteinases that induce target cell apoptosis. *Immunol. Today*, 16, 202-206.
- [93] Berthou, C., Marolleau, J. P., LaFaurie, C., Soulie, A., Dal Cortivo, L., Bourge, J.-F., Benbunan, M. and Sespportes, M. (1995). Granzyme B and perforin lytic proteins are expressed in CD34+ peripheral blood progenitor cells mobilized by chemotherapy and granulocyte colony-stimulating factor. *Blood*, 86, 3500-3506.
- [94] Irmeler, M., Hertig, S., Robson, M., Sadoul, R., Becherer, J. D., Proudfoot, A., Solari, R. and Tschopp, J. (1995). Granzyme A is an interleukin-1 β -converting enzyme. *J. Exp. Med.*, 181, 1917-1922.
- [95] Xue, D. and Horvitz, R. (1995). Inhibition of the *Caenorhabditis elegans* cell-death protease CED-3 by a Ced-3 cleavage site in baculovirus p35 protein. *Nature*, 377, 248-251.
- [96] Wang, Z. Q., Auer, B., Stingl, L., Berghammer, H., Haidacher, D., Schweiger, M. and Wagner, E. F. (1995). Mice lacking ADPRT and poly(ADP-ribosyl)ation develop normally but are susceptible to skin disease. *Genes Dev.*, 9, 509-20.
- [97] Lazebnik, Y. A., Takahashi, A., Moir, R. D., Goldman, R. D., Poirier, G. G., Kaufmann, S. H. and Earnshaw, W. C. (1995). Studies of the lamin proteinase reveal multiple parallel biochemical pathways during apoptotic execution. *Proc. Natl. Acad. Sci. USA*, 92, 9042-9046.
- [98] Pushkareva, M., Obeid, L. M. and Hannun, Y. A. (1995). Ceramid: an endogenous regulator of apoptosis and growth suppression. *Immunol. Today*, 16, 294-297.
- [99] Kolesnick, R. N., Haimovitz-Freedman, A. and Fuks, Z. (1994). The sphingomyelin signal transduction pathway mediates apoptosis for tumor necrosis factor, Fas, and ionizing radiation. *Biochem. Cell Biol.*, 72, 471-474.
- [100] Chinnaiyan, A. M., Tepper, C. G., Seldin, M. F., O'Rourke, K., Kischkel, F. C., Hellbardt, S., Krammer, P. H., Peter, M. E. and Dixit, V. M. FADD/MORT1 is a common mediator of CD95 (Fas/APO-1)- and TNF-receptor-induced apoptosis. *J. Biol. Chem.*, (in press).
- [101] Li, P., Allen, H., Banerjee, S., Franklin, S., Herzog, L., McDowell, J., Paskind, M., Rodman, L., Salfeled, J., Towne, E., Tracey, D., Wardwell, S., Wei, F.-Y., Wong, W., Kamen, R. and Seshardi, T. (1995). Mice deficient in IL-1 β -converting enzyme are defective in production of mature IL-1 β and resistant to endotoxic shock. *Cell*, 80, 401-411.
- [102] Kuida, K., Lippke, J. A., Ku, G., Harding, M. W., Livingston, D. J., Su, M. S. and Flavell, R. A. (1995). Altered cytokine export and apoptosis in mice deficient in interleukin-1 β converting enzyme. *Science*, 267, 2000-2003.
- [103] Komiyama, T., Ray, C. A., Pickup, D. J., Howard, A. D., Thornberry, N. A., Peterson, E. P. and Salvesen, G. (1994). Inhibition of interleukin-1 β converting enzyme by the cowpox virus serpin crmA. *J. Biol. Chem.*, 269, 19331-19337.
- [104] Clem, R. J., Fechheimer, M. and Miller, L. K. (1991). Prevention of apoptosis by a baculovirus gene during infection of insect cells. *Science*, 254, 1388-1390.
- [105] Sugimoto, A., Friesen, P. D. and Rothman, J. H. (1994). Baculovirus p35 prevents developmentally programmed cell death and rescues a ced-9 mutant in the nematode *Caenorhabditis elegans*. *EMBO J.*, 13, 2023-2028.
- [106] Shaw, E. (1990). Cysteine proteinases and their selective inactivation. *Adv. Enzymol.*, 63, 271-347.
- [107] Miller, B. E., Krasney, P. A., Gauvin, D. M., Holbrook, K. B., Koonz, D. J., Abruzzese, R. V., Miller, R. V., Pagani, K. A., Dole, R. E., Ator, M. A. and Gilman, S. C. (1995). Inhibition of mature IL-1 β production in mature macrophages and a murine model of inflammation by WIN 67694, an inhibitor of IL-1 β converting enzyme. *J. Immunol.*, 154, 1331-1338.
- [108] Robinson, R. P. and Donahue, K. M. (1992). Synthesis of a peptidyl difluoro ketone bearing the aspartic acid side chain: An inhibitor of interleukin-1 β converting enzyme. *J. Org. Chem.*, 57, 7309-7314.
- [109] Rambaldi, A., Torcia, M., Bettoni, S., Vannier, E., Barbui, T., Shaw, A. R., Dinarello, C. A. and Cozzolino, F. (1991). Modulation of cell proliferation and cytokine production in acute myeloblastic leukemia by interleukin-1 receptor antagonist and lack of its expression by leukemic cells. *Blood*, 78, 3248-3253.
- [110] Yin, M., Gopal, V., Banavali, S., Gartside, P. and Preisler, H. (1992). Effect of an IL-1 receptor antagonist on acute myeloid leukemia cells. *Leukemia*, 6, 898-901.
- [111] Estrov, Z., Black, R., Sleath, P. R., Harris, D., Van, Q., LaPushin, R., Estey, E. and Talpaz, M. (1995). Effect of interleukin-1 β converting enzyme inhibitor on acute myelogenous leukemia progenitor proliferation. *Blood*, 86, 4594-4602.
- [112] Kettner, C. and Shaw, E. (1989). Inactivation of trypsin-like enzymes with peptides of arginine chloromethyl ketone. In *Methods in Enzymology*, Vol. 80, *Proteolytic Enzymes*, Part C, edited by L. Lorand L. pp. 826-842. Orlando FL: Academic Press Inc. pp. 826-842.
- [113] Stosic-Grujicic, S., Basara, N., Milenkovic, P., Dimarello, C. A. (1995). Modulation of acute myeloblastic leukemia (AML) cell proliferation and blast colony formation by antisense oligomer for IL-1 beta converting enzyme (ICE) and IL-1 receptor antagonist (IL-1ra). *J. Chemother.*, 7, 67-70.

Inhibition of Interleukin-1 by an Interleukin-1 Receptor Antagonist Prevents Graft-Versus-Host Disease

By Philip L. McCarthy Jr, Sunil Abhyankar, Steven Neben, Gale Newman, Colin Sieff, Robert C. Thompson, Steven J. Burakoff, and James L.M. Ferrara

Graft-versus-host disease (GVHD) is the major complication of allogeneic bone marrow transplantation (BMT). Dysregulation of inflammatory monokines such as tumor necrosis factor α (TNF α) has been noted in both clinical and experimental GVHD. We present evidence that interleukin-1 (IL-1), another inflammatory monokine, is an important mediator of GVHD. Expression of the gene for IL-1 α as well as the gene for TNF α is increased in the skin of mice with GVHD. Inhibition of IL-1 function by the *in vivo* administration of IL-1 receptor

antagonist (IL-1ra) reduces the immunosuppression and mortality of GVHD without impairing the engraftment of hematopoietic stem cells. GVHD thus appears to be a systemic inflammatory process in which monokines, especially IL-1, appear to be important mediators. Inhibition of IL-1 by IL-1ra represents a novel approach to the understanding and control of GVHD.

© 1991 by The American Society of Hematology.

GRAFT-VERSUS-HOST disease (GVHD) is the primary complication of allogeneic bone marrow transplantation (BMT). Although GVHD is caused by T cells in the donor graft, one manifestation of the disease is the dysregulation of inflammatory monokines such as tumor necrosis factor α (TNF α).^{1,2} In an experimental model of GVHD, TNF α has been shown to induce GVHD lesions and inhibition of TNF reduces GVHD in both experimental and clinical BMT.^{3,4} Several cytokines are dysregulated in models of *in vivo* alloreactivity, including graft rejection and GVHD.^{5,6} Interleukin-1 (IL-1) is a potent cytokine mediator of a variety of inflammatory conditions^{7,8} and has similar effects to TNF α both *in vitro* and *in vivo*.^{9,10} We wished to examine the role of IL-1 in the pathogenesis of GVHD and asked whether GVHD could be prevented by a molecule that inhibits the action of IL-1.

The human IL-1 receptor antagonist (IL-1ra) is a recombinant protein that, like its natural analog, competes with IL-1 for binding to the type I IL-1 receptor but has no agonist activity.^{11,12} IL-1ra has been shown to prevent the effects of exogenous IL-1 α in mice,¹³ but it has no direct effect on the activity of other monokines such as TNF α (P. Kilian, unpublished results). Thus, this protein is a useful probe of the involvement of IL-1 in the pathology of a complex disease such as GVHD in which multiple cytokines are dysregulated. In this study, we investigated the role of IL-1 in the pathogenesis of GVHD and show that IL-1ra blocks the mortality and immunosuppression associated with GVHD.

MATERIALS AND METHODS

Mice and BMT. CBA and B10.BR mice were obtained from Jackson Labs (Bar Harbor, ME). BMT was performed as previously described.^{12,14} Briefly, CBA or B10.BR mice were administered 1,300 cGy total body irradiation in a split dose and injected intravenously with 1×10^7 B10.BR BM cells and 2×10^6 nylon wool-passaged B10.BR splenocytes. Mice were given acidified drinking water and kept in isolator cages after transplantation.

IL-1ra administration. Human IL-1ra was purified as previously described.¹⁵ The allogeneic CBA mice were administered twice daily injections of saline or 3 mg/kg of IL-1ra intraperitoneally (IP) from day 0 through day 10. Syngeneic B10.BR mice were administered only saline injections. The dose of IL-1ra of 3 mg/kg injected twice a day was chosen for this study because a dose of 2 mg/kg injected twice a day had no detectable toxicity and provided

complete protection against reactivation arthritis in response to streptococcal cell wall challenge in rats¹⁶ (J. Schwab, manuscript submitted). No toxicities were observed either at this dose and schedule of IL-1ra or at 10 times the dose (20 mg/kg injected twice a day). The administration of IL-1ra at 0.5 mg/kg twice a day gave only 50% protection in the arthritis system. In addition, bioavailability studies in rats have shown that plasma levels of IL-1ra greater than 25 ng/mL can be maintained for at least 8 hours after a 2 mg/kg subcutaneous injection (D. Bloedow, unpublished data). The dose of 3.0 mg/kg injected twice a day was chosen for use in the murine GVHD studies based on the rat data and the different ratio of body surface area to weight in mice. All mice were monitored for potential toxicities with particular reference to lymphohematopoietic reconstitution.

Messenger RNA (mRNA) detection. RNA was isolated by guanidinium thiocyanate/phenol/chloroform extraction, reverse transcribed into cDNA and amplified by polymerase chain reaction (PCR) as described.¹⁷ The PCR protocol consisted of the following conditions: denaturation at 95°C for 30 seconds, annealing at 55°C for 30 seconds, and primer extension at 72°C for 60 seconds. The reactions were performed for 30 cycles. Sense and antisense oligonucleotide primers for TNF α , IL-1 α , and β actin yielded PCR products of 310, 300, and 348 bp, respectively, as previously published.¹⁸ PCR products were electrophoresed in a 2% agarose gel and stained with ethidium bromide.

Peripheral blood count determinations. Two hundred microliters

From the Division of Hematology and the Department of Immunology, Brigham and Women's Hospital; the Department of Pediatric Oncology, DFCI and Children's Hospital; the Joint Center for Radiation Therapy, Harvard Medical School, Boston, MA; and Synergen Inc. Boulder, CO.

Submitted June 20, 1991; accepted August 1, 1991.

Supported by National Institutes of Health (NIH) Program Project Award 5-PO1-CA39542. P.L.M. is supported by an NIH Clinical Investigator Award No. 1-K08AI00926. J.L.M.F. is a recipient of an American Cancer Society Junior Faculty Research Award and a Claudia Adams Barr Investigator.

Address reprint requests to Philip L. McCarthy, Jr, MD, Division of Hematology, Baylor College of Medicine, Methodist Hospital M902, 6565 Fannin, Houston, TX 77030.

The publication costs of this article were defrayed in part by page charge payment. This article must therefore be hereby marked "advertisement" in accordance with 18 U.S.C. section 1734 solely to indicate this fact.

© 1991 by The American Society of Hematology.
0006-4971/91/7808-0035\$3.00/0

of heparinized blood was obtained from the retroorbital plexus and complete blood count analysis was obtained by a Technicon H-1 analyzer (Technicon, Tarrytown, NY).

Progenitor assays. Mice were killed by cervical dislocation. BM was harvested, prepared as single cell suspensions, and counted. Progenitors were cultured in duplicate for 7 days using the methyl cellulose technique and the total number of colonies calculated (colony-forming unit granulocyte-macrophage [CFU-GM], $\times 10^{-3}/2$ hind limbs) as described.²² Hematopoietic stem cells were measured by injection of BM into irradiated (950 cGy) B10.BR mice as described.²³ Spleens were harvested at 12 days ($n = 6$) and the total number of stem cells calculated (CFU-S $\times 10^{-3}/2$ hind limbs).

T-lymphocyte precursor assay. Four weeks after transplantation, mice were killed, and thymus and spleens were prepared as single cell suspensions and counted. Splenocytes were placed in culture for seven days in 96-well plates with the mitogen concanavalin A (3 $\mu\text{g}/\text{mL}$) under limiting dilution conditions as described.¹⁹ Wells were pulsed with ^3H -thymidine (New England Nuclear, Boston, MA), harvested, and counted in a beta scintillation counter. Wells scored as positive when the counts per minute were higher than negative controls by at least 3 standard deviations. The frequency of splenic proliferating T-lymphocyte precursors (pPTL) was determined by limiting dilution analysis and the total number of precursors per spleen was calculated by multiplying their frequency by the splenocyte count.

RESULTS

Monokine expression in GVHD skin. We first examined whether the IL-1 α gene is transcribed in the skin, a principle target organ, using a murine model of GVHD to minor histocompatibility antigens.¹⁷ As shown in Fig 1, mRNA specific for both TNF α and IL-1 α are detectable by PCR amplification of RNA from the skin of animals with GVHD. Neither monokine mRNA is amplified from normal skin. Band fidelity was confirmed by hybridization of the blotted PCR products to the respective γ - ^{32}P -labeled internal oligonucleotide probes (data not shown). Negative controls included amplification of RNA without reverse transcriptase that showed no PCR product for β actin. The induction of these inflammatory monokines during GVHD appears to be specific because no PCR product from the mRNA of the lymphokine IL-2 could be detected in the skin of animals with GVHD (data not shown). PCR analysis was used for this study due to the difficulty in discerning TNF α mRNA in the skin of GVHD mice.²⁴ In addition, we were unable to detect significant differences in TNF protein production from splenocytes of control and GVHD mice using the L929 bioassay (data not shown). Studies are in

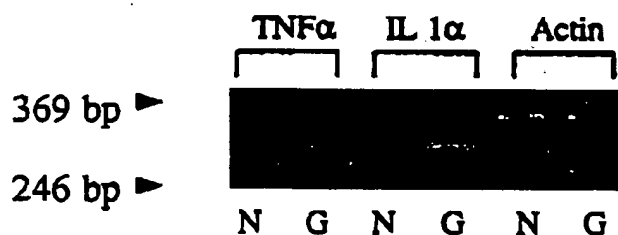


Fig 1. Induction of IL-1 α and TNF α mRNA in GVHD skin. RNA was isolated from epithelial cells of normal CBA mice (N) or transplanted (B10.BR \rightarrow CBA) mice with GVHD (G), reverse transcribed into cDNA, and amplified by PCR with primers for TNF α , IL-1 α , and β actin.

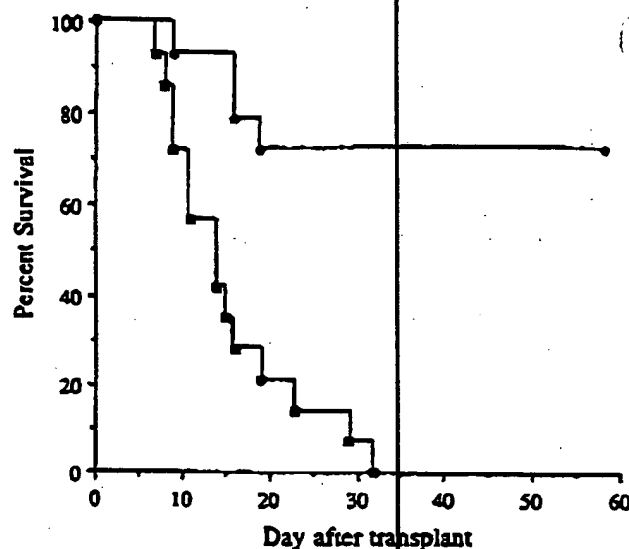


Fig 2. IL-1ra reduces mortality from GVHD. BM and T cells from B10.BR donor mice were injected into lethally irradiated allogeneic CBA recipients. The CBA mice were given twice daily injections of saline (○, $n = 14$) or 3 mg/kg of IL-1ra IP (●, $n = 14$) from day 0 through day 10. Survival was significantly improved in the mice receiving IL-1ra ($P = .0001$, exact log rank test).

progress to localize the specific cell populations in the skin that produce both TNF α and IL-1 and the effect of IL-1ra on such production.

Effect of blocking IL-1 on GVHD. To examine further the role of IL-1 in GVHD, we tested the effects of an IL-1 inhibitor, IL-1ra,^{13,14} for its effects on systemic GVHD in the same murine BMT model. Transplants of BM and splenic T cells were conducted between donor B10.BR and lethally irradiated recipient CBA mouse strains (B10.BR \rightarrow CBA) that are H-2 identical but differ at multiple minor histocompatibility loci that are stimuli for GVHD.¹⁷ GVHD induces profound immunosuppression and the mice die within 6 weeks. Transplanted mice received either saline or IL-1ra injections for 10 days after transplantation and were monitored for signs of GVHD and survival (Fig 2). We chose a dose and schedule of IL-1ra treatment based on a regimen that gave complete efficacy and no toxicity in a rat model of arthritic inflammation (see Materials and Methods). The saline-treated (B10.BR \rightarrow CBA) mice developed evidence of GVHD within 14 to 21 days after BMT and all animals were dead by 40 days after transplantation. By contrast, 80% of the IL-1ra-treated (B10.BR \rightarrow CBA) mice were alive at day 15 and showed no evidence of GVHD as manifested by weight loss or fur ruffling (data not shown). Survival levelled off at 70% after 60 days after BMT and showed long-term protection by IL-1ra ($P = .0001$). Syngeneic B10.BR transplant recipients had a 100% survival at 40 days (data not shown). These results argue for an important pathologic role for IL-1 in GVHD.

Effect of blocking GVHD on immune reconstitution. Immunologic dysfunction is another manifestation of GVHD, and we wished to see if blocking IL-1 would ameliorate the immunosuppressive effects of GVHD (Table 1).

Table 1. IL-1ra Prevents the Immunologic Suppression of GVHD

| Recipient | Injection | n | Thymocyte Counts ($\times 10^{-4}$) | pPTL Total/Spleen ($\times 10^{-4}$) |
|-----------------------------|-----------|---|---------------------------------------|--|
| B10.BR \rightarrow CBA | Saline | 3 | 0.13 (0.1) | 1.14 (0.48) |
| B10.BR \rightarrow CBA | IL-1ra | 4 | 2.45 (1.49) | 3.52 (0.99) |
| B10.BR \rightarrow B10.BR | Saline | 4 | 4.78 (1.09) | 7.02 (1.83) |

CBA (B10.BR \rightarrow CBA) and B10.BR (B10.BR \rightarrow B10.BR) mice were transplanted with B10.BR BM and spleen cells as described in Materials and Methods. The frequency of splenic pPTL was determined by limiting dilution analysis and the total number of precursors per spleen was calculated by multiplying their frequency by the splenocyte count. The standard error is in parentheses.

(B10.BR \rightarrow CBA) control mice treated with saline showed severely diminished thymic cellularity and low numbers of pPTL, as previously reported.¹⁸ By contrast, (B10.BR \rightarrow CBA) mice receiving IL-1ra had 20 times as many thymocytes and three times as many pPTL per spleen ($P = .03$) when compared with saline-treated (B10.BR \rightarrow CBA) controls. These data show that IL-1 either directly or indirectly plays an important role in the immunosuppression of GVHD.

Effect of blocking GVHD by IL-1ra on hematopoietic reconstitution. IL-1 is known to be an important factor in hematopoiesis. Exogenous IL-1 protects mice against radiation-induced BM aplasia and enhances BM engraftment in mice receiving T-cell-depleted BMT.^{3a,27} Recombinant human IL-1ra can block the effect of IL-1 on certain aspects of hematopoiesis in mice.¹⁹ To determine whether blocking the action of endogenous IL-1 might impede engraftment of hematopoietic stem cells, we examined engraftment and hematopoietic reconstitution in IL-1ra-treated animals at 4 weeks after transplantation. Donor B10.BR marrow engrafted completely in CBA mice receiving IL-1ra as determined by the presence of donor B10.BR hemoglobin and thymocytes at 4 and 8 weeks after BMT (data not shown). In addition, IL-1ra had no deleterious effect on peripheral blood counts (Fig 3A). Hematopoietic reconstitution was further quantitated by BM cellularity and the measurement of progenitor cells (CFU-GM) and stem cells (day 12 CFU-S) (Fig 3B). IL-1ra had no detrimental effects on any aspect of hematopoiesis; (B10.BR \rightarrow CBA) mice receiving IL-1ra had significantly more day 12 CFU-S than the saline-treated (B10.BR \rightarrow CBA) animals ($P = .05$) and approximately 60% of the day 12 CFU-S of syngeneic (B10.BR \rightarrow B10.BR) mice. This increase confirms the ability of IL-1ra to block systemic effects of GVHD and to enhance hematopoietic engraftment.

DISCUSSION

Current efforts to prevent GVHD have focused on the inhibition or elimination of T-cell lymphocytes from the donor BM. However, T-cell depletion of donor BM has led to an increase in graft failure, poor immunologic reconstitution, and relapse of primary BM disease.²⁸ We have shown

that IL-1 is an important mediator of GVHD, confirming and extending the observation that exogenous IL-1 appeared to intensify GVHD in another experimental murine model of BMT.³ The neutralization of endogenous IL-1 by IL-1ra in vivo improved survival from GVHD and reconstitution of cell-mediated immunity without retarding hematopoietic engraftment.

Both TNF α and IL-1 are induced during a variety of inflammatory states and are intimately involved in the pathogenesis of inflammation in such disorders as sepsis and allograft rejection.⁷⁻¹³ Inhibition of TNF α by anti-TNF antibodies in mice with GVHD has led to highly significant but incomplete inhibition of GVHD mortality.⁴ Similarly, in this study, blockade of IL-1 by IL-1ra led to highly significant but not complete inhibition of GVHD mortality. Both cytokines appear to play significant roles in the development and propagation of GVHD. Studies are in progress to determine whether both anti-TNF and anti-IL-1 agents synergize to reduce GVHD mortality. Studies are also in progress to determine the optimal dose and schedule of IL-1ra administration as well as to determine whether IL-1ra will prevent mortality of GVHD that is induced by

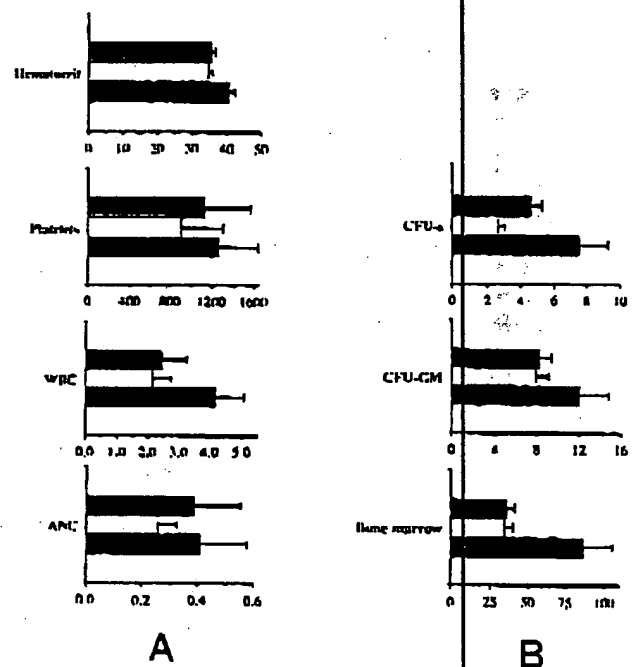


Fig 3. Effect of IL-1ra on hematopoietic reconstitution. (A) Peripheral blood counts from (B10.BR \rightarrow CBA) recipients treated with IL-1ra (□) were not significantly different from those of (B10.BR \rightarrow CBA) mice given saline (■) or from (B10.BR \rightarrow B10.BR) recipients given saline (■). Peripheral blood counts are expressed as: hematocrit (%), platelets ($\times 10^9/L$), white blood count (WBC, $\times 10^3/L$), and absolute neutrophil count ($\times 10^3/L$). (B) BM reconstitution was greater in syngeneic (B10.BR \rightarrow B10.BR) recipients than in either group of (B10.BR \rightarrow CBA) recipients. Hematopoietic stem cell numbers (CFU-S day 12) were greater in mice receiving IL-1ra than in saline-treated controls ($P = .05$). Total stem cells are expressed as day 12 CFU-S $\times 10^{-3}/2$ hind limbs. Colony-forming units of granulocyte-macrophage precursors are expressed as CFU-GM $\times 10^{-3}/2$ hind limbs. Nucleated BM cells are expressed as cells $\times 10^4/2$ hind limbs.

MHC differences. Inhibition of IL-1 may permit maintenance of certain critical functions such as immune surveillance while preventing the nonspecific and deleterious effects of systemic inflammation. This drug would be another alternative to T-cell depletion as a means of controlling GVHD. IL-1ra may represent a prototype of a class of cytokine antagonists that will serve not only as a probe for the pathology of a complex disease process, such

as GVHD, but also as a new agent for prophylaxis and treatment of clinical GVHD.

ACKNOWLEDGMENT

The authors acknowledge the expert technical assistance of Linda Callahan and Ellen Moore as well as Drs Joseph Antin, Alan D'Andrea, Ilonna Rimm, and Gary Tanigawa for critically reviewing the manuscript.

REFERENCES

1. Ferrara JLM, Deeg HJ: Graft versus host disease. *N Engl J Med* 324:667, 1991
2. Holler E, Kolb HJ, Moller A, Kempeni J, Liesenfeld S, Pechumer H, Lehman W, Ruckdeschel G, Gleixner B, Riedner C, Ledderose G, Brehm G, Mittermuller J, Wilmanns W: Increased serum levels of tumor necrosis factor alpha precede major complications of bone marrow transplantation. *Blood* 75:1011, 1990
3. Symington FW, Pepe MS, Chen A, Deliganis A: Serum tumor necrosis factor alpha associated with acute graft-versus-host disease in humans. *Transplantation* 50:518, 1990
4. Piguet PF, Grau GE, Allet B, Vassalli PJ: Tumor necrosis factor/cachectin is an effector of skin and gut lesions of the acute phase of graft-versus-host disease. *J Exp Med* 166:1280, 1987
5. Bianco J, Nemunaitis J, Almgren J, Andrews F, Ballard B, Appelbaum FR, Buckner CD, Shields A, Singer J: Pentoxifylline (PTX) diminishes regimen related toxicity (RRT) in patients undergoing bone marrow transplantation. *Blood* 76:528a, 1990 (abstr, suppl 1)
6. Herve P, Wijdenes J, Flesch M, Tiberghien P, Bordignon P, Holler E, Lioure B, Racador E, Stephan JL, Powles R, Bourdeau H, Bergerat JP, Roche C, Cahn JY: Anti-TNF α monoclonal antibody (B-C7) in the treatment of severe forms of acute GVHD. *Blood* 76:554a, 1990 (abstr, suppl 1)
7. Ford HR, Hoffman RA, Wing EJ, Magee DM, McIntyre LA, Simmons RL: Tumor necrosis factor, macrophage-colony stimulating factor, and interleukin 1 production within sponge matrix allografts. *Transplantation* 50:460, 1990
8. Smith SR, Terminelli C, Kenworthy-Bott L, Phillips DL: A study of cytokine production in acute graft-vs-host disease. *Cell Immunol* 134:336, 1991
9. Pober JS, Cotran RS: The role of endothelial cells in inflammation. *Transplantation* 50:537, 1990
10. Dinarello CA: Biology of interleukin 1. *FASEB J* 2:108, 1988
11. Okusawa S, Gelfand JA, Ikejima T, Connolly RJ, Dinarello CA: Interleukin 1 induces a shock-like state in rabbits. Synergism with tumor necrosis factor and the effect of cyclooxygenase inhibition. *J Clin Invest* 81:1162, 1988
12. Le J, Vilcek J: Tumor necrosis factor and interleukin 1: Cytokines with multiple overlapping biological activities. *Lab Invest* 56:234, 1987
13. Eisenberg SP, Evans RJ, Arend WP, Verderbert E, Brewer MT, Hannum CH, Thompson RC: Primary structure and functional expression from complementary DNA of a human interleukin-1 receptor antagonist. *Nature* 343:341, 1990
14. Hannum CH, Wilcox CJ, Arend WP, Joslin FG, Dripps DJ, Heimdahl PL, Armes LG, Sommer A, Eisenberg SP, Thompson RC: Interleukin-1 receptor antagonist activity of a human interleukin-1 inhibitor. *Nature* 343:336, 1990
15. McIntyre KW, Stepan GJ, Kolinsky KD, Kolinsky WR, Benjamin WR, Plocinski JM, Kafka KL, Campen CA, Chizzonite RA, Kilian PL: Inhibition of interleukin 1 (IL-1) binding and biological activity in vitro and modulation of acute inflammation in vivo by IL-1 receptor antagonist and anti-IL-1 receptor monoclonal antibody. *J Exp Med* 173:931, 1991
16. Seckinger P, Williamson K, Balavoine JF, Mach B, Mazzei G, Shaw A, Dayer JM: A urine inhibitor of interleukin 1 activity affects both interleukin 1 alpha and 1 beta but not tumor necrosis factor. *J Immunol* 139:1541, 1987
17. Korngold R, Sprent J: Lethal graft-versus-host disease after bone marrow transplantation across minor histocompatibility barriers in mice. Prevention by removing mature T-cells from marrow. *J Exp Med* 148:1687, 1987
18. Ferrara JLM, Daley JP, Burakoff SJ, Miller RG: Functional T-cell deficits after bone marrow transplantation across minor histocompatibility barriers: Effects of graft-vs-host disease on precursor frequency of reactive cells. *J Immunol* 138:3598, 1987
19. Esser RE, Stimpson SA, Cromartie WJ, Schwab JH: Reactivation of streptococcal cell wall-induced arthritis by homologous and heterologous cell wall polymers. *Arthritis Rheum* 28:1402, 1985
20. Innis MA, Gelfand DH: Optimization of PCRs. In Innis MA, Gelfand DH, Sininsky JJ, White TJ (eds): *PCR Protocols*. San Diego, CA, Academic, 1989, p 3
21. Murray LJ, Lee R, Martens C: In vivo cytokine gene expression in T cell subsets of the autoimmune MRL/Mp-lpr/lpr mouse. *Eur J Immunol* 20:163, 1990
22. Iscove NN, Sieber F: Erythroid progenitors in mouse bone marrow detected by macroscopic colony formation in culture. *Exp Haematol* 3:32, 1975
23. Till JE, McCulloch EA: A direct measurement of the radiation sensitivity of normal mouse bone marrow cells. *Radiat Res* 14:213, 1961
24. Piguet PF: Tumor necrosis factor and graft-vs-host disease. In Burakoff SJ, Deeg HJ, Ferrara J, Atkinson K (eds): *Graft-vs-Host Disease*. New York, NY, Dekker, 1990, p 255
25. Lapp WS, Ghayur T, Mendez M, Seddik M, Seemeyer TA: The functional and histological basis for graft-versus-host-induced immunosuppression. *Immunol Rev* 88:107, 1985
26. Oppenheim JJ, Nera R, Tiberghien P, Gress R, Kenney JJ, Longo DL: Interleukin-1 enhances survival of lethally irradiated mice treated with allogeneic bone marrow cells. *Blood* 74:2257, 1989
27. Blazar BR, Widmer MB, Valleria DA: Improved survival, hematological recovery and engraftment in murine recipients of IL-1 alpha infusions post-bone marrow transplantation. *Blood* 76:529a, 1990 (abstr, suppl 1)
28. Champlin R: T-cell depletion to prevent graft-versus-host disease after bone marrow transplantation. *Hematol Oncol Clin N Am* 4:687, 1990
29. Atkinson K, Matias C, Guiffre A, Seymour R, Cooley M, Biggs J, Munro V, Gillis S: In vivo administration of granulocyte colony-stimulating (G-CSF), granulocyte-macrophage CSF, interleukin-1 (IL-1), and IL-4, alone and in combination, after allogeneic murine hematopoietic stem cell transplantation. *Blood* 1376, 1991

Interleukin-1 receptor antagonist halts the progression of established crescentic glomerulonephritis in the rat

HUI Y. LAN, DAVID J. NIKOLIC-PATERSON, WEI MU, JAMES L. VANNICE, and ROBERT C. ATKINS

Department of Nephrology, Monash Medical Centre, Clayton, Victoria, Australia, and Synergen, Boulder, Colorado, USA

Interleukin-1 receptor antagonist halts the progression of established crescentic glomerulonephritis in the rat. The pathogenic role of interleukin-1 (IL-1) in the progression of established rat crescentic glomerulonephritis was investigated by administration of the interleukin-1 receptor antagonist (IL-1ra). Passive accelerated antiglomerular basement membrane (GBM) disease was induced in three groups of six rats. One group was killed on day 7 with no treatment. The other groups received a constant infusion of IL-1ra or saline from day 7 until being killed on day 21. All animals developed moderate glomerular injury, a significant loss of renal function and marked histological damage including crescent formation by day 7. Saline treated animals showed a significant deterioration in these parameters over days 7 to 21. In contrast, animals treated with the IL-1ra over this period showed stabilization of glomerular injury (proteinuria; $P < 0.001$) and a recovery of normal renal function (creatinine clearance; $P < 0.05$). Histologically, IL-1ra treatment suppressed glomerular cell proliferation (PCNA expression; $P < 0.001$) and significantly inhibited crescent formation ($P < 0.005$), glomerular sclerosis ($P < 0.005$), tubular atrophy ($P < 0.05$) and interstitial fibrosis ($P < 0.05$). A key finding was that IL-1ra treatment not only stopped renal leukocyte accumulation over days 7 to 21 ($P < 0.01$), but that treatment also suppressed immune activation of the infiltrate ($P < 0.01$). In conclusion, this study provides direct evidence that IL-1 plays a key role in the progressive/chronic phase of renal injury in experimental crescentic glomerulonephritis and indicates that IL-1ra treatment may be of therapeutic benefit in human rapidly progressive crescentic glomerulonephritis.

Interleukin-1 (IL-1) is a cytokine which elicits a wide range of pro-inflammatory and immunologic effects, including: activation of endothelium; stimulation of T and B cell activation; up-regulation of leukocyte adhesion molecule expression by many cell types; and the induction of a range of cytokines and growth factors including interleukins 1, 2, 6 and 8, tumor necrosis factor- α , monocyte chemotactic protein-1, platelet-derived growth factor, and transforming growth factor- β , which regulate events such as leukocyte chemotaxis and the fibrotic response [1, 2]. A potential role for IL-1 in proliferative forms of glomerulonephritis was first suggested by studies in which macrophage-derived IL-1 was found to stimulate mesangial cell proliferation *in vitro* [3]. Since then, renal IL-1 production has been detected during acute and progressive/chronic phases of experimental [4-10] and human glomerulonephritis [11-13]. The main source of renal IL-1 production appears to be infiltrating macrophages

[5, 7, 10-13] which are a common feature of almost all forms of human and experimental glomerulonephritis [14], although other renal cell types such as mesangial cells and tubular epithelial cells can also synthesize IL-1 [12, 15].

To demonstrate a pathogenic role for IL-1 in glomerulonephritis it is necessary to block the action of IL-1 *in vivo*. Such an approach has been made possible by the identification and characterization of a specific IL-1 receptor antagonist (IL-1ra) [1, 16, 17]. Initial studies using the IL-1ra targeted acute glomerular injury in rat anti-GBM glomerulonephritis which is mediated by a transient glomerular neutrophil influx following deposition of antibodies on the GBM [18-20]. IL-1ra treatment during this period had no discernible effect upon neutrophil influx or glomerular injury. However, an important finding was that a 14 day treatment with the IL-1ra from the time of anti-GBM serum injection produced a marked suppression of the monocyte-dependent phase of glomerular injury and renal impairment [20]. Having demonstrated a key role for IL-1 in the induction of monocyte-dependent renal injury, the next question was whether blocking IL-1 could intervene in the progressive phase of established crescentic glomerulonephritis. This is an important issue because of its relevance to treatment of human disease and in identifying pathogenic mechanisms of renal damage, as a range of other mediators of renal injury are produced during the progressive phase. Hence, this study examined the ability of IL-1ra treatment to intervene in the progression of established rat anti-GBM glomerulonephritis.

Methods

Animals

Inbred male Sprague-Dawley rats (150 g) were obtained from the Monash University Animal House.

Nephrotoxic serum

Rabbit anti-rat GBM nephrotoxic serum was raised by repeated immunization of New Zealand white rabbits with particulate rat GBM, as previously described [21]. The anti-GBM serum was pooled, decomplexed and adsorbed extensively against normal rat erythrocytes.

Experimental design

Passive accelerated anti-GBM disease was induced in 18 rats as previously described [20, 22, 23]. Animals were immunized subcutaneously with 5 mg normal rabbit IgG in Freund's complete adjuvant and injected intravenously with 10 ml/kg body weight

Received for publication July 25, 1994
and in revised form December 12, 1994
Accepted for publication December 12, 1994

© 1995 by the International Society of Nephrology

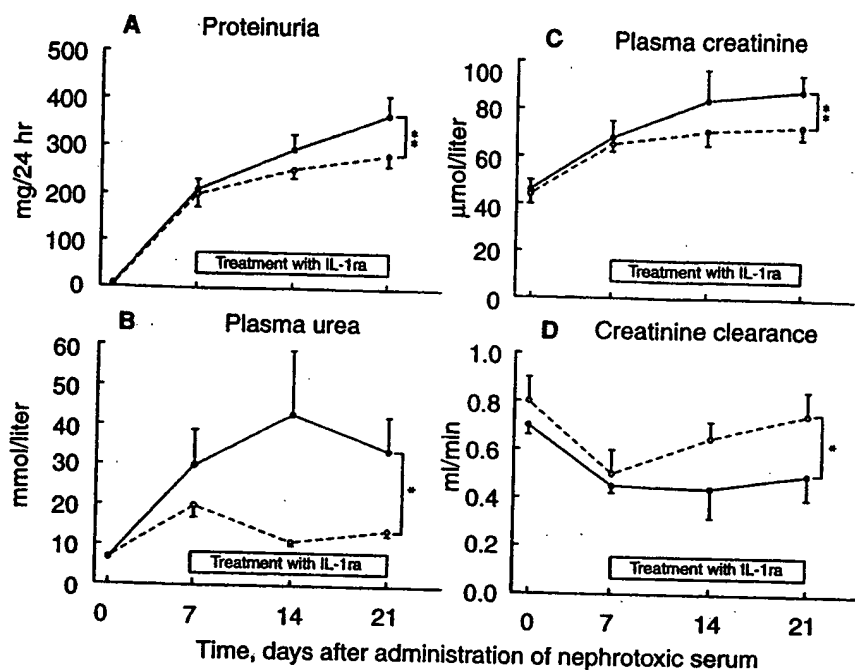


Fig. 1. Suppression of renal injury by IL-1ra treatment. Data for (A) 24-hour urinary protein excretion, (B) plasma urea levels, (C) plasma creatinine levels, and (D) creatinine clearance are shown. Symbols are: saline treated animals (●), IL-1ra treated animals (○). Data are expressed as the mean \pm SEM for each experimental group of 6 animals. Untreated animals killed on day 7 of anti-GBM disease had proteinuria of 228 ± 25 mg/24 hr, plasma urea of 18.5 ± 1.2 mmol/liter, plasma creatinine of 72.5 ± 5.8 μmol/liter, and creatinine clearance of 0.57 ± 0.08 ml/min. Statistical differences between untreated and IL-1ra treated groups was assessed by one way analysis of variance (ANOVA); * $P < 0.05$, ** $P < 0.001$.

rabbit anti-rat GBM serum (12.5 mg IgG/ml) five days later (termed day 0). One group of six rats was killed on day 7 with no treatment. The remaining animals received a constant infusion of either human recombinant IL-1ra (Synergen, Colorado, USA) or saline from day 7 until being killed at day 21 by means of an Alzet 2002 miniosmotic pump implanted under the skin of the back which delivered 0.5 μl/hr of 50 mg/ml IL-1ra in saline. Following pump implantation, all wounds healed cleanly and there were no signs of infection when pumps were removed at the end of the experiment.

Blood samples and 24-hour urine collections were taken on days 0, 7, 14, and 21. Plasma levels of hrIL-1ra were measured by a commercial ELISA (R&D Systems, MN, USA) and were 671 ± 175 ng/ml (mean \pm SEM) on day 14 and 643 ± 112 ng/ml on day 21. In addition, one group of six normal rats was also examined.

Analysis of renal function and proteinuria

Urinary protein excretion was determined using the Manual Pnceau Red method. Urinary blood (hematuria) was determined by a standard Combur's stick test (Boehringer Mannheim) and semi-quantitated into four scores: (1) trace or minor, (2) mild, (3) moderate, and (4) severe. Concentrations of plasma and urine creatinine were measured using the standard Jaffe rate reaction (alkaline picrate), while plasma urea concentrations were measured by the NED/OPA assay. All analyses were performed in the Department of Biochemistry, Monash Medical Centre.

Immunofluorescence

Tissues for direct immunofluorescence staining were frozen in liquid nitrogen and 6 μm cryostat sections were stained with fluorescein isothiocyanate (FITC)-conjugated goat polyclonal antibodies to rat IgG, C3 and fibrinogen or FITC-conjugated sheep anti-rabbit IgG (Nordic, the Netherlands). The intensity of antibody staining was semi-quantitatively assessed as: nil (0), mild (+), moderate (++), and strong (+++). In addition, day 21 tissues were assessed for deposition of immune reactants by

semi-quantitative immunofluorescence staining using a blinded antibody titration method as previously described [23]. Briefly, consecutive cryostat sections from each animal were incubated with serial dilutions of FITC-conjugated antibodies against rabbit IgG, rat IgG or rat C3. Blinded sections were examined on the same day and the titer at which antibody staining became undetectably scored. Results are expressed in terms of mean \pm SEM of the inverse antibody titer for groups of six animals.

Measurement of plasma antibodies

Plasma levels of rabbit IgG, rat anti-rabbit IgG, rat anti-human rIL-1ra IgG and total rat IgG were determined by capture ELISA as previously described [23]. Briefly, 96-well ELISA plates were coated with 100 μl of swine anti-rabbit IgG, normal rabbit IgG, human recombinant IL-1ra or normal rat IgG (10 μg/ml in 0.1 M carbonate-bicarbonate buffer, pH 9.0) overnight at 4°C, blocked with 2% bovine serum albumin and washed ($\times 4$) with 0.05% Tween 20 in PBS. Triplicate serum samples (1:1000 dilution) were added to wells, incubated for two hours and washed ($\times 4$) with 0.05% Tween 20 in PBS. Bound rabbit or rat IgG was detected using a peroxidase-conjugated sheep anti-rabbit IgG or peroxidase-conjugated sheep anti-rat IgG (Sigma Chemical Co., St. Louis, MO, USA) and color development with the OPD substrate for 10 minutes in the dark. The reaction was terminated with 3 M H_2SO_4 and optical density (OD) was read at 490 nm on a Dynatec MR 5000 ELISA plate reader. The background reading obtained with normal rat serum, which was the same as the buffer blank, was subtracted from the readings, except for measurement of total rat IgG when the buffer blank was subtracted.

Histopathology

Tissues for histology were fixed in formalin and 4 μm paraffin sections were stained with hematoxylin and eosin or periodic acid-Schiff. Glomerular and tubulointerstitial damage was scored as follows: the percentage of glomeruli exhibiting atrophy/segmental sclerosis, global sclerosis or glomerular crescent formation

was assessed by examination of at least 100 glomerular cross sections per animal in periodic acid-Schiff-stained sections. Glomerular hypercellularity was assessed on the basis of total glomerular cell counts/glomerular cross section (gcs). At least 100 glomeruli per animal were scored in hematoxylin and eosin-stained sections and ranked as follows: (0), normal (less than 50 cells/gcs); (1), mild (60 to 80 cells/gcs); (2), moderate (80 to 120 cells/gcs); (3), severe hypercellularity (more than 120 cells/gcs).

Tubulointerstitial lesions of tubular atrophy and fibrosis were semi-quantitatively analyzed on hematoxylin and eosin-stained sections and graded on a scale of 0 to 3 as follows: (0) no apparent damage; (1) mild damage, with lesions involving less than 15% of the cortex; (2) moderate damage, involving 15 to 30% of the cortex; and (3) severe damage, that is, involving more than 30% of the cortex and focal accumulation of leukocytes at sites of damage.

Immunoperoxidase staining

Monoclonal antibodies (mAb) used for immunoperoxidase staining were as follows: OX-1, leukocyte common antigen [24]; ED1, monocytes, macrophages and some dendritic cells [25]; R73, non-polymorphic $\alpha\beta$ T cell receptor [26]; OX-8, anti-rat CD8, cytotoxic T lymphocytes and NK cells [27]; F17-23-2, MHC class II Ia antigen (RT1-B) [28]; NDS-61, p55 chain of the interleukin-2 receptor (IL-2R) [29]; PC-10, proliferating cell nuclear antigen (PCNA) [30].

Tissues for immunoperoxidase staining were fixed in 2% paraformaldehyde-lysine-periodate and serial 6 μ m cryostat sections were labeled with monoclonal antibodies (mAbs) using a standard three layer peroxidase-anti-peroxidase method and developed with diaminobenzidine as previously described [20, 22]. Three layer immunoperoxidase staining with the PC-10 mAb was performed on cryostat tissue sections which were pre-treated with microwave oven heating for 2×5 minutes in 0.01 M sodium citrate pH 6.0 at 800 watts as previously described [31, 32]. This treatment facilitates antigen retrieval, thereby increasing the sensitivity of PCNA detection.

Quantitation of leukocytes in tissue sections

Leukocyte subpopulations infiltrating the glomerulus and interstitium were analyzed by mAb labeling of cryostat tissue sections. Cells labeled by each mAb were counted in high power fields ($\times 400$) of 20 consecutive glomeruli for each animal (this minimized variation in cell counts caused by differences in glomerular cross section areas). The mean of 20 glomerular counts from each group of six animals was expressed as cells \pm standard error of mean (SEM) per glomerular cross section. To assess tubulointerstitial leukocyte infiltration, cortical areas were selected at random. The number of labeled cells was assessed from 20 consecutive high power fields by means of a 0.02 mm² graticule fitted in the eyepiece of the microscope. These fields progressed from the outer to inner cortex, avoiding only large vessels, glomerular and immediate periglomerular areas. For each tissue, the same area was examined in serial sections labeled with different mAbs. No adjustment of the cell count was made for tubules or the luminal space. The mean of 20 field counts from each group of six animals was expressed as cells per mm² \pm SEM.

Scoring of histological changes, immunofluorescence and immunoperoxidase staining was performed on coded slides by an experienced renal pathologist (HYL).

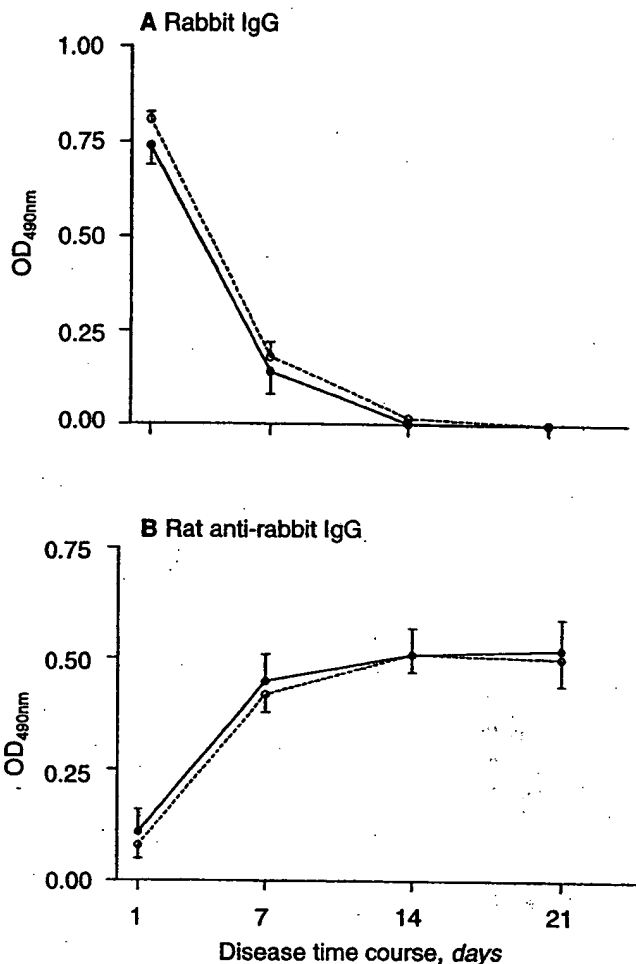


Fig. 2. Effect of IL-1ra treatment on the plasma antibody levels. Plasma levels of (A) rabbit IgG, and (B) rat anti-rabbit IgG, were quantitated at different times by ELISA. Symbols are: saline treated animals (●); IL-1ra treated animals (○). Data are expressed as the mean optical density (OD₄₉₀) \pm SEM for each group of 6 animals with background subtracted. Untreated animals killed on day 7 had 0.85 ± 0.04 and 0.04 ± 0.05 OD₄₉₀ plasma rabbit IgG and 0.05 ± 0.05 and 0.44 ± 0.13 OD₄₉₀ plasma rat anti-rabbit IgG on days 1 and 7, respectively.

Statistical analysis

Data from the measurement of renal function and proteinuria over the experimental course were analyzed using the one way analysis of variance (ANOVA) program from Complete Statistical System (CSS, Statsoft, USA), and individual time points were also compared using the unpaired *t*-test. Data from leukocyte infiltration in the two renal compartments was compared using an unpaired *t*-test. Measurements of hematuria and histological changes were compared by the non-parametric Mann-Whitney U test.

Results

Renal function and proteinuria

On day 7 of anti-GBM disease, all animals exhibited moderate proteinuria, a significant increase in plasma levels of creatinine and urea, and a 37% reduction in creatinine clearance (Fig. 1). Over days 7 to 21 there was a significant deterioration in saline

Table 1. Inhibition of histopathological damage by IL-1ra treatment

| | Glomerulus | | | | | | | Tubulointerstitium | |
|-----------------------------|-------------------------|-------------------------|-----------------------|--------------------------------|-------------------------|-------------------------|-------------------------|------------------------|------------------------|
| | Hypercellularity % | | | PCNA ⁺ cells/gcs | Sclerosis % | | Crescents % | Atrophy (0-3) | Fibrosis (0-3) |
| | + | ++ | +++ | | Segmental | Global | | | |
| Untreated Day 7 | 25.3 ± 2.4 | 24.5 ± 1.6 | 10.3 ± 1.5 | 12.8 ± 1.2 | 21.0 ± 3.8 | 0.6 ± 0.2 | 14.0 ± 3.2 | 1.2 ± 0.2 | 1.5 ± 0.2 |
| Saline treated Day 21 | 16.7 ± 3.2 ^a | 44.5 ± 3.6 ^b | 29.5 ± 6 ^a | 12.0 ± 0.9 | 49.0 ± 5.1 ^b | 13.8 ± 5.8 ^b | 58.5 ± 4.9 ^b | 2.8 ± 0.2 ^a | 2.7 ± 0.2 ^a |
| IL-1ra treated Day 21 | 18.2 ± 1.4 ^a | 25.0 ± 3.5 ^b | 13.5 ± 2.3 | 5.8 ± 0.6 ^{bc} | 24.5 ± 3.6 ^a | 3.2 ± 1.1 ^a | 25.0 ± 4.0 ^b | 1.3 ± 0.2 ^b | 1.5 ± 0.2 ^a |

^a $P < 0.05$, ^b $P < 0.005$, compared to untreated day 7 animals, ^c $P < 0.001$, compared to saline treated day 21 animals

treated animals which developed severe proteinuria, a further increase in plasma levels of creatinine and urea, while creatinine clearance remained impaired (Fig. 1). This is consistent with previous studies in this model in which a very similar disease progression was evident in untreated animals over this time course [22, 23].

IL-1ra treatment over days 7 to 21 prevented the increase in proteinuria seen in saline treated animals, stabilized plasma creatinine and reduced plasma urea to normal levels (Fig. 1). Of particular note was the finding that IL-1ra treatment produced a gradual recovery to a normal rate of creatinine clearance (Fig. 1D).

On day 7 of anti-GBM disease, all animals exhibited moderate to severe hematuria (2.3 ± 0.8). In saline treated animals, there was an increase in hematuria over days 7 to 21 (3.0 ± 0.4 on day 21). However, IL-1ra treatment resulted in a marked improvement in hematuria with all animals showing only trace to mild hematuria on day 21 (1.0 ± 0 ; $P < 0.05$ vs. saline treated).

Deposition of immune reactants

Deposition of immune reactants within the kidney was assessed by direct immunofluorescence staining of cryostat tissue sections. In untreated animals killed on day 7 of anti-GBM disease, there was strong (+++) linear deposition of rabbit IgG and moderate (++) linear deposition of rat IgG, and C3 along the GBM. In addition, moderate (++) fibrinogen deposition was seen within Bowman's space in some glomeruli and within the interstitium. At day 21, saline treated animals exhibited strong (+++) linear deposition of rabbit IgG, rat IgG and C3 along the GBM. There was also a strong patchy deposition of fibrinogen, rat IgG and C3 within Bowman's space, crescents and necrotic glomerular capillary tufts and strong fibrinogen deposition throughout the interstitium.

The effect of IL-1ra treatment on the intensity of immune deposits on the GBM on day 21 of anti-GBM disease was assessed by a serial dilution immunofluorescence technique as described in the Methods section. There was no difference in the intensity of rabbit IgG deposition on the GBM in saline treated and IL-1ra treated animals (12000 ± 1454 vs. 12800 ± 1905 ; mean inverse antibody titer \pm SEM, respectively). Similarly, there was no difference in the intensity of rat IgG deposition (900 ± 73 vs. 940 ± 39) or C3 deposition (4800 ± 762 vs. 3290 ± 953) in saline and IL-1ra treated animals, respectively. However, IL-1ra treated animals showed little, if any, deposition of rat IgG, C3 and fibrinogen

within Bowman's space and had only mild (+) fibrinogen deposition throughout the interstitium.

Quantitation of plasma antibody titers by ELISA was performed to check that all animals received an equivalent dose of rabbit anti-GBM serum and to examine whether IL-1ra treatment had any suppressive effect on the humoral immune response. Figure 2A shows that high plasma levels of rabbit IgG were still evident 24 hours after injection of anti-GBM serum and had almost disappeared by day 7. There was no difference in plasma rabbit IgG levels in any of the experimental groups. The time course of the rat anti-rabbit IgG response is shown in Figure 2B. Rat anti-rabbit IgG was detected on day 1 reflecting the fact that these animals were primed with rabbit IgG. There was a fourfold increase in rat anti-rabbit IgG levels on day 7 and the response remained at this level to day 21. No differences in rat anti-rabbit IgG levels were apparent between the saline and IL-1ra treated groups. Similarly, there was no difference in plasma levels of total rat IgG on day 21 (0.566 ± 0.017 vs. 0.577 ± 0.024 OD₄₉₀ in saline and IL-1ra treated animals respectively; $P = \text{NS}$). Of note was a small antibody response to the administered human IL-1ra on day 21 (0.013 ± 0.004 OD₄₉₀) which was absent in saline treated animals.

Histopathology

A detailed evaluation of renal histopathology was made on all three groups of animals (Table 1). On day 7 of anti-GBM disease, untreated animals displayed significant renal lesions. These untreated animals exhibited mild to severe hypercellularity in 60% of glomeruli and there was marked glomerular cell proliferation as assessed by PCNA expression (12.8 ± 1.2 vs. 2.0 ± 1.8 PCNA⁺ cells/gcs in normal rats; $P < 0.01$). Segmental glomerular sclerosis and crescent formation were also evident on day 7 of disease as was mild tubular atrophy and fibrosis (Table 1). In saline treated animals, there was a pronounced deterioration in renal histopathology by day 21 of the disease. Both the percentage and severity of glomerular hypercellularity increased while the number of PCNA⁺ glomerular cells remained high. In addition, there was a marked increase in glomerular segmental and global sclerosis and crescent formation as well as severe tubular atrophy and fibrosis.

Renal histopathology changes between IL-1ra and saline treated animals at day 21. IL-1ra treatment essentially halted deterioration of renal histopathology over the days 7 to 21 period (Table 1). The percentage of hypercellular glomeruli and the severity of glomerular hypercellularity was similar in IL-1ra

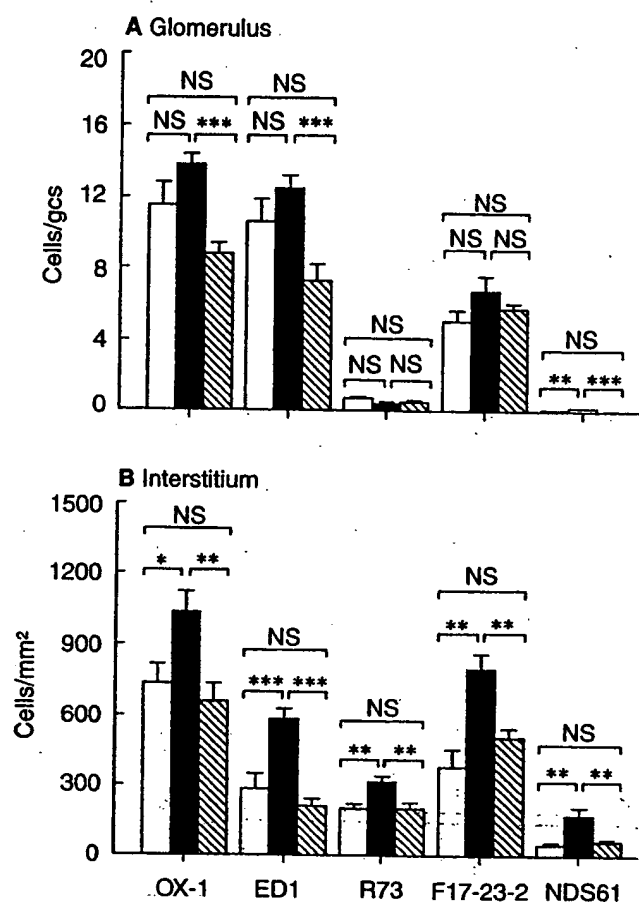


Fig. 3. Suppression of renal leukocytic infiltration and immune activation by IL-1ra treatment. Total leukocytes and leukocyte subsets were analyzed by labeling serial tissue sections with mAbs. Abbreviations are: OX-1, total leukocytes; ED1, macrophages; R73, total T cells; F.17.23.2, MHC class II I-A antigen; NDS 61, IL-2R. (a) Quantitation of leukocyte infiltration in the glomerulus. (b) Quantitation of leukocyte infiltration in the tubulointerstitium. Data are expressed as the mean \pm SEM for each group of 6 animals. Open bars represent untreated day 7 anti-GBM disease. Closed bars represent day 21 saline treated animals. Hatched bars represent day 21 IL-1ra treated animals. Data for antibody labeling of normal rat glomeruli are as follows: 0.94 ± 0.10 OX-1⁺ cells/gcs; 0.76 ± 0.10 ED1⁺ cells/gcs; 0.34 ± 0.10 R73⁺ cells/gcs; 1.1 ± 0.21 F.17.23.2⁺ cells/gcs; 0 ± 0 NDS 61⁺ cells/gcs. Data for antibody labeling of normal rat interstitium are as follows: 99.4 ± 10.2 OX-1⁺ cells/mm²; 26.0 ± 1.4 ED1⁺ cells/mm²; 31.4 ± 6.7 R73⁺ cells/mm²; 99.0 ± 7.0 F.17.23.2⁺ cells/mm²; 0 ± 0 NDS 61⁺ cells/mm². Statistical differences between the different groups was assessed by unpaired *t*-test: * $P < 0.05$, ** $P < 0.01$, *** $P < 0.001$, or not significant (NS).

treated animals at day 21 and untreated animals at day 7, while glomerular cell proliferation was markedly inhibited by IL-1ra treatment (Table 1). Glomerular segmental and global sclerosis and crescent formation were not different in IL-1ra treated animals compared to untreated animals at day 7. Similarly, tubular atrophy and interstitial fibrosis were also unchanged. An example of histological damage in an IL-1ra treated animals is shown in Figure 3b.

Glomerular leukocytic infiltration

Renal leukocytic accumulation and immune activation was examined by mAb labeling of cryostat tissue sections. There was a

prominent glomerular leukocyte infiltrate on day 7 of anti-GBM disease (11.4 ± 1.3 vs. 1.1 ± 0.2 OX-1⁺ cells/gcs in normal rats; $P < 0.001$) which was composed of ED1⁺ macrophages (Fig. 3a). There was no significant increase in glomeruli R73⁺ T cells (Fig. 3a) or CD8⁺ cells (0.53 ± 0.1 vs. 0.24 ± 0.1 CD8⁺ cells/gcs in normal; $P = NS$), although there was an increase in the number of CD4⁺ cells (3.47 ± 0.3 vs. 0.56 ± 0.12 CD4⁺ cells/gcs in normal; $P < 0.05$) which presumably reflects a subpopulation of CD4⁺ macrophages. There was also a significant increase in the number of glomerular cells expressing MHC class II antigens (5.1 ± 0.6 vs. 1.2 ± 0.2 MHC class II⁺ cells/gcs in normal rats; $P < 0.05$) which may be "activated" macrophages or mesangial cells.

In saline treated animals, there was no significant change in the pattern of glomerular leukocytic infiltration or MHC class II expression over days 7 to 21 (Fig. 3a). However, IL-1ra treatment over this period significantly reduced glomerular macrophage infiltration in comparison to saline treated animals (Fig. 3a).

Interstitial leukocytic infiltration

The composition of interstitial leukocytic infiltration was different to that seen in the glomerulus (Fig. 3). On day 7 of anti-GBM disease there was a significant interstitial leukocyte infiltrate (735 ± 81 vs. 102 ± 16 OX-1⁺ cells/mm² in normal rats; $P < 0.001$) which was composed of both ED1⁺ macrophages and R73⁺ T cells. There was evidence of immune activation of the mononuclear cell infiltrate as shown by interleukin-2 receptor (IL-2R) expression and the prominent accumulation of MHC class II⁺ cells within the interstitium (Fig. 3b). The T cell infiltrate contained both CD8⁺ cells (109 ± 8.5 at day 7 vs. 38.0 ± 8.0 CD8⁺ cells/gcs in normal; $P < 0.05$) and CD4⁺ cells (570.5 ± 94 vs. 92.0 ± 23.8 CD4⁺ cells/gcs in normal; $P < 0.01$), although many macrophages also expressed the CD4 antigen.

There was a significant increase in the number of interstitial ED1⁺ macrophages and R73⁺ T cells in saline treated animals over days 7 to 21. Of particular note was the marked increase in the number of immune-activated mononuclear cells—both IL-2R⁺ cells ($\uparrow 283\%$) and MHC class II⁺ cells ($\uparrow 111\%$)—during this period. Many of these activated cells were seen in focal infiltrates of T cells and macrophages around and within damaged tubules and immediately adjacent to areas of Bowman's capsule rupture. However, there was no change in the number of CD8⁺ cells (109 ± 8.5 at day 7 vs. 103 ± 9.4 CD8⁺ cells/mm² at day 21; $P = NS$) while the number of CD4⁺ cells was increased (570.5 ± 94 at day 7 vs. 846.5 ± 41 CD4⁺ cells/mm² at day 21; $P < 0.01$). This indicated that the increased number of R73⁺ T cells seen in saline treated animals was due to accumulation of CD4⁺ T cells.

IL-1ra treatment completely stopped interstitial leukocyte accumulation and immune activation over the 7 to 21 day period (Fig. 3b). The suppression of aggressive focal leukocytic infiltrates was associated with a marked reduction in tubular damage and interstitial fibrosis.

Discussion

This study has evaluated the effect of IL-1ra treatment on the progression of established rat accelerated anti-GBM disease—a severe model of glomerulonephritis which exhibits many features similar to that of human rapidly progressive glomerulonephritis. In this model, significant glomerular injury, renal function impairment and histological damage was evident on day 7 which rapidly progressed to a severe form of crescentic glomerulonephritis by

day 21. IL-1ra treatment over days 7 to 21 halted the progression of established disease as demonstrated by: (i) stabilization of proteinuria and reduction of hematuria, (ii) reversal of renal function impairment, and (iii) inhibition of renal histopathological damage. The ability of IL-1ra treatment to intervene and halt disease progression in this model demonstrates a key pathogenic role for IL-1 in crescentic glomerulonephritis. Indeed, the ability to halt disease progression by targeting just one cytokine is most impressive considering that a range of other cytokines and mediators of renal injury are also produced during the disease process [33]. This argues that the cytokine network *in vivo* operates in an interdependent fashion rather than exhibiting functional redundancy as suggested by their many overlapping functions *in vitro*.

The suppression of rat anti-GBM disease by IL-1ra treatment indicates that IL-1 acts at several levels in disease pathogenesis. Possible mechanisms of IL-1ra mediated suppression of disease progression are discussed below.

T cells and macrophages play a crucial role in the induction and progression of experimental anti-GBM disease [22, 34–38]. Glomerular macrophages are associated with glomerular hypercellularity, crescent formation and glomerulosclerosis, while in the interstitium aggressive focal accumulation of activated T cells (IL-2R+) and macrophages is associated with tubular atrophy, Bowman's capsule rupture, granuloma formation and interstitial fibrosis. This disease is different to the NK (CD8+) cell-dependent anti-GBM disease induced in the susceptible WKY rat strain [39], as it features a progressive accumulation and activation of CD4+ T cells within the interstitium, while CD8+ cell numbers do not change during disease progression over days 1 to 21 [22]. The ability of IL-1ra treatment of established anti-GBM disease to reduce glomerular macrophage accumulation compared to saline treated animals and to completely halt interstitial T cell and macrophage accumulation and activation over this period was associated with the stabilization of glomerular injury and the cessation of histological damage. This suppression of leukocyte infiltration and activation is consistent with previous studies in which IL-1ra treatment prevented the development of glomerular, and in particular, interstitial leukocyte infiltration during the induction phase of rat anti-GBM disease by suppressing up-regulation of renal ICAM-1 (CD54) expression [20, 40].

Glomerular hypercellularity is a feature of proliferative forms of glomerulonephritis and results from an increased number of mesangial cells and glomerular leukocyte infiltration [41]. The use of double immunohistochemistry staining has demonstrated that most glomerular PCNA+ cells detected in human and experimental models of glomerulonephritis are proliferating mesangial cells [41, 42]. In our study, IL-1ra treatment appeared to suppress glomerular hypercellularity through inhibition of mesangial cell proliferation as evidenced by the marked reduction in the number of glomerular PCNA+ cells. This could be a direct effect since IL-1 is a mesangial cell growth factor *in vitro* [3]. However, IL-1ra treatment could also act indirectly through suppression of production of other mesangial cell growth factors such as IL-6 or platelet-derived growth factor (PDGF) by mesangial cells or infiltrating macrophages [31, 43].

One further mechanism by which blocking IL-1 action could inhibit rat anti-GBM disease is through modulation of the humoral immune response. In this model, there is a strong systemic immune response to the immunizing rabbit IgG and the subse-

quent challenge with rabbit nephrotoxic serum [44]. Semi-quantitative immunofluorescence staining found that IL-1ra treatment had no effect upon the deposition of rabbit IgG, rat IgG or C3 on the GBM. In addition, IL-1ra treatment had no measurable effect upon plasma levels of rat anti-rabbit IgG antibody throughout the disease course. Thus, blocking IL-1 did not affect the systemic humoral immune response. Indeed, a mild antibody response to the administered human IL-1ra was detected, consistent with a report that the IL-1ra does not inhibit antigen specific responses *in vivo* [45].

Further studies of established experimental crescentic glomerulonephritis are warranted to determine: (1) whether disease remains suppressed when IL-1ra treatment is stopped, and (2) how rapidly IL-1ra treatment is able to halt disease progression.

In conclusion, this study provides the first direct evidence that IL-1 plays a key pathogenic role in the progressive/chronic phase of renal injury in experimental crescentic glomerulonephritis. This study also demonstrates the therapeutic potential of the IL-1ra for treatment of human rapidly progressive glomerulonephritis.

Acknowledgments

This work was funded in part by an NH&MRC grant (#930825) and a grant from the Baxter Extramural Grant Program. The NDS 61 cell line was the kind gift of Dr. M. Dallman, University of Oxford. Part of this work was presented at the 30th meeting of the Australia and New Zealand Society of Nephrology, Adelaide, 1994. We acknowledge the assistance of Song Qing with the ELISA studies.

Reprint requests to Robert C. Atkins, M.D., Department of Nephrology, Monash Medical Centre, Clayton, Victoria 3168, Australia.

References

1. DINARELLO CA: Interleukin-1 and interleukin-1 antagonism. *Blood* 77:1627–1652, 1991
2. DINARELLO CA, WOLFF SM: The role of interleukin-1 in disease. *N Engl J Med* 328:106–113, 1993
3. LOVETT DH, RYAN JL, STERZEL B: Stimulation of rat mesangial cell proliferation by macrophage interleukin-1. *J Immunol* 131:2830–2836, 1983
4. MATSUMOTO K, ATKINS RC: Glomerular cells and macrophages in the progression of experimental focal glomerulosclerosis. *Am J Pathol* 134:933–945, 1989
5. BOSWELL JM, YUI MA, BURT DW, KELLEY VE: Increased tumor necrosis factor and IL-1 β gene expression in the kidneys of mice with lupus nephritis. *J Immunol* 141:3050–3054, 1988
6. MATSUMOTO K, HATANO M: Production of interleukin-1 in glomerular cultures from rats with nephrotoxic serum nephritis. *Clin Exp Immunol* 75:123–128, 1989
7. MATSUMOTO K: Production of interleukin-1 by glomerular macrophages in nephrotoxic serum nephritis. *Am J Nephrol* 10:502–506, 1990
8. CAMUSSI G, TETTA C, BUSSOLINO F, TURELLO E, BRENTIENS J, MONTRUCCHIO G, ANDRES G: Effect of leukocyte stimulation on rabbit immune complex glomerulonephritis. *Kidney Int* 38:1047–1055, 1990
9. DIAMOND JR, PESEK I: Glomerular tumor necrosis factor and interleukin 1 production during acute aminonucleoside nephrosis. *Lab Invest* 64:21–28, 1991
10. TIPPING PG, LOWE MG, HOLDSWORTH SR: Glomerular interleukin-1 production is dependent on macrophage infiltration in anti-GBM glomerulonephritis. *Kidney Int* 39:103–110, 1991
11. MATSUMOTO K, DOWLING J, ATKINS RC: Production of interleukin-1 in glomerular cell cultures from patients with rapidly progressive crescentic glomerulonephritis. *Am J Nephrol* 8:463–470, 1988
12. NORONHA IL, KRUGER C, ANDRASSY K, RITZ E, WALDHERR R: In situ production of TNF- α , IL-1 β and IL-2R in ANCA-positive glomerulonephritis. *Kidney Int* 43:682–692, 1993
13. YOSHIOKA K, TAKEMURA T, MURAKAMI K, OKADA M, YAGI K,

- MIYAZATO H, MATSUSHIMA K, MAKI S: In situ expression of cytokines in IgA nephritis. *Kidney Int* 44:825-833, 1993
14. NIKOLIC-PATERSON DJ, LAN HY, HILL PA, ATKINS RC: Macrophages in renal injury. *Kidney Int* 45 (Suppl 45):S79-S82, 1994
15. LOVETT DH, LARSEN A: Cell-cycle-dependent interleukin-1 gene expression by cultured glomerular mesangial cells. *J Clin Invest* 82:115-122, 1988
16. EISENBERG SP, EVANS RJ, AREND WP, VERDERBER E, BREWER MT, HANNUM CH, THOMPSON RC: Primary structure and functional expression from complementary DNA of a human interleukin-1 receptor antagonist. *Nature* 343:341-346, 1990
17. DINARELLO CA, THOMPSON RC: Blocking IL-1: interleukin 1 receptor antagonist in vivo and in vitro. *Immunol Today* 12:404-410, 1991
18. MULLIGAN MS, JOHNSON KJ, TODD III RF, ISSEKUTZ TB, MIYASAKA M, TAMATANI T, SMITH CW, ANDERSON DC, WARD PA: Requirements for leukocyte adhesion molecules in nephrotoxic nephritis. *J Clin Invest* 91:577-587, 1993
19. TANG WW, FENG L, VANNICE JL, WILSON CB: Interleukin-1 receptor antagonist ameliorates experimental anti-glomerular basement membrane antibody-associated glomerulonephritis. *J Clin Invest* 93:273-279, 1994
20. LAN HY, NIKOLIC-PATERSON DJ, ZARAMA M, VANNICE JL, ATKINS RC: Suppression of experimental crescentic glomerulonephritis by the interleukin-1 receptor antagonist. *Kidney Int* 43:479-485, 1993
21. HOLDSWORTH SR, THOMSON NM, GLASGOW EF, DOWLING JP, ATKINS RC: Tissue culture of isolated glomeruli in experimental crescentic glomerulonephritis. *J Exp Med* 147:98-109, 1978
22. LAN HY, PATERSON DJ, ATKINS RC: Initiation and evolution of interstitial leukocytic infiltration in experimental glomerulonephritis. *Kidney Int* 40:425-433, 1991
23. LAN HY, ZARAMA M, NIKOLIC-PATERSON DJ, KERR PG, ATKINS RC: Suppression of experimental crescentic glomerulonephritis by deoxyspergualin. *J Am Soc Nephrol* 3:1765-1774, 1993
24. SUNDERLAND CA, MCMASTER WR, WILLIAMS AF: Purification with monoclonal antibody of a predominant leukocyte-common antigen and glycoprotein from rat thymocytes. *Eur J Immunol* 9:155-159, 1979
25. DIJKSTRA CD, DOPP EA, JOLING P, KRAAL G: The heterogeneity of mononuclear phagocytes in lymphoid organs: Distinct macrophage subpopulations in the rat recognized by monoclonal antibodies ED1, ED2, ED3. *Immunology* 54:589-599, 1985
26. HUING T, WALLNY HJ, HARTLEY JK, LAWETZTY A, TIEFENTHALER G: A monoclonal antibody to a constant region determinant of the rat T cell antigen receptor that induces T cell activation. *J Exp Med* 169:73-86, 1989
27. BRIDEAU RJ, CARTER PB, MCMASTER WR, MASON DW, WILLIAMS AF: Two subsets of rat T lymphocytes defined with monoclonal antibodies. *Eur J Immunol* 10:609-615, 1980
28. HART DNJ, FABRE JW: Endogenously produced Ia antigens within cells of convoluted tubules or rat kidney. *J Immunol* 126:2109-2113, 1981
29. TELLIDES G, DALLMAN MJ, MORRIS PJ: Mechanism of action of interleukin-2 receptor (IL-2R) monoclonal antibody (MAb) therapy: Target cell depletion or inhibition of function? *Transplant Proc* 21:997-998, 1989
30. WASEEM NH, LANE DP: Monoclonal antibody analysis of the proliferating cell nuclear antigen (PCNA). *J Cell Sci* 96:121-129, 1990
31. SHI S-R, CHAIWUN B, YOUNG L, COTE RJ, TAYLOR CR: Antigen retrieval technique utilizing citrate buffer or urea solution for immunohistochemical demonstration of androgen receptor in formalin-fixed paraffin sections. *J Histochem Cytochem* 41:1599-1604, 1993
32. LAN HY, MU W, NIKOLIC-PATERSON DJ, ATKINS RC: A novel, simple, reliable and sensitive method of multiple immunoenzymic staining: Use of microwave oven heating to block antibody cross-reactivity and retrieve antigens. *J Histochem Cytochem* 43:97-102, 1995
33. SEDOR JR: Cytokines and growth factors in renal injury. *Semin Nephrol* 12:428-440, 1992
34. LAN HY, NIKOLIC-PATERSON DJ, ATKINS RC: Involvement of activated periglomerular leucocytes in the rupture of Bowman's capsule and crescent progression in experimental glomerulonephritis. *Lab Invest* 67:743-751, 1992
35. SCHREINER GF, COTRAN RS, PARDO V, UNANUE ER: A mononuclear cell component to experimental immunological glomerulonephritis. *J Exp Med* 147:369-384, 1978
36. HOLDSWORTH SR, NEALE TJ: Macrophage induced glomerular injury: Cell transfer studies in passive autologous antglomerular basement membrane antibody-initiated experimental glomerulonephritis. *Lab Invest* 51:172-180, 1984
37. HUANG XR, HOLDSWORTH SR, TIPPING PG: Evidence for delayed-type hypersensitivity mechanisms in glomerular crescent formation. *Kidney Int* 46:69-78, 1994
38. MAIN IW, NIKOLIC-PATERSON DJ, ATKINS RC: T Cells and macrophages and their role in renal injury. *Semin Nephrol* 12:428-440, 1992
39. KAWASAKI K, YAOITA E, YAMAMOTO T, KIHARA I: Depletion of CD8 positive cells in nephrotoxic serum nephritis of WKY rats. *Kidney Int* 41:1517-1526, 1992
40. NIKOLIC-PATERSON DJ, LAN HY, HILL PA, VANNICE JL, ATKINS RC: Interleukin-1 receptor antagonist inhibits ICAM-1 upregulation and leukocyte infiltration in experimental glomerulonephritis. *J Am Soc Nephrol* 4:1695-1700, 1994
41. JOHNSON RJ: The glomerular response to injury: Progression or resolution? *Kidney Int* 45:1769-1782, 1994
42. ALPERS CE, HUDKINS KL, GOWN AM, JOHNSON RJ: Enhanced expression of "muscle-specific" actin in glomerulonephritis. *Kidney Int* 41:1134-1142, 1992
43. ABOUD HE: Growth factors and the mesangium. *J Am Soc Nephrol* 2:S185-S189, 1992
44. LAN HY, NIKOLIC-PATERSON DJ, ATKINS RC: Immune events in lymphoid tissues during experimental glomerulonephritis. *Pathology* 25:159-166, 1993
45. FAHERTY DA, CLAUDY V, PLOCINSKI JM, KAFFKA K, KILIAN P, THOMPSON RC: Failure of IL-1 receptor antagonism to inhibit antigen-specific immune responses in vivo. *J Immunol* 148:766-771, 1992

Attenuation of Delayed Neuronal Death After Mild Focal Ischemia in Mice by Inhibition of the Caspase Family

Matthias Endres, Shobu Namura, Masao Shimizu-Sasamata, Christian Waeber, Lin Zhang,
*Teresa Gómez-Isla, *Bradley T. Hyman, and Michael A. Moskowitz

Stroke and Neurovascular Regulation and *Alzheimer Research Group, Neurosurgery and Neurology Department, Massachusetts General Hospital, Harvard Medical School, Charlestown, Massachusetts, U.S.A.

Summary: Inhibitors of apoptosis and of excitotoxic cell death reduce brain damage after transient and permanent middle cerebral artery occlusion. We compared the neuroprotective effects of two caspase family inhibitors with the *N*-methyl-D-aspartate receptor antagonist (+)-MK-801 hydrogen maleate (MK-801) in a newly characterized cycloheximide-sensitive murine model of transient middle cerebral artery occlusion (30 minutes) in which apoptotic cell death is prominent. Ischemic infarction, undetected by 2,3,5-triphenyltetrazolium chloride staining at 24-hour reperfusion, featured prominently in the striatum at 72 hours and 7 days on hematoxylin-eosin-stained sections. Markers of apoptosis, such as oligonucleosomal DNA damage (laddering) and terminal deoxynucleotidyl transferase-mediated dUTP-biotin nick-end labeling (TUNEL)-positive cells first appeared at 24 hours and increased significantly at 72 hours and 7 days after reperfusion. The TUNEL-labeled cells were mostly neurons and stained negative for glial (GFAP, glial fibrillary acid protein) and leukocyte specific markers (CD-45). The caspase inhibitors, *N*-benzyloxycarbonyl-Val-Ala-Asp-fluoromethyl ketone (z-VAD.FMK; 120 ng intracerebroventricularly) or *N*-benzyloxycarbonyl-Asp-Glu-Val-Asp-fluoromethyl ketone (z-DEVD.FMK; 480 ng intracerebroventricularly) decreased infarct size and neurologic deficits when administered 6 hours

after reperfusion. The extent of protection was greater than in models of more prolonged ischemia or after permanent occlusion, and the therapeutic window was extended from 0 to 1 hours after 2-hour middle cerebral artery occlusion to at least 6 hours after brief ischemia. Also, z-VAD.FMK and z-DEVD.FMK treatment decreased oligonucleosomal DNA damage (DNA laddering) as assessed by quantitative autoradiography after gel electrophoresis. By contrast, MK-801 protected brain tissue only when given before ischemia (3 mg/kg intraperitoneally), but not at 3 or 6 hours after reperfusion. Despite a decrease in infarct size after MK-801 pretreatment, the amount of DNA laddering did not decrease 72 hours after reperfusion, thereby suggesting a mechanism distinct from inhibition of apoptosis. Hence, 30 minutes of reversible ischemia augments apoptotic cell death, which can be attenuated by delayed z-VAD.FMK and z-DEVD.FMK administration with preservation of neurologic function. By contrast, the therapeutic window for MK-801 does not extend beyond the time of occlusion, probably because its primary mechanism of action does not block the development of apoptotic cell death. **Key Words:** interleukin-1 β converting enzyme family caspases—Apoptosis—Cerebral ischemia—Delayed neuronal death—Mice.

Received June 2, 1997; final revision received September 11, 1997; accepted September 13, 1997.

Supported by Massachusetts General Hospital Interdepartmental Stroke Project Grants (NS10828) and an unrestricted award in Neuroscience from Bristol Myers Squibb (M.A. Moskowitz). Dr. M. Endres was supported by the Deutsche Forschungsgemeinschaft (En343/1-1). Dr. S. Namura by the Uehara Memorial Foundation, and Drs. T. Gómez-Isla and B. Hyman were supported by NIH (AG05134 and AG11337) and a generous gift from the Walters Family Foundation.

Address correspondence and reprint requests to Dr. Michael A. Moskowitz, Neurosurgery and Neurology Department, Massachusetts General Hospital, Harvard Medical School, 149 13th Street, Room 6403, Charlestown, MA 02129, U.S.A.

Abbreviations used: DMSO, dimethylsulfoxide; GFAP, glial fibrillary acid protein; H&E, hematoxylin-eosin; ICE, interleukin-1 β converting enzyme; MCAO, middle cerebral artery occlusion; MK-801, (+)-MK-801 hydrogen maleate; NMDA, *N*-methyl-D-aspartate; PBS, phosphate-buffered saline; rCBF, regional cerebral blood flow; TTC, 2,3,5-triphenyltetrazolium chloride; TTC, triphenyltetrazolium chloride; TUNEL, terminal deoxynucleotidyl transferase-mediated dUTP nick-end labeling; z-DEVD.FMK, *N*-benzyloxycarbonyl-Asp-Glu-Val-Asp-fluoromethyl ketone; z-VAD.FMK, *N*-benzyloxycarbonyl-Val-Ala-Asp-fluoromethyl ketone.

Several laboratories provide evidence for cell death by an apoptotic mechanism in animal models of cerebral ischemia (Li et al., 1995a,b,c; MacManus et al., 1995a,b; Charriaut-Marlangue et al., 1996). Apoptosis is a cell suicide program under active cell control. The interleukin-1 β converting enzyme (ICE) family caspases, implicated in apoptotic cell death (Yuan and Horvitz, 1990; Ellis et al., 1991), are the human homologues of the nematode *Caenorhabditis elegans* CED-3. Eleven members of this family have been identified, which share a common QACXG consensus sequence (Alnemri et al., 1996). Caspase 1 (ICE) cleaves a pro-interleukin-1 β 31-kilodalton (kd) protein to generate mature 17.5-kd interleukin-1 β , which is involved in inflammatory reactions (Dinarello, 1994), apoptosis (Friedlander et al., 1996), as well as focal and global cerebral ischemia (Saito et al., 1996; Liu et al., 1993). Caspase 3 (CPP32), another important family member implicated in apoptotic cell

death, cleaves poly(ADP-ribose)polymerase and DNA-dependent protein kinase delta, among other substrates (Tewari et al., 1995; Nicholson et al., 1995).

Reports from our laboratory show that peptide inhibitors of the caspase family (*N*-benzyloxycarbonyl-Val-Ala-Asp-fluoromethyl ketone [z-VAD.FMK] and *N*-benzyloxycarbonyl-Asp-Glu-Val-Asp-fluoromethyl ketone [z-DEVD.FMK]) are neuroprotective after focal reversible cerebral ischemia in mice and rats (Hara et al., 1997a). Both drugs reduced tissue injury and associated neurologic deficits after 2-hour middle cerebral artery occlusion (MCAO) when assessed at 24 and 72 hours (Hara et al., 1997a). Interleukin-1 β formation, a product of ICE cleavage, was significantly blocked by z-VAD.FMK, a rather unselective caspase inhibitor, but not by the putative caspase 3 inhibitor z-DEVD.FMK. Smaller infarcts also were observed in transgenic mice expressing a dominant negative mutation of ICE (Friedlander et al., 1997; Hara et al., 1997b). Cleavage of pro-interleukin-1 β is important to the development of ischemic damage (Relton and Rothwell, 1992; Yamasaki et al., 1995) as is a cascade that may involve activation of caspase 3. We speculated that an important mechanism by which z-VAD and z-DEVD decrease infarct size relates to blockade of ischemia-induced apoptosis and in this report, we tested the effects of peptide methylketones in a murine model of brief (30 minutes) transient focal cerebral ischemia.

Mild injury augments apoptotic cell death in *in vitro* and *in vivo* models of cell injury, including brain ischemia. In the rat, infarct development is delayed until 3 days after 30 minutes of distal middle cerebral artery occlusion whereas tissue damage develops much earlier (within 24 hours) after 90 minutes or 2 hours of reversible MCAO. In this rat model, terminal deoxynucleotidyl transferase-mediated dUTP nick-end labeling (TUNEL)-positive cells and ladder DNA are present in the perinfarct zone, suggesting a role for apoptotic cell death (Du et al., 1996).

In the current study, we developed a model of mild ischemia in mice showing delayed infarct development and delayed appearance of several apoptosis markers (TUNEL staining, DNA laddering). We then evaluated the efficacy and the treatment window of two caspase inhibitors. We determined whether inhibition of caspase family members by the use of peptide methylketones decreases DNA laddering in ischemic tissue as measured by densitometry on agarose gels. Delayed therapeutic intervention—possibly directed against apoptotic death—may become an important therapeutic strategy to reduce mild ischemic insults (Du et al., 1996).

METHODS

Drugs

Both z-VAD.FMK and z-DEVD.FMK were obtained from Enzyme Systems Products (Dublin, CA, U.S.A.). The com-

pounds were dissolved in 0.3% dimethylsulfoxide (DMSO; MC/B, Norwood, OH, U.S.A.) prepared with 0.1 M phosphate-buffered saline [PBS] pH 7.4. Cycloheximide (Chex) was purchased from Sigma (St. Louis, MO, U.S.A.) and dissolved in PBS. We obtained (+)-MK-801 hydrogen maleate (MK-801) from Research Biochemicals International (Natick, MA, U.S.A.) and dissolved it in PBS.

Physiology

Regional cerebral blood flow (rCBF) was measured by Laser-Doppler flowmetry (PF2B, Perimed, Stockholm, Sweden) along with arterial blood pressure and heart rate as described (Hara et al., 1996, 1997a,b). Arterial blood samples (50 μ L) were analyzed for pH, oxygen (Pao₂), and carbon dioxide (Paco₂) using a blood gas/pH analyzer (Corning 178, Ciba-Corning Diagnostics, Medford, MA, U.S.A.). Core temperature was maintained at $36.5^{\circ} \pm 1^{\circ}\text{C}$ with a temperature control unit (FHC, Brunswick, ME, U.S.A.) and a heating lamp (Skytron, Daiichi Shomei, Tokyo, Japan) until 1 hour after reperfusion and during the treatment and monitoring period. With the exception of MK-801 experiments (see treatment protocol), animals were kept at room temperature during the reperfusion period. For physiologic monitoring, animals (selected randomly) were monitored for rCBF and physiologic parameters before and during ischemia, and until 30 minutes after reperfusion for different reperfusion protocols (24 and 72 hours; $n = 4$ per group). In an earlier study, we determined that intracerebroventricular pretreatment with peptide methylketones had no obvious effects on rCBF, mean arterial blood pressure, heart rate, core temperature, and arterial blood gases (Hara et al., 1997a).

Ischemia model

Adult male 129/SV mice (18 to 20 g, Taconic farms, Germantown, NY, U.S.A.) were anesthetized with 1.5% halothane for induction and maintained on 1.0% halothane in 70% N₂O and 30% O₂ using a Fluotec 3 vaporizer (Colonial Medical, Amherst, NH, U.S.A.). Ischemia was induced with a 8.0 nylon monofilament coated with silicone resin/hardener mixture (Xantopren and Elastomer Activator, Bayer Dental, Osaka, Japan), as described previously (Hara et al., 1996). The filament was introduced into the left internal carotid artery up to the anterior cerebral artery. For filament withdrawal, the animals were briefly reanesthetized. The MCAO procedures were performed by two investigators (M. E. examined the effects of z-VAD.FMK and MK-801 experiments, whereas M. S. tested z-DEVD.FMK).

Treatment protocol

Both z-VAD.FMK (120 ng) and z-DEVD.FMK (160 ng or 480 ng) were injected intracerebroventricularly (2 μ L; bregma -0.9 mm lateral, -0.1 mm posterior, -3.1 mm deep) either 10 minutes before ischemia or 6, 12, or 18 hours after reperfusion. Control animals were injected with 2 μ L of 0.3% DMSO. Cycloheximide (10 mg/kg) was administered intraperitoneally 1 day before ischemia. MK-801 (3 mg/kg) was administered intraperitoneally 10 minutes before ischemia or 3 or 6 hours after reperfusion. Control animals were injected intraperitoneally with a corresponding volume of PBS. Since hypothermia is a well known consequence of MK-801 treatment, animals were kept in an incubator (ThermoCare System, Incline Village, NV, U.S.A.) at 30 to 31°C for 6 hours after treatment to maintain a body temperature of 37°C. Core temperatures were measured using a thermometer (BAT-12, Physitemp, Clifton, NJ, U.S.A.) after 3 and 6 hours. Control mice ($36.8^{\circ} \pm 0.2^{\circ}\text{C}$ at 3 hours and $36.7^{\circ} \pm 0.2^{\circ}\text{C}$ at 6 hours) did not differ from

MK-801-injected animals ($36.7 \pm 0.1^\circ\text{C}$ at 3 hours and $36.7 \pm 0.2^\circ\text{C}$ at 6 hours).

Infarct measurement

For survival longer than 24 hours, infarct size was measured from hematoxylin-eosin (H&E)-stained sections, whereas triphenyltetrazolium chloride (TTC; Sigma, St. Louis, MO, U.S.A.) stained 2-mm coronal sections were used to assess injury after shorter periods of occlusion. For H&E-stained sections, the brains were first immediately frozen in 2-methylbutane on dry ice and then sectioned. For TTC staining, animals were decapitated, and the brains were divided into five coronal 2-mm sections using a mouse brain matrix (RBM-2000C, Activational Systems, MI, U.S.A.) and stained with 2% 2,3,5-TTC. Infarction volume was quantitated in TTC-stained sections or in H&E-stained cryostat section ($12\ \mu\text{m}$) with an image analysis system (M4, Imaging Research, St. Catharines, Ontario, Canada) and calculated by summing the volumes of each section determined directly (Huang et al., 1994) or indirectly using the following formula: contralateral hemisphere (in cubic millimeters) minus undamaged ipsilateral hemisphere (in cubic millimeters) (Swanson et al., 1990). Differences between "direct" and "indirect" volumes are likely to be accounted for by brain swelling.

Neurologic deficits

Mice were tested for neurologic deficits and scored as described by Bederson and others (1986) with the following minor modifications (Hara et al., 1996): 0, no observable neurologic deficit (normal); 1, failure to extend right forepaw (mild); 2, circling to the contralateral side (moderate); 3, loss of walking or righting reflex (severe). The rater was naive to the treatment protocol and to the group's identity. Assessments were made at 30 minutes after onset of ischemia and 24 and 72 hours (if necessary) after reperfusion.

DNA analysis

Samples were obtained at different time points after 30 minutes of transient MCAO. Ischemic striatal tissue was taken from the third 2-mm section along with homologous tissue from contralateral side after the brain was cut coronally with a brain matrix. For quantitation of DNA damage, a terminal transferase-dependent [^{32}P]ddATP end-labeling method was used (Tilly and Hsueh, 1993) with minor modifications, as described previously (Hara et al., 1997b). Three micrograms of DNA were used in the labeling procedure together with 35 ng of a 100-base pair (bp) DNA fragment as an internal standard. Electrophoresis was performed on the DNA on a 2.0% agarose gel (agarose 3:1, Amresco, Solon, OH, U.S.A.), autoradiographed together with a [^{32}P] standard, and analyzed with the M4 image analysis system. DNA less than 10 kb was used as an index of total DNA fragmentation. To measure oligonucleosomal damage more specifically, ladder DNA less than 1000 bp was measured by summing the areas of each peak (areas under the curve) minus baseline densitometry readings. The method of quantitation was validated using an artificial "smear-ladder" system in which smeared DNA was extracted from a decapitated mouse brain and incubated at 37°C for 48 hours (MacManus et al., 1995b). In a total amount of $1\ \mu\text{g}$ of DNA, 0.02, 0.04, 0.08, and $0.12\ \mu\text{g}$ of a commercially available 200-bp ladder (Invitrogen, Carlsbad, CA, U.S.A.) were added to a constant amount of smeared DNA (Fig. 1). In another experiment, increasing amounts of smeared DNA (0.3, 0.5, 0.7, 0.9 μg) were added to a constant amount of ladder (0.1 μg). The measurements for "total DNA fragmentation" and

"DNA laddering" were related linearly to the amount of total (smeared) and ladder DNA (error < 10%).

Terminal deoxynucleotidyl transferase-mediated dUTP nick-end labeling

The TUNEL staining was carried out according to the method of Gavrieli and others (1992) with minor modifications according to Wood and associates (1993). Terminal deoxynucleotidyl transferase and biotinylated dUTP were obtained from Boehringer Mannheim (Mannheim, Germany). The biotinylated dUTP was visualized by the avidin-biotin method with 3'-3' diaminobenzidine as chromogene. The reaction was intensified with 0.04% nickel chloride. For negative controls, either terminal deoxynucleotidyl transferase or biotinylated dUTP was omitted. For positive controls, the sections were treated with DNase I.

For cell counts, sections were counterstained lightly with H&E. Following a systematically random sampling scheme and based on stereologic techniques (Gundersen, 1992; West, 1993; Gómez-Isla et al., 1996), five coronal sections ($12\ \mu\text{m}$) were selected, taken at equally spaced intervals (2 mm) through the full rostrocaudal extent of the brain. The boundaries of the area occupied by TUNEL-positive cells within each section were marked using the Bioquant Image analysis system (Nashville, TN, U.S.A.). The entire volume of the lesion occupied by TUNEL-positive cells was calculated according to the principle of Cavalieri (Cavalieri, 1966). Within each section with TUNEL-positive cells, a systematically random sampling scheme was applied to count cells. The total number of TUNEL-positive cells in each brain was estimated by using ~80 optical dissectors and a $40\times$ objective. Each optical disector was a $100 \times 100\ \mu\text{m}$ sampling box with extended exclusion edges. The appropriateness of the sampling scheme chosen was evaluated by calculating the precision of the estimates in each animal, expressed as the coefficient of error (West and Gundersen, 1990). In all cases, the coefficient of error was less than 0.10, suggesting that a minimal amount of variance in the counts can be attributed to the technique. The calculation of total number of TUNEL-positive cells was performed by multiplying the volume density of TUNEL-positive cells by the total volume occupied by TUNEL-positive staining.

Glial fibrillary acid protein immunohistochemistry/TUNEL double staining and CD-45 (leukocyte common antigen) immunohistochemistry

Glial fibrillary acid protein (GFAP)/TUNEL double staining was performed to determine if glial cells show TUNEL staining. The TUNEL staining protocol was performed as described earlier. Subsequently, sections were washed and blocked with 10% normal goat serum in PBS. GFAP double labeling was performed with a rabbit GFAP polyclonal antibody (1:500, Dako Corporation, Carpinteria, CA, U.S.A.) using a three-stage avidin-biotin method and biotinylated goat anti-rabbit IgG as secondary antibody. The reaction product was visualized with 3-amino-9-ethylcarbazole reagent (Elite PK 6101 Kit, Vector Laboratories, Burlingame, CA, U.S.A.). For controls, single GFAP immunostaining was performed in adjacent sections.

To identify inflammatory cells, CD-45 (leukocyte common antigen) immunohistochemical study was performed on adjacent sections with a purified rat anti-mouse antibody (1:500, Clone 30F11.1, Pharmingen, San Diego, CA, U.S.A.) and a three-stage avidin-biotin method with a biotinylated rabbit anti-rat IgG (BA 4001, Vector Laboratories) as secondary antibody.

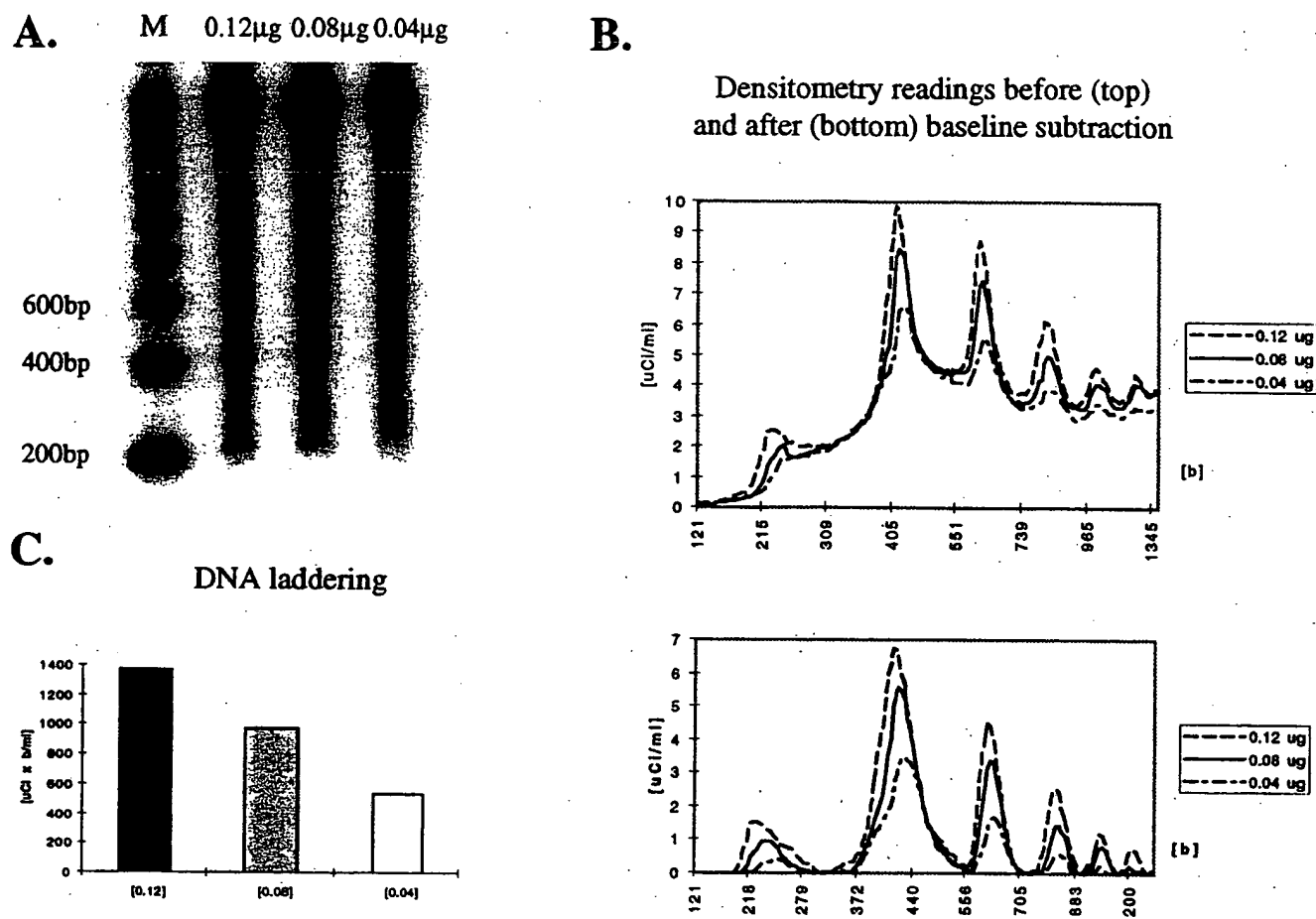


FIG. 1. Quantitative evaluation of "laddered" and "smeared" DNA by agarose gel electrophoresis. To validate the method, decreasing amounts of laddered DNA (0.12 µg, 0.08 µg, 0.04 µg) were added to constant amounts of smeared brain DNA (MacManus et al, 1995b), and labeled with [32 P]ddATP, separated by agarose gels (A), and compared with a 200-bp standard (M). Each lane was analyzed by densitometry with an image analysis system (B, top). The abscissa represents the length in base pairs [bp]; the ordinate represents µCi/mL compared with a radioactive standard (not shown). To demonstrate peak heights corresponding to laddered DNA, a baseline subtraction was performed (B, bottom). The areas under each peak provide a measure of DNA laddering. A linear relation was found between the amount of laddered DNA used in the labeling procedure and the densitometry readings (C). Readings also were linear when increasing amounts of smeared DNA were mixed with a constant amount of laddered DNA (not shown).

Statistical analysis

Data are presented as mean \pm SD. Statistical comparisons were made by one-way analysis of variance and followed by Dunnett test (rCBF) or Tukey test (physiology). For neurologic deficits, Mann-Whitney rank sum test was applied for two groups, and Kruskal-Wallis one-way analysis of variance on ranks followed by Dunn test for three or more groups. For unpaired data (infarction volume and area, DNA laddering, cell counts) two-tailed Student's *t* test was applied. Analysis was made using the software SigmaStat (Jandel Corporation, San Rafael, CA, U.S.A.) or Excel (Microsoft, Redmond, WA, U.S.A.). *P* < 0.05 was considered statistically significant.

RESULTS

Mouse model of mild focal cerebral ischemia

Physiologic parameters before, during, and after ischemia were within the normal range and did not differ between groups. Mean arterial blood pressure remained stable at 110 ± 12 mm Hg, and heart rate at 480 ± 70 beats per minute. Blood gases were stable at pH 7.4 \pm

0.1, P_{aCO_2} at 45 ± 5 mm Hg, and P_{aO_2} at 125 ± 25 mm Hg. After MCAO, rCBF decreased to 20% of baseline ($20\% \pm 8\%$) and was sustained during 30 minutes of ischemia. The rCBF immediately returned to more than 100% of baseline ($116\% \pm 20\%$) after suture removal.

No evidence for injury was detected 24 or 72 hours (TTC staining) after 10 minutes of MCAO in pilot experiments ($n = 5$ each). Twenty-four hours after 30 minutes of MCAO, ischemic changes were not detected by TTC ($n = 5$) or grossly by H&E ($n = 5$), although infrequent striatal cells showed light microscopic changes consistent with ischemia.

At 72 hours of reperfusion after 30 minutes of MCAO, clear evidence for infarction was found. Infarct size was 32.7 ± 8.3 mm³ ($n = 17$) after vehicle (DMSO) was injected intracerebroventricularly 6 hours after reperfusion. Vehicle injection did not alter infarct size, since noninjected animals showed the same injury volume (31.4 ± 19.2 mm³, $n = 12$). The lesion was located

TABLE 1. Effects of the nonselective caspase inhibitor z-VAD.FMK, the putative caspase 3 inhibitor z-DEVD.FMK, and the NMDA-antagonist MK-801 on infarct volume after 30 minutes of MCAO

| Treatment (n) | Rx time (h) | Sacrifice (h) | Infarct volume (mm ³) |
|---------------|-------------|---------------|-----------------------------------|
| Vehicle (9) | 6 | 72 | 38.1 ± 6.4 |
| z-VAD (8) | 6 | 72 | 11.2 ± 5.4* |
| Vehicle (4) | 6 | 7 days | 27.1 ± 1.9 |
| z-VAD (4) | 6 | 7 days | 9.8 ± 5.0* |
| Vehicle (6) | 18 | 72 | 37.5 ± 9.5 |
| z-VAD (4) | 18 | 72 | 38.3 ± 12.7 |
| Vehicle (7) | before | 72 | 25.0 ± 5.0 |
| z-DEVD (7) | before | 72 | 11.2 ± 2.3* |
| Vehicle (8) | 6 | 72 | 26.5 ± 5.3 |
| z-DEVD (9) | 6 | 72 | 11.2 ± 8.0* |
| Vehicle (5) | 12 | 72 | 22.6 ± 5.2 |
| z-DEVD (6) | 12 | 72 | 15.8 ± 9.2 |
| Vehicle (5)† | before | 72 | 33.4 ± 4.2 |
| MK-801 (5)† | before | 72 | 14.5 ± 5.8* |
| MK801 (5) † | 3 | 72 | 29.1 ± 6.2 |
| MK-801 (5) † | 6 | 72 | 31.1 ± 6.0 |

Time refers to drug injection after reperfusion except when noted for z-DEVD.FMK and MK-801 (given 10 minutes before MCA occlusion). z-VAD.FMK (120 ng) and z-DEVD.FMK (480 ng) were administered intracerebroventricularly, MK-801 (3 mg/kg) was given intraperitoneally. Data are presented as mean ± SD.

* $P < 0.01$ versus vehicle group.

† MK-801/vehicle-treated mice were held at a constant temperature (31°C) for 6 hours after treatment.

predominantly in the striatum where cells were severely pyknotic. Cortical injury, by comparison, was minor. Lesion volume did not increase significantly by 7 days ($33.5 \pm 21.1 \text{ mm}^3$, $n = 8$, no intracerebroventricular injection), and brain swelling did not contribute significantly to infarct size, as assessed by an indirect method for measurement of infarct size. Cycloheximide (Chex) pretreatment (10 mg/kg, $n = 7$) reduced infarct size ($10.5 \pm 9.0 \text{ mm}^3$ versus $31.4 \pm 19.2 \text{ mm}^3$, $P < 0.05$) at 72 hours, suggesting the importance of protein synthesis inhibition.

Inhibitors of the caspase family reduce infarct size

Table 1 contains the data for experiments using caspase inhibitors and MK-801. Infarct size in vehicle-treated controls were smaller in the z-DEVD.FMK experiments (22.6 to 26.5 mm^3) versus the other two vehicle groups (27.1 to 38.1 mm^3), probably because the

TABLE 2. rCBF during and after 30 minutes of filamentous middle cerebral artery occlusion in z-VAD.FMK and vehicle (0.3% DMSO) groups

| | z-VAD.FMK | Vehicle |
|---------------|-----------|----------|
| rCBF (during) | 18 ± 4 | 18 ± 12 |
| rCBF (after) | 105 ± 15 | 105 ± 18 |

z-VAD.FMK (120 ng) or vehicle were administered intracerebroventricularly in a volume of 2 μL 6 hours after reperfusion following 30 minutes of MCAO. rCBF was measured by Laser-Doppler-flowmetry (expressed as % of baseline). Data represent mean ± SD ($n = 5-6$). There are no significant differences between groups.

TABLE 3. Physiologic variables 10 minutes before and until 1 hour after injections of z-VAD.FMK or vehicle (0.3% DMSO)

| | z-VAD.FMK | Vehicle |
|-------------------|-----------|-----------|
| MABP (before) | 115 ± 9 | 115 ± 6 |
| MABP (after) | 112 ± 4 | 118 ± 12 |
| pH | 7.3 ± 0.1 | 7.3 ± 0.1 |
| Paco ₂ | 47 ± 5 | 43 ± 5 |
| Pao ₂ | 151 ± 17 | 133 ± 24 |

z-VAD.FMK (120 ng) or vehicle were administered intracerebroventricularly in a volume of 2 μL 6 hours after reperfusion following 30 minutes of MCAO. Mean arterial blood pressure (MABP, in mm Hg) was measured before and until 1 hour after drug injection. Fifty microliter blood was withdrawn 30 minutes after drug administration. Paco₂ and Pao₂ are given in mm Hg. Data represent mean ± SD ($n = 5-6$). There are no significant differences between groups.

surgical procedure for z-DEVD.FMK was performed by a different investigator (see Methods).

A dose of z-VAD.FMK (120 ng intracerebroventricularly) given 6 hours after reperfusion decreased infarct size (Table 1) and neurologic deficits at 72 hours (1.0 ± 0.9 versus 2.4 ± 0.9 , $P < 0.05$). The protective effects sustained for at least 7 days (Table 1). When given at 18 hours after reperfusion, however, the drug was not effective in reducing gross infarct size (Table 1); neurologic deficits did show some improvements in this group, however (1.2 ± 0.8 versus 2.4 ± 0.9).

A dose of z-DEVD.FMK (480 ng given intracerebro-

TABLE 4. Physiologic parameters before, during and after 30 minutes of ischemia (129/SV mice) after z-DEVD.FMK or vehicle (0.3% DMSO) pretreatment

| | z-DEVD.FMK | Vehicle |
|----------------------------|------------|------------|
| rCBF (during) | 23 ± 7 | 17 ± 6 |
| rCBF (after) | 111 ± 22 | 101 ± 27 |
| CT (before) | 37.0 ± 0.3 | 36.7 ± 0.9 |
| CT (after) | 36.9 ± 0.3 | 36.4 ± 0.4 |
| CT (72 h) | 36.0 ± 1.0 | 35.2 ± 1.0 |
| MABP (before) | 102 ± 11 | 107 ± 13 |
| MABP (during) | 103 ± 12 | 108 ± 11 |
| MABP (after) | 100 ± 14 | 104 ± 17 |
| HR (before) | 494 ± 32 | 486 ± 36 |
| HR (during) | 508 ± 45 | 461 ± 62 |
| HR (after) | 504 ± 25 | 516 ± 84 |
| pH (before) | 7.4 ± 0.1 | 7.4 ± 0.1 |
| pH (after) | 7.4 ± 0.1 | 7.4 ± 0.1 |
| Pcco ₂ (before) | 45 ± 4 | 45 ± 3 |
| Paco ₂ (after) | 48 ± 6 | 43 ± 5 |
| Pao ₂ (before) | 121 ± 12 | 124 ± 19 |
| Pao ₂ (after) | 116 ± 20 | 130 ± 33 |

Mean arterial blood pressure (MABP, in mm Hg) and heart rate (HR) were measured before, during and until 30 min after ischemia. Core temperature (CT, in °C) was measured before and until 30 minutes after ischemia and again after 72 hours, just before sacrifice. Fifty microliter blood was withdrawn twice, before ischemia and 30 minutes after reperfusion. Paco₂ and Pao₂ are given in mm Hg. rCBF was measured by Laser-Doppler-flowmetry (expressed as % of baseline). z-DEVD.FMK (480 ng) or vehicle were administered intracerebroventricularly in a volume of 2 μL 10 minutes before ischemia ($n = 5$ each). Data represent mean ± SD. There are no significant differences between groups.

ventriculally 10 minutes before ischemia) significantly reduced infarction volume at 72 hours (Table 1). A lower dose (160 ng) did not reach statistical significance ($18.0 \pm 3.3 \text{ mm}^3$ versus $24.7 \pm 5.0 \text{ mm}^3$, $n = 7$). Infarct size and neurologic deficits (0.4 ± 0.5 versus 1.7 ± 0.5 , $P < 0.05$) were reduced when 480 ng z-DEVD.FMK was administered at 6 hours after reperfusion (Table 1). Infarct volumes, although decreased, did not reach statistical significance when z-DEVD was given 12 hours after reperfusion (Table 1).

The rCBF during ischemia and after reperfusion did not differ between groups (Tables 2 and 4). There were also no significant group differences in physiologic parameters after z-VAD.FMK (Table 3) or z-DEVD.FMK treatment (Table 4).

Treatment with MK-801 significantly reduced infarct size if given before MCAO but not when given 3 or 6 hours after reperfusion (Tables 2 and 3). Neurologic deficits tended to be lower after pretreatment but did not differ from controls when MK-801 was given at 3 or 6 hours after reperfusion (0.4 ± 0.6 [pretreatment], 1.0 ± 0.8 [3 hours], 1.2 ± 0.8 [6 hours] versus 1.0 ± 0.7 [control], $n = 4$ to 5 per group).

DNA fragmentation

The TUNEL-positive cells, present in low numbers throughout the striatum at 24 hours, profoundly increased at 72 hours. The TUNEL-positive cells were identified morphologically as neurons, many of them with nuclear condensation and apoptotic bodies. Almost no TUNEL-positive cells contained GFAP double staining (Fig. 2, $n = 3$ for each time point). At 72 hours, low numbers of CD-45-positive inflammatory cells were found within the vasculature; however, only single cells were located within ischemic brain tissue (not shown).

Laddered DNA, detected first at 24 hours, increased 16-fold at 72 hours and 46-fold at 7 days compared with 24 hours (Fig. 3, $n = 3$ per group). DNA damage was already present at 6 hours as smeared DNA and increased substantially between 24 and 72 hours (Fig. 3). Total DNA damage and laddering were significantly inhibited at 72 hours by Chex pretreatment (Figs. 3 and 4).

To test the hypothesis that caspase inhibitors block

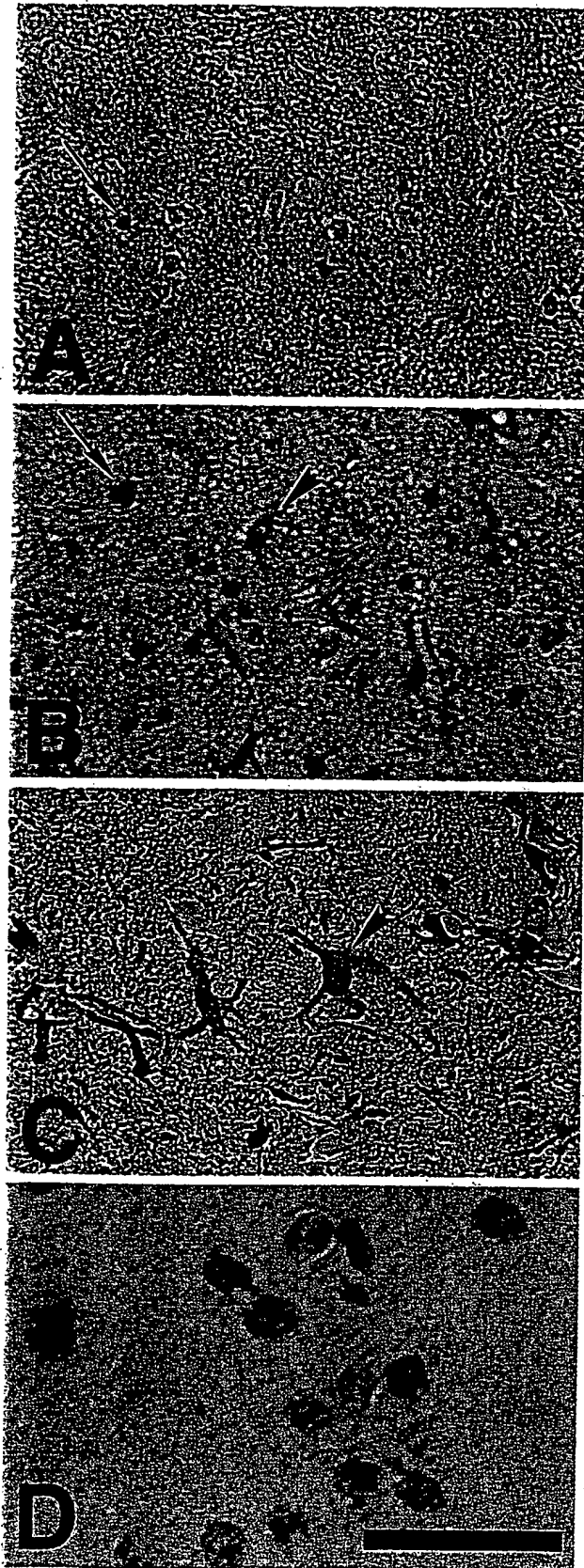


FIG. 2. Time-dependent changes in the appearance of terminal deoxynucleotidyl transferase-mediated dUTP nick-end labeling (TUNEL)-positive cells and glial fibrillary acid protein (GFAP) staining in striatum after reperfusion following 30 minutes of middle cerebral artery occlusion (MCAO). Tissue sections (6 μm) obtained at 24 hours (A), 72 hours (B), and 7 days (C) were co-stained by TUNEL and GFAP immunohistochemical methods. The TUNEL-positive cells (arrow) were infrequent at 24 hours, increased at 72 hours, and decreased at 7 days. The number of GFAP-positive glial cells (arrowhead) increased over time, but GFAP-labeled cells did not show TUNEL staining (B, C). At a higher magnification (D), TUNEL-positive cells show nuclear condensation and apoptotic bodies (section thickness 40 μm). Scale bar = 50 μm (A, B, C) and 30 μm (D).

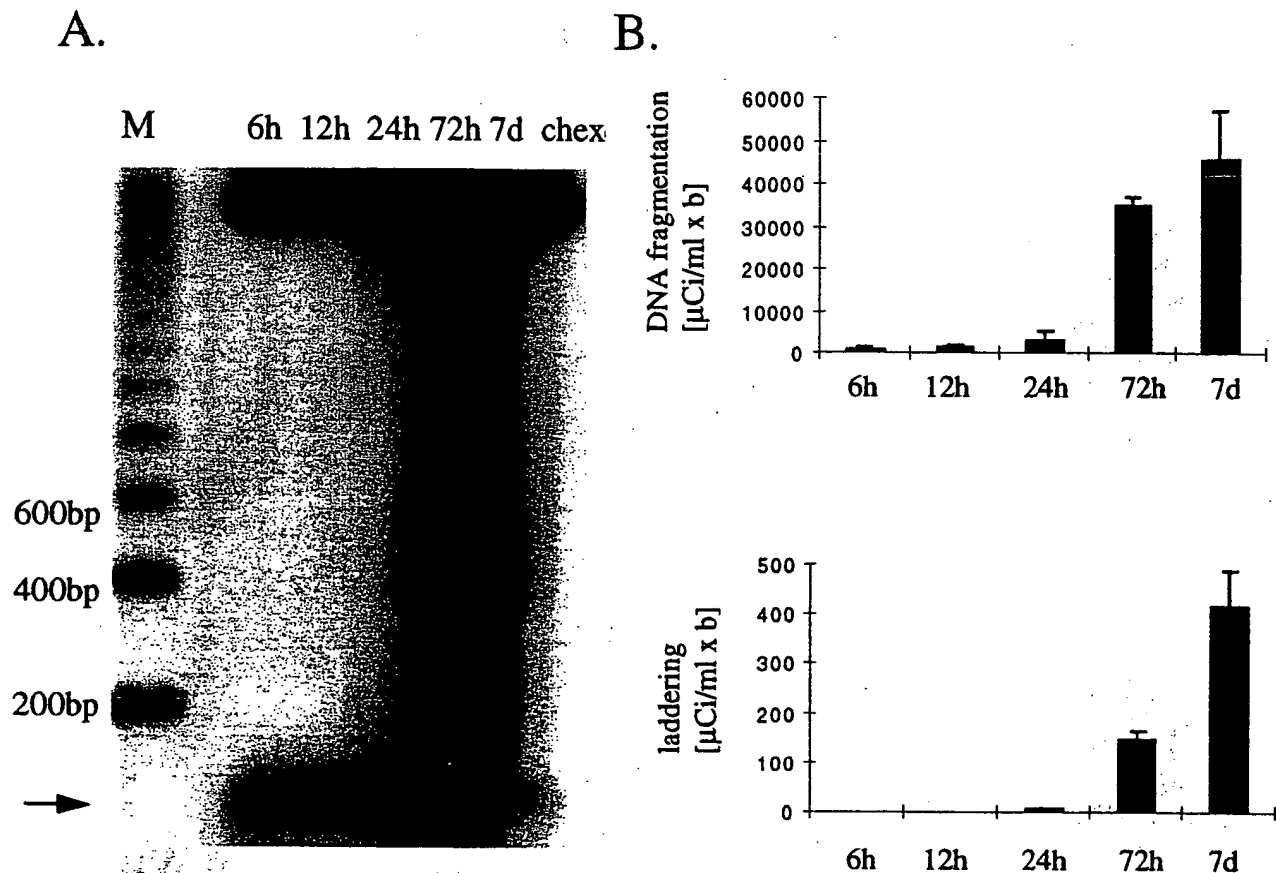


FIG. 3. Cycloheximide (Chex, 10 mg/kg) pretreatment inhibited DNA laddering during reperfusion after 30 minutes of MCAO. DNA was isolated from ischemic striatal tissue after various times after reperfusion, end-labeled with [^{32}P]ddATP, electrophoresed on a 2% agarose gel, and autoradiographed. The autoradiogram (A) shows a 200-bp standard (M) DNA prepared at 6, 12, 24, 72 hours, or 7 days, or at 72 hours after Chex pretreatment. Arrow indicates the location of a 100-bp internal standard. B: Quantitation of "DNA damage" (top) and "DNA laddering" (bottom) was performed as described in Fig. 1. Laddering was first visible after 24 hours and increased by 72 hours (16-fold) and 7 days (46-fold). Each group represents the mean \pm SD of three animals from independent labeling procedures.

apoptosis after ischemia, we compared the number of TUNEL-positive cells in z-VAD.FMK-treated animals (120 ng, given at 6 hours, $n = 4$) versus DMSO ($n = 4$) at 72 hours. Total number of TUNEL-positive cells was significantly reduced in the treatment group ($540,000 \pm 258,000$ versus $1,390,000 \pm 446,000$, $P < 0.05$), and the lesion volume containing TUNEL-positive cells was reduced by 60%. The density of TUNEL-positive cells did not decrease, however ($82,700/\text{mm}^3 \pm 6500/\text{mm}^3$ versus $84,900/\text{mm}^3 \pm 9200/\text{mm}^3$).

A significant reduction in total DNA fragmentation and DNA laddering within ischemic tissue was found at 72 hours in z-VAD.FMK-treated ($n = 4$) and z-DEVD.FMK-treated ($n = 5$) animals (administered 6 hours after reperfusion) compared with controls ($n = 9$) (Figs. 4 and 5), whereas MK-801 pretreatment (3 mg/kg, $n = 4$) did not reduce DNA fragmentation or DNA laddering compared with saline-injected controls ($n = 4$) (Figs. 4 and 5).

DISCUSSION

We provide evidence for the importance of apoptosis to the delayed development of tissue injury after mild

focal cerebral ischemia (30 minutes of MCAO) in the mouse. In this model, ischemic brain damage became grossly visible at 72 hours and did not expand at 7 days after reperfusion. The TUNEL-positive cells and DNA laddering were observed first 24 hours after reperfusion. Cells staining TUNEL-positive probably were neurons, since they did not stain positive for GFAP or CD-45. In fact, Li and colleagues (1995a,b) came to a similar conclusion, since they found GFAP co-staining in only a few TUNEL-positive cells (10%) after 2 hours of MCAO in the rat. Treatment with inhibitors of apoptosis such as cycloheximide, z-VAD.FMK, or z-DEVD.FMK reduced ischemic injury after 30 minutes of MCAO, and peptide methylketones were more effective after mild (30 minutes) than after more prolonged ischemia (2 hours of MCAO). In the 30-minute model, z-VAD.FMK and z-DEVD.FMK decreased infarct volume by 70% and 57%, respectively, whereas the degree of protection was 45% and 35%, respectively, after 2-hour MCAO (Hara et al., 1997a; Moskowitz and Ma, 1997). Peptide methylketones also were more successful many hours (6 hours) after 30 minutes of MCAO compared with 0 to 1 hours after more prolonged (2 hours) MCAO (Hara et al.,

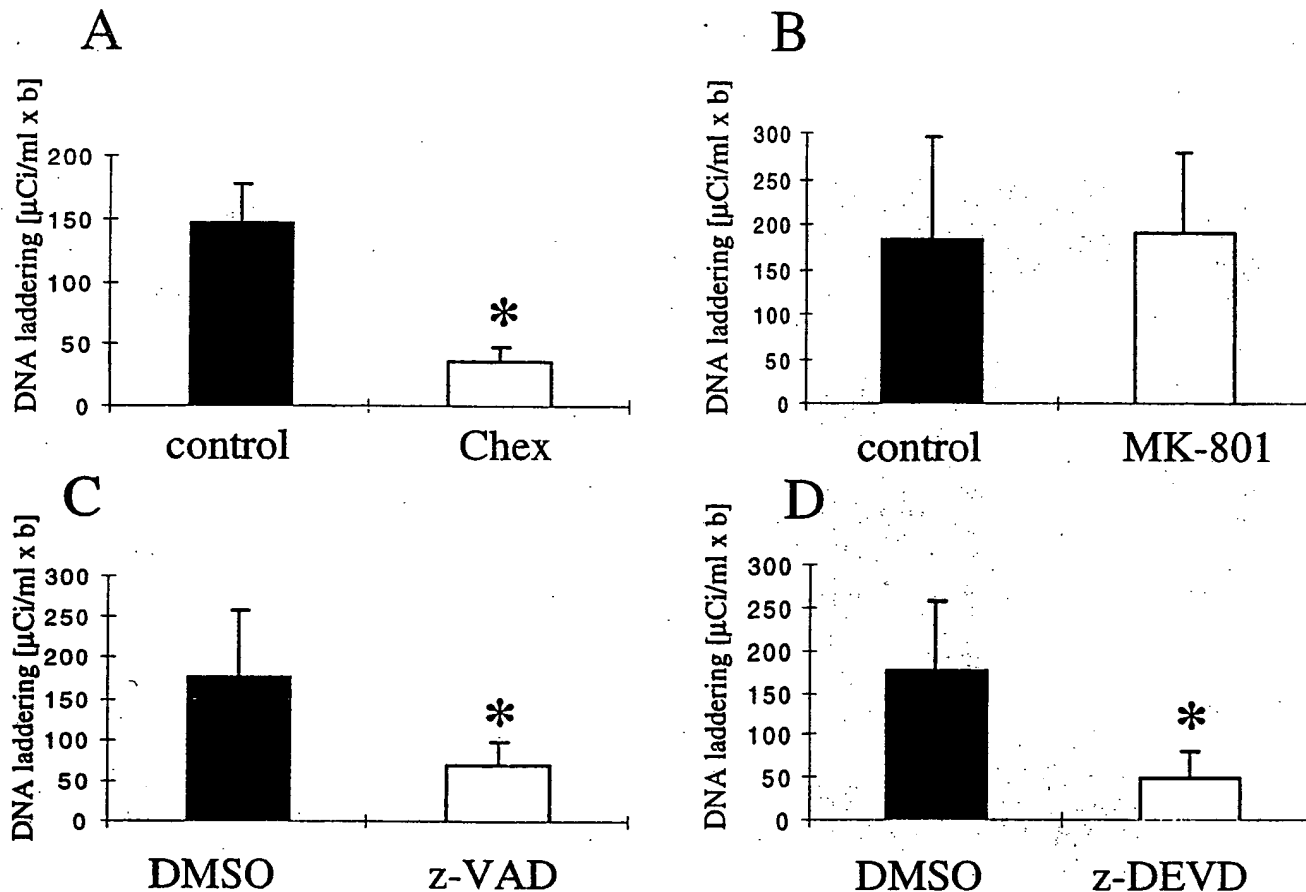


FIG. 4. Cycloheximide (Chex) pretreatment (A), z-VAD.FMK (C), or z-DEVD.FMK (D) given 6 hours after reperfusion, but not MK-801 pretreatment (B) decreased DNA laddering in ischemic tissue. Animals were subjected to 30 minutes of MCAO and reperfusion for 72 hours. DNA was extracted and separated on agarose gels (see Methods; Figs. 1 and 3). Chex also decreased total DNA damage (3299 ± 696 [drug] versus $35,426 \pm 2099$ [vehicle], $P < 0.01$), as did z-VAD.FMK ($14,394 \pm 8101$ [drug] versus $32,102 \pm 10,353$ [vehicle], $P < 0.05$) and z-DEVD.FMK ($13,341 \pm 5627$ [drug] versus $32,102 \pm 10,353$ [vehicle], $P < 0.01$). Total DNA damage did not differ after MK-801 pretreatment ($24,697 \pm 5229$ [drug] versus $20,264 \pm 8552$ [vehicle]). Units are $\mu\text{Ci/mL} \times \text{b}$. * $P < 0.05$, each group represents the mean \pm SD of four to nine animals from independent experiments.

1997a; Moskowitz and Ma, 1997). Hence, mild focal cerebral ischemia provides a useful experimental tool to assess the contribution of apoptosis to delayed mechanisms of cell death.

DNA laddering may reflect the consequences of a specific cascade promoting tissue injury after ischemia, which is distinct from necrosis. We found that oligonucleosomal damage was a useful indicator of apoptotic cell death and that a newly developed method for quantitation was reliable and reproducible. A linear relation was found between the amount of ladder DNA used in the labeling procedure and the densitometry readings in validation experiments (Fig. 1). Decreases in ladder DNA did not always accompany decreases in infarct size but depended on whether apoptosis was inhibited. For example, MK-801 pretreatment decreased ischemic damage but not DNA laddering (Figs. 4 and 5). Similar findings were observed after administering 3-amino-benzamide, a widely-used inhibitor of poly(ADP-ribose)polymerase (Endres et al., 1997). On the other

hand, inhibitors of apoptotic cell death such as cycloheximide, z-VAD.FMK, or z-DEVD.FMK clearly inhibited oligonucleosomal DNA damage and decreased infarct size (Figs. 3 through 5; Table 1).

The protective mechanisms of peptide methylketones and MK-801 are different. As observed, MK-801 did not decrease DNA laddering, and its therapeutic window was relatively short in mild ischemia when apoptotic cell death is prominent. We infer that apoptosis probably is not the predominant mechanism of cell death after *N*-methyl-D-aspartate (NMDA) excitotoxicity. Not surprisingly then, z-VAD.FMK and z-DEVD.FMK blocked damage induced by intrastriatal NMDA microinjections only weakly (Hara et al., 1997a). Moreover, TUNEL staining and DNA laddering appear late (24 to 48 hours) after NMDA microinjections (Ayata et al., 1997), suggesting that apoptosis was not primarily a direct NMDA-induced event. Nevertheless, pretreatment with MK-801 protected brain in mild ischemia, suggesting that delayed ischemic death contains both necrotic and apoptotic

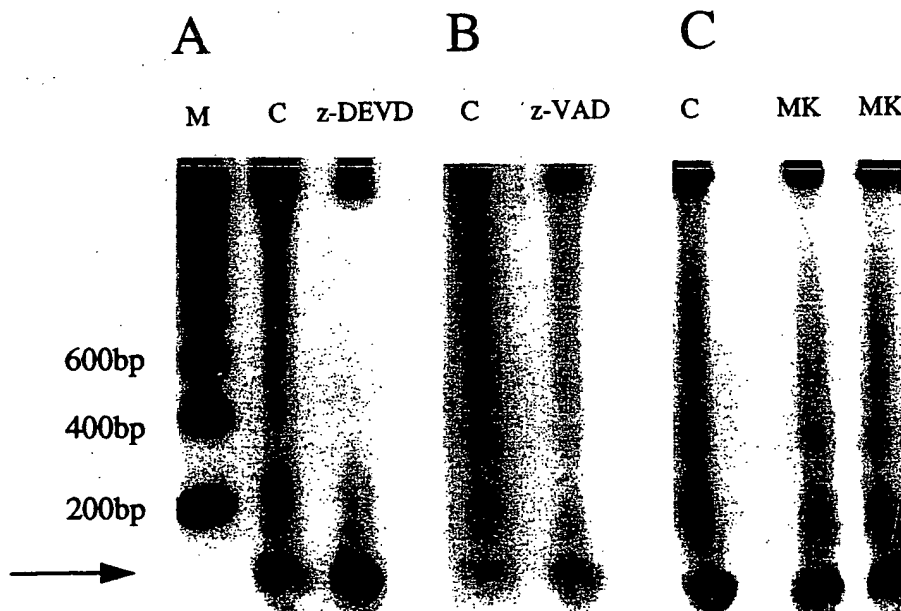


FIG. 5. The z-DEVD.FMK (480 ng) (A) or z-VAD.FMK (120 ng) (B) given intracerebroventricularly 6 hours after reperfusion but not MK-801 pretreatment (3 mg/kg) (C) inhibited DNA laddering within ischemic tissue compared with controls (C). Animals were subjected to 30 minutes of MCAO and 72 hours of reperfusion. DNA laddering was performed as shown (Figs. 1 and 3) and compared with a 200-bp DNA standard (M). The figure shows results for each treatment from representative experiments repeated in four to nine animals. A, B, and C were photographed from separate gels. Arrow indicates a 100-bp internal standard.

mechanisms (as suggested by smeared plus ladder DNA on agarose gels [Figs. 3 and 5]). Because injury is slowly evolving, and MK-801 reduced infarct size when given as a pretreatment, it must mean that NMDA-receptor activation initiates early (within 3 hours) a delayed mechanism of ischemic cell death that is not exclusively apoptosis (DNA laddering does not decrease) and cannot be inhibited by blocking the NMDA receptor after the fact.

The literature supports the notion that MK-801 and caspase inhibitors act through distinct yet complementary and synergistic mechanisms. Choi and colleagues found that NMDA receptor antagonists unmask apoptosis after oxygen-glucose deprivation in neuronal cell cultures *in vitro*. Caspase inhibitors are protective in culture only after MK-801 pretreatment (Gwag et al., 1995). *In vivo*, we demonstrated synergistic protective effects after treatment with MK-801 plus caspase inhibitors (Moskowitz and Ma, 1997). A 35% decrease in infarct size was observed in a mouse model of focal ischemia after combining doses and treatment times when neither compound provided protection alone.

Both the mouse and rat model (30 minutes of ischemia) (Du et al, 1996) show delayed infarct development, prominent DNA laddering, and TUNEL-stained cells. Damage in the mouse, however, was primarily within striatum, whereas injury was mostly within cortex in the rat model. Additionally, the lesion in the mouse did not expand after 3 days as it did in the rat. These differences may relate to greater collateral blood flow in the mouse, as well as differences in vascular anatomy or suture placement, with attendant differences in blood flow reduction. Cycloheximide reduced injury in both species, emphasizing the importance of protein synthe-

sis. The ability of cycloheximide to inhibit apoptosis is well documented in ischemia (Linnik et al., 1993; Du et al, 1996). Cycloheximide may at the same time increase *bcl-2* expression, which also would reduce tissue injury (Furukawa et al., 1997). In general, cycloheximide suppresses synthesis of all proteins, including those that may afford neuroprotection (e.g., superoxide dismutase, growth factors). Hence, it may be difficult to predict the effects of cycloheximide on tissue injury. In our studies, we demonstrate the relevance of caspases to injury development in a model in which cycloheximide reduces infarct size.

Our data could have important implications for the treatment of stroke or other evolving CNS injuries in humans, or even for procedures that carry a risk of brain damage (e.g., neurosurgical procedures or cardiopulmonary bypass). Caspase inhibitors administered at relatively late time points after mild brain injury or ischemia may protect injured tissue. We conclude that inhibitors of ICE family caspases might become valuable drugs to treat stroke in humans.

Acknowledgment: The authors thank Dr. H. Hara for advice.

REFERENCES

- Alnemri ES, Livingston DJ, Nicholson DW, Salvesen G, Thornberry NA, Wong WW, Yuan J (1996) Human ICE/CED-3 protease nomenclature. *Cell* 87:171
- Ayata C, Ayata G, Hara H, Matthews RT, Beal MF, Ferrante RJ, Endres M, Kim A, Christie R, Waeber C, Huang PL, Hyman BT, Moskowitz MA (1997) Reduced striatal NMDA excitotoxicity in type I nitric oxide synthase knockout mice. *J Neurosci* 17:6908-6917
- Bederson JB, Pitts LH, Tsuji M, Nishimura MC, Davis RL, Bartkowski HM (1986) Rat middle cerebral artery occlusion: evaluation of the

- model and development of a quantification of experimental cerebral infarction in rats. *Stroke* 17:472-476
- Cavalieri B (1966) Geometria degli indivisibili. Torino, Unione Tipografico, Edetrice
- Charriaud-Marlangue C, Margaill I, Represa A, Popovici T, Plotkine M, Ben-Ari Y (1996) Apoptosis and necrosis after reversible focal ischemia: an in situ DNA fragmentation analysis. *J Cereb Blood Flow Metab* 16:186-194
- Dinarello CA (1994) The biological properties of IL-1. *Eur Cytokine New* 5:517-531
- Du C, Hu R, Csernansky CA, Hsu CY, Choi D (1996) Very delayed infarction after mild focal cerebral ischemia: a role for apoptosis? *J Cereb Blood Flow Metab* 16:195-201
- Ellis RE, Yuan J, Horvitz HR (1991) Mechanisms and functions of cell death. *Ann Rev Cell Biol* 7:663-698
- Endres M, Wang Z-Q, Namura S, Waeber C, Moskowitz MA (1997) Ischemic brain injury is mediated by the activation of poly(ADP-ribose)polymerase. *J Cereb Blood Flow Metab* 17:1143-1151
- Fink K, Endres M, Hara H, Waeber C, Moskowitz MA (1997) Early peak IL-1 β formation in transient focal ischemia precedes DNA fragmentation and is inhibitable by caspase inhibitors. *J Cereb Blood Flow Metab* 17(suppl 1):S443
- Friedlander RM, Gagliardini V, Hara H, Fink KB, Li W, MacDonald G, Fishman MC, Greenberg AH, Moskowitz MA, Yuan J (1997) Expression of a dominant negative mutant of ICE in transgenic mice prevents neuronal cell death induced by trophic factor withdrawal and ischemic brain injury. *J Exp Med* 185:933-940
- Friedlander RM, Gagliardini V, Rotello RJ, Yuan J (1996) Functional role of interleukin-1 β (IL-1 β) in IL-1 β -converting enzyme-mediated apoptosis. *J Exp Med* 184:717-724
- Furukawa K, Estus S, Fu W, Mark RJ, Mattson MP (1997) Neuroprotective action of cycloheximide involves induction of bcl-2 and antioxidant pathways. *J Cell Biol* 136:1137-1149
- Gavrieli Y, Sherman Y, Ben-sasson SA (1992) Identification of programmed cell death in situ via specific labeling of nuclear DNA fragmentation. *J Cell Biol* 199:493-501
- Gómez-Isla T, Price JL, McKeel DW Jr, Morris JC, Growdon JH, Hyman BT (1995) Profound loss of layer II entorhinal cortex neurons occurs in very mild Alzheimer's disease. *J Neurosci* 16:4491-4500
- Gundersen HJG (1992) Stereology: the fast lane between neuroanatomy and brain function or still only a tightrope? *Acta Neurol Scand* 137:8-13
- Gwag BJ, Lobner D, Koh JY, Wie MB, Choi DW (1995) Blockade of glutamate receptors unmasks neuronal apoptosis after oxygen-glucose deprivation in vitro. *Neuroscience* 3:615-619
- Hara H, Fink K, Endres M, Friedlander RM, Gagliardini V, Yuan J, Moskowitz MA (1997b) Attenuation of transient focal cerebral ischemic injury in transgenic mice expressing a mutant ICE inhibitory protein. *J Cereb Blood Flow Metab* 17:370-375
- Hara H, Friedlander RM, Gagliardini V, Ayata C, Fink K, Huang Z, Shimizu-Sasamata M, Yuan J, Moskowitz MA (1997a). Inhibition of interleukin 1 β converting enzyme family proteases reduces ischemic and excitotoxic damage. *Proc Natl Acad Sci USA* 94:2007-2012
- Hara H, Huang PL, Panahian N, Fishman MC, Moskowitz MA (1996) Reduced brain edema and infarction volume in mice lacking the neuronal isoform of nitric oxide synthase after transient MCA occlusion. *J Cereb Blood Flow Metab* 16:605-611
- Huang Z, Huang PL, Panahian N, Dalkara T, Fishman MC, Moskowitz MA (1994) Effects of cerebral ischemia in mice deficient in neuronal nitric oxide synthase. *Science* 265:1883-1885
- Li Y, Chopp M, Jiang N, Yao F, Zaloga C (1995a) Temporal profile of in situ DNA fragmentation after transient middle cerebral artery occlusion in the rat. *J Cereb Blood Flow Metab* 15:389-397
- Li Y, Chopp M, Jiang N, Zaloga C (1995b) In situ detection of DNA fragmentation after focal ischemia in mice. *Mol Brain Res* 28:164-168
- Li Y, Chopp M, Jiang N, Zhang ZG, Zaloga C (1995c) Induction of DNA fragmentation after 10 to 120 minutes of focal cerebral ischemia in rats. *Stroke* 26:1252-1258
- Linnik MD, Zobrist RH, Hatfield MD (1993) Evidence supporting a role for programmed cell death in focal cerebral ischemia in rats. *Stroke* 24:2002-2009
- Liu T, McDonnell PC, Young PR, White RF, Siren AL, Hallenbeck JM, Barone FC, Feuerstein GZ (1993) Interleukin-1 β mRNA expression in ischemic rat cortex. *Stroke* 24:1746-1751
- MacManus JP, Hill IE, Huang ZG, Rasquinha I, Xue Dong, Buchan AM (1995a) DNA damage consistent with apoptosis in transient focal ischaemic neocortex. *Mol Neurosci* 5:493-496
- MacManus JP, Hill IE, Preston E, Rasquinha I, Walker T, Buchan AM (1995b) Differences in DNA fragmentation following transient cerebral or decapitation ischemia in rats. *J Cereb Blood Flow Metab* 15:728-737
- Moskowitz MA, Ma J (1997) Synergistic decrease in infarct volume when an ICE family inhibitor and MK-801 are combined to treat cerebral ischemia. *J Cereb Blood Flow Metab* 17(suppl 1):S434
- Nicholson DW, Ali A, Thornberry NA, Vailancourt JP, Ding CK, Gallant M, Gareau Y, Griffin PR, Labelle M, Lazebnik YA, Munday NA, Raju SM, Smulson ME, Yamin TT, Yu VL, Miller DK (1995) Identification and inhibition of the ICE/CED-3 protease necessary for mammalian apoptosis. *Nature* 376:37-43
- Refton JK, Rothwell NJ (1992) Interleukin-1 receptor antagonist inhibits ischaemic and excitotoxic neuronal damage in rats. *Brain Res Bull* 29:243-246
- Saito K, Suyama K, Nishida K, Sei Y, Basile AS (1996) Early increases in TNF- β , IL-6 and IL-1 β levels following transient cerebral ischemia in gerbil brain. *Neurosci Lett* 206:149-152
- Swanson RA, Morton MT, Tsao-Wu G, Savalos RA, Davidson C, Sharp FR (1990) A semiautomated method for measuring brain infarct volume. *J Cereb Blood Flow Metab* 10:290-293
- Tewari M, Quan LT, O'Rourke K, Desnoyers S, Zeng Z, Beidler DR, Poirier GG, Salvesen GS, Dixit VM (1995) Yama/CPP32, a mammalian homolog of CED-3, is a crmA-inhibitable protease that cleaves the death substrate poly(ADP-ribose)polymerase. *Cell* 81:801-809
- Tilly JL, Hsueh AJW (1993) Microscale autoradiographic method for the qualitative and quantitative analysis of apoptotic DNA fragmentation. *J Cell Physiol* 154:519-526
- West MJ (1993) New stereological methods for counting neurons. *Neurobiol Aging* 14:275-285
- West MJ, Gundersen HJG (1990) Unbiased stereological estimation of the number of neurons in the human hippocampus. *J Comp Neurol* 296:1-22
- Wood KA, Dipsquale B, Youle RJ (1993) In situ labeling of granule cells for apoptosis-associated DNA fragmentation reveals different mechanisms of cell loss in developing cerebellum. *Neuron* 11:621-632
- Yamasaki Y, Matsuura N, Shozuhara H, Onodera H, Itoyama Y, Kogure K (1995) Interleukin-1 as a pathogenetic mediator of ischemic brain damage in rats. *Stroke* 26:676-681
- Yuan J, Horvitz HR (1990) The Caenorhabditis elegans genes ced-3 and ced-4 act cell autonomously to cause programmed cell death. *Dev Biol* 138:33-41

ICE inhibitor YVADcmk is a potent therapeutic agent against *in vivo* liver apoptosis

Nicolas Rouquet*, Jean-Christophe Pagès*, Thierry Molina†, Pascale Briand* and Virginie Joulin*

EXHIBIT

14

In liver, apoptosis is a physiological process involved in the clearance of injured cells and in homeostatic control [1]. However, in patients with viral fulminant hepatitis or with nonacute liver diseases [2], dramatic liver failure or secondary cirrhosis results from the death of hepatocytes, which express the cell-surface receptor Fas, by apoptosis. To date, treatment of fulminant hepatitis relies mainly on orthotopic liver transplantation, which is limited by immunological complications and graft availability. Unravelling the molecular mechanisms that underlie acute liver failure could allow the design of an appropriate therapy. Ligand-bound Fas and tumour necrosis factor α (TNF- α) induce hepatic apoptosis in mice [3–6]. In various cell types, Fas- or TNF- α -induced apoptosis is blocked by viral proteins (such as p35 and CrmA) as well as by a decoy peptide (YVADcmk) [7–11], suggesting that these mechanisms of apoptosis involve ICE (interleukin-1 β converting enzyme)-like proteases. Here, we report that, *in vivo*, pre-treatment of mice with YVADcmk protects them from the lethal effect of anti-Fas antibody and from liver failure induced by injection of TNF- α . Remarkably, YVADcmk administration is also highly effective in rescuing mice that have been pretreated with anti-Fas antibody from rapid death, despite extensive hepatic apoptosis. This dramatic curative effect could be of clinical benefit for the treatment of viral and inflammatory liver diseases.

Addresses: *INSERM U-380, ICGM, 22 rue Méchain, 75014, Paris, France. †Laboratoire Universitaire de Recherche en Histopathologie, 15 rue de l'Ecole de Médecine, 75006, Paris, France.

Correspondence: Virginie Joulin. E-mail: joulin@icgm.cochin.inserm.fr

Received: 19 June 1996

Revised: 17 July 1996

Accepted: 17 July 1996

Current Biology 1996, Vol 6 No 9:1192–1195

© Current Biology Ltd ISSN 0960-9822

Results and discussion

ICE-like proteases, mammalian homologs of the nematode cell death protein Ced-3, have apoptotic properties when overexpressed in various cell lines [12–19]. *In vitro*, the inhibition of these proteases by certain viral proteins, as well as by the YVADcmk peptide [7], results in protection against TNF α - and Fas-mediated apoptosis [8–11,20,21].

Primary cultured mouse hepatocytes undergo apoptosis after incubation with anti-Fas antibody in combination with cycloheximide (CHX) [22,23]. To investigate the role of ICE-like proteases in Fas-mediated apoptosis, primary hepatocytes were incubated with YVADcmk and then treated with anti-Fas antibody supplemented with CHX. In the absence of YVADcmk, 90 % of the cells had undergone apoptosis after 36 hours of incubation with anti-Fas antibody, whereas more than 90 % of the cells were resistant to Fas-induced apoptosis in the presence of 200 μ M YVADcmk, even after a 60 hour incubation (Fig. 1a,b). The addition of YVADcmk inhibited apoptosis in a dose-dependent manner (Fig. 1c,d): in the presence of 50 μ M YVADcmk, 50 % of the cells treated with anti-Fas antibody died within 24 hours; in the presence of 300 μ M YVADcmk, 100 % of the cells survived. Note that YVADcmk was diluted in DMSO, which is known to act as a differentiating agent for primary cultures of hepatocytes; at the concentrations used here, however, DMSO *per se* conferred no protective effect against Fas-mediated apoptosis (data not shown).

The intraperitoneal or intravenous administration of anti-Fas antibody in mice leads to death [3]. That this results from severe liver damage was shown by the liver-specific expression of a *Bcl-2* transgene, which prevented the lethal effects of the antibody [24]. To evaluate the effect of ICE inhibitor on Fas-mediated apoptosis *in vivo*, mice were treated with YVADcmk (4 μ mole) 2 hours before injection of anti-Fas antibody. Most of the mice (93 %) survived and were healthy, whereas all untreated mice died 3–4 hours after antibody injection (Fig. 2a). Histological tissue sections of surviving mice were examined for liver damage and regenerative features. The livers of YVADcmk-treated mice were protected against lethal hepatic cytolysis, but had many areas of hepatocyte injury 12 and 24 hours after antibody injection. This damage consisted of numerous typical apoptotic bodies surrounded by polynuclear granulocyte, lymphocyte and macrophage infiltrates; no such damage was seen in control mice (treated with YVADcmk but not exposed to anti-Fas antibody; data not shown). The anti-apoptotic properties of YVADcmk *in vivo* were confirmed by the TUNEL assay (terminal deoxynucleotidyl transferase (TdT)-mediated dUTPbiotin nick end-labeling), which detects DNA fragmentation — a hallmark of apoptosis. By 1.5 hours after anti-Fas antibody injection, the livers of unprotected mice had numerous TUNEL-positive cells

Figur 1

Effect of YVADcmk on Fas- and TNF- α -mediated hepatocyte cytotoxicity *in vitro*. (a,b) Primary mouse hepatocytes were incubated with anti-Fas antibody in the presence (open bars and open circles) or absence (filled bars and filled circles) of YVADcmk. (c,d) Dose-dependent inhibition of Fas-induced apoptosis by YVADcmk. Primary hepatocytes were incubated for 24 h with various concentrations of YVADcmk in the presence (filled bars and filled circles) or absence (open bars and open circles) of anti-Fas antibody. (e,f) Primary hepatocytes were incubated with recombinant murine TNF- α and actinomycin D (ActD) in the presence (open bars and open circles) or absence (closed bars and filled circles) of YVADcmk. Control experiments showed that YVADcmk solvent (DMSO) did not interfere with hepatocyte apoptosis (see text). Percent apoptotic hepatocytes (Hoechst staining) and viability (blue trypan exclusion) were obtained from triplicate experiments.

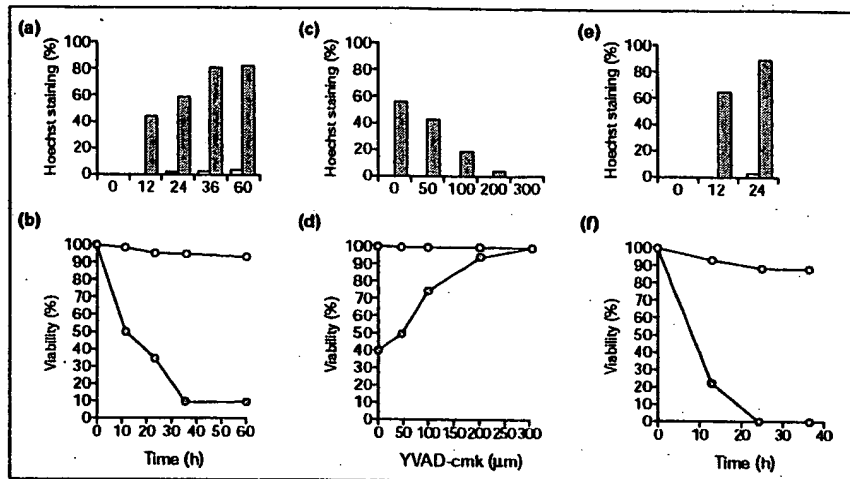


(Fig. 3a), whereas the extent of the apoptosis was reduced significantly in livers from YVADcmk-protected mice (Fig. 3b). Mitoses appeared in the parenchyma without any obvious zonal distribution within 1 day and persisted at day 4 (Fig. 3c). Progressively, apoptotic bodies disappeared within 6 days and, at day 13, liver architecture was indistinguishable from that of normal liver. Plasmatic transaminase levels increased and then decreased progressively to reach normal values concomitant with the disappearance of the apoptotic process (data not shown). The increase in transaminase levels during this process, a process which is usually described as a nonlytic event, probably results from insufficient phagocytosis [3].

The duration of the YVADcmk protective effect was tested by injecting anti-Fas antibody at day 1, 2 or 3 after administration of YVADcmk. Only the mice injected at day 3 died, suggesting that the effect of YVADcmk was transient. Histological examination of liver, heart, lung, spleen, thymus, lymph nodes, kidney and brain was performed in three mice one month after a single YVADcmk treatment, revealing no apparent cytotoxicity. Finally, the long-term

survival of protected mice confirms that blockage of ICE-like proteases, and thereby inhibition of massive hepatic apoptosis, is highly efficient in preventing lethality induced by anti-Fas antibody injection.

TNF- α is a potent mediator of hepatocyte apoptosis and liver failure [4,5]. As the signalling pathway of the TNF type I-receptor requires an ICE-like protease [9,11], we examined whether YVADcmk treatment could protect against TNF-induced hepatocyte apoptosis and liver damage. As shown above for Fas-induced apoptosis, addition of YVADcmk (200 μ M) blocked TNF-induced apoptosis of primary hepatocytes, which occurred within 24 hours in the absence of YVADcmk (Fig. 1e,f). YVADcmk protection against TNF-induced liver damage *in vivo* was tested by injection of YVADcmk and TNF- α . As the *in vivo* hepatic apoptosis mediated by TNF- α is known to require transcriptional arrest [4], mice were co-treated with ActD. The high dose (9 μ g kg⁻¹) of TNF- α injected into ActD-sensitized mice induced liver damage (Fig. 3e) and death of all the mice in less than 7 hours. Interestingly, YVADcmk administered before TNF- α into ActD-sensitized mice

Figure 2

In vivo protective effect of YVADcmk on Fas-induced mortality. (a) Preventive effect of YVADcmk. Mice were injected intraperitoneally with YVADcmk 2 h before intravenous injection of anti-Fas antibody (open circles). (b) Curative effect of YVADcmk. Mice were injected intraperitoneally with YVADcmk 2 h after intravenous injection of anti-Fas antibody (open circles). Control mice received anti-Fas antibody alone (filled squares and filled circles) or YVADcmk alone (open squares).

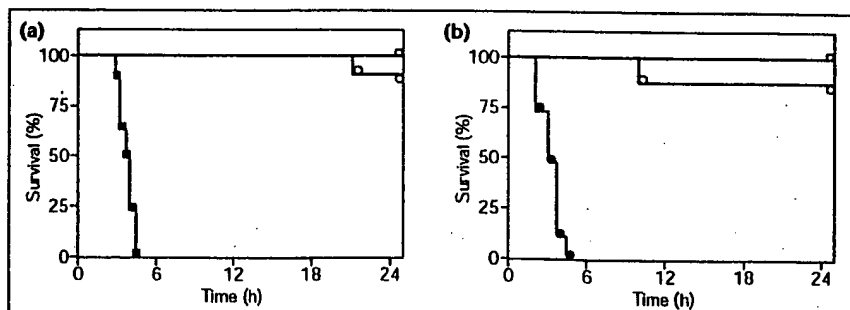
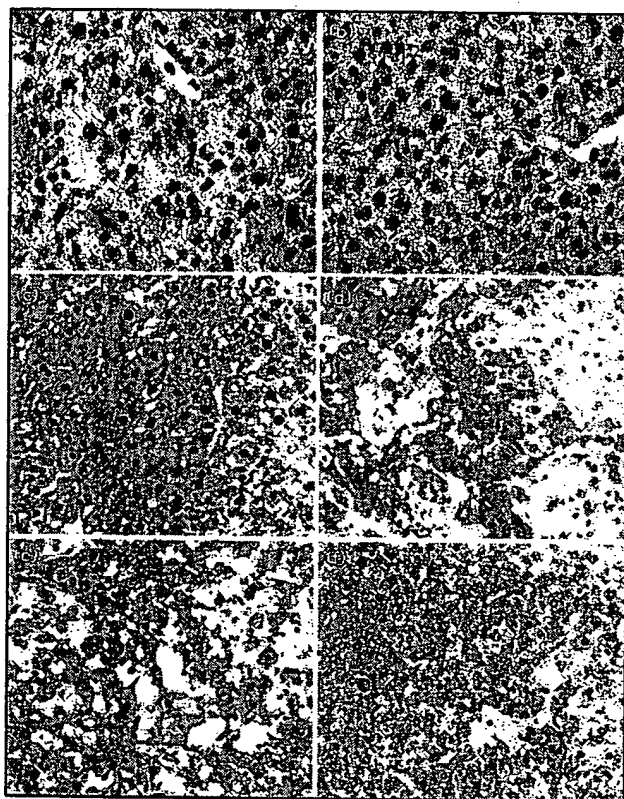


Figure 3



Liver sections from untreated and YVAD-cmk-treated mice. (a,b) TUNEL *in situ* detection of apoptosis, $\times 250$. (a) Liver section from a YVADcmk-untreated mouse 1.5 h after intravenous injection of anti-Fas antibody. Note the presence of multiple stained nuclei (arrows). (b) Liver section from YVAD-cmk-pretreated mouse 1.5 h after intravenous injection of anti-Fas antibody. Rare stained nuclei are detected (arrows). (c,d) Histological analysis, $\times 200$. (c) Liver section from YVAD-cmk-pretreated mouse prepared 4 days after intravenous injection of anti-Fas antibody. The liver has partially recovered its normal organization, despite the presence of mononuclear cell infiltrates and some hepatocyte mitosis. The same histological features were observed with liver sections of rescued mice, which had received YVAD-cmk 2 h after anti-Fas antibody injection. (d) Liver section from untreated mouse prepared 2 h after a single intravenous injection of anti-Fas antibody. The liver exhibits architectural disorganization, numerous apoptotic bodies (arrows) and infiltration of blood cells. (e) Liver section from untreated mice prepared upon death, 7 h after co-injection of ActD and TNF- α . The liver section shows a total disorganization of tissue architecture with numerous apoptotic bodies (arrows). (f) Liver section from YVADcmk-treated mouse was performed 7 h after injection of YVADcmk followed by ActD and TNF- α . The liver displays few scattered apoptotic bodies.

blocked the appearance of liver damage characterized by apoptosis (Fig. 3f) and prevented the death of animals. Considering the wide range of cells sensitive to TNF cytotoxicity [25], the causal relationship between TNF-induced death and TNF-induced liver damage has not yet been demonstrated formally. The ability of YVADcmk to protect against TNF-lethal cytotoxicity could thus be related to its

protection of other cell types *in vivo*. Note that inflammatory response syndrome observed in septic shock is mainly related to TNF- α production [26–28] and is attenuated in ICE-deficient mice [29]. It will be thus of great interest to assess the ability of YVADcmk to abolish multiple organ failure in septic shock experimental models.

To evaluate the curative potential of YVADcmk treatment against Fas-induced liver damage, we tested its ability to stop an ongoing lethal hepatic cytolysis. Time-course analysis of hepatic histological damage induced by anti-Fas antibody administration showed that 50–70 % of the liver was destroyed within 2 hours (Fig. 3d). As this experimental damage could be relevant to clinical lesions observed during liver failure [3], YVADcmk was administered 2 hours after anti-Fas antibody injection. Under these conditions, 86 % of the mice were rescued, whereas all animals died in the control group, untreated with YVADcmk (Fig. 2b). It is noteworthy that YVADcmk treatment is rapidly effective, considering the short survival of mice treated with anti-Fas antibody (3–4 hours). Biochemical analysis of hepatic transaminases and liver histology of rescued mice showed apoptosis followed by a regenerative process similar to that described for protected mice in the preventive protocol (data not shown). These data demonstrate that YVADcmk is able to overcome the rapid progression of dramatic hepatic damage induced by Fas activation.

Our results suggest that *in vivo* inhibition of ICE-dependent apoptosis mediated by Fas or TNF- α represents an attractive approach for treating liver injuries, including those caused by inflammatory, viral and autoimmune diseases [1]. As we can assume that, during fulminant hepatitis, multiple signals account for massive hepatic destruction, it would be of interest to assess ICE-mediated protection in other models. This hypothesis is supported by our preliminary experiments demonstrating an *in vivo* protective effect of YVADcmk against LPS-induced fulminant hepatitis (N.R. and A. Mignon, unpublished data). Recently, transgenic liver-specific expression of Bcl-2 has proven its efficacy in protecting mice against Fas-induced lethality [24]. However, therapeutic application of Bcl-2 will encounter the difficulties inherent to gene-transfer approaches. Our results provide evidence that a simple galenic formulation of ICE-inhibiting drugs has a curative effect on Fas-mediated liver apoptosis. This opens the field for new treatments of viral fulminant hepatitis.

Materials and methods

In vitro experiments

Hepatocytes were isolated by *in situ* collagenase perfusion [23]. The perfused liver was minced, cells were suspended in M199 medium with 10 % fetal calf serum (FCS; Gibco-BRL) and filtered through a 70 μ m mesh filter. Viability was over 90 % according to trypan blue exclusion. Cells were counted and plated at a density of 5×10^5 cells per 35 mm dishes in M199 medium containing 10 % FCS. The cells were allowed to adhere for 3 h; the medium was then removed and replaced by M199 containing 10^{-8} M insulin, 10^{-6} M thyroid hormone and 10^{-6} M dexamethasone. The *ex vivo*

protective effect of YVADcmk (Ac-Tyr-Val-Ala-Asp-chloromethylketone) (Bachem Biochimie SARL, Bale) was explored by culturing primary hepatocytes in the presence or absence of 200 μ M YVADcmk in dimethyl sulfoxide (DMSO). At the same time anti-Fas antibody (1 μ g ml⁻¹) (Pharmingen), supplemented with 10 μ g ml⁻¹ CHX or recombinant murine TNF- α (20 ng ml⁻¹) (Genzyme) supplemented with ActD (333 nM) (Sigma) were added. Cells were monitored at times up to 60 h and the percentage of viable cells assessed by trypan blue exclusion. Approximately 200 cells were counted in each sample. To monitor apoptosis, Hoechst 33258 staining was performed as described [23].

In vivo experiments

To explore the *in vivo* preventive effect of YVADcmk, a group of 14 mice were injected intraperitoneally with YVADcmk (4 μ mole in 200 μ l PBS) 2 h prior to intravenous injection of anti-Fas antibody (10 μ g in 100 μ l 0.9 % NaCl) or prior to intravenous injection of 9 μ g kg⁻¹ of TNF- α and intraperitoneal administration of ActD (16 μ g in 200 μ l PBS). To explore the *in vivo* curative effect of YVADcmk, a group of 7 mice were injected intraperitoneally with YVADcmk (4 μ mole in 200 μ l PBS) 2 h after intravenous injection of anti-Fas antibody (10 μ g in 100 μ l 0.9 % NaCl). As controls, 15 mice received anti-Fas antibody alone (10 μ g in 100 μ l 0.9 % NaCl) and 3 mice received YVADcmk alone (4 μ mole in 200 μ l PBS). 8-week-old B6D2/F1 mice were used in all experiments.

Histological examinations, TUNEL and serum analysis

Livers were excised and immediately transferred to Bouin's and formalin-acetic acid-alcohol fixatives. Samples embedded in Paraplast were cut at 5 μ m and stained with hematoxylin and eosin. Using light microscopy, 3 fields of each sample were analyzed for typical apoptotic features: marked condensation of chromatin, cell shrinkage and apoptotic bodies. Apoptosis severity was evaluated by a ratio of the number of apoptotic hepatocytes to the total hepatocytes of the field. The TUNEL procedure was performed with the 'In situ cell death detection kit, POD' (Boehringer Mannheim). For serum analysis, biochemical parameters of the serum (ALT, alanine aminotransferase, and AST, aspartate aminotransferase) were quantified using a standard clinical automatic analyzer (Hitachi, Type 7150).

Acknowledgements

All animal procedures reported in this paper were carried out in accordance with French government regulations (Services Vétérinaires de la Santé et de la Production Animale, Ministère de l'Agriculture). N.R. is a recipient of a fellowship from IFSBM and JCP from AP-HP CANA M. We thank P. Benaroch for critical comments on the manuscript. This work was supported by l'Institut National de la Santé et de la Recherche Médicale, La ligue contre le Cancer and l'Association pour la Recherche contre le Cancer.

References

- Patel T, Gores GJ: Apoptosis and hepatobiliary disease. *Hepatology* 1995, 21:1725-1741.
- Galle PR, Hofmann WJ, Walczak H, Schaller H, Otto G, Stremmel W, et al.: Involvement of the CD95 (APO-1/Fas) receptor and ligand in liver damage. *J Exp Med* 1995, 182:1223-1230.
- Ogasawara J, Watanabe FR, Adachi M, Matsuzawa A, Kasugai T, Kitamura Y, et al.: Lethal effect of the anti-Fas antibody in mice. *Nature* 1993, 364:806-809.
- Leist M, Gantner F, Böhlinger I, Germann PG, Tiegs G, Wendel A: Murine hepatocyte apoptosis induced *in vitro* and *in vivo* by TNF- α requires transcriptional arrest. *J Immunol* 1994, 153:1778-1788.
- Leist M, Gantner F, Jilg S, Wendel A: Activation of the 55 kDa receptor is necessary and sufficient for TNF-induced liver failure, hepatocyte apoptosis, and nitrite release. *J Immunol* 1995, 154:1307-1316.
- Leist M, Gantner F, Böhlinger I, Tiegs G, Germann PJ, Wendel A: Tumor necrosis factor-induced hepatocyte apoptosis precedes liver failure in experimental murine shock models. *Am J Pathol* 1995, 146:1220-1234.
- Thornberry NA, Bull HG, Calaycay JR, Chapman KT, Howard AD, Kostura MJ, et al.: A novel heterodimeric cysteine protease is required for Interleukin-1 β processing in monocytes. *Nature* 1992, 356:768-774.
- Beldier DR, Tewari M, Friesen PD, Poirier G, Dixit VM: The baculovirus p35 protein inhibits Fas- and tumor necrosis factor-induced apoptosis. *J Biol Chem* 1995, 270:16526-16528.
- Tewari M, Dixit VM: Fas- and tumor necrosis factor-induced apoptosis is inhibited by the poxvirus gene product. *J Biol Chem* 1995, 270:3255-3260.
- Los M, Van de Craen M, Penning LC, Schenk H, Westendorp M, Baeuerle PA, et al.: Requirement of an ICE/ced-3 protease for Fas/APO-1-mediated apoptosis. *Nature* 1995, 375:81-83.
- Enari M, Hug H, Nagata S: Involvement of an ICE-like protease in Fas-mediated apoptosis. *Nature* 1995, 375:78-81.
- Kumar S, Kinoshita M, Noda M, Copeland NG, Jenkins NA: Induction of apoptosis by the mouse *Nedd2* gene, which encodes a protein similar to the product of the *Caenorhabditis elegans* cell death gene *ced-3* and the mammalian IL-1 β -converting enzyme. *Genes Dev* 1994, 8:1613-1626.
- Fernandes Alnemri T, Litwack G, Alnemri ES: CPP32, a novel human apoptotic protein with homology to *Caenorhabditis elegans* cell death protein Ced-3 and mammalian interleukin-1 β -converting enzyme. *J Biol Chem* 1994, 269:30761-30764.
- Wang L, Miura M, Bergeron L, Zhu H, Yuan J: Ich-1, an Ice/ced-3-related gene, encodes both positive and negative regulators of programmed cell death. *Cell* 1994, 78:739-750.
- Fernandes Alnemri T, Litwack G, Alnemri ES: Mch2, a new member of the apoptotic Ced-3/Ice cysteine protease gene family. *Cancer Res* 1995, 55:2737-2742.
- Kamens J, Paskind M, Hugunin M, Talanian RV, Allen H, Banach D, et al.: Identification and characterization of ICH-2, a novel member of the interleukin-1 β -converting enzyme family of cysteine proteases. *J Biol Chem* 1995, 270:15250-15256.
- Nicholson DW, Ali A, Thornberry NA, Vaillancourt JP, Ding CK, Gallant M, et al.: Identification and inhibition of the ICE/CED-3 protease necessary for mammalian apoptosis. *Nature* 1995, 376:37-43.
- Tewari M, Quan LT, O'Rourke K, Desnoyers S, Zeng Z, Beldier DR, et al.: Yama/CPP32 beta, a mammalian homolog of CED3, is a CrmA-inhibitable protease that cleaves the death substrate poly(ADP-ribose) polymerase. *Cell* 1995, 81:801-809.
- Faucheu C, Diu A, Chan AW, Blanchet AM, Miossec C, Herve F, et al.: A novel human protease similar to the interleukin-1 β converting enzyme induces apoptosis in transfected cells. *EMBO J* 1995, 14:1914-1922.
- Gagliardini V, Fernandez PA, Lee RK, Drexler HC, Rotello RJ, Fishman MC, et al.: Prevention of vertebrate neuronal death by the *crmA* gene [erratum appears in *Science* 1994, 264:1388]. *Science* 1994, 263:826-828.
- Miura M, Friedlander RM, Yuan J: Tumor necrosis factor-induced apoptosis is mediated by a CrmA-sensitive cell death pathway. *Proc Natl Acad Sci USA* 1995, 92:8318-8322.
- Ni R, Tomita Y, Matsuda K, Ichihara A, Ishimura K, Ogasawara J, et al.: Fas-mediated apoptosis in primary cultured mouse hepatocytes. *Exp Cell Res* 1994, 215:332-337.
- Rouquet N, Allemand I, Molina T, Bennoun M, Briand P, Joulin V: Fas-dependent apoptosis is impaired by SV40 T-antigen in transgenic liver. *Oncogene* 1995, 11:1061-1067.
- Lacronique V, Mignon A, Fabre M, Viollet B, Rouquet N, Molina T, et al.: Bcl-2 protects from lethal hepatic apoptosis induced by an anti-Fas antibody in mice. *Nat Med* 1996, 2:80-86.
- Vassalli P: The pathophysiology of tumor necrosis factors. *Annu Rev Immunol* 1992, 10:411-452.
- Lehman V, Freudenberg MA, Galanos C: Lethal toxicity of lipopolysaccharide and tumor necrosis factor in normal and D-galactosamine-treated mice. *J Exp Med* 1987, 165:657-663.
- Dinarello CA, Gelfand JA, Wolff SM: Anticytokine strategies in the treatment of the systemic inflammatory response syndrome. *J Am Med Assoc* 1993, 269:1829-1835.
- Pfeffer K, Matsuyama T, Kündig TM, Wakeham A, Kishihara K, Weigmann K, et al.: Mice deficient for the 55 kD tumor necrosis factor receptor are resistant to endotoxic shock, yet succumb to *L. monocytogenes* infection. *Cell* 1993, 73:457-467.
- Li P, Allen H, Banerjee S, Franklin S, Herzog L, Johnston C, et al.: Mice deficient in IL-1 β -converting enzyme are defective in production of mature IL-1 β and resistant to endotoxic shock. *Cell* 1995, 80:401-411.

Attenuation of Ischemia/Reperfusion Injury in Rats by a Caspase Inhibitor

Hiroyuki Yaoita, MD; Kazuei Ogawa, MD; Kazuhira Maehara, MD; Yukio Maruyama, MD

Background—Z-Val-Ala-Asp(OMe)-CH₂F (ZVAD-fmk), a tripeptide inhibitor of the caspase interleukin-1 β -converting enzyme family of cysteine proteases, may reduce myocardial reperfusion injury in vivo by attenuating cardiomyocyte apoptosis within the ischemic area at risk.

Methods and Results—Sprague-Dawley rats were subjected to a 30-minute coronary occlusion followed by a 24-hour reperfusion. An inert vehicle (dimethylsulfoxide; group 1, n=8) or ZVAD-fmk, at a total dose of 3.3 mg/kg (group 2, n=8), was administered intravenously every 6 hours starting at 30 minutes before coronary occlusion until 24 hours of reperfusion. At this 24-hour point, hemodynamics were assessed by means of cardiac catheterization; then, the rats were killed, and the left ventricle was excised and sliced. The myocardial infarct size/ischemic area at risk and the count of presumed apoptotic cardiomyocytes (terminal deoxynucleotidyl transferase-mediated dUTP-biotin nick end labeling [TUNEL]-positive cells) within the ischemic area at risk were assessed through triphenyltetrazolium chloride staining and TUNEL methods, respectively. Peak positive left ventricular dP/dt was higher ($P=.02$) and left ventricular end-diastolic pressure was lower ($P=.04$) in group 2 than in group 1. The infarct size/ischemic area at risk of group 2 ($52.4\pm4.0\%$) was smaller ($P=.02$) than that of group 1 ($66.6\pm3.7\%$), and TUNEL-positive cells were fewer ($P=.0002$) (group 2, $3.1\pm0.9\%$; group 1, $11.1\pm1.0\%$). Agarose gel electrophoresis revealed DNA laddering in the border zone myocardium of group 1, but DNA ladder formation was attenuated in group 2.

Conclusions—ZVAD-fmk was effective in reducing myocardial reperfusion injury, which could at least be partially attributed to the attenuation of cardiomyocyte apoptosis. (*Circulation*. 1998;97:276-281.)

Key Words: myocardium ■ reperfusion ■ apoptosis ■ caspase

Attempts to reduce the extent of myocardial reperfusion injury have included lowering the risk posed by certain injurious factors and potentiating various aspects of cardioprotection relating to ischemic duration,¹ oxygen free radicals,^{2,3} proinflammatory cytokines,^{4,5} and preconditioning.⁶⁻¹⁰ It has been reported that apoptosis is a significant contributor to myocardial cell death as a result of reperfusion injury.¹ Therefore, it might be hypothesized that this type of injury could be attenuated if a portion of the injured myocardial cells could be rescued from an apoptotic death.

See p 227

The caspase inhibitors, that is, ICE-like protease inhibitors,¹¹ interfere with apoptosis at a point subsequent to the initiation of the proapoptotic process in cells that have already received apoptosis-promoting signals. As opposed to reducing the exposure of cardiomyocytes to injurious stimuli, apoptosis of these cells is attenuated through modulation of the caspase-related proapoptotic process, and this may allow ischemic myocardium to survive even after receiving significant injury. ZVAD-fmk (fluoro-methylketone), a tripeptide inhibitor of the caspase, is reported to attenuate cardiomyocyte apoptosis in

vitro.⁶ In the present study, we investigated whether ZVAD-fmk lowers the extent of experimental myocardial reperfusion injury in vivo by attenuating cardiomyocyte apoptosis. In a rat model for myocardial reperfusion injury, infarct size and the appearance of presumed apoptotic cardiomyocytes were assessed in two groups that were or were not administered this protease inhibitor.

Methods

This study was carried out under the supervision of the Animal Research Committee in accordance with the Guideline on Animal Experiments of Fukushima Medical College and Japanese Government Animal Protection and Management Law (No. 105).

Animal Model

Twenty-six of 36 adult male (290 to 310 g body weight) Sprague-Dawley rats were anesthetized through intraperitoneal administration of 30 mg/kg sodium pentobarbital. Under artificial ventilation with a rodent ventilator, a left thoracotomy was performed. The proximal portion of the left coronary artery was surgically occluded for 30 minutes through ligation with a suture (size 6.0) followed by coronary reperfusion through release of the tie. Coronary occlusion was confirmed through elevation of the ST segment on the ECG obtained from a limb lead. Transient ventricular arrhythmias were evoked in all

Received July 21, 1997; revision received October 2, 1997; accepted October 2, 1997.

From the First Department of Internal Medicine, Fukushima Medical College, Hikarigaoka 1, Fukushima 960-12, Japan.

Correspondence to Yukio Maruyama, MD, Professor and Chairman, First Department of Internal Medicine, Fukushima Medical College, Hikarigaoka 1, Fukushima, 960-12, Japan.

E-mail yaoita@cc.fmu.ac.jp

© 1998 American Heart Association, Inc.

Selected Abbreviations and Acronyms

| | |
|--------------------|---|
| DMSO | = dimethylsulfoxide |
| ICE | = interleukin-1 β -converting enzyme |
| I/R | = infarct size/ischemic area at risk |
| (\pm)-LV dP/dt | = peak positive (+) and negative (-) first derivatives of left ventricular pressure |
| LVEDP | = left ventricular end-diastolic pressure |
| LVSP | = left ventricular peak systolic pressure |
| PMN | = polymorphonuclear leukocyte |
| TdT | = terminal deoxynucleotidyl transferase |
| TTC | = triphenyltetrazolium chloride |
| TUNEL | = terminal deoxynucleotidyl transferase-mediated dUTP-biotin nick end labeling |
| ZVAD-fmk | = Z-Val-Ala-Asp(OMe)-CH ₂ F |

rats \approx 5 minutes after coronary occlusion, but these usually disappeared after 10 minutes of occlusion. After coronary reperfusion, the tie was left loose on the surface of the heart, the chest was closed, and the intratracheal tube and ECG electrodes were removed. The rats were returned to their cages, where they awakened, and they were allowed free access to food and water until they were killed 24 hours later.

One milligram of ZVAD-fmk (Enzyme Systems Products) was dissolved in 107 μ L of DMSO (Wako Pure Chemicals). In group 2 animals ($n=8$), ZVAD-fmk, at one fourth of a total dose of 3.3 mg/kg body weight, was administered as a bolus into the tail vein four times during the study (first 30 minutes before coronary occlusion and then three times every 6 hours after reperfusion). The same amount of an inert vehicle (DMSO) was administered in the same manner to rats of group 1 ($n=8$).

To assess whether the amount of DMSO used as a vehicle would have a toxic effect *in vivo*, one fourth of a total DMSO volume of 353 μ L/kg body weight ($n=5$) or the same volume of saline ($n=5$) was administered four times to sham-operated rats in the same manner as to groups 1 and 2.

Leukocytes are known to be involved in the formation of myocardial reperfusion injury.¹² As a positive control for this model of coronary reperfusion injury, 4 rats were administered absorbed polyclonal rabbit anti-rat PMN antisera at a dose of 3 mL/kg (Inter-Cell Technologies) 36 hours before coronary occlusion. Each was subjected to the 30-minute coronary occlusion and 24-hour reperfusion protocol, and 0.5 mL of blood was taken before occlusion and just before death.

Hemodynamic Assessment

Twenty-four hours after coronary reperfusion, rats were anesthetized again through intraperitoneal administration of 30 mg/kg sodium pentobarbital. ECG readings were monitored, and a polyethylene tube (PE 50; Becton-Dickinson) was inserted into the left ventricular cavity via the right carotid artery. LVSP, LVEDP, and (\pm)-LV dP/dt were measured using a polygraph system (AP601G; Nihon Koden).

Assessment of Infarcted Area and Detection of TUNEL-Positive Cardiomyocytes

After hemodynamics were assessed at 24 hours of coronary reperfusion, 0.5 mL of blood was obtained from the catheter for measurement of blood cells. Then, an intratracheal tube was inserted, and the chest was reopened under artificial ventilation. The coronary artery was again briefly occluded through ligation of the tie that remained at the site of the previous occlusion. Immediately after the ligation, 1% Evans blue solution was infused through the catheter into the beating left ventricular cavity to delineate the ischemic area at risk (underperfused and then reperfused area) of the left ventricle. After administration of an excessive dose of sodium pentobarbital into the left ventricular cavity, the heart was excised and cross-sectioned from the apex to the atrioventricular groove into five specimens of \approx 2 mm in thickness with the use of a stereoscope. Because there may be some anatomic

differences in the left coronary artery of each rat, the three middle slices were prepared for morphometry to determine the ischemic area at risk. These slices were incubated with a 4% TTC¹³ solution for 30 minutes at 37°C in a dark room. Then, ischemic but viable (TTC-stained) and infarcted (TTC-unstained) zones within the underperfused and then reperfused area (Evans blue-unstained) and the nonischemic area (Evans blue-stained) were stereoscopically measured using the point-counting method of Weibel¹⁴ with an eyepiece equipped with a 25-square grid (Integration No. 1; Zeiss) under 100 \times magnification, and I/R was calculated. These slices were then fixed in 10% neutral-buffered formalin. Using paraffin sections that were 4 μ m thick, TUNEL was performed as described previously¹⁵ with minor modifications. Briefly, nuclei of tissue sections were stripped of proteins through incubation with 20 μ g/mL proteinase K (Sigma Chemical) for 15 minutes at room temperature. The slides were incubated with 2% H₂O₂ for 5 minutes to allow inactivation of endogenous peroxidase and then incubated for 60 minutes at 37°C with 0.3 EU/ μ L TdT (Takara Shuzo Co) and 0.04 nmol/ μ L biotinylated dUTP (Boehringer-Mannheim Biochemica) in TdT buffer containing 30 mmol/L Tris-HCl, pH 7.2, 140 mmol/L sodium cacodylate, and 1 mmol/L cobalt chloride. The reaction was terminated with buffer containing 300 mmol/L NaCl and 30 mmol/L sodium citrate. The slides were coated with avidin-conjugated peroxidase (Medical and Biological Laboratories) diluted 1:3000 in PBS and visualized with the use of chromogen 3,3'-diaminobenzidine (Dojindo) and H₂O₂. Counterstaining was performed with 2% methyl green. Using this method, each cardiomyocyte could be defined, and TdT-positive or -negative nuclei were stained dark brown or light green, respectively, under light microscopy. When the TUNEL method was performed, positive controls were always included. For DNase treatment *in situ*,¹⁵ sections were processed with proteinase K, and peroxidase inactivation was carried out as described above. Next, the sections were pretreated with DN buffer (30 mmol/L Tris-HCl, pH 7.2, 140 mmol/L K cacodylate, 4 mmol/L MgCl₂, and 0.1 mmol/L dithiothreitol); then, DNase I (Sigma) at 100 ng/mL was dissolved in this buffer and used to cover each section. After a 15-minute incubation at room temperature, the slides were washed extensively with double-distilled water, and DNA nick end labeling was carried out.

Using an eyepiece for the point-counting method (Integration No. 1, Zeiss), which was performed under a light microscope at a magnification of 400 \times , we determined the count ratio of the area of cardiomyocytes with TdT-stained nuclei with that of total cardiomyocytes (TUNEL-positive cardiomyocytes) within the ischemic area at risk. The entire area was searched through an orderly shifting of the visual field using the outer grids of the eyepiece for orientation. TUNEL-positive cardiomyocytes were carefully distinguished from TUNEL-positive noncardiomyocytes, such as macrophages.

To assess the distribution of the infarcted area and TUNEL-positive cardiomyocytes in the left ventricular wall, we subdivided the ischemic area at risk into three transmural stratified layers of equal thickness (epicardial, middle, and endocardial) in each slice mentioned above (Fig 1). We also divided the ischemic area at risk into five radial segments, and then these five radial segments were rearranged as (Fig 1) a right lateral border segment adjacent to the interventricular septum; a total of three central segments; and a left lateral border segment adjacent to the left ventricular posterior wall. For each of the segments or layers, I/R and TUNEL-positive cardiomyocytes were calculated, as well as for the entire ischemic area at risk.

Using some of the paraffin sections of groups 1 and 2, hematoxylin and eosin staining was also performed for confirmation of myocardial reperfusion injury, such as myocardial cell coagulation, contraction bands, bleeding, and inflammatory cell infiltration.

Genomic DNA Extraction and Agarose Gel Electrophoresis

Rats subjected to the same occlusion and reperfusion protocol as groups 1 and 2, respectively ($n=3$ each group), had their hearts excised at 24 hours after reperfusion, and underperfused myocardium was delineated using Evans blue. The excised heart was sliced immediately as described above. Because TUNEL-positive cardio-

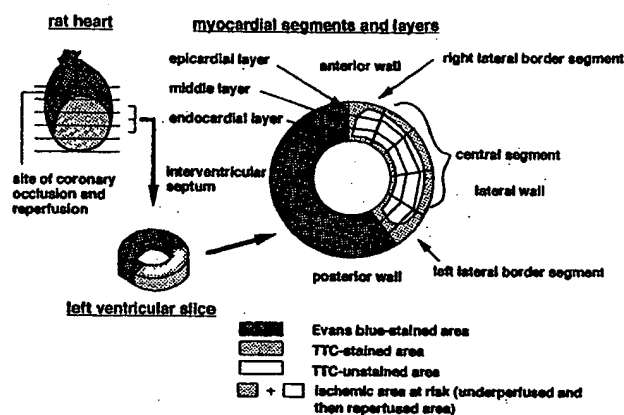


Figure 1. Myocardial segments and layers for assessment of distribution of the infarcted area and TUNEL-positive cardiomyocytes. The three middle slices of the five left ventricular slices of each heart were analyzed for measurements of the infarcted area and TUNEL-positive cardiomyocytes. The entire ischemic area at risk was first divided into five radial segments and then classified into three segments (right lateral border, central three radial segments, and left lateral border segment). The ischemic area at risk (R) was also divided into three myocardial layers (endocardial, middle, and epicardial layers). The measurements of I/R and TUNEL-positive cardiomyocytes were done in the entire ischemic area at risk, as well as in each ischemic portion.

myocytes were found mainly in the lateral border zones and the endocardial side of the ischemic area at risk (as noted in "Results"), we isolated fresh myocardial specimens from these zones and from the core of infarcted zones (mainly corresponding to the zone of the central segment, including middle and epicardial layers in Fig 1) for DNA extraction. Each myocardial specimen weighed ≈ 0.2 mg and was minced in homogenization buffer (10 mmol/L Tris-HCl, 150 mmol/L NaCl, and 10 mmol/L EDTA, pH 8.0) at 0°C and homogenized for 15 seconds at 10 000 rpm using a Polytron homogenizer (Kinematica AG). The homogenate was then treated with 100 $\mu\text{g}/\text{mL}$ proteinase K and 0.1% SDS for 90 minutes at 50°C . The DNA was extracted with phenol and chloroform followed by ethanol precipitation. The pellet was resuspended in TE buffer (10 mmol/L Tris-HCl, pH 8.0, and 1 mmol/L EDTA) and treated with DNase-free RNase (Boehringer-Mannheim) for 2 hours at 37°C . The concentration of DNA was measured through spectrophotometry, and 10 μg of each DNA sample was then electrophoretically fractionated on a 1.5% agarose gel containing ethidium bromide at a concentration of 0.4 $\mu\text{g}/\text{mL}$. DNA was visualized with a UV (302 nm) transilluminator, and the gel was photographed with the use of a Polaroid camera.

Statistical Analysis

Data are expressed as mean \pm SEM. To compare group 1 (control ischemia/reperfusion) with group 2 or to compare the two groups of sham-operated rats, an unpaired *t* test was performed. For comparisons

between the positive anti-PMN control and the other groups, one-way ANOVA followed by Fisher's posthoc comparison was carried out. For comparisons in I/R and TUNEL-positive cardiomyocytes among different myocardial portions, two-way ANOVA followed by Fisher's posthoc comparison was carried out. A value of $P < .05$ was considered statistically significant.

Results

Hemograms

White blood cell counts just before death revealed no difference between group 1 ($9502 \pm 351/\mu\text{L}$) and group 2 ($9350 \pm 435/\mu\text{L}$). In anti-PMN-treated rats, white blood cell counts were $956 \pm 132/\mu\text{L}$ ($P < .0001$ versus group 1 and group 2) before coronary occlusion and $1081 \pm 156/\mu\text{L}$ ($P < .0001$ versus group 1 and group 2) just before death. In this positive control group, lymphocytes made up most of the white blood cells ($>99\%$).

Positive Control for the Rat Model of Reperfusion Injury

The ischemic area at risk was $53.0 \pm 2.5\%$ (NS versus group 1 and group 2), and the I/R was $51.0 \pm 1.7\%$ ($P < .05$ versus group 1, NS versus group 2).

Hemodynamics

Although the LVSP did not differ between groups 1 and 2, the LVEDP of group 2 was lower ($P = .04$) than that of group 1 (Table). The positive LV dP/dt of group 2 was greater ($P = .02$) than that of group 1, but the heart rates of the two groups did not differ.

For the sham-operated rats, administration of DMSO or saline resulted in no differences in LVSP/EDP or LV dP/dt value or in the heart rate.

Myocardial Infarct Size and TUNEL-Positive Cardiomyocytes

The ischemic areas at risk of groups 1 and 2 were similar ($53.9 \pm 2.9\%$ in group 1 and $55.4 \pm 3.0\%$ in group 2, NS). In the entire ischemic area at risk, the I/R of group 2 ($52.4 \pm 4.0\%$) was significantly ($P = .02$) smaller than that of group 1 ($66.6 \pm 3.7\%$) (Fig 2, left). The I/Rs of left and right lateral border segments or endocardial and epicardial layers were smaller ($P < .05$, $< .05$, or $P < .05$, $< .01$, respectively) than that of the central segment or that of the middle layer in group 1 (Fig 3). In group 2, the I/Rs of all of three myocardial segments and all of three layers were smaller ($P < .05$, each) than those of group 1.

We confirmed that all nuclei of cardiomyocytes on sections subjected to DNase treatment (as a positive control for the TUNEL

Hemodynamics Before Death

| Group | LVSP/LVEDP, mm Hg | LV dP/dt, mm Hg/s | Heart Rate, bpm |
|----------------------------------|-------------------------------|---|-----------------|
| 1 | $133 \pm 5/9 \pm 1$ | $+4296 \pm 204/-4385 \pm 337$ | 428 ± 18 |
| 2 | $136 \pm 8/5 \pm 1^*$ | $+4907 \pm 129^*/-4715 \pm 227$ | 409 ± 14 |
| PMN-depleted (positive controls) | $126 \pm 1/6 \pm 1$ | $+4716 \pm 143/-4684 \pm 130$ | 410 ± 10 |
| Sham with DMSO | $139 \pm 5/2 \pm 1^{\dagger}$ | $+5545 \pm 205^{\dagger}/-5468 \pm 131^{\dagger}$ | 390 ± 10 |
| Sham with saline | $137 \pm 2/2 \pm 1^{\dagger}$ | $+5440 \pm 147^{\dagger}/-5088 \pm 316$ | 398 ± 14 |

* $P < .05$, $^{\dagger}P < .01$ vs group 1.

In group 2, LVEDP was lower and +LV dP/dt was higher than in group 1.

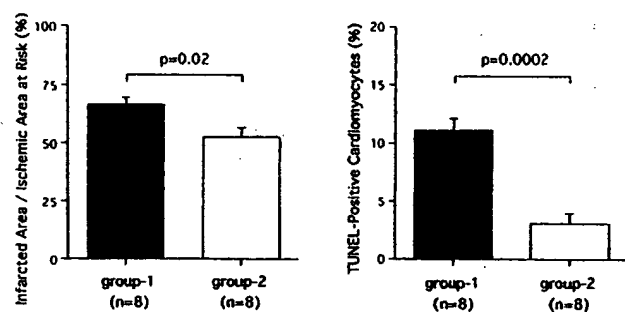


Figure 2. Infarct size and TUNEL-positive cardiomyocytes in the entire underperfused and then reperfused area. Left, I/R. Right, TUNEL-positive cardiomyocytes in the ischemic area at risk. The column representing the infarcted area was lower ($P=0.02$) for group 2 than for group 1. The counts of TUNEL-positive cardiomyocytes in group 2 were lower ($P=0.0002$) than in group 1. Group 1, infarcted rats ($n=8$) administered vehicle; group 2, infarcted rats ($n=8$) treated with ZVAD-fmk at a total dose of 3.3 mg/kg.

method) were stained dark brown each time the TUNEL method was performed. The concentration of the TUNEL-positive cardiomyocytes of group 2 ($3.1 \pm 0.9\%$) was significantly ($P=0.0002$) less than that of group 1 ($11.1 \pm 1.0\%$) (Fig 2, right). In group 1, TUNEL-positive cardiomyocytes were greater in left and right lateral segments ($P<0.05$, <0.01 , respectively) than in the central segment and greater in the endocardial layer ($P<0.01$) but smaller in the epicardial layer ($P<0.01$) than in the middle layer (Fig 4). In group 2, TUNEL-positive cardiomyocytes of all of three segments ($P<0.01$, each) and of endocardial, middle, and epicardial layers ($P<0.01$, <0.01 , <0.05 , respectively) were smaller than those of group 1 (Figs 4 and 5). Therefore, there were no significant differences of TUNEL-positive cardiomyocytes in group 2 among the three myocardial segments or three myocardial layers (Fig 4).

Neither TTC-negative zones nor TUNEL-positive cardiomyocytes were detected in the sham-operated rats administered DMSO or saline.

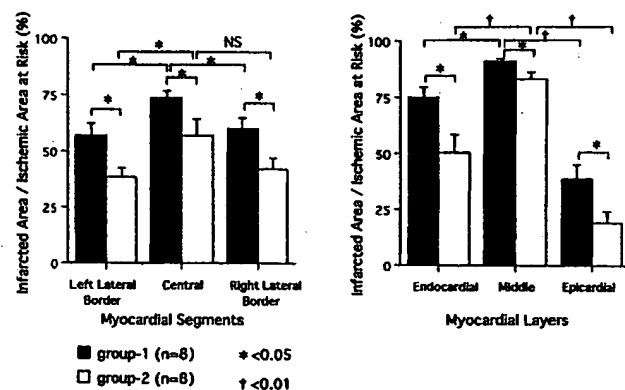


Figure 3. The I/R in myocardial segments or myocardial layers. In group 1, the I/R was smaller in left and right lateral border segments ($P<0.05$, respectively) than the central segment (left). Furthermore, in this group, the I/R was smaller in endocardial and epicardial layers ($P<0.05$, <0.01 , respectively) than the middle layer (right). In group 2, the I/R of three myocardial segments (left) and of three myocardial layers (right) was smaller than that of the corresponding segments or layers of group 1 ($P<0.05$, respectively).

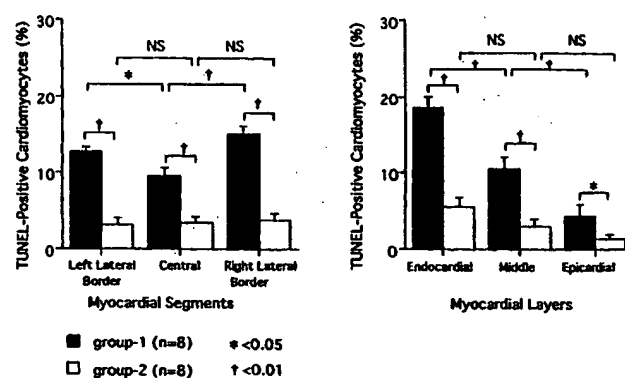


Figure 4. The TUNEL-positive cardiomyocytes in myocardial segments or myocardial layers within the ischemic area at risk. In group 1, TUNEL-positive cardiomyocytes of left and right lateral border segments (left) were greater than that of the central segment ($P<0.05$, <0.01 , respectively). In this group, TUNEL-positive cardiomyocytes of the endocardial layer or those of the epicardial layer were greater ($P<0.01$) or smaller ($P<0.01$) than those of the middle layer, respectively (right). In group 2, TUNEL-positive cardiomyocytes were smaller than those of group 1 in all of three myocardial segments and three myocardial layers ($P<0.05$ or <0.01).

Agarose Gel Electrophoresis

DNA laddering indicative of fragmented DNA was clearly demonstrated in myocardial specimens sampled from the lateral border zones and the endocardial side of the ischemic area at risk in group 1 (lane 4) but was attenuated in group 2 (lane 3), as shown in Fig 6. DNA laddering in the core of infarction was attenuated in group 1 (lane 2) and was absent in group 2 (lane 1).

Discussion

The present study revealed that administration of ZVAD-fmk reduced both the size of the myocardial infarct, as assessed through TTC staining, and the number of TUNEL-positive cardiomyocytes, with significant hemodynamic improvement in vivo in rats that underwent the 30-minute coronary occlusion and 24-hour reperfusion procedure. TUNEL-positive cardiomyocytes appeared to be apoptotic in this study because well-defined (group 1) or attenuated (group 2) DNA laddering on electrophoresis was consistent with a higher or lower value of TUNEL-positive cardiomyocytes, respectively, in the ischemic area at risk of the two groups. In a preliminary study using frozen sections, we confirmed that none of the TUNEL-positive cardiomyocytes were stained with TTC. Therefore, a reduction in their number appeared to contribute to a reduction in the myocardial infarct size. These results suggested that ZVAD-fmk was effective in reducing myocardial reperfusion injury, which could be at least partially attributed to the attenuation of cardiomyocyte apoptosis.

ZVAD-fmk achieved $\approx 21\%$ decrease in the I/R and $\approx 72\%$ decrease in TUNEL-positive cardiomyocytes, as ratios compared with the control ischemia/reperfusion. However, the absolute value for decrease in TTC unstained area ($\approx 14\%$) appeared somewhat greater than that of TUNEL-positive cardiomyocytes ($\approx 8\%$) (Fig 2); we must be careful to simply compare the absolute values of TUNEL-positive cardiomyocytes with the I/R because the methodology for quantification

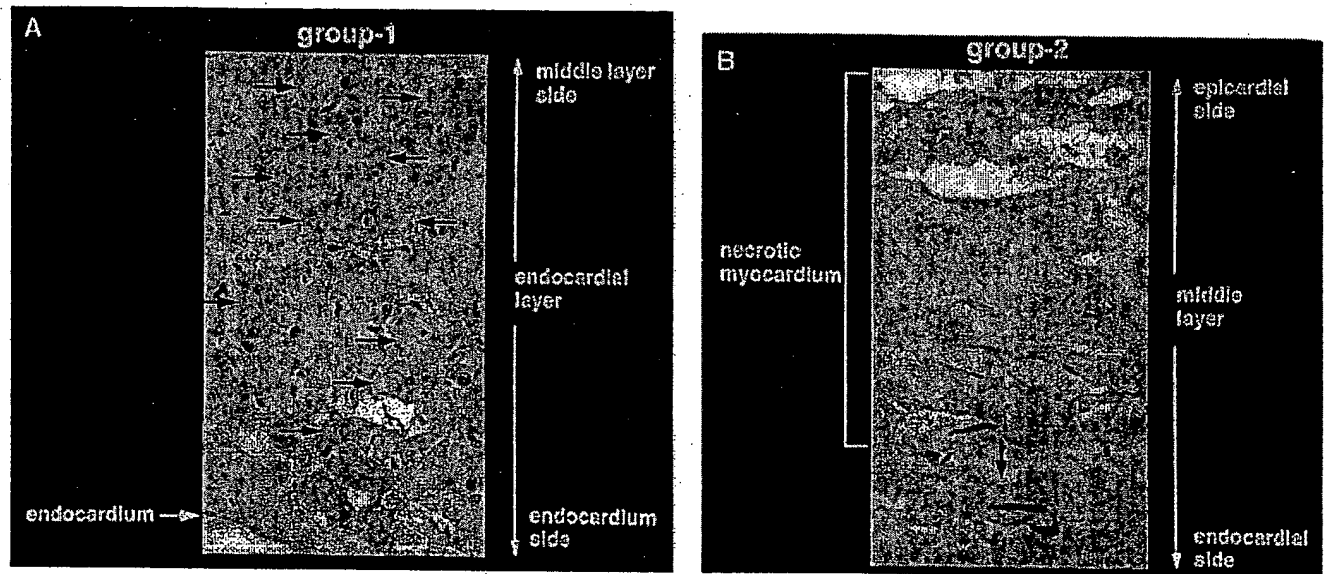


Figure 5. Light microscopic findings on the distribution of TUNEL-positive cardiomyocytes at 24 hours after reperfusion. A, TUNEL-positive cardiomyocytes (arrows) in the endocardial layer of ischemic area at risk on the section from group 1 at a high magnification. B, TUNEL-positive cardiomyocytes (top to middle) and a TUNEL-positive cardiomyocyte (bottom) in the middle layer on the section from group 2. TUNEL-positive cardiomyocytes were frequently detected in the endocardial layer in group 1 (control ischemia/reperfusion) (A). In this group, TUNEL-positive cardiomyocytes were widely spread close to endocardium. In contrast, only a few TUNEL-positive cardiomyocytes were detected mainly in the endocardial side close to the core of infarction in group 2 (ischemia/reperfusion with administration of ZVAD-fmk). The core of infarction consisted of possibly necrotic cardiomyocytes with appearance of disappeared nuclei and degenerated cytoplasm (B). TUNEL-positive cardiomyocytes did not coexist with the mass of these degenerated cardiomyocytes but were present in the surrounding area within central segments or middle layers.

was not the same between TTC staining (histochemical area measurement on myocardial slices) and the TUNEL method (histological cell counting on paraffin sections). Furthermore, we cannot exclude the possibility that ZVAD-fmk interferes

with myocardial necrotic process as well as the apoptotic process.¹⁶⁻¹⁸ Tsujimoto and colleagues^{17,18} recently revealed that ICE inhibitors retarded necrotic cell death as well as apoptotic cell death in their *in vitro* system of chemical hypoxia. The authors speculated that there was possible involvement of common mediators in apoptotic and necrotic signal transductions, although their detailed mechanisms remain to be determined. In the present study, we might have observed effects of ZVAD-fmk on these possible but undetermined common mediators. However, our examination in an *in vivo* system is not suited for approach to signal transductions of these two forms of cell death. The third possibility is the difference in time from initiation of cellular change until elimination between apoptosis and other types of cell death, both forming the infarction. Apoptotic cells are eliminated through phagocytosis in a few minutes in an *in vitro* condition¹⁹ and in a few hours in an *in vivo* condition.²⁰ In contrast, necrotic cardiomyocytes are eliminated much slowly by infiltrating inflammatory cells. Although a turnover of apoptotic cardiomyocytes *in vivo* has not been clarified so far, it may be speculated that the amount of TUNEL-positive cells quantified at a death stage may not equal the total amount of apoptotic cardiomyocytes that appear during a 24-hour reperfusion period.

To date, nothing is known about the fate of cardiomyocytes that have been exposed to ZVAD-fmk but have not undergone a proapoptotic process, such as initiation of apoptotic signal transduction via TNF receptor. These cardiomyocytes may continue to survive or may undergo an early death because of injury already sustained. Myocardial infarct size was assessed only at 24 hours after reperfusion in the present study. Future studies will be needed to evaluate the viability of cardiomyocytes that escape apoptosis through assessment of infarct extension in the later phase of reperfusion.

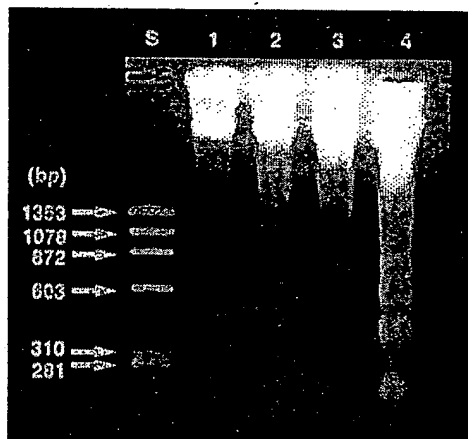


Figure 6. Agarose gel electrophoresis. S indicates size marker (bp). Lane 1, sampled from the core of infarction in myocardium with the same experimental protocol as group 2; lane 2, sampled from the core of infarction in myocardium with the same experimental protocol as group 1; lane 3, sampled from endocardial and lateral border zones of the ischemic area at risk in myocardium with the same experimental protocol as group 2; and lane 4, sampled from endocardial and lateral border zones of the ischemic area at risk in myocardium with the same experimental protocol as group 1. DNA laddering was well defined in the sample from peripheral zone of the ischemic area at risk in control ischemia/reperfusion (lane 4), but DNA ladder formation was attenuated in peripheral zone of the ischemic area at risk in the ZVAD-fmk-treated ischemia/reperfusion (lane 3) or in the core of infarction in control ischemia/reperfusion (lane 2). DNA ladder was not detected in the core of infarction in ZVAD-fmk-treated ischemia/reperfusion (lane 1).

References

1. Fliss H, Gattinger D. Apoptosis in ischemic and reperfused rat myocardium. *Circ Res*. 1996;79:949-956.
2. Ambrosio G, Flaherty JT, Duilio C, Tritto I, Santoro G, Elia PP, Condorelli M, Chiariello M. Oxygen radicals generated at reflow induce peroxidation of membrane lipids in reperfused hearts. *J Clin Invest*. 1991;87:2056-2066.
3. Bolli R, Zughbib M, Li XY, Tang XL, Sun JZ, Triana JF, McCay PB. Recurrent ischemia in the canine heart causes recurrent bursts of free radical production that have a cumulative effect on contractile function: a pathophysiological basis for chronic myocardial 'stunning.' *J Clin Invest*. 1995;96:1066-1084.
4. Kukiellka GL, Smith CW, Manning AM, Youker KA, Michael LH, Entman ML. Induction of interleukin-6 synthesis in the myocardium: potential role in postreperfusion inflammatory injury. *Circulation*. 1995;92:1866-1875.
5. Krown KA, Page MT, Nguyen C, Zechner D, Gutierrez V, Comstock KL, Glembotski CC, Quintana PJ, Sabbadini RA. Tumor necrosis factor alpha-induced apoptosis in cardiac myocytes: involvement of the sphingolipid signaling cascade in cardiac cell death. *J Clin Invest*. 1996;98:2854-2865.
6. Gottlieb RA, Gruol DL, Zhu JY, Engler RL. Preconditioning rabbit cardiomyocytes: role of pH, vacuolar proton ATPase, and apoptosis. *J Clin Invest*. 1996;97:2391-2398.
7. Przyklenk K, Zhao L, Kloner RA, Elliott GT. Cardioprotection with ischemic preconditioning and MLA: role of adenosine-regulating enzymes? *Am J Physiol*. 1996;271:H1004-1014.
8. Woolfson RG, Patel VC, Neild GH, Yellon DM. Inhibition of nitric oxide synthesis reduces infarct size by an adenosine-dependent mechanism. *Circulation*. 1995;91:1545-1551.
9. Yao Z, Gross GJ. A comparison of adenosine-induced cardioprotection and ischemic preconditioning in dogs: efficacy, time course, and role of KATP channels. *Circulation*. 1994;89:1229-1236.
10. Homeister JW, Hoff PT, Fletcher DD, Lucchesi BR. Combined adenosine and lidocaine administration limits myocardial reperfusion injury. *Circulation*. 1990;82:595-608.
11. Tatsuta T, Cheng J, Mountz JD. Intracellular IL-1 beta is an inhibitor of Fas-mediated apoptosis. *J Immunol*. 1996;157:3949-3957.
12. Romson JL, Hook BG, Kunkel SL, Abrams GD, Schork MA, Lucchesi BR. Reduction of the extent of ischemic myocardial injury by neutrophil depletion in the dog. *Circulation*. 1983;67:1016-1023.
13. Vivaldi MT, Kloner RA, Schoen FJ. Triphenyltetrazolium staining of irreversible ischemic injury following coronary occlusion in rats. *Am J Pathol*. 1985;121:522-530.
14. Weibel ER. Principles and methods for the morphometric study of the lung and other organs. *Lab Invest*. 1963;12:131-155.
15. Gavrieli Y, Sherman Y, Ben-Sasson SA. Identification of programmed cell death in situ via specific labeling of nuclear DNA fragmentation. *J Cell Biol*. 1992;119:493-501.
16. Shimizu S, Eguchi Y, Kamiike W, Waguri S, Uchiyama Y, Matsuda H, Tsujimoto Y. Bcl-2 expression prevents activation of the ICE protease cascade. *Oncogene*. 1996;12:2251-2257.
17. Shimizu S, Eguchi Y, Kamiike W, Waguri S, Uchiyama Y, Matsuda H, Tsujimoto Y. Retardation of chemical hypoxia-induced necrotic cell death by Bcl-2 and ICE inhibitors: possible involvement of common mediators in apoptotic and necrotic signal transductions. *Oncogene*. 1996;12:2045-2050.
18. Shimizu S, Eguchi Y, Kamiike W, Waguri S, Uchiyama Y, Matsuda H, Tsujimoto Y. Bcl-2 blocks loss of mitochondrial membrane potential while ICE inhibitors act at a different step during inhibition of death induced by respiratory chain inhibitors. *Oncogene*. 1996;13:21-29.
19. Russell SW, Rosenau W, Lee JC. Cytolysis induced by human lymphotoxin. *Am J Pathol*. 1972;69:103-111.
20. Perlman H, Maillard L, Krasinski K, Walsh K. Evidence for the rapid onset of apoptosis in medial smooth muscle cells after balloon injury. *Circulation*. 1997;95:981-987.

Interleukin-1 β converting enzyme (caspase-1) in intestinal inflammation

Britta Siegmund*

University of Colorado Health Sciences Center, Division of Infectious Diseases B168,
4200 East Ninth Avenue, Denver, CO 80262, USA

Abstract

An imbalance of T helper cell type 1 (Th1) versus type 2 (Th2) polarization in favor of Th1 cell subsets appears to be a key pathogenic mechanism in chronic inflammatory bowel disease (IBD), in particular in Crohn's disease. The interferon γ -inducing factor interleukin (IL)-18 acts in strong synergism with the Th1 polarizing cytokine IL-12. Recent studies provide evidence for the participation of IL-18 in the pathogenesis of IBD: IL-18 expression is increased in inflamed lesions of Crohn's disease patients and neutralization of IL-18 in different models of experimental colitis resulted in a dramatic amelioration of disease severity. IL-18 and IL-1 β are cleaved and thereby activated by the interleukin-1 β converting enzyme (ICE). Activation of ICE also occurs during different types of infectious colitis, and ICE expression and subsequent release of IL-1 β and IL-18 significantly contribute to intestinal inflammation. ICE knockout mice as well as mice treated with the ICE inhibitor pralnacasan are protected against experimental mucosal inflammation. Thus, inhibition of ICE represents an intriguing new target that requires further investigation in animal models. © 2002 Elsevier Science Inc. All rights reserved.

Keywords: Inflammatory bowel disease; Interleukin-1 β converting enzyme; IL-18; IL-1 β ; Experimental colitis

1. Introduction

Human IBD is a chronic, relapsing, and remitting inflammatory condition of unknown origin that afflicts individuals of both sexes throughout life. Studies in humans with IBD suggest that genetic and environmental factors contribute to the pathogenesis of these disorders [1]. Studies in experimental models of mucosal inflammation provide profound insight into the understanding of pathologies of mucosal immunity, thereby guiding investigators towards new innovative therapeutic strategies for IBD.

Several approaches focusing on the inhibition of the pro-inflammatory Th1 response, such as treatment with a chimeric antibody against TNF α in patients with Crohn's disease [2] or administration of antibodies against IL-12 in experimental mucosal inflammation, have been shown to be dramatically effective [3,4]. Studies from the recent literature suggest that inhibition of the IFN γ -inducing

factor IL-18, which strongly synergizes with IL-12, might be of therapeutic significance as well. IL-18 and IL-1 β require cleavage by the ICE, also named caspase-1 [5], to become active mediators. The availability of ICE inhibitors offers a strong pharmacological tool for *in vivo* evaluation. The present review will focus on ICE, the biological activities of IL-18, the relevance of IL-18 neutralization during intestinal inflammation, and, hence, the possible significance of ICE inhibition.

2. ICE

2.1. Definition of ICE

ICE or caspase-1 is a member of a large family of intracellular cysteine proteases known as caspases. The term caspase stands for cysteine proteases cutting after aspartic acid [6]. The ICE gene codes for a 45 kDa inactive precursor protein that is constitutively expressed in many cell types. Whereas most caspases appear to be involved in the enzymatic pathways leading to apoptosis, ICE probably plays a lesser role in that function, and its predominant role is in the processing of IL-1 β and IL-18. As with most caspases, the 45 kDa precursor of ICE requires two internal

*Tel.: +1-303-315-3558; fax: +1-303-315-8054.

E-mail address: britta.siegmund@gmx.net (B. Siegmund).

Abbreviations: ICE, interleukin-1 β converting enzyme; Th1/2, T helper cell type 1/2; IL, interleukin; IBD, inflammatory bowel disease; IFN γ , interferon- γ ; TNF α , tumor necrosis factor- α ; DSS, dextran sulfate sodium; TNBS, trinitrobenzene sulfonic acid; IL-18BP, IL-18 binding protein; and hIL-18BP α , human IL-18BP isoform α .

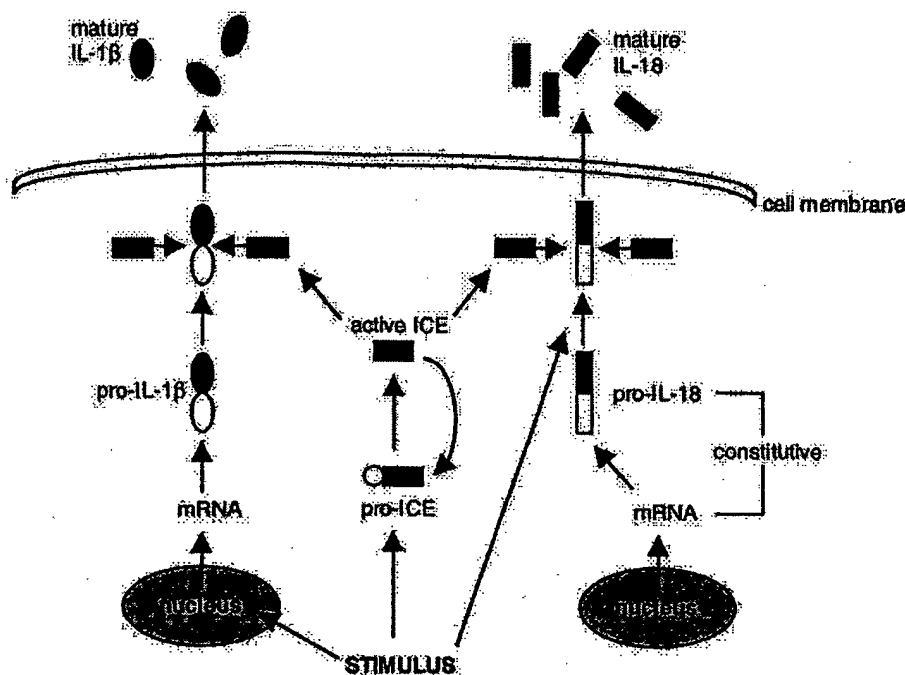


Fig. 1. Synthesis, ICE processing, and secretion of IL-1 β and IL-18. A human monocyte is shown. After cell stimulation, mRNA for pro-IL-1 β is induced and enters the cytosol. Pro-ICE is cleaved into active ICE by members of the caspase family including ICE itself. Pro-IL-1 β is found diffusely in the cytosol and is cleaved by active ICE into mature IL-1 β , which is secreted from the cell. Pro-IL-18 is expressed constitutively, as is the IL-18 mRNA. After stimulation of the monocyte, pro-IL-18 is cleaved by activated ICE and released.

cleavages before being enzymatically active as a heterodimer comprised of a 10 and 20 kDa chain. ICE itself contributes to autoprocessing of the ICE precursor by undergoing oligomerization with itself or other members of the caspase family, such as caspase-3 [7,8]. Each caspase appears to have limited substrate specificity: pro-IL-1 β and pro-IL-18 have been identified as substrates for ICE. The activation of ICE and the subsequent activation of IL-1 β and IL-18 are illustrated in Fig. 1 and will be discussed in more detail below.

2.2. Regulation of ICE

Activation of ICE is often associated with generalized cell activation and IL-1 β and IL-18 production. Although endotoxin activates ICE as well as the synthesis of IL-1 β , endogenous cytokines also possess this dual property. For example, the CD40 ligand, a member of the TNF α superfamily of ligands, activates ICE and leads to secretion of IL-1 β from human endothelial and smooth muscle cells [9]. IFN γ also induces ICE expression, but not activation, in macrophages [10]. Not surprisingly, there is evidence that the regulation of ICE activity is affected by intracellular inhibitors. One such inhibitor is the serine proteinase inhibitor 9, which reduces ICE activity in cultured human smooth muscle cells [11]. Nitric oxide is a potent inhibitor of caspase activity through a mechanism that involves S-nitrosylation [12,13]. Accordingly, nitric oxide prevents the release of both IL-1 β and IL-18 in the extracellular space [14].

2.3. Blockade of ICE in disease

The role of ICE has been characterized in several models of *in vivo* inflammation. ICE-deficient mice are resistant to lethal endotoxemia, but this is due to a failure to process pro-IL-18 and induce IFN γ rather than to inhibition of IL-1 β [15,16]. In different models of acute pancreatitis, inhibition of ICE by the administration of an irreversible ICE inhibitor was shown to be protective [17,18]. Moreover, ICE knockout mice were found not to develop acute pancreatitis despite induction [19]. In addition, administration of an irreversible ICE inhibitor resulted in reduced inflammation in the mouse model of collagen-induced arthritis [20]. Furthermore, in melanoma studies, the number of hepatic metastases after intrasplenically injected mouse B16 melanoma cells was 84–95% lower in ICE knockout than in wild-type mice [21].

2.4. ICE in infectious intestinal inflammation

Three examples in the recent literature provide evidence that infection with distinct microorganisms and concurrent intestinal inflammation strongly depend on ICE activity. Enterobacteria of the genus *Shigella* are the causative agents of bacillary dysentery, manifested by painful abdominal cramps, fever, and characteristic blood and mucus in the stools [22]. Resident macrophages infected with *Shigella flexneri* undergo apoptosis [23,24] and release IL-1 β , thereby initiating an inflammatory cascade [25–27]. Apoptosis induction as well as IL-1 β maturation can be prevented by ICE inhibitors [28].

The protozoan parasite *Entamoeba histolytica*, which causes amoebic dysentery and amoebic liver abscesses, is one of the leading causes of death from parasitic diseases worldwide [29]. Intestinal inflammation and ulceration are the hallmarks of amoebic dysentery [30–32]. Amoebic cysteine proteases are mandatory as virulent factors, as cysteine proteinase-deficient amoeba failed to induce intestinal epithelial cell production of IL-1 β and IL-18, accompanied by significantly reduced gut inflammation and damage to the intestinal permeability barrier [33].

Salmonella typhimurium invades host macrophages and can either induce rapid cell death or establish an intracellular niche within the phagocytic vacuole [34]. SipB, a protein translocated by *Salmonella* into the cytoplasm of macrophages, is required for the activation of ICE [35]. ICE knockout mice have an oral *Salmonella typhimurium* LD₅₀ that is 100-fold higher than that of wild-type mice, accompanied by a decrease in apoptotic cells and decreased *Salmonella* dissemination [36,37]. These three examples point out that the activation of ICE and the subsequent release of IL-1 β and IL-18 play a significant role in intestinal inflammation during infection.

2.5. ICE in IBD

A study on ICE in the context of IBD by McAlindon and colleagues [10] led to an important observation. Exposure of normal colonic macrophages to lipopolysaccharide induced only the production of the precursor of IL-1 β , because the cells failed to activate ICE. In contrast, colonic macrophages from patients with IBD were able to activate ICE and hence release mature IL-1 β in a manner similar to circulating monocytes. This is consistent with recent recruitment of IBD macrophages from the circulating monocyte population. Recent studies from our group examined the acute and chronic model of DSS-induced colitis in ICE knockout mice [38]. In particular, during chronic administration of DSS over 4 weeks, ICE knockout mice presented with an almost complete absence of colitis. This significant amelioration was accompanied by reduced cell activation in the draining mesenteric lymph nodes and a significant reduction of the pro-inflammatory cytokines IL-18, IFN γ , and IL-1 β in the colon.

Several ICE inhibitors are available for experimental use *in vivo* or *in vitro*. Pralnacasan, an orally active inhibitor of human ICE, has been administered to healthy volunteers in phase I trials. The phase I and phase II clinical programs have confirmed that pralnacasan is well absorbed from oral solutions and tablet formulations and achieves plasma levels sufficient to inhibit production of IL-1 β in an *ex vivo* assay. The preliminary safety profile from these studies in healthy volunteers and rheumatoid arthritis patients is excellent. Pralnacasan is currently in phase II trials in rheumatoid arthritis. No toxic side-effects have been observed [39]. Pralnacasan has also been adminis-

tered to mice during acute DSS-induced colitis, resulting in significant amelioration of disease activity [40].

3. Possible mechanisms for the protective role of ICE inhibition in IBD

3.1. Biological activities of IL-1 β and IL-18

Monocytes/macrophages are the best studied source of IL-18 [41]. Most of the information on the production of IL-18 is derived from mice preconditioned with *Propionibacterium acnes* and subsequently challenged with lipopolysaccharide, the original model used to isolate and clone this cytokine [42]. In this particular model, Kupffer cells in the liver are the major producers of IL-18 [42,43]. Differently from what was previously observed for IL-1 β [44,45], constitutive gene expression for IL-18 is present in unstimulated, freshly isolated human peripheral blood mononuclear cells as well as murine splenocytes [46] (see also Fig. 1). Constitutive expression of IL-18 mRNA has been observed in many hematopoietic cell lines [47]. The structure of the promoter region of the *IL-18* gene provides insight into these observations. The promoter for *IL-18* does not contain a TATA box, and promoter activity upstream of exon 2 acts constitutively [48]. The additional finding that the 3' untranslated region of human *IL-18* lacks the AUUUA destabilization sequence is also consistent with these observations [48].

IL-18 acts via an IL-18 receptor complex. The IL-18 receptor complex consists of two non-identical chains: a ligand binding chain termed IL-18 α and a non-ligand binding chain termed IL-18 β [49–51]. IL-18 does not directly induce IFN γ and other Th1 cytokines [52], but acts together with IL-2 or IL-12 as a costimulant. The synergism between IL-12 and IL-18 and the subsequent effects on the immune system are illustrated in Fig. 2.

IL-1 β is not constitutively expressed in healthy subjects [53,54]. Intracellularly, IL-1 β is found diffusely in the cytosol rather than localized in the endoplasmic reticulum or Golgi structures [55,56] (Fig. 1). Nearly all microbes and microbial products induce production of IL-1 β , but stimulants of nonmicrobial origin can also stimulate transcription [57]. Stimuli such as complement factor 5a, hypoxia, adherence to surfaces, and clotting blood induce the synthesis of large amounts of IL-1 β mRNA in monocytic cells without significant translation into IL-1 β protein. A second stimulus, such as pro-inflammatory cytokines including IL-1 β itself, activates translational mechanisms resulting in translation of the IL-1 β mRNA. A review on the biological actions of IL-1 β can be found in Ref. [57].

3.2. Cleavage of IL-1 β and IL-18 by ICE

Posttranslational, enzymatic processing is a critical step in the modulation of the activity of several cytokines. The

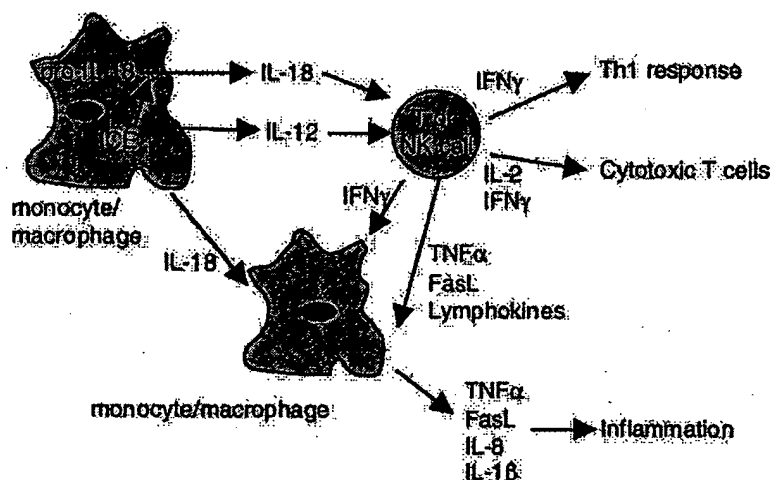


Fig. 2. Biological activities of IL-18 and cell activation. Starting at the upper left, monocytic/macrophagic cells use ICE to cleave inactive pro-IL-18 into active IL-18, which is then secreted from the cell. The same cells also release IL-12 by an ICE-independent mechanism. The combination of IL-18 and IL-12 causes T lymphocytes and natural killer (NK) cells to produce IFN γ , which (a) acts on macrophages to increase ICE expression and further activates the macrophage, and (b) activates CD4 $^{+}$ T lymphocytes as part of the Th1 response. The IL-18/IL-12-stimulated T cell or NK cell releases several lymphokines, TNF α , and/or Fas ligand (FasL). In turn, these cytokines stimulate macrophages to release TNF α , FasL, IL-8, and IL-1 β , which result in increased inflammation. The IL-18/IL-12-stimulated T lymphocyte or NK cell also releases IFN γ and IL-2, which result in the generation of cytotoxic T cells.

genes for some cytokines do not encode for a typical signal sequence common to the vast number of secretory, structural, and membrane-bound proteins. IL-1 β and IL-18 are examples of cytokines lacking a leader peptide [7,57,58]. These cytokines gain access to the extracellular environment via secretory mechanisms that are linked to their processing. The relationship between the unprocessed IL-1 β and IL-18 and the mature form of both cytokines is essential to identify the pleiotropic functions of these molecules. Both pro-IL-1 β and pro-IL-18 are biologically inactive [57].

Following synthesis, pro-IL-1 β remains primarily cytosolic until it is cleaved and transported out of the cell (Fig. 1). Release of mature IL-1 β is often linked to the cleavage at the aspartic acid–alanine (amino acid 116–117) site by ICE [59]. If pro-IL-1 β is released into the extracellular space, for example, following cell death or necrosis, there are several extracellular proteases that can cleave pro-IL-1 β into an active cytokine [60–63].

3.3. IL-1 β and intestinal inflammation

The role of IL-1 β in intestinal inflammation depends upon both the up-regulation of IL-1 β production and the level of its naturally occurring inhibitor, the IL-1 receptor antagonist (IL-1Ra). Indeed, there is evidence that the balance of IL-1 and IL-1Ra may affect disease outcome. For example, mice deficient in IL-1Ra develop spontaneous rheumatoid arthritis and lethal arteritis [64,65]. Administration of IL-1Ra reduces disease severity in several models of intestinal inflammation [57], including decreased immune complex-induced colitis severity in rabbits [66]. A review of the role of IL-1 β in intestinal inflammation has been provided in Ref. [67].

3.4. IL-18 and intestinal inflammation

Several studies provide strong direct and indirect evidence for a significant role of IL-18 in intestinal inflammation. Nakamura and colleagues confirmed *in vivo* the synergistic effect of IL-12 and IL-18, originally described *in vitro* [68], by concomitant injection of both cytokines or either one alone [69]. While mice injected with IL-18 alone did not present with macroscopic changes, IL-12-injected mice showed significant weight loss and colitis. However, the combined administration of both cytokines resulted in severe colitis and high mortality. Chikano and colleagues [70] confirmed this *in vivo* synergism and showed, in addition, that the intestinal inflammation occurs in an IFN γ -dependent but TNF α -, NO- and Fas ligand-independent manner. Consistent with an increased Th1 response in Crohn's disease, several groups could independently demonstrate a significant up-regulation of IL-18 expression in the inflamed lesions of the intestine, mostly localized to macrophages and epithelial cells [71,72]. Interestingly, no increase in IL-18 expression could be observed in inflamed lesions from patients with ulcerative colitis, which is partly characterized by an increase of Th2 cytokines [72]. While increased IL-18 expression is providing first evidence for a possible role in disease, in order to prove that IL-18 participates in the inflammatory process of intestinal inflammation it has to be demonstrated that blockade of IL-18 results in amelioration of disease severity.

In the recent literature, four studies using different animal models of colitis and different ways of IL-18 blockade approach this question. An overview is provided in Table 1, and the studies are summarized in the subsequent paragraphs. Our group examined the role of IL-18

Table 1

Blockade of IL-18 in experimental colitis in mice

| Animal model of colitis | IL-18 blocking strategy | Study results | References |
|--|--|---|------------|
| Dextran sulfate sodium | Anti-IL-18 antiserum | <ul style="list-style-type: none"> IL-18 expression localized to intestinal epithelial cells Colitis aggravation accompanied by IL-18 increase Histological amelioration of colitis by anti-IL-18 treatment Significant decrease in IFNγ, IL-18, and TNFα in the colon after anti-IL-18 treatment | [73] |
| Trinitrobenzene sulfonic acid | Anti-IL-18 antibody | <ul style="list-style-type: none"> IL-18 expression localized to macrophages Anti-Mac1-saporin antibody as well as neutralizing antibody against IL-18 resulted in a dramatic histological attenuation of colitis TNBS cannot induce significant colitis in the IL-18 knockout mice Reduction in IFNγ in IL-18 knockout, anti-IL-18 or anti-Mac1-saporin-treated mice | [77] |
| Trinitrobenzene sulfonic acid | IL-18 binding protein | <ul style="list-style-type: none"> Significantly less histological signs of inflammation after hIL-18BPα treatment Significant reduction in TNFα, IL-1β, and IL-6, but no decrease in IFNγ, IL-10, and IL-4 in colon homogenates | [78] |
| CD62L ⁺ CD4 ⁺ transfer model | Local administration of adenovirus expressing IL-18 antisense mRNA | <ul style="list-style-type: none"> IL-18 expression localized to intestinal epithelial and some mononuclear cells in the lamina propria Significant decrease in inflammation after treatment, as evaluated histologically and endoscopically Attenuation of IL-18 synthesis in lamina propria mononuclear cells after treatment | [81] |

blockade in the model of DSS-induced colitis [73]. In this model, colitis is induced chemically and is associated with the up-regulation of pro-inflammatory cytokines [74]. Colitis can be induced in *severe combined immunodeficiency* mice by DSS administration and hence is not T cell-dependent [75]. However, during the course of DSS-induced colitis, T cells become activated at the inflammation site and participate in the inflammatory process [76]. In this model, an anti-IL-18 antiserum was administered to achieve IL-18 blockade. IL-18 expression could be localized to the epithelial cells and was reduced significantly in anti-IL-18-treated mice. Blockade of IL-18 was accompanied by a significant reduction in the release of other pro-inflammatory cytokines. In addition, histological signs of inflammation were decreased significantly by blockade with anti-IL-18.

Kanai and colleagues [77] investigated the model of TNBS-induced colitis and focused in particular on the role of IL-18 produced by macrophages. It is hypothesized that the ethanol used as a vehicle in the rectal administration of TNBS disrupts the mucosal epithelial barrier, enabling this hapten to bind covalently to proteins of colonic epithelial cells and modify cell surface proteins. Fragments of these altered cells can be taken up by macrophages and dendritic cells for presentation to T cells as antigens, resulting in a Th1-dominated colitis. Earlier studies showed that administration of neutralizing IL-12 antibodies and thereby blockade of the Th1 pathway is protective [3]. In mice treated with an anti-IL-18 antibody as well as in IL-18 knockout mice, TNBS was unable to induce significant colitis. An increase in IL-18 synthesis in this model could be localized to the macrophages. In fact, administration of an antibody conjugated to the ribosome-inactivating

protein saporin directed against macrophages also resulted in protection against TNBS-induced colitis.

Ten Hove and colleagues [78] also examined the model of TNBS-induced colitis; however, they applied a different strategy to neutralize IL-18. In this study, IL-18BP, a naturally occurring IL-18 antagonist, was administered [79]. The human IL-18BP gene encodes for four different isoforms (a–d) generated by alternative mRNA splicing [80]. These isoforms vary in their ability to bind IL-18; only human IL-18BP isoform a (hIL-18BP α) and isoform c have a neutralizing ability, and recombinant hIL-18BP α neutralizes murine IL-18. In this study, mice were treated with recombinant hIL-18BP α during the course of TNBS-induced colitis. Blockade of IL-18 by the recombinant hIL-18BP α resulted in a reduced clinical score accompanied by reduction of TNF α , IL-6, and IL-1 β in the colon homogenate, while IFN γ , IL-10, and IL-4 remained unchanged.

Finally, Wirtz and colleagues [81] neutralized IL-18 by local administration of an adenovirus expressing IL-18 antisense mRNA in the T cell-dependent transfer model of colitis. This model is based on the transfer of CD62L⁺ CD4⁺ T cells in *severe combined immunodeficiency* mice resulting, after 6–12 weeks, in chronic colitis, which is histologically similar to Crohn's disease in humans [82]. In this study, a significant reduction in IL-18 by adenovirus infected mice expressing IL-18 antisense mRNA was accompanied by a decrease in endoscopically and histologically evaluated inflammation as well as in IFN γ production.

Interestingly, when comparing these four studies, the IL-18 knockout mice as well as the administration of the neutralizing antibody, the antiserum, or the adenovirus expressing IL-18 antisense mRNA seem to result in a more

dramatic amelioration than the administration of recombinant hIL-18BP. In particular, in the *IL-18* knockout mice, as well as in the studies with the neutralizing anti-IL-18 antibody/antiserum or after local administration of the adenovirus expressing IL-18 antisense mRNA, a significant reduction in colonic IFN γ concentrations was observed. However, no suppression could be measured in mice after recombinant hIL-18BP treatment [73,77,78,81]. These differences are of significance and may point out that, although in theory all strategies described aim at the neutralization of IL-18, the IL-18BP might exert additional biological functions that are currently unknown and require further investigations in the future.

The pathogenesis of inflammatory bowel diseases remains elusive. However, results from these experimental models, in combination with the descriptive data from patients with Crohn's disease, suggest an important function of IL-18.

4. Conclusions

The studies in the chronic and acute DSS model suggest that the ICE may contribute to IBD. However, further investigations on the effect of ICE inhibitors in other animal models of experimental colitis are necessary to evaluate whether a similar efficacy can be achieved when compared with the results obtained from single IL-18 or IL-1 β blockade. In addition, an IL-1 β - and IL-18-independent, yet unknown, mechanism might contribute to the anti-inflammatory function of ICE blockade. Compared to currently used strategies to suppress specific cytokines, which mostly implicate antibody therapy, the possibility of having an orally available drug whose half-life can be easily controlled is highly intriguing.

Acknowledgments

Supported by a grant from the Deutsche Forschungsgemeinschaft (DFG Si 749/2-1). I wish to thank Drs. Giamila Fantuzzi and Charles Dinarello for their support and critical review of the manuscript.

References

- [1] Fiocchi C. Inflammatory bowel disease: etiology and pathogenesis. *Gastroenterology* 1998;115:182–205.
- [2] Sandborn WJ, Hanauer SB. Antitumor necrosis factor therapy for inflammatory bowel disease: a review of agents, pharmacology, clinical results, and safety. *Inflamm Bowel Dis* 1999;5:119–33.
- [3] Neurath MF, Fuss I, Kelsall BL, Stuber E, Strober W. Antibodies to interleukin 12 abrogate established experimental colitis in mice. *J Exp Med* 1995;182:1281–90.
- [4] Simpson SJ, Shah S, Comiskey M, de Jong YP, Wang B, Mizoguchi E, Bhan AK, Terhorst C. T cell-mediated pathology in two models of experimental colitis depends predominantly on the interleukin 12/signal transducer and activator of transcription (Stat)-4 pathway, but is not conditional on interferon γ expression by T cells. *J Exp Med* 1998;187:1225–34.
- [5] Fantuzzi G, Dinarello CA. Interleukin-18 and interleukin-1 β : two cytokine substrates for ICE (caspase-1). *J Clin Immunol* 1999;19:1–11.
- [6] Alnemri ES, Livingston DJ, Nicholson DW, Salvesen G, Thornberry NA, Wong WW, Yuan J. Human ICE/CED-3 protease nomenclature. *Cell* 1996;87:171.
- [7] Gu Y, Kuida K, Tsutsui H, Ku G, Hsiao K, Fleming MA, Hayashi N, Higashino K, Okamura H, Nakanishi K, Kurimoto M, Tanimoto T, Flavell RA, Sato V, Harding MW, Livingston DJ, Su MS-S. Activation of interferon- γ inducing factor mediated by interleukin-1 β converting enzyme. *Science* 1997;275:206–9.
- [8] Wilson KP, Black J-AF, Thomson JA, Kim EE, Griffith JP, Navia MA, Murcko MA, Chambers SP, Aldape RA, Raybuck SA, Livingston DJ. Structure and mechanism of interleukin-1 β converting enzyme. *Nature* 1994;370:270–5.
- [9] Schönbeck U, Mach F, Bonnefoy J-Y, Loppnow H, Flad H-D, Libby P. Ligation of CD40 activates interleukin 1 β -converting enzyme (caspase-1) activity in vascular smooth muscle and endothelial cells and promotes elaboration of active interleukin 1 β . *J Biol Chem* 1997;272:19569–74.
- [10] McAlindon ME, Hawkey CJ, Mahida YR. Expression of interleukin 1 β and interleukin 1 β converting enzyme by intestinal macrophages in health and inflammatory bowel disease. *Gut* 1998;42:214–9.
- [11] Young JL, Sukhova GK, Foster D, Kiesel W, Libby P, Schonbeck U. The serpin proteinase inhibitor 9 is an endogenous inhibitor of interleukin 1 β -converting enzyme (caspase-1) activity in human vascular smooth muscle cells. *J Exp Med* 2000;191:1535–44.
- [12] Dimmeler S, Haendeler J, Nehls M, Zeiher AM. Suppression of apoptosis by nitric oxide via inhibition of interleukin-1 β -converting enzyme (ICE)-like and cysteine protease protein (CPP)-32-like proteases. *J Exp Med* 1997;185:601–7.
- [13] Li J, Billiar TR, Talanian RV, Kim YM. Nitric oxide reversibly inhibits seven members of the caspase family via S-nitrosylation. *Biochem Biophys Res Commun* 1997;240:419–24.
- [14] Kim Y-M, Talanian RV, Li J, Billiar TR. Nitric oxide prevents IL-1 β and IFN- γ -inducing factor (IL-18) release from macrophages by inhibiting caspase-1 (IL-1 β -converting enzyme). *J Immunol* 1998;161:4122–8.
- [15] Fantuzzi G, Puren AJ, Harding MW, Livingston DJ, Dinarello CA. Interleukin-18 regulation of interferon γ production and cell proliferation as shown in interleukin-1 β -converting enzyme (caspase-1)-deficient mice. *Blood* 1998;91:2118–25.
- [16] Netea MG, Fantuzzi G, Kullberg BJ, Stuyt RJL, Pulido EJ, McIntyre Jr RC, Joosten LAB, Van der Meer JWM, Dinarello CA. Neutralization of IL-18 reduces neutrophil tissue accumulation and protects mice against lethal *Escherichia coli* and *Salmonella typhimurium* endotoxemia. *J Immunol* 2000;164:2644–9.
- [17] Norman J, Yang J, Fink G, Carter G, Ku G, Denham W, Livingston D. Severity and mortality of experimental pancreatitis are dependent on interleukin-1 converting enzyme (ICE). *J Interferon Cytokine Res* 1997;17:113–8.
- [18] Rau B, Paszkowski A, Lillich S, Baumgart K, Möller P, Beger HG. Differential effects of caspase-1/interleukin-1 β -converting enzyme on acinar cell necrosis and apoptosis in severe acute experimental pancreatitis. *Lab Invest* 2001;81:1001–13.
- [19] Paszkowski AS, Rau B, Mayer JM, Möller P, Beger HG. Therapeutic application of caspase 1/interleukin-1 β -converting enzyme inhibitor decreases the death rate in severe acute experimental pancreatitis. *Ann Surg* 2002;235:68–76.
- [20] Ku G, Ford P, Raybuck SA, Harding MW, Randle JCR. Selective interleukin-1 converting enzyme (ICE/Caspase-1) inhibition with pralnacasan (HMR3480/VX-740) reduces inflammation and joint destruction in murine type II collagen-induced arthritis (CIA). *Arthritis Rheum* 2001;44:S241.

- [21] Vidal-Vanaclocha F, Fantuzzi G, Mendoza L, Fuentes AM, Anasagasti MJ, Martin J, Carrascal T, Walsh P, Reznikov LL, Kim S-H, Novick D, Rubinstein M, Dinarello CA. IL-18 regulates IL-1 β -dependent hepatic melanoma metastasis via vascular cell adhesion molecule-1. *Proc Natl Acad Sci USA* 2000;97:734–9.
- [22] Mathan MM, Mathan VI. Morphology of rectal mucosa of patients with shigellosis. *Rev Infect Dis* 1991;13(Suppl 4):S314–8.
- [23] Islam D, Veress B, Bardhan PK, Lindberg AA, Christensson B. In situ characterization of inflammatory responses in the rectal mucosae of patients with shigellosis. *Infect Immun* 1997;65:739–49.
- [24] Zychlinsky A, Prevost MC, Sansonetti PJ. *Shigella flexneri* induces apoptosis in infected macrophages. *Nature* 1992;358:167–9.
- [25] Sansonetti PJ, Arondel J, Cavaillon J-M, Huerre M. Role of interleukin-1 in the pathogenesis of experimental shigellosis. *J Clin Invest* 1995;96:884–92.
- [26] Zychlinsky A, Fitting C, Cavaillon J-M, Sansonetti PJ. Interleukin 1 is released by murine macrophages during apoptosis induced by *Shigella flexneri*. *J Clin Invest* 1994;94:1328–32.
- [27] Zychlinsky A, Thirumalai K, Arondel J, Cantey JR, Aliprantis AO, Sansonetti PJ. In vivo apoptosis in *Shigella flexneri* infections. *Infect Immun* 1996;64:5357–65.
- [28] Hilbi H, Chen Y, Thirumalai K, Zychlinsky A. The interleukin 1 β -converting enzyme, caspase 1, is activated during *Shigella flexneri*-induced apoptosis in human monocyte-derived macrophages. *Infect Immun* 1997;65:5165–70.
- [29] Walsh JA. Problems in recognition and diagnosis of amebiasis: estimation of the global magnitude of morbidity and mortality. *Rev Infect Dis* 1986;8:228–38.
- [30] Kanani SR, Knight R. Relapsing amoebic colitis of 12 year's standing exacerbated by corticosteroids. *Br Med J* 1969;2:613–4.
- [31] Li E, Stanley Jr SL. Protozoa. Amebiasis. *Gastroenterol Clin North Am* 1996;25:471–92.
- [32] Tucker PC, Webster PD, Kilpatrick ZM. Amebic colitis mistaken for inflammatory bowel disease. *Arch Intern Med* 1975;135:681–5.
- [33] Zhang Z, Yan L, Wang L, Seydel KB, Li E, Ankri S, Mirelman D, Stanley Jr SL. *Entamoeba histolytica* cysteine proteinases with interleukin-1 beta converting enzyme (ICE) activity cause intestinal inflammation and tissue damage in amebiasis. *Mol Microbiol* 2000;37:542–8.
- [34] Darwin KH, Miller VL. Molecular basis of the interaction of *Salmonella* with the intestinal mucosa. *Clin Microbiol Rev* 1999;12:405–28.
- [35] Monack DM, Detweiler CS, Falkow S. Salmonella pathogenicity island 2-dependent macrophage death is mediated in part by the host cysteine protease caspase-1. *Cell Microbiol* 2001;3:825–37.
- [36] Monack DM, Hersh D, Ghori N, Bouley D, Zychlinsky A, Falkow S. Salmonella exploits caspase-1 to colonize Peyer's patches in a murine typhoid model. *J Exp Med* 2000;192:249–58.
- [37] Monack DM, Navarre WW, Falkow S. Salmonella-induced macrophage death: the role of caspase-1 in death and inflammation. *Microbes Infect* 2001;3:1201–12.
- [38] Siegmund B, Lehr H-A, Fantuzzi G, Dinarello CA. IL-1 β -converting enzyme (caspase-1) in intestinal inflammation. *Proc Natl Acad Sci USA* 2001;98:13249–54.
- [39] Randle JC, Harding MW, Ku G, Schönharting M, Kurrle R. ICE/Caspase-1 inhibitors as novel anti-inflammatory drugs. *Expert Opin Investig Drugs* 2001;10:1207–9.
- [40] Bauer C, Loher F, Schmall K, Hallwachs R, Loehr C, Siegmund B, Daur M, Lehr HA, Schönharting M, Endres S, Eigler A. In vivo efficacy of the IL-1 β converting enzyme inhibitor pralnacasan in DSS-induced murine colitis. *Gastroenterology* 2002;122(Suppl. 1):T971.
- [41] Dinarello CA. IL-18: a TH1-inducing, proinflammatory cytokine and new member of the IL-1 family. *J Allergy Clin Immunol* 1999;103:11–24.
- [42] Okamura H, Tsutsi H, Komatsu T, Yutsudo M, Hakura A, Tanimoto T, Torigoe K, Okura T, Nukada Y, Hattori K, Akita K, Namba M, Tanabe F, Konishi K, Fukuda S, Kurimoto M. Cloning of a new cytokine that induces IFN- γ production by T cells. *Nature* 1995;378:88–91.
- [43] Tsutsui H, Nakanishi K, Matsui K, Higashino K, Okamura H, Miyazawa Y, Kaneda K. IFN- γ -inducing factor up-regulates Fas ligand-mediated cytotoxic activity of murine natural killer cell clones. *J Immunol* 1996;157:3967–73.
- [44] Mileno MD, Margolis NH, Clark BD, Dinarello CA, Burke JF, Gelfand JA. Coagulation of whole blood stimulates interleukin-1 β gene expression. *J Infect Dis* 1995;172:308–11.
- [45] Shapiro L, Dinarello CA. Hyperosmotic stress as a stimulant for proinflammatory cytokine production. *Exp Cell Res* 1997;231:354–62.
- [46] Puren AJ, Fantuzzi G, Dinarello CA. Gene expression, synthesis, and secretion of interleukin 18 and interleukin 1 β are differentially regulated in human blood mononuclear cells and mouse spleen cells. *Proc Natl Acad Sci USA* 1999;96:2256–61.
- [47] Akita K, Ohtsuki T, Nukada Y, Tanimoto T, Namba M, Okura T, Takakura-Yamamoto R, Torigoe K, Gu Y, Su MS, Fujii M, Satoh-Itoh M, Yamamoto K, Kohno K, Ikeda M, Kurimoto M. Involvement of caspase-1 and caspase-3 in the production and processing of mature human interleukin 18 in monocytic THP.1 cells. *J Biol Chem* 1997;272:26595–603.
- [48] Tone M, Thompson SAJ, Tone Y, Fairchild PJ, Waldmann H. Regulation of IL-18 (IFN- γ -inducing factor) gene expression. *J Immunol* 1997;159:6156–63.
- [49] Born TL, Thomassen E, Bird TA, Sims JE. Cloning of a novel receptor subunit, AcPL, required for interleukin-18 signaling. *J Biol Chem* 1998;273:29445–50.
- [50] Parnet P, Garka KE, Bonnett TP, Dower SK, Sims JE. IL-1Rrp is a novel receptor-like molecule similar to the type I interleukin-1 receptor and its homologues T1/ST2 and IL-1R AcP. *J Biol Chem* 1996;271:3967–70.
- [51] Torigoe K, Ushio S, Okura T, Kobayashi S, Taniai M, Kunikata T, Murakami T, Sanou O, Kojima H, Fujii M, Ohta T, Ikeda M, Ikegami H, Kurimoto M. Purification and characterization of the human interleukin-18 receptor. *J Biol Chem* 1997;272:25737–42.
- [52] Ushio S, Namba M, Okura T, Hattori K, Nukada Y, Akita K, Tanabe F, Konishi K, Micallef M, Fujii M, Torigoe K, Tanimoto T, Fukuda S, Ikeda M, Okamura H, Kurimoto M. Cloning of the cDNA for human IFN- γ -inducing factor, expression in *Escherichia coli*, and studies on the biologic activities of the protein. *J Immunol* 1996;156:4274–9.
- [53] Fenton MJ, Clark BD, Collins KL, Webb AC, Rich A, Auron PE. Transcriptional regulation of the human prointerleukin 1 β gene. *J Immunol* 1987;138:3972–9.
- [54] Fenton MJ, Vermeulen MW, Clark BD, Webb AC, Auron PE. Human pro-IL-1 β gene expression in monocytic cells is regulated by two distinct pathways. *J Immunol* 1988;140:2267–73.
- [55] Rubartelli A, Cozzolino F, Talio M, Sitia R. A novel secretory pathway for interleukin-1 β , a protein lacking a signal sequence. *EMBO J* 1990;9:1503–10.
- [56] Stevenson FT, Torrano F, Locksley RM, Lovett DH. Interleukin 1: the patterns of translation and intracellular distribution support alternative secretory mechanisms. *J Cell Physiol* 1992;152:223–31.
- [57] Dinarello CA. Biologic basis for interleukin-1 in disease. *Blood* 1996;87:2095–147.
- [58] Zhang Y, Center DM, Wu DM, Cruikshank WW, Yuan J, Andrews DW, Kornfeld H. Processing and activation of pro-interleukin-16 by caspase-3. *J Biol Chem* 1998;273:1144–9.
- [59] Black RA, Kronheim SR, Cantrell M, Deeley MC, March CJ, Prickett KS, Wignall J, Conlon PJ, Cosman D, Hopp TP, Mochizuki DY. Generation of biologically active interleukin-1 β by proteolytic cleavage of the inactive precursor. *J Biol Chem* 1988;263:9437–42.
- [60] Coeshott C, Ohnemus C, Pilyavskaya A, Ross S, Wiczorek M, Kroona H, Leimer AH, Cheronis J. Converting enzyme-independent release of tumor necrosis factor α and IL-1 β from a stimulated human monocytic cell line in the presence of activated neutrophils or purified proteinase 3. *Proc Natl Acad Sci USA* 1999;96:6261–6.
- [61] Dinarello CA, Cannon JG, Mier JW, Bernheim HA, LoPreste G, Lynn DL, Love RN, Webb AC, Auron PE, Reuben RC, Rich A, Wolff SM,

- Putney SD. Multiple biological activities of human recombinant interleukin 1. *J Clin Invest* 1986;77:1734–9.
- [62] Mizutani H, Black R, Kupper TS. Human keratinocytes produce but do not process pro-interleukin-1 (IL-1) beta. Different strategies of IL-1 production and processing in monocytes and keratinocytes. *J Clin Invest* 1991;87:1066–71.
- [63] Mizutani H, Schechter N, Lazarus G, Black RA, Kupper TS. Rapid and specific conversion of precursor interleukin 1 β (IL-1 β) to an active IL-1 species by human mast cell chymase. *J Exp Med* 1991;174:821–5.
- [64] Horai R, Saijo S, Tanioka H, Nakae S, Sudo K, Okahara A, Ikuse T, Asano M, Iwakura Y. Development of chronic inflammatory arthropathy resembling rheumatoid arthritis in interleukin 1 receptor antagonist-deficient mice. *J Exp Med* 2000;191:313–20.
- [65] Nicklin MJ, Hughes DE, Barton JL, Ure JM, Duff GW. Arterial inflammation in mice lacking the interleukin 1 receptor antagonist gene. *J Exp Med* 2000;191:303–12.
- [66] Cominelli F, Nast CC, Duchini A, Lee M. Recombinant interleukin-1 receptor antagonist blocks the proinflammatory activity of endogenous interleukin-1 in rabbit immune colitis. *Gastroenterology* 1992;103:65–71.
- [67] Cominelli F, Pizarro TT. Interleukin-1 and interleukin-1 receptor antagonist in inflammatory bowel disease. *Aliment Pharmacol Ther* 1996;10:49–53.
- [68] Barbulescu K, Becker C, Schlaak JF, Schmitt E, Meyer zum Büschenfelde K-H, Neurath MF. Cutting edge: IL-12 and IL-18 differentially regulate the transcriptional activity of the human IFN- γ promoter in primary CD4 $^{+}$ T lymphocytes. *J Immunol* 1998;160:3642–7.
- [69] Nakamura S, Otani T, Ijiri Y, Motoda R, Kurimoto M, Orita K. IFN- γ -dependent and -independent mechanisms in adverse effects caused by concomitant administration of IL-18 and IL-12. *J Immunol* 2000;164:3330–6.
- [70] Chikano S, Sawada K, Shimoyama T, Kashiwamura S-I, Sugihara A, Sekikawa K, Terada N, Nakanishi K, Okamura H. IL-18 and IL-12 induce intestinal inflammation and fatty liver in mice in an IFN- γ dependent manner. *Gut* 2000;47:779–86.
- [71] Monteleone G, Trapasso F, Parrello T, Biancone L, Stella A, Iuliano R, Luzzo F, Fusco A, Pallone F. Bioactive IL-18 expression is up-regulated in Crohn's disease. *J Immunol* 1999;163:143–7.
- [72] Pizarro TT, Michie MH, Bentz M, Woraratanadharm J, Smith Jr MF, Foley E, Moskaluk CA, Bickston SJ, Cominelli F. IL-18, a novel immunoregulatory cytokine, is up-regulated in Crohn's disease: expression and localization in intestinal mucosal cells. *J Immunol* 1999;162:6829–35.
- [73] Siegmund B, Fantuzzi G, Rieder F, Gamboni-Robertson F, Lehr H-A, Hartmann G, Dinarello CA, Endres S, Eigler A. Neutralization of interleukin-18 reduces severity in murine colitis and intestinal IFN- γ and TNF- α production. *Am J Physiol Regul Integr Comp Physiol* 2001;281:R1264–73.
- [74] Dieleman LA, Palmen MJ, Akol H, Bloemena E, Pena AS, Meuwissen SG, Van Rees EP. Chronic experimental colitis induced by dextran sulphate sodium (DSS) is characterized by Th1 and Th2 cytokines. *Clin Exp Immunol* 1998;114:385–91.
- [75] Dieleman LA, Ridwan BU, Tennyson GS, Beagley KW, Bucy RP, Elson CO. Dextran sulfate sodium-induced colitis occurs in severe combined immunodeficient mice. *Gastroenterology* 1994;107:1643–52.
- [76] Saubermann LJ, Beck P, De Jong YP, Pitman RS, Ryan MS, Kim HS, Exley M, Snapper S, Balk SP, Hagen SJ, Kanauchi O, Motoki K, Sakai T, Terhorst C, Koezuka Y, Podolsky DK, Blumberg RS. Activation of natural killer T cells by α -galactosylceramide in the presence of CD1d provides protection against colitis in mice. *Gastroenterology* 2000;119:119–28.
- [77] Kanai T, Watanabe M, Okazawa A, Sato T, Yamazaki M, Okamoto S, Ishii H, Totsuka T, Iiyama R, Okamoto R, Ikeda M, Kurimoto M, Takeda K, Akira S, Hibi T. Macrophage-derived IL-18-mediated intestinal inflammation in the murine model of Crohn's disease. *Gastroenterology* 2001;121:875–88.
- [78] Ten Hove T, Corbaz A, Amitai H, Aloni S, Belzer I, Graber P, Drillenburger P, van Deventer SJH, Chvatchko Y, Te Velde AA. Blockade of endogenous IL-18 ameliorates TNBS-induced colitis by decreasing local TNF- α production in mice. *Gastroenterology* 2001;121:1372–9.
- [79] Novick D, Kim SH, Fantuzzi G, Reznikov LL, Dinarello CA, Rubinstein M. Interleukin-18 binding protein: a novel modulator of the Th1 cytokine response. *Immunity* 1999;10:127–36.
- [80] Kim SH, Eisenstein M, Reznikov L, Fantuzzi G, Novick D, Rubinstein M, Dinarello CA. Structural requirements of six naturally occurring isoforms of the IL-18 binding protein to inhibit IL-18. *Proc Natl Acad Sci USA* 2000;97:1190–5.
- [81] Wirtz S, Becker C, Blumberg R, Galle PR, Neurath MF. Treatment of T cell-dependent experimental colitis in SCID mice by local administration of an adenovirus expressing IL-18 antisense mRNA. *J Immunol* 2002;168:411–20.
- [82] Atreya R, Mudter J, Finotto S, Müllberg J, Jostock T, Wirtz S, Schütz M, Bartsch B, Holtmann M, Becker C, Strand D, Czaja J, Schlaak JF, Lehr HA, Autschbach F, Schürmann G, Nishimoto N, Yoshizaki K, Ito H, Kishimoto T, Galle PR, Rose-John S, Neurath MF. Blockade of interleukin 6 *trans* signaling suppresses T-cell resistance against apoptosis in chronic intestinal inflammation: evidence in Crohn disease and experimental colitis in vivo. *Nat Med* 2000;6:583–8.

Inhibition of caspase 1 reduces human myocardial ischemic dysfunction via inhibition of IL-18 and IL-1 β

EXHIBIT

17

Benjamin J. Pomerantz^{*†}, Leonid L. Reznikov[†], Alden H. Harken^{*}, and Charles A. Dinarello^{*†}

Departments of ^{*}Surgery and [†]Medicine, University of Colorado Health Sciences Center, Denver, CO 80262

Contributed by Charles A. Dinarello, December 22, 2000

The proinflammatory cytokine IL-18 was investigated for its role in human myocardial function. An ischemia/reperfusion (I/R) model of suprafused human atrial myocardium was used to assess myocardial contractile force. Addition of IL-18 binding protein (IL-18BP), the constitutive inhibitor of IL-18 activity, to the perfusate during and after I/R resulted in improved contractile function after I/R from 35% of control to 76% with IL-18BP. IL-18BP treatment also preserved intracellular tissue creatine kinase levels (by 420%). Steady-state mRNA levels for IL-18 were elevated after I/R, and the concentration of IL-18 in myocardial homogenates was increased (control, 5.8 pg/mg vs. I/R, 26 pg/mg; $P < 0.01$). Active IL-18 requires cleavage of its precursor form by the IL-1 β -converting enzyme (caspase 1); inhibition of caspase 1 also attenuated the depression in contractile force after I/R (from 35% of control to 75.8% in treated atrial muscle; $P < 0.01$). Because caspase 1 also cleaves the precursor IL-1 β , IL-1 receptor blockade was accomplished by using the IL-1 receptor antagonist. IL-1 receptor antagonist added to the perfusate also resulted in a reduction of ischemia-induced contractile dysfunction. These studies demonstrate that endogenous IL-18 and IL-1 β play a significant role in I/R-induced human myocardial injury and that inhibition of caspase 1 reduces the processing of endogenous precursors of IL-18 and IL-1 β and thereby prevents ischemia-induced myocardial dysfunction.

During ischemia and reperfusion, numerous endogenous mediators, such as small-molecule second messengers, are produced that affect myocardial function. Within minutes of an ischemic episode, myocardial contractile force diminishes, and the overall recovery of contractile force largely depends on the duration of the ischemic period (1). For example, during an ischemic event, Ca²⁺ homeostasis is perturbed, oxygen-derived free radicals are generated, and nitric oxide (NO) synthesis and release takes place. In addition, there is also local production of cytokines, particularly tumor necrosis factor α (TNF- α) and IL-1 β (2). In the intact heart, these cytokines contribute to ischemia-induced myocardial dysfunction by inducing expression of the genes for inducible NO synthase (1), cyclooxygenase 2, and phospholipase A2, as well as vascular adhesion molecules and several chemokines. As a result, there is immediate depression of myocardial contractile force mediated by small-molecule messengers, followed by cytokine-mediated neutrophil infiltration that further damages heart muscle. Animal hearts studied in the absence of blood or blood products elaborate TNF- α (3) and IL-1 β during an ischemic challenge. Cardiomyocytes also lose contractile force because of the action of these endogenous cytokines (4).

Most of the experimental data concerning TNF- α - and IL-1 β -mediated myocardial dysfunction are derived from animal studies. However, human myocardial tissues obtained from patients undergoing elective cardiopulmonary bypass procedures have been studied under controlled *ex vivo* conditions (5, 6). In this experimental model, human atrial trabeculae are suspended in a blood-free physiologically oxygenated buffer bath and then exposed to an episode of simulated ischemia. During

this time, contractile force decreases dramatically; when the tissue is reexposed to oxygen, the contractile force returns but is diminished (60%–70% reduction) and evidence of myocardial damage is observed by release of creatine kinase (CK) (5, 6). When TNF bioactivity is specifically neutralized during ischemia/reperfusion (I/R), a greater return of contractile force is observed, suggesting that endogenous myocardial TNF activity contributes to the contractile dysfunction induced by the ischemic event (7).

In the present study, we asked whether the cytokine IL-18 contributes to human ischemia-induced myocardial dysfunction. IL-18 is a proinflammatory cytokine structurally and functionally related to IL-1 β (8–10). IL-1 β and IL-18 are initially synthesized as inactive precursors requiring the IL-1 β -converting enzyme (ICE or caspase 1) for cleavage to mature biologically active molecules (11, 12). Although IL-1 β and IL-18 have distinct cell surface receptors, the receptor chains for each cytokine are members of the same receptor superfamily (13, 14), and signal transduction is similar (15). For IL-18, however, there is a third receptor-like chain, the IL-18 binding protein (IL-18BP), that has no transmembrane domain (16). IL-18BP is a constitutively produced, secreted, and potent inhibitor of IL-18 activity (16, 17). To assess a role for endogenous IL-18 in the heart, a specific natural inhibitor of IL-18 activity, IL-18BP, was added to the suprafusing bath during I/R.

Materials and Methods

Reagents. IL-18BP α isoform was expressed with a N-terminal (His)₆ tag in Chinese hamster ovary cells and purified to homogeneity (supplied by Interpharm Laboratories, Nes Ziona, Israel). The ability of IL-18BP α -(His)₆ to neutralize IL-18 has been described (17). The IL-1 receptor antagonist (IL-1Ra) was supplied by Amgen Biologicals. The ICE inhibitor (ICEi) Ac-Try-Val-Ala-Asp-chloromethylketone (YVAD) was purchased from Alexis Biochemicals (San Diego) and solubilized in DMSO at 10 mg/ml. The ICEi was diluted in Tyrode's solution before being used. On human peripheral blood mononuclear cells, the ICEi reduces endotoxin-induced secretion of mature IL-1 β by 92%, as measured by ELISA (Cistron Biotechnology, Pine Brook, NJ).

Isolated Atrial Trabeculae. Patients undergoing elective coronary artery bypass surgery with a pump oxygenator require insertion of a canula into the right atrium. At that time, a small segment of the right atrial appendage is routinely excised and discarded. Trabeculae were obtained from this discarded tissue. Human

Abbreviations: I/R, ischemia/reperfusion; CK, creatine kinase; ICE, IL-1 β -converting enzyme; ICEi, ICE inhibitor; IL-18BP, IL-18 binding protein; IL-1Ra, IL-1 receptor antagonist; YVAD, Ac-Try-Val-Ala-Asp-chloromethylketone; TNF, tumor necrosis factor.

[†]To whom reprint requests should be addressed at: University of Colorado Health Sciences Center, 4200 East Ninth Avenue, B168, Denver, CO 80262.

The publication costs of this article were defrayed in part by page charge payment. This article must therefore be hereby marked "advertisement" in accordance with 18 U.S.C. §1734 solely to indicate this fact.

atrial tissue was placed in oxygenated modified Tyrode's buffer solution at 4°C. Modified Tyrode's solution was prepared daily with deionized distilled water and contained D-glucose at 5.0 mmol/liter, CaCl_2 at 2.0 mmol/liter, NaCl at 118.0 mmol/liter, KCl at 4.0 mmol/liter, $\text{MgSO}_4 \cdot 7\text{H}_2\text{O}$ at 1.2 mmol/liter, NaHCO_3 at 25.0 mmol/liter, and NaH_2PO_4 at 1.2 mmol/liter. The substrate-free Tyrode's solution contained choline chloride at 7 mmol/liter to maintain osmolarity. Unless otherwise indicated, chemicals and reagents were obtained from Sigma. Two to four trabeculae (4–7 mm long and <1.0 mm in diameter) were attached to a force transducer and immersed in a heated (37°C) 30-ml bath of modified Tyrode's solution; a 92.5% O_2 /7.5% CO_2 mixture was bubbled during normoxia. This gas mixture provided an O_2 partial pressure of >350 mmHg (1 mmHg = 133 Pa), a partial pressure of CO_2 of 36–40 mmHg, and a pH of 7.35–7.45. Each parameter was checked routinely with an automated blood gas analyzer. The organ bath temperature was maintained at 37°C throughout the experiment. During simulated ischemia, the gas mixture was switched to 92.5% N_2 /7.5% CO_2 . This mixture produced an O_2 partial pressure of <50 mmHg. The buffer solution was changed every 20 min except during the 30-min period of simulated ischemia.

Experimental Design. Trabeculae were equilibrated for 90 min to increase the baseline stretch force to 1,000 mg and to allow stabilization of developed force. Trabeculae that failed to generate more than 250 mg of developed force were excluded from the study. During the 90 min of equilibration, pacing was performed with platinum electrodes (Radnoti Glass, Monrovia, CA) for field stimulation. The electrodes were placed on either side of the trabeculae, stimulated (Grass SD9 stimulator, Warwick, RI) with 6-ms pulses at a voltage 20% above threshold, and paced at 1 Hz during normoxia and at 3 Hz during ischemia. Contractions were monitored by force transducers (Grass FT03) and recorded with a computerized preamplifier and digitizer (MacLab Quad Bridge, MacLab/8e, AD Instruments, Milford, MA) and continuously monitored with a Macintosh computer.

After equilibration, trabeculae from a single patient were studied under three experimental conditions: control conditions consisted of 90 min of normoxic suprafusion; I/R consisted of 30 min of simulated ischemia followed by 45 min of reperfusion; and the third condition consisted of an anticytokine intervention. In the latter case, the anticytokine was added to the suprafusion bath just before the onset of ischemia and was present throughout the 45 min of reperfusion.

Preserved Trabecular CK Activity. End reperfusion tissue (90 min) CK activity was determined as described (18). Tissues were homogenized in 100 vol of ice-cold isotonic extraction buffer (5, 18). The assay was performed with a CK kit (Sigma) by using an automated spectrophotometer. Results are presented as units of CK activity per mg (wet weight of tissue).

RNA Isolation and Reverse Transcription-Coupled PCR. Fresh trabeculae were homogenized in Tri-Reagent (Molecular Research Center, Cincinnati), and total RNA was isolated with chloroform extraction and isopropanol precipitation. The RNA was solubilized in diethyl-pyrocyanate-treated water, DNase-treated, and quantitated by using GeneQuant (Amersham Pharmacia Biotech). cDNA methods have been described (19). For each PCR, the following sequence was used: preheat at 95°C for 15 min, then cycles of 94°C for 40 s, 55°C for 45 s, and 72°C for 1 min, with a final extension phase at 72°C for 10 min. The optimal number of cycles was determined as 35. The primers for glyceraldehyde-3-phosphate dehydrogenase (GAPDH) and human IL-18 (19) and for human IL-18BP (17) have been reported. The PCR products were separated on a 1.5% agarose gel containing 0.5× TBE (50 mM Tris/45 mM boric acid/0.5 mM

EDTA, pH 8.3) with ethidium bromide at 0.5 mg/ml, visualized by UV illumination, and photographed. Densitometry was performed on the negative image (IMAGEQUANT software, Molecular Dynamics), and the relative absorbance of the IL-18 and IL-18BP PCR products was corrected against the absorbance obtained for GAPDH.

IL-18 Determinations. Fresh trabeculae were homogenized as described above for CK measurements. IL-18 was analyzed with liquid-phase electrochemiluminescence (ECL, Igen, Gaithersburg, MD). Mouse anti-human IL-18 mAb (R & D Systems) was labeled with ruthenium (Igen). In addition, affinity-purified goat anti-human IL-18 antibody (R & D) was labeled with biotin (Igen). The biotinylated antibody was diluted to a final concentration of 1 $\mu\text{g}/\text{ml}$ in PBS (pH 7.4) containing 0.25% BSA, 0.5% Tween-20, and 0.01% azide (ECL buffer). Per assay tube, 25 μl of the biotinylated antibody was preincubated at room temperature with 25 μl of streptavidin-coated paramagnetic beads (Dynal, Great Neck, NY) at 1 $\mu\text{g}/\mu\text{l}$ for 30 min by vigorous shaking. Samples to be tested (25 μl) or standards were added to tubes followed by 25 μl of ruthenylated antibody (final concentration, 1 $\mu\text{g}/\mu\text{l}$, diluted in ECL buffer). The tubes were then shaken for 24 h. The reaction was quenched by the addition of PBS at 200 μl per tube and the amount of chemiluminescence was determined with an Origin Analyzer (Igen). The limit of detection for IL-18 is 16 pg/ml.

Confocal Microscopy. Human atrial tissue obtained during insertion of the canula of the pump oxygenator was placed in a plastic holder of 1 cm (3), embedded, and frozen in tissue-freezing medium (Triangle Biomedical Sciences, Durham, NC) on isopentane cooled with dry ice. Frozen sections (5 μm) were cut on a Leica CM 1850 cryostat (Leica, Deerfield, IL). The slides were fixed for 10 min in 4% paraformaldehyde, air-dried, and incubated for 20 min in PBS supplemented with 10% normal goat serum. Sections were incubated in a 1:100 dilution of rabbit anti-human IL-18 antibody (Peprtech, Rocky Hill, NJ) or nonimmune rabbit IgG at 1 $\mu\text{g}/\text{ml}$ as negative control. The antibodies were diluted in PBS containing 1% BSA. After an overnight incubation at 4°C, the sections were washed three times with 0.5% BSA in PBS. The sections were then incubated with a secondary goat anti-rabbit antibody conjugated to Alexa488 (Molecular Probes) for 60 min at room temperature in the dark. Nuclei were stained blue with bisbenzimidazole (Sigma) at 1 $\mu\text{g}/100\text{ ml}$. After staining, sections were washed and examined with the Leica DM RXA (Leica) confocal laser scanning system and analyzed with SLIDEBOOK software for Macintosh (Intelligent Imaging Innovations, Denver).

Statistical Analysis. Data are expressed as the mean \pm SEM. Mean changes in developed force were calculated relative to the control value at 90 min for each patient's tissue. Statistical significance of differences between groups were determined by factorial ANOVA with Bonferroni–Dunn post hoc analysis. Statistical analyses were performed with STAT-VIEW 4.51 software (Abacus Concepts, Calabasas, CA).

Results

The Effect of Neutralization of Endogenous IL-18 with IL-18BP on Postischemic Developed Force. Fig. 1A demonstrates the kinetic response of trabeculae to I/R injury. The final 15 min of equilibration are shown and normalized to 100% at the beginning of the experimental period. Control trabeculae are suprafused under normoxic conditions throughout the experiment. As shown, there is a reduction (10%) in the developed force in the control trabeculae. Trabeculae subjected to ischemia exhibit a rapid decline in contractile function; on reperfusion, contractile force returns to approximately 25% of the control developed

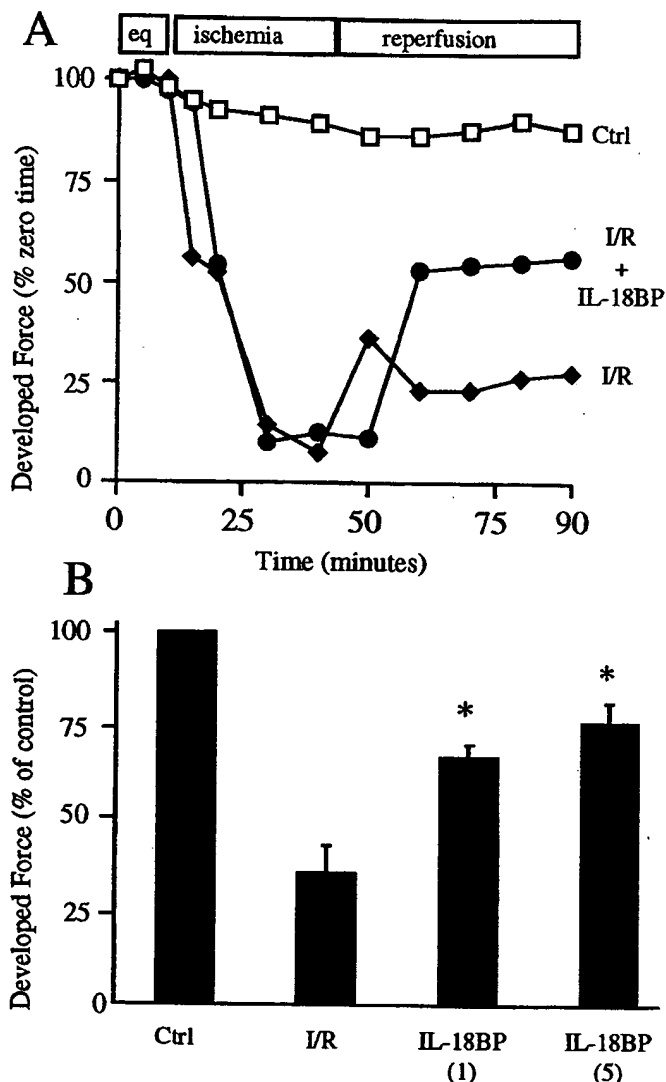


Fig. 1. Effect of IL-18BP on ischemia-induced myocardial contractile dysfunction. (A) Kinetic response to ischemic injury. After equilibration (eq), control (Ctrl) trabeculae were superfused under normoxic conditions throughout the experiment. Trabeculae were subjected to I/R in the absence or presence of IL-18BP (5 μ g/ml) as described in the experimental model. The vertical axis indicates percent of developed force compared with initiation of the experiment (time 0). The data are derived from trabeculae of a single patient and are representative of the methods used to calculate the mean change in developed force at 90 min. (B) Postischemic developed force after neutralization of IL-18 with IL-18BP. Results are expressed as the mean percent change in developed force relative to Ctrl after completion of reperfusion (90 min). Numbers in parentheses indicate IL-18BP in μ g/ml ($n = 6$). *, $P < 0.01$ compared with I/R.

force. In contrast, trabeculae exposed to ischemia but in the presence of IL-18BP returned to 55% of the control developed force. To assess the I/R response of heart tissues from several patients, the level of developed force in the control trabeculae at 90 min was set at 100% for each patient's sample, and the relative percent change in developed force for the experimental groups was calculated.

As shown in Fig. 1B, postischemic developed force in untreated trabeculae (I/R) was reduced to a mean of 35% of control. However, in the presence of IL-18BP, this reduction was attenuated to a mean of 66.2% of control at 1 μ g/ml and 76% of control at 5 μ g/ml, respectively. These results suggest that I/R

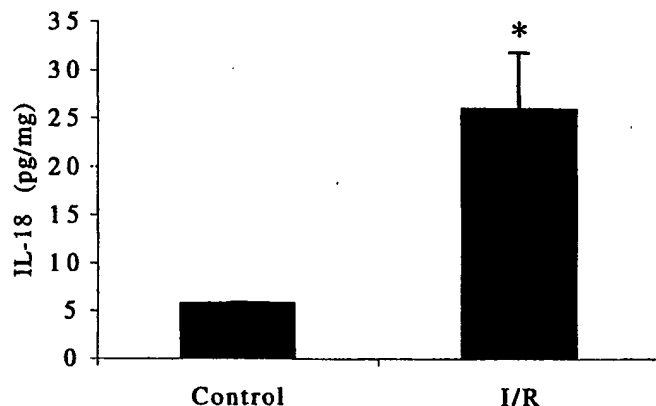


Fig. 2. Myocardial IL-18 protein content. Trabeculae were homogenized after 90 min of superfusion under normoxic conditions (Control) or 45 min after 30 min of ischemia. Trabeculae were matched from the same subjects. IL-18 levels are indicated on the vertical axis in pg/ml ($n = 4$). *, $P < 0.01$.

leads to release of biologically active IL-18 after processing endogenous precursor IL-18 by ICE. Therefore, IL-18 was measured in freshly obtained atrial tissue. As shown in Fig. 2, basal IL-18 was present in trabeculae obtained before the insertion of the of pump-oxygenator canula into the right atrium. After 90 min of equilibration, 30 min of ischemia, and 45 min of reoxygenation, trabeculae were homogenized, and IL-18 levels determined. There was a 4.5-fold increase in IL-18 in the tissue after I/R (Fig. 2).

Steady-state mRNA levels for IL-18 and IL-18BP were also determined in these tissues. We observed basal gene expression for IL-18 and IL-18BP in the freshly obtained preischemic atrial homogenates (Fig. 3). Similar to the increase in IL-18 protein, I/R induced a further increase in steady-state IL-18 mRNA levels (4.7-fold increase). IL-18BP gene expression was also observed in freshly obtained atrial tissue and increased only modestly (1.3-fold) after I/R.

Location of IL-18 in Human Myocardium. Because IL-18 protein, as measured by ECL, and IL-18 mRNA are present in freshly obtained myocardial homogenates, we used histochemical staining to determine the location of IL-18. Atrial tissues was obtained just before insertion of the pump-oxygenator canula and was immediately snap-frozen. As shown in Fig. 4, IL-18 was observed in resident myocardial macrophages and within the vascular endothelial cells. The IL-18 in macrophages and endo-

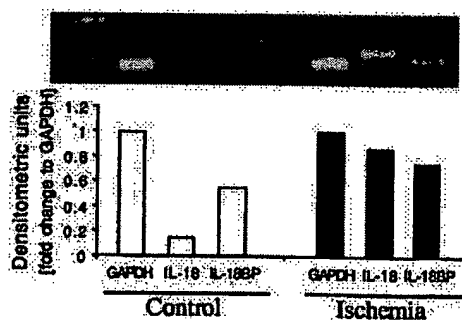


Fig. 3. Steady-state IL-18 and IL-18BP mRNA levels in control and ischemic atrial tissue. Tissues obtain after conditions described in Fig. 2 were snap-frozen in liquid nitrogen and kept frozen at -70°C . After homogenization in Tri-Reagent and mRNA isolation, levels of IL-18 and IL-18BP mRNA were determined by reverse transcription-coupled PCR. Data are from one of two subjects evaluated. GAPDH, glyceraldehyde-3-phosphate dehydrogenase.

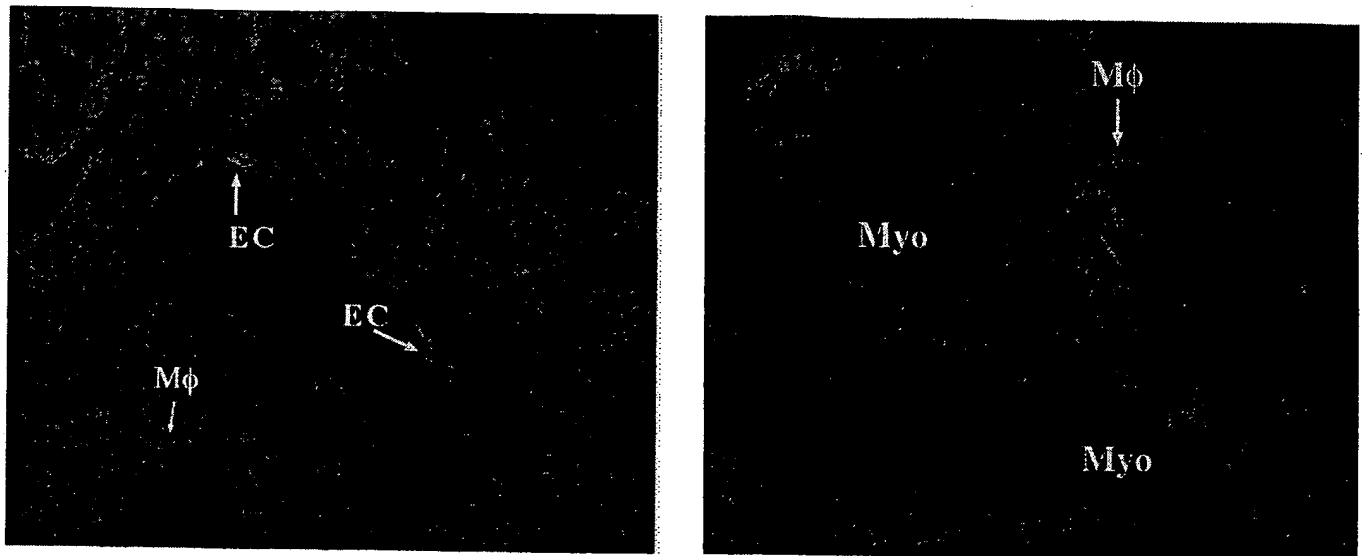


Fig. 4. Location of IL-18 in human myocardium. Immunohistochemical staining of human atrial tissue before insertion of atrial canula. (Left) Section through an atrial blood vessel. IL-18 is present within vascular endothelial cells (EC) and in resident myocardial macrophages (Mφ) (Right) Section through atrial muscle. Myocytes (Myo) are identified and IL-18 is observed in the resident macrophages. In this staining technique, IL-18 appears pink.

thelial cells is present before any operation-related ischemia takes place and is present in the absence of contact with any foreign surfaces. The localization of IL-18 in resident macrophages and endothelial cells is consistent with previous studies of constitutive preformed precursor IL-18 in freshly obtained human peripheral monocytes from healthy subjects (20). Therefore, we conclude that preformed precursor IL-18 exists in the myocardium of patients scheduled for coronary artery bypass for ischemic heart disease.

The Effect of ICE Inhibition on Postischemic Developed Force. Because IL-18BP effectively attenuated ischemia-induced myocardial dysfunction, we hypothesized that inhibition of the conversion of preformed precursor IL-18 to mature IL-18 would also attenuate ischemia-induced myocardial dysfunction. Therefore, the specific ICE inhibitor YVAD was added to the suprafusion bath before the onset of ischemia. ICE inhibition by the addition of YVAD was continued throughout the ischemic period and during reperfusion. YVAD-mediated inhibition of ICE resulted in attenuation of ischemia-induced myocardial dysfunction, as shown by the improvement in contractile function from 35% of control in I/R to 60% at 10 $\mu\text{g/ml}$ and 75.8% at 20 $\mu\text{g/ml}$ (Fig. 5). These results confirm that biologically active IL-18 in human myocardium is the result of cleavage of preformed precursor

IL-18 by ICE. In addition, these results suggest that myocardial ischemia may activate latent ICE.

The Effect of IL-1Ra on Postischemic Developed Force. Given that the inhibition of ICE may also reduce processing of endogenous IL-1 β , inhibition of IL-1 β under saturating concentrations of IL-1Ra will prevent biologically active IL-1 β from exerting its effect. As shown in Fig. 6, blockade of IL-1R with IL-1Ra increased the contractile force after I/R from 35% to 61%. Therefore, inhibition of ICE likely exerts its effects via inhibition of the processing of both pro-IL-1 β and pro-IL-18.

Preservation of Cellular Viability. Intracellular levels of CK were used to assess the degree of cellular viability after I/R. In this assay, the higher the CK value, the greater the number of viable cells. Each of the anticytokine interventions resulted in the preservation cellular viability. As demonstrated in Fig. 7, IL-18BP, ICE inhibition (10 and 20 $\mu\text{g/ml}$), and IL-1Ra increased intracellular CK levels after I/R from 1,399 to 5,921, 5,675, 6,624, and 4,662 units of CK activity per mg (wet tissue), respectively. These observations suggest that inhibition of I/R-induced activation of IL-18 and IL-1 β preserves myocellular viability in this *ex vivo* model.

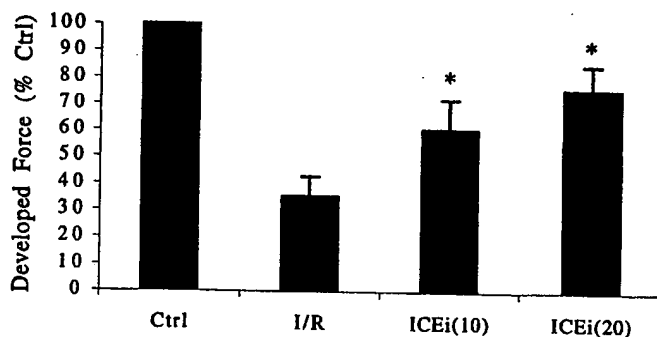


Fig. 5. Effect of ICE inhibition on postischemic developed force. Results are expressed as the mean percent change in developed force relative to control (Ctrl) after I/R. Numbers in parentheses indicate the concentration of ICEi in $\mu\text{g/ml}$ ($n = 7$). *, $P < 0.01$ compared with I/R.

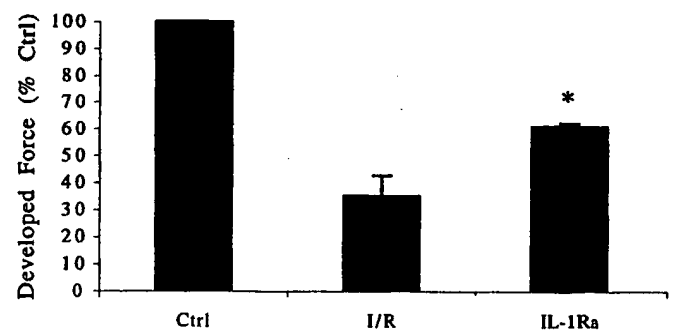


Fig. 6. Preservation of contractile function after I/R and blockade of IL-1 receptors with IL-1Ra. Results are expressed as the mean percent change in developed force relative to control (Ctrl) after completion of reperfusion. The concentration of IL-1Ra is 20 $\mu\text{g/ml}$ ($n = 5$). *, $P < 0.01$ compared with I/R.

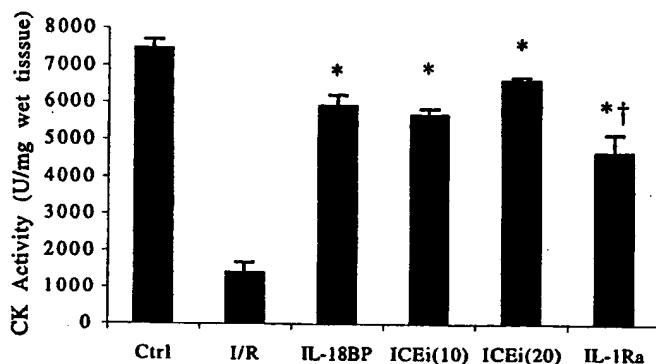


Fig. 7. Tissue CK activity after I/R. CK is expressed in units of activity per mg (wet weight of tissue). The experimental conditions are indicated under the horizontal axis. Ctrl and I/R ($n = 6$); IL-18BP at 5 $\mu\text{g/ml}$ ($n = 5$); ICEi at 10 and 20 $\mu\text{g/ml}$ ($n = 5$, each group); IL-1Ra at 20 $\mu\text{g/ml}$ ($n = 6$). *, $P < 0.05$ compared with I/R; †, $P < 0.05$ for ICEi (20) compared with IL-1Ra.

Discussion

Generation of oxygen-derived free radicals, NO, calcium overload, or decreased responsiveness of the myofilaments to calcium may contribute to contractile dysfunction after I/R (1). In addition to these immediate-acting mediators, the relationship of cytokines to myocellular dysfunction after I/R remains unclear. Data from the present study suggest that IL-18 and IL-1 β are processed and released from their endogenous precursor forms in human heart tissue during ischemic injury and function to suppress contractile force. Furthermore, the processing of the precursors appears to be ICE-dependent, and latent ICE is likely activated by ischemia. Previously, neutralization of endogenous TNF- α was shown to protect human trabeculae from ischemia-induced dysfunction (6). At present, it is likely that the combination of IL-18, IL-1 β , and TNF- α accounts for the ischemia-induced dysfunction.

Oxygen metabolites present after ischemia depress myocardial contractile function in several animal models *in vitro* and *in vivo* (1). The source of the oxygen radicals is unclear, although xanthine oxidase may be an important mediator of oxyradical production (21). Oxyradicals may interact with cellular proteins, lipids, calcium, and myofilaments to induce contractile depression. In addition to xanthine oxidase, TNF- α is an inducer of oxygen metabolites. In addition, recent data indicate that IL-18 primes human neutrophils for superoxide production (C. Sillman, personal communication).

Ischemia is a direct stress signal to the myocyte and, as a result, gene expression of stress-related molecules is elevated. For example, after 15 min of ischemia in rodent hearts perfused with Krebs's buffer, TNF- α gene expression is up-regulated (2). However, the sudden and marked reduction in atrial trabecular function in the present study is apparent within minutes and it is unlikely that cytokines account for the early dysfunction. During reperfusion, however, the failure to return completely to functionality appears to be cytokine-mediated because specific cytokine blockade or neutralization restores functionality to a greater degree than ischemic controls. Depressed function during reperfusion may be caused by oxygen radical-induced loss of myocyte integrity, increased production of NO, or altered calcium flux. Therefore, do IL-1 β and/or IL-18 trigger the above changes? The addition of IL-1 β to oxygenated human trabeculae suppresses function (22), and it is known that IL-1 β induces NOS in cardiac myocytes (23). However, it is not known whether IL-18 acts similarly.

NO is a myocardial depressant. However, the effect of NO after ischemia is controversial. This controversy stems from the different tissue levels NO present depending on which pathway of NO

synthesis is activated. Lower levels of NO resulting from synthesis via the constitutive NO synthase pathway appears to protect the myocardium (24), whereas the NO produced from inducible NO synthase, which is significantly higher, leads to myocardial injury (25). After a moderate ischemic insult, induction of inducible NO synthase occurs in the rat myocardium followed by increased NO production (26). This NO subsequently leads to myocardial contractile depression. Using the same trabeculae model as the present study, Cain *et al.* (22) demonstrated that specific inhibition of NO synthase attenuated TNF- α - and IL-1 β -induced human myocardial dysfunction. As discussed, endogenous TNF- α accounts for some of the postischemic myocardial dysfunction. There are numerous hypotheses on how TNF- α mediates ischemia induced myocardial dysfunction. Finkel *et al.* (25) demonstrated TNF- α induced contractile dysfunction in isolated hamster papillary muscle. This effect was abolished with inhibition of NO synthase. NO has been demonstrated to play a role in TNF- α -induced myocardial dysfunction via desensitization of the myofilaments to calcium (23). In addition, TNF- α may also lead to phosphorylation of troponin, which further desensitizes the myofilaments to calcium.

Calcium is a vital mediator of myocardial contractile function. Changes in intracellular Ca^{2+} , cellular calcium overload, and modulation of the myofilaments response to Ca^{2+} affect contractile force. The majority of investigations has focused on the role of calcium as the effector of myocardial contractile dysfunction. The relationship between myocardial calcium changes and myocellular contractile dysfunction has been well described (1). After an I/R injury, the myofilaments responsiveness to calcium decreases and is thought to account for most of the decrease in contractile function after ischemia. In addition to calcium overload, an ischemic insult leads to the production and activation of intracellular calcium-dependent proteases. Upon activation, these proteases begin intracellular myofilament proteolysis leading to postischemic contractile dysfunction. Given the protection afforded by the anticytokine interventions in the present study, it is likely that IL-1 β and/or IL-18 alter intracellular calcium homeostasis during and after ischemia.

Although mature IL-1 β has been shown to directly suppress function when added to human atrial trabeculae (22), it has not been shown whether endogenous IL-1 β in the heart participates in ischemia-induced dysfunction. In the present study, inhibition of IL-1 β activity by IL-1 receptor blockade indicates that biologically active endogenous IL-1 β is present in the heart after ischemia. Furthermore, the formation of active IL-1 β in the ischemic heart is ICE-dependent. The data are consistent with the concept that synthesis of the precursor for IL-1 β and activation of ICE takes place during I/R.

The present studies support the concepts that human atrial myocardium is highly sensitive to IL-18 and IL-1 β and that the combination of these two cytokines appear to synergistically depress myocardial function. We have demonstrated (22) that the presence of exogenous IL-1 β or TNF- α decreases contractile force in human trabeculae in the absence of ischemia. In addition, the combination of these two cytokines have a synergistic effect on the depression of myocardial contractility. Furthermore, we have preliminary data to suggest that exogenous IL-18 under normoxic conditions also depresses myocardial contractile function.

The ability of ICE inhibition to reduce postischemic dysfunction suggests that the processing of precursor IL-1 β and IL-18 are necessary for cytokine-mediated myocardial suppression. The immunohistochemical studies revealed that IL-18 is preformed in the resident macrophages and endothelial cells of atrial tissues from patients with ischemic heart disease but it is not clear whether the precursor IL-1 β is also preformed. However, IL-1 β mRNA is rapidly increased in rat hearts within 15 min after an ischemic insult (2), and therefore it is likely that there is also increased precursor IL-1 β synthesis in atrial trabeculae during ischemia. Ischemia itself may be an activator of

latent ICE activity in heart tissue. Several investigators have reported that ICE inhibition during myocardial I/R injury in animals reduces apoptotic cell death. The criteria used for determining cell death was DNA fragmentation and cleavage of poly(ADP)-ribose polymerase (27–29). Importantly, the present studies expand these observations by demonstration that ICE inhibition preserves functionality within the injured tissue immediately after I/R. ICE inhibition also preserves cell viability because CK levels remained high in postischemic tissues treated with an ICE inhibitor.

IL-1 β and TNF- α have also been implicated in the pathogenesis of human myocardial suppression in sepsis (30, 31). The mechanism(s) by which IL-1 β and TNF- α induce contractile dysfunction has also been linked to NO and changes in cellular calcium handling (31). In addition, inhibition of the sphingomyelin signaling pathway abrogated TNF- α /IL-1 β -induced myocardial contractile dysfunction (22). Although the present study does not address the role of NO in IL-18-mediated ischemia-induced dysfunction, TNF- α depresses the myocardium in a NO-dependant pathway (6). Blockade of IL-1 receptors revealed a role for endogenous IL-1 β in I/R injury, a finding that was not unanticipated given the large amount of animal data. That endogenous IL-18 also plays a role in the injury was unanticipated but based on the fact that IL-18BP only neutralizes mature IL-18 (16, 17). Because ICE inhibition prevents the cleavage of both precursor IL-1 β and IL-18, it would not be surprising that

IL-18 and IL-1 β act synergistically in suppressing myocardial function. In fact, the specific blockade of TNF- α , IL-1 β , or IL-18 attenuates, but does not entirely reverse, I/R-induced myocardial dysfunction, suggesting that the three cytokines act together to suppress myocardial function.

The ability to modulate or interrupt cytokine signaling has been demonstrated in numerous disease states in animal models and clinically in humans (e.g., rheumatoid arthritis and Crohn's disease). IL-1 β and TNF- α have been associated with acute myocardial dysfunction and hence are logical targets in patients. However, IL-18, a member of the IL-1 superfamily, has to date not been associated with myocardial dysfunction but should also be considered a target for ischemic therapy based on the present studies. IL-1 β and IL-18 share numerous properties including the cleavage of the inactive precursor forms to the active forms by ICE (caspase 1). Given the myocardium's response to proinflammatory cytokines and the ability to interrupt the inflammatory process, we hypothesize that the inhibition of caspase 1 protects ischemia-induced human myocardial dysfunction via inhibition of IL-1 β and IL-18 processing.

We thank Fabia Gamboni-Robertson for the IL-18 immunohistochemical studies, Dr. Ron Pincus (Interpharm, Nes Ziona, Israel) for the recombinant human IL-18BP, and Amgen for IL-1Ra. These studies are supported by National Institutes of Health Grants AI-15614 and GM-4922.

- Bolli, R. (1990) *Circulation* 82, 723–738.
- Herskowitz, A., Choi, S., Ansari, A. A. & Wesselingh, S. (1995) *Am. J. Pathol.* 146, 419–428.
- Meldrum, D. R., Cleveland, J. C., Jr., Cain, B. S., Meng, X. & Harken, A. H. (1998) *Ann. Thorac. Surg.* 65, 439–443.
- Gurevitch, J., Frolkis, I., Yuh, Y., Paz, Y., Matsa, M., Mohr, R. & Yakirevich, V. (1996) *J. Am. Coll. Cardiol.* 28, 247–252.
- Cleveland, J. C. J., Meldrum, D. R., Cain, B. S., Banerjee, A. & Harken, A. H. (1997) *Circulation* 96, 29–32.
- Cain, B. S., Meldrum, D. R., Dinarello, C. A., Meng, X., Banerjee, A. & Harken, A. H. (1998) *J. Surg. Res.* 76, 117–123.
- Cain, B. S., Meldrum, D. R., Meng, X., Dinarello, C. A., Shames, B. D., Banerjee, A. & Harken, A. H. (1999) *J. Surg. Res.* 83, 7–12.
- Okamura, H., Nagata, K., Komatsu, T., Tanimoto, T., Nukata, Y., Tanabe, F., Akita, K., Torigoe, K., Okura, T., Fukuda, S., et al. (1995) *Infect. Immun.* 63, 3966–3972.
- Bazan, J. F., Timans, J. C. & Kaselein, R. A. (1996) *Nature (London)* 379, 591.
- Dinarello, C. A. (1999) *J. Allergy Clin. Immunol.* 103, 11–24.
- Gu, Y., Kuida, K., Tsutsui, H., Ku, G., Hsiao, K., Fleming, M. A., Hayashi, N., Higashino, K., Okamura, H., Nakanishi, K., et al. (1997) *Science* 275, 206–209.
- Ghayur, T., Banerjee, S., Hugunin, M., Butler, D., Herzog, L., Carter, A., Quintal, L., Sekut, L., Talanian, R., Paskind, M., et al. (1997) *Nature (London)* 386, 619–623.
- Born, T. L., Thomassen, E., Bird, T. A. & Sims, J. E. (1998) *J. Biol. Chem.* 273, 29445–29450.
- Torigoe, K., Ushio, S., Okura, T., Kobayashi, S., Taniai, M., Kunikate, T., Murakami, T., Sanou, O., Kojima, H., Fuji, M., et al. (1997) *J. Biol. Chem.* 272, 25737–25742.
- Robinson, D., Shibuya, K., Mui, A., Zonin, F., Murphy, E., Sana, T., Hartley, S. B., Menon, S., Kastelein, R., Bazan, F., et al. (1997) *Immunity* 7, 571–581.
- Novick, D., Kim, S.-H., Fantuzzi, G., Reznikov, L., Dinarello, C. A. & Rubinstein, M. (1999) *Immunity* 10, 127–136.
- Kim, S.-H., Eisenstein, M., Reznikov, L., Fantuzzi, G., Novick, D., Rubinstein, M. & Dinarello, C. A. (2000) *Proc. Natl. Acad. Sci. USA* 97, 1190–1195.
- Kaplan, L. J., Blum, H., Banerjee, A. & Whitman, G. J. (1993) *J. Surg. Res.* 54, 311–315.
- Reznikov, L. L., Kim, S. H., Westcott, J. Y., Frishman, J., Fantuzzi, G., Novick, D., Rubinstein, M. & Dinarello, C. A. (2000) *Proc. Natl. Acad. Sci. USA* 97, 2174–2179. (First Published February 11, 2000; 10.1073/pnas.040582597)
- Puren, A. J., Fantuzzi, G. & Dinarello, C. A. (1999) *Proc. Natl. Acad. Sci. USA* 96, 2256–2261.
- Charlat, M. I., O'Neill, P. G., Egan, J. M., Abernethy, D. R., Michael, L. H., Myers, M. L., Roberts, R. & Bolli, R. (1987) *Am. J. Physiol.* 252, H566–H577.
- Cain, B. S., Meldrum, D. R., Dinarello, C. A., Meng, X., Joo, K. S., Banerjee, A. & Harken, A. H. (1999) *Crit. Care Med.* 27, 1309–1318.
- Kelly, R. A. & Smith, T. W. (1997) *Circulation* 95, 778–781.
- Schluter, K. D., Weber, M., Schraven, E. & Piper, H. M. (1994) *Am. J. Physiol.* 267, H1461–H1466.
- Finkel, M. S., Oddis, C. V., Jacob, T. D., Watkins, S. C., Hattler, B. G. & Simmons, R. L. (1992) *Science* 257, 387–389.
- Chandrasekar, B., Streitman, J. E., Colston, J. T. & Freeman, G. L. (1998) *Biochim. Biophys. Acta* 1406, 91–106.
- Holly, T. A., Drincic, A., Byun, Y., Nakamura, S., Harris, K., Klocke, F. J. & Cryns, V. L. (1999) *J. Mol. Cell. Cardiol.* 31, 1709–1715.
- Okamura, T., Miura, T., Takemura, G., Fujiwara, H., Iwamoto, H., Kawamura, S., Kimura, M., Ikeda, Y., Iwatate, M. & Matsuzaki, M. (2000) *Cardiovasc. Res.* 45, 642–650.
- Piot, C. A., Martini, J. F., Bui, S. K. & Wolfe, C. L. (1999) *Cardiovasc. Res.* 44, 536–542.
- Kumar, A., Thota, V., Dee, L., Olson, J., Uretz, E. & Parrillo, J. E. (1996) *J. Exp. Med.* 183, 949–958.
- Schulz, R., Panas, D. L., Catena, R., Moncada, S., Olley, P. M. & Lopaschuk, G. D. (1995) *Br. J. Pharmacol.* 114, 27–34.

IL-18 regulates IL-1 β -dependent hepatic melanoma metastasis via vascular cell adhesion molecule-1

Fernando Vidal-Vanaclocha^{*,†}, Giamila Fantuzzi[‡], Lorea Mendoza^{*}, Angela M. Fuentes[†], Miren J. Anasagasti[†], Javier Martín^{*}, Teresa Carrascal^{*}, Patrick Walsh[‡], Leonid L. Reznikov[‡], Soo-Hyun Kim[‡], Daniela Novick[§], Menachem Rubinstein[§], and Charles A. Dinarello^{†¶}

^{*}School of Medicine and Dentistry, University of the Basque Country, 48940 Vizcaya, Spain; [†]University of Colorado Health Sciences Center, Denver, CO 80262; [‡]Biomedical Research and Technological Development Institute, 20009 Gipuzkoa, Spain; and [§]The Weizmann Institute, 76100 Rehovot, Israel

Contributed by Charles A. Dinarello, October 27, 1999

Proinflammatory cytokines, including IL-1 β and tumor necrosis factor- α (TNF- α), promote cancer cell adhesion and liver metastases by up-regulating the expression of vascular cell adhesion molecule-1 (VCAM-1) on hepatic sinusoidal endothelium (HSE). In this study, hepatic metastasis after intrasplenically injected mouse B16 melanoma (B16M) cells was reduced 84–95% in mice with null mutations for either IL-1 β or the IL-1 β -converting enzyme (ICE, caspase-1) compared with wild-type mice. On day 12, 47% of wild-type mice were dead compared with 19% of either IL-1 β or ICE-deficient mice. *In vitro*, conditioned medium from B16M cells (B16M-CM) induced the release of TNF- α and IL-1 β from cultures of primary murine HSE. The effect of B16M-CM on HSE resulted in increased numbers of B16M cells adhering to HSE, which was completely abrogated by a specific inhibitor of ICE, anti-IL-18 or IL-18-binding protein. Exogenous IL-18 added to HSE also increased the number of adhering melanoma cells; however, this was not affected by IL-1 receptor blockade or TNF neutralization but rather by anti-VCAM-1. These results demonstrate a role for IL-1 β and IL-18 in the development of hepatic metastases of B16M *in vivo*. *In vitro*, soluble products from B16M cells stimulate HSE to sequentially release TNF- α , IL-1 β , and IL-18. The IL-18 cytokine increases expression of VCAM-1 and the adherence of melanoma cells.

The adhesion of circulating cancer cells to capillary endothelia is a critical step in the initiation of metastasis (1). Vascular cell adhesion molecule-1 (VCAM-1), up-regulated by proinflammatory cytokines, facilitates the binding of leukocytes to activated endothelial cells. The adhesive function of VCAM-1 is also used by cancer cells to enhance metastatic implantation and spread (2). For example, IL-1 β and tumor necrosis factor- α (TNF- α) are known to potentiate the metastasis of very late antigen-4-expressing mouse B16 melanoma (B16M) cells in lung tissue by a mechanism which involves the up-regulation of VCAM-1 expression on endothelial cells (3, 4). We also have demonstrated that IL-1 significantly contributes to hepatic colonization of B16M cells both in normal and lipopolysaccharide-treated mice (5, 6). In addition, mannose receptor-mediated murine hepatic sinusoidal endothelium (HSE) activation involves endogenous IL-1-mediated expression of VCAM-1, leading to increased B16M cell adhesion and metastasis (7). IL-1 β -activated HSE cells release very late antigen-4-stimulating factors that potentiate B16M cell adhesion to HSE (8). Thus, IL-1 can create a prometastatic microenvironment for certain intrasplenicly arrested very late antigen-4-expressing cancer cells.

In the present study, the role of the IL-1 β -converting enzyme (ICE, caspase-1) in B16M melanoma metastasis in mice was investigated. ICE cleaves the precursors of both IL-1 β and IL-18 (9, 10), and hence, inhibitors of ICE or mice with a null mutation for ICE result in a deficiency in the release of biologically active IL-1 β as well as biologically active IL-18. To differentiate between the role of either cytokine in ICE-deficient mice, we compared B16M metastasis after intrasplenic injection of B16M cells into mice deficient in ICE or IL-1 β . The role of IL-18 in metastatic spread via activation of HSE is unknown, although

IL-18 is a proinflammatory cytokine with several similarities to IL-1 β (11), including up-regulation of adhesion molecules (12). However, IL-18 is different from IL-1 in that IL-18 plays an essential role as an interferon- γ (IFN- γ)-inducing factor (13–15). IL-18 is a product of macrophages and particularly the Kupffer cells (13), and therefore may play a role in hepatic metastasis by altering the microenvironment of the hepatic sinusoidal wall.

The conditioned medium from B16M cells (B16M-CM) contains spontaneously released, unknown soluble “factors” that, in turn, stimulate the production of IL-1 β and TNF- α as well as the expression of VCAM-1 on HSE (16). Inhibitors of ICE, IL-1 receptor blockade, and neutralization of TNF were employed to characterize the cytokine cascade induced by these soluble factors on HSE activation. In addition, the role of IL-18 in B16M adhesion to HSE was investigated by using the newly described, naturally occurring IL-18 binding protein (IL-18BP) (17). Although IL-18BP circulates in healthy subjects and appears to be a natural inhibitor of production of the T-cell helper cytokine IFN- γ (17), there may be a role for IL-18BP in regulating host resistance to cancer by either affecting the adhesion of cancer cells to vascular endothelium or suppressing the T-cell helper function of immunosurveillance to malignant cells.

Materials and Methods

Reagents. Rat anti-mouse IgG and rat anti-mouse VCAM-1 mAb were obtained from Serotec. Recombinant murine IL-1 β was obtained from R & D Systems. Recombinant human IL-1 receptor antagonist (IL-1Ra) was a kind gift from Amgen Biologicals, and recombinant human TNF-binding protein (TNFbp), the native p55 TNF soluble receptor (18, 19) was a kind gift from Serono Laboratories (Randolph, MA). ICE inhibitor (ICEi) was purchased from Alexis Co. (San Diego, CA). Recombinant murine IL-18 and rabbit anti-mouse IL-18 IgG were purchased from PeproTech EC (London, U.K.). Recombinant human IL-18BP was produced as described (17). Reverse transcription-PCR for murine IL-18 was determined as described (20).

Culture of B16M Cells. B16M cells intended for intrasplenic injection were cultured, maintained, and passaged as described (8). B16M-CM was prepared as follows: 5×10^5 B16M cells were plated in a 25-cm² T-flask and cultured for 24 h in 5% FCS. Cells were cultured for an additional 24 h in serum-free medium (final

Abbreviations: IL-1 β –/–, IL-1 β deficient; IL-1Ra, IL-1 receptor antagonist; ICE, IL-1 β -converting enzyme; ICE–/–, ICE deficient; ICEi, ICE inhibitor; TNF, tumor necrosis factor; TNFbp, TNF-binding protein; IL-18BP, IL-18-binding protein; HSE, hepatic sinusoidal endothelium; B16M, B16 melanoma; B16M-CM, B16M-conditioned medium; VCAM-1, vascular cell adhesion molecule-1; IFN- γ , interferon- γ ; WT, wild-type.

[¶]To whom reprint requests should be addressed.

The publication costs of this article were defrayed in part by page charge payment. This article must therefore be hereby marked “advertisement” in accordance with 18 U.S.C. §1734 solely to indicate this fact.

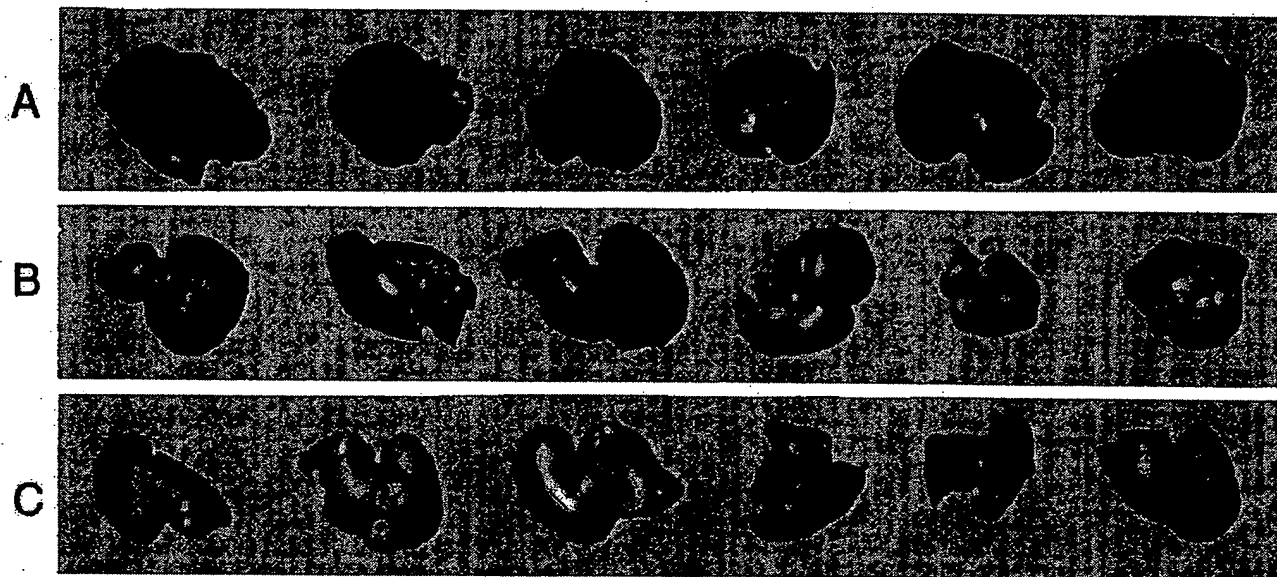


Fig. 1. Experimental hepatic colonization after intrasplenic injection of B16M cells into WT (A), IL-1 β ^{-/-} (B), or ICE^{-/-} (C) mice. Livers were removed on day 10 after injection of melanoma cells, fixed, and photographed. Metastases can be identified by black melanotic nodules. These livers are taken from mice depicted in Table 1, Experiment 1.

cellular density of 6×10^4 cells/cm²). Supernatants were collected, diluted 1:3 in fresh serum-free medium, and passed through a 0.22 μ m filter.

Quantitative B16M Cell Adhesion to Primary HSE Cultures. HSE cells were separated from syngeneic mice, identified, and cultured as described (21). B16M cells were labeled with 2',7'-bis-(2-carboxyethyl)-5,6-carboxyfluorescein-acetoxymethylester solution (Molecular Probes, Eugene, OR) as reported (6). HSE cells were incubated with various stimulants or inhibitors as indicated in each figure legend. Following the incubation times, the HSE was washed and the number of labeled cells determined. For the adherence cell assay, 2×10^5 -labeled B16M cells were added to wells. After an 8-min incubation at 37°C, HSE cells were washed three times with fresh medium. The number of adhering cells was determined by using a quantitative method based on a previously described fluorescence measurement system (6). The percentage of B16M cells adhering to HSE was calculated as the relative value with respect to the initial number of added cells.

Cytokine Analysis. Release of cytokines from cultures of primary HSE cells and B16M cells was measured by using specific ELISA kits for mouse IL-1 β and TNF- α (R & D Systems). Circulating IFN- γ and IL-1 β in mice was measured as described (22).

Hepatic Metastasis Assay. The protocol was approved by the University of Colorado Health Sciences Animal Care Committee. IL-1 β ^{-/-} and ICE^{-/-} male mice were generated as described (23, 24). Six- to eight-week-old mice (housed five per cage) were used. Hepatic metastases were produced by the intrasplenic injection into anesthetized mice of 3×10^5 viable B16M melanoma cells suspended in 0.1 ml Hanks' balanced salt solution (6). Mice were killed under anesthesia on the 10th day after the injection of cancer cells. Liver tissue was fixed in PBS with 10% formaldehyde, pH 7.4, and processed for routine histology. Densitometric analysis of digitized microscopic images was used to discriminate metastatic B16M from normal hepatic tissue. The mean number of melanoma foci in 15 10×10 mm² sections per liver was determined. The density of liver metastasis, which

is the number of metastases per 100 mm³ of liver, was calculated with the stereological procedures described (5).

Results

Reduced Metastasis and Growth of B16M Cells Injected into IL-1 β - and ICE-Deficient Mice. Initial experiments examined mortality. Seven of 15 wild-type (WT) mice injected intrasplenicly were dead on day 12, whereas only 3 out of 16 of both the IL-1 β ^{-/-} and ICE^{-/-} were dead on day 12. However, to quantitate the degree of hepatic metastasis ante mortem, the experiment was repeated and mice were killed on day 10 after the injection of tumor cells. Separated by 1 year, in two independent experiments and by using two different cultures of B16M cells, mice were injected intrasplenicly into WT background, IL-1 β ^{-/-} and ICE^{-/-} mice. Ten days later, gross inspection demonstrated visible melanotic tumors in the spleen from all mice, without significant differences in size as evaluated by splenic weight. In contrast, a marked decrease in metastasis was present in the livers of IL-1 β ^{-/-} and ICE^{-/-} mice compared with WT mice (Fig. 1). Quantitative histological analyses on number and size of metastatic foci were performed to determine metastasis density (as number of foci per 100 mm³) and metastasis volume (percent organ occupancy). As shown in Table 1, compared with WT mice, hepatic metastasis density was significantly reduced (84–95%, $P < 0.01$) in the livers of IL-1 β ^{-/-} and ICE^{-/-} mice. These results indicate that most of the injected B16M cells were unable to implant in the hepatic tissue of the mutant mice. In addition, metastasis volume, an indicator of metastatic growth, was also significantly reduced in IL-1 β ^{-/-} and ICE^{-/-} mice six- to sevenfold ($P < 0.01$, Table 1). We also observed a difference in these metastasis parameters between IL-1 β ^{-/-} and ICE^{-/-} mice, particularly in experiment 1. The mean number of metastatic foci in the WT mice was 234; the IL-1 β ^{-/-} mice, 25; and only 13 in the ICE^{-/-} mice, which was a 95% reduction.

Autocrine IL-18 Mediates TNF- α - and IL-1 β -Induced Adhesiveness on B16M-CM-Activated HSE. Incubation of B16M-CM with HSE resulted in a significant ($P < 0.01$) increase in the adhesiveness of B16M cells as well as release of TNF- α and IL-1 β into the HSE

Table 1. Hepatic colonization following intrasplenically injected B16M cells into WT, IL-1 β ^{-/-}, or ICE^{-/-} mice

| Mouse group | Metastasis density, no. foci per 100 mm ³ | Metastasis volume, % liver volume |
|-----------------------------|--|-----------------------------------|
| Experiment I | | |
| WT | 234.16 \pm 58.36* | 66.18% |
| IL-1 β ^{-/-} | 25.18 \pm 21.02† | 10.05% |
| ICE ^{-/-} | 13.56 \pm 16.20† | 2.1% |
| Experiment II | | |
| WT | 198.40 \pm 100.54 | 59.62% |
| IL-1 β ^{-/-} | 33.79 \pm 19.89† | 9.70% |
| ICE ^{-/-} | 27.73 \pm 15.68† | 8.08% |

*Means \pm SD of two independent experiments performed one year apart (7–15 mice per group).

†P < 0.01 with respect to WT mice by ANOVA and the Scheffe F test.

supernatant (Fig. 2). In the presence of ICEi, both the increased release in IL-1 β as well as the increase in melanoma cell adhesiveness was completely abrogated, without decreasing TNF- α . The addition of anti-IL-18 IgG also completely abrogated the increase in adhesiveness but did not affect the release of IL-1 β or TNF- α . There were no statistically significant changes in IL-1 β or TNF- α levels or in the number of adhering B16M cells to HSE cells when these cells were treated with ICEi or anti-IL-18 IgG in the absence of B16M-CM (data not shown). These results suggest that soluble factors present in the B16M-CM induce a cascade that begins with the release of TNF- α and is followed sequentially by ICE-dependent release of IL-1 β and IL-18. Because antimurine IL-18 completely reduced the increase in HSE adhesiveness, IL-18 appears to be responsible for the expression of VCAM-1 in activated HSE.

In the next experiment shown in Fig. 3, exogenously added murine IL-1 β did not reverse the effect of ICEi on HSE (Fig. 3A). This suggests that in addition to inhibiting the processing of the IL-1 β precursor, the ICEi is also inhibiting the processing of the IL-18 precursor. Reverse transcription-PCR confirmed that HSE cells constitutively express IL-18 mRNA, as observed in murine spleen cells (20). The ability of murine IL-1 β to directly increase the adherence of B16M cells is shown in Fig. 3B; however, in the presence of antimurine IL-18, this increase is reversed, again suggesting that IL-1 β -induced IL-18 is increasing the expression of VCAM-1 on HSE. In a similar fashion, TNF- α added to HSE up-regulates melanoma cell adhesion (Fig. 3C), but this is reduced by the presence of anti-IL-18.

The above data provide evidence that B16M-CM contains soluble factors that trigger a cascade in HSE in which the last steps leading to increased adhesiveness for melanoma cells involve release of biologically active IL-18. To demonstrate this, B16M-CM was incubated with HSE in the presence of recombinant human IL-18BP, which binds and neutralizes murine IL-18 (17). As shown in Table 2, IL-18BP prevents the adhesion of B16M melanoma cells induced by B16M-CM. The addition of IL-18BP to HSE reduced the percent of adhering cells from 35.1 to 8.7% (P < 0.01). This represents a 100% inhibition and is consistent with the high affinity binding of IL-18BP to IL-18 and complete neutralization of its biological activities at a molar excess of two (25). In fact, the number of adhering cells was below the number of adhering cells incubated with basal medium, suggesting IL-18BP suppression of constitutive as well as inducible IL-18 from HSE. These results demonstrate that IL-18-activated HSE is an essential component of adhesion of melanoma cells to HSE cells. In preliminary studies, *in vivo* administration of IL-18BP or anti-IL-18 antibodies before intrasplenic injection of B16M reduced the number of hepatic metastatic foci and metastatic density on day 10 by >50%.

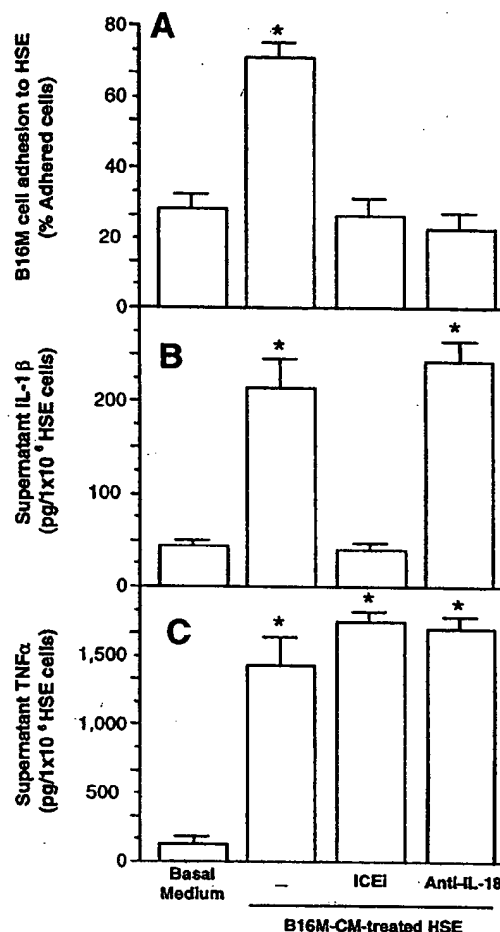


Fig. 2. Effect of B16M-CM on adhesion of B16M cells to HSE. Cultured HSE cells were incubated in the presence of B16M-CM for 10 h. (A) Percent of adhering B16M cells to HSE incubated with B16M-CM in the presence of ICEi (10 μ M) or anti-IL-18 (10 μ g/ml). (B) Level of IL-1 β in HSE supernatants before adhesion assay. (C) Level of TNF- α in HSE supernatants before adhesion assay. After the removal of the HSE supernatants, the adhesion cell assay was performed as described in *Materials and Methods*. Data represent the means \pm SD of four separate experiments performed by using four different preparations of HSE cells, each in six replicates (n = 24). *, P < 0.01 for the percentage of B16M cells adhering to B16M-CM-treated HSE and of IL-1 β and TNF- α production with respect to the basal medium. The Student's two-tailed, unpaired t test was used.

Direct evidence that IL-18 increases the expression of VCAM-1 on HSE is shown in Fig. 4. Murine IL-18 was incubated with HSE cells in the presence of TNFbp, IL-1Ra, or anti-VCAM-1. IL-18 increased the adhesiveness of B16M cells (P < 0.01) which was not affected by the presence of TNFbp or IL-1Ra, both present in high concentrations. However, anti-VCAM-1 completely reduced the IL-18-induced increase in the number of melanoma cells adhering to HSE cells. A nonspecific IgG did not affect the up-regulation of B16M cell adhesion to IL-18-treated HSE (data not shown).

Discussion

Inflammatory mechanisms facilitate cancer metastasis. Previous work has focused on IL-1 (4–6, 8, 26–30) and TNF (3, 31–33) as prometastatic cytokines. Although specific blockade of endogenous IL-1 and TNF reduce metastasis, other factors or cyto-

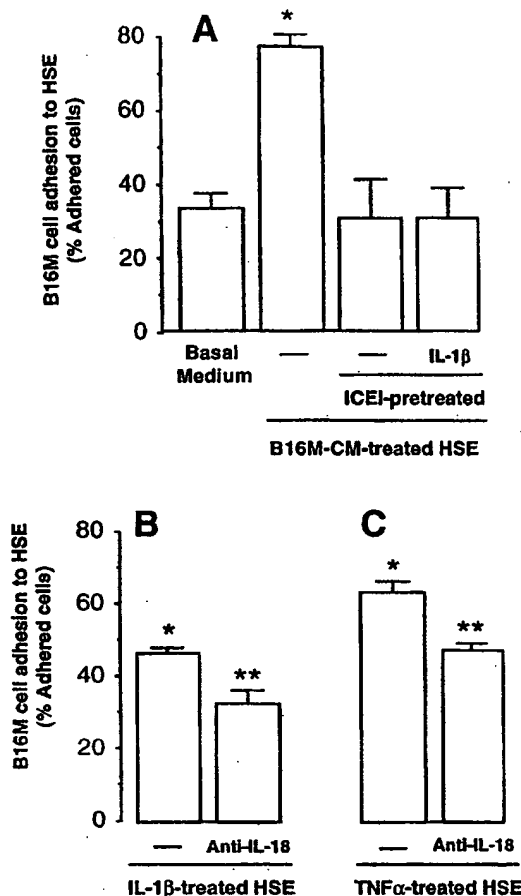


Fig. 3. B16M cell adhesion to cytokine-activated HSE. (A) HSE cells were incubated with basal medium or stimulated with B16M-CM for 8 h. ICEI (10 μ M) was added to some wells 18 h before stimulation with B16M-CM. Recombinant murine IL-1 β (1 ng/ml) was added together with B16M-CM. (B) The HSE was stimulated with 1 ng/ml murine IL-1 β for 6 h with and without antimurine IL-18 IgG (10 μ g/ml) added 1 h before the IL-1 β . (C) The HSE was stimulated with 100 pg/ml murine TNF- α for 6 h with and without antimurine IL-18 IgG (10 μ g/ml) added 1 h before the TNF- α . After each of the indicated incubation times, the adherence cell assay was performed as described in *Materials and Methods*. The results represent the means \pm SD of three separate experiments, each in six replicates ($n = 18$). Differences in the percent of adhering cells with respect to untreated HSE (*) and IL-1 β - or TNF- α -treated HSE (**) were statistically significant ($P < 0.01$) by the Student's two-tailed, unpaired t test.

kines, acting via the same or alternative pathways, are surely involved. In the present study, we have identified IL-18 as a proinflammatory cytokine with an unexpected pivotal position

Table 2. Inhibitory effect of IL-18BP on B16M-CM-induced adhesion of B16M melanoma cells to hepatic sinusoidal endothelial cells

| | % Melanoma cell adhesion* |
|------------------------------|---------------------------|
| Basal medium | 10.15 \pm 1.5 |
| B16M-CM | 35.10 \pm 4.4 |
| B16M-CM + IL-18BP (1 ng/ml) | 15.00 \pm 2.5* |
| B16M-CM + IL-18BP (10 ng/ml) | 8.70 \pm 1.1* |

*Means \pm SD of two independent experiments performed in six replicates ($n = 12$ for each condition).

* $P < 0.01$ with respect to B16-CM by ANOVA and the Scheffe F-test.

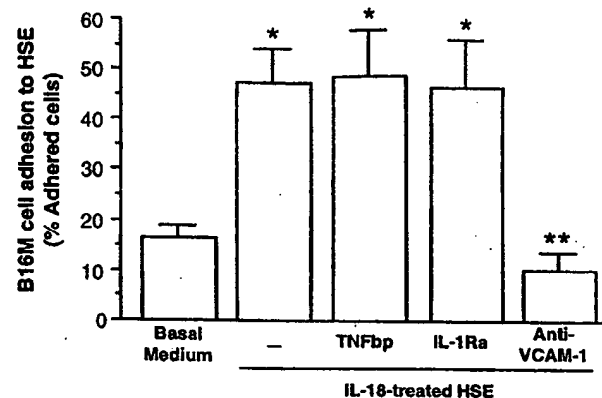


Fig. 4. Effect of anti-VCAM-1 on B16M cell adhesion to IL-18-treated HSE. HSE cells were incubated with 1 ng/ml recombinant murine IL-18 for 6 h. In some wells, 1 μ g/ml TNFbp or 100 ng/ml IL-1Ra were added 10 min before IL-18. In other wells, 10 μ g/ml anti-VCAM-1 antibody or 10 μ g/ml anti-mouse IgG was added to HSE cells 30 min before the B16M cell adhesion assay. The percent of adhering B16M cells was determined as described in *Materials and Methods*. The results represent the means \pm SD of three separate experiments, each in six replicates ($n = 18$). Differences in the percent of adhering cells with respect to basal medium-treated HSE (*) or IL-18-treated HSE (**) were statistically significant ($P < 0.01$ by the Student's two-tailed, unpaired t test).

in the cytokine hierarchy that functions to increase metastatic spread in this model. We show that hepatic metastasis of intrasplenically injected B16M cells is dramatically reduced in IL-1 β -/- and almost completely inhibited in ICE-/- mice. Splenic weights were not different, suggesting that the cytokine effects were at the level of hepatic implantation rather than on tumor growth at the injection site. Because ICE regulates the processing of both the IL-1 β as well as the IL-18 precursors into biologically active molecules, the ICE-/- mice represent a quasi double knock-out mutant.

Although the present data showing reduced hepatic metastases in IL-1 β -deficient mice confirm previous data demonstrating a role for IL-1 in hepatic spread of B16 (6, 34), those studies did not discriminate between a role for IL-1 α or IL-1 β . The present observation in IL-1 β -deficient mice demonstrates that IL-1 β and not IL-1 α participates in the metastatic process. In fact, others have shown that IL-1 α can protect against tumor growth (35). Similarly, IL-1 β and not IL-1 α is responsible for the development of the acute-phase response following turpentine-induced tissue damage and inflammation (36, 37).

From *in vitro* experiments, the data also indicate that the prometastatic effect of IL-18 depends on VCAM-1 expression, because VCAM-1 up-regulation accounts for all the adhesion-stimulating activity of B16M-CM-treated HSE. In this regard, preliminary studies by Western blot analysis confirm that recombinant murine IL-18 induces HSE expression of VCAM-1. In macrophagic cells, IL-18 increases expression of ICAM-1 (12). Thus, it is likely that IL-18-induced VCAM-1 expression itself can account for cancer cell adhesion to inflamed HSE and, hence, for inflammation-augmented hepatic metastases.

We also found that IL-18 neutralization did not reduce B16M-CM-induced TNF- α or IL-1 β release from HSE, suggesting that their production was IL-18 independent. Conversely, neither TNFbp nor IL-1Ra was able to inhibit the increase in adhesiveness in IL-18-treated HSE, confirming that neither endogenous TNF nor IL-1 accounted for IL-18-induced HSE adhesiveness. This is in contrast to the effect of IL-18 in human peripheral blood mononuclear cells where the primary target cell of IL-18 is the non-CD14 $^{+}$ T and natural killer cell (38). These cells express receptors for IL-18, which, after stimulation by

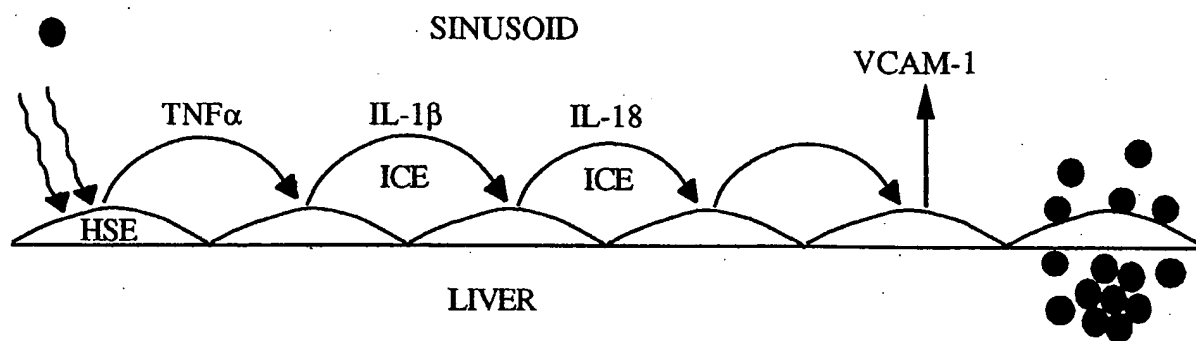


Fig. 5. Proposed mechanism for B16M adhesion to HSE. From left, melanoma cells (●) release a prometastatic substance(s) that increases TNF- α production in HSE. TNF- α in turn stimulates IL-1 β release via ICE and mature IL-1 β stimulates IL-18 release, also via an ICE-dependent pathway. Mature IL-18 induces VCAM-1, which facilitates the adhesion of melanoma cells to HSE.

IL-18, release TNF. However, in the case of more typical reticuloendothelial cells such as the HSE cell, IL-18 is downstream from IL-1 β and TNF. Thus, in HSE, a proinflammatory cytokine cascade exists in which TNF- α induces IL-1 β ; then, IL-1 β , either alone or with TNF- α , induces IL-18 release. As such, TNF- α and IL-1 β use the production of IL-18 to facilitate the increase in expression of VCAM-1 (Fig. 5).

Unlike murine HSE, B16M cells did not constitutively express IL-18 mRNA as determined by reverse transcription-PCR, and incubation with ICEi for 18 h did not abrogate cytokine- and adhesion-stimulating activities of B16M-CM on HSE (data not shown). Therefore, there is no IL-18 in the B16M-CM to account for these findings. However, local production of IL-18 by HSE may arrest B16M cells during transit through the hepatic microvasculature. Additional findings were that B16M cells incubated with 1 ng/ml murine IL-18 for 6 h increased their adhesion to untreated HSE by twofold and increased their proliferation, suggesting that very late antigen-4 interaction was involved (data not shown). These findings are also in agreement with the reduction in metastasis volume observed in IL-1 β ^{-/-} and ICE^{-/-} mice (Table 1).

The role of IL-18 as an IFN- γ -inducing factor in the present study remains unknown. Following intrasplenic injection of 3×10^5 viable B16M cells, there was no increase in circulating IL-1 β or IFN- γ in WT mice. However, IFN- γ plays both an agonist as well as an antagonist role in experimental models of various diseases (39). There is ample evidence that IFN- γ contributes to the immunostimulating, antitumor effects of several biological modifiers in murine cancer models. Indeed, the expression of mature IL-18 by genetically altered murine mammary carcinoma cells reduced the local growth of the tumor. This was caused by the production of IFN- γ (40). Because a reduction in IFN- γ production in ICE^{-/-} mice is likely and since neutralization of IL-18 *in vitro* contributes to the findings of the present study, the role of IFN- γ in this model must be one of proinflammatory and

not one of immunostimulation. IFN- γ is known to increase the expression of endothelial cell adhesion molecules.

IL-18BP is a unique, naturally occurring inhibitor of the biological activity of IL-18. IL-18BP resembles a soluble receptor for IL-18 but is unique in that it lacks a transmembrane and cytosolic domain (17). Recombinant IL-18BP completely reduced the adhesiveness of B16M-CM-stimulated HSE for melanoma cells, placing IL-18 in a strategic role for up-regulating the metastatic microenvironment of the liver sinusoids. IL-18BP is a constitutively expressed, circulating molecule but the levels of IL-18BP in patients with melanoma are presently unknown. Nevertheless, the balance between the naturally occurring agonist and antagonist may affect the outcome of melanoma implantation in the liver.

IL-18BP administration may also be useful in patients with melanoma or other cancer cells that employ VCAM-1-mediated adhesion to endothelia as a mechanism for invasion. However, IL-18 plays an essential role in regulating the production of the T-cell helper type 1 cytokine, IFN- γ . Several studies, in fact, show that administration of IFN- γ in various animal models of cancer growth serves to augment the immune response to the malignant cells. In fact, IL-18 has been used to increase the immune response against certain cancers in mice (41). Assuming the inhibition of IFN- γ production by IL-18BP does not impact on the immune response to the malignant cells, IL-18BP may be useful as adjuvant therapy in reducing adhesion of malignant cells to vascular endothelia, particularly in the liver.

We thank Interpharm Laboratories (Nes Ziona, Israel) for providing the IL-18BP. This work was supported in part by grants from the National Institutes of Health (AI-15614) and Colorado Cancer Center (CA-46934) to C.A.D., and by a grant from the National Institutes of Health (AI-2532359) to L.L.R. Grants from University of the Basque Country (EB214/95 and G17/98) and Comision Interministerial de Ciencia y Tecnologia (SAF99-0042) were to F.V.V. Fellowships from the Ministerio de Educación y Ciencia (Madrid) went to L.M., T.C., and M.A.A., and a fellowship from the University of the Basque Country was received by J.M.

- Nicolson, G. L. & Winkelhake, J. L. (1975) *Nature (London)* 255, 230-232.
- Rice, G. E. & Bevilacqua, M. P. (1989) *Science* 246, 1303-1306.
- Okahara, H., Yagita, H., Miyake, K. & Okumura, K. (1994) *Cancer Res.* 54, 3233-3236.
- Garofalo, A., Chirivì, R. G. S., Foglieni, C., Pigot, R., Mortarini, R., Martin-Padura, I., Anichini, A., Gearing, A. J., Sanchez-Madrid, F., Dejana, E., et al. (1995) *Cancer Res.* 55, 414-419.
- Vidal-Vanaclocha, F., Alvarez, A., Asumendi, A., Urcelay, B., Tonino, P. & Dinarello, C. A. (1996) *J. Natl. Cancer Inst.* 88, 198-205.
- Vidal-Vanaclocha, F., Amézaga, C., Asumendi, A., Kaplanski, G. & Dinarello, C. A. (1994) *Cancer Res.* 54, 2667-2672.
- Mendoza, L., Olaso, E., Anasagasti, M. J., Fuentes, A. & Vidal-Vanaclocha, F. (1998) *J. Cell. Physiol.* 174, 322-330.
- Anasagasti, M. J., Alvarez, A., Martín, J. J., Mendoza, L. & Vidal-Vanaclocha, F. (1997) *Hepatology* 25, 840-846.

- Gu, Y., Kuida, K., Tsutsui, H., Ku, G., Hsiao, K., Fleming, M. A., Hayashi, N., Higashino, K., Okamura, H., Nakanishi, K., et al. (1997) *Science* 275, 206-209.
- Ghayur, T., Banerjee, S., Hugunin, M., Butler, D., Herzog, L., Carter, A., Quintal, L., Sekut, L., Talanian, R., Paskind, M., et al. (1997) *Nature (London)* 386, 619-623.
- Dinarello, C. A. (1999) *J. Allergy Clin. Immunol.* 103, 11-24.
- Kohka, H., Yoshino, T., Iwagaki, H., Sakuma, I., Tanimoto, T., Matsuo, Y., Kurimoto, M., Orita, K., Akagi, T. & Tanaka, N. (1998) *J. Leukocyte Biol.* 64, 519-527.
- Nakamura, K., Okamura, H., Wada, M., Nagata, K. & Tamura, T. (1989) *Infect. Immun.* 57, 590-595.
- Okamura, H., Tsutsui, H., Komatsu, T., Yutsudo, M., Hakura, A., Tanimoto, J. M. (1997) *Hepatology* 25, 840-846.

- T., Torigoe, K., Okura, T., Nukada, Y., Hattori, K., *et al.* (1995) *Nature (London)* 378, 88–91.
15. Takeda, K., Tsutsui, H., Yoshimoto, T., Adachi, O., Yoshida, N., Kishimoto, K., Okamura, H., Nakanishi, K. & Akira, S. (1998) *Immunity* 8, 383–390.
16. Mendoza, L., Carrascal, T., Fuentes, A., Anasagasti, M. J., Martin, J. J., DeLuca, M., Dinarello, C. A. & Vidal-Vanaclocha, F. (1999) *Proc. Am. Assoc. Cancer Res.* 40, 449 (abstr.).
17. Novick, D., Kim, S.-H., Fantuzzi, G., Reznikov, L. L., Dinarello, C. A. & Rubinstein, M. (1999) *Immunity* 10, 127–136.
18. Engelmann, H., Novick, D. & Wallach, D. (1990) *J. Biol. Chem.* 265, 1531–1536.
19. Porat, R., Paddock, H. N., Schwaitzberg, S. D., Connolly, R. J., Wilkens, T., Dasch, J. R., Gascon, M.-P., Hutchison, J. S., Ythier, A., Wallach, D., *et al.* (1995) *Crit. Care Med.* 23, 1080–1089.
20. Puren, A. J., Fantuzzi, G. & Dinarello, C. A. (1999) *Proc. Natl. Acad. Sci. USA* 96, 2256–2261.
21. Vidal-Vanaclocha, F., Rocha, M., Asumendi, A. & Barbera-Guillem, E. (1993) *Hepatology* 18, 328–339.
22. Fantuzzi, G., Puren, A. J., Harding, M. W., Livingston, D. J. & Dinarello, C. A. (1998) *Blood* 91, 2118–2125.
23. Zheng, H., Fletcher, D., Kozak, W., Jiang, M., Hofmann, K., Conn, C. C., Siszynski, D., Grabcic, C., Trumbauer, M. A., Shaw, A. R., *et al.* (1995) *Immunity* 3, 9–19.
24. Kuida, K., Lippke, J. A., Ku, G., Harding, M. W., Livingston, D. J., Su, M. S.-S. & Flavell, R. A. (1995) *Science* 267, 2000–2003.
25. Kim, S.-H., Eisenstein, M., Reznikov, L. L., Fantuzzi, G., Novick, D., Rubinstein, M. & Dinarello, C. A. (2000) *Proc. Natl. Acad. Sci. USA*, in press.
26. Lauri, D., Bertomeu, M.-C. & Orr, F. W. (1990) *Clin. Exp. Metastasis* 8, 27–32.
27. Bani, M. R., Garofalo, A., Scanziani, E. & Giavazzi, R. (1991) *J. Natl. Cancer Inst.* 83, 119–123.
28. Bertomeu, M. C., Gallo, S., Lauri, D., Haas, T. A., Orr, F. W., Bastida, E. & Buchanan, M. R. (1993) *Clin. Exp. Metastasis* 11, 243–250.
29. Burrows, F. J., Haskard, D. O., Hart, I. R., Marshall, J. F., Selkirk, S., Poole, S. & Thorpe, P. E. (1991) *Cancer Res.* 51, 4768–4775.
30. Chirivì, R. G. S., Garofalo, A., Padura, I. M., Mantovani, A. & Giavazzi, R. (1993) *Cancer Res.* 53, 5051–5054.
31. Malik, S. T., Naylor, M. S., East, N., Oliff, A. & Balkwill, F. R. (1990) *Eur. J. Cancer* 26, 1031–1034.
32. Orosz, P., Echtenacher, B., Falk, W., Ruschoff, J., Weber, D. & Mannel, D. N. (1993) *J. Exp. Med.* 177, 1391–1398.
33. Orosz, P., Krüger, A., Hubbe, M., Rüschhoff, J., Von Hoegen, P. & Mannel, D. N. (1995) *Int. J. Cancer* 60, 867–871.
34. Vidal-Vanaclocha, F., Alvarez, A., Asumendi, A., Urcelay, B., Tonino, P. & Dinarello, C. A. (1996) *J. Natl. Cancer Inst.* 88, 198–205.
35. Voronov, E., Weinstein, Y., Benharroch, D., Cagnano, E., Ofir, R., Dobkin, M., White, R. M., Zoller, M., Barak, V., Segal, S., *et al.* (1999) *Cancer Res.* 59, 1029–1035.
36. Fantuzzi, G., Ku, G., Harding, M. W., Livingston, D. L., Sipe, J. D., Kuida, K., Flavell, R. A. & Dinarello, C. A. (1997) *J. Immunol.* 158, 1818–1824.
37. Horai, R., Asano, M., Sudo, K., Kanuka, H., Suzuki, M., Nishihara, M., Takahashi, M. & Iwakura, Y. (1998) *J. Exp. Med.* 187, 1463–1475.
38. Puren, A. J., Fantuzzi, G., Gu, Y., Su, M. S.-S. & Dinarello, C. A. (1998) *J. Clin. Invest.* 101, 711–724.
39. Froyen, G. & Billiau, F. (1997) *Biotherapy* 10, 49–57.
40. Coughlin, C. M., Salhany, K. E., Wysocka, M., Aruga, E., Kurzawa, H., Chang, A. E., Hunter, C. A., Fox, J. C., Trinchieri, G. & Lee, W. M. F. (1998) *J. Clin. Invest.* 101, 1441–1452.
41. Osaki, T., Peron, J. M., Cai, Q., Okamura, H., Robbins, P. D., Kurimoto, M., Lotze, M. T. & Tahara, H. (1998) *J. Immunol.* 160, 1742–1749.

Minocycline inhibits caspase-1 and caspase-3 expression and delays mortality in a transgenic mouse model of Huntington disease

MINGHUA CHEN¹, VICTOR O. ONA¹, MINGWEI LI¹, ROBERT J. FERRANTE^{2,3}, KLAUS B. FINK⁴, SHAN ZHU¹, JIE BIAN¹, LEI GUO⁵, LAURIE A. FARRELL⁶, STEVE M. HERSCH⁷, WENDY HOBBS⁸, JEAN-PAUL VONSATTEL⁸, JANG-HO J. CHA⁶ & ROBERT M. FRIEDLANDER¹

¹Neuroapoptosis Laboratory, Neurosurgical Service, Department of Surgery, Brigham and Women's Hospital, Harvard Medical School, Boston, Massachusetts 02115, USA

²Geriatric Research Education and Clinical Center, Bedford VA Medical Center, Bedford, Massachusetts and Boston University School of Medicine, Bedford, Massachusetts 01730, USA

³Neurology, Pathology, and Psychiatry Departments, Boston University School of Medicine, Boston, Massachusetts

⁴Department of Pharmacology, University of Bonn Medical School, Bonn, Germany.

⁵Department of Medicine, Brigham and Women's Hospital, Harvard Medical School, Boston, Massachusetts 02115, USA

⁶Department of Neurology, Massachusetts General Hospital, Harvard Medical School, Boston, Massachusetts 02114, USA

⁷Department of Neurology, Emory University School of Medicine, Atlanta Georgia 30322, USA

⁸Department of Neuropathology, Massachusetts General Hospital, Harvard Medical School, Boston, Massachusetts 02114, USA

Correspondence should be addressed to R.M.F.; email: rfriedlander@rics.bwh.harvard.edu

Huntington disease is an autosomal dominant neurodegenerative disease with no effective treatment. Minocycline is a tetracycline derivative with proven safety. After ischemia, minocycline inhibits caspase-1 and inducible nitric oxide synthetase upregulation, and reduces infarction. As caspase-1 and nitric oxide seem to play a role in Huntington disease, we evaluated the therapeutic efficacy of minocycline in the R6/2 mouse model of Huntington disease. We report that minocycline delays disease progression, inhibits caspase-1 and caspase-3 mRNA upregulation, and decreases inducible nitric oxide synthetase activity. In addition, effective pharmacotherapy in R6/2 mice requires caspase-1 and caspase-3 inhibition. This is the first demonstration of caspase-1 and caspase-3 transcriptional regulation in a Huntington disease model.

Despite significant advances in understanding the mechanistic pathways mediating progression of Huntington disease (HD) and cloning the mutant gene, effective pharmacotherapy remains elusive¹. HD is caused by a mutation consisting of an expanded CAG repeat in the 5' coding region of the huntingtin gene¹. Evidence points to the caspases as important mediators of apoptosis^{2,3}. We have demonstrated that caspase-1 is activated in brains of humans and mice with HD⁴. In addition, blocking caspase function either by expression of a caspase-1 dominant negative mutant, or by intracerebroventricular administration of a broad caspase inhibitor, delays disease onset and mortality in a transgenic HD mouse model⁴. Huntingtin is itself a substrate of caspase-1 and caspase-3^{5,6}. As evidence indicates a toxic gain of function of huntingtin cleavage fragments, these data provide a direct link between caspase-1 and caspase-3 and the mechanism of disease progression. However, unlike for caspase-1, direct *in vivo* evidence for a role of caspase-3 in HD has not been demonstrated.

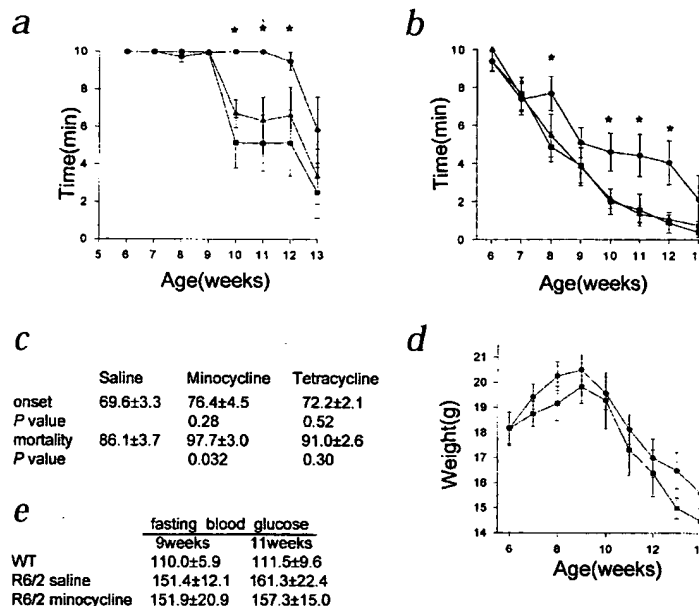
Minocycline is a second-generation tetracycline used in humans, which effectively crosses the blood-brain barrier⁷. After experimental ischemia, minocycline inhibits caspase-1 and inducible nitric oxide synthetase (iNOS) upregulation, and decreases infarct size^{8,9}. As a detrimental role for caspase-1 and iNOS

has been proposed in HD, we evaluated minocycline using the R6/2 HD mouse^{4,10,11}. We report that in R6/2 mice, minocycline delays disease progression and death, as well as inhibits caspase-1 and iNOS activation. In addition, we demonstrate that caspase-1 and caspase-3 gene expression are not only upregulated in this mouse model, but also are remarkably inhibited by minocycline. To provide further relevance to these findings we demonstrate elevated iNOS immunoreactivity in human HD striatum.

Minocycline slows progression and delays mortality in R6/2 mice

To evaluate a potential role for minocycline in HD, we used the R6/2 transgenic model¹². R6/2 mice express exon-1 of huntingtin with an expanded polyglutamine repeat under the control of its native promoter. R6/2 mice develop a progressive neurological phenotype with features of HD, neuronal intranuclear inclusions (NII), decreased neurotransmitter receptor binding and early mortality^{13,14}. At 6 weeks of age, we began daily minocycline administration. At this age, R6/2 mice are in the late presymptomatic stage, and early histopathology can be demonstrated^{12,14}. Minocycline significantly delayed the characteristic decline of Rotarod performance (Fig. 1a and b), and extended survival by 14% when compared to saline-treated mice (Fig. 1c). As a control, we evaluated whether tetracycline, which does not effectively

Fig. 1 Progression of disease in R6/2 mice is inhibited by minocycline. Mice were evaluated on the Rotarod at **a**, 5 and **b**, 15 rpm. Testing was terminated either when the mouse fell from the rod or at 10 min if it remained on the rod (minocycline = ● [*n* = 12], saline = ■ [*n* = 12] and tetracycline = ▲ [*n* = 6]). **c**, Onset and mortality in days are recorded as mean ± s.e.m. (minocycline [*n* = 7], saline [*n* = 7] and tetracycline [*n* = 6]). **d**, Body weight (minocycline = ●, saline = ■). **e**, Fasting blood glucose recorded as mean ± s.e.m. (R6/2 minocycline [*n* = 15], R6/2 saline [*n* = 15] and wild-type [*n* = 6]).



cross the blood-brain barrier, affected disease progression⁷. Tetracycline-treated mice did not demonstrate neuroprotection or significantly increased survival (Fig. 1a, b, and c). The characteristic weight loss and fasting blood glucose elevation observed in R6/2 mice were not altered by minocycline (Fig. 1d and e). Lack of protection by tetracycline, and lack of alteration of the systemic phenotype (that is, weight and blood glucose), indicate that the protective effect of minocycline does not result from a systemic effect, but rather from direct action on the brain.

Caspase-1 is inhibited in minocycline-treated R6/2 mice

Caspase-1 is activated in brains of humans with HD and of R6/2 mice, and caspase-1 inhibition correlates with increased survival in mice⁴. As caspase-1 is required in mice for processing of pro-interleukin-1 β (pro-IL-1 β), measurements of mature IL-1 β provide direct evidence of caspase-1 activation^{4,15-18}. Mature IL-1 β levels in brains of minocycline-treated mice were 43.1% lower than in saline-treated mice, demonstrating that minocycline inhibited caspase-1 activation (Fig. 2a). As huntingtin is cleaved *in vitro* by caspase-1 and caspase-3, and caspase inhibition blocks cleavage of endogenous huntingtin in R6/2 mice, we evaluated whether minocycline would inhibit endogenous huntingtin cleavage⁴⁻⁶. We reported that endogenous huntingtin is cleaved in brain samples of 9-week-old R6/2 mice and not in samples from wild-type littermates⁴. Generation of the endogenous huntingtin cleavage fragment is significantly inhibited in nine-week old minocycline-treated R6/2 mice (Fig. 2b). As huntingtin is important for normal development, depleting endogenous huntingtin likely has a detrimental role on cellular homeostasis¹⁹.

Minocycline does not affect NII formation or receptor-binding

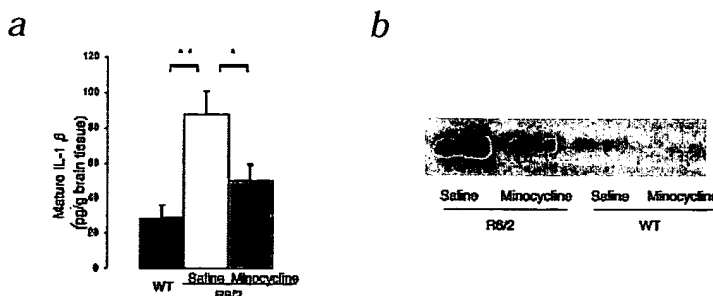
Similar to humans with HD, R6/2 mice develop NII and a progressive decrease in neurotransmitter receptor binding^{4,13,14,20}. Minocycline treatment did not inhibit the formation of NII or the decrease of adenosine A2a, forskolin, dopamine D1 and dopamine D2 neurotransmitter receptor binding in nine-week old R6/2 (data not shown). These results indicate that minocycline-mediated

neuroprotection is not related to the effect that NII or decrease in neurotransmitter receptor binding have on the disease. We demonstrated a delay of NII formation and neuroreceptor down-regulation in R6/2 mice mediated by expression of the caspase-1 dominant negative transgene⁴. NII are detected in R6/2 mice as early as three weeks of age (R.J.F., unpublished data). NII detection is delayed by the caspase-1 dominant negative transgene, and, as expression of this transgene is detected during embryogenesis, it indicates that an early caspase-dependent pathway is required for the initial formation of the NII²¹. This caspase-dependent step may be cleavage of full-length huntingtin and, thereafter, aggregation of the mutant huntingtin fragment for generation of NII. Once NII begins to form, then their growth in R6/2 mice is caspase-independent, as the transgene fragment does not require, as well as lacks sites for, caspase cleavage. Minocycline probably did not inhibit NII formation, as it was administered after the caspase-dependent step of NII generation at 6 weeks of age.

Minocycline inhibits iNOS activation in R6/2 mice

Elevated iNOS expression has been demonstrated in R6/2 mice resulting in pathologic protein nitration¹⁰. As in brains of R6/2 mice, human HD brains also demonstrate elevated iNOS expression when compared with normal age-matched controls (Fig. 3a and b). Marked increased iNOS immunoreactivity is present in glial, neuronal and vascular elements of HD striatum. Elevation

Fig. 2 Minocycline inhibits caspase-1 activation as well as endogenous huntingtin cleavage in R6/2 mice. **a**, Mature IL-1 β levels in 12-week-old mice (*n* = 7-9/group). Error bars indicate SEM * *P* < 0.05, ** *P* < 0.01. **b**, Cleavage of endogenous huntingtin in 9-week-old R6/2 mice is inhibited by minocycline. A large N-terminal cleavage fragment (approx. 210 kDa) was observed in lysates from R6/2 mice using an antibody directed against amino acids 181-810 of mouse huntingtin (results are representative of 5 mice/group).



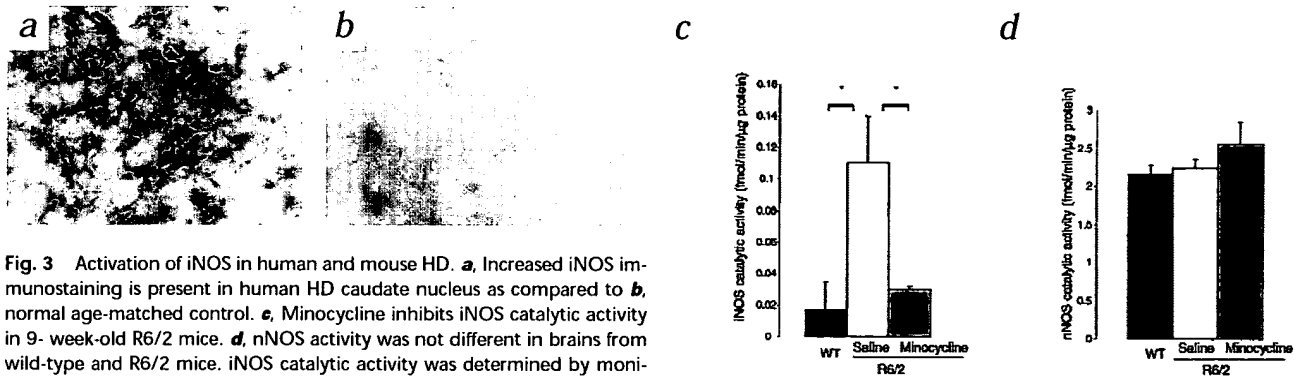


Fig. 3 Activation of iNOS in human and mouse HD. **a**, Increased iNOS immunostaining is present in human HD caudate nucleus as compared to **b**, normal age-matched control. **c**, Minocycline inhibits iNOS catalytic activity in 9-week-old R6/2 mice. **d**, nNOS activity was not different in brains from wild-type and R6/2 mice. iNOS catalytic activity was determined by monitoring the conversion of [3 H]arginine to [3 H]citrulline in brain homogenates in Ca^{2+} -free medium. $n = 5/\text{group}$; Saline = saline-treated R6/2 mice; minocycline = minocycline-treated R6/2 mice; WT = wild-type mice.

of brain iNOS immunoreactivity in humans with HD and in R6/2 mice provides further validation for this transgenic model as relevant to the human disease. As minocycline inhibits cerebral ischemia-mediated iNOS upregulation, its effect on catalytic iNOS activity in brains of R6/2 mice was evaluated. Ca^{2+} -independent NOS activity, representing iNOS activity, was elevated 6.5-fold in R6/2 mice when compared with wild-type mice. Minocycline treatment resulted in a 72% inhibition of iNOS activity in brains of R6/2 mice when compared to saline-treated controls (Fig. 3c). Constitutive Ca^{2+} -dependent NOS activity, representing nNOS activity, was not different in brains from wild-type or saline- and minocycline-treated mice R6/2 mice (Fig. 3d). These results indi-

cate that minocycline-mediated neuroprotection results in part from inhibition of iNOS activity, likely resulting in decreased free-radical damage.

Minocycline inhibits caspase-1 and -3 upregulation in R6/2 mice

We then evaluated whether transcription of caspase-1 and caspase-3 were regulated in R6/2 mice. Using RT-PCR we detected a peak of caspase-1 mRNA elevation at 7 weeks of age, which was 2.1-fold higher than wild-type levels (Fig. 4a). Thereafter, caspase-1 mRNA levels remained stably elevated throughout the disease. Caspase-3 mRNA elevation began 2 weeks after caspase-1 at 9 weeks, being 3.6-fold of wild-type levels, and peaking at 5.5-fold at

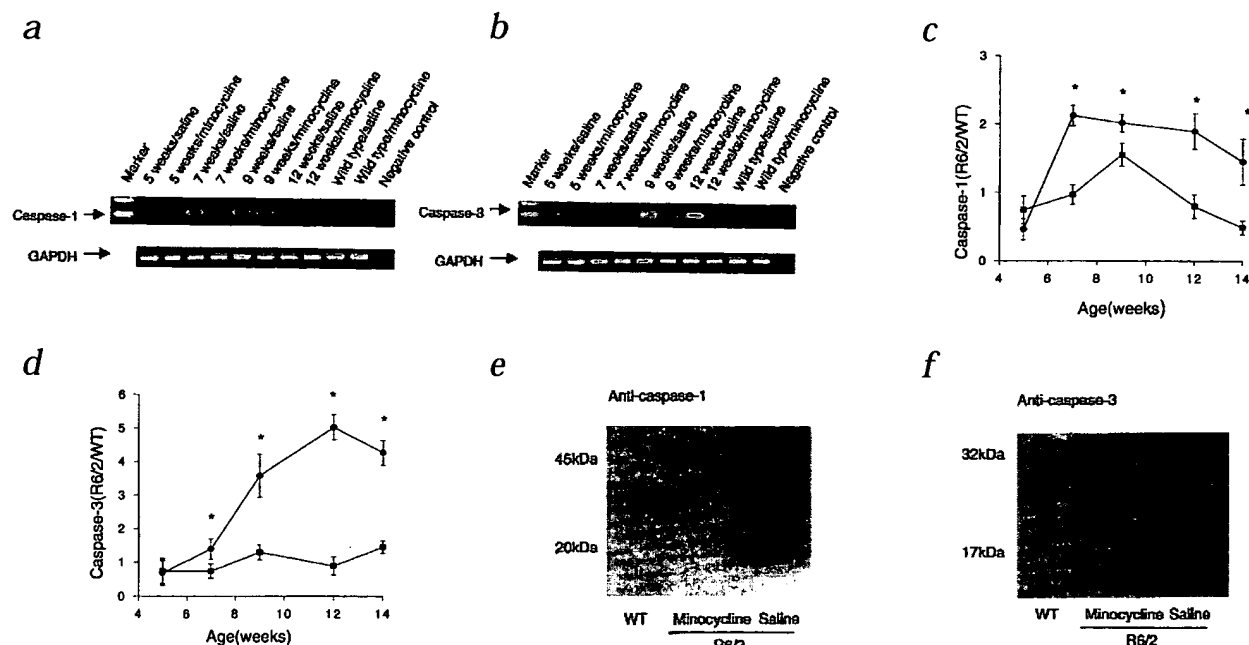


Fig. 4 Minocycline inhibits caspase-1 and caspase-3 expression. Ethidium bromide-stained gels of RT-PCR analysis of caspase-1 **a**, and caspase-3 **b**, mRNA run in parallel with GAPDH mRNA. Time-dependent upregulation of caspase-1 **c**, and caspase-3 **d**, mRNA expression in R6/2 mice, compared with age-matched wild-type mice. Caspase levels represent the ratio of the caspase/GAPDH signal. Samples were amplified and run in parallel. Saline = \bullet ; Minocycline = \blacksquare . Error bars indicate SEM, * $P <$

0.05, $n = 5/\text{group}$. Caspase-1 (**e**) and caspase-3 (**f**) Western blot analysis of 12-week-old wild-type and R6/2 mouse brain lysates. R6/2 mice show a minocycline-sensitive increase in activated caspase-1 (p20) and activated caspase-3 (p17) subunits. There is faint pro-caspase-1 (p45) band in saline-treated brain lysates of R6/2 mice. As with RT-PCR results, there is increased amount of pro-caspase-3 (p32) in the R6/2 samples. Each lane 50 μg protein.

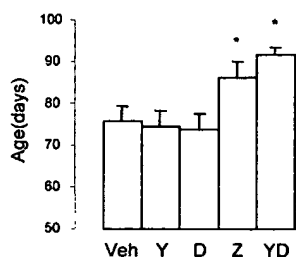


Fig. 5 Caspase-1 and caspase-3 inhibition are required to delay mortality of R6/2 mice. Beginning at 7 weeks of age, caspase inhibitors were intracerebroventricularly administered for 4 weeks in R6/2 mice. Veh = vehicle ($n = 13$); Y = YVAD-cmk ($n = 6$); D = DEVD-fmk ($n = 8$); Z = zVAD ($n = 15$); YD = combined YVAD-cmk and DEVD-fmk ($n = 5$). * $P < 0.05$.

12 weeks of age (Fig. 4b). Unlike caspase-1, caspase-3 mRNA elevation was progressive throughout the disease. These results are consistent with *in vitro* evidence demonstrating early caspase-1 and delayed caspase-3 activation during apoptosis²². Similarly, in a mouse model of amyotrophic lateral sclerosis, caspase-1 mRNA is elevated before caspase-3 mRNA²³. Caspase-1 and caspase-3 mRNA elevation in R6/2 mice were remarkably inhibited in minocycline-treated mice (Fig. 4c and d). Despite almost complete inhibition of elevation of caspase-3 mRNA, the disease continues to progress likely due to the less thorough caspase-1 inhibition, as well as due to additional cell death mediators. By western blot we confirmed a minocycline-sensitive elevation of caspase-1 and caspase-3 protein, in particular, elevation of activated subunits in brain lysates of 12-week old R6/2 mice (Fig. 4e and f). Fluorogenic caspase-1 and caspase-3 assays were done using HeLa cell-free extracts to rule out a direct enzymatic effect of minocycline. Caspase-1 and caspase-3 activities were not directly inhibited by minocycline (data not shown). As a control, it was evaluated whether minocycline inhibited expression of the R6/2 transgene. RT-PCR demonstrated that minocycline did not alter R6/2 transgene expression (data not shown).

Inhibition of both caspase-1 and -3 required for neuroprotection

So that the specific functional contribution of caspase-1 and caspase-3 to disease progression could be evaluated, R6/2 mice were treated with intracerebroventricular administration of either zVAD-fmk (Val-Ala-Asp-fluoromethyl ketone) (a broad caspase inhibitor), Tyr-Val-Ala-Asp-chloromethylketone (YVAD-cmk [a caspase-1-like inhibitor]), Asp-Glu-Val-Asp-aldehyde-fmk (DEVD-fmk, a caspase-3-like inhibitor), or with a combination of YVAD-cmk and DEVD-fmk. As we reported, zVAD-fmk extended survival of R6/2 mice⁴. Neither YVAD-cmk nor DEVD-fmk demonstrated neuroprotection. However, the combination of YVAD-cmk and DEVD-fmk resulted in improved Rotarod performance and significantly extended survival comparable to zVAD-fmk treated mice (17.3% and 12.2% respectively) when compared to vehicle-treatment (Fig. 5). To rule out that neuroprotection mediated by the combination of YVAD-cmk and DEVD-fmk is not a result of simply doubling the dose of caspase inhibitors, we independently evaluated higher doses of YVAD-cmk and DEVD-fmk. Higher concentrations of YVAD-cmk or DEVD-fmk were toxic causing earlier death than in vehicle-treated mice (data not shown). As caspase-1 and caspase-3 are upregulated, and their combined inhibition is required for therapeutic efficacy, effective therapy for HD (and likely other chronic neurodegenerative dis-

eases) may ultimately require inhibition of both caspase-1 and caspase-3. However, as YVAD-cmk and DEVD-fmk inhibit caspases in addition to caspase-1 and caspase-3, albeit with lower affinities, we can not rule out that the neuroprotection mediated by these drugs might result from inhibiting other caspases in addition to caspase-1 and caspase-3.

Discussion

It is demonstrated for the first time in R6/2 mice that caspase-1 and caspase-3 are transcriptionally regulated. As caspase expression in HD is regulated rather than constitutive, caspase transcriptional modulation provides a new target for therapeutic manipulation. The mechanism of mutant huntingtin-mediated toxicity is at present not clearly understood. A role for mitochondrial dysfunction and toxic nitric oxide metabolites have been proposed^{10,11,24,25}. Beginning in the late presymptomatic stage of the disease mutant huntingtin-mediated intracellular toxicity induces caspase-1 upregulation and activation, resulting in mature IL-1 β production. As disease progresses, caspase-3 is upregulated, further exacerbating toxicity. Interestingly, caspase-1 activates caspase-3 *in vitro*²⁶. The early upregulation of caspase-1 with respect to caspase-3 provides evidence that caspase-1 is not merely an inflammatory mediator, but rather an important early trigger of the apoptotic cascade. Minocycline inhibits caspase-1 and caspase-3 upregulation, although the later more thoroughly. As caspase-1 and caspase-3 are upregulated, an effective therapeutic intervention in HD will likely require inhibition of at least both of these caspases. Our data are consistent with a detrimental role of iNOS in HD. Minocycline has been used in humans for extended periods of time with relatively few side effects^{27,28}. With the described results, and with the relatively low toxicity, minocycline represents a new potential therapeutic agent for the treatment of HD.

Methods

Mice and treatment regimen. R6/2 mice (Jackson Laboratories, Bar Harbor, Maine) were randomly assigned to three groups. At 6 weeks of age, mice were treated with daily intraperitoneal injections of either saline, minocycline hydrochloride (5 mg/kg, Sigma, St. Louis, Missouri), or with tetracycline hydrochloride (5 mg/kg, Sigma) in 0.5 ml of saline. Experiments were in accordance with protocols approved by the Harvard Medical School Animal Care Committee.

Mature IL-1 β determination. Mature IL-1 β quantification was done as described using an enzyme-linked immunosorbent assay kit specific for the mature form of the cytokine (R&D Systems, Minneapolis, Minnesota)¹⁸.

Assay of NOS catalytic activity. NOS activity was measured by conversion of L-[³H] arginine to [³H]citrulline as described by Bredt and Snyder²⁹ and Yoshida *et al.*³⁰ with modifications. Brain samples were homogenized in 10 vol Tris buffer (25 mM; pH 7.4; 4 °C) containing 1 mM ethylenediaminetetraacetic acid and 1 mM ethyleneglucoctetraacetic acid and centrifuged (20,000g for 5 min at 4 °C). For total NOS or iNOS activity, 10 μ l aliquots of the supernatant were incubated with or without 0.6 mM Ca²⁺, respectively, in 25 mM Tris (pH 7.4), 3 μ M tetrahydrobiopterin, 1 μ M flavin mononucleotide, 1 μ M flavin adenine dinucleotide, 1 mM nicotinamide adenine dinucleotide phosphate, 0.1 μ M calmodulin and 22 μ M L-[2,3,4-³H] arginine (specific activity 45.2 Ci/mmol; NEN, Boston, Massachusetts) for 15 min at 37 °C. The assays were terminated by addition of 400 μ l N-(2-hydroxyethyl)piperazine-N'-2-ethanesulfonic acid buffer (50 mM; pH 5.5; 4 °C) containing 5 mM ethylenediaminetetraacetic acid and 1 mM ethyleneglucoctetraacetic acid and centrifuged (20,000g, applied to 100 μ l Dowex AG50WX-8 resin (Na⁺ form; Bio-Rad, Hercules, California) in spin cups (Sigma, St. Louis, Missouri) and centrifuged (20,000g for 30 s at 4 °C). [³H]citrulline was quantitated by liquid scintillation counting of the eluate

(LS 6000; Beckman Instruments, Palo Alto, California). Protein concentration in the reaction mix was measured with a Bio-Rad assay.

Histochemical staining. Human postmortem striatal tissue specimens from 6 HD (grades 3 and 4; mean age, 64.8 yr; range, 54–73 yr) and 6 neurologic age-matched controls (mean age, 67.5; range 58–76) were dissected fresh and placed in cold (4 °C) 2% paraformaldehyde-lysine-periodate solution for 24–36 h. Brain tissue specimens were received from the Bedford VA Medical Center Brain Tissue Archive (Bedford, Massachusetts). The post-mortem intervals did not exceed 18 h (mean time, 8.3 h; range, 4–18 h). Each HD patient had been clinically diagnosed based upon known family history and phenotypic symptoms of HD. The diagnosis of HD was confirmed by neuropathologic examination and graded by severity. Tissue blocks were rinsed in 0.1 M sodium phosphate buffer and placed in cold cryoprotectant in increasing concentrations of 10% and 20% glycerol/2% dimethyl sulfoxide solution over 36 h. Frozen serial sections of the striatal tissue block were cut at 50 µm intervals in the coronal plane. The cut sections were stored in 0.1 M sodium phosphate buffer/0.08% sodium azide at 4 °C and subsequently immunostained for iNOS (Upstate, dilution 1:500) using the conjugated second antibody method³¹.

Western blot. Huntingtin western blot accomplished as described using an antibody (MAB2166) raised against a mouse huntingtin fusion protein (amino acids 181–810)(Chemicon, Temecula, California) ⁴. Antibodies for caspase western blots were purchased from Santa Cruz (Santa Cruz, California).

Reverse transcription-polymerase chain reaction (RT-PCR). Total RNA from the brains of R6/2 and wild-type mice was prepared using TRIZOL Reagent (Gibco-BRL, Grand Island, New York) according to the manufacturer's instructions. RNA concentration and purity were determined by measuring the absorbance at 260 and 280 nm, respectively. First-strand cDNA was synthesized from total RNA using the Superscript Preamplification system with Superscript II RNase H-reverse transcriptase (Gibco-BRL) according to the manufacturer's instructions. Then 1 µl of cDNA template was amplified by PCR in 20 µl of total reaction volume containing 18 µl of Supremix (Gibco-BRL) and 4–10 pmol of each specific primer. Caspase-1 primer sequences were 5'-TGGTCTGTGACTGGAGGA-3'(forward) and 5'-TG-GCTTCTTATTGGCAGAT-3' (reverse). Caspase-3 primer sequences were 5'-TGTCATCTCGCTCTGGTACG-3' (forward) and 5'-AAATGACCCCTTCAT-CACCA-3' (reverse). As an internal control, glyceraldehyde-3-phosphate-dehydrogenase (GAPDH) was amplified using primer sequences 5'-AACCTTGGCATTGTGGAAGG-3' (forward) and 5'-GGAGACAACCTGGTC-CTCAG-3' (reverse). GAPDH levels were not altered in R6/2 mice when compared to the wild-type controls. Each PCR cycle consisted of 45 s at 94 °C, 45 s at 60 °C and 1 min at 72 °C. PCR amplification was carried out for 30 cycles for caspase-1, 35 cycles for caspase-3 and 28 cycles for GAPDH. Using these protocols DNA amplification was within its linear range. After amplification, the products were separated in a 1.5% agarose gel containing 0.03% ethidium bromide. The PCR results were analyzed by using a Bio-Rad Imaging Densitometer Quantity One-4.1.0 (Bio-Rad, Hercules, California)

Rotarod test. Motor performance was evaluated weekly from 5 to 13 weeks on a Rotarod (Columbus Instruments, Columbus, Ohio), at 5 and 15 rpm. If the mouse remained on the rod for 10 min the test was completed and scored as 10 min.

Placement of osmotic pumps. Pumps were inserted at 7 weeks of age as described by Ona *et al.*⁴. Concentrations were for zVAD-fmk 100 µg/20 g body weight/28 d, for YVAD-cmk and DEVD-fmk 50 µg/20 g body weight/28 d for the low dose, and 100 µg/20 g body weight/28 d for the high dose. Combined YVAD-cmk and DEVD-fmk were used at 50 µg/20 g body weight/28 d each.

Data analysis. Data are presented as mean ± standard error of the mean (SEM). Statistical comparisons were made by Student's *t*-test.

Acknowledgments

The authors thank E. Friedlander for editorial assistance. This work was

supported by a grant from the Hereditary Disease Foundation (to R.M.F. and J.H.J.C.), the Huntington Disease Society of America (to R.M.F. and J.H.J.C.), the National Institutes of Health (to R.M.F., J.H.J.C., R.J.F. and S.M.H.) and the Veterans Administration (R.J.F.). R.M.F. is a member of the Cure Huntington's Disease Initiative of the Hereditary Disease Foundation and of the Coalition for the Cure from the Huntington's Disease Society of America.

RECEIVED 7 MARCH; ACCEPTED 12 MAY 2000

1. The Huntington's Disease Collaborative Research Group. A novel gene containing a trinucleotide repeat that is expanded and unstable on Huntington's disease chromosomes. *Cell* **72**, 971–983 (1993).
2. Alnemri, E.S. *et al.* Human ICE/CED-3 protease nomenclature. *Cell* **87**, 171 (1996).
3. Friedlander, R.M. & Yuan, J. ICE, neuronal apoptosis and neurodegeneration. *Cell Death Differ.* **5**, 823–831 (1998).
4. Ona, V.O. *et al.* Inhibition of caspase-1 slows disease progression in a mouse model of Huntington's disease. *Nature* **399**, 263–267 (1999).
5. Goldberg, Y.P. *et al.* Cleavage of huntingtin by apoptosis, a proapoptotic cysteine protease, is modulated by the polyglutamine tract. *Nature Genet.* **13**, 442–449 (1996).
6. Wellington, C.L. *et al.* Caspase cleavage of gene products associated with triplet expansion disorders generates truncated fragments containing the polyglutamine tract. *J. Biol. Chem.* **273**, 9158–9167 (1998).
7. Aronson, A.L. Pharmacotherapeutics of the newer tetracyclines. *J. Am. Vet. Med. Assoc.* **176**, 1061–1068 (1980).
8. Yrjanheikki, J., Keinanen, R., Pellikka, M., Hokfelt, T. & Koistinaho, J. Tetracyclines inhibit microglial activation and are neuroprotective in global brain ischemia. *Proc. Natl. Acad. Sci. USA* **95**, 15769–15774 (1998).
9. Yrjanheikki, J. *et al.* A tetracycline derivative, minocycline, reduces inflammation and protects against focal cerebral ischemia with a wide therapeutic window. *Proc. Natl. Acad. Sci. USA* **96**, 13496–13500 (1999).
10. Tabrizi, S.J. *et al.* Mitochondrial dysfunction and free radical damage in the Huntington R6/2 transgenic mouse. *Ann. Neurol.* **47**, 80–86 (2000).
11. Tabrizi, S.J. *et al.* Biochemical abnormalities and excitotoxicity in Huntington's disease brain. *Ann. Neurol.* **45**, 25–32 (1999).
12. Mangiarini, L. *et al.* Exon 1 of the HD gene with an expanded CAG repeat is sufficient to cause a progressive neurological phenotype in transgenic mice. *Cell* **87**, 493–506 (1996).
13. Davies, S.W. *et al.* Formation of neuronal intranuclear inclusions underlies the neurological dysfunction in mice transgenic for the HD mutation. *Cell* **90**, 537–548 (1997).
14. Cha, J.H. *et al.* Altered brain neurotransmitter receptors in transgenic mice expressing a portion of an abnormal human huntington disease gene. *Proc. Natl. Acad. Sci. USA* **95**, 6480–6485 (1998).
15. Li, P. *et al.* Mice deficient in IL-1 beta-converting enzyme are defective in production of mature IL-1 beta and resistant to endotoxic shock. *Cell* **80**, 401–411 (1995).
16. Kuida, K. *et al.* Altered cytokine export and apoptosis in mice deficient in interleukin-1 beta converting enzyme. *Science* **267**, 2000–2003 (1995).
17. Friedlander, R.M. *et al.* Expression of a dominant negative mutant of interleukin-1 beta converting enzyme in transgenic mice prevents neuronal cell death induced by trophic factor withdrawal and ischemic brain injury. *J. Exp. Med.* **185**, 933–940 (1997).
18. Hara, H. *et al.* Inhibition of interleukin 1beta converting enzyme family proteases reduces ischemic and excitotoxic neuronal damage. *Proc. Natl. Acad. Sci. USA* **94**, 2007–2012 (1997).
19. White, J.K. *et al.* Huntingtin is required for neurogenesis and is not impaired by the Huntington's disease CAG expansion. *Nature Genet.* **17**, 404–410 (1997).
20. DiFiglia, M. *et al.* Aggregation of huntingtin in neuronal intranuclear inclusions and dystrophic neurites in brain. *Science* **277**, 1990–1993 (1997).
21. Forss-Petter, S. *et al.* Transgenic mice expressing beta-galactosidase in mature neurons under neuron-specific enolase promoter control. *Neuron* **5**, 187–197 (1990).
22. Enari, M., Talianian, R.V., Wong, W.W. & Nagata, S. Sequential activation of ICE-like and CPP32-like proteases during Fas-mediated apoptosis. *Nature* **380**, 723–736 (1996).
23. Li, M. *et al.* Functional role of caspase-1 and caspase-3 in an ALS transgenic mouse model. *Science* **288**, 335–339 (2000).
24. Browne, S.E. *et al.* Oxidative damage and metabolic dysfunction in Huntington's disease: selective vulnerability of the basal ganglia. *Ann. Neurol.* **41**, 646–653 (1997).
25. Schapira, A.H. Mitochondrial dysfunction in neurodegenerative disorders. *Biochim. Biophys. Acta* **1366**, 225–233 (1998).
26. Tewari, M. *et al.* Yama/CPP32 beta, a mammalian homolog of CED-3, is a CrmA-inhibitable protease that cleaves the death substrate poly(ADP-ribose) polymerase. *Cell* **81**, 801–809 (1995).
27. Goulden, V., Glass, D. & Cunliffe, W.J. Safety of long-term high-dose minocycline in the treatment of acne. *Br. J. Dermatol.* **134**, 693–695 (1996).
28. Gottlieb, A. Safety of minocycline for acne. *Lancet* **349**, 374 (1997).
29. Bredt, D.S. & Snyder, S.H. Isolation of nitric oxide synthetase, a calmodulin-requiring enzyme. *Proc. Natl. Acad. Sci. USA* **87**, 682–685 (1990).
30. Yoshida, T., Waeber, C., Huang, Z. & Moskowitz, M.A. Induction of nitric oxide synthase activity in rodent brain following middle cerebral artery occlusion. *Neurosci. Lett.* **194**, 214–218 (1995).
31. Ferrante, R.J. *et al.* Heterogeneous topographic and cellular distribution of huntingtin expression in the normal human neostriatum. *J. Neurosci.* **17**, 3052–3063 (1997).

Androgen induced cell death in SHSY5Y neuroblastoma cells expressing wild-type and spinal bulbar muscular atrophy mutant androgen receptors

Andrew J. Grierson, Christopher E. Shaw, Christopher C.J. Miller *

Departments of Neuroscience and Neurology, Institute of Psychiatry, De Crespigny Park, Denmark Hill, London SE5 8AF, UK

Received 14 September 2000; received in revised form 23 January 2001; accepted 31 January 2001

Abstract

Spinal bulbar muscular atrophy (SBMA) is one of a family of inherited neurodegenerative diseases caused by expansion of CAG encoding polyglutamine repeats; in SBMA the affected gene is the androgen receptor. To understand further the mechanisms that lead to neuronal cell death in SBMA, we generated SHSY5Y neuroblastoma cell lines that stably express identical levels of wild-type (19 polyglutamine repeat) or SBMA (52 polyglutamine repeat) androgen receptor. Parental SHSY5Y cells do not express detectable levels of the androgen receptor. In the absence of androgen, the transfected cell lines have similar phenotypes and growth characteristics to parental SHSY5Y cells. However, upon treatment with androgen, both cell lines undergo a marked dose-dependent loss of viability; this loss was significantly greater in cells expressing the SBMA receptor. Morphological analyses of the androgen treated cells revealed that cell death bore hallmarks of apoptosis involving altered nuclear morphology and cleavage of poly(ADP-ribose) polymerase and of caspase 3 in both wild-type and SBMA cell lines. The caspase inhibitor VAD-fmk was able to decrease loss of viability of both cell lines on exposure to androgen. © 2001 Elsevier Science B.V. All rights reserved.

Keywords: Kennedy's disease; Apoptosis; Polyglutamine; CAG repeat

1. Introduction

Spinal bulbar muscular atrophy (SBMA), also known as Kennedy's disease, is an adult onset genetic form of motor neurone disease that is caused by mutations in the androgen receptor gene [1]. The mutations involve expansion of a polymorphic CAG repeat that encodes a polyglutamine tract located towards the amino terminus of the androgen receptor. In the normal population, this polyglutamine tract varies between approx. 11 and 33 repeats

with a modal length of about 20 [2,3]; expansion of the repeat to beyond approx. 40 causes disease [1].

SBMA is one of a group of inherited neurodegenerative diseases that are caused by expansion of CAG encoding polyglutamine repeats and which include Huntington's disease [4], dentatorubralpallidoluysian atrophy (DRPLA) [5,6] and the spinocerebellar ataxias [7–13]. The molecular mechanisms by which expansion of polyglutamine tracts cause neuronal cell death in these disorders are not understood although favoured hypotheses are that the expansion causes a gain of toxic function(s). Indeed, expanded polyglutamine tracts have been shown to be toxic in both cultured cells and transgenic mice [14–16].

A further complication to our understanding of the mechanism of cell death in these polyglutamine

* Corresponding author. Fax: +44-207-708-0017;
E-mail: chris.miller@iop.kcl.ac.uk

disorders is that the normal function of most of the polyglutamine containing proteins are not known. However, this is not the case for SBMA; the androgen receptor belongs to the nuclear receptor superfamily and mediates the effects of androgens (see for review [17]). In common with other members of this family, the androgen receptor comprises a carboxy-terminal ligand binding domain which binds androgens, a conserved centrally located DNA binding domain that interacts with androgen response elements in androgen-responsive genes, and an amino-terminal transactivation domain. The polyglutamine tract is located within the transactivation domain and its expansion is now known to inhibit androgen receptor function [18–20] and also to influence its interactions with other transcription factors and activators [21,22]. Decreased receptor function probably accounts for the partial androgen insensitivity that is a further common phenotype of SBMA [23].

The mechanism(s) by which the SBMA receptor causes motor neurone cell death is far from clear (see Section 4). However, one suggestion is that polyglutamine expansion causes altered expression of androgen receptor regulated genes and that this contributes to SBMA [18–22,24,25]. As such, modulating androgen receptor function might be therapeutic for SBMA although it is not clear whether treatment with androgens or anti-androgens would be beneficial. In order to understand more fully how androgens can influence neuronal cell survival, we created SHSY5Y neuroblastoma cells that stably express wild-type (19 polyglutamines) or SBMA (52 polyglutamines) androgen receptor. We find that androgen stimulation of these cells induces a marked loss of viability.

2. Materials and methods

2.1. Plasmids and SHSY5Y cell culture and transfection

Expression vectors for human androgen receptors harbouring 19 and 52 CAG repeats in pCMVneo were as described [24]. SHSY5Y cells were routinely cultured in DMEM/F12 mix containing 10% (v/v) charcoal stripped foetal calf serum supplemented with 2 mM glutamine, 100 IU ml⁻¹ penicillin and

100 µg ml⁻¹ streptomycin (Life Technologies). For transfection, cells were plated onto 100 mm diameter dishes and transfected using a Profection CaPO₄ transfection kit (Promega) according to the manufacturer's instructions. Plasmids were linearised prior to transfection with *Xba*I. 48 h post transfection, the medium was replaced with selection medium (as above, containing 600 µg ml⁻¹ Genetecin (Life Technologies)), and colonies picked and expanded 2–3 weeks later [26]. Thereafter, cells were maintained in medium containing 300 µg ml⁻¹ Genetecin.

Testosterone was obtained from Sigma, the non-metabolisable androgen R1881 from NEN DuPont and staurosporine from Alexis.

2.2. Western blotting and indirect immunofluorescence

The androgen receptor was detected using antibody N20 (Santa Cruz), poly(ADP-ribose) polymerase (PARP) detected using antibody C-2-10 (Biomol), and caspase 3 was detected using a rabbit polyclonal antibody (Santa Cruz). Cells were harvested for SDS-PAGE by washing twice with ice-cold phosphate buffered saline (PBS) and then scraping into the appropriate buffer. For analyses of androgen receptor expression and caspase 3 cleavage, this was ice-cold 50 mM Tris-HCl pH 6.8 containing 1 mM EDTA, 0.6 mM PMSF, 0.5 mM bacitracin, 10 mM dithiothreitol and 10% (w/v) glycerol. Thereafter, an equal volume of SDS-PAGE sample buffer containing 4% SDS was added and the samples heated in a boiling water bath. For detection of PARP, samples were prepared according to the manufacturer's instructions for use of PARP antibody C-2-10 (Biomol). All samples were separated on 10% (w/v) acrylamide gels and transferred to Protran nitrocellulose membranes (Schleicher & Schuell) using a Bio-Rad TransBlot system. Following blocking in PBS containing 3% skimmed milk and 0.2% Tween 20, the blots were incubated with primary antibodies, washed in PBS/0.2% Tween 20, incubated with horseradish peroxidase conjugated anti-mouse or anti-rabbit immunoglobulins (Igs) (Amersham) and following further washes developed using an enhanced chemiluminescence system (Amersham) according to the manufacturer's instructions.

To compare androgen receptor expression levels in the different transfected cell clones, quantitative

Western blots were performed following methods similar to those previously described by us [27]. Briefly, 5×10^6 cells from each population were processed identically for SDS-PAGE and equal volumes of these samples then loaded on SDS-PAGE gels and probed for the androgen receptor by Western blotting as described above. To confirm that equal amounts of protein were loaded, identically loaded gels were Coomassie stained and three selected bands from each sample quantified by densitometric analyses using a Bio-Rad GS-710 Imaging Densitometer equipped with Quantity One software. The signals from these scans were then compared with the signals obtained from the androgen receptor Western blots.

For immunocytochemical and nuclear morphology studies, cells were fixed in 4% (w/v) paraformaldehyde in PBS for 20 min, permeabilised in 0.1% (w/v) Triton X-100 in PBS for 10 min and then processed for immunofluorescence. Following blocking with 5% (v/v) foetal bovine serum/0.2% (w/v) Tween 20 in PBS for 1 h, cells were probed with primary antibody N20 to the androgen receptor diluted in blocking solution. Antibodies were detected using goat anti-rabbit Igs coupled to Oregon Green or Texas red (Molecular Probes). Nuclear morphology

was analysed by labelling with Hoechst 33342 stain. Cells were mounted in Vectashield (Vector Labs).

2.3. Cell viability assays

Cell viability was assayed using a commercial (3-(4,5-dimethylthiazol-2-yl)-5-(carboxymethoxyphenyl)-2-(4-sulphophenyl)-2H-tetrazolium, inner salt (MTS)) assay according to the manufacturer's instructions (CellTiter 96, Promega). Lactate dehydrogenase (LDH) assays were also performed using a commercial kit (CytoTox 96, Promega).

3. Results

We utilised SHSY5Y cells since pilot studies revealed that these human neuroblastoma cells do not express detectable levels of androgen receptor (see also Figs. 1a and 2d). Studies on the effect of expressing wild-type or SBMA mutant androgen receptor by transfection in these cells would not therefore be complicated by co-expression of the endogenous receptor.

We generated several different transfected SHSY5Y cell clones and screened these by quantitative Western blotting to identify ones that expressed similar levels of wild-type and SBMA receptors. These studies identified two clones that expressed levels of wild-type and SBMA receptors that were indistinguishable (clones C28 and K6 respectively) (Fig. 1). These two clones were therefore selected for further investigations.

Both C28 and K6 cells had morphologies that were similar to parental non-transfected cells and grew in androgen free medium in a fashion that was not noticeably different to parental SHSY5Y cells (Fig. 2a–c). Treatment of C28 and K6 cells with 1 nM R1881 for 2 h induced nuclear translocation of the androgen receptor (Fig. 2d–i) but no evidence of cytoplasmic or nuclear aggregates was observed in any of the cells either prior to, or after androgen treatment. Similarly, we did not detect inclusions in any of the other cell lines expressing wild-type or SBMA receptor that were examined.

Upon treatment with R1881 for longer periods, both of the transfected cell lines displayed a marked time- and dose-dependent loss in cell viability as de-

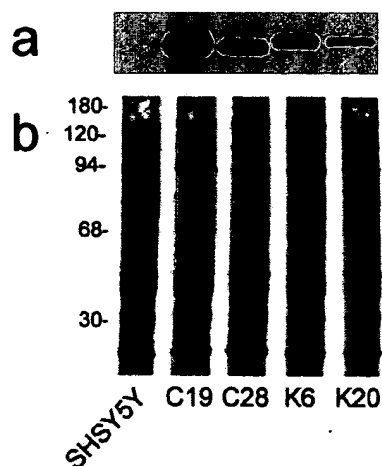


Fig. 1. Androgen receptor expression in non-transfected parental SHSY5Y cells and SHSY5Y cells stably expressing either a wild-type androgen receptor (C19 and C28 cells) or an SBMA mutant androgen receptor (K6 and K20 cells). (a) Western blot to detect the androgen receptor; (b) full length identically loaded Coomassie stained gel to demonstrate equal protein loadings. Molecular masses in kDa are indicated on the left in panel b.

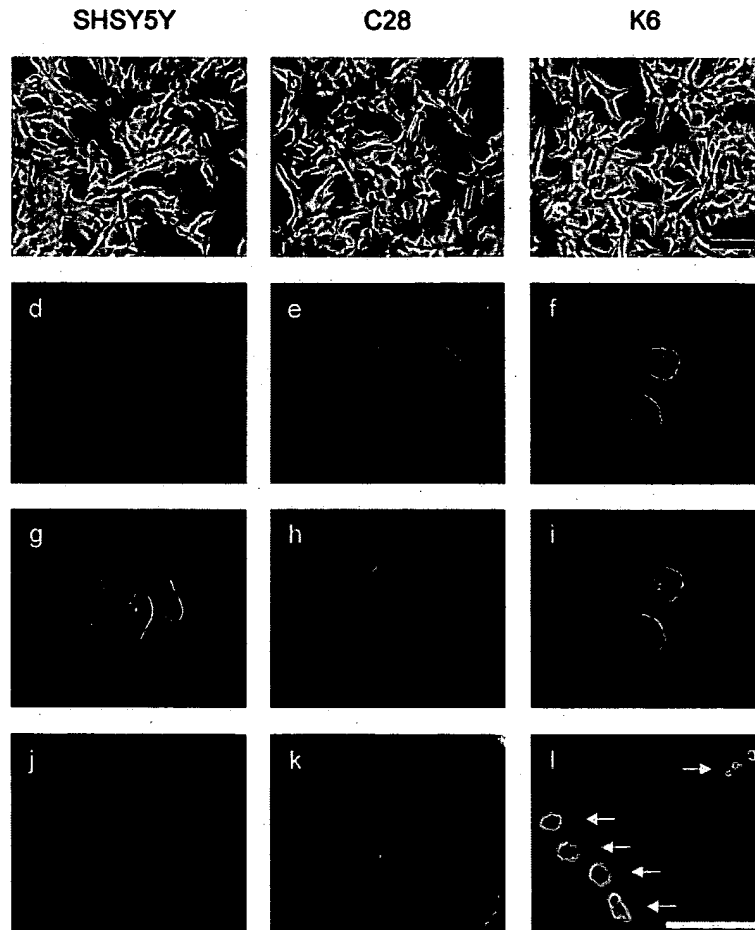


Fig. 2. Morphology and immunocytochemical analyses of parental SHSY5Y cells and SHSY5Y cells stably expressing either a wild-type androgen receptor (C28 cells) or an SBMA mutant androgen receptor (K6 cells). (a–c) Phase contrast images of SHSY5Y, C28, and K6 cells respectively. (d–f) SHSY5Y, C28, and K6 cells stained with androgen receptor antibody N20 following treatment with 1 nM R1881 for 2 h to demonstrate nuclear localisation; (g–i) the same fields stained with Hoechst 33342 to show nuclei. (j–l) SHSY5Y, C28, and K6 cells stained with Hoechst 33342 following 10 pM R1881 treatment for 3 days; pyknotic and fragmenting nuclei typical of apoptotic cells are arrowed in the K6 cells. Scale bars: 50 μ m.

terminated by MTS assays; non-transfected parental cells were unaffected by androgen (Fig. 3). Similar results were obtained using LDH assays (data not shown). This loss in viability was significantly greater in clone K6 expressing the SBMA mutant androgen receptor than in clone C28 expressing the wild-type receptor. Similar results were obtained with testosterone treatment.

Analyses of two further clones that expressed the androgen receptor at different levels (C19 expressing the wild-type receptor and K20 expressing the SBMA receptor (Fig. 1)) revealed that they too exhibited a loss of viability following androgen treat-

ment. Following a 5 day treatment with 1 nM R1881, C19 cells displayed 20% and K20 cells 65% survival (relative to non-transfected SHSY5Y cells) as determined by MTS assays. Under the same experimental conditions, C28 and K6 cells displayed 50% and 20% survival respectively (Fig. 3). Quantitative Western blots (see Fig. 1) revealed that C19 cells expressed 1.8 times and K20 cells 0.23 times the level of receptor as C28 and K6 cells. Thus, several SHSY5Y cell lines expressing differing levels of the androgen receptor display a loss of viability in response to androgen treatment and this loss is at least partially related to the expression level of the recep-

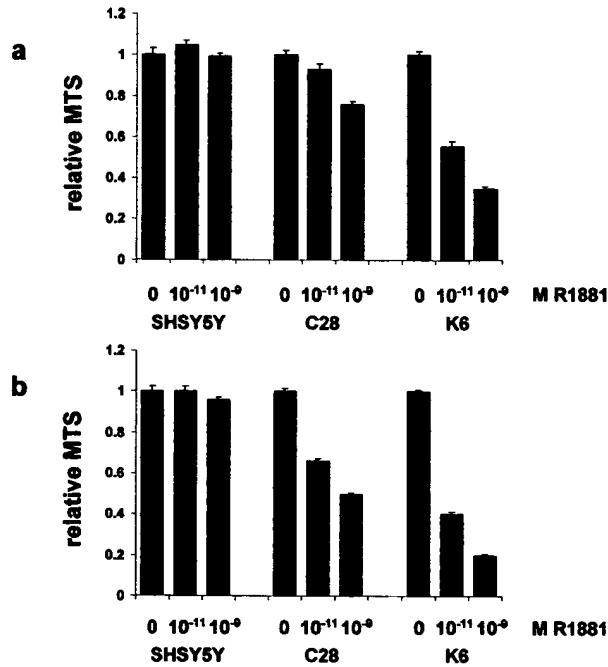


Fig. 3. MTS cell viability assays of SHSY5Y cells and SHSY5Y cells expressing either a wild-type androgen receptor (C28 cells) or an SBMA mutant androgen receptor (K6 cells). Cell viability is expressed relative to untreated cells in each case. Cells were either untreated or treated with 10 pM (10^{-11} M) or 1 nM (10^{-9} M) R1881 for 3 days (a) or 5 days (b). Error bars are S.E.M.

tor. These studies also provide further evidence that cells expressing the SBMA receptor are more sensitive to androgen than cells expressing the wild-type receptor although this relationship is not linear (C19 cells are equally susceptible to androgen as K6 cells despite expressing 1.8 times the level of receptor and K20 cells are only moderately less sensitive to androgen than C28 cells despite expressing only 0.23 times their level).

The mechanism(s) that lead to neuronal cell loss in SBMA or indeed in any of the polyglutamine repeat diseases are not known. However, apoptosis is one proposed method of cell death for these disorders (see for example [15,28,29]). Since altered nuclear morphology is a marker for apoptosis, we analysed nuclear shape in the androgen treated cells by staining with Hoechst 33342. For these studies, we focused on cells exposed to 10 pM R1881 for 3 days since this particular treatment produced the most marked differences in survival between the cell types as determined by the MTS assays (see Fig. 3). Nuclei

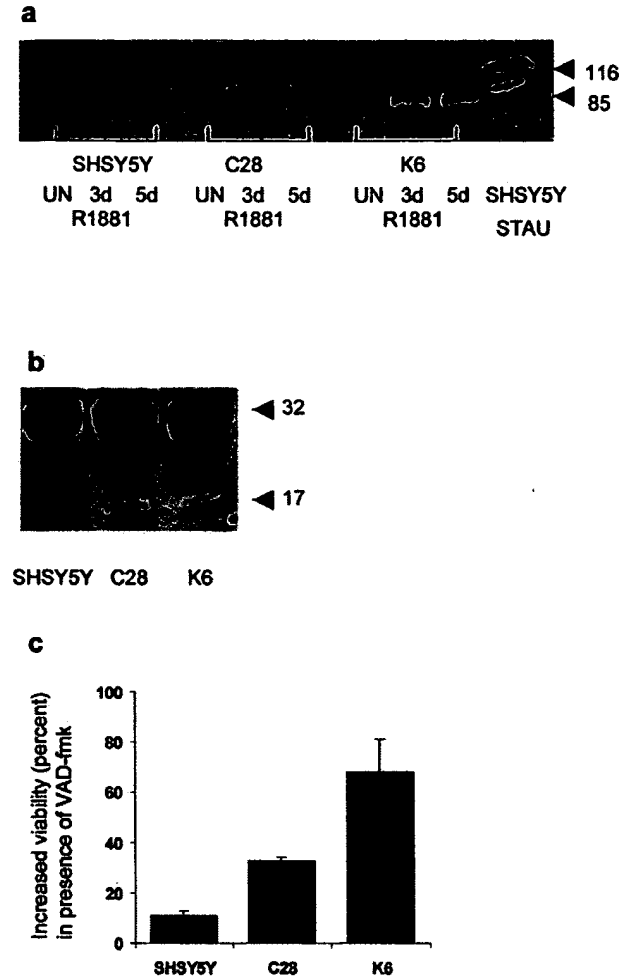


Fig. 4. Androgen stimulation causes cleavage of proteins associated with apoptosis in SHSY5Y cells expressing either a wild-type androgen receptor (C28 cells) or an SBMA mutant androgen receptor (K6 cells). (a) PARP cleavage in cells that were untreated (UN) or treated with 0.1 nM R1881 for either 3 or 5 days (3d, 5d). As a positive control, parental SHSY5Y cells (SHSY5Y) were also treated with 10 μ M staurosporine (STAU) for 2 h to induce apoptosis. The 116 and 85 kDa PARP species are indicated. (b) Caspase 3 cleavage in C28 and K6 cells, but not parental SHSY5Y cells exposed to 1 nM R1881 for 5 days. Cleaved (17 kDa) and uncleaved (32 kDa) caspase 3 bands are identified. (c) The caspase inhibitor VAD-fmk increases viability of cells exposed to 1 nM R1881 for 5 days. Cells were treated with 1 nM R1881 in the presence and absence of VAD-fmk. Cell viabilities were determined by MTS assays and are expressed relative to cells without VAD-fmk in each case.

were scored for apoptotic changes (pyknotic/fragmenting nuclei) and these studies revealed that R1881 treatment resulted in 3.6% abnormal nuclei in C28 cells ($n=443$) and 35.5% abnormal nuclei

induced in K6 cells ($n = 327$) as compared to parental SHSY5Y cells (see Fig. 2j–l for representative images). These figures are similar to those obtained by the MTS assays (cf. Fig. 3) which show 7.5% and 45% losses of viability in C28 and K6 cells respectively.

Proteolytic cleavage of PARP to generate an 85 kDa fragment is a further marker for apoptosis [30,31]. We therefore analysed PARP cleavage by Western blotting in the SHSY5Y, C28 and K6 cells following treatment with 1 nM R1881 for 3 and 5 days. Following R1881 treatment, the 85 kDa cleaved product was clearly discernible in both K6 and C28 cells with the level being lower in C28 cells (Fig. 4a).

To further investigate the possibility that death in response to androgen stimulation was by apoptosis we utilised an antibody against caspase 3. On activation, caspase 3 is cleaved to generate a faster migrating species on a Western blot. After stimulation with 1 nM R1881 for 5 days both cell lines showed cleaved caspase 3, whereas parental cells did not (Fig. 4b). We also used the caspase inhibitor VAD-fmk to inhibit cell death in cells exposed to 1 nM R1881 (Fig. 4c). This increased survival of both cell lines; K6 and C28 viability was increased by 68% and 33% respectively. The small increase in viability seen in parental cells (11%) is probably due to inhibition of naturally occurring apoptosis in the cells.

4. Discussion

A number of other groups have now studied the effects of wild-type and SBMA androgen receptor expression on cell survival in transfected cells [29,32–37]. The results of these studies are variable. Some groups have reported little if any effect on viability of either the wild-type or SBMA receptor [32,33] whereas other reports demonstrate toxicity of both wild-type and SBMA receptors with SBMA receptors exhibiting increased toxicity [29,35]. However, in one of these studies, androgens have little effect on the toxicity [35] whereas in the other study, androgen treatment rescues cells from toxicity [29]. A further study suggests that toxicity requires proteolytic cleavage of the receptor and formation of aggregates containing the polyglutamine tract [34]. It

has also been shown that formation of aggregates requires androgens [37,38]. Most recently, it has been suggested that androgen stimulation promotes aggregate formation but may also be neuroprotective [37]. These different results probably reflect the different cell types used for investigation, the different levels of expression of the androgen receptor in the cells including whether the cells express endogenous receptor, and finally whether stable or transient transfection methods were used.

In the studies reported here, we have stably expressed wild-type (19 polyglutamine repeats) and SBMA (52 polyglutamine repeats) androgen receptors in SHSY5Y cells. These are a human neuronal cell type that have been extensively used to study mechanisms of cell death in neurodegenerative diseases (see for example [39,40]). We selected for study two clones that express identical levels of wild-type and SBMA receptors (clones C28 and K6 respectively). Since parental SHSY5Y cells do not express the androgen receptor, we were therefore able to compare directly how polyglutamine repeat length influenced cell viability in the absence of an endogenous receptor. This is an important feature of our experimental approach since only one copy of the androgen receptor gene is expressed per cell in vivo in humans (the androgen receptor is located on the X-chromosome and so one copy is silenced in females due to X-inactivation). The transfected SHSY5Y cells we have generated therefore model in vivo androgen receptor expression more closely than in some earlier studies.

In the absence of androgen, C28 and K6 cells have similar morphologies and growth rates to parental SHSY5Y cells. However, upon treatment with androgens, C28 and K6 cells both undergo a dose-dependent loss of viability; no such loss is seen in the parental cells. Furthermore, analyses of several other SHSY5Y cell clones stably transfected with either wild-type or SBMA androgen receptor but expressing differing levels of the receptors also revealed losses of viability following androgen treatment (data not shown). Alterations to expression of androgen-responsive gene(s) is thus toxic to SHSY5Y cells. The identification of the gene(s) that mediate this toxicity is therefore an important avenue for future investigation.

Interestingly, although androgens induced a loss of

viability in both C28 and K6 cells, stimulation of the SBMA receptor induced a significantly higher rate of cell death. Studies of two further clones expressing wild-type and SBMA receptors (C19 and K20) provided further support for this notion. Stimulation of the SBMA receptor is therefore more toxic than stimulation of the wild-type receptor in SHSY5Y cells. This may be because the wild-type and SBMA receptors induce expression of different gene(s) following androgen stimulation which then leads to cell death, or that they induce expression of androgen-responsive genes to differing levels which again induces a toxic effect. Alternatively, the SBMA receptor may cause cell death in a manner that is unrelated to expression of androgen-responsive genes but that is dependent upon androgen stimulation. Indeed, the mechanism(s) of cell death in SBMA and all of the polyglutamine repeat diseases are far from clear. One suggestion is that polyglutamine tract expansion induces the formation of aggregates that are toxic to neurones [24,34,38]. However, we were unable to detect androgen receptor aggregates in the transfected cells studied here (either before or after androgen treatment) although we cannot exclude the possibility that submicroscopic aggregates are present in the cells. Recent data have suggested that polyglutamine containing aggregates may not be toxic to cells [28,41,42] and this includes aggregates containing the SBMA receptor [37].

A further proposed toxic mechanism involves activation of apoptotic pathways since expression of SBMA receptors has been shown to induce morphological changes that are characteristic of apoptosis [29,35]. Our findings are in agreement with these studies since we too observe altered nuclear morphology consistent with apoptosis in the androgen treated K6 cells. In addition, we also detected proteolytic cleavage of PARP, a biochemical marker for apoptosis [30,31] upon androgen stimulation and this cleavage was more prominent in K6 cells. PARP is cleaved by caspases (caspase 3 and 7) as part of the apoptotic process (for reviews see [43,44]). We also detected cleavage of caspase 3 upon androgen stimulation of our stable cells, suggesting that this caspase is involved in the cell death induced by androgen treatment. Interestingly the androgen receptor has been shown to undergo proteolysis by members of the caspase family of proteases, including

caspase 3 [29,45]. It has also been suggested that cleavage of the SBMA androgen receptor may mediate its toxicity [24,29]. We were able to detect a faster migrating species with the N20 androgen receptor antibody; however, we did not detect any increase in this band upon androgen treatment, or observe any *de novo* cleavage products after 5 days of 1 nM R1881 (data not shown). Since we had used several criteria to demonstrate apoptosis in these cells, we chose to try and prevent cell death using a well characterised caspase inhibitor. Treatment with VAD-fmk was able to increase cellular survival in both cell lines after 5 days of 1 nM R1881. The results presented here therefore suggest that androgen induced death of SHSY5Y cells expressing the SBMA androgen receptor may well involve apoptotic mechanisms.

Acknowledgements

This work was supported by grants from the UK Motor Neurone Disease Association and Wellcome Trust. We thank L. Pinsky, Montreal, for the kind gift of androgen receptor plasmids containing 19 and 52 CAG repeats.

References

- [1] A.R. La Spada, E.M. Wilson, D.B. Lubahn, A.E. Harding, K.H. Fischbeck, *Nature* 352 (1991) 77–79.
- [2] A. Edwards, H.A.J. Hammond, L. Jun, T. Caskey, R. Chakraborty, *Genomics* 12 (1992) 241–253.
- [3] V. Biancalana, F. Serville, J. Pommier, J. Julien, A. Hanauer, J.L. Mandel, *Hum. Mol. Genet.* 1 (1992) 255–258.
- [4] The Huntington's Disease Collaborative Research Group, *Cell* 72 (1993) 971–983.
- [5] R. Koide, T. Ikeuchi, O. Onodera, H. Tanaka, S. Igarishi, K. Endo, H. Takahashi, R. Kondo, A. Ishikawa, T. Hayashi, M. Saito, A. Tomoda, T. Miike, H. Naito, F. Ikuta, S. Tsuji, *Nat. Genet.* 6 (1994) 9–13.
- [6] S. Nagafuchi, H. Yanagisawa, K. Sato, T. Shirayama, E. Ohsaki, M. Bundo, T. Takeda, K. Tadokora, I. Kondo, N. Murayama, Y. Tanaka, H. Kikushima, K. Umino, H. Kurosawa, T. Furukawa, K. Nihei, T. Inoue, A. Sano, O. Komure, M. Takahashi, T. Yoshizawa, I. Kanazawa, M. Yamada, *Nat. Genet.* 6 (1994) 14–18.
- [7] Y. Kawaguchi, T. Okamoto, M. Taniwaka, M. Aizawa, M. Inoue, S. Katayama, H. Kawakami, S. Nakamura, M. Nishimura, I. Akiyuchi, J. Kimura, S. Narumiya, A. Kakizuka, *Nat. Genet.* 8 (1994) 221–228.

- [8] H.T. Orr, M.-Y. Chung, S. Banfi, J.J. Kwiatkowski, A. Servadio, A.L. Beaudet, A.E. McCall, L.A. Duvick, L.P.W. Ranum, H.Y. Zoghbi, *Nat. Genet.* 4 (1993) 221–225.
- [9] S.M. Pulst, A. Nechiporuk, T. Nechiporuk, S. Gispert, X.N. Chen, I. Lopes-Sendes, S. Pearlman, S. Starkman, G. Orozco-Diaz, A. Lunkes, *Nat. Genet.* 14 (1996) 269–276.
- [10] K. Sanpei, H. Takano, S. Igarishi, T. Sato, M. Oyake, H. Sasaki, A. Wakisaka, K. Tashiro, Y. Ishida, T. Ikeuchi, R. Koide, M. Saito, A. Sato, T. Tanaka, S. Hanyu, Y. Takiyama, M. Nishizawa, N. Shimizu, Y. Nomura, M. Segawa, K. Iwabuchi, I. Eguchi, H. Tanaka, H. Takahashi, S. Tsuji, *Nat. Genet.* 14 (1996) 277–284.
- [11] G. Imbert, F. Sadou, G. Yvert, D. Devys, Y. Trottier, J.M. Garnier, C. Weber, J.-L. Mandel, G. Cancel, N. Abbas, A. Durr, O. Didierjean, G. Stevanin, Y. Agid, A. Brice, *Nat. Genet.* 14 (1996) 285–291.
- [12] O. Zhuchenko, J. Bailey, P. Bonnen, T. Ashizawa, D.W. Stockton, C. Amos, W.B. Dobyns, S.H. Subramony, H.Y. Zoghbi, C.C. Lee, *Nat. Genet.* 15 (1997) 62–69.
- [13] G. David, N. Abbas, G. Stevanin, A. Dürr, G. Yvert, G. Cancel, C. Weber, G. Imbert, F. Saudou, E. Antoniou, H. Drabkin, R. Gemmill, P. Giunti, A. Benomar, N. Wood, M. Ruberg, Y. Agid, J.L. Mandel, A. Brice, *Nat. Genet.* 17 (1997) 65–70.
- [14] H. Ikeda, M. Yamaguchi, S. Sugai, Y. Aze, S. Narumiya, A. Kakizuka, *Nat. Genet.* 13 (1996) 196–202.
- [15] S. Igarashi, R. Koide, T. Shimohata, M. Yamada, Y. Hayashi, H. Takano, H. Date, M. Oyake, T. Sato, A. Sato, S. Egawa, T. Ikeuchi, H. Tanaka, R. Nakano, K. Tanaka, I. Hozumi, T. Inuzuka, S. Tsuji, *Nat. Genet.* 18 (1998) 111–117.
- [16] D. Martindale, A. Hackman, A. Wiczorek, L. Ellerby, C. Wellington, K. McCutcheon, R. Singaraja, P. Kazemi-Esfarjani, R. Devon, S.U. Kim, D.E. Bredesen, F. Tufaro, M.R. Hayden, *Nat. Genet.* 18 (1998) 150–154.
- [17] D.J. Mangelsdorf, C. Thummel, M. Beato, P. Herrlich, G. Schultz, K. Umesono, B. Blumberg, P. Kastner, M. Mark, P. Chambon, R.M. Evans, *Cell* 83 (1995) 835–839.
- [18] A. Mhatre, M.A. Trifiro, M. Kaufman, P. Kazemi-Esfarjani, D. Figelwicz, G. Rouleau, L. Pinsky, *Nat. Genet.* 7 (1993) 513–520.
- [19] N.L. Chamberlain, E.D. Driver, R.L. Miesfeld, *Nucleic Acids Res.* 22 (1994) 3181–3186.
- [20] P. Kazemi-Esfarjani, M.A. Trifiro, L. Pinsky, *Hum. Mol. Genet.* 4 (1995) 523–527.
- [21] A.J. Grierson, R.C. Mootsoosamy, C.C.J. Miller, *Neurosci. Lett.* 277 (1999) 9–12.
- [22] R.A. Irvine, H. Ma, M.C. Yu, R.K. Ross, M.R. Stallcup, G.A. Coetzee, *Hum. Mol. Genet.* 9 (2000) 267–274.
- [23] K.H. Fischbeck, D. Souders, A. La Spada, *Adv. Neurol.* 56 (1991) 209–213.
- [24] R. Butler, P.N. Leigh, M.J. McPhaul, J.-M. Gallo, *Hum. Mol. Genet.* 7 (1998) 121–127.
- [25] P.W. Haiao, D.L. Lin, R. Nakao, C. Chang, *J. Biol. Chem.* 274 (1999) 20229–20234.
- [26] J.C. McPheat, W.J. Potts, C.C.J. Miller, *Methods Mol. Cell. Biol.* 2 (1991) 289–291.
- [27] B.J.M. Gibb, J.-P. Brion, J. Brownlee, B.H. Anderton, C.C.J. Miller, *J. Neurochem.* 70 (1998) 492–500.
- [28] F. Saudou, S. Finkbeiner, D. Devys, M.E. Greenberg, *Cell* 95 (1998) 55–66.
- [29] L.M. Ellerby, A.S. Hackam, S.S. Propp, H.M. Ellerby, S. Rabizadeh, N.R. Cashman, M.A. Trifiro, L. Pinsky, C.L. Wellington, G.S. Salvesen, M.R. Hayden, D.E. Bredesen, *J. Neurochem.* 72 (1999) 185–195.
- [30] S.H. Kaufmann, S. Desnoyers, Y. Ottaviano, N.E. Davidson, G.G. Poirier, *Cancer Res.* 53 (1993) 3976–3985.
- [31] M. Tewari, L.T. Quan, K. O'Rourke, S. Desnoyers, Z. Zheng, D.R. Beidler, G.G. Poirier, G.S. Slavesen, V.M. Dixit, *Cell* 81 (1995) 801–809.
- [32] H. Nakajima, F. Kimura, T. Nakagawa, T. Ikemoto, D. Furutama, K. Shinoda, S. Kato, A. Shimizu, N. Ohsawa, *Neurosci. Lett.* 222 (1997) 83–86.
- [33] B.P. Brooks, H.L. Paulson, D.E. Merry, E.F. Salazar-Gruesso, A.O. Brinkmann, E.M. Wilson, K.H. Fischbeck, *Neurobiol. Dis.* 4 (1997) 313–323.
- [34] D.E. Merry, Y. Kobayashi, C.K. Bailey, A.A. Taye, K.H. Fischbeck, *Hum. Mol. Genet.* 7 (1998) 693–701.
- [35] A.R.A. Abdullah, M.A. Trifiro, V. Panet-Raymond, C. Alvarado, S. de Turreil, D. Frankel, H.M. Schipper, L. Pinsky, *Hum. Mol. Genet.* 7 (1998) 379–384.
- [36] B.P. Brooks, D.E. Merry, H.L. Paulson, A.P. Lieberman, D.L. Kolson, K.H. Fischbeck, *J. Neurochem.* 70 (1998) 1054–1060.
- [37] S. Simeoni, M.A. Mancini, D.L. Stenoien, M. Marcelli, N.L. Weigel, L. Martini, A. Poletti, *Hum. Mol. Genet.* 9 (2000) 133–144.
- [38] D.L. Stenoien, C.J. Cummings, H.P. Adams, M.G. Mancini, K. Patel, G.N. DeMartino, M. Marcelli, N.L. Weigel, M.A. Mancini, *Hum. Mol. Genet.* 8 (1999) 731–741.
- [39] H. Martin, M.P. Lambert, K. Barber, S. Hinton, W.L. Klein, *Neuroscience* 66 (1995) 769–779.
- [40] R.V. Ward, J.B. Davis, C.W. Gray, A.J.L. Barton, L.G. Bresciani, M. Caivano, V.F. Murphy, K. Duff, M. Hutton, J. Hardy, G.W. Roberts, E.H. Karran, *Neurodegeneration* 5 (1996) 293–298.
- [41] I.A. Klement, P.J. Skinner, M.D. Kaytor, H. Yi, S.M. Hersch, H.B. Clark, H.Y. Zoghbi, H.T. Orr, *Cell* 95 (1998) 41–53.
- [42] S.S. Sisodia, *Cell* 95 (1998) 1–4.
- [43] B.B. Wolf, D.R. Green, *J. Biol. Chem.* 274 (1999) 20049–20052.
- [44] J.B. Schulz, M. Weller, M.A. Moskowitz, *Ann. Neurol.* 45 (1999) 421–429.
- [45] C.L. Wellington, L.M. Ellerby, A.S. Hackam, R.L. Margolis, M.A. Trifiro, R. Singaraja, K. McCutcheon, G.S. Salvesen, S.S. Propp, M. Bromm, K.J. Rowland, T. Zhang, D. Rasper, S. Roy, N. Thornberry, L. Pinsky, A. Kakizuka, C.A. Ross, D.W. Nicholson, D.E. Bredesen, M.R. Hayden, *J. Biol. Chem.* 273 (1998) 9158–9167.

Kennedy's Disease: Caspase Cleavage of the Androgen Receptor Is a Crucial Event in Cytotoxicity

*†Lisa M. Ellerby, ‡Abigail S. Hackam, *†Stephanie S. Propp, *†H. Michael Ellerby, †§Shahrooz Rabizadeh, ||Neil R. Cashman, ¶Mark A. Trifiro, ¶Leonard Pinsky, ‡Cheryl L. Wellington, *†Guy S. Salvesen, ‡Michael R. Hayden, and *†#Dale E. Bredesen

*Program on Apoptosis and Cell Death; and †Program on Aging, Burnham Institute, La Jolla; §Interdepartmental Program in Neuroscience, University of California, Los Angeles; #Neuroscience Department, University of California, San Diego, California, U.S.A.; ‡Centre for Molecular Medicine and Therapeutics, Department of Medical Genetics, University of British Columbia, Vancouver, British Columbia; ¶Lady Davis Institute, Department of Human Genetics, McGill University, Montreal, Quebec; and ||Center for Research in Neurodegenerative Diseases, University of Toronto, Toronto, Ontario, Canada

Abstract: X-linked spinal and bulbar muscular atrophy (SBMA), Kennedy's disease, is a degenerative disease of the motor neurons that is associated with an increase in the number of CAG repeats encoding a polyglutamine stretch within the androgen receptor (AR). Recent work has demonstrated that the gene products associated with open reading frame triplet repeat expansions may be substrates for the cysteine protease cell death executioners, the caspases. However, the role that caspase cleavage plays in the cytotoxicity associated with expression of the disease-associated alleles is unknown. Here, we report the first conclusive evidence that caspase cleavage is a critical step in cytotoxicity; the expression of the AR with an expanded polyglutamine stretch enhances its ability to induce apoptosis when compared with the normal AR. The AR is cleaved by a caspase-3 subfamily protease at Asp¹⁴⁶, and this cleavage is increased during apoptosis. Cleavage of the AR at Asp¹⁴⁶ is critical for the induction of apoptosis by AR, as mutation of the cleavage site blocks the ability of the AR to induce cell death. Further, mutation of the caspase cleavage site at Asp¹⁴⁶ blocks the ability of the SBMA AR to form perinuclear aggregates. These studies define a fundamental role for caspase cleavage in the induction of neural cell death by proteins displaying expanded polyglutamine tracts, and therefore suggest a strategy that may be useful to treat neurodegenerative diseases associated with polyglutamine repeat expansions. **Key Words:** Triplet repeat disease—Caspase—Kennedy's disease—Androgen receptor—Aggregates.

J. Neurochem. **72**, 185–195 (1999).

that was originally described to underlie developmental cell death (Lockshin and Williams, 1964; Kerr et al., 1972). For example, presenilin-2 (PS2) appears to play a fundamental role in apoptosis regulation (Wolozin et al., 1996), and mutations of PS2 associated with familial Alzheimer's disease increase apoptosis. Furthermore, both presenilin-1 (PS1) and PS2 protein products are substrates for the caspases (Kim et al., 1997), which are cysteine proteases required for apoptosis (Salvesen and Dixit, 1997). Mutations in the β -amyloid precursor protein at residue 717 that are associated with Alzheimer's disease are also proapoptotic (Yamatsuji et al., 1996). Spinal muscular atrophy is caused by mutations in the neuronal IAP gene (NIAP), an IAP (inhibitor of apoptosis)-related protein (Roy et al., 1995). XIAP has been shown to be a direct inhibitor of some caspases (Deveraux et al., 1997). How and at what point in the progression of these neurodegenerative diseases the apoptotic process is invoked, however, remain to be clarified.

Perhaps the most convincing evidence for involvement of the apoptotic pathway in neurodegeneration comes from studies of the CAG trinucleotide expansion diseases. Huntington's disease (HD) and other polyglutamine expansion diseases have an interesting relationship to the apoptotic process, as Huntingtin, as well as at least four other polyglutamine disease proteins, is a sub-

Received April 30, 1998; revised manuscript received July 22, 1998; accepted July 24, 1998.

Address correspondence and reprint requests to Dr. D. E. Bredesen at Program on Aging, Burnham Institute, 10901 N. Torrey Pines Rd., La Jolla, CA 92037, U.S.A.

Abbreviations used: AR, androgen receptor; DRPLA, dentatorubropallidolusian atrophy; HD, Huntington's disease; MJD, Machado-Joseph disease; NIAP, neuronal inhibitor of apoptosis; PBS, phosphate-buffered saline; PIPES, piperazine-*N,N'*-bis(2-ethanesulfonic acid); PS, presenilin; SBMA, spinal and bulbar muscular atrophy; SCA, spinocerebellar ataxia.

The basic mechanisms that underlie neurodegenerative diseases are unknown. However, over the last few years more evidence has accumulated, suggesting that the neuronal cell death in at least some neurodegenerative diseases may involve an inappropriate activation of the programmed cell death pathway (apoptotic pathway)

strate for the proapoptotic caspase-3 (Goldberg et al., 1996; Miyashita et al., 1997; Wellington et al., 1998; Sheldon et al., unpublished data).

Thus far, eight different dominantly inherited neurodegenerative diseases are associated with polyglutamine tract expansions in their respective proteins (Ross, 1995; Perutz, 1996; Nance, 1997). These include HD, spinal and bulbar muscular atrophy (SBMA; or Kennedy's disease), Machado-Joseph disease (MJD; or SCA-3), dentatorubropallidoluysian atrophy (DRPLA), and spinocerebellar ataxia types 1, 2, 6, and 7 (SCA-1, SCA-2, SCA-6, and SCA-7) (La Spada et al., 1991; Huntington's Disease Collaborative Research Group, 1993; Orr et al., 1993; Kawaguchi et al., 1994; Koide et al., 1994; Imbert et al., 1996; Sanpei et al., 1996; David et al., 1997; Zhuchenko et al., 1997). In all cases, there is selective death of neurons in different regions of the brain, and the clinical symptoms correlate with the affected regions. These neurodegenerative disorders show a strong correlation between polyglutamine tract length and age at onset of the disease (for review, see Nance, 1997). Anticipation, the phenomenon of progressively earlier onset of symptoms in succeeding generations, is a second common feature of these disorders.

As each of these disease-associated proteins shares a similar mutation, they may have a common pathological mechanism leading to neuronal cytotoxicity. This mechanism must involve the expansion of the polyglutamine repeat, as the causative proteins do not share other structural or functional similarities. Recent studies from several groups suggest that a critical step in the pathogenic mechanism shared among several of these triplet repeat proteins is the generation of a truncated protein containing the polyglutamine repeat, with the subsequent formation of intracellular aggregates. Perinuclear aggregates and intranuclear aggregates of truncated huntingtin are found in the brains of HD patients and HD transgenic mice expressing an N-terminal mutant fragment for HD (Davies et al., 1997; DiFiglia et al., 1997; Scherzinger et al., 1997; Martindale et al., 1998). Neuronal intranuclear inclusions are also found in the brains of MJD and DRPLA patients, and in vitro studies again have shown these inclusions to be present only with truncated forms of these proteins (Paulson et al., 1997; Igarashi et al., 1998).

We have recently reported that four of the polyglutamine-containing proteins, i.e., huntingtin, the androgen receptor (AR), atrophin-1 (DRPLA), and ataxin-3 (MJD), are cleaved by caspases (Wellington et al., 1998), suggesting that a caspase-dependent apoptotic pathway may be a critical factor in the generation of truncated proteins in some of these polyglutamine repeat disease proteins.

Given our recent findings, we wished to determine if the caspase cleavage is required for the cytotoxicity exhibited by these proteins. Further, we wished to address whether the caspase cleavage site is required for the formation of the protein aggregates characteristic of these diseases. Here, we report the first conclusive evi-

dence that caspase cleavage is a critical step in the cytotoxicity of one polyglutamine disease protein, the AR. We show that expression of the AR with an expanded polyglutamine stretch enhances its cytotoxicity when compared with the normal AR. Protein aggregates are formed on apoptosis induction only for the expanded repeat protein, suggesting a gain-of-function for the proapoptotic fragment with an expanded polyglutamine stretch. Further, mutation of the caspase cleavage site at Asp¹⁴⁶ blocks the ability of the SBMA androgen receptor to form perinuclear aggregates, and substantially blocks its cellular cytotoxicity. Caspase cleavage of SBMA AR and other polyglutamine-containing disease proteins may thus be a required step leading to the progression of polyglutamine expansion disorders.

MATERIALS AND METHODS

Culture and transfection of cells

Cells from the human embryonic kidney cell line 293T were cultured in Dulbecco's modified Eagle's medium containing 10% fetal bovine serum with 1% penicillin/streptomycin. Transient transfection was performed with control plasmid pRc/CMV, full-length androgen constructs pRc/CMV-AR12, pRc/CMV-AR50, pRc/CMV-AR12D146N, pRc/CMV-AR50D146N, pRc/CMV-ARΔQ₅₈₋₈₀, and control plasmid pRc/CMV-*LacZ* according to Jordan et al. (1996). Optimal transfection efficiency was determined to occur with the following procedure: DNA (5 μ l, 1 μ g/ μ l) was mixed with 2 M CaCl₂ (6.2 μ l) and tissue culture water (38.8 μ l) in polystyrene tubes and incubated at room temperature for 10 min. During the 10-min incubation, the medium in the six-well plates was replaced with 1 ml of fresh medium. Then, 50 μ l of 2 \times HBS (280 mM NaCl, 10 mM KCl, 1.5 mM sodium phosphate, 12 mM dextrose, 50 mM HEPES, pH 7.05) was added to the polystyrene tube. The DNA mixture was incubated for 2 min at 37°C and then carefully added to the cells. After incubation overnight, the cells were washed twice with fresh medium. Using pRc/CMV-*LacZ*, transfection efficiency was determined by staining for the expression of β -galactosidase. Cell death was measured by trypan blue exclusion, acridine orange/ethidium bromide, and *LacZ* reporter gene cotransfection, either in the presence of testosterone (1 μ M) or in its absence. To assess cell viability, 1.5 ml of medium was gently removed from the six-well dish, leaving 0.5 ml behind. Then, 0.5 ml of trypan blue dye solution (0.1%) was added to the adherent cells. Cells were incubated briefly at room temperature to allow for dye uptake. Cells were scored for dye uptake in three separate fields with a minimum of 300 cells counted. Values for percentages of viable cells were corrected for transfection efficiency, which was determined by *LacZ* staining. Testosterone was added to some cultures 12 h after transfection, and cell death was measured 36–50 h after transfection. Cellular death in confluent cells was induced with tamoxifen citrate at a concentration of 35 μ M 36–48 h after transfection (Ellerby et al., 1997). Data were collected for three to five experiments and then compared by Student's *t* test for statistical significance.

Death was established as apoptotic based on acridine orange/ethidium bromide staining and activation of caspase-3. For adherent cells undergoing early apoptosis, morphological changes associated with apoptotic cell death were monitored using an acridine orange/ethidium bromide solution by a procedure based on the method of McGahon et al. (1995) with

modifications. At certain time points, cell culture medium was aspirated from adherent cells growing in 24-well plates, and the cells were washed gently once with room temperature phosphate-buffered saline (PBS). Then 1–2 ml of a 20-fold dilution of the dye mixture (composed of 100 mg/ml acridine orange and 100 mg/ml ethidium bromide), in PBS with formalin, was gently pipetted on the cells and viewed on an inverted fluorescence microscope.

Acridine orange passes freely through the plasma membrane, so it intercalates into the DNA, giving it, and therefore the nucleus, a green appearance. This dye also binds the RNA, but because it cannot intercalate, the RNA, and therefore the cytoplasm, appears red. Early apoptotic cells whose membranes are still intact, but which have started to fragment their DNA, still have green nuclei, because ethidium bromide still cannot enter the cell, but chromatin condensation will become visible as bright green patches in the nuclei. As the cell progresses through apoptosis, membrane blebbing occurs, so that in late apoptosis, ethidium bromide enters the cell and stains the nuclei so that they fluoresce bright orange. Nuclei were scored as apoptotic if they exhibited margination and condensation of the chromatin, and/or nuclear fragmentation similar to that observed in normal apoptotic cells (Kerr et al., 1972). A minimum of 200 cells were scored for each time point. Necrotic cells can be identified by ethidium bromide staining in the absence of the apoptotic features described above. Necrotic cells are typically stained bright orange with uniform color.

Western blot analysis

Western blot analysis was performed as described previously by Ellerby et al. (1997), using N-terminal and C-terminal AR antibody from Santa Cruz Biotech (Santa Cruz, CA, U.S.A.).

In vitro translation reactions

Plasmids pRc/CMV, pRc/CMV-AR12, pRc/CMV-AR50, pRc/CMV-AR12D146N, pRc/CMV-AR50D146N, and pRc/CMV-ARΔQ_{58–80} were transcribed by using T7 polymerase, then translated by using the TNT system (Promega) in the presence of [³⁵S]methionine. Translations were incubated with the indicated caspase for 2 h, at identical specific activities, in the following buffer: 20 mM piperazine-*N,N'*-bis(2-ethanesulfonic acid) (PIPES), 100 mM NaCl, 1% 3-[(3-cholamidopropyl)dimethylammonio]-1-propanesulfonate (CHAPS), 10% sucrose, 10 mM dithiothreitol, and 0.1 mM EDTA, pH 7.2, at 37°C.

Purification of caspases and preparation of cell-free extracts

His-tagged caspases were purified by nickel-affinity chromatography as previously described (Orth et al., 1996; Cardone et al., 1997; Zhou et al., 1997). Translated AR constructs were treated with control extract, tamoxifen-primed neuronal cell-free extract, or cytochrome c/dATP extract as previously described (Ellerby et al., 1997).

Site-directed mutagenesis and plasmid construction

Human AR12D146N and AR50D146N were created using the QuikChange site-directed mutagenesis system from Stratagene. pRc/CMV-AR constructs were used as templates with the following synthetic primers according to manufacturer instructions: 5'-CCGGACGAGGATAACTCAGCTGCCCATCC-3'; 5'-GGATGGGGCAGCTGAGTTATCCTCGTCCGG-3'; and 5'-GCTCTAGACCAATGCTTCACTGGGTGTGG-3'. Site-directed mutagenesis was used to prepare

N-terminal fragments representing caspase cleavage products. AR12 and AR50 N-terminal constructs designated pLME443-12 and pLME443-50, encoding amino acids 1–146, were constructed by introducing termination codons with the following mutagenic primers: 5'-CCGGACGAGGATGACTGAGCTGCCCCATCCAC-3' and 5'-GTGGATGGGGCAGCTCAGTCATCCTCGTCCGG-3'. C-terminal construct pLME2316, encoding amino acids 147–919 of AR was constructed by PCR amplification, using the following oligonucleotides containing *Xba*I and *Nor*I restriction sites, respectively: 5'-GCTCTAGACCAATGCTTCACTGGGTGTGG-3' and 5'-ATAAGAATGCGGCCGCGCAGATGGACTCAGCTGCCCCATCCAC-3'.

pRc/CMV-ARΔQ_{58–80} was constructed, using overlap PCR. Using four oligonucleotides, two fragments of the AR gene were created via PCR. Fragment A was created, using the following oligonucleotides: 5'-CCGCTCGAGGCGGCCGCTAGCTGCAGCGACTAC-3' and 5'-CTCACCAGCAGCAGCAAAGTGGCGCCG-3' as the reverse primer. The former primes a region within the 5' untranslated region of the AR and contains an *Nhe*I restriction site. The latter primes up to the 5' end of the CAG region of AR and includes six nucleotides 3' to the AR. Fragment B was created with the following oligonucleotides: 5'-CTGCTGGGTGAGGATGGTTCTCCCCAAAG-3' as the forward primer and 5'-CAGCTGCTTAAGCCGGGAAAGTG-3' as the reverse primer. The former primes six nucleotides 5' upstream of the CAG region and 22 nucleotides downstream from the 3' end of the region. The latter primes a region within the open reading frame of AR and contains an *Afl*II site. The PCR products, fragment A and fragment B, were then purified and used in a third PCR reaction. Using the forward primer used to make fragment A and the reverse primer for fragment B, a third PCR product was created using fragments A and B, which overlap by 12 nucleotides, as the template. This fragment (AB) was purified, digested with *Nhe*I and *Afl*II, and subsequently ligated into pRc/CMV-AR digested by the same enzymes.

Mapping of caspase cleavage sites by radiosequencing

Radiosequencing was performed as previously described (Salvesen and Enghild, 1990; Cardone et al., 1997). Plasmid pRc/CMV-AR12 was transcribed and translated with T7 polymerase, using the TNT system (Promega) with either [³⁵S]methionine or [³H]leucine. The translation was treated with caspase-3, separated by sodium dodecyl sulfate–polyacrylamide gel electrophoresis, and electroblotted onto a polyvinylidene difluoride membrane. After autoradiography, the position of the [³⁵S]methionine-labeled AR fragments was used to cut out the [³H]leucine AR bands from the polyvinylidene difluoride membrane. The samples were subjected to automated sequencing, using an Applied Biosystems 476A sequencer, and the anilinothiazolinone derivatives in each cycle were counted in a scintillation counter. Comparison of the known positions of leucines relative to the caspase cleavage site aspartate allowed identification of one of the AR cleavage sites.

Immunofluorescence microscopy

293T cells were grown on glass coverslips and transiently transfected with the indicated AR construct as described above. At 36 h after transfection, the cells were treated with 35 μM tamoxifen for 1 h. After fixation in 3% paraformaldehyde/PBS [or PHEM (60 mM PIPES, 25 mM HEPES, 5 mM glycine, 10 mM EGTA, 2 mM MgSO₄, pH 6.9)] solution for 20 min, the cells were permeabilized in 0.5% Triton/PBS (or PHEM) for

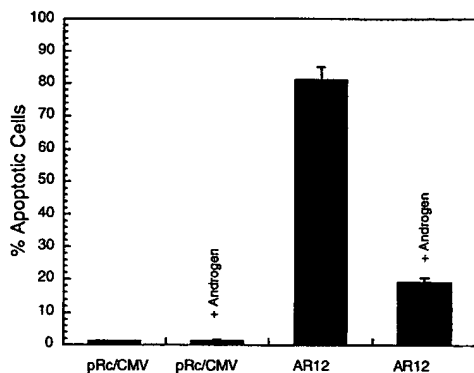


FIG. 1. Expression of the wild-type AR (AR12) is proapoptotic, with testosterone inhibiting the proapoptotic effect. 293T cells were transiently transfected at low confluency (10%) with pRc/CMV-AR12, and cellular death was assessed using trypan blue exclusion in the presence and absence of testosterone (1 μ M). Testosterone was added 12 h after transfection, and death was measured 48 h after transfection. Differences between control and pRc/CMV-AR12 and pRc/CMV-AR12 with and without testosterone were statistically significant ($p < 0.01$). Very similar results were obtained with the motor neuronal cell line NSC-19; transient transfection of AR12 resulted in apoptotic cell death and addition of testosterone blocked cell death.

5 min. The cells were incubated at room temperature with anti-AR antibody from Santa Cruz Biotech (1:200) for 1 h, washed with PBS (3 \times or PHEM), and then incubated in Texas Red-conjugated anti-rabbit antibody (1:1,000) for 30 min. PBS- (or PHEM-) washed cells on coverslips were then mounted onto slides with 4',6'-diamidino-2-phenylindole (DAPI; Sigma) as a nuclear counterstain. Either PHEM or PBS solutions were used for these studies. Immunofluorescence was observed by using a Zeiss confocal microscope. Control experiments were performed, including incubation with secondary antibody only, and immunofluorescence of cells transfected with control plasmids.

RESULTS

Increased cytotoxicity of SBMA mutant AR

To investigate the cytotoxicity of the AR and SBMA mutant AR, we transiently transfected 293T cells as well as motor neuronal cell line NSC-19 (Cashman et al., 1992) with expression constructs encoding the full-length human AR gene (Jordan et al., 1996). Untransfected 293T cells do not express the AR and are not dependent on androgen. The expression of wild-type AR in 293T cells enhanced apoptosis in the absence of androgen, whereas apoptosis was inhibited by the addition of testosterone (Fig. 1). The viability of the cells was measured by trypan blue exclusion and the mode of death was shown to be apoptotic, based on acridine orange/ethidium bromide staining. Expression of β -galactosidase was used as a control and used to determine transfection efficiency.

As the syndrome of complete androgen insensitivity is not associated with a motor neuron syndrome similar to that displayed by SBMA patients (Fischbeck, 1997), Kennedy's disease is more likely to be caused by a

gain-of-function rather than a loss-of-function mutation. Gain-of-function can entail enhancement of a normal function and/or establishment of a novel function. We hypothesized that the AR mutations associated with Kennedy's disease may enhance the proapoptotic effect of the wild-type AR. Therefore, we compared the cytotoxic effect of the wild-type AR (AR12) to that of a mutant form of AR with an expanded polyglutamine tract (AR50) in our tissue culture model. As shown in Fig. 2, cell death was increased by expansion of the polyglutamine repeat (AR50), and decreased by deletion of the polyglutamine tract in 293T cells. Vector alone or *LacZ*-transfected 293T cells served as controls.

Furthermore, stable transfections of AR12 and AR50 into the motor neuronal cell line NSC-19 (Cashman et al., 1992) confirmed that the cytotoxicity of the AR expression increases with expansion of the polyglutamine tract. In this case, transfection of the motor neuronal cell line NSC-19 with pRc/CMV-AR12 gave 21% death in the controls (pRc/CMV), 36% cell death with AR12 expression, and 54% death with AR50 expression. It is noteworthy that stable transfections of AR24 and AR65 into motor neurons, which are androgen responsive, have demonstrated poor expression of AR65 in comparison with AR24, which may have obscured a potential proapoptotic effect of AR65 (Brooks et al., 1997).

Cleavage of the AR by caspases

Because the AR had been shown previously to be processed proteolytically in the intracellular compartment (Kemppainen et al., 1992), we evaluated its cleavage in a cell-free system of neuronal apoptosis (Ellerby et al., 1997). We showed previously that extracts prepared from neurons and neuronal cell lines committed to

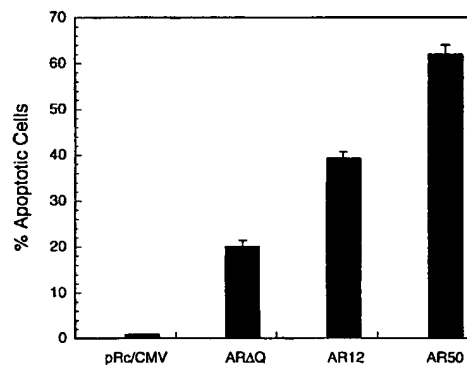


FIG. 2. Expansion of the polyglutamine repeat within the AR, from 12 to 50 glutamines, enhances the proapoptotic effect of AR expression. 293T cells were transiently transfected with pRc/CMV-AR Δ Q, pRc/CMV-AR12, or pRc/CMV-AR50 at 25% confluency. Death was induced 48 h after transfection with tamoxifen (35 μ M). Cellular death was assessed by using trypan blue exclusion in the presence and absence of testosterone (1 μ M) 5 h after tamoxifen treatment at 80% confluency. The difference between AR Δ Q, AR12, and AR50 was statistically significant ($p < 0.01$). Expression of the AR lacking the polyglutamine tract is less cytotoxic than the expression of wild-type or expanded AR. See Materials and Methods.

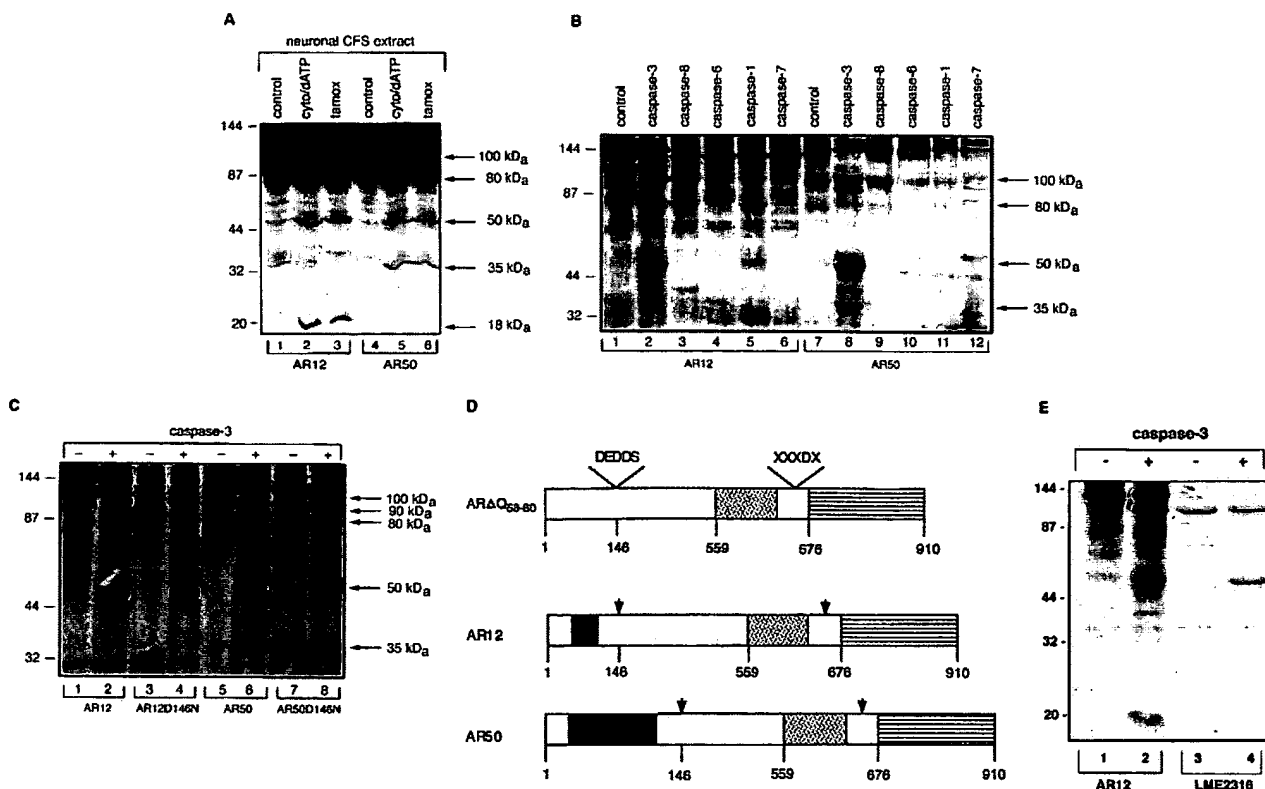


FIG. 3. **A:** In vitro translated wild-type AR12 (lanes 1, 2, and 3) and AR50 (lanes 4, 5, and 6) were treated with neuronal cell-free extracts. Control and activated extracts are noted (see Ellerby et al., 1997). cyto/dATP, cytochrome c/dATP; tamox, tamoxifen. **B:** In vitro translated AR12 (lanes 1–6) and AR50 (lanes 7–12) were treated with the indicated purified caspases (20 nM). **C:** In vitro translated AR12 (lanes 1 and 2), AR12D146N (lanes 3 and 4), AR50 (lanes 5 and 6), and AR50D146N (lanes 7 and 8) were treated with caspase-3. **D:** Diagrams of the primary structure of the normal and mutant (SBMA-derived) human AR protein are shown: ■, polyglutamine tract; □, DNA binding domain; ▨, hormone binding domain. Caspases cleave the AR in the N-terminal and C-terminal regions of the protein. Radiosequencing of in vitro translated AR with [3 H]leucine was used to map the N-terminal cleavage site. The cleavage site in the N-terminal region and the approximate location of the C-terminal cleavage site are indicated (†). AR functional domains are noted. The predicted molecular masses of the fragments resulting from cleavage near the N terminus of the AR12 are 82 kDa (for both AR12 and AR50) and 16 kDa (21 kDa for AR50). **E:** In vitro translated AR12 (lanes 1 and 2) and C-terminal AR construct pLME2316 (lanes 3 and 4) were treated with caspase-3.

apoptosis cleave several cellular death substrates (e.g., poly-ADP-ribose polymerase, the δ isoform of protein kinase C, and lamin-B) specifically, and that this cleavage is caspase dependent (Ellerby et al., 1997). Therefore, we tested whether in vitro translated AR is cleaved by activated neuronal extracts. As shown in Fig. 3A, both AR12 (lane 1) and AR50 (lane 4) remained intact when incubated with nonapoptotic extracts. In contrast, incubation of AR12 (Fig. 3A, lanes 2 and 3) or AR50 (Fig. 3A, lanes 5 and 6) with neuronal extracts committed to undergoing apoptosis yielded four AR fragments. These fragments had apparent sizes of 100 kDa (AR12 and AR50), 80 kDa (90 kDa for AR50), 50 kDa (AR12 and AR50), and 18 kDa (35 kDa for AR50). As shown in Fig. 3A, the predominant fragments generated in neuronal cell-free extracts are the 100 kDa (AR12 and AR50), 50 kDa (AR12 and AR50), and the 18 kDa (35 kDa for AR50). The fragment generated at 80 kDa (90 kDa for AR50) is cleaved considerably less efficiently in our neuronal cell-free extracts. Therefore, characterization of

the former (i.e., major) cleavage products was pursued further.

The finding that the AR is cleaved by apoptotic extracts but not by nonapoptotic extracts suggested, but did not prove, that the cleavage was mediated by caspases. This is because both caspases and noncaspase proteases may be activated during apoptosis (Zhivotovsky et al., 1996, 1997). However, previous work by Goldberg et al. (1996) had shown that huntingtin is cleaved in vitro by caspase-3, and the AR, like huntingtin, contains consensus caspase-3 cleavage sites. Therefore, we determined whether AR12 and AR50 are caspase substrates, by incubating in vitro translated AR products with purified caspases. As shown in Fig. 3B, we found that caspase-3 (CPP32/YAMA/apopain), caspase-1 (ICE), and caspase-8 (FLICE/Mach-1), but not caspase-6 (Mch2) or caspase-7 (Mch3), are capable of cleaving the AR (AR12 or AR50) in vitro. Caspase-3 cleavage of AR was more efficient than that catalyzed by either caspase-6 or caspase-8, based on both protein concentra-

tion and specific activity of these enzymes. We found no evidence that the expanded polyglutamine tract of AR influenced the susceptibility of AR to cleavage by purified caspases, and the results of these studies have been reported elsewhere (Wellington et al., 1998).

We next sought to determine whether this potential cleavage event plays a role in the *in vivo* proapoptotic effect of the AR. To determine this, we first used radio-sequence analysis to map the site of cleavage of the AR by caspase-3 to Asp¹⁴⁶ (see Fig. 3D). We localized this site to the N-terminal transcription modulatory domain of AR, ~70 residues C-terminal to the polyglutamine region of the protein. Cleavage at this site gave two cleavage products, with apparent sizes of 100 kDa (C-terminal product) and 18 kDa (N-terminal product) for AR12 (see Fig. 3A, lane 2). For AR50, a 35-kDa product containing the glutamine repeat was generated, as well as the same 100-kDa product (see Fig. 3A, lane 5). In addition, a second site was identified between the receptor steroid binding domain and DNA binding domain (see Fig. 3D). This second site yields a large N-terminal 80-kDa fragment with polyglutamine repeat for AR12 (90 kDa for AR50).

As shown in Fig. 3C, mutation of Asp¹⁴⁶ to Asn (D146N) blocked the *in vitro* cleavage by caspase-3 at this site. The cleavage products at 100 and 18 kDa (35 kDa for AR50) for AR12 are no longer present in the *in vitro* translated mutant proteins (see Fig. 3C). Mutation to Asn was chosen rather than to Glu because of the structural similarity of Asn to Asp and the previous finding that Glu in the P1 position may in some cases still allow caspase cleavage, although with lower efficiency than with Asp in the P1 position (Howard et al., 1991; Kayalar et al., 1996). Substitution of Asn for Asp at position 146 also blocked the AR cleavage in apoptotic neuronal extracts, providing confirmation that AR proteolytic processing in these extracts is mediated by caspases, and that Asp¹⁴⁶ is a caspase cleavage site (data not shown).

To test further whether the cleavage products of AR at Asp¹⁴⁶ were consistent with the observed cleavage products generated in neuronal apoptotic extracts and in cell culture, a series of truncated cDNAs representing the caspase cleavage products of normal and SBMA AR were prepared. *In vitro* translation of plasmids representing N-terminal cleavage product for AR12 (18 kDa) and AR50 (35 kDa) resulted in translated products identical to those generated from caspase cleavage of full-length AR (data not shown). As shown in Fig. 3E, *in vitro* translation of a plasmid coding for the C-terminal fragment (amino acids 147–919) produced a 100-kDa product identical to that generated during caspase cleavage of the full-length AR (Fig. 3E, lane 2 and 3). It is interesting that incubation of the C-terminal fragment with purified caspase-3 generates two 50-kDa fragments (Fig. 3E, lane 4). Thus, AR cleavage at Asp¹⁴⁶ generates a small N-terminal product and a large C-terminal product. The C-terminal product is further cleaved to generate the two 50-kDa products. As shown in Fig. 4A and B, western

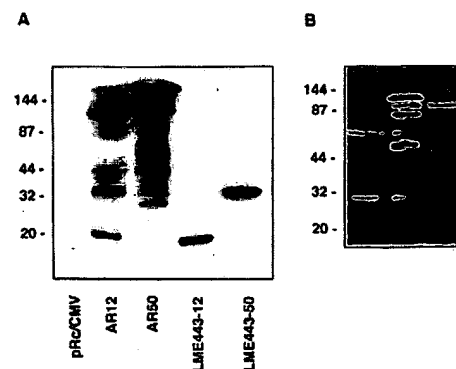


FIG. 4. Western analysis of 293T cells transfected with truncated or full-length AR constructs. **A:** Western blot of tamoxifen (35 μ M)-treated 293T cells transfected with pRc/CMV (lane 1), AR12 (lane 2), AR50 (lane 3), pLME443-12 (lane 4), and pLME443-50 (lane 5). Truncated N-terminal AR cDNAs were prepared as described in Materials and Methods and N-terminal AR antibody was used to detect expression of these constructs. **B:** Western blot of pRc/CMV (lane 1), AR12 (lane 2), and pLME2316 (lane 3) transfected into 293T cells treated with tamoxifen (35 μ M). C-terminal AR antibody was used to detect expression of AR and the C-terminal fragment.

analysis of the various truncated AR cDNAs and full-length AR cDNA introduced into 293T cells confirmed that these fragments are generated during apoptotic death. Similar cleavage products were observed in numerous cell lines undergoing apoptosis, e.g., NT2, NSC-19, and COS-7 (data not shown).

The proapoptotic effect of the AR requires caspase cleavage

Having determined that a caspase cleavage site is located just carboxy-terminal to the polyglutamine tract in the AR, and that mutation of this site blocks caspase cleavage, we assessed the effect of blocking caspase cleavage of AR12 and AR50 on the proapoptotic effects of these proteins in culture. As shown in Fig. 5A, transient transfection of AR12D146N and AR50D146N resulted in a two- to threefold reduction in apoptotic cell death when compared with AR12 and AR50. The expression level of all four proteins was similar in the transient expression assay (see Fig. 5B), suggesting that the reduction in proapoptotic effect was not simply due to a decrease in the expression of the transfected mutant genes. Further, western blot analysis using an antibody directed against the N-terminal domain of AR12 confirmed the generation of caspase cleavage product of 18 kDa (35 kDa for AR50), and substitution of Asn for Asp at position 146 in AR blocked the generation of these cleavage products in 293T cells.

Increased cytotoxicity of SBMA AR correlates with formation of large perinuclear aggregates

As our cytotoxicity studies indicated that the caspase cleavage site is crucial to the proapoptotic effect of AR, we investigated whether apoptosis induction with tamoxifen modulated the formation of

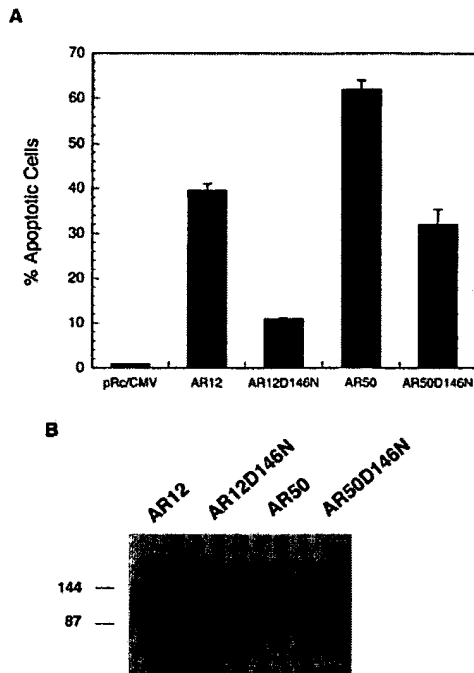


FIG. 5. Inhibition of the cytotoxic effect of both wild-type and expanded ARs by mutation of the N-terminal caspase cleavage site. **A:** 293T cells were transiently transfected with pRc/CMV-AR12, pRc/CMV-AR50, pRc/CMV-AR12D146N, and pRc/CMV-AR50D146N. Death was induced 48 h after transfection with tamoxifen (35 μ M). Cellular death was assessed by using trypan blue exclusion 5 h after tamoxifen treatment at 80% confluency. Differences between AR12 and AR12D146N as well as AR50 and AR50D146N were statistically significant ($p < 0.01$). **B:** Western analysis of transiently transfected 293T cells with pRc/CMV-AR12, pRc/CMV-AR50, pRc/CMV-AR12D146N, and pRc/CMV-AR50D146N demonstrates a similar level of expression of androgen receptor.

aggregates. Expression of the AR50, but not AR12, led to formation of large perinuclear aggregates in the cytoplasm, as determined by confocal microscopy (Fig. 6C and D) on apoptosis induction. Modulation of aggregate formation did not occur in the absence of apoptosis induction (Fig. 6A and C) for AR50 or AR12. The perinuclear aggregates described in these studies are observed in several cell culture models of triplet repeat expansion disease proteins and in patients with HD (DiFiglia et al., 1997; Paulson et al., 1997; Martindale et al., 1998). Transfection of 293T cells with truncated MJD resulted in perinuclear and intranuclear clusters (Paulson et al., 1997). In a similar manner, we have recently reported that cells transfected with amino-terminal huntingtin constructs contain both perinuclear and intranuclear aggregates, depending on the size of the fragment (Martindale et al., 1998). The fact that initial studies on patients with Kennedy's disease have shown aggregates in the nucleus rather than perinuclear may reflect further truncation or specific neuronal protein interactions with AR fragments that localize the inclusions to the nucleus.

Mutation of caspase cleavage site in SBMA AR blocks formation of aggregates

To test whether the caspase cleavage site is required for the formation of aggregates in cell culture, we evaluated whether mutation of the caspase cleavage site in the AR affects the formation of aggregates. Cells transfected with pRc/CMV-AR12 expressed AR protein diffusely in the cytoplasm with a homogeneous pattern during apoptotic cell death with tamoxifen (Fig. 6C). Cells transfected with pRc/CMV-AR50 showed large aggregates in perinuclear locations (Fig. 6D) during apoptotic cell death. In sharp contrast, cells transfected with pRc/CMV-AR50D146N did not form these large aggregates, suggesting that, at least in this system, caspase cleavage of SBMA AR is required for aggregation (Fig. 6F). Cells transfected with pRc/CMV-AR12D146N also showed a homogeneous cytoplasmic distribution of AR (Fig. 6E).

To determine whether the formation of aggregates correlated with the cytotoxicity of SBMA AR and caspase cleavage, we quantified the frequency of aggregate bodies in 293T cells transfected with each of the AR constructs. During apoptotic stimulation with tamoxifen, aggregate formation was observed at high frequency for SBMA AR (38–43%) when compared with normal AR (5–10%) (Fig. 7). Mutation of the caspase cleavage site Asp¹⁴⁶ of the expanded AR substantially blocked aggregate formation (12–18%) (Fig. 7).

Androgen blocks cleavage of AR and prevents formation of aggregates in SBMA AR

The AR functions as a transcription factor after nuclear translocation that is initiated by binding to androgen. We have shown that the wild-type AR is proapoptotic (Fig. 1), and that this cytotoxicity is completely blocked by the addition of androgen (Fig. 1). In separate experiments, we have shown that the cytotoxicity of the AR is blocked by mutation of the caspase cleavage site Asp¹⁴⁶, suggesting that the generation of a proapoptotic fragment is responsible for this effect. Together these data suggest that testosterone may block the cleavage of the AR. As shown in Fig. 8A and B, addition of testosterone to 293T cells transfected with AR results in translocation of AR into the nucleus. Western analysis reveals that testosterone addition blocks cleavage of AR during apoptotic stimulation (Fig. 8C).

Given our findings, we assessed whether androgen was a critical factor in the formation of aggregates in cells transfected with SBMA AR. As shown in Fig. 9, aggregate formation was observed at high frequency for SBMA AR (38–43%) when compared with normal AR (5–10%). Addition of testosterone blocked aggregate formation (13–18%) in cells transfected with SBMA AR.

DISCUSSION

In this study, we show that cells transfected with expression constructs encoding the AR undergo enhanced apoptotic cell death that is mediated by a pro-

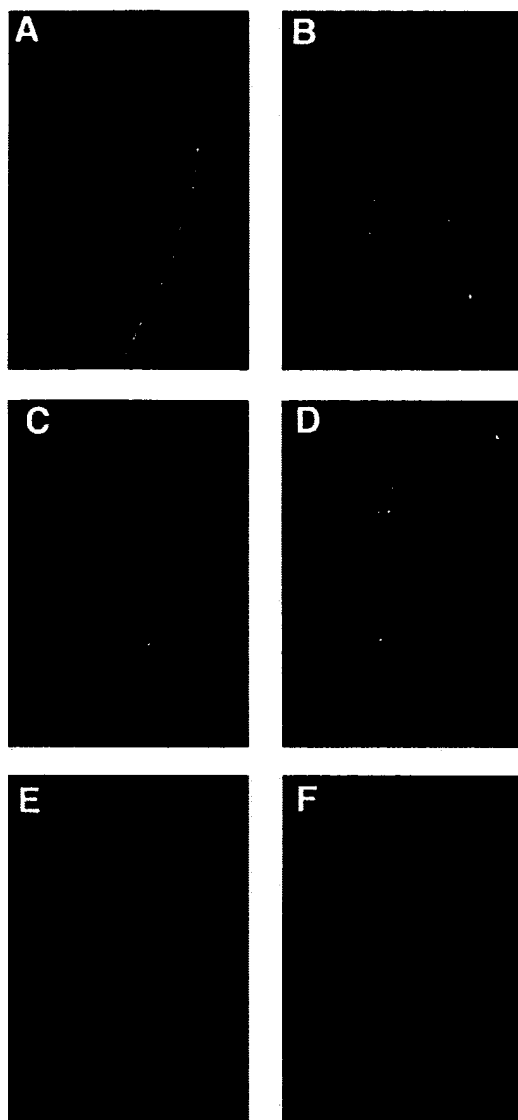


FIG. 6. Immunofluorescence of AR with expanded polyglutamine repeat shows the formation of protein aggregates in 293T cells. **A:** Untreated 293T cells transfected with AR (AR12). **B:** Tamoxifen treated (1 h, 35 μ M) 293T cells transfected with normal AR (AR12). Immunofluorescence of AR in 293T cells transfected with wild-type AR before tamoxifen treatment was identical to tamoxifen-treated cells. **C:** Untreated 293T cells transfected with disease-associated AR (AR50). **D:** Tamoxifen-treated (1 h, 35 μ M) 293T cells transfected with disease-associated AR (AR50). Immunofluorescence studies show that mutation of the N-terminal caspase cleavage site in SBMA AR blocks formation of perinuclear aggregates. **E:** Tamoxifen-treated (1 h, 35 μ M) 293T cells transfected with AR12D146N. **F:** Tamoxifen-treated (1 h, 35 μ M) 293T cells transfected with AR50D146N.

apoptotic caspase cleavage product. In vitro mutagenesis of the N-terminal caspase site blocks production of this proapoptotic fragment and dramatically reduces cellular toxicity. Further, we show that caspase cleavage of SBMA AR plays a central role in the formation of perinuclear aggregates in cell culture. Our results suggest

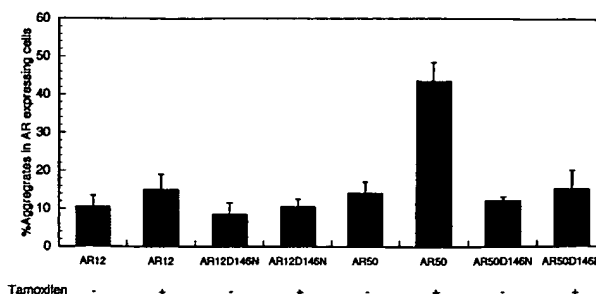


FIG. 7. Mutation of the caspase cleavage site abolishes formation of perinuclear aggregates in SBMA AR. 293T cells were transfected with the indicated AR constructs. AR was detected by immunofluorescence. The total number of cells containing aggregates relative to the total number of cells expressing AR were counted. The percentage aggregates in AR-expressing cells are presented for each construct before and after tamoxifen addition. Differences between AR50 and the other AR constructs were statistically significant ($p < 0.01$).

that the enhanced cytotoxicity of SMBA AR observed in our tissue culture paradigm may relate to the cause of neuronal cell death in patients with Kennedy's disease. Our initial characterization of the SBMA AR in 293T cells demonstrated a marked reduction in cytotoxicity after mutation of the caspase cleavage site. However, this reduction was not a proportionally greater reduction in cytotoxicity when compared with the wild-type protein. The reason for this is likely to be related to the following three factors: (1) the cytotoxicity of normal AR and expanded form are modulated by androgen levels; (2) we



FIG. 8. The subcellular distribution of AR is modulated by androgen, and addition of androgen blocks cleavage of the AR. **A:** Immunofluorescence microscopy of 293T cells transfected with AR12 shows a cytoplasmic distribution of AR. **B:** 293T cells transfected with AR12 treated with testosterone shows a nuclear localization. **C:** Western analysis of AR12 shows that the addition of testosterone blocks cleavage of the AR.

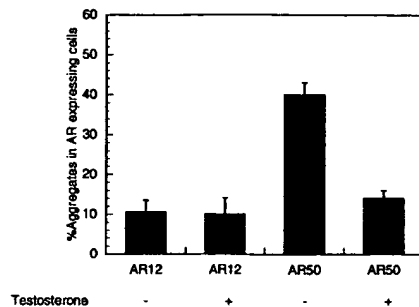


FIG. 9. Addition of testosterone modulates aggregate formation in SBMA AR. 293T cells were transfected with the indicated AR constructs. AR was detected by immunofluorescence. The total number of cells containing aggregates relative to the total number of cells expressing AR were counted. The percentages of aggregates in AR-expressing cells treated with tamoxifen are presented for each construct without and with testosterone (100 nM) addition. Differences between AR50 with and without androgen were statistically significant ($p < 0.01$).

have mutated only one of the two caspase cleavage sites contained within the AR; (3) the SBMA AR is transcriptionally less active than the wild-type form.

One intriguing finding is the effect of androgen addition on the formation of aggregates by SBMA (i.e., expanded) AR. We found that addition of testosterone reduces cleavage of AR, and this correlates with the ability of androgen to reduce the frequency of aggregates found in cells transfected with SBMA AR. Androgen treatment results in translocation of AR into the nucleus and high levels of transcriptional activity. SBMA AR is similarly translocated into the nucleus, with a slightly reduced transactivation activity (50–80%) (Kazemi-Esfarjani et al., 1995). One possible explanation for our results is that the transcriptionally active form of AR may bind to proteins and/or DNA in a fashion that blocks cleavage by caspases. An alternative possibility is that transcriptional activation of AR by androgen may result in the expression of antiapoptotic proteins such as BCL2 or IAPs.

The results reported here, coupled with our recent reports (Martindale et al., 1998; Wellington et al., 1998), suggest that one potential similarity between the eight different proteins for which expanded polyglutamine regions are associated with neurodegenerative disease states is that they are cleaved by caspases to produce proapoptotic fragments; i.e., they may function as caspase amplifiers. In this model, initial cleavage would produce a toxic fragment with a gain of toxic function, e.g., aggregation. This initial generation of toxic fragment would lead to amplification of caspases through a feedback loop. This amplification loop would be highly dependent on cellular context such as caspase/inhibitor distribution within the cell, protein–protein, and/or protein–ligand interaction with each type of polyglutamine repeat protein. Thus, generation of a proapoptotic fragment may be specifically blocked by binding to the appropriate substrates (such as androgen for the AR).

The physiological role of caspase cleavage of these proteins is unknown. However, the reported results demonstrate that caspase cleavage is crucial to the cytotoxic effect of the expanded repeat AR, as well as to its aggregation. In contrast, expression of the wild-type AR did not lead to aggregation, whether or not caspase activation was induced. These results do not, however, exclude the possibility that noncaspase proteases may also play a role in processing of the AR or other polyglutamine tract proteins.

The results also do not offer an explanation for the specific pattern of neuronal loss in Kennedy's disease or other CAG repeat diseases. It is possible that alterations in caspase expression, androgen concentration, AR expression, or downstream targets may determine the selective vulnerability of motor neurons in Kennedy's disease. The effect of testosterone to block both AR cleavage and the proapoptotic effect suggests that physiological inhibitors and enhancers of caspase cleavage of polyglutamine-containing proteins may explain the selective vulnerability of specific neuronal populations in this group of diseases.

Finally, as blocking the cleavage of the AR inhibits its proapoptotic effect, such a strategy may prove useful for the treatment of neurodegenerative diseases associated with polyglutamine repeat expansions. It is noteworthy that general caspase inhibitors have been developed, but not substrate-specific caspase inhibitors. The latter may prove to be effective in halting the continued progression of neurodegenerative diseases associated with polyglutamine tract expansions.

Note added in proof: Recent studies by Butler et al. (1998) and Abdullah et al. (1998) have demonstrated a 74-kDa C-terminally truncated fragment of the AR, which is increased in cells expressing polyglutamine-expanded AR. It is possible that this corresponds to the fragment generated by cleavage at the C-terminal caspase site, between the DNA binding domain and the hormone binding domain (referred to as an 80-kDa fragment in the current article).

Acknowledgment: This study was supported by NIH grants AG12282 and CA69381 to D.E.B., and by the Glendon Foundation (Catherine Dorn, trustee). The work of G.S.S. was supported by NIH HL51399. H.M.E. is a NIH Senior Research Fellow (NS10050). The work of M.R.H. and L.P. is supported by the Canadian Networks of Centres of Excellence (NCE-Genetics) and MRC (Canada) operating grants. M.R.H. is an established investigator of the B.C. Children's Hospital. C.L.W. and A.S.H. are Alberta Heritage Foundation for Medical Research postdoctoral fellows. We thank E. Wilson for providing a wild-type androgen receptor cDNA.

REFERENCES

- Abdullah A. A. R., Trifiro M. A., Panet-Raymond V., Alvarado C., de Tourreil S., Frankel D., Schipper H. M., and Pinsky L. (1998) Spinobulbar muscular atrophy: polyglutamine-expanded androgen receptor is proteolytically resistant *in vitro* and processed abnormally in transfected cells. *Hum. Mol. Genet.* 7, 379–384.

- Brooks B. P., Paulsen H. L., Merry D. E., Salazar-Gruoso E. F., Brinkmann A. O., Wilson E. M., and Fishbeck K. H. (1997) Characterization of an expanded glutamine repeat androgen receptor in a neuronal cell culture system. *Neurobiol. Dis.* **4**, 313–323.
- Butler R., Leigh P. N., McPhaul M. J., and Gallo J.-M. (1998) Truncated forms of the androgen receptor are associated with polyglutamine expansion in X-linked spinal and bulbar muscular atrophy. *Hum. Mol. Genet.* **7**, 121–127.
- Cardone M. H., Salvesen G. S., Widmann C., Johnson G., and Frisch S. M. (1997) The regulation of anoikis: MEKK-1 activation requires cleavage by caspases. *Cell* **90**, 315–323.
- Cashman N. R., Durham H. D., Blusztajn J. K., Oda K., Tabira T., Shaw I. T., Dahrouge S., and Antel J. P. (1992) Neuroblastoma X spinal cord (NSC) hybrid cell lines resemble developing motor neurons. *Dev. Dyn.* **194**, 209–221.
- David G., Abbas N., Stevanin G., Durr A., Yvert G., Cancel G., Weber C., Imbert G., Saudou F., et al. (1997) Cloning of the SCA7 gene reveals a highly unstable CAG repeat expansion. *Nat. Genet.* **17**, 65–70.
- Davies S. W., Turmaine M., Cozens B. A., DiFiglia M., Sharp A. H., Ross C. R., Scherzinger E., Wanker E. E., Mangiarini L., and Bates G. P. (1997) Formation of neuronal intranuclear inclusions underlies the neurological dysfunction in mice transgenic for the HD mutation. *Cell* **90**, 537–548.
- Deveraux Q. L., Takahashi R., Salvesen G. S., and Reed J. C. (1997) X-linked IAP is direct inhibitor of cell death proteases. *Nature* **388**, 300–304.
- DiFiglia M., Sapp E., Chase K. O., Davies S. W., Bates G. P., Vonsattel J. P., and Aronin N. (1997) Aggregation of huntingtin in neuronal intranuclear inclusions and dystrophic neurites in brain. *Science* **277**, 1990–1993.
- Ellerby H. M., Martin S. J., Ellerby L. M., Naiem S. S., Rabizadeh S., Salvesen G. S., Casiano N. R., Green D. R., and Bredesen D. E. (1997) Establishment of a cell-free system of apoptosis: comparison of premitochondrial, mitochondrial, and post mitochondrial phases. *J. Neurosci.* **17**, 6165–6178.
- Fischbeck K. H. (1997) Kennedy disease. *J. Inherit. Metab. Dis.* **20**, 152–158.
- Goldberg Y. P., Nicholson D. W., Rasper D. M., Kalchman M. A., Koide H. B., Graham R. K., Bromm M., Kazemi-Esfarjani P., Thornberry N. A., Vaillancourt J. P., and Hayden M. R. (1996) Cleavage of huntingtin by apopain, a proapoptotic cysteine protease, is modulated by the polyglutamine tract. *Nat. Genet.* **13**, 442–449.
- Howard A. D., Kostura M. J., Thornberry N., Ding G. J., Limjuco G., Weidner J., Salley J. P., Hogquist K. A., Chaplin D. D., Mumford R. A., et al. (1991) IL-1-converting enzyme requires aspartic acid residues for processing of the IL-1 beta precursor at two distinct sites and does not cleave 31-kDa IL-1 alpha. *J. Immunol.* **147**, 2964–2969.
- Huntington's Disease Collaborative Research Group (1993) A novel gene containing a trinucleotide repeat that is expanded and unstable on Huntington's disease chromosomes. *Cell* **72**, 971–983.
- Igarashi S., Koide R., Shimohata T., Yamada M., Hayashi Y., Takano H., Date H., Oyake M., Sato T., Sato A., Egawa S., Ikeuchi T., Tanaka H., Nakano R., Tanaka K., Hozumi I., Inuzuka T., Takahashi H., and Tsuji S. (1998) Suppression of aggregate and apoptosis by transglutaminase inhibitors in cells expressing truncated DRPLA protein with an expanded polyglutamine stretch. *Nat. Genet.* **18**, 111–117.
- Ikeda H., Yamaguchi M., Sugai S., Aze Y., Narumiya S., and Kakizuka A. (1996) Expanded polyglutamine in the Machado-Joseph disease protein induces cell death *in vitro* and *in vivo*. *Nat. Genet.* **13**, 196–202.
- Imbert G., Saudou F., Yvert G., Devys D., Trottier Y., Garnier J. M., Weber C., Mandel J. L., Cancel G., Abbas N., Durr A., Didierjean O., Stevanin G., Agid Y., and Brice A. (1996) Cloning of the gene for spinocerebellar ataxia 2 reveals a locus with high sensitivity to expanded CAG/glutamine repeats. *Nat. Genet.* **14**, 285–291.
- Jordan M., Schallhorn A., and Wurm F. M. (1996) Transfecting mammalian cells: optimization of critical parameters affecting calcium-phosphate precipitate formation. *Nucleic Acids Res.* **24**, 596–601.
- Kawaguchi Y., Okamoto T., Taniwaki M., Aizawa M., Inoue M., Katayama S., Kawakami H., Nakamura S., Nishimura M., Akiguchi I., Kimura J., Narumiya S., and Kakizuka A. (1994) CAG expansions in a novel gene for Machado-Joseph disease at chromosome 14q32.1. *Nat. Genet.* **8**, 221–227.
- Kayalar C., Ord T., Testa M. P., Zhong L. T., and Bredesen D. E. (1996) Cleavage of actin by interleukin 1 beta-converting enzyme to reverse DNase I inhibition. *Proc. Natl. Acad. Sci. USA* **93**, 2234–2238.
- Kazemi-Esfarjani P., Trifiro M. A., and Pinsky L. (1995) Evidence for a repressive function of the long polyglutamine tract in the human androgen receptor: possible pathogenetic relevance for the (CAG)_n-expanded neuropathies. *Hum. Mol. Genet.* **4**, 523–527.
- Kempainen J. A., Lane M. V., Sar M., and Wilson E. M. (1992) Androgen receptor phosphorylation, turnover, nuclear transport, and transcriptional activation. *J. Biol. Chem.* **267**, 968–974.
- Kerr J. F. R., Wyllie A. H., and Currie A. R. (1972) Apoptosis: a basic biological phenomenon with wide-ranging implications in tissue kinetics. *Br. J. Cancer* **26**, 239–257.
- Kim T.-W., Pettingell W. H., Jung Y.-K., Kovacs D. M., and Tanzi R. E. (1997) Alternative cleavage of Alzheimer-associated presenilins during apoptosis by a caspase-3 family protease. *Science* **277**, 373–376.
- Koide R., Ikeuchi T., Onodera O., Tanaka H., Igarashi S., Endo K., Takahashi H., Kondo R., Ishikawa A., Hayashi T., et al. (1994) Unstable expansion of CAG repeat in hereditary dentatorubral-pallidolysian atrophy (DRPLA). *Nat. Genet.* **6**, 9–13.
- La Spada A. R., Wilson E. M., Lubahn D. B., Harding A. E., and Fischbeck K. H. (1991) Androgen receptor gene mutations in X-linked spinal and bulbar muscular atrophy. *Nature* **352**, 77–79.
- Lockshin R. A. and Williams C. M. (1964) Programmed cell death. II. Endocrine potentiation of the breakdown of the intersegmental muscles of silkworms. *J. Insect Physiol.* **10**, 643–649.
- Martindale D., Hackam A., Wiczorek A., Ellerby L. M., Wellington C., McCutcheon K., Devon R., Sinaraja R., Bredesen D., Tufaro F., and Hayden M. R. (1998) Length of huntingtin and its polyglutamine tract influences localization and frequency of intracellular aggregates. *Nat. Genet.* **18**, 150–154.
- McGahon A. J., Martin S. J., Bissonnette R. P., Mahboubi R. P., Mahboubi A., Shi Y., Mogil R. J., Nishioka W. K., and Green D. R. (1995) The end of the (cell) line: methods for the study of apoptosis *in vitro*. *Methods Cell Biol.* **46**, 153–185.
- Miyashita T., Okamuraho Y., Mito Y., Nagafuchi S., and Yamada M. (1997) Dentatorubral pallidolysian atrophy (DRPLA) protein is cleaved by caspase-3 during apoptosis. *J. Biol. Chem.* **272**, 29238–29242.
- Nance M. A. (1997) Clinical aspects of CAG repeat diseases. *Brain Pathol.* **7**, 881–900.
- Orr H. T., Chung M., Banfi S., Kwiatkowski T. J., Servadio A., Beaudet A. L., McCalli A. E., Duveck L. A., Ranum L. P. W., and Zoghbi H. Y. (1993) Expansion of the unstable trinucleotide CAG repeat in spinocerebellar ataxia type 1. *Nat. Genet.* **4**, 221–226.
- Orth K., O'Rourke K., Salvesen G. S., and Dixit V. M. (1996) Molecular ordering of apoptotic mammalian CED-3/ICE-like proteases. *J. Biol. Chem.* **271**, 20977–20980.
- Paulson H. L., Perez M. K., Trotter Y., Trojanowski S. H., Subramony S. H., Das S. S., Vig P., Mandel J.-L., Fischbeck K. H., and Pittman R. N. (1997) Intranuclear inclusions of expanded polyglutamine protein in spinocerebellar ataxia type 3. *Neuron* **19**, 333–334.
- Perutz M. F. (1996) Glutamine repeats and inherited neurodegenerative diseases: molecular aspects. *Curr. Opin. Struct. Biol.* **6**, 848–858.
- Ross C. A. (1995) When more is less: pathogenesis of glutamine repeat neurodegenerative diseases. *Neuron* **15**, 493–496.
- Roy N., Mahadevan M. S., McLean M., Shutler G., Yaraghi Z., Farhani R., Baird S., Besner-Johnston A., Lefebvre C., Kang X., et al. (1995) The gene for neuronal apoptosis inhibitory protein is partially deleted in individuals with spinal muscular atrophy. *Cell* **80**, 167–178.

- Salvesen G. S. and Dixit V. M. (1997) Caspases: intracellular signaling by proteolysis. *Cell* **91**, 443–446.
- Salvesen G. and Enghild J. (1990) An unusual specificity in the activation of neutrophil serine protease zymogens. *Biochemistry* **29**, 5304–5308.
- Sanpei K., Takano H., Igarashi S., Sato T., Oyake M., Sasaki H., Wakisaka A., Tashiro K., Ishida Y., Ikeuchi T., Koide R., Saito M., Sato A., and Tanaka T. (1996) Identification of the gene for spinocerebellar ataxia type 2 (SCA2) using a direct identification of repeat expansion and cloning technique (DIRECT). *Nat. Genet.* **14**, 277–284.
- Scherzinger E., Lurz R., Turmaine M., Mangiarini L., Hollenbach B., Hasenbank R., Bates G. P., Davies S. W., Lehrach H., and Wanker E. E. (1997) Huntington-encoded polyglutamine expansions form amyloid-like protein aggregates *in vitro* and *in vivo*. *Cell* **90**, 549–558.
- Wellington C. L., Ellerby L. M., Hackam A. S., Margolis R. L., Trifiro M. A., Singaraja R., McCutcheon K., Salvesen G. S., Propp S. S., Bromm M., Rowland K. J., Zhang T. Q., Rasper D., Roy S., Thornberry N., Pinsky L., Kakizuka A., Ross C. A., Nicholson D. W., Bredesen D. E., and Hayden M. R. (1998) Caspase cleavage of gene products associated with triplet expansion disorders generates truncated fragments containing the polyglutamine tract. *J. Biol. Chem.* **273**, 9158–9167.
- Wolozin B., Iwasaki K., Vito P., Ganjei J. K., Lacana E., Sunderland T., Zhao B., Kusiak J. W., Wasco W., and D'Adamio L. (1996) Participation of presenilin 2 in apoptosis: enhanced basal activity conferred by an Alzheimer mutation. *Science* **274**, 1710–1713.
- Yamatsuji T., Matsui T., Okamoto T., Komatsuzaki K., Takeda S., Fukumoto H., Iwatsubo T., Suzuki N., Asami-Odaka A., and Ireland S. (1996) G protein-mediated neuronal DNA fragmentation induced by familial Alzheimer's disease-associated mutants of APP. *Science* **272**, 1349–1352.
- Zhivotovsky B., Burgess D. H., and Orrenius S. (1996) Proteases in apoptosis. *Experientia* **52**, 968–978.
- Zhivotovsky B., Gahm A., and Orrenius S. (1997) Two different proteases are involved in the proteolysis of lamin during apoptosis. *Biochem. Biophys. Res. Commun.* **233**, 96–101.
- Zhou Q., Snipas S., Orth K., Dixit V. M., and Salvesen G. S. (1997) Target protease specificity of the viral serpin CrmA. Analysis of five caspases. *J. Biol. Chem.* **272**, 7797–7800.
- Zhuchenko O., Bailey J., Bonnen P., Ashizawa T., Stockton D. W., Amos C., Dobyns W. B., Subramony S. H., Zoghbi H. Y., and Lee C. C. (1997) Autosomal dominant cerebellar ataxia (SCA6) associated with small polyglutamine expansions in the α_{1A} -voltage-dependent calcium channel. *Nat. Genet.* **15**, 62–69.

Research report

Intracerebral injection of caspase-3 inhibitor prevents neuronal apoptosis after kainic acid-evoked status epilepticus

Alexei Kondratyev *, Karen Gale

Department of Pharmacology, Georgetown University Medical Center, Washington, DC, 20007, USA

Accepted 28 September 1999

Abstract

In the aftermath of prolonged continuous seizure activity (status epilepticus, SE), neuronal cell death occurs in the brain regions through which the seizure propagates. Recent studies have implicated apoptotic processes in this seizure-related injury. Because activation of caspase-3-like cysteine proteases plays a crucial role in mammalian neuronal apoptosis, we explored the possibility that activation of caspase-3 is involved in the neuronal apoptotic cell death that occurs in rat brain following SE induced by systemic kainic acid. Caspase-3 activity was determined immunocytochemically using CM1 antibodies specific for catalytically active subunit (p17) of the enzyme. We found an induction of caspase-3 activity in rhinal cortex and amygdala at 24 h after SE. To determine whether activation of caspase-3-like proteases is a *necessary* component of the injury process, we delivered a caspase-3 inhibitor, z-DEVD-fmk, into the lateral ventricle prior to, and following SE. z-DEVD-fmk treatment substantially attenuated apoptotic cell death after SE, both in hippocampus and rhinal cortex, as evaluated by analysis of internucleosomal DNA fragmentation and neuronal nuclear morphology. Our findings implicate caspase-3 cysteine protease in the neurodegenerative response to SE and suggest that this degeneration can be attenuated by inhibition of caspase-3-like enzyme activity. © 2000 Elsevier Science B.V. All rights reserved.

Keywords: Epilepsy; Limbic system; Rhinal cortex; Caspase-3; Neuronal apoptosis; DNA fragmentation

1. Introduction

Prolonged continuous seizure activity, as occurs during status epilepticus (SE), triggers neuronal cell death in the brain regions through which the seizure propagates. Experimental SE evoked by the systemic administration of kainic acid is associated with neuronal damage preferentially localized to limbic areas, including hippocampal CA subfields and rhinal cortex [37,38].

There is reason to suspect that programmed cell death (PCD) is responsible for a significant component of the neural degeneration that occurs in the aftermath of prolonged seizures. Molecular and histopathological markers of PCD, some of which characterize apoptosis, have been reported as sequelae of SE evoked by either kainic acid or pilocarpine [13–15,19,20,32–34,44].

Apoptotic PCD depends to a significant extent on the activation of cysteine proteases. The *ced-3* gene, initially

identified in the nematode, *Caenorhabditis elegans*, provided the first evidence for an essential role of cysteine proteases in promoting apoptosis [45]. Multiple mammalian homologues of Ced-3, or “caspases”, have since been identified and fall into two distinct subclasses: caspase-1-like and caspase-3-like proteases. Among those related to caspase-1 are caspases 4, and 5 [8,18,28]. Those similar to caspase-3 include caspases 2, and 6–10 [6,9–12,23,29,42].

In mammalian systems, a crucial role for caspases in neuronal apoptosis has been documented through the use of specific inhibitors of cysteine proteases in cell cultures [4,5,7,14,26,36,40]. Moreover, caspases have been implicated in the pathogenesis associated with several models of brain damage, including ischemia [2,3], traumatic brain injury [43], and epilepsy [16]. In particular, induction of caspase-3 mRNA has been reported in rat hippocampal neurons following systemic administration of kainic acid [16], after transient global ischemia [2,16], and in response to fluid percussion-induced traumatic brain injury [43]. Furthermore, inhibitors of caspase-1-like or caspase-3-like cysteine proteases proved neuroprotective against ischemic

* Corresponding author. Fax: +1-801-469-5580; e-mail: kondrata@gusun.georgetown.edu

insults in vivo [2,3] and against ischemic and excitotoxic treatments in vitro [17].

Post-translational activation of caspases requires proteolytic cleavage of the precursor protein. In the case of caspase-3, two subunits (p17 and p12) are generated, the larger of which contains the catalytic site [10]. This process (and the resulting generation of proteolytic fragments) leads to enzyme activation and can therefore be used as a reliable and sensitive indicator of caspase activation. In the present study, we examined apoptosis and proteolytic cleavage of caspase-3 in rat hippocampus and rhinal cortex following kainic acid-evoked SE of durations sufficient to cause mild to moderate degrees of neuronal injury. To determine whether caspase-3 activation is a *necessary* component of SE-induced apoptosis, we evaluated the effect of a specific caspase-3 inhibitor, z-DEVD-fmk, applied by intracerebroventricular microinjection (according to a protocol established by Yakovlev et al. [43]), on the extent of apoptotic cell death following SE. Our findings indicate that caspase-3-like cysteine protease is a necessary component of the neurodegenerative response to prolonged seizure activity.

2. Materials and methods

2.1. Animals

Sprague–Dawley male rats weighing 175–200 g (Harlan Sprague Dawley, Indianapolis, IN) were used. Rats were maintained four per cage in a temperature-controlled room with a 12-h light cycle. Food and water were provided ad libitum. All experimental protocols used were in compliance with AALAC standards and were approved by the Georgetown University Animal Care and Use Committee.

2.2. Surgical procedures

Animals were anesthetized with Equithesin (3 mg/kg) and placed in a Kopf stereotaxic apparatus. A stainless steel guide cannula (0.71 mm external diameter, 3 mm length) aimed at the left lateral ventricle was placed through a hole drilled in the skull and secured to the skull with dental acrylic and jeweler's screws. A stainless steel stylet (0.36 mm external diameter) was inserted into the guide cannula and kept in place prior to, and in between, injections. Surgery was performed on the rats at least 3 days before experiments were initiated.

2.3. Treatment groups

Rats were randomly assigned to vehicle-treated control or z-DEVD-fmk groups ($n = 4$ for each group). A specific caspase-3 tetrapeptide inhibitor, z-DEVD-fmk (*N*-benzyloxycarbonyl-Asp(OMe)-Glu(OMe)-Val-Asp(OMe)-fluoromethylketone), 240 pmol, was infused into the left lateral

ventricle in a volume of 5 μ l. The infusion cannula, which protruded 1 mm below the indwelling guide cannula, was connected by polyethylene tubing to a 10 μ l Hamilton syringe mounted in a Sage infusion pump. The treatment regimen we selected was identical to that used by Yakovlev et al. [43] for the prevention of neuronal death after traumatic brain injury. The treatment was given 30 min before kainic acid injection, and again at 4 and 20 h after the onset of SE (which occurred between 45 and 90 min after kainic acid injection, see below). Vehicle-treated control animals were infused at the same time points (before and after SE) with 5 μ l of vehicle alone (50% DMSO). Animals were sacrificed by decapitation at 6 h after the last intraventricular injection (i.e., 24 h after termination of SE). Brains were either quickly dissected (for DNA isolation) or frozen for subsequent cryostat sectioning (for immunohistochemistry). The basis for selecting the 24-h time point (after SE termination) for measurements of caspase-3 activation and apoptosis included: (1) The fact that following kainic acid, DNA fragmentation in rhinal cortex and hippocampus has an onset between 12 and 24 h (with continued rise in fragmentation for up to 48 h or longer) [unpublished observations]; 24 h is the earliest time at which all animals exhibit consistent robust DNA fragmentation (a marker of irreversible stage of apoptosis); (2) Caspase-3 activation is known to precede the triggering of DNA fragmentation [31,39]. By choosing the earliest time point when fragmentation was robust, we increased our chances of detecting *both* caspase-3 activation *and* DNA fragmentation, thus allowing us to evaluate the protective effect of z-DEVD-fmk with maximum sensitivity.

In addition, two separate groups of saline-treated controls (see Induction of SE) and SE-treated rats ($n = 3$ for each group) were used for caspase-3 activity measurements.

2.4. Induction of SE

To induce SE, kainic acid (Sigma) was administered i.p. in a dose of 10–15 mg/kg, titrated as necessary for each group of animals to ensure that continuous SE developed within 90 min of injection. SE was allowed to continue for 2 h, after which it was terminated by an i.p. injection of 30 mg/kg diazepam (Elkins-Sinn, Cherry Hill, NJ). SE was defined as continuous seizure activity (facial and forelimb clonus, head bobbing, and facial twitching) uninterrupted by normal behavior. The animals were observed closely for at least 2 h following seizure termination to verify seizure cessation. We have previously established (in studies with EEG recordings) that in diazepam-treated rats, signs of mild head twitching and/or forelimb twitching are indicative of resumption of electrographic seizure activity. Consequently, additional doses of diazepam (10 mg/kg) were given, as needed, to ensure that all signs of seizure activity (including subtle twitching) were pre-

vented. Control (seizure naïve) rats received i.p. injection of saline (“saline control treatment”) instead of kainic acid, and were given diazepam (30 mg/kg i.p.) 3 h later.

2.5. Immunocytochemistry

2.5.1. Perfusion/fixation

For immunocytochemical detection of caspase activation, perfusion/fixation was performed. After completion of each experiment, animals were given an i.p. injection of pentobarbital (150 mg/kg) to induce deep anesthesia as assessed by loss of the “toe-pinch reflex”. Fixation was then initiated by perfusion with a rinsing solution (phosphate-buffered saline, PBS, pH 7.4, Gibco). This was followed by perfusion with 4% formaldehyde in PBS (pH 7.4). Brains were then removed from the skull, soaked overnight in the same buffer, and then transferred to a formol-saline solution containing 20% sucrose for an additional 24 h.

2.5.2. Detection of caspase-3 activation

Caspase-3 activation was determined using CM1 rabbit polyclonal antibodies (IDUN Pharmaceuticals, La Jolla, CA) which specifically recognize the fragment (17 kDa) containing the catalytic site of the enzyme [21,41]. Procedures followed those recommended by the company, as previously described [41]. Briefly, coronal cryosections (10 μ m) from perfusion-fixed brains were rinsed twice in PBS and incubated for 30 min in PBS containing 3% hydrogen peroxide to inhibit endogenous peroxidase activity. Sections were then incubated for 1 h at room temperature in blocking buffer consisting of 2% bovine serum albumin (Sigma), 0.2% non-fat milk powder, 2% normal goat serum (Sigma) and 0.8% Triton X-100 in PBS, and then overnight with primary antibodies (1:2000) at 4°C. Sections were washed three times in wash buffer (PBS containing 0.2% Tween-20), incubated with biotinylated goat anti-rabbit antibodies, and then incubated with avidin-horseradish peroxidase (HRP) conjugate (Vector Laboratories, Burlingame, CA), according to the manufacturer's recommendations for the Vecstain ABC kit. Active caspase-3-positive cells were visualized using chromogenic HRP substrate from the AEC kit (Vector Laboratories) as recommended by the manufacturer. To control for reaction specificity and residual endogenous peroxidase activity, adjacent brain sections were treated as described above with the omission of either CM1 antibody or goat anti-rabbit antibodies. Sections were counterstained with Hematoxylin (Vector Laboratories) to visualize nuclei and then examined under a microscope.

2.5.3. Double labeling for Hoechst 33258 and Texas Red / NeuN

Immunohistochemical detection of apoptotic neurons (double labeling) was performed according to the procedures described previously [43]. Coronal cryosections (10

μ m) containing ventral hippocampus were thaw-mounted onto Superfrost Plus slides (Fisher Scientific). The sections were immersion fixed for 5 min in 10% buffered formalin (pH 7.1), rinsed twice in PBS and then permeabilized by a 15 min immersion in PBS containing 0.1% saponin (Calbiochem). For identification of neurons, sections were incubated in a PBS buffer containing mouse antibodies to rat neuronal nuclear protein (NeuN, 1:100; Chemicon, Temecula, CA), 1% bovine serum albumin, and 1% normal goat serum (Sigma). After 20 h, the sections were washed in PBS and incubated for 1 h with fluorescent (Texas Red) goat anti-mouse IgG (1:100; Sigma) and then washed 3 \times in PBS. All sections were then incubated for 1 min with a 1:5000 dilution of 10 mg/ml bis-benzimide (Hoechst 33258; Sigma) to resolve nuclear morphology, mounted in Citifluor (Ted Pella, Redding, CA), and examined under a fluorescent microscope with excitation/emission wavelengths of 345/425 (Hoechst) and 590/615 (Texas Red).

2.6. Analysis of DNA fragmentation

Apoptotic DNA was isolated and labeled as previously described [43], with minor modifications. Briefly, genomic DNA was extracted from rhinal cortex and hippocampus in 7 M guanidine hydrochloride. Extracts were mixed with 1 ml of Wizard Maxiprep Resin (Promega) and the suspension was pelleted by centrifugation. The pellets were resuspended in 1 ml of washing solution (90 mM NaCl, 9 mM Tris-HCl, pH 7.4, 2.25 mM EDTA, and 55% ethanol), and drawn by vacuum through Wizard Midicolumns (Promega). Columns were washed with 6 ml of washing solution and vacuum dried. DNA was eluted with 50 μ l of water. Residual RNA was removed by incubation with 1 μ g of RNase A at 37°C for 30 min. DNA (100 ng) was added to each 20 μ l of labeling mixture comprised of 10 mM Tris-HCl, pH 9.0, 50 mM KCl, 0.1% Triton X-100, 10 mM MgCl₂, 2 μ Ci [α -³²P]dATP (3,000 Ci/mmol, Amersham) and 1 U *Taq* DNA polymerase (Perkin-Elmer). Reactions were incubated at 72°C for 20 min and terminated by the addition of the gel loading buffer. Samples were loaded onto a 1.3% agarose gel and electrophoresed at 4 V/cm. Labeled DNA fragments were visualized by autoradiography of the dried gel. Multiple autoradiographic exposure durations were used to determine and ensure that visualized DNA fragments were in the linear range of optical density. Optical density of the nucleosomal dimer areas on the autoradiograph was measured using an AlphaImager 2000 image capturing computer (Alpha Innotech, San Leandro, CA) and image analyzing software (Scion Image 3b, Scion, Frederick, MD).

A two-way ANOVA with a post-hoc Fishers test was used for statistical analysis of the DNA fragmentation detected in hippocampus and rhinal cortex in the different treatment groups. The following groups of animals and

samples were compared: (a) vehicle-treated control group was compared with SE or SE + zDEVD-fmk treated groups; (b) SE-treated group was compared with SE + z-DEVD-fmk treated group; and (c) samples from hemisphere ipsilateral to the z-DEVD-fmk infusion site were compared to samples from contralateral side within the same treatment group.

3. Results

3.1. Induction of caspase-3 activity by SE

The induction of caspase-3 activity after SE was examined immunohistochemically using CM1 antibodies [41]. These antibodies selectively recognize the active (17 kDa) catalytic subunit of the enzyme, which is released by the proteolytic digestion of an inactive precursor protein. CM1

antibody staining of brain sections obtained from rats at 24 h after a 2-h period of kainic acid-induced SE revealed cells strongly positive for the active subunit of caspase-3 localized throughout rhinal cortex (Fig. 1d,d*). In addition, a modest level of immunoreactivity was seen in the medial and lateral mammillary body. No positive cells were detected in hippocampus (Fig. 1b), mediodorsal thalamus, parietal cortex or striatum (not shown) of the same animals. Rhinal cortex and hippocampus in brain sections from animals that did not experience SE, contained no cells that were positive for the active subunit of caspase-3 (Fig. 1a,c,c*).

3.2. z-DEVD-fmk prevents apoptosis induced by SE

The extent of apoptosis after SE was examined by electrophoretic analysis of internucleosomal DNA fragmentation and by immunohistochemical labeling of neu-

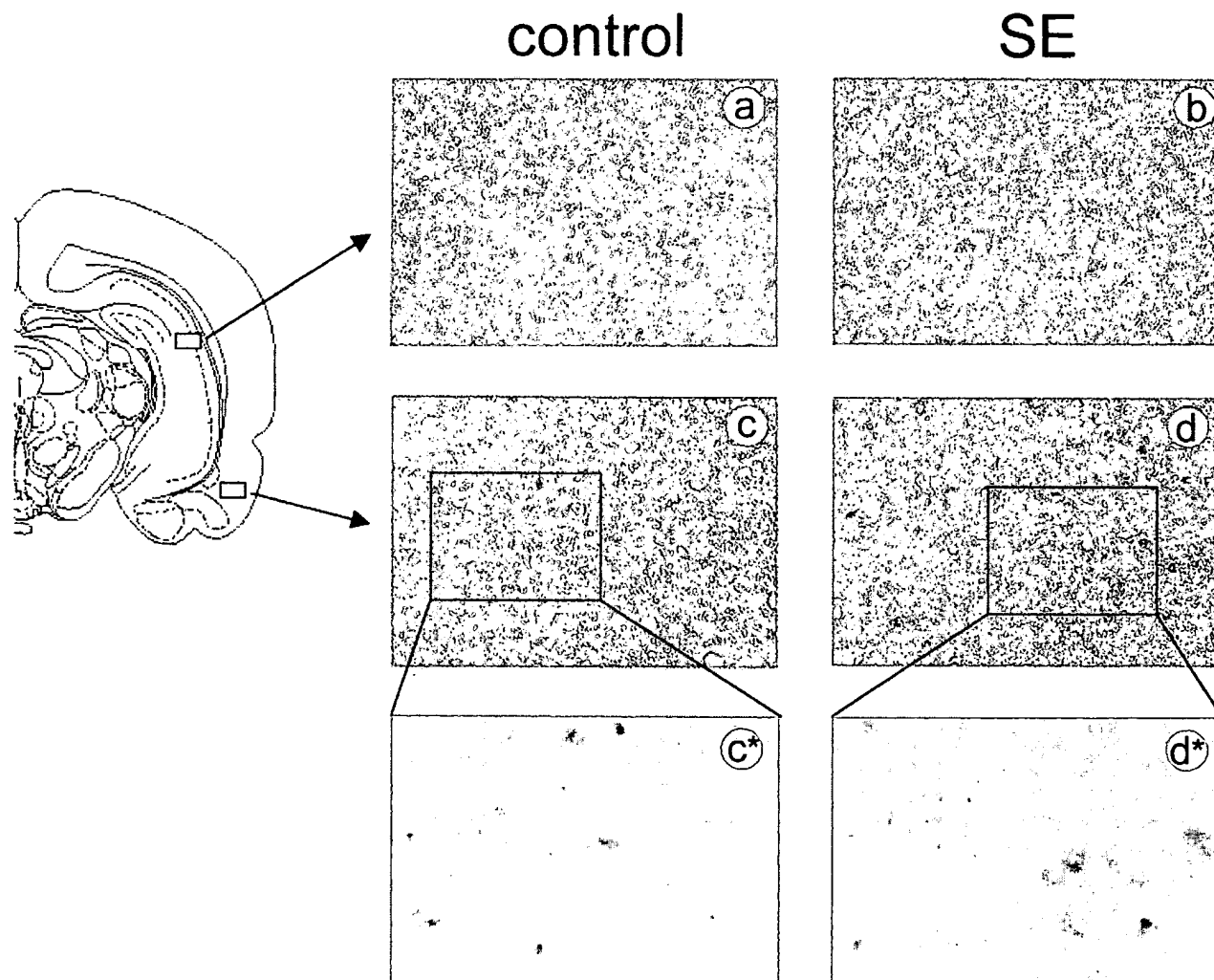


Fig. 1. Activation of caspase-3 24 h after a 2-h period of SE, as compared to saline-treated control animals not experiencing seizures. Sections from hippocampus (a, b) and entorhinal cortex (c, d) were stained with CM1 anti-p17 as described in Section 2. Cells positive for active caspase-3 (d, d*) seen as brown-red on gray-blue background. Photographs a, b, c, and d were taken at 200 \times magnification. Insets c* and d* are photomicrographs of entorhinal cortex taken at 400 \times magnification.

ronal nuclear morphology. Robust DNA fragmentation was detected by agarose gel electrophoresis from rhinal cortex and hippocampus taken at 24 h after a 2-h period of SE (Fig. 2A, lanes 3 and 4). Control brains (sham-operated, vehicle and diazepam-treated, without SE) exhibited barely detectable DNA fragmentation (Fig. 2A, lanes 1 and 2). In all groups of rats, the optical density of radiolabeled DNA bands was equivalent across the two hemispheres (Fig. 2B), indicating that the extent of DNA fragmentation is bilaterally symmetrical.

For immunohistochemical labeling, we used Hoechst 33258 to resolve nuclear morphology and to identify cells undergoing apoptosis. Double immunofluorescence stain-

ing with antibodies to neuron-specific nuclear protein NeuN performed on tissue taken 24-h after a 2-h period of SE confirmed that the majority of cells with apoptosis-like nuclear morphology were neurons of CA pyramidal cell layers of the hippocampus (Fig. 3A), as well as cells throughout rhinal cortex (not shown). No apoptotic-like cells were found in the brain sections from sham-operated, vehicle-treated animals not experiencing SE (not shown).

In animals treated with z-DEVD-fmk, in the hemisphere ipsilateral to the intracerebroventricular infusion of z-DEVD-fmk (see Section 2 for injection schedule), the neuronal apoptosis associated with SE was markedly attenuated (Fig. 3B); DNA fragmentation was not significantly

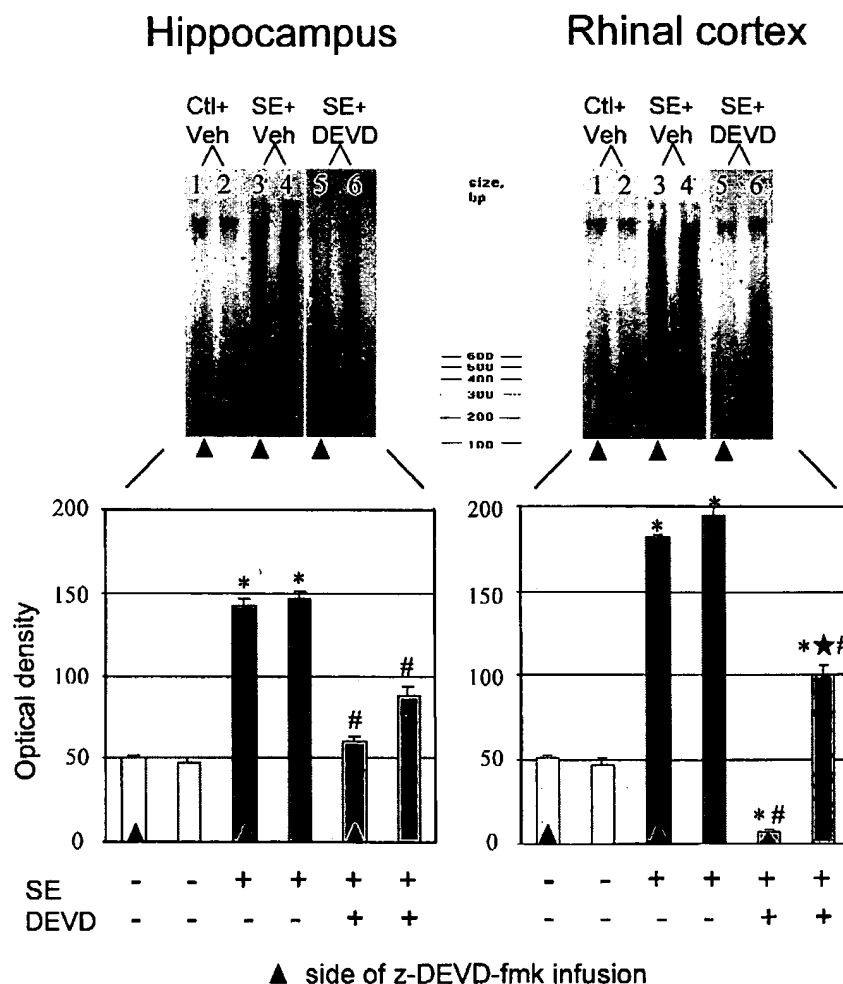


Fig. 2. DNA fragmentation evaluated 24 h after a 2-h period of SE in rats with and without z-DEVD-fmk (DEVD) treatment (see Section 2 for treatment regimen). Genomic DNA was analyzed by agarose gel electrophoresis of tissue extracts obtained from hippocampus and rhinal cortex taken from seizure-naïve control animals 6 h after the last intraventricular vehicle (DMSO) treatment (see Section 2), (Ctl + Veh, lanes 1, 2), 24 h after termination of SE in rats treated with intraventricular DMSO (SE + Veh, lanes 3, 4), and 24 h after termination of SE in rats treated with intraventricular z-DEVD-fmk (SE + DEVD, lanes 5, 6). Odd numbered lanes represent the hemisphere ipsilateral to treatment infusion. Even numbered lanes are from the contralateral side. Gel photographs are representative of the other gels run for the same experiment. Note the residual DNA laddering present in hippocampal samples and in sample from rhinal cortex contralateral to the injection side taken from rats that were treated with z-DEVD-fmk. Charts below photographs represent changes in optical density (OD) of nucleosomal dimer after SE (solid bars) and after SE in the presence of z-DEVD-fmk (gray bars), as compared to vehicle-treated controls (white bars). Significant difference ($p < 0.05$) between vehicle-treated controls and SE + vehicle or SE + z-DEVD-fmk treated animals is marked by “*”, between SE treated and z-DEVD-fmk treated animals marked by “#”, and between hemispheres within the same treatment group, marked by “★”.

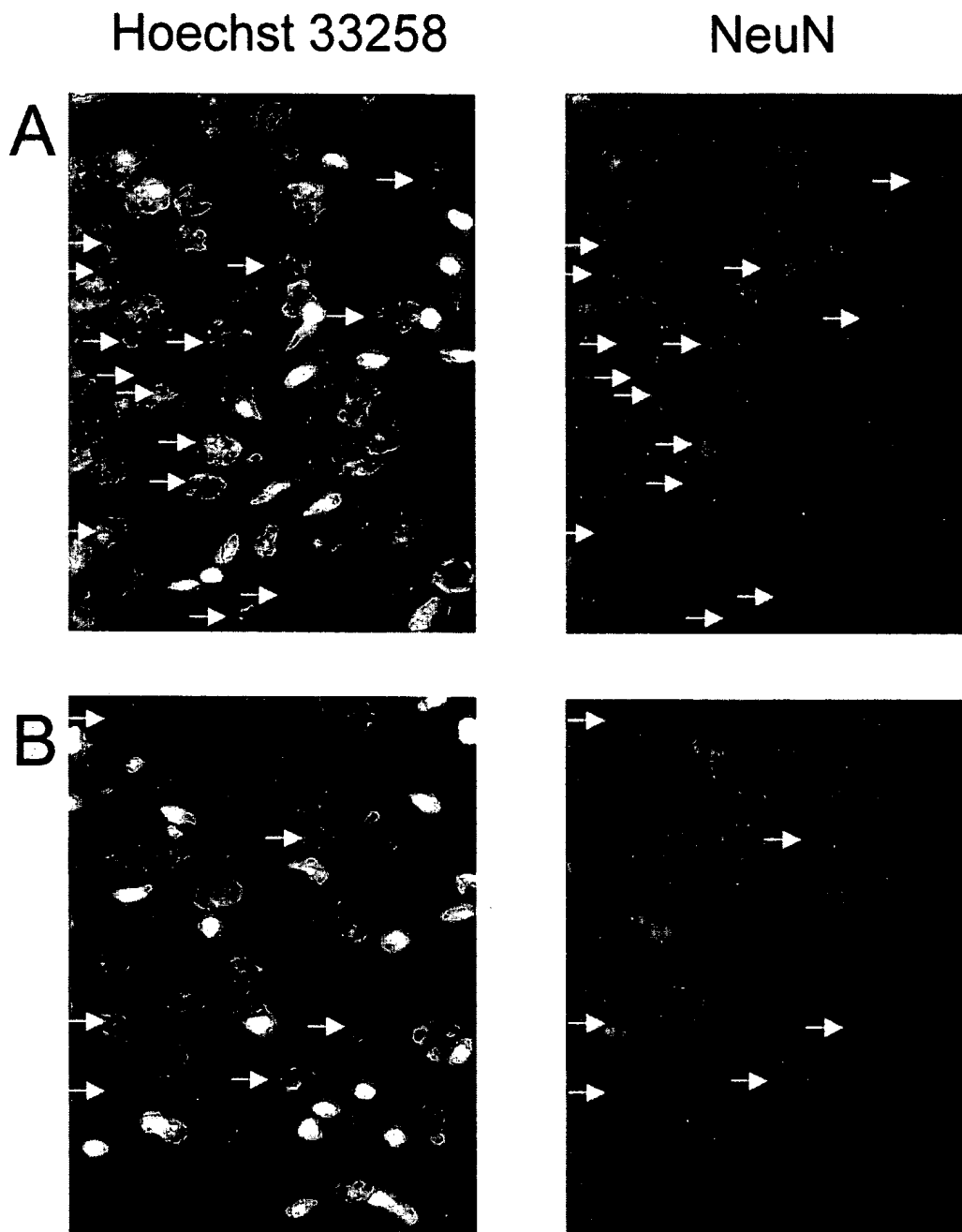


Fig. 3. Effect of z-DEVD-fmk on neuronal apoptosis in CA2 pyramidal cells. SE was induced by administration of kainic acid in (A) vehicle-treated (intraventricular DMSO) rats or (B) rats treated with intraventricular z-DEVD-fmk. Cells with apoptosis-like morphology are indicated by arrows. As evidenced by the Hoechst 33258 staining, sections obtained from control (saline-treated, seizure-naïve) animals exhibited no apoptotic morphology (not shown). Many cells exhibited apoptosis-like morphology after SE as demonstrated by nuclear staining with Hoechst 33258 (left panels). The same microscopic fields were stained for antineuronal nuclear protein (NeuN) (right panels). Double immunofluorescence revealed that a majority of apoptotic cells were neurons. Photographs were taken at 400 \times magnification. Note the presence of apoptotic like neurons still present after SE in the presence of z-DEVD-fmk. These cells may be responsible for residual DNA fragmentation seen on Fig. 2 (lanes 5, 6).

above the control level in the hippocampus, and completely undetectable in rhinal cortex (Fig. 2A, lanes 5). Partial protection was observed in the hemisphere contralateral to the z-DEVD-fmk infusion (Fig. 2, lanes 6), where the optical density indicative of DNA fragmentation in hippocampus and in rhinal cortex, was 39% and 51%

lower, respectively, than the DNA fragmentation in the same brain regions of animals exposed to SE without z-DEVD-fmk. The extent of DNA fragmentation observed in the rhinal cortex homolateral to the z-DEVD-fmk injected ventricle was significantly less than that on the contralateral side. In contrast, there was no significant

difference between the DNA fragmentation obtained in the hippocampus of the injected hemisphere vs. contralateral hemisphere. The z-DEVD-fmk injections did not alter seizure severity, latency to seizure onset, or duration of SE following administration of kainic acid.

4. Discussion

Our results demonstrate that administration of a specific caspase-3 inhibitor, z-DEVD-fmk, significantly reduces vulnerability to the neuronal cell death that occurs in the aftermath of kainic acid-evoked SE. Furthermore, the z-DEVD-fmk exposure appears to ameliorate the apoptotic component of the neurodegenerative response, as evidenced by a significant reduction in the internucleosomal DNA fragmentation and a decreased incidence of apoptosis-like neuronal morphology in hippocampus and rhinal cortex. These data suggest that caspase-3 plays a *necessary* role in seizure-induced neurodegeneration.

The molecular and histopathological evidence presented here extends previous observations that programmed cell death (PCD) participates in the neuronal loss following experimental SE, and indicates that caspase-3-like protease plays an important role in this process. In the present study, the induction of caspase-3 activity following SE was evidenced by an increase in the amount of immunoreactive catalytic subunit (p17) in rhinal cortex and amygdala, brain areas that are especially vulnerable to SE-induced neurodegeneration. These same brain areas exhibited apoptosis-like morphological changes accompanied by internucleosomal DNA fragmentation. While we do not know the mechanism by which the cleavage of the caspase-3 precursor is initiated following SE, it is conceivable that SE-induced glutamate release could be a trigger [5]. Regions resistant to SE-evoked neurodegeneration (i.e., parietal cortex and striatum) showed no signs of p17 immunoreactivity following SE. However, two other areas that exhibit marked SE-induced apoptotic neurodegeneration (CA subfields of hippocampus and dorsomedial thalamus) (Fig. 3A and Fig. 2) also showed no signs of caspase-3 activation (Fig. 1b). Thus, whereas cell death in rhinal cortex and amygdala after SE is associated with caspase-3 activation, cell death in other areas may depend upon different members of the caspase-like protease family.

The fact that caspase-3 is activated by prolonged seizure activity leads to the question of whether caspase-3 is a necessary component of the apoptotic response following SE. Consequently, we examined the effect of caspase-3 inhibition in vivo on the histological and biochemical manifestations of apoptosis following SE. Intracerebroventricular injection of the tetrapeptide inhibitor of caspase-3-like proteases, z-DEVD-fmk, significantly decreased the intranucleosomal DNA fragmentation and the incidence of apoptotic-like neuronal morphology following SE. The protection was observed to extend to regions (rhinal cor-

tex) that were located a considerable distance from the intracerebroventricular injection site, indicating that the inhibition of caspase activity is effective over a several millimeter range of drug diffusion. The DMSO vehicle is likely to facilitate drug diffusion from the ventricle and throughout the brain tissue. However, while equivalent protection was observed in the hippocampus of both hemispheres, the protection observed in rhinal cortex was markedly asymmetrical, with the rhinal cortex in the hemisphere in which the infusions were made showing a significantly greater neuroprotective response (Fig. 2) than that on the contralateral side. This suggests that the concentration of z-DEVD-fmk is less than maximally inhibitory in tissues located more than 7 mm away from the intracerebroventricular injection site.

While inhibition of caspase-3 is a plausible explanation for the neuroprotective action of z-DEVD-fmk, other related proteases may also be inhibited by this agent. z-DEVD-fmk was designed to mimic the cleavage site on poly(ADP-ribose) polymerase (PARP) [22], which is a substrate for caspase-3. However, PARP is also a substrate for several caspase-3-related proteases, including caspase-6 and caspase-7 [11]. Caspase-4 and caspase-2 can also cleave PARP, albeit with very high enzyme-substrate ratios [46]. Thus, we cannot exclude the possibility that the protective effect achieved by z-DEVD-fmk is via the inhibition of a group of enzymes with caspase-3-like activity. In fact, one or more of these enzymes may play a role in cell death in hippocampus. Our failure to detect p17 immunoreactivity in hippocampus following SE suggests that caspase-3 is not the major cysteine protease in this region. Nevertheless, z-DEVD-fmk protected against cell death in the hippocampus. This apparent inconsistency may be explained by an inhibitory action of z-DEVD-fmk on enzymes with caspase-3-like activity other than caspase-3 itself. In contrast, in rhinal cortex, the elevation of p17 immunoreactivity after SE is consistent with caspase-3 inhibition accounting for the neuroprotective effect of z-DEVD-fmk in this area.

The fact that z-DEVD-fmk is also protective against neuronal death associated with other injury models, namely traumatic brain injury [43] and transient cerebral ischemia [2], indicates that the effect we have observed is not specific to the injury model. This is consistent with z-DEVD-fmk working via a common mechanism of cell death.

What is the potential mechanism by which the activation of caspase-3-like proteases may contribute to SE-evoked apoptotic cell death? It has been suggested that the activation of caspase-3, followed by cleavage of specific substrates, may contribute to the process of apoptosis by a combination of changes in signaling molecules and structural changes. One early biochemical event that accompanies apoptosis in many cell types is the caspase-3-mediated proteolytic cleavage of nuclear proteins, including PARP [25,30] and DNA-dependent protein kinase (DNA-PK) [1].

The significance of cleavage of these proteins in apoptosis currently is uncertain, although PARP and DNA-PK are involved in DNA repair and protection of fragmented DNA [27,35]. At least two important components of the cytoskeleton, β -actin and actin-associated protein α -fodrin, also are cleaved during apoptosis by caspase-3-like proteases. When cleaved by caspase-3, actin loses its ability to polymerize and to inhibit DNase I activity [24]. Thus, an activation of caspase-3-like enzyme or enzymes may contribute to both the morphological changes and the DNA fragmentation that we have observed to follow SE.

In summary, we have demonstrated that the occurrence of apoptosis in selected brain regions after SE is accompanied by the induction of caspase-3 activity. Moreover, in vivo administration of a specific tetrapeptide inhibitor of caspase-3 markedly attenuated the SE-evoked apoptosis in rhinal cortex and hippocampus. These results implicate caspase-3-like proteases as important agents in the process of neuronal apoptosis after SE, and suggest that members of the caspase-3-like protease family may regulate neuronal PCD in a regionally-specific fashion.

Acknowledgements

The authors thank IDUN Pharmaceuticals, for supplying us with the CM1 antibodies. We are especially grateful to Dr. Anu Srinivasan for providing the detailed protocol that we followed for immunocytochemistry and for her expert advice in the execution of the protocol. The authors also thank Nguen Lan for assistance with preparation of brain sections and Dr. Alexander Yakovlev for reviewing the manuscript and providing suggestions. This work was supported by NIH grant NS 36035.

References

- [1] L.A. Casciola-Rosen, G.J. Anhalt, A. Rosen, DNA-dependent protein kinase is one of a subset of autoantigens specifically cleaved early during apoptosis, *J. Exp. Med.* 182 (1995) 1625–1634.
- [2] J. Chen, T. Nagayama, K. Jin, R.A. Stetler, R.L. Zhu, S.H. Graham, R.P. Simon, Induction of caspase-3-like protease may mediate delayed neuronal death in the hippocampus after transient cerebral ischemia, *J. Neurosci.* 18 (1998) 4914–4928.
- [3] Y. Cheng, M. Deshmukh, A. D'Costa, J.A. Demaro, J.M. Gidday, A. Shah, Y. Sun, M.F. Jacquin, E.M. Johnson, D.M. Holtzman, Caspase inhibitor affords neuroprotection with delayed administration in a rat model of neonatal hypoxic-ischemic brain injury, *J. Clin. Invest.* 101 (1998) 1992–1999.
- [4] M. Deshmukh, J. Vasilakos, T.L. Deckwerth, P.A. Lampe, B.D. Shivers, E.M. Johnson Jr., Genetic and metabolic status of NGF-deprived sympathetic neurons saved by an inhibitor of ICE family proteases, *J. Cell Biol.* 135 (1996) 1341–1354.
- [5] Y. Du, K.R. Bales, R.C. Dodel, E. Hamilton-Byrd, J.W. Horn, D.L. Czilli, L.K. Simmons, B. Ni, S.M. Paul, Activation of a caspase 3-related cysteine protease is required for glutamate-mediated apoptosis of cultured cerebellar granule neurons, *Proc. Natl. Acad. Sci. U.S.A.* 94 (1997) 11657–11662.
- [6] H. Duan, A.M. Chinnaiyan, P.L. Hudson, J.P. Wing, W.W. He, V.M. Dixit, ICE-LAP3, a novel mammalian homologue of the *Caenorhabditis elegans* cell death protein Ced-3 is activated during Fas- and tumor necrosis factor-induced apoptosis, *J. Biol. Chem.* 271 (1996) 1621–1625.
- [7] B.A. Eldadah, A.G. Yakovlev, A.I. Faden, The role of CED-3-related cysteine proteases in apoptosis of cerebellar granule cells, *J. Neurosci.* 17 (1997) 6105–6113.
- [8] C. Faucheu, A. Diu, A.W. Chan, A.M. Blanchet, C. Miossec, F. Herve, V. Collard-Dutilleul, Y. Gu, R.A. Aldape, J.A. Lippke, A novel human protease similar to the interleukin-1 beta converting enzyme induces apoptosis in transfected cells, *EMBO J.* 14 (1995) 1914–1922.
- [9] T. Fernandes-Alnemri, R.C. Armstrong, J. Krebs, S.M. Srinivasula, L. Wang, F. Bultrich, L.C. Fritz, J.A. Trapani, K.J. Tomaselli, G. Litwack, E.S. Alnemri, In vitro activation of CPP32 and Mch3 by Mch4, a novel human apoptotic cysteine protease containing two FADD-like domains, *Proc. Natl. Acad. Sci. U.S.A.* 93 (1996) 7464–7469.
- [10] T. Fernandes-Alnemri, G. Litwack, E.S. Alnemri, CPP32, a novel human apoptotic protein with homology to *Caenorhabditis elegans* cell death protein Ced-3 and mammalian interleukin-1 beta-converting enzyme, *J. Biol. Chem.* 269 (1994) 30761–30764.
- [11] T. Fernandes-Alnemri, G. Litwack, E.S. Alnemri, Mch2, a new member of the apoptotic Ced-3/Ice cysteine protease gene family, *Cancer Res.* 55 (1995) 2737–2742.
- [12] T. Fernandes-Alnemri, A. Takahashi, R. Armstrong, J. Krebs, L. Fritz, K.J. Tomaselli, L. Wang, Z. Yu, C.M. Croce, G. Salveson, Mch3, a novel human apoptotic cysteine protease highly related to CPP32, *Cancer Res.* 55 (1995) 6045–6052.
- [13] R.K. Filipkowski, M. Hetman, B. Kaminska, L. Kaczmarek, DNA fragmentation in rat brain after intraperitoneal administration of kainate, *NeuroReport* 5 (1994) 1538–1540.
- [14] V. Gagliardini, P.A. Fernandez, R.K. Lee, H.C. Drexler, R.J. Rotello, M.C. Fishman, J. Yuan, Prevention of vertebrate neuronal death by the crmA gene, *Science* 263 (1994) 826–828.
- [15] S.F. Giardina, N.S. Cheung, M.T. Reid, P.M. Beart, Kainate-induced apoptosis in cultured murine cerebellar granule cells elevates expression of the cell cycle gene cyclin D1, *J. Neurochem.* 71 (1998) 1325–1328.
- [16] F. Gillardon, B. Bottiger, B. Schmitz, M. Zimmermann, K.A. Hossmann, Activation of CPP-32 protease in hippocampal neurons following ischemia and epilepsy, *Brain Res. Mol. Brain Res.* 50 (1997) 16–22.
- [17] H. Hara, R.M. Friedlander, V. Gagliardini, C. Ayata, K. Fink, Z. Huang, M. Shimizu-Sasamata, J. Yuan, M.A. Moskowitz, Inhibition of interleukin 1beta converting enzyme family proteases reduces ischemic and excitotoxic neuronal damage, *Proc. Natl. Acad. Sci. U.S.A.* 94 (1997) 2007–2012.
- [18] J. Kamens, M. Paskind, M. Hugunin, R.V. Talanian, H. Allen, D. Banach, N. Bump, M. Hackett, C.G. Johnston, P. Li, Identification and characterization of ICH-2, a novel member of the interleukin-1 beta-converting enzyme family of cysteine proteases, *J. Biol. Chem.* 270 (1995) 15250–15256.
- [19] Y. Kitamura, T. Ota, Y. Matsuoka, M. Okazaki, J. Kakimura, I. Tooyama, H. Kimura, S. Shimohama, P.J. Gebicke-Haerter, Y. Nomura, T. Taniguchi, Kainic acid-induced neuronal loss and glial changes in the hippocampal CA3 of p53-deficient mouse, *Neurosci. Lett.* 255 (1998) 57–60.
- [20] A.D. Kondratyev, N. Sahibzada, K. Gale, An inhibitor of caspase-3 prevents neuronal cell death following status epilepticus, *Epilepsia* 39 (Suppl. 6) (1998) 5.
- [21] K. Kuida, T.F. Haydar, C.Y. Kuan, Y. Gu, C. Taya, H. Karasuyama, M.S. Su, P. Rakic, R.A. Flavell, Reduced apoptosis and cytochrome c-mediated caspase activation in mice lacking caspase 9, *Cell* 94 (1998) 325–337.
- [22] Y.A. Lazebnik, S.H. Kaufmann, S. Desnoyers, G.G. Poirier, W.C.

- Earnshaw, Cleavage of poly(ADP-ribose) polymerase by a proteinase with properties like ICE, *Nature* 371 (1994) 346–347.
- [23] J.A. Lippke, Y. Gu, C. Samecki, P.R. Caron, M.S. Su, Identification and characterization of CPP32/Mch2 homolog 1, a novel cysteine protease similar to CPP32, *J. Biol. Chem.* 271 (1996) 1825–1828.
- [24] T. Mashima, M. Naito, N. Fujita, K. Noguchi, T. Tsuruo, Identification of actin as a substrate of ICE and an ICE-like protease and involvement of an ICE-like protease but not ICE in VP-16-induced U937 apoptosis, *Biochem. Biophys. Res. Commun.* 217 (1995) 1185–1192.
- [25] M. Masson, V. Rolli, F. Dantzer, C. Trucco, V. Schreiber, S. Fribourg, M. Molinete, A. Ruf, E.A. Miranda, C. Niedergang, Poly(ADP-ribose) polymerase: structure-function relationship, *Biochimie* 77 (1995) 456–461.
- [26] C.E. Milligan, D. Prevette, H. Yaginuma, S. Homma, C. Cardwell, L.C. Fritz, K.J. Tomaselli, R.W. Oppenheim, L.M. Schwartz, Peptide inhibitors of the ICE protease family arrest programmed cell death of motoneurons in vivo and in vitro, *Neuron* 15 (1995) 385–393.
- [27] V.E. Morozov, M. Falzon, C.W. Anderson, E.L. Kuff, DNA-dependent protein kinase is activated by nicks and larger single-stranded gaps, *J. Biol. Chem.* 269 (1994) 16684–16688.
- [28] N.A. Munday, J.P. Vaillancourt, A. Ali, F.J. Casano, D.K. Miller, S.M. Molineaux, T.T. Yamin, V.L. Yu, D.W. Nicholson, Molecular cloning and pro-apoptotic activity of ICERell and ICERelll, members of the ICE/CED-3 family of cysteine proteases, *J. Biol. Chem.* 270 (1995) 15870–15876.
- [29] M. Muzio, A.M. Chinnaiyan, F.C. Kischkel, K. O'Rourke, A. Shevchenko, J. Ni, C. Scaffidi, J.D. Bretz, M. Zhang, R. Gentz, M. Mann, P.H. Krammer, M.E. Peter, V.M. Dixit, FLICE, a novel FADD-homologous ICE/CED-3-like protease, is recruited to the CD95 (Fas/APO-1) death-inducing signaling complex, *Cell* 85 (1996) 817–827.
- [30] D.W. Nicholson, A. Ali, N.A. Thornberry, J.P. Vaillancourt, C.K. Ding, M. Gallant, Y. Gareau, P.R. Griffin, M. Labelle, Y.A. Lazebnik, Identification and inhibition of the ICE/CED-3 protease necessary for mammalian apoptosis, *Nature* 376 (1995) 37–43.
- [31] A.G. Porter, R.U. Janicke, Emerging roles of caspase-3 in apoptosis, *Cell Death. Differ.* 6 (1999) 99–104.
- [32] S. Sakhi, A. Bruce, N. Sun, G. Tocco, M. Baudry, S.S. Schreiber, p53 induction is associated with neuronal damage in the central nervous system, *Proc. Natl. Acad. Sci. U.S.A.* 91 (1994) 7525–7529.
- [33] S. Sakhi, N. Sun, L.L. Wing, P. Mehta, S.S. Schreiber, Nuclear accumulation of p53 protein following kainic acid-induced seizures, *NeuroReport* 7 (1996) 493–496.
- [34] R. Sankar, D.H. Shin, H. Liu, A. Mazarati, D. Pereira, V.C.G. Wasterlain, Patterns of status epilepticus-induced neuronal injury during development and long-term consequences, *J. Neurosci.* 18 (1998) 8382–8393.
- [35] M.S. Satoh, T. Lindahl, Role of poly(ADP-ribose) formation in DNA repair, *Nature* 356 (1992) 356–358.
- [36] J.B. Schulz, M. Weller, T. Klockgether, Potassium deprivation-induced apoptosis of cerebellar granule neurons: a sequential requirement for new mRNA and protein synthesis, ICE-like protease activity, and reactive oxygen species, *J. Neurosci.* 16 (1996) 4696–4706.
- [37] J.E. Schwob, T. Fuller, J.L. Price, J.W. Olney, Widespread patterns of neuronal damage following systemic or intracerebral injections of kainic acid: a histological study, *Neuroscience* 5 (1980) 991–1014.
- [38] G. Sperk, H. Lassmann, H. Baran, S.J. Kish, F. Seitelberger, O. Hornykiewicz, Kainic acid induced seizures: neurochemical and histopathological changes, *Neuroscience* 10 (1983) 1301–1315.
- [39] J.E. Springer, R.D. Azbill, P.E. Knapp, Activation of the caspase-3 apoptotic cascade in traumatic spinal cord injury, *Nat. Med.* 5 (1999) 943–946.
- [40] A. Srinivasan, L.M. Foster, M.P. Testa, T. Ord, R.W. Keane, D.E. Bredesen, C. Kayalar, Bcl-2 expression in neural cells blocks activation of ICE/CED-3 family proteases during apoptosis, *J. Neurosci.* 16 (1996) 5654–5660.
- [41] A. Srinivasan, K.A. Roth, R.O. Sayers, K.S. Shindler, A.M. Wong, L.C. Fritz, K.J. Tomaselli, In situ immunodetection of activated caspase-3 in apoptotic neurons in the developing nervous system, *Cell Death. Differ.* 5 (1998) 1004–1016.
- [42] L. Wang, M. Miura, L. Bergeron, H. Zhu, J. Yuan, Ich-1, an Ice/ced-3-related gene, encodes both positive and negative regulators of programmed cell death, *Cell* 78 (1994) 739–750.
- [43] A.G. Yakovlev, S.M. Knoblach, L. Fan, G.B. Fox, R. Goodnight, A.I. Faden, Activation of CPP32-like caspases contributes to neuronal apoptosis and neurological dysfunction after traumatic brain injury, *J. Neurosci.* 17 (1997) 7415–7424.
- [44] D.D. Yang, C.Y. Kuan, A.J. Whitmarsh, M. Rincon, T.S. Zheng, R.J. Davis, P. Rakic, R.A. Flavell, Absence of excitotoxicity-induced apoptosis in the hippocampus of mice lacking the Jnk3 gene, *Nature* 389 (1997) 865–870.
- [45] J. Yuan, S. Shaham, S. Ledoux, H.M. Ellis, H.R. Horvitz, The *C. elegans* cell death gene *ced-3* encodes a protein similar to mammalian interleukin-1 beta-converting enzyme, *Cell* 75 (1993) 641–652.
- [46] B. Zhivotovsky, D.H. Burgess, S. Orrenius, Proteases in apoptosis, *Experientia* 52 (1996) 968–978.

Involvement of Caspase-3-Like Protease in the Mechanism of Cell Death Following Focally Evoked Limbic Seizures

David C. Henshall, Jun Chen, and Roger P. Simon

Department of Neurology, University of Pittsburgh, Pittsburgh, Pennsylvania, U.S.A.

Abstract: The cysteine protease caspase-3 may be involved in the mechanism of cell death following seizures. Using a rat model of focally evoked limbic epilepsy with continuous electroencephalography monitoring, we investigated seizure-induced changes in caspase-3 protein expression and processing, enzyme activity, and the *in vivo* effect of caspase-3 inhibition. Seizures were induced by intraamygdaloid injection of kainic acid (0.1 μ g) and were terminated after 45 min by diazepam (30 mg/kg) administration. Animals were killed 0–72 h following diazepam administration. Levels of the 32-kDa proenzyme form of caspase-3 were unaffected by seizures. Levels of the 17-kDa cleaved (active) fragment of caspase-3 were almost undetectable in control brain, but were increased significantly at 4 and 24 h within ipsilateral hippocampus and cortex in seizure animals. Caspase-3-like protease activity was increased within the ipsilateral hippocampus at 8 and 24 h following seizures. Caspase-3 immunoreactivity was increased within the vulnerable ipsilateral CA3/CA4 subfield at 24 and 72 h following seizures and was associated predominantly, but not exclusively, with neurons exhibiting DNA fragmentation. The putatively selective caspase-3 inhibitor *N*-benzyloxycarbonyl-Asp(OMe)-Glu(OMe)-Val-Asp(OMe)-fluoromethyl ketone significantly improved neuronal survival bilaterally within the hippocampal CA3/CA4 subfields following seizures. Collectively, these data suggest that caspase-3 may play a significant role in the mechanism by which neurons die following seizures. **Key Words:** Caspase-3—Seizure—Kainic acid—DNA fragmentation—z-DEVD-fmk. *J. Neurochem.* **74**, 1215–1223 (2000).

The caspase family of cell death effector proteases may have pivotal roles in the execution of neuronal death in many neurological diseases (Thornberry and Lazebnik, 1998; Schulz et al., 1999). Of the 14 identified members (Van de Craen et al., 1998), caspase-3 (CPP32/Yama/Apopain) has been shown to mediate cell death in a large number of biological systems (Fernandes-Alnemri et al., 1994; Nicholson et al., 1995; Tewari et al., 1995), in experimental models of ischemia (Chen et al., 1998; Namura et al., 1998), and in human traumatic brain injury (Clark et al., 1999). Caspase-3 is expressed as a 32-kDa proenzyme, which is cleaved to form 17- and 12-kDa fragments (Fernandes-Alnemri et al., 1994; Ni-

cholson et al., 1995). Activated caspase-3 has been shown to cleave a number of targets, including poly(ADP-ribose) polymerase (PARP) (Nicholson et al., 1995) and the caspase-activated DNase/inhibitor complex (CAD/ICAD) (Enari et al., 1998). A number of pathways have been identified by which caspase-3 activation occurs, including caspase-8- and caspase-9-dependent cleavage (Enari et al., 1996; Kuida et al., 1998; Slee et al., 1999). Caspase-9 activation occurs following formation of a complex with Apaf-1 and mitochondrial-released cytochrome *c* (Zou et al., 1997; Slee et al., 1999), and deletion of caspase-9 inhibits caspase-3 activation and apoptosis (Kuida et al., 1998). However, activation of caspase-8 may also be promoted by cytochrome *c* release (Kuwana et al., 1998).

Recent studies have implied a role for cell death regulatory genes in the mechanism by which seizures induce cell death. Following experimental seizures, the cell death inhibitory protein Bcl-2 was down-regulated within injured cell populations (Gillardon et al., 1995), whereas the cell death effector protein Bax may be increased in vulnerable regions (Gillardon et al., 1995; Zhang et al., 1998). The involvement of the caspase cell death pathway in seizure-induced brain injury was suggested recently by observations that systemically administered kainic acid (KA) increased caspase-3 mRNA, protein expression, and caspase-3-like enzyme activity (Gillardon et al., 1997; Faherty et al., 1999). However, the use of systemically administered excitotoxins to elicit seizures may confound separation of injury arising from

Received September 30, 1999; revised manuscript received November 9, 1999; accepted November 10, 1999.

Address correspondence and reprint requests to Dr. R. P. Simon at Legacy Clinical Research and Technology Center, 1225 NE 2nd Avenue, P.O. Box 3950, Portland, OR 97208-3950, U.S.A. E-mail: rsimon@lhs.org

Abbreviations used: Ac-DEVD-pNA, acetyl-Asp-Glu-Val-Asp-p-nitroanilide; CAD/ICAD, caspase-activated DNase/inhibitor complex; EEG, electroencephalography; i.c.v., intracerebroventricular; KA, kainic acid; PARP, poly(ADP-ribose) polymerase; PBS, phosphate-buffered saline; PFA, paraformaldehyde; PMSF, phenylmethylsulfonyl fluoride; SDS, sodium dodecyl sulfate; TUNEL, terminal deoxynucleotidyl transferase-mediated dUTP nick end-labeling; z-DEVD-fmk, *N*-benzyloxycarbonyl-Asp(OMe)-Glu(OMe)-Val-Asp(OMe)-fluoromethyl ketone.

seizure activity from the direct neurotoxic actions of such agents. In addition, identification and quantification of the electrographic events responsible for seizure-induced recruitment of caspase-3 remain unexplored.

Presently, we have used a model of focally evoked limbic seizures induced by intraamygdaloid injection of KA with continuous electroencephalography (EEG) monitoring and seizure quantification to address the role of caspase-3 in cell death resulting from experimental seizures. Our data strongly support the involvement of caspase-3 as a pivotal enzyme in the response of the brain to seizures and the execution of seizure-induced cell death.

MATERIALS AND METHODS

Seizure model

All animal procedures were performed in accordance with protocols approved by the Animal Care Committee of the University of Pittsburgh and in accordance with the principles outlined in the National Institutes of Health *Guide for the Care and Use of Laboratory Animals*. All studies were performed on male Sprague-Dawley rats (Harlan) within the weight range 280–350 g, which were allowed access to food and water ad libitum. Animals were anesthetized with 4% isoflurane, then intubated, and ventilated with a mixture containing 68.5% N₂O, 30% O₂, and 1.5% isoflurane. A catheter was inserted into the right femoral vein for drug administration, and the animal was then placed in a stereotaxic frame and maintained normothermic ($37 \pm 1^\circ\text{C}$) by means of a thermostatically controlled heating pad (Harvard Instruments, Holliston, MA, U.S.A.). Following a midline incision, a craniotomy (1-mm diameter) was performed (coordinates relative to bregma: AP = -2.8 mm; L = -4.0 mm) (Paxinos and Watson, 1997) and a 26-gauge steel guide cannula held in position over the surface of the dura. Additional burr holes were drilled to accommodate a securing screw and three recording electrodes with mounting screws (Plastics One Inc., Roanoke, VA, U.S.A.). Electrodes were skull-mounted over both hippocampi and over frontal cortex. The electrode-cannula assembly was then secured in place using dental cement, and animals were removed from the frame, extubated, and placed in a restraining chamber (restraining height, 50.8 mm; length, 150 mm; Harvard Instruments). A connector cable (Plastics One) was then attached to the electrode sockets and baseline EEG recordings made (Grass model 8-16; Grass Instruments Co., Quincy, MA, U.S.A.). A 31-gauge cannula (Plastics One) was then inserted into the guide and lowered 7.8 mm below the dura to enable intraamygdaloid injection of KA (0.1 μg) or vehicle [phosphate-buffered saline (PBS), pH 7.4] in a 0.5- μl volume into the right amygdala. EEG monitoring continued until diazepam (30 mg/kg) was administered intravenously 45 min following KA/vehicle injection to terminate seizures. The EEG was monitored for 1 h following diazepam to confirm seizure cessation. During recovery, animals were placed in an incubator to maintain normothermia.

EEG records were analyzed by an observer blinded to treatment, and the duration of four identifiable EEG patterns in this model was quantified as previously described (Henshall et al., 1999). Type I activity was designated baseline, type II comprised ictal fast activity, type III was high-voltage spikes of <1 -Hz frequency over type II background, and type IV seizures were high-voltage, high-frequency polyspike paroxysmal discharges.

Western blotting

Animals were killed 4 or 24 h following administration of diazepam in seizure or control animals, and the entire ipsilateral hippocampus and piriform cortex were quickly dissected free. Pooled brain samples ($n = 3$ per group) were homogenized and lysed in buffer containing 0.1 M NaCl, 0.01 M Tris, 0.1 mM EDTA, and the protease inhibitors phenylmethylsulfonyl fluoride (PMSF; 100 $\mu\text{g}/\text{ml}$) and aprotinin. Samples were then centrifuged at 14,000 rpm for 30 min at 4°C . Protein concentration was determined spectrophotometrically at A_{280} nm, and samples (50 μg) were then denatured in gel-loading buffer containing 4% sodium dodecyl sulfate (SDS), 100 mM Tris-HCl, 200 mM dithiothreitol, 0.2% bromophenol blue, and 20% glycerol at 100°C for 6 min and then separated on a 15% SDS-polyacrylamide gel. Proteins were transferred to polyvinylidene difluoride membranes (Bio-Rad) and then incubated with a polyclonal antibody against caspase-3, which has been shown previously to detect both 32- and 17-kDa fragments [dilution 1:750; Biosynthesis, Dallas, TX, U.S.A. (Chen et al., 1998)]. Membranes were then incubated with a secondary antibody (1:3,000 dilution) followed by chemiluminescence detection (NEN Life Science Products, Boston, MA, U.S.A.), and then exposed to Fuji RX film (Fuji, Tokyo, Japan).

Cytochrome c translocation

Animals were killed 0, 2, 4, 8, or 24 h following seizure termination by diazepam or 0 h following diazepam in control animals. The ipsilateral hippocampus was dissected free for isolation of mitochondrial and cytoplasmic protein fractions as previously described (Sun and Gilboe, 1994), with modifications. Pooled brain samples were homogenized in an extraction buffer containing 0.21 M mannitol, 0.07 M sucrose, 10 mM HEPES (pH 7.4), 1 mM EDTA, 0.15 mM spermine, 0.75 mM spermidine, and the protease inhibitors dithiothreitol (1 mM), PMSF (1 mM), leupeptin (1 $\mu\text{g}/\text{ml}$), and pepstatin (1 $\mu\text{g}/\text{ml}$) at 4°C . After lysis for 30 min, samples were centrifuged at 1,200 g for 25 min. The supernatant was then centrifuged at 10,000 g for 15 min, and the supernatant containing the cytoplasmic fraction was removed. The pellet containing the mitochondrial fraction was added to a solution containing 3% Ficoll 400, 0.12 M mannitol, 0.03 M sucrose, and 25 μM EDTA (pH 7.4), and gently layered twice in 6% Ficoll 400 solution to produce a discontinuous density gradient. The fraction was then centrifuged at 10,500 g for 25 min and the sediment resuspended in the lysis buffer containing 10 mM HEPES (pH 7.4), 142.5 mM KCl, 5 mM MgCl₂, 1 mM EGTA, 0.5% Nonidet P-40, 0.5 mM PMSF, 10 $\mu\text{g}/\text{ml}$ aprotinin, and 1 $\mu\text{g}/\text{ml}$ each of leupeptin, chymostatin, antipain, and pepstatin. Samples were then sonicated and the solution centrifuged at 130,000 g for 1 h to obtain the mitochondrial fraction. Cytoplasmic and mitochondrial fractions were run on 15% SDS-polyacrylamide gels using the previously described western blotting protocol, and membranes were probed with an antibody to cytochrome c (Pharmingen, San Diego, CA, U.S.A.).

Caspase-3-like protease activity

Assay of caspase-3-like protease activity was performed according to previously described techniques (Nicholson et al., 1995; Chen et al., 1998) with modifications. In brief, ipsilateral and contralateral hippocampus and piriform cortex were obtained from animals killed 4, 8, 24, or 72 h following diazepam or after 24 h for control animals. Protein was extracted in lysis buffer containing 25 mM HEPES, 5 mM EDTA, 1 mM EGTA, 5 mM MgCl₂, 5 mM dithiothreitol, and 10 $\mu\text{g}/\text{ml}$ each of pepstatin, leupeptin, and PMSF (Sigma, St. Louis, MO,

U.S.A.). Lysates were then centrifuged at 1,500 g for 10 min, and the supernatant was extracted and assayed for activity. Samples (100 μ g) of the extracted protein were incubated with the reaction buffer (25 mM HEPES, 10% sucrose, 0.1% 3-[(3-cholamidopropyl)dimethylammonio]-1-propane sulfonate, 5 mM dithiothreitol, and 5 mM EDTA) to 200- μ l volume containing 25 μ M acetyl-Asp-Glu-Val-Asp-*p*-nitroanilide (Ac-DEVD-*p*Na) (Biomol, Plymouth Meeting, PA, U.S.A.). Enzyme-catalyzed release of *p*-nitroanilide was measured at 405 nm using a microtiter plate reader (Molecular Devices, Palo Alto, CA, U.S.A.). Activity was expressed as the fold change over control once corrected for baseline. The protease inhibitor DEVD-aldehyde (5 μ M; Biomol) was incubated with alternate samples to determine nonspecific activity.

DNA fragmentation

Detection of DNA fragmentation was performed using the terminal deoxynucleotidyl transferase-mediated dUTP nick end-labeling (TUNEL) technique as previously described (Chen et al., 1998) with modifications. In brief, fresh frozen sections from animals killed 24 and 72 h following diazepam were air-dried (15 min) and then postfixed in 10% formalin (15 min) followed by ethanol/acetic acid (1:2, vol/vol) for 10 min. Sections were washed twice in PBS and then permeabilized with 3% Triton X-100 for 20 min followed by immersion in 3% hydrogen peroxide for 15 min. Sections were then incubated in an equilibration buffer for 20 min containing the following: 200 mM potassium cacodylate (pH 7.2), 4 mM potassium chloride, and 1 mM 2-mercaptoethanol. Sections were then transferred to a mixture containing, in addition, 30 μ M biotin-16-dUTP (Boehringer Mannheim Corp., Indianapolis, IN, U.S.A.) and 300 U/ml TdT (GibcoBRL) for 90 min at 37°C and washed four times in PBS. Sections were then incubated with fluorescein-D avidin (Vector Laboratories, Burlingame, CA, U.S.A.). Positive control sections were incubated with 200 U/ml DNase I for 5 min before fixation. Negative control sections underwent the same procedure, but TdT was omitted from the reaction buffer to assess nonspecific labeling.

Immunocytochemistry

Sections previously stained for DNA fragmentation using the TUNEL protocol were preblocked in 2% goat serum and then incubated for 2 h at 37°C in a 1:250 dilution of the polyclonal caspase-3 antibody. Sections were then washed three times in PBS and incubated for 2 h at 37°C in a 1:500 dilution of goat anti-rabbit Cy3.18 immunconjugate (Jackson ImmunoResearch, West Grove, PA, U.S.A.). Sections were subsequently washed, mounted in Gelvatol, and coverslipped. In additional sections, the primary antibody was omitted to assess nonspecific binding. A Zeiss microscope equipped for epifluorescent illumination was used for examining TUNEL labeling and caspase-3 immunoreactivity under excitation/emission wavelengths of 495/515 nm (green-yellow) and 550/565 nm (red), respectively. Images were collected using a Xillix digital camera and analyzed using an MCID system (St. Catharines, Ontario, Canada, U.S.A.).

Effect of the caspase-3 inhibitor on seizure-induced cell death

To examine the effects of caspase-3 inhibition *in vivo*, additional animals received intracerebroventricular (i.c.v.) administration of the putatively selective caspase-3 inhibitor *N*-benzyloxycarbonyl-Asp(OMe)-Glu(OMe)-Val-Asp(OMe)-fluoromethyl ketone (z-DEVD-fmk) (Enzyme Systems Products, Livermore, CA, U.S.A.). Animals ($n = 8$ per treatment)

were implanted with a cannula (coordinates from bregma: AP = -0.8 mm; L = -1.4 mm) to allow i.c.v. infusion (Harvard pump) of 4.5 μ g of z-DEVD-fmk at a rate of 0.75 μ g/min (Chen et al., 1998). Infusions were performed 30 min before KA administration and 1 and 24 h after diazepam. Animals were killed 72 h following diazepam by chloral hydrate overdose (400 mg/kg). Animals were then perfused transcardially with 100 ml of heparinized saline followed by 400 ml of 4% paraformaldehyde (PFA) in PBS (pH 7.4). Brains were then excised, placed in 4% PFA in PBS for 2–3 days, then cut into 2-mm slices using a brain matrix, and processed for paraffin embedding according to standard techniques. Ten-micrometer sections were cut on a microtome and stained with 0.1% cresyl violet. Assessment of seizure-induced brain injury within the selectively vulnerable hippocampus was performed bilaterally at the level of bregma -3.6 mm according to anatomical locations defined in a rat brain atlas (Paxinos and Watson, 1997). CA3/CA4 cell counts were performed by an observer blinded to treatment, using grid morphometric techniques under low- and high-power magnification fields (Henshall et al., 1999). Surviving neurons exhibiting normal morphology within the anatomically defined field of interest were included in counts, whereas shrunken and rounded or irregularly shaped neurons were omitted. Results were compared with cell counts in sham-operated animals.

Statistical analysis

Data are shown as mean \pm SEM values. Changes in caspase-3 protease activity and the effects of z-DEVD-fmk were compared by ANOVA with post hoc Fisher's PLSD test. A value of $p < 0.05$ was considered significant.

RESULTS

EEG

Four patterns of EEG activity previously defined in this model (Henshall et al., 1999) were quantified in all studies. All types of seizure activity were detected bilaterally. In the present studies, type II ictal fast activity preceded all other seizure activity without exception and typically began 2–10 min following KA injection. Type III high-voltage spikes over ictal fast background occurred over brief periods, often following type IV activity. Type IV high-voltage, high-frequency paroxysmal discharges, which are responsible for injury in this model (Henshall et al., 1999), typically occurred in defined bursts of 10–100-s duration. Administration of diazepam terminated all seizure activity, although low-level type II EEG persisted in some cases. The duration of injurious type IV epileptiform activity in KA-injected groups at each time point and for each study was equivalent.

Expression and processing of caspase-3 following seizures

The 32-kDa proenzyme form of caspase-3 was detected in both hippocampal and cortical samples from control and seizure brain (Fig. 1A). Seizures induced by intraamygdaloid KA injection did not alter levels of the 32-kDa form of caspase-3 in any brain region. In contrast, the 17-kDa cleaved fragment of caspase-3 was detected in both ipsilateral hippocampus and cortex at 4 and 24 h following seizures (Fig. 1A). The 17-kDa

FIG. 1. Caspase-3 protein expression and cytochrome *c* translocation following seizures. **A:** Representative western blot showing 32- and 17-kDa (cleaved) bands of caspase-3, in control hippocampus at 4 h (lane 1), seizure hippocampus at 4 h (lane 2), control cortex at 4 h (lane 3), seizure cortex at 4 h (lane 4), control hippocampus at 24 h (lane 5), seizure hippocampus at 24 h (lane 6), control cortex at 24 h (lane 7), and seizure hippocampus at 24 h (lane 8). Data represent pooled samples ($n = 3$ per lane). **B:** Detection of cytochrome *c* within hippocampal mitochondrial fractions from control brain at 0 h (lane 1) and after 0 h (lane 2), 2 h (lane 3), 4 h (lane 4), 8 h (lane 5), and 24 h (lane 6) in seizure brain. Data represent pooled samples ($n = 2$ per lane). **C:** Detection of cytochrome *c* within hippocampal cytoplasmic fractions from control brain at 0 h (lane 1) and after 0 h (lane 2), 2 h (lane 3), 4 h (lane 4), 8 h (lane 5), and 24 h (lane 6) in seizure brain. Data represent pooled samples ($n = 2$ per lane).

fragment was not found in control brain regions at either 4 or 24 h (Fig. 1A).

Seizure-induced translocation of cytochrome *c*

Cytochrome *c* was detected within all mitochondrial fractions from hippocampal samples (Fig. 1B) from control (lane 1) and seizure brain (lanes 2–6) samples, and levels were relatively unaffected by seizures. In contrast, cytochrome *c* was almost undetectable in cytoplasmic extracts from control animals (lane 1) and immediately following seizures (lane 2), but was increased in brain samples from rats killed 2–24 h following seizures (lanes 3–6) (Fig. 1C).

Seizure-induced increase in caspase-3-like protease activity

Caspase-3-like protease activity was increased significantly within the ipsilateral hippocampus at 8 and 24 h and declined thereafter (Fig. 2A). In contrast, there was little change in enzyme activity within the contralateral hippocampus (Fig. 2B) or bilaterally within cortical brain samples.

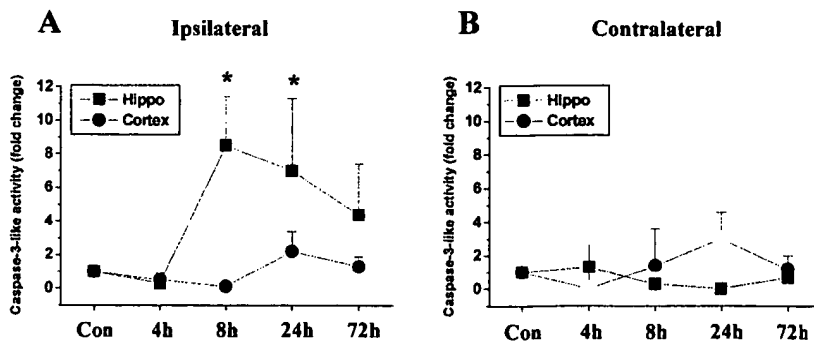


FIG. 2. Caspase-3-like protease activity following seizures. Quantification of changes in caspase-3-like protease activity within hippocampal and cortical extracts is shown. **A:** Ipsilateral caspase-3-like activity in control brain (Con) or 4, 8, 24, or 72 h following seizures. **B:** Contralateral caspase-3-like protease activity in control brain at 24 h or 4, 8, 24, or 72 h following seizures. Data are shown as means \pm SEM. Changes in enzyme activity are expressed as fold change versus control for $n = 3$ –4 per group. * $p < 0.05$, one-way ANOVA with post hoc Fisher's PLSD test.

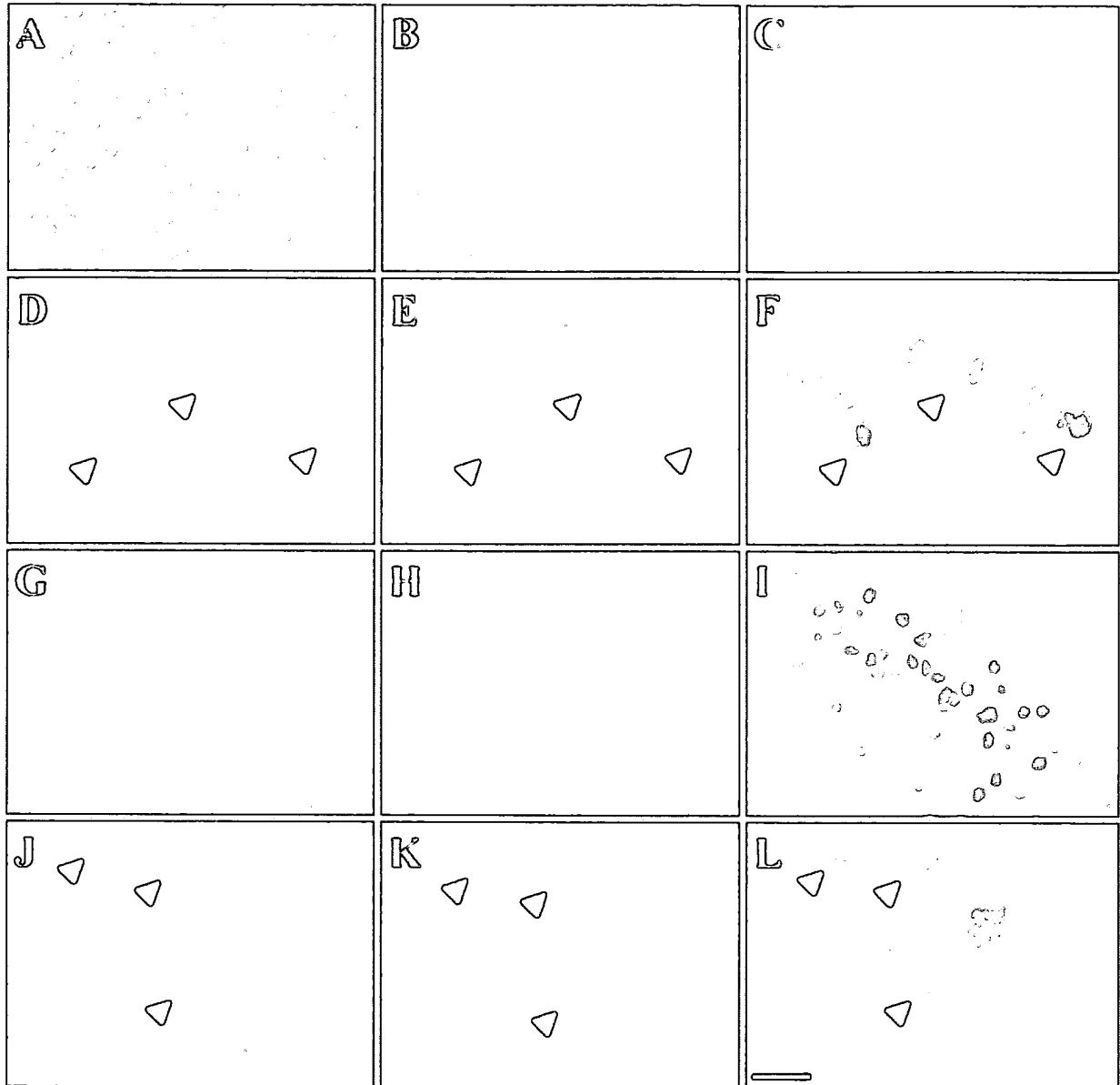


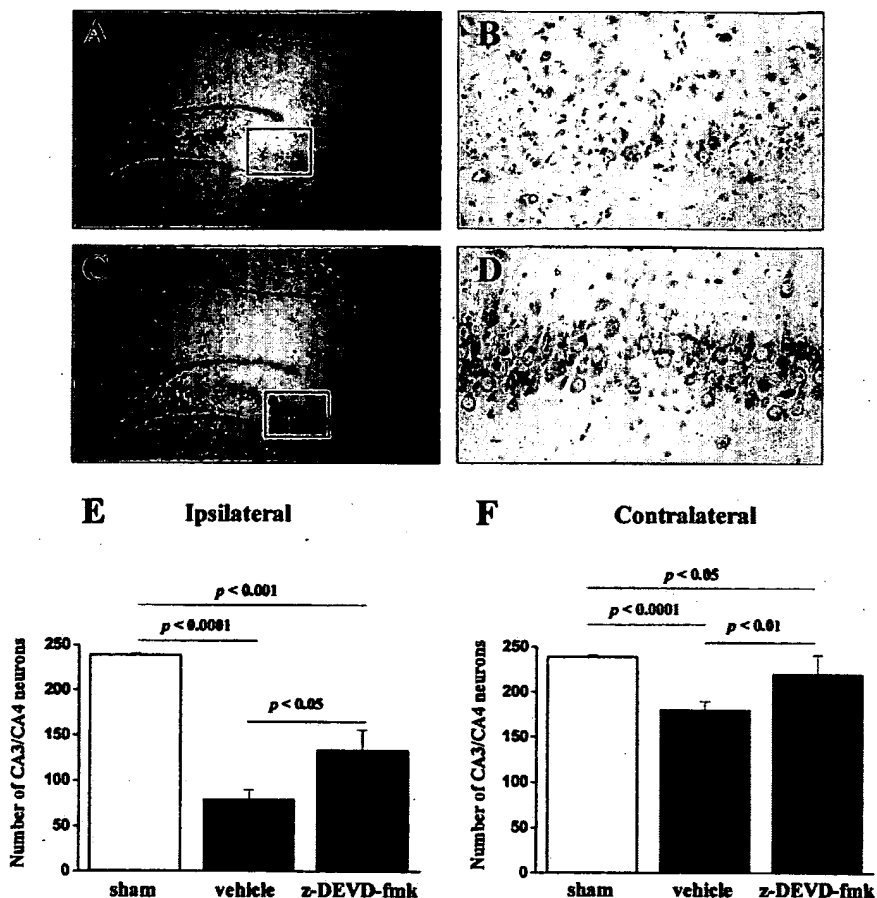
FIG. 3. Immunofluorescent images of caspase-3 protein (C, E, H, and K) and DNA fragmentation (D, G, and J) following seizures. **A:** TUNEL-positive labeling within the piriform cortex following treatment of sections with the DNA-damaging enzyme DNase I. **B:** TUNEL labeling of DNA fragmentation within the CA3 subfield of the ipsilateral hippocampus from control brain at 72 h. **C:** Caspase-3 immunoreactivity within corresponding control CA3 subfield. **D:** TUNEL labeling within ipsilateral CA3 subfield 24 h following seizures showing emergence of DNA fragmentation. **E:** Caspase-3 immunoreactivity within corresponding CA3 subfield 24 h following seizures. **F:** Image overlay of D and E showing colocalization of DNA fragmentation with caspase-3 immunoreactivity. **G:** TUNEL labeling within ipsilateral CA3 subfield 72 h following seizures showing extensive DNA fragmentation. **H:** Caspase-3 immunoreactivity within the corresponding CA3 subfield 72 h following seizures. **I:** Image overlay of G and H showing colocalization of DNA fragmentation with caspase-3 immunoreactivity. **J:** High-power magnification of TUNEL-positive CA3 pyramidal neurons 72 h following seizures. **K:** Corresponding high-power image of caspase-3 labeling of CA3 neurons within the same field. **L:** High-power overlay image of J and K, showing colocalization of TUNEL labeling and caspase-3 immunoreactivity within CA3 neurons 72 h following seizures. Note predominantly nuclear localization of caspase-3 immunoreactivity. Arrowheads indicate examples of neurons exhibiting TUNEL and caspase-3 labeling. Scale bar = 40 μ m.

Neur protective effects of the caspase-3 inhibitor z-DEVD-fmk in vivo

The duration of injurious type IV seizure activity in animals subject to KA-induced seizures was equivalent between animals receiving z-DEVD-fmk (359 ± 64 s)

and those receiving i.c.v. vehicle (352 ± 46 s). Representative low- and high-power field micrographs showing the widespread loss of neurons within the CA3/CA4 subfields of the ipsilateral hippocampus from an animal subject to KA-induced seizures with i.c.v. administration

FIG. 4. In vivo effects of the caspase-3 inhibitor z-DEVD-fmk on seizure-induced cell death. Animals received i.c.v. infusion of vehicle or z-DEVD-fmk 30 min before KA-induced seizures and 1 and 24 h following diazepam and were killed after 72 h. **A:** Low-power micrograph showing seizure-induced injury within the ipsilateral hippocampus from an animal that received i.c.v. vehicle. The box indicates high-power micrograph field. **B:** Corresponding high-power field showing large loss of ipsilateral CA3 pyramidal neurons in animals subject to seizures that received infusion of vehicle. **C:** Low-power micrograph showing representative ipsilateral hippocampus from an animal that received z-DEVD-fmk. The box indicates site of high-power micrograph. **D:** High-power field showing increased survival of pyramidal neurons within the CA3 subfield from an animal that received z-DEVD-fmk. **E:** Quantification of CA3/CA4 survival within the ipsilateral hippocampus in sham-operated animals (left column) or following seizures in animals that received infusion of vehicle (middle column) or z-DEVD-fmk (right column). Numbers of CA3/CA4 neurons were reduced significantly in animals that underwent seizures and received vehicle. Numbers of CA3/CA4 neurons were also reduced in the z-DEVD-fmk treatment group compared with sham, but were significantly higher than in the vehicle group. **F:** Quantification of CA3/CA4 survival within the contralateral hippocampus in sham-operated animals (left column) or following seizures in animals that received infusion of vehicle (middle column) or z-DEVD-fmk (right column). Numbers of CA3/CA4 neurons were reduced significantly in animals that underwent seizures and received vehicle compared with sham. Numbers of CA3/CA4 neurons were also reduced in the z-DEVD-fmk treatment group compared with sham, but were significantly higher than in the vehicle group. Data are shown as means \pm SEM for $n = 8$ animals per group and were analyzed by one-way ANOVA with post hoc Fisher's PLSD test.



of vehicle are shown in Fig. 4A and B. Figure 4C is a low-power field micrograph from an animal that received i.c.v. administration of z-DEVD-fmk, illustrating the improved survival of neurons within the CA3/CA4 area. Figure 4D shows a high-power field from the CA3 subfield of the same animal.

Quantification of CA3/CA4 neuron survival 72 h following KA-induced seizures with or without administration of z-DEVD-fmk (4.5 μ g) is shown in Fig. 4E and F. The number of ipsilateral CA3/CA4 neurons was significantly reduced by 44% (range 4–67%; $p < 0.001$) in z-DEVD-fmk-treated ($n = 8$) and by 67% (range 51–85%; $p < 0.0001$) in i.c.v. vehicle-treated ($n = 8$) seizure animals compared with sham-operated controls. Numbers of contralateral CA3/CA4 neurons were significantly reduced by 8% (range 0–19%; $p < 0.05$) in z-DEVD-fmk-treated ($n = 8$) and by 25% (range 9–38%; $p < 0.0001$) in i.c.v. vehicle-treated ($n = 8$) seizure animals compared with sham-operated controls. Comparison of CA3/CA4 cell counts between seizure animals that received either z-DEVD-fmk or vehicle

determined that neuron survival was improved by 23% within ipsilateral CA3/CA4 ($p < 0.05$) and 17% within contralateral CA3/CA4 ($p < 0.01$) in z-DEVD-fmk-treated animals over animals that received vehicle.

DISCUSSION

The present studies suggest that neuronal death following focally evoked limbic seizures may involve the activation of the cysteine protease caspase-3. Activation of caspase-3 was determined by detection of the cleaved 17-kDa fragment of caspase-3 and an increase in caspase-3-like enzymatic activity within vulnerable brain regions. We also detected translocation of the mitochondrial enzyme cytochrome *c* to the cytoplasm, an important upstream activator of the caspase cascade. Caspase-3-like immunoreactivity was increased within the selectively vulnerable CA3/CA4 subfield of the hippocampus 24–72 h following seizures, and was predominantly colocalized with DNA fragmentation within the nucleus. Finally, inhibition of caspase-3 in vivo by the putatively

selective inhibitor z-DEVD-fmk reduced neuronal death within the selectively vulnerable CA3/CA4 subfields. These data support a role for caspase-3 in mediating seizure-induced neuronal death and suggest that therapeutic treatments targeted at the caspase cascade may prove useful as an adjunct to anticonvulsant therapy in human epileptics.

Investigation of the mechanism of cell death underlying many neurodegenerative diseases has yielded a demonstrable role for the caspase family of cell death effector proteases in many cases (Thornberry and Lazebnik, 1998; Schulz et al., 1999). Caspase-3 is an essential effector of the caspase cascade (Slee et al., 1999) and among the best understood. Caspase-3 is produced as an inactive 32-kDa proenzyme, which yields 17- and 12-kDa fragments on cleavage (Nicholson et al., 1995). Activated caspase-3 cleaves a number of substrates, including structural proteins, PARP, and the CAD/ICAD endonuclease complex responsible for DNA fragmentation (Nicholson et al., 1995; Enari et al., 1998), and inhibition of this enzyme reduces neuronal death in experimental models of ischemia and traumatic brain injury (Yakovlev et al., 1997; Chen et al., 1998; Namura et al., 1998).

The role of cell death regulatory genes in the neuropathology of epilepsy has been explored only recently. Studies support the involvement of cell death effectors and repressors of the *bcl-2* gene family in the control of seizure-induced brain injury (Gillardon et al., 1995; Graham et al., 1996; Zhang et al., 1998). Whether the caspase family of cell death effector proteases plays a role in seizure-induced cell death remains little explored. However, Gillardon et al. (1995) demonstrated caspase-3 mRNA up-regulation and increased caspase-3-like enzyme activity within vulnerable regions following systemic KA administration, and increased caspase-3 immunoreactivity was reported recently in a similar model (Faherty et al., 1999). However, the use of systemic convulsants in these studies complicates separation of seizure-induced injury from the direct neurotoxic effects of KA. Furthermore, the electrographic (EEG) activity responsible for activation of caspase-3 has not been addressed.

The seizure model used in the present study involves intraamygdaloid injection of KA with assessment of seizure injury in the anatomically remote target neurons of the hippocampal CA3/CA4 subfields. This avoids the confounding influence systemic convulsants may have in separation of seizure-induced injury from that caused by direct neurotoxicity (Ben-Ari et al., 1980). Brain injury in this model is characterized by a 60–70% loss of CA3/CA4 neurons from the ipsilateral hippocampus with milder (~20%) loss of neurons on the contralateral side, whereas cell death outside this brain region is restricted to the amygdala site of injection (Henshall et al., 1999). Previous studies in multiple models have shown that seizure-induced brain injury (heat-shock protein expression), DNA damage (Klenow polymerase-labeled DNA fragmentation), and neuronal death are directly corre-

lated with the duration of polyspike paroxysmal discharges (here termed type IV seizures), but not to any other EEG pattern (Lowenstein et al., 1990, 1991; Tanaka et al., 1998; Henshall et al., 1999). As behavioral monitoring of seizure activity yields only limited insight into underlying electrographic events in brain (Ben-Ari, 1985), quantification of the duration of injurious EEG activity in the present studies also ensures that treatment groups underwent an equivalent duration of injurious seizures.

In the present study, the 32-kDa proenzyme form of caspase-3 was detected in cortical and hippocampal samples from both control and seizure animals, and levels remained unaffected following seizures in both brain regions. In contrast, the 17-kDa (active) fragment of caspase-3 was detected only within the ipsilateral hippocampus and cortex from animals that underwent seizures at 4 and 24 h, regions that exhibit neuronal death in this model (Henshall et al., 1999). These data therefore suggest that cleavage of caspase-3 is an early event following seizures.

The cell death-promoting factor cytochrome *c* has been shown to be an important upstream activator of caspase-3 through pathways involving caspase-9 and, to a lesser extent, caspase-8 (Kuida et al., 1998; Kuwana et al., 1998; Slee et al., 1999). Cytochrome *c* normally resides within the outer surface of the mitochondrial inner membrane and is not present within the cytoplasm (Skulachev, 1998). In our studies, cytochrome *c* was detectable within all mitochondrial extracts from the ipsilateral hippocampus of control and seizure animals, but was almost undetectable within the cytoplasm of control animals. Cytochrome *c* appeared within cytoplasmic extracts from seizure animals within 2 h and remained elevated until 24 h. These data therefore suggest that cytochrome *c* release could be a factor in the mechanism of seizure-induced caspase-3 activation. As cytochrome *c* may be a factor in the upstream mechanism of both caspase-8 and caspase-9 (Li et al., 1997; Kuwana et al., 1998; Skulachev, 1998), the present data do not allow further insight into the role these caspases might play upstream of caspase-3 activation.

Caspase-3-like enzyme activity was investigated in the present study using a previously described assay based on the enzyme-catalyzed release of the fluorimetric substrate *p*-nitroanilide from Ac-DEVD-*p*Na (Chen et al., 1998). Caspase-3-like activity was increased significantly only within the ipsilateral hippocampus, although small increases were found within cortical samples. Increased activation was detected 8 h following seizures, remaining elevated until 24 h and declining thereafter (Fig. 2A). Therefore, increased caspase-3-like protease activity occurs after caspase-3 cleavage, as has been reported previously in experimental ischemia (Chen et al., 1998).

DNA fragmentation within the ipsilateral CA3/CA4 subfield detected by the Klenow fragment of DNA polymerase I has been shown previously to emerge 16–24 h following seizures in this model (Henshall et al., 1999).

In the present study, TUNEL-positive cells were also restricted to the ipsilateral CA3/CA4 and appeared after a similar 24–72-h time delay. Caspase-3 immunoreactivity was very low within the ipsilateral CA3/CA4 subfield in control brain samples in the present study, but was increased in brain sections 24 and 72 h following seizures. Colocalization of TUNEL and caspase-3 immunoreactivity determined that a large number of TUNEL-positive neurons were also strongly caspase-3-immunoreactive, suggesting most but not all DNA fragmentation may be mediated by a caspase-3-dependent mechanism. This is supported by previous studies that have shown caspase-3 colocalization with DNA fragmentation following ischemia (Chen et al., 1998; Namura et al., 1998). Cell death may proceed in the absence of caspase involvement, however (Kitanaka and Kuchino, 1999), and this is supported by morphologic studies showing that more than one form of cell death occurs in neuronal populations subject to seizures (Sloviter et al., 1996). An additional observation of significance in the present study was that caspase-3 immunoreactivity was localized predominantly within the nucleus at 24 and 72 h, with little detected within the cytoplasm. As caspase-3 is found mainly within the cytoplasm and mitochondria in normal cells (Zhovotovskiy et al., 1999), these data suggest that caspase-3 translocates to the nucleus following seizures, as has been suggested recently in other systems (Zhovotovskiy et al., 1999).

In vivo inhibition of caspase-3 by the putatively selective inhibitor z-DEVD-fmk significantly improved neuron survival by ~20% within the vulnerable CA3/CA4 of both ipsilateral and contralateral hippocampi following seizures. The tetrapeptide inhibitor z-DEVD-fmk has been shown previously to be a potent inhibitor of caspase-3-like protease activity in vivo (Chen et al., 1998), which under the same dosing regime reduced DNA fragmentation and neuronal death following global cerebral ischemia (Chen et al., 1998). This is the first study to investigate the effects of this inhibitor on seizure-induced neuronal death, and the data support the effectiveness of z-DEVD-fmk as a neuroprotectant against seizure-induced neuronal death. That z-DEVD-fmk was effective in reducing neuronal loss from the contralateral CA3/CA4 was surprising, however, because significant caspase-3 enzyme activity, immunoreactivity, and DNA fragmentation were not detected within this region. The explanation is unclear but may reside with different cell death processes within this brain region, inhibition of non-caspase-3-dependent cell death processes, or through a nonspecific action.

A number of limitations should be considered when interpreting the findings in the present study. The specificity of the substrate used in the caspase-3 enzyme assay (Ac-DEVD-pNa) may not be absolute (Chen et al., 1998). Also, the caspase-3 inhibitor z-DEVD-fmk may inhibit additional caspases that recognize a DEVD cleavage motif. Further, the detection of caspase-3 cleavage, enzyme activity, and immunochemical colocalization with DNA fragmentation cannot be taken as implicit

involvement of caspase-3 in seizure-induced cell death nor exclude multiple cell-death mechanisms.

The present study shows that caspase-3 is cleaved and becomes active within brain regions exhibiting cell death following seizures induced by intraamygdaloid KA. These events occurred in a sequential manner over a time course compatible with downstream consequences of caspase-3 activation, such as DNA fragmentation. Further, caspase-3 protein likely translocates to the nucleus where it is colocalized with fragmented DNA. Selective inhibition of caspase-3 in vivo may confer significant protection against seizure-induced brain injury, and inhibition of caspase-3 may therefore provide a novel neuroprotective approach as an adjunct to anticonvulsant therapy.

Acknowledgment: The authors would like to thank Jennifer L. Sinclair, Shu-Feng Yang, and Christine O'Hara for technical help. This work was supported by NIH grant NS39016 (R.P.S., D.C.H.).

REFERENCES

- Ben-Ari Y. (1985) Limbic seizure and brain damage produced by kainic acid: mechanisms and relevance to human temporal lobe epilepsy. *Neuroscience* **14**, 375–403.
- Ben-Ari Y., Tremblay E., and Ottersen O. P. (1980) Injections of kainic acid into the amygdaloid complex of the rat: an electrographic, clinical and histological study in relation to the pathology of epilepsy. *Neuroscience* **5**, 515–528.
- Chen J., Nagayama T., Jin K., Stetler R. A., Zhu R. L., Graham S. H., and Simon R. P. (1998) Induction of caspase-3-like protease may mediate delayed neuronal death in the hippocampus after transient cerebral ischemia. *J. Neurosci.* **18**, 4914–4928.
- Clark R. S., Kochanek P. M., Chen M., Watkins S. C., Marion D. W., Chen J., Hamilton R. L., Loeffert J. E., and Graham S. H. (1999) Increases in Bcl-2 and cleavage of caspase-1 and caspase-3 in human brain after head injury. *FASEB J.* **13**, 813–821.
- Enari M., Talianian R. V., Wong W. W., and Nagata S. (1996) Sequential activation of ICE-like and CPP32-like proteases during Fas-mediated apoptosis. *Nature* **380**, 723–726.
- Enari M., Sakahira H., Yokoyama H., Okawa K., Iwamatsu A., and Nagata S. (1998) A caspase-activated DNase that degrades DNA during apoptosis, and its inhibitor ICAD. *Nature* **391**, 43–50.
- Faherty C. J., Xanthoudakis S., and Smeyne R. J. (1999) Caspase-3-dependent neuronal death in the hippocampus following kainic acid treatment. *Mol. Brain Res.* **70**, 159–163.
- Fernandes-Alnemri T., Litwack G., and Alnemri E. S. (1994) CPP32, a novel human apoptotic protein with homology to *Caenorhabditis elegans* cell death protein Ced-3 and mammalian interleukin-1 β -converting enzyme. *J. Biol. Chem.* **269**, 30761–30764.
- Gillardon F., Wickert H., and Zimmermann M. (1995) Up-regulation of bax and down-regulation of bcl-2 is associated with kainate-induced apoptosis in mouse brain. *Neurosci. Lett.* **192**, 85–88.
- Gillardon F., Bottiger B., Schmitz B., Zimmermann M., and Hossmann K.-A. (1997) Activation of CPP32 protease in hippocampal neurons following ischemia and epilepsy. *Mol. Brain Res.* **50**, 16–22.
- Graham S. H., Chen J., Stetler R. A., Zhu R. L., Jin K. L., and Simon R. P. (1996) Expression of the proto-oncogene bcl-2 is increased in the rat brain following kainate-induced seizures. *Rest. Neurol. Neurosci.* **9**, 243–250.
- Henshall D. C., Sinclair J. S., and Simon R. P. (1999) Relationship between seizure-induced transcription of the DNA damage-inducible gene GADD45, DNA fragmentation, and neuronal death in focally evoked limbic epilepsy. *J. Neurochem.* **73**, 1573–1583.
- Kitanaka C. and Kuchino Y. (1999) Caspase-independent programmed cell death with necrotic morphology. *Cell Death Differ.* **6**, 508–515.

- Kuida K., Haydar T. F., Kuan C. Y., Gu Y., Taya C., Karasuyama H., Su M. S., Rakic P., and Flavell R. A. (1998) Reduced apoptosis and cytochrome *c*-mediated caspase activation in mice lacking caspase 9. *Cell* **94**, 325–337.
- Kuwana T., Smith J. J., Muzio M., Dixit V., Newmeyer D. D., and Kornbluth S. (1998) Apoptosis induction by caspase-8 is amplified through the mitochondrial release of cytochrome *c*. *J. Biol. Chem.* **273**, 16589–16594.
- Li P., Nijhawan D., Budihardjo I., Srinivasula S. M., Ahmad M., Alnemri E. S., and Wang X. (1997) Cytochrome *c* and dATP-dependent formation of Apaf-1/caspase-9 complex initiates an apoptotic protease cascade. *Cell* **91**, 479–489.
- Lowenstein D. H., Simon R. P., and Sharp F. R. (1990) The pattern of 72-kDa heat shock protein-like immunoreactivity in the rat brain following fluoroethyl-induced status epilepticus. *Brain Res.* **531**, 173–182.
- Lowenstein D. W., Shimosaka S., So Y. T., and Simon R. P. (1991) The relationship between electrographic seizure activity and neuronal injury. *Epilepsy Res.* **10**, 49–54.
- Namura S., Zhu J., Fink K., Endres M., Srinivasan A., Tomaselli K. J., Yuan J., and Moskowitz M. A. (1998) Activation and cleavage of caspase-3 in apoptosis induced by experimental cerebral ischemia. *J. Neurosci.* **18**, 3659–3668.
- Nicholson D. W., Ali A., Thornberry N. A., Vaillancourt J. P., Ding C. K., Gallant M., Gareau Y., Griffin P. R., Labelle M., Lazebnik Y. A., Munday N. A., Raju S. M., Smulson M. E., Yamin T.-T., Yu V. L., and Miller D. K. (1995) Identification and inhibition of the ICE/CED-3 protease necessary for mammalian apoptosis. *Nature* **376**, 37–43.
- Paxinos P. and Watson C. (1997) *The Rat Brain in Stereotaxic Coordinates*, 3rd edit. Academic Press, San Diego.
- Schulz J. B., Weller M., and Moskowitz M. A. (1999) Caspases as treatment targets in stroke and neurodegenerative diseases. *Ann. Neurol.* **45**, 421–429.
- Skulachev V. P. (1998) Cytochrome *c* in the apoptotic and antioxidant cascades. *FEBS Lett.* **423**, 275–280.
- Slee E. A., Harte M. T., Kluck R. M., Wolf B. B., Casiano C. A., Newmeyer D. D., Wang H.-G., Reed J. C., Nicholson D. W., Alnemri E. S., Green D. R., and Martin S. J. (1999) Ordering the cytochrome *c*-initiated caspase cascade: hierarchical activation of caspases-2, -3, -6, -7, -8 and -10 in a caspase-9-dependent manner. *J. Cell Biol.* **144**, 281–292.
- Sloviter R. S., Dean E., Sollas A. L., and Goodman J. H. (1996) Apoptosis and necrosis induced in different hippocampal neuron populations by repetitive perforant path stimulation in the rat. *J. Comp. Neurol.* **366**, 516–533.
- Sun D. and Gilboe D. D. (1994) Ischemia-induced changes in cerebral mitochondrial free fatty acids, phospholipids, and respiration in the rat. *J. Neurochem.* **62**, 1921–1928.
- Tanaka K., Henshall D. C., Waga S., Shimosaka S., and Simon R. P. (1998) Bilateral intranigral NMDA infusion suppresses neuronal injury without affecting the duration of kainic acid-induced seizures in rats. *Neurosci. Lett.* **251**, 69–71.
- Tewari M., Quan L. T., O'Rourke K., Desnoyers S., Zeng Z., Beidler D. R., Poirier G. G., Salvesen G. S., and Dixit V. M. (1995) Yama/CPP32 beta, a mammalian homolog of CED-3, is a CrmA-inhibitable protease that cleaves the death substrate poly(ADP-ribose) polymerase. *Cell* **81**, 801–809.
- Thornberry N. A. and Lazebnik Y. (1998) Caspases: enemies within. *Science* **281**, 1312–1316.
- Van de Craen M., Van Loo G., Declercq W., Schotte P., Van den Brande I., Mandruzzato S., van der Bruggen P., Fiers W., and Vandenabeele P. (1998) Molecular cloning and identification of murine caspase-8. *J. Mol. Biol.* **284**, 1017–1026.
- Yakovlev A. G., Knoblach S. M., Fan L., Fox G. B., Goodnight R., and Faden A. I. (1997) Activation of CPP32-like caspases contributes to neuronal apoptosis and neurological dysfunction after traumatic brain injury. *J. Neurosci.* **17**, 7415–7424.
- Zhang L. X., Smith M. A., Li X. L., Weiss S. R., and Post R. M. (1998) Apoptosis of hippocampal neurons after amygdala kindled seizures. *Mol. Brain Res.* **55**, 198–208.
- Zhivotovsky B., Samali A., Gahm A., and Orrenius S. (1999) Caspases: their intracellular localization and translocation during apoptosis. *Cell Death Differ.* **6**, 644–651.
- Zou H., Henzel W. J., Liu X., Lutschg A., and Wang X. (1997) Apaf-1, a human protein homologous to *C. elegans* CED-4, participates in cytochrome *c*-dependent activation of caspase-3. *Cell* **90**, 405–413.

Activation of Fas and caspase 3 precedes PrP accumulation in 87V scrapie

Elizabeth Jamieson,^{CA} Martin Jeffrey,¹ James W. Ironside² and Janet R. Fraser

Institute for Animal Health, Neuropathogenesis Unit, Ougston Building, West Mains Road, Edinburgh EH9 3JF; ¹VLA Lasswade Veterinary Laboratory, Pentlands Science Park, Bush Loan, Penicuik, Edinburgh EH26 OPZ; ²National CJD Surveillance Unit, University of Edinburgh, Western General Hospital, Edinburgh EH4 2XU, UK

^{CA}Corresponding Author

Received 17 August 2001; accepted 5 September 2001

The sequence of events involved in the neurodegeneration caused by transmissible spongiform encephalopathies is not yet known. Using a murine scrapie model in which neurodegeneration in the hippocampus is restricted to the CA2, we show an up-regulation of the proapoptotic markers Fas and caspase 3 early in the incubation period prior to disease-specific prion

protein (PrP) deposition and clinical signs. These results suggest that activation of Fas and caspase 3 are involved in the early pathological sequence of events during murine scrapie, and that these proapoptotic markers may be a specific method for early detection of neurodegeneration. *NeuroReport* 12:3567–3572 © 2001 Lippincott Williams & Wilkins.

Key words: Apoptosis; Caspase; Fas; Prion; PrP; Scrapie

INTRODUCTION

The neurodegenerative transmissible spongiform encephalopathies (TSEs) include scrapie in sheep and goats, bovine spongiform encephalopathy in cattle, and Creutzfeldt-Jakob disease in humans. These diseases are characterised by central nervous system (CNS) spongiosis, neuronal loss and accumulation of PrP^{Sc}, an abnormal protease-resistant isomer of the cellular prion protein, PrP^C. The relationship between neuronal loss and PrP deposition in TSEs remains unclear [1–3]. The molecular nature of the TSE infectious agent is thought to be associated with PrP^{Sc} [4]. The normal cellular function of PrP^C is unknown, but studies suggest it is involved in survival of Purkinje neurons [5], synaptic plasticity [6] and superoxide dismutase-like activity [7,8].

Cell death by apoptosis is a regulated process exerted by the coordinated action of many different gene products. An important physiological mediator of apoptosis is Fas (CD95, APO-1), a 48 kDa cell surface receptor belonging to a family of receptors that includes nerve growth factors and tumour necrosis factor receptors [9,10]. Increased levels of Fas and Fas ligand have been reported in Alzheimer's disease (AD) [11]. However, the Fas/Fas ligand pathway is not involved in cell loss during other neurodegenerative diseases such as Huntington's or Parkinson's diseases [12]. Increased levels of Fas have been observed in neurons of apoptotic areas following middle cerebral artery occlusion [13]. Recent work has also shown that Fas induction is associated with neuronal death and p53 accumulation in the rat brain after kainic-acid-induced seizures [14].

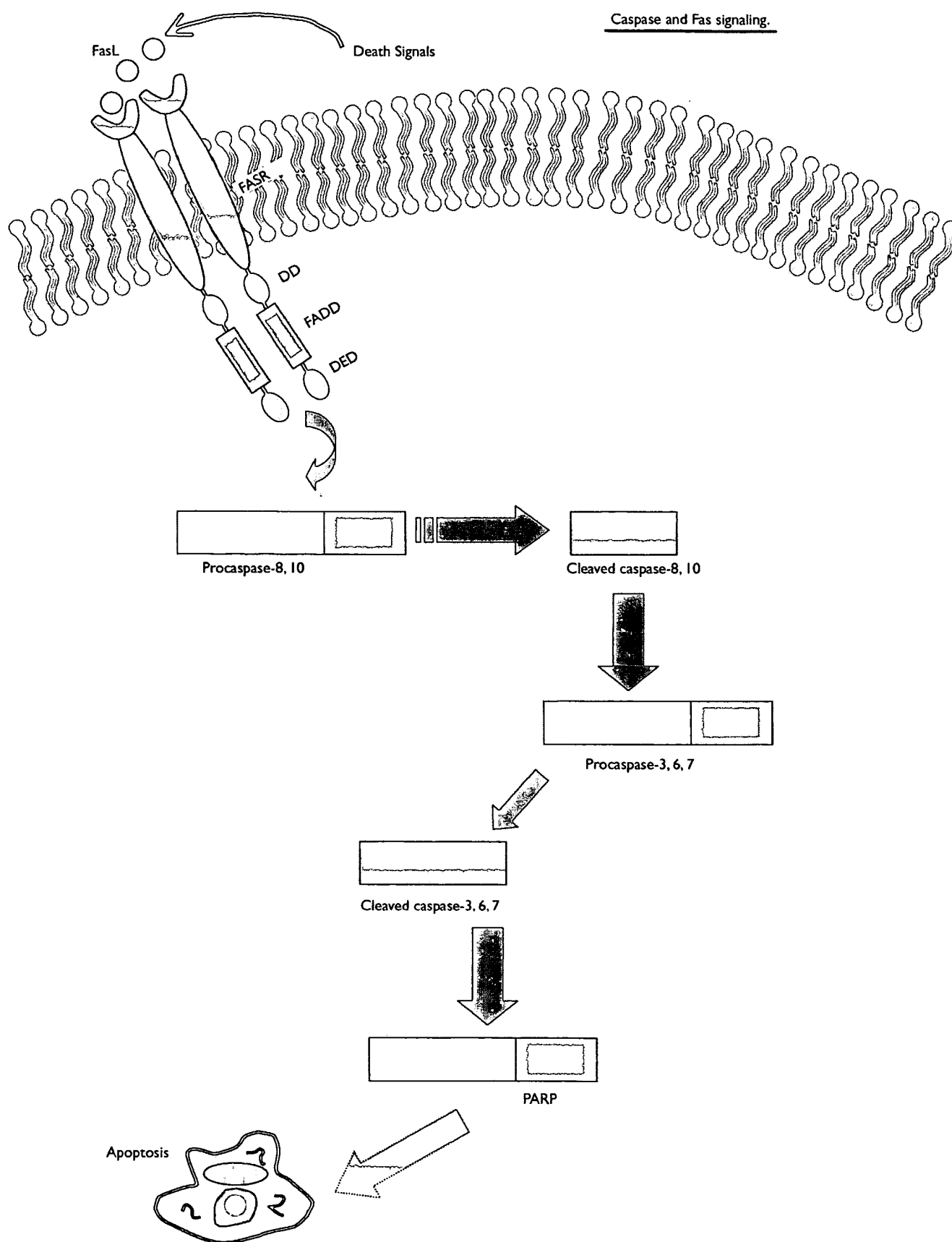
Upon binding of Fas ligand to the extracellular domain of the Fas receptor, the receptor is thought to link via its cytosolic death domain to adaptor proteins such as the

intracellular Fas-associated death domain (FADD) which in turn initiates the apoptotic cascade. This is thought to occur via activation of initiator caspases (caspases 8 and 10) by effector proteins (Fig. 1). Activated caspases 8 and 10 then cleave and activate downstream effector caspases such as 3, 6 and 7 [15,16]. Activated caspases 3, 6 and 7 are then thought to cleave and activate various proteins including poly(ADP-ribose) polymerase (PARP), leading to DNA damage and apoptosis. Increased levels of caspase 3 and other proapoptotic markers have been observed in AD tissue [17,18], and caspases have been suggested to play a dual role in proteolytic processing of amyloid precursor protein and apoptotic death of neurons in AD [19]. Elevated caspase 3 has been observed in primary cortical neurons exposed to the amyloidogenic peptides A β 1–40 and A β 1–42 [20,21].

Recent studies have shown that low concentrations of the amyloidogenic prion protein peptide PrP106–126 can induce activation of proapoptotic markers in cell culture [22], and that a substrate of caspase 3, poly (ADP-ribose) polymerase, cleavage is induced by PrP 106–126 [23]. However, neither Fas nor caspase up-regulation have been reported in prion diseases. We now report early induction of Fas and caspase 3 prior to disease specific PrP deposition during 87V scrapie infection.

MATERIALS AND METHODS

Murine scrapie model: Mice of VM/Dk strain encoding the PrP^{a/b} genotype were intracerebrally inoculated with 20 μ l 1% (w/v) brain homogenate from a VM/Dk mouse terminally infected with 87V scrapie by the standard procedure [24]. Uninfected brain tissue was used as control



homogenate. Scoring for clinical signs of illness during the incubation period was performed as described [25], and first clinical signs were apparent at 260 days post-injection (dpi). At specific time points throughout the incubation period: 50, 100, 150, 200, 250 dpi, and at terminal point of disease (320 dpi), six scrapie-infected and four age-matched normal brain-injected mice were culled by cervical dislocation and their brains removed for further analysis.

Immunohistochemistry: Following removal, brains were fixed in 10% formal saline, dehydrated in alcohol and embedded in paraffin wax during a 7 h automated processing cycle. Microtome sections were cut at 6 µm and mounted onto Superfrost plus slides (Shandon). Fas was detected using a polyclonal antibody (Santa Cruz Biotechnology, USA, se-1023), and activated caspase-3 was detected using a polyclonal antibody that detects the p17 active subunit of caspase 3 (R and D Systems, Europe, AF835). The secondary label used in both cases was a biotinylated goat anti-rabbit antibody (Jackson's, PA, USA, 111-065-003). The reaction products were visualised with DAB. Normal serum was used in place of primary antibody as a control.

Western blot analysis: 10% (w/v) homogenates of whole brain tissue were prepared in NP-40 buffer (0.5% (v/v) NP-40, 0.5% (w/v) sodium deoxycholate, 150 mM NaCl, 50 mM Tris-HCl pH 7.5). Homogenates were centrifuged at 1300 × g for 20 min to remove cellular debris. Supernatant samples were incubated with sample buffer (Invitrogen, CA, USA) at 70°C for 15 min and separated on 4–12% Bis-Tris gradient gels (Invitrogen, CA, USA). Proteins were transferred onto PVDF membrane by electroblotting and incubated with polyclonal rabbit antisera (those used for immunohistochemistry) for 2 h at room temperature. Proteins were visualised with horseradish peroxidase conjugated secondary antibody and a chemiluminescence detection kit (Roches Diagnostics, Mannheim, Germany). Membranes were exposed to X-ray film for 3 min.

RESULTS

Fas immunolabelling: The intensity of Fas immunolabelling was assessed at time points during the incubation period. No difference between 87V scrapie-infected and control tissue was observed at 50 dpi (data not shown). Immunohistochemistry showed an increase in Fas immunoreactivity in 87V-scrapie infected CA2 at 100 dpi (Fig. 2b) compared to the low basal level in age-matched normal brain injected control tissue (Fig. 2a). This increase is maintained at 150 and 200 dpi (data not shown) and at the terminal stage of disease in 87V-infected CA2 (Fig. 2d) compared to control normal brain-injected tissue (Fig. 2c). Fas immunolabelling was present in the neuropil surrounding cell bodies.

Immunoblotting with antisera to Fas confirmed that increased levels of Fas were first detectable from 100 dpi in

87V scrapie-infected tissue (Fig. 2e, lane 2) compared to basal levels in control tissue (Fig. 2e, lane 1). Fas was abundant in 87V scrapie-infected tissue at the terminal stage of disease (320 dpi, Fig. 2c, lane 4) when compared to the basal level in normal brain-injected control tissue (Fig. 2c, lane 3).

Caspase-3 immunolabelling: The level of cleaved p17 fragment of caspase 3 was assessed throughout the incubation period. No difference in caspase-3-cleaved fragment immunoreactivity was observed in the CA2 region of 87V scrapie-infected and normal brain-injected control tissue at 50 dpi (data not shown). However, immunohistochemistry showed an increase in caspase-3-cleaved fragment immunoreactivity in 87V scrapie-infected CA2 at 100 dpi (Fig. 3b) compared to age-matched control tissue (Fig. 3a). This increase is maintained at 150 and 200 dpi (data not shown), and at the terminal stage of disease in 87V scrapie-infected CA2 (Fig. 3d) compared to control tissue (Fig. 3c). Caspase 3 staining was seen as granular intracellular inclusions within the large CA2 pyramidal neurons.

These findings were confirmed by immunoblot analysis, which demonstrated increased levels of caspase-3-cleaved fragment from 100 dpi in 87V-infected tissue (Fig. 3e, lanes 5, 6, 7) compared to control tissue (Fig. 3e, lane 8). At the terminal stage of disease (320 dpi), 87V scrapie-infected tissue has an increase in caspase 3 (Fig. 3e, lanes 1, 3, 4) compared to control tissue (Fig. 3e, lane 2).

DISCUSSION

Our results show that during 87V scrapie infection, early up-regulation of the proapoptotic markers Fas and caspase 3 occurs at 100 dpi, significantly prior to the detection of disease-specific PrP deposition at 200 dpi, and onset of clinical signs at 260 dpi. These results suggest that Fas and caspase 3 may be specific early indicators of apoptosis induction in murine scrapie. Previous work showed positive TUNEL staining of isolated CA2 neurons at 100 dpi during 87V scrapie infection [3] and, together with the current results, there thus appears to be a positive relationship between the expression of Fas, caspase 3- and TUNEL-positive cells in 87V scrapie infection.

The previously reported dendritic damage at 70 dpi in 87V scrapie infection [3] remains the earliest pathological abnormality in the CA2 during 87V scrapie infection. This occurs 30 dpi prior to the up-regulation of Fas and caspase, and the appearance of TUNEL-positive cells at 100 dpi. The influence of the dendritic and cytoskeletal systems on apoptosis is unclear, however tau protein phosphorylation [26], microfilament reorganisation, and tubulin and actin polymerisation [27] are all thought to accelerate apoptosis. The dendritic swelling and contortion is suggestive of cytoskeletal dysfunction, and additional studies on the 87V/VM murine scrapie model will aim to elucidate the relationship between early dendritic and cytoskeletal damage and activation of proapoptotic markers. In AD an

Fig. 1. Fas and caspase signalling. Upon binding of Fas ligand (FasL) to the Fas receptor (FasR), the receptor links via its cytosolic death domain (DD) to adaptor proteins such as intracellular Fas-associated death domain (FADD). This then binds via its death effector domain (DED) to initiator caspases (caspases 8 and 10). Activated caspases 8 and 10 then cleave and activate downstream effector caspases (caspases 3, 6, 7), which in turn cleave various proteins including poly(ADP-ribose) polymerase (PARP) which results in DNA damage and apoptosis.

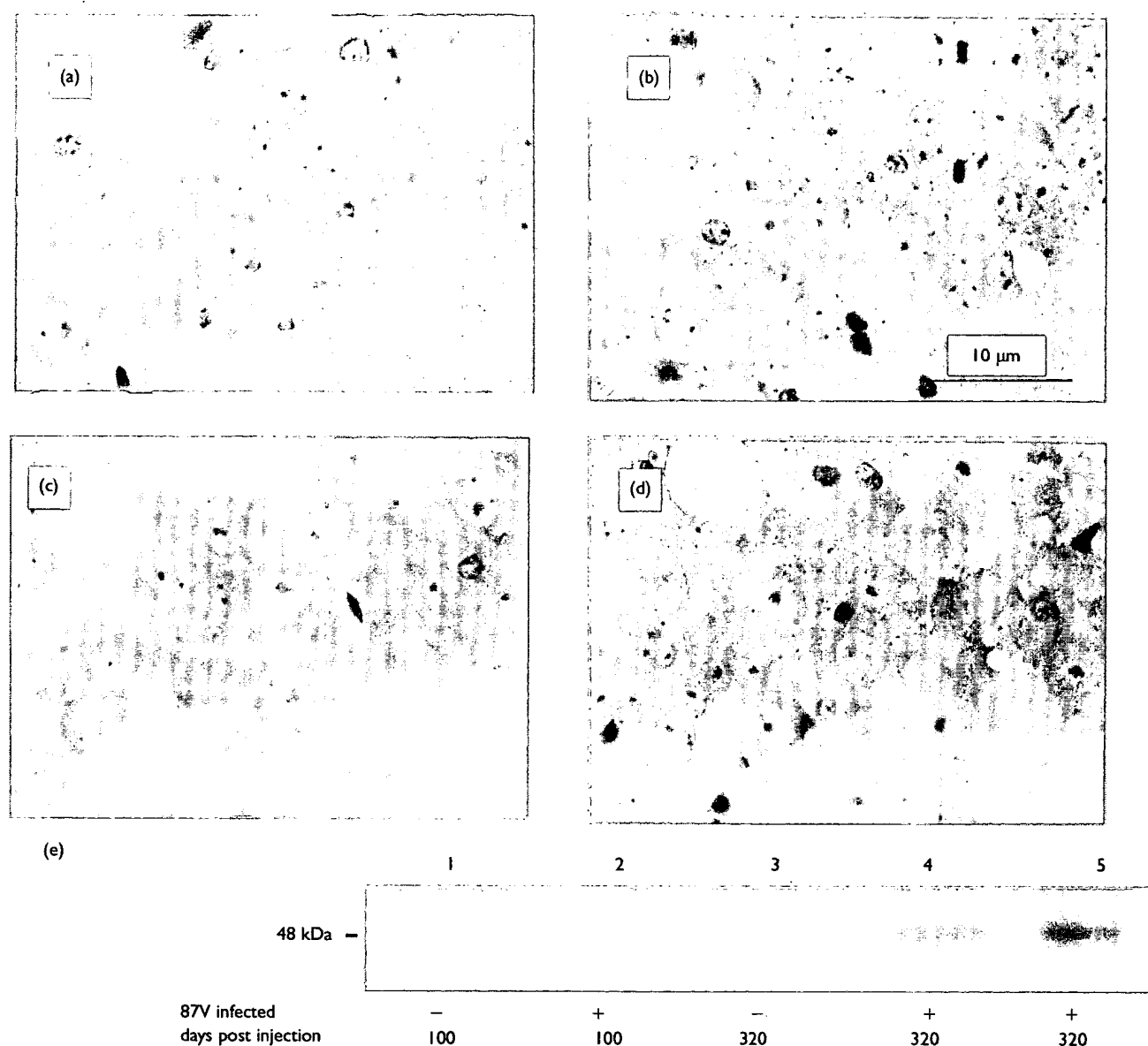


Fig. 2. Increased Fas expression in the CA2 during 87V scrapie infection. Immunocytochemistry in 87V scrapie-infected CA2 at 100 dpi (b), and age-matched normal brain-injected control tissue (a). Terminal 87V-infected CA2 (d), and age-matched control CA2 (c). Terminal stage (TM) is 320 dpi. Bar, 10 µm. Western blot using the same Fas antibody shows increased levels 100 dpi in 87V scrapie-infected tissue (e, lane 2) compared to normal brain-injected control tissue (e, lane 1). At the terminal stage, 87V-infected tissue has a marked increase in caspase 3 level (e, lanes 4 and 5) compared to normal brain-injected control tissue (e, lane 3). Terminal stage (TM) is 320 dpi.

analogous neurodegenerative disease with deposition of an amyloidogenic protein, neuronal loss and gliosis, the relationship between the formation of neurofibrillary tangles, deposition of A β and neuronal loss remains unclear. It has been suggested that there is an association between neurofibrillary tangle formation and the activation of apoptotic pathways [28], and it is possible that a similar relationship is present in 87V scrapie infection.

During 87V scrapie infection, dendritic damage and induction of apoptosis all occur significantly prior to detectable disease-specific PrP deposition within the hippo-

campus. The increase in caspase 3 first evident at 100 dpi does not appear to significantly increase further by the terminal stage of disease. It is possible that during 87V scrapie infection low levels of PrP^{Sc} or pre-amyloidogenic PrP are generating neuronal dysfunction and isolated TUNEL-positive cells prior to widespread neuronal loss. This has been shown *in vitro* using PrP106-126 where low levels of the peptide induce and maintain a prolonged increase in proapoptotic markers, including caspase 3, without a commitment to cell death [22]. It is also possible that a slow progression of the early induction of proapop-

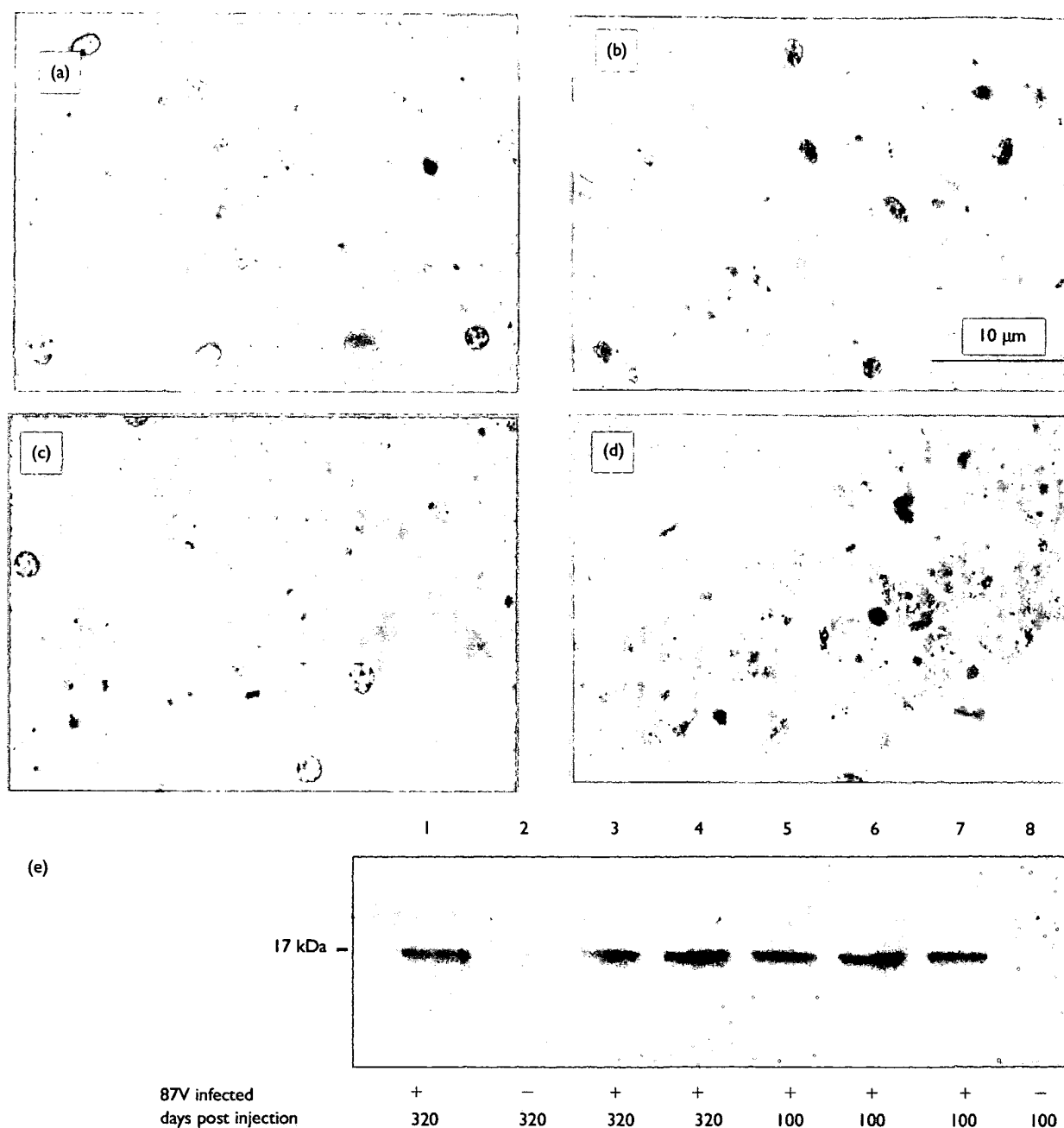


Fig. 3. Increased caspase 3 expression in the CA2 during 87V scrapie infection. Immunocytochemistry in 87V scrapie-infected CA2 at 100 dpi (b), and age-matched normal brain-injected control tissue (a). Terminal 87V-infected CA2 (d), and age-matched normal brain-injected control CA2 (c). Terminal stage (TM) is 320 dpi. Bar = 10 µm. Western blot using the same caspase 3 antibody shows increased levels 100 dpi in 87V-infected tissue (e, lanes 5, 6 and 7) compared to normal brain injected control tissue (e, lane 8). At terminal stage, 87V infected tissue has a marked increase in caspase 3 level (e, lanes 1, 3 and 4) compared to normal brain injected control tissue (e, lane 2). Terminal stage (TM) is 320 dpi.

otic markers leaves neurons susceptible to further damage from disease-specific PrP rather than causing immediate widespread cell loss. During ME7 scrapie infection, PrP^{Sc}-associated synaptic and dendritic spine loss occurs prior to cell death [1,2]. The 320 dpi incubation period of 87V scrapie is significantly longer than that of ME7 scrapie, and it is possible that a slow progression of proapoptotic marker induction occurs over time. Future studies on

murine scrapie will aim to further elucidate the temporal relationship between proapoptotic marker activation, PrP deposition and cell death.

CONCLUSION

The present study has shown early induction of Fas and caspase 3 during 87V scrapie infection. These data suggest that proapoptotic markers may be specific early indicators

of neurodegeneration in murine scrapie. A thorough understanding of the initial events in the neurodegenerative process is critical for the development of therapeutic strategies for the treatment of TSE diseases.

REFERENCES

1. Brown D, Belichenko PV, Sales J *et al.* *Neuroreport* **12**, 179–183 (2001).
2. Jeffrey M, Halliday WG, Bell J *et al.* *Neuropathol Appl Neurobiol* **26**, 41–44 (2000).
3. Jamieson E, Jeffrey M, Ironside JW *et al.* *Neuroreport* **12**, 2147–2153 (2001).
4. Prusiner SB. *TIBS* **12**, 482–487 (1996).
5. Sakaguchi S, Katamine S, Nishida N *et al.* *Nature* **380**, 528–531 (1996).
6. Collinge J, Whittington MA, Sidle KCL *et al.* *Nature* **370**, 295–297 (1994).
7. Brown DR, Wong B-S, Hafiz F *et al.* *Biochem J* **344**, 1–5 (1999).
8. Brown DR, Clive C and Haswell SJ. *J Neurochem* **76**, 69–76 (2001).
9. Nagata S and Golstein P. *Science* **267**, 1449–1456 (1995).
10. Orlinick JR, Vaishnav K and Elkon KB. *Int Rev Immunol* **18**, 293–308 (1999).
11. Nishimura T, Akiyama H, Yonehara S *et al.* *Brain Res* **695**, 137–145 (1995).
12. Ferrer I, Blanco R, Cutillas B and Ambrosio S. *Neuropathol Appl Neurobiol* **26**, 424–433 (2000).
13. Martin-Villalba A, Herr I and Jeremais I. *J Neurosci* **19**, 3809–3817 (1999).
14. Tan Z, Levid J and Schreiber SS. *Neuroreport* **12**, 1979–1982 (2001).
15. Nagata S. *Prog Mol Sub Cell Biol* **16**, 87–103 (1996).
16. Peter ME and Krammer PH. *Curr Op Immunol* **10**, 545–551 (1998).
17. Engidawork E, Gulesserian T, Seidl R *et al.* *Neurosci Lett* **303**, 79–82 (2001).
18. Engidawork E, Gulesserian T, Yoo BC *et al.* *Biochem Biophys Res Commun* **281**, 84–93 (2001).
19. Gervais FG, Xu D, Robertson GS *et al.* *Cell* **97**, 395–406 (1999).
20. Harada J and Sugimoto M. *Brain Res* **842**, 311–323 (1999).
21. Ivins KJ, Bui ETN and Cotman CW. *Neurobiol Dis* **5**, 365–378 (1998).
22. White AR, Guirguis R, Brazier MW *et al.* *Neurobiol Dis* **8**, 229–316 (2001).
23. Burkle A, Kretzschmar HA and Brown DR. *Histochem J* **3**, 1711–1716 (1999).
24. Bruce ME. *Methods Mol Med Prion Dis* **13**, 223–236 (1996).
25. Dickinson AG, Meikle VM and Fraser H J. *Comp Pathol* **78**, 293–299 (1968).
26. Davis PK and Johnson GV. *J Biochem Chem* **274**, 35686–35692 (1999).
27. Yamazaki T, Tsuruga M, Zhou D *et al.* *Exp Cell Res* **259**, 64–78 (2000).
28. Rohn TT, Head E, Su JH *et al.* *Am J Pathol* **158**, 189–198 (2001).

Acknowledgements: We thank Emma Murdoch and Christine Clink (Institute for Animal Health) for animal husbandry. This work is funded by the BBSRC (Grant no. 201/BS 410537).

B. Puig · I. Ferrer

Cell death signaling in the cerebellum in Creutzfeldt-Jakob disease

FILE COPY

Received: 12 September 2000 / Revised, accepted: 9 January 2001 / Published online: 9 August 2001
© Springer-Verlag 2001

Abstract Examination of the expression of proteins linked with signaling pathways commanding cell death and cell survival has been carried out to increase understanding on the mechanisms leading to cell death in the cerebellum in Creutzfeldt-Jakob disease (CJD). Expression of Fas, Fas ligand (Fas-L), ERK, MEK, Bcl-2, Bax, N-myc, c-myc, pro-caspase-2 and active caspase-3 was examined by immunohistochemistry in the cerebellum of six patients with sporadic CJD, three patients with olivopontocerebellar atrophy (OPCA) and six age-matched controls. No modifications in the expression of these proteins were observed in granule cells in CJD and OPCA when compared with controls, except in a few cells in the molecular and granular layers in CJD that displayed dense homogeneous active caspase-3 immunostaining. This suggests selective activation of caspase-3 in association with increased cellular vulnerability in CJD. No modifications in pro-caspase-2 and c-myc immunoreactivity were observed in Purkinje cells in diseased brains when compared with controls. However, increased diffuse Fas, Fas-L, MEK, ERK and Bax expression, and enhanced granular active caspase-3 immunoreactivity was found in the cytoplasm of Purkinje cells in CJD. Increase in Bcl-2 and N-myc occurred in Purkinje cells in CJD and OPCA. These results indicate that enhanced Fas, Fas-L, MERK, ERK, Bax and granular active caspase-3 expression is not lethal to Purkinje cells in CJD, whereas increased Bcl-2 and N-myc does not preclude per se cell death or death survival in CJD and OPCA. These findings point to the likelihood that expression of these cell death proteins in neurodegeneration has functional roles differing from those related with apoptosis.

Keywords Creutzfeldt-Jakob disease · Olivopontocerebellar atrophy · Cell death/survival pathway proteins · Caspase · Apoptosis

Introduction

Creutzfeldt-Jakob disease (CJD), Gerstmann-Sträussler-Scheinker syndrome and fatal familial insomnia (FFI) in humans, and scrapie and bovine spongiform encephalopathy in animals are neurodegenerative diseases characterized by the accumulation of an abnormal, protease-resistant and amyloidogenic isoform of the prion protein known as PrP^{CJD} or PrP^{Sc} [10, 48]. Pathological hallmarks of prion diseases are spongiform degeneration of neurons and their processes, reactive astrocytic gliosis, abnormal protease-resistant PrP deposition, and loss of neurons [10, 48]. It has been suggested that neuronal cell death in scrapie-infected mice is due to apoptosis [23, 36]. However, studies in CJD and FFI, mainly based on the method of in situ end-labeling of nuclear DNA fragmentation, are controversial [12, 15, 25]. For this reason, studies focused on the expression of proteins commanding specific cell-death pathways are useful to investigate mechanisms leading to cell death in CJD.

A common feature of cells undergoing apoptosis is the activation of caspases, the cysteine proteases constitutively expressed as zymogens or pro-caspases that, after activation, can cleave substrates (including pro-caspases) at aspartic acid residues. From a functional point of view, caspases can be divided into two groups: upstream instigators (caspase 8, 9 and 10), the cascade initiators that can activate other caspases; and downstream terminators that cleave distinct cellular substrates, thus destroying the cell (caspase 3, 6 and 7). Caspases 1, 2, 4, 5 and 11 can act as initiators and executioners [22, 42, 53, 54, 55, 57]. The Fas/Fas ligand (Fas-L) signaling pathway is one of the mechanisms that, once activated, may trigger the apoptotic caspase cascade. The Fas (CD95, APO-1) receptor is a 44-kDa type-1 membrane glycoprotein of the TNF receptor superfamily, which has an extracellular domain for

B. Puig · I. Ferrer (✉)
Unitat de Neuropatologia Experimental,
Departament de Biologia Cel·lular i Anatomia Patològica,
Universitat de Barcelona, Campus de Bellvitge,
carrer Feixa Llarga sn, 08907 Hospitalet de Llobregat, Spain
e-mail: iferrer@sakma.es, Fax: +34-93-2045065

ligand binding and an intracellular death domain. The cross-linking with its specific ligand Fas-L triggers Fas trimerization and recruits the Fas-associated death domain (FADD). This is followed by FLICE/caspase-8 binding via interactions between the death-effector domains of FADD and caspase-8, and by activation of caspase-8. Activation of caspase-8, in turn, activates the caspase cascade, leading to apoptosis [41, 47, 52, 54, 59, 62]. Bcl-2 and Bax proteins play a role in the control of cell survival and apoptosis. Bcl-2 promotes cell survival, whereas Bax promotes cell death [9, 31, 38]. Members of the Bcl-2 family regulate cell death upstream of caspase proteases [32, 49].

Other proteins have been implicated in the signaling of cell death and cell survival. The oncogene myc family encodes the transcription factor proteins N-myc, c-myc and L-myc, which are implicated in the regulation of cell proliferation and differentiation [8, 43], as well as apoptosis [26, 46, 56]. The family of mitogen-activated protein (MAP) kinases is composed of different members, including ERKs, c-Jun N-terminal kinases and p38 kinases [7, 39, 50]. ERKs are activated by MAP/ERK kinases (MEKs) which, in turn, are activated by MEK kinases (MEKKs). The best characterized MAPK cascade is regulated by Ras, and consists of Raf isoforms, particularly Raf-1, MEK1/2 and ERK1/2 [7, 50]. The role of MEK and ERK in the control of cell death and cell survival is not clear, and it is probably dependent on the cell type as well as on the signal that triggers apoptosis [4, 34, 44].

Severe spongiform degeneration and marked loss of cerebellar granule cells is a characteristic lesion in the ataxic form of CJD [5, 24, 29]. However, moderate spongiform degeneration in the molecular layer, mild or moderate granule cell loss, and reactive astrocytosis are common features in classical CJD [1, 10]. Loss of dendritic spines and reduction of dendritic arbors have been shown with the Golgi method in relatively resistant Purkinje cells in CJD [2, 17]. The present study examines by immunohistochemistry the expression of Fas, Fas-L, Bcl-2, Bax, N-myc, c-myc, MEK, ERK, pro-caspase-2, and active caspase-3 in the cerebellum of patients with CJD, and compares these observations with those encountered in olivopontocerebellar atrophy (OPCA) and age-matched controls.

Material and methods

Samples of the cerebellum from six patients with sporadic CJD, three patients with OPCA and six age-matched controls were obtained at autopsy and immediately immersed in 10% buffered formalin. The delay between death and tissue processing was between 3 and 8 h. The clinical and pathological details of CJD and OPCA cases have been described in detail elsewhere [18, 20]. Samples were embedded in paraffin or cut with a vibratome. Paraffin sections, 5 µm thick, which were obtained with a sliding microtome, were stained with hematoxylin and eosin or processed for immunohistochemistry following the avidin-biotin-peroxidase (ABC) method (ABC kit, Vectastain, Vector). Sections were slightly counterstained with hematoxylin. In some cases, sections were first boiled in citrate buffer and then stored overnight at room temperature. Endogenous peroxidase was blocked with 2% hydrogen peroxide and 10% methanol followed by incubation with normal serum for 2 h at room temperature. Sections were incubated at 40°C overnight with one of the primary antibodies. The sections were then incubated with specific biotinylated secondary antibody diluted 1:200, and with ABC diluted 1:100 for 1 h for each step. The immunoreaction was visualized with 0.05% diaminobenzidine (DAB) and 0.01% hydrogen peroxide. Table 1 shows specifications of the antibodies used.

For PrP immunohistochemistry, a different procedure was carried out. Dewaxed paraffin sections were first boiled in 35% HCl for 2 min and then treated with 96% formic acid for 10 min. After blocking endogenous peroxidase with 0.03% hydrogen peroxide, sections were incubated at 40°C overnight with mouse monoclonal PrP antibody (clone 3F4, Dako) at a dilution of 1:30 in TRIS-buffer (pH 7.2) containing 15 mM Na₂N₃. After washing, sections were processed with the EnVision+ System Peroxidase (DAB) procedure (Dako). Sections were incubated with EnVision mouse labeled polymer horseradish peroxidase for 30 min and the reaction was visualized with 0.05% DAB and 0.01% hydrogen peroxide. Sections with and without pre-incubation with proteinase K were processed in parallel.

Finally, vibratome sections, 50 µm thick, were processed free-floating for pro-caspase-2 immunohistochemistry following the LSAB method (Dako LSAB+Kit) following the instructions of the supplier. Incubation with the primary antibody was carried out at 40°C overnight. The goat polyclonal antibody to pro-caspase-2 (Santa Cruz Biotechnology) was used at a dilution of 1:1,000. Sections were then incubated with link solution (LSAB) and with streptavidin-peroxidase solution, 15 min each at room temperature. The peroxidase reaction was visualized with the DAB chromogen.

All the antibodies were analyzed on Western blots of brain homogenates of control brains. The antibodies recognized specific bands at the expected molecular masses. In addition, antibodies from Santa Cruz Biotechnology (Fas, Fas-L, N-Myc, c-myc, Bcl-2 and Bax) were tested by pre-absorption with the corresponding antigenic peptides (also available from Santa Cruz Biotechnol-

Table 1 Summary of the antibodies used in paraffin sections processed with the avidin-biotin-peroxidase (ABC) method

| | Pre-treatment with citrate buffer | Mono-/polyclonal antibody | Dilution | Source |
|-------------------------------|-----------------------------------|---------------------------|----------|---------------------|
| Fas | Yes | Rabbit polyclonal | 1:100 | Santa Cruz, sc-715 |
| Fas-L | Yes | Rabbit polyclonal | 1:50 | Santa Cruz, sc-834 |
| N-Myc | Yes | Rabbit polyclonal | 1:50 | Santa Cruz, sc-791 |
| c-myc | Yes | Monoclonal | 1:40 | Santa Cruz, sc-42 |
| Bcl-2 | Yes | Rabbit polyclonal | 1:100 | Santa Cruz, sc-492 |
| Bax | Yes | Rabbit polyclonal | 1:200 | Santa Cruz, sc-493 |
| Active caspase-3 | Yes | Rabbit polyclonal | 1:25 | Cell Signaling |
| MEK | No | Monoclonal clone 25 | 1:100 | Transduction |
| ERK | No | Monoclonal clone 16 | 1:1,000 | Transduction |
| Phosphorylated neurofilaments | No | Monoclonal clone BF10 | 1:50 | Boehringer-Mannheim |

ogy). The immunoreactive signal was abolished in sections processed with the pre-absorbed antibodies.

Results

General morphological findings

Mild spongiform degeneration in the molecular layer, granule cell loss, and astrocytic gliosis were encountered, although with variable intensity, in CJD. The number of Purkinje cells was preserved, although axonal torpedoes were seldom observed. In addition, abnormal punctate protease-resistant PrP deposition in the molecular layer, and granular protease-resistant PrP deposition, reminiscent of glomeruli, in the granular layer was found in every case. Small numbers of diffuse PrP plaques were present in the molecular layer and upper border of the granular layer, as described in detail [20].

Loss of Purkinje cells, accompanied by axonal torpedoes in the remaining Purkinje cells, together with reactive astrocytic gliosis, were the major pathological findings in OPCA, as reported elsewhere [18].

Increased cellular vulnerability was not associated with morphological characteristics of apoptosis, including pe-

ripheral chromatin condensation, or extreme chromatin condensation and formation of apoptotic bodies, in CJD and OPCA.

Fas and Fas-L immunohistochemistry

In controls, moderate Fas and Fas-L immunoreactivity decorated the soma of Purkinje cells and the neuropil of the molecular layer. Faint Fas-L immunoreactivity was found in the granular layer (Fig. 1A, D).

Marked increase in Fas and Fas-L immunoreactivity was found in Purkinje cells, and Fas in Golgi cells in CJD (Fig. 1B, E). Reactive astrocytes showed moderate Fas-L immunoreactivity. In contrast, Fas and Fas-L immunoreactivity was low in Purkinje cells in OPCA, although Fas-L was strongly expressed in reactive astrocytes (Fig. 1C, F). No modifications in the expression of Fas and Fas-L were seen in the remaining granule cells in diseased brains when compared with controls.

Fig. 1 Fas (A–C) and Fas-L (D–F) immunoreactivity in control (A, D), CJD (B, E) and OPCA (C, F) cases. Marked increase in Fas and Fas-L immunoreactivity is found in Purkinje cells, and Fas (arrow in B) in Golgi cells in CJD. Fas-L immunoreactivity is also increased in reactive astrocytes (arrowheads in E and F) in CJD and OPCA. An asterisk marks an axonal ballooning in OPCA (CJD Creutzfeldt Jakob disease, OPCA olivopontocerebellar atrophy, Fas-L Fas ligand). A–F Paraffin sections counterstained with hematoxylin; bar 25 μ m

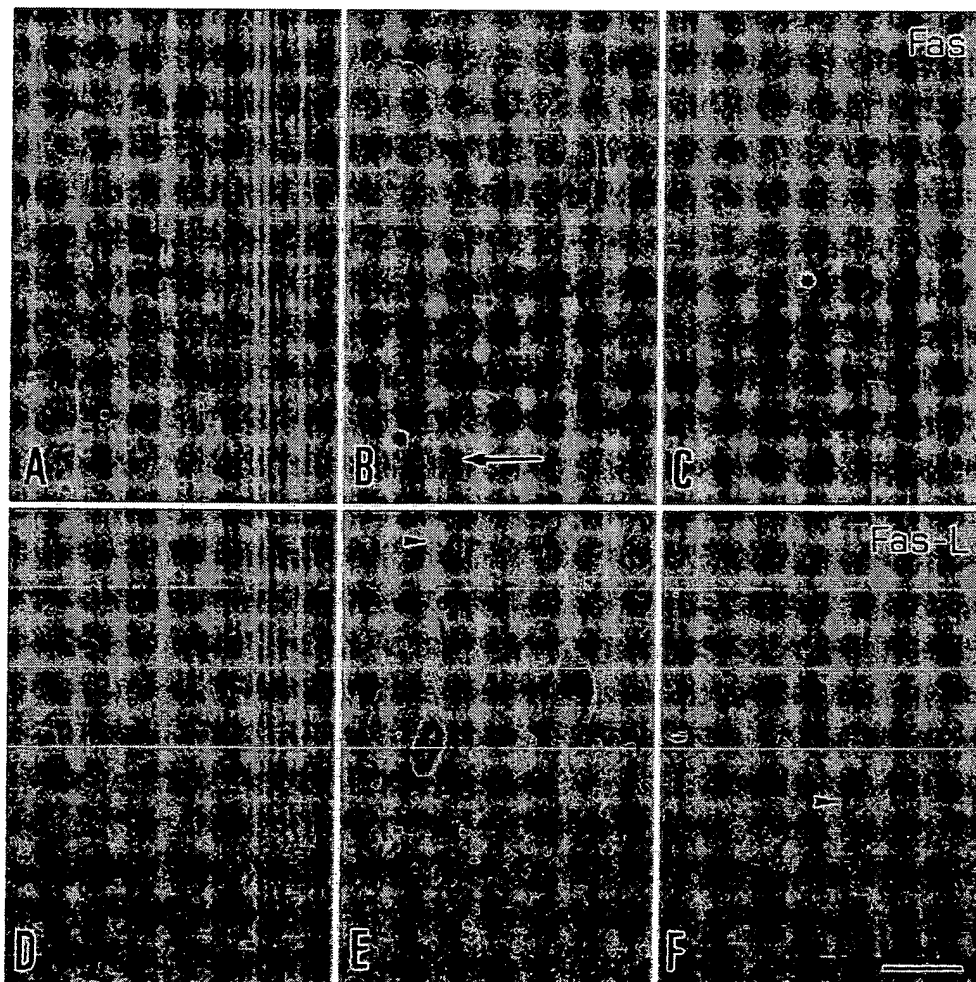
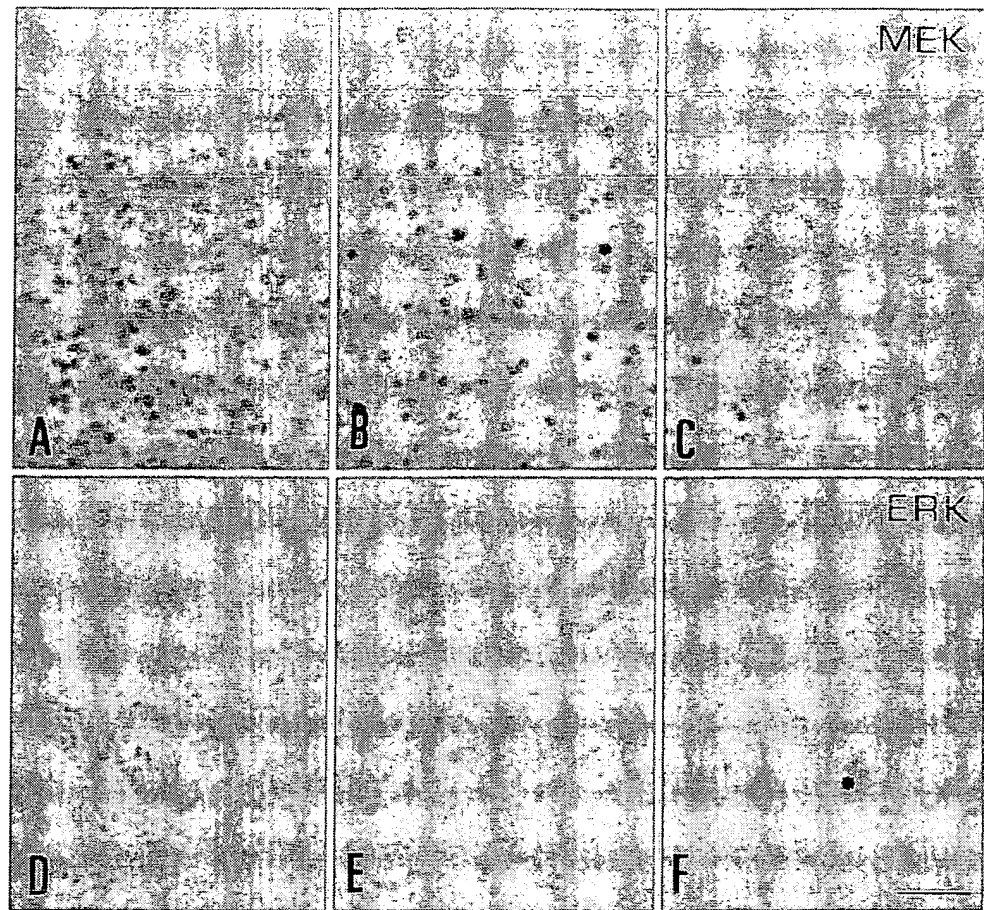


Fig. 2 MEK (A–C) and ERK (D–F) immunoreactivity in control (A, D), CJD (B, E) and OPCA (C, F) cases. Slight increase in MEK and ERK immunoreactivity is found in Purkinje cells in CJD but not in OPCA. ERK antibodies decorate an axonal torpedo in a Purkinje cell (*asterisk* in F). A–F Paraffin sections, hematoxylin counterstaining; bar 25 μ m



MEK and ERK immunohistochemistry

In controls, strong MEK immunoreactivity was present in granule cells, whereas Purkinje cells were slightly, or not at all, stained with anti-MEK antibodies (Fig. 2A). However, a slight increase in MEK immunoreactivity occurred in Purkinje cells in CJD (Fig. 2B). No modifications were seen in the remaining granule cells. MEK expression in OPCA was similar to controls (Fig. 2C).

Faint ERK immunoreactivity was present in Purkinje cells in control cases (Fig. 2D). However, increased ERK expression was found in Purkinje cells in CJD (Fig. 2E) but not in OPCA (Fig. 2F). ERK expression was very low or almost absent in granule cells in control and diseased cases.

Axonal torpedoes in OPCA and CJD, as visualized with anti-phosphorylated neurofilament antibodies (clone BF10) in consecutive sections, were faintly stained with anti-MEK and anti-ERK antibodies (Fig. 2F).

Bcl-2 and Bax immunohistochemistry

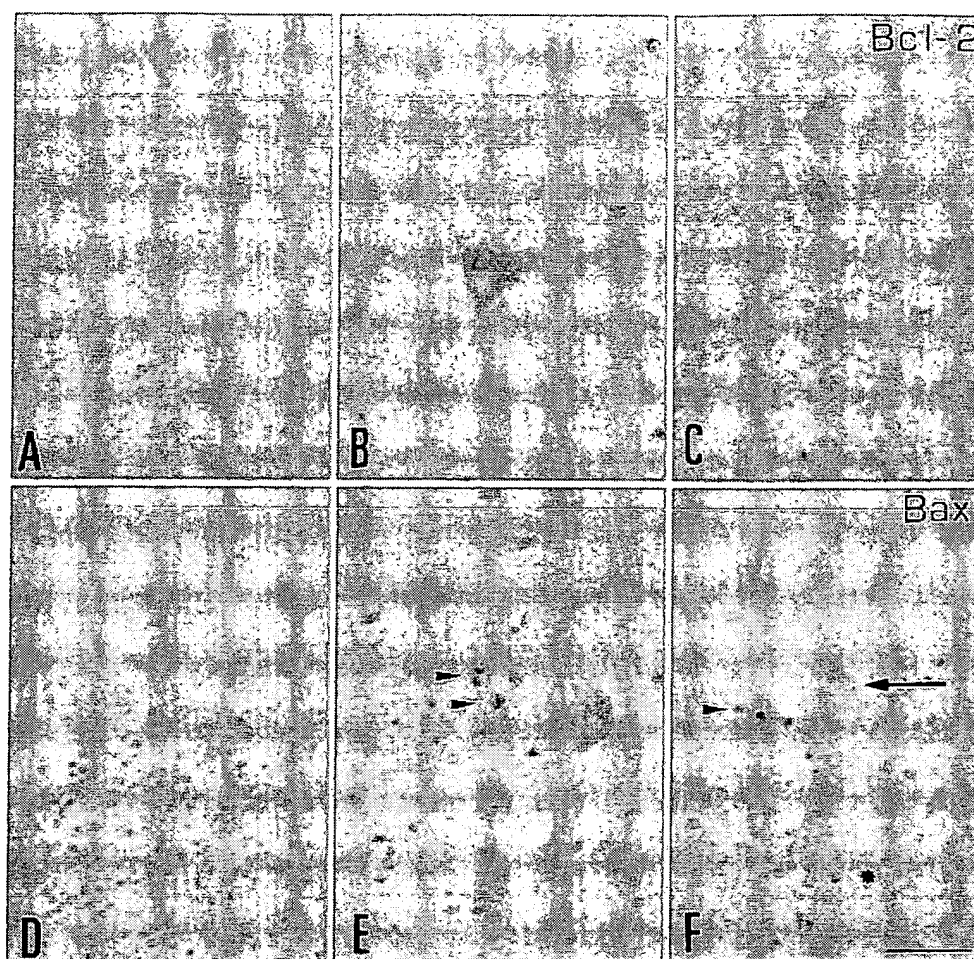
Weak Bcl-2 immunoreactivity in stellate cells of the molecular layer and in Golgi cells, but not in Purkinje cells, was present in controls (Fig. 3A). Increased Bcl-2 im-

munoactivity was observed in Purkinje cells in CJD and, to a lesser extent, in OPCA (Fig. 3B, C). Weak Bax immunoreactivity occurred in Purkinje cells, but not in granule and stellate cells, in control cases (Fig. 3D). A moderate increase in Bax was observed in the cytoplasm of Purkinje cells in CJD, but not in OPCA (Fig. 3E, F). Moreover, an increase in Bax immunoreactivity occurred in non-identified cell processes in the vicinity of Purkinje cells in diseased brains (Fig. 3E, F). No changes in the expression of Bcl-2 and Bax were noticed in granule cells in CJD and OPCA.

N-myc and c-myc immunohistochemistry

Faint c-myc immunoreactivity was found in neurons of the molecular layer, Purkinje cells and granule cells in control samples. No differences in c-myc expression were seen between control and diseased brains (data not shown). However, enhanced N-myc immunoreactivity was seen in Purkinje cells in CJD and OPCA when compared with controls (Fig. 4A–C). N-myc expression was not changed in granule cells in diseased brains.

Fig. 3 Bcl-2 (A–C) and Bax (D–F) immunoreactivity in control (A, D), CJD (B, E) and OPCA (C, F). Enhanced Bcl-2 immunoreactivity is found in Purkinje cells in CJD and OPCA. Slight increase in Bax immunoreactivity is found in the cytoplasm of Purkinje cells in CJD. Lipofuscin in a Purkinje cell in OPCA is labeled with an *arrow*. Bax-immunoreactive non-identified cell processes are shown in E and F (*arrowheads*). A–F Paraffin sections counterstained with hematoxylin; bar 25 μ m



Pro-caspase-2 and active caspase-3 immunohistochemistry

Strong pro-caspase-2 immunoreactivity was observed in Purkinje cells in control and CJD (Fig. 4D, E). Mild reduction of pro-caspase-2 immunoreactivity occurred in one case of OPCA (Fig. 4F). No pro-caspase-2 immunostaining was seen in the granular layer in control and pathological cases.

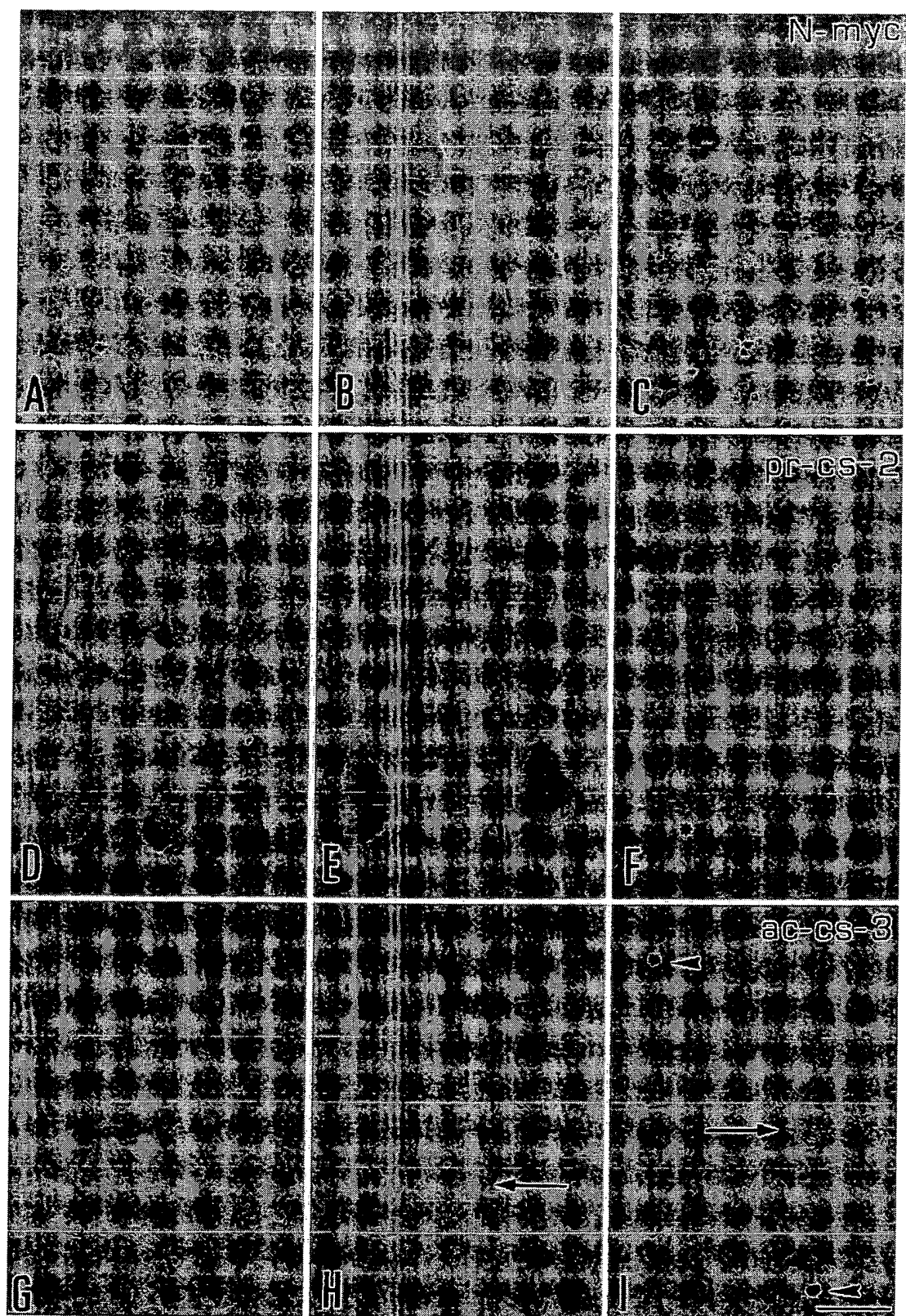
Active caspase-3 expression was not seen in controls and OPCA. However, strong granular active caspase-3 immunoreactivity was observed in the cytoplasm of Purkinje cells in CJD (Fig. 4H, I). In addition, dense homogeneous active caspase-3 immunoreactivity was recognized in a few cells, representing about 1 per 1,000 of the total number of cells, in the molecular and granular layers in CJD (Fig. 4I).

Discussion

The study was designed to delineate putative pathways involved in cell death in CJD. No modifications in the expression of Fas, Fas-L, MEK, ERK, Bcl-2, Bax, c-myc and N-myc were found in vulnerable granule cells in this

disease. The exception was active caspase-3 that was expressed in a few cells in the molecular and granular layers in CJD, but not in control and OPCA cases. It is tempting to suggest caspase-3 activation in vulnerable cells in CJD, and caspase-mediated cell death as the mechanism of granular dropout in CJD. However, such a possibility has to be confirmed with additional data from *in vivo* and *in vitro* models. Lack of active caspase-3 expression in OPCA may be due to the lack of involvement of caspase-3 or to the difficulty in finding a single caspase-3-immunoreactive cell in such long-lasting disease.

Unexpectedly, the present results have shown a complex scenario of protein expression in Purkinje cells. Increased Fas and Fas-L immunoreactivity in Purkinje cells, and Fas immunoreactivity in Golgi cells was found in CJD. Interestingly, Purkinje and Golgi cells are relatively resistant, whereas granule cells are largely vulnerable to CJD. This pattern appears to be specific as no similar increase in Fas and Fas-L expression was encountered in OPCA, a condition in which Purkinje cells degenerate and are committed to die [18, 30]. Increased Fas and Fas-L expression has been found in association with neuron death following focal ischemia in adult and developing animal models [14, 37, 51]. Yet a transient increase in Fas-L immunoreactivity occurs in surviving granule cells of the



dentate gyrus following transient forebrain ischemia in gerbils (unpublished observations), thus indicating that increased Fas and Fas-L expression in neurons is not sufficient to promote cell death. In addition, increased Fas-L immunoreactivity was found in reactive astrocytes in CJD and OPCA. Previous studies have shown that Fas and Fas-L are constitutively expressed in fetal and adult human astrocytes; various cytokines, including IL-1, IL-6, or TNF- α , stimulate Fas and Fas-L expression [6]. Moreover, increased Fas and Fas-L expression in reactive astrocytes has also been described in several unrelated human neurodegenerative disorders [19].

Increased active caspase-3 immunoreactivity was found in the cytoplasm of Purkinje cells in CJD but not in control and OPCA cases. It is known that activation of caspase-3 is associated with morphological hallmarks of apoptosis, covering nuclear chromatin condensation, nuclear shrinkage and formation of apoptotic bodies [28]. However, there is emerging evidence of caspase-3 activation without cell death in several paradigms [64]. Stimulation of T lymphocytes is accompanied by caspase-3 activation without apoptosis [40, 61]. Furthermore, IL-16 production following caspase-3 activation has been detected in resting and activated CD8⁺ T cells and in inactivated CD4⁺ T cells, without any apparent sign of apoptosis [63]. It is interesting to note that increased caspase-3 expression in Purkinje cells in CJD had a granular appearance that differed from the dense homogeneous staining of active caspase-3 in isolated cells of the molecular and granular layers. These findings, together with the lack of involvement of Purkinje cells in caspase-3 knockout mice [33], suggest alternative functions of caspase-3 in surviving Purkinje cells in CJD.

Strong pro-caspase-2 immunoreactivity was found in Purkinje cells in control and diseased brains. Two isoforms of caspase-2, caspase-2_s and caspase-2_L, which can induce and antagonize cell death, respectively, have been described. Caspase-2_L is predominantly expressed in brain, skeletal muscle and heart [60]. Caspase-2 knockouts further delineate sub-populations of neurons that are selectively involved or spared during the process of cell death following deletion of the caspase-2 gene [3]. It can be speculated that strong expression of caspase-2 in Purkinje cells is associated with cell death endurance. How-

ever, additional information is needed to elucidate which caspase-2 isoform is predominant in Purkinje cells.

MEK and ERK immunoreactivity was found in Purkinje cells in CJD but not in OPCA. Although the MEK/ERK pathway is involved in several paradigms of neuron death, MEK and ERK are also involved in neurotrophic factor-dependent neurite outgrowth in vitro [11, 13]. Since MEK/ERK are implicated in neurofilament phosphorylation [58], there is the possibility that ERK may participate in the maintenance of the microtubule cytoskeleton of hampered Purkinje cells in CJD. In line with this possibility is the presence of ERK and MEK in axonal torpedoes of Purkinje cells in OPCA and CJD; axonal torpedoes accumulate phosphorylated neurofilaments.

Increased Bcl-2 expression was found in Purkinje cells in CJD and OPCA, thus indicating that these cells are enriched with an anti-apoptotic protein. Yet the presence of Bcl-2 does not discriminate between Purkinje cells that are relatively resistant in CJD from cells that are vulnerable in OPCA. On the other hand, increased Bax immunoreactivity was found in Purkinje cells in CJD. The latter finding would suggest increased vulnerability to apoptosis. However, it is worth noting that increased Bax mRNA and protein was also detected in granule cells of the dentate gyrus following kainic acid administration at convulsant doses to the rat, and that this particular cell population is resistant to the excitotoxic insult [35]. Heterodimerization of Bcl-2 and Bax is critical for Bcl-2 functions in regulating certain forms of cell death [38, 45]. Furthermore, intracellular Bax redistribution seems to play a pivotal role in cell death and cell survival [27]. Therefore, interactions of Bcl-2 and Bax, rather than the mere modifications in the total levels of Bcl-2 and Bax in individual cells, appear to be crucial in determining whether a cell survives or dies.

No differences in c-myc immunoreactivity were found in Purkinje cells in CJD and OPCA when compared with controls. These results indicate that the fate of Purkinje cells in these disorders is not associated with modifications in the steady state expression of c-myc in individual neurons. This is in agreement with observations in vitro showing no modifications in the expression levels of c-myc in neuronal cells treated with PrP 106–126 [21]. Moreover, similar findings have been reported in other human neurodegenerative diseases, including Alzheimer's disease, Parkinson's disease and Huntington's disease [16]. In contrast, N-myc is increased in Purkinje cells in CJD and OPCA. However, modifications in the expression of N-myc are not predictors of cell death or cell survival.

In summary, the present findings show that Purkinje cells are sensitive to CJD as expression of several proteins regulating cell death and cell survival is increased in these cells. Yet enhanced expression of proteins linked to putative cell death pathways is not associated with apoptosis of Purkinje cells in CJD. It is important to stress that Purkinje cells in CJD are subjected to loss of dendritic spines, reduction of dendritic arbors, occasional torpedoes, and formation of abnormal varicose or club-shaped

◀ **Fig. 4** N-myc (A–C), pro-caspase-2 (D–F) and active caspase-3 (G–I) in control (A, D, G), CJD (B, E, H, I) and OPCA (C, F) cases. Increased N-myc immunoreactivity is observed in Purkinje cells in CJD and OPCA. Strong pro-caspase-2 immunoreactivity is seen in Purkinje cells in controls and CJD, but pro-caspase-2 expression is slightly reduced in this particular case of OPCA. Note pro-caspase-2 immunoreactivity in an axonal torpedo in OPCA (*asterisk* in F). No active caspase-3 expression is found in the control cerebellum, but granular active caspase-3 expression is seen in the cytoplasm of Purkinje cells in CJD (*arrows* in H and I). In addition, dense homogeneous active caspase-3 immunoreactivity is found in isolated cells in the molecular and granular layers in CJD (*arrowheads* in I). A–C, G–I Paraffin sections counterstained with hematoxylin; D–F vibratome sections without counterstaining; bar 25 μ m

proximal collateral axon branches and axon terminals [2, 17, 20]. Present results point to the likelihood that overexpression of selected proteins involved in cell death pathways in neurodegeneration has functional roles differing from those related with apoptosis.

Acknowledgement This study was supported in part by UE contract BIO4-1998-6060. B.P. is the recipient of a grant from the Pi Sunyer Foundation. We wish to thank T. Yohannan for editorial assistance.

References

- Bell JE, Ironside JW (1993) Neuropathology of spongiform encephalopathies in humans. *Br Med Bull* 49:738-777
- Berciano J, Berciano MT, Polo J, Figols J, Ciudad J, Lafarga M (1990) Creutzfeldt-Jakob disease with severe involvement of the cerebral white matter and cerebellum. *Virchows Arch [A]* 417:533-538
- Bergeron L, Perez G, MacDonald G, Shi L, Sun Y, Jurisicova A, Varmuza S, Latham K, Flaws J, Salter J, Hara H, Moskovitz M, Li E, Greenberg A, Tilly J, Yuan J (1998) Defects in regulation of apoptosis in caspase-2-deficient mice. *Genes Dev* 12:1304-1314
- Bhat NR, Zhang P (1999) Hydrogen peroxide activation of multiple mitogen-activated protein kinases in an oligodendrocyte cell line: role of extracellular signal-regulated kinase in hydrogen peroxide-induced cell death. *J Neurochem* 72:112-119
- Brownell B, Oppenheimer DR (1965) An ataxic form of subacute presenile poliomyelopathy (Creutzfeldt-Jakob disease). *J Neurol Neurosurg Psychiatry* 28:350-361
- Choi C, Park JY, Lee J, Lim JH, Shin EC, Ahn YS, Kim CH, Kim SJ, Kim JD, Choi IS, Choi IH (1999) Fas ligand and Fas are expressed constitutively in human astrocytes and the expression increases with IL-1, IL-6, TNF- α , or IFN- γ . *J Immunol* 162:1889-1895
- Cobb MH, Goldsmith EJ (1995) How MAP kinases are regulated. *J Biol Chem* 270:14843-14846
- Cole MD, MacMahon SB (1999) The Myc oncoprotein: a critical evaluation of transactivation and target gene regulation. *Oncogene* 18:2916-2924
- Craig RW (1995) The bcl-2 gene family. *Semin Cancer Biol* 6:35-43
- DeArmond SJ, Prusiner SB (1997) Prion Diseases. In: Graham DI, Lantos PL (eds) *Greenfield's neuropathology*, vol 2. Arnold, London, pp 235-280
- Dolcet X, Egea J, Soler RM, Martín-Zanca D, Comella JX (1999) Activation of phosphatidylinositol 3-kinase, but not extracellular-regulated kinases, is necessary to mediate brain-derived neurotrophic factor-induced motoneuron survival. *J Neurochem* 73:521-531
- Dorandeu A, Wingerstmann L, Chrétien F, Delisle MB, Vital C, Parchi P, Montagna P, Lugaresi E, Ironside JW, Budka H, Gambetti P, Gray F (1998) Neuronal apoptosis in fatal familial insomnia. *Brain Pathol* 8:531-537
- Encinas M, Iglesias M, Lecha N, Comella J (1999) Extracellular-regulated kinases and phosphatidylinositol 3-kinase are involved in brain-derived neurotrophic factor-mediated survival and neuritogenesis of the neuroblastoma cell line SH-SY5Y. *J Neurochem* 73:1409-1421
- Felderhoff-Mueser U, Taylor DL, Greenwood K, Kozma M, Stibenz D, Joashi UC, Edwards AD, Mehmet H (2000) Fas/CD95/APO-1 can function as a death receptor for neuronal cells in vitro and in vivo, and is upregulated following cerebral hypoxic-ischemic injury to the developing rat brain. *Brain Pathol* 10:17-29
- Ferrer I (1999) Nuclear DNA fragmentation in Creutzfeldt-Jakob disease: does a mere positive in situ nuclear end-labeling indicate apoptosis? *Acta Neuropathol* 97:5-12
- Ferrer I, Blanco R (2000) N-myc and c-myc expression in Alzheimer disease, Huntington disease and Parkinson disease. *Mol Brain Res* 77:270-276
- Ferrer I, Kulisevski J, Vazquez J, Gonzalez A, Pineda M (1988) Purkinje cells in degenerative diseases of the cerebellum and its connections. *Clin Neuropathol* 7:237-242
- Ferrer I, Genis D, Dávalos A, Bernadó L, Sant F, Serrano T (1994) The Purkinje cell in olivopontocerebellar atrophy. A Golgi and immunohistochemical study. *Neuropathol Appl Neurobiol* 20:38-46
- Ferrer I, Blanco R, Cutillas B, Ambrosio S (2000) Fas and Fas-L expression in Huntington disease and Parkinson disease. *Neuropathol Appl Neurobiol* 26:424-433
- Ferrer I, Puig B, Blanco R, Martí E (2000) Prion protein deposition and abnormal synaptic protein expression in the cerebellum in Creutzfeldt-Jakob disease. *Neuroscience* 97:715-726
- Forloni G, Tagliavini F, Bugiani O, Salmona M (1996) Amyloid in Alzheimer's disease and prion-related encephalopathies: studies with synthetic peptides. *Prog Neurobiol* 49:287-315
- Friedlander RM, Yuan J (1998) ICE, neuronal apoptosis and neurodegeneration. *Cell Death Differ* 5:823-831
- Giese A, Groschup M, Hess B, Kretzschmar H (1995) Neuronal cell death in scrapie-infected mice is due to apoptosis. *Brain Pathol* 5:213-221
- Gomori AJ, Partnow MJ, Horoupian DS, Hirano A (1973) The ataxic form of Creutzfeldt-Jakob disease. *Arch Neurol* 29:318-323
- Gray F, Delisle MB, Vital A, Wingerstmann L, Julien J, Géraud G, Vital C (1997) Neuronal apoptosis in human prion diseases. *Brain Pathol* 7:1268
- Hoffman B, Liebermann DA (1998) The proto-oncogene c-myc and apoptosis. *Oncogene* 17:3351-3357
- Hsu Y, Wolter KG, Youle RJ (1997) Cytosol-to-membrane redistribution of Bax and Bcl-XL during apoptosis. *Proc Natl Acad Sci USA* 94:3688-3692
- Jänike R, Sprengart M, Wati M, Porter A (1998) Caspase-3 is required for DNA fragmentation and morphological changes associated with apoptosis. *J Biol Chem* 273:9357-9360
- Jellinger KA, Heiss WD, Deisenhammer E (1974) The ataxic (cerebellar) form of Creutzfeldt-Jakob disease. *J Neurol* 207:289-305
- Koeppen AH (1991) The Purkinje cell and its afferents in human hereditary ataxia. *J Neuropathol Exp Neurol* 50:505-514
- Korsmeyer SJ (1995) Regulators of cell death. *Trends Genet* 11:101-105
- Kuan CY, Roth KA, Flavell RA, Rakic P (2000) Mechanisms of programmed cell death in the developing glia. *Trends Neurosci* 23:291-297
- Kuida K, Zheng TS, Na S, Kuan C, Yang D, Karasuyama H, Rakic P, Flavell RA (1996) Decreased apoptosis in the brain and premature lethality in CPP-32-deficient mice. *Nature* 384:368-372
- Lannuzel A, Barnier JV, Hery C, Huynh VT, Guibert B, Gray F, Vincent JD, Tardieu M (1997) Human immunodeficiency virus type 1 and its coat protein gp120 induce apoptosis and activate JNK and ERK mitogen-activated protein kinases in human neurons. *Ann Neurol* 42:847-856
- López E, Pozas E, Rivera R, Ferrer I (1999) Bcl-2, Bax and Bcl-x expression following kainic acid administration at convulsant doses in the rat. *Neuroscience* 91:1461-1470
- Lucassen PJ, Williams A, Chung WC, Fraser H (1995) Detection of apoptosis in murine scrapie. *Neurosci Lett* 198:185-188
- Martin-Villalba A, Herr I, Jeremias I, Hahne M, Brandt R, Vogel J, Schenkel J, Herdegen T, Debakin (1999) CD95 ligand (Fas-L/APO-1L) and tumor necrosis factor-related apoptosis-inducing ligand mediate ischemia-induced apoptosis in neurons. *J Neurosci* 19:3809-3817
- Merry DE, Korsmeyer SJ (1997) Bcl-2 gene family in the nervous system. *Annu Rev Neurosci* 20:245-267
- Mielke K, Herdegen T (2000) JNK and p38 stress kinases-degenerative effectors of signal-transduction-cascades in the nervous system. *Prog Neurobiol* 61:45-60

40. Miossec C, Dutilleul V, Fassy F, Dru-Hercend A (1997) Evidence of CPP32 activation in the absence of apoptosis during T lymphocyte stimulation. *J Biol Chem* 272:13459-13462
41. Muzio M (1998) Signalling by proteolysis: death receptors induce apoptosis. *Int J Clin Lab Res* 28:141-147
42. Nicholson DW, Thornberry NA (1997) Caspases: killer proteases. *Trends Neurosci* 22:299-306
43. O'Byrne AJ, Mateyak MK, Sedivy JM (1999) Mysterious liaisons: the relationship between c-Myc and the cell cycle. *Oncogene* 18:2934-2941
44. Oh-Hashi K, Maruyama W, Yi H, Takahashi T, Naoi M, Isobe K (1999) Mitogen-activated protein kinase pathway mediates peroxynitrite-induced apoptosis in human dopaminergic neuroblastoma SH-SY5Y cells. *Biochem Biophys Res Commun* 263:504-509
45. Oltvai Z, Millman CL, Korsmeyer SJ (1993) Bcl-2 heterodimerizes in vivo with a conserved homologue, Bax, that accelerates cell death. *Cell* 74:609-619
46. Pendergast GC (1999) Mechanisms of apoptosis by c-myc. *Oncogene* 18:2967-2987
47. Peter ME, Krammer PH (1998) Mechanisms of CD95 (APO-1/Fas)-mediated apoptosis. *Curr Opin Immunol* 10:545-551
48. Prusiner SB (1997) Cell biology and transgenic models of prion diseases. In: Collinge J, Palmer MS (eds) *Prion diseases*. Oxford University Press, Oxford, pp 130-162
49. Rao L, White E (1997) Bcl-2 and the ICE family of apoptotic regulators: making a connection. *Curr Opin Genet Dev* 7:52-58
50. Robinson MJ, Cobb MH (1997) Mitogen-activated protein kinase pathways. *Curr Opin Cell Biol* 9:180-186
51. Sakurai M, Hayashi T, Abe K, Sadahiro M, Tabayashi K (1998) Delayed selective motor neuron death by fas antigen induction after spinal cord ischemia in rabbits. *Brain Res* 797: 23-28
52. Scaffidi C, Fulda S, Srinivasan A, Friesen C, Li F, Tomaselli K, Debatin KM, Krammer P, Peter M (1998) Two CD95 (APO-1/Fas) signaling pathways. *EMBO J* 17:1675-1687
53. Schülze-Osthoff K, Ferrari D, Los M, Wesselborg S, Peter ME (1998) Apoptosis signaling by death receptors. *Eur J Biochem* 254:439-459
54. Slec EA, Adrain C, Martin SJ (1999) Serial killers: ordering caspase activation events in apoptosis. *Cell Death Differ* 6: 1067-1074
55. Stroh C, Schülze-Osthoff K (1998) Death by thousand cuts: an even increasing list of caspase substrates. *Cell Death Differ* 5: 997-1000
56. Thompson B (1998) The many roles of c-Myc in apoptosis. *Annu Rev Physiol* 60:575-600
57. Thornberry NA, Lazebnik Y (1998) Caspases: enemies within. *Science* 281:1312-1316
58. Veeranna GJ, Amin ND, Ahn NG, Jaffe J, Winters CA, Grant P, Pant HC (1998) Mitogen activated protein kinases (Erk1, 2) phosphorylate Lys-Ser-Pro (KSP) repeats in neurofilament proteins NF-H and NF-M. *J Neurochem* 18:4008-4021
59. Wallach D, Varfolomeev EE, Malinin NL, Goltsev YV, Kovalenko AV, Boldin MP (1999) Tumor necrosis factor receptor and Fas signaling mechanisms. *Annu Rev Immunol* 17:331-367
60. Wang L, Miura M, Bergeron L, Zhu H, Yuan J (1994) Ich1, and Ice/ced-3-related gene, encodes both positive and negative regulators of programmed cell death. *Cell* 78:739-750
61. Wilhelm S, Wagner H, Hacker G (1998) Activation of caspase-3-like enzymes in non-apoptotic T cells. *Eur J Immunol* 28: 891-900
62. Wilson MR (1998) Apoptotic signal transduction: emerging pathways. *Biochem Cell Biol* 76:573-582
63. Wu DM, Zhang Y, Parada NA, Kornfeld H, Nicoll J, Center DM, Cruikshank WW (1999) Processing and release of IL-16 from CD4⁺ but not CD8⁺ T cells is activation dependent. *J Immunol* 162:1287-1293
64. Zeuner A, Eramo A, Peschle C, María R de (1999) Caspase activation without death. *Cell Death Differ* 6:1075-1080

Cell death signaling in the cerebellum in Creutzfeldt-Jakob disease.

Puig B, Ferrer I.

Acta Neuropathol (Berl). 2001 Sep;102(3):207-15.

Departament de Biologia Cel·lular i Anatomia Patològica, Universitat de Barcelona, Hospitalet de Llobregat, Spain.

Examination of the expression of proteins linked with signaling pathways commanding cell death and cell survival has been carried out to increase understanding on the mechanisms leading to cell death in the cerebellum in Creutzfeldt-Jakob disease (CJD). Expression of Fas, Fas ligand (Fas-L), ERK, MEK, Bcl-2, Bax, N-myc, c-myc, pro-caspase-2 and active caspase-3 was examined by immunohistochemistry in the cerebellum of six patients with sporadic CJD, three patients with olivopontocerebellar atrophy (OPCA) and six age-matched controls. No modifications in the expression of these proteins were observed in granule cells in CJD and OPCA when compared with controls, except in a few cells in the molecular and granular layers in CJD that displayed dense homogeneous active caspase-3 immunostaining. This suggests selective activation of caspase-3 in association with increased cellular vulnerability in CJD. No modifications in pro-caspase-2 and c-myc immunoreactivity were observed in Purkinje cells in diseased brains when compared with controls. However, increased diffuse Fas, Fas-L, MEK, ERK and Bax expression, and enhanced granular active caspase-3 immunoreactivity was found in the cytoplasm of Purkinje cells in CJD. Increase in Bcl-2 and N-myc occurred in Purkinje cells in CJD and OPCA. These results indicate that enhanced Fas, Fas-L, MEK, ERK, Bax and granular active caspase-3 expression is not lethal to Purkinje cells in CJD, whereas increased Bcl-2 and N-myc does not preclude per se cell death or death survival in CJD and OPCA. These findings point to the likelihood that expression of these cell death proteins in neurodegeneration has functional roles differing from those related with apoptosis.



FUNCTIONAL ROLE AND THERAPEUTIC IMPLICATIONS OF NEURONAL CASPASE-1 AND -3 IN A MOUSE MODEL OF TRAUMATIC SPINAL CORD INJURY

M. LI,* V. O. ONA,* M. CHEN,* M. KAUL,†‡ L. TENNETI,†‡ X. ZHANG,§ P. E. STIEG,* S. A. LIPTON†‡ and R. M. FRIEDLANDER*||

*Neuroapoptosis Laboratory and Neurosurgical Service, Department of Surgery, †Cerebrovascular and Neuroscience Research Institute, and §Cardiovascular Division, Department of Medicine, Brigham and Women's Hospital, Harvard Medical School, Boston, MA 02115, USA

Abstract—Evidence indicates that both necrotic and apoptotic cell death contribute to tissue injury and neurological dysfunction following spinal cord injury. Caspases have been implicated as important mediators of apoptosis following acute central nervous system insults. We investigated whether caspase-1 and caspase-3 are involved in spinal cord injury-mediated cell death, and whether caspase inhibition may reduce tissue damage and improve outcome following spinal cord injury. We demonstrate a 17-fold increase in caspase-1 activity in traumatized spinal cord samples when compared with samples from sham-operated mice. Caspase-1 and caspase-3 activation were also detected by western blot following spinal cord injury, which was significantly inhibited by the broad caspase inhibitor *N*-benzyloxycarbonyl-Val-Ala-Asp-fluoromethylketone. By immunofluorescence or *in situ* fluorogenic substrate assay, caspase-1 and caspase-3 expression were detected in neuronal and non-neuronal cells following spinal cord injury. *N*-Benzyloxycarbonyl-Val-Ala-Asp-fluoromethylketone treated mice, and transgenic mice expressing a caspase-1 dominant negative mutant, demonstrated a significant improvement of motor function and a reduction of lesion size compared with vehicle-treated mice.

Our results demonstrate for the first time that both caspase-1 and caspase-3 are activated in neurons following spinal cord injury, and that caspase inhibition reduces post-traumatic lesion size and improves motor performance. Caspase inhibitors may be one of the agents to be used for the treatment of spinal cord injury. © 2000 IBRO. Published by Elsevier Science Ltd. All rights reserved.

Key words: apoptosis, ICE, zVAD-fmk, interleukin-1 β , neuroprotection.

In the United States, there are 183,000–230,000 people surviving with disabilities resulting from spinal cord injury (SCI) with approximately 10,000 new cases occurring each year.¹ More than half of SCI survivors cannot return to their normal life.² This disappointing prognosis results in part due to the poor understanding of the mechanism mediating secondary degeneration. Neurological damage after acute SCI results from both the primary mechanical injury as well as the subsequent activation of cell death cascades mediating delayed tissue damage.³ The primary injury results from actual mechanical tissue disruption, as well as necrotic cell death. Secondary degeneration results from a cascade of events triggered by the injury, resulting in activation of endogenous cell death pathways.^{4,5} High dose steroids, the widely used treatment for SCI, target many mediators of secondary degeneration, but outcome remains disappointing.⁶ Reports have identified apoptosis or programmed cell death as an important component contributing to tissue damage following SCI in rats, monkeys, as well as humans.^{4,5,7–10}

Apoptotic cell death has been detected up to three weeks following SCI.⁸ Since apoptosis is a tightly regulated process, this finding provides the opportunity to manipulate apoptotic pathways for the treatment of SCI.

The critical role of the caspases in apoptosis is well known.^{11,12} Caspase-1 [interleukin-1 β converting enzyme, (ICE)] has been implicated as a critical mediator of apoptosis following both acute CNS insults (ischemia and trauma) as well as models of chronic neurodegeneration (amyotrophic lateral sclerosis, Parkinson's disease and Huntington's disease).^{13,19} In these animal models, caspase-1 activation has been demonstrated, and caspase inhibition not only reduced tissue damage, but also resulted in improved neurological function.^{13,15} Caspase-3 activation has also been demonstrated in ischemia and trauma as well as in humans following SCI.^{9,10,20,21} Significant insight regarding *in vivo* neuronal cell death has been generated using a transgenic mouse expressing a caspase-1-dominant negative mutant.^{14,16–18} The transgene is caspase-1 with its active site cysteine (C285) substituted for a glycine (M17Z). The caspase-1 mutant is an effective caspase-1-dominant negative inhibitor (and possibly of other caspase family members). The neuron-specific enolase promoter targets transgene expression to neurons, oligodendrocytes, and astrocytes (NSE-M17Z).^{14,22,23} Using this mouse, as well as a pharmacologic approach to inhibit caspases, we investigated whether caspase-1 and caspase-3 are activated following SCI, and if their inhibition would reduce post-traumatic lesion size and improve neurological recovery.

EXPERIMENTAL PROCEDURES

Spinal cord injury model

A total of 110 mice (20–25 g) of the C57BL/6 strain (Jackson Lab,

†Present address: The Burnham Institute, 10901 North Torrey Pines Road La Jolla, CA 92037, USA.

|| To whom correspondence should be addressed. Tel.: +1-617-732-7676; fax: +1-617-734-8342.

E-mail address: rfriedlander@rics.bwh.harvard.edu (R. M. Friedlander).

Abbreviations: ANOVA, analysis of variance; DEVD-CHO, *N*-acetyl-Asp-Glu-Val-Asp-CHO; DMSO, dimethylsulfoxide; EDTA, ethylenediaminetetraacetate; ELISA, enzyme-linked immunosorbent assay; HRP, horseradish peroxidase; ICE, interleukin-1 β converting enzyme; IL-1 β , interleukin-1 β ; NeuN, neuronal nuclei; NSE, neuron specific enolase; PBS, phosphate-buffered saline; PMSF, phenylmethylsulfonyl fluoride; SCI, spinal cord injury; SDS-PAGE, sodium dodecylsulfate-polyacrylamide gel electrophoresis; TE, tris ethylenediaminetetraacetic acid; TUNEL, TdT-mediated dUTP nick-end labeling; zVAD-fmk, *N*-benzyloxycarbonyl-Val-Ala-Asp-fluoromethylketone.

Bar Harbor, ME, USA), or NSE-M17Z mice and wild-type littermates, which we generated in a C57BL/6 background, were used in this study. Transgenic mice were genotyped as previously described.¹⁴ All efforts were made to minimize both suffering and number of animals used. All experimental procedures were in accordance with protocols approved by the Harvard Medical School Animal Care Committee. Mice were anesthetized with an i.p. injection of 2,2,2-tribromoethanol (0.02 ml of a 2.5% solution/g body weight). After the depth of anesthesia was adequate, the mouse was placed prone in a modified spinal stereotactic apparatus with vertebral column fixation under a stereomicroscope. The skin was shaved and decontaminated. A 15–20-mm midline incision was made, and the T7–T12 levels were exposed by laterally separating the dorsal para-spinal muscles. Trauma was performed using a modification of the weight-drop method.²⁴ Briefly, a T8, T9, and T10 laminectomy was made with a high-speed micro drill (Harvard apparatus, Inc. Holliston, MA, USA) and a micro-rongeur (Fine Science Tools, Inc. Foster City, CA, USA). Following the laminectomy, a window over the dura of at least 1.6 mm in diameter was made to accommodate a stainless steel impact rod with a diameter of 1.4 mm and weight of 1.8 g. Part of the dura mater was carefully removed though the window for better drug penetration. Two horizontal bars of the stereotactic frame were used for vertebral column stabilization by clamping the T9–T10 transverse processes bilaterally. A vertical bar of the stereotactic frame held the cylinder supporting the weight rod, which was raised 10 mm above the dura and dropped onto the spinal cord at the T9 level. Following trauma, mice were randomly divided into two groups and treated with *N*-benzyloxycarbonyl-Val-Ala-Asp-fluoromethylketone (zVAD-fmk) or vehicle [dimethylsulfoxide (DMSO) 0.4%] (Enzyme Systems, Livermore, CA, USA). A piece of surgical gelfoam (2 × 2 × 6 mm³) presoaked in 10 μ l of zVAD-fmk (10 μ g) or vehicle was placed over the contused spinal cord. The muscle and skin were sutured in layers. During surgery, mice were kept on a 37°C warming blanket, and after surgery recovered in a 37°C incubator until fully alert. The bladder was manually expressed twice daily until return of reflexive bladder control. Animals had free access to food and water. The trauma model was equivalent in the NSE-M17Z and wild-type mice, with all the mice receiving vehicle treatment.

TdT-mediated dUTP nick-end labeling and immunohistochemistry

NSE-M17Z, zVAD-fmk or wild-type vehicle-treated mice were transcardially perfused with 4% paraformaldehyde (pH 7.4) in phosphate buffer 8, 24 and 48 h after trauma. Samples were embedded in paraffin, and cut in 10- μ m sections. TdT-mediated dUTP nick-end labeling (TUNEL) assay was carried out using a Fluorescein Apoptosis Detection Kit (Promega, Madison, WI, USA) Hoechst 33342 (Molecular Probe, Eugene, OR, USA) was used to evaluate nuclear morphology. Neurons were identified using anti-neuronal nuclei (NeuN) antibody (Chemicon, Temecula, CA, USA).

Mature interleukin-1 β determination

Mature interleukin-1 β (IL-1 β) concentration was measured using an enzyme-linked immunosorbent assay (ELISA) kit (R&D Minneapolis, MN, USA) which is specific for mature IL-1 β . Spinal cord tissue 15 mm long, centered upon the impact area, was removed from mice treated with zVAD-fmk or vehicle for 24 h after SCI or from sham-operated mice on which only a laminectomy and dural opening were performed without trauma ($n = 3$). Tissue was processed as previously described.¹⁴

Western blot analysis

Spinal cord tissue was lysed in RIPA buffer (150 mM NaCl, 1% Nonidet P-40, 12 mM sodium deoxycolate, 0.1% sodium dodecyl-sulfate (SDS), 50 mM Tris-HCl, pH 7.2), supplemented with protease inhibitors (PMSF, leupeptin, pepstatin A, and aprotinin). Lysates were centrifuged and protein concentration was determined using a protein assay (Bio-Rad, Hercules, CA, USA). Samples were loaded (50 μ g of protein/lane), electrophoresed on a 15% SDS-polyacrylamide gel electrophoresis (SDS-PAGE) gel, and blotted to an Immobilon-P transfer membrane (Millipore, Bedford, MA, USA). Blots were probed with a monoclonal antibody against the caspase-1 p20 subunit (generously provided by Dr. Junying Yuan), or with a polyclonal antibody against the p17 subunit of caspase-3 (generously provided by Anu Srinivasan, Idu, La Jolla, CA, USA) and visualized with

horseradish peroxidase-conjugated secondary antibodies by ECL (Amersham).

DNA laddering

Spinal cord DNA was isolated according to published methods.²⁵ Briefly, sham-operated mice and mice receiving zVAD-fmk or vehicle were euthanized 24 h after trauma. The tissue was homogenized in lysis buffer (10 mM Tris-HCl, 100 mM EDTA, and 0.5% SDS) and incubated with proteinase K (100 μ g/ml). DNA was extracted by phenol/chloroform/ethyl alcohol (25:24:1), precipitated with 70% ethanol, and resuspended in TE buffer. The samples were digested with DNase-free RNase, and separated by electrophoresis on a 1.5% agarose gel.

Detection of conformationally active caspase-3-like and caspase-1 proteases

To demonstrate activation of caspase-3 in SCI-induced neuronal apoptosis, we used an affinity-labeling technique with biotinylated-*N*-acetyl-Asp-Glu-Val-Asp-CHO (DEVD-CHO) (BIOMOL Research Laboratories, Inc., Plymouth Meeting, PA, USA), as previously described with some modifications.^{26,27} At indicated times, following deparaffinization and rehydration, sections were washed with phosphate-buffered saline (PBS) containing 0.05% Tween-20 and blocked in 10% normal goat serum for 1 h. Next, tissue was incubated with 50 μ M biotinylated-DEVD-CHO for 48 h at 4°C. Following three washes with PBS, tissue was incubated with fluorescein avidin DCS (1:1000, Vector Laboratories, Burlingame, CA, USA) for 30 min. For double staining with anti-caspase-3 antibody, CM1 (Idun, La Jolla, CA, USA) and biotinylated-DEVD-CHO, sections were incubated with primary antibody CM1 (1:6000) overnight after biotinylated-DEVD-CHO incubation and followed by a 1-h incubation with anti-rabbit TEXRED (1:200, Vector Laboratories, Burlingame, CA, USA). For co-staining with anti-NeuN and biotinylated-DEVD-CHO, the sections were incubated with anti-NeuN antibody (Chemicon, Temecula, CA, USA) in dilution of 1:100 for 1 h and then probed with anti-mouse TEXRED (1:200, Vector Laboratories, CA, USA). Hoechst 33342 (0.2 μ g/ml, Molecular Probe, Eugene, OR, USA) was used for counterstaining. DEVD-associated fluorescence was detected using epifluorescence microscopy. For controls, tissue not treated with biotinylated-DEVD-CHO did not display staining, indicating that the affinity-labeling technique specifically detects conformationally active caspase-3-like proteases. Furthermore, preincubation with unlabeled DEVD-CHO (300 μ M) greatly reduced biotinylated-DEVD-associated cellular fluorescence. For caspase-1 protease detection, specimens were incubated with a monoclonal antibody against the caspase-1 p20 subunit (generously provided by Dr Junying Yuan) at 1:3 dilution and probed with biotinylated anti-rat immunoglobulin followed by incubation in 1:1000 fluorescein avidin DCS for 1 h. The primary antibody was eliminated in controls, which did not reveal a detectable signal.

Quantification of apoptotic cells following spinal cord injury

To quantitatively compare the extent of apoptosis following SCI in vehicle-treated, zVAD-fmk-treated, and caspase-1-dominant negative mice, we performed apoptotic cell counting on TUNEL-stained sections from each of these groups ($n = 3$). The sections (10 μ m thick) were obtained from the epicenter and 3 mm rostral and caudal to the impact site 24 h following SCI. A blinded researcher counted TUNEL-positive cells in five random high-power fields (40 \times) from each section using epifluorescence microscopy, without discriminating between white and gray matter.

Behavioral assessment

All animals were blindly scored on three different behavioral tests adopted from previously described methods for the evaluation of mouse SCI models,²⁴ including open field, pain withdrawal, and platform tests. Mice were evaluated on the day before surgery, on post-surgical days 3 and 7, and weekly thereafter for three weeks.

Lesion size measurement

On post-trauma day 28, animals were euthanized with isoflurane and transcardially perfused with heparinized saline followed by 4%

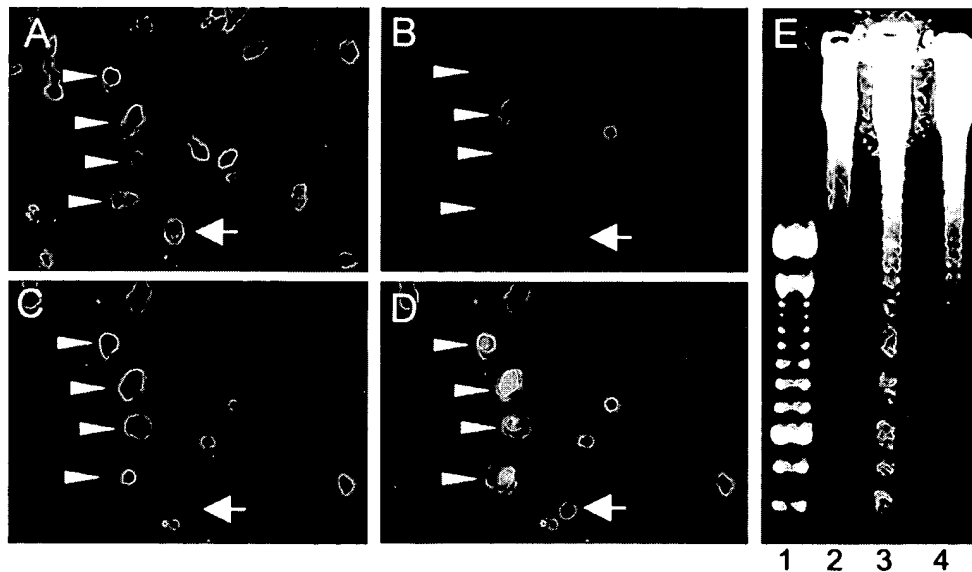


Fig. 1. Post-SCI neuronal apoptosis. (A–D) A traumatized spinal cord section at the lesion epicenter 24 h after SCI was stained with Hoechst 33342 (A), NeuN (B), and TUNEL (C); (D) is a superimposed image of (B) and (C). Yellow or orange cells in (D) (arrowheads) represent apoptotic neurons since they are TUNEL- and NeuN-positive. Green cells in (D) most likely represent non-neuronal apoptotic cells since they do not stain for NeuN. Non-apoptotic neurons in (D) are red (arrow). These results demonstrate that post-SCI apoptosis occurs in both neuronal and non-neuronal cells. (E) Ethidium bromide-stained agarose gel demonstrates a DNA ladder from a vehicle-treated mouse (lane 3) at 24 h after SCI. Laddering was virtually undetectable in traumatized zVAD-fmk-treated mice (lane 4) and was not visible in sham-operated mice (lane 2). Lane 1 shows 100-bp DNA ladder standard (this experiment was independently performed with three different sets of mice).

paraformaldehyde (pH 7.4) in PBS. Spinal cord segments 5 mm long (2.5 mm rostral and caudal to the impact site) were removed and post-fixed in paraformaldehyde overnight and then embedded in paraffin. Serial transverse sections (20 μ m thick) were cut, and one of every 40 sections was saved for lesion size measurement. The sections were stained with Luxol Fast Blue, by which residual white and gray matter are easily distinguished from the lesioned area, and Cresyl Violet to visualize neurons.²⁴ The damaged area of spinal cord was characterized by neuronal loss and weakly stained tissue (Fig. 6B–E). The images of the stained specimen were captured by a digital photographic camera (Sony DKC-5000) and analysed with a Scion Image System (NIH image 6.1) for morphometric measurement. Total lesion volumes were computed by integrating the lesion area of each section and the distance between two sections (0.8 mm) (Total lesion volume = lesion area of section 1 \times 0.8/2 + lesion area of section 2 \times 0.8/2 + lesion area of section 3 \times 0.8/2 + ... + lesion area of section 10 \times 0.8/2). All lesion volume analyses were performed by a blinded investigator.

Data analysis

Data are presented as mean \pm S.E.M. Statistical comparisons among three different groups (vehicle-treated, zVAD-treated and NSE-M17Z) for lesion volumes were made by one-way analysis of variance (ANOVA) with post-test. The behavioral outcomes were analysed by a two-way ANOVA with repeated measures and significant two-way ANOVA was followed by the Scheffe test (acceptable $P < 0.05$) to perform a series of the mean comparisons. The statistical programs Statistical Analysis System and GraphPad InStar were used in the statistic analysis.

RESULTS

N-Benzylloxycarbonyl-Val-Ala-Asp-fluoromethylketone treatment and caspase-1-dominant negative mutant expression inhibit post-spinal cord injury-mediated apoptosis

To determine whether apoptotic cell death played a role in the mouse SCI weight drop model, we performed TUNEL staining and evaluated the presence of oligonucleosomal DNA degradation in traumatized spinal cord tissue. Apoptotic cells, some of which were stained with neuronal-specific

markers, were incrementally detected at 8, 24 and 48 h following trauma (Figs 1A–D, 2A–C). Distinct oligonucleosomal DNA fragmentation was detected superimposed on random DNA degradation, represented as a smear of various molecular weights, suggesting that both apoptotic and necrotic cell death played a role in our mouse SCI model, which was reduced in zVAD-fmk- (a broad spectrum caspase inhibitor) treated mice (Fig. 1E). The extent of apoptotic cell death, as evaluated by TUNEL staining, was reduced in mice treated with zVAD-fmk and in the caspase-1-dominant negative mutant transgenic mice by 50.2% and 54.0%, respectively ($n = 3/\text{group}$, $P < 0.0001$; Fig. 2A–C vs G–I, M–O and Table 1). Treatment with the caspase inhibitor was performed by placing a collagen sponge loaded with either zVAD-fmk (10 μ g) or vehicle solvent and placing it over the spinal cord following the injury. TUNEL-positive cells and DNA degradation were not detected in sham-operated mice.

Caspase-1 and caspase-3 are activated following spinal cord injury

Detection of mature IL-1 β has been used as a sensitive and specific marker to determine caspase-1 activation since, in mice, caspase-1 is the major (if not the only) enzyme able to cleave pro-IL-1 β .^{14,15,28–30} Twenty-four hours following trauma, mature IL-1 β levels were 17-fold higher in vehicle-treated mice when compared with sham-operated mice ($P < 0.001$). Following SCI, zVAD-fmk treatment or mutant caspase-1 expression resulted in a 52.3% and 60.4% reduction in caspase-1 activity, respectively, when compared with traumatized wild-type untreated samples. These results demonstrate SCI-mediated caspase-1 activation, which is inhibited by local zVAD-fmk delivery or mutant caspase-1 expression (Table 2).

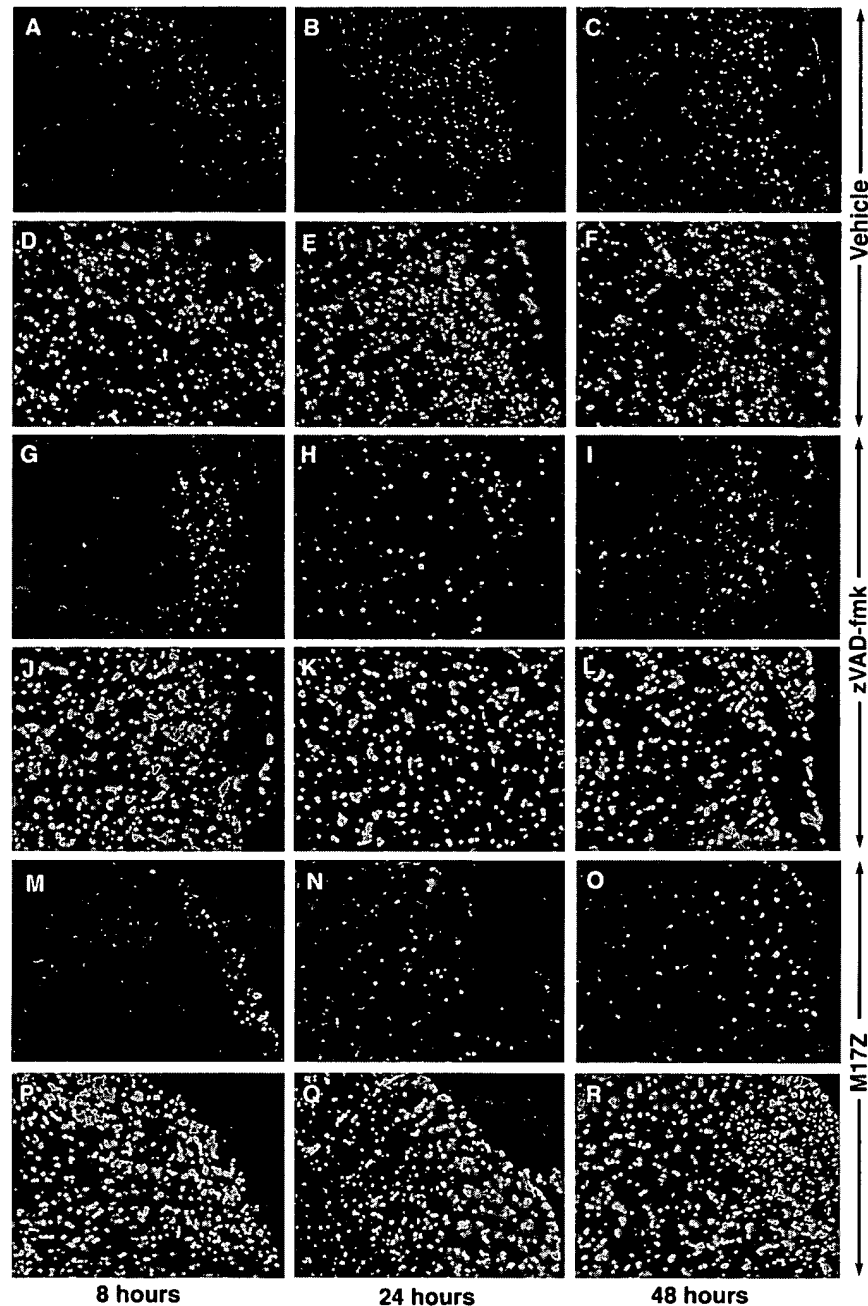


Fig. 2. Post-SCI apoptosis is inhibited by zVAD-fmk or mutant caspase-1. Under lower magnification ($\times 5$), the sections obtained from the lesion epicenter at 8 h (A, G, M), 24 h (B, H, N), and 48 h (C, I, O) following SCI show that the number of TUNEL-positive cells (green) increased over time but was reduced by zVAD-fmk treatment (G–I), or by mutant caspase-1 expression (M–O), when compared with wild-type vehicle-treated mice (A–C). (D–F, J–L, P–R) Images of the same sections as (A–C, G–I, M–O) counter-stained with Hoechst 33342.

We assayed for the active subunits of caspase-1 and caspase-3 after SCI by western blotting. The immunoreactive bands of caspase-1 (20,000 mol. wt) and caspase-3 (17,000 mol. wt) were detected in spinal cord lysates 24 h after SCI. No evidence of the active subunits was demonstrated in sham-operated mice. Detection of cleaved caspase-1 and caspase-3 immunoreactive subunits was significantly decreased in zVAD-fmk-treated mice (Fig. 3). Caspase activation can result both from autocatalysis or activation by other activated caspases.^{31,32} zVAD-fmk broadly inhibits caspase activity, blocking both processing of general caspase substrates, as well as generation of activated caspase-1 and caspase-3.³³

Table 1. Number of TUNEL-positive cells 24 h post-SCI was significantly inhibited in zVAD-fmk-treated and NSE-M17Z mice, compared with vehicle-treated wild-type mice

| | Number of TUNEL-positive cells | P-value |
|--------------------|--------------------------------|---------|
| Wild-type/vehicle | 127.7 \pm 11.1 | |
| Wild-type/zVAD-fmk | 63.6 \pm 6.7 | < 0.001 |
| NSE-M17Z | 58.7 \pm 5 | < 0.001 |

Cells were counted under $\times 40$ magnification ($n = 3/\text{group}$, ANOVA).

Table 2. Mature IL-1 β levels were measured using an ELISA specific for the mature form of the cytokine

| | Mature IL-1 β (pg/mg tissue weight) | P-value |
|--------------|---|-----------|
| Sham | 0.07 \pm 0.01 | |
| SCI/vehicle | 1.21 \pm 0.25 | < 0.001* |
| SCI/zVAD-fmk | 0.58 \pm 0.03 | = 0.01** |
| SCI/NSE-M17Z | 0.48 \pm 0.12 | = 0.02*** |

Following spinal cord injury, mature IL-1 β levels in vehicle-treated mice were 17-fold higher than in sham-operated mice. zVAD-fmk treatment and NSE-M17Z expression produced a 52.3% and 60.4% decrease, respectively, in post-SCI mature IL-1 β production compared with wild-type vehicle-treated mice. Data are presented as mean \pm S.E.M. and analysed by one-way ($n=3$, ANOVA).

*P-value for comparison to sham-operated wild-type mice.

**P-value for comparison to vehicle-treated wild-type mice after spinal cord injury.

***P-value for comparison to vehicle-treated wild-type mice after spinal cord injury.

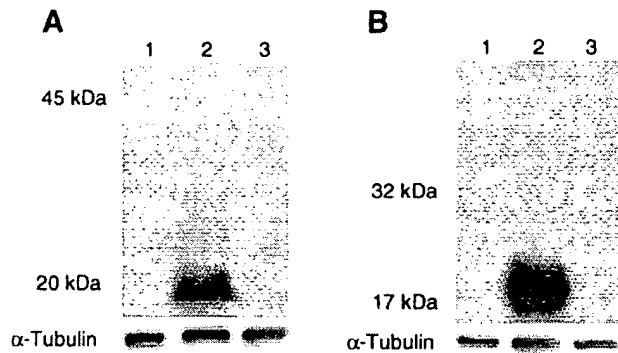


Fig. 3. Post-SCI caspase-1 and caspase-3 activation. (A) Detection of the caspase-1 active p20 subunit. (B) The caspase-3 active p17 subunit by western blot from spinal cord lysates 24 h after trauma. The active subunit was significantly reduced in zVAD-fmk-treated mice (lane 3) when compared with vehicle-treated mice (lane 2). No immunoreactive product was detected in sham-operated mouse (lane 1). These blots are representative of three independent experiments.

Detection of neuronal and non-neuronal caspase-1- and caspase-3-like signal following spinal cord injury

Significant controversy exists regarding the cell types expressing caspase-1 and caspase-3 in the central nervous system. Using the caspase-1 antibody and biotinylated DEVD-CHO (an activated caspase-3-like marker), and a specific neuronal marker to identify neurons (anti-NeuN),³⁴ we stained spinal cord sections from sham-operated mice. No caspase-1- or caspase-3-like staining was detected in sections from sham-operated mice (Figs 4C, 5C). However, clear caspase-1- and caspase-3-like staining was detected in both NeuN-positive and NeuN-negative cells demonstrating caspase-1- and caspase-3-like induction following SCI (Figs 4E–L, 5E–L). At the epicenter of the lesion, caspase-1- and caspase-3-like staining was detected in 77% and 69% respectively of NeuN-positive cells (345 neurons counted in three mice). As a control, preincubation with DEVD-CHO significantly blocked subsequent biotinylated DEVD-CHO binding (Fig. 5M–P). In addition, biotinylated DEVD-CHO binding colocalized with caspase-3 immunostaining (Fig. 5Q–T). No staining was detected in sections incubated with the fluorescent ligand without the caspase-1 antibody or biotinylated DEVD-CHO. Cytoplasmic and nuclear caspase stainings were both detected, likely demonstrating cells in different stages of cell death. Caspase-1 contains a nuclear localization signal, and cell death-associated nuclear translocation has been previously described *in vitro*.³⁵ These findings are consistent with the ELISA and western blot results. In sham-operated mice, minimal mature IL-1 β was detected (Table 2), and there were no detectable caspase-1 or caspase-3 immunoreactive bands (Fig. 3A, lane 1; Fig. 3B, lane 1). Furthermore, post-SCI samples demonstrated a robust increase in caspase-1 activity (Table 2) as well as marked caspase-1 p20 (Fig. 3A, lane 2) and caspase-3 p17 (Fig. 3B, lane 2) immunoreactivity. These findings show that caspase-1- and caspase-3-like signals are induced in both neuronal and non-neuronal cells following SCI.

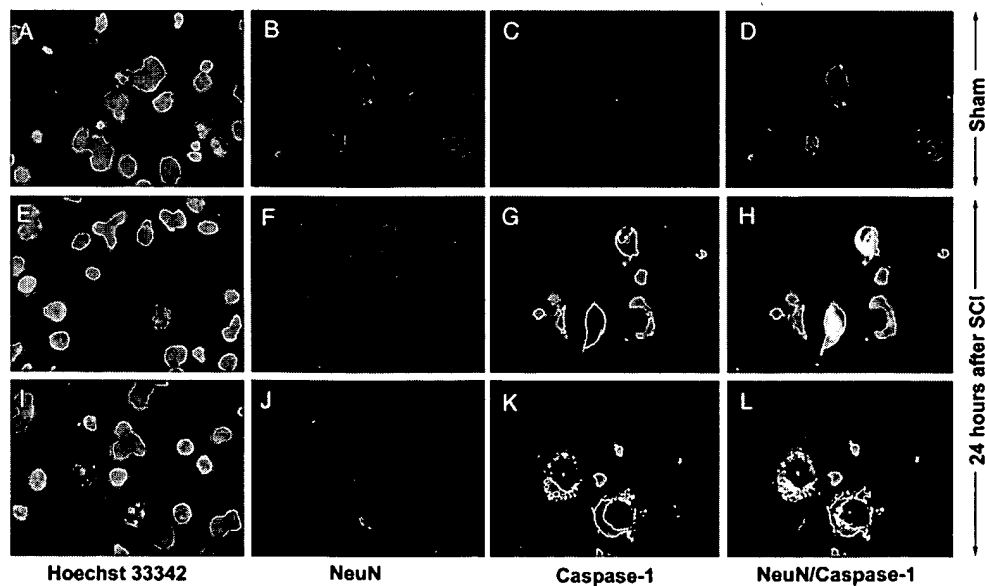


Fig. 4. Induction of neuronal and non-neuronal post-SCI caspase-1. (A–D) Spinal cord sections of a sham-operated mouse. (E–H and I–L) Two spinal cord sections at the lesion epicenter from traumatized mice 24 h following the injury. (A, E, I) Hoechst 33342 staining. (B, F, J) NeuN staining. (C, G, K) Caspase-1 staining. (D, H, L) Merged images of NeuN and caspase-1. In the merged images, both caspase-1 cytoplasmic and nuclear stainings were evident in neuronal and non-neuronal cells.

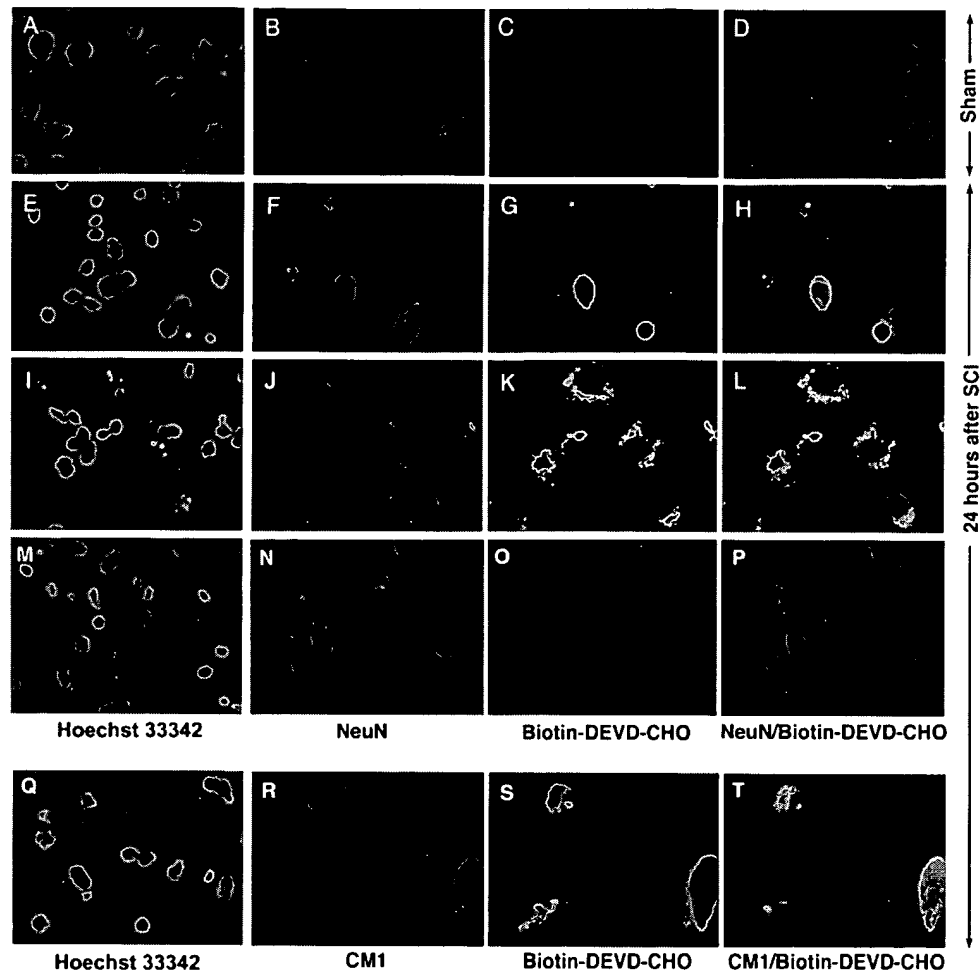


Fig. 5. Induction of neuronal and non-neuronal post-SCI caspase-3 like activity. (A–D) Spinal cord sections of a sham-operated mouse. (E–T) Spinal cord sections at the lesion epicenter from traumatized mice 24 h following the injury. (A, E, I, M, Q) Hoechst 33342 dye staining. (B, F, J, N, R) NeuN staining. (C, G, K, O, S) Active caspase-3-like staining (biotinylated DEVD-CHO). (D, H, L, P) Merged images of NeuN and caspase-3-like staining. In the merged images caspase-3-like cytoplasmic and nuclear staining were demonstrated in neuronal and non-neuronal cells. (M–P) Sections preincubated with non-biotinylated DEVD-CHO prior to biotinylated DEVD-CHO revealed blocking of specific DEVD binding (O). (Q–T) Colocalization of activated caspase-3 antibody binding (CM1) with biotinylated DEVD-CHO (T).

Post-spinal cord injury neurological deficits and lesion size are inhibited by N-benzoyloxycarbonyl-Val-Ala-Asp-fluoromethylketone and by expression of a caspase-1-dominant negative mutant

To assess post-SCI neurological deficits following trauma, as well as the effect of zVAD-fmk treatment (Fig. 6A–C) and mutant caspase-1 expression (Fig. 6D–F) on motor function, a battery of tests was used by a blinded observer to evaluate the mice for a period of three weeks. All mice were paraplegic following trauma, with gradual neurological recovery over 21 days. A two-way ANOVA with repeated measures revealed significant interaction between SCI group and test time in all behavioral tests: pain withdrawal test (zVAD/control) $F_{16,79} = 42.54$, $P < 0.0001$; pain withdrawal test (M17Z/WT) $F_{13,49} = 12.78$, $P < 0.0001$; platform (zVAD/control) $F_{16,78} = 9.69$, $P < 0.0001$; platform (M17Z/WT) $F_{13,49} = 7.41$, $P < 0.0001$; open-field (zVAD/control) $F_{16,79} = 14.81$, $P < 0.0001$; open-field (M17Z/WT) $F_{13,49} = 15.39$; $P < 0.0001$.

All behavior tests, except for the platform test (zVAD-fmk/control), demonstrated a significant improvement following

SCI by either zVAD-fmk treatment or mutant caspase-1 expression when compared with vehicle-treated wild-type mice. Of the zVAD-fmk-treated and caspase-1-dominant negative mice, 80% and 83%, respectively, achieved a weight bearing functional recovery (grade 3 or better on the open-field testing), compared with 13% in the control group (Fig. 6C, F). Significant differences between the two groups were not detected in any of the tests prior to day 5, suggesting that caspase inhibition does not affect the symptomatic manifestation resulting from the initial injury. However, delayed cell death, likely resulting from caspase-mediated apoptotic mechanisms, was inhibited by zVAD-fmk and by mutant caspase-1, therefore providing neurological protection from the delayed consequences of the initial injury.

To evaluate the effect of caspase inhibition, serial sections stained with Luxol Fast Blue and Cresyl Violet were examined by light microscopy for morphometric lesion analysis. The injured tissue was easily distinguished from spared tissue by a clear boundary, as demonstrated in Luxol Fast Blue-stained sections. The lesioned area was replaced by a dense astroglial scar (Fig. 7A–D). Mice treated with zVAD-fmk or expressing

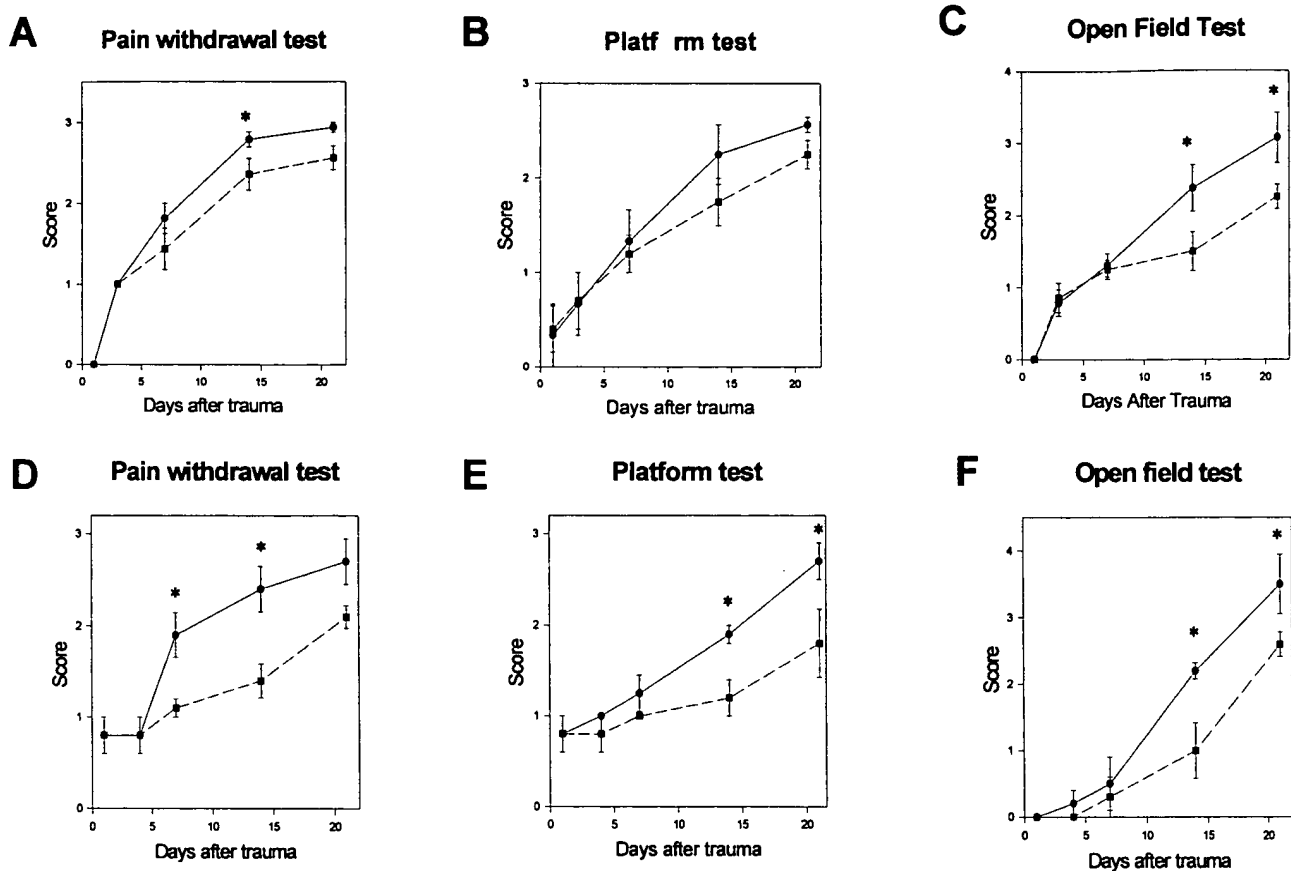


Fig. 6. zVAD-fmk and mutant caspase-1 expression improve post-SCI neurological outcome. zVAD-fmk-treated (A–C) and mutant caspase-1 transgenic (D–F) mice were blindly evaluated for a period of three weeks following trauma using the pain withdrawal test (A, D), the platform test (B, E), and the open field test (C, F). All mice were paraplegic following trauma, with gradual neurological recovery over 21 days. All three functional tests, except for the platform test (B), demonstrated a significant improvement in the zVAD-fmk-treated and mutant caspase-1 transgenic groups (circles, solid line) compared with the control (squares, dashed line) ($n=5-8/\text{group}$, Scheffe test, $*P < 0.05$). Significant differences were not detected prior to day five.

mutant caspase-1 had a 38.2% and 49.3% reduction in lesion size, respectively, when compared with wild-type vehicle-treated mice (Table 3, $n=5-8/\text{group}$, ANOVA, $P < 0.05$, $P < 0.01$). In addition, to further validate our trauma model as well as the relation of the lesion size and the behavioral score, the Pearson product moment correlation was calculated between the two variables. We found a high degree of correlation between behavioral score and lesion size ($r = -0.94$, $P < 0.001$, Fig. 7E).

DISCUSSION

This study demonstrates for the first time both caspase-1 and caspase-3 activation in neuronal and non-neuronal cells following SCI. Adding therapeutic relevance to this finding, local delivery of zVAD-fmk, or use of a caspase-1-dominant negative transgenic mouse, reduced post-traumatic tissue damage and improved neurological recovery. Recently, apoptotic cell death has been detected following SCI in rats, monkeys and humans.^{4,8,9} Apoptotic cell death following SCI was first detected in an experimental rat model. In a rat model, TUNEL-positive cells were detected from 4 h to three weeks after SCI, suggesting that a prolonged post-traumatic therapeutic window might exist for intervention.^{4,8} Apoptotic cell death was also detected in remote degenerating fiber tracts in monkey, suggesting that apoptosis is associated

with Wallerian degeneration of long spinal tracts.⁴ More recently, a study of 15 patients who died between 3 h and two months after SCI reported apoptotic cell death in human spinal cords.⁹ Cycloheximide, an inhibitor of protein synthesis, has been demonstrated to reduce SCI-mediated tissue damage and improve motor recovery. The beneficial effect of cycloheximide treatment might have resulted from inhibition of protein synthesis-dependent apoptosis.⁸

Since apoptotic cell death occurs in all the spinal cord cellular components, including neurons, astrocytes, oligodendrocytes, and microglia, decreased lesion size as well as improved motor function likely result from inhibition of cell death in all the different cell types.^{8,36} Neuronal protection is clearly important because of the inability of neurons in the spinal cord to regenerate. Despite the fact that glia can regenerate, inhibiting glial death confers neuroprotection by at least two likely mechanisms. First, glia supply neurotrophic and metabolic support to injured neurons as well as to axonal pathways likely required for recovery of sublethal injured cells.³⁷⁻³⁹ Second, during apoptosis, dying cells secrete additional mediators of apoptosis, such as cytokines, and free radicals, which have an additive toxic effect to other adjacent cells, likely enhancing further neurodegeneration.⁴⁰⁻⁴³

In the present study, we demonstrate that, following SCI, TUNEL-positive cells were detected in increasing numbers at 8, 24 and 48 h. TUNEL-positive cells were first detected (8 h)

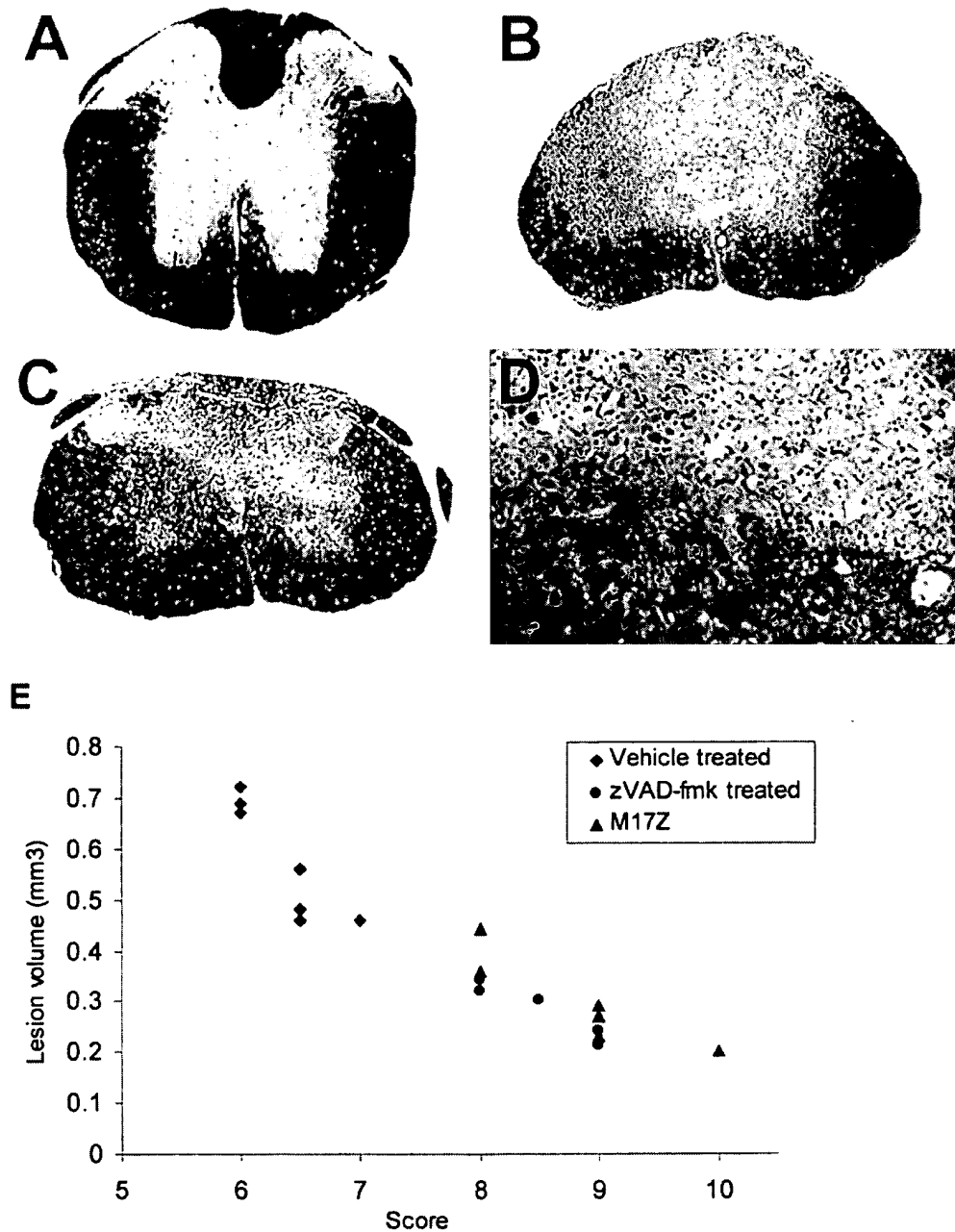


Fig. 7. zVAD-fmk and mutant caspase-1 expression reduce post-SCI tissue injury. (A–D) Spinal cord sections stained with Luxol Fast Blue and Cresyl Violet. (A) Normal spinal cord. (B, C) Representative slices at the lesion epicenter in vehicle (B) and zVAD-fmk-treated mice (C). (D) Under high magnification, there is a clear border between post-traumatic scar and normal tissue (white arrows). (E) Analysis of the correlation factor on individual mice between total behavior score (sum of the three behavioral tests at day 21) and lesion size (diamond = vehicle-treated wild type, circle = zVAD-fmk treated, and triangle = NSE-M17Z) ($r = -0.94$, $P < 0.001$, Pearson product moment correlation test).

adjacent to the site of injury where the magnitude of the triggering event is maximum. However, TUNEL-positive cells were also detected at later times (24 and 48 h) at increasing distances from the site of impact. As seen in cerebral ischemia models, this finding is consistent with a graded activation of apoptotic pathways, wherein the time for detection of TUNEL positivity is proportional to the severity of the insult.^{18,44} With immunohistochemistry we demonstrated that apoptosis occurs in both neuronal and non-neuronal cells. Consistent with experimental SCI models in rats,⁸ we demonstrated DNA fragmentation in the mouse weight-drop SCI model. In addition, this is the first study to

demonstrate specific neuronal expression of both caspase-1 and caspase-3 following spinal cord injury.

Caspase-1 appears to play a role in tissue injury by participating in both apoptotic and inflammatory pathways. Caspase-1-mediated generation of mature IL-1 β has been demonstrated to play a role in neuronal cell death as well as in inflammatory pathways.^{40,42,45} Decreased tissue damage and improved neurological outcome resulting from caspase-1 inhibition likely result from interfering with both apoptotic and inflammatory pathways. Our findings do not distinguish the possible contributions to delayed neurodegeneration resulting from these two important mechanistic pathways.

Table 3. Total lesion volume four weeks after SCI in mice treated with zVAD-fmk and NSE-M17Z mice had a 38.2% and 49.3% reduction, respectively, when compared with those in vehicle-treated mice ($n = 5-8$ /group, ANOVA)

| | Lesion volume (mm ³) | P-value |
|--------------------|----------------------------------|---------|
| Wild-type/vehicle | 0.55 ± 0.04 | |
| Wild type/zVAD-fmk | 0.34 ± 0.08 | < 0.05 |
| NSE-M17Z | 0.28 ± 0.03 | < 0.01 |

Effective therapy following SCI requires a comprehensive approach targeting several potential reversible factors contributing to delayed neurological dysfunction. Local components responsible for acute post-SCI neurological deficits can be reversible or irreversible. At present, irreversible factors include cord transection and interruption of axonal pathways. If treated sufficiently early, potentially reversible factors include compression-mediated ischemia, astroglial scar formation, cell death, damage resulting from swelling, inflammation and oxidative stress.³ Potential agents targeting different reversible factors include inhibitors of swelling and inflammation (steroids, caspase-1 inhibitors), inhibitors of scar formation (CM101), apoptosis inhibitors (caspase inhibitors), inhibitors of excitotoxins (memantine), among others.^{37,46-49} As demonstrated in this study, following acute surgical decompression and stabilization, local delivery of caspase inhibitors can be one of the components of an SCI treatment protocol in humans. Unlike the case in traumatic brain injury, the localized nature of the injury makes the spinal cord particularly suited for the local delivery of a therapeutic agent such as a caspase inhibitor.

Using *in vivo* models, previous studies have demonstrated

in mice that caspases are important mediators of apoptosis induced by both acute and chronic CNS insults, including brain trauma, cerebral ischemia, amyotrophic lateral sclerosis, Huntington's disease, and Parkinson's disease.¹⁴⁻¹⁸ Pharmacological inhibition of caspase-1 or expression of a dominant negative caspase-1 inhibitor in transgenic mice produced substantial neurological and survival improvement in the above cell-death paradigms. Caspase-3, another important mediator of apoptosis, has also been implicated to contribute to neuronal apoptotic cell death in trauma and ischemia as well as in neurodegenerative diseases.^{10,20,21,50,51} Caspase-3 activation has recently been demonstrated in human spinal cord samples following SCI.⁹ Data presented here demonstrate in a mouse model that both caspase-1 and caspase-3 are activated after SCI and that pharmacological inhibition with zVAD-fmk significantly blocked their activation as well as decreased the extent of SCI-induced apoptosis. Moreover, caspase inhibition by either local delivery of zVAD-fmk or expression of a caspase-1-dominant negative mutant significantly reduced lesion size and improved motor function following SCI. These results demonstrate for the first time an important functional role for caspase-mediated apoptosis in tissue damage and neurological dysfunction following SCI. Therefore, caspase inhibition could be a rational targeted strategy for the treatment of SCI.

Acknowledgements—We thank Junying Yuan (Harvard Medical School) for providing the caspase-1 antibody and Anu Srinivasan for providing the active-caspase-3 (CM1) antibody (Idun Pharmaceuticals), Joseph R. Madsen for helpful comments, and Eugenia Friedlander for editorial assistance. This work was supported by a departmental grant and PO1 HD29587.

REFERENCES

- Price C., Makintubee S., Herndon W. and Istre G. R. (1994) Epidemiology of traumatic spinal cord injury and acute hospitalization and rehabilitation charges for spinal cord injuries in Oklahoma, 1988–1990. *Am. J. Epidemiol.* **139**, 37–47.
- Gerhart K. A. (1991) Spinal cord injury outcomes in a population-based sample. *J. Trauma* **31**, 1529–1535.
- Amar A. P. and Levy M. L. (1999) Pathogenesis and pharmacological strategies for mitigating secondary damage in acute spinal cord injury. *Neurosurgery* **44**, 1027–1039.
- Crowe M. J., Bresnahan J. C., Shuman S. L., Masters J. N. and Beattie M. S. (1997) Apoptosis and delayed degeneration after spinal cord injury in rats and monkeys. *Nat. Med.* **3**, 73–76.
- Lou J., Lenke L. G., Ludwig F. J. and O'Brien M. F. (1998) Apoptosis as a mechanism of neuronal cell death following acute experimental spinal cord injury. *Spinal Cord* **36**, 683–690.
- Braughler J. M. and Hall E. D. (1985) Current application of "high-dose" steroid therapy for CNS injury. A pharmacological perspective. *J. Neurosurg.* **62**, 806–810.
- Yong C., Arnold P. M., Zoubine M. N., Citron B. A., Watanabe I., Berman N. E. and Festoff B. W. (1998) Apoptosis in cellular compartments of rat spinal cord after severe contusion injury. *J. Neurotrauma* **15**, 459–472.
- Liu X. Z., Xu X. M., Hu R., Du C., Zhang S. X., McDonald J. W., Dong H. X., Wu Y. J., Fan G. S., Jacquin M. F., Hsu C. Y. and Choi D. W. (1997) Neuronal and glial apoptosis after traumatic spinal cord injury. *J. Neurosci.* **17**, 5395–5406.
- Emery E., Aldana P., Bunge M. B., Puckett W., Srinivasan A., Keane R. W., Bethea J. and Levi A. D. (1998) Apoptosis after traumatic human spinal cord injury. *J. Neurosurg.* **89**, 911–920.
- Springer J. E., Azbill R. D. and Knapp P. E. (1999) Activation of the caspase-3 apoptotic cascade in traumatic spinal cord injury. *Nat. Med.* **5**, 943–946.
- Miura M., Zhu H., Rotello R., Hartwig E. A. and Yuan J. (1993) Induction of apoptosis in fibroblasts by IL-1 beta-converting enzyme, a mammalian homolog of the *C. elegans* cell death gene *ced-3*. *Cell* **75**, 653–660.
- Friedlander R. M. and Yuan J. (1998) ICE, neuronal apoptosis and neurodegeneration. *Cell Death Differ.* **5**, 823–831.
- Friedlander R. M., Brown R. H., Gagliardini V., Wang J. and Yuan J. (1997) Inhibition of ICE slows ALS in mice. *Nature* **388**, 31.
- Friedlander R. M., Gagliardini V., Hara H., Fink K. B., Li W., MacDonald G., Fishman M. C., Greenberg A. H., Moskowitz M. A. and Yuan J. (1997) Expression of a dominant negative mutant of interleukin-1 beta converting enzyme in transgenic mice prevents neuronal cell death induced by trophic factor withdrawal and ischemic brain injury. *J. exp. Med.* **185**, 933–940.
- Hara H., Friedlander R. M., Gagliardini V., Ayata C., Fink K., Huang Z., Shimizu-Sasamata M., Yuan J. and Moskowitz M. A. (1997) Inhibition of interleukin-1beta converting enzyme family proteases reduces ischemic and excitotoxic neuronal damage. *Proc. natn. Acad. Sci. USA* **94**, 2007–2012.
- Ona V. O., Li M., Vonsattel J. P., Andrews L. J., Khan S. Q., Chung W. M., Frey A. S., Menon A. S., Li X. J., Stieg P. E., Yuan J., Penney J. B., Young A. B., Cha J. H. and Friedlander R. M. (1999) Inhibition of caspase-1 slows disease progression in a mouse model of Huntington's disease. *Nature* **399**, 263–267.
- Klevenyi P., Andreassen O., Ferrante R. J., Schleicher J. R. Jr., Friedlander R. M. and Beal M. F. (1999) Transgenic mice expressing a dominant negative mutant interleukin-1beta converting enzyme show resistance to MPTP neurotoxicity. *NeuroReport* **10**, 635–638.

18. Hara H., Fink K., Endres M., Friedlander R. M., Gagliardini V., Yuan J. and Moskowitz M. A. (1997) Attenuation of transient focal cerebral ischemic injury in transgenic mice expressing a mutant ICE inhibitory protein. *J. cerebr. Blood Flow Metab.* **17**, 370–375.
19. Fink K. B., Andrews L. J., Butler W. E., Ona V. O., Li M., Bogdanov M., Endres M., Khan S. Q., Namura S., Stieg P. E., Beal M. F., Moskowitz M. A., Yuan J. and Friedlander R. M. (1999) Reduction of post-traumatic brain injury and free radical production by inhibition of the caspase-1 cascade. *Neuroscience* **94**, 1213–1218.
20. Yakovlev A. G., Knoblach S. M., Fan L., Fox G. B., Goodnight R. and Faden A. I. (1997) Activation of CPP32-like caspases contributes to neuronal apoptosis and neurological dysfunction after traumatic brain injury. *J. Neurosci.* **17**, 7415–7424.
21. Namura S., Zhu J., Fink K., Endres M., Srinivasan A., Tomaselli K. J., Yuan J. and Moskowitz M. A. (1998) Activation and cleavage of caspase-3 in apoptosis induced by experimental cerebral ischemia. *J. Neurosci.* **18**, 3659–3668.
22. Burne J. F., Staple J. K. and Raff M. C. (1996) Glial cells are increased proportionally in transgenic optic nerves with increased numbers of axons. *J. Neurosci.* **16**, 2064–2073.
23. Forss-Petter S., Danielson P. E., Catsicas S., Battenberg E., Price J., Nerenberg M. and Sutcliffe J. G. (1990) Transgenic mice expressing beta-galactosidase in mature neurons under neuron-specific enolase promoter control. *Neuron* **5**, 187–197.
24. Kuhn P. L. and Wrathall J. R. (1998) A mouse model of graded contusive spinal cord injury. *J. Neurotrauma* **15**, 125–140.
25. Sambrook J., Fritsch E. F. and Maniatis T. (1989) Analysis and cloning of eukaryotic genomic DNA. In *Molecular Cloning* (eds Ford N., Nolan C. and Ferguson M.), pp. 9.16–9.19. Cold Spring Harbour Laboratory Press, New York.
26. Mattson M. P., Keller J. N. and Begley J. G. (1998) Evidence for synaptic apoptosis. *Expl Neurol.* **153**, 35–48.
27. Xu D., Bureau Y., McIntyre D. C., Nicholson D. W., Liston P., Zhu Y., Fong W. G., Crocker S. J., Korneluk R. G. and Robertson G. S. (1999) Attenuation of ischemia-induced cellular and behavioral deficits by X chromosome-linked inhibitor of apoptosis protein overexpression in the rat hippocampus. *J. Neurosci.* **19**, 5026–5033.
28. Li P., Allen H., Banerjee S., Franklin S., Herzog L., Johnston C., McDowell J., Paskind M., Rodman L. and Salfeld J. (1995) Mice deficient in IL-1 beta-converting enzyme are defective in production of mature IL-1 beta and resistant to endotoxic shock. *Cell* **80**, 401–411.
29. Kuida K., Lippke J. A., Ku G., Harding M. W., Livingston D. J., Su M. S. and Flavell R. A. (1995) Altered cytokine export and apoptosis in mice deficient in interleukin-1 beta converting enzyme. *Science* **267**, 2000–2003.
30. Miura M., Friedlander R. M. and Yuan J. (1995) Tumor necrosis factor-induced apoptosis is mediated by a CrmA-sensitive cell death pathway. *Proc. natn. Acad. Sci. USA* **92**, 8318–8322.
31. Thornberry N. A., Bull H. G., Calaycay J. R., Chapman K. T., Howard A. D., Kostura M. J., Miller D. K., Molineaux S. M., Weidner J. R. and Aunins J. (1992) A novel heterodimeric cysteine protease is required for interleukin-1 beta processing in monocytes. *Nature* **356**, 768–774.
32. Nicholson D. W. (1999) Caspase structure, proteolytic substrates, and function during apoptotic cell death. *Cell Death Differ.* **6**, 1028–1042.
33. Garcia-Calvo M., Peterson E. P., Leiting B., Ruel R., Nicholson D. W. and Thornberry N. A. (1998) Inhibition of human caspases by peptide-based and macromolecular inhibitors. *J. biol. Chem.* **273**, 32608–32613.
34. Mullen R. J., Buck C. R. and Smith A. M. (1992) NeuN, a neuronal specific nuclear protein in vertebrates. *Development* **116**, 201–211.
35. Mao P. L., Jiang Y., Wee B. Y. and Porter A. G. (1998) Activation of caspase-1 in the nucleus requires nuclear translocation of pro-caspase-1 mediated by its prodomain. *J. biol. Chem.* **273**, 23621–23624.
36. Shuman S. L., Bresnahan J. C. and Beattie M. S. (1997) Apoptosis of microglia and oligodendrocytes after spinal cord contusion in rats. *J. Neurosci. Res.* **50**, 798–808.
37. Lee T. T., Green B. A., Dietrich W. D. and Yeziarski R. P. (1999) Neuroprotective effects of basic fibroblast growth factor following spinal cord contusion injury in the rat. *J. Neurotrauma* **16**, 347–356.
38. McTigue D. M., Horner P. J., Stokes B. T. and Gage F. H. (1998) Neurotrophin-3 and brain-derived neurotrophic factor induce oligodendrocyte proliferation and myelination of regenerating axons in the contused adult rat spinal cord. *J. Neurosci.* **18**, 5354–5365.
39. Abe Y., Yamamoto T., Sugiyama Y., Watanabe T., Saito N., Kayama H. and Kumagai T. (1999) Apoptotic cells associated with Wallerian degeneration after experimental spinal cord injury: a possible mechanism of oligodendroglial death. *J. Neurotrauma* **16**, 945–952.
40. Friedlander R. M., Gagliardini V., Rotello R. J. and Yuan J. (1996) Functional role of interleukin 1 beta (IL-1 beta) in IL-1 beta-converting enzyme-mediated apoptosis. *J. exp. Med.* **184**, 717–724.
41. Prehn J. H., Jordan J., Ghadge G. D., Preis E., Galindo M. F., Roos R. P., Kriegstein J. and Miller R. J. (1997) Ca²⁺ and reactive oxygen species in staurosporine-induced neuronal apoptosis. *J. Neurochem.* **68**, 1679–1685.
42. Troy C. M., Stefanis L., Prochiantz A., Greene L. A. and Shelanski M. L. (1996) The contrasting roles of ICE family proteases and interleukin-1beta in apoptosis induced by trophic factor withdrawal and by copper/zinc superoxide dismutase down-regulation. *Proc. natn. Acad. Sci. USA* **93**, 5635–5640.
43. Diaz-Ruiz A., Rios C., Duarte I., Correa D., Guizar-Sahagun G., Grijalva I. and Ibarra A. (1999) Cyclosporin-A inhibits lipid peroxidation after spinal cord injury in rats. *Neurosci. Lett.* **266**, 61–64.
44. Endres M., Namura S., Shimizu-Sasamata M., Waeber C., Zhang L., Gomez-Isla T., Hyman B. T. and Moskowitz M. A. (1998) Attenuation of delayed neuronal death after mild focal ischemia in mice by inhibition of the caspase family. *J. cerebr. Blood Flow Metab.* **18**, 238–247.
45. Dinarello C. A. (1998) Interleukin-1 beta, interleukin-18, and the interleukin-1 beta converting enzyme. *Ann. N. Y. Acad. Sci.* **856**, 1–11.
46. Bracken M. B., Shepard M. J., Holford T. R., Leo-Summers L., Aldrich E. F., Fazl M., Fehlings M., Herr D. L., Hitchon P. W., Marshall L. F., Nockels R. P., Pascale V., Perot P. L. Jr., Piepmeyer J., Sonntag V. K., Wagner F., Wilberger J. E., Winn H. R. and Young W. (1997) Administration of methylprednisolone for 24 or 48 hours or tirilazad mesylate for 48 hours in the treatment of acute spinal cord injury. Results of the Third National Acute Spinal Cord Injury Randomized Controlled Trial. National Acute Spinal Cord Injury Study. *J. Am. med. Ass.* **277**, 1597–1604.
47. Wamil A. W., Wamil B. D. and Hellerqvist C. G. (1998) CM101-mediated recovery of walking ability in adult mice paralyzed by spinal cord injury. *Proc. natn. Acad. Sci. USA* **95**, 13188–13193.
48. Chen H. S. and Lipton S. A. (1997) Mechanism of memantine block of NMDA-activated channels in rat retinal ganglion cells: uncompetitive antagonism. *J. Physiol., Lond.* **499**, 27–46.
49. Chen H. S., Pellegrini J. W., Aggarwal S. K., Lei S. Z., Warach S., Jensen F. E. and Lipton S. A. (1992) Open-channel block of N-methyl-D-aspartate (NMDA) responses by memantine: therapeutic advantage against NMDA receptor-mediated neurotoxicity. *J. Neurosci.* **12**, 4427–4436.
50. Goldberg Y. P., Nicholson D. W., Rasper D. M., Kalchman M. A., Koide H. B., Graham R. K., Bromm M., Kazemi-Esfarjani P., Thornberry N. A., Vaillancourt J. P. and Hayden M. R. (1996) Cleavage of huntingtin by apopain, a proapoptotic cysteine protease, is modulated by the polyglutamine tract. *Nat. Genet.* **13**, 442–449.
51. Gervais F. G., Xu D., Robertson G. S., Vaillancourt J. P., Zhu Y., Huang J., LeBlanc A., Smith D., Rigby M., Shearman M. S., Clarke E. E., Zheng H., Van Der Ploeg L. H., Ruffolo S. C., Thornberry N. A., Xanthoudakis S., Zamboni R. J., Roy S. and Nicholson D. W. (1999) Involvement of caspases in proteolytic cleavage of Alzheimer's amyloid-beta precursor protein and amyloidogenic A beta peptide formation. *Cell* **97**, 395–406.

Apoptosis after traumatic human spinal cord injury

EVELYNE EMERY, M.D., PHILIPP ALDANA, M.D., MARY BARTLETT BUNGE, PH.D.,
WILLIAM PUCKETT, ANU SRINIVASAN, PH.D., ROBERT W. KEANE, PH.D.,
JOHN BETHEA, PH.D., AND ALLAN D. O. LEVI, M.D., PH.D., F.R.C.S.(C)

Department of Neurological Surgery and the Miami Project to Cure Paralysis, and Department of Physiology and Biophysics, University of Miami School of Medicine, Miami, Florida; and IDUN Pharmaceuticals, Inc., La Jolla, California

Object. Apoptosis is a form of programmed cell death seen in a variety of developmental and disease states, including traumatic injuries. The main objective of this study was to determine whether apoptosis is observed after human spinal cord injury (SCI). The spatial and temporal expression of apoptotic cells as well as the nature of the cells involved in programmed cell death were also investigated.

Methods. The authors examined the spinal cords of 15 patients who died between 3 hours and 2 months after a traumatic SCI. Apoptotic cells were found at the edges of the lesion epicenter and in the adjacent white matter, particularly in the ascending tracts, by using histological (cresyl violet, hematoxylin and eosin) and nuclear staining (Hoechst 33342). The presence of apoptotic cells was supported by staining with the terminal deoxynucleotidyl transferase-mediated deoxyuridinetriphosphate nick-end labeling technique and confirmed by immunostaining for the processed form of caspase-3 (CPP-32), a member of the interleukin-1 β -converting enzyme/*Caenorhabditis elegans* D 3 (ICE/CED-3) family of proteases that plays an essential role in programmed cell death. Apoptosis in this series of human SCIs was a prominent pathological finding in 14 of the 15 spinal cords examined when compared with five uninjured control spinal cords. To determine the type of cells undergoing apoptosis, the authors immunostained specimens with a variety of antibodies, including glial fibrillary acidic protein, 2',3'-cyclic nucleotide 3'-phosphohydrolase (CNPase), and CD45/68. Oligodendrocytes stained with CNPase and a number of apoptotic nuclei colocalized with positive staining for this antibody.

Conclusions. These results support the hypothesis that apoptosis occurs in human SCIs and is accompanied by the activation of caspase-3 of the cysteine protease family. This mechanism of cell death contributes to the secondary injury processes seen after human SCI and may have important clinical implications for the further development of protease inhibitors to prevent programmed cell death.

KEY WORDS • apoptosis • human spinal cord injury • caspase-3

APOPTOSIS is an important biological process in eukaryotes in which individual cells die by activating an intrinsic suicide mechanism. Apoptosis is distinguished from necrotic cell death by morphological and biochemical criteria. Apoptosis is an active process of cell destruction characterized by cell shrinkage, chromatin aggregation with genomic fragmentation, and nuclear pyknosis.^{27,31} In contrast, necrosis is characterized by passive cell swelling, intense mitochondrial damage with rapid energy loss, and disruption of internal homeostasis. Necrosis leads to membrane lysis and release of intracellular constituents that evoke an inflammatory reaction.^{10,37,43}

Apoptosis has long been known to occur as a form of neuronal cell death during embryonic development^{22,25} and has been observed more recently following damage to the nervous system caused by ischemia, neurodegenera-

tive conditions, inflammatory diseases, and traumatic injuries.^{3,6,22,24,41,44,46,50,54} Caspases are a family of cysteine proteases that play an important role in the effector phase of apoptosis. Caspase-3, in particular, has been shown to be important in neural development and injury. Germline deletions of this protease led to severe neurological defects in mice.³⁴ The contribution of caspase-3 activity and apoptosis to neuronal cell death after traumatic brain injury⁵⁴ and experimental transient ischemia^{24,41} has been reported. In both injury paradigms, the use of caspase inhibitors not only reduced the extent of apoptosis, but also resulted in functional behavioral improvement in the animals.

The presence of apoptosis in spinal cord injury (SCI) following a contusion has been reported recently in rats and monkeys.^{11,32,35,36} In these studies, it was shown that

TABLE 1
Summary of the clinical data of the 15 patients with SCI*

| Case No. | Survival Time | Age (yrs), Sex | Injury Level | Cause of Injury | Neurological Status | Classification of Injury | Histopathological Findings at Lesion Epicenter | Presence & Location of Wallerian Degeneration |
|----------|---------------|----------------|--------------|-----------------|---------------------|--------------------------|---|---|
| 1 | 3 hrs | 72, M | T-6 | fall | complete | massive compression | maceration & hemorrhagic components | no wallerian degeneration |
| 2 | 3 days | 67, M | C-6 | fall | incomplete | solid cord | minor increase in interstitial spaces | subtle, above |
| 3 | 6 days | 74, M | C6-7 | MVA | complete | massive compression | all neural tissue damaged at epicenter | mild, above |
| 4† | 8 days | 20, F | C7-8 | GSW | complete | laceration | subtotal destruction of neural tissue at epicenter | moderate, above & below |
| 5† | 10 days | 22, M | C-7 | diving | incomplete | contusion | macerated tissue & phagocytic response at epicenter | mild, asymmetric; above & below |
| 6 | 12 days | 59, M | C-6 | MVA | complete | contusion | major loss of neural tissue at epicenter | severe, above & below |
| 7 | 12 days | 16, F | T-11 | GSW | complete | laceration | all neural tissue damaged at epicenter | very subtle, above & below |
| 8 | 12 days | 19, M | L-1 | GSW | complete | contusion | macerated tissue at epicenter; vascular infarction proximal to epicenter | severe, up to C-3 & below |
| 9 | 15 days | 38, M | T-5 | GSW | complete | laceration | spinal cord transected at T-5; necrotic tissue at T-4 w/ invasion of macrophages | moderate, above & below |
| 10 | 16 days | 43, M | C5-6 | fall | complete | contusion | large blood-filled cavities w/ macrophage invasion at epicenter; preserved axon/myelin units in extreme periphery of most of cord | mild |
| 11 | 16 days | 80, M | C-6 | fall | complete | contusion | large destruction of cord tissue w/ macrophages & hemorrhage | mild, more present above than below |
| 12 | 17 days | 70, M | C-8 | MVA | complete | contusion | loss of neural tissue at epicenter | moderate, above & below |
| 13 | 17 days | 17, F | C6-7 | MVA | complete | contusion | macerated tissue in ventral & central portions of cord at epicenter | moderate, more present above than below |
| 14 | 45 days | 67, M | C5-7 | fall | complete | contusion | large destruction of cord tissue at epicenter | moderate, above & below |
| 15 | 60 days | 68, F | T-5 | fall | incomplete | contusion | loss of motor neurons at epicenter & diffuse axonal injury throughout dorsal columns & lateral & ventral corticospinal tracts | severe in dorsal columns |

* GSW = gunshot wound; MVA = motor vehicle accident.

† Received methylprednisolone according to the Second National Acute Spinal Cord Injury Study protocol.

apoptosis contributed to the tissue damage seen after SCI. Apoptotic cell death was observed in both neurons and oligodendrocytes^{11,36} and was prominent in the white matter, in which wallerian degeneration was simultaneously observed. A time course analysis in rats³⁶ revealed that apoptosis occurred as early as 4 hours postinjury and could be seen in decreasing amounts as late as 3 weeks after SCI.

We initiated this study to determine whether apoptosis is an important factor after human SCI by examining the spinal cords of patients who died between 3 hours and 2 months postinjury. Apoptosis in these 15 patients was assessed using multiple criteria, including nuclear morphology, chromatin staining techniques, and immunostaining for a processed form of caspase-3. We also determined the spatial and temporal expression of apoptotic cells and the nature of the cells involved in programmed cell death.

Clinical Material and Methods

Patient Population

This study was based on postmortem examination of spinal cord tissue from five control patients without SCI and 15 patients who died at different time points after an SCI. Fifteen specimens were obtained from the Miami Project's Human Spinal Cord Injury Bank, which contains more than 100 injured human spinal cords. The cases were

selected based on the short interval between SCI and death (0–2 months) and the availability of tissue above and below the lesion site.

Preparation of Specimens

The spinal cords had been removed at autopsy, usually within 16 hours after death. They were then fixed in 10% neutral buffered formalin for a minimum of 15 days, after which they were stored in 0.1 M phosphate buffer at 4°C. Selected tissue blocks were taken at the epicenter and at three consecutive root levels above and below the injury. Samples from each of these regions were dehydrated, embedded in paraffin, and cut in 7- μ m-thick cross-sections.

Sections were stained with hematoxylin and eosin and cresyl violet (15 samples), terminal deoxynucleotidyl transferase (TdT)-mediated deoxyuridinetriphosphate nick-end labeling ([TUNEL], five samples), or Hoechst 33342 (four samples), and immunostained with CM 1, an antibody that preferentially recognizes the processed form of caspase-3 (10 samples). Sections from control spinal cords (five samples) were stained with cresyl violet and immunostained with the CM 1 antibody. Wallerian degeneration in white matter tracts was assessed using a silver stain for axons (Sevier–Munger) and a myelin stain (solochrome–cyanine) on adjacent sections. Regions undergoing wallerian degeneration contained swollen, fragmented, or absent axons in the same areas in which myelin

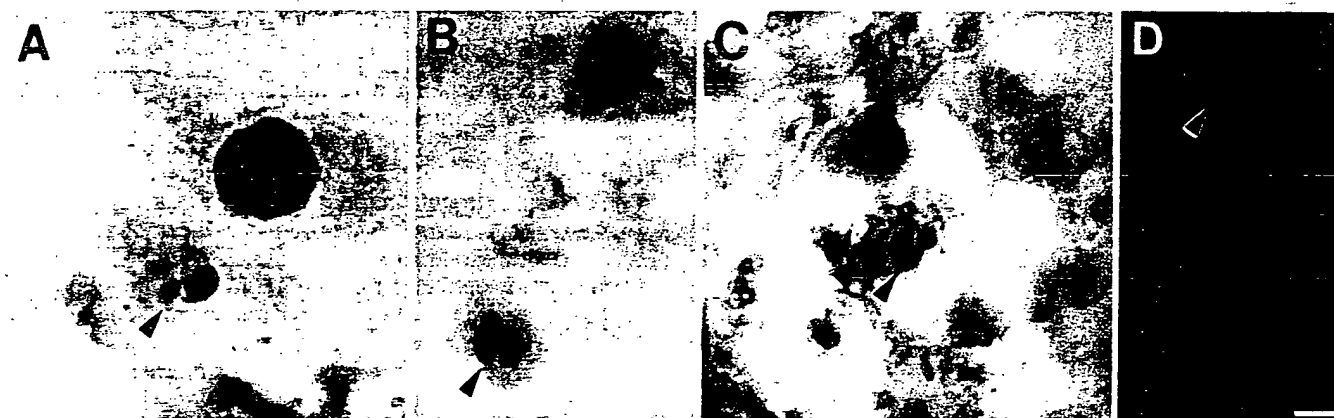


FIG. 1. Photomicrographs showing apoptotic nuclei (arrowheads) within the traumatized human spinal cord stained with cresyl violet (A and B), H & E (C), and Hoechst 33342 (D). Apoptotic nuclei appear as condensed, clumped fragments. Bar = 20 μ m.

was distorted or collapsed. Wallerian degeneration was quantified in the white matter above and below the lesion according to four levels of severity: subtle, mild, moderate, and severe.

Staining With the TUNEL Technique

To determine whether DNA fragmentation characteristic of apoptosis occurs, we stained spinal cord tissue by using the in situ TUNEL technique.¹⁹ Spinal cord sections were deparaffinized in xylene for 5 minutes and then rehydrated sequentially in 100%, 95%, 75%, and 50% ethanol. The sections were incubated with 50 μ g/ml proteinase K for 5 minutes to strip off nuclear proteins. The TUNEL staining was completed using the apoptosis in situ kit according to the manufacturer's instructions.

Briefly, sections were immersed in equilibration buffer for 10 minutes and then incubated with TdT and deoxyuridinetriphosphate-fluorescein isothiocyanate in a humidified chamber at 37°C for 1 hour. The sections were

washed with 0.1 M phosphate-buffered saline (PBS) at pH 7.4 and counterstained with propidium iodide (a nuclear stain) for 10 minutes. As a positive control we pretreated slides with DNAase to produce TUNEL-positive staining of all nuclei, and the negative controls were incubated without TdT enzyme. Sections were examined and photographed using fluorescence microscopy.

Hoechst 33342 Staining

Spinal cord sections were deparaffinized with xylene for 5 minutes, rehydrated, and rinsed with 0.1 M PBS. The sections were stained with one drop of glycerol/PBS solution containing 5 μ l Hoechst 33342 dye (5.6 mg in 10 ml PBS).

Immunostaining for Processed Form of Caspase-3 With the CM 1 Antibody

Spinal cord sections were deparaffinized as described earlier, rinsed in 0.01 M PBS, and treated for 30 minutes

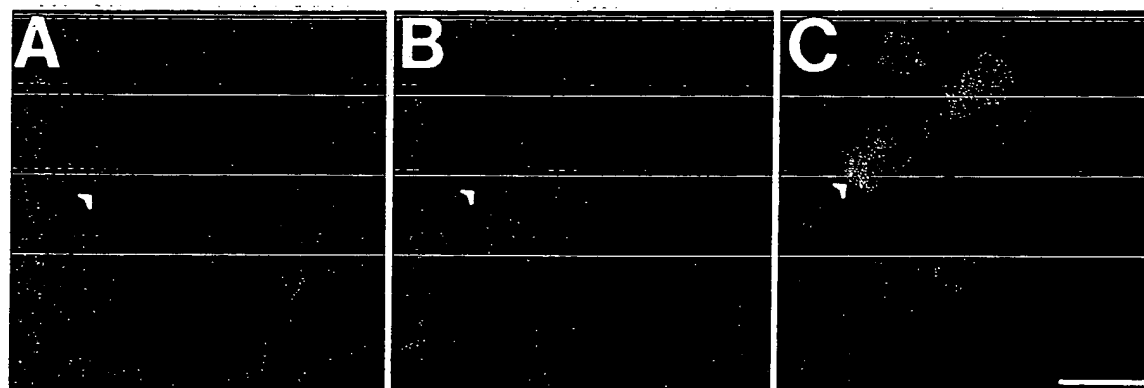


FIG. 2. Photomicrographs showing TUNEL-labeled cells in the spinal cord at the epicenter level. Cross-sections of the spinal cord demonstrate a single TUNEL-positive labeled nucleus that appears small and fragmented (A and B, arrowhead), among numerous normal nuclei counterstained by propidium iodide nuclear dye (B). On double exposure (C), the apoptotic cell is yellow (arrowhead), whereas the normal nuclei remain red. Bar = 50 μ m.

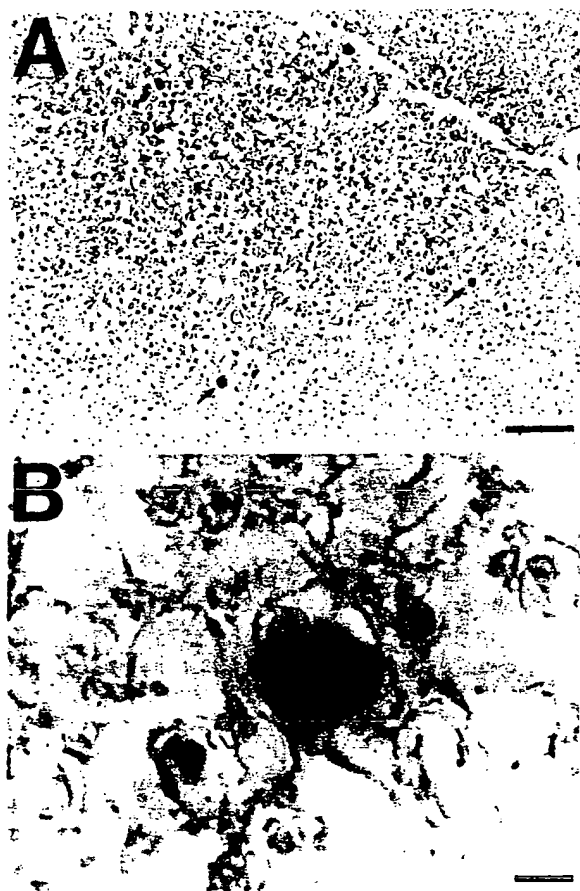


FIG. 3. Photomicrographs showing CM 1 immunostaining of the dorsal columns at low (A) and high magnification (B) demonstrating a number of dark and shrunken cells (arrows) containing condensed and clumped chromatin. The staining for processed CPP-32 is evident within the nucleus (B). Bar = 200 μ m (A), 10 μ m (B).

with 3% H_2O_2 in 10% methanol. The sections were blocked for 1 hour in 5% normal goat serum with 0.1 M PBS and 0.1% Triton X-100. The primary antibody CM 1 (0.012 μ g/ml) was applied and the preparations were left overnight. The following morning, the sections were fixed for 10 minutes in 0.01 M PBS containing 0.1% glutaraldehyde. The sections were incubated for 1 hour with a biotinylated secondary antibody, followed by a 1-hour incubation with an avidin-biotin complex (ABC) reagent. Sections were then incubated for 10 minutes in 0.5% biotinylated tyramine 1% H_2O_2 solution in 0.01 M PBS. They were reincubated in the ABC reagent for 30 minutes. The stain was developed in diaminobenzidine and H_2O_2 , and enhanced by nickel chloride in PBS. The sections were rinsed, dehydrated, mounted on a coverslip, and examined under the light microscope. Sections from uninjured control cases were processed using the same protocol.

Immunostaining for Glial Fibrillary Acidic Protein, CNPase, CD45, and CD68

Immunohistochemical techniques were used to detect the following antigens: glial fibrillary acidic protein (GFAP), 2', 3'-cyclic nucleotide 3'-phosphohydrolase (CNPase), and CD45/CD68. Glial fibrillary acidic protein GFAP is an astrocyte marker; CNPase is a myelin protein in the central nervous system and has been shown to be specific for oligodendrocytes;⁴⁵ and CD45 and CD68 were used to study activated microglia and macrophages.

Tissue sections were deparaffinized and endogenous peroxidase activity was blocked with 0.3% H_2O_2 in 100% methanol. Sections were incubated with either 0.3% Triton X-100 in 0.1 M PBS (GFAP) or with Tris (pH 7.6) containing 10% normal goat serum. The sections were incubated overnight at room temperature with the following monoclonal antibodies: GFAP 1:200, CD45 1:100, CD68 1:100, and CNPase 1:800. This was followed by sequential incubation with biotinylated secondary antibody, ABC with horseradish peroxidase, 3,3'-diaminobenzidine, and H_2O_2 . The slides were then counterstained with 2% cresyl violet, dehydrated, and mounted. Omission of the primary antibody served as a negative control.

Sources of Supplies and Equipment

The proteinase K and Hoechst 33342 dye were purchased from Sigma Chemical Co., St. Louis, MO. The apoptosis in situ kit was acquired from Chemicon International, Inc., Temecula, CA. The Axiophot fluorescent microscope was obtained from Zeiss, Inc., Oberkochen, Germany. The primary antibody CM 1 was a generous gift from IDUN Pharmaceuticals, Inc., La Jolla, CA. The biotinylated secondary antibody and ABC reagent (Vectastain) were acquired from Vector Laboratories, Burlingame, CA. The monoclonal antibodies GFAP, CD45, and CD68 were purchased from Dako Corp., Carpinteria, CA, and the CNPase from Sternberger Monoclonals, Inc., Baltimore, MD.

Results

Clinical Data

The mean age of the 15 patients with SCIs (Table 1) was 49 years (range 16–80 years) and the mean age of the five control patients was 55 years (range 33–77 years). The principal causes of death in the patients with SCIs were pulmonary embolism (six patients), pneumonia (six patients), hemothorax with cardiac arrest in one, and an unknown cause in two patients. The causes of death for the control patients were cardiovascular disease in two and a motor vehicle accident (without head injury or SCI) in three. Only two patients with SCI (Cases 4 and 5) received methylprednisolone according to the Second National Acute Spinal Cord Injury Study protocol.⁸

Ten patients suffered a cervical and four a thoracic SCI, and one case consisted of a conus medullaris injury. Twelve patients presented with a complete motor and sensory loss below the level of their injury, whereas three experienced incomplete loss. The cause of injury was variable and included falls (six patients), motor vehicle

TABLE 2
Distribution and quantification of apoptotic cells per section†

| Case No. | Injury Level | Apoptotic Cells | Epicenter Level | 1-3 Levels Above Epicenter | 1-3 Levels Below Epicenter |
|----------|--------------|-----------------|--------------------|--|--|
| 1 | T-6 | yes | no viable tissue | normal tissue* T-5: no apoptotic cells above T-5 | normal tissue; no apoptotic cells |
| 2 | C-6 | yes | edges of lesion* | dorsal columns* | ventral CST, lat CST*; no apoptotic cells below C-8 |
| 3 | C6-7 | yes | no viable tissue | dorsal columns** | at edges of central cavity* |
| 4 | C7-8 | yes | edges of lesion** | dorsal columns (fx gracilis)* | ventral CST (T-1)*; no apoptotic cells below T-2 |
| 5 | C-7 | yes | edges of cavity* | no apoptotic cells from C5-7 | dispersed at C-8*; no apoptotic cells at T-1 & below |
| 6 | C-6 | yes | edges of lesion* | dorsal columns, spinocerebellar tracts** | ventral CST* |
| 7 | T-11 | yes | edges of lesion* | dorsal columns* | dispersed T12-L1*; no apoptotic cells below L-2 |
| 8 | L-1 | yes | no viable tissue | dorsal columns (T-11) & a few cells in CST & spinocerebellar tracts*** | ventral CST L3-5** |
| 9 | T-5 | yes | no viable tissue | spinothalamic tract (T-3)* | no apoptotic cells T4-8 |
| 10 | C5-6 | no | — | — | — |
| 11 | C-6 | yes | edges of lesion** | dorsal columns (fx gracilis); spinothalamic tracts* | ventral CST** |
| 12 | C-8 | yes | edges of lesion** | dorsal columns & spinocerebellar tracts** | no apoptotic cells at T-1 & below |
| 13 | C6-7 | yes | edges of lesion*** | dorsal columns & spinothalamic tracts** | ventral CST & lat CST** |
| 14 | C5-7 | yes | edges of lesion* | dorsal columns* | ventral CST & lat CST* |
| 15 | T-5 | yes | edges of lesion* | dorsal columns*; no apoptotic cells above T-3 | ventral CST* |

† Asterisks represent the stratification of cell counts per section: * = 1-15; ** = 15-30; *** = 30-45. Abbreviations: CST = corticospinal tract; fx = funiculus; — = not applicable.

accidents (four patients), gunshot wounds (four patients), and a diving accident (one patient).

Histological Data

We analyzed cross-sections of the lesion epicenter and rostral and caudal levels in tissue obtained in 15 patients who died between 3 hours and 60 days after their SCI. According to the classification established by Bunge, et al.,⁹ nine patients presented with a contusion/cavity lesion, two with a massive compression, three with a laceration lesion, and one with a solid spinal cord syndrome.

All patients except the one in Case 2 showed significant destruction of the spinal cord parenchyma at the epicenter of the injury. Signs of wallerian degeneration in the white matter occurred as early as Day 3 postinjury and thereafter spread rostral and caudal to the lesion, with more advanced degeneration of the ascending tracts. In one patient (Case 8), the contusion was associated with a vascular infarction proximal to the epicenter and a pattern of obvious wallerian degeneration.

Morphological Appearance of Apoptotic Cells

Apoptotic nuclei were found in 14 of the 15 cases on hematoxylin and eosin- and cresyl violet-stained sections (Fig. 1A-C). Cells containing apoptotic nuclei exhibited evidence of cytoplasmic shrinkage. The nuclei themselves demonstrated chromatin condensation or aggregation into small and dark nuclear fragments. Staining with Hoechst 33342 revealed typically small and bright fragmented nuclei (Fig. 1D). No apoptotic bodies were detected on cresyl violet-stained sections from the five uninjured control patients.

The in situ TUNEL technique (Fig. 2A) combined with propidium iodide (Fig. 2B) also demonstrated apoptotic

TUNEL-positive nuclei as double-stained (yellow), fragmented nuclei (Fig. 2C) among numerous propidium iodide-positive cells. The location and quantity of apoptotic nuclei observed using this technique correlated with the number of apoptotic nuclei observed with hematoxylin and eosin- and cresyl violet-stained sections (paired t-test, $p = 0.16$; correlation coefficient 0.83).

The presence of apoptotic cells was also demonstrated in sections immunostained with the CM 1 antibody. Most positive nuclei were dark and shrunken and contained condensed, clumped chromatin (Fig. 3A and B). Relatively more apoptotic cells were detected after CM 1 antibody staining compared with cresyl violet staining. As cresyl violet staining was used to detect apoptotic bodies and caspase-3-positive cells did not necessarily contain these bodies, the implication is that immunostaining for caspase-3 activation detects apoptosis at an earlier stage. Staining with caspase-3 was also negative in Case 10, in which no apoptotic cells were shown in cresyl violet-stained sections. Staining with caspase-3 showed one to two positive cells per section in tissue obtained in one control patient (73 years old, died of cardiovascular disease), whereas tissue from the four other uninjured control patients was negative. Other potential explanations for the few apoptotic cells seen in tissue obtained in the one control case are the patient's advanced age and associated vascular disease.

Temporal and Spatial Distribution of Apoptotic Cells

Apoptotic cells were seen between 3 hours and 2 months postinjury. Although too few cases were analyzed to allow a correlation between the time after SCI and the number of apoptotic cells, most of these cells were seen in tissue obtained in patients who died between 3 days and 3

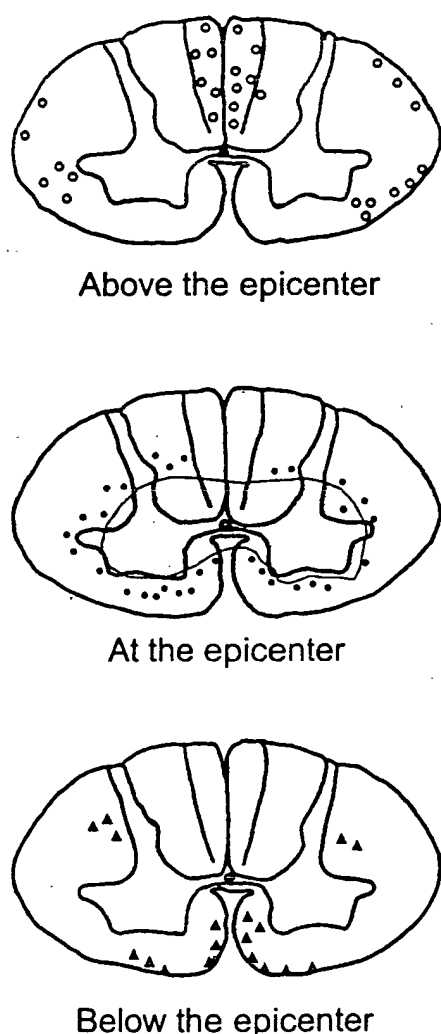


FIG. 4. Schematic diagram demonstrating the spatial distribution of apoptotic cells in the spinal cord of the patient in Case 13, who died 17 days postinjury. The apoptotic bodies were identified on cresyl violet-stained sections and are represented as either filled circles at the epicenter level, empty circles above, or filled triangles below the lesion.

weeks after the SCI. Incomplete neurological injury was associated with fewer apoptotic bodies (Cases 2, 5, and 15). When ischemia was associated with the primary injury, as in Case 8, a large number of apoptotic nuclei were observed throughout the levels studied.

Most apoptotic cells were randomly distributed in the rim of surviving tissue around the epicenter of the SCI and within the adjacent white matter (Table 2), and none was identified in the gray matter. Apoptotic cells were seen in areas of wallerian degeneration in the white matter above and below the epicenter. Rostral to the lesion epicenter, apoptosis was associated with axonal degeneration in ascending tracts, especially the funiculus gracilis, the spinoreticular, the spinothalamic, and the spinocerebellar tracts. Degeneration and apoptosis were absent in the regions containing descending motor pathways. Apoptosis was associated with the degenerating axons in the de-

scending tracts caudal to the lesion, especially the ventral corticospinal, reticulospinal, and vestibulospinal tracts; it was less prevalent in the lateral corticospinal or rubrospinal, and no apoptotic cells were seen in the caudal ascending tracts. Apoptotic cells were seen in much larger numbers in ascending than in descending tracts, and wallerian degeneration was present earlier in the ascending tracts than in the descending tracts. There appeared to be a good correlation between apoptosis and wallerian degeneration. A schematic diagram (Fig. 4) demonstrates the spatial distribution of apoptotic cells at the SCI epicenter as well as above and below the lesion in the spinal cord of the patient in Case 13, who died 17 days postinjury.

Apoptotic Cell Type

To identify the type of cells undergoing apoptosis, different antibodies directed against astrocytes (GFAP), oligodendrocytes (CNPase), and macrophages or activated microglia markers (CD45, CD68) were assayed. Apoptotic bodies were not seen in astrocytes (data not shown). Immunostaining with CNPase demonstrated that apoptotic cells (identified using cresyl violet counterstain) were present within oligodendrocytes adjacent to myelin sheaths in degenerating white matter tracts (Fig. 5). Macrophages or activated microglia were seen engulfing fragments of apoptotic cells. Apoptotic bodies in proximity to cells unstained with microglia markers were also observed (Fig. 6).

Discussion

Apoptosis is a form of physiological cell death, also defined as programmed cell death, in which cells die and are engulfed by phagocytes without discharging cytosolic contents into the extracellular space and without initiating an inflammatory reaction.¹⁰ The cell surface membrane begins to form blebs and express prophagocytic signals, the cell shrinks and severs contact with its neighbors, chromatin becomes condensed and cleared, and eventually the whole cell fragments into membrane-bound vesicles that are rapidly ingested by neighboring cells. The apoptotic process can be rapid when compared with necrotic cell death, and the debris is removed with similar swiftness.^{27,37} Because the process is rapid, quantification of the number of apoptotic cells on any given cross-section underestimates the extent to which apoptosis contributes to the death of cells at the injury site.⁵²

The genetic control and the biochemical markers of apoptotic cell death were initially elucidated in the roundworm *Caenorhabditis elegans*, and *CED 3* was identified as a gene encoding a protein involved in programmed cell death in this maturing roundworm.²⁹ The mammalian homologs of cell death mechanisms consist of the CED 3/ICE (interleukin-1 β -converting enzyme) family of cysteine proteases (caspases),^{17,38,40} in which the prototype is the ICE. The mammalian caspase family is composed of at least 10 known members.² One of these is caspase-3 (Yama, apopain), which has been definitively implicated in apoptosis.^{16,26} The essential role of caspases in vertebrate apoptosis is consistent with their activity as the principal effectors of apoptosis through their proteolytic

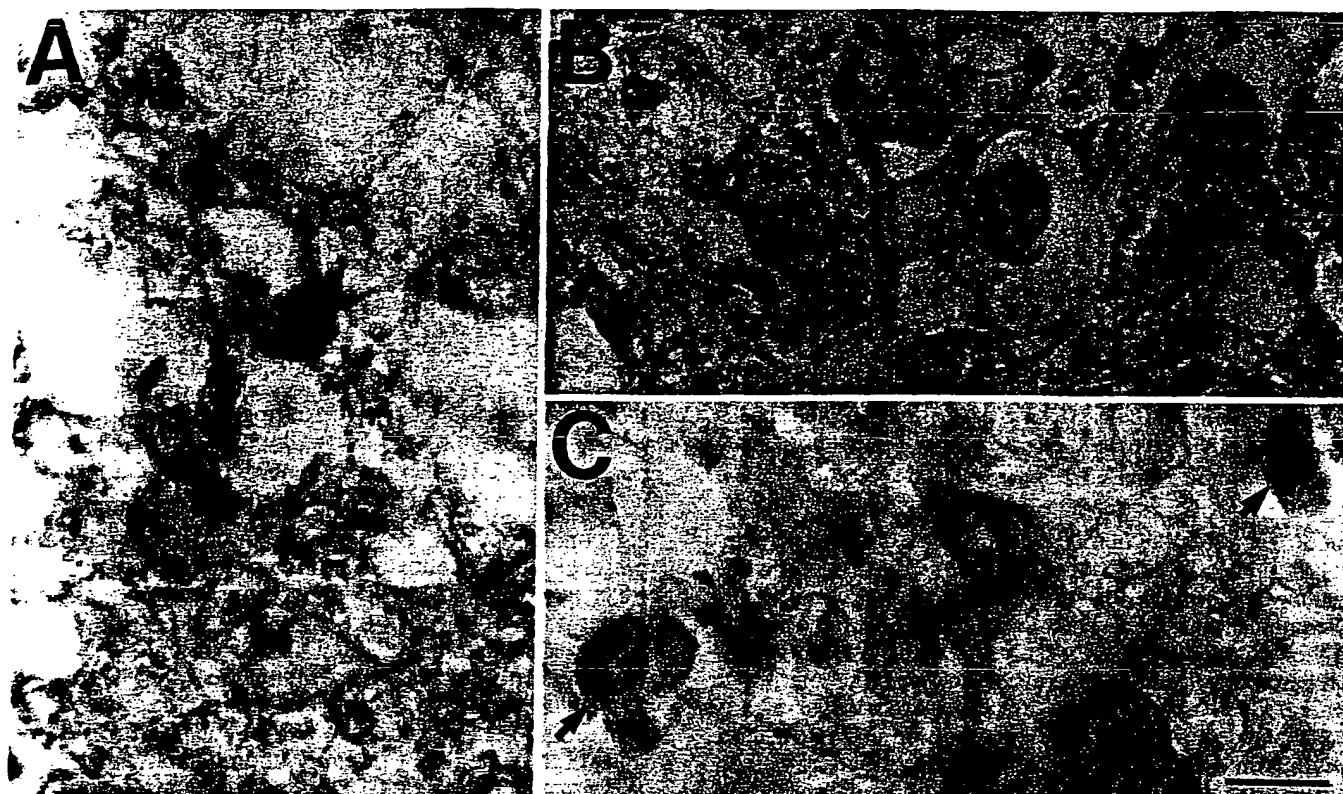


FIG. 5. Photomicrographs showing oligodendrocytes immunostained with CNPase and nuclei counterstained with cresyl violet. Normal oligodendrocytes are seen (A), as well as multiple apoptotic oligodendrocytes (arrows) (B and C). Bar = 50 μ m.

action on specific targets. One of the final effectors of cell death is activation of endonucleases that induce fragmentation of nuclear DNA into 185-bp fragments.³⁰ In a number of reports caspases have been implicated as important during apoptosis of neurons and astrocytes, and it has been suggested that caspase-3 was the principal effector in the apoptotic pathway.^{4,33} Moreover, caspase-3 activation was never observed in necrotic cell death.^{4,26} Hisahara, et al.,²⁶ demonstrated that caspase-1 (ICE) and caspase-3 (CPP-32) were expressed in oligodendrocytes and that their inhibition prevented apoptotic cell death.

Secondary injury processes are believed to be an important, remediable component of SCI.^{8,49} Many of the basic research advances that have reached the clinical arena focus on the prevention of these secondary injury mechanisms.^{21,55} Apoptotic cell death has been recognized for many years; however, this process has now gained increasing attention in the basic science literature as a mechanism by which cells die in a number of neurological diseases.⁴⁷ Apoptotic cell death appears to be yet another mechanism in which cells may die in a delayed fashion after injury, that is, a secondary injury mechanism.

There is evidence that apoptotic cell death contributes to tissue damage, and prevention of this process results in neurological recovery after SCI³⁶ and brain injury in rats.⁵⁴ Data presented here indicate for the first time that apoptosis is associated with the tissue damage observed after human SCI. Our determination of apoptosis relied on mul-

tiiple criteria: morphological staining (cresyl violet, hematoxylin and eosin), nuclear chromatin staining with Hoechst 33342 dye, and the TUNEL test, all of which have been widely used for assessment of apoptosis. These results were confirmed using immunostaining with the CM 1 antibody that is specific for the processed form of caspase-3 (A Srinivasan, et al., unpublished data). Caspase-3 is required for DNA fragmentation and the morphological changes associated with apoptosis.³⁰

Crowe, et al.,¹² presented the first evidence for the presence of apoptosis in SCIs in the rat. Li, et al.,³⁵ demonstrated that compression trauma to the spinal cord was associated with apoptosis of glial cells preferentially located in degenerating longitudinal tracts of the white matter. The apoptotic cells were most likely oligodendrocytes, a conclusion based on morphological data and negative GFAP staining. Further studies demonstrated the occurrence of apoptosis in SCI in rats and monkeys and showed that oligodendrocytes were the major cell population undergoing apoptosis based on immunohistochemical analysis.^{11,35} Apoptosis of oligodendrocytes was seen in areas of wallerian degeneration and was detected from 24 hours to 3 weeks postinjury.^{11,12} Liu, et al.,³⁶ also observed a burst of neuronal and glial apoptosis in gray and white matter at the lesion site within the first 24 hours postinjury and a delayed wave of oligodendrocyte apoptosis in distant white matter several days later.

In our study, the lesion epicenter demonstrated the pres-



FIG. 6. Photomicrographs showing activated microglia immunostained with CD68 before the section was counterstained with cresyl violet to demonstrate apoptotic bodies. Cells that did not stain with the activated microglia marker (A, arrow) as well as CD68-positive cells ingesting apoptotic bodies (B, arrow) were observed. Bar = 50 μ m.

ence of multifocal hemorrhages and necrotic tissue involving the central gray matter and the contiguous white matter. Apoptotic cells were identified surrounding the lesion epicenter. As early wallerian degeneration occurred in the white matter tracts, a second phase of apoptotic cells appeared and these were positive for an oligodendrocyte marker (CNPase). Oligodendrocyte apoptosis was clearly associated with wallerian degeneration and was more obvious in ascending than in descending tracts. This corresponds to the pattern of progression of wallerian degeneration in which the ascending tracts show signs of degeneration before the descending tracts.⁹

We found no relationship between the average number of apoptotic bodies and time from injury because the injury mechanism and severity were different in each case. Nonetheless, it seemed that apoptosis was less severe in patients with incomplete neurological injuries. Liu, et al.,³⁶ demonstrated that after rat SCI, apoptotic glial cells were more abundant above than below the site of compression and that apoptotic cells were more numerous after moderate and severe injury compared with mild compression. We found no evidence of apoptosis within the spinal cord neurons. This indicates that any neuronal loss was the result of necrosis rather than apoptosis or that it occurred at an early stage before we could detect it. Tissue in only one of our cases was examined within 24 hours of death. Li, et al.,³⁵ demonstrated that neuronal apoptosis was complete within the first 24 hours, whereas Liu and colleagues³⁶ saw no evidence of apoptosis in the spinal cord neurons at 4 hours or 1, 4, and 9 days after compression trauma. We suspect that activated microglia (macrophages) clear apoptotic bodies, as has been observed by others,^{13,14,48,51} but may also be partly responsible for the induction of apoptosis by secreting cytotoxic substances such as cytokines (tumor necrosis factor- α) and nitric oxide.⁵³ Other investigators have also demonstrated that microglia can undergo apoptosis following damage to the nervous system.^{20,42}

The mechanisms responsible for oligodendrocyte apoptosis remain unclear. It may occur as a result of loss of axonally derived survival signals (wallerian degeneration)⁵ and/or as a result of evolving adverse changes in the cellular milieu¹³ resulting in axonal demyelination. If these axons are in continuity across the injury site, electri-

cal conduction will be impaired through the axon. The presence of demyelinated axons around the epicenter of SCIs has received attention recently.^{7,8} One therapeutic strategy for SCIs relies on the use of the drug 4-aminopyridine (a potassium channel blocker) to enhance axonal conduction through areas of demyelination.²³ Thus, prevention of axonal demyelination after SCI by the reduction of apoptotic oligodendrocyte cell death may result in an overall reduction of partially injured axons.

The contribution of CPP-32 activity and apoptosis to neuronal cell death after traumatic brain injury⁵⁴ and experimental transient ischemia^{24,41} has been reported. In both injury paradigms, the use of caspase inhibitors not only reduced the extent of apoptosis, but also resulted in functional behavioral improvement in the animals. In that regard, therapeutic interventions aimed at blocking apoptosis may be useful in reducing tissue damage after SCI and ultimately in improving functional outcomes. Liu, et al.,³⁶ reported that intraperitoneal injections of cycloheximide, a protein synthesis inhibitor, improved behavioral outcomes after spinal cord contusion injury in rats. Partial inhibition of protein synthesis can induce the production of *Bcl-2*,²⁸ an antiapoptotic human protooncogene important in cell survival that was shown to be upregulated in injured axons of the white matter following compression injury of the spinal cord.^{18,35} Hisahara, et al.,²⁶ demonstrated that caspases were involved in tumor necrosis factor-mediated cell death of oligodendrocytes and that inhibition of these proteases can prevent apoptosis. Milligan, et al.,³⁹ identified peptide inhibitors of the ICE protease family that arrest programmed cell death of motor neurons *in vivo* and *in vitro*. In that regard, it would be useful to test drugs that inhibit caspases in the treatment of SCI.

Conclusions

This work demonstrates for the first time that apoptotic cell death is observed from 3 hours to 8 weeks after traumatic human SCIs. Apoptosis occurs around the lesion epicenter as well as within areas of wallerian degeneration in both ascending and descending white matter tracts. Oligodendrocytes were definitely implicated as cells undergoing apoptosis on sections of injured spinal cord in which immunohistochemical markers were used. Apop-

Apoptosis in human spinal cord injury

osis after human SCI appears to be dependent on activation of CPP-32. Inhibition of this process may have potential therapeutic benefits for reducing tissue damage and improving the outcome after SCI.

Acknowledgments

We are grateful to Tesha Monteith for her technical assistance and to Dr. Alexander Marcillo for his assistance in preparing the manuscript. We also thank Drs. Jacqueline Bresnahan and Hans Lassmann for their helpful advice.

References

- Adams JC: Biotin amplification of biotin and horseradish peroxidase signals in histochemical stains. *J Histochem Cytochem* 40:1457-1463, 1992
- Alnemri ES, Livingston DJ, Nicholson DW, et al: Human ICE/CED-3 protease nomenclature. *Cell* 87:171, 1996 (Letter)
- Arends MJ, Wyllie AH: Apoptosis: mechanisms and roles in pathology. *Int Rev Exp Pathol* 32:223-254, 1991
- Armstrong RC, Aja TJ, Hoang KD, et al: Activation of the CED3/ICE-related protease CPP32 in cerebellar granule neurons undergoing apoptosis but not necrosis. *J Neurosci* 17:553-562, 1997
- Barres BA, Jacobson MD, Schmid R: Does oligodendrocyte survival depend on axons? *Curr Biol* 3:489-497, 1993
- Bauer J, Wekerle H, Lassmann H: Apoptosis in brain-specific autoimmune disease. *Curr Opin Immunol* 7:839-843, 1995
- Blight AR: Effect of 4-aminopyridine on axonal conduction-block in chronic spinal cord injury. *Brain Res Bull* 22:47-52, 1989
- Bracken MB, Shepard MJ, Collins WF, et al: A randomized, controlled trial of methylprednisolone or naloxone in the treatment of acute spinal-cord injury. Results of the second National Acute Spinal Cord Injury Study. *N Engl J Med* 322:1405-1411, 1990
- Bunge RP, Puckett WR, Becerra JL, et al: Observations on the pathology of human spinal cord injury. A review and classification of 22 new cases with details from a case of chronic cord compression with extensive focal demyelination. *Adv Neurol* 59:75-89, 1993
- Cohen JJ: Apoptosis. *Immunol Today* 14:126-130, 1993
- Crowe MJ, Bresnahan JC, Shuman SL: Apoptosis and delayed degeneration after spinal cord injury in rats and monkeys. *Nature Med* 3:73-76, 1997
- Crowe MJ, Shuman SL, Masters JN, et al: Morphological evidence suggesting apoptotic nuclei in spinal cord injury. *Soc Neurosci Abstr* 21:232, 1995 (Abstract)
- Dusart I, Schwab ME: Secondary cell death and the inflammatory reaction after dorsal hemisection of the rat spinal cord. *Eur J Neurosci* 6:712-724, 1994
- Duvall E, Wyllie AH, Morris RG: Macrophage recognition of cells undergoing programmed cell death (apoptosis). *Immunology* 56:351-358, 1985
- Ellis RE, Yvan J, Horvitz HR: Mechanisms and functions of cell death. *Annu Rev Cell Biol* 7:663-698, 1991
- Enari M, Talanian RV, Wong WW, et al: Sequential activation of ICE-like and CPP32-like proteases during Fas-mediated apoptosis. *Nature* 380:723-726, 1996 (Letter)
- Fraser A, Evan G: A license to kill. *Cell* 85:781-784, 1996
- Furukawa K, Estus S, Fu WM, et al: Neuroprotective action of cycloheximide involves induction of Bcl-2 and antioxidant pathways. *J Cell Biol* 136:1137-1149, 1997
- Gavrieli Y, Sherman Y, Ben-Sasson SA: Identification of programmed cell death *in situ* via specific labeling of nuclear DNA fragmentation. *J Cell Biol* 119:493-501, 1992
- Gehrmann J, Banati RB: Microglial turnover in the injured CNS: activated microglia undergo delayed DNA fragmentation following peripheral nerve injury. *J Neuropathol Exp Neurol* 54:680-688, 1995
- Hall ED, Yonkers PA, Andrus PK, et al: Biochemistry and pharmacology of lipid antioxidants in acute brain and spinal cord injury. *J Neurotrauma* 9 (Suppl):S425-S442, 1992
- Hamburger V: Cell death in the development of the lateral motor column of the chick embryo. *J Comp Neurol* 160:535-546, 1975
- Hansebout RR, Blight AR, Fawcett S, et al: 4-Aminopyridine in chronic spinal cord injury: a controlled, double-blind, crossover study in eight patients. *J Neurotrauma* 10:1-18, 1993
- Hara H, Friedlander RM, Gagliardini V, et al: Inhibition of interleukin 1 β converting enzyme family proteases reduce ischemic and excitotoxic neuronal damage. *Proc Natl Acad Sci USA* 94:2007-2012, 1997
- Henderson CE: Programmed cell death in the developing nervous system. *Neuron* 17:579-585, 1997
- Hisahara S, Shoji S, Okano H, et al: ICE/CED-3 family executes oligodendrocyte apoptosis by tumor necrosis factor. *J Neurochem* 69:10-20, 1997
- Hockenberry D: Defining apoptosis. *Am J Pathol* 146:16-19, 1995
- Hockenberry DM, Oltvai ZN, Yin XM, et al: Bcl-2 functions in an antioxidant pathway to prevent apoptosis. *Cell* 75:241-251, 1993
- Horwitz HR, Ellis HM, Sternberg DW: Programmed cell death in nematode development. *Neurosci Comment* 1:56-65, 1982
- Jänicke RU, Sprengart ML, Wati MR, et al: Caspase-3 is required for DNA fragmentation and morphological changes associated with apoptosis. *J Biol Chem* 273:9357-9360, 1997
- Kane AB: Redefining cell death. *Am J Pathol* 146:1-2, 1995
- Katoh K, Ikata T, Katoh S, et al: Induction and its spread of apoptosis in rat spinal cord after mechanical trauma. *Neurosci Lett* 216:9-12, 1996
- Keane RW, Srinivasan A, Foster LM, et al: Activation of CPP32 during apoptosis of neurons and astrocytes. *J Neurosci Res* 48:168-180, 1997
- Kuida K, Zheng TS, Na S, et al: Decreased apoptosis in the brain and premature lethality in CPP32-deficient mice. *Nature* 384:368-372, 1996
- Li GI, Brodin G, Farooque M, et al: Apoptosis and expression of Bcl-2 after compression trauma to rat spinal cord. *J Neuropathol Exp Neurol* 55:280-289, 1996
- Liu XZ, Xu XM, Hu R, et al: Neuronal and glial apoptosis after traumatic spinal cord injury. *J Neurosci* 17:5395-5406, 1997
- Majno G, Joris I: Apoptosis, oncosis, and necrosis. An overview of cell death. *Am J Pathol* 146:3-15, 1995
- Martin SJ, Green DR: Protease activation during apoptosis: death by a thousand cuts. *Cell* 82:349-352, 1995
- Milligan CE, Prevette D, Yaginuma H, et al: Peptide inhibitors of the ICE protease family arrest programmed cell death of motoneurons *in vivo* and *in vitro*. *Neuron* 15:385-393, 1995
- Nagata S: Apoptosis by death factor. *Cell* 88:355-365, 1997
- Namura S, Zhu J, Fink K, et al: Activation and cleavage of caspase-3 in apoptosis induced by experimental cerebral ischemia. *J Neurosci* 18:3659-3668, 1998
- Nguyen KB, McCombe PA, Pender MP: Macrophage apoptosis in the central nervous system in experimental autoimmune encephalomyelitis. *J Autoimmun* 17:145-152, 1994
- Nicotera P, Ankarcrona M, Bonfoco E, et al: Neuronal necrosis and apoptosis: two distinct events induced by exposure to glutamate or oxidative stress. *Adv Neurol* 72:95-101, 1997
- Pender MP, Nguyen KB, McCombe PA, et al: Apoptosis in the nervous system in experimental allergic encephalomyelitis. *J Neurol Sci* 104:81-87, 1991
- Prineas JW, Kwon EE, Goldenberg PZ, et al: Multiple sclerosis. Oligodendrocyte proliferation and differentiation in fresh lesions. *Lab Invest* 61:489-503, 1989
- Rink A, Fung KM, Trojanowski JQ, et al: Evidence of apoptot-

- ic cell death after experimental traumatic brain injury in the rat. *Am J Pathol* 147:1575-1583, 1995
47. Savitz SI, Rosenbaum DM: Apoptosis in neurological disease. *Neurosurgery* 42:555-574, 1998
 48. Shuman SL, Bresnahan JC, Beattie NS: Apoptosis of microglia and oligodendrocytes after spinal cord injury in rats. *J Neurosci Res* 50:798-808, 1997
 49. Tator CH, Fehlings MG: Review of the secondary injury theory of acute spinal cord trauma with emphasis on vascular mechanisms. *J Neurosurg* 75:15-26, 1991
 50. Thompson CB: Apoptosis in the pathogenesis and treatment of disease. *Science* 267:1456-1462, 1995
 51. Vela JM, Dalmau I, González B, et al: The microglial reaction in spinal cords of jimpy mice is related to apoptotic oligodendrocytes. *Brain Res* 712:134-142, 1996
 52. Weedon D, Searle J, Kerr JF: Apoptosis. Its nature and implications for dermatopathology. *Am J Dermatopathol* 1: 133-144, 1979
 53. Wood PL: Microglia as a unique cellular target in the treatment of stroke: potential neurotoxic mediators produced by activated microglia. *Neurol Res* 17:242-248, 1995
 54. Yakovlev AG, Knoblich SM, Fan L, et al: Activation of CPP32-like caspases contributes to neuronal apoptosis and neurological dysfunction after traumatic brain injury. *J Neurosci* 17:7415-7424, 1997
 55. Young W: Secondary injury mechanisms in acute spinal cord injury. *J Emerg Med* 11 (Suppl 1):13-22, 1993

Manuscript received January 7, 1998.

Accepted in final form August 4, 1998.

Address for Dr. Emery: Hôpital Beaujon, Clichy, France.

Address reprint requests to: Allan D. O. Levi, M.D., The Miami Project to Cure Paralysis, 1600 NW 10th Avenue, R-48, Miami, Florida 33136. email: alevi@mednet.med.miami.edu.

Caspase-3 activity is present in cerebrospinal fluid from patients with traumatic brain injury

Luc Härter^{a,*}, Marius Keel^a, Hannes Hentze^b, Marcel Leist^c, Wolfgang Ertel^a

^a Department of Trauma Surgery, University Hospital Zürich, Zürich, Switzerland

^b Institute of Molecular and Cell Biology, 117609 Singapore, Singapore

^c H. Lundbeck A/S, 2500 Valby, Denmark

Received 13 March 2001; received in revised form 23 July 2001; accepted 2 August 2001

Abstract

Loss of neurons after traumatic brain injury (TBI) might involve dysregulated apoptosis. Activation of caspase-3 is one hallmark of apoptosis. Therefore, caspase-3 activity (cleavage of DEVD-afc) was measured in cerebrospinal fluid (CSF) samples ($n = 113$) from 27 patients with TBI at day 1 to 14 after trauma. Caspase-3 activity was detected in 31 (27.4%) CSF samples with highest values ($> 5.5 \mu\text{M}/\text{min}$) seen at day 2–5 after trauma. No caspase-3 activity was found in serum from patients or CSF from controls. The presence of activated caspase-3 in CSF suggests ongoing apoptotic processes during traumatic brain injury. © 2001 Elsevier Science B.V. All rights reserved.

Keywords: Apoptosis; Neurons; Trauma; Brain; DEVD-afc; zVAD

Neuronal cell loss after traumatic brain injury (TBI) has been formerly attributed to necrosis of neurons as a result of secondary insults. More recent evidence from animal models (Rink et al., 1995) and findings in human patient tissues (Ng et al., 2000; Clark et al., 1999) point towards an involvement of apoptosis in the mechanism of neuronal destruction following TBI. Apoptosis in neurons, endothelial cells, and astrocytes is triggered through the CD95 system (Leist and Nicotera, 1998). Because high concentrations of CD95-ligand were found in cerebrospinal fluid (CSF) from patients with severe TBI (Ertel et al., 1997), this points to the involvement of apoptotic processes responsible for brain damage following TBI.

A group of intracellular cysteine proteases, called caspases has been shown to play a pivotal role in the regulation and execution of apoptosis. Within this group, caspase-3 is the main executioner protease and its activation marks a point-of-no-return in the complicated cascade of apoptosis induction. Thus, the presence of active caspase-3 is a good indicator of apoptosis. To date, it is unknown whether active caspase-3 can be released from cells dying by apoptosis into CSF following TBI.

Therefore, caspase-3 activity was examined in the CSF of 27 patients with severe TBI. All patients were treated

according to our standard protocol for TBI (Stocker et al., 1995), which was approved by the University Hospital Medical Ethics Board. Three patients (11.1%) succumbed to death due to TBI. As a control, the CSF from seven patients requiring spinal anesthesia for elective orthopedic surgery (with normal CSF protein content and cell count) were included in this study after written informed consent. The control group was comparable to the trauma patients with regard to age and gender (Table 1).

CSF drained from an indwelling ventricular catheter was collected from all patients each day at 8 am between days 1 and 14 after trauma. However, in some patients, it was not possible to obtain CSF on consecutive days due to failure of the intraventricular catheter, collapsed ventricles due to extensive brain edema or death of the patient. The preflow (0.5 ml) was discarded and 1–2 ml of the sterile CSF centrifuged ($300 \times g$, 10 min, 4°C) and then frozen immediately at -80°C until further processing.

Caspase-3 activity in the CSF was measured by a fluorimetric assay based on the specific hydrolysis of DEVD-7-amino-4-trifluoromethylcoumarin (DEVD-afc, $60 \mu\text{M}$) in substrate buffer (50 mM HEPES, pH 7.4, 1% sucrose, 0.1% Chaps, 10 mM DDT, Thornberry, 1994). Caspase-3 activity (μM afc/min) was determined by measuring the increase of afc-fluorescence (excitation at 385 nm; fluorescence emission at 505 nm) over 30 min at 37°C , and calculation of the afc formation/time based on an

* Corresponding author.

Table 1
Demographic data of patients and controls

| Group | n | Age ^a | Gender ^b | Mortality | AIS | ISS | GCS |
|----------|----|------------------|---------------------|-----------|-----------|-------------|-----------|
| Patients | 27 | 36.1 ± 12.9 | 24/3 | 11.1% | 4.8 ± 0.4 | 29.2 ± 11.9 | 7.9 ± 4.2 |
| Controls | 7 | 41.6 ± 9.8 | 6/1 | – | – | – | – |

AIS: abbreviated injury score (points), ISS: injury severity score (points). GCS: Glasgow coma scale (points).

^aMean age ± SD.

^bGender is given as male/female.

afc standard curve. The specificity of the assay for caspase-3 activity was confirmed by the block of fluorescence increase when samples were re-measured in the presence of the caspase inhibitors DEVD-CHO (1 μ M) or zVAD-fmk (5 μ M). Recovery ($105 \pm 10\%$ at a mixture of sample:caspase-3 (300 μ M/min) of 96:4) and sensitivity (≥ 0.5 μ M/min) of the assay was regularly controlled by addition of active recombinant human caspase-3 to control CSF samples.

Caspase-3 activity was detected in 31 of 113 (27.4%) CSF samples from 20 out of 27 patients (74.1%) with TBI (Fig. 1). The highest levels of caspase-3 activity were detected between day 2 (6.5 μ M/min), day 4 (5.5 μ M/min) and day 5 (6.3 μ M/min) after trauma and declined thereafter. In contrast to CSF from patients, caspase-3 activity was undetectable in CSF from the seven controls or in parallel serum samples from patients and controls despite addition of DTT (10 mM) to the samples which is known to reactivate caspases previously inactivated by mild oxidants or nitric oxide (NO).

The data presented here show that caspase-3 activity is present in CSF of patients with severe TBI, indicating the involvement of apoptotic processes in the brain following

TBI. Undetectable caspase-3 activity in the circulation excludes secondary migration of caspase-3 through the blood–brain barrier. The identification of the mode of death in human TBI has been complicated by the fact that only post mortem material can be used where the mechanisms of death are difficult to study. Since the only form of cell death associated with caspase-3 activation is apoptosis (Leist and Jäätelä, 2001), the observation of increased activity of this protease in CSF of patients adds further evidence for the contribution of apoptosis to TBI. Thus, our results refute arguments that caspase-3 detected in post-mortem brain tissues from patients with TBI were a post-mortem artifact (Love et al., 2000).

Sampling of CSF has been used frequently as a minimally invasive method or readily available source to draw conclusions on the state of injury to the brain, and to obtain markers of predictive or diagnostic value. Besides various cytokines indicating inflammatory processes, also increased concentrations of the apoptosis-inducing CD95L have been detected (Ertel et al., 1997). This finding is now complemented by even closer evidence of ongoing apoptotic processes indicated by the release of activated caspase-3. It should be emphasized that our results do not allow localization or identification of specific cells undergoing apoptosis in the injured brain or differentiation between active involvement of caspase-3 and its release due to cell death. Although preliminary, our study demonstrates for the first time the presence of active caspase-3 in CSF from patients with severe head injuries.

Acknowledgements

We thank Heike Naumann and Andreas Rassow for expert technical assistance. This work was supported by grant 32-52932.97 from the Swiss National Science Foundation.

References

- Clark, R.S., Kochanek, P.M., Chen, M., Watkins, S.C., Marion, D.W., Chen, J., Hamilton, R.L., Loeffert, J.E., Graham, S.H., 1999. Increases in Bcl-2 and cleavage of caspase-1 and caspase-3 in human brain after head injury. *FASEB J.* 13, 813–821.
- Ertel, W., Keel, M., Stocker, R., Imhof, H.G., Leist, M., Steckholzer, U., Tanaka, M., Trentz, O., Nagata, S., 1997. Detectable concentrations

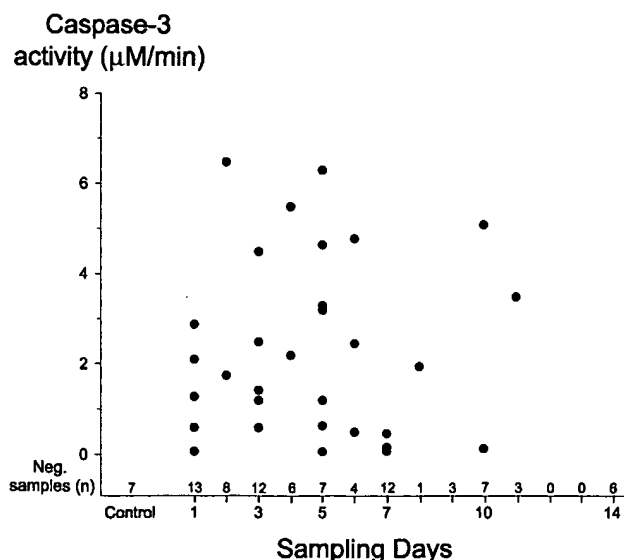


Fig. 1. Caspase-3 activity in CSF from patients with severe traumatic brain injury compared to controls. Sterile CSF was collected from patients between day 1 and 14 after trauma and from controls and immediately frozen until measurement of caspase-3 activity (μ M/min).

- of Fas ligand in cerebrospinal fluid after severe head injury. *J. Neuroimmunol.* 80, 93–96.
- Leist, M., Nicotera, P., 1998. Apoptosis versus necrosis: the shape of neuronal cell death. *Results Probl. Cell Differ.* 24, 105–135.
- Leist, M., Jäättelä, M., 2001. *Nat. Rev. Mol. Cell. Biol.* 2 (8), 1–12.
- Love, S., Barber, R., Wilcock, G.K., 2000. Neuronal death in brain infarcts in man. *Neuropathol. Appl. Neurobiol.* 26, 55–66.
- Ng, I., Yeo, T.T., Tang, W.Y., Soong, R., Ng, P.Y., Smith, D.R., 2000. Apoptosis occurs after cerebral contusions in humans. *Neurosurgery* 46, 949–956.
- Rink, A., Fung, K.M., Trojanowski, J.Q., Lee, V.M., Neugebauer, E., McIntosh, T.K., 1995. Evidence of apoptotic cell death after experimental traumatic brain injury in the rat. *Am. J. Pathol.* 147, 1575–1583.
- Stocker, R., Bernays, R., Kossmann, T., Imhof, H.G., 1995. Monitoring and treatment of acute head injury. *Update Intensive Care Emerg. Med.* 22, 196–210.
- Thornberry, N.A., 1994. Interleukin-1beta converting enzyme. *Methods Enzymol.* 244, 615–631.

Multiple Caspases Are Activated after Traumatic Brain Injury: Evidence for Involvement in Functional Outcome

SUSAN M. KNOBLACH,¹ MARIA NIKOLAEVA,¹ XIULING HUANG,¹ LEI FAN,¹
STANISLAW KRAJEWSKI,² JOHN C. REED,² and ALAN I. FADEN¹

ABSTRACT

Caspase-3 is a cysteine protease that is strongly implicated in neuronal apoptosis. Activation of caspase-3 may be induced by at least two major initiator pathways: a caspase-8-mediated pathway activated through cell surface death receptors (extrinsic pathway), and a caspase-9-mediated pathway activated by signals from the mitochondria that lead to formation of an apoptosomal complex (intrinsic pathway). In the present studies, we compare the activation of caspases-3, -8, and -9 after lateral fluid-percussion traumatic brain injury (TBI) in rats. Immunoblot analysis identified cleaved forms of caspases-3 and -9, but not caspase-8, at 1, 12, and 48 h after injury. Immunocytochemistry specific for cleaved caspases-3 and -9 revealed their expression primarily in neurons. These caspases were also frequently localized in TUNEL-positive cells, some of which demonstrated morphological features of apoptosis. However, caspases-3 and -9 were also found in neurons that were not TUNEL-positive, and other TUNEL-positive cells did not show activated caspases. In contrast to caspases-3 or -9, caspase-8 expression was only minimally changed by injury. An increase in expression of this caspase was undetectable by immunoblotting methods, and appeared as positive immunostaining restricted to a few cells within the injured cortex. Treatment with the pan-caspase inhibitor z-VAD-fmk at 15 min after TBI improved performance on motor and spatial learning tests. These data suggest that several caspases may be involved in the pathophysiology of TBI and that pan-caspase inhibition strategies may improve neurological outcomes.

Key words: brain injury; caspase; cysteine protease; mitochondria; neuron; trauma

INTRODUCTION

TRAUMATIC BRAIN INJURY (TBI) initiates physiological and cellular secondary injury responses that ultimately lead to neuronal death and neurological dysfunction. Although necrosis has long been acknowledged as a major cell death mechanism after TBI, a significant role for apoptotic cell death has recently been described (Rink et al., 1995; Yakovlev et al., 1997; Fox et al., 1998; Clark et al., 1999; Newcomb et al., 1999; Ng et al., 2000).

Activation of caspase proteases has been strongly implicated in apoptosis after CNS injuries, including TBI (Yakovlev et al., 1997; Namura et al., 1998; Clark et al., 1999, 2000; Fink et al., 1999; Krajewski et al., 1999; Springer et al., 1999; Beer et al., 2000b; Buki et al., 2000; Li et al., 2000; Lu et al., 2000). Caspases are cysteine proteases that are expressed as inactive pro-forms (zymogens) that, upon activation, are cleaved into large and small subunits that form heterotetramers with enzymatic activity (for caspase review, see Eldadah and Faden,

¹Department of Neuroscience, Georgetown University, Washington, D.C.

²The Burnham Institute, La Jolla, California.

2000; Reed, 2000). Caspases have been categorized into three groups, based on function: (1) initiator/apical caspases (caspases -2, -8, -9, -10); (2) executioner/effector caspases (caspases-3, -6, -7); (3) inflammatory caspases (caspases-1, -4, -5, -11). Initiator/apical caspases are so-named because of their relative position upstream of other caspases in putative apoptotic pathways. Executioner/effector caspases primarily function downstream of apical caspases, and directly cleave various substrate proteins responsible for apoptosis. Inflammatory caspases play dual roles as both cell-death proteins and processors of pro-inflammatory cytokines.

To date, two major routes of caspase activation have been described. An extrinsic pathway involves binding of cell surface receptors by specific ligands, that directly trigger caspase activation through adaptor proteins. Thus, apoptosis is induced through signals received at the cell surface. This pathway is utilized by members of the tumor necrosis factor (TNF) superfamily. Examples include binding of TNF receptor I by TNF/lymphotoxin, and binding of Fas by Fas ligand (Chinnaiyan et al., 1995; Juo et al., 1998; Varfolomeev et al., 1998). Either of these events can serve to activate pro-caspase-8, which subsequently activates pro-caspase-3 (Stennicke et al., 1998). In contrast, the intrinsic pathway is triggered by intracellular activation through signals derived from mitochondria. Cytochrome c is released from mitochondria and, in turn, binds the caspase-activating protein Apaf-1, which oligomerizes and binds pro-caspase-9, resulting in its cleavage/activation (Li et al., 1997; Hakem et al., 1998; Saleh et al., 1999; Zou et al., 1999). Subsequently, caspase-9 activates pro-caspase-3 (Slee et al., 1999). Although this classification of extrinsic and intrinsic pathways has proved generally useful, it should be noted that the scheme is somewhat oversimplified, as evidenced by cross-talk and feed-forward amplification of these pathways (Saleh et al., 1999; Zou et al., 1999; Reed, 2000).

Activated caspases cleave a diverse group of substrates, including other enzymes, and proteins involved in cell structure, signal transduction, transcription and DNA repair (reviewed in Eldadah and Faden, 2000). Effector caspases, in particular, cleave proteins that maintain the integrity of nucleic acids (ICAD, PARP) and cell structure (lamins, α -fodrin). Degradation of such proteins leads to membrane blebbing, nuclear fragmentation or condensation, cell shrinkage and/or formation of apoptotic bodies, all of which are morphological hallmarks of apoptotic demise.

Information about caspase activation, and its potential effect on neurological recovery and tissue loss after traumatic brain injury is primarily confined to caspases-1, -2, and -3 (Yakovlev et al., 1997; Beer et al., 2000b; Buki

et al., 2000; Clark et al., 2000). Recently, the activation of caspases-8 and -9, was described in models of cerebral ischemia and traumatic spinal cord injury (Krajewski et al., 1999; Springer et al., 1999; Velier et al., 1999; Keane et al., 2001b). As these caspases are initiators of well-described intrinsic and extrinsic apoptotic pathways, respectively, information about them provides particular insight into the type of apoptotic mechanisms that may be important in secondary injury responses. To address this issue, we evaluated the activation of caspase-8, -9, and -3 after TBI induced by the rat lateral fluid-percussion model via temporal immunoblot analysis of cleaved fragments of caspases-3, -8, and -9. In addition, we performed immunocytochemistry utilizing antibodies specific for active caspases, to determine their relative distribution and cell-type specific expression, as well as their association with a late event associated with apoptotic cell death—namely, DNA fragmentation as assessed by the TUNEL assay. Lastly, we evaluated the effect of treatment with a broad-spectrum caspase inhibitor on motor and cognitive function over time after injury.

MATERIALS AND METHODS

Traumatic Brain Injury

The lateral fluid-percussion model of rat brain injury has been previously detailed (McIntosh et al., 1989). Briefly, a craniotomy was performed over the left parietal cortex of anesthetized (70 mg/kg sodium pentobarbital, i.p.), intubated, male Sprague-Dawley rats (400 \pm 25 g, Harlan) ventilated on room air. Injury was induced by a brief, pressurized (2.5–2.6 atm), saline pulse delivered through the craniotomy to the intact dura. Sham controls were subjected to identical surgical procedures, with the exception that no fluid pulse was delivered. The caudal artery was cannulated to monitor blood gas and pressure throughout the procedure. Body (rectal) (37.5–38.5°C) and brain temperature (lateralis muscle) (36.5–37.5°C) were assessed and maintained within normal ranges. Three different sets of animals were prepared: (1) for immunoblot and activity assay studies, rats were subjected to the brain injury procedure and then sacrificed either 1, 12, 48, or 168 h later ($n = 5$ –6/group); naive rats were used as controls ($n = 5$ –6); (2) for immunocytochemical studies, rats were subjected to brain injury and then sacrificed either 4 or 24 h later ($n = 3$ /group); controls were sacrificed either 4 or 24 h after sham injury performed as described above ($n = 3$ /group); (3) for the drug treatment study, 25 mM z-VAD-fmk was dissolved in DMSO and injected intracerebroventricularly (5 μ L/2 min) at 15 min after injury ($n = 12$); con-

trols received equi-volume injections of DMSO vehicle ($n = 13$).

All procedures involving live animals were approved by the Georgetown University Animal Care and Use Committee, and were performed according to principles enumerated in the Guide for the Care and Use of Laboratory Animals, prepared by the Committee on the Care and Use of Laboratory Animals of the Institute of Laboratory Resources, National Research Council (DHEW publication NIH 85-23-2985).

Preparation of Tissue Homogenates and Immunoblotting

After decapitation, rat cortices were resected on ice and immediately frozen (-70°C). Later, the samples were weighed and homogenized in a 5:1 (wt/v) ratio of RIPA buffer (1% Na deoxycholate, 0.1% SDS, 1% Triton X-100, 0.01 M Tris HCl, pH 8.0, 0.14 M NaCl, 1 mM iodoacetamide, 1 mM AEBSF, 1 mM Aprotinin). Homogenates were centrifuged ($10,000 \times g$, 4°C) for 15 min and the resulting supernatant removed and frozen in $50\text{-}\mu\text{L}$ aliquots. One aliquot was used to determine protein concentration via the method of Bradford (Bradford, 1976). Protein lysates were normalized for total protein content ($50\text{ }\mu\text{g/lane}$) and loaded into 16% (caspase-3) or 4–20% (caspases-9 or -8) Tris-glycine gels and electrophoresed at 100 V for 2–3 h in a Tris/glycine/SDS running buffer. Proteins were transferred to PVDF membranes (25 V for 2 h, 4°C) in Tris/glycine buffer. The membrane was blocked for 2 h with 5% dried milk in Tris/borate/1% Tween 20 buffer at room temperature, then incubated overnight with primary polyclonal rabbit antisera. The next day, membranes were washed three times for 10 min each in Tris/borate buffer, and the protein bands were detected by enhanced chemiluminescence-based ECL methods using Hyperfilm (Amersham). The following primary antibodies were used: caspase-3 (Bur1797, 1:2,000; Burnham Institute, La Jolla, CA); caspase-9 (Bur81, 1:2,000); and caspase-8 (SK440, 1:2,000; SmithKline Beecham, King of Prussia, PA). The specificity of these antibodies has been demonstrated previously (Velier et al., 1999; Krajewski et al., 1999), except for Bur81, which was prepared and specificity demonstrated as described below. Recombinant active caspases and/or cells that are known to highly express caspases were used as positive controls. All blots were directly re-probed with anti- β -actin antibody as an internal control for loading and transfer of proteins (Liao et al., 2000). Blots shown are representative of experiments that were repeated on samples taken from three to five different animals/timepoint.

Production and Specificity of Bur81 Antibody

Anti-caspase-9 serum B81 was produced using recombinant human caspase-9 full-length His 6 protein as an immunogen. Recombinant C9/B81 was produced as a fusion protein with a C-terminal his 6 tag. This protein was expressed in BL21 (DE3) cells by induction with 1 mM IPTG. Following cell growth and lysis, the clarified cell lysate was applied to a Ni-NTA column and eluted with an imidazole gradient. The pooled C9 fractions were dialyzed against 50 mM Tris at pH 8.8 and applied to a 10/10 FPLC mono Q column (Pharmacia, Piscataway, NJ) and eluted with a NaCl gradient. New Zealand white female rabbits were injected subcutaneously with a mixture of recombinant protein (0.1–0.25 mg protein per immunization) and 0.5 mL of Freund's complete adjuvant (dose divided over 10 injections sites) and then boosted three times at weekly intervals, followed by another 3–20 boostings at monthly intervals of recombinant protein immunogens in Freund's incomplete adjuvant, before collecting blood and obtaining immune serum. Specificity of the antisera was tested for reactivity to *in vitro* translated caspases as follows. Caspase-3, -6, -7, -8, -9, and -10 cDNAs subcloned into pcDNA-3 (Invitrogen, Carlsbad, CA) were transcribed and translated *in vitro* using 1 μg of plasmid DNA, T7 RNA polymerase and TNT reticulocyte lysates (Promega, Madison, WI), according to the manufacturer's protocol, in the presence of [^{35}S]-labeled L-methionine ($\sim 1\text{ mCi/mmol}$) (Amersham, Piscataway, NJ). The *in vitro* translated caspase proteins were then subjected to SDS-PAGE/immunoblot analysis using Bur81 antisera.

Immunocytochemistry

Animals were anesthetized and intracardially perfused with saline and 4% paraformaldehyde at selected times after injury. Brains were removed, protected in sucrose, frozen in O.C.T. media, sectioned serially ($40\text{ }\mu\text{m}$), and stored free-floating in 2% paraformaldehyde. Approximately four to six sections distributed evenly within the area of the lesion (approximately -2.3 to -3.9 relative to Bregma) (Paxinos and Watson, 1986) were used for staining.

For immunocytochemistry, sections were placed in 4% paraformaldehyde for 5 min, rinsed twice in phosphate-buffered saline (PBS) and blocked in 10% goat serum/0.3% triton for 1 h at room temperature. Primary antibodies specific for cleaved forms of either caspase-3 or -9 (9661S, 9501S; Cell Signaling, Beverly, MA) were diluted 1:100 in PBS containing 2% goat serum/0.2% triton. Antibody 9661S detects only the 17–20-kDa fragment of caspase-3 in human, rat and mouse. Antibody

9501S detects only 37- and 17-kDa fragments of caspase-9 in human and rat. Neither antibody recognizes full-length forms of these caspases. Alternatively, some sections were incubated with SK398 (anti-cleaved caspase-3), SK440 (anti-cleaved caspase-8) (both from SmithKline Beecham), or Bur81 (anti-caspase-9) (Burnham Institute) at a dilution of 1:1000. Antibody SK398 is a neo-epitope peptide antibody generated to the C terminus of the p20 subunit of caspase-3 (GIETD). It detects only an 18-kDa fragment of caspase-3 in rodents. Antibody SK440 was raised against a p20/p10 fusion protein purified from *E. coli*. It recognizes epitopes in the p20 fragment of caspase-8. It does not react with endogenous caspase-8 expressed by Jurkat cells, or with recombinant full-length caspase-8-spiked Jurkat extracts (Velier et al., 1999). Bur81 reacts preferentially with 32–33- and 15-kDa fragments of caspase-9, but also detects the 48-kDa proform of this caspase, as shown in Figure 2 below. Sections were incubated in these solutions overnight (16 h/4°C). In some cases, mouse monoclonal antibodies against neuronal nuclear protein (NeuN) (Chemicon, Temecula, CA) or glial fibrillary acidic protein (GFAP) (Sigma, St. Louis, MO) were diluted at 1:100 in solution with caspase primary antibodies to serve as cell-type specific markers. After incubation, sections were rinsed twice (5 min each) in PBS (4°C) and then incubated with secondary antibodies (1:50) for 1 h (room temperature). Either goat anti-rabbit FITC (Sigma) or goat anti-mouse Texas Red (Accurate Chemicals, Westbury, NY) served as secondary antibodies. Finally, the sections were rinsed twice (5 min each), mounted, covered with anti-fade mounting medium, sealed with glass coverslips, and visualized with a confocal microscope. Confocal parameters were kept constant to allow valid comparisons between experimental groups. Method controls omitted either primary or secondary antibodies.

For sections co-labeled with TUNEL, Tdt reaction mix was applied for 1 h (37°C) after rinsing off primary antibodies. Tdt reaction mix consisted of dNTPs, Tdt buffer, and Tdt enzyme (Life Technologies, Rockville, MD) in sterile, ultrapure H₂O. The TUNEL reaction was stopped in 0.1 M EDTA, pH 8.0 for 2–5 min. Sections were rinsed twice in PBS (5 min each), and incubated with secondary antibody + DN-Avidin-FITC (Vector Labs, Burlingame, CA) for 1 h (room temperature). Thereafter, sections were rinsed, sealed with coverslips, and viewed with a Nikon TE300 inverted fluorescent microscope.

Neurological Evaluation

All neurological examinations were performed by an individual blinded to treatment. Complete methods for motor and cognitive testing have previously been de-

scribed (McIntosh et al., 1989; Fox et al., 1998). Motor testing was performed at 7 and 14 days after trauma (McIntosh et al., 1989). Composite scores were derived from three separate motor tests: (1) flexion test—measures forelimb and paw (left and right) extension and placement in response to a perceived fall, (2) lateral pulsion test—measures body and leg resistance (left and right) to a lateral push, (3) inclined plane test—assesses the ability to maintain balance (in the vertical, left lateral and right lateral positions) on a progressively inclined surface. Scores for each limb on the individual tests range from 0 (maximal deficit) to 5 (no deficit). These were combined for a possible total maximal composite neuroscore of 35.

Morris water maze training began at day 14 after injury, and concluded after a total of 16 trials were completed in blocks of 4/day. For each trial, rats were gently placed into a tank of opaque water that had extramaze visual cues. The latency, or time required to locate a hidden, submerged, platform was recorded. After reaching the platform, animals were allowed to remain on it for 10 sec before they were removed, dried and kept in a warm environment until the next trial. Animals that failed

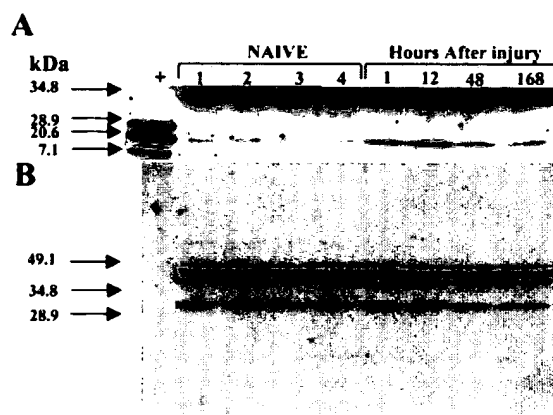


FIG. 1. Temporal expression of caspase-3 cleavage fragments in injured cortex after traumatic brain injury (TBI). Anesthetized rats ($n = 5$ –6/group) were subjected to lateral fluid-percussion trauma (2.5–2.6 ATM). Injured cortex was analyzed by immunoblot at various times after injury (1–168 h). (A) A blot shows results from one animal at each time point, which is representative of results obtained from all animals in each group. The molecular weight of each cleavage fragment appears on the left. Bands corresponding to a 32-kDa proform and a 17-kDa cleavage fragment are present; expression of the 17-kDa fragment increased after trauma. Recombinant active caspase-3 was used as a positive control. Naive rats served as injury controls. (B) β -actin was directly assessed as an internal methods control. As β -actin may itself be cleaved by caspases, some control blots were overexposed, revealing a ~31 kDa cleaved fragment of β -actin which was unchanged by trauma.

INTRINSIC APOPTOTIC PATHWAYS AFTER BRAIN INJURY

to reach the platform within 2 min after placement in the tank, were gently placed on the platform for 10 sec before removal. Data are presented as the average latencies for the treated or untreated groups on each individual day of training.

Data Analysis

Densitometric immunoblot analysis data were assessed by ANOVA followed by post-hoc Dunnett's test. Motor neuroscores were analyzed by nonparametric Mann-Whitney *U* tests. Morris water maze data were analyzed by repeated measures ANOVA followed by multiple two-tailed *t* tests with Bonferroni (Dunn's) correction. A *p* value of <0.05 was considered statistically significant.

RESULTS

Immunoblot analysis of caspase-3 indicated the presence of a 32-kDa proform in all brain samples (Fig. 1A), but not in a recombinant active caspase-3-positive control. A 17-kDa cleavage fragment of caspase-3 was evident at 1, 12, and 48 h after injury. Blots were directly reprobed with β -actin antibody (without stripping) (Liao et al., 2000) which served as an internal control for protein loading and transfer. Loading and transfer of proteins was equal in all wells, as shown by equivalent signal intensity of a 42-kDa β -actin internal control (Fig. 1B; also see Fig. 3C below). However, because caspases are known to cleave β -actin, some control blots were overexposed to determine whether cleavage fragments of this protein were present. In some cases, a 30-kDa β -actin cleavage fragment was detected under this condition, but it was neither robust, nor trauma-dependent (Fig. 1B), thus verifying that β -actin was a suitable internal control.

Specificity studies showed that antibody Bur-81 did not react with either full-length or cleaved forms of caspases-3, -6, -7, -8, or -10, expressed by *in vitro* translation. Bur-81 preferentially reacted with the 32–33- or 15-kDa cleaved forms of caspase-9, but also detected the 48-kDa pro-form of this caspase (Fig. 2A). Similarly, the antibody detected the 48-kDa pro-form of caspase-9 in all brain extracts, as well as 32–33-kDa cleaved fragment (Fig. 2B). Expression of the 15-kDa cleavage fragment was low in naive controls, but increased after TBI. Densitometric analysis of the 15-kDa subunit revealed significant elevations over uninjured controls at 1 and 12 h after injury (Fig. 2C). The appearance of the 32–33-kDa cleaved fragment in both naive and injured cortex is consistent with observations that caspase-9 is auto-processed in brain and peripheral nerve (Krajewski et al., 1999).

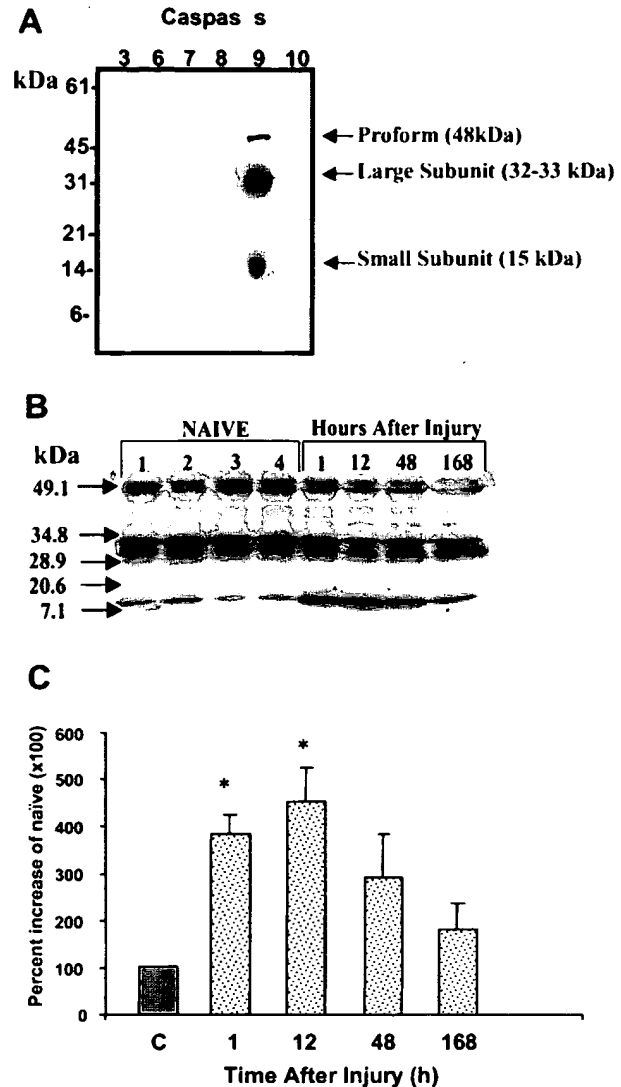


FIG. 2. Specificity of the Bur81 anti-caspase-9 antibody and temporal expression of caspase-9 cleavage fragments in cytosolic extracts of injured cortex after traumatic brain injury (TBI). (A) Immunoblots utilizing extracts from cells expressing *in vitro* translated caspases-3, -6, -7, -8, -9, and -10 show that Bur81 reacts primarily with the ~32–33 and 15-kDa processed (cleaved) forms of caspase-9, and also with the 48-kDa pro-caspase-9. (B,C) Rats (*n* = 5–6/group) were subjected to lateral fluid-percussion trauma, and the injured cortex assessed by immunoblotting with Bur81 as described for Fig. 1. A representative immunoblot is shown in B. Bands corresponding to a 48-kDa proform and 32–33- or 15-kDa cleavage fragments are present; expression of the 15-kDa fragment increased after trauma. A 32–33-kDa subunit of processed caspase-9 is known to be present in naive cortex and in peripheral nerve. (C) Immunoreactivity of the 15-kDa cleavage fragment is expressed as arbitrary densitometric units. Data were transformed to the percentage of densitometric levels from naive animals visualized on the same scanned blot. Bars indicate means \pm SEM for each timepoint. **p* < 0.05 versus controls by ANOVA and Dunnett's post-hoc test.

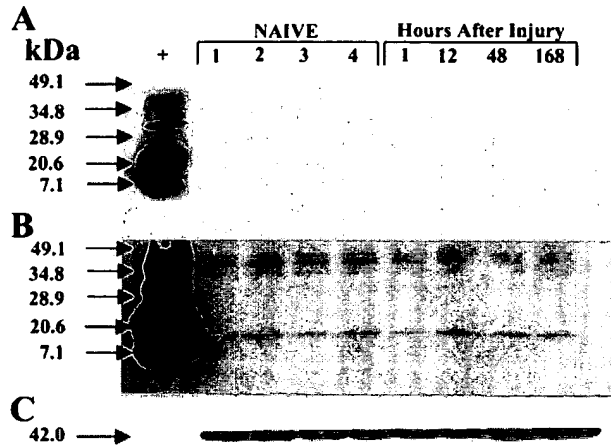


FIG. 3. Temporal expression of caspase-8 cleavage fragments in cytosolic extracts of injured cortex after traumatic brain injury (TBI). Rats ($n = 5$ – 6 /group) were subjected to lateral fluid-percussion trauma, and the injured cortex assessed by immunoblotting as described for Fig. 1. (A–C) The blot shows results from one animal at each time point, which is representative of results obtained from all animals in each group. The molecular weight of each cleavage fragment appears on the left. In A, the blot was exposed for 15 sec to detect cleaved products present in the recombinant caspase-8 control, which undergoes auto-processing. In B, the same blot was exposed for 8 min to determine whether caspase-8 cleavage fragments were present. At this exposure, bands corresponding to 38–40- or 14-kDa cleavage fragments were detected, although a p55-kDa proform was not. Expression of the 38–40- or 14-kDa cleavage fragments was unchanged by trauma. The β -actin internal control is shown in C.

There was no evidence for injury-induced cleavage of caspase-8, despite the fact that antibody SK440 detected several cleavage fragments in recombinant active caspase-8–positive control samples run on the same gels (Fig. 3A). Blots were subjected to multiple exposures, the longest of which revealed the presence of 38–40- and 14-kDa cleavage fragments in all brain samples, regardless of injury status (Fig. 3B).

To determine the distribution and cell-type expression patterns of caspases within the injured cortex and hippocampus we performed qualitative immunocytochemistry. Four to six sections distributed evenly within the extent of the lesion were chosen and stained for caspases-3, -9, or -8. For caspases-3 and -9, commercially available (Cell Signaling) antibodies, designated 9661S and 9501S, respectively, were used. The antibodies do not detect pro-forms of these caspases; they are specific for cleaved forms, and thus can be used as a cellular marker of caspase activation. Cleaved forms of caspases-3 and -9 were expressed mainly in the inner cortex along the border of the corpus callosum at 4 h after injury (Fig. 4), but were distributed widely throughout the entire region of injured cortex by 24 h after injury (Fig. 5). Active forms of caspases-3 and -9 were also expressed in the CA3 and CA2 regions of the hippocampus, particularly at 24 h after injury (Fig. 6). Selective cell loss was also evident in the CA3 region at this time.

In contrast to the relatively widespread distribution of active caspases-3 and -9 at 4 and 24 h after injury, expression of caspase-8 was limited to only a few cells within the injured cortex at either time (Fig. 7A). These

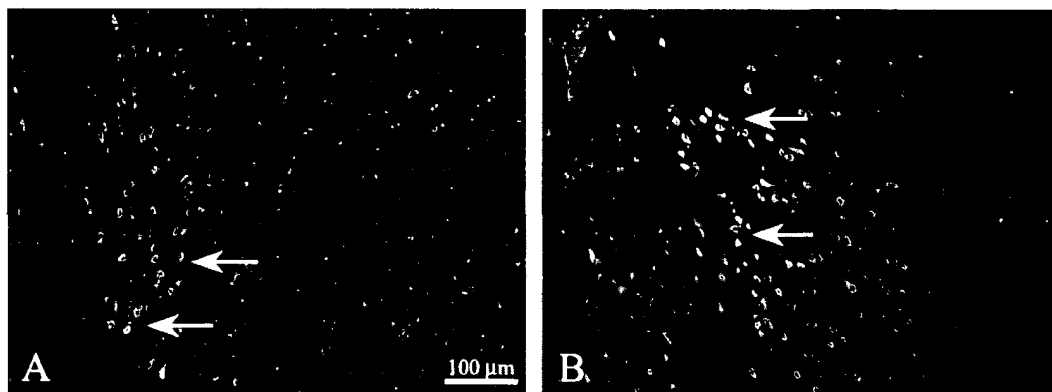


FIG. 4. Distribution of active caspase-3 (A) or caspase-9 (B) (antibodies 9661S or 9501S, respectively) in the inner cortex after lateral fluid-percussion injury, as visualized by fluorescent immunohistochemistry. Injury was produced as described in Fig. 1. At 4 or 24 h after injury, sham-injury brains were removed and stained as described in methods. Low-power images ($\times 10$) of the inner injured cortex at 4 h after injury are shown. Arrows indicate positively stained cells near the border of the corpus callosum. Images are representative of data obtained from $n = 3$ rats/group.

INTRINSIC APOPTOTIC PATHWAYS AFTER BRAIN INJURY

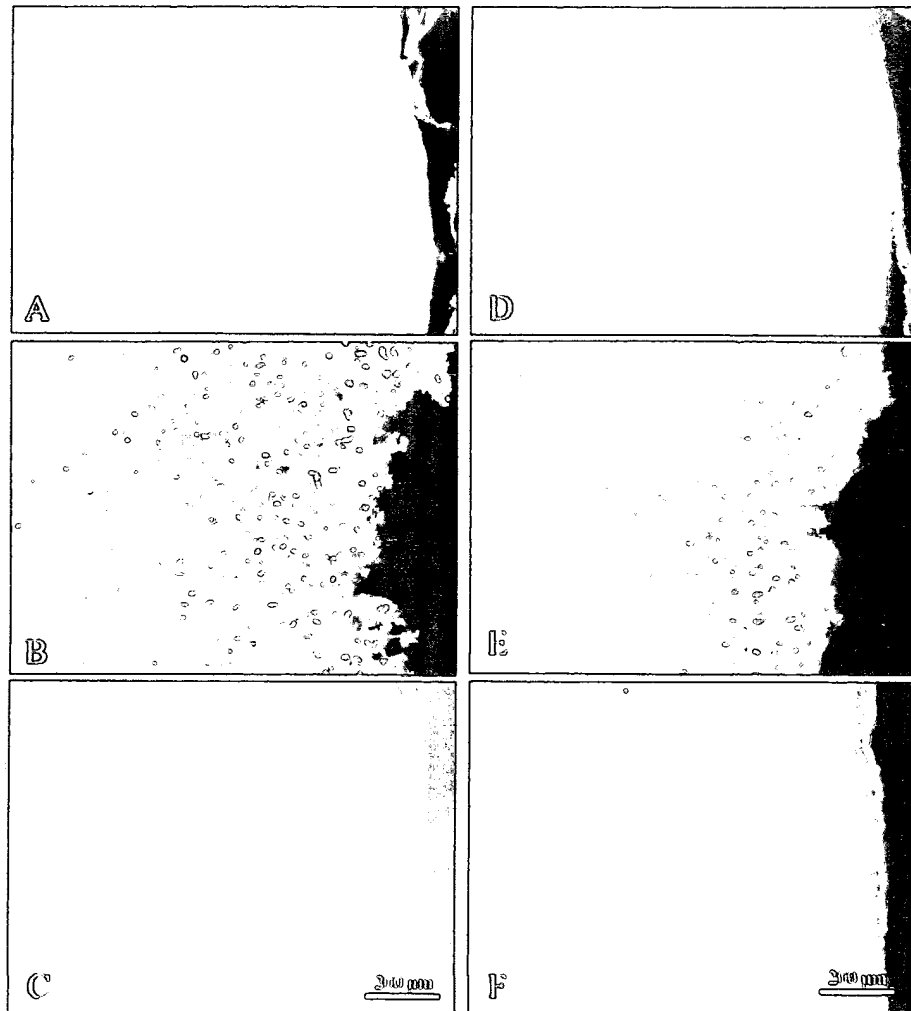


FIG. 5. Distribution of active caspase-3 (A–C) (antibody 9661S) or -9 (D–F) (antibody 9501S) in the outer cortex after lateral fluid-percussion injury. Data were obtained from the same rats described in Fig. 4. Low-power images ($\times 10$) of outer injured cortex were obtained at 4 h (A,D) and 24 h (B,E) after TBI, or 24 h after sham-TBI (C,F).

cells morphologically resembled neurons and glia. Even though few cells stained positively, such staining was associated with injury, as sham-injury controls showed no evidence of any positive staining (Fig. 7B).

Double-label immunocytochemistry revealed that cleaved caspases-3 and -9 were expressed by neurons, but not astrocytes of the injured cortex (Figs. 8 and 9). Staining in neurons was diffuse, cytosolic and present in the soma as well as what appeared to be dendrites, on some occasions (Figs. 5, 8, and 9). Caspase-9 and the cleaved fragment of caspase-3 were also colocalized to some extent with TUNEL-positive cortical cells that showed apoptotic-like condensed or punctate nuclear morphology (Fig. 10). However, this colocalization was not exclusive, as many TUNEL-positive and TUNEL-

positive cells with apoptotic-like phenotypes did not express active subunits of either caspase, and some caspase positive cells were not TUNEL-positive.

To evaluate the effect of caspase inhibition on functional recovery after injury, animals were treated 15 min after injury with z-VAD-fmk, a pan-caspase inhibitor. This treatment significantly improved performance on a series of three separate motor tests administered 2 weeks later (Fig. 11A). In addition, in daily comparisons, z-VAD-fmk treated animals performed significantly better than controls in the Morris water maze test on days 2 and 4 of training (Fig. 11B). There was no significant difference in latencies on the first day of training, indicating that swim speeds were not significantly different between treated and control groups.

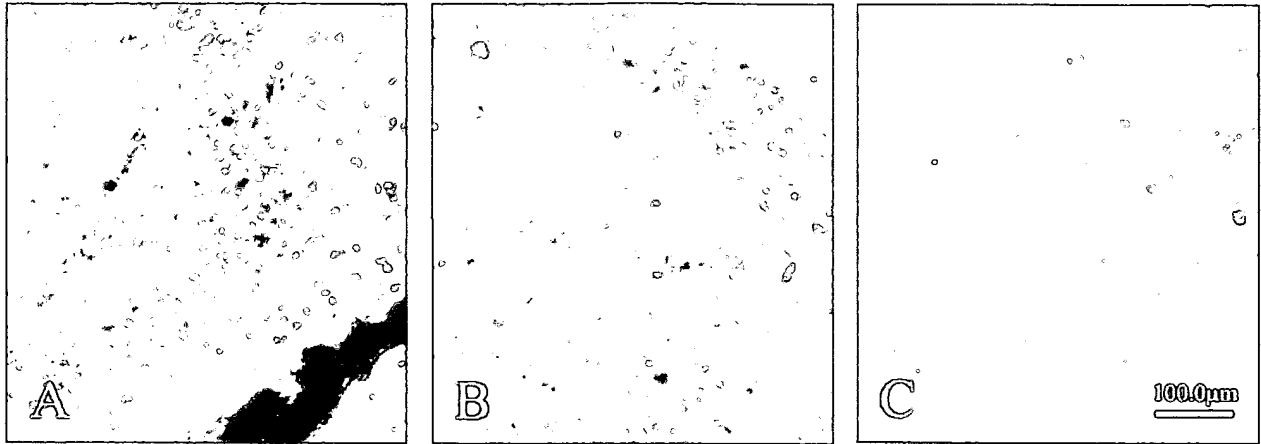


FIG. 6. Distribution of active caspase-3 (A) (9661S) or caspase-9 (B) (9501S) in the hippocampus 24 h after TBI. Many CA3 pyramidal cells stained positively for caspase-3 (A) or caspase-9 (B). Note that some cell loss is also visible in the CA3 region. The majority of CA2 cells at the junction with CA1 were caspase-3 or -9 positive, although most CA1 cells were not (data not shown). Few caspase-positive cells were observed in the hippocampus at 2 h after sham-TBI (C) or at 4 h after injury (data not shown).

DISCUSSION

Our studies show that caspases-3 and -9 are activated in injured cortex and hippocampus after traumatic injury. Cleavage products of these caspases were expressed throughout the cortex, primarily in neurons, and frequently co-localized with TUNEL-positive labeling. The latter associates these caspases with neuronal cell death that is likely to be, at least in part, apoptotic. In contrast, the presence of active caspase-8 was more difficult to detect than either caspase-3 or -9. Cleavage fragments for this caspase were not observed on immunoblots, and were only localized to a few cells by immunocytochemistry.

Caspase activation after brain injury has been assessed by a variety of methods, ranging from accumulation of degraded downstream substrates unique to a particular caspase (Pike et al., 1998; Beer et al., 2000b; Clark et al., 2000), to direct activity measurements utilizing oligopeptide substrates tagged with a fluorogen that produces an optical change upon cleavage (Yakovlev et al., 1997; Clark et al., 2000). In preliminary experiments, we found that, in the case of caspases-8 and -9, such fluorescence-based activity assays were nonspecific. In assays with Ac-LETD-afc (caspase-8) and Ac-LEHD-afc (caspase-9), the recognized substrate sequences for these caspases (Talanian et al., 1997; Thornberry et al., 1997), submicro-

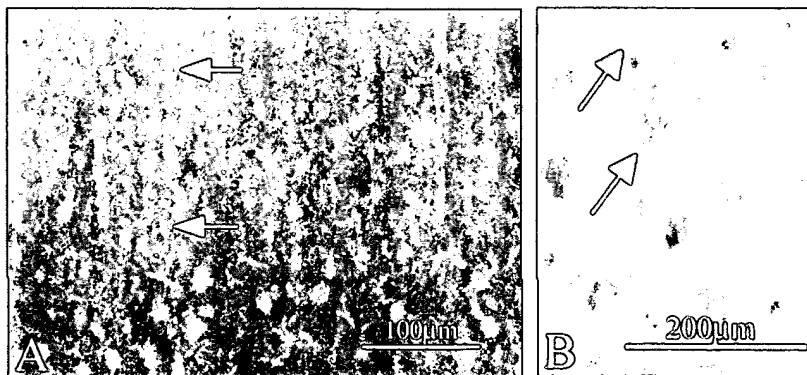


FIG. 7. Distribution of caspase-8 (antibody SK440) in the injured parietal cortex at 24 h after TBI. Low-power image shows that only a few cells distributed within the cortex expressed caspase-8 after injury (A; some positive cells indicated by arrows). Under higher power magnification, such cells resembled glia or neurons (B; cells indicated by arrows). Results are representative of $n = 3$ animals. Sections from 4 h after injury were also evaluated (including sections adjacent to those which showed positive staining for caspases-9 and -3), and showed a distribution of staining similar to that shown in A.

INTRINSIC APOPTOTIC PATHWAYS AFTER BRAIN INJURY

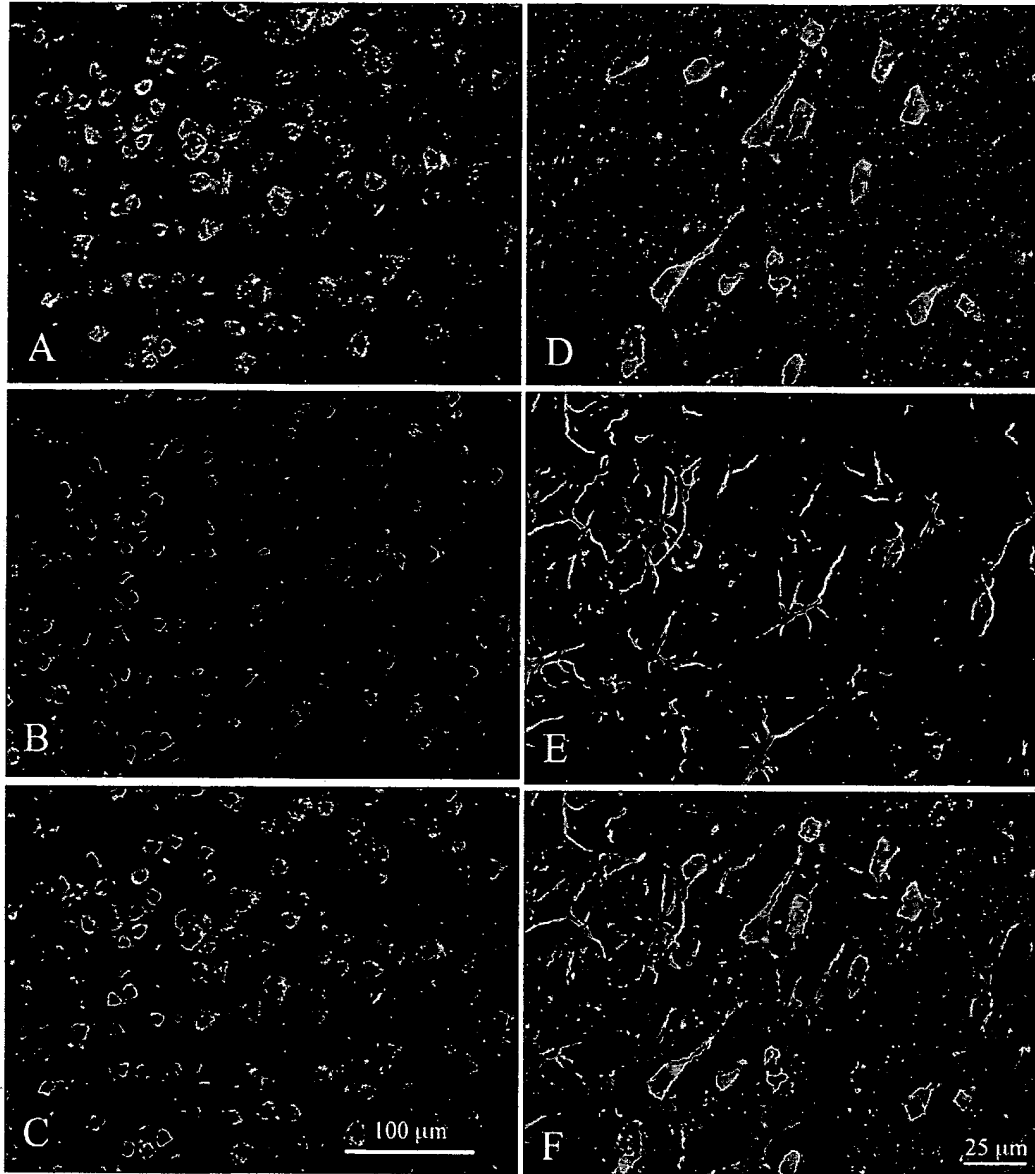


FIG. 8. Double-label immunocytochemistry for active caspase-3 (A,D) (antibody 9661S) combined with either NeuN, a neuronal marker (B) or GFAP (E), a marker for astrocytes. Staining for active caspase-3 was diffuse, cytosolic (A), and was localized to neuronal cell bodies (B,C), and in some instances, dendrites (A). Active caspase-3 was not frequently expressed by astrocytes (E,F). Images were taken from the injured parietal cortex at 24 h after TBI. They are representative of data from $n = 3$ animals.

molar concentrations of either recombinant caspase-3 or z-DEVD added to control (sham) samples respectively markedly increased or decreased apparent caspase-8 or -9 activity. Therefore, this method was replaced with detection of active caspases via immunoblot.

Our data indicated that caspases-3 and -9 were activated from 1 to at least 12 h after lateral fluid-percussion injury. These results are consistent with both the time-course for activation of caspase-3 we reported previously

using a fluorogenic activity assay (Yakovlev et al., 1997), and with recently reported time-courses for caspases-3 or -9 utilizing immunoblotting methods (Beer et al., 2000b; Clark et al., 2000). Together, such findings suggest that cortical apoptosis occurs over an extended time-course, in agreement with studies which showed increased TUNEL-staining in the same model from 24 to 168 h after injury (Rink et al., 1995; Conti et al., 1998). These results are also consistent with the time course for acti-

vation of caspase-3 and apoptotic cell death reported in cortical contusion models (Yakovlev et al., 1997; Fox et al., 1998; Newcomb et al., 1999; Beer et al., 2000b; Clark et al., 2000).

In undisturbed neurons, the location of procaspase-9 is frequently mitochondrial, giving rise to a distinct organellar staining pattern (Krajewski et al., 1999). After ischemic injury, caspase-9 translocates from the mitochondria to the cytosol and nucleus, resulting in diffuse staining throughout the cell (Krajewski et al., 1999), which resembles that pattern we observed, suggesting that a similar translocation of caspase-9 occurs in both ischemic and traumatic injuries. Caspase-3 primarily resides in the cytosol (Krajewska et al., 1997), and thus staining for this caspase is usually diffuse, as seen here, and reported previously in other models of trauma (Beer et al., 2000b; Clark et al., 2000) or ischemia (Namura et al., 1998). Apart from visualization in the soma, we observed some expression of caspase-9 (and caspase-3) in what appeared to be dendrites. Dendritic expression of active caspase has been associated with synaptic loss and cell death due to excessive glutamate stimulation (Mattson et al., 1998). Thus, it is possible that caspase activation through this route could be a factor in traumatic injury. Expression of cytochrome c, calpain and active caspase-3 have also been observed in cortical axons, where they are hypothesized to contribute to neuronal demise in models of axonal injury (Buki et al., 2000). Together, these data suggest that activated caspases are not limited to somatic expression in injured neurons, and may reflect several different local routes through which neuronal death or synaptic reorganization could be initiated.

Qualitatively, the regional and cell-type distributions of active caspases-3 and -9 appeared similar, as they were evident in all layers of injured cortex, albeit somewhat preferentially in the inner cortex adjacent to the corpus callosum at 4 h after injury, but distributed throughout the region at 24 h after injury. Both caspases were expressed primarily by neurons rather than astrocytes, in agreement with findings from cortical contusion models, which also mainly located active caspase-3 expression to neurons trauma (Beer et al., 2000b; Clark et al., 2000). Caspase-3 appeared to be expressed in more cells than caspase-9 at both 4 and 24 h after injury. In this regard, it is worth noting that caspase-3 may be activated not only through extrinsic and intrinsic cascades, but also by additional factors, including granzyme B, caspase-11, and others, whose role in injury, if any, is uncertain (Yang et al., 1998; Kang et al., 2000).

We could not use antibodies 9661S or 9501S in the TUNEL double-label study, because these antibodies did not perform well on thin, mounted sections, but TUNEL-

staining did not work well on thick free-floating sections. Therefore, antibodies SK398 and Bur81 were used in the TUNEL double-label experiments. In this regard, it is worth noting that SK398 is specific only for active caspase-3, whereas Bur81 preferentially stains cleaved fragments of caspase-9, but also reacts to a lesser extent with the pro-form of this caspase. Data from this experiment indicate that active caspase-3, and likely, active caspase-9, are expressed by either type I or type II TUNEL-labeled cells, but this association was not complete, as noted previously for caspase-3 by others (Beer et al., 2000b; Clark et al., 2000). This result may reflect the fact that active caspases are short-lived, and their temporal expression may not completely overlap the DNA fragmentation that gives rise to the TUNEL signal, but rather (and particularly in the case of caspase-9) precede it. Other factors may also contribute to the discrepancy. These would include observations that: some TUNEL positive cells are actually necrotic (Rink et al., 1995; de Torres et al., 1997); there may be a mixed apoptotic-necrotic phenotype (Allen et al., 1999); there is likely to be cross-talk between cell death mechanisms, and/or activation of certain apoptotic pathways may not be mediated by caspases (Susin et al., 2000; Thomas et al., 2000).

Presumptive involvement of the extrinsic apoptotic pathway in TBI is supported by evidence that Fas and Fas ligand are increased after TBI (Ertel et al., 1997; Beer et al., 2000a), as is TNF (Shohami et al., 1996; Knoblach et al., 1999). Yet, the present data show only limited caspase-8 activation. It is unlikely that our findings are due to antibody specificity issues. This antibody, which has previously been extensively characterized (Velier et al., 1999), strongly detected a positive caspase-8 control. In addition, we have utilized the antibody in an identical protocol to evaluate active caspase-8 expression after spinal cord injury (Huang et al., 2000), and others have used it in models of spinal ischemia and focal stroke (Velier et al., 1999; Matsushita et al., 2000). In all these studies, substantial expression of active caspase-8 was detected. More likely, the data reflect injury level or model issues. Caspase-8 activation was recently shown after more moderate fluid percussion injury (1.7–2.2 atm), where its temporal elevation correlated well with the time course of TNF α we observed after severe injury (2.6–2.7 atm) (Keane et al., 2001a). In our hands, more moderate injury (2.0 atm) did not consistently elevate TNF α . Thus, there are apparent differences in actual injury levels between laboratories, and it is possible that our severe injury level may be required to induce substantial caspase-8 activation. This is supported indirectly by a recent study in the cortical impact injury model, which demonstrated increases in both caspase-8 mRNA and activation, and in

INTRINSIC APOPTOTIC PATHWAYS AFTER BRAIN INJURY

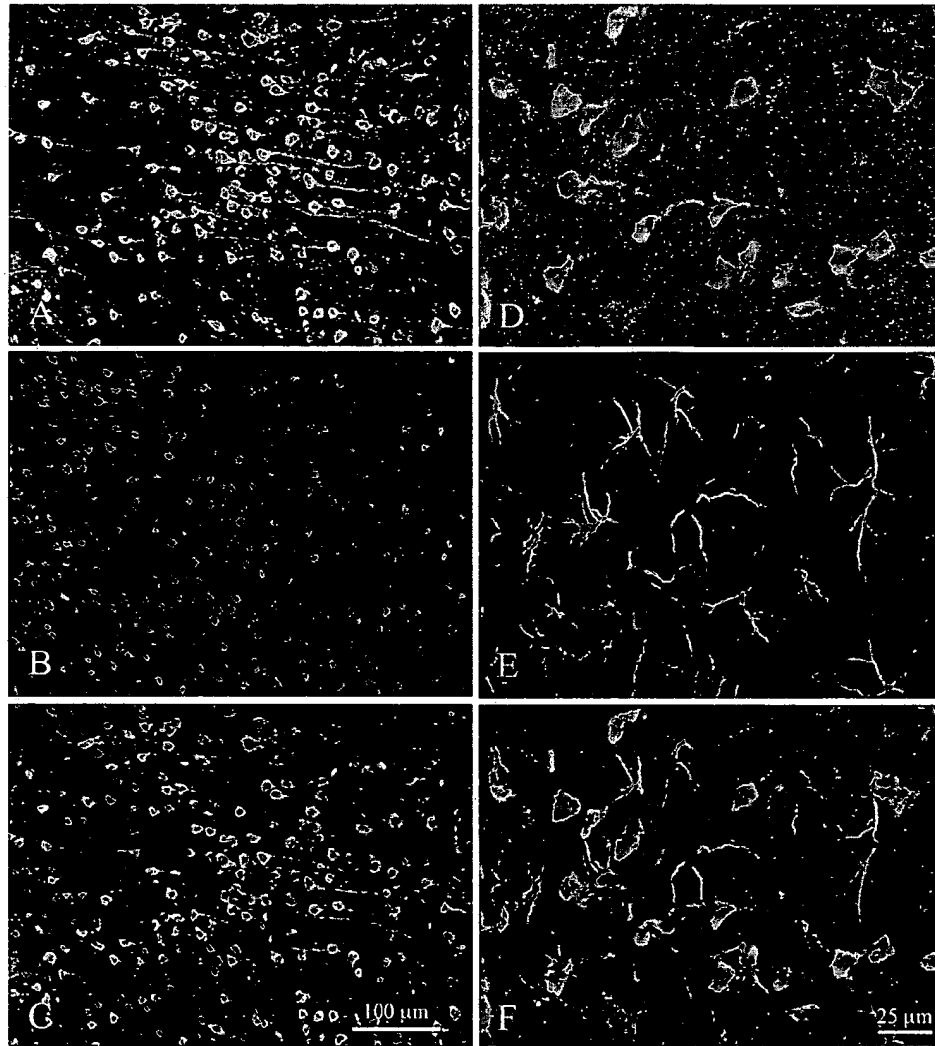


FIG. 9. Double-label immunocytochemistry for active caspase-9 (A,D) (antibody 9501S) combined with either NeuN, a neuronal marker (B) or GFAP (E), a marker for astrocytes. As with caspase-3, staining was diffuse, cytosolic and was localized to neuronal bodies and in some instances, dendrites (A,D,C). Active caspase-9 was not frequently expressed by astrocytes (F). Images were taken from the injured parietal cortex 24 h after TBI. They are representative of data from $n = 3$ animals.

addition, associated caspase-8 with neurons and glia (Beer et al., 2001). This injury model is known to invoke an ischemic response that may only be present at severe levels of fluid percussion injury (Bryan et al., 1995).

Our caspase-9 data are the first to show the cortical distribution of this caspase after injury, as well as to evaluate its expression in specific cell-types, or in conjunction with TUNEL staining. The results are consistent with reports of increased expression of apaf-1 and cytochrome c after trauma (Yakovlev et al., 2001), as well as alterations of endogenous inhibitors of this pathway, such as bcl-2 or XIAP (Clark et al., 1999; Lu et al., 2000; Keane et al., 2001a,b). Together, these data collectively provide

strong support for the intrinsic pathway of apoptotic cell death after TBI.

Treatment with the pan-caspase inhibitor z-VAD-fmk improved motor and cognitive function, compared to vehicle controls. This likely relates to caspase expression both in cortex and hippocampus, as shown here for caspase-9 and previously for caspase-3 (Yakovlev et al., 1997). Z-VAD-fmk was also neuroprotective in a mouse model of controlled cortical impact, where it reduced lesion volume (Fink et al., 1999), and in mouse and rat models of ischemia, where it both reduced lesion volume and improved neurological function (Loddick et al., 1996; Hara et al., 1997; Fink et al., 1998; Ma et al., 1998).

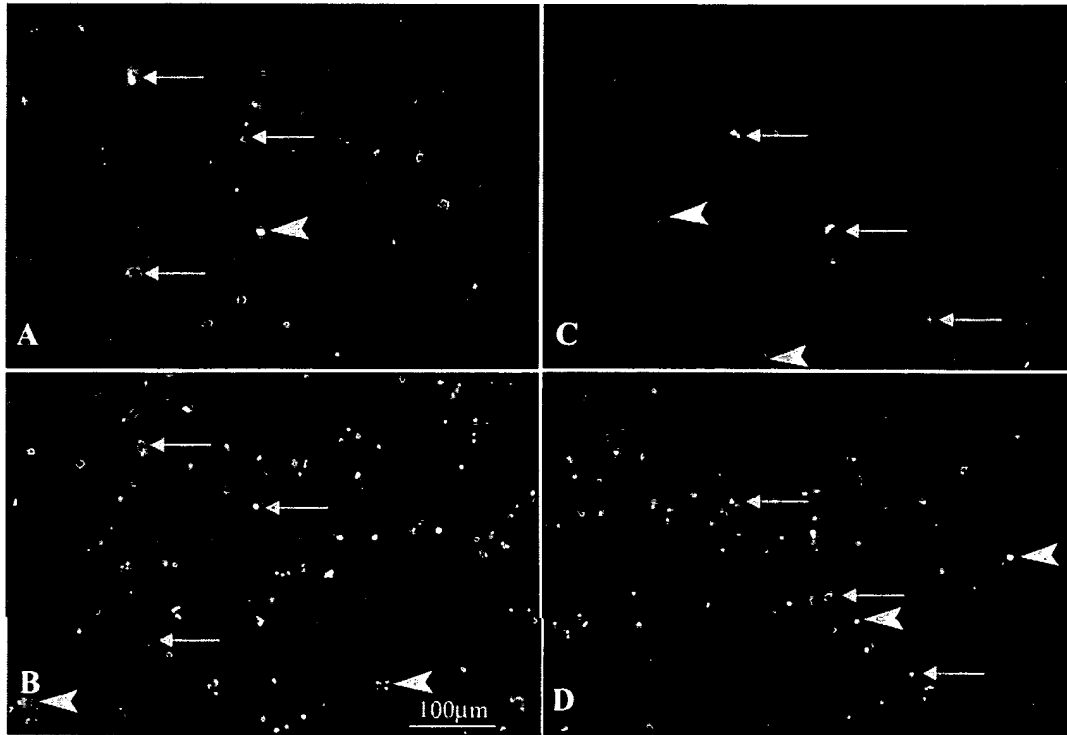


FIG. 10. Colocalization of caspases and TUNEL staining in rat cortex at 24 h after TBI. Fluorescent immunostaining was used to detect either active caspase-3 (SK398 antibody) (A) or caspase-9 (Bur81 antibody) (C) as indicated in representative fields ($\times 40$). (B,D) Images show TUNEL-positive staining observed in the same fields as A and C, respectively. Arrows denote cells positive for caspase as well as TUNEL labeling. Chevrons denote cells positive for either caspase or TUNEL labeling, but not both.

Z-VAD-fmk is an irreversible inhibitor of most caspases, showing greatest inhibition of caspases-1, -5, -8, and -9, but also significant inhibition of caspases-3, -4, -6, and -7 (Thornberry et al., 1997). Of these, caspases-4, -5, -6, and -7 have not yet been associated with TBI, and may not even be present in the CNS (Eldadah and Faden, 2000). However, we previously observed improved neurological recovery concurrent with reductions in TUNEL-labeled cells and DNA laddering after selective inhibition of caspase-3 with z-DEVD-fmk in our model (Yakovlev et al., 1997), implicating this caspase in tissue damage and functional deterioration. Similar findings were reported after caspase-3 inhibition in a model of controlled cortical impact, although behavioral status was unchanged (Clark et al., 2000). The parenchymal injection scheme employed in the latter study may have led to local tissue preservation, but prevented diffusion of z-DEVD-fmk to brain regions (cortex, hippocampus) that are represented in behavioral outcome measures. Caspase-1 has also been implicated in TBI, but here again, the data are mixed. The selective caspase-1 inhibitor z-YVAD-fmk reduced lesion volume in a mouse cortical contusion model, and dominant-negative caspase-1 mu-

tant mice showed improved neurological function and reduced lesion volumes (Fink et al., 1999). However, activation of caspase-1 was not significantly elevated after lateral fluid-percussion injury, though mRNA for the pro-form did increase (Yakovlev et al., 1997). Nonetheless, caspase-1 activation has been observed after clinical head injury (Clark et al., 1999). Whether such discrepancies reflect potential ischemic/metabolic complications associated with clinical head injury and/or model specific anomalies remains to be determined. Specific proof of an important role for caspases-8 or -9 awaits additional studies, perhaps with ribozyme constructs, given issues with the specificity of currently available selective inhibitors for these caspases.

In addition to inhibition of caspases, z-VAD-fmk was recently found to inhibit calpains (Wolf et al., 1999; Blomgren et al., 2001), enzymes which are independently recognized as important mediators of necrotic cell death, tissue loss and dysfunction in both traumatic and ischemic injuries (Kampfl et al., 1996; Saatman et al., 1996; Pike et al., 1998; McCracken et al., 1999; Zhao et al., 1999; Buki et al., 2000). The IC₅₀ of z-VAD is actually lower for m- and u-calpain (15 μ M) than for caspase-3

INTRINSIC APOPTOTIC PATHWAYS AFTER BRAIN INJURY

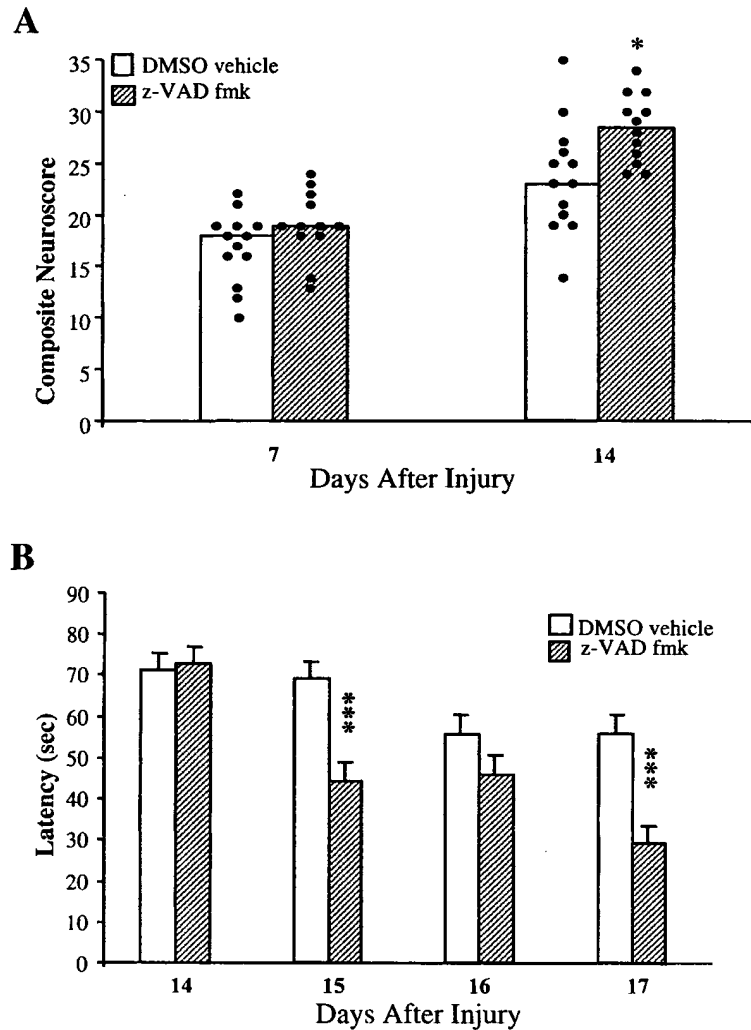


FIG. 11. Pan-caspase inhibitor z-VAD-fmk improves neurological recovery after traumatic brain injury. Z-VAD-fmk (25 mM in 5 μ L), was injected intracerebroventricularly 15 min after lateral fluid-percussion-induced brain injury. **(A)** Bars represent median combined score on three separate tests of motor function (flexion, pulsion, and inclined plane). Dots represent scores of individual animals (z-VAD-fmk, $n = 12$; vehicle [DMSO], $n = 13$). The best possible combined score is 35. Animals treated with z-VAD-fmk scored significantly better than DMSO controls 14 days after injury. * $p < 0.05$ versus vehicle by Mann-Whitney U comparison. **(B)** Bars represent the daily mean \pm SEM of latency to find a hidden platform for each group over four trials of a Morris water maze visuospatial learning paradigm. Four consecutive days of training (for a total of 16 trials) commenced 14 days after traumatic brain injury. Data are from the same animals/experiment shown in A. Z-VAD-fmk-treated animals performed significantly better on days 2 and 4 of water maze testing than did vehicle (DMSO)-treated controls. *** $p < 0.001$ for z-VAD-fmk versus vehicle from the same day. Maze data were analyzed by repeated measures ANOVA followed by post-hoc t tests with Bonferroni correction.

(60 μ M) (Blomgren et al., 2001); thus, it is possible that some of the beneficial effects of z-VAD-fmk may reflect inhibition of calpains. From a treatment perspective, an agent which inhibits both calpains and caspases may be optimal for clinical use, as it would target both necrotic and apoptotic cell death. This may be particularly important, since evidence suggests that prevention of either necrosis or apoptosis may shunt the injury response toward the alternate death pathway (Pohl et al., 1999;

Lewen et al., 2001; Susin et al., 1998). In addition, calpain- and caspase-mediated cell death pathways appear to share points of intersection as well as common features (reviewed in Wang, 2000). Illustrative examples include that the endogenous calpain inhibitor calpastatin is degraded by active caspases (Wang et al., 1998a), and that both enzymes degrade spectrin, a major component of cytoskeleton (Wang et al., 1998b).

In summary, we show evidence for the activation of

several caspases after TBI. Activation of caspases-3 and -9 was significantly elevated from hours to days after injury, in contrast to active caspase-8, which was expressed in only a few cells. In addition, the pan-caspase inhibitor z-VAD-fmk improved motor and cognitive neurological dysfunction after TBI. Together, these data support an involvement of several caspases in secondary cell death and neurological dysfunction after TBI, and suggest that anti-caspase treatment strategies may be potentially useful after traumatic brain injury in humans.

ACKNOWLEDGMENTS

We thank Sadia Aden, Anu Singh, and Tong Zhang for technical assistance. Grant support was provided by NIH NS36537 and DAMD17-99-2-9007 to A.I.F., KA1-9905-02 from the Christopher Reeve Paralysis Foundation to S.M.K., and NIH NS36821 to S. Krajewski.

REFERENCES

- ALLEN, J.W., KNOBLACH, S.M., and FADEN, A.I. (1999). Combined mechanical trauma and metabolic impairment *in vitro* induces NMDA receptor-dependent neuronal cell death and caspase-3-dependent apoptosis. *FASEB J.* **13**, 1875–1882.
- BEER, R., FRANZ, G., KRAJEWSKI, S., et al. (2001). Temporal and spatial profile of caspase 8 expression and proteolysis after experimental traumatic brain injury. *J. Neurochem.* **78**, 862–873.
- BEER, R., FRANZ, G., SCHOPF, M., et al. (2000a). Expression of Fas and Fas ligand after experimental traumatic brain injury in the rat. *J. Cereb. Blood Flow Metab.* **20**, 669–677.
- BEER, R., FRANZ, G., SRINIVASAN, A., et al. (2000b). Temporal profile and cell subtype distribution of activated caspase-3 following experimental traumatic brain injury. *J. Neurochem.* **75**, 1264–1273.
- BLOMGREN, K., ZHU, C., WANG, X., et al. (2001). Synergistic activation of caspase-3 by m-calpain after neonatal hypoxia-ischemia: a mechanism of “pathological apoptosis”? *J. Biol. Chem.* **276**, 10191–10198.
- BRADFORD, M.M. (1976). A rapid and sensitive method for the quantitation of microgram quantities of protein utilizing the principle of protein-dye binding. *Anal. Biochem.* **72**, 248–254.
- BRYAN, R.M., JR., CHERIAN, L., and ROBERTSON, C. (1995). Regional cerebral blood flow after controlled cortical impact injury in rats. *Anesth. Analg.* **80**, 687–695.
- BUKI, A., OKONKWO, D., WANG, K., et al. (2000). Cytochrome c release and caspase activation in traumatic axonal injury. *J. Neurosci.* **20**, 2825–2834.
- CHINNAIYAN, A.M., O’ROURKE, K., TEWARI, M., et al. (1995). FADD, a novel death domain-containing protein, interacts with the death domain of Fas and initiates apoptosis. *Cell* **81**, 505–512.
- CLARK, R., KOCHANNEK, P., CHEN, M., et al. (1999). Increases in Bcl-2 and cleavage of caspase-1 and caspase-3 in human brain after head injury. *FASEB J.* **13**, 813–821.
- CLARK, R., KOCHANNEK, P., WATKINS, S., et al. (2000). Caspase-3-mediated neuronal death after traumatic brain injury in rats. *J. Neurochem.* **74**, 740–753.
- CONTI, A.C., RAGHUPATHI, R., TROJANOWSKI, J.Q., et al. (1998). Experimental brain injury induces regionally distinct apoptosis during the acute and delayed post-traumatic period. *J. Neurosci.* **18**, 5663–5672.
- DE TORRES, C., MUNELL, F., FERRER, I., et al. (1997). Identification of necrotic cell death by the TUNEL assay in the hypoxic-ischemic neonatal rat brain. *Neurosci. Lett.* **230**, 1–4.
- ELDADAH, B.A., and FADEN, A.I. (2000). Caspase pathways, neuronal apoptosis, and CNS injury. *J. Neurotrauma* **17**, 811–829.
- ERTEL, W., KEEL, M., STOCKER, R., et al. (1997). Detectable concentrations of Fas ligand in cerebrospinal fluid after severe head injury. *J. Neuroimmunol.* **80**, 93–96.
- FINK, K., ZHU, J., NAMURA, S., et al. (1998). Prolonged therapeutic window for ischemic brain damage caused by delayed caspase activation. *J. Cereb. Blood Flow Metab.* **18**, 1071–1076.
- FINK, K., ANDREWS, L., BUTLER, W., et al. (1999). Reduction of post-traumatic brain injury and free radical production by inhibition of the caspase-1 cascade. *Neuroscience* **94**, 1213–1218.
- FOX, G.B., FAN, L., LEVASSEUR, R.A., et al. (1998). Sustained sensory/motor and cognitive deficits with neuronal apoptosis following controlled cortical impact brain injury in the mouse. *J. Neurotrauma* **15**, 599–614.
- HAKEM, R., HAKEM, A., DUNCAN, G.S., et al. (1998). Differential requirement for caspase 9 in apoptotic pathways *in vivo*. *Cell* **94**, 339–352.
- HARA, H., FRIEDLANDER, R.M., GAGLIARDINI, V., et al. (1997). Inhibition of interleukin 1 β converting enzyme family proteases reduces ischemic and excitotoxic neuronal damage. *Proc. Natl. Acad. Sci. U.S.A.* **94**, 2007–2012.
- HUANG, X., VANGELDEREN, J., CALVA-CERQUIERA, D., et al. (2000). Differential activation of caspases after traumatic spinal cord injury in the rat. In: *Society for Neuroscience*. Society for Neuroscience, 30th Annual Meeting, New Orleans, LA.
- JUO, P., KUO, C.J., YUAN, J., et al. (1998). Essential requirement for caspase-8/FLICE in the initiation of the Fas-induced apoptotic cascade. *Curr. Biol.* **8**, 1001–1008.

INTRINSIC APOPTOTIC PATHWAYS AFTER BRAIN INJURY

- KAMPFL, A., POSMANTUR, R., NIXON, R., et al. (1996). mu-Calpain activation and calpain-mediated cytoskeletal proteolysis following traumatic brain injury. *J. Neurochem.* **67**, 1575–1583.
- KANG, S.J., WANG, S., HARA, H., et al. (2000). Dual role of caspase-11 in mediating activation of caspase-1 and caspase-3 under pathological conditions. *J. Cell Biol.* **149**, 613–622.
- KEANE, R.W., KRAYDIEH, S., LOTOCKI, G., et al. (2001a). Apoptotic and antiapoptotic mechanisms after traumatic brain injury. *J. Cereb. Blood Flow Metab.* **21**, 1189–1198.
- KEANE, R.W., KRAYDIEH, S., LOTOCKI, G., et al. (2001b). Apoptotic and anti-apoptotic mechanisms following spinal cord injury. *J. Neuropathol. Exp. Neurol.* **60**, 422–429.
- KNOBLACH, S., FAN, L., and FADEN, A. (1999). Early neuronal expression of tumor necrosis factor- α after experimental brain injury contributes to neurological impairment. *J. Neuroimmunol.* **95**, 115–125.
- KRAJEWSKA, M., WANG, H.G., KRAJEWSKI, S., et al. (1997). Immunohistochemical analysis of *in vivo* patterns of expression of CPP32 (Caspase-3), a cell death protease. *Cancer Res.* **57**, 1605–1613.
- KRAJEWSKI, S., KRAJEWSKA, M., ELLERBY, L.M., et al. (1999). Release of caspase-9 from mitochondria during neuronal apoptosis and cerebral ischemia. *Proc. Natl. Acad. Sci. U.S.A.* **96**, 5752–5757.
- LEWEN, A., SKOGLOSA, Y., CLAUSEN, F., et al. (2001). Paradoxical increase in neuronal DNA fragmentation after neuroprotective free radical scavenger treatment in experimental traumatic brain injury. *J. Cereb. Blood Flow Metab.* **21**, 344–350.
- LI, M., ONA, V.O., CHEN, M., et al. (2000). Functional role and therapeutic implications of neuronal caspase-1 and -3 in a mouse model of traumatic spinal cord injury. *Neuroscience* **99**, 333–342.
- LI, P., NIJHAWAN, D., BUDIHARDJO, I., et al. (1997). Cytochrome c and dATP-dependent formation of Apaf-1/caspase-9 complex initiates an apoptotic protease cascade. *Cell* **91**, 479–489.
- LIAO, J., XU, X., and WARGOVICH, M.J. (2000). Direct reprobing with anti- β -actin antibody as an internal control for western blotting analysis. *Biotechniques* **28**, 216–218.
- LODDICK, S.A., MACKENZIE, A., and ROTHWELL, N.J. (1996). An ICE inhibitor, z-VAD-DCB attenuates ischaemic brain damage in the rat. *Neuroreport* **7**, 1465–1468.
- LU, J., MOOCHHALA, S., KAUR, C., et al. (2000). Changes in apoptosis-related protein (p53, Bax, Bcl-2 and Fos) expression with DNA fragmentation in the central nervous system in rats after closed head injury. *Neurosci. Lett.* **290**, 89–92.
- MA, J., ENDRES, M., and MOSKOWITZ, M.A. (1998). Synergistic effects of caspase inhibitors and MK-801 in brain injury after transient focal cerebral ischaemia in mice. *Br. J. Pharmacol.* **124**, 756–762.
- MATSUSHITA, K., WU, Y., QIU, J., et al. (2000). Fas receptor and neuronal cell death after spinal cord ischemia. *J. Neurosci.* **20**, 6879–6887.
- MATTSON, M.P., KELLER, J.N., and BEGLEY, J.G. (1998). Evidence for synaptic apoptosis. *Exp. Neurol.* **153**, 35–48.
- MCCRACKEN, E., HUNTER, A., PATEL, S., et al. (1999). Calpain activation and cytoskeletal protein breakdown in the corpus callosum of head-injured patients. *J. Neurotrauma.* **16**, 749–761.
- MCINTOSH, T.K., VINK, R., NOBLE, L., et al. (1989). Traumatic brain injury in the rat: characterization of a lateral fluid-percussion model. *Neuroscience* **28**, 233–244.
- NAMURA, S., ZHU, J., FNK, K., et al. (1998). Activation and cleavage of caspase-3 in apoptosis induced by experimental cerebral ischemia. *J. Neurosci.* **18**, 3659–3668.
- NEWCOMB, J., ZHAO, X., PIKE, B., et al. (1999). Temporal profile of apoptotic-like changes in neurons and astrocytes following controlled cortical impact injury in the rat. *Exp. Neurol.* **158**, 76–88.
- NG, I., YEO, T., TANG, W., et al. (2000). Apoptosis occurs after cerebral contusions in humans. *Neurosurgery* **46**, 949–956.
- PAXINOS, G., and WATSON, C. (1986). *The Rat and Brain in Stereotaxic Coordinates*. Academic Press: Sydney.
- PIKE, B.R., ZHAO, X., NEWCOMB, J.K., et al. (1998). Regional calpain and caspase-3 proteolysis of α -spectrin after traumatic brain injury. *Neuroreport* **9**, 2437–2442.
- POHL, D., BITTIGAU, P., ISHIMARU, M.J., et al. (1999). N-Methyl-D-aspartate antagonists and apoptotic cell death triggered by head trauma in developing rat brain. *Proc. Natl. Acad. Sci. U.S.A.* **96**, 2508–2513.
- REED, J.C. (2000). Mechanisms of apoptosis. *Am. J. Pathol.* **157**, 1415–1430.
- RINK, A., FUNG, K.M., TROJANOWSKI, J.Q., et al. (1995). Evidence of apoptotic cell death after experimental traumatic brain injury in the rat. *Am. J. Pathol.* **147**, 1575–1583.
- SAATMAN, K.E., MURAI, H., BARTUS, R.T., et al. (1996). Calpain inhibitor AK295 attenuates motor and cognitive deficits following experimental brain injury in the rat. *Proc. Natl. Acad. Sci. U.S.A.* **93**, 3428–3433.
- SALEH, A., SRINIVASULA, S.M., ACHARYA, S., et al. (1999). Cytochrome c and dATP-mediated oligomerization of Apaf-1 is a prerequisite for procaspase-9 activation. *J. Biol. Chem.* **274**, 17941–17945.
- SHOHAMI, E., BASS, R., WALLACH, D., et al. (1996). Inhibition of tumor necrosis factor α (TNF α) activity in rat brain is associated with cerebroprotection after closed head injury. *J. Cereb. Blood Flow Metab.* **16**, 378–384.

- SLEE, E.A., HARTE, M.T., KLUCK, R.M., et al. (1999). Ordering the cytochrome c-initiated caspase cascade: hierarchical activation of caspases-2, -3, -6, -7, -8, and -10 in a caspase-9-dependent manner. *J. Cell Biol.* **144**, 281–292.
- SPRINGER, J.E., AZBILL, R.D., and KNAPP, P.E. (1999). Activation of the caspase-3 apoptotic cascade in traumatic spinal cord injury. *Nat. Med.* **5**, 943–946.
- STENNICKE, H.R., JURGENSMEIER, J.M., SHIN, H., et al. (1998). Pro-caspase-3 is a major physiologic target of caspase-8. *J. Biol. Chem.* **273**, 27084–27090.
- SUSIN, S.A., DAUGAS, E., RAVAGNAN, L., et al. (2000). Two distinct pathways leading to nuclear apoptosis. *J. Exp. Med.* **192**, 571–580.
- SUSIN, S.A., ZAMZAMI, N., and KROEMER, G. (1998). Mitochondria as regulators of apoptosis: doubt no more. *Biochim. Biophys. Acta* **1366**, 151–165.
- TALANIAN, R.V., QUINLAN, C., TRAUTZ, S., et al. (1997). Substrate specificities of caspase family proteases. *J. Biol. Chem.* **272**, 9677–9682.
- THOMAS, D.A., DU, C., XU, M., et al. (2000). DFF45/ICAD can be directly processed by granzyme B during the induction of apoptosis. *Immunity* **12**, 621–632.
- THORNBERRY, N.A., RANO, T.A., PETERSON, E.P., et al. (1997). A combinatorial approach defines specificities of members of the caspase family and granzyme B. Functional relationships established for key mediators of apoptosis. *J. Biol. Chem.* **272**, 17907–17911.
- VARFOLOMEEV, E.E., SCHUCHMANN, M., LURIA, V., et al. (1998). Targeted disruption of the mouse caspase 8 gene ablates cell death induction by the TNF receptors, Fas/Apo1, and DR3 and is lethal prenatally. *Immunity* **9**, 267–276.
- VELIER, J.J., ELLISON, J.A., KIKLY, K.K., et al. (1999). Caspase-8 and caspase-3 are expressed by different populations of cortical neurons undergoing delayed cell death after focal stroke in the rat. *J. Neurosci.* **19**, 5932–5941.
- WANG, K.K. (2000). Calpain and caspase: can you tell the difference? *Trends Neurosci.* **23**, 20–26.
- WANG, K.K., POSMANTUR, R., NATH, R., et al. (1998b). Simultaneous degradation of alphaII- and betaII-spectrin by caspase 3 (CPP32) in apoptotic cells. *J. Biol. Chem.* **273**, 22490–22497.
- WANG, K.K., POSMANTUR, R., NADIMPALLI, R., et al. (1998a). Caspase-mediated fragmentation of calpain inhibitor protein calpastatin during apoptosis. *Arch. Biochem. Biophys.* **356**, 187–196.
- WOLF, B.B., GOLDSTEIN, J.C., STENNICKE, H.R., et al. (1999). Calpain functions in a caspase-independent manner to promote apoptosis-like events during platelet activation. *Blood* **94**, 1683–1692.
- YAKOVLEV, A.G., KNOBLACH, S.M., FAN, L., et al. (1997). Activation of CPP32-like caspases contributes to neuronal apoptosis and neurological dysfunction after traumatic brain injury. *J. Neurosci.* **17**, 7415–7424.
- YANG, X., STENNICKE, H.R., WANG, B., et al. (1998). Granzyme B mimics apical caspases. Description of a unified pathway for trans-activation of executioner caspase-3 and -7. *J. Biol. Chem.* **273**, 34278–34283.
- ZHAO, X., PIKE, B.R., NEWCOMB, J.K., et al. (1999). Mito-toxin induces calpain but not caspase-3 activation and necrotic cell death in primary septo-hippocampal cultures. *Neurochem. Res.* **24**, 371–382.
- ZOU, H., LI, Y., LIU, X., et al. (1999). An APAF-1/cytochrome c multimeric complex is a functional apoptosome that activates procaspase-9. *J. Biol. Chem.* **274**, 11549–11556.

Address reprint requests to:
Susan M. Knoblach, Ph.D.

Georgetown University Medical Center
EP-16, New Research Building
3970 Reservoir Rd. NW
Washington, DC 20007

E-mail: knoblachs@giccs.georgetown.edu

REPORTS

We propose the following model for CTX phage secretion. CTX ϕ 's homolog of fl pI, Zot, a presumed inner membrane protein (21), interacts with a multimer of the outer membrane protein EpsD and thereby induces opening of this outer membrane channel, through which the phage is released. Additional interactions between Zot, EpsD, and phage coat proteins are also likely; interactions between CTX phage-encoded proteins and proteins of the *eps* apparatus other than EpsD are probably not required. It is not known whether a single EpsD multimer can interact simultaneously with components of both secretory pathways or whether the phage and protein secretory processes compete for access to the outer membrane channel.

Phage exploitation of a host secretin has not been demonstrated previously; however, analyses of the genomes of additional filamentous phages suggest that reliance upon a chromosome-encoded secretin may be a common strategy for phage secretion. Within the GenBank database, there are at least five filamentous phages other than CTX ϕ —fsl1, Vf12, Vf33, Cf1c, and Pf1—that do not appear to encode a pIV homolog and thus may rely upon a chromosomal protein instead. All these phages infect bacterial species that contain type II secretion systems. In contrast, the filamentous coliphages that encode a phage-specific secretin infect a host that generally does not produce a secretory apparatus (22). Thus, coliphages may have been constrained during their evolution to rely upon a phage-encoded secretin. Alternatively, phage-encoded secretins may grant access to a broader range of host species or confer some other evolutionary advantage.

It is somewhat surprising that EpsD can mediate both CTX ϕ and CT secretion. Most secretins are unable to function within heterologous systems, even systems composed of very similar proteins with highly related substrates (9, 23). Furthermore, the two secretory processes to which EpsD contributes are markedly different. Phage export releases a cytoplasmic DNA molecule coated with inner membrane-derived coat proteins, whereas type II secretion systems export only free, periplasmic proteins. Nonetheless, in *V. cholerae*, these two disparate classes of secretion substrates both appear to pass through an outer membrane pore composed of EpsD. The convergence of phage and protein secretion pathways may be a clue that structurally similar periplasmic complexes are assembled during each process. Indirect evidence in support of this hypothesis has already been provided by the findings that both pathways bear similarities, at either the sequence or structural level, to type IV pilus assembly (2). Our finding that a filamentous phage and a type II secretion apparatus use the same secretin provides additional evidence that the two export systems have a common evolutionary origin and suggests that they may still maintain mechanistic similarities.

References and Notes

1. B. B. Finlay and S. Falkow, *Microbiol. Mol. Biol. Rev.* **61**, 136 (1997).
2. M. Russel, *J. Mol. Biol.* **279**, 485 (1998).
3. P. J. Christie, *J. Bacteriol.* **179**, 3085 (1997).
4. R. Binet, S. Letoffe, J. M. Ghigo, P. Deleplaire, C. Wandersman, *Gene* **192**, 7 (1997).
5. K. J. Fullner and J. J. Mekalanos, *Infect. Immun.* **67**, 1393 (1999).
6. M. K. Waldor and J. J. Mekalanos, *Science* **272**, 1910 (1996).
7. D. K. Marciano, M. Russel, S. M. Simon, *Science* **284**, 1516 (1999).
8. M. Russel, *Trends Microbiol.* **3**, 223 (1995).
9. ———, *J. Mol. Biol.* **231**, 689 (1993).
10. We searched the *V. cholerae* database with the Institute for Genome Research's BLAST Search Engine for Unfinished Microbial Genomes (www.tigr.org/cgi-bin/BlastSearch/blast.cgi).
11. M. Sandkvist et al., *J. Bacteriol.* **179**, 6994 (1997).
12. J. B. Kaper, J. G. Morris Jr., M. M. Levine, *Clin. Microbiol. Rev.* **8**, 48 (1995).
13. The targeting vector is described by A. Ali et al., *Infect. Immun.* **68**, 1967 (2000).
14. B. M. Davis, E. H. Lawson, M. Sandkvist, M. K. Waldor, H. H. Kimsey, unpublished data.
15. G. D. Pearson, A. Woods, S. L. Chiang, J. J. Mekalanos, *Proc. Natl. Acad. Sci. U.S.A.* **90**, 3750 (1993).
16. C. C. Hase and R. A. Finkelstein, *J. Bacteriol.* **173**, 3311 (1991).
17. EpsD (base pairs 1159 to 3245 of the *eps* gene cluster; GenBank accession number L33796) was cloned into the Cm^R, isopropyl- β -D-thiogalactopyranoside (IPTG)-inducible plasmid pGZ119HE (24).
18. M. Judson and J. J. Mekalanos, unpublished data.
19. pMS43 and pMS42 are equivalent to pMS27 and pMS12 (25), except that they are Cm^R.
20. pCTX-Kn is a more stable replicon than pCTX-Ap; this probably accounts for the consistently higher phage titers from strains containing pCTX-Kn. Transduction assays were performed as described in Table 1.
21. E. V. Koonin, *FEBS Lett.* **312**, 3 (1992).
22. A. P. Pugsley and O. Francetic, *Cell Mol. Life Sci.* **54**, 347 (1998).
23. M. Lindeberg, G. P. Salmond, A. Collmer, *Mol. Microbiol.* **20**, 175 (1996).
24. M. Lessl et al., *J. Bacteriol.* **174**, 2493 (1992).
25. M. Sandkvist, M. Bagdasarian, S. P. Howard, V. J. DiRita, *EMBO J.* **14**, 1664 (1995).
26. M. Sandkvist, L. P. Hough, M. M. Bagdasarian, M. Bagdasarian, *J. Bacteriol.* **181**, 3129 (1999).
27. We thank M. Russel, A. Camilli, A. L. Sonenshein, and Waldor lab colleagues for helpful suggestions and critical reading of the manuscript and A. Kane and the New England Medical Center GRASP Center for preparation of plates and media. S.S. thanks G. Morris and J. Johnson for research support. This work was supported by NIH grant AI-42347 to M.K.W. M.K.W. is a Pew Scholar in the Biomedical Sciences. M.S. was supported by funds from the American Red Cross. S.S. was supported by a University of Maryland Intramural Grant.

23 November 1999; accepted 25 February 2000

Functional Role of Caspase-1 and Caspase-3 in an ALS Transgenic Mouse Model

Mingwei Li,¹ Victor O. Ona,¹ Christelle Guégan,² Minghua Chen,¹ Vernice Jackson-Lewis,² L. John Andrews,¹ Adam J. Olszewski,¹ Philip E. Stieg,¹ Jean-Pyo. Lee,⁴ Serge Przedborski,^{2,3} Robert M. Friedlander^{1*}

Mutations in the copper/zinc superoxide dismutase (SOD1) gene produce an animal model of familial amyotrophic lateral sclerosis (ALS), a fatal neurodegenerative disorder. To test a new therapeutic strategy for ALS, we examined the effect of caspase inhibition in transgenic mice expressing mutant human SOD1 with a substitution of glycine to alanine in position 93 (mSOD1^{G93A}). Intracerebroventricular administration of zVAD-fmk, a broad caspase inhibitor, delays disease onset and mortality. Moreover, zVAD-fmk inhibits caspase-1 activity as well as caspase-1 and caspase-3 mRNA up-regulation, providing evidence for a non-cell-autonomous pathway regulating caspase expression. Caspases play an instrumental role in neurodegeneration in transgenic mSOD1^{G93A} mice, which suggests that caspase inhibition may have a protective role in ALS.

ALS is a neurodegenerative disorder involving motor neuron loss in the brain, brainstem, and spinal cord and resulting in progressive paralysis. ALS is universally fatal, with an average mortality of 5 years after onset (1).

Familial ALS accounts for 10 to 20% of all cases; the remaining cases are sporadic. Both forms of the disease have indistinguishable clinical and histopathological features (2). Mutations of the SOD1 (mSOD1) gene have been identified in some cases of familial ALS (3, 4). Transgenic mice have been generated expressing different mSOD1 genes identified in ALS patients (5, 6). Like humans with ALS, these mice develop an adult-onset progressive motor deterioration universally leading to early death and have been used as models for the disease (5, 7). Although the mechanisms leading to motor neuron degen-

¹Neuroapoptosis Laboratory and Neurosurgical Service, Department of Surgery, Brigham and Women's Hospital, Harvard Medical School, Boston, MA 02115, USA. ²Department of Neurology, ³Department of Pathology, Columbia University, New York, NY 10032, USA. ⁴Department of Medicine, University of Chicago, Chicago, IL 60637, USA.

*To whom correspondence should be addressed. E-mail: rfriedlander@rics.bwh.harvard.edu

REPORTS

eration in ALS are not thoroughly understood, evidence points to apoptotic pathways playing a role in human and mouse models of the disease (8–10). The caspase family plays an important role in the pathogenesis of central nervous system (CNS) disorders featuring apoptosis (11–17). Recent reports provide evidence for caspase-3 activation in human ALS (18). In addition, mSOD1 expression induces caspase-dependent neuronal apoptosis *in vitro* (19). The importance of apoptotic pathways in the pathogenesis of ALS is supported by the neuroprotective effects of both the Bcl-2 transgene and the dominant-negative caspase-1 inhibitor transgene in transgenic mSOD1^{G93A} mice (9, 10). Evidence exists of caspase-1 and caspase-3 activation in ALS mice (20). Here we provide direct evidence for a functional role of caspase-1 and caspase-3 in presymptomatic and end-stage mSOD1^{G93A} mice and demonstrate a therapeutic benefit of pharmacologic caspase inhibition (21). In addition, we demonstrate that caspase-1 is activated in the human ALS spinal cord.

Because caspase-1 activity has been detected in spinal cords of mSOD1^{G93A} mice and caspase-3 activity has been detected in the same mice and in humans with ALS, we evaluated the expression of activated caspase-1 and caspase-3 in spinal motor neurons of mSOD1^{G93A} mice (8, 20, 22). We performed double staining with a neuron-specific antibody

(NeuN) and either an antibody to activated caspase-1 or to activated caspase-3 (23). Beginning at 70 days of age and thereafter at 90 and 110 days, caspase-1 and caspase-3 staining were shown primarily in NeuN-positive cells in the ventral horn of the spinal cord of transgenic mSOD1^{G93A} mice (Fig. 1, A through P). Caspase-positive NeuN-positive cells tended to be smaller than caspase-negative NeuN-positive cells, suggesting a more advanced apoptotic phenotype. Caspase-1 or caspase-3 staining was not detected in spinal cord sections of wild-type littermates or in the brain, spinal cord white matter, or dorsal horn of transgenic mSOD1^{G93A} mice. We evaluated by Western blot the caspase-1 and caspase-3 antibodies used for immunostaining to confirm their specificity in spinal cord tissue for the activated caspase subunits (Fig. 1, Q and S). We compared spinal cord lysates of presymptomatic (50 days) and symptomatic (90 days) mSOD1^{G93A} mice using other caspase-1 and caspase-3 antibodies that recognize both the procaspase and the cleaved activated subunit (Fig. 1, R and T). Activated caspase-1 and caspase-3 were detected in symptomatic mice and not in presymptomatic mice. In addition, the activated caspase antibodies specifically recognized the cleaved form of caspase-1 and caspase-3 and not the procaspase (Fig. 1, Q and S).

In light of the fact that caspase-1 and caspase-3 are activated in spinal cord motor

neurons of transgenic mSOD1^{G93A} mice, we evaluated their functional contribution to the progression of the disease by pharmacologically inhibiting them. *N*-benzyloxycarbonyl-Val-Asp-fluoromethylketone (zVAD-fmk) was selected as the agent to be evaluated because it is a broad caspase inhibitor that is well tolerated by mice in prolonged administration protocols, and it has a proven efficacy in other neurodegenerative disease models (14). We used osmotic pumps for delivery of zVAD-fmk into the cerebral ventricle (24). Osmotic pumps were implanted into 60-day-old mice. At this age there has been no significant neuronal loss, clinically representing the late presymptomatic stage of the disease. Pumps continuously delivered the drug for 56 days. The onset of motor and/or coordination deficits was defined as the first day that a mouse could not remain on the Rotarod for 7 min at a speed of 20 rpm (25). Mortality was scored as the age of death or the age when the mouse was unable to right itself within 30 s. The length of time before disease onset in transgenic mice treated with either vehicle or 300 μ g of zVAD-fmk per 20 g of body weight for 28 days (300 μ g/20 g body weight/28 days) was 103.5 ± 2.8 days and 123.7 ± 6.8 days, respectively. zVAD-fmk delayed the disease-induced onset of Rotarod deficit by 20.2 ± 6.4 days. In addition, zVAD-fmk treatment prolonged survival from 126.1 ± 3.0 days to 153.3 ± 8.8 days as compared with

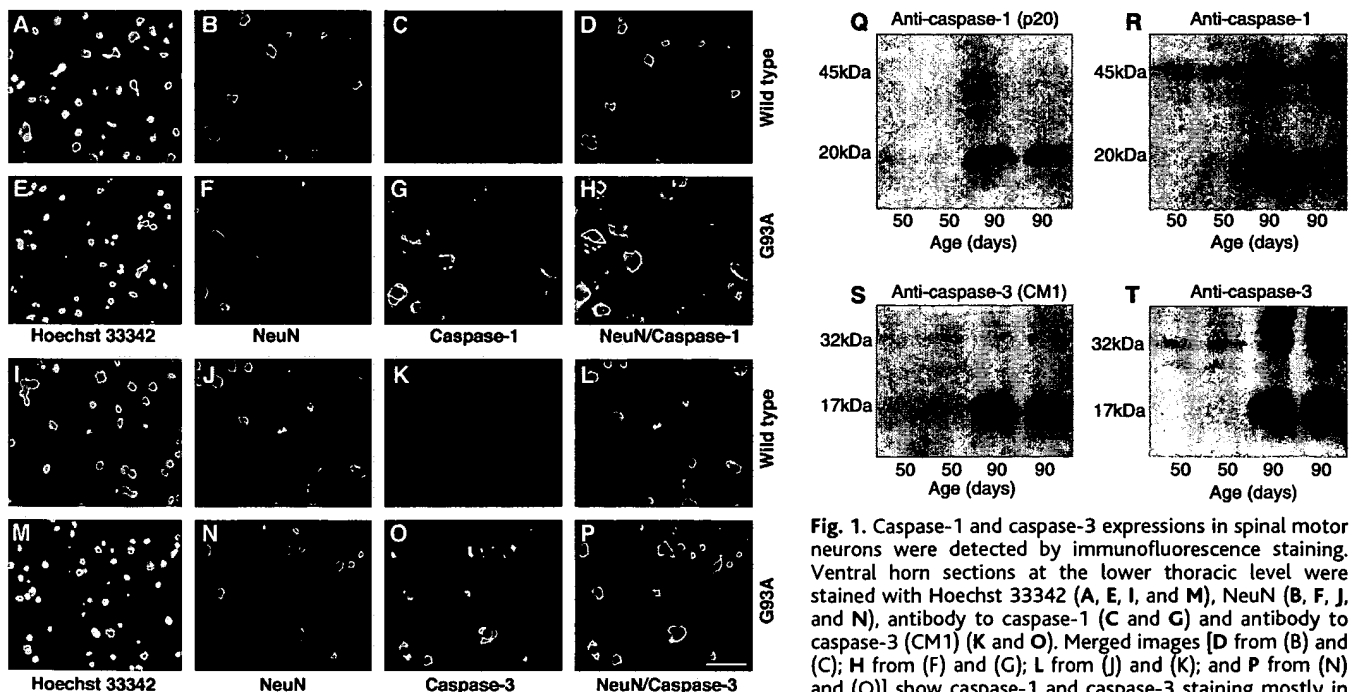


Fig. 1. Caspase-1 and caspase-3 expressions in spinal motor neurons were detected by immunofluorescence staining. Ventral horn sections at the lower thoracic level were stained with Hoechst 33342 (A, E, I, and M), NeuN (B, F, J, and N), antibody to caspase-1 (C and G) and antibody to caspase-3 (CM1) (K and O). Merged images [D from (B) and (C); H from (F) and (G); L from (J) and (K); and P from (N) and (O)] show caspase-1 and caspase-3 staining mostly in NeuN-positive but also in NeuN-negative cells, demonstrating

induction of both caspases in mSOD1 mice. No caspase-1 or caspase-3 staining was detected in the dorsal horn or in spinal cord sections from wild-type littermates [(C) and (K)]. The staining is representative of 70-, 90-, and 110-day-old wild-type and mSOD1 mice ($n = 3$ mice per group). Scale bar, 30 μ m. (Q through T) Western blot of lysates from 50- and 90-day-old mSOD1^{G93A} mice. (Q) Activated caspase-1 antibody (p20) used in the immunostaining; (R) caspase-1 antibody, which recognizes procaspase-1 (p45) and activated caspase-1; (S) activated caspase-3 antibody (p17) used in the immunostaining; and (T) caspase-3 antibody, which recognizes procaspase-3 (p32) and activated caspase-3. Each lane was loaded with 50 μ g of protein.

REPORTS

vehicle-treated littermates, representing a life-span prolonged by 22% (Fig. 2, A through C). zVAD-fmk-mediated neuroprotection was dose-dependent because mice treated with a lower dose (100 $\mu\text{g}/20\text{ g body weight}/28\text{ days}$) survived 11% longer than vehicle-treated mice. However, this protection did not reach statistical significance. Motor strength and coordination, as evaluated by Rotarod performance, were significantly improved in zVAD-fmk-treated mice (Fig. 2, D through F).

A hallmark of ALS in humans, as well as in mSOD1^{G93A} transgenic mice, is a progressive loss of spinal motor neurons (2, 5, 6). To evaluate the effect of zVAD-fmk on motor neuron loss, we compared the numbers of cervical and lumbar motor neurons in both zVAD-fmk- and vehicle-treated mSOD1^{G93A} mice at 110 days of age (26). At this stage, vehicle-treated mice are at the end stage of the disease. zVAD-fmk-treated mice had a significantly greater number of motor neurons at the cervical level as compared with vehicle-treated mice (Fig. 3A). At the lumbar level, zVAD-fmk-treated mice also had a greater number of motor neurons; however, this did not reach statistical significance (Fig. 3B). The greater protection from motor neuron loss at the cervical level likely represents a zVAD-fmk concentration effect. Because zVAD-fmk is delivered to the cerebral ventricle, the concentration reaching cervical motor neurons is higher than in the lumbar area, demonstrating a concentration-dependent effect of

zVAD-fmk neuroprotection. Degeneration of phrenic nerve axons was also significantly inhibited in zVAD-fmk-treated mice (Fig. 3C). zVAD-fmk extends survival of mSOD1 mice by inhibiting motor neuron cell death.

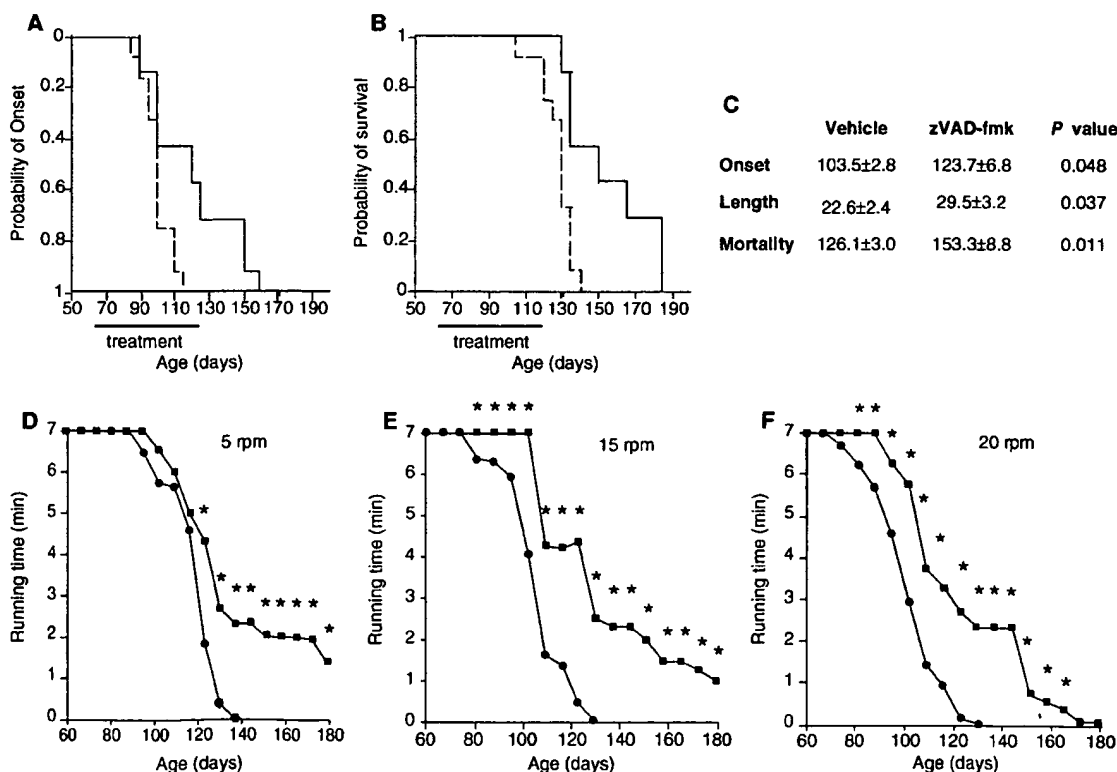
Given that caspase-1 is activated in the spinal cords of mSOD1^{G93A} mice, we evaluated whether zVAD-fmk inhibits caspase-1 activity (22). Detection of mature interleukin 1- β (IL-1 β) has been used as a sensitive and specific marker of caspase-1 activation (11–14, 27). Mature IL-1 β levels were 2.4-fold higher in spinal cord samples of 100-day-old mSOD1^{G93A} mice when compared with age-matched wild-type littermates, indicating caspase-1 activation (28). zVAD-fmk treatment resulted in a 37% reduction of caspase-1 activity in the spinal cords of mSOD1^{G93A} mice (Fig. 3D). We next evaluated whether caspase-1 activation is also detected in the spinal cords of humans with ALS. We demonstrated an 81.5% elevation of caspase-1 activity in the spinal cord of humans with ALS when compared with normal controls (Fig. 3E). These results further validate this mouse as a relevant disease model. Because mature IL-1 β plays a functional role in neuronal cell death, zVAD-fmk-mediated neuroprotection in mSOD1 mice is likely mediated in part by inhibiting activation of this cytokine (19, 29, 30).

Because increased caspase-1 and caspase-3 activity in transgenic mSOD1^{G93A} mice has been demonstrated, we investigated whether

these caspases might also be regulated at the transcription level (20, 22). Using reverse transcriptase-polymerase chain reaction (RT-PCR), we quantified caspase-1 and caspase-3 mRNA expression in transgenic mSOD1^{G93A} mice and evaluated the effect of caspase inhibition on their expression (31). Beginning at 70 days of age, caspase-1 mRNA levels began to increase, peaking at 3.2-fold above wild-type levels at 90 days (Fig. 4, A and B). Caspase-3 mRNA elevation began at 90 days of age and peaked at 110 days with levels 2.6-fold above those in the wild-type mice (Fig. 4, C and D). Caspase-1 and caspase-3 mRNA levels were significantly reduced in zVAD-fmk-treated mice by 27 and 34%, respectively, as compared with vehicle-treated mSOD1 littermates.

zVAD-fmk is an enzymatic caspase inhibitor. However, decreased caspase mRNA expression levels mediated by zVAD-fmk are consistent with a detrimental role of intracellular and extracellular diffusible factors resulting from caspase activation (19, 30). Caspase inhibition decreases the production of diffusible factors such as mature IL-1 β and free radicals (11–14). In addition, blocking extracellular binding of endogenously produced IL-1 β inhibits cell death, suggesting a proapoptotic role of extracellular caspase downstream mediators (19, 30). Furthermore, direct injection of IL-1 β into the rat brain induces neuronal apoptosis (32). As in human neurodegeneration, cell loss in mSOD1 mice is not synchronized—it occurs over a pro-

Fig. 2. Cumulative probability of onset of Rotarod deficits (A) and survival (B) in mSOD1 mice. Survival was significantly prolonged and the onset of Rotarod deficit was significantly delayed in mSOD1 mice treated with zVAD-fmk when compared with vehicle-treated transgenic littermates. Solid line, zVAD-fmk; dashed line, vehicle. (C) Table of onset of motor deficit and mortality. Motor function was tested with the Rotarod at 5 (D), 15 (E), and 20 rpm (F). Testing was terminated either when the mice fell from the rod or at 7 min if the mouse remained on the rod. Mice treated with zVAD-fmk performed significantly better than vehicle-treated mice (* $P < 0.05$; vehicle, $n = 12$ mice; zVAD-fmk, $n = 7$ mice). Square, zVAD-fmk; circle, vehicle.



REPORTS

longed period of time. Therefore, because neighboring cells are at different stages of the apoptotic pathway, diffusible factors produced by cells in which caspases are activated likely have a detrimental effect on neighboring cells,

resulting in caspase up-regulation. Hence, caspase inhibition in one cell likely delays a neighboring cell from initiating the caspase cascade. Thus, unlike in *Caenorhabditis elegans*, the caspase cascade in vertebrates is not cell-auton-

omous but rather is influenced in a paracrine fashion by the extracellular microenvironment (33).

We demonstrate inhibition of disease progression and extended survival in a transgenic mouse model of ALS by pharmacologic caspase inhibition, and we show that caspase-1 and caspase-3 are expressed in neurons in transgenic mSOD1^{G93A} mice. Furthermore, we demonstrate that caspase-1 is activated in spinal cord samples from humans affected by ALS. Consistent with in vitro evidence in nonneuronal cell lines, we demonstrate that caspase-1 mRNA is up-regulated before that of caspase-3, suggesting that caspase-1 mediates early disease processes and that caspase-3 may be involved in the terminal stage of the apoptotic pathway (34, 35). Interestingly, in vitro caspase-1 activates caspase-3 (36). In addition to an inflammatory role of caspase-1, early caspase-1 neuronal expression indicates its importance as an early mediator of the neuronal apoptotic cascade. Because of the extensive similarities in the behavioral, histologic, and molecular mechanisms between the mSOD1^{G93A} transgenic mouse and humans with ALS (familial and sporadic), these results provide therapeutic information relevant to the human disease. These results indicate that caspases play a role not only in the end stage of ALS but also in the presymptomatic progression of the disease, which suggests that therapy targeted at inhibiting caspase function should begin in the presymptomatic stage of ALS.

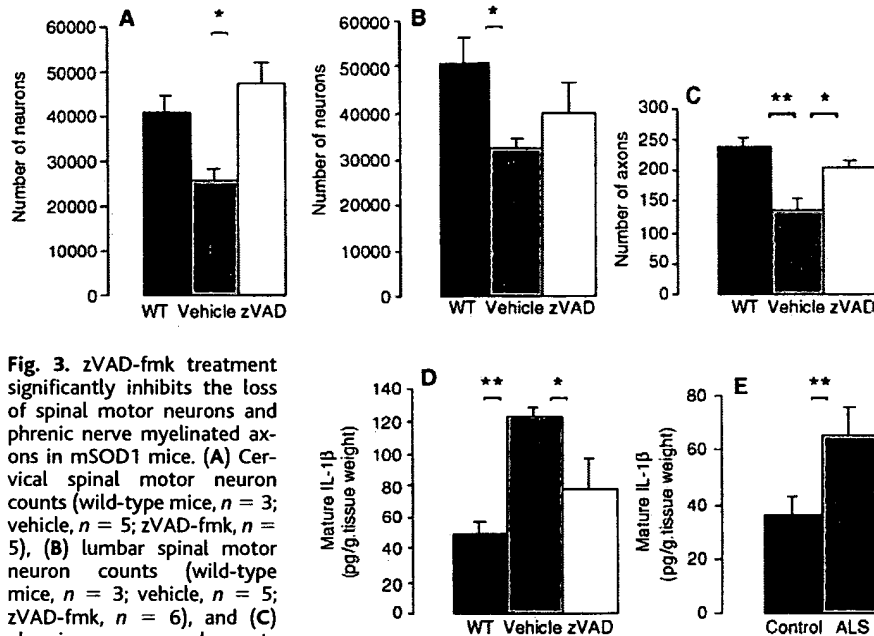


Fig. 3. zVAD-fmk treatment significantly inhibits the loss of spinal motor neurons and phrenic nerve myelinated axons in mSOD1 mice. (A) Cervical spinal motor neuron counts (wild-type mice, $n = 3$; vehicle, $n = 5$; zVAD-fmk, $n = 5$), (B) lumbar spinal motor neuron counts (wild-type mice, $n = 3$; vehicle, $n = 5$; zVAD-fmk, $n = 6$), and (C) phrenic nerve axonal counts ($n = 6$ mice per group) in 110-day old mice. Mature IL-1 β levels, indicating caspase-1 activation in (D) mSOD1 mice at 100 days of age ($n = 4$ mice per group) and in (E) human spinal cord normal control and ALS patients ($n = 4$ humans per group). Mature IL-1 β levels significantly increased in mSOD1 transgenic mice and in human ALS patients as compared with wild-type age-matched littermates and control spinal cord tissue. zVAD-fmk treatment reduced caspase-1 activity in the spinal cords of mSOD1 mice ($*P < 0.05$, $**P < 0.01$). Error bars indicate SEM.

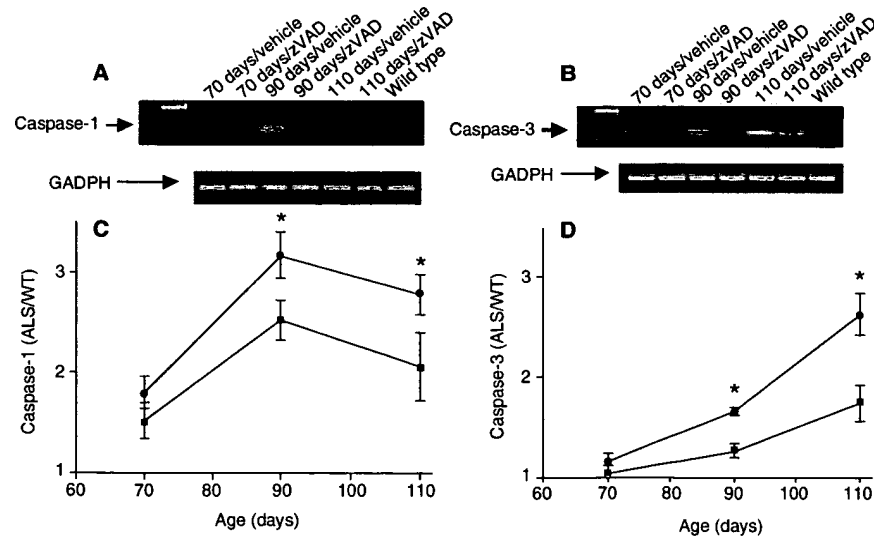


Fig. 4. Caspase-1 and caspase-3 mRNA levels were quantified in spinal cord specimens of mSOD1 mice. Ethidium bromide-stained gels of RT-PCR analysis of (A) caspase-1 and (B) caspase-3 mRNA run in parallel with those of GAPDH mRNA. (C) and (D) show time-dependent up-regulation of (C) caspase-1 and (D) caspase-3 mRNA expression in mSOD1 transgenic mice compared with age-matched wild-type mice ($*P > 0.05$, $n = 6$ mice per time point). Caspase levels are normalized to GAPDH expression and tabulated as the caspase ratio of SOD^{G93A} to wild-type mice. Square, zVAD-fmk; circle, vehicle. Error bars indicate SEM.

References and Notes

1. D. B. Williams and J. A. Windebank, *Peripheral Neuropathy*, P. J. Dyck, P. K. Thoma, J. W. Griffin, P. A. Low, J. F. Poduslo, Eds. (Saunders, Philadelphia, ed. 3, 1993).
2. L. P. Rowland, in *Merritt's Textbook of Neurology*, L. P. Rowland, Ed. (Williams & Wilkins, Philadelphia PA, 1995), pp. 742-749.
3. D. R. Rosen et al., *Nature* **362**, 59 (1993).
4. H. X. Deng et al., *Science* **261**, 1047 (1993).
5. M. E. Gurney et al., *Science* **264**, 1772 (1994).
6. D. R. Borchelt et al., *Neurobiol. Dis.* **5**, 27 (1998).
7. M. E. Gurney, T. J. Fleck, C. S. Himes, E. D. Hall, *Neurology* **50**, 62 (1998).
8. L. J. Martin, *J. Neuropathol. Exp. Neurol.* **58**, 459 (1999).
9. R. M. Friedlander, R. H. Brown, V. Gagliardini, J. Wang, J. Yuan, *Nature* **388**, 31 (1997).
10. V. Kostic, V. Jackson-Lewis, F. de Bilbao, M. Dubois-Dauphin, S. Przedborski, *Science* **277**, 559 (1997).
11. H. Hara et al., *Proc. Natl. Acad. Sci. U.S.A.* **94**, 2007 (1997).
12. K. B. Fink et al., *Neuroscience* **94**, 1213 (1999).
13. R. M. Friedlander et al., *J. Exp. Med.* **185**, 933 (1997).
14. V. O. Ona et al., *Nature* **399**, 263 (1999).
15. S. Namura et al., *J. Neurosci.* **18**, 3659 (1998).
16. J. E. Springer, R. D. Azbill, P. E. Knapp, *Nature Med.* **5**, 943 (1999).
17. A. G. Yakovlev et al., *J. Neurosci.* **17**, 7415 (1997).
18. L. J. Martin, A. C. Price, A. Kaiser, A. Y. Shaikh, Z. Liu, *Int. J. Mol. Med.* **5**, 3 (2000).
19. C. M. Troy, L. Stefanis, A. Prochiantz, L. A. Greene, M. L. Shelanski, *Proc. Natl. Acad. Sci. U.S.A.* **93**, 5635 (1996).
20. S. Vukosavic, L. Stefanis, S. Przedborski, *Soc. Neurosci. Abstr.* **25**, 1304 (1999).
21. Male transgenic mice expressing the human mSOD1^{G93A} were bred with background-matched B6SJL wild-type females (Jackson Laboratories, Bar Harbor, ME). The progeny were genotyped and used

- for subsequent studies. Experiments were conducted in accordance with protocols approved by the Harvard Medical School Animal Care Committee.
22. P. Pasinelli, D. R. Borchelt, M. K. Houseweart, D. W. Cleveland, R. H. Brown Jr., *Proc. Natl. Acad. Sci. U.S.A.* **95**, 15763 (1998).
 23. To investigate whether caspase-1 and caspase-3 are activated in the mSOD1 mouse spinal cord, we performed immunohistochemical staining with an antibody specific for activated caspase-1 (provided by J. Yuan, Harvard Medical School, Boston, MA) and an antibody specific to activated caspase-3, which is also known as CM1 (provided by A. Srinivasan, Idun Pharmaceutical, La Jolla, CA). In addition, a neuron-specific marker, anti-NeuN antibody (Chemicon, Temecula, CA), was used in a double staining procedure to identify neuronal cells. At 70, 90, and 110 days of age, mice were killed and perfused with 4% paraformaldehyde. Spinal cords were removed under a dissecting microscope. Tissue was frozen in cold isopentane after cryoprotection in 30% sucrose. Frozen sections (10 μ m thick) were washed with phosphate-buffered saline (PBS) containing 0.05% Tween-20 and were incubated with 5% normal goat serum. The sections were incubated overnight with rat polyclonal antibody to caspase-1 (1:5) or rabbit polyclonal antibody to caspase-3 (CM1) (1:2000), washed overnight, then washed three times with PBS, and finally probed with a biotinylated secondary antibody to rat immunoglobulin G (IgG) or a biotinylated secondary antibody to rabbit IgG (1:300; Vector, Burlingame, CA) for 2 hours. Next, specimens were incubated in Fluorescein Avidin DCS (1:1000; Vector). Sections were also double stained with the NeuN antibody (1:100) followed by Texas Red antibody to mouse (1:200; Vector). Hoechst 33342 was used for counterstaining. The fluorescent stained sections were evaluated with epifluorescence microscopy.
 24. At 60 days of age, osmotic pumps (Alzet, Palo Alto, CA) were used for the intracerebroventricular delivery of zVAD-fmk (Enzyme Systems, Livermore, CA). Pumps were filled with vehicle (0.4% dimethyl sulfoxide, 0.1 M Pipes, pH 6.9), 100 μ g of zVAG-fmk per 20g body weight, or 300 μ g of zVAG-fmk per 20 g of body weight. Pumps continuously delivered the drug for 28 days and were then exchanged for new pumps filled with fresh drug or vehicle for an additional 28-day treatment. The investigator was blind to the identity of the drug or vehicle used in the pump until the death of all mice.
 25. A Rotarod (Columbus Instruments, Columbus, OH) was used to evaluate motor function. Mice were first evaluated the day before placement of the osmotic pumps and thereafter on a weekly basis. Mice were placed on the rotating rod at speeds of 5, 15, and 20 rpm. The time each mouse remained on the rod was registered automatically. If the mouse remained on the rod for 7 min, the test was completed and scored as 7 min.
 26. Spinal cord and phrenic nerve samples were collected and processed as described (10). Motor neurons were counted on cryostat-cut sections (40 μ m thick) stained with thionin. Quantification was performed by stereology as described by Liberatore *et al.* [*Nature Med.* **5**, 1403 1999] on every 10th spinal cord section, spanning the entire cervical and lumbar enlargements.
 27. K. Kuida *et al.*, *Science* **267**, 2000 (1995).
 28. Mature IL-1 β concentration was measured with an enzyme-linked immunosorbent assay (ELISA) kit (R&D, Minneapolis, MN), which is specific for the mature form of the cytokine. Full-length spinal cord tissue was removed from mice treated with zVAD-fmk or vehicle at 100 days of age. Tissue was processed as previously described (20). Human spinal cord samples were generously provided by the Harvard, Massachusetts General Hospital, and Columbia brain banks.
 29. R. M. Friedlander and J. Yuan, *Cell Death Differ.* **5**, 823 (1998).
 30. R. M. Friedlander, V. Gagliardini, R. J. Rotello, J. Yuan, *J. Exp. Med.* **184**, 717 (1996).
 31. Spinal cord tissue was obtained from 70-, 90-, and 110-day-old mice. Total RNA was extracted with Trizol (Life Technologies, Rockville, MD), and 1 mg was used as a template for first-strand synthesis. Primers were designed from published sequences (Life Technologies). Primers used to amplify caspase-1 were 5'-TGG TCT TGT GAC TTG GAG GA-3' and 5'-TGG CTT CTT ATT GGC ACG AT-3', resulting in a 191-base pair (bp) amplified product. For caspase-3, primer sequences were 5'-TGT CAT CTC GCT CTG GTA CG-3' and 5'-AAA TGA CCC CTT CAT CAC CA-3', resulting in a 200-bp amplified product. To confirm cDNA integrity and to standardize expression levels, we amplified fragments of glyceraldehyde phosphate-3-dehydrogenase (GAPDH) in parallel. Products were analyzed by electrophoresis in a 1.5% agarose gel and were visualized by ethidium bromide staining. A Chemi Doc imaging system (BioRad) was used for signal quantification. Signals are expressed as the ratio of band densities (caspase/GAPDH) of caspase expression in ALS and wild-type mice.
 32. S. Holmin and T. Mathiesen, *J. Neurosurg.* **92**, 108 (2000).
 33. J. Y. Yuan and H. R. Horvitz, *Dev. Biol.* **138**, 33 (1990).
 34. M. Enari, R. V. Talanian, W. W. Wong, S. Nagata, *Nature* **380**, 723 (1996).
 35. A. Ali *et al.*, *J. Hematother. Stem Cell Res.* **8**, 343 (1999).
 36. M. Tewari *et al.*, *Cell* **81**, 801 (1995).
 37. We thank A. Srinivasan for providing the CM1 antibody and J. Yuan for providing the caspase-1 antibody; M. Schoenebeck for expert preparation of the phrenic nerve samples; J. Yuan for insightful comments on the manuscript; and E. Friedlander for editorial assistance. Supported by the Muscular Dystrophy Association; the ALS Association; Project-ALS; the National Institute of Neurological Disorders and Stroke (grants R01 NS38586, R29 NS37345, and P50 NS38370); the U.S. Department of Defense (grant DAMD 17-99-1-9471); the Lowenstein Foundation; the Smart Foundation; and the Parkinson's Disease Foundation. C.G. is the recipient of a scholarship from the French ISERM. S.P. is a recipient of the Cotzias Award from the American Parkinson Disease Association.
- 4 February 2000; accepted 15 March 2000

The Outcome of Acute Hepatitis C Predicted by the Evolution of the Viral Quasispecies

Patrizia Farci,^{1,2*} Atsushi Shimoda,³ Alessandra Coiana,¹ Giacomo Diaz,⁴ Giovanna Peddis,¹ Jacqueline C. Melpolder,⁵ Antonello Strazzer,¹ David Y. Chien,⁶ Santiago J. Munoz,⁷ Angelo Balestrieri,¹ Robert H. Purcell,² Harvey J. Alter⁵

The mechanisms by which hepatitis C virus (HCV) induces chronic infection in the vast majority of infected individuals are unknown. Sequences within the HCV E1 and E2 envelope genes were analyzed during the acute phase of hepatitis C in 12 patients with different clinical outcomes. Acute resolving hepatitis was associated with relative evolutionary stasis of the heterogeneous viral population (quasispecies), whereas progressing hepatitis correlated with genetic evolution of HCV. Consistent with the hypothesis of selective pressure by the host immune system, the sequence changes occurred almost exclusively within the hypervariable region 1 of the E2 gene and were temporally correlated with antibody seroconversion. These data indicate that the evolutionary dynamics of the HCV quasispecies during the acute phase of hepatitis C predict whether the infection will resolve or become chronic.

HCV infection is an important public health problem worldwide (1) because it is a major cause of chronic hepatitis, cirrhosis, and hepatocellular carcinoma (2). Very rarely, HCV causes fulminant hepatitis (FH), the most severe

form of acute hepatitis. Although the infection resolves in 15% of cases, it becomes chronic in up to 85% of infected individuals (3). The clinical course of chronic hepatitis C is highly variable. In about 70% of the patients the disease is mild and stable over several decades, whereas in the remaining 30% it is more rapidly progressive. Prospective studies of hepatitis C have failed to identify any clinical, serologic, or virologic features that predict the outcome of the disease (4).

The mechanisms responsible for the high rate of viral persistence and for the variable clinical course of hepatitis C are unknown, but are thought to represent a complex interplay between viral diversity and host immunity (5). Although HCV infection induces strong cellular and humoral immune responses (6, 7), they are generally insufficient to

¹Department of Medical Sciences, University of Cagliari, Via San Giorgio 12, 09124 Cagliari, Italy. ²Hepatitis Viruses Section, Laboratory of Infectious Diseases, National Institute of Allergy and Infectious Diseases, National Institutes of Health (NIH), Bethesda, MD 20892, USA. ³Department of Internal Medicine, Kanazawa University, Kanazawa 920-8641, Japan. ⁴Department of Cytopathology, University of Cagliari, 09124 Cagliari, Italy. ⁵Department of Transfusion Medicine, Warren G. Magnuson Clinical Center, NIH, Bethesda, MD 20892, USA. ⁶Chiron Corporation, Emeryville, CA 94507, USA. ⁷Albert Einstein Medical Center, Philadelphia, PA 19141, USA.

*To whom correspondence should be addressed. E-mail: farci@pacs.unica.it

Short communication

Interleukin-1 β converting enzyme/Caspase-1 (ICE/Caspase-1) and soluble APO-1/Fas/CD 95 receptor in amyotrophic lateral sclerosis patients

Hłzecka J, Stelmasiak Z, Dobosz B. Interleukin-1 β converting enzyme/Caspase-1 (ICE/Caspase-1) and soluble APO-1/Fas/CD 95 receptor in amyotrophic lateral sclerosis patients.

Acta Neurol Scand 2001; 103: 255–258. © Munksgaard 2001.

Objectives – The aim of the study was to investigate the role of ICE/Caspase-1 and soluble APO-1/Fas/CD 95 receptor in amyotrophic lateral sclerosis patients. **Material and methods** – The apoptosis parameters were measured by enzyme-linked immunosorbent assay (ELISA) in serum and cerebrospinal fluid from 25 amyotrophic lateral sclerosis and 15 control patients. **Results** – There has been shown a significant increase of ICE/Caspase-1 level in serum, and significant decrease of this parameter in cerebrospinal fluid from amyotrophic lateral sclerosis patients. Soluble APO-1/Fas/CD 95 level in amyotrophic lateral sclerosis patients did not differ from the control group. There was no significant correlation between clinical status, duration of amyotrophic lateral sclerosis, and levels of ICE/Caspase-1 and soluble APO-1/Fas/CD 95. **Conclusion** – Our study suggests that ICE/Caspase-1 may play a role in neurodegeneration in ALS. Due to ethical difficulties we cannot include patients suffering from progressive neurological diseases, who are a more appropriate control group for the amyotrophic lateral sclerosis patients. Therefore we are limited in drawing conclusions from the research.

J. Hłzecka, Z. Stelmasiak, B. Dobosz

Department of Neurology, Lublin Medical School,
Poland

Key words: apoptosis; Caspase-1; sAPO-1;
amyotrophic lateral sclerosis

Joanna Hłzecka, Department of Neurology, Lublin
Medical School, Jaczewskiego 8, 20–954 Lublin, Poland

Accepted for publication December 29, 2000

It has been suggested that apoptosis may play a role in the mechanism of neurodegeneration in amyotrophic lateral sclerosis (ALS) (1). Interleukin-1 β converting enzyme/Caspase-1 (ICE/Caspase-1) is a cysteine protease that shares sequence homology with the protein product of *ced-3*, the gene responsible for cell death of the *Caenorhabditis elegans*. Its homology initiated studies about the role of ICE/Caspase-1 in apoptosis (2, 3). The activation of caspases appears to play a key role in this process (4). APO-1/Fas/CD 95, a member of the tumor necrosis factor receptor superfamily, is a transmembranous protein that can transduce cell death signals via a proteolytic cascade upon cross-linking or ligand binding (5, 6). Soluble APO-1/Fas/CD 95 (sAPO-1/Fas/CD 95) is able to protect cells

from Fas-mediated apoptosis (7). Triggering of CD 95 rapidly stimulates the proteolytic activity of ICE. Overexpression of ICE potentiates Fas-mediated cell death (8, 9). Determination of apoptotic parameters could help to explain the mechanism of neurodegeneration in ALS.

Material and methods

Twenty-five patients with clinically definite ALS were studied. ALS was recognized on the basis of El Escorial Criteria WFN of ALS (10). The mean duration of the disease was 1.4 years (range 3 months–4 years). According to Munsat, the ALS Health State Scale (11), the patients were divided into 4 groups: mild, moderate, severe and terminal,

and into 3 groups in dependence on time of ALS duration. Group characteristics are summarized in Table 1.

The control group consisted of 15 patients (8 males/7 females) with lumbosacral disc disease. The mean age was 55 years (range 32–69). Blood and cerebrospinal fluid were taken for examination from the patients of the control group during diagnosis. The cerebrospinal fluid was collected from a lumbar puncture performed on radiculography. Lumbosacral disc disease was confirmed by means of computer tomography or magnetic resonance imaging. The history, neurological examination and additional tests (biochemical test of blood serum, urine analysis, general examination of the cerebrospinal fluid, X-ray of the chest) allowed us to exclude other diseases which could affect the levels of ICE and sAPO-1.

The measurements were performed one time in serum and cerebrospinal fluid (CSF) from ALS and control group patients. The study was approved by the ethics committee of the Lublin Medical School.

Clinical samples were kept at 2–8°C and centrifuged rapidly before storing at –20°C to avoid loss of bioactive sAPO-1 and ICE. ICE and sAPO-1 levels were measured by sandwich enzyme-linked immunosorbent assay (ELISA) (12) using the sAPO-1/Fas ELISA and IL-1 β converting enzyme (ICE/Caspase-1) ELISA (human kits from Bender MedSystems Diagnostics GmbH). Sensitivity of sAPO-1/Fas ELISA method was 20 pg/ml, and ICE/Caspase-1 ELISA method – 5 pg/ml.

For statistical analysis the Mann–Whitney *U*-test, ANOVA procedure (Kruskal–Wallis test), and Spearman rank correlation were used. *P* values <0.05 were considered significant.

Results

The mean ICE level from serum of ALS patients was significantly higher than controls (*P*<0.05), however the mean ICE level from CSF of ALS patients was significantly lower than controls

Table 1. Characteristics of ALS patients

| | |
|-----------------------------------|------------|
| Number of patients | 25 |
| Male/female | 13/12 |
| Age of patients | 57 (34–77) |
| Munsat the ALS Health State Scale | |
| Mild | 5 |
| Moderate | 7 |
| Severe | 8 |
| Terminal | 5 |
| Time of ALS duration | |
| 0–6 months | 9 |
| 7–24 months | 10 |
| 25–48 months | 6 |

Table 2. Comparative analysis of Caspase-1 and sAPO-1 levels (pg/ml) in ALS patients with controls

| Parameter | ALS patients | Controls | <i>P</i> |
|-----------------|-----------------|-----------------|----------|
| ICE in serum | 89.3 SD 33.1 | 56.0 SD 14.5 | 0.0002* |
| ICE in CSF | 6.36 SD 4.55 | 16.4 SD 9.9 | 0.0027* |
| sAPO-1 in serum | 1781.6 SD 702.6 | 1530.2 SD 431.3 | 0.605 |
| sAPO-1 in CSF | 188.2 SD 36.0 | 184.6 SD 28.6 | 0.730 |

Mann–Whitney *U*-test. * *P*<0.05 statistical significance versus control group.

(*P*<0.05). sAPO-1 levels in serum and CSF of ALS patients did not differ significantly from controls (*P*>0.05) (Table 2).

The study has shown that ICE and sAPO-1 levels in serum of ALS patients had a tendency to increase with the time of ALS duration. ICE in CSF of ALS patients has been increasing with the time of duration of ALS and with the advance of the disease, but it has been decreasing in the groups of patients with terminal clinical status and with the longest time of ALS duration. Statistical analysis showed that there was no significant correlation between clinical status, time of ALS duration, and levels of ICE and sAPO-1. The clinical status of patients and time of duration of the disease did not influence significantly ICE and sAPO-1 levels in serum and CSF of ALS patients (*P*>0.05) (Table 3).

Discussion

Experimental research conducted with the model of a transgenic SOD 1 mutant mouse and *in vitro* suggests that apoptosis may play a role in the process of the death of neurons in ALS. The mutations in Cu/Zn superoxide dismutase 1 (SOD-1) have a significant role in the pathogenesis of ALS (13). Pasinelli et al. (14) showed increased activity of ICE in motoneurons limits with expression of mutated SOD-1. ICE is activated by xanthine/xanthine oxidase which increases production and secretion of pro-interleukin 1 β . Activation of ICE in SOD-1 transgenic mouse, causes changes characteristic of apoptosis process in the spinal cord area.

Table 3. Relationship of Caspase-1 and sAPO-1 levels [pg/ml] with clinical status and time of ALS duration

| Parameter | Clinical status | | ALS duration | |
|-----------------|-----------------|----------|--------------|----------|
| | H | <i>P</i> | H | <i>P</i> |
| ICE in serum | 0.49 | 0.93 | 0.69 | 0.70 |
| ICE in CSF | 2.17 | 0.53 | 2.54 | 0.28 |
| sAPO-1 in serum | 0.81 | 0.84 | 1.30 | 0.52 |
| sAPO-1 in CSF | 0.43 | 0.93 | 1.77 | 0.41 |

H: value of Kruskal–Wallis test. *P*<0.05 statistical significance.

APO-1 can mediate cytotoxicity, and play a role in cell survival in the immune system and in the nervous system. It is presumed that in neurodegenerative diseases, among others, in ALS increased expression of CD 95-CD 95L on glial cells may lead to apoptosis (15). De la Monte et al. (16) state that death cell mechanism dependent on Fas receptor may be important in ALS. APO-1 expression increase and nuclear DNA fragmentation were shown in the motor cortex and spinal ventral horns in ALS.

Gamen et al. (17) reported that caspases play the leading role in apoptosis depending on Fas receptor. Activation of caspases takes place under the influence of the adapter protein Fas-associated death domain (FADD), as the outcome of Fas receptor stimulation by its ligand (18). This process leads to mitochondrial transmembrane potential damage. It was shown that Caspase-1-treated mitochondria release an apoptosis-inducing factor causing DNA fragmentation (19).

Caspases play an important role in the process of neurodegeneration of SOD-1 transgenic mice, which suggests that caspases inhibition may play a protective role in ALS. Intracerebroventricular administration of VAD-fmk, a caspase inhibitor, delays ALS onset and mortality (20). Milligan et al. (21) reported that peptide inhibitors of ICE proteases prevent apoptosis in motoneurons *in vivo* and *in vitro*. ICE-like proteases might affect disease progression in ALS mouse model and suggest that ICE inhibitors may be a useful treatment for ALS (22).

Vercammen et al. (23) demonstrated the existence of two different pathways originating from the Fas receptor. If one pathway is blocked by caspase inhibitors, a second leads to necrosis and oxygen radical production. That is why in ALS a combined therapy which influences different potential neurodegeneration mechanisms is most recommended.

Our study suggests that ICE may be considered when we deal with the case of the death of neurons in ALS. There are no essential differences in the levels of sAPO-1 in blood serum and in the cerebrospinal fluid of the ALS patients in comparison with the control group, but we cannot exclude that sAPO-1 receptor may play a role in the pathomechanism of the disease. No significant correlation has been found between the levels of the apoptosis parameters and the duration of the disease and the clinical state of the patients. It is difficult to interpret the findings and the conclusions are limited. We could not include into the control group the patients with other progressive neurological conditions. Due to ethical reasons we did not take the cerebrospinal fluid from them. The control group consisted of patients with lumbosacral disc disease, in whose case it was possible to take the cerebrospinal fluid during examination. In view of

the fact that there is not a more appropriate control group for the ALS patients, which would be patients with progressive neurological diseases, it is difficult to say whether the findings are specific of ALS. The conclusions are also limited by a very small number of patients who took part in the research. Therefore if we want to know the potential mechanisms of the death of neurons in ALS we need further research.

References

1. RABIZADEH S, GRALLA EB, BORCHELT DR et al. Mutations associated with amyotrophic lateral sclerosis convert superoxide dismutase from an antiapoptotic gene to a proapoptotic gene: studies in yeast and neural cells. *Proc Natl Acad Sci USA* 1995;92:3024-8.
2. YUAN J, SHAHAMS S, LEDOUX S, ELLIS HM, HORVITZ HR. The *C. elegans* cell death gene *ced-3* encodes a protein similar to mammalian interleukin-1 β converting enzyme. *Cell* 1993;75:641-52.
3. MARKS N, BERG MJ. Recent advances on neuronal caspases in development and neurodegeneration. *Neurochem Int* 1999;35(3):195-220.
4. SCHWARTZ LM, MILLIGAN CE. Cold thoughts of death: the role of ICE proteases in neuronal cell death. *Trends Neurosci* 1996;19:555-62.
5. SUDA T, TAKAHASHI T, GOLSTEIN P, NAGATA S. Molecular cloning and expression of the Fas ligand, a novel member of the tumor necrosis factor family. *Cell* 1993;75:1169-78.
6. HOFMANN K. The modular nature of apoptotic signaling proteins. *Cell Mol Life Sci* 1999;55:1113-28.
7. CHENG J, ZHOU T, LIN C et al. Protection from Fas-mediated apoptosis by a soluble form of the Fas molecule. *Science* 1994;263:1759-62.
8. LOS M, CRAEN M, PENNING LC et al. Requirement of an ICE/CED-3 protease for Fas/APO-1-mediated apoptosis. *Nature* 1995;375:81-3.
9. WARING P, MULLBACHER A. Cell death induced by the Fas/Fas ligand and its role in pathology. *Immunol Cell Biol* 1999;77(4):312-17.
10. BROOKS BR. El Escorial World Federation of Neurology criteria for the diagnosis of amyotrophic lateral sclerosis. *J Neurol Sci [Suppl]* 1994;124:96-107.
11. RIVIERE M, MEININGER V, ZEISSER P, MUNSAT T. An analysis of extended survival in patients with amyotrophic lateral sclerosis treated with riluzole. *Arch Neurol* 1998;55:526-8.
12. SEISHIMA H, TAKEMURA M, SAITO K et al. Highly sensitive ELISA for soluble Fas in serum: increased soluble Fas in the elderly. *Clin Chem* 1996;42(12):1911-14.
13. RADUNOVIC A, LEIGH PN. Cu/Zn superoxide dismutase gene mutations in amyotrophic lateral sclerosis: correlation between genotype and clinical features. *J Neurol Neurosurg Psych* 1996;61:565-71.
14. PASINELLI P, BORCHELT DR, HOUSEWEART MK, CLEVELAND DW, BROWN RH. Caspase-1 is activated in neural cells and tissue with amyotrophic lateral sclerosis-associated mutations in copper-superoxide dismutase. *Proc Natl Acad Sci USA* 1998;95(26):15763-8.
15. BECHER B, BARKER PA, OWENS T, ANTEL JP. CD 95-CD 95 L: can the brain learn from the immune system? *Trends Neurosci* 1998;21(3):114-17.
16. DE LA MONTE SM, SOHN YK, GANJU N, WANDS JR. P 53 and CD 95-associated apoptosis in neurodegenerative diseases. *Lab Invest* 1998;78(4):401-11.
17. GAMEN S, ANEL A, PINEIRO A, NAVAL J. Caspases are the main executioners of Fas-mediated apoptosis, irrespective of the

- ceramide signaling pathway. *Cell Death Differ* 1998;5(3): 241–9.
18. TATSUTA T, SHIVAISHI A, MOUNTZ JD. The prodomain of caspase-1 enhances Fas-mediated apoptosis through facilitation of caspase-8 activation. *J Biol Chem* 2000; 275:14248–54.
 19. SUSIN SA, ZAMZAMI N, CASTEDO M et al. The central executioner of apoptosis: multiple connections between protease activation and mitochondria in Fas/APO-1/CD 95- and ceramide-induced apoptosis. *J Exp Med* 1997;186(1): 25–37.
 20. LI M, ONA VO, GUEGAN C et al. Functional role of caspase-1 and caspase-3 in an ALS transgenic mouse model. *Science* 2000;288:335–9.
 21. MILLIGAN CE, PREVETTE D, YAGINUMA H et al. Peptide inhibitors of ICE proteases family arrest programmed cell death of motoneurons *in vivo* and *in vitro*. *Neuron* 1995; 15:385–93.
 22. FRIEDLANDER RM, BROWN RH, GAGLIARDINI V, WANG J, YUAN J. Inhibition of ICE slows ALS in mice. *Nature* 1997;388 (6637):31.
 23. VERCAMMEN D, BROUCKAERT G, DENECKER G et al. Dual signaling of the Fas receptor: initiation of both apoptotic and necrotic cell death pathways. *J Exp Med* 1998;188(5):919–30.

Multiple Caspases Are Involved in β -Amyloid-Induced Neuronal Apoptosis

Jason W. Allen,^{1,2} Basil A. Eldadah,^{1,2} Xiuling Huang,^{1,3} Susan M. Knoblach,^{1,3} and Alan I. Faden^{1-3*}

¹Institute for Cognitive and Computational Sciences, Georgetown University, Washington, DC

²Interdisciplinary Program in Neuroscience, Georgetown University, Washington, DC

³Department of Neuroscience, Georgetown University, Washington, DC

β -amyloid peptide (A β) has been implicated in the pathogenesis of Alzheimer disease and has been reported to induce apoptotic death in cell culture. Cysteine proteases, a family of enzymes known as caspases, mediate cell death in many models of apoptosis. Multiple caspases have been implicated in A β toxicity; these reports are conflicting. We show that treatment of cerebellar granule cells (CGC) with A β_{25-35} causes apoptosis associated with increased activity of caspases-2, -3 and -6. Selective inhibition of each of these three caspases provides significant protection against A β -mediated apoptosis. In contrast, no change in caspase-1 activity was seen after A β_{25-35} application, nor was inhibition of caspase-1 neuroprotective. Similar to CGC, cortical neuronal cultures treated with A β_{25-35} demonstrate increased caspase-3 activity but not caspase-1 activity. Furthermore, significant neuroprotection is elicited by selective inhibition of caspase-3 in cortical neurons administered A β_{25-35} , whereas selective caspase-1 inhibition has no effect. Taken together, these findings indicate that multiple executioner caspases may be involved in neuronal apoptosis induced by A β . *J. Neurosci. Res.* 65: 45–53, 2001. © 2001 Wiley-Liss, Inc.

Key words: caspase inhibitors; cerebellar granule cells; cortical neurons; in vitro

Alzheimer disease (AD) is characterized by morphological changes, such as the development of neurofibrillary tangles and the extracellular accumulation of β -amyloid (A β), and by neuronal loss leading to cognitive deficits (Terry et al., 1994). Numerous studies have demonstrated the toxicity of exogenous A β in cultured neurons, suggesting that A β may have a primary role in the neuronal loss associated with AD (for review see Iversen et al., 1995). Application of A β to cultured neurons induces cell death that has the characteristic features of apoptosis, such as nuclear condensation and fragmentation as well as membrane blebbing (Loo et al., 1993; Copani et al., 1995; Cagnoli et al., 1996; Estus et al., 1997; Ivins et al., 1998; Allen et al., 1999).

In addition to the changes listed above, apoptosis is characterized by the selective activation of cell death pro-

grams. Certain cysteine proteases, known as caspases, are believed to be essential mediators of many of the pathways involved in executing the apoptotic program. Mammalian caspases belong to a rapidly expanding family of enzymes that may be functionally subdivided into a three broad categories (for review see Eldadah and Faden, 2000). Initiator caspases include caspases-8, -9 and -10, and possibly caspase-2. The executioner caspases include caspases-3, -6 and -7. Caspase-2 has also been classified within this group (Thornberry et al., 1997). Hypothesized to be located downstream from the initiator caspases, executioner caspases may directly implement the apoptotic death program. The third group, termed pro-inflammatory caspases, include caspase-1 and caspase-11. As their name implies, they are intimately involved in inflammatory cytokine processing.

Recent studies suggest that various caspases may be activated or upregulated in postmortem tissue from patients with verified AD. Increases in caspase-1 protein level and activity have been reported in hippocampal homogenates from AD brains (Chan et al., 1999), and caspase-3 immunoreactivity is increased in brain tissue from AD patients (Masliah et al., 1998; Chan et al., 1999). In vitro studies have also demonstrated increases in caspase activity after A β administration. Application of non-specific caspase inhibitors is protective against A β -mediated neuronal apoptosis (Jordán et al., 1997; Keller et al., 1998; Mattson et al., 1998; Chan et al., 1999; Harada and Sugimoto, 1999; Ivins et al., 1999a; Troy et al., 2000). Considerable controversy exists however in the literature as to which specific caspases are involved. Caspase-1 (Jordán et al., 1997), -2 (Troy et al., 2000), -3 (Jordán et al., 1997; Mattson et al., 1998; Michaelis et al., 1998; Harada et al., 1999; Selznick et al., 2000; Troy et al., 2000), -8

Contract grant sponsor: NIH, Contract grant number: R01 NS36537; Contract grant sponsor: Department of Defense, Contract grant number: DAMD17-99-2-9117.

*Correspondence to: Alan I. Faden, MD, Department of Neuroscience, EP-12 Research Building, 3970 Reservoir Road, NW, Washington, DC 20007. E-mail: fadenai@georgetown.edu

Received 23 February 2001; Revised 23 March 2001; Accepted 26 March 2001

(Ivins et al., 1999b), and -12 (Nakagawa et al., 2000) have all been implicated in the pathogenesis of A β toxicity in vitro

The present study sought to determine which of the executioner caspases are involved in A β -induced neuronal apoptosis. Activity assays and inhibitor studies were carried out for caspase-2, -3, and -6. Caspase-7 was not included because it has been reported to be undetectable in brain tissue (Fernandes-Alnemri et al., 1995; Desjardins and Ledoux, 1998). In addition, we investigated the role of caspase-1, as this caspase has been reported to be upregulated in postmortem AD brain tissue (Chan et al., 1999). Selected studies were carried out in both cerebellar granule cell and cortical neuronal cultures to determine whether differences in the literature may reflect the cell type studied.

MATERIALS AND METHODS

Cerebellar Granule Cells

Primary cerebellar granule cell (CGC) cultures were prepared as described previously (Eldadah et al., 1997). Briefly, cerebella from 8-day-old Sprague-Dawley rat pups (Taconic Farms, Germantown, NY) were dissected in Krebs-Ringer bicarbonate buffer containing 0.3% bovine serum albumin (BSA, Life Technologies, Gaithersburg, MD). Cerebella were then minced and dissociated in 1,800 U/ml trypsin (Sigma, St. Louis, MO) at 37°C for 20 min. Addition of 200 U/ml DNase I (Sigma) and 3,600 U/ml soybean trypsin inhibitor (Life Technologies) halted trypsinization. Individual cells were obtained by multiple rounds of trituration. After settling, supernatant was centrifuged through a 4% BSA layer. Cell pellets were then resuspended in seeding medium comprised of basal medium Eagle (BME, Life Technologies) supplemented with 2 mM glutamine (Biofluids, Rockville, MD), 50 μ g/ml gentamicin sulfate (Biofluids), 10% fetal bovine serum (FBS, Hyclone Laboratories, Logan, UT), and 25 mM KCl (Sigma). Cells were seeded at 1.5×10^5 cells/cm² onto 6-well, 24-well or 96-well microplates (Corning, Corning, NY) precoated with poly-L-lysine (30–70 kDa, Sigma). Ten micromolar cytosine- β -arabinofuranoside (ara-C, Sigma) was added after 24 hr to stop glia proliferation. Cultures were incubated at 37°C in 5% CO₂ and were used for experiments between 5 and 7 days in vitro (DIV).

Cortical Neuronal Cultures

Neocortices from 18-day-old Sprague-Dawley rat embryos (Taconic Farms, Germantown, NY) were used to prepare cortical neuronal cultures. Neurons were prepared as described previously in detail (Mukhin et al., 1998). Briefly, cortices were dissociated in Hank's balanced salt solution without calcium or magnesium (Mediatech, Herndon, VA) supplemented with 10 mM HEPES (pH 7.0, Biofluids) and 1 mM sodium pyruvate (Biofluids). Individual cells were obtained by dissociation, after that cell suspension was diluted with neurobasal medium (NBM, Life Technologies) supplemented with 25 μ M glutamate (Sigma), 0.5 mM glutamine, 1% antibiotic-antimycotic, and 2% B27 supplement (Life Technologies). Cells were seeded at 1×10^6 cells/ml onto 24-well or 96-well microplates precoated with 10 μ g/ml poly-D-lysine (Sigma). Cultures were fed at 4 DIV by

the addition of an equal volume of NBM supplemented with 0.5 mM glutamine, 1% antibiotic-antimycotic, and 2% B27 supplement. Cortical neuronal cultures were used for experiments at 11–14 DIV.

Induction of β -Amyloid Apoptosis In Vitro

β -Amyloid peptide fragment 25–35 (A β _{25–35}, Bachem, King of Prussia, PA) was resuspended in DW to 2.5 mM, aliquoted, and stored at –20°C. Aliquots were thawed only once and used immediately or discarded. For CGC, media was replaced with BME supplemented with 2 mM glutamine, 50 μ g/ml gentamicin sulfate, 10% dialyzed FBS (Hyclone Laboratories), 25 mM KCl, and 10 μ M ara-C as appropriate. For cortical neuronal cultures, media was replaced with NBM supplemented with 0.5 mM glutamine, 1% antibiotic-antimycotic, and 2% B27 supplement. A β _{25–35} was diluted in a small amount of DW and added directly to culture media to the desired concentration. This amount of DW was added to control cultures. Cultures were incubated at 37°C before cell death assessment by calcein AM fluorescence.

Calcein AM Staining

Cell viability was estimated by the retention and deesterification of calcein AM (Molecular Probes, Eugene, OR) as described previously (Eldadah et al., 1997). Cells were washed with Locke's buffer containing 154 mM NaCl (Sigma), 5.6 mM KCl, 3.6 mM NaHCO₃ (Sigma), 2.3 mM CaCl₂ (Sigma), 1.2 mM MgCl₂ (Sigma), 5.6 mM glucose (Biofluids), and 5 mM HEPES (pH 7.4, Biofluids). Cells were then loaded with 5 μ M calcein AM in Locke's buffer for 30 min at 37°C. Fluorescence was quantified using a CytoFluor II Fluorescence Multi-well Plate Reader (PerSeptive Biosystems, Inc., Framington, MA). To account for variability in number of cells between wells and platings, one culture from each plating was washed and the number of viable cells in each well was estimated by the calcein assay described above. All subsequent experimental manipulations were normalized to this control plate by dividing each condition by the results of the corresponding wells on the control plate.

DNA Fragmentation Analysis

DNA was extracted and analyzed after a previously established protocol with minimal modifications (Eldadah et al., 1996). Briefly, cells were lysed in 7 M guanidine hydrochloride (Life Technologies). Nucleic acids were extracted by adding lysate to Wizard Miniprep DNA Purification Resin (Promega, Madison, WI), followed by centrifugation at $2,000 \times g$. Pellets were resuspended in washing solution containing 90 mM NaCl, 9 mM Tris-HCl (pH 7.4, Sigma), 2.25 mM EDTA (Sigma) and 55% ethanol (Sigma). This solution was filtered through a Wizard Minicolumn (Promega) mounted onto a vacuum manifold and then washed with washing solution. Columns were then dried by centrifugation at $5,000 \times g$ for 2 min. Nucleic acids were eluted with deionized water and centrifugation at $5,000 \times g$ for 2 min. RNA was destroyed by incubation with 2 μ g RNase A (5 Prime \rightarrow 3 Prime, Boulder, CO) for 15 min at 37°C. DNA was loaded onto a 1.5% agarose gel (United States Biochemicals, Cleveland, OH) in TBE buffer (Digene Diagnostics, Beltsville, MD) containing 0.5 μ g/ml ethidium bromide (Sig-

ma) Electrophoresis was carried out at 5 V/cm and DNA was visualized by 300 nm transillumination on a Speedlight Gel Documentation System (Hofer, San Francisco, CA)

Caspase Activity Assay

Caspase-1 and -3 activity were estimated using a fluorogenic assay after minor modifications of an established method (Eldadah et al., 1997). In brief, media was completely aspirated from 24-well microplates and Locke's buffer was added to each well, followed by saponin (0.03%, Sigma). Plates were then incubated at room temperature for 10 min with gentle agitation. A small volume of crude cell extract was removed for protein quantitation (see below). Ac-DEVD-AMC (20 μ M) or Ac-YVAD-AMC (20 μ M) was added to each well and plates were briefly agitated. Free aminomethylcoumarin accumulation was measured over time using a CytoFluor II Fluorescence Multi-well Plate Reader with excitation at 360 nm and emission at 460 nm. Specific activity was determined by linear regression analysis. Protein quantitation was carried out using the CBQCA Protein Quantitation Kit (Molecular Probes, Eugene, OR) following manufacturer's guidelines. Specific activity from each sample was then corrected for protein content.

Caspase-2 activity was estimated using specific fluorogenic substrate and by immunoblot analysis. Caspase-6 activity was estimated using a fluorogenic substrate. Protein extracts were obtained from 24-well microplates by aspirating media and replacing it with reaction buffer containing 10 mM HEPES, 2 mM EDTA (Biofluids), 0.1% CHAPS (Sigma) and 5 mM DTT (Sigma). Iodoacetamide (0.1 mM, Calbiochem, San Diego, CA), AEBSF (1 mM, Calbiochem) and aprotinin (1 mM, Calbiochem) were added to inhibit endogenous proteinases. Protein quantitation was carried out via Bradford method (Bio-Rad, Hercules, CA) following manufacturer's recommendations. Each sample was incubated with reaction buffer and appropriate substrate (0.04 mg/ml). Results were corrected for protein content after linear regression. For immunoblot analysis, samples were obtained from 96-well plates and protein content of each sample was quantified using the Bradford method. Samples were stored at -80°C . Twenty micrograms of protein was then loaded on 4–20% Tris-Glycine gel (Novex, San Diego, CA) and subjected to electrophoresis at 100 V for 2–3 hr in a running buffer comprised of Tris/Glycine/SDS (BioRad). Mouse spleen tissue extract (50 μ g, StressGen, Victoria, BC, Canada) was used as a positive control. Samples were then transferred to a PVDF membrane (BioRad) in Tris/Glycine buffer (BioRad) at 25 V for 2 hr. Membranes were blocked at room temperature for 2 hr with 5% milk in TBS containing 1% Tween-20 (Sigma). Membranes were incubated with rabbit anti-caspase-2 (4 μ g/ml, StressGen) or mouse monoclonal anti- β -actin (Sigma) antibodies overnight at 4°C with gentle agitation. After washing three times for 10 min each in TTBS, membranes were incubated with HRP-linked anti-rabbit immunoglobulin (1:2,000 dilution, Amersham, Piscataway, NJ) for 1 hr at room temperature. Membranes were washed using TTBS and signal was detected using enhanced chemiluminescences ECL Western blot kit (Amersham) and Hyperfilm ECL (Amersham).

Drugs

Z-DEVD-FMK, Ac-DEVD-CHO and Z-YVAD-FMK were obtained from Enzyme Systems Products (Livermore, CA). Ac-YVAD-AMC and Ac-DEVD-AMC were obtained from Bachem. Ac-VDVAD-AFC, Z-VDVAD-FMK, Ac-VEID-AFC, Z-VEID-FMK and Z-Boc-D-FMK were obtained from Bio-Rad, Richmond, CA. These substrates and inhibitors represent the optimal peptide recognition sequences for each respective caspase, or all caspases (Z-Boc-D-FMK), as defined previously (Thornberry et al., 1997).

RESULTS

β -Amyloid Induces Cerebellar Granule Cell (CGC) Apoptosis

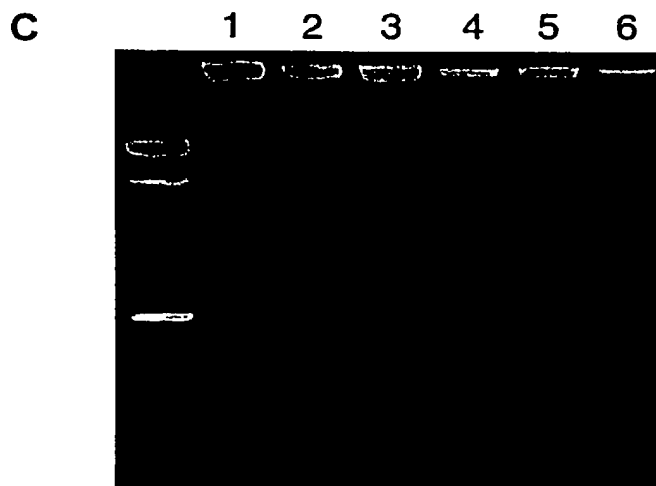
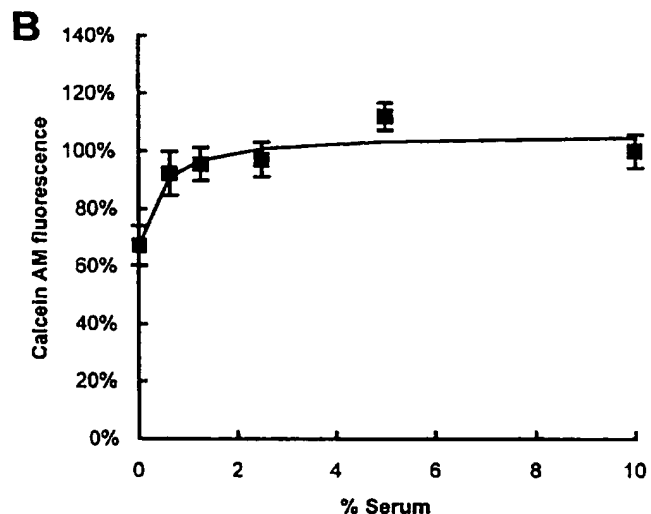
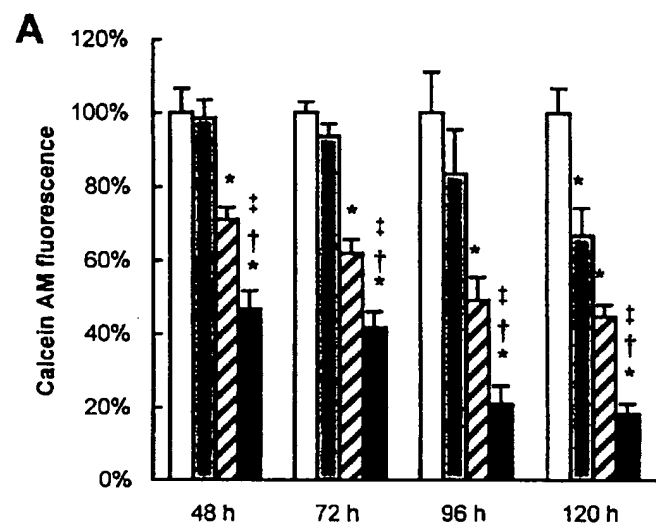
$\text{A}\beta_{25-35}$ (25 μ M) treatment of CGC in the presence of serum produces neuronal death that is detectable only after 120 hr (Fig. 1A). In contrast, CGC deprived of serum exhibit significant cell death by 48 hr (Fig. 1A). Concurrent serum deprivation and $\text{A}\beta_{25-35}$ (25 μ M) application induces significantly greater levels of CGC death as compared with either treatment alone (Fig. 1A). Dose response curve for serum in the presence of $\text{A}\beta_{25-35}$ (25 μ M) exhibits an EC_{50} of 0.391% (Fig. 1B).

We have shown previously that both serum deprivation and administration of $\text{A}\beta_{25-35}$ with serum withdrawal produces significant CGC death that is characterized by morphological changes consistent with apoptosis as detected by calcein AM and Hoechst 33258 staining (Eldadah et al., 1997; Allen et al., 1999). Analysis of DNA extracts at 48 hr reveals the absence of laddering in both control cultures and CGC treated with $\text{A}\beta_{25-35}$ (25 μ M), and minimal DNA laddering in extracts from CGC deprived of serum. In contrast, prominent laddering is seen in extracts from CGC simultaneously treated with $\text{A}\beta_{25-35}$ and serum deprivation at both 24 and 48 hr (Fig. 1C).

Selective Caspase Activation Occurs in CGC Exposed to $\text{A}\beta_{25-35}$ in the Absence of Serum

We have demonstrated previously that CGC simultaneously deprived of serum and potassium exhibit increased activity of caspase-3 with no change in caspase-1 activity (Eldadah et al., 1997). Using relatively selective fluorogenic substrates for caspase-1, 2, 3, and 6 we examined the profile of caspase activation in CGC treated with $\text{A}\beta_{25-35}$ (25 μ M) and concomitant serum deprivation. No difference is seen in cleavage of the caspase-1 substrate Ac-YVAD-AMC in extracts from CGC exposed to $\text{A}\beta_{25-35}$ and serum deprivation for 24 hr as compared with control CGC extracts (Fig. 2). In contrast, significant increases in cleavage of the substrates for caspase-2 (Ac-VDVAD-AFC), caspase-3 (Ac-DEVD-AMC), and caspase-6 (Ac-VEID-AFC) occur after 24 hr of treatment of CGC with $\text{A}\beta_{25-35}$ in the absence of serum (Fig. 2).

Extracts from control cultures and CGC exposed to $\text{A}\beta_{25-35}$ (25 μ M) with simultaneous serum deprivation were subjected to immunoblot analysis using anti-caspase-2 antibody. Mouse spleen tissue extract was used as a positive control. Consistent with our data using Ac-VDVAD-AFC, a caspase-2 substrate, CGC treated with



Aβ₂₅₋₃₅ and serum withdrawal exhibit loss of procaspase-2 bands and increases in bands corresponding to activated caspase-2 fragments at both 12 and 24 hr (Fig. 3)

Selective Caspase Inhibition Rescues CGC From Combined Aβ₂₅₋₃₅ and Serum Deprivation Toxicity

To determine the functional relevance of the selective caspase activation reported in the present study, CGC cultures exposed to Aβ₂₅₋₃₅ (25 μM) with concurrent serum withdrawal were treated with selective caspase inhibitors and cell viability was determined at 24 hr. The pan-caspase inhibitor Z-Boc-D-FMK (150 μM) provided significant protection against this insult (Fig. 4). As predicted by the lack of caspase-1 activity, the caspase-1 inhibitor Z-YVAD-FMK (150 μM) had no effect of toxicity induced by Aβ₂₅₋₃₅ with serum deprivation (Fig. 4). In contrast, and again consistent with our data using fluorogenic substrate assays, the inhibitors of caspase-2 (Z-VDVAD-FMK, 30 μM), caspase-3 (Z-DEVD-FMK, 160 μM), and caspase-6 (Z-VEID-FMK, 150 μM) all provided significant protection against Aβ₂₅₋₃₅-toxicity in the absence of serum (Fig. 4).

Fig. 1 Aβ₂₅₋₃₅ with concurrent serum deprivation induces CGC apoptosis. **A:** Cell survival as determined by calcein AM fluorescence in control CGC cultures (open bars) was compared with viability of CGC exposed to Aβ₂₅₋₃₅ (25 μM, gray bars), serum deprivation (hatched bars), and Aβ₂₅₋₃₅ (25 μM) with concurrent serum deprivation (black bars) at various time points. Significant cell death in Aβ₂₅₋₃₅-treated CGC is not detectable until after 5 days of exposure, whereas significant toxicity is seen at 48 hr for both serum deprived CGC and cultures incubated with Aβ₂₅₋₃₅ in the absence of serum. At all time points studied, combined treatment with Aβ₂₅₋₃₅ and serum deprivation induces significantly greater cell death than either insult alone. Data are expressed as a percentage of control calcein AM values. Scale bars = mean + SEM, n = 10 cultures per condition. *P < 0.05 vs control; †P < 0.05 vs Aβ₂₅₋₃₅; ‡P < 0.05 vs serum deprivation. ANOVA followed by Student-Newman-Keuls test. **B:** Dose response curve was generated for serum. Serial dilutions of serum were carried out and CGC were incubated with Aβ₂₅₋₃₅ (25 μM) in the presence of the indicated concentration of serum before cell viability was determined at 48 hr. Aβ₂₅₋₃₅-toxicity exhibits a significant serum dose-dependent correlation (r = 0.943, P < 0.01, Spearman's Rank Correlation test). Non-linear regression analysis estimates EC₅₀ at 0.391%. Data are expressed as a percentage of calcein AM. Values represent mean + SEM, n = 10 cultures per condition. **C:** DNA was extracted and subjected to gel electrophoresis as detailed in Materials and Methods. Equal amounts of DNA were loaded to each lane. DNA isolated from control CGC (lane 1) or CGC treated with Aβ₂₅₋₃₅ (25 μM) in the presence of serum (lane 2) does not demonstrate identifiable fragmentation at 48 hr. In contrast, minimal DNA fragmentation is visible after serum deprivation at 48 hr (lane 3). More prominent DNA fragmentation was observed in DNA isolated from CGC incubated with Aβ₂₅₋₃₅ (25 μM) with concurrent serum deprivation at both 24 hr (lane 4) and 48 hr (lane 5). Positive control is provided by depriving CGC of both serum and potassium for 24 hr (lane 6), a well-studied apoptotic insult (Eldadah et al., 1997).

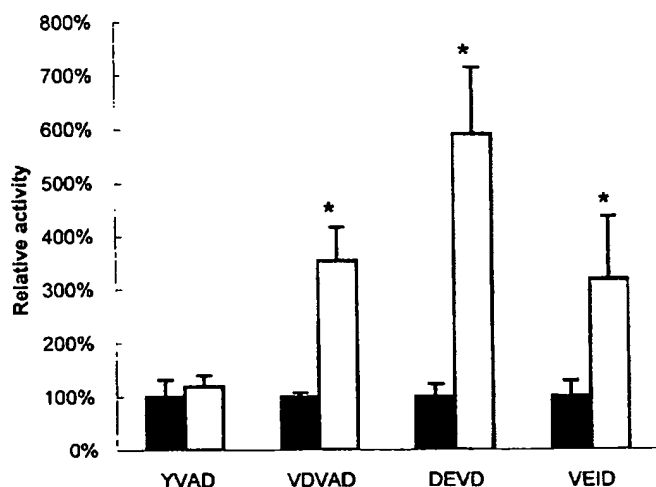


Fig 2 Significant increases in executioner caspases occurs in CGC exposed to $A\beta_{25-35}$ in the absence of serum. CGC were incubated with $A\beta_{25-35}$ (25 μ M) with concurrent serum withdrawal for 24 hr and caspase activity was estimated from protein extracts using selective fluorogenic substrates as detailed in Materials and Methods. No change in caspase-1 activity (YVAD) is observed after $A\beta_{25-35}$ treatment with serum deprivation (open bars) as compared with control levels (filled bars). In contrast, the activity of all three executioner caspases, caspase-2 (VDVAD), -3 (DEVD) and -6 (VEID), is significantly increased in CGC exposed to $A\beta_{25-35}$, in the absence of serum (open bars) as compared with control CGC (filled bars). Data are expressed as a percentage of control activity levels. Scale bars = mean + SEM, $n = 5$. * $P < 0.05$ vs control. ANOVA followed by Student-Newman-Keuls test.

β -Amyloid Induces Cortical Neuronal Apoptosis

Significant cell death occurs after incubation of rat cortical neurons with $A\beta_{25-35}$ (50 μ M) at 48 and 72 hr (Fig. 5). Approximately equal levels of cell death at 48 hr are seen in cortical neurons exposed to $A\beta_{25-35}$ as compared with CGC treated with $A\beta_{25-35}$ with serum deprivation. Little or no baseline DNA fragmentation is detected in extracts from control cortical neurons, whereas treatment with $A\beta_{25-35}$ (50 μ M) for 24 hr induces prominent DNA laddering (Fig. 5). Similar levels of cortical neuronal death are seen after application of pre-aggregated $A\beta_{1-42}$ for 48 hr (data not shown).

Role of Caspase-3 in $A\beta_{25-35}$ -Induced Cortical Neuronal Apoptosis

Significant cleavage of the caspase-3 substrate Ac-DEVD-AMC occurs after treatment of cortical neurons with $A\beta_{25-35}$ (50 μ M) for 24 hr (Fig. 6). In contrast, no change in Ac-YVAD-AMC cleavage, a substrate for caspase-1, is seen with the same insult at 24 hr. Consistent with increased caspase-3 activity, cortical neurons are rescued from $A\beta_{25-35}$ -mediated apoptosis by administration of the caspase-3 inhibitor Ac-DEVD-CHO (400 μ M) (Fig. 6). As expected, application of the caspase-1 inhibitor Z-YVAD-FMK (160 μ M) had no effect on cortical neuronal death induced by $A\beta_{25-35}$ (Fig. 6).

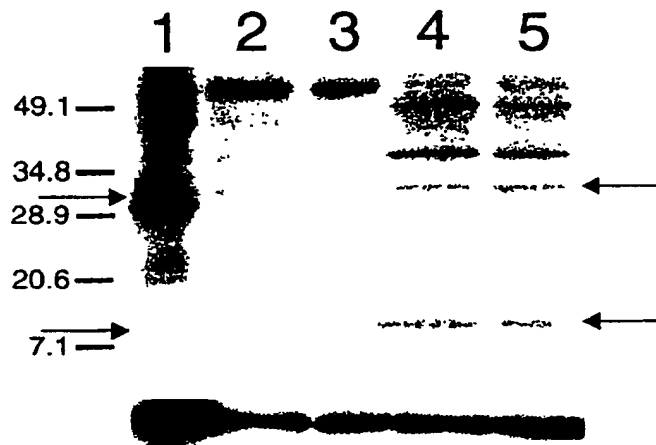


Fig 3 Caspase-2 activation in CGC treated with $A25-35$ with serum deprivation. Immunoblot analysis of extracts from mouse spleen extract (lane 1, positive control), control CGC at 12 hr (lane 2) and 24 hr (lane 3), and CGC treated with $A25-35$ for 12 hr (lane 4) and 24 hr (lane 5) was carried out as described in Materials and Methods. Cleavage of procaspase-2 into active caspase-2 occurs after 12 and 24 hr of exposure to $A25-35$. Prominent procaspase-2 is detected as a band around 50 kDa in extracts from mouse spleen tissue and control CGC at 12 hr and 24 hr. Activated caspase-2 is detected in mouse spleen tissue extract as bands around 33 and 32 kDa (arrows). Mild caspase-2 activation is also detected in control CGC at 12 and 24 hr. Further processing of active caspase-2 is detected as a faint band around 11 kDa in control CGC at 12 and 24 hr (arrows). CGC treated with $A25-35$ for 12 hr or 24 hr exhibit loss of the procaspase-2 band with increased caspase-2 activity as evidenced by more prominent signal at 33, 32 and 11 kDa as compared with control CGC. Lower bands depict staining of the same blot with anti-actin to confirm equal loading of protein between control and $A25-35$ -treated CGC.

DISCUSSION

Although it is generally well-accepted that $A\beta$ induces apoptotic neuronal death, at least in vitro, the particular pathways of the apoptotic cell death program that are involved in $A\beta$ toxicity remain unclear. Caspases have been widely implicated as essential mediators of many types of neuronal apoptosis, including $A\beta$ -mediated cell death. In the present study, we demonstrate selective activation of three executioner caspases in CGC exposed to $A\beta$ in the absence of serum: caspase-2, -3 and -6. Moreover, rescue from $A\beta$ -mediated CGC apoptosis is found with selective inhibition of each of these caspases. Activation of caspase-3 is also confirmed in cortical neuronal cultures treated with $A\beta$, and similar increases in cell survival are found after selective inhibition of this caspase. In contrast, we demonstrate that $A\beta$ application does not elicit activation of caspase-1 in either CGC or cortical neurons, and selective inhibition of caspase-1 has no effect on $A\beta$ -mediated toxicity in either cell type.

We have demonstrated previously that application of $A\beta_{25-35}$ in the absence of serum induces nuclear changes consistent with apoptosis (Allen et al., 1999). A recent study using rat cortical neuronal-glial cultures reported

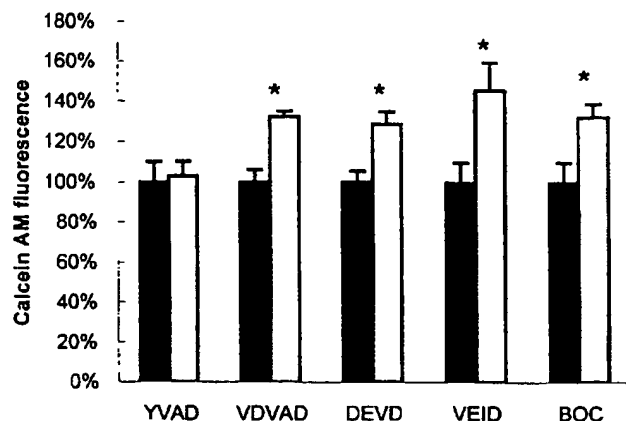


Fig. 4 Selective inhibition of executioner caspases rescues CGC from $A\beta_{25-35}$ toxicity with serum withdrawal. $A\beta_{25-35}$ (25 μ M) was applied to CGC in the absence of serum for 48 hr (filled bars) and the level of cell death was compared with 48 hr of treatment with various caspase inhibitors (open bars) as detailed in Materials and Methods. Non-selective inhibition of caspases by Z-Boc-D-FMK (150 μ M, BOC) significantly reduces $A\beta_{25-35}$ toxicity in the absence of serum. No significant difference in cell viability occurs after inhibition of caspase-1 by Z-YVAD-FMK (150 μ M, YVAD). In contrast, selective inhibition of the executioner caspases, caspase-2 by Z-VDVAD-FMK (30 μ M, VDVAD), caspase-3 by Z-DEVD-FMK (160 μ M, DEVD) and caspase-6 by Z-VEID-FMK (150 μ M, VEID), significantly rescues CGC from $A\beta_{25-35}$ with concurrent serum deprivation toxicity. Data are expressed as a percentage of calcein AM levels of CGC incubated with $A\beta_{25-35}$ and simultaneous serum withdrawal in the absence of treatment (control). Scale bars = mean + SEM, $n = 10-15$. * $P < 0.05$ vs. control. ANOVA followed by Student-Newman-Keuls test.

that $A\beta_{25-35}$ toxicity was increased in serum-free media as compared with conditioned (serum-containing) media (Harada et al., 1999). We present similar results in CGC. Although serum deprivation in the absence of $A\beta$ induces cell death in CGC, application of $A\beta_{25-35}$ with concurrent serum withdrawal causes significantly greater cell death than either $A\beta_{25-35}$ or serum deprivation alone. Dose-response curves indicate that $A\beta_{25-35}$ toxicity is very sensitive to the presence of serum, with an EC_{50} of approximately 0.4%. One hypothesis is that serum may be stimulating the release of an endogenous neuroprotective factor. As this effect has now been seen in two neuronal cell types, it is also possible however that serum contains a factor that is directly providing protection against $A\beta$. One possible mechanism may relate to binding of $A\beta$ by serum proteins thereby sequestering $A\beta$ from its cellular targets. To control for this effect, we carried out all of our experiments in the absence of serum.

AD is characterized by $A\beta$ deposition and manifests itself with cognitive deficits that may be a result of neuronal loss (Terry et al., 1994). Increases in the numbers of apoptotic neurons have been reported in postmortem tissue from confirmed AD patients (Smale et al., 1995; Anderson et al., 1996; Li et al., 1997), although interpretative questions have been raised in this regard (Perry et al.,

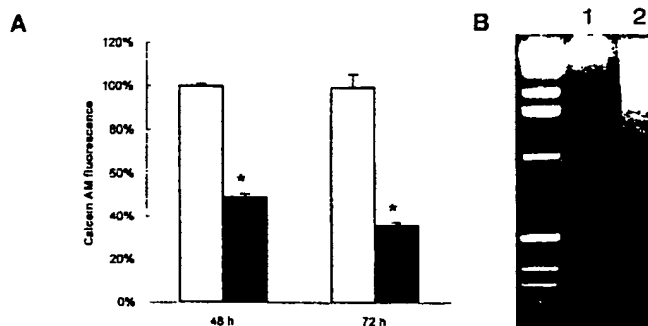


Fig. 5 $A\beta_{25-35}$ induces cortical neuronal apoptosis. (A) Cortical neurons were treated with $A\beta_{25-35}$ (50 μ M) for 48 or 72 hr (filled bars) and cell viability was determined by calcein AM assay as detailed in Materials and Methods and was compared with control cortical neurons (open bars). Significant cell loss is seen at both 48 and 72 hr of incubation with $A\beta_{25-35}$. Data are expressed as a percentage of control calcein AM levels. Scale bars = mean + SEM, $n = 22-24$. * $P < 0.05$ vs. control. ANOVA followed by Student-Newman-Keuls test. (B) DNA extracted from control (lane 1) and cortical neurons exposed to $A\beta_{25-35}$ for 24 hr (lane 2) were subjected to electrophoresis as detailed in Materials and Methods. Minimal DNA fragmentation is seen in control DNA, whereas cortical neurons treated with $A\beta_{25-35}$ demonstrate more prominent DNA laddering.

2001). Increased activation of caspases has also been reported in postmortem tissue from AD patients. As noted above, a recent report demonstrated increases in caspase-1 protein levels and activity in AD postmortem brain tissue (Chan et al., 1999). An earlier study reported however no significant differences in caspase-1 immunoreactivity between control and AD postmortem brain tissue (Masliah et al., 1998). The role of caspase-3 in AD has similarly been questioned. A number of studies indicate that caspase-3 immunoreactivity is increased in brain tissue from AD patients (Masliah et al., 1998; Chan et al., 1999; Selznick et al., 1999). In contrast, one study reported no change in caspase-3 mRNA or protein levels in brain homogenates from AD patients as compared with controls (Desjardins and Ledoux, 1998). Therefore, whereas the presence of caspase-mediated apoptosis in postmortem AD brain tissue is supported by recent studies (Rohn et al., 2001), the role of specific caspases in this process remains unclear.

Similarly, conflicting results have also been reported for in vitro studies of $A\beta$ -mediated caspase activation. $A\beta$ has been demonstrated to induce neuronal apoptosis in various in vitro models (Loo et al., 1993; Copani et al., 1995; Cagnoli et al., 1996; Estus et al., 1997; Allen et al., 1999), suggesting that the apoptosis seen in vivo may be related to the increases in $A\beta$ levels. In addition, an important role for caspases in $A\beta$ -induced cell death has been firmly established by in vitro studies using non-selective caspase inhibitors (Jordán et al., 1997; Keller et al., 1998; Mattson et al., 1998; Chan et al., 1999; Harada et al., 1999; Ivins et al., 1999a; Troy et al., 2000). Studies using selective caspases in the setting of $A\beta$ toxicity have however, produced conflicting results. Protection of rat

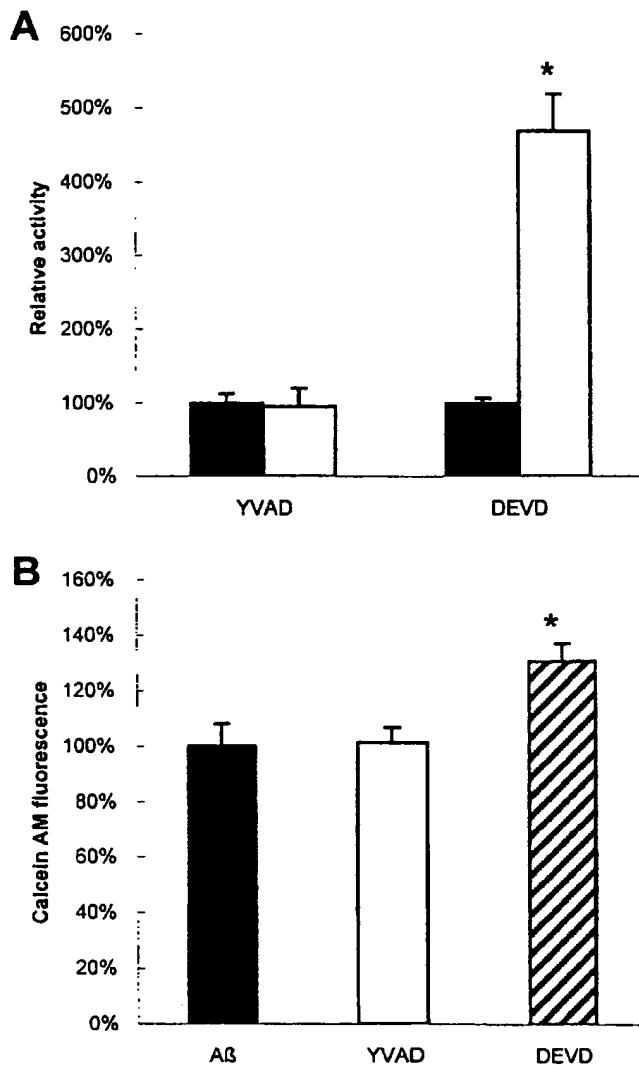


Fig 6 Selective activation of caspase-3 is involved in $A\beta_{25-35}$ -induced apoptosis of cortical neurons (A) Cortical neurons were treated with $A\beta_{25-35}$ (50 μ M) for 24 hr (open bars) and caspase activity as determined by fluorogenic substrates was compared with control cortical neurons (filled bars). No change in Ac-YVAD-AMC cleavage, a substrate for caspase-1, is seen after $A\beta_{25-35}$ application. In contrast, significant cleavage of the caspase-3 substrate, Ac-DEVD-AMC, occurs with this treatment. Data are expressed as level of substrate cleavage in control. Scale bars = mean \pm SEM, $n = 5-12$. * $P < 0.05$ vs control. ANOVA followed by Student-Newman-Keuls test (B) Cortical neurons were incubated with $A\beta_{25-35}$ (50 μ M) in the presence or absence of selective caspase inhibitors. Cell viability was determined at 48 hr and compared with cultures incubated with $A\beta_{25-35}$ in the absence of treatment (filled bar). No change in cell death is seen after inhibition of caspase-1 by Z-YVAD-FMK (160 μ M, open bar), whereas significant increase in cell survival occurs after inhibition of caspase-3 by Ac-DEVD-CHO (400 μ M, hatched bar). Data are expressed as a percentage of calcein AM levels in cortical neurons exposed to $A\beta_{25-35}$ in the absence of treatment (control). Scale bars = mean \pm SEM, $n = 14-20$. * $P < 0.05$ vs control. ANOVA followed by Student-Newman-Keuls test.

hippocampal neurons against $A\beta_{25-35}$ has been reported after pre-application of Ac-YVAD-CMK, a caspase-1 inhibitor (Jordán et al., 1997). A recent study using rat hippocampal neurons and PC12 cells incubated with $A\beta_{1-42}$ however failed to find an increase in caspase-1 activity, as evidenced by no change in YVAD-AFC cleavage (Troy et al., 2000), furthermore, inhibition of caspase-1 by Z-YVAD-FMK had no effect on cell survival (Troy et al., 2000). The results presented here are consistent with the latter study. No change in Ac-YVAD-AMC cleavage was found in either CGC or cortical neurons treated with $A\beta_{25-35}$. Furthermore, $A\beta_{25-35}$ -mediated cell death was not modified by administration of Z-YVAD-FMK in CGC or cortical neurons. As similar concentrations of caspase-1 inhibitors were used in all three studies, the lack of effect is not likely due to inadequate inhibition.

Caspase-2 has also recently been implicated in $A\beta$ toxicity. Caspase-2 activity was increased in hippocampal neurons treated with $A\beta_{1-42}$ as evidenced by more prominent bands correlating with intermediate forms of caspase-2 on immunoblot analysis (Troy et al., 2000). In addition, antisense directed against caspase-2 protected PC12 cells treated with $A\beta_{1-42}$ and sympathetic neurons cultured from caspase-2 null mice similarly exhibited resistance to $A\beta_{1-42}$ (Troy et al., 2000). These results are corroborated in the present study. Using CGC treated with $A\beta_{25-35}$ in the absence of serum, we demonstrated increased cleavage of Ac-VDVAD-AFC, a caspase-2 substrate, and increased intensity of bands representing activated subunits of caspase-2 by immunoblot analysis. Furthermore, increased cell viability was observed after application of the selective caspase-2 inhibitor Z-VDVAD-FMK. Taken together, these multiple lines of evidence indicate that caspase-2 plays an important role in $A\beta$ -mediated toxicity in vitro.

Caspase-3 is the caspase most strongly implicated in the pathogenesis of $A\beta$ -induced apoptosis. Activation of caspase-3 occurs in multiple cell types after $A\beta$ application, as demonstrated by increased cleavage of selective fluorogenic substrates (Jordán et al., 1997; Mattson et al., 1998; Michaelis et al., 1998; Harada et al., 1999; Troy et al., 2000), increased levels of activated subunits by immunoblot analysis (Harada et al., 1999; Troy et al., 2000), increased immunohistochemical staining with antibodies directed against activated subunits (Selznick et al., 2000) or with biotinylated substrates (Mattson et al., 1998; Chan et al., 1999), and increased cleavage of caspase-3 endogenous substrates (Harada et al., 1999). Moreover, protection with a caspase-3 inhibitor has been reported (Harada et al., 1999). In contrast, one study failed to find a protective effect for a selective inhibitor of caspase-3 against $A\beta$ -mediated cell death (Troy et al., 2000). In the present study, we show increased activity of caspase-3 in CGC and cortical neurons treated with $A\beta_{25-35}$ as demonstrated by increased cleavage of Ac-DEVD-AMC. Furthermore, our results support an important role for caspase-3 in $A\beta$ toxicity as inhibition of caspase-3 by Z-DEVD-FMK or Ac-DEVD-CHO provides significant protection against such injury.

Although caspase-6, along with caspase-3 and -7 and possibly caspase-2, is considered a member of the executioner group of caspases, it has been recently suggested that caspase-6 may be upstream of caspase-3 in CGC and may therefore serve as an initiator caspase (Allsopp et al., 2000). Extracts from CGC treated with $A\beta_{25-35}$ with concurrent serum deprivation exhibit increased cleavage of the caspase-6 selective substrate Ac-VEID-AFC. Furthermore, significant rescue of CGC from $A\beta$ toxicity was found after administration of Z-VEID-FMK, a selective caspase-6 inhibitor. Caspase-6 has been shown to induce apoptosis directly in human primary neurons (Zhang et al., 2000). Moreover, caspase-6, but not caspase-3, is activated in serum-deprived mediated apoptosis of human neurons, and is correlated with increased $A\beta$ production (LeBlanc et al., 1999).

It was recently reported that caspase-12 mediates endoplasmic-reticulum-specific apoptosis as well as cytotoxicity induced by $A\beta$ (Nakagawa et al., 2000). Neurons from caspase-12 knockout animals or neurons treated with antisense to caspase-12 showed protection against $A\beta$ -induced apoptosis. The relationship of caspase-12 to executioner caspases remains to be established.

This study was designed to address the role of executioner caspases in the pathogenesis of $A\beta$ -mediated neuronal apoptosis. Our data indicate that all of the three caspases belonging to this group that are expressed in brain - caspase-2, -3 and -6 - are probably involved in mediating the apoptotic cell death program initiated by $A\beta$. Thus, it is not surprising that although high levels of caspase activity have been reported after $A\beta$ administration, the levels of neuroprotection provided by selective caspase inhibitors has been modest. It is possible that the blockade of one of the executioner caspases may be offset by the activity of the remaining members. Nonetheless, delineating which caspases are involved with $A\beta$ -mediated toxicity has important potential implications for the treatment of AD.

ACKNOWLEDGMENTS

This research was supported by NIH Grant R01 NS36537 and Department of Defense Cooperative Agreement DAMD17-99-2-9007.

REFERENCES

- Allen JW, Eldadah BA, Faden AI 1999 Beta-amyloid-induced apoptosis of cerebellar granule cells and cortical neurons: exacerbation by selective inhibition of group I metabotropic glutamate receptors. *Neuropharmacology* 38:1243-1252.
- Allsopp TE, McLuckie J, Kerr LE, Macleod M, Sharkey J, Kelly JS 2000 Caspase 6 activity initiates caspase 3 activation in cerebellar granule cell apoptosis. *Cell Death Differ* 7:984-993.
- Anderson AJ, Su JH, Cotman CW 1996 DNA damage and apoptosis in Alzheimer disease: colocalization with c-Jun immunoreactivity, relationship to brain area and effect of postmortem delay. *J Neurosci* 16:1710-1719.
- Cagnoli CM, Attnby C, Marek H 1996 Protective action of isoquinoline-sulfonamides in vitro models of neuronal apoptosis. *Life Sci* 58:295-301.
- Chan SL, Griffin WST, Mattson MP 1999 Evidence for caspase-mediated cleavage of AMPA receptor subunits in neuronal apoptosis and Alzheimer disease. *J Neurosci Res* 57:315-323.
- Copani A, Bruno V, Battaglia G, Leanza G, Pellicani R, Russo A, Stanzani S, Nicoletti F 1995 Activation of metabotropic glutamate receptors protects cultured neurons against apoptosis induced by β -amyloid peptide. *Mol Pharmacol* 47:891-897.
- Desjardins P, Ledoux S 1998 Expression of ced-3 and ced-9 homologs in Alzheimer disease cerebral cortex. *Neurosci Lett* 244:69-72.
- Eldadah BA, Yakovlev AG, Faden AI 1996 A new approach for the electrophoretic detection of apoptosis. *Nucleic Acids Res* 24:4092-4093.
- Eldadah BA, Yakovlev AG, Faden AI 1997 The role of CED-3-related cysteine proteases in apoptosis of cerebellar granule cells. *J Neurosci* 17:6105-6113.
- Eldadah BA, Faden AI 2000 Caspase pathways, neuronal apoptosis, and CNS injury. *J Neurotrauma* 17:811-829.
- Estus S, Tucker HM, van Rooyen C, Wright S, Bringham EF, Wogulis M, Rydel RE 1997 Aggregated amyloid- β protein induces cortical neuronal apoptosis and concomitant 'apoptotic' pattern of gene induction. *J Neurosci* 17:7736-7745.
- Fernandes-Alnemri T, Takahashi A, Armstrong R, Krebs J, Fritz L, Tomaselli KJ, Wang L, Yu Z, Croce CM, Salvesen G, Earnshaw WC, Litwack G, Alnemri ES 1995 Mch3, a novel human apoptotic cysteine protease highly related to CPP32. *Cancer Res* 55:6045-6052.
- Harada J, Sugimoto M 1999 Activation of caspase-3 in β -amyloid-induced apoptosis of cultured rat cortical neurons. *Brain Res* 842:311-323.
- Iversen LL, Mortishier-Smith RJ, Pollack SJ, Shearman MS 1995 The toxicity in vitro of β -amyloid protein. *Biochem J* 311:1-16.
- Ivins KJ, Bui ETN, Cotman CW 1998 β -amyloid induces local neurite degeneration in cultured hippocampal neurons: evidence for neuritic apoptosis. *Neurobiol Dis* 5:365-378.
- Ivins KJ, Ivins JK, Sharp JP, Cotman CW 1999a Multiple pathways of apoptosis in PC12 cells. *J Biol Chem* 274:2107-2112.
- Ivins KJ, Thornton PL, Rohn TT, Cotman CW 1999b Neuronal apoptosis induced by β -amyloid is mediated by caspase-8. *Neurobiol Dis* 6:440-449.
- Jordan J, Galindo MF, Müller RJ 1997 Role of calpain- and interleukin-1 β converting enzyme-like proteases in the β -amyloid-induced death of rat hippocampal neurons in culture. *J Neurochem* 68:1612-1621.
- Keller JN, Kindy MS, Holtsberg FW, St Clair DK, Yen H-C, Germeyer A, Steiner SM, Bruce-Keller AJ, Hutchins JB, Mattson MP 1998 Mitochondrial manganese superoxide dismutase prevents neural apoptosis and reduces ischemic brain injury: suppression of peroxynitrite production, lipid peroxidation, and mitochondrial dysfunction. *J Neurosci* 18:687-697.
- LeBlanc A, Liu H, Goodver C, Bergeron C, Hammond J 1999 Caspase-6 role in apoptosis of human neurons, amyloidogenesis, and Alzheimer disease. *J Biol Chem* 274:23426-23436.
- Li WP, Chan WY, Lai HWL, Yew DT 1997 Terminal dUTP nick end labeling (TUNEL) positive cells in the different regions of the brain in normal aging and Alzheimer patients. *J Mol Neurosci* 8:75-82.
- Loo DT, Copani A, Pike CJ, Whittemore ER, Walencewicz AJ, Cotman CW 1993 Apoptosis is induced by β -amyloid in cultured central nervous system neurons. *Proc Natl Acad Sci USA* 90:7951-7955.
- Masliah E, Mallory M, Alford M, Tanaka S, Hansen LA 1998 Caspase dependent DNA fragmentation might be associated with excitotoxicity in Alzheimer disease. *J Neuropathol Exp Neurol* 57:1041-1052.
- Mattson MP, Pirtin J, Begley JG 1998 Amyloid β -peptide induces apoptosis-related events in synapses and dendrites. *Brain Res* 807:167-176.
- Michaelis ML, Ranciar N, Chen Y, Bechtel M, Ragan R, Hepperle M, Liu Y, George G 1998 Protection against β -amyloid toxicity in primary neurons by paclitaxel (taxol). *J Neurochem* 70:1623-1627.
- Mukhin AG, Ivanova SA, Allen JW, Faden AI 1998 Mechanical injury to neuronal/glial cultures in microplates: role of NMDA receptors and pH in secondary neuronal cell death. *J Neurosci Res* 51:748-758.

- Nakagawa T, Zhu H, Morishima N, Li E, Xu J, Yankner BA, Yuan J 2000 Caspase-12 mediates endoplasmic-reticulum-specific apoptosis and cytotoxicity by amyloid- β . *Nature* 403 98–103
- Perry G, Zhu X, Smith MA 2001 Do neurons have a choice in death? *Am J Pathol* 158 1–2
- Rohn TT, Head E, Su JH, Anderson AJ, Bahr BA, Cotman CW, Conboy DH 2001 Correlation between caspase activation and neurofibrillary tangle formation in Alzheimer diseases. *Am J Pathol* 158 189–198
- Selznick LA, Zheng TS, Flavell RA, Rakic P 2000 Amyloid beta-induced neuronal death is bax-dependent but caspase independent. *J Neuropathol Exp Neurol* 59 271–279
- Smale G, Nichols NR, Brady DR, Finch CE, Horton WE Jr 1995 Evidence for apoptotic cell death in Alzheimer disease. *Exp Neurol* 133 225–230
- Terry RD, Masliah E, Hansen LA 1994 Structural basis of the cognitive alterations in Alzheimer disease. In Terry RD, Katzman R, Bick KL, editors. *Alzheimer disease*. New York: Raven Press, Ltd. p 179–196
- Thornberry NA, Tano TA, Peterson EP, Rasper DM, Timkey T, Garcia-Calvo M, Houtzager VM, Nordstrom PA, Roy S, Vaillancourt JP, Chapman KT, Nicholson DW 1997 A combinatorial approach defines specificities of members of the caspase family and granzyme B. Functional relationships established for key mediators of apoptosis. *J Biol Chem* 272 17907–17911
- Trov CM, Rabacchi SA, Friedman WJ, Frappier TF, Brown K, Shelanski ML 2000 Caspase-2 mediates neuronal cell death induced by β -amyloid. *J Neurosci* 20 1386–1392
- Zhang Y, Goodover C, LeBlanc A 2000 Selected and protected apoptosis in human primary neurons microinjected with active caspase-3, -6, -7, and -8. *J Neurosci* 20 8384–8389

Caspase-9 Activation and Caspase Cleavage of tau in the Alzheimer's Disease Brain

Troy T. Rohn,^{*,1} Robert A. Rissman,[†] Michael C. Davis,^{*}
Young Eun Kim,^{*} Carl W. Cotman,[†] and Elizabeth Head[†]

^{*}Department of Biology, Science/Nursing Building, Room 228, Boise State University,
Boise, Idaho 83725 and [†]Institute for Brain Aging and Dementia,
University of California at Irvine, Irvine, California 92697

Received March 21, 2002; revised July 15, 2002; accepted for publication August 29, 2002

Accumulating evidence supports a role for the activation of proteolytic enzymes, caspases, in the Alzheimer's disease (AD) brain. Neurons committed to apoptosis may do so through a mitochondrial pathway employing caspase-9 or through an alternative, receptor-mediated pathway involving caspase-8. Considering the role of mitochondrial dysfunction in AD, we examined the possible activation of caspase-9 in the AD brain using an antibody that recognizes the active fragments of caspase-9, but not the full-length proform of the enzyme. *In vivo* immunohistochemical analysis demonstrated little caspase-9 activation in the majority of hippocampal brain sections from control brains. However, labeling of neurons as well as dystrophic neurites within plaque regions was observed in all AD hippocampal brain sections examined. In addition, active caspase-9 was colocalized with active caspase-8 and the accumulation of caspase-3-cleavage products of fodrin. The activation of caspase-9 was also observed in neurons positive for oxidative damage to DNA/RNA. A quantitative analysis indicates that as the number of neurons containing neurofibrillary tangles (NFTs) increases, the extent of caspase-9 activation decreases, supporting the idea that caspase-9 activation may precede NFT formation. In addition, a site-directed caspase-cleavage antibody was designed to the amino-terminal caspase-3 consensus cleavage site located in tau, and shown to be an effective marker for caspase-cleaved fragments of tau *in vitro*. Analysis with this antibody using age-matched control or AD brain sections demonstrated no staining in control brains while widespread labeling of NFTs, neuropil threads, and dystrophic neurites was observed in AD sections. Taken together, these results demonstrate the activation of caspases and cleavage of tau in the AD brain, events which may precede and lead to the formation of NFTs. © 2002 Elsevier Science (USA)

Key Words: Alzheimer's disease; tau; caspase-9; caspase-3; neurofibrillary tangles.

INTRODUCTION

One mechanism responsible for the extensive neuronal cell loss associated with Alzheimer's disease (AD) may be the activation of apoptotic pathways (Marx, 2001). Apoptosis is a highly conserved form of cell death that is characterized by chromatin condensation, nuclear fragmentation, cytoplasmic membrane blebbing, and cell shrinkage (Kerr *et al.*, 1972). Critical to the execution of apoptosis is a family of aspartate proteases, known as caspases, that are activated from

procaspases to their active form by proteolysis (Thornberry & Lazebnik, 1998). Caspases can serve both as initial transducers of apoptotic stimuli and also as final executioners of death. Two major pathways of apoptosis have been characterized: the death-receptor pathway in which caspase-8 plays a pivotal role and the mitochondrial pathway involving oxidative damage and activation of caspase-9 (Ashkenazi & Dixit, 1999). In both pathways, caspase-8 and -9, respectively, act as initiator caspases leading to downstream activation of executioner caspases, particularly caspase-3.

Several recent studies have employed caspase-cleavage site-directed antibodies as specific probes for apoptosis and demonstrated the activation of apopto-

¹ To whom correspondence should be addressed. Fax: 208-426-4267. E-mail: trohn@boisestate.edu.

tic pathways in the AD brain (Yang *et al.*, 1998; Gervais *et al.*, 1999; Rohn *et al.*, 2001b). Using this approach, we have recently developed an antibody to the active 18-kDa fragment of caspase-8 and demonstrated the localization of this fragment within neurofibrillary tangles (NFTs) and in neurites in plaque-rich regions in the AD brain (Rohn *et al.*, 2001a). On the basis of this study, it was suggested that cell-surface interaction of β -amyloid in neurons might trigger stimulation of the receptor-mediated pathway of apoptosis and cleavage of critical cellular proteins (Rohn *et al.*, 2001a). However, evidence also suggests significant oxidative damage in the AD brain possibly related to direct oxidizing effects of β -amyloid (Mattson *et al.*, 1999; Nunomura *et al.*, 2001), leading to the hypothesis that the mitochondrial pathway of apoptosis may also be activated in selected neurons within the AD brain.

In the present study, the role of activated caspase-9 was investigated in the AD brain using a caspase-cleavage site-directed antibody directed toward the N-terminus of the auto activation cleavage site of caspase-9. This commercial antibody recognizes the active fragments of caspase-9, but not the inactive, precursor form of the enzyme. A recent study, using this antibody, has demonstrated the presence of activated caspase-9 in the AD brain by western blot analysis (Lu *et al.*, 2000). By immunohistochemical analysis, we now show the presence of activated caspase-9 in the AD brain and within tangle-bearing neurons. Furthermore, active caspase-9 colocalized with active caspase-8 and caspase-3 cleavage products of fodrin within neurons exhibiting NFT morphology. These results support a role for the activation of both the receptor-mediated and mitochondrial-mediated pathways of apoptosis in the AD brain. In addition, evidence is presented demonstrating caspase cleavage of tau in the AD brain. Based on this study and along with previous studies (Rohn *et al.*, 2001a,b; Su *et al.*, 2001), a putative model is discussed whereby the role of caspases in the cleavage of important cellular proteins, per se, and not the full execution of apoptosis may actually be more important for driving neuron dysfunction and pathology observed in AD.

MATERIALS AND METHODS

Materials

All chemicals used were of the highest grade available. The rabbit (polyclonal) anti-caspase-9 cleavage site (315/316) specific antibody (caspase-9 CSSA) was

purchased from Biosource International (Camarillo, CA). The monoclonal antibody, AT8 (neurofibrillary tangles) was purchased from Innogenetics (Ghent, Belgium) and 6E10 (anti-A β -16) was purchased from Signet Laboratories, Inc. (Dedham, MA). Apopain/YAMA/caspase-3 (nickel-NTA-agarose associated) expressed in *E. coli* was from Upstate Biotechnology (Lake Placid, NY). The monoclonal antibody, 8oxodG, was from QED Bioscience, (San Diego, CA). This antibody recognizes 8-hydroxy-2'-deoxyguanosine (oh⁸dG), 8-hydroxyguanine (oh⁸G), as well as 8-hydroxyguanosine (oh⁸G), and serves as a marker of oxidative damage to DNA and RNA. A multiple antigen peptide (MAP) containing the QGGYTMHQDQ sequence to the amino terminal caspase-3 cleavage site of tau was used for the generation of polyclonal antibodies and was synthesized by Research Genetics, Inc. (Huntsville, AL). The peptide was injected into two different rabbits and collected sera were monitored for antibody titer by ELISA. All injections and collection of antisera were contracted out to Research Genetics, Inc. (Huntsville, AL). A Sulfolink kit used to affinity purify antibody was purchased from Pierce (Rockford, IL).

Human Subjects

Autopsy brain tissue from the hippocampus and entorhinal cortex of seven neuropathologically confirmed AD cases and seven nondemented cases with no evidence of senile plaques or NFTs was studied. Preliminary studies indicated that paraformaldehyde-fixed tissue samples were necessary to visualize caspase-9 CCSA with either no or weak labeling observed in formalin-fixed tissue. In addition, cases with short post mortem intervals (PMI) were selected to minimize possible post mortem effects leading to caspase activation. Case demographics are presented in Table 1. Age at death was not significantly different between AD (mean, 68 ± 8.29) and controls (mean, 74 ± 11.1). For quantification experiments, autopsy brain tissue from the hippocampus, parahippocampal, and frontal cortex of 13 cases with a range of Mini Mental Status Examination Scores (MMSE) between 0 and 30 (mean, 10.46 ± 2.21) was examined. Ages ranged from 69 to 92 years (mean, 77.31 ± 1.94) and post mortem intervals ranged from 2.75 to 7.5 h (mean, 4.61 ± 0.41). Frontal cortex was available from 9/13 cases and the hippocampus was available on 8/13 cases with 6/13 cases having both regions available for study. Case demographics are presented in Table 2. Human brain tissues used in this study were pro-

TABLE 1

Case Demographics

| Case | Group | Age (yrs) | Sex | PMI | MMSE | Neuropathological diagnosis | Braak & Braak stage | Cause of death |
|------|---------|-----------|-----|-----|------|-----------------------------|---------------------|-----------------------|
| 1 | AD | 66 | M | 7 | 7 | AD | N/A | Respiratory failure |
| 2 | AD | 71 | F | 7 | 7 | AD | VI | Unknown |
| 3 | AD | 51 | F | 2.5 | 3 | AD | N/A | Respiratory failure |
| 4 | AD | 77 | M | 3.6 | 22 | AD | V | Respiratory failure |
| 5 | AD | 68 | F | 5 | 5 | AD | VI | Cardiac Arrest |
| 6 | AD | 70 | M | 3.8 | 9 | AD | VI | End stage AD |
| 7 | AD | 73 | M | 2.7 | 7 | AD | VI | End stage AD |
| 8 | Control | 69 | M | 6.6 | N/A | Normal | 0 | N/A |
| 9 | Control | 68 | F | 6 | N/A | Normal | II | N/A |
| 10 | Control | 90 | F | 6.5 | N/A | Normal | N/A | Heart failure |
| 11 | Control | 70 | M | 5.2 | N/A | Normal | 0 | N/A |
| 12 | Control | 64 | F | 8 | N/A | Normal | N/A | Myocardial infarction |
| 13 | Control | 90 | F | 8 | N/A | Normal | I | N/A |
| 14 | Control | 67 | M | 2.7 | N/A | Normal | N/A | Cardiomyopathy |

Note: PMI, post mortem interval; MMSE, Mini Mental State Examination; N/A, not available.

vided by the Institute for Brain Aging and Dementia Tissue Repositories at the University of California, Irvine.

Cell Culture

Rat PC12 cells (ATCC, Manassas, VA) were grown on rat tail collagen-coated dishes in F12K media (Life Technologies, Inc.) containing 15% horse serum, 2.5% fetal bovine serum, 100 units/ml penicillin, and 100 µg/ml streptomycin. To induce differentiation to a

neuronal phenotype, PC12 cells were maintained in medium containing 100 ng/ml NGF for 10–12 days.

Western Blot Analysis

Western blot analysis was performed as previously described (Rohn *et al.*, 2000). PC12 extracts were prepared by adding ice-cold lysis buffer (50 mM Tris-HCL, 150 mM NaCl, 1% NP-40, 0.25% deoxycholate, 1 mM EGTA, pH 7.4), followed by centrifugation. The resulting supernatant was analyzed for protein con-

TABLE 2

Case Demographics for Quantification Study

| Case | Age (yrs) | Sex | PMI | MMSE | Neuropathological diagnosis | Braak & Braak stage | Cause of death |
|------|-----------|-----|------|------|-----------------------------|---------------------|---------------------|
| 1 | 74 | M | 2.75 | 0 | AD | V | Dehydration |
| 2 | 88 | F | 4.33 | 0 | AD | V | N/A |
| 3 | 85 | M | 5.3 | 4 | AD | V | AD |
| 4 | 73 | M | 4.3 | 7 | AD | V | Respiratory failure |
| 5 | 69 | M | 7 | 8 | AD | VI | N/A |
| 6 | 73 | M | 4 | 8 | AD | N/A | N/A |
| 7 | 70 | M | 3.75 | 9 | AD | VI | AD |
| 8 | 92 | F | 3.8 | 10 | AD | V | Respiratory failure |
| 9 | 74 | F | 7.5 | 13 | AD | N/A | N/A |
| 10 | 77 | M | 6.17 | 14 | AD | IV | Pneumonia |
| 11 | 77 | M | 3.6 | 16 | AD | V | Respiratory failure |
| 12 | 79 | F | 4.75 | 17 | AD | V | N/A |
| 13 | 74 | F | 2.8 | 30 | Normal | II | Cancer |

Note: PMI, post mortem interval; MMSE, Mini Mental State Examination; N/A, not available.

tent using the BCA assay (Pierce) to ensure equal protein loading. Blots were developed using an enhanced chemiluminescence system (Amersham).

Immunohistochemistry

Free-floating 50- μ m-thick serial sections were used for immunohistochemical studies as previously described (Rohn *et al.*, 2001b). For single-labeling experiments, sections were incubated overnight in either caspase-9 CSSA (5–10 μ g/ml) or anti-A β 1-16 (6E10, 1:1000). For immunostaining with β -amyloid, sections were pretreated in 90% formic acid for 4 min prior to incubation in 6E10. For double-labeling experiments, sections were incubated with caspase-9 CSSA (2.5 μ g/ml) and either AT8 (1:30,000) or an antibody to the active 18 kDa fragment of caspase-8 (CASP-8p18, 1:200). To determine if cross-reactivity to reagents was a factor in double-labeling experiments, experiments were replicated with the antibodies in reverse. Antigen visualization was determined using ABC complex (ABC Elite immunoperoxidase kit, Vector labs, Burlingame, CA) followed by reaction with diaminobenzidine (DAB, Vector Labs, Burlingame, CA).

For quantification studies involving cell counts, sections were incubated overnight in caspase-9 CSSA (1:100) and visualized with biotinylated anti-rabbit IgG, avidin–biotin complex and finally with DAB (1 h each incubation at RT). After a series of washes, sections were subsequently incubated in anti-PHF-1 (1:1000; provided by Dr. P. Davies, Albert Einstein College of Medicine, Bronx, NY) with a blue SG substrate. Both brain regions and all cases were immunostained in one study to reduce experimental variability. For quantification involving load values, two sections were incubated in either anti-caspase-9 CSSA or in 6E10 and similar areas were outlined and captured for image analysis. A load analysis was used for determining the relationship between active caspase-9 CSSA and β -amyloid because several cases showed extensive diffuse plaque formation leading to low plaque counts that did not accurately represent the extent of β -amyloid accumulation. Thus loads were obtained for both caspase-9 activation and β -amyloid to provide numbers that were comparable for the two different markers.

Immunofluorescence and Confocal Microscopy

Immunofluorescence studies were performed by incubating sections with caspase-9 CSSA (20 μ g/ml) overnight at room temperature, followed by ABC

complex containing a secondary rabbit-HRP antibody (ABC Elite immunoperoxidase). Antigen visualization was accomplished using a tyramide signal amplification kit (Molecular Probes, Eugene, OR) consisting of Alexa fluor 488-labeled tyramide (Ex/Em = 495/519). Caspase-9 CSSA labeled sections were further incubated with anti-fodrin caspase-cleavage product (CCP) antibody overnight at room temperature (0.4 to 0.5 μ g/ml). This antibody specifically recognizes caspase-3 cleavage products of fodrin but not full-length fodrin (Rohn *et al.*, 2001b). A secondary biotinylated antibody was incubated for 1 h followed by streptavidin Cy-3 (1:200) for an additional hour and observed under fluorescent optics or with a confocal microscope. Confocal images were collected on an Olympus IX70 inverted microscope using both a 20 \times and 40 \times objective for image analysis and barrier filters at 510 and 605 nm. A z-series at 1- μ m intervals was captured to determine the spatial colocalization characteristics of staining within individual neurons. To determine whether cross-reactivity to reagents was a factor in double-labeling experiments, experiments were replicated in reverse. The order of primary antibody application did not affect the results.

Quantification

Cell counts using double-labeled sections included five brain regions: CA3, hilus, the average of two areas of CA1, superficial/deep layers of the parahippocampal cortex, and superficial/deep layers of frontal cortex. Photographs of double-labeled regions for each case were taken at 20 \times and two independent counts by EH and RR was obtained while blind with respect to disease severity. The number of caspase-9 CSSA-only, PHF-1-only, and colocalized cells was counted. Reliability correlations between the two independent counts were significant and ranged between 0.805 and 0.997. The average of the two counts was used as raw data and analyzed using SPSS for Windows with an alpha of 0.05. Load values for single labels of either active-caspase 9 CSSA or A β 1-16 were obtained using previously described methods (Cummings *et al.*, 1996).

RESULTS

Caspase-9 Activation in the AD Brain

To examine a possible role for the activation of caspase-9 in the AD brain, hippocampal sections from AD or aged-matched control brains were analyzed by

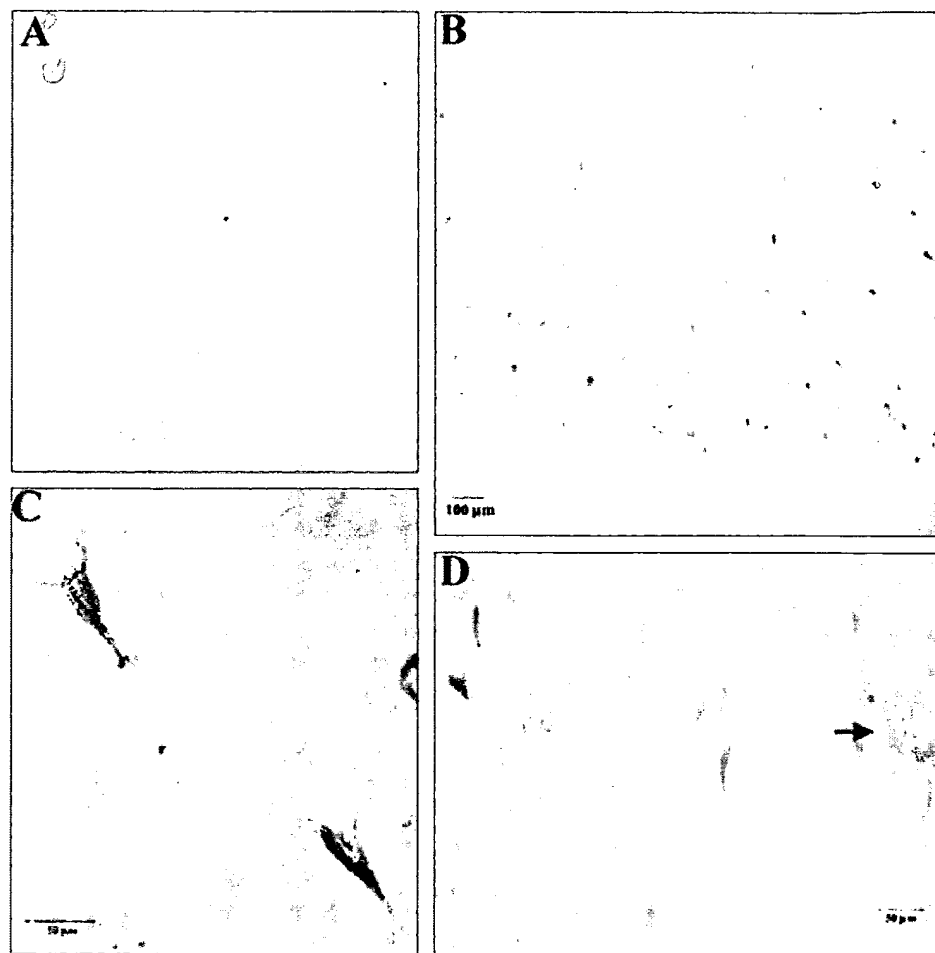


FIG. 1. Caspase-9 CSSA immunoreactivity in Alzheimer's disease. (A) Representative immunohistochemical staining with caspase-9 CSSA in a control case showing absence of staining. (B) Low magnification (4x) of a brain section from a representative AD case depicting labeling of neurons in the hippocampus. (C) High magnification (60x) of a brain section from a representative AD case showing labeling of two neurons with apparent tangle morphology. (D) Immunolabeling of caspase-9 CSSA in a representative AD case demonstrating labeling of apparent NFTs and neurites within a plaque-rich region (arrow).

immunohistochemistry. Little immunoreactivity was seen following incubation of caspase-9 CSSA in sections from age-matched control brains (Fig. 1A). Of the seven control cases examined, one case (64 years, PMI = 8 h, myocardial infarction) showed extensive neuronal staining within the hippocampus (data not shown). In contrast, extensive labeling of neurons in the hippocampus (CA1, CA2, and subiculum) and entorhinal cortex was observed in all tissue sections examined from severe AD brains (Fig. 1B, C, and D). In addition, swollen dystrophic neurites within plaque-rich regions was also observed following incubation with caspase-9 CSSA (Fig. 1D arrow and Fig. 2D). In a previous study, we demonstrated the activation of caspase-8 in NFTs, as well as in reactive astro-

cytes of the AD brain (Rohn *et al.*, 2001a). In the present study, there was no evidence for the activation of caspase-9 within reactive astrocytes in any of the AD cases examined (data not shown).

Caspase-9 Activation Colocalized with AT8 and Additional Markers of Caspase Activation

Neuronal staining by caspase-9 CSSA in the AD brain appeared to be within neurons containing NFTs. To examine a possible relationship between caspase-9 activation and NFTs, double-labeling experiments were performed using the NFT marker, AT8. Colocalization of these two antibodies was evident in neurons with clear NFT morphology (Fig. 2A).

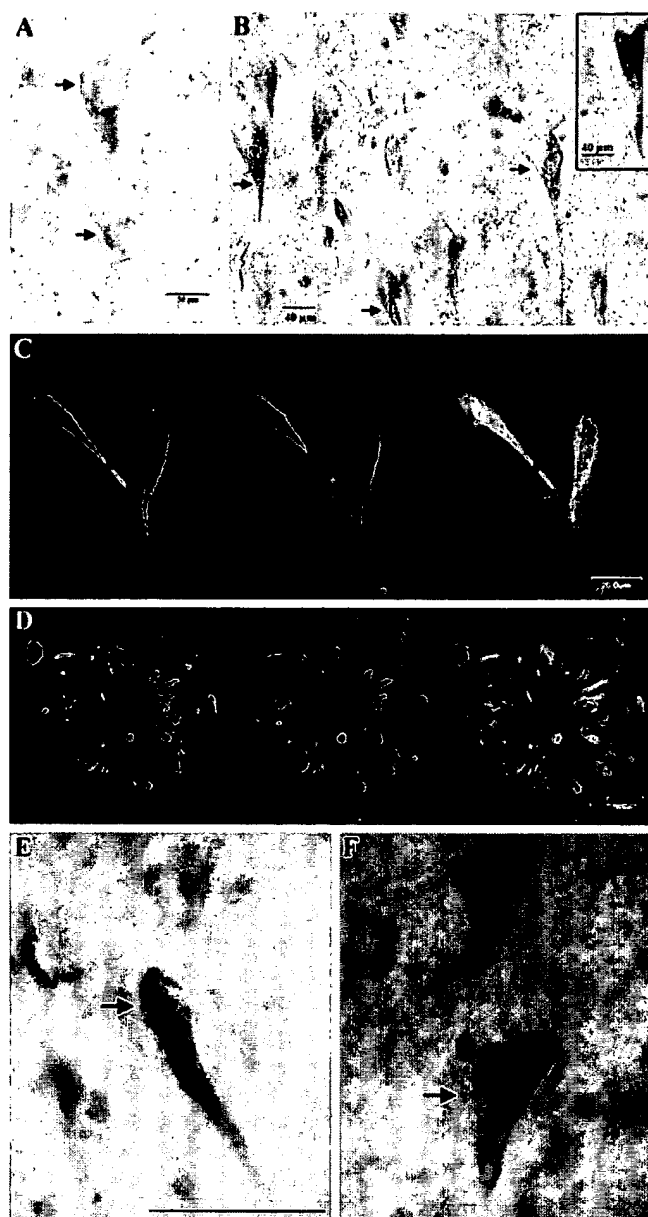


FIG. 2. Colocalization of the caspase-9 CSSA with a NFT marker and antibodies to the active fragments of caspase-8 as well as caspase-3 cleavage products of fodrin. (A) Double-labeling immunohistochemical analysis for caspase-9 CSSA and AT8 demonstrate colocalization of active caspase-9 (brown) and AT8 (blue) in hippocampal neurons from the AD brain. (B) Double-labeling immunohistochemical analysis for caspase-9 CSSA and CASP-8p18 antibody demonstrate colocalization of active caspase-9 (brown) and active caspase-8 (blue) in hippocampal neurons. Inset represents colocalization of active caspase-8 and -9 in a hippocampal brain section from an additional AD case. (C) Confocal fluorescent microscopy with the fodrin CCP antibody (red) and caspase-9 CSSA (green) in a severe AD case illustrating the high degree of colocalization between these two markers. (D) Identical to panel C, with fodrin CCP antibody (red) and caspase-9 CSSA (green) colocalizing

To examine a possible relationship between the activation of caspase-8 and caspase-9, experiments were performed using caspase-9 CSSA and CASP-8p18, an antibody that specifically recognizes the activated 18 kDa fragment of caspase-8 (Rohn *et al.*, 2001a). Colocalization of these two antibodies was seen in sections from the AD brain (Fig. 2B, arrows and inset), supporting the hypothesis that activation of both caspase-8 and -9 occurs within the same neurons of the AD brain. In addition, the colocalization of these two markers appeared to be delegated to neurons exhibiting a "flame-like" morphology consistent with NFTs (Fig. 2B).

We have previously demonstrated that fodrin CCP antibody is a specific marker for caspase-3 cleavage fragments for fodrin, a neuronal cytoskeleton protein (Rohn *et al.*, 2001b). Initial attempts to perform double-labeling immunohistochemical analysis using brown DAB and blue SG staining proved difficult due to a lack of color separation in neurons that were double-labeled (data not shown). Therefore, immunofluorescence double-labeling experiments were undertaken followed by confocal analysis. In this case, clear demonstration of colocalization of activated caspase-9 with caspase-3 products of fodrin within neurons of the AD brain was observed (Fig. 2C). In addition, colocalization of these two markers was observed within dystrophic neurites within plaque-rich regions in the AD brain (Fig. 2D). Thus, not only is activated caspase-9 localized together with activated caspase-8, but is also found in close association with stable CCPs of fodrin formed following cleavage by caspase-3. It should be noted that no pretreatment to abolish autofluorescence was necessary to observe fodrin CCP or activated caspase-9 immunofluorescence as the staining patterns of both these antibodies could be clearly differentiated from the characteristic morphological features associated with autofluorescence.

Caspase-9 Activation, DNA/RNA Oxidative Damage and Mitochondrial Dysfunction

Because caspase-9 is a key member of the mitochondrial pathway of apoptosis, we examined whether it is

within dystrophic neurites within a cored plaque of a severe AD case. (E and F) Double-labeling immunohistochemical analysis for caspase-9 CSSA (blue) and 8oxodG (brown) in two separate AD cases demonstrates colocalization of active caspase-9 with markers for oxidative DNA/RNA damage. Scale bars are equivalent to 50 μ m.

active in neurons exhibiting oxidative damage. To determine this, we performed colocalization experiments with caspase-9 CSSA and anti-8oxodG, an antibody that detects oxidative damage to either DNA (nuclear or mitochondrial) or RNA. In previous studies, 8oxodG was observed in association with dysfunctional mitochondria, which may serve as a stimulus for the activation of caspase-9 (Aliev *et al.*, 2002). As shown in Fig. 2E and F, the activation of caspase-9 occurred in neurons positive for oxidized DNA/RNA in the AD brain. Whereas 8oxodG staining appeared to be punctate within the cell body, the majority of caspase-9 CSSA labeling appeared to be more concentrated in the apical dendrites.

Caspase-9 Activation, NFT and Senile Plaque Formation in the AD Brain

A consistent feature of caspase-9 CSSA labeling in the AD brain was immunolabeling of neurons with "flame-like" inclusions, consistent with tangle formation. Therefore, to examine in further detail a possible relationship between caspase-9 activation and NFTs, quantitative analysis of 13 cases with a range of MMSE scores between 0 and 30 was performed using caspase-9 CSSA and PHF-1, a marker for mature NFTs. The number of cells containing both caspase-9 CSSA and PHF-1 was relatively small and ranged from 0 to a maximum of 18.6% across all the brain regions sampled. In a control case with a MMSE of 30 used for the quantification study, no tangles were observed but a significant number of caspase-9 CSSA positive neurons were identified, suggesting that caspase-9 activation can occur in the absence of overt tangle formation. Further, a significant negative correlation was observed for the number of PHF-1 positive neurons and those positive for caspase-9 CSSA in the parahippocampal cortex ($r = -0.75$, $P < .053$) and the frontal cortex ($r = -0.688$, $P < .013$), and for area CA1 ($r = -0.94$, $P < .002$) (Fig. 3, top) but not in the hilus ($r = 0.42$, $P = \text{n.s.}$) or in the CA3 subregion ($r = 0.40$, $P = \text{n.s.}$) (data not shown). Thus, as tangle formation increased, the extent of caspase-9 activation decreased. Figure 3 (lower panel) shows representative staining of caspase-9 CSSA and PHF-1 in area CA1 and the frontal cortex in cases with increasing numbers of NFTs (left to right) illustrating the inverse relationship between caspase-9 activation and NFT formation in the AD brain. No significant correlation was observed between caspase-9 CSSA and MMSE, age at death, or post mortem interval.

To determine the relationship between active caspase-9 CCSA and β -amyloid deposition, loads were obtained from single label experiments for each antibody. No significant correlations were found between these two variables (data not shown). Thus, more extensive β -amyloid was not associated with higher levels of caspase-9 activation.

Synthesis and Characterization of a Caspase-Cleavage Site-Directed Antibody to the Microtubule-Associated Protein, tau

Based upon the previous results indicating a relationship between the activation of the enzyme caspase-9 and NFT formation, experiments were undertaken to examine if tau, whose modification leads to PHFs and NFTs in AD, is cleaved by caspases and whether fragments accumulate in the AD brain. To determine if tau is cleaved by caspases, *in vivo*, we designed a caspase-cleavage site-directed antibody to tau based upon a known consensus caspase-cleavage site within the tau sequence located toward the amino-terminal end, DRKD-QGGYTMHQDQ (Canu *et al.*, 1998). Following purification of this antibody (herein termed tauCCP antibody) by affinity chromatography, its validity as a specific probe for tau CCPs was examined using a cell-free system. Human brain or primary cultured rat cortical neuron extracts were incubated with or without caspase-3. Following digestion with caspase-3, samples were immunoblotted with the tau-CCP antibody to determine if recognition of CCPs occurred. Two prominent bands were immunolabeled with the tau-CCP antibody in digested extracts corresponding to 67 and 28 kDa, that were not present under control conditions (Fig. 4A, left panel). Under these conditions, the tau CCP antibody did not label full-length tau in control lanes, which normally has a molecular weight of 70 kDa. To verify that full-length tau was indeed present in these extracts the same blot was stripped and reprobed with an anti-tau antibody that recognizes both full-length tau and its associated caspase-cleaved fragments. Numerous bands corresponding to full-length tau and CCPs were detected following western blot analysis with this antibody (Fig. 4A, right panel). These initial results suggest that the tau-CCP antibody recognizes CCPs of tau, but does not recognize full-length tau.

To further characterize the tau-CCP antibody, experiments were undertaken using differentiated PC12 cells. To verify the presence of tau in PC12 cells, extracts from both nondifferentiated and differentiated

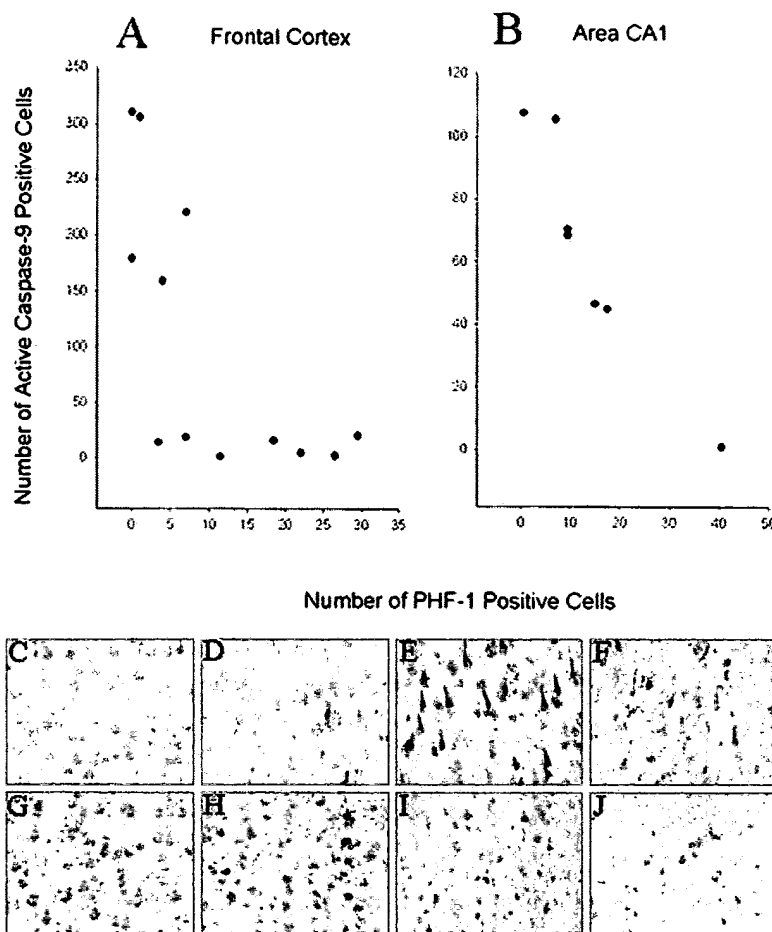


FIG. 3. Negative correlation between caspase-9 activation and PHF-1 immunolabeling. Significant negative correlations were observed for the number of PHF-1 positive neurons and those positive for caspase-9 CCSA in the frontal cortex ($r = -0.69$, $P < .013$) (A) and for area CA1 ($r = -0.94$, $P < .002$) (B). Caspase-9 activation decreases with increasing neurofibrillary tangle accumulation in area CA1 of the hippocampus (C-F) and frontal cortex (G-J). Cases were selected with increasing tangle-bearing neuron counts (lowest to highest, left-right) to illustrate that caspase-9 activation (brown) also appears to precede tangle formation (blue) and decline as the extent of tangle formation increases. Note, however, that in a severe AD case (F and J), extensive cell loss may also account for loss of active-caspase-9 containing neurons.

PC12 cells were immunoblotted with the anti-tau antibody that recognizes full-length tau. Figure 4B (left panel) depicts the results of such an experiment showing the expression of tau following differentiation of PC12 cells in the presence of NGF. The full-length antibody also recognized numerous CCPs of tau following digestion with caspase-3 (Fig. 4B, left panel). In separate experiments, NGF-treated PC12 cells were incubated in the presence or absence of caspase-3, and probed with the tau-CCP antibody. Although the tau-CCP antibody recognized several caspase-cleaved fragments including a prominent band running at 28 kDa, it did not recognize full-length tau in nondigested extracts (Fig. 4B, right panel).

Tau-CCP Antibody as a Marker for Caspase Activation in the AD Brain

Following validation of the tau-CCP antibody as a specific probe for the caspase-cleavage of tau *in vitro*, immunohistochemistry experiments were performed using hippocampal sections from AD or age-matched control brains. In all control sections examined, little staining was observed following application of the tau-CCP antibody (Fig. 4C). In contrast, widespread labeling of NFTs, neuropil threads, and dystrophic neurites within plaque-rich regions was observed following immunohistochemical analysis with the tau-CCP antibody in all severe AD brain sections exam-

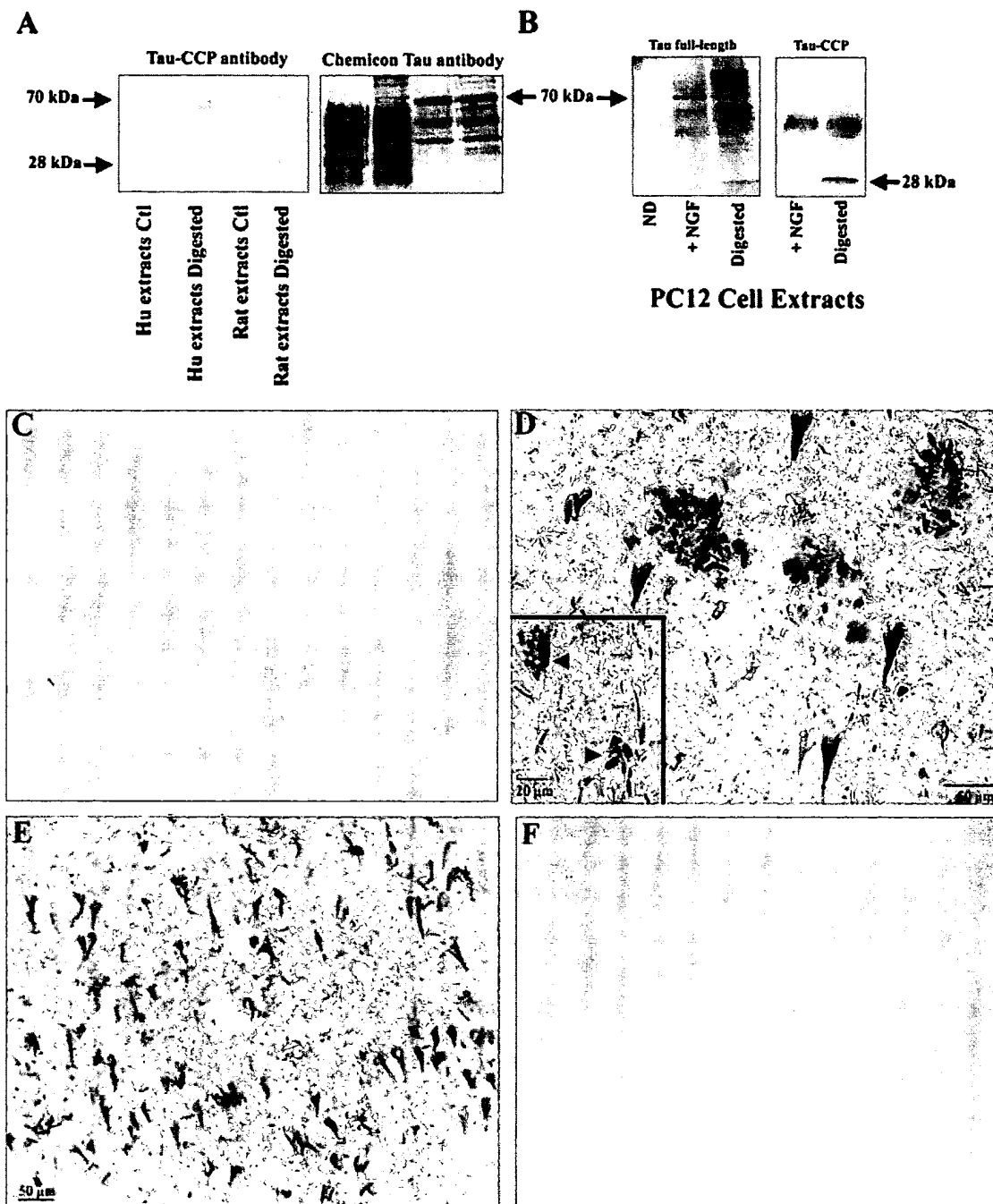


FIG. 4. Caspase cleavage of tau in the AD brain. (A) Brain extracts from human or primary cultured rat cortical neurons were digested with 1.88 μ g of caspase-3 overnight at RT. Proteins were separated by a 12% SDS-PAGE gel, transferred to nitrocellulose, and probed with 0.5–1.0 μ g/ml of purified tau-CCP antibody (left panel) or with a commercial antibody (1:100) that recognizes both full-length tau (70 kDa), as well as any associated cleaved fragments (right panel). Unlike the commercial antibody, which recognized full-length tau and caspase-cleaved fragments, the tau-CCP antibody labeled two prominent caspase-3-cleaved fragments without labeling full-length tau corresponding to 70 kDa. (B) NGF-treated PC12 cell extracts were prepared, digested with caspase-3, and analyzed with either a commercial antibody to tau (left panel) or with the tau-CCP antibody (right panel) as described above. The tau-CCP antibody recognized caspase-3 digested fragments but did not recognize full-length tau. (C) Representative immunohistochemical staining with anti-tau CCP purified antibody in a control case showing lack of immunoreactivity. (D) High-field magnification (40X) of a hippocampal section from a severe AD case depicting tau-CCP immunoreactivity within NFTs, neuropil threads, and dystrophic neurites within plaque regions. Inset (D) indicates the granular nature of tau-CCP immunoreactivity (arrowheads). (E and F) Serial hippocampal tissue sections from a severe AD case showing extensive neuronal labeling using tau-CCP, which is absent after staining with preabsorbed antibody (panel F).

ined (Fig. 4D). Interestingly, numerous tau-CCP-positive neurons displayed staining that was granular in nature, and appeared to be membrane-bound (inset, arrowheads, Fig. 4D). This type of staining has also been observed in a previous study demonstrating the activation of caspase-3 in the AD brain (Stadelmann et al., 1999). Importantly, staining with the tau-CCP antibody was completely prevented following preabsorption with free peptide (Fig. 4E and F), illustrating the specificity of the tau-CCP antibody. In addition, we also tested purified tau-CCP antibody derived from a second rabbit immunized with the same amino-terminal peptide and obtained identical results following immunohistochemistry (data not shown).

DISCUSSION

Several recent studies have reported increased levels of caspase-3-cleaved substrates, including APP, fodrin, and actin in the AD brain (Yang et al., 1998; Gervais et al., 1999; Rohn et al., 2001b). All of these studies relied on the use of site-directed caspase-cleavage antibodies, which take advantage of the fact that caspases are specific, cleaving after aspartic residues thereby generating caspase-cleavage products (CCPs) that are antigenically distinct. Using this approach, we have synthesized antibodies against one of the active fragments of caspase-8, compared these results with a commercially available active-caspase-8 antibody, and demonstrated colocalization of this antibody together with caspase-3 cleaved products of fodrin in the AD brain (Rohn et al., 2001a). The goal of the present study was to further dissect out the pathways of apoptosis activated in the AD brain. Presently, there are two major pathways leading to apoptosis: the death-receptor pathway in which caspase-8 plays a pivotal initiator role, and the mitochondrial pathway (or chemical pathway) where caspase-9 is the key initiator caspase (Ashkenazi and Dixit, 1999). Both pathways converge and activate the executioner caspase, caspase-3.

Data presented in the present manuscript suggests a role for the activation caspase-9 in the AD brain. These results are supported by a recent study demonstrating an immunoreactive band consistent with cleaved caspase-9 in synaptosomal preparations from five of five AD brains but only in one of five control brain preparations using caspase-9 CSSA (Lu et al., 2000). Taken together, these results implicate the mitochondrial pathway of apoptosis as a mechanism leading to activation of caspase-3 in the AD brain. Furthermore, the observation of caspase-9 activation in one of five

control cases in the Lu et al., study (2000) is consistent with our observations of a subset of control cases showing active caspase-9 immunoreactivity.

A Link between Oxidative Damage and Pathways Associated with Apoptosis in AD

Oxidative damage is a key feature of normal aging and is more extensive in the AD brain (Smith et al., 2000). It is possible that neurons accumulating extensive oxidative insults may selectively undergo apoptosis (Lu et al., 2000). Mitochondria are particularly vulnerable to oxidative damage because they are the major source of oxidants produced through normal metabolic processes. Mitochondrial dysfunction has been observed in AD brain (Hirai et al., 2001), and as a consequence, stimulation of the mitochondrial pathway of apoptosis may be elicited through oxidative damage leading to the release of cytochrome *c*. Released cytochrome *c* interacts with Apaf-1 and this complex recruits caspase-9 leading to its activation (Kuida, 2000). Studies have shown that if caspase-9 is inactivated or is not expressed, full activation of the mitochondrial pathway does not occur (Kuida, 2000). For example, caspase-9 null mice are deficient in activation of caspase-3 *in vivo* and cytochrome *c*-mediated cleavage of caspase-3 is absent in cytosolic extracts but can be restored after reconstitution with *in vitro*-translated caspase-9 (Kuida et al., 1998). Thus, the observation of neurons containing both oxidatively damaged DNA/RNA, most likely associated with mitochondrial dysfunction, and the activation of caspase-9 suggests a link between these two events *in vivo*. Further experiments will help clarify the strength of the association between these two markers of cell dysfunction.

Stimulation of Apoptotic Pathways by Multiple Insults May Ultimately Lead to the Activation of Caspase-3

Another outcome of the present study was the demonstration of colocalization of activated caspase-9 and caspase-8 within individual neurons in the AD brain. This suggests the possibility of concurrent activation of both major pathways of apoptosis within the same neuron possibly by different stimuli. Caspase-8 has been implicated in Fas/CD95 or tumor necrosis factor (TNF) receptor cell death program. In this regard, caspase-8 is thought to be the most apical member of the family of caspases that is recruited by adapter proteins (e.g., Fas-associated death domain, FADD) and converted to an active form by auto proteolysis

(Muzio *et al.*, 1996). Cleavage of caspase-8 results in two active fragments of 11 and 18 kDa, both of which represent the activated form of the enzyme. Caspase-8 in turn, is thought to activate downstream caspases, particularly caspase-3 (Takahashi, 1999).

What mechanism occurring in the AD brain could possibly lead to the activation of both pathways of apoptosis within the same neuron? In a previous study, we presented a model proposing that β -amyloid may induce neuronal cell death by inducing apoptosis following cross-linking of death-receptors and concomitant activation of caspase-8 and caspase-3 (Rohn *et al.*, 2001a). Several *in vitro* studies support this as a possible mechanism for β -amyloid-induced neurotoxicity (Ivins *et al.*, 1999a,b). In addition to the possible activation of death receptors by a cross-linking mechanism, evidence suggests that β -amyloid may also induce significant oxidative stress within neurons by the formation of reactive oxygen species (Miranda *et al.*, 2000; Varadarajan *et al.*, 2000). The formation of reactive oxygen species and subsequent oxidative damage may lead to the stimulation of the mitochondrial pathway of apoptosis. Evidence given in the present report, indicating the activation of caspase-9 and caspase-8, suggests that activation of both pathways of apoptosis may occur within neurons in the AD brain.

However, the current study indicates a closer association between NFT formation rather than β -amyloid deposition and the extent of caspase-9 activation. The simplest interpretation is that β -amyloid does not serve as a stimulus for the activation of either caspase. This may, however, be a difficult hypothesis to test using post mortem tissue because β -amyloid is a long-lived protein and will be present in the brain at much longer time intervals than would be expected for the activity of any single enzyme. Experiments using neuronal cultures and *in vitro* methodologies would be better able to address this question directly.

An Association between Caspase Activation and tau Pathology?

Regardless of the exact pathway of apoptosis stimulated, the end result will be the activation of executioner caspases, such as caspase-3, and the cleavage of critical cellular proteins. One susceptible protein that may be a target for caspase-3 cleavage relevant to AD is the microtubule-associated protein, tau. In AD, tau becomes hyperphosphorylated leading to the formation of NFTs and destabilization of the cytoskeleton network (Bramblett *et al.*, 1993). NFTs consist of paired

helical filaments (PHFs) resulting from the hyperphosphorylation of tau in select neuronal populations. In the brains of patients with AD, the cytoskeleton is gradually damaged and replaced by bundles of PHFs, which are largely composed of abnormally processed forms of tau (Wischik *et al.*, 1988; Alonso *et al.*, 1996). Until recently, it was thought that an abnormal phosphorylation of tau proteins was responsible for their aggregation in AD. However, normal tau proteins are also phosphorylated in fetal and adult brain, and they do not aggregate to form filamentous inclusions (Buee *et al.*, 2000). Moreover, nonphosphorylated recombinant tau proteins form filamentous structures under physiological conditions *in vitro* (Buee *et al.*, 2000). In light of these observations, it has been proposed that modifications of tau independent of phosphorylation may also be involved in the formation of pathological tau filaments.

One recurrent theme demonstrated in the present study along with our previous studies is activation of caspases within tangle-bearing neurons (Rohn *et al.*, 2001a,b; Su *et al.*, 2001). Thus, we have previously demonstrated a strong positive correlation ($R = 0.84$) between the presence of CCPs of fodrin and NFTs (Rohn *et al.*, 2001b). In the present study we actually observed a *negative* correlation between the activation of caspase-9 and NFTs in the CA1, parahippocampal regions, and the frontal cortex of the AD brain. There are a number of possible interpretations of this result: (1) the stimuli to drive mitochondrial-dependent caspase-9 activation are no longer present in tangle bearing neurons; (2) caspase-9 activation is independent of tangle formation; (3) caspase-9 activation precedes tangle formation. We favor the last interpretation because it is clear that the activation of caspase-9 and tangle formation is related based on the results following quantitative analysis. These results are consistent with the appearance of activated caspase-9, followed by increasing numbers of neurons developing tangles.

The negative correlation in the present study between caspase-9 activation and NFTs and the positive correlation between caspase cleavage of fodrin and NFTs in our previous report (Rohn *et al.*, 2001b) would seem to be contradictory. However, it is important to realize the distinction between the two antibodies used for each of these studies. The fodrin CCP antibody recognizes cleavage products of fodrin that are stable, which accumulate over time and are present even when the neuron dies. It seems plausible that only when sufficient amounts of these CCPs of fodrin accumulate, does the fodrin CCP antibody give a

strong signal following immunohistochemical analysis. We hypothesize that the accumulation of CCPs of fodrin may take many years to develop and this is why it is so strongly correlated with PHF-1 immunolabeling. On the other hand, an antibody against the active fragment of caspase-9 would be expected to provide a maximum signal as soon as it was activated in the AD brain, and might actually be attenuated in late stages of AD as the neurons die.

Based on these results and other evidence in the literature, it is possible that the activation of caspases within neurons in the AD brain may lead to tau cleavage and its modification may contribute to the formation of PHFs and NFT formation. In order for this to be true, it must be first demonstrated that tau is cleaved by caspases *in vivo*. Data in the present study indicate the labeling of neurons with a site-directed caspase-cleavage antibody to tau in the AD brain, supporting the conclusion that tau is cleaved by caspases in the AD brain. The implications of these data are that caspases play an earlier role in the pathology associated with AD than originally described and do not represent simply end stage processes associated with neuronal cell death. Therefore, pharmacological intervention using caspase inhibitors may be a potential beneficial therapeutic target for the treatment of AD.

In some instances, staining with the tau-CCP antibody revealed labeling of neurons that was granular and vesicular in nature (Fig. 4D, inset). Previous studies have shown that tau is not only a substrate for caspase cleavage, but in turn, this produces a tau fragment that is an effector of apoptosis generating a positive-feedback loop that is self-propagating (Fasulo et al., 2000; Chung et al., 2001). Therefore, the compartmentalization of caspase-cleaved fragments of tau would suggest that these fragments are somehow toxic to the neuron and are being segregated as a possible means of protection. These results are supported by a previous study, which demonstrated the activation of caspase-3 in autophagic granules in single neurons in the AD brain (Stadelmann et al., 1999). The authors concluded that activation of caspases in neurons is counteracted by the seclusion of damaged areas into autophagic vacuoles (Stadelmann et al., 1999).

A Hypothetical Sequence of Events Linking β -Amyloid Deposition and NFT Formation in the AD Brain

We propose that individual neurons within the AD brain may have a number of caspases that have been

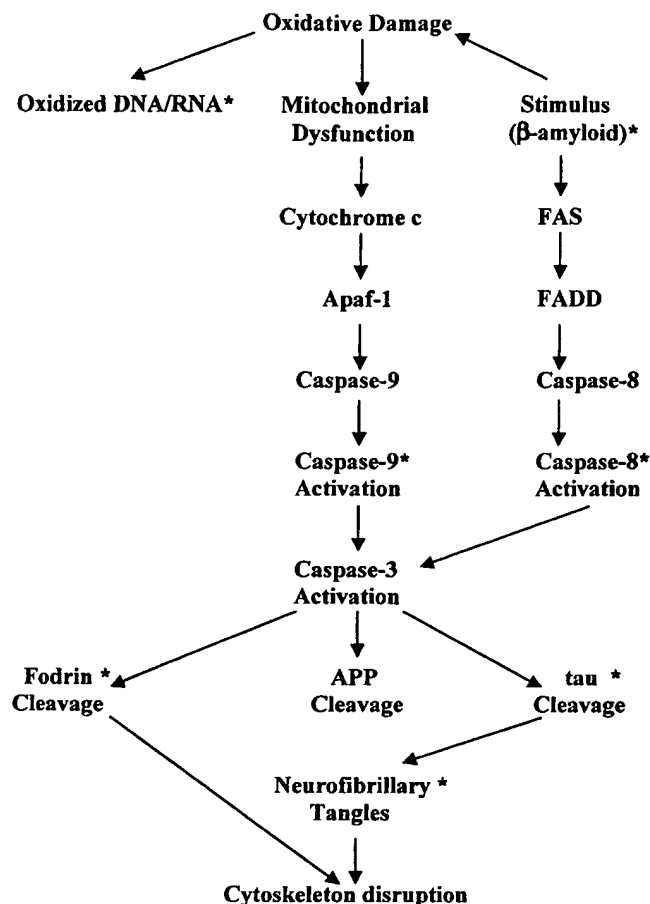


FIG. 5. A hypothetical sequence of events leading to caspase activation and possibly tau cleavage. Two parallel pathways, activated by different stimuli, may operate within individual neurons. The accumulation of β -amyloid may lead to the cross-linking and activation of receptors resulting in caspase-8 activation. An additional mechanism is that β -amyloid may modify lipids by oxidation in the cell membrane that may also increase or exacerbate existing oxidative damage within neurons. Mitochondrial dysfunction is also a consequence of oxidative damage that can be detected by oxidative modifications to DNA/RNA, which may accumulate within neurons and in turn lead to further mitochondrial dysfunction. Cytochrome c is released by dysfunctional mitochondria and activates caspase-9. Both pathways may then converge by activating the effector enzyme, caspase-3. Tangle formation may be occurring independently or as a consequence of caspase-3 activation and cleavage of tau. Asterisks indicate markers used in the current study.

activated by several possible stimuli (Fig. 5). The deposition of β -amyloid may lead to caspase-8 activation through cross-linking of death receptors such as Fas. In parallel, oxidative damage accumulating with both age and with disease may lead to mitochondrial dysfunction, the release of cytochrome c, and finally,

caspase-9 activation. Thus, it is possible that the cumulative events of β -amyloid accumulation and oxidative damage may converge and become additive when levels of caspase-3 rise. In this model, tangle formation would be a relatively late event and is more closely associated in time with caspase-3 activation and the accumulation of caspase-3 cleavage products, such as fodrin. Caspase cleavage of proteins that are constituents of the cytoskeleton, such as fodrin and tau, may result in the disassembly of the cytoskeleton, leading to disruption of synaptic vesicle transport as well as altering cell morphology.

In conclusion, we have demonstrated the activation of caspase-9 together with caspase-8 and products of caspase-3 cleavage in the AD brain. The colocalization of caspase-9 together with caspase-8 within individual neurons would suggest the activation of multiple pathways of apoptosis within neurons in the AD brain. It is possible that β -amyloid may initiate the activation of both apoptotic pathways through either cross-linking of death receptors or through the generation of oxidative damage. The activation of either pathway within neurons of the AD brain may lead to the concomitant activation of caspase-3 and subsequent cleavage of cellular proteins, including tau. Caspase-cleavage of tau may induce modifications of tau that facilitate the formation of PHFs and ultimately NFTs. However, the exact role of caspase cleavage of tau, *in vivo*, and the formation of NFTs will require additional studies.

ACKNOWLEDGMENTS

This work was supported in part by NIA grants; R15AG19642-01 and R03AG19386-01 (T.T. Rohn), a grant from the Aging Federation of Aging Research (T.T. Rohn), and NIA grant P50 AG16573 to CWC.

REFERENCES

- Aliev, G., Smith, M. A., Seyidov, D., Neal, M. L., Lamb, B. T., Nunomura, A., Gasimov, E. K., Vinters, H. V., Perry, G., LaManna, J. C., & Friedland, R. P. (2002) The role of oxidative stress in the pathophysiology of cerebrovascular lesions in Alzheimer's disease. *Brain Pathol.* 12, 21-35.
- Alonso, A. C., Grundke-Iqbal, I., & Iqbal, K. (1996) Alzheimer's disease hyperphosphorylated tau sequesters normal tau into tangles of filaments and disassembles microtubules. *Nat. Med.* 2, 783-787.
- Ashkenazi, A., & Dixit, V. M. (1999) Apoptosis control by death and decoy receptors. *Curr. Opin. Cell Biol.* 11, 255-260.
- Bramblett, G. T., Goedert, M., Jakes, R., Merrick, S. E., Trojanowski, J. Q., & Lee, V. M. (1993) Abnormal tau phosphorylation at Ser396 in Alzheimer's disease recapitulates development and contributes to reduced microtubule binding. *Neuron* 10, 1089-1099.
- Buee, L., Bussiere, T., Buee-Scherrer, V., Delacourte, A., & Hof, P. R. (2000) Tau protein isoforms, phosphorylation and role in neurodegenerative disorders. *Brain Res. Brain Res. Rev.* 33, 95-130.
- Canu, N., Dus, L., Barbato, C., Ciotti, M. T., Brancolini, C., Rinaldi, A. M., Novak, M., Cattaneo, A., Bradbury, A., & Calissano, P. (1998) Tau cleavage and dephosphorylation in cerebellar granule neurons undergoing apoptosis. *J. Neurosci.* 18, 7061-7074.
- Chung, C. W., Song, Y. H., Kim, I. K., Yoon, W. J., Ryu, B. R., Jo, D. C., Woo, H. N., Kwon, Y. K., Kim, H. H., Gwag, B. J., Mook-Jung, I. H., & Jung, Y. K. (2001) Proapoptotic effects of tau cleavage product generated by caspase-3. *Neurobiol. Dis.* 8, 162-172.
- Cummings, B. J., Head, E., Afagh, A. J., Milgram, N. W., & Cotman, C. W. (1996) Beta-amyloid accumulation correlates with cognitive dysfunction in the aged canine. *Neurobiol. Learn. Mem.* 66, 11-23.
- Fasulo, L., Ugolini, G., Visintin, M., Bradbury, A., Brancolini, C., Verzillo, V., Novak, M., & Cattaneo, A. (2000) The neuronal microtubule-associated protein tau is a substrate for caspase-3 and an effector of apoptosis. *J. Neurochem.* 75, 624-633.
- Gervais, F. G., Xu, D., Robertson, G. S., Vaillancourt, J. P., Zhu, Y., Huang, J., LeBlanc, A., Smith, D., Rigby, M., Shearman, M. S., Clarke, E. E., Zheng, H., Van Der Ploeg, L. H., Ruffolo, S. C., Thornberry, N. A., Xanthoudakis, S., Zamboni, R. J., Roy, S., & Nicholson, D. W. (1999) Involvement of caspases in proteolytic cleavage of Alzheimer's amyloid-beta precursor protein and amyloidogenic A beta peptide formation. *Cell* 97, 395-406.
- Hirai, K., Aliev, G., Nunomura, A., Fujioka, H., Russell, R. L., Atwood, C. S., Johnson, A. B., Kress, Y., Vinters, H. V., Tabaton, M., Shimohama, S., Cash, A. D., Siedlak, S. L., Harris, P. L., Jones, P. K., Petersen, R. B., Perry, G., & Smith, M. A. (2001) Mitochondrial abnormalities in Alzheimer's disease. *J. Neurosci.* 21, 3017-3023.
- Ivins, K. J., Ivins, J. K., Sharp, J. P., & Cotman, C. W. (1999a) Multiple pathways of apoptosis in PC12 cells. CrmA inhibits apoptosis induced by beta-amyloid. *J. Biol. Chem.* 274, 2107-2112.
- Ivins, K. J., Thornton, P. L., Rohn, T. T., & Cotman, C. W. (1999b) Neuronal apoptosis induced by beta-amyloid is mediated by caspase-8. *Neurobiol. Dis.* 6, 440-449.
- Kerr, J. F., Wyllie, A. H., & Currie, A. R. (1972) Apoptosis: A basic biological phenomenon with wide-ranging implications in tissue kinetics. *Br. J. Cancer* 26, 239-257.
- Kuida, K. (2000) Caspase-9. *Int. J. Biochem. Cell Biol.* 32, 121-124.
- Kuida, K., Haydar, T. F., Kuan, C. Y., Gu, Y., Taya, C., Karasuyama, H., Su, M. S., Rakic, P., & Flavell, R. A. (1998) Reduced apoptosis and cytochrome c-mediated caspase activation in mice lacking caspase 9. *Cell* 94, 325-337.
- Lu, D. C., Rabizadeh, S., Chandra, S., Shayya, R. F., Ellerby, L. M., Ye, X., Salvesen, G. S., Koo, E. H., & Bredesen, D. E. (2000) A second cytotoxic proteolytic peptide derived from amyloid beta-protein precursor. *Nat. Med.* 6, 397-404.
- Marx, J. (2001) Neuroscience. New leads on the 'how' of Alzheimer's. *Science* 293, 2192-2194.
- Mattson, M. P., Pedersen, W. A., Duan, W., Culmsee, C., & Camandola, S. (1999) Cellular and molecular mechanisms underlying perturbed energy metabolism and neuronal degeneration in Alzheimer's and Parkinson's diseases. *Ann. NY Acad. Sci.* 893, 154-175.
- Miranda, S., Opazo, C., Larrondo, L. F., Munoz, F. J., Ruiz, F., Leighton, F., & Inestrosa, N. C. (2000) The role of oxidative stress

- in the toxicity induced by amyloid beta-peptide in Alzheimer's disease. *Prog. Neurobiol.* **62**, 633–648.
- Muzio, M., Chinnaiyan, A. M., Kischkel, F. C., O'Rourke, K., Shevchenko, A., Ni, J., Scaffidi, C., Bretz, J. D., Zhang, M., Gentz, R., Mann, M., Krammer, P. H., Peter, M. E., & Dixit, V. M. (1996) FLICE, a novel FADD-homologous ICE/CED-3-like protease, is recruited to the CD95 (Fas/APO-1) death-inducing signaling complex. *Cell* **85**, 817–827.
- Nunomura, A., Perry, G., Aliev, G., Hirai, K., Takeda, A., Balraj, E. K., Jones, P. K., Ghanbari, H., Wataya, T., Shimohama, S., Chiba, S., Atwood, C. S., Petersen, R. B., & Smith, M. A. (2001) Oxidative damage is the earliest event in Alzheimer disease. *J. Neuropathol. Exp. Neurol.* **60**, 759–767.
- Rohn, T. T., Head, E., Nesse, W. H., Cotman, C. W., & Cribbs, D. H. (2001a) Activation of caspase-8 in the Alzheimer's disease brain. *Neurobiol. Dis.* **8**, 1006–1016.
- Rohn, T. T., Head, E., Su, J. H., Anderson, A. J., Bahr, B. A., Cotman, C. W., & Cribbs, D. H. (2001b) Correlation between caspase activation and neurofibrillary tangle formation in Alzheimer's disease. *Am. J. Pathol.* **158**, 189–198.
- Rohn, T. T., Ivins, K. J., Bahr, B. A., Cotman, C. W., & Cribbs, D. H. (2000) A monoclonal antibody to amyloid precursor protein induces neuronal apoptosis. *J. Neurochem.* **74**, 2331–2342.
- Smith, M. A., Rottkamp, C. A., Nunomura, A., Raina, A. K., & Perry, G. (2000) Oxidative stress in Alzheimer's disease. *Biochim. Biophys. Acta* **1502**, 139–144.
- Stadelmann, C., Deckwerth, T. L., Srinivasan, A., Bancher, C., Bruck, W., Jellinger, K., & Lassmann, H. (1999) Activation of caspase-3 in single neurons and autophagic granules of granulovacuolar degeneration in Alzheimer's disease. Evidence for apoptotic cell death. *Am. J. Pathol.* **155**, 1459–1466.
- Su, J. H., Zhao, M., Anderson, A. J., Srinivasan, A., & Cotman, C. W. (2001) Activated caspase-3 expression in Alzheimer's and aged control brain: Correlation with Alzheimer pathology. *Brain Res.* **898**, 350–357.
- Takahashi, A. (1999) Caspase: Executioner and undertaker of apoptosis. *Int. J. Hematol.* **70**, 226–232.
- Thornberry, N. A., & Lazebnik, Y. (1998) Caspases: Enemies within. *Science* **281**, 1312–1316.
- Varadarajan, S., Yatin, S., Aksenova, M., & Butterfield, D. A. (2000) Review: Alzheimer's amyloid beta-peptide-associated free radical oxidative stress and neurotoxicity. *J. Struct. Biol.* **130**, 184–208.
- Wischik, C. M., Novak, M., Thogersen, H. C., Edwards, P. C., Runswick, M. J., Jakes, R., Walker, J. E., Milstein, C., Roth, M., & Klug, A. (1988) Isolation of a fragment of tau derived from the core of the paired helical filament of Alzheimer disease. *Proc. Natl. Acad. Sci. USA* **85**, 4506–4510.
- Yang, F., Sun, X., Beech, W., Teter, B., Wu, S., Sigel, J., Vinters, H. V., Frautschy, S. A., & Cole, G. M. (1998) Antibody to caspase-cleaved actin detects apoptosis in differentiated neuroblastoma and plaque-associated neurons and microglia in Alzheimer's disease [see comments]. *Am. J. Pathol.* **152**, 379–389.

Short communication

Activated caspase-3 expression in Alzheimer's and aged control brain: correlation with Alzheimer pathology

Joseph H. Su^{a,*}, Ming Zhao^{a,1}, Aileen J. Anderson^a, Anu Srinivasan^b, Carl W. Cotman^a

^a*Institute for Brain Aging and Dementia, University of California, Irvine, CA 92697-4540, USA*

^b*IDUN Pharmaceuticals, Inc., La Jolla, CA 92037, USA*

Accepted 19 December 2000

Abstract

Several studies have suggested that activated caspase-3 has properties of a cell death executioner protease. In this study, we examined the expression of activated caspase-3 in AD and aged control brains. Activated caspase-3 immunoreactivity was seen in neurons, astrocytes, and blood vessels, was elevated in AD, and exhibited a high degree of colocalization with neurofibrillary tangles and senile plaques. These data suggest that activated caspase-3 may be a factor in functional decline and may have an important role in neuronal cell death and plaque formation in AD brain. © 2001 Elsevier Science B.V. All rights reserved.

Theme: Disorders of the nervous system

Topic: Degenerative disease: Alzheimer's — other

Keywords: Activated caspase-3; Neurofibrillary tangle; Senile plaque; Neuropathology; Alzheimer's disease; Cell death

Alzheimer's disease (AD) is a neurodegenerative disease characterized by massive neuronal death, extracellular senile plaques (SPs), and intracellular neurofibrillary tangles (NFTs). The major protein component of SPs is β -amyloid ($A\beta$), which is derived from a much larger transmembrane amyloid precursor protein (APP). $A\beta$ is initially soluble but under the influence of local environmental changes, soluble $A\beta$ aggregates. The aggregated form of $A\beta$ is neurotoxic and accumulates in plaques in AD brain (for reviews, see Refs. [11,20]). NFTs are intracellular intermediate filaments that appear to originate from the hyperphosphorylation of the protein tau. As paired helical filaments (PHF) accumulate, they disrupt intracellular transport and are thought to contribute to neurodegeneration (for review, see Ref. [28]). Thus, a wide variety of recent data suggest that SPs and NFTs may be active participants in the neuronal death associated with AD. We and others have suggested that apoptosis may be one of the mechanisms leading to neuronal cell death in

AD [8,12,25]. In this regard, cultured neurons exposed to $A\beta$ undergo apoptotic cell death, and histochemical techniques for the demonstration of fragmented DNA reveal a large number of positive neurons in postmortem AD brain. Many cells that exhibit DNA damage also exhibit apoptotic-like morphological characteristics, including chromatin aggregation, nuclear shrinkage and formation of apoptotic bodies. Furthermore, there is altered expression of apoptosis-related proteins, such as Bcl-2 and Bax in AD brains. Finally, recent evidence suggests that some genetic factors such as Presenilin 1 and Presenilin 2 may increase neuronal vulnerability to apoptosis (for review, see Ref. [4]).

A central component of the machinery of apoptosis is an aspartate-specific cysteine class of proteases called caspases. Caspases function in both cell disassembly (effectors) and in initiating this disassembly in response to pro-apoptotic signals (initiators). Multiple lines of evidence indicate that caspase-3 plays an important role in several models of apoptosis (for review, see Refs. [15,27]). Caspase-3 normally exists in the cytosolic fraction of cells as an inactive precursor that is activated by enzymatic cleavage in early apoptosis. Activated caspase-3 is found only in cells undergoing apoptosis, and consists of p18

*Corresponding author. Tel.: +1-949-824-6324; fax: +1-949-824-2071.

E-mail address: josephsu@uci.edu (J.H. Su).

¹These authors contributed equally to the manuscript.

(amino acids 29–175) and p12 subunits (amino acids 176–277) [17], which are derived from the 32-kDa pro-enzyme (pro-caspase-3). Several studies have suggested that caspase-3 activation is both necessary and sufficient to trigger apoptosis. Additionally, multiple apoptotic signals have been shown to activate this protease [5,6]. In the cell death pathway, activated caspase-3 is thought to be responsible for dismantling cellular proteins and activation of caspase-3 cannot be reversed. Thus, caspase-3 has properties of a cell death executioner protease (for review, see Refs. [14,27]). However, little is known about the expression of active caspase-3 in AD brain. Such information is important for understanding the molecular mechanisms of neuronal cell death in AD and could be critical for developing strategies for managing this protease with inhibitors. We have recently shown that activated caspase-3 immunoreactivity was detected in both neurons and astrocytes and was elevated in frontotemporal dementia cases [26]. This led us to investigate activated caspase-3 expression in AD brain. The results demonstrate that activated caspase-3 immunoreactivity is elevated in AD cases and exhibits a high degree of colocalization with NFTs and SPs in AD brain.

Postmortem tissue was obtained from the Institute for Brain Aging and Dementia Tissue Repository. The hippocampal formation and frontal cortex from seven AD and four control cases was examined. Fresh brain tissue was fixed in 10% formalin or 4% paraformaldehyde in 0.1 M Sorensen's buffer (pH 7.3) for 48–72 h, and stored in 0.1 M PBS (0.02% sodium azide) at 4°C. All experiments were performed using free-floating 40–50- μ m sections cut on a Vibratome and collected in PBS, pH 7.4. AD and control cases were matched for age and PMD as closely as possible. Mean age AD=79 \pm 9 years, control=76 \pm 12 years; mean PMD AD=2.6 \pm 1.5 h, control=4.9 \pm 2.5 h. There were no statistically significant differences in these variables.

Tissue was processed as described previously [25,26]. Briefly, tissue sections were treated for 20 min. with 1% H₂O₂ to inactivate endogenous peroxidases. Before incubation with antibodies to caspase-3, some sections were immersed in 50% formic acid for 5 min. Sections were incubated overnight at room temperature in primary antibody, rinsed, and incubated in biotinylated secondary antibody and avidin–biotin complex for 1 h, respectively (Vector Labs, CA). The final color product for single labeling was visualized by diaminobenzidine (DAB) for a brown reaction product or a SG kit (Vector Labs, CA) for a blue-gray reaction product. Some sections were counter stained with Neutral Red. In double-labeling experiments, bound antibodies were detected using a DAB kit for the first antigen and an SG kit for the second antigen or using FITC-conjugated IgG (green fluorescence) and CY3-conjugated IgG (red fluorescence) (Jackson ImmunoResearch, PA). Sections incubated in parallel without primary antibody failed to develop specific staining. For the purpose of

quantitative estimation a series of sections was used. Free floating sections from seven AD and four control brains were processed in parallel with the same batch of antibody dilution.

A species anti-species antibody (CM1, 1:8000) was used to identify activated caspase-3 (IDUN Pharmaceuticals, La Jolla, CA). The protocols employed for the production of CM1 antibody and its characterization have been described elsewhere [23]. Briefly, this antibody was raised against a 13-amino acid peptide sequence from the C terminus of the p18 subunit of cleaved caspase-3. On Western blot analysis, this antibody recognizes the large (p18) subunit of cleaved caspase-3 and does not recognize the unprocessed p32 zymogen form or the cleaved small (p12) subunit of caspase-3. CM1 immunolabeled apoptotic, but not normal or necrotic, neurons in vitro. CM1 immunoreactivity was absent in the nervous system of caspase-3-deficient mouse embryos and in neurons cultured from caspase-3-deficient mice and was verified by Western blot analysis and immunohistochemistry [10,24,26]. These data strongly support the specificity of CM1 antibody. In addition, one commercially available anti-active caspase-3 polyclonal antibody (PharMingen 67341A, 1:700) was also used to recognize active caspase-3 (17-kDa form). This affinity-purified antibody was made against an active human caspase-3 fragment and was characterized by immunohistochemistry of vibratome sections [7]. Two well-characterized monoclonal antibodies, AT8 (1:10,000) and PHF-1 (1:1000), were used to detect PHF. The specificity of these antibodies has been described in detail previously [1,2]. In addition, mouse anti-human A β , designated 6E10 (Senetek, Maryland Heights, NJ), mouse anti-S-100 (β -subunit) (Sigma, St. Louis, MO), and mouse anti-human neurofilament (SMI-33; Sternberger Monoclonals, Lutherville MD) were used to identify SPs, astrocytes and neurons, respectively.

Three $\times 20$ fields of CM1-stained sections, each field corresponding to an approximate area of 0.3 mm² from each CA1 area, were randomly captured using an Olympus BX60 microscope with a UPLAN objective ($\times 20/0.70$). All counted neurons were double-labeled with either CM1 and SMI-33, or CM1 and PHF. In order to normalize for the loss of cells in AD and analyze these data relative to an unbiased index, results were expressed in terms of 'labeling index', that is, the number of activated caspase-3-labeled neurons per 100 SMI-33-positive or NFT-bearing neurons. The labeling indices of double-labeled activated caspase-3 and SMI-33 or phosphorylated τ were analyzed using Image-Pro Plus (version 4.0, Media cybernetics). To work out the index of tangle-bearing neurons a series of neighboring sections were used to minimize the variance in imaging analysis. The means from AD and controls were statistically analyzed using ANOVA/*t*-test with a software of StatView 4.5 (Abacus Concepts, 1995). *P* values less than 0.05 were accepted as statistically significant.

In general, neurons and senile plaques were immuno-

reactive to both of the antibodies against active caspase-3 used in the present study. However, 67341A (PharMingen) produced less robust neuronal staining than CM1. Thus, CM1 was employed in all double-labeling experiments. The most robust labeling with the least background was observed in cases with shorter PMD and paraformaldehyde fixation. Quantitative labeling indices exhibited a strong significant difference between AD and control brains ($P < 0.01$) in both CM1/PHF and CM1/SMI-33 neuron subgroups.

1. Activated caspase-3 immunoreactivity in age-matched control brain

CM1 and 67341A, which detect activated caspase-3 expression, were examined in four non-demented normal control cases. Activated caspase-3 immunoreactivity was present in a small subset of neurons in three out of four of these cases. Neurons positive for activated caspase-3 showed weak to moderate staining in a fine punctate pattern within the cytoplasm/soma, nucleus, and proximal neurites of neurons in layers 2–3 of entorhinal cortex and the CA1 region of hippocampus. In frontal cortex, positive neurons were observed mainly in the pyramidal neurons in layers 2–3 (Fig. 1).

Activated caspase-3 immunoreactivity was also found within scattered plaque-like structures (Fig. 1) in all control cases examined. Doubling labeling with CM1 or 67341A and 6E10 (A β marker) in controls demonstrated that many caspase-3 immunoreactive plaque-like structures were also A β immunoreactive (not shown).

2. Proportion of CM1-positive neurons to SMI-33-positive neurons and NFT-bearing neurons in control brain

In order to investigate the relationship between activated caspase-3-positive cells and neuronal labeling in controls, double labeling for CM1 or 67341A and SMI-33 was conducted in sections from frontal cortex. All activated caspase-3 immunoreactive cells were also labeled with the neuronal marker SMI-33 (data not shown). Additionally, double labeling for CM1 or 67341A and AT8/PHF-1 was conducted in order to investigate the relationship between activated caspase-3-positive neurons and neurofibrillary degeneration. Scattered AT8/PHF-1-positive NFTs were apparent in control cases; however, most neurons that exhibited activated caspase-3 immunoreactivity were negative for AT8/PHF-1 immunoreactivity (not shown). Neurons double-labeled for CM1 and AT8/PHF-1 exhibited a punctate pattern of CM1 staining. The labeling index of CM1-positive/SMI-33-positive neurons was 10.66%,

while that of CM1-positive/PHF-positive neurons was 3.28% (Fig. 2 and Table 1).

3. Activated caspase-3 expression in AD brain

Overall, immunoreactivity to CM1 or 67341A (PharMingen) was much more extensive in AD brains as compared to control cases. Activated caspase-3 immunoreactivity was found to be present in a large subset of neurons, senile plaques, blood vessels, and glial cells with astrocytic morphologies (Fig. 3a–d). In neurons, CM1 activated caspase-3 immunoreactivity was found within the cytoplasm/soma, nucleus, and proximal processes, as observed in aged control cases. Interestingly, 67341A immunoreactivity within the nuclei was usually stronger than that within the cytoplasm/soma (Fig. 3a, insets). Long activated caspase-3-positive neurites could be seen extending more than 300 μ m through the neuropil. Activated caspase-3-positive neurons were observed mainly in the CA1 subfield of hippocampus, the entorhinal cortex, and the superficial layers of frontal cortex; however, activated caspase-3 immunoreactivity was rare in dentate granule cells. In accordance with observations in aged control brain (above), activated caspase-3-positive staining appeared as small punctate granules in a subset of neurons (Fig. 3a, insets). However, in contrast to these findings, active caspase-3 immunoreactivity in a subset of neurons in AD brain was in the form of fibrillar deposits which resembled the appearance of NFTs and dystrophic neurites as seen with immunostaining for phosphorylated tau (Fig. 3b, right inset). Activated caspase-3 immunoreactivity was also detected in the granules of neurons exhibiting swollen morphologies with granulovacuolar degeneration, although other cytoplasmic compartments remained unstained in these cells (Fig. 3b, left inset), which is consistent with recent *in vivo* studies [22,24].

Immunoreactivity for activated caspase-3 was also seen in punctate or granular deposits and neurites in plaque-like structures in AD brain (Fig. 3c,d). Critically, diffuse plaque-associated immunoreactivity for active caspase-3 was not observed with either of the antibodies employed in this study (CM1 or 67341A), suggesting that active caspase-3 in plaques was present in association with defined structures rather than reflecting neuropil deposition or non-specific staining. Doubling labeling with CM1 or 67341A and 6E10 or AT8/PHF-1 demonstrated that many caspase-3-positive plaque-like structures were also A β -immunoreactive (Fig. 3d). Moreover, these caspase-3-positive structures in AD plaques were associated with PHF-positive dystrophic neurites (Fig. 3d, left inset). Additionally, in contrast to observations in control brain, activated caspase-3-positive astrocytes were also detected in AD plaques (Fig. 3d, right inset).

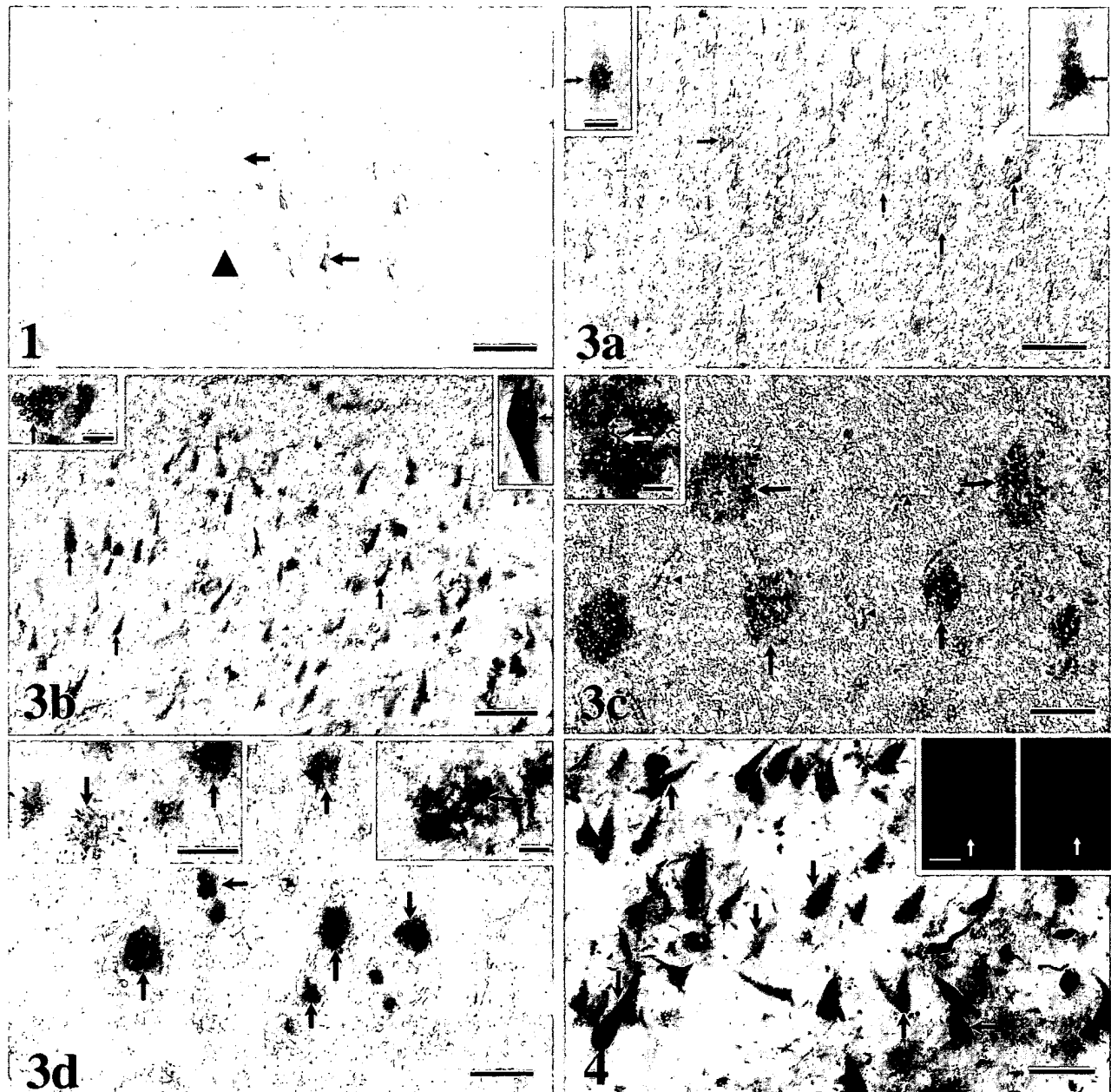


Fig. 1. Activated caspase-3 immunoreactivity is present in a small subset of neurons in three of four age-matched control brains. Arrows indicate neurons. Arrowhead indicates SP. Scale bar=290 μ m.

Fig. 3. Activated caspase-3 expression in AD brain. (A) Activated caspase-3 immunoreactivity is present in a large subset of neurons in all AD brains examined. Arrows indicate positive neurons. Scale bar: 290 μ m. Insets: high magnification showing activated caspase-3 immunoreactivity in neurons stained with PharMingen active caspase-3 antibody (67341A). Note that activated caspase-3 immunoreactivity is localized in nucleus and positive staining appears as small punctates. Scale bar: (insets) 54 μ m. (B) Activated caspase-3 expression in neurons where many of them are NFT-bearing neurons as revealed by immunofluorescence staining. Scale bar: 290 μ m. Note that the immunostaining appears to be fibrillar deposits. Arrows indicate positive neurons. Right inset: high magnification showing fibrillar pattern (arrow). Left inset: high magnification showing that strong activated caspase-3 immunoreactivity is detected in granules of granulovacuolar degeneration of a swollen neurons. Scale bar: (insets) 54 μ m. (C) Activated caspase-3 expression in plaque-like structure (arrows) and blood vessels (arrowhead). Scale bar: 290 μ m. Inset: high magnification showing activated caspase-3-positive neurites in plaque-like structure (arrow). Scale bar: 72 μ m. (D) Many activated caspase-3-positive plaques (blue) are co-localized with A β (brown). Arrows indicate double-labeled SPs. Scale bar: 290 μ m. Left inset: high magnification showing that PHF-positive dystrophic neurites (blue) are associated with activated caspase-3-positive SPs (brown). Scale bar: 290 μ m. Right inset: two astrocytes (arrow, labeled with S-100 β , blue) are double-labeled with CM1 (brown) in plaque area. Scale bar: 54 μ m.

Fig. 4. There is a prominent co-localization of activated caspase-3 (brown) and PHF (blue). Arrows indicate tangle-bearing neurons double-labeled with CM1 and AT8/PHF-1. Scale bar: 145 μ m. Insets: double immunofluorescence staining showing a CM1-positive neuron (red, arrow, CY3 labeling) is co-localized with neurofibrillary tangle (green, arrow, FITC labeling). Note: CM1 positive neuron is slightly larger than tangle. Scale bar: 54 μ m.

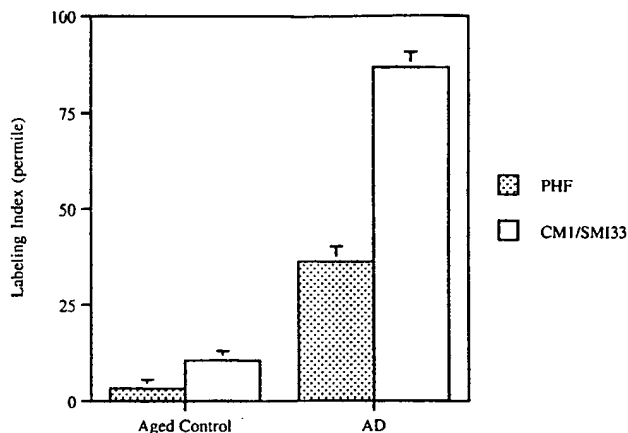


Fig. 2. Labeling indices of double-labeled neurons in control and AD brains. The differences between AD and control brains in both neuron subgroups double-labeled with CM1/SMI-33 or CM1/PHF are highly significant ($P < 0.01$).

4. Proportion of CM1-positive neurons to SMI-33-positive neurons and NFT-bearing neurons in AD brains

In order to investigate the relationship between activated caspase-3-positive cells and neuronal labeling in AD, double labeling for CM1 or 67341A and SMI-33 was conducted in sections from frontal cortex. All of the AD cases examined in this study exhibited a prominent colocalization between neurons exhibiting CM1 and SMI-33 immunoreactivity (not shown). The majority of cells double labeled for CM1 and SMI-33 were pyramidal neurons and were distributed in layers 2–4. Additionally, double labeling for CM1 and AT8/PHF-1 was used to investigate the relationship between activated caspase-3 immunoreactivity and neurofibrillary degeneration. All of the AD brains examined exhibited a strong co-localization between CM1-positive neurons and PHF-positive neurons (Fig. 4). The majority of neurons double-labeled for CM1 and AT8/PHF-1 were pre-NFT, early NFT, or mature NFT-bearing neurons (Fig. 4, inset). Non-NFT-bearing neurons and pre- or early NFT-bearing neurons usually exhibited punctate CM1 immunoreactivity in the cytoplasm, whereas mature NFT-bearing neurons usually exhibited fibrillar deposits of CM1 immunoreactivity in the

cytoplasm. Activated caspase-3 immunoreactivity was generally not observed in extracellular NFTs. While activated caspase-3 immunoreactivity was detected within a large subset of NFT-bearing neurons, a few activated caspase-3-positive neurons did not co-localize with NFTs. Neurons single-labeled for CM1 generally exhibited a punctate pattern of staining, and were predominantly distributed in hippocampal fields CA2–3 and adjacent regions, or dispersed among neurons double-labeled for CM1 and AT8/PHF-1. The labeling index of CM1-positive/SMI-33-positive neurons was 86.72%, while that of CM1-positive/PHF-1-positive neurons was 36.20% (Fig. 2 and Table 1). These labeling indices were 8 to 11 times higher in AD as compared to control brain ($P < 0.01$).

The principal goals of this study were to examine whether activated caspase-3 is present in neurons in AD brain, and the relationship of NFT-bearing neurons to activated caspase-3-positive neurons in AD. In contrast to a recent study [22], we demonstrate clear evidence that activated caspase-3 immunoreactivity is present in neurons in both control and AD brain, and that there is a significant up-regulation of activated caspase-3 immunoreactivity in AD compared with control cases. In this regard, the labeling index of activated caspase-3 was approximately 8 times higher in AD brain than in control brain ($P < 0.01$). Activated caspase-3-immunoreactive neurons appeared unhealthy. Most of these neurons were pyramidal in type, and were distributed in entorhinal cortex, CA1, and the superficial layers of frontal cortex, roughly corresponding to vulnerable areas of AD brain. Additionally, over one-third of NFT-bearing neurons were active caspase-3-positive; these double-labeled neurons consisted of pre-tangle neurons, early stage NFTs, and mature NFTs. These findings support the suggestion that active caspase-3 might mediate or contribute to NFT formation and associated neuronal death in AD brain, and are consistent with recent studies demonstrating that caspase-3 is involved in τ and APP cleavage [3,9].

Neurons labeled for active caspase-3 exhibited several characteristics. First, active caspase-3 immunoreactivity was present in neuronal nuclei, this observation is in agreement with our previous findings in frontal-temporal dementia neurons [26]. These results are also consistent with recent animal model studies [16,29], in which nuclear localization of active caspase-3 was reported in neurons undergoing apoptosis. Nuclear localization of active caspase-3 as observed here suggests that activated caspase-3 is translocated from the cytoplasm to the nucleus in AD neurons, and may contribute to an apoptotic program. Nuclear proteins such as the DNA repair or degrading enzymes PARP and ICAD/DFF45 have been shown to be caspase-3 substrates (for review, see Ref. [13]). Presumably, one role of nuclear activated caspase-3 might be to cleave these substrates, resulting in nuclear DNA fragmentation and ultimately contributing to neuronal death.

A second characteristic of active caspase-3 immuno-

Table 1

Labeling indices^a of activated caspase-3 and hyperphosphorylated τ (PHF)^b in CA1 of aged control and AD brains (mean \pm S.E.)^{*}

| | N | CM1/SMI-33 | CM1/PHF |
|---------|---|------------------|------------------|
| Control | 4 | 10.66 \pm 1.34 | 3.28 \pm 1.20 |
| AD | 7 | 86.72 \pm 2.96 | 36.20 \pm 7.39 |

^a Labeling index was estimated based on double-labeling for CM1/SMI-33 or CM1/PHF, as described in the text.

^b PHF labeling was conducted with mixed antiserum containing AT8 and PHF-1 antibodies, as described in the text.

^{*} $P < 0.006$ for all comparisons.

reactivity was that two staining patterns, punctate and fibrillar, were observed within the cytoplasm of AD neurons. Surprisingly, fibrillar caspase-3 staining bore a marked similarity to the pattern of staining observed with PHF-1. Double labeling experiments showed that punctate deposits were usually detected in non NFT-bearing neurons and pre- or early NFT-bearing neurons, whereas fibrillar deposits were usually observed in mature NFT-bearing neurons. Furthermore, only punctate deposits of active caspase-3 were detected in control brain, and these were observed in only a small subset of neurons. No fibrillar active caspase-3 immunoreactivity was observed in control brain neurons. Caspase-3 is the leading candidate as the primary effector protease in neuronal apoptosis. More than 40 protein substrates for caspase-3 have been identified, including cytoskeletal, regulatory, and neuro-pathological proteins such as τ , Bcl-2, APP, and presenilins (for review, see Ref. [13]). Furthermore, during neurofibrillary degeneration the N-terminal half of the τ molecule in the most superficial part of the PHF coat is cleaved or degraded [31]. Presumably, the intracytoplasmic redistribution of active caspase-3 immunoreactivity from a granular to a fibrillar pattern could reflect the cleavage of neurofilament-associated substrates during chronic neuronal degeneration in AD. Further studies are needed to confirm this hypothesis.

An unexpected finding of the present study was that activated caspase-3 immunoreactivity was present in a small subset of neurons in control brain, although the number of these cells was approximately eight times lower than that found in AD brain ($P < 0.01$). These results are consistent with a recent *in vivo* study, which reported activated caspase-3-immunoreactive neurons in the substantia nigra of control human brain [10]. In parallel with our findings, activated caspase-3-positive neurons in that study also appeared unhealthy and were detected in areas susceptible to degeneration. Interestingly, double-labeling experiments demonstrated that most of active caspase-3-positive neurons in control brain in the present study were not labeled with AT8/PHF-1. In contrast, activated caspase-3 immunoreactivity was observed in 87% of all neurons, and 36% of AT8/PHF-1-positive neurons, in AD. Taken together with the change in cellular distribution of activated caspase-3 in AD as compared with control brain, these results suggest that alterations in neuronal active caspase-3 expression may occur prior to NFT formation.

Recent studies have shown that caspase-3 is activated in early apoptosis and its activation precedes the appearance of DNA damage [10,16]. However, CM1 and 67341A immunoreactivity in neurons could simply reflect caspase-3 activation; concurrent expression of caspase-3 inhibitory proteins, such as the inhibitor of apoptosis proteins (IAPs) or other molecules, could mitigate the impact of caspase-3 activation, blocking immediate apoptotic neuronal loss but contributing to cellular dysfunction. Hence, activation of caspase-3 would not necessarily predetermine an apoptotic

cell fate. Furthermore, CM1 and 67341A recognize an epitope of caspase-3 exposed by activation, this epitope is not the active site for caspase-3-mediated cleavage of other proteins. Immunocytochemical staining with these antibodies therefore provides evidence that caspase activation has occurred, however, it is theoretically possible that this epitope accumulates in AD neurons, and could thus reflect previous, rather than current, caspase activation.

Accordingly, we hypothesize that the majority of active caspase-3-immunoreactive neurons in AD brain have suffered sublethal insults, resulting in impaired cellular signaling, dysfunction, and the initiation of early mechanisms associated with apoptosis — without commitment to apoptotic cell death. In this light, some proportion of these neurons may ultimately undergo one of several cell fates, including necrosis, apoptosis, or degeneration via NFT mechanisms that differ from either of these cell death pathways. In support of this possibility, while caspase-3 activation has been shown to be necessary and sufficient for neuronal cell death, recent work suggests that caspase activation in T cells can occur in the absence of cell death and apoptosis [30,32]. Moreover, the possibility that caspase activation could play a role in normal cellular functions in some cell types cannot be excluded (for review, see Ref. [33]).

Given the injured state of AD neurons and potential for rapid caspase activation it is also important to note that the detection of activated caspase-3 could be influenced by variables related to postmortem delay, agonal state, or tissue archival. We have previously investigated the contribution of these variables to the detection of DNA damage by terminal transferase-mediated dUTP nick-end labeling (TUNEL) in AD brain, another rapidly initiated marker of cellular injury. Our findings suggest that TUNEL detection is not affected by postmortem delays less than 6–8 h or archival in formalin less than 4 years (for review, see Ref. [4]). In accordance with our findings in these studies, we selected cases for the current study that are of the shortest possible postmortem delay and archival lengths. The dramatic differences in active caspase-3 labeling between short postmortem delay, high quality AD and control brain tissue observed in the present study support a specific, pathology-related source of caspase activation as the basis for these findings. However, the potential for postmortem or agonal activation of caspase-3 cannot be excluded on the basis of *in situ* tissue analyses.

Another goal of this study was to examine the expression of activated caspase-3 in A β plaques, and the relationship of activated caspase-3 expression to dystrophic neurites and glial cells. In this study, we observed strong active caspase-3 immunoreactivity in numerous senile plaques (SPs), and demonstrated that this immunoreactivity is detected in SP-associated astrocytes and dystrophic neurites. A β , the major protein component of SPs, is derived from a much larger transmembrane precursor APP. It is likely that extracellular A β can arise from APP in

neurites and astrocytes (for review, see Refs. [20,21]). Based on in vitro and in vivo observations of A β generation via caspase-mediated APP cleavage, and co-localization of a caspase-3 APP cleavage product with A β in SPs in AD, at least one recent study has concluded that caspase-3 is the predominant caspase involved in APP cleavage [9]. This suggests that active caspase-3 in SP-associated astrocytes and neurites, as observed in the present study, may contribute to plaque maturation. The lack of active caspase-3 immunoreactivity in diffuse plaques, which contain few astrocytes or dystrophic neurites, is consistent with the intracellular generation of A β via such a mechanism. However, because it is generally thought that diffuse plaques progress to form SPs over time, it seems reasonable to hypothesize that APP cleavage by astrocytic and neuritic caspase-3 may play a contributory, rather than a causative, role in plaque pathogenesis. As discussed above, the presence of active caspase-3 in plaque-associated dystrophic neurites suggests that this protease may also be involved in τ cleavage in these structures.

Accumulating evidence suggests that caspase inhibitors play a key role in the control and regulation of cell death protease cascades. Several neuronal inhibitors of apoptosis proteins have been identified (for review, see Refs. [18,19]), and a clear link between a failure of caspase inhibition and the hereditary neurodegenerative disorder spinal muscular atrophy has recently been reported (for reviews, see Refs. [18,19]). Recent studies have also shown that peptidyl caspase inhibitors can prevent neuronal loss in animal models of stroke, myocardial ischemia-reperfusion, liver disease, and traumatic brain injury (for reviews, see Refs. [13,18,27]). However, many questions remain to be answered if these promising results are to be applied to neurodegenerative disease, including identifying what the best targets for apoptosis inhibition are in AD. In this study, we demonstrate clear evidence that active caspase-3 is co-localized and elevated in NFT-bearing neurons and SPs, two primary pathological hallmarks of AD. Considering the close co-localization and marked elevation of active caspase-3 within NFTs and SPs, we suggest that caspase-3 inhibition may be a viable therapeutic target for slowing the progression of AD.

In conclusion, our findings suggest that activated caspase-3 immunoreactivity is elevated in AD and exhibits a high degree of colocalization with NFTs and SPs in AD brain. These data suggest that activated caspase-3 may have an important role in neuronal cell death, as well as NFT and plaque formation in the AD brain.

References

- [1] J. Biernat, E.-M. Mandelkow, C. Schroter, B. Lichtenberg-Kraag, B. Steiner, B. Berling, H. Meyer, M. Merchen, A. Vandermeeren, M. Goedert, E. Mandelkow, The switch of tau protein to an Alzheimer-like state includes the phosphorylation of two serine-proline motif upstream of the microtubule binding region, *EMBO J* 11 (1992) 1593–1597.
- [2] G.T. Bramblett, M. Goedert, R. Jakes, S.E. Merrick, J.Q. Trojanowski, V.M.-Y. Lee, Abnormal tau phosphorylation at Ser396 in Alzheimer's disease recapitulates development and contributes to reduced microtubule binding, *Neuron* 10 (1993) 1089–1099.
- [3] N. Canu, L. Dus, C. Barbato, M.T. Ciotti, C. Brancolini, A.M. Rinaldi, M. Novak, A. Cattaneo, A. Bradbury, P. Calissano, Tau cleavage and dephosphorylation in cerebellar granule neurons undergoing apoptosis, *J. Neurosci.* 18 (1998) 7061–7074.
- [4] C.W. Cotman, J.H. Su, Mechanisms of neuronal death in Alzheimer's disease, *Brain Pathol.* 6 (1996) 493–506.
- [5] A.J. Darmon, T.J. Ley, D.W. Nicholson, R.C. Bleackley, Cleavage of cyp32 by granzyme b represents a critical role for granzyme B in the induction of target cell dna fragmentation, *J. Biol. Chem.* 271 (1996) 21709–21712.
- [6] R. Datta, H. Kojima, D. Banach, N.J. Bump, R.V. Talanian, E.S. Alnemri, R.R. Weichselbaum, W.W. Wong, D.W. Kufe, Activation of a CrmA-insensitive, p35-sensitive pathway in ionizing radiation-induced apoptosis, *J. Biol. Chem.* 272 (1997) 1965–1969.
- [7] I. Ferrer, Role of caspases in ionizing radiation-induced apoptosis in the developing cerebellum, *J. Neurobiol.* 41 (1999) 549–558.
- [8] G. Forloni, R. Chiesa, S. Smiriglio, L. Verga, M. Salmona, F. Tagliavini, N. Angeretti, Apoptosis mediated neurotoxicity induced by chronic application of beta amyloid fragment 25–35, *Neuroreport* 4 (1993) 523–526.
- [9] F.G. Gervais, D. Xu, G.S. Robertson, J.P. Vaillancourt, Y. Zhu, J. Huang, A. LeBlanc, D. Smith, M. Rigby, M.S. Shearman, E.E. Clarke, H. Zheng, L.H. Van Der Ploeg, S.C. Ruffolo, N.A. Thornberry, S. Xanthoudakis, R.J. Zamboni, S. Roy, D.W. Nicholson, Involvement of caspases in proteolytic cleavage of Alzheimer's amyloid-beta precursor protein and amyloidogenic A beta peptide formation, *Cell* 97 (1999) 395–406.
- [10] A. Hartmann, S. Hunot, P.P. Michel, M.P. Muriel, S. Vyas, B.A. Faucheux, A. Mouatt-Prigent, H. Turnel, A. Srinivasan, M. Ruberg, G.I. Evan, Y. Agid, E.C. Hirsch, Caspase-3: a vulnerability factor and final effector in apoptotic death of dopaminergic neurons in Parkinson's disease, *Proc Natl Acad Sci USA* 97 (2000) 2875–2880.
- [11] L.L. Iversen, R.J. Mortishire-Smith, S.J. Pollack, M.S. Shearman, The toxicity in vitro of β -amyloid protein, *Biochem. J.* 311 (1995) 1–16.
- [12] D.T. Loo, A. Copani, C.J. Pike, R.E. Whittemore, A.J. Walencewicz, C.W. Cotman, Apoptosis is induced by β -amyloid in cultured central nervous system neurons, *Proc. Natl. Acad. Sci. USA* 90 (1993) 7951–7955.
- [13] N. Marks, M.J. Berg, Recent advances on neuronal caspases in development and neurodegeneration, *Neurochem Int.* 35 (1999) 195–220.
- [14] H. Mehmet, Caspases find a new place to hide, *Nature* 403 (2000) 29–30.
- [15] S. Nagata, Apoptosis by death factor, *Cell* 88 (1997) 355–365.
- [16] S. Namura, J. Zhu, K. Fink, M. Endres, A. Srinivasan, K.J. Tomaselli, J. Yuan, M.A. Moskowitz, Activation and cleavage of caspase-3 in apoptosis induced by experimental cerebral ischemia, *J. Neurosci.* 18 (1998) 3659–3668.
- [17] D.W. Nicholson, A. Ali, N.A. Thornberry, J.P. Vaillancourt, C.K. Ding, M. Gallan, Y. Gareau, P.R. Griffin, M. Labelle, Y.A. Lazebnik, N.A. Munday, S.M. Raja, M.E. Smulson, T.-T. Yamin, V.L. Yu, D.K. Miller, Identification and inhibition of the ICE/CED-3 protease necessary for mammalian apoptosis [see comments], *Nature* 376 (1995) 37–43.
- [18] G.S. Robertson, S.J. Crocker, D.W. Nicholson, J.B. Schulz, Neuroprotection by the inhibition of apoptosis, *Brain Pathol.* 10 (2000) 283–292.
- [19] J.B. Schulz, M. Weller, M.A. Moskowitz, Caspases as treatment

- targets in stroke and neurodegenerative diseases, *Ann Neurol.* 45 (1999) 421–429.
- [20] D.J. Selkoe, The molecular pathology of Alzheimer's disease, *Neuron* 6 (1991) 487–498.
- [21] D.J. Selkoe, Physiological production of the β -amyloid protein and the mechanism of Alzheimer's disease, *Trends Neurosci.* 16 (1993) 403–408.
- [22] L.A. Selznick, D.M. Holtzman, B.H. Han, M. Gokden, A.N. Srinivasan, E.M. Johnson Jr., K.A. Roth, In situ immunodetection of neuronal caspase-3 activation in Alzheimer disease, *J. Neuropathol. Exp. Neurol.* 58 (1999) 1020–1026.
- [23] A. Srinivasan, K.A. Roth, R.O. Sayers, K.S. Shindler, A.M. Wong, L.C. Fritze, K.J. Tomaselli, In Situ immunodetection of activated caspase-3 in apoptotic neurons in the developing nervous system, *Cell Death Diff.* 5 (1998) 1004–1016.
- [24] C. Stadelmann, T.L. Deckwerth, A. Srinivasan, C. Bancher, W. Bruck, K. Jellinger, H. Lassmann, Activation of caspase-3 in single neurons and autophagic granules of granulovacuolar degeneration in Alzheimer's disease. Evidence for apoptotic cell death, *Am. J. Pathol.* 155 (1999) 1459–1466.
- [25] J.H. Su, A.J. Anderson, B.J. Cummings, C.W. Cotman, Immunohistochemical evidence for apoptosis in Alzheimer's disease, *Neuro-Report* 5 (1994) 2529–2533.
- [26] J.H. Su, K.E. Nichol, T. Sitch, P. Sheu, C. Chubb, B.L. Miller, K.J. Tomaselli, R.C. Kim, C.W. Cotman, DNA damage and activated caspase-3 expression in neurons and astrocytes: evidence for apoptosis in frontotemporal dementia, *Exp. Neurol.* 163 (2000) 9–19.
- [27] N.A. Thornberry, Y. Lazebnik, Caspases: enemies within, *Science* 281 (1998) 1312–1316.
- [28] J.Q. Trojanowski, M.L. Schmidt, R.-W. Shin, G.T. Bramblett, M. Goedert, V.M.-Y. Lee, PHF (A68) From pathological marker to potential mediator of neuronal dysfunction and degeneration in Alzheimer's disease, *Clin. Neurosci.* 1 (1993) 1–4.
- [29] J.J. Velier, J.A. Ellison, K.K. Kikly, P.A. Spera, F.C. Barone, G.Z. Feuerstein, Caspase-8 and caspase-3 are expressed by different populations of cortical neurons undergoing delayed cell death after focal stroke in the rat, *J. Neurosci.* 19 (1999) 5932–5941.
- [30] S. Wilhelm, H. Wagner, G. Hacker, Activation of caspase-3-like enzymes in non-apoptotic T cells, *Eur. J. Immunol.* 28 (1998) 891–900.
- [31] C.M. Wischik, M. Novak, P.C. Edwards, A. Klug, W. Tichelaar, R.A. Crowther, Structural characterization of the core of the paired helical filament of Alzheimer disease, *Proc. Natl. Acad. Sci. USA* 85 (1988) 4884–4888.
- [32] D.M. Wu, Y. Zhang, N.A. Prada, H. Kornfeld, J. Nicoll, D.M. Center, W.W. Cruikshank, Processing and release of IL-16 from CD4+ but not CD8+ T cell is activation dependent, *J. Immunol.* 163 (1999) 1287–1293.
- [33] A. Zeuner, A. Eramo, C. Peschle, R. De Maria, Caspase activation without death, *Cell Death Diff.* 6 (1999) 1075–1080.

A Role for Caspase-1 and -3 in the Pathology of Experimental Allergic Encephalomyelitis

Inflammation Versus Degeneration

Zubair Ahmed,* Anne I. Doward,* Gareth Pryce,*
Deanna L. Taylor,* Jennifer M. Pocock,*
John P. Leonard,[†] David Baker,* and
M. Louise Cuzner*

From the Department of Neuroinflammation,* Institute of
Neurology, University College London, London, United Kingdom;
and Wyeth Research,[†] Andover, Massachusetts

Axonal loss, already present in the acute and first relapse phases of experimental allergic encephalomyelitis (EAE) in the ABH mouse, only becomes apparent in the third relapse in the interleukin-12 model of relapsing EAE in the Lewis rat. Caspase-1 immunostaining in the spinal cord of Lewis rats was mainly localized to inflammatory cuffs with the greatest proportion of active caspase-1-positive cells detected during the first and second relapses, correlating with enzyme activity and protein on Western blots. However, in the spinal cord of ABH mice during acute EAE, caspase-1 immunostaining was localized both on inflammatory and neuronal cells, again correlating with enzyme activity and protein production. In contrast, caspase-3 expression in the spinal cord of Lewis rats did not increase significantly until the third relapse when inflammatory and neuronal cells and axons became positive in line with a significant increase in caspase activity. In ABH mice active caspase-3 was already immunolocalized on axons and apoptotic neurons in the spinal cord during the acute stage of EAE. Because caspase-3 is a downstream cell death signal it may be possible to reduce apoptosis by selectively blocking caspase-3 and therefore provide a therapeutic target for EAE and potentially, multiple sclerosis. (*Am J Pathol* 2002, 161:1577–1586)

We have previously shown that interleukin (IL)-12, a proinflammatory cytokine, can induce serial paralytic relapses of experimental allergic encephalomyelitis (EAE) in the Lewis rat¹ with the appearance of myelin basic protein-laden macrophages, indicating myelin processing.^{1,2} Signs of limited axonal death together with localization of tissue plasminogen activator (tPA) were observed on axons by the third relapse.² In ABH mice,

however, chronic relapsing EAE (CREAE) can be induced by a single sensitization with spinal cord homogenate and animals undergo relapsing-remitting disease. This is characterized by progressive inflammatory demyelination but also by axonal loss even during the acute stage.³ Interestingly, Lewis rats showed no clinical signs of disease between the relapses whereas ABH mice showed cumulative deficits after each bout of disease.

Caspases, a family of cysteine proteases mainly involved in the apoptotic pathway⁴ are essential for the control of cell populations not only during development but also in pathology.^{5,6} Apoptosis is recognized by distinct morphological changes, including cell shrinkage, nuclear condensation, and fragmentation.⁷ Caspases are synthesized as inactive proenzymes releasing active subunits when they are catalytically activated.^{8–12} The active caspases hydrolyze a number of key structural and housekeeping proteins in the progression of apoptosis.^{8,13,14} Among these, caspase-1, also known as IL-1 β -converting enzyme, is less involved in the apoptotic cascade but prominent in inflammation in which it plays a key role in regulating cellular export of proinflammatory cytokines such as IL-1 β .¹⁵ However, overexpression of caspase-1 can lead to apoptotic cell death and may mediate microglial apoptosis after inflammatory microglial activation *in vitro*.^{16–18} Caspase-3 or CPP32, another member of the caspase family, appears to be the main effector caspase involved in neuronal apoptosis.^{19,20} Activation of caspase-3 has been shown to be a critical event in neuronal apoptosis in the brain during development and after acute injury and after exposure to the cytokines produced from activated microglia.^{17,19,20}

Because there is limited axonal death in Lewis rats after three relapses of EAE and ABH mice undergo axonal damage and demyelination, particularly after the first relapse, the aim of the study was to test the hypothesis that the axonal death observed might be mediated by caspases, caspase-1 and in particular caspase-3.

Supported by the Brain Research Trust, UK.

Accepted for publication June 20, 2002.

Address reprint requests to Prof. L. Cuzner, Department of Neuroinflammation, Institute of Neurology, University College London, 1 Wakefield St., London, WC1N 1PJ, UK. E-mail: l.cuzner@ion.ucl.ac.uk.

Materials and Methods

Induction of Active EAE

Female Lewis rats (180 to 200 g) (Charles River, Kent, UK) were immunized in each hind foot with a mixture of purified guinea pig myelin basic protein (final concentration, 1 mg/ml), emulsified in Freund's complete adjuvant (myelin basic protein-complete Freund's adjuvant) containing *Mycobacterium tuberculosis* H37Ra (final concentration, 5 mg/ml; Difco Laboratories, Detroit, MI) in a final volume of 50 μ l. Animals were weighed and monitored daily for clinical signs of EAE using the earlier published criteria.²

CREAE was induced in 6- to 8-week-old Biozzi ABH mice (bred at the Institute of Neurology) by injection with mouse spinal cord homogenate emulsified in complete Freund's adjuvant on days 0 and 7.³ Animals with complete hindlimb paralysis were examined during the initial acute paralytic attack on day 18 after immunization and the first clinical relapse on days 37 to 42 after immunization. Animals were also examined during the first clinical remission on days 27 to 28 after immunization in which animals exhibited only minimal tail paresis and chronically affected remission animals after three relapses on days 80 to 100, in which animals had residual hindlimb paresis.^{21,22}

IL-12 Administration to Lewis Rats

Recombinant murine IL-12 (Genetics Institute, Cambridge, MA) was administered intraperitoneally as described before.²

Immunocytochemistry

Rats and mice were culled at different stages after immunization and the brain and spinal cord were removed and rapidly frozen on solid CO₂. Longitudinal frozen sections were cut, adhered to Vectabond-coated slides (Vector Laboratories, Peterborough, UK) and processed for immunohistochemistry using the following antibodies to caspases: rabbit anti-caspase-1 (p10 subunit, diluted 1:200) and goat anti-caspase-3 (1:200) (both from Santa Cruz Biotechnology Inc., Santa Cruz, CA). Tissues were fixed in ethanol for 1 minute at room temperature and washed twice in phosphate-buffered saline (PBS) followed by incubation with the appropriate primary antibody diluted in PBS, pH 7.4. For caspase-3 immunostaining an additional step was included in which tissues were permeabilized in 0.1% Triton X-100 for 5 minutes after fixation. After incubation with the primary antibody sections were washed in PBS before incubation with either biotinylated anti-goat or anti-rabbit IgG (Vector Laboratories) diluted 1:200 for 30 minutes at room temperature. Peroxidase-labeled avidin-biotin complex solution was added to the sections (Vector Laboratories) for 45 minutes, washed, and peroxidase activity detected by placing the slides in a solution of 0.5 mg/ml of 3,3'-diaminobenzidine (Sigma, Poole, UK) in PBS containing 0.01%

hydrogen peroxide for 5 minutes. For caspase-3 immunostaining, nickel chloride was added to the 3,3'-diaminobenzidine and hydrogen peroxide solution and sections were not counterstained. Other sections were rinsed and counterstained in Mayer's hematoxylin (30 seconds), dehydrated through a graded series of alcohols, and mounted in DPX (BDH, Poole, UK). Appropriate antibody control sections were included with each run, including preabsorption of caspase-1 and -3 with the appropriate blocking peptide (Santa Cruz Biotechnology) for 2 hours at room temperature before incubating with sections.

Identification of the Cell Types Expressing Cleaved Caspase-3 by Double-Immunofluorescent Staining

Fixed sections were permeabilized with 1% Triton X-100 for 10 minutes followed by three washes on PBS for 5 minutes each before incubating with polyclonal cleaved caspase-3 antibody (1:100 dilution in PBS containing 1% bovine serum albumin; Cell Signaling Technology, Beverly, MA). Sections were then washed in PBS and incubated with fluorescein isothiocyanate-conjugated anti-rabbit IgG (Sigma). Sections were allowed to react with one of the following monoclonal antibodies: ED-1 (macrophage), OX-42 (macrophages/microglia), glial fibrillary acidic protein (astrocytes), SMI-32 (1:1000, neurons/axons), OX-34 (1:500, T cells); or the following polyclonal antibodies: CNPase (1:1000, gift from Dr. T. J. Sprinkle, Veterans Affairs Medical Centre, Augusta, USA) and neurofilament 200 (1:500, neurons/axons, Sigma) or rat anti-mouse CD4 (1:50, CD4 T cells), F4/80 (1:50, macrophages) (Serotec). Appropriate secondary antibodies (diluted 1:50 in PBS) used for the above markers were: tetramethyl-rhodamine isothiocyanate-conjugated anti-mouse, anti-rat, anti-rabbit, and anti-goat IgG (all from Sigma). Finally sections were mounted using Citifluor (Citifluor Ltd., London, UK) and viewed under the Radiance 2100 confocal laser microscope using Lasersharp 2000 software system (Bio-Rad, Hertfordshire, UK). Captured images were converted to TIFF files using Confocal Assistant (Version 4.02, Todd Clark Brelje) and assembled using Adobe Photoshop (Adobe Systems Inc., San Jose, CA). Appropriate control sections were included in each run.

Western Blotting

Chopped spinal cord tissue was homogenized for 25 seconds in cold lysis buffer consisting of: 20 mmol/L Tris/acetate (pH 7), 1 mmol/L EGTA, 10 mmol/L sodium β -glycerophosphate (pH 7.4), 1 mmol/L sodium orthovanadate, 5% glycerol, 1% Triton X-100, and 0.27 mol/L sucrose with 1 μ mol/L microcystin LR, 1 mmol/L benzamidine, 4 μ g/ml leupeptin, and 0.1% β -mercaptoethanol (Bio-Rad, UK). The tissue suspension was centrifuged at 1500 rpm at 4°C and the supernatant and pellet separated. Supernatant protein was assayed using the Lowry method with bovine serum albumin as a standard.

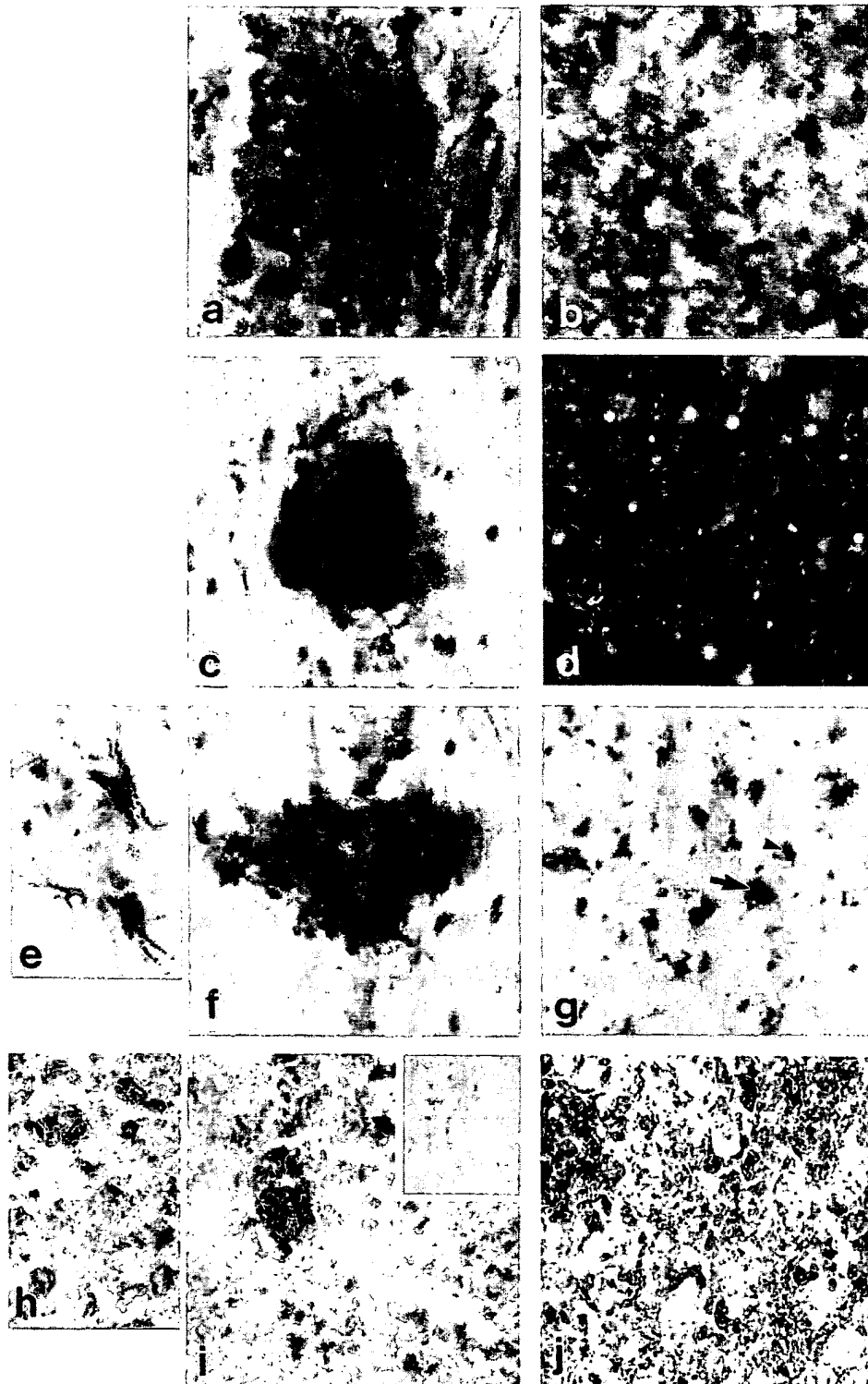


Figure 1. Caspase and CaspaTag-1 immunostaining. **a:** Spinal cord section from Lewis rat acute EAE immunostained with caspase-1. **b:** CaspaTag-1 immunostaining in a serial section. **c:** First relapse. **d:** Caspatag-1 in a serial section. **e:** Caspase-1 immunostaining in parenchymal astrocytes. **f:** White matter inflammatory cuff. **g:** Gray matter neurons of third relapse animals. **h:** Caspase-1-positive neurons in gray matter of ABH mice. **i:** Inflammatory cuff in acute EAE. **j:** Immunostaining in first relapse animals. Original magnifications: $\times 500$ (**a–d**, **f**, **g**, **i**, and **j**); $\times 1000$ (**e** and **h**). Inset to **i** shows caspase-1-negative staining in control mice.

Fifty μg of the supernatant protein including sodium dodecyl sulfate containing sample buffer was run on either 7.5% (Bio-Rad), 12%, or 16% (both from Autogen Bioclear, Wiltshire, UK) Tris-glycine precast gels and

then transferred onto Immobilon P polyvinylidene difluoride membrane (Millipore, Bedford, MA). The membrane was blocked in 2% bovine serum albumin in Tween-Tris-buffered saline (T-TBS) and incubated with secondary

antibody for 2 hours diluted 1:2000 in 2% bovine serum albumin T-TBS. Membranes were washed in T-TBS before incubating with horseradish peroxidase-labeled anti-mouse or rabbit IgG. After further washes in T-TBS, membranes were developed using an enhanced chemiluminescent kit (Amersham, Buckingham, UK). For control experiments, caspase-1 or -3 antibody was pre-blocked as described above before applying onto Western blots.

Detection of Active Caspases by CaspaTag

CaspaTag detection kits (Intergen Company, Oxford, UK) were used to detect activated caspase-1 and -3 in sections from experimental animals²³ according to the manufacturer's instructions. Sections were incubated with the appropriate detection kit in a humidified chamber at 37°C for 1 hour in the dark. Sections were washed three times in PBS followed by fixation for 10 minutes and two further washes in PBS. Sections were then counterstained with Hoechst 33342 to indicate apoptotic cells and viewed under a fluorescent microscope at 490 excitation to observe green fluorescence of caspase-positive cells and a UV filter to view Hoechst staining.

The number of CaspaTag-positive cells in spinal cord sections from Lewis rats were counted using a 100- μm^2 graticule in five different random fields for each section. A total of two sections from three animals in each group were counted and the results expressed as the mean \pm SD. The results were analyzed statistically using GraphPad Prism software (GraphPad Prism, San Diego, CA). Sample means were analyzed using a one-way analysis of variance with Bonferroni's post hoc testing.

Detection of Fragmented DNA in Cells Indicative of Apoptosis

The Fluorescein-FragEL (QIA-39; Oncogene Research Products, San Diego, CA) system was used to evaluate DNA fragmentation in apoptotic cells according to the manufacturer's instructions. Briefly, sections were fixed in 4% formaldehyde, permeabilized with proteinase K, and incubated with a fluorescent-labeled terminal deoxynucleotidyl transferase. Finally, sections were washed and mounted using the media provided and viewed under a confocal laser-scanning microscope (Bio-Rad).

Results

Disease Course and Pathology

The samples for this study came from the same spinal cord tissue used in the previous report of IL-12-induced relapses in the Lewis rat.² Tissues from the representative acute and the three subsequent relapses of EAE were used in this study. The clinical course and pathology of CREAE in the ABH mouse has been described.³ Here we selected animals during the peak of acute EAE,

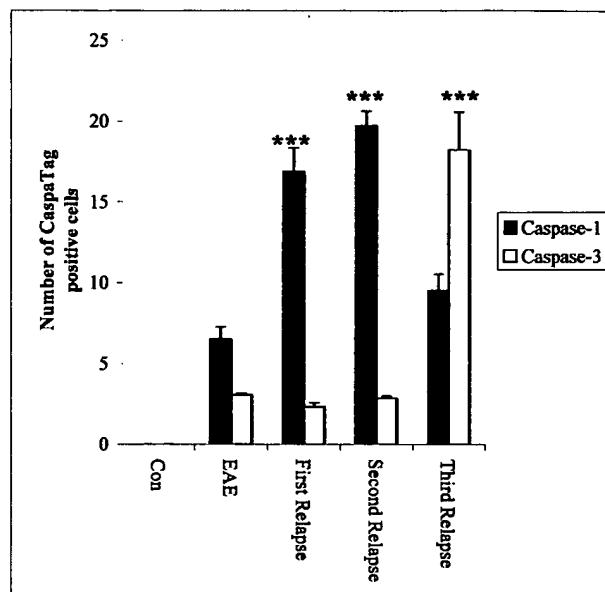


Figure 2. Quantitation of the number of CaspaTag-1 and -3⁺ cells in the spinal cord of Lewis rats during the relapses. ***, $P < 0.0001$ versus acute EAE.

after remission from acute attack, first relapse, and atypical chronic stages.

Caspase-1 Immunostaining

Caspase-1 immunostaining in Lewis rats was localized to a few cells in the spinal cord of control rats (not shown), none of which were positive by the CaspaTag-1 for active caspase-1. In acute EAE, caspase-1-positive cells were restricted to inflammatory cuffs (Figure 1a) with some also staining with CaspaTag-1 (Figure 1b). During IL-12-induced relapses, numbers of both immunopositive and CaspaTag-1-positive cells were localized in inflammatory cuffs as well as individual cells in the parenchyma, peaking during the second relapse (Figure 1, c and d, respectively, and Figure 2). During the second and third relapse, immunopositive astrocytes were localized (Figure 1e) in close proximity to the inflammatory cuffs (Figure 1f) and also further into the parenchyma, whereas caspase-1-positive neurons were observed in third relapse animals (Figure 1g).

In contrast, Caspase-1 immunostaining in CREAE mice was abundant even during the acute phase within inflammatory cells (Figure 1i) and neurons (Figure 1h). Caspase-1-positive immunostaining was also observed on axonal surfaces predominantly during the relapse phase as well as neurons (arrow) and inflammatory cells (Figure 1j, arrowhead). CaspaTag-1 immunostaining for active caspase-1 activity was also strongly localized on axons and cells in all of the different phases studied, however it was difficult to distinguish between cellular and axonal staining (not shown). Weak caspase-1 and CaspaTag-1 immunostaining was also present in control ABH mice (not shown). Control sections were negative.

Caspase-3 Immunostaining

During acute EAE there were immunopositive cells in inflammatory cuffs (Figure 3a) with only a few of these

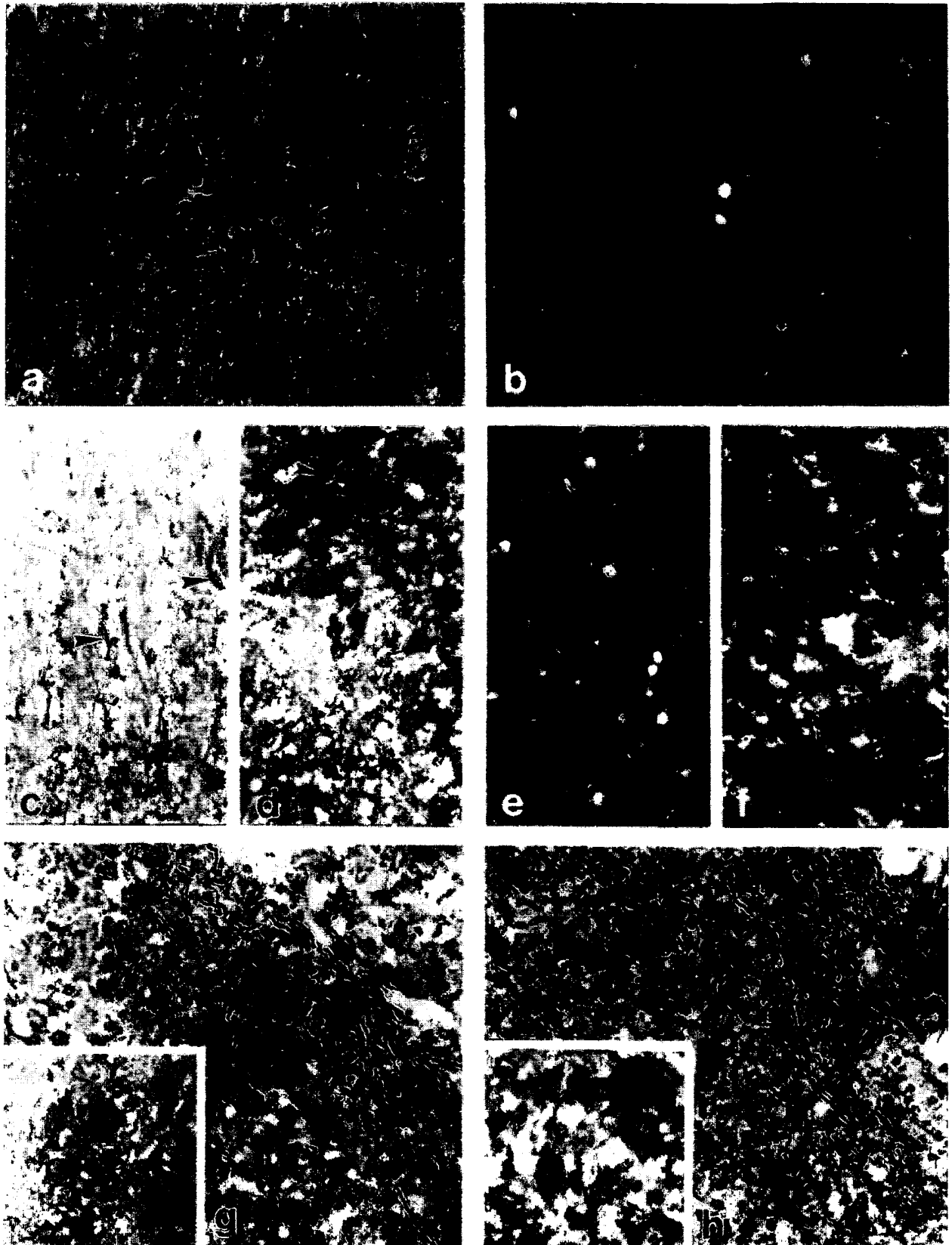


Figure 3. Caspase-3 immunostaining in Lewis rat spinal cords from EAE (a), third relapse white matter (c), and third relapse (d) gray matter neuronal cells and axons (arrowhead). The corresponding CaspaTag-3 immunostaining is shown in b, e, and f, respectively. g and h: Caspase-3-immunostained axons in ABH mice acute EAE and first relapse animals, respectively. Inset to h shows caspase-3-positive immunostaining in neurons in gray matter of ABH mice. Original magnifications: $\times 500$ (a–h); $\times 1000$ (inset). Inset to g shows caspase-3-positive immunostaining in control mice.

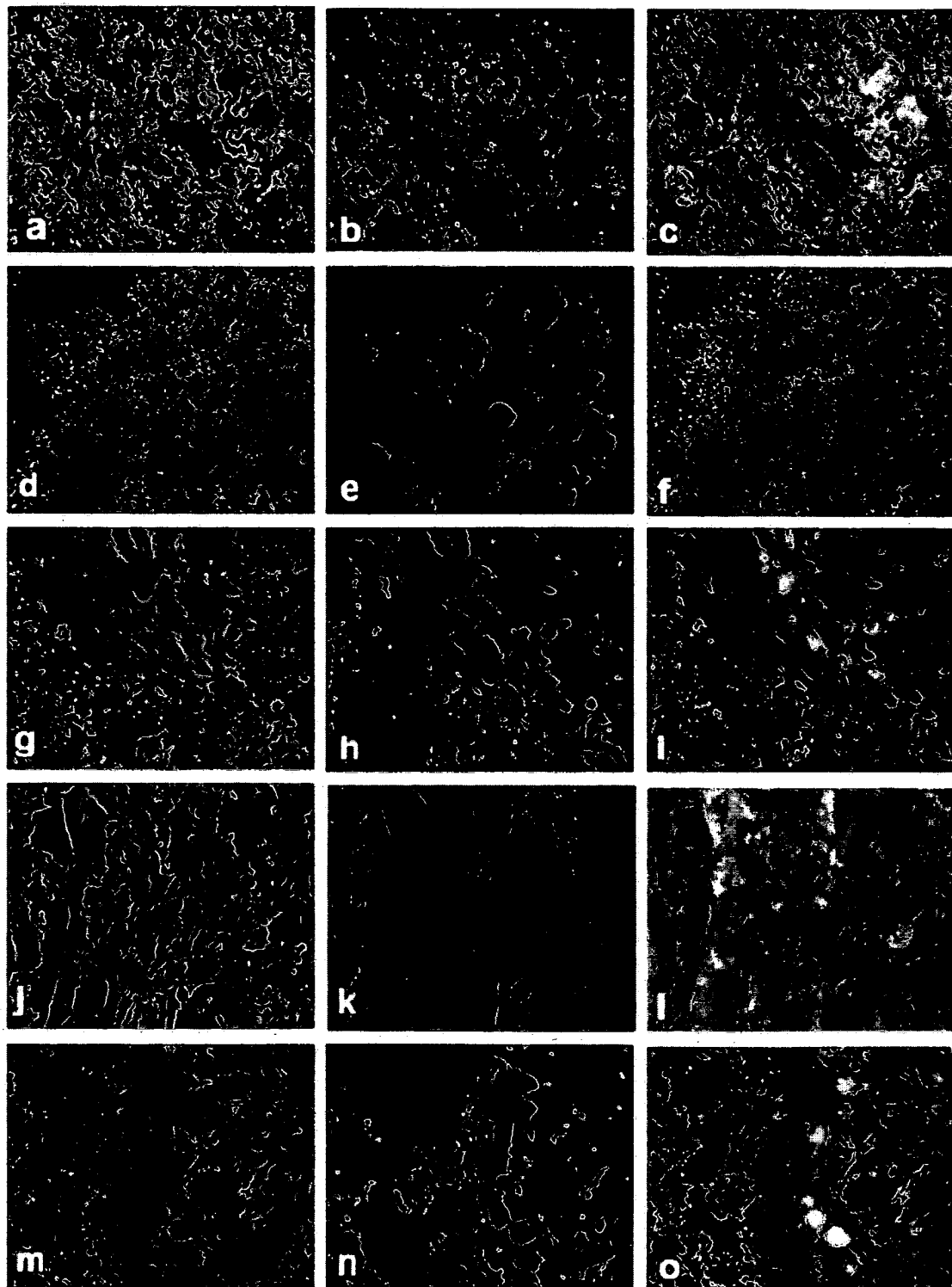


Figure 4. Phenotypic characterization of active caspase-3⁺ cells. **a** and **d** show double staining for active caspase-3 in ED-1⁺ macrophages (**b**) and NF⁺ neuronal cells (**e**) and **c** and **f** are merged images of **a** and **b** and **d** and **e**, respectively, in the spinal cord of Lewis rats from the third relapse. **g**, **j**, and **m** show activated caspase-3 in CD4⁺ T cells (**h**), NF⁺ axons (**k**), and CNPase⁺ oligodendrocytes (**n**). **i**, **l**, and **o** are merged images of **g** and **h**, **j** and **k**, and **m** and **n**, respectively. Original magnifications, $\times 1500$. White matter in all panels except **d-f**.

cells positive for active caspase-3 in a serial section (Figure 3b) whereas very few cells were positive during the first and second relapse with caspase-3 and its active component (not shown). However, during the third re-

lapse numerous microglial cells in white matter (Figure 3c) and neuronal cells in gray matter (Figure 3d) were stained positive with caspase-3 and CaspaTag-3, together with small sections of axons in white matter and

gray matter (Figure 3, c and d, arrowheads). Control animals did not show any immunostaining for caspase or CaspaTag-3.

Caspase-3 immunostaining in ABH mice showed that small sections of axons were immunopositive even in control animals (Figure 3g, inset). Once disease was induced, many white matter axons were immunopositive for caspase-3 (Figure 3g) and CaspaTag-3 activity was also localized to these axons (not shown). After remission from acute EAE small sections of axons remained positive but by the first relapse phase, there was extensive detection of axonal and neuronal caspase-3 (Figure 3h and inset). Active caspase-1- and -3-positive cells could not be counted in ABH mice because there was such overwhelming positive immunostaining on axons such that it was difficult to decipher individual cells. In all CaspaTag-1- and -3-positive cells, bright pyknotic nuclei, indicative of apoptosis, were observed when sections were counterstained with Hoechst 33342 (not shown).

Double-immunofluorescent staining for activated caspase-3 and a range of cell markers showed similar cell-type localization from the spinal cord of Lewis rats in the third relapse and in ABH mouse EAE. In the Lewis rat, inflammatory cells including macrophages (Figure 4; a, b, and c) and neuronal cells (Figure 4, d and f) in the gray matter of the spinal cord were immunopositive for activated caspase-3. Similarly, inflammatory cells including CD4⁺ T cells (Figure 4, g and h) were immunopositive for activated caspase-3, localized in both in the parenchyma and in inflammatory cuffs in the spinal cord of the mouse, with the greatest amount of positive staining during the relapse stage of mouse EAE. Additionally there was prominent activated caspase-3 staining in axons (Figure 4; j, k, and l) and oligodendrocytes (Figure 4; m, n, and o), particularly during the relapse stage in the mouse. Control spinal cord sections from rat and mouse were negative (see supplemental figures).

Presence of Fragmented DNA within Cells Indicating Apoptosis

Fragmented DNA was present only during the third relapse in Lewis rat spinal cords localized within inflammatory (Figure 5a) and neuronal (Figure 5b) cells. However, many more inflammatory (Figure 5, c and e) and neuronal (Figure 5, d and e) cells with fragmented DNA were localized in the mouse spinal cord with the highest number present during the relapse stage of mouse EAE. Sections from the spinal cord of control mice (Figure 5g) showed rare weakly positive cells whereas control rat samples were totally negative (Figure 5h).

Changes in Caspase-1 and -3 Protein in Lewis Rat and ABH Mouse

Immunohistochemical changes were reflected in Western blots of spinal cord samples during the different stages of EAE in the two models. Caspase-1 protein was induced during acute EAE in Lewis rats (Figure 6a) and increased

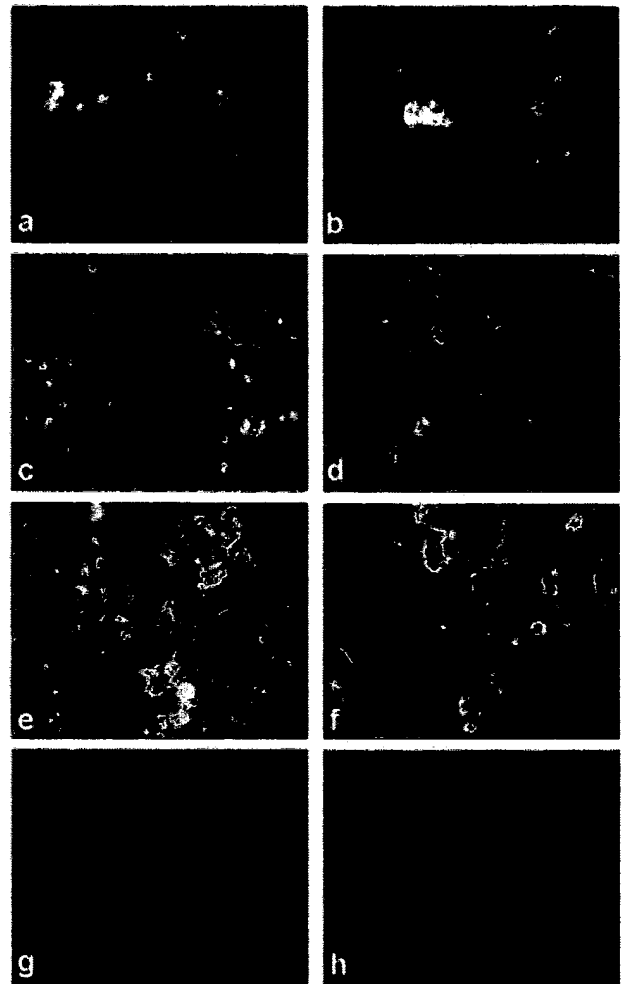


Figure 5. a, c, e, f, and h: White matter sections. b, d, and f: Gray matter section. a, b, and h: Lewis rat spinal cord. c–g: ABH mice. a, c, and e show fragmented DNA in inflammatory cells in white matter and b, d, and f show neuronal cells in gray matter from the spinal cords of third relapse Lewis rat and acute and relapse ABH mice, respectively. g and h: Negative control for DNA fragmentation in the spinal cord of normal animals. Original magnifications, $\times 1500$.

further after the relapses peaking during the second relapse and finally decreasing during the third relapse. However, the greatest amount of caspase-3 together with 12-kd cleaved active caspase-3 protein was found during the third relapse in Lewis rats compared with any other stage of disease (Figure 6a). Caspase-1 and caspase-3 proteins were undetectable in control Lewis rat spinal cords and peptide blocking eliminated staining in the test samples.

In contrast to the Lewis rat model, some caspase-1 and -3 protein was detected even in normal control ABH mouse spinal cord (Figure 6b). However, the greatest amount of caspase-1 protein was found during acute EAE whereas that of caspase-3 protein and the 20- and 12-kd active caspase fragments was found during the first relapse (Figure 6b).

Discussion

In this study, we have shown that caspase-1 protein and activity were induced in inflammatory cells during the

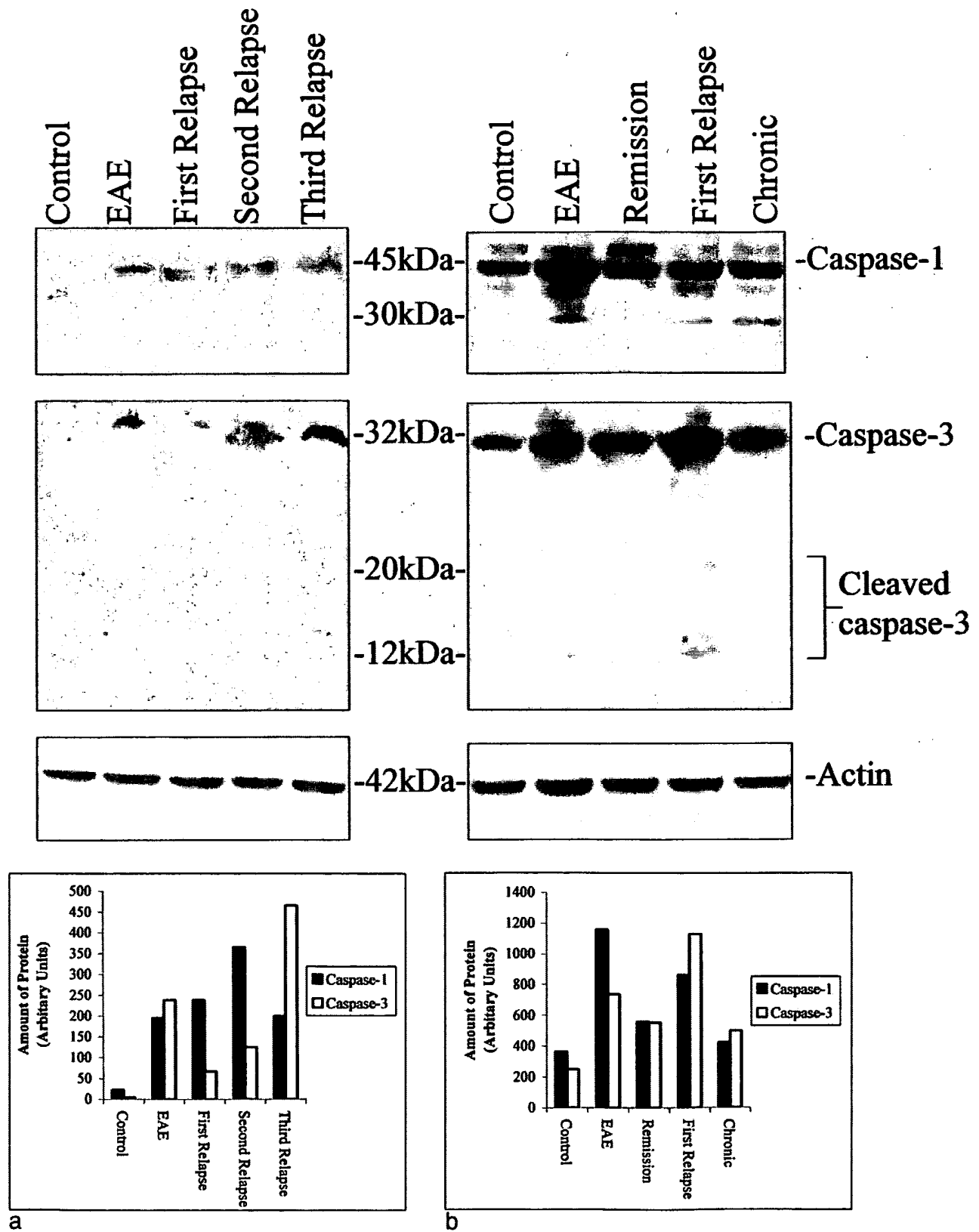


Figure 6. **a:** Western Blot of caspase-1 and -3 protein expression during the relapses in Lewis rat EAE and a corresponding graph to show the relative amounts of protein in each band determined by gel analysis using ScionImage 4.0.2 (Scion Corporation, MD). **b:** Western blot in ABH mice and a graph to show the relative amounts of protein in each band. Actin blots of the same gels are shown for control of protein loading.

initial acute episodes of EAE in both the Lewis rat (mainly inflammatory) and ABH mouse (mainly degenerative) models. By the third relapse in the Lewis rat, neuronal cells in the spinal cord were positive for caspase-1 whereas even during the acute phase in the ABH mouse, immunostained neurons were detectable that increased during relapses. In agreement with this the greatest amount of caspase activity was observed during the inflammatory stages of the disease (first and second relapse in the Lewis rat and the acute EAE stage in the ABH mouse). In contrast caspase-3 protein and activity did not increase significantly until the third relapse in the Lewis rat with immunostaining initially restricted to macrophages and T cells in inflammatory cuffs and extending to neuronal cells at later stages. However, in the ABH mouse, caspase-3 expression and activity was already high in acute EAE and during the first relapse, predominantly localized to axons and neuronal cells but also in oligodendrocytes.

These results are in conformity with the idea that caspase-1 has dual biological roles in that it can participate in the cellular induction of apoptosis as well as the processing of pro-IL-1 β to the active form.^{17,24} In our experiments, it is suggested that in the inflammatory model, caspase-1 may primarily function as a processor of pro-IL-1 β because there was no evidence from our earlier study using electron microscopic criteria² of cellular or axonal death during first and second relapse. It has been reported that during maximum EAE severity in the mouse, expression of caspase-1 mRNA mirrors that of proinflammatory cytokines such as IL-1 β , IL-6, tumor necrosis factor- α , and interferon- γ .¹⁵ In the same study, a reduction of the incidence and severity of EAE was observed both in caspase-1-deficient mice ($-/-$) and with pharmacological blockers, suggesting a key involvement of the enzyme in the development of EAE.¹⁵ However, the observation of caspase-1-positive astrocytes in second and third relapse of Lewis rats suggests that these cells undergo apoptosis during this stage of the disease. Furthermore, caspase-1-positive neurons in the spinal cord of third relapse animals in the Lewis rat and immediately after disease induction in the ABH mouse suggests that caspase-1 can contribute to apoptotic cell death by blocking DNA repair mechanisms.¹⁶

The localization of caspase-3 in axons and neurons with increased enzyme activity in the third IL-12-induced relapse of EAE in the Lewis rat correlates with the limited axonal loss observed in our earlier study,² implicating a caspase-3-mediated mechanism. This is strengthened further by observations in the ABH mouse in which the highest amount of active caspase-3 was found in the spinal cord of relapse animals with immunostaining predominantly localized to axons and neurons but also in oligodendrocytes. This correlates well with a previous study in which axonal loss together with demyelination was found to be prominent during the first relapse compared to acute EAE.³ Caspase-3 has been shown to be the major executioner caspase involved in neuronal apoptosis and *in vitro* when microglia are activated.^{17,19,20} Procaspases are also found within axons and caspase-3 can be activated within the axon itself or transported from

the neuronal cell body.^{25,26} Activation of caspase-3 can occur by the release from mitochondria of cytochrome c causing hydrolysis of key structural and housekeeping genes which leads to DNA fragmentation and apoptosis.^{8,13,14} The degenerative changes in axons through activation of caspase-3 can therefore be attributed to the cytochrome c release with consequent dysfunction of mitochondria that are distributed along axons as well as in the neuronal soma.^{27,28} Although demyelination is predominantly executed by inflammatory macrophages, the detection of active caspase-3 oligodendrocytes in the ABH mouse suggests additional mechanisms of myelin breakdown.

The fundamental difference between the two models is that in EAE in the ABH mouse, extensive axonal pathology and demyelination are observed whereas myelin basic protein-induced EAE in Lewis rats is predominantly inflammatory. Even after three relapses of EAE induced by IL-12, only limited axonal death could be observed in the Lewis rat model.² ABH mice however, may be particularly susceptible to EAE because both caspase-1 and caspase-3 protein and immunostaining are already detected in control animals. This may represent a primed response system or enhanced gene transcription of these cell death proteins in the ABH mice such that in the early stages of EAE, abundant caspase-1 and -3 protein can be synthesized. Furthermore, the axonal localization of caspases in the ABH mouse during EAE reinforces the disease susceptibility in this strain, in which the production of caspases was many fold higher than in the Lewis rat.

In conclusion, the current study suggests that caspase-1 and caspase-3 can mediate axonal damage and cell death in EAE, especially in degenerative CREAE in the ABH mouse where axons are particularly susceptible. Caspase-3, being a downstream executioner of neuronal cell death could be an important target for specific caspase-3 inhibitors, reducing axonal damage and degeneration in multiple sclerosis and in EAE and is being investigated further.

References

1. Smith T, Hewson AK, Kingsley CI, Leonard JP, Cuzner ML: Interleukin-12 induces relapse in experimental allergic encephalomyelitis in the Lewis rat. *Am J Pathol* 1997, 150:1909-1917
2. Ahmed Z, Gveric D, Pryce G, Baker D, Leonard JP, Cuzner ML: Myelin/axonal pathology in interleukin-12 induced serial relapses of experimental allergic encephalomyelitis in the Lewis rat. *Am J Pathol* 2001, 158:2127-2138
3. Baker D, O'Neill JK, Gschmeissner SE, Wilcox CE, Butter C, Turk JL: Induction of chronic relapsing experimental allergic encephalomyelitis in Biozzi mice. *J Neuroimmunol* 1990, 28:261-270
4. Thornberry NA, Lazebnik Y: Caspases: enemies within. *Science* 1998, 281:1312-1316
5. Arends MJ, Wyllie AH: Apoptosis: mechanisms and roles in pathology. *Int Rev Exp Pathol* 1991, 32:223-254
6. Raff MC: Social controls on cell survival and cell death. *Nature* 1992, 356:397-400
7. MacFarlane M, Cain K, Sun XM, Alnemri ES, Cohen GM: Processing/activation of at least four interleukin-1 β converting enzyme-like proteases occurs during the execution phase of apoptosis in human monocytic tumor cells. *J Cell Biol* 1997, 137:469-479
8. Cohen GM: Caspases: the executioners of apoptosis. *Biochem J* 1997, 326:1-16

9. Slee EA, Harte MT, Kluck RM, Wolf BB, Casiano CA, Newmeyer DD, Wang HG, Reed JC, Nicholson DW, Alnemri ES, Green DR, Martin SJ: Ordering the cytochrome c-initiated caspase cascade: hierarchical activation of caspases-2, -3, -6, -7, -8, and -10 in a caspase-9-dependent manner. *J Cell Biol* 1999, 144:281-292
10. Gu Y, Wu J, Faucheu C, Lallanne JL, Diu A, Livingston DJ, Su MS: Interleukin-1 beta converting enzyme requires oligomerization for activity of processed forms in vivo. *EMBO J* 1995, 14:1923-1931
11. Darmon AJ, Nicholson DW, Bleackley RC: Activation of the apoptotic protease CPP32 by cytotoxic T-cell-derived granzyme B. *Nature* 1995, 377:446-448
12. Walker NP, Talanian RV, Brady KD, Dang LC, Bump NJ, Ferenz CR, Franklin S, Ghayur T, Hackett MC, Hammill LD: Crystal structure of the cysteine protease interleukin-1 beta-converting enzyme: a (p20/p10)₂ homodimer. *Cell* 1994, 78:343-352
13. Takahashi A, Alnemri ES, Lazebnik YA, Fernandes-Alnemri T, Litwack G, Moir RD, Goldman RD, Poirier GG, Kaufmann SH, Earnshaw WC: Cleavage of lamin A by Mch2 alpha but not CPP32: multiple interleukin 1 beta-converting enzyme-related proteases with distinct substrate recognition properties are active in apoptosis. *Proc Natl Acad Sci USA* 1996, 93:8395-8400
14. Weaver VM, Carson CE, Walker PR, Chaly N, Lach B, Raymond Y, Brown DL, Sikorska M: Degradation of nuclear matrix and DNA cleavage in apoptotic thymocytes. *J Cell Sci* 1996, 109:45-56
15. Furlan R, Martino G, Galbiati F, Poliani PL, Smirardo S, Bergami A, Desina G, Comi G, Flavell R, Su MS, Adorini L: Caspase-1 regulates the inflammatory process leading to autoimmune demyelination. *J Immunol* 1999, 163:2403-2409
16. Kumar S: ICE-like proteases in apoptosis. *Trends Biochem Sci* 1995, 20:198-202
17. Kingham PJ, Cuzner ML, Pocock JM: Apoptotic pathways mobilized in microglia and neurones as a consequence of chromogranin A-induced microglial activation. *J Neurochem* 1999, 73:538-547
18. Kingham PJ, Pocock JM: Microglial apoptosis induced by chromogranin A is mediated by mitochondrial depolarization and the permeability transition but not by cytochrome c release. *J Neurochem* 2000, 74:1452-1462
19. Bredesen DE: Apoptosis: overview and signal transduction pathways. *J Neurotrauma* 2000, 17:801-810
20. Eldadah BA, Faden AI: Caspase pathways, neuronal apoptosis, and CNS injury. *J Neurotrauma* 2000, 17:811-829
21. Baker D, Pryce G, Croxford JL, Brown P, Pertwee RG, Huffman JW, Layward L: Cannabinoids control spasticity and tremor in a multiple sclerosis model. *Nature* 2000, 404:84-87
22. Allen SJ, Baker D, O'Neill JK, Davison AN, Turk JL: Isolation and characterization of cells infiltrating the spinal cord during the course of chronic relapsing experimental allergic encephalomyelitis in the Biozzi AB/H mouse. *Cell Immunol* 1993, 146:335-350
23. Kingham PJ, Pocock JM: Microglial secreted cathepsin B induces neuronal apoptosis. *J Neurochem* 2001, 76:1475-1484
24. Schumann RR, Belka C, Reuter D, Lamping N, Kirschning CJ, Weber JR, Pfeil D: Lipopolysaccharide activates caspase-1 (interleukin-1-converting enzyme) in cultured monocytic and endothelial cells. *Blood* 1998, 91:577-584
25. Krupinski J, Lopez E, Marti E, Ferrer I: Expression of caspases and their substrates in the rat model of focal cerebral ischemia. *Neurobiol Dis* 2000, 7:332-342
26. Finn JT, Weil M, Archer F, Siman R, Srinivasan A, Raff MC: Evidence that Wallerian degeneration and localized axon degeneration induced by local neurotrophin deprivation do not involve caspases. *J Neurosci* 2000, 20:1333-1341
27. Springer JE, Azbill RD, Knapp PE: Activation of the caspase-3 apoptotic cascade in traumatic spinal cord injury. *Nat Med* 1999, 5:943-946
28. Van Vliet BJ, Sebben M, Dumuis A, Gabrion J, Bockaert J, Pin JP: Endogenous amino acid release from cultured cerebellar neuronal cells: effect of tetanus toxin on glutamate release. *J Neurochem* 1989, 52:1229-1239

Caspase-1 Regulates the Inflammatory Process Leading to Autoimmune Demyelination¹

Roberto Furlan,* Gianvito Martino,^{2*†} Francesca Galbiati,[‡] Pietro L. Poliani,*
Simona Smirardo,[‡] Alessandra Bergami,* Gaetano Desina,^{**§} Giancarlo Comi,[†] Richard Flavell,[¶]
Michael S. Su,^{||} and Luciano Adorini[‡]

T cell-mediated inflammation is considered to play a key role in the pathogenic mechanisms sustaining multiple sclerosis (MS). Caspase-1, formerly designated IL-1 β -converting enzyme, is crucially involved in immune-mediated inflammation because of its pivotal role in regulating the cellular export of IL-1 β and IL-18. We studied the role of caspase-1 in experimental autoimmune encephalomyelitis (EAE), the animal model for MS. Caspase-1 is transcriptionally induced during EAE, and its levels correlate with the clinical course and transcription rate of proinflammatory cytokines such as TNF- α , IL-1 β , IFN- γ , and IL-6. A reduction of EAE incidence and severity is observed in caspase-1-deficient mice, depending on the immunogenicity and on the amount of the encephalitogenic myelin oligodendrocyte glycoprotein (MOG) peptide used. In caspase-1-deficient mice, reduced EAE incidence correlates with defective development of anti-MOG IFN- γ -producing Th1 cells. Finally, pharmacological blockade of caspase-1 in Biozzi AB/H mice, immunized with spinal cord homogenate or MOG₃₅₋₅₅ peptide, by the caspase-1-inhibitor Z-Val-Ala-DL-Asp-fluoromethylketone, significantly reduces EAE incidence in a preventive but not in a therapeutic protocol. These results indicate that caspase-1 plays an important role in the early stage of the immune-mediated inflammatory process leading to EAE, thus representing a possible therapeutic target in the acute phase of relapsing remitting MS. *The Journal of Immunology*, 1999, 163: 2403-2409.

The caspase family comprises thus far 13 different cysteine proteases that are mainly involved in the apoptotic pathway (1). Among them, caspase-1, formerly named IL-1 β -converting enzyme, which is activated by caspase-11-mediated proteolytic cleavage (2), is less involved in the apoptotic cascade but is prominent in inflammation because of its pivotal role in regulating the cellular export of proinflammatory cytokines such as IL-1 β . Caspase-1 is elevated in intestinal macrophages during inflammatory bowel disease (3) and in a variety of organs, including the brain, in response to bacterial LPS administration (4). Further evidence on the role played by caspase-1 in inflammation comes from studies on caspase-1-deficient ($-/-$) mice and caspase-1 pharmacological inhibitors. Caspase-1 $-/-$ mice display an alteration in the export of several proinflammatory cytokines, namely IL-1 β , IL-1 α , IL-6, and TNF- α , although neither IL-1 α nor IL-6 nor TNF- α are substrates for caspase-1 (5). Furthermore, caspase-1 proteolytically activates IL-18, and caspase-1 $-/-$ mice have also reduced serum levels of IL-18 and IFN- γ in response to LPS administration (6). Caspase-1 $-/-$ mice are resistant to LPS-induced endotoxic shock (7) and to the induction of experimental

pancreatitis (8). In vivo pharmacological inhibition of caspase-1 protects mice from TNF- α -induced liver failure (9) and collagen-induced arthritis (10).

MS³ is an immune-mediated demyelinating disease of the CNS of unknown etiology (11). The pathological hallmark of the disease is the presence within the CNS of inflammatory infiltrates containing few autoreactive T cells and many pathogenic nonspecific mononuclear cells (12). It is currently believed that Ag-specific T cells provide the organ specificity of the pathogenic process and regulate the recirculation within the CNS of activated mononuclear cells releasing inflammatory myelinotoxic substances. These latter cells can be activated in the periphery by polyclonal inflammatory stimuli, thus determining disease recurrence (12, 13). Proinflammatory cytokines participate either in Ag-specific T cell activation or in peripheral activation of nonspecific mononuclear cells. TNF- α , IFN- γ , and IL-6 levels increase before disease relapses (13, 14). An increased number of disease relapses was observed in MS patients treated with IFN- γ (15). Moreover, TNF- α , IFN- γ , and IL-1 β are present in demyelinating plaques (16), and IL-1 β has been shown to be a mediator of the inflammatory process sustaining EAE, the animal model for MS (17).

We evaluated the role of caspase-1 in EAE. We found that caspase-1 mRNA blood levels parallel those of proinflammatory cytokines, such as IL-1 β , IL-6, TNF- α , and IFN- γ , during EAE and peak at the time of maximal EAE severity. A reduction of EAE incidence and severity was observed in caspase-1 $-/-$ mice depending on the immunogenicity and on the amount of the encephalitogenic MOG peptide used. Finally, pharmacological blockade of caspase-1 reduced the incidence of EAE, induced either with SCH or MOG₃₅₋₅₅ peptide, in a preventive but not therapeutic

*Experimental Neuroimmunotherapy Unit, Department of Biotechnology, and [†]Department of Neurology, San Raffaele Scientific Institute, Milan, Italy; [‡]Roche Milano Ricerche, Milan, Italy; [§]Department of Neurology, Casa Sollievo della Sofferenza Scientific Institute, San Giovanni Rotondo (FG), Italy; [¶]Howard Hughes Medical Institute, Yale University School of Medicine, New Haven, CT 06510; and ^{||}Vertex Pharmaceuticals, Inc., Cambridge, MA 02139

Received for publication April 12, 1999. Accepted for publication June 10, 1999.

The costs of publication of this article were defrayed in part by the payment of page charges. This article must therefore be hereby marked *advertisement* in accordance with 18 U.S.C. Section 1734 solely to indicate this fact.

¹ This work was supported by Istituto Superiore di Sanità (Target project: Multiple Sclerosis), and Ministero dell'Università e della Ricerca Scientifica e Tecnologica.

² Address correspondence and reprint requests to Dr. Gianvito Martino, Department of Biotechnology-San Raffaele Scientific Institute, Via Olgettina 58, 20132 Milan, Italy. E-mail address: g.martino@hsr.it

³ Abbreviations used in this paper: MS, multiple sclerosis; EAE, experimental autoimmune encephalomyelitis; MOG, myelin oligodendrocyte glycoprotein; SCH, spinal cord homogenate; AU, arbitrary units; p.i., postimmunization.

protocol. These results indicate that caspase-1 plays an important role in the immune-mediated pathogenic events leading to EAE and might represent a suitable therapeutic target of the active phase of the immune-mediated inflammatory demyelination.

Materials and Methods

Mice and immunizations

Female Biozzi AB/H mice, 4–6 wk old, were purchased from Harlan U.K. (Blackthorn, U.K.). Female C57BL/6 mice, 4–6 wk old were obtained by Charles River (Calco, Italy). Female (SV129 × C57BL/6)_{F1} mice, hereafter designated (SV129 × B6)_{F1}, 4–6 wk old, were obtained by The Jackson Laboratory (Bar Harbor, ME). Caspase-1^{-/-} mice had been obtained as previously described (5). Briefly, chimeric mice were obtained by injection of embryonic stem cells, in which the caspase-1 gene was disrupted and replaced with a neomycin resistance gene cassette, into C57BL/6 blastocysts. The chimeric males were then mated with C57BL/6 mice. Homozygous mice with two copies of the disrupted caspase-1 gene were identified by Southern blot of genomic DNA, and the absence of caspase-1 mRNA in caspase-1^{-/-} mice was confirmed by RT-PCR analysis. Homozygous mice were then interbred and used for the experiments.

All animals were housed in specific pathogen-free conditions and treated according to the guidelines of the Animal Ethical Committee of our Institute. Mice were immunized with IFA (Difco, Detroit, MI) supplemented with 4 mg/ml *Mycobacterium tuberculosis* (strain H37Ra; Difco) and MOG_{35–55} (Multiple Peptide Systems, San Diego, CA), MOG_{40–55} (Roche Milano Recherche, Milan, Italy), or SCH from Biozzi AB/H mice. Two immunization schedules were used for peptides: a single injection of 200 µg or two injections of 300 µg peptide 7 days apart. For SCH immunization, 1 mg of Ag was given twice, at days 0 and 7. All injections were followed by i.p. administration of 500 ng pertussis toxin (Sigma, St. Louis, MI) the same day and 48 h later. Body weight and clinical score (0 = healthy, 1 = flaccid tail, 2 = ataxia and/or paresis of hind limbs, 3 = paralysis of hind limbs and/or paresis of forelimbs, 4 = tetraparesis, 5 = moribund or death) were recorded daily.

Miniosmotic pumps

Miniosmotic pumps (Alzet 2001, Alza, Palo Alto, CA) were implanted s.c. in the dorsal flank of mice. The mean fill volume of pumps was ~220 µl, and the mean pumping rate was ~1 µl/h, delivering continuously for ~10 days. Pumps were filled with 50 mg/ml of the caspase-1 inhibitor Z-Val-Ala-DL-Asp-fluoromethylketone (Bachem, Bubendorf, Switzerland) obtaining a delivery of 1.2 mg/day. Pumps were implanted 1 day before immunization (preventive protocol) or 1 week after (therapeutic protocol). Dosage of Z-Val-Ala-DL-Asp-fluoromethylketone has been deducted from previous reports showing that in vivo administration of 25–50 mg/kg of specific caspase-1 inhibitors (i.e., Z-Val-Ala-DL-Asp-fluoromethylketone, VE 13.045) completely inhibits caspase-1 enzymatic activity for several days (18, 19).

Semiquantitative RT-PCR for cytokines

Blood samples were obtained from mice by tail bleeding every week. RNA was recovered from these samples in guanidinium thiocyanate by acid phenol extraction. A T-primed first strand kit was used for the reverse transcription of total RNA into cDNA (Ready-to-go kit, Pharmacia, Uppsala, Sweden). PCR amplification (30 cycles: 1 min 95°C, 1 min 55°C, 1 min 72°C) of cDNA sequences specific for caspase-1 and cytokines was performed using 20 pmol of each primer, 200 mM concentrations of each dNTP, 25 mM KCl, 10 mM Tris-HCl (pH 8.3), 1.5 mM MgCl₂, and 2.5 U *Taq* polymerase. Amplified PCR products were hybridized with the specific ³²P-labeled oligonucleotide probe (caspase-1 and cytokines) or ³²P-labeled probe obtained from a plasmid containing the mouse GAPDH cDNA, followed by analysis on a PhosphorImager (Molecular Dynamics, Sunnyvale, CA; Image Quant Software, version 3.3). Values were normalized against the GAPDH gene. For interanimal comparisons, the normalized intensities were further corrected with the use of the normalized intensities of the bands resulting from RT-PCR amplification of a cDNA derived from mouse LPS-activated splenocytes (positive control). The following primers and probes were used: caspase-1 (product: 343 bp), antisense 5'-GTGTTGAAGAGCAGAAAGCA-3', sense 5'-GAGATGGTGAAA GAGGTGAA-3', probe 5'-TGAAAGACAAGCCCAAGG TG-3'; IL-1β (product: 563 bp), antisense 5'-CAGGACAGGTATAGATTCTTCTTT-3', sense 5'-ATGGCAACTGTTTCTGAACTCAACT-3', probe 5'-AGCTTTCAGCTCATATGGGTCGACAGCAC-3'; IL-6 (product: 634 bp), antisense 5'-CAGTAGGTTTGCCGAGTAGATCTC-3', sense 5'-ATGAAGTTCCTCTCTGCAAGAGACT-3', probe 5'-CTCCAGAAGAC

CAGAGGAAATTTCAATAG-3'; TNF-α (product: 373 bp), antisense 5'-GTATGAGATAGCAATGCGCTGACGGTGTGGG-3', sense 5'-TTCTGTCTACTGAACCTCGGGGTGATCGGTCC-3', probe 5'-GCCGTGGGC CAGGAGGGCGTTGGCGCGCTG-3'; IFN-γ (product: 450 bp), antisense 5'-ACACTGCATCTTGGCTTTGC-3', sense 5'-CGACTCTTTTCCGCT TCCT-3', probe 5'-TTCTTCAGCAACAGCAAGGC-3'; GAPDH (product: 710 bp), antisense 5'-CGCATCTTCTTGTGCAAGT-3', sense 5'-GT TCAGCTCTGGGATGAC-3'. RT-PCR results were expressed as fold induction of AU from basal levels.

Ag-specific proliferation assays

For T cell proliferation assays, draining lymph nodes were removed, and 4 × 10⁵ lymph node cells per well were cultured in 96-well culture plates (Costar, Cambridge, MA) in synthetic HL-1 medium (Ventrex Laboratories, Portland, ME) supplemented with 2 mM L-glutamine and 50 µg/ml gentamicin (Sigma, St. Louis, MO) and serial concentrations (1, 3, 10 µM) of MOG_{40–55} peptide. Cultures were incubated for 3 days in 5% CO₂ in air and pulsed 8 h before harvesting with 1 µCi [³H]TdR (40 Ci/nmol, Pharmacia Biotech, Amersham, Cologno Monzese, Italy). Incorporation of [³H]TdR was measured by liquid scintillation spectrometry.

Intracytoplasmic staining for cytokine production

Lymph node cells (6 × 10⁵ cells/well) were cultured in 96-well culture plates in synthetic HL-1 medium with 10 µM MOG_{40–55}. After 72 h of culture cells were harvested, washed, and recultured for additional 72 h in RPMI 1640 supplemented with 2 mM L-glutamine, 50 µg/ml gentamicin, 50 µM 2-ME (Fluka Chemical, Ronkonkoma, NY), and 10% FCS (Sigma). After culture, living cells separated on a Ficoll gradient were restimulated with PMA (1 µg/ml) and ionomycin (50 ng/ml) for 4 h at 37°C, with 10 µg/ml brefeldin A (Novartis, Basel, Switzerland) added for the last 2 h to prevent egress of newly synthesized proteins from the endoplasmic reticulum. After fixation with 4% paraformaldehyde for 20 min at room temperature, cells were stained for IFN-γ and IL-4 using the method of Openshaw et al. (20) and Galbiati et al. (21). Cells were washed, preincubated for 10 min with PBS/FCS/saponin, and then incubated with FITC rat anti-mouse IFN-γ (XMG1.2, PharMingen, San Diego, CA) and PE rat anti-mouse IL-4 (11B11, PharMingen) or with isotype controls FITC- and PE-labeled rat IgG1, κ (R3-34, PharMingen). After 30 min, cells were washed twice with PBS/FCS/saponin and then with PBS containing 5% of FCS without saponin to allow membrane closure. Cell membranes were then stained with Cy-Chrome-labeled anti-CD4 (L3T4, PharMingen) for 15 min at room temperature. Analysis was performed with a FACScan flow cytometer (Becton Dickinson, Mountain View, CA) equipped with CellQuest software, and 50,000 events were acquired.

ELISA for IFN-γ secretion

IFN-γ was quantified by two-sites sandwich ELISA using polyvinyl microtiter plates (Falcon 3012) coated with AN-18.17.24 mAb in carbonate buffer as previously described (21). Samples (50 µl/well) diluted in test solution (PBS containing 5% FCS and 1 g/l phenol) were incubated together with 50 µl peroxidase-conjugated XMG1.2 mAb. After overnight incubation at room temperature, bound peroxidase was detected by 3,3',5,5'-tetramethylbenzidine (Fluka Chemical), and absorbance was read at 450 nm with an automated microplate ELISA reader (MR5000, Dynatech Laboratories, Chantilly, VA). IFN-γ was quantified from two to three titration points using standard curves generated by purified recombinant mouse IFN-γ, and results were expressed as cytokine concentration in ng/ml. Detection limit was 15 pg/ml.

Neuropathological features in EAE mice

At the time of sacrifice, mice were transcardially perfused with 4% paraformaldehyde. Brains and spinal cords were removed and postfixed in the same fixative for 2–4 h, washed in PBS, and then embedded in paraffin. Tissue sections were cut at 4 µm on a microtome and stained for histological examination. Hematoxylin and eosin staining was used to reveal perivascular inflammatory infiltrates, Luxol Fast Blue staining was used to reveal demyelinated areas, and Bielschowsky staining was used to detect axonal loss. Macrophages were stained using peroxidase-labeled BS-I isolectin B4 (Sigma), whereas T cells using a rat anti-CD3 Ab (pan-T cell marker; Serotec Ltd, Oxford, U.K.) revealed using a biotin-labeled secondary anti-rat Ab (Amersham). Neuropathological findings were quantified on an average of 10 complete cross-sections of spinal cord per mouse. The number of perivascular inflammatory infiltrates was calculated and expressed as the numbers of inflammatory infiltrates per mm², whereas demyelinated areas and axonal loss were expressed as the percentage of

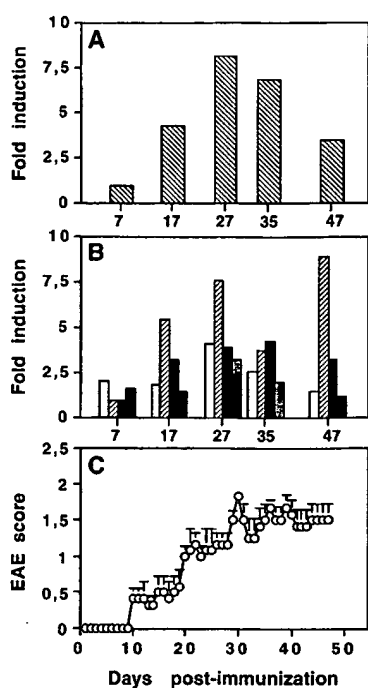


FIGURE 1. Caspase-1 and proinflammatory cytokine mRNAs are up-regulated during the course of EAE in blood from C57BL/6 mice immunized with 200 μ g of MOG_{40–55}. **A**, Caspase-1 mRNA levels. **B**, mRNA levels of IL-1 β (□), IL-6 (▨), IFN- γ (■), and TNF- α (▤) from the same mice. mRNA levels were measured by a semiquantitative RT-PCR on blood samples obtained from the tail vein of mice once a week. mRNA levels have been normalized against GAPDH mRNA levels and expressed as fold induction (AU increase over basal level recorded 7 days p.i.). Blood samples were obtained every week after immunization as indicated on x-axis. **C**, Clinical course of EAE in blood donors ($n = 12$ mice). Each circle represents the mean EAE score registered. Bars represent the SE.

damaged area per mm² (22). T cells and macrophages were counted and expressed as the number of cells per mm².

Statistical analysis

Data are expressed as mean \pm SE. Student's t test for unpaired data was used to compare cytokine and caspase-1 mRNA levels and the cytokine protein levels. EAE cumulative score was calculated by summing up each individual score registered in any group of mice studied during the follow-up period levels. Comparison between cumulative scores was performed using Student's t test. A χ^2 test was used to compare EAE incidence in the different groups of mice. $p < 0.05$ was considered significant.

Results

Caspase-1 mRNA is up-regulated in the course of EAE

C57BL/6 mice immunized with MOG_{40–55} were bled once a week for 5 weeks after immunization. RT-PCR was performed on blood samples to determine caspase-1, IL-1 β , IL-6, TNF- α , and IFN- γ mRNA levels. Caspase-1 mRNA levels increased almost 8-fold (Fig. 1A) during EAE from basal levels recorded at day 7 p.i. This increase paralleled disease severity, peaking 4 wk p.i. (day 27 p.i., 52.9 ± 16.8 AU; $p = 0.01$ vs day 7 p.i.) (Fig. 1A) when EAE clinical score reached its maximum (Fig. 1C). Caspase-1 mRNA level increase paralleled that of the caspase-1 substrate IL-1 β , which showed a 2-fold increase (day 27 p.i., 3.3 ± 0.9 AU; $p = 0.03$ vs day 7 p.i.) (Fig. 1B); IL-6 mRNA increased almost 8-fold (day 27 p.i., 15.4 ± 7.6 AU; $p = 0.04$) (Fig. 1B); TNF- α mRNA increased almost 3-fold (day 27 p.i., 12.2 ± 5.4 ; $p = \text{n.s.}$ vs day 7 p.i.) (Fig. 1B), and IFN- γ mRNA 4-fold (day 27 p.i., 1.6 ± 0.5 AU; $p = 0.02$ vs day 7 p.i.) (Fig. 1B). These data indicate that

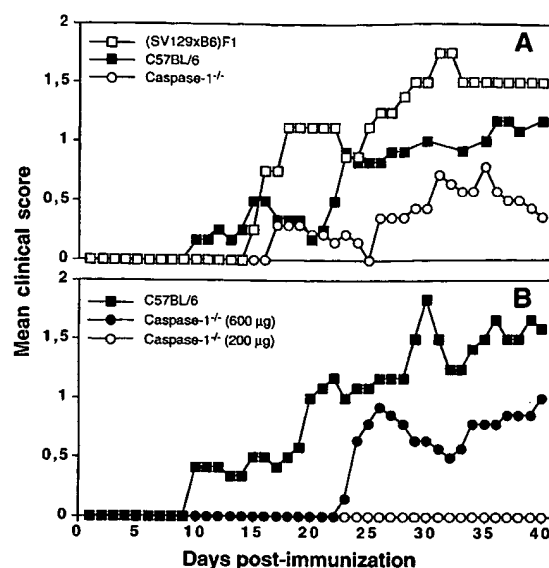


FIGURE 2. Clinical course of EAE in MOG peptide-immunized (SV129 \times B6)F₁, caspase-1^{-/-}, and C57BL/6 mice. In caspase-1^{-/-} mice, the EAE course and severity varies depending on the amount and length of the MOG peptide used. **A**, EAE immunization protocol with 200 μ g MOG_{35–55} in (SV129 \times B6)F₁, C57BL/6, and caspase-1^{-/-} mice. Caspase-1^{-/-} mice are susceptible to EAE induction but develop a less severe disease than control mice. **B**, EAE immunization protocol with 200 or 600 μ g MOG_{40–55} in C57BL/6 (■ = 200 μ g MOG_{40–55}) and caspase-1^{-/-} mice (○ = 200 μ g MOG_{40–55}; ● = 600 μ g MOG_{40–55}). Immunization of caspase-1^{-/-} mice with the low amount (200 μ g) of the shorter peptide (MOG_{40–55}) does not lead to EAE development. Irrespective of the dose of MOG_{40–55} used, C57BL/6 mice always show a more severe EAE than do caspase-1^{-/-} mice.

caspase-1 is up-regulated at the transcriptional level during the course of EAE and that this up-regulation parallels that of proinflammatory cytokines such as IL-1 β , IFN- γ , TNF- α , and IL-6.

Caspase-1^{-/-} mice are less susceptible to EAE induction

To further explore the role of caspase-1 in EAE, we studied the susceptibility of caspase-1^{-/-} mice to MOG peptide-induced EAE. We first analyzed EAE susceptibility of (SV129 \times B6)F₁ and C57BL/6 mice, which have a genetic background comparable with that of the caspase-1^{-/-} mice using 200 μ g of MOG_{35–55}. The two groups of mice showed similar disease courses (Fig. 2A, Table I) confirming results previously reported (23).

To analyze EAE susceptibility in caspase-1^{-/-} mice, we used two different amounts (200 μ g once or 300 μ g twice, 7 days apart) of two MOG overlapping peptides (MOG_{35–55} and MOG_{40–55}). MOG peptides were chosen because of their previously described difference in immunogenicity and encephalitogenicity in C57BL/6 mice (24). Low dose immunization (200 μ g) with MOG_{40–55} failed to induce EAE in caspase-1^{-/-} mice (0 of 12 sick animals) compared with C57BL/6 mice (11 of 12) ($p < 0.0001$) (Fig. 2B, Table I). Caspase-1^{-/-} mice developed EAE when immunized with the low dose (200 μ g) of MOG_{35–55} (Fig. 2A, Table I) or the high dose (600 μ g) of MOG_{40–55} (Fig. 2B, Table I); the incidence, however, was lower and the onset delayed compared with (SV129 \times B6)F₁ or C57BL/6 mice. Therefore, caspase-1^{-/-} mice are less susceptible to MOG-induced EAE compared with C57BL/6 or (SV129 \times B6)F₁ mice. However, caspase-1^{-/-} mice can develop EAE when the immunogenicity of the encephalitogenic peptide is increased.

Table I. EAE in (SV129 × B6)F₁, C57BL/6, and caspase-1^{-/-} mice

| Mouse Strain | MOG Peptide (amount) | EAE Incidence (%) | EAE Onset (range) ^a | Maximum EAE Score (range) ^b |
|----------------------------|--|-----------------------|--------------------------------|--|
| (SV129 × B6)F ₁ | MOG ₃₅₋₅₅ (200 μg) | 4/4 (100) | 20.0 ± 3.7 (16–31) | 1.9 ± 0.6 (1–2.5) |
| C57BL/6 | MOG ₃₅₋₅₅ (200 μg) | 6/6 (100) | 19.2 ± 3.0 (10–31) | 1.5 ± 0.2 (1–2) |
| | MOG ₄₀₋₅₅ (200 μg) | 11/12 (92) | 17.3 ± 2.6 (10–30) | 2.0 ± 0.1 (1.5–2.0) |
| Caspase-1 ^{-/-} | MOG ₄₀₋₅₅ (600 μg) ^c | 5/7 (71) | 27.8 ± 2.4 (23–34) | 1.8 ± 0.4 (1.0–3.0) |
| | MOG ₃₅₋₅₅ (200 μg) | 4/7 (57) | 27.2 ± 3.9 (18–35) | 1.9 ± 0.1 (1.5–2.0) |
| | MOG ₄₀₋₅₅ (200 μg) | 0/12 ^d (0) | NA ^e | NA |

^a EAE onset is expressed as day post immunization ± SE.^b EAE score is expressed as mean maximum score ± SE.^c MOG₄₀₋₅₅ has been administered twice 1 wk apart (300 + 300 μg).^d $p < 0.0001$ vs C57BL/6 mice immunized with 200 μg MOG₄₀₋₅₅, $p = 0.03$ and $p = 0.006$ vs caspase-1^{-/-} mice immunized with 200 μg MOG₃₅₋₅₅ or 600 μg MOG₄₀₋₅₅, respectively.^e NA, not applicable.

Inhibition of the Th1 response in caspase-1-deficient mice

To elucidate the possible causes of reduced susceptibility of caspase-1^{-/-} mice to EAE, we analyzed mice immunized with 200 μg of MOG₄₀₋₅₅ peptide in which the most striking difference between caspase-1^{-/-} and C57BL/6 was observed (Fig. 2B, Table I). Five caspase-1^{-/-} mice and 5 C57BL/6 mice were sacrificed 10 days after immunization with MOG₄₀₋₅₅, and cells from the draining lymph nodes were obtained. Proliferation assays to MOG₄₀₋₅₅ showed no impairment in the responsiveness of T cells from caspase-1^{-/-} compared with C57BL/6 mice (Fig. 3A). We detected, however, decreased levels of IFN-γ secreted in the supernatant of MOG₄₀₋₅₅ restimulated cells (Fig. 3B) from caspase-1^{-/-} compared with C57BL/6 mice ($p = 0.01$). Intracytoplasmic staining for IFN-γ and IL-4 of MOG₄₀₋₅₅-restimulated cells showed reduced IFN-γ-producing cells and no induction of IL-4-producing cells (Fig. 3, C–E). These results suggest that cells from caspase-1^{-/-} mice efficiently present the encephalitogenic peptide to T cells but are defective in Th1 development.

Caspase-1 inhibitor administration prevents but does not treat EAE

Pharmacological blockade of EAE with caspase-1 inhibitors was tested in Biozzi AB/H mice immunized with SCH or MOG₃₅₋₅₅. In Biozzi mice, SCH induces a very aggressive relapsing-remitting EAE (25), whereas MOG₃₅₋₅₅ induces a more chronic progressive disease. We administered vehicle or Z-Val-Ala-DL-Asp-fluoromethylketone, a highly specific, cell-permeable, and irreversible inhibitor of caspase-1-like proteases (26) to Biozzi mice before immunization with SCH or MOG₃₅₋₅₅. Because this caspase-1 inhibitor is a peptide with a very short half-life in vivo, we implanted s.c. mini-osmotic pumps able to continuously release the inhibitor for 10 days. Continuous administration of the caspase-1 inhibitor induced a clearcut suppression of either SCH-induced or MOG₃₅₋₅₅-induced EAE compared with vehicle-treated mice (Table II). The cumulative EAE score, representing the disease burden, was significantly lower in caspase-1 inhibitor-treated mice than in vehicle-treated mice in both immunization protocols (Table II).

FIGURE 3. Reduced Th1 cell development in caspase-1^{-/-} mice immunized with 200 μg of MOG₄₀₋₅₅. **A**, Proliferation of draining lymph nodes cells from caspase-1^{-/-} (○) and C57BL/6 (●) mice restimulated in vitro with the indicated concentrations of MOG₄₀₋₅₅. The background cpm values were subtracted (Δ cpm). **B**, IFN-γ levels (±SE) in supernatants from cell cultures from caspase-1^{-/-} (○) and C57BL/6 (●) in response to the indicated concentrations of MOG₄₀₋₅₅. **C**, Intracellular staining for IFN-γ and IL-4 of MOG₄₀₋₅₅-stimulated cells from a representative C57BL/6 mouse. **D**, Intracellular staining for IFN-γ and IL-4 of MOG₄₀₋₅₅-stimulated cells from a representative caspase-1^{-/-} mouse. In **C** and **D**, the percentage of IFN-γ-producing cells are reported in the lower right corner. In **E**, the percentage of IFN-γ-producing cells from MOG₄₀₋₅₅-immunized C57BL/6 (○) and caspase-1^{-/-} (●) mice. Each circle represents a single mouse, and mean values are indicated by the horizontal bars. Caspase-1^{-/-} mice display a significant ($p = 0.01$) reduction of IFN-γ production.

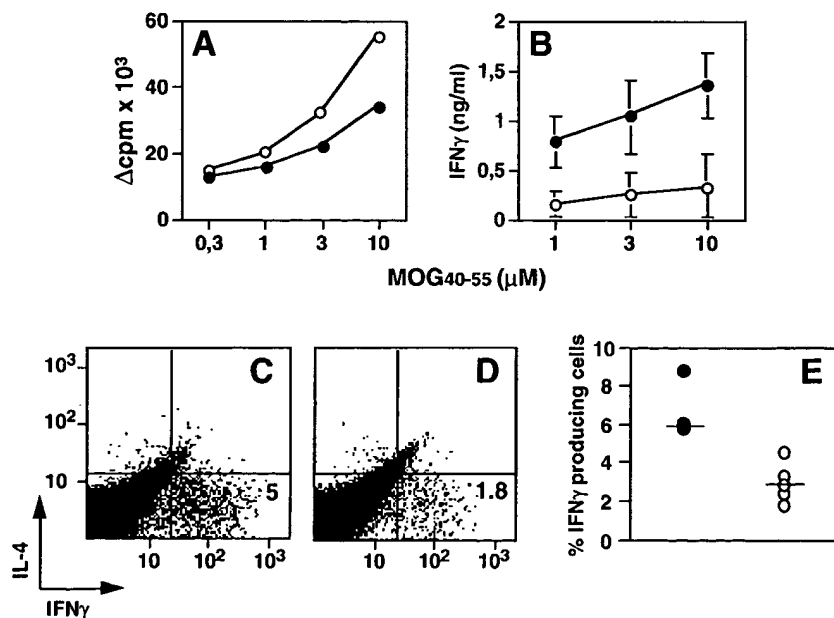


Table II. EAE in Biozzi AB/H mice immunized with SCH or MOG₃₅₋₅₅ and treated with vehicle or the caspase-1 inhibitor Z-Val-Ala-DL-fluoromethylketone

| Treatment Schedule ^a | EAE Incidence (%) | EAE Onset (range) ^b | Maximum EAE Score (range) ^c | Cumulative Score (days of follow-up) ^d |
|-----------------------------------|---------------------------|--------------------------------|--|---|
| MOG ₃₅₋₅₅ (preventive) | | | | |
| Vehicle | 5/7 (71) | 22.4 ± 2.9 (16–30) | 2.1 ± 0.5 (1–4) | 89.5 (40) |
| Caspase-1 inhibitor | 2/7 (29) | 23.5 ± 5.5 (18–29) | 2.2 ± 1.2 (1–3.5) | 32 (40) |
| SCH (preventive) | | | | |
| Vehicle | 10/10 (100) | 14.2 ± 0.5 (12–16) | 3.7 ± 0.2 (1.5–5.0) | 282 (25) |
| Caspase-1 inhibitor | 4/10 ^e (40) | 15.0 ± 0.7 (13–16) | 3.6 ± 0.4 (2.5–4.0) | 82 ^f (25) |
| SCH (therapeutic) | | | | |
| Vehicle | 10/10 (100) | 14.5 ± 0.6 (13–19) | 3.8 ± 0.3 (1.5–5.0) | NA ^g |
| Caspase-1 inhibitor | 9/10 (90) | 14.3 ± 0.3 (13–16) | 3.0 ± 0.3 (1.5–4.0) | NA |

^a Treatment was performed by implantation of mini-osmotic pumps releasing for 10 days vehicle or the caspase-1 inhibitor Z-Val-Ala-DL-fluoromethylketone (1.2 mg/day) from the day before immunization (preventive) or day 7 (therapeutic) after immunization.

^b EAE onset is expressed as day post immunization ± SE.

^c EAE score is expressed as mean maximum score ± SE.

^d Cumulative score was calculated by summing up each individual score registered during the follow-up period.

^e $p = 0.003$ vs vehicle-treated mice.

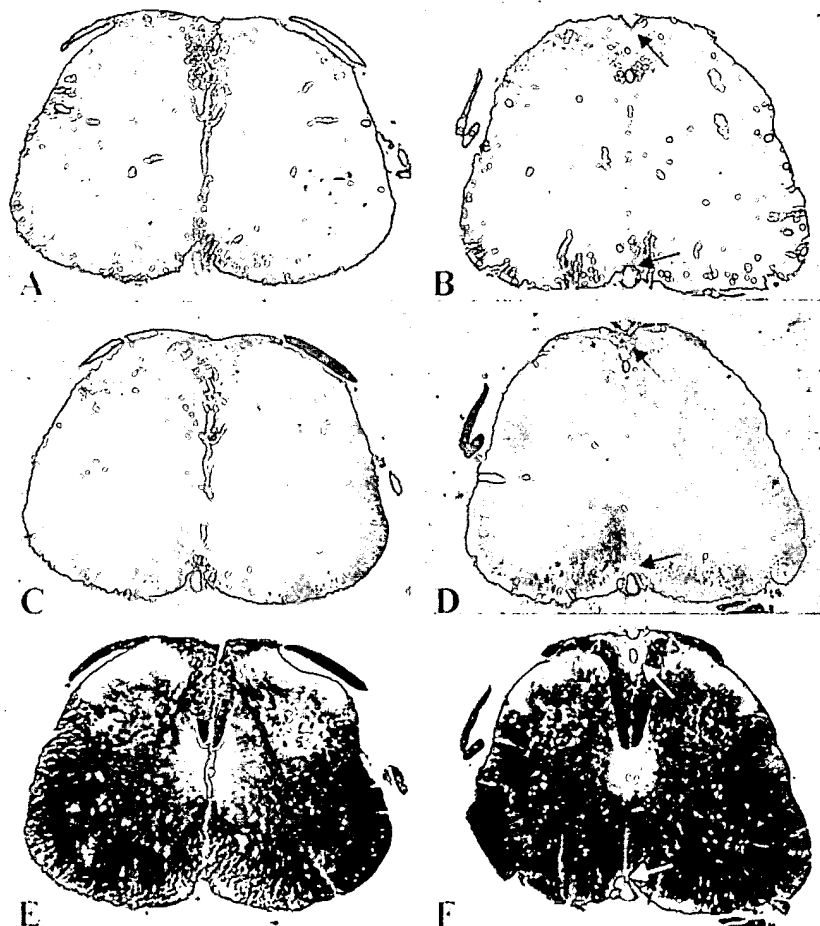
^f $p = 0.0007$ vs vehicle-treated mice.

^g NA, not applicable because in the therapeutic administration one mouse died during the follow-up period.

However, the mean day of onset and the mean clinical score of sick animals were comparable between groups (Table II). In the SCH-induced group, two animals for each treatment were sacrificed for

neuropathology examination. Animals treated with the inhibitor had less infiltrates per mm² than did vehicle-treated controls (0.4 and 1.6 vs 6.6 and 3.1, respectively) (Fig. 4, A and B), less demy-

FIGURE 4. Neuropathological findings of SCH-induced EAE in two representative Biozzi mice treated with vehicle or caspase-1 inhibitor Z-Val-Ala-DL-Asp-fluoromethylketone, respectively. Spinal cord sections stained with hematoxylin and eosin (×5) are shown in A and B; perivascular infiltrates (arrowheads) are less evident in the caspase-1 inhibitor-treated (A) vs vehicle-treated (B) mouse. Spinal cord sections stained with Luxol Fast Blue (×5) are shown in C and D; demyelinated areas (arrowheads) are less prominent in the caspase-1 inhibitor-treated (C) vs vehicle-treated (D) mouse. Spinal cord sections stained with Bielschowsky staining (×5) are shown in E and F; axonal loss (arrowheads) is decreased in the caspase-1 inhibitor-treated mouse (E) vs the vehicle-treated (F) mouse. Tissue sections of each mouse are from the same spinal cord area and have been obtained serially.



elination (0.6% and 0.8% vs 9.8% and 2.2%, respectively) (Fig. 4, C and D), reduced axonal loss (0.4% and 0.6% vs 8.3% and 1.5%, respectively) (Fig. 4, E and F), less infiltrating CD3⁺ cells/mm² (39.9 and 90.5 vs 291 and 138.2, respectively), and reduced numbers of infiltrating macrophages per mm² (21.8 and 52.5 vs 211.9 and 84.9, respectively).

By contrast, when the mini-osmotic pumps were implanted 7 days p.i. in Biozzi mice immunized with SCH, EAE development was similar in inhibitor- and vehicle-treated mice (Table II). Only 1 of the 10 mice treated with the inhibitor from 7 days p.i. did not develop a full-blown EAE. These results suggest that caspase-1 is crucial in the induction phase of EAE, when peripheral inflammation leads to the recruitment of effector cells into the CNS.

Discussion

The central role of proinflammatory cytokines in orchestrating the pathogenic process leading to EAE has been extensively studied (27–29), but few data are thus far available on the posttranslational mechanisms of regulation of cytokine secretion during this experimental autoimmune CNS-confined disease. We focused our attention on the proteolytic enzyme caspase-1, because previous studies showed that its pharmacological inhibition or its absence (i.e., deletion mutant mice) mainly affects the secretion of proinflammatory cytokines such as IL-1 β , IL-1 α , IL-6, TNF- α , IL-18, and IFN- γ (5–7). We found that caspase-1 transcription is up-regulated during mouse EAE, reaching a peak at maximal disease severity. This induction is higher compared with other proinflammatory cytokines previously shown to be up-regulated during EAE (27) and is similar to that found in the Lewis rat EAE (30). These data suggest that proteolytic activation of proinflammatory cytokines is a crucial step in the immune-mediated process leading to EAE.

Caspase-1^{-/-} mice were susceptible to MOG peptide-induced EAE. Disease susceptibility was associated with the number of immunizations and the dose and the MHC-binding affinity of the encephalitogenic MOG-peptide. In our hands, MOG_{40–55} showed a 3-fold weaker binding (IC₅₀ = 360 pM) compared with MOG_{35–55} (IC₅₀ = 1 nM) to the I-A^{b7} molecule (data not shown). However, the disease induced in caspase-1^{-/-} mice was always less severe than in C57BL/6 or (SV129 \times B6)F₁ mice and did not develop at all when a low dose of the weaker MHC binder MOG peptide was used. The reduced EAE in caspase-1-deficient mice was not caused by inefficient Ag presentation to T cells, as shown by the Ag-specific proliferation assays, but to an impairment in Th1 cell development as indicated by the lower percentage of IFN- γ -producing cells from caspase-1^{-/-} vs C57BL/6 mice. The most likely explanation of this finding possibly resides in the cleavage activity of caspase-1 on the precursor of IL-18 into its mature form (6). Although IL-18 in itself does not induce Th1 cell development (31, 32), which is mostly driven by IL-12 (33), Th1 cell development independent from IL-12 could be induced by the cooperative action of IL-18 and other factors (34). These factors may include IFN- γ itself (35) and IL-1 $\alpha\beta$ (33). Thus, the simultaneous caspase-1-dependent defect in IL-18 and IL-1 $\alpha\beta$ production could explain the impaired Th1 development and the reduced EAE in caspase-1^{-/-} mice. A more aggressive immunization protocol, however, is able to overcome this limiting step in EAE induction, likely because other proteases may replace caspase-1 in the cleavage of pro-IL-1 β and pro-IL-18.

Results obtained with caspase-1 inhibitor administration are consistent with the lower susceptibility to EAE of caspase-1^{-/-} mice. The preventive administration of the caspase-1 inhibitor Z-Val-Ala-DL-Asp-fluoromethylketone dramatically reduced both re-

lapsing-remitting or chronic-progressive EAE in two different mouse strains. However, the small proportion (35%) of mice not protected from EAE by caspase-1 inhibitor treatment developed a clinical course of EAE indistinguishable from that of controls. As in inflammatory fluids other proteases (i.e., trypsin, chymotrypsin, elastase, granzyme A) (36) can replace caspase-1 enzymatic activity, an immunization protocol able to induce a potent local inflammation may bypass its requirement. Nevertheless, recent data indicate that Z-Val-Ala-DL-Asp-fluoromethylketone is active also on other cysteine proteases involved in inflammatory reactions but not in the apoptotic cascade, such as caspases-4 and -5 (37).

Administration of Z-Val-Ala-DL-Asp-fluoromethylketone during the effector phase of SCH-induced EAE (i.e., therapeutic protocol) had no effect on the disease course and severity. These data are suggestive for a crucial role played by caspase-1 in the peripheral activation of proinflammatory cytokines during the induction phase of EAE. The lack of efficacy of caspase-1 inhibitors once the inflammatory cascade has already determined CNS infiltration and damage might be also explained by the impaired blood-brain barrier crossing of caspase-1 inhibitors (26).

In conclusion, our results indicate that caspase-1 plays a crucial role in the development of the immune-mediated inflammatory process leading to CNS demyelination. EAE development is impaired in caspase-1^{-/-} mice, although the requirement for caspase-1 in the inflammatory phase of EAE can be bypassed. The role of caspase-1 in autoimmune demyelination is further corroborated by the significant reduction of EAE incidence in mice preventively treated with the caspase-1-inhibitor Z-Val-Ala-DL-Asp-fluoromethylketone. However, the inefficacy of caspase-1 inhibitors in blocking ongoing EAE suggests that this enzyme is crucial in the early phase of the inflammatory process leading to immune-mediated demyelination. Thus, caspase-1 could represent both a marker of inflammation sustaining immune-mediated demyelination and a possible therapeutic target of the acute phase of relapsing-remitting MS.

Acknowledgments

We thank Drs. Adriano Fontana, Hans-Pietro Eugster, and Hans Lassmann for helpful discussion, and Silvia Gregori for performing the MHC-binding assay.

References

1. Thornberry, N. A., and Y. Lazebnik. 1998. Caspases: enemies within. *Science* 281:1312.
2. Wang, S., M. Miura, Y. Jung, H. Zhu, E. Li, and J. Yuan. 1998. Murine caspase-11, an ICE-interacting protease, is essential for the activation of ICE. *Cell* 92:501.
3. McAlidon, M. E., C. J. Hawkey, and Y. R. Mahida. 1998. Expression of interleukin-1 β and interleukin-1 β converting enzyme by intestinal macrophages in health and inflammatory bowel disease. *Gut* 42:214.
4. Tingsborg, S., M. Zetterstrom, K. Alheim, H. Hasanvan, M. Schultzberg, and T. Bartfai. 1996. Regionally specific induction of ICE mRNA and enzyme activity in the rat brain and adrenal gland by LPS. *Brain Res.* 712:153.
5. Kuida, K., J. A. Lippke, G. Ku, M. W. Harding, D. J. Livingston, M. S. Su, and R. A. Flavell. 1995. Altered cytokine export and apoptosis in mice deficient in interleukin-1 β converting enzyme. *Science* 267:2000.
6. Gu, Y., K. Kuida, H. Tsutsui, G. Ku, K. Hsiao, M. A. Fleming, N. Hayashi, K. Higashino, H. Okamura, K. Nakanishi, et al. 1997. Activation of interferon- γ inducing factor mediated by interleukin-1 β converting enzyme. *Science* 275:206.
7. Li, P., H. Allen, S. Banerjee, and T. Seshadri. 1997. Characterization of mice deficient in interleukin-1 β converting enzyme. *J. Cell. Biochem.* 64:27.
8. Norman, J., J. Yang, G. Fink, G. Carter, G. Ku, W. Denham, and D. Livingston. 1997. Severity and mortality of experimental pancreatitis are dependent on interleukin-1 converting enzyme (ICE). *J. Interferon Cytokine Res.* 17:113.
9. Rouquet, N., J. C. Pages, T. Molina, P. Briand, and V. Joulin. 1996. ICE inhibitor YVADcmk is a potent therapeutic agent against in vivo liver apoptosis. *Curr. Biol.* 6:1192.
10. Ku, G., T. Faust, L. L. Lauffer, D. J. Livingston, and M. W. Harding. 1996. Interleukin-1 β converting enzyme inhibition blocks progression of type II collagen-induced arthritis in mice. *Cytokine* 8:377.
11. Martin, R., H. F. McFarland, and D. E. McFarlin. 1992. Immunological aspects of demyelinating diseases. *Annu. Rev. Immunol.* 10:153.

12. Steinman, L. 1996. A few autoreactive cells in an autoimmune infiltrate control a vast population of nonspecific cells: a tale of smart bombs and the infantry. *Proc. Natl. Acad. Sci. USA* 93:2253.
13. Martino, G., F. Grohovaz, E. Brambilla, F. Codazzi, A. Consiglio, E. Clementi, M. Filippi, G. Comi, and L. M. E. Grimaldi. 1998. Proinflammatory cytokines regulate antigen-independent T-cell activation by two separate calcium-signaling pathways in multiple sclerosis patients. *Ann. Neurol.* 43:340.
14. Beck, J., P. Rondot, L. Catinot, E. Falcoff, H. Kirchner, and J. Wietzerbin. 1988. Increased production of interferon γ and tumor necrosis factor precedes clinical manifestation in multiple sclerosis: do cytokines trigger off exacerbations? *Acta Neurol. Scand.* 78:318.
15. Panitch, H. S., R. L. Hirsch, A. S. Haley, and K. P. Johnson. 1987. Exacerbations of multiple sclerosis in patients treated with γ interferon. *Lancet* 1:893.
16. Brosnan, C. F., B. Cannella, L. Battistini, and C. S. Raine. 1995. Cytokine localization in multiple sclerosis lesions: correlation with adhesion molecule expression and reactive nitrogen species. *Neurology* 45:S16.
17. Martin, D., and S. L. Near. 1995. Protective effect of the interleukin-1 receptor antagonist (IL-1ra) on experimental allergic encephalomyelitis in rats. *J. Neuroimmunol.* 61:241.
18. Zhu, H., H. O. Fearnhead, and G. M. Cohen. 1995. An ICE-like protease is a common mediator of apoptosis induced by diverse stimuli in human monocytic THP-1 cells. *FEBS Lett.* 374:303.
19. Rodriguez, I., K. Matsuura, C. Ody, S. Nagata, and P. Vassalli. 1996. Systemic injection of a tripeptide inhibits the intracellular activation of CPP32-like proteases in vivo and fully protects mice against Fas-mediated fulminant liver destruction and death. *J. Exp. Med.* 184:2067.
20. Openshaw, P., E. E. Murphy, N. A. Hosken, V. Maino, K. Davis, K. Murphy, and A. O'Garra. 1995. Heterogeneity of intracellular cytokine synthesis at the single-cell level in polarized T helper 1 and T helper 2 populations. *J. Exp. Med.* 182:1357.
21. Galbiati, F., L. Rogge, J. C. Guery, S. Smirardo, and L. Adorini. 1998. Regulation of the IL-12 receptor β -2 subunit by soluble antigen and IL-12 in vivo. *Eur. J. Immunol.* 28:209.
22. Piddlesden, S. J., M. K. Storch, M. Hibbs, A. M. Freeman, H. Lassmann, and B. P. Morgan. 1994. Soluble recombinant complement receptor 1 inhibits inflammation and demyelination in antibody-mediated demyelinating experimental allergic encephalomyelitis. *J. Immunol.* 152:5477.
23. Eugster, H.-P., K. Frei, M. Kopf, H. Lassmann, and A. Fontana. 1998. IL-6-deficient mice resist myelin oligodendrocyte glycoprotein-induced autoimmune encephalomyelitis. *Eur. J. Immunol.* 28:2178.
24. Mendel, I., N. Kerlero de Rosbo, and A. Ben-Nun. 1995. A myelin oligodendrocyte glycoprotein peptide induces typical chronic experimental autoimmune encephalomyelitis in H-2^b mice: fine specificity and T cell receptor V β expression of encephalitogenic T cells. *Eur. J. Immunol.* 25:1951.
25. O'Neil, J. K., D. Baker, A. N. Davison, K. K. Maggon, B. D. Jaffee, and J. L. Turk. 1992. Therapy of chronic relapsing experimental allergic encephalomyelitis and the role of the blood-brain barrier: elucidation by the action of Brequinar sodium. *J. Neuroimmunol.* 38:53.
26. Livingston, D. J. 1997. In vitro and in vivo studies of ICE inhibitors. *J. Cell. Biochem.* 64:19.
27. Olsson, T. 1995. Critical influences of the cytokine orchestration on the outcome of myelin antigen-specific T-cell autoimmunity in experimental autoimmune encephalomyelitis and multiple sclerosis. *Immunol. Rev.* 144:245.
28. Ewing, C., and C. C. Bernard. 1998. Insights into the aetiology and pathogenesis of multiple sclerosis. *Immunol. Cell. Biol.* 76:47.
29. Ruuls, S. R., and J. D. Sedgwick. 1998. Cytokine-directed therapies in multiple sclerosis and experimental autoimmune encephalomyelitis. *Immunol. Cell. Biol.* 76:65.
30. Jander, S., and G. Stoll. 1998. Differential induction of interleukin-12, interleukin-18 and interleukin-1 β converting enzyme mRNA in experimental autoimmune encephalomyelitis of the Lewis rat. *J. Neuroimmunol.* 91:93.
31. Matsui, K., T. Yoshimoto, H. Tsutsui, Y. Hyodo, N. Hayashi, K. Hiroishi, N. Kawada, H. Okamura, K. Nakanishi, and K. Higashino. 1997. *Propionibacterium acnes* treatment diminishes CD4⁺ NK1.1⁺ T cells but induces type 1 T cells in the liver by induction of IL-12 and IL-18 production from Kupffer cells. *J. Immunol.* 159:97.
32. Robinson, D., K. Shibuya, A. Mui, F. Zonin, E. Murphy, T. Sana, S. B. Hartley, S. Menon, R. Kastelein, F. Bazan, and A. O'Garra. 1997. IGIF does not drive Th1 development but synergizes with IL-12 for interferon- γ production and activates IRAK and NF κ B. *Immunity* 7:571.
33. Gately, M. K., L. M. Renzetti, J. Magram, A. S. Stern, L. Adorini, U. Gubler, and D. H. Presky. 1998. The interleukin-12/interleukin-12-receptor system: role in normal and pathologic immune responses. *Annu. Rev. Immunol.* 16:495.
34. Takeda, K., H. Tsutsui, T. Yoshimoto, O. Adachi, N. Yoshida, T. Kishimoto, H. Okamura, K. Nakanishi, and S. Akira. 1998. Defective NK cell activity and Th1 response in IL-18-deficient mice. *Immunity* 8:383.
35. Szabo, S. J., A. S. Dighe, U. Gubler, and K. M. Murphy. 1997. Regulation of the interleukin (IL)-12R β 2 subunit expression in developing T helper 1 (Th1) and Th2 cells. *J. Exp. Med.* 185:817.
36. Fantuzzi, G., G. Ku, M. W. Harding, D. J. Livingston, J. D. Sipe, K. Kuida, R. A. Flavell, and C. A. Dinarello. 1997. Response to local inflammation of IL-1 β -converting enzyme-deficient mice. *J. Immunol.* 158:1818.
37. Schulz, J. B., M. Weller, and M. A. Moskowitz. 1999. Caspases as treatment targets in stroke and neurodegenerative diseases. *Ann. Neurol.* 45:421.

Caspase-1 expression in multiple sclerosis plaques and cultured glial cells

Xue Ming^{a,1}, Weiping Li^{b,1}, Yasuhiro Maeda^{a,b}, Benjamin Blumberg^b, Sumul Raval^a,
Stuart D. Cook^{a,b}, Peter C. Dowling^{a,b,*}

^aDepartment of Neurosciences, UMDNJ-New Jersey Medical School, Newark, NJ, USA

^bNeurology Service, VA New Jersey Health Care System, East Orange, NJ 07018, USA

Received 20 July 2001; received in revised form 15 January 2002; accepted 28 January 2002

Abstract

Caspase-1 is responsible for processing inflammatory cytokines and is associated with the induction of apoptosis. Using RT-PCR, we found that caspase-1 mRNA transcripts from frozen brain extracts were significantly elevated in multiple sclerosis (MS) compared to controls. Immunohistochemical staining using a specific antiserum confirmed the marked up regulation of caspase-1 within acute and chronic MS plaques, while little staining was seen in control brains. In addition to the expected caspase-1 expression in microglia and infiltrating perivascular mononuclear cells, we found that cytoplasmic caspase-1 expression was sharply increased in the resident oligodendrocytes of MS lesions. The TUNEL reaction for fragmented DNA co-localized over an occasional caspase-1-expressing cell and large numbers of caspase-1-positive “corpses” were observed within phagocytic macrophages of an acute evolving MS lesion. Studies using an immortalized human oligodendroglial hybrid cell line exposed to cytokine challenge showed that death induction was blocked by the caspase-1-like inhibitor Z-YVAD-fmk, while the caspase-3-like inhibitor Z-DEVD-fmk was less effective. Cellular levels of procaspase-1 were reduced compared to controls in oligodendroglia induced to die by cytokine challenge, as judged by Western immunoblotting. Our results suggest that caspase-1 may play a role in the inflammatory and apoptotic processes associated with MS pathogenesis. © 2002 Elsevier Science B.V. All rights reserved.

Keywords: Caspase-1; Multiple sclerosis; Plaques; Oligodendrocyte; Cultures

1. Introduction

Multiple sclerosis (MS) is a chronic inflammatory demyelinating disease and its neuropathology is characterized by CNS white matter plaques displaying myelin loss and gliosis [1,2]. Inflammatory cytokines such as tumor necrosis factor alpha (TNF- α), interleukin-1 beta (IL-1 β), and interferon-gamma (IFN- γ) are upregulated in MS plaques [3], although the precise link between the inflammatory process and myelin sheath destruction is unclear. In previous investigations on the fate of glial cells, we identified substantial numbers of apoptotic oligodendrocytes within developing

and mature MS lesions by the in situ TUNEL reaction [4,5]. We also found that glial cells in MS plaques often strongly express both Fas receptor and ligand on their plasma membrane surface, suggesting that the Fas death pathway may be active during MS lesion formation [6]. However, the precise molecules and intracellular pathways responsible for glial cell death in MS remain ill-defined.

Caspase-1, previously named interleukin-1 β converting enzyme (ICE), is a cysteine protease whose proteolytic activity makes it a key molecule in myriad cellular processes, including mediation of the inflammatory response through cleavage activation of IL-1 β and IFN- γ promolecules. In addition, developmental studies in the nematode *C. elegans* have shown that the caspase-1 homolog CED-3 is chief among the genes required to induce programmed cell death [7–9]. We investigated caspase-1 expression in MS white matter lesions and tested for its activation in response to death induction by cytokine stimulation on immortalized cultures of oligodendrocytes.

* Corresponding author. Neurology Service (127), Veterans Administration New Jersey Health Care System, 385 Tremont Avenue, East Orange, NJ 07018, USA. Tel.: +1-973-676-1000x3596; fax: +1-973-395-7233.

E-mail address: dowlincp@umdnj.edu (P.C. Dowling).

¹ The first two authors contributed equally to this study.

2. Methods

2.1. Autopsy specimens

This study was performed on frozen and paraffin-embedded formalin-fixed MS and control brains obtained from the Rocky Mountain Multiple Sclerosis Center (Englewood, CO), the MS Human Neurospecimen Bank (West Los Angeles, CA), Dr. John Prineas (UMDNJ, NJ) and St. Vincent's Hospital (New York, NY). The frozen control specimens ($n=14$) included white matter samples from chronic CNS measles virus infection (subacute sclerosing panencephalitis, SSPE; $n=9$), cerebrovascular disease ($n=2$), Parkinson's disease ($n=2$), and amyotrophic lateral sclerosis (ALS). The average postmortem interval for the MS brains ($n=18$) was 17.8 h, and five brains were obtained within 7 h of death. The paraffin-embedded fixed brains consisted of MS ($n=11$), ALS ($n=4$), cerebrovascular disease, Parkinson's disease, and AIDS-associated progressive multifocal leukoencephalopathy (PML). The disease diagnosis was established from patient clinical records and neuropathological examination.

2.2. RT-PCR and liquid hybridization

RNA was extracted from 500-mg fragments of frozen MS and control white matter by the GITC/CsCl method as previously described [10]. A one-tube 50- μ l RT-PCR reaction was performed in buffer containing 20 mM KCl, 6 mM MgCl₂, 40 mM Tris-HCl (pH 8.3), 1 mM DTT, 0.1% gelatin, 40 U RNasin, 100 U Superscript II, and 5 U of Taq polymerase (Gibco, Life Technologies, Grand Island, NY). Total RNA (3 μ g) was used as template. A 50-pmol amount of caspase-1 mRNA reverse primer 5'-CATGAACACCAG-GAACGTGCTGTC-3' (position 698–722) was used for reverse transcription (15 min each at 37 and 42 °C), and an equal amount of forward primer 5'-GGAAATTACCT-TAATATGCAAGAC-3' (position 303–329) was used for PCR (50 cycles of 95, 42, and 72 °C/60 s). RT-PCR was performed to measure expression of glyceraldehyde-3-phosphate dehydrogenase (GAPDH) as an internal control of cellular mRNA levels and integrity using the reverse primer 5'-ATAGGATCCTCAGTGTAGCCCAGGATGC-3' and the forward primer 5'-ATAAAGCTTACCATGGA-GAAGGCTGG-3' [11]. For detection and semiquantification of PCR products, oligonucleotide probes representing internal portions of the caspase-1 (5'-GTCGGCAGAGATT-TATCCAA-3'; 430-bp product) and GAPDH (5'-GTGGAAGGACTCATGACCACAGTCCATGCC-3'; 508-bp product) amplicons were 5'-end-labeled with [³²P]-ATP using T4 polynucleotide kinase. A 1- μ l aliquot of probe (150,000 cpm) was mixed with 20 μ l of the PCR product in buffer containing 0.15 M NaCl and 2.5 mM EDTA, and was hybridized (5 min at 98 °C and 15 min at 25 °C). The hybridization products were analyzed by electrophoresis on a 3.5% agarose gel in 0.5 \times TBE buffer. The gel was dried

with a vacuum and the radioactivity of the caspase-1 and GAPDH mRNA bands was quantified by digital autoradiography and integration using a Packard Instant Imager (Packard, Meriden, CT).

2.3. Caspase-1 antigen detection by immunohistochemistry

Three-micron paraffin-embedded sections were attached to Vectabond treated slides (Vector Labs, Burlingame, CA) by heat fixation. After dewaxing and rehydration through graded alcohols, sections were washed in PBS, subjected to antigen retrieval (95 °C for 10 min) in Target Unmasking Fluid (TUF; Zymed Laboratory, South San Francisco, CA), and then incubated further in hot TUF for 10 min on the benchtop. Sections were then reacted for 2 h at room temperature with a rabbit polyclonal antiserum (R105, 1:300 dilution) that recognizes both the intact procaspase and the cleaved forms of human caspase-1 (kindly provided by Dr. Douglas K. Miller, Merck Research Laboratories). Staining was done as previously described [5,6] using standard horseradish peroxidase-conjugated avidin-biotin methods (ABC kit, Vector Labs) and visualized with the chromogen diaminobenzidine (DAB). To identify glial-specific antigens in caspase-1/DAB-stained sections, multi-labeling with several fluorescent stains was performed. A goat polyclonal antibody against CNPase (a gift from Dr. T.J. Sprinkle of the Medical College of Georgia) was used to label oligodendrocytes (diluted at 1:500 and incubated for 1 h) and was visualized by an FITC-conjugated donkey anti-goat antibody (diluted at 1:600 and incubated for 30 min). A 1-h incubation with a mouse monoclonal antibody against GFAP (DAKO, Carpinteria, CA) diluted to 1:25 was used to label astrocytes and was visualized with a Cy3-conjugated rabbit anti-mouse antibody (1:500 dilution for 30 min). Finally, a biotinylated *Ricinus communis* agglutinin 1 lectin (RCA-1, Vector Labs) was used for macrophage/microglia (1:500 for 1 h) and was visualized with a Cy5-conjugated mouse anti-biotin antibody (1:500 for 30 min). All secondary antibodies were obtained from Jackson Laboratories (West Grove, PA). Omission of the primary antibody was used to control for specificity. Fluorescent-labeled sections were mounted in glycerol/PBS.

2.4. In situ TUNEL detection of apoptotic cells and colocalization with caspase-1

Cells containing fragmented DNA were labeled with digoxigenin-11-dUTP by terminal transferase (TdT) tailing, and subsequently detected by immunoperoxidase staining (Intergen ApopTag kit, Purchase, NY) [12,13]. We previously used a modification of this method on both fixed and frozen MS brain, and confirmed the specificity of this assay by demonstrating laddering in DNA extracted from TUNEL-positive frozen MS brain [5]. Immunohistochemistry for caspase-1 using DAB chromogen detection was combined

with FITC-fluorescent staining for cell-specific identification of inflammatory and glial cells. For determining the colocalization of TUNEL-positive cells with caspase-1 expression, sections were reassayed with a caspase-1 antibody (a gift from Dr. Douglas K. Miller; diluted at 1:300). A Cy3-conjugated goat anti-rabbit secondary antibody (Jackson Laboratories; diluted at 1:100 and incubated for 30 min) was used to visualize caspase-1 reactivity. The sections were then evaluated using a four-channel Zeiss Model 410 series confocal microscope.

2.5. *In vitro studies on the oligodendroglial hybrid cell line*

The MO3.13 human oligodendroglial hybrid cell line (a kind gift of Dr. P.J. Talbot, University of Quebec, Canada) was maintained in Dulbecco's modified Eagle's medium (DMEM) supplemented with 10% fetal calf serum (FCS), 100 U/ml penicillin, and 100 µg/ml streptomycin in a 5% (v/v) CO₂ incubator at 37 °C. The MO3.13 oligodendrocyte hybrid cell line was characterized by immunohistochemistry under the culture conditions described above. The cells were collected, washed in PBS, and then spun down using a cell preparation system, Cytospin 3 (Shandon, Pittsburgh, PA) onto microscope slides. After air-drying, cells were fixed in 2% formalin in PBS for 10 min at room temperature, then treated with ethanol/acetic acid at –20 °C for 5 min. The cellular endogenous peroxidase was blocked using 0.3% H₂O₂ for 10 min and 10% normal horse serum was used to block nonspecific immunoglobulin binding sites. A battery of glial cell markers was employed for the immunohistochemical staining using a previously published method [6]. These markers included CNPase (a gift from Dr. Terry Sprinkle, 1:600 dilution, incubated at room temperature for 1 h.), PLP (Chemicon, 1:200, at room temperature for 1 h.), PDGFα-R (Santa Cruz Biotechnology, Santa Cruz, CA, 1:150, at 4 °C overnight) and GFAP (DAKO, 1:200, at 4 °C overnight). The MBP (1:500), O1 (1:25), and A2B5 (1:25) were all gifts from Dr. Steven Pfeiffer and were incubated at 4 °C overnight. The NCTC929 connective tissue cell line was used as a negative control.

In the caspase-inhibitor blocking experiments, MO3.13 cells were preincubated with either a caspase-1-like inhibitor (Z-YVAD-fmk; Enzyme Systems, Livermore, CA) or a caspase-3-like inhibitor (Z-DEVD-fmk; Enzyme Systems) for 3 h at a dose range of 0–500 µM, and then challenged with TNF-α/IL-1β (100 and 10 ng/ml) combined with cycloheximide (5 µg/ml). Each determination was made in duplicate. Challenged cells were harvested after 24 or 48 h and assayed for Annexin V staining following the manufacturer's protocol (Vybrant™ Apoptosis Assay Kit #1, Molecular Probes, Eugene, OR). The apoptotic and viable cells were then quantified by flow cytometry (FACSCalibur, Becton-Dickinson, San Jose, CA). A comparison was made between numbers of apoptotic cells in cytokine-challenged groups and those of controls. Data were analyzed using

Histogram Statistics by LYSYS II software (Becton-Dickinson) gated for 10,000 events. The experiment was replicated six times and a one-way ANOVA was used for statistical analysis.

For the lower molecular weight DNA analysis, DNA was extracted from cultured cells with 10 mM Tris-HCl (pH 8.0), 0.5% SDS, 0.1 M NaCl, and 5 mM EDTA containing 100 µg/ml of proteinase K (Sigma) for 2 h at 37 °C. Sodium chloride was added to a final concentration of 1 M, and samples were incubated overnight at 4 °C. Then the samples were centrifuged for 15 min and the supernatant was ethanol-precipitated after phenol-chloroform extraction. In order to enhance the detection system, we used a radiolabeling method that is capable of detecting very low levels of apoptotic DNA. A 1-µg sample of DNA was labeled with 0.5 µCi of [³²P]-labeled dATP in the presence of 10 mM Tris-HCl (pH 7.5), 5 mM MgCl₂, and 5 U of Klenow polymerase (Gibco). The mixture was incubated for 10 min at room temperature and then the reaction was terminated by adding EDTA to a final concentration of 10 mM. Unincorporated nucleotides were removed by a Microcon centrifugal filter device (Amicon Bioseparations, Millipore, Bedford, MA). Identical amounts of control and test DNA were electrophoresed on 1.5% agarose gels. The gels were then dried on DEAE cellulose filters and developed by autoradiography.

2.6. *Western blotting*

Cultures were lysed in radio-immuno-protein assay (RIPA) buffer containing 150 mM NaCl, 1% NP-40, 0.5% deoxycholate, 0.1% SDS, 50 mM Tris (pH 8.0), and proteinase inhibitors (2 mg/ml aprotinin, 1 mg/ml leupeptin, and 25 µg/ml phenylmethylsulfonyl fluoride) at 0 °C for 30 min. The cell lysates were then incubated in 1 µl of PMSF on ice for another 30 min and centrifuged at 4 °C for 10 min. The protein concentration in the supernatant was determined by the Bio-Rad assay using BSA as the standard. A 50-µg sample of protein from cell lysates was run on a 10–20% Tris-glycine gel and transferred to a nitrocellulose membrane (Invitrogen/Novex Electrophoresis, Carlsbad, CA). The membrane was blocked for nonspecific binding in 5% milk at 4 °C overnight and washed in 1 × T-TBS (Tris-buffered saline and 0.1% Tween 20). The membranes were incubated for 1 h with a caspase-1 p20 polyclonal rabbit antibody at a 1:300 dilution (Santa Cruz Biotechnology, Cat #sc-1780). They were then rinsed three times with T-TBS and incubated with an HRP-conjugated donkey anti-rabbit secondary antibody (Amersham, Arlington Heights, IL) diluted 1:3000 for 1 h at room temperature. Immunoreactive bands were visualized by chemiluminescence using the ECL-kit (Amersham) and then exposed to Hyperfilm (Amersham). An antiserum to β-actin (Santa Cruz Biotechnology) was also tested on blots as a control for equal loading of lanes.

3. Results

3.1. Caspase-1 mRNA upregulation in MS white matter

To measure caspase-1 gene expression in white matter, RNA was extracted from the white matter of 18 MS and 14 control frozen brains and subjected to an RT-PCR assay that targeted a 420-bp segment of the caspase-1 mRNA. The PCR products were solution-hybridized with a radio-labeled oligonucleotide corresponding to an internal sequence of the amplicon and electrophoresed on agarose gels. Fig. 1A shows an autoradiograph of this gel. Caspase-1 mRNA was present in all the MS brains tested, and the bands generated from MS RNA were usually more intense than those amplified from controls. To quantify the amount of caspase-1 transcript in these samples, caspase-1 amplicon radioactivity was normalized to that of GAPDH in each extract, as is shown in the bottom panel of Fig. 1A. A graph of the normalized caspase-1 PCR product (Fig. 1B) shows significantly more caspase-1 mRNA expression in the MS group than in the control ($p < 0.03$), and the average caspase-1 transcript expression in controls was half of that in MS white matter. It is important to note that the controls included white matter from nine SSPE brains (open circles) that were known from a previous study to contain large numbers of inflammatory T-cells and activated macrophage/microglia [10]. While the SSPE samples might be expected to overexpress caspase-1, the mean mRNA expression in these brains was still lower than in many MS brains.

3.2. Caspase-1 protein is upregulated in MS plaques

We next investigated caspase-1 expression and localization in MS brains by immunohistochemistry using a polyclonal antiserum that recognizes both the procaspase (uncleaved) and active tetrameric (cleaved) forms. Fig. 2 compares caspase-1 expression in normal control white

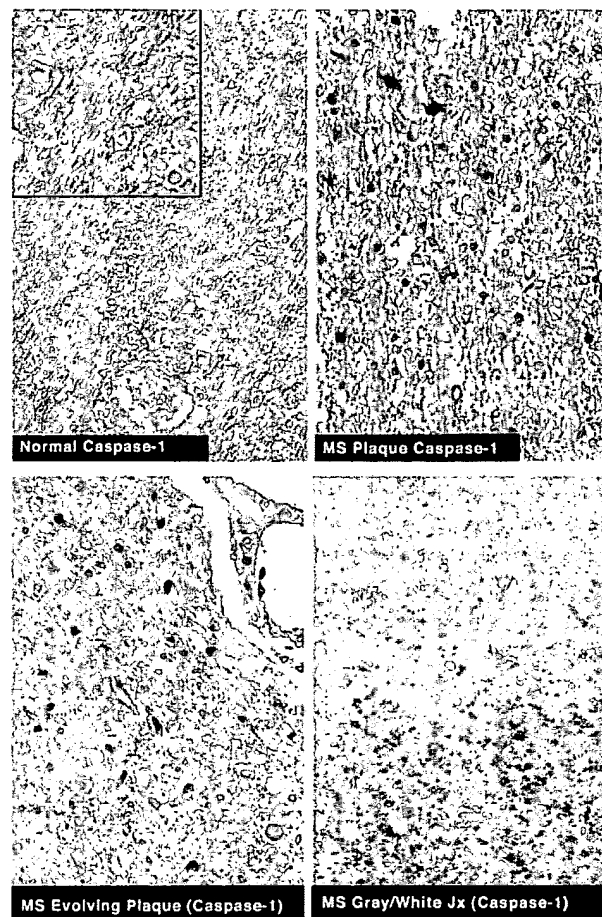


Fig. 2. Immunohistochemical study of caspase-1 expression in normal control white matter and MS plaques. Caspase-1 staining was rarely seen in normal white matter (upper left panel and enhanced inset photograph). By contrast, strong cytoplasmic caspase-1 staining was detected in many oligodendroglia, macrophage/microglia, and some enlarged reactive astrocytes of MS plaques (upper right and lower left panels). Some caspase-1-positive cells have strong nuclear staining. Neurites within another plaque located at the gray/white matter junction also stained for caspase-1 (lower right).

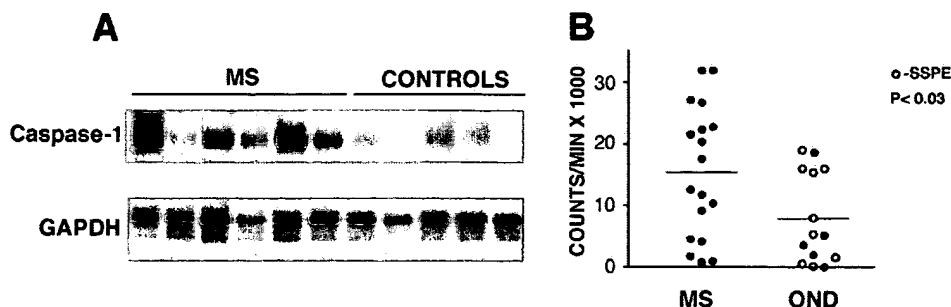


Fig. 1. Determination of caspase-1 gene expression in MS white matter and controls. (A) Semi-quantitative RT-PCR and liquid hybridization for caspase-1 and control GAPDH transcripts in RNA extracts from MS and control brains. The agarose gel regions containing bands for the GAPDH and caspase-1 PCR products are shown. Lanes 1–6: MS brains. Lanes 7–11: control brains. The radioactivity of the mRNA bands was measured and caspase-1 mRNA values were normalized to those of GAPDH for each sample. (B) Graph of normalized caspase-1 gene expression in MS brain and other neurologic disease controls (OND). Mean value for each group: MS=15,240; OND=7818. The MS group was significantly different from the ONDs according to a Student's *t*-test ($p < 0.03$). Open circles (O) represent values derived from a group of nine SSPE brains containing considerable chronic inflammation.

Table 1
Identity of caspase-1-expressing cells in MS white matter plaque

| Patient number | Caspase-1-positive cells (total counted) | Oligodendrocytes (CNPase-positive) | Macrophages/microglia (RCA-1 lectin-positive) |
|--------------------------------|--|------------------------------------|---|
| First experiment | | | |
| Patient 1 | 152 | 44 (29%) | 59 (38%) |
| Patient 2 | 148 | 46 (31%) | none seen (0%) |
| Patient 3 | 119 | 27 (23%) | 47 (39%) |
| Patient 4 | 135 | 40 (30%) | 40 (30%) |
| Second experiment ^a | | | |
| Patient 1 | 151 | 63 (42%) | 42 (28%) |
| Patient 4 | 149 | 77 (52%) | 42 (28%) |
| Average | 142 | 50 (35%) | 38 (27%) |

^a Sections from different levels of the blocks were used in the two experiments, so variation in the percentage of counted oligodendrocytes and macrophage/microglia is expected. The difference is within experimental error.

matter to that in MS brain. We found that this protein was readily detectable in most MS lesions, and that many plaques contained far more caspase-1-positive cells than control white matter. Normal white matter failed to exhibit immunoreactivity to the caspase-1 antiserum (top left panel). The inset shows an enhanced photograph of negative staining oligodendroglial cells in normal brain. The same section was subsequently reacted with CNPase to assure that the small round caspase-1-negative cells were indeed oligodendrocytes. By contrast, the MS plaques (top right and lower left panels) show strong caspase-1 staining in many cells possessing oligodendrocyte morphology. There were also caspase-1-positive astrocytes, and although most caspase staining was cytoplasmic, in some cells, prominent nuclear staining was observed. The lower right panel shows the gray/white matter junction in an MS brain where marked caspase-1 immunoreactivity was observed within nerve fibers along the plaque edge.

As previously mentioned, we superimposed fluorescent antisera specific for oligodendrocytes (CNPase) or macrophage/microglial-lineage cells (RCA-1 lectin) on sections previously subjected to caspase-1/DAB staining to determine precisely which cell types express caspase-1 in MS plaques. The experimental results are summarized in Table 1. Fig. 3 illustrates caspase-1 immunostaining at the active margin of a chronic active plaque (left panel) co-labeled with the oligodendrocyte marker CNPase (middle panel), and with the macrophage/microglia marker RCA-1 lectin (right panel). A comparison of the left and middle panels of Fig. 3 shows that caspase-1 is prominently upregulated in the cytoplasm of oligodendrocytes within the thin zone of active demyelination at the plaque margin (black arrows). Comparison of the left panel with the right panel shows that caspase-1 is also upregulated within the perivascular and parenchymal lectin-positive macrophage/microglia (white arrow) as expected. The upper region of the plaque has undergone complete myelin loss. These findings demonstrate that caspase-1 is upregulated throughout evolving early MS plaques, and that caspase-1 is also upregulated at the active margin in chronic plaques in comparison to normal brain.

The largest average number of caspase-1-positive cells belonged to the oligodendrocyte population (35%) and this was closely followed by the average in caspase-1-positive macrophages/microglia (27%, see Table 1). Cytoplasmic caspase-1 staining was often more intense in oligodendrocytes than in macrophage/microglia, and expression varied greatly among cells. GFAP-positive astrocytes usually constituted only 10–15% of caspase-1-positive cells, and their stain was also of variable intensity (data not shown).

3.3. Macrophages engulf caspase-1-positive cell bodies in acute MS brain

To address the possible relationship between caspase-1 expression and cell death in MS lesions, we used fluorescent

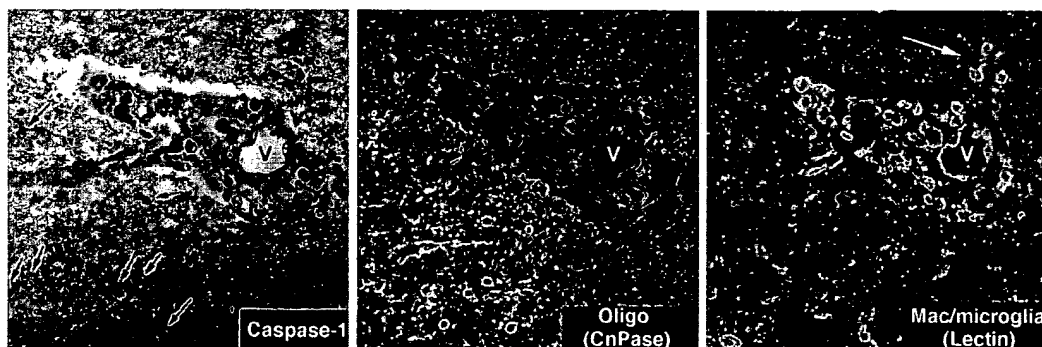


Fig. 3. Chronic MS plaque with active margin showing caspase-1 expression in oligodendrocytes and macrophage/microglia lineage cells. Left panel: Caspase-1 staining using DAB (dark cells; arrows). Arrows point to field of caspase-1-positive oligodendrocytes that are restricted to the active margin of the plaque. Additionally, many caspase-1-positive mononuclear cells are found in the perivascular infiltrate around the blood vessel (V). Middle panel: Confocal image of the same field showing FITC-labeled CNPase-positive oligodendrocytes within a partially demyelinated region of the plaque. Right panel: Confocal image of the same field now labeled with Cy5 RCA-1 lectin that shows positive macrophage/microglia around the vessel. This area of the plaque is totally devoid of myelin.

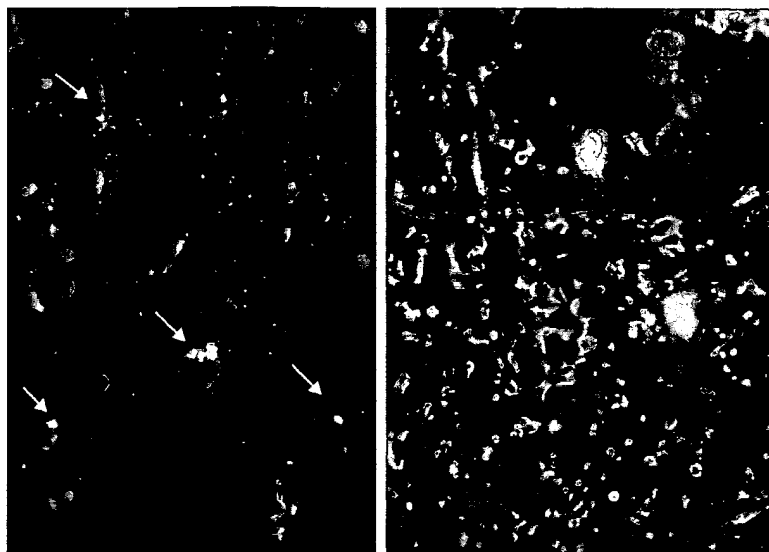


Fig. 4. Confocal fluorescent microscopic images showing FITC-labeled TUNEL-positive cells containing fragmented DNA (yellow) and Cy-3-labeled caspase-1-positive cells (red). Left panel: Arrows indicate caspase-1-positive cells with condensed TUNEL-positive nuclei. Right panel: Higher power image of two additional TUNEL-positive cells with marked expression of caspase-1.

immunohistochemistry for caspase-1 in conjunction with in situ TUNEL staining, which is a nuclear marker for fragmented DNA that is highly characteristic of cell death. Fig. 4 (left panel) shows a chronic MS plaque with many caspase-1-positive cells (red signal) and a few contain TUNEL-positive nuclei (yellow signal; arrows). In another field at higher magnification, a few cells expressing caspase-1 again labeled with the TUNEL stain (right panel). The majority of cells that stained heavily for caspase-1, however, failed to react with the TUNEL assay, indicating that increased

caspase-1 expression alone is not sufficient to induce cell death.

We performed caspase-1 immunohistochemistry on an early evolving acute MS plaque where the cell death process was very aggressive, as judged by TUNEL staining. Fig. 5 shows intense caspase-1 staining (DAB) of multiple internalized cell bodies within several large phagocytic cells of this lesion. These bodies probably represent caspase-1-positive cell corpses being phagocytosed by macrophages (arrows).

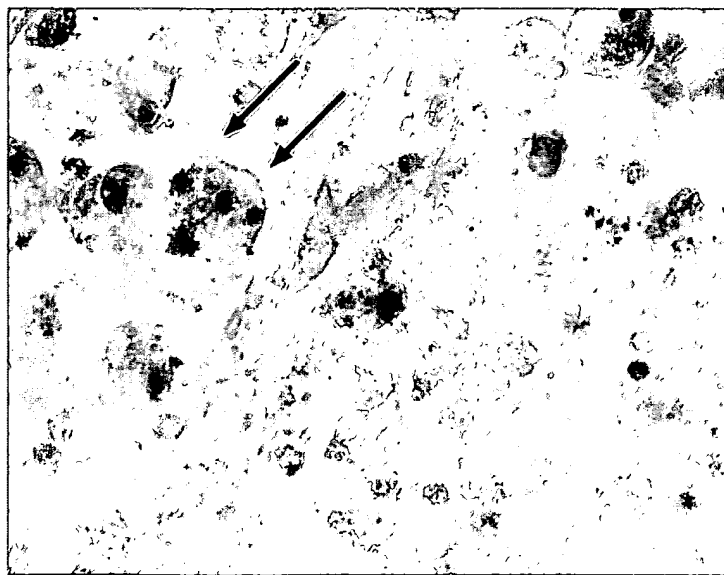


Fig. 5. Phagocytosis of caspase-1-positive cells in a very acute MS lesion. Caspase-1 immunohistochemistry (DAB chromogen, brown stain) showing highly edematous white matter and several large phagocytic cells with multiple caspase-1-positive corpses (arrows).

3.4. In vitro caspase-1 studies on oligodendrocyte hybrid cultures

The majority of MO3.13 cells expressed mature oligodendroglial cell markers including MBP, PLP, CNPase, and O1 when tested by immunohistochemistry. A small portion (up to 5%) expressed progenitor oligodendroglia markers including PDGF α -receptor and A2B5. The MO3.13 cells failed to react with the astrocyte marker GFAP. A nonneural connective tissue cell line (NCTC929) was simultaneously tested with the same marker panel and found to be non-reactive for all markers tested.

The TNF- α /IL-1 β cytokine combination induced 47% of the cycloheximide-sensitized cells to die compared to control levels of 20%, as judged by flow cytometry (Fig. 6). The caspase-1-like inhibitor Z-YVAD-fmk blocked most of the cell death induced by this cytokine combination (24%), and was therefore quite effective. Fig. 6 also shows that DNA extracted from the control cells described in the experiment above contained mostly high molecular weight intact DNA and only modest amounts of the low molecular weight banding pattern that is characteristic of apoptosis. In contrast, cultures that were challenged with inflammatory cytokines showed far larger amounts of this low molecular weight banding pattern (middle lane). The companion culture treated with Z-YVAD-fmk exhibited a marked reduction in low molecular weight DNA (right lane).

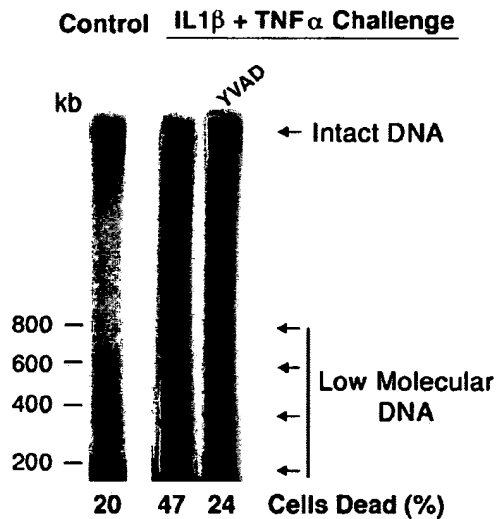


Fig. 6. Autoradiograph showing DNA analysis by 1.5% agarose gel electrophoresis. Lane 1: DNA extracted from control cells showing background apoptosis (20% cells dead). Lane 2: DNA extracted from cells exposed to cytokine challenge showing marked increase in low molecular weight DNA banding pattern (47% cells dead). Lane 3: DNA from challenged cells that were pretreated with the inhibitor Z-YVAD-fmk (60 μ M). A strong low molecular weight DNA apoptotic ladder is present in the cytokine-challenged DNA, which is much less prominent in the control lane. Pretreatment with the inhibitor Z-YVAD-fmk blocks cell death, as reflected by the preservation of high molecular weight DNA species and a drop in spacers of low molecular weight. Cell death levels also dropped to 24% in the presence of the inhibitors.

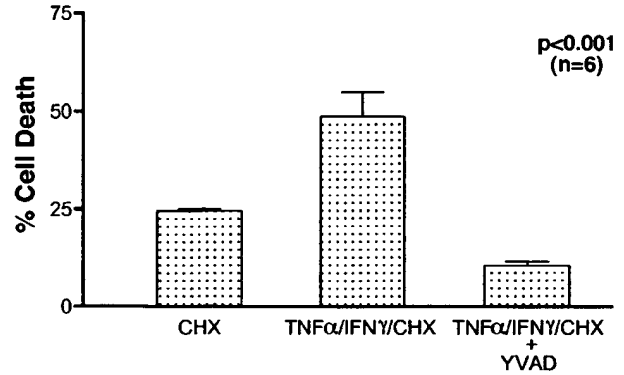


Fig. 7. Graph showing data from six independent experiments where oligodendroglial cultures were challenged with a combination of TNF- α and IFN- γ . Death induction by cytokine exposure averaged nearly 50%, and in this case, inhibition using Z-YVAD-fmk reduced the number of dead cells to less than background control values. Bars represent mean percentages of cell death \pm 1 S.E.M. Data were analyzed using a one-way ANOVA ($F=495$; $p<0.001$).

Fig. 7 summarizes the in vitro results of TNF- α /IFN- γ /CHX induced cell death in six independent trials, as judged by flow cytometry using Annexin V staining. This cytokine-stimulated death was blocked by Z-YVAD-fmk, and cell death levels even dropped below the levels of CHX-treated control cultures. A one-way ANOVA showed all three groups

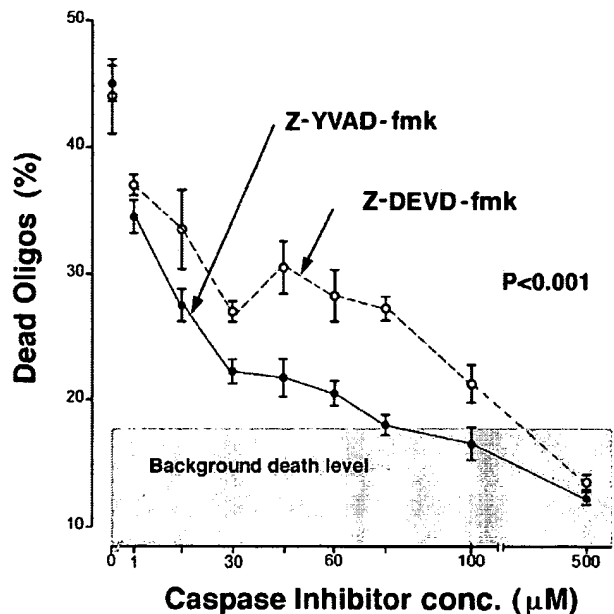


Fig. 8. Comparison of Z-YVAD-fmk and Z-DEVD-fmk dose-response curves after induction of cell death by exposure to TNF- α /IL-1 β . The baseline cell death value induced after 24 h was 45% as determined by flow cytometry. Both Z-YVAD-fmk and Z-DEVD-fmk caused modest inhibition at concentrations as low as 1 μ M, and both were quite effective at blocking cell death at 500 μ M. Z-YVAD-fmk was more effective at blocking cell death at low concentrations (15–100 μ M) than Z-DEVD-fmk. A two-way ANOVA was used for statistical analysis, and the difference between the two inhibitors was found to be highly significant ($F=163$, $p<0.001$).

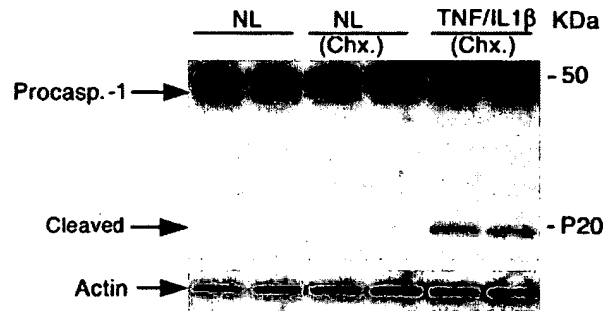


Fig. 9. Western blot showing effect of TNF- α /IL-1 β activation on the immortalized MO3 oligodendrocyte culture. These immunoblots were reacted with an antibody to caspase-1 that is capable of detecting the intact promolecule and a 20-kDa cleavage activation product. The intact promolecule of caspase-1 migrates at 47 to 53 kDa depending on the cell line. The control MO3.13 cell cultures (left lanes) show a prominent caspase-1 promolecule band that is substantially reduced following exposure to TNF- α /IL-1 β death induction. An activated fragment of caspase-1 is seen only in the cytokine-challenged lanes (right two lanes).

to be significantly different ($p < 0.001$), indicating that cytokine challenge resulted in increased cell death, and that Z-YVAD-fmk was highly effective in blocking this process.

We titrated the effectiveness of the two different caspase inhibitors on blocking oligodendrocyte death by determining their dose–response curves (Fig. 8). The MO3.13 cells were pretreated for 3 h with Z-YVAD-fmk or Z-DEVD-fmk at a dose range of 0–500 μ M, and then challenged with 100 ng/ml of TNF- α and 10 ng/ml of IL-1 β . A two-way ANOVA test was used to compare the efficacy of the two inhibitors, and Z-YVAD-fmk was found to be a more potent inhibitor of cell death than Z-DEVD-fmk ($F = 163$, $p < 0.001$). While inhibition was detectable with both Z-YVAD-fmk and Z-DEVD-fmk at a concentration of 1 μ M, Z-YVAD-fmk retained increased effectiveness at much lower concentrations, indicating that Z-YVAD-fmk inhibits oligodendrocyte death induced by the cytokines in a dose-dependent manner resembling but more potent than Z-DEVD-fmk.

3.5. Caspase-1 is consumed in cytokine-challenged oligodendrocyte hybrid cells

Western blot analysis indicated that caspase-1 was activated by cytokine challenge in MO3 cells. Fig. 9 shows that challenge with TNF- α /IL-1 β resulted in both a marked reduction of the procaspase-1 band compared to the control lane and the appearance of a lower molecular weight p20 cleavage activation product restricted to the cytokine-challenge lanes.

4. Discussion

A major finding in this study is that caspase-1 is commonly overexpressed in white matter oligodendrocytes of

MS brain. We found that caspase-1 mRNA transcripts were significantly more abundant in MS white matter than in control brain tissue as measured by semiquantitative RT-PCR. We extended this finding at the single-cell level by using immunohistochemistry to determine the pattern of caspase-1 expression in chronic and acute MS plaques. The expression of caspase-1 was negligible in both normal control white matter and in normal appearing areas of MS brain. In contrast, a striking upregulation of caspase-1 was observed in oligodendrocytes of early evolving MS plaques, and this increased expression was often widespread throughout the lesion. In other plaques, however, positive cells were largely restricted to the active plaque margin. As expected, caspase-1 was also upregulated in infiltrating perivascular mononuclear cells and parenchymal macrophage/microglia.

Caspase-1 commonly mediates inflammatory effects through cleavage activation of the IL-1 β and IFN- γ promolecules, and these inflammatory cytokines are widely distributed in MS white matter. IFN- γ and TNF- α , both toxic to oligodendrocytes in tissue culture, are produced by macrophages/microglia in the CNS of MS patients [14,15]. IFN- γ is found at the margin of active plaques, while TNF- α is prominent in macrophages at the center of lesions and in the perivascular microglia outside lesions [15]. IL-1 β provokes inflammation in the CNS as demonstrated by the acute inflammation involving hemorrhage and edema observed after its injection into the brain of experimental animals [14]. Caspase-1-deficient mice have a major defect in the generation of mature IL-1 β and demonstrate impaired production of IFN- γ and IFN- γ -inducing factor (IGIF), thus making them resistant to LPS-induced endotoxic shock [16–18]. These previous studies suggest that caspase-1 may play an important role in the regulation of multiple cytokines implicated in the inflammatory aspects of the MS disease process.

Recently, Furlan et al. [19] found that caspase-1 could regulate the inflammatory process leading to experimental autoimmune encephalomyelitis (EAE), an animal model of MS. In this experiment, caspase-1 mRNA blood levels parallel those of proinflammatory cytokines during EAE and peak at the time of maximal EAE severity, and a reduction of EAE incidence and severity was observed in caspase-1 knockout mice. They also found pharmacological inhibition of caspase-1 using the caspase-1-inhibitor Z-Val-Ala-DL-Asp-fluoromethylketone (Z-VADA-fmk) which could block the induction of EAE if administered early, but could not stop the latter progressive phases of the disease. This experiment clearly indicates that caspase-1 plays an important role in the early phases of the immune-mediated inflammatory process leading to EAE.

Caspase-1 is one of the few caspases with characterized activities both in the cleavage activation of proinflammatory cytokines and in apoptosis. Since caspase-1 knockout mice show no defect in development, some investigators have concluded that caspase-1 may play a redundant role in apoptosis [16]. However, one recent study has shown activation

of caspase-1 in association with apoptosis, even in the nuclei of dying cells. In Mao's report, TNF challenge of Hela cells induced apoptosis without detectable proteolytic activation of caspase-1 in the cytosol. Instead, TNF induced the translocation of procaspase-1 to the nucleus where it was proteolytically activated, releasing the intact prodomain. These findings suggest that caspase-1 may have a nuclear function in some cell types undergoing apoptosis [20], and in our experiment, a number of caspase-1-positive cells in MS plaques showed prominent nuclear expression. Other reports also indicate that caspase-1 may be implicated in cytokine-mediated glial cell death. Under some conditions, TNF induced considerable cytotoxicity in cultured oligodendrocytes. This effect was blocked by the caspase-1 inhibitor Ac-YVAD-CHO, suggesting that TNF-induced death in glial cells is mediated via a death pathway involving caspase-1 [21]. In yet another in vitro study, oligodendrocyte apoptosis was induced with a different stimulus, the neurotrophin NGF. Caspase-1 was again found to be activated in this study, as was the downstream executioner protein caspase-3 [22].

In the present study, an occasional dying TUNEL-positive cell was found in MS brain expressing large amounts of caspase-1. However, the vast majority of caspase-1-expressing cells were TUNEL-negative, so it is unclear precisely what role caspase-1 plays in the process of cell death within postmortem MS brain lesions. On the other hand, high levels of caspase-1 expression in the resident glial population at the active margin of chronic MS plaques as well as the presence of caspase-1-positive corpses within phagocytic macrophages of acute MS plaques are consistent with the operation of multiple caspase-1-mediated processes, including inflammation and perhaps apoptosis in MS lesion development.

In our in vitro studies, MO3.13 cells were used as an oligodendroglial cell model. The immortalized oligodendroglial human-human hybrid MO3.13 cell line has been utilized in previous reports to study caspase activation and apoptosis [23,24]. The cells have been shown to display several of the morphological and biochemical characteristics of human oligodendroglia [25]. We tested the cell line with a battery of glial cell markers and found that the majority of MO3.13 cells expressed markers of mature oligodendrocytes including MBP, PLP, CNPase, and O1 antigen, and none expressed the astrocyte marker GFAP. These findings indicate that the MO3.13 cells share many of the characteristics of human oligodendrocytes. The results of our in vitro study showed that the caspase-1-like inhibitor Z-YVAD-fmk was able to block the cytotoxic effects of TNF- α /IL-1 β in a dose-dependent manner. These findings suggest that caspase-1-like signaling is involved in in vitro cytokine-induced oligodendrocyte death and are strongly supported by the Western immunoblot data that revealed consumption of caspase-1 and the appearance of cleavage activation fragments in the cells subjected to death induction by TNF- α /IL-1 β . While the increased expression of caspase-1 message

and the caspase-1 product in MS plaques is likely associated with inflammation, the in vitro data suggest that under some circumstances, caspase-1 may be involved in the apoptosis of oligodendrocytes.

Acknowledgements

We gratefully acknowledge Dr. Douglas K. Miller from Merck Research Laboratories for his gift of caspase-1 antiserum. This work was supported in part by the L'Hommedieu Multiple Sclerosis Fund, VA Merit Review grant (#0017), National MS Society grant (RG954-A-10/1), the Kirby Fund, and the Segal Fund.

References

- [1] Lassmann H. Comparative Neuropathology of Chronic Experimental Allergic Encephalomyelitis and Multiple Sclerosis. New York: Springer-Verlag, 1983. p. 47–62.
- [2] Prineas JW. The neuropathology of multiple sclerosis. In: Vinken PJ, Bruyn GW, Koetsier JC, editors. Handbook of Clinical Neurology: Demyelinating Diseases, vol. 47. Amsterdam: Elsevier, 1985. pp. 213–57.
- [3] Merrill JE, Benveniste EN. Cytokines in inflammatory brain lesions: helpful and harmful. *TINS* 1996;19:331–8.
- [4] Dowling P, Bansil S, Menonna J, Husar W, Cook S. Programmed cell death in multiple sclerosis brain (abstract). *Ann Neurol* 1995;38:341.
- [5] Dowling P, Husar W, Menonna J, Donnemfeld H, Cook S, Sidhu M. Cell death and birth in multiple sclerosis brain. *J Neurol Sci* 1997;149:1–11.
- [6] Dowling P, Shang G, Raval S, Menonna J, Cook S, Husar W. Involvement of the CD95(APO-1/Fas) receptor/ligand system in multiple sclerosis brain. *J Exp Med* 1996;184:1513–8.
- [7] Ellis HM, Horvitz HR. Genetic control of programmed cell death in the nematode *C. elegans*. *Cell* 1986;44:817–29.
- [8] Cerretti DP, Kozlosky CJ, Mosley B, et al. Molecular cloning of the interleukin-1 β converting enzyme. *Science* 1992;256:97–100.
- [9] Thornberry NA, Bull HG, Calaycay JR, et al. A novel heterodimeric cysteine protease is required for interleukin-1 β processing in monocytes. *Nature* 1992;356:768–74.
- [10] Sidhu MS, Crowley J, Lowenthal A, et al. Defective measles virus in human subacute sclerosing panencephalitis brain. *Virology* 1994;202:631–41.
- [11] Wesselingh SI, Power C, Glass JD, et al. Intracerebral cytokine messenger RNA expression in acquired immunodeficiency syndrome dementia. *Ann Neurol* 1993;33:576–82.
- [12] Schmitz G, Walter T, Seibl R, Kessler C. Nonradioactive labeling of oligonucleotides in vitro with the haptens digoxigenin by tailing with terminal transferase. *Anal Biochem* 1991;192:222–31.
- [13] Gavrieli Y, Sherman Y, Ben-Sasson SA. Identification of programmed cell death in situ via specific labeling of nuclear DNA fragmentation. *J Cell Biol* 1992;119:493–501.
- [14] Brosnan CF, Cannella B, Battistini L, Raine CS. Cytokine localization in multiple sclerosis lesions: correlation with adhesion molecule expression and reactive nitrogen species. *Neurology* 1995;45:S16–21.
- [15] Vartanian T, Li Y, Zhao M, Stefansson K. Interferon- γ -induced oligodendrocyte cell death: implication for the pathogenesis of multiple sclerosis. *Mol Med* 1995;3:732–43.
- [16] Li P, Allen H, Banerjee S, et al. Mice deficient in IL-1 β -converting enzyme are defective in production of mature IL-1 β and resistant to endotoxic shock. *Cell* 1995;80:401–11.
- [17] Ghayur T, Banerjee S, Huganin M, et al. Caspase-1 processes IFN-

- gamma-inducing factor and regulates LPS-induced IFN-gamma production. *Nature* 1997;386:619–23.
- [18] Gu Y, Kuida K, Tsutsue H, et al. Activation of interferon- γ inducing factor mediated by interleukin-1 β converting enzyme. *Science* 1997;275:206–9.
- [19] Furlan R, Martino G, Galbiati F, et al. Caspase-1 regulates the inflammatory process leading to autoimmune demyelination. *J Immunol* 1999;163:2403–9.
- [20] Mao PL, Jiang Y, Wee BY, Porter AG. Activation of caspase-1 in the nucleus requires nuclear translocation of pro-caspase-1 mediated by its prodomain. *J Biol Chem* 1998;273:23621–4.
- [21] Hisahara S, Shoji SI, Okano H, Miura M. Caspase-1/CED-3 family executes oligodendrocyte apoptosis by tumor necrosis factor. *J Neurochem* 1997;69:10–20.
- [22] Gu C, Casaccia-Bonnel P, Srinivasan A, Chao MV. Oligodendrocyte apoptosis mediated by caspase activation. *J Neurosci* 1999;19:3043–9.
- [23] Craighead M, Pole J, Waters C. Caspases mediate C2-ceramide-induced apoptosis of the human oligodendroglial cell line, MO3.13. *Neurosci Lett* 2000;278:125–8.
- [24] Craighead MW, Tiwari P, Keynes RG, Waters CM. Human oligodendroglial cell line, MO3.13, can be protected from apoptosis using the general caspase inhibitor zVAD-FMK. *J Neurosci Res* 1999;57:236–43.
- [25] McLaurin J, Trudel GC, Shaw IT, Antel JP, Cashman NR. A human glial hybrid cell line differentially expressing genes subserving oligodendrocyte and astrocyte phenotype. *J Neurobiol* 1995;26:283–93.

Caspase-9 Activation Results in Downstream Caspase-8 Activation and Bid Cleavage in 1-Methyl-4-Phenyl-1,2,3,6-Tetrahydropyridine-Induced Parkinson's Disease

Veena Viswanath,² Yongqin Wu,¹ Rapee Boonplueang,^{1,2} Sylvia Chen,¹ Fang Feng Stevenson,¹ Ferda Yantiri,² Lichuan Yang,³ M. Flint Beal,³ and Julie K. Andersen^{1,2}

¹Buck Institute for Age Research, Novato, California 94945, ²Division of Neurogerontology, Andrus Gerontology Center and Program in Molecular Biology, Department of Biological Sciences, University of Southern California, Los Angeles, California 90089, and ³Department of Neurology, Cornell University Medical College, New York, New York 10021

Parkinson's disease (PD) and 1-methyl-4-phenyl-1,2,3,6-tetrahydropyridine (MPTP) toxicity are both associated with dopaminergic neuron death in the substantia nigra (SN). Apoptosis has been implicated in this cell loss; however, whether or not it is a major component of disease pathology remains controversial. Caspases are a major class of proteases involved in the apoptotic process. To evaluate the role of caspases in PD, we analyzed caspase activation in MPTP-treated mice, in cultured dopaminergic cells, and in postmortem PD brain tissue. MPTP was found to elicit not only the activation of the effector caspase-3 but also the initiators caspase-8 and caspase-9, mitochondrial cytochrome *c* release, and Bid cleavage in the SN of wild-type mice. These changes were attenuated in transgenic mice neuronally expressing the general caspase inhibitor protein baculoviral p35. These mice also displayed increased resistance to the cytotoxic effects of the drug. MPTP-associated toxicity in culture was found temporally to involve cytochrome *c* release,

activation of caspase-9, caspase-3, and caspase-8, and Bid cleavage. Caspase-9 inhibition prevented the activation of both caspase-3 and caspase-8 and also inhibited Bid cleavage, but not cytochrome *c* release. Activated caspase-8 and caspase-9 were immunologically detectable within MPP⁺-treated mesencephalic dopaminergic neurons, dopaminergic nigral neurons from MPTP-treated mice, and autopsied Parkinsonian tissue from late-onset sporadic cases of the disease. These data demonstrate that MPTP-mediated activation of caspase-9 via cytochrome *c* release results in the activation of caspase-8 and Bid cleavage, which we speculate may be involved in the amplification of caspase-mediated dopaminergic cell death. These data suggest that caspase inhibitors constitute a plausible therapeutic for PD.

Key words: caspases; substantia nigra; Parkinson's disease; MPTP; mesencephalic cultures; PC12

Parkinson's disease (PD) is characterized by a progressive degeneration of dopaminergic neurons of the substantia nigra (SN). In postmortem Parkinsonian brain dying neurons are present that have been reported to display morphological characteristics of apoptosis, including cell shrinkage, chromatin condensation, and DNA fragmentation (Mochizuki et al., 1996; Hajimohamadreza and Treherne, 1997; Tatton et al., 1998). In addition, the expression of known effectors of neuronal apoptosis, including the major downstream executioner caspase, caspase-3, has been re-

ported in autopsied SN tissue isolated from PD patients (Anglade et al., 1997; Hartmann et al., 2000). *In vivo* and *in vitro* models of PD also have suggested a role for apoptosis in the related human disease pathology (for review, see Andersen, 2001). 1-Methyl-4-phenyl-1,2,3,6-tetrahydropyridine (MPTP) administration in mice, for example, produces selective degeneration of dopaminergic neurons of the SN, and the presence of DNA fragmentation has been reported after its administration along with the induction of caspase-3 activity (Tatton and Kish, 1997; Hartmann et al., 2000). In addition, proapoptotic Bax expression is found to be elevated after MPTP administration, and mice in which Bax has been ablated or the expression of the anti-apoptotic protein Bcl-2 has been elevated have been shown to be resistant to this agent (Hassouna et al., 1996; Offen et al., 1998; Yang et al., 1998; Choi et al., 2001). 1-Methyl-4-phenylpyridinium ion (MPP⁺), a metabolite of MPTP, has been found at low dosages to cause apoptotic cell death in dopaminergic PC12 cells and mesencephalic cultures via the activation of caspase-3 (Hartley et al., 1994; Mochizuki et al., 1996; Dodel et al., 1998). Caspase-3, therefore, has been suggested to be the final effector of apoptotic cell death in Parkinson's-associated neurodegeneration, but the exact biochemical pathways involved in its activation are unclear.

Previously, we have reported the creation of transgenic mice that neuronally express the baculoviral protein p35 (Viswanath et al., 2000). This protein acts as a potent irreversible caspase inhibitor with broad effectiveness against all classes of these

Received July 16, 2001; revised Sept. 20, 2001; accepted Sept. 24, 2001.

This work was funded in part by National Institutes of Health Grants AG12141 and AG09793 (J.K.A.). We thank Dr. John O. Archambeau (Loma Linda, CA) for the use of his stereology setup for performing the neuronal cell counts and Dr. Jytte Larsen (University of Aarhus, Aarhus, Denmark) for advice regarding this procedure. We also thank Dr. Carlos Arruda (SmithKline Beecham, Philadelphia, PA) for the gift of the activated caspase-8 antibody and Julie Schneider and Beth Howard at the Brain Bank (Rush University, Chicago, IL) and Carole Miller at the University of Southern California (USC; Los Angeles, CA) Brain Bank for providing us with human postmortem Parkinsonian and age-matched control tissue. In addition, we acknowledge Dr. Junying Yuan (Harvard University, Cambridge, MA) for advice regarding use of the Bid antibody, Dr. Hadi Zanjani (USC) for assistance with mouse brain dissections and immunohistochemistry protocols performed on human tissues, and Dr. Christian Pike (USC) for use of his fluorescent scope and advice on fluorescent immunohistochemistry.

V.V. and Y.W. contributed equally to this work.

Correspondence should be addressed to Dr. Julie K. Andersen, Associate Professor, Buck Institute for Age Research, 8001 Redwood Boulevard, Novato, CA 94948. E-mail: jandersen@buckinstitute.org.

Copyright © 2001 Society for Neuroscience 0270-6474/01/219519-10\$15.00/0

proteases (Bump et al., 1995; Zhou et al., 1998; Fisher et al., 1999). Expression of the p35 protein *in vivo* has been shown to confer functional caspase inhibitory activity and to attenuate apoptosis in a variety of different paradigms (Hay et al., 1994; Sugimoto et al., 1994; Davidson and Steller, 1998; Izquierdo et al., 1999; Hisahara et al., 2000; Viswanath et al., 2000). Unlike animals deficient in the expression of specific caspases (i.e., caspase-3, caspase-8, and caspase-9; Kuida et al., 1996, 1998; Varfolomeev et al., 1998; Colussi and Kumar, 1999; Zheng et al., 1999), p35 transgenics appear phenotypically normal and are viable, and embryonic development does not appear to be affected in these animals (Viswanath et al., 2000). These animals were studied along with the examination of dopaminergic cell lines, primary mesencephalic cultures, and PD brain tissue to assess the possible regulatory role of other caspases in the activation of caspase-3 in the molecular pathway leading to apoptotic cell death in MPTP toxicity and sporadic late-onset PD.

MATERIALS AND METHODS

MPTP treatment of mice. MPTP-HCl (Sigma Aldrich, St. Louis, MO) in 0.9% NaCl was administered to 10- to 16-week-old wild-type and p35 transgenic mice, using an acute dosing regimen of 15 mg/kg intraperitoneally every 2 hr for four doses ($n = 5$ –7 mice in each group) as described previously (Yang et al., 1998). Control animals in both paradigms were treated with equal volumes of saline.

Stereological counts of tyrosine hydroxylase-immunopositive neurons. MPTP and saline-treated animals ($n = 5$ –7) were perfused transcardially with 4% paraformaldehyde. Brain tissue containing SN was sectioned coronally at 40 μ m on a sliding microtome. Immunohistochemistry was performed with a rabbit polyclonal anti-tyrosine hydroxylase antibody (Chemicon, Temecula, CA). Briefly, fixed tissue was preincubated with 1% hydrogen peroxide/methanol to reduce background staining, and then the tissue was exposed to a 1:500 dilution of primary antibody in appropriate buffer overnight at 4°C. Sections were washed with PBS, incubated with biotinylated anti-rabbit IgG secondary antibody (Vector Laboratories, Burlingame, CA), rinsed, placed for 1 hr in avidin–biotin peroxidase solution (Vectastain ABC kit, Vector Laboratories), and then developed in 0.01% hydrogen peroxide, 0.01% diaminobenzidine tetrahydrochloride (DAB; Sigma Aldrich) for 5 min. Sections were rinsed, mounted on glass slides in 50% glycerol, and coverslipped. Slides were coded, and calculations of the cell numbers were performed by using the unbiased disector method (West et al., 1991). Hydroxylase-immunopositive (TH⁺) cells were counted from a total of 14–18 sections in each field per brain (i.e., every second section) at a magnification of 100 \times in a 0.2 mm² area, using the optical fractionator approach.

Measurement of levels of dopamine and homovanillic acid. MPTP and saline-treated animals ($n = 5$ –7) were killed 7 d after the last MPTP injection. For each mouse the striatum was dissected, immediately frozen in dry ice, and then stored at -80°C for the measurement of dopamine and its metabolites. Dissected striatal tissues were sonicated and centrifuged in chilled 0.1 M perchloric acid (PCA; 30 μ l/mg tissue). The supernatants were analyzed for levels of dopamine and homovanillic acid (HVA) by using 16-electrode electrochemical detection as described previously (Beal et al., 1990). Concentrations of dopamine and HVA are expressed as picomoles per milligram of protein.

Measurement of caspase activities. Caspase activities were measured in PC12 cells and murine SN tissues at the indicated time points after toxin treatment by using specific fluorogenic tetrapeptide substrates. Caspase-3 activity was measured with a fluorace apopain assay kit (Bio-Rad, Hercules, CA) that used the substrate DEVD-AFC according to the manufacturer's directions. Caspase-8 and caspase-1 activities were measured by using the substrates IETD-AFC and YVAD-AFC (Calbiochem, La Jolla, CA), respectively. Caspase-9 activity was measured with an assay kit (Oncogene, Cambridge, MA), using the specific substrate LEHD-AFC. Cells or tissues were lysed in 100–250 μ l of lysis buffer [containing (in mM) 10 HEPES-KOH, pH 7.2, 2 EDTA, 5 dithiothreitol (DTT), and 1 phenylmethylsulfonyl fluoride (PMSF) plus 0.1% CHAPS, 10 μ g/ml pepstatin A, 10 μ g/ml aprotinin, 20 μ g/ml leupeptin], vortexed gently, and freeze-thawed four to five times. Lysates were centrifuged at 13,000 \times g for 30 min at 4°C, and the supernatants were collected. Protein concentrations were estimated by using Bradford reagent (Bio-Rad).

Supernatant aliquots were incubated with the fluorescent substrates at 37°C for 1–2 hr. Free AFC accumulation resulting from cleavage of the aspartate–AFC bond was measured with a Cytofluor II fluorometer at 360 nm excitation and 515 nm emission wavelengths.

Western blot analysis of cytochrome *c* levels and Bid cleavage. For analysis of Bid cleavage, tissue extracts were prepared as described above for the measurement of caspase activities. To analyze cytochrome *c* release, we performed protein extraction of both the mitochondrial and cytosolic fractions as described previously (Kirsch et al., 1999). Cells or tissues were rinsed twice with cold PBS and lysed in cold MSHE buffer [0.21 M mannitol (and in mM) 70 sucrose, 10 HEPES-KOH, pH 7.2, 1 EGTA, 1 EDTA, 0.15 spermine, 0.75 spermidine, and 5 DTT plus 2 μ g/ml leupeptin, 2 μ M benzamide-HCl, 1 μ g/ml pepstatin]. Cells were homogenized with Dounce on ice. Nuclei and unlysed cells were removed by centrifugation at 500 \times g at 4°C for 12 min. The supernatant was centrifuged at 9500 \times g for 9 min at 4°C to pellet mitochondria. The supernatant contained the cytosolic fraction; the mitochondrial pellet was resuspended in MSHE buffer and was also used for immunoblot analysis. Protein (5 μ g) from the cytosolic fraction and 2.2 μ g from the mitochondrial fraction were loaded per lane. The primary antibodies were either a 1:1000 dilution of polyclonal anti-human/mouse Bid (R&D Systems, Minneapolis, MN) or a 1:1000 dilution of monoclonal cytochrome *c* (PharMingen, San Diego, CA), followed by horseradish peroxidase-conjugated secondary antibody (Vector Laboratories) and autoradiography with enhanced chemiluminescence (ECL; Amersham Pharmacia Biotech, Arlington Heights, IL). Cytosolic extracts also were analyzed with Cox IV antibody, which serves as an indicator of mitochondrial contamination of cytosolic extracts (Clontech, Palo Alto, CA).

PC12 cell culture and treatment with MPP⁺. PC12 cells were grown in DMEM supplemented with 10% heat-inactivated horse serum, 5% fetal bovine serum, and 2% penicillin/streptomycin (Life Technologies, Gaithersburg, MD). Typically, the cells were plated in 100 \times 200 mm culture dishes or six-well plates at a confluency of 50–80% and grown at 37°C in 5% CO₂. Cultures were used for no more than 20 passages. Cells were treated with 150 μ M MPP⁺ (Sigma Aldrich) for 4–24 hr; untreated cells were used as controls. MPP⁺ stock was made freshly before its addition to DMEM. For each set of experiments the samples were run in triplicate and repeated three times. For experiments that used the caspase-8 and caspase-9 inhibitors (25 μ M in DMSO; Calbiochem-Novabiochem, San Diego, CA and PharMingen, respectively), the cells were preincubated with the inhibitors for 1 hr before treatment with MPP⁺.

Mesencephalic cultures and MPP⁺ treatment. All experiments were performed by following an institutionally approved protocol in accordance with National Institutes of Health *Guide for the Care and Use of Laboratory Animals*. Ventral mesencephalon was dissected from embryonic gestation day 14 (E14) wild-type and p35 transgenic mice. Neurons were dissociated mechanically and incubated for 5 min at room temperature (RT) in 0.05% trypsin-EDTA (Life Technologies) in HBSS without calcium and magnesium (Life Technologies). The digestion reaction was stopped by the addition of 10% fetal bovine serum (FBS; Life Technologies) in high-glucose DMEM (Life Technologies). Cells were plated onto poly-D-lysine-coated eight-well culture slides (Becton Dickinson Labware, Bedford, MA) at a density of 3.5×10^5 cells/well. Neurons were grown in neurobasal medium (NBM) supplemented with 2% B-27, 0.5 mM glutamine, and 1% antibiotic–antimycotic solution (all from Life Technologies). All cultures were incubated at 37°C at 5% CO₂. After 4 d one-half of the medium was removed and replaced with an equal volume of medium. Cells were grown an additional 2 d and then treated with 5 μ M MPP⁺ (Sigma Aldrich) for 6, 12, 18, 24, and 48 hr. The caspase-9 inhibitor Z-LEHD-FMK (25 μ M; PharMingen) was added 1 hr before MPP⁺ treatment. Cells were fixed with 4% paraformaldehyde in PBS for 30 min.

Immunocytochemistry for activated caspase-3, caspase-9, and caspase-8 and TH and DAPI staining in cultured TH⁺ SN neurons. To address the time course of MPP⁺-induced activation of caspase-3, caspase-9, and caspase-8 in apoptotic TH⁺ SN neurons, we used double immunolabeling for both the activated caspases and TH and DAPI staining in this study. After fixation the cells were blocked with 10% normal goat serum (NGS) containing 0.3% H₂O₂ and 0.3% Triton X-100 for 1 hr at RT. After being washed three times in PBS, the cells were incubated with rabbit polyclonal antibodies that recognize the active forms of caspase-3 (1:50; New England Biolabs, Beverly, MA), caspase-9 (1:100; New England Biolabs), and caspase-8 (1:500; SK440, gift from SmithKline Beecham, Philadelphia, PA) at 4°C overnight. After being washed with

PBS, the cells were incubated with BODIPY FL goat anti-rabbit IgG conjugates (1:200; Molecular Probes, Eugene, OR) at RT for 1 hr. Then the cells were washed with PBS and incubated with sheep anti-tyrosine hydroxylase polyclonal antibody (1:100; Chemicon) at RT for 1 hr. After being washed with PBS, the cells were incubated with Cy-3-conjugated anti-sheep IgG (1:500; Jackson ImmunoResearch, West Grove, PA) at RT for 1 hr. Finally, the cells were washed with PBS and mounted with VectaShield mounting medium with DAPI (Vector Laboratories).

Cell counts in cultured TH⁺ SN neurons from p35 transgenic versus wild-type mice treated with MPP⁺. The total number of TH⁺ neurons in mesencephalic cultures from both p35 transgenic and wild-type animals was counted in every well in at least three wells per time point (0, 6, 12, and 24 hr after MPP⁺ treatment). The percentage of TH⁺ neurons compared with that of the untreated wild type was used to evaluate MPP⁺ toxicity. Experiments were repeated three times with cultures isolated from independent dissections.

Immunohistochemistry of activated caspase-8 and caspase-9 and TH⁺ SN neurons in vivo. For mouse tissue, free-floating 40- μ m-thick sections were treated first with sheep polyclonal anti-tyrosine hydroxylase antibody (1:500; Chemicon), followed by biotinylated anti-sheep IgG secondary antibody and cy3 streptavidin (Jackson ImmunoResearch). TH⁺ neurons were localized, and then the sections were reincubated with either rabbit polyclonal anti-activated caspase-9 antibody (1:100; New England Biolabs) or rabbit polyclonal anti-activated caspase-8 antibody (1:2500; gift from SmithKline Beecham), followed by biotinylated anti-rabbit IgG and cy2 streptavidin (Jackson ImmunoResearch); the sections were visualized under fluorescence microscopy. Control experiments were performed in which one or the other of the primary antisera was omitted. No staining was observed under these conditions. Immunostaining was performed similarly with human brain sections (25 μ m thick) from both late-onset PD patients with mild-to-moderate focal loss of melanized neurons in ventral and caudal parts of the SN pars compacta (SNpc) and age-matched controls fixed in formaldehyde ($n = 3$ for each; average postmortem period, 7.25 ± 5 hr; average age, 69.7 ± 9 years). All PD cases were diagnosed clinically and neuropathologically confirmed, whereas controls had no clinical or neuropathological signs of PD or dementia. Caspase expression was not found to be affected by postmortem delay (Stadelmann et al., 1999).

Statistical analysis. Results were expressed as means \pm SD of the difference between wild type and p35 transgenics as assessed by ANOVA. Values of $p < 0.01$ were taken as being statistically significant.

RESULTS

Transgenic mice expressing the general caspase inhibitory protein p35 are resistant to the toxicity associated with the Parkinson's-inducing agent MPTP

Apoptosis has been shown to play a role in MPTP-induced neurotoxicity (Hassouna et al., 1996; Offen et al., 1998). Because caspase-3 has been demonstrated previously to be activated during this process both *in vitro* and *in vivo*, we examined whether expression of the general caspase inhibitor p35 in our transgenic animals would act to inhibit the death of dopaminergic SN neurons induced by MPTP treatment. Stereological cell counts of TH⁺ dopaminergic neurons were performed on coronal sections isolated from the SN of p35 transgenics versus wild-type animals injected with either MPTP or saline ($n = 5$ –7). TH⁺ cells were counted in every alternate section via the optical fractionator method that combines the optical disector method and systematic uniform random sampling (West et al., 1991). The number of TH⁺ neurons in the SNpc of wild-type animals was found to be decreased by $\sim 37 \pm 6.2\%$ after MPTP administration compared with animals injected with saline alone ($p < 0.01$; Fig. 1A). In contrast, a decrease of only $15 \pm 4.8\%$ in the number of TH⁺ cells was observed in the SNpc of p35 transgenics that were injected with MPTP compared with saline-injected animals ($p < 0.01$).

The effects of acute administration of MPTP on striatal dopamine and HVA levels also was assessed in wild-type versus p35

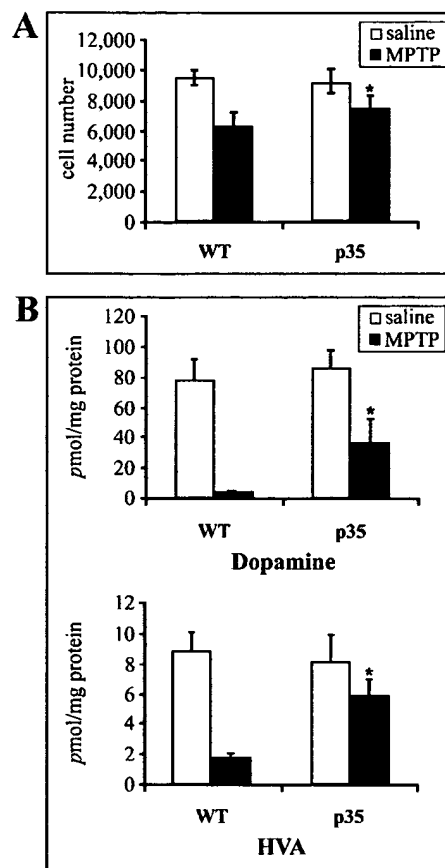


Figure 1. Toxicity induced by MPTP is attenuated in transgenic mice neuronally expressing the general caspase inhibitor protein baculoviral p35. *A*, Stereological counts of TH⁺ neurons from wild-type (WT) versus p35 transgenic mice after MPTP administration. Both wild-type and p35 transgenics were killed 7 d after MPTP injection, and SN tissue was immunostained with TH antibody. The cell number was assessed stereologically in every alternate section. Data are means \pm SD of five to seven animals per group; $*p < 0.01$. *B*, Effects of MPTP administration on dopamine and HVA levels in WT versus p35. For all animals the striatum was dissected for measurement of dopamine and HVA 7 d after MPTP administration. Data are means \pm SD from three to four mice per group; $*p < 0.01$.

transgenic mice (Fig. 1B). No significant differences were noted in striatal dopamine or HVA concentrations after the administration of saline in wild-type versus p35 transgenic animals ($p = 0.10$; Fig. 1B). However, a large reduction in concentrations of both dopamine and its metabolite was observed in the wild-type animals after drug administration. In the p35 transgenics these depletions were attenuated significantly for both dopamine or HVA ($p < 0.01$).

MPTP elicits cytochrome c release, caspase-3, caspase-9, and caspase-8 activation, and Bid cleavage in the SN of wild-type mice that are attenuated in p35 transgenics

The inhibition of cell death elicited by MPTP administration in p35 transgenic mice suggests a role for caspases in this process. *In vitro* kinetic analysis demonstrates that p35 inhibits caspase-1, caspase-3, caspase-6, caspase-7, caspase-8, caspase-9, and caspase-10 most potently (Zhou et al., 1998). The attenuation of MPTP-induced cell death in p35 transgenics implies that either

upstream activator or downstream effector caspases or both may be involved in this process.

To determine which caspases are activated in MPTP-induced neuronal degeneration, we injected wild-type and p35 transgenic mice with either MPTP or saline; the SNs were dissected 24 hr later, and cell lysates were prepared to assess caspase activities with the use of specific tetrapeptide fluorogenic substrates. This particular time point was chosen because, according to previous work, this is when the maximum number of apoptotic cells can be observed after MPTP administration, and this time point precedes that of maximal cell death (Hartmann et al., 2001).

Caspase-3 appears to be an essential component of the apoptotic machinery in many cell types and a key player in many types of neuronal apoptosis (Salvesen and Dixit, 1997). We analyzed the ability of MPTP to trigger the activation of caspase-3 activity in SN dissected from p35 transgenics versus wild-type animals. In keeping with previous results (Hartmann et al., 2000), we observed significant activation of caspase-3 in wild-type animals after MPTP injection, approximately threefold (Fig. 2*A*). Expression of p35 was found to attenuate the MPTP-induced activation of caspase-3 activity significantly ($p < 0.01$).

MPTP is a known mitochondrial toxin (Hartley et al., 1994). Damage to the mitochondria in other paradigms has been demonstrated to result in the release of mitochondrial cytochrome *c* into the cytoplasm and subsequent activation of caspase-9, which in turn can elicit the activation of caspase-3 (Li et al., 1997). To evaluate whether mitochondrial release of cytochrome *c* is involved in MPTP-induced cell death, we prepared cytosolic and mitochondrial extracts from SN of wild types and p35 transgenics at various time points after MPTP treatment, and cytochrome *c* protein levels were measured by immunoblot analysis. Cytosol from tissues isolated from either saline-treated wild-type or p35 animals did not contain any detectable cytochrome *c* protein (data not shown). In contrast, cytosolic cytochrome *c* accumulated significantly in wild-type animals treated with MPTP and to a lesser degree in tissue from p35 transgenics (Fig. 2*B*). The absence of Cox IV in cytosolic extracts confirmed that our preparations were free of mitochondrial contamination (data not shown). Along with mitochondrial cytochrome *c* release, SN caspase-9 activity was increased by approximately twofold at 24 hr after the induction of apoptosis by *in vivo* MPTP administration in the wild-type animals; this increase in activity was found to be inhibited greatly in the presence of p35 ($p < 0.01$; Fig. 2*A*).

Caspase-8 is another caspase that, like caspase-9, appears to be activated upstream of caspase-3 and in addition recently has been implicated possibly to play a role in the cell death associated with neurodegenerative paradigms, including PD (Sanchez et al., 1999; Velier et al., 1999; Hartmann et al., 2001). In wild-type animals caspase-8 activity was found to be induced twofold after treatment with MPTP; this activity increase was attenuated greatly in the p35 transgenics ($p < 0.01$; Fig. 2*A*). Bid, a Bcl-2 family member, has been shown to be a specific substrate of caspase-8 and to play a role in caspase 8-mediated mitochondrial damage and cell death (Li et al., 1998). To investigate the possible involvement of Bid in MPTP-mediated neurodegeneration, we analyzed Bid cleavage in SN tissue lysates from wild-type and p35 mice after MPTP versus saline injection. Bid was

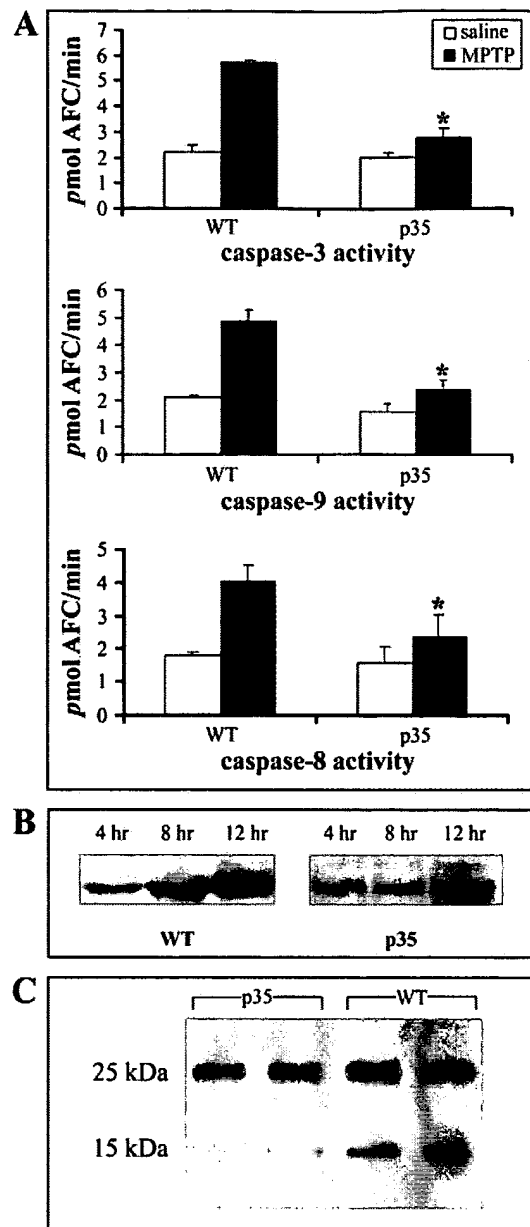


Figure 2. Caspase-3, caspase-8, and caspase-9 activation, cytochrome *c* release, and Bid cleavage after MPTP administration. *A*, Caspase-3, caspase-9, and caspase-8 activities. Substantia nigra (SN) dissected from MPTP versus saline-treated wild-type and p35 transgenic animals was used to measure caspase activities with specific fluorogenic tetrapeptide substrates ($n = 5$ –7 animals per group for all assays). The caspase activities were measured 24 hr after MPTP injection. Values represent the means \pm SD from three individual experiments; $*p < 0.01$. *B*, MPTP-induced cytochrome *c* release from the mitochondria. Cytosolic extracts were prepared at the indicated times, and cytochrome *c* was evaluated by Western blot analysis with the use of a monoclonal antibody. *C*, *In vivo* Bid cleavage 24 hr after MPTP administration in WT and p35 mice. SN was dissected, and total cell lysates were subjected to immunoblotting. Molecular weights are shown on the left. The 25 kDa band represents full-length Bid; the 15 kDa fragment represents the cleaved form.

found to be cleaved to a 15 kDa fragment in SN tissue homogenates isolated from MPTP-treated wild-type animals, and this cleavage was attenuated partially in tissues from p35 transgenic animals (Fig. 2*C*).

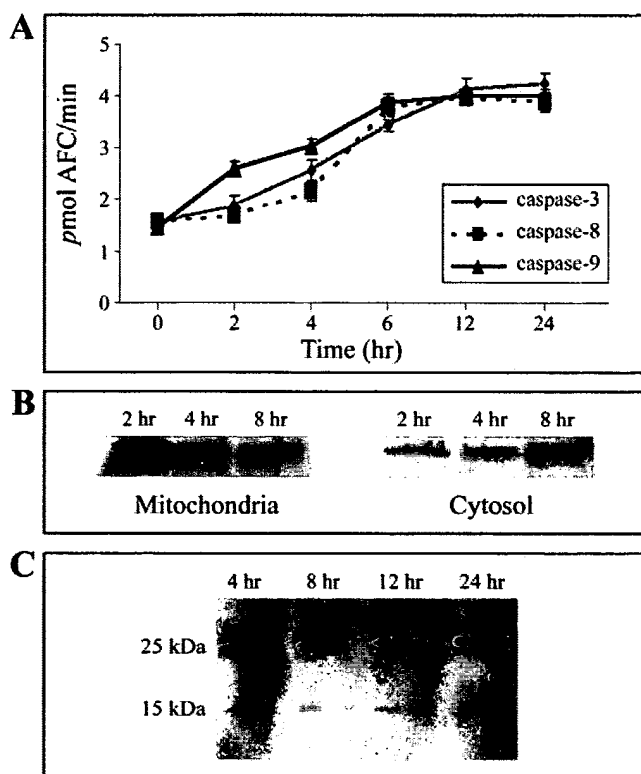


Figure 3. MPP⁺ induces time-dependent activation of various caspases, cytochrome *c* release, and Bid cleavage in PC12 cells. Values represent the means \pm SD from three experiments; $p < 0.01$. *A*, PC12 cells were incubated with 150 μ M MPP⁺ for the indicated times. Then the cell lysates were analyzed for caspase activities with the use of specific fluorogenic substrates. *B*, MPP⁺-induced cytochrome *c* release from the mitochondria. Mitochondrial and cytosolic extracts were prepared as described, and cytochrome *c* release was evaluated by using a monoclonal antibody at 2, 4, and 8 hr after MPP⁺ treatment. *C*, Cleavage of Bid in PC12 cells at various times after treatment with MPP⁺; the 15 kDa fragment was not observed at either 0 or 2 hr after MPP⁺ application (data not shown).

MPTP-associated toxicity in dopaminergic cells in culture sequentially involves cytochrome *c* release, activation of caspase-9, caspase-3, and caspase-8, and Bid cleavage

To determine further the pathway of activation of caspase-3, caspase-9, and caspase-8 in MPTP-induced neurodegeneration, we temporally examined the sequential order of their inductions *in vitro* by administration of MPP⁺, the active metabolite of MPTP, to dopaminergic PC12 cells. PC12 cells are a noradrenergic line derived from the rat adrenal medulla that secrete, store, synthesize, and uptake dopamine and are therefore a commonly used model for studying catecholaminergic neurons (Greene and Tischler, 1976). PC12 cells were treated at a dosage of 150 μ M MPP⁺, as described previously (Hartley et al., 1994), and caspase activities were analyzed at various time points (0, 2, 4, 6, 12, and 24 hr after MPP⁺). At 150 μ M MPP⁺ caspase-9 was activated significantly between 0 and 2 hr and caspase-3 activation between 2 and 4 hr after MPP⁺ treatment, respectively ($p < 0.01$; Fig. 3*A*). In contrast, caspase-8 activation did not show significant activation until between 4 and 6 hr after 150 μ M MPP⁺ treatment ($p < 0.01$). This implies that caspase-9 is likely the apical caspase in MPP⁺-induced toxicity and may be responsible for caspase-8 activation. In agreement with this conclusion, cytochrome *c* re-

lease from the mitochondria was observed by 2 hr after MPP⁺ treatment (Fig. 3*B*). Bid cleavage, in contrast, was not seen in MPP⁺-treated cells until at least 4–6 hr after drug administration (Fig. 3*C*).

Caspase-9 activation is necessary for caspase-8 activation and Bid cleavage

To elucidate further the order of caspase activation, we used a specific inhibitor against caspase-9 and examined its effect on caspase-8 activation and Bid cleavage after MPP⁺ treatment of PC12 cells. LEHD-FMK, a cell-permeable caspase-9 specific inhibitor, was applied 1 hr before the exposure of PC12 cells to 150 μ M MPP⁺ for various periods of time. The dose of the inhibitor used here was predetermined by a set of dose–response experiments in which the ability of LEHD-FMK to inhibit the activity of caspase-9 and the effects of this inhibitor on cell viability were examined (data not shown). Because previous work has implicated a nonspecific caspase inhibition at doses higher than a 50 μ M concentration of the inhibitor (Thornberry and Lazebnik, 1998) and because lower dosages (5–20 μ M) failed to inhibit caspase-9 activity effectively, a dosage of 25 μ M was chosen. Pharmacological inhibition of caspase-9 before MPP⁺ treatment resulted in inhibition not only of caspase-9 activity but also of both caspase-8 and caspase-3 activities, indicating that the activation of caspase-9 is necessary for the activation of both (Fig. 4*A*). Inhibition of caspase-9 also prevented Bid cleavage (Fig. 4*C*). However, it did not prevent the release of cytochrome *c* into the cytosol, an event normally considered to occur upstream of caspase-9 activation (Fig. 4*C*). Pretreatment with a 5 μ M concentration of the cell-permeable caspase-8 specific inhibitor IETD-CHO led to the inhibition of caspase-8 activity and small but significant inhibitions in activities of both caspase-9 and caspase-3 by 6–12 hr after MPP⁺ treatment ($p < 0.01$; compare Figs. 4*B* and 3*A*).

Primary mesencephalic cultures isolated from p35 transgenics demonstrate decreased MPP⁺-mediated loss of primary TH⁺ neurons

PC12 is a transformed cell line that may have survival mechanisms that are absent in normal primary dopaminergic neurons. Therefore, to verify the role of caspase activation in toxin-induced dopaminergic cell death on a cellular level in primary TH⁺ neurons, we explored the effects of MPP⁺ treatment in primary mesencephalic cultures isolated from both p35 transgenic and wild-type animals. A concentration of 5 μ M MPP⁺ was chosen for these studies because this dosage is in the range previously reported to elicit primarily apoptotic versus necrotic cell death in dopaminergic cells in these cultures (Hartmann et al., 2001). Preliminary dosage experiments conducted in our own laboratory at MPP⁺ concentrations of 5, 10, and 50 μ M verified this phenomenon. Cells were stained for TH at 0, 6, 12, and 24 hr after MPP⁺ treatment, and TH⁺ cells were counted. The percentage of TH⁺ neurons present versus untreated cultures was $62.0 \pm 16.6\%$ for wild-type versus $77.0 \pm 28.9\%$ for p35 cultures at 6 hr, $52.7 \pm 12.7\%$ wild-type versus $78.6 \pm 11.3\%$ p35 at 12 hr, and $28.3 \pm 4.8\%$ wild-type versus $38.3 \pm 2.7\%$ p35 at 24 hr ($p < 0.01$; Fig. 5*A*). As previously observed by Hartmann et al. (2001), this cell loss was found to be accompanied by a noticeable loss in neuritic extensions, especially by the 24 hr time point in the remaining TH⁺ neurons (Fig. 5*B*). However, unlike the results of Hartmann and colleagues that used the broad pharmacological caspase inhibitor zVAD-FMK, expression of the broad caspase inhibitor p35 was found to attenuate rather than to exacerbate

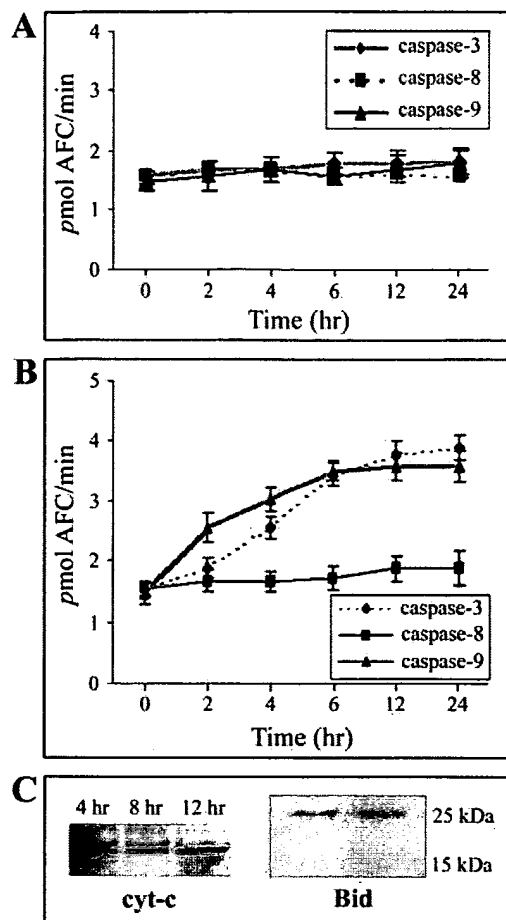


Figure 4. Effects of treatment of PC12 cells with specific cell-permeable inhibitors of caspase-9 and caspase-8 before treatment with MPP⁺ on the activation of caspase-9, caspase-3, and caspase-8, cytochrome c release, and Bid cleavage. Values for all assays represent the means \pm SD from three experiments; $p < 0.01$. *A*, Effects of pretreatment with a caspase-9 specific inhibitor on the activation of caspase-8, caspase-9, and caspase-3. PC12 cells were incubated with 25 μM LEHD-CHO 1 hr before treatment with MPP⁺. *B*, Effects of pretreatment with the specific peptide inhibitor to caspase-8 on the activation of caspase-8, caspase-3, and caspase-9. PC12 cells were incubated with 25 μM IETD-CHO at 1 hr before treatment with MPP⁺. *C*, Bid cleavage, but not cytochrome c release, is attenuated in PC12 cells after preincubation with LEHD-CHO. Data represent three individual experiments.

this cell loss, in keeping with our *in vivo* data. MPP⁺-treated wild-type cultures also were pretreated with a 25 μM concentration of the caspase-9 specific inhibitor LEHD-FMK. Although preliminary, results from treatment of wild-type cultures with caspase-9 specific inhibitor suggest that cell loss is attenuated after MPP⁺ treatment compared with untreated cultures at both 24 and 48 hr after MPP⁺ ($28.0 \pm 4.80\%$ wild-type versus $35.3 \pm 3.9\%$ wild-type plus inhibitor at 24 hr; $12.7 \pm 4.5\%$ wild-type versus $26.0 \pm 4.1\%$ wild-type plus inhibitor at 48 hr).

Pattern of caspase inductions in mesencephalic cultures that is observed in the primary PC12 cell line

To verify the temporal pattern of caspase induction after MPP⁺ on a cellular level in apoptotic primary dopaminergic neurons, we monitored the induction of caspase-9, caspase-3, and caspase-8 in primary mesencephalic cultures after treatment for 0, 2, 4, 6, 8,

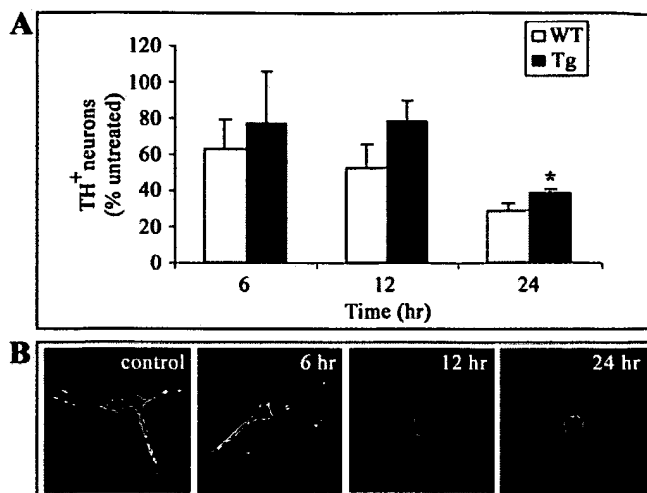


Figure 5. TH⁺ cell counts in MPP⁺-treated mesencephalic cultures from p35 transgenics (Tg) versus wild-type (WT) animals. *A*, Percentage of TH⁺ neurons in p35 transgenic versus wild-type mice mesencephalic cultures after 6, 12, and 24 hr of MPP⁺ (5 μM) treatment compared with untreated WT; * $p < 0.01$. *B*, Representative morphology of TH⁺ neurons in MPP⁺-treated wild-type cultures after 0, 6, 12, and 24 hr. Magnification, 40 \times . Data represent three independent experiments.

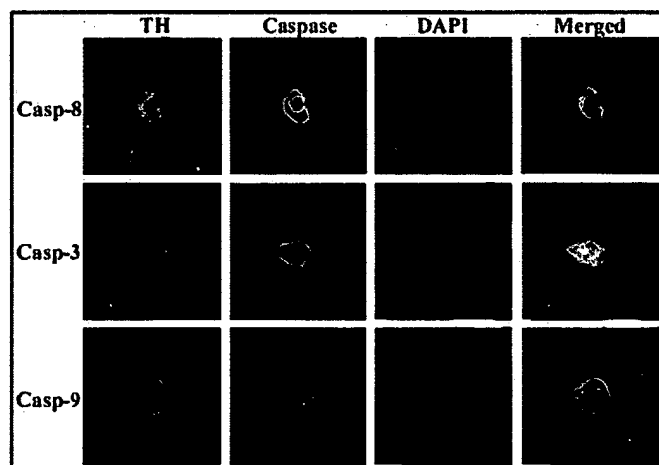


Figure 6. Temporal MPP⁺-induced activation of caspase-9, caspase-3, and caspase-8 in TH⁺ neurons in mesencephalic cultures. Triple labeling shows immunostaining for the active forms of caspase-9, caspase-3, and caspase-8 in apoptotic (DAPI-stained) TH⁺ neurons at the time of first induction, i.e., 2, 6, and 12 hr, respectively. Magnification, 60 \times . Data represent three independent experiments.

12, 18, 24, and 48 hr with 5 μM MPP⁺ via immunofluorescence with antibodies specific for both TH⁺ and the activated forms of each of the enzymes, coupled with DAPI staining. As with the PC12 cells, caspase-9 induction as monitored by immunofluorescence in the TH⁺ cells occurred first at 2 hr, followed by caspase-3 induction at 6 hr, which in turn preceded caspase-8 induction at 12 hr, demonstrating that MPP⁺-mediated cell death temporally involves the activation of caspase-9, caspase-3, and then caspase-8 (Fig. 6). The number of TH⁺ cells at any given time point displaying caspase activation was limited (1–10% or 2–5 per every 50 cells); however, this is in keeping with the findings of others and reflects the fact that only a small subset of dopaminergic neurons is undergoing apoptosis at any given time

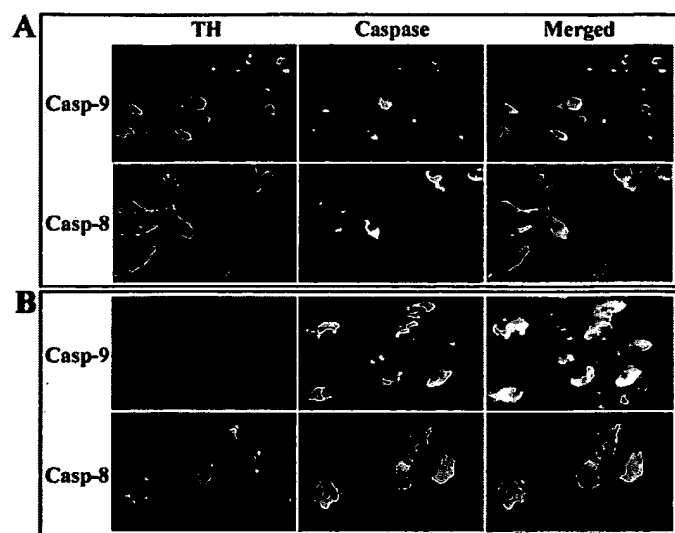


Figure 7. Presence of activated caspase-8 and caspase-9 in TH⁺ neurons of the substantia nigra of MPTP-treated mice and Parkinsonian brain. *A*, Wild-type mice were treated with MPTP, and 40 μ m sections were double immunolabeled for antibody against TH and the activated form of either caspase-9 or caspase-8. *B*, Postmortem human brain samples from Parkinson's patients were double immunostained for TH and activated caspase-9 or activated caspase-8. Magnification, 40 \times .

point (Hartmann et al., 2001). Caspase activation was accompanied by morphological changes in these cells compatible with apoptosis, including chromatin condensation as observed by DAPI staining, apoptotic bodies, and shrunken soma. Although treatment of cultures with caspase-9 specific inhibitor appeared to show a trend toward attenuation of caspase-9, caspase-3, and caspase-8 activation as monitored by immunofluorescence, it was not possible to access this statistically, given the low numbers of caspase-positive TH⁺ cells present at any of the examined time points (data not shown).

Activated caspase-8 and caspase-9 are found within dopaminergic neurons of the substantia nigra in both MPTP-treated mice and Parkinson's patients

To examine caspase activation after MPTP administration on a cellular level *in vivo*, we used antibodies specific to activated caspase-8 and caspase-9 in conjunction with anti-TH antibodies in MPTP-treated mice. Cellular expression of MPTP-induced activated caspase-3 and caspase-8 has been shown previously to occur in TH⁺ SN neurons of MPTP-treated mice as well as in PD patients (Hartmann et al., 2000, 2001). In the present study we found that several TH⁺ SN neurons in the MPTP-treated animals were also positive for immunostaining with both activated anti-caspase-8 and anti-caspase-9 antibodies (Fig. 7*A*).

To determine whether activated caspase-8 and caspase-9 were present in dopaminergic neurons of the Parkinsonian SN and therefore may play a role in the disease pathology, we performed similar experiments on tissues from late-onset sporadic PD cases versus age-matched controls. TH⁺ SN neurons that also were stained positively for antibodies against activated caspase-8 and caspase-9 were found in the SN isolated from autopsied PD patients (Fig. 7*B*). Although some caspase-8- and caspase-9-positive SN dopaminergic neurons also were detected in tissue from age-matched controls, this was observed less frequently (data not shown).

DISCUSSION

In this study we have demonstrated that neuronal expression of the general caspase inhibitor protein p35 in transgenic mice results in significant reduction in the effects of MPP⁺/MPTP-induced Parkinsonism both *in vitro* and *in vivo*. Given that neuronal expression of p35 is not completely protective against TH⁺ SN neuronal cell loss either *in vitro* or *in vivo* raises the possibility that other caspase-independent pathways also may be involved in toxin-induced cell death. An alternative explanation is that levels of p35 may not have been elevated sufficiently in our transgenic model to counteract all of the MPP⁺/MPTP-induced caspase induction and subsequent cell death.

MPTP was found to elicit cytochrome *c* release, activation of caspase-3, caspase-9, and caspase-8, and Bid cleavage in the SN of wild-type mice, and these events were found to be attenuated in the p35 transgenics *in vivo*. Studies in dopaminergic PC12 cells and primary mesencephalic cultures revealed that this toxicity appears to involve, sequentially, cytochrome *c* release, activation of caspase-9, caspase-3, and caspase-8, and Bid cleavage. Furthermore, the inhibition of MPTP-mediated caspase-9 activation appears to prevent caspase-3 and caspase-8 activation and Bid cleavage, but not cytochrome *c* release. On a cellular level the activation of caspase-9 and caspase-3 in TH⁺ cells in mesencephalic cultures was found to precede that of caspase-8, and either general caspase inhibition via p35 expression or specific pharmacological inhibition of caspase-9 resulted in attenuated MPP⁺-mediated TH⁺ cell loss. Both active caspase-8 and caspase-9 were found to be present within dopaminergic SN neurons of MPP⁺-treated mesencephalic cultures, MPTP-treated mice, and in late-onset Parkinson's patients to a greater extent than in controls. Taken together, these data suggest that caspase-8 activation in dopaminergic neurons occurs downstream of activation of both caspase-9 and caspase-3. Furthermore, caspase-9 activation appears to be required for both caspase-8 activation and Bid cleavage as well as for MPTP-mediated dopaminergic cell death.

MPTP is a mitochondrial toxin that elicits its actions first via monoamine oxidase B-catalyzed conversion to MPP⁺, which is taken up selectively into nigral dopaminergic neurons by the dopamine transporter. Here it acts to kill these cells by specifically inhibiting mitochondrial complex I activity (for review, see Przedborski and Jackson-Lewis, 1998). Cell death associated with PD also appears to involve a decrease in mitochondrial function via inhibition of the activity of mitochondrial complex I (Mizuno et al., 1998; Schapira et al., 1998). There is evidence both after MPTP administration in mice and in PD that mitochondrial dysfunction results in apoptotic cell death in dopaminergic neurons of the SN (Mochizuki et al., 1996; Hajimohamadreza and Treherne, 1997; Tatton and Kish, 1997; Tatton et al., 1998; Hartmann et al., 2000, 2001; Andersen, 2001). Mitochondrial injury can elicit apoptosis by disruption of mitochondrial membrane potential, resulting in the release of mitochondrial cytochrome *c* into the cytoplasm where it can complex with apoptosis-activating factor 1 (Apaf-1) and caspase-9, causing the activation of this initiator caspase (Li et al., 1997). Caspase-9 in turn can cleave and activate the downstream executioner caspases, including caspase-3. This leads to cleavage of additional cellular substrates, resulting in the morphological changes associated with apoptosis, including DNA fragmentation and cytoskeletal disruption (for review, see Nuñez et al., 1998; Stennicke and Salvesen, 2000).

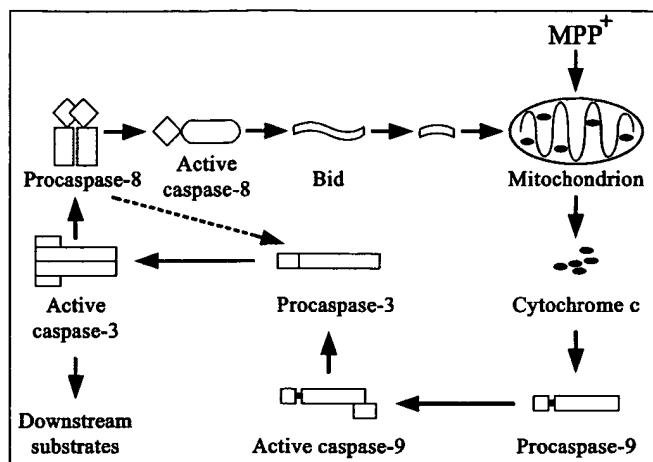


Figure 8. Possible pathway of caspase activation in MPTP-induced dopaminergic cell death. MPTP administration results in the release of mitochondrial cytochrome *c* and the activation of procaspase-9, leading to the subsequent activation of procaspase-3. Active caspase-3 can cleave downstream substrates, resulting in apoptosis. Active caspase-3 also can activate procaspase-8. Active caspase-8 in turn can cleave Bid, leading to cytochrome *c* release and setting up a self-amplification loop. Caspase-8 also has been reported to lead directly to the cleavage of caspase-3 (Kumar, 1999). A similar pattern may be at work in the SN of PD patients; alternatively, protein aggregates may lead to caspase-8 oligomerization and activation.

Recent evidence from cell-free and *in vitro* expression systems has suggested that, besides being a final effector in neuronal apoptosis, caspase-3 is also capable of eliciting cleavage and activation of the upstream initiator caspase-8 (Slee et al., 1999; Wolf and Green, 1999; Tang et al., 2000). Caspase-8 traditionally is associated with Fas receptor-induced apoptosis. In this system caspase-8 activation results in the cleavage of Bid, a proapoptotic BH3 domain-containing member of the Bcl-2 family, to produce a truncated form of the protein. Truncated Bid translocates from the cytoplasm to the mitochondria, where it appears to interact with and antagonize the actions of anti-apoptotic members of the Bcl-2 family, thereby causing an efflux of cytochrome *c* from the mitochondria (Kuwana et al., 1998; Li et al., 1998; Luo et al., 1998; Schendel et al., 1999; Wei et al., 2001). This in turn can result in the activation of caspase-9. Therefore, theoretically, caspase-8 acting via the translocation of cleaved Bid to the mitochondria could amplify apoptotic signals via the continued release of cytochrome *c* and subsequent activation of caspase-9 and caspase-3. Coupled with our data, this leads to the speculation that the initial activation of mitochondrially associated caspase-9 by MPTP may be potentiated via a feedback amplification loop involving the caspase 8/Bid pathway (Fig. 8). In our studies caspase-8 inhibition appeared to have a small but significant effect on activities of caspase-9 or caspase-3 in MPP⁺-treated dopaminergic cells in culture by 6–12 hr after MPP⁺ treatment (Fig. 4). It is conceivable that periods of >24 hr are required for more significant effects of caspase-8 inhibition, i.e., for the inhibition of Bid cleavage and cytochrome *c* release, thereby inhibiting additional activation of caspase-9 and caspase-3. Bid cleavage itself does not occur until ~4–6 hr after MPP⁺ application.

Caspase-8 recently has been shown to be involved in cell death induced by expanded polyglutamine repeats associated with such conditions as Huntington's disease (HD) and spino-

cerebellar ataxia, possibly by production of protein fragments that form toxic aggregates in affected neurons, although this is somewhat controversial (Kuemmerle et al., 1999; Sanchez et al., 1999; Wellington and Hayden, 2000). Intracellular aggregates also occur in PD in the form of Lewy bodies (Hughes, 1997; Olanow and Tatton, 1999). It is possible in PD that Lewy body aggregation itself may contribute to the recruitment and activation of caspase-8 similar to that which occurs in HD. Indeed, activated caspase-8 recently has been reported to be present in neuromelanin-containing SN neurons in autopsied tissues from PD patients (Hartmann et al., 2001). There also have been reports that both the cell death receptor-associated Fas and FADD are expressed in cells in the adult human SN that undergo degeneration in PD (de la Monte et al., 1998; Hartmann et al., 1998; Michel et al., 1999), although this has been disputed (Jellinger, 2000). This can initiate downstream apoptotic events including the activation of caspase-3 via direct proteolytic cleavage as well as via caspase-9 (Kumar, 1999).

Parkinson's disease develops over a period of several years; however, caspase-mediated apoptosis has been shown to occur within hours or days of initiation. The initiating event in neurodegeneration that is associated with PD appears to be mitochondrial dysfunction. In the MPTP model of PD in which the mitochondrial effects are acute and rapid, apoptosis occurs within 24 hr of drug administration. The delayed development of apoptosis in PD may reflect a slower accumulation of age-related mitochondrial damage over decades. Histological analysis of SN tissue from late-onset PD patients reveals a shrunken, condensed appearance in the remaining neurons and a lack of inflammation (Beal et al., 1993; Ziv et al., 1997). This is in contrast to the type of morphology expected if the associated cell death were necrotic in nature, i.e., cell swelling, rupture, and spillage of cell contents into the extracellular space eliciting significant local immune response. This suggests that cell death is likely apoptotic. Furthermore, the ability of dopaminergic cells of the substantia nigra to undergo PD-related apoptosis is likely dependent on the availability and concentration of activatable caspases in the affected neurons that may be altered over time (Velier et al., 1999). Recent publications have reported that neither the addition of pharmacological caspase inhibitors nor the expression of baculoviral p35 in either cultured primary dopaminergic neurons or dopaminergic cell lines protected them against MPP⁺-induced cell death (Choi et al., 2001; Hartmann et al., 2001). Indeed, Hartmann and colleagues have reported that both general caspase inhibition and inhibition selective for caspase-8 result in an increase in MPP⁺-mediated toxicity in rat mesencephalic cultures 24 hr after the addition of toxin, which they have attributed to a switch from apoptotic to necrotic cell death. We found, in contrast, that both the expression of baculoviral p35 and the administration of the caspase-9 specific inhibitor LEHD-FMK resulted in an attenuation of TH⁺ cell death in murine mesencephalic cultures *in vitro* up to 24 hr after MPP⁺ addition. In addition and in agreement with these data, we found that neuronal expression of p35 *in vivo* resulted in significant attenuation of dopaminergic SN cell loss and striatal dopamine/HVA levels up to 7 d after MPTP administration. Our studies clearly imply that caspase inhibition is protective against MPTP-induced cell death and suggest that strategies involving specific caspase inhibition could have utility in the treatment of Parkinson's disease.

REFERENCES

- Andersen J (2001) Does neuronal loss in Parkinson's disease involve programmed cell death? *BioEssays* 23:640–646.
- Anglade P, Vyas S, Javoy-Agid F, Herrero MT, Michel PP, Marquez J, Mouatt-Prigent A, Ruberg M, Hirsch EC, Agid Y (1997) Apoptosis and autophagy in nigral neurons of patients with Parkinson's disease. *Histol Histopathol* 12:25–31.
- Beal MF, Kowall NW, Swartz KJ, Ferrante R (1990) Homocysteic acid striatal lesions in rats spare somatostatin-neuropeptide Y neurons. *Neurosci Lett* 108:36–42.
- Beal MF, Hyman BT, Koroshetz W (1993) Do defects in mitochondrial energy metabolism underlie the pathology of neurodegenerative diseases? *Trends Neurosci* 16:125–131.
- Bump NJ, Hackett M, Huginin M, Seshagiri S, Brady K, Chen P, Ferenz C, Franklin S, Ghayur T, Li P, Licari P, Mankovitch J, Shi L, Greenberg AH, Miller LK, Wong W (1995) Inhibition of ICE family proteases by baculovirus anti-apoptotic protein p35. *Science* 269:1885–1888.
- Choi WS, Lee EH, Chung CW, Jung YK, Jin BK, Kim SU, Oh TH, Saido TC, Oh YJ (2001) Cleavage of Bax is mediated by caspase-dependent or -independent calpain activation in dopaminergic neuronal cells: protective role of Bcl-2. *J Neurochem* 77:1531–1541.
- Colussi PA, Kumar S (1999) Targeted disruption of caspase genes in mice: what they tell us about the functions of individual caspases in apoptosis. *Immunol Cell Biol* 77:58–63.
- Davidson FF, Steller H (1998) Blocking apoptosis prevents blindness in *Drosophila* retinal degeneration mutants. *Nature* 391:587–591.
- de la Monte SM, Sohn JM, Ganju N, Wands JR (1998) P53- and CD95-associated apoptosis in neurodegenerative diseases. *Lab Invest* 78:401–411.
- Dodel RC, Du Y, Bales KR, Ling ZD, Carvey PM, Paul SM (1998) Peptide inhibitors of caspase-3-like proteases attenuate 1-methyl-4-phenylpyridinium-induced toxicity of cultured fetal rat mesencephalic dopamine neurons. *Neuroscience* 86:701–707.
- Fisher AJ, Dela Cruz W, Zoog SJ, Schneider CL, Friesen PD (1999) Crystal structure of baculovirus p35: role of a novel reactive site loop in apoptotic caspase inhibition. *EMBO J* 18:2031–2039.
- Greene LA, Tischler AS (1976) Establishment of a noradrenergic clonal line of rat adrenal pheochromocytoma cells which respond to nerve growth factor. *Proc Natl Acad Sci USA* 73:2424–2428.
- Hajimohamadreza I, Treherne JM (1997) The role of apoptosis in neurodegenerative disease. *Prog Drug Res* 48:55–98.
- Hartley A, Stone JM, Heron C, Cooper JM, Schapira AH (1994) Complex I inhibitors induce dose-dependent apoptosis in PC12 cells: relevance to Parkinson's disease. *J Neurochem* 63:1987–1990.
- Hartmann A, Hunot S, Hirsch EC (1998) CD95 (APO-1/Fas) and Parkinson's disease. *Ann Neurol* 44:425–426.
- Hartmann A, Hunot S, Michel PP, Muriel MP, Vyas S, Faucheux BA, Mouatt-Prigent A, Turmel H, Srinivasan A, Ruberg M, Evan GI, Agid Y, Hirsch E (2000) Caspase 3: a vulnerability factor and final effector in apoptotic cell death of dopaminergic neurons in Parkinson's disease. *Proc Natl Acad Sci USA* 97:2875–2880.
- Hartmann A, Troade J-D, Hunot S, Kikly K, Faucheux BA, Prigent A-M, Ruberg M, Agid Y, Hirsch EC (2001) Caspase 8 is an effector in apoptotic death of dopaminergic neurons in Parkinson's disease, but pathway inhibition results in neuronal necrosis. *J Neurosci* 21:2247–2255.
- Hassouna I, Wickert H, Zimmermann M, Gillardon F (1996) Increase in Bax expression in substantia nigra following 1-methyl-4-phenyl-1,2,3,6-tetrahydropyridine (MPTP) treatment of mice. *Neurosci Lett* 204:85–88.
- Hay BA, Wolff T, Rubin GM (1994) Expression of baculovirus P35 prevents cell death in *Drosophila*. *Development* 120:2121–2129.
- Hisahara S, Araki T, Sugiyama F, Yagami KI, Suzuki M, Abe K, Yamamura K, Miyazaki J, Momoi T, Saruta T, Bernard CC, Okano H, Miura M (2000) Targeted expression of baculovirus p35 caspase inhibitor in oligodendrocytes protects mice against autoimmune-mediated demyelination. *EMBO J* 19:341–348.
- Hughes AJ (1997) Clinicopathological aspects of Parkinson's disease. *Eur Neurol* 38[Suppl 2]:13–20.
- Izquierdo M, Grandien A, Criado LM, Robles S, Leonardo E, Albar JP, de Buitrago GG, Martínez-AC (1999) Blocked negative selection of developing T-cells in mice expressing the baculovirus p35 caspase inhibitor. *EMBO J* 18:156–166.
- Jellinger KA (2000) Cell death mechanisms in Parkinson's disease. *J Neural Transm* 107:1–29.
- Kirsch DG, Doseff A, Chau BN, Lim DS, de Souza-Pinto NC, Hansford R, Kastan MB, Lazebnik YA, Hardwick JM (1999) Caspase-3-dependent cleavage of Bcl-2 promotes release of cyt c. *J Biol Chem* 274:21155–21161.
- Kuemmerle S, Gutekunst CA, Klein AM, Li XJ, Li SH, Beal MF, Hersch SM, Ferrante RJ (1999) Huntington aggregates may not predict neuronal death in Huntington's disease. *Ann Neurol* 46:842–849.
- Kuida K, Zhen TS, Na S, Kuan C, Yang D, Karasuyama H, Rakic P, Flavell RA (1996) Decreased apoptosis in the brain and premature lethality in CPP-32 deficient mice. *Nature* 384:368–372.
- Kuida K, Haydar TF, Kuan CY, Gu Y, Taya C, Karasuyama H, Su MSS, Rakic P, Flavell RA (1998) Reduced apoptosis and cytochrome c-mediated caspase activation in mice lacking caspase 9. *Cell* 94:325–337.
- Kumar S (1999) Mechanisms mediating caspase activation in cell death. *Cell Death Differ* 6:1060–1066.
- Kuwana T, Smith JJ, Muzio M, Dixit V, Newmeyer DD (1998) Apoptosis induction by caspase 8 is amplified through the mitochondrial release of cytochrome c. *J Biol Chem* 273:16589–16594.
- Li H, Zhu H, Xu C, Yuan J (1998) Cleavage of BID by caspase 8 mediates the mitochondrial damage in the Fas pathway of apoptosis. *Cell* 94:491–501.
- Li P, Nijhawan D, Budihardjo I, Srinivasula SM, Ahmed M, Alnemri ES, Wang X (1997) Cytochrome c and dATP-dependent formation of apaf-1/caspase 9 complex initiates an apoptotic protease cascade. *Cell* 91:479–489.
- Luo X, Budihardjo I, Zou H, Slaughter C, Wang X (1998) Bid, a Bcl2 interacting protein, mediates cytochrome c release from mitochondria in response to activation of cell surface death receptors. *Cell* 94:481–490.
- Michel PP, Lambeng N, Rugerg M (1999) Neuropharmacological aspects of apoptosis: significance for neurodegenerative diseases. *Clin Neuropharmacol* 22:137–150.
- Mizuno Y, Yoshino H, Ikebe S, Hattori N, Kobayashi T, Shimoda-Matsubayashi S, Matsumine H, Kondo T (1998) Mitochondrial dysfunction in Parkinson's disease. *Ann Neurol* 44:99–109.
- Mochizuki H, Goto K, Mori H, Mizuno Y (1996) Histochemical detection of apoptosis in Parkinson's disease. *J Neurol Sci* 137:120–123.
- Núñez G, Benedict MA, Hu Y, Inohara N (1998) Caspases: the proteases of the apoptotic pathway. *Oncogene* 17:3237–3245.
- Offen D, Beart PM, Cheung NS, Pascoe CJ, Hochman A, Gorodin S, Melamed E, Bernard R, Bernard O (1998) Transgenic mice expressing human Bcl-2 in their neurons are resistant to 6-hydroxydopamine and 1-methyl-4-phenyl-1,2,3,6-tetrahydropyridine neurotoxicity. *Proc Natl Acad Sci USA* 95:5789–5794.
- Olanow CW, Tatton WG (1999) Etiology and pathogenesis of Parkinson's disease. *Annu Rev Neurosci* 22:123–144.
- Przedborski S, Jackson-Lewis V (1998) Mechanisms of MPTP toxicity. *Mov Disord* 13:35–38.
- Salvesen GS, Dixit VM (1997) Caspases: intracellular signaling by proteolysis. *Cell* 91:443–446.
- Sanchez I, Xu CJ, Joo P, Kakizaka A, Blenis J, Yuan J (1999) Caspase 8 is required for cell death induced by expanding polyglutamine repeats. *Neuron* 22:623–633.
- Schapira AH, Gu M, Taanman JW, Tabrizi SJ, Seaton T, Cleeter M, Cooper JM (1998) Mitochondria in the etiology and pathogenesis of Parkinson's disease. *Ann Neurol* 44:89–98.
- Schendel SL, Azimov R, Pawlowski K, Godzik A, Kagan BL, Reed JC (1999) Ion channel activity of the BH3 only Bcl-2 family member, BID. *J Biol Chem* 274:21932–21936.
- Slee EA, Harte MT, Kluck RM, Wolf BB, Casiano CA, Newmeyer DD, Wang HG, Reed JC, Nicholson DW, Alnemri ES, Green DR, Martin SJ (1999) Ordering the cytochrome c-initiated caspase cascade: hierarchical activation of caspases-2, -3, -6, -7, -8 and -10 in a caspase-9-dependent manner. *J Cell Biol* 144:281–292.
- Stadelmann C, Deckwerth TL, Srinivasan A, Bancher C, Brück W, Jellinger K, Lassmann H (1999) Activation of caspase-3 in single neurons and autophagic granules of granulovacuolar degeneration in Alzheimer's disease. Evidence for apoptotic cell death. *Am J Pathol* 155:1459–1466.
- Stennicke HR, Salvesen GS (2000) Caspases—controlling intracellular signals by protease zymogen activation. *Biochim Biophys Acta* 1477:299–306.
- Sugimoto A, Friesen PD, Rothman JH (1994) Baculovirus p35 prevents developmentally programmed cell death and rescues a *ced-9* mutant in the nematode *Caenorhabditis elegans*. *EMBO J* 13:2023–2028.
- Tang D, Lahti JM, Kidd VJ (2000) Caspase 8 activation and BID cleavage contribute to MCF7 cellular execution in a caspase 3-dependent manner during staurosporin-mediated apoptosis. *J Biol Chem* 275:9303–9307.
- Tatton NA, Kish SJ (1997) *In situ* detection of apoptotic nuclei in the substantia nigra compacta of 1-methyl-4-phenyl-1,2,3,6-tetrahydropyridine-treated mice using terminal deoxynucleotidyl transferase labeling and acridine orange staining. *Neuroscience* 77:1037–1048.
- Tatton NA, Maclean-Fraser A, Tatton WG, Perl DP, Olanow CW (1998) A fluorescent double-labeling method to detect and confirm apoptotic nuclei in Parkinson's disease. *Ann Neurol* 44:142–148.
- Thornberry NA, Lazebnik Y (1998) Caspases: enemies within. *Science* 281:1312–1316.
- Varfolomeev EE, Schuchmann M, Luria V, Chiannilkulchai N, Beckmann JS, Mett IL, Rebrikov D, Brodianski VM, Kemper OC, Kollet O, Lapidot T, Soffer D, Sobe T, Avraham KB, Goncharov T, Holtmann H,

- Lonai P, Wallach D (1998) Targeted disruption of the mouse caspase 8 gene ablates cell death induction by the TNF receptors, Fas/Apo1, and DR3 and is lethal prenatally. *Immunity* 9:267–276.
- Velier JJ, Ellison JA, Kikly KK, Spera PA, Barone FC, Feuerstein GZ (1999) Caspase-8 and caspase-3 are expressed by different populations of cortical neurons undergoing delayed cell death after focal stroke in the rat. *J Neurosci* 19:5932–5941.
- Viswanath V, Wu Z, Wei Q, Fonck C, Andersen JK (2000) Transgenic mice neuronally expressing baculoviral p35 are resistant to diverse types of induced apoptosis including seizure-associated neurodegeneration. *Proc Natl Acad Sci USA* 97:2270–2275.
- Wei MC, Zong W-X, Cheng EH-Y, Lindsen T, Panoutsakopoulou V, Ross AJ, Roth KA, MacGregor GR, Thompson CB, Korsmeyer SJ (2001) Proapoptotic BAX and BAK: a requisite gateway to mitochondrial dysfunction. *Science* 292:727–730.
- Wellington CL, Hayden MR (2000) Caspases and neurodegeneration: on the cutting edge of new therapeutic approaches. *Clin Genet* 57:1–10.
- West MJ, Slomianka L, Gundersen HJG (1991) Unbiased stereological estimation of the total number of neurons in the subdivisions of the rat hippocampus using the optical fractionator. *Anat Rec* 231:482–497.
- Wolf BB, Green DR (1999) Suicidal tendencies: apoptotic cell death by caspase family proteinases. *J Biol Chem* 274:20049–20052.
- Yang L, Matthews RT, Schulz JB, Klockgether T, Liao AW, Martinou JC, Penney Jr JB, Hyman BT, Beal MF (1998) 1-Methyl-4-phenyl-1,2,3,6-tetrahydropyridine neurotoxicity is attenuated in mice overexpressing Bcl-2. *J Neurosci* 18:8145–8152.
- Zheng TS, Hunot S, Kuida K, Flavell RA (1999) Caspase knockouts: matters of life and death. *Cell Death Differ* 6:1043–1053.
- Zhou Q, Krebs JF, Snipas SJ, Price A, Alnemri ES, Tomaselli KJ, Salvesen GS (1998) Interaction of the baculovirus anti-apoptotic protein p35 with caspases. Specificity, kinetics, and characterization of the caspase/p35 complex. *Biochemistry* 37:10757–10765.
- Ziv I, Offen D, Barzilai A, Haviv R, Stein R, Zilkha-Falb R, Shirvan A, Melamed E (1997) Modulation of control mechanisms of dopamine-induced apoptosis—a future approach to the treatment of Parkinson's disease? *J Neural Transm [Suppl]* 49:195–202.

Caspase-3: A vulnerability factor and final effector in apoptotic death of dopaminergic neurons in Parkinson's disease

EXHIBIT

39

Andreas Hartmann*, Stéphane Hunot*, Patrick P. Michel*, Marie-Paule Muriel*, Sheela Vyas†, Baptiste Annick Mouatt-Prigent*, Hélène Turmel*, Anu Srinivasan‡, Merle Ruberg*, Gerard I. Evan†, Yves Agid*, and Etienne C. Hirsch*[§]

*Institut National de la Santé et de la Recherche Médicale U 289, Hôpital de la Salpêtrière, 47 Boulevard de l'Hôpital, 75013 Paris, France; †Imperial Cancer Research Fund Laboratories, 44 Lincoln's Inn Field, London WC2A 3PX, United Kingdom; and ‡IDUN Pharmaceuticals Inc., 11085 North Pines Road, La Jolla, CA 92037

Communicated by Jean-Pierre Changeux, Institut Pasteur, Paris, France, December 20, 1999 (received for review August 20, 1999)

Caspase-3 is an effector of apoptosis in experimental models of Parkinson's disease (PD). However, its potential role in the human pathology remains to be demonstrated. Using caspase-3 immunohistochemistry on the postmortem human brain, we observed a positive correlation between the degree of neuronal loss in dopaminergic (DA) cell groups affected in the mesencephalon of PD patients and the percentage of caspase-3-positive neurons in these cell groups in control subjects and a significant decrease of caspase-3-positive pigmented neurons in the substantia nigra pars compacta of PD patients compared with controls that also could be observed in an animal model of PD. This suggests that neurons expressing caspase-3 are more sensitive to the pathological process than those that do not express the protein. In addition, using an antibody raised against activated caspase-3, the percentage of active caspase-3-positive neurons among DA neurons was significantly higher in PD patients than in controls. Finally, electron microscopy analysis in the human brain and *in vitro* data suggest that caspase-3 activation precedes and is not a consequence of apoptotic cell death in PD.

The pathological hallmarks of Parkinson's disease (PD) are a loss of dopaminergic (DA) neurons in the mesencephalon and the presence of Lewy bodies in altered neurons. The exact cause of this neuronal loss is still unknown, but recent human postmortem studies have suggested that, in PD, nigral DA neurons die by apoptosis (1–3) as do DA neurons in 1-methyl-4-phenyl-1,2,3,6-tetrahydropyridine (MPTP)-treated mice (4, 5), an *in vivo* model of PD. However, the significance of purely morphological human postmortem features suggestive of apoptosis remained controversial, and the results of investigations into molecular apoptotic markers in PD brains are awaited to confirm the morphologic studies (6).

Extensive *in vitro* studies in nonneuronal and neuronal cell systems indicate that aspartate-specific cysteine proteases (caspases) are effectors of apoptosis (7). In neurons, several lines of evidence indicate that caspase-3 (CPP32/Yama/Apopain), a 32-kDa cytosolic protein, plays a major role in the executive phase of apoptosis (8, 9). First, cerebral hyperplasia and cellular disorganization are observed in caspase-3-deficient mice (10). Second, neuronal death in experimental models of several acute and chronic neurodegenerative disorders has been associated with activation of caspase-3 (11–13). Third, with special reference to PD, neurotoxins commonly used to induce experimental parkinsonian syndromes, e.g., 1-methyl-4-phenylpyridinium (MPP⁺) and 6-hydroxydopamine (6-OHDA), have been shown to exert their proapoptotic actions via activation of caspase-3-like proteases in neuronal *in vitro* models (14–16). To date, however, cellular expression of caspase-3 has not been studied in postmortem brain from patients with PD or any other neurologic disorders. In the present study, we thus analyzed caspase-3

distribution and activation in PD and experimental models of the disease.

Materials and Methods

Patients and Human Brain Tissue. Mesencephalons were obtained at autopsy from five individuals with no known history of psychiatric or neurologic disorders (control group) and from five patients with histologically confirmed PD (PD group). Age at death and time interval from death to tissue fixation did not differ significantly between the control group [79.6 ± 9.6 years and 25.4 ± 6.4 hr, respectively (mean \pm SEM)] and the PD group (70.4 ± 5.3 years and 24.2 ± 5.8 hr, respectively). Within 2 hr of autopsy, tissue was dissected and processed as described previously (17).

For the quantitative caspase-3 analysis, free-floating, 40- μ m-thick sections taken at the level of the oculomotor nerve fibers were used. For the quantitative analysis using the CM1 antibody (18), four to five sections covering the whole extent of the substantia nigra pars compacta (SNpc) from its rostral to its caudal pole of four control and four parkinsonian patients were used. Finally, for the ultrastructural analysis using the CM1 antibody, SN tissue fixed according to a different protocol for electron microscopy (19) from one PD patient not included in the previous analysis was analyzed.

MPTP-Intoxicated Mice. Mice were intoxicated subchronically with MPTP as described elsewhere (5). In brief, 8-week-old male C57BL/6 mice were injected at a 30-mg/kg per day i.p. dosage over a period of 5 days and sacrificed after 21 days ($n = 6$). A control group was injected with equivalent volumes of 0.9% NaCl ($n = 6$). The animals were perfused with 4% paraformaldehyde, the brains were removed, and the mesencephalon was cut into 20- μ m-thick sections.

Primary Cultures of Rat Mesencephalon. Primary cultures of rat mesencephalon were prepared as described previously (20). Apoptosis was induced after 6 days of differentiation, with cell-permeant MPP⁺ (Sigma) at a concentration of 1 μ M. Cultures were fixed 12, 24, and 72 hr after initiation of treatment. All experiments were repeated six times.

Abbreviations: CGS, central gray substance; DA, dopaminergic; MPP⁺, 1-methyl-4-phenylpyridinium; MPTP, 1-methyl-4-phenyl-1,2,3,6-tetrahydropyridine; PD, Parkinson's disease; TH, tyrosine hydroxylase; SNpc, substantia nigra pars compacta; VTA, ventral tegmental area.

[§]To whom reprint requests should be addressed. E-mail: hirsch@ccr.jussieu.fr.

The publication costs of this article were defrayed in part by page charge payment. This article must therefore be hereby marked "advertisement" in accordance with 18 U.S.C. §1734 solely to indicate this fact.

Article published online before print: *Proc. Natl. Acad. Sci. USA*, 10.1073/pnas.040556599. Article and publication date are at www.pnas.org/cgi/doi/10.1073/pnas.040556599

Immunohistochemistry. Free-floating, 40- μ m-thick sections were pretreated as described previously (17) and incubated with a polyclonal rabbit antibody (1:250, 48 hr at 4°C) raised against amino acid residues ⁵¹NNKNFHKSTGMTSRSGT⁶⁷ located within the caspase-3 p20 subunit for quantitative analysis. In addition, trial experiments were conducted by using a rabbit polyclonal antibody (65906E; PharMingen; 1:250, 48 hr at 4°C) raised against recombinant human caspase-3-His6 as immunogen (21) (1:250, 48 hr at 4°C) or the CM1 antibody raised against the C terminus of the human p17 caspase-3 fragment, ¹⁶³CRGTELDGIEDT¹⁷⁵, specifically recognizing activated (cleaved) caspase-3 (18) (1:2,500, 48 hr at 4°C). The sections were revealed as described previously (19). Sequential double-labeling experiments were performed by using a rabbit polyclonal anti-ubiquitin antibody (Dako; 1:250, 48 hr at 4°C) and the anti-caspase-3 antiserum used for the quantitative analysis or the CM1 antibody as described (22). Because the two antigens were detected with a different localization within the cell, some sections were coincubated with the two antibodies (anti-ubiquitin and caspase-3 or CM1) at the same time for the illustrations. Similarly, mesencephalon sections from MPTP-treated and control mice first were incubated for 48 hr at 4°C with an anti-tyrosine hydroxylase (anti-TH) mouse mAb (1:500; Instar, Stillwater, MN), TH-positive neurons were localized and counted, and then sections were unstained and reincubated with a rabbit polyclonal antibody (67341A; PharMingen; 1:500, 48 hr at 4°C) recognizing murine procaspase-3, previously tested by Western immunoblotting (data not shown). Control experiments were performed in which one or the other of the primary antisera was omitted. No staining was observed under these conditions.

Fluorescent double-staining experiments were performed on mesencephalic sections mounted on gelatin-double-coated slides, as described previously (23), to analyze simultaneously caspase-3 and TH.

TH immunocytochemistry in primary cultures of rat mesencephalon was performed as described previously by using FITC as fluorochrome (20). Cultures then were incubated with the CM1 antibody at 1:2,500 for 24 hr at 4°C and revealed by using TRITC as fluorochrome. The cell-permeant fluorescent marker Hoechst 33258 (1 μ M; Boehringer Mannheim) was added to the cultures for 15 min at room temperature to assess the morphology of normal and apoptotic (i.e., condensed, fragmented) cells.

Western Immunoblotting. Specificity of the antibodies was analyzed on Western blots of human SN homogenates from control and parkinsonian patients. Homogenates of SNpc were fractionated, and the proteins (50 μ g) were separated by PAGE and transferred onto nitrocellulose membranes. Jurkat cell lysates (15 μ g) were used as positive control. To positively detect the cleaved p17 fragment of caspase-3 using the CM1 antibody, 15 μ g of Jurkat cell lysates was preincubated with 500 ng of human recombinant caspase-3 (PharMingen) for 60 min at 37°C. The membranes were incubated for 48 hr at 4°C with the caspase-3 polyclonal antibody (1:1,000) or the CM1 antibody (1:5,000) and revealed as described (23).

Electron Microscopy. Ultrastructural analysis of CM1-immunopositive DA neurons was performed as described previously with minor modifications (24).

Regional Quantification and Image Analysis. For each stained section, caspase-3-positive and -negative pigmented DA neurons were counted in the central gray substance (CGS), ventral tegmental area (VTA), and SNpc by using a computer-based image analysis system (VISIOSCAN; Biocom, Les Ulis) (19). The SNpc was subdivided into lateroventral, medioventral, and dorsal tiers according to the regional vulnerability of nigral DA neurons established by Fearnley and Lees (25). Because the

degree of neuronal loss and, thus, the absolute number of pigmented neurons varies between PD patients, the results were expressed as the percentage of pigmented neurons that were stained for caspase-3. For activated caspase-3 staining, immunoreactive DA neurons were counted exclusively in the SNpc without regional subdivisions because of the low numbers of immunoreactive neurons detected, which made a statistical analysis of SNpc subdivisions irrelevant. The total number of DA neurons in the mesencephalon was estimated as described previously (19), and the mean percentage of neuronal loss within the CGS, VTA, and SNpc in our sample was calculated. The total number of CM1-positive neurons in the SNpc was estimated by using the same method.

For the mice, the SNpc was delineated based on the distribution of TH-positive cells at identical levels for all mice and analyzed by using the same methodology as for the human postmortem sections.

Cultures were analyzed by phase-contrast and standard epillumination fluorescence microscopy and by computer-assisted image analysis (IMSTAR, Paris). Counting was performed at $\times 20$ in eight fields per horizontal axis and eight fields per vertical axis per well. Six wells were analyzed per experimental condition.

Statistical Analysis. Intergroup differences (control vs. PD) in the percentage of caspase-3 immunoreactive neurons were compared by Student's *t* test or, in the event of failure in normality test, by Mann-Whitney rank sum test. Correlations were determined by linear regression analysis.

Results

Specificity of Antibodies Directed Against the p20 Subunit of Human Caspase-3 and the Cleaved Caspase-3 p17 Subunit. On Western blots of proteins extracted from the SNpc of three control subjects and three PD patients, two bands were observed by using the antibody directed against the caspase-3 p20 subunit: a 32-kDa band corresponding to the caspase-3 precursor protein and a 30-kDa band representing the processed form of caspase-3 without its prodomain, as described by Kuida *et al.* (10) (Fig. 1A). No cleaved p10 or p20 caspase-3 fragments were detected either in control or in parkinsonian SNpc protein extracts. The same result was obtained by using the CM1 antibody with regard to pooled SNpc extracts from four parkinsonian patients, as well as untreated Jurkat cell lysates. However, when Jurkat cell lysates were preincubated with human recombinant caspase-3, a cleaved caspase-3 p17 subunit could readily be detected (Fig. 3A). On tissue sections, staining intensity decreased with lower antibody dilutions. No staining was observed when the primary antibody was omitted. Using a commercial antibody directed against caspase-3, an identical pattern of staining was observed on transverse mesencephalon sections from two control subjects and two PD patients (data not shown).

Immunohistochemical Detection of Caspase-3 in Control and Parkinsonian Mesencephalon. At the macroscopic level, caspase-3 immunostaining was observed in all mesencephalic subregions. Among DA cell groups, staining intensity was high in the SNpc (Fig. 1B), moderate in the VTA, and undetectable in the CGS. At the cellular level, both pigmented and nonpigmented neurons were stained. Immunoreactive glial cells were also observed in all mesencephalic subregions. Fluorescent double-staining experiments with caspase-3 and TH in control human mesencephalon sections evidenced the expression of caspase-3 in TH-immunoreactive neurons in the SNpc and VTA but not in the CGS. Whereas TH immunoreactivity was observed in cell perikarya and dendrites, caspase-3 immunoreactivity was confined to the cytosol of the neuronal perikarya (Fig. 1 C and D).

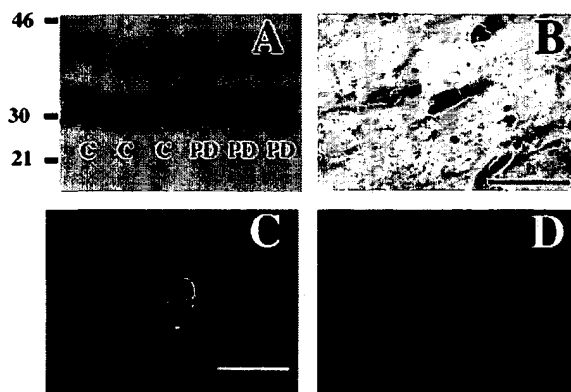


Fig. 1. Characterization of caspase-3 staining. (A) Specificity of the anti-caspase-3 p20 polyclonal rabbit antibody. Western immunoblot of caspase-3 from 50 µg of SNpc protein extracted from three control and three parkinsonian mesencephalons after SDS/PAGE. Molecular mass markers in the first lane are given in kDa and allow identification of caspase-3 protein at molecular masses of 32 kDa (including prodomain) and 30 kDa (without prodomain). (B) High-power photomicrograph showing cytosolic caspase-3 immunostaining of SNpc neuromelanin-containing neurons in transverse sections of control SNpc. (C and D) Immunofluorescent dopaminergic neurons in transverse SNpc sections of a control subject stained with a caspase-3 polyclonal rabbit antibody revealed by fluorescein (C) and a TH monoclonal mouse antibody revealed by rhodamine₆₆₀ (D). Whereas caspase-3 immunoreactivity is confined to the cytosol, TH staining can be observed in the perikarya and dendrites. The middle portion of the neuron is occupied by neuromelanin. (Bars = 30 µm.)

Quantitative Analysis of Caspase-3-Positive Pigmented Neurons in the SNpc and VTA of Control and PD Patients. The mean total numbers (\pm SEM) of caspase-3-positive and -negative melanized neurons in the SNpc and VTA of controls and PD patients are given in Table 1. A variable percentage of caspase-3-positive neurons was observed within the different mesencephalic catecholaminergic cell groups in the mesencephalon of control subjects. These percentages showed a positive linear regression with the degree of neuronal loss within the CGS, VTA, and SNpc (df: 1; $r = 0.997$; $P < 0.001$), suggesting that expression of caspase-3 in certain populations of DA neurons may contribute to their vulnerability in this neurodegenerative disorder. This finding was in line with the reduced percentage of pigmented neurons that were caspase-3-immunoreactive in the SNpc of patients with PD ($10.8 \pm 2.4\%$) as compared with control subjects ($45.2 \pm 3.8\%$) ($P < 0.001$). In contrast, there was no statistically significant difference between these percentages in the VTA (controls: $15.8 \pm 3.9\%$; PD: $17.0 \pm 7.0\%$), which is less affected in PD (17). The percentage of caspase-3-positive neurons among pigmented neurons was also analyzed in subsectors of the SNpc. It was significantly lower in PD patients than in controls in the lateroventral part ($P < 0.001$) (controls: $68.4 \pm 5.5\%$; PD: $3.8 \pm 3.8\%$), in the medioventral part ($P < 0.006$) (controls: $30.4 \pm$

Table 1. Analysis of caspase-3-positive and caspase-3-negative neurons in PD

| Group | No. (mean \pm SEM) of melanized caspase-3-positive neurons | | No. (mean \pm SEM) of melanized caspase-3-negative neurons | |
|---------|--|------------|--|--------------|
| | SNpc | VTA | SNpc | VTA |
| Control | 388 \pm 77 | 20 \pm 7 | 442 \pm 43 | 120 \pm 47 |
| PD | 7 \pm 2 | 3 \pm 1 | 68 \pm 15 | 16 \pm 4 |



Fig. 2. High-power photomicrograph showing Lewy bodies stained for ubiquitin (single arrow) and caspase-3 (triple arrows) in a SNpc neuromelanin-containing (thick arrow) neuron in a transverse section of PD SNpc. Note that ubiquitin-containing fibers and extraneuronal melanin can be seen. (Bar = 30 µm.)

4.9%; PD: $7.4 \pm 3.8\%$), and in the dorsal part ($P < 0.001$) (controls: $47.2 \pm 4.2\%$; PD: $12.4 \pm 3.6\%$).

An analysis of Lewy body-containing DA neurons detected by anti-ubiquitin staining within the SNpc of the five PD patients revealed that $52.5 \pm 4.0\%$ of the neurons containing Lewy bodies were also immunoreactive for caspase-3 (Fig. 2). This percentage was significantly higher than the overall percentage of caspase-3-positive neurons among all DA neurons ($10.8 \pm 2.4\%$) in the same group of PD patients ($P < 0.001$).

Quantitative Analysis of Caspase-3-Positive DA Neurons in the SNpc of MPTP-Treated and Control Mice. To test whether similar decreases in caspase-3 immunoreactivity in DA neurons could be observed in an animal model of PD, C57BL/6 mice were treated with a subchronic regimen of MPTP reported to induce apoptotic degeneration of DA SNpc neurons (5) and sacrificed after 21 days when the degeneration process of DA neurons is completed (data not shown). The MPTP group had a significantly lower percentage of caspase-3-positive neurons among TH-positive neurons ($53.0 \pm 3.7\%$) than control mice ($67.7 \pm 2.4\%$) ($P = 0.008$).

Quantitative Analysis of Activated, Caspase-3-Positive Pigmented Neurons in the SNpc of Control and PD Patients. Using an antibody directed against the C terminus of the p17 fragment of caspase-3 (CM1) and, thus, specific for the activated form of caspase-3 (Fig. 3 B–E), we observed 13.6 ± 1.7 CM1-positive, melanized neurons per SNpc section in control subjects and 7.2 ± 1.1 in PD patients. In the SNpc, based on the estimated total numbers, the proportion of DA neurons that were CM1-positive was significantly higher in PD patients than in control subjects (PD: $6.5 \pm 3.9\%$; controls: $1.2 \pm 0.2\%$; Mann–Whitney rank sum test: $P = 0.03$). Occasionally, it was possible to detect activated caspase-3 in Lewy body-containing neurons (Fig. 3F).

Electron Microscopy Analysis of Nigral DA Neurons Expressing Activated Caspase-3 in PD. Cytosolic, activated caspase-3 staining was observed in DA SNpc neurons at the ultrastructural level. These neurons typically exhibited a condensed perinuclear endoplasmic reticulum (ER) that was suggestive of increased protein synthesis (Fig. 4A). DA neurons displaying classical morphological features of apoptosis, i.e., chromatin condensation, were CM1-negative (Fig. 4B). Finally, dopaminergic neurons negative for CM1 and without apoptotic features did not display dense perinuclear ER aggregates (Fig. 4C).

Does Caspase-3 Activation Precede Cell Death in Primary DA Cultures Treated with MPP⁺? To test whether caspase-3 activation precedes morphological features of apoptosis as suggested by our electron microscopy study, low concentrations (1 µM) of MPP⁺, reported to induce apoptosis, were applied in primary DA neurons (14).



Fig. 3. Characterization of CM1 staining. (A) Specificity of the anti-CM1 polyclonal rabbit antibody. Western immunoblot of activated caspase-3 from 50 μ g of SNpc protein extracted from four parkinsonian mesencephalons (lane a), 15 μ g of untreated Jurkat cell lysate (lane b), and 15 μ g of Jurkat cell lysate preincubated with 500 ng of human recombinant caspase-3 for 60 min at 37°C (lane c) after SDS/PAGE. Molecular mass markers in the first lane are given in kDa and allow identification of the cleaved p17 subunit at molecular masses of 17 kDa in lane c (A). Note that in the homogenate of the parkinsonian SNpc, activated caspase-3 is not detectable because of its presence in only a few cells. (B–D) High-power photomicrograph showing cytosolic-activated caspase-3 immunostaining (CM1 antibody) of SNpc neuromelanin-containing neurons in transverse sections of control SNpc. (E) High-power photomicrograph showing Lewy bodies stained with antiubiquitin (arrow) and co-CM1 immunostaining of SNpc neuromelanin-containing neurons in transverse sections of PD SNpc. Note the presence of both Lewy bodies and CM1 staining in a single neuron. (Bar = 30 μ m.)

Cultures fixed 12 hr after treatment showed a significantly higher percentage of CM1-positive neurons among TH-positive neurons ($32.4 \pm 3.6\%$) than control cultures ($13.1 \pm 3.3\%$) ($P = 0.004$) whereas neuronal cell loss represented only 3.8% at this time point. After 24 hr, this percentage of CM1-positive neurons was lower but still significantly higher ($P = 0.015$) in the MPP⁺-treated cultures ($13.9 \pm 1.2\%$) than in the control cultures ($8.4 \pm 1.4\%$) whereas neuronal cell loss represented 18.8%. Finally, at 72 hr after treatment, this percentage was even higher in the control cultures ($7.9 \pm 1.7\%$) than in the MPP⁺-treated cultures ($4.6 \pm 3.0\%$). At this time, neuronal loss reached 78.5%. Concomitant Hoechst 33258 staining did not allow DNA condensation to be detected in CM1-positive DA neurons after 12 hr of MPP⁺ treatment (Fig. 5 A–C). In contrast, DNA condensation within DA neurons was observed after 72 hr and accompanied by CM1 staining (Fig. 5 D–F).

Discussion

Caspase-3 Is Expressed in Postmitotic DA Neurons. Activation of caspase-3 has been reported in several models of neuronal apoptosis *in vitro* or *in vivo* (11–13), but only one study has reported caspase-3 expression in the human central nervous system (21). In the present study, almost half of the pigmented DA neurons expressed caspase-3, indicating that proapoptotic effectors indeed are present in a latent state and do not require to be newly synthesized should a proapoptotic pathway be engaged. This is in agreement with recent *in vitro* studies showing that caspase-3 activation in various neuronal cell death paradigms is posttranscriptional (26, 27).

Caspase-3 May Be a Vulnerability Factor for Pigmented DA Neurons. A relationship between the presence of caspase-3 in DA neurons and their sensitivity to PD is supported by the analysis of the different catecholaminergic cell groups in the control mesencephalon. Indeed, a positive correlation between the estimated percentage of caspase-3-positive neurons among pigmented neurons in the CGS, VTA, and SNpc in control subjects and the percentage loss of pigmented neurons in these regions in PD was shown in our study (19). Such a relationship also was observed in the subregions of the SNpc, but only partially. Whereas the highest percentage of caspase-3-positive neurons was observed in the lateroventral part of the structure (68.4%), where neuronal loss is most severe in PD [91% according to Fearnley and

Lees (25)], it is higher in the dorsal part of the SNpc (47.2%) than in the ventromedial part (30.4%), where neuronal loss is 56% and 71%, respectively. This apparent discrepancy may be due either to differences in delineation of the SNpc subregions or to the presence of additional factors in one of these subregions (28). Of course, these speculative arguments leave the possibility open that, within the SNpc, the distribution of caspase-3 does not contribute to regional vulnerability. Alternatively, the regional vulnerability of DA neurons in the parkinsonian SNpc probably observes a more complex distribution (29) than reported initially by Fearnley and Lees (25). The relationship between the presence of caspase-3 in DA neurons and their sensitivity to PD is supported further by a 76% decrease in melanized SNpc neurons that are caspase-3-positive in PD patients compared with controls. A significant, 22% decrease of DA neurons expressing caspase-3 also was observed in mice subchronically intoxicated with MPTP. Yet, this decrease was less pronounced than in the human sample. This is probably due to the less severe degeneration of DA neurons in the SNpc in mice (20%) compared with that observed in PD patients (85%). Furthermore, the percentage of caspase-3-positive neurons was increased 3.9-fold in Lewy body-containing DA neurons as compared with DA neurons without Lewy bodies. Given the suggestion that the presence of Lewy bodies represents an indicator of neuronal suffering and/or damage (30) and the fact that incidental Lewy body disease is considered by some authors to be a presymptomatic form of PD (31), the increased expression of caspase-3 in Lewy body-containing neurons is in line with the hypothesis that caspase-3 is a probable effector of apoptotic cell demise. Taken together, these findings suggest that caspase-3-expressing neurons are particularly prone to degenerate in PD if caspase-3 is activated during the course of the disease. However, it should be emphasized that term “vulnerability factor” is based on a probabilistic rather than deterministic definition. Because about 50% of neurons that degenerate in PD do not express caspase-3 in control SNpc neurons—at least on a detectable scale—our assumption is that the presence or absence of caspase-3 does not dictate cell fate but may, however, be a necessary cofactor for eventual cell death. Furthermore, the presence in control subjects of caspase-3 in DA cell groups that are more susceptible in PD and its absence in cell groups that are preserved in PD also reinforces this notion. However, this argument is purely correlative and does not exclude that another effector caspase, such as

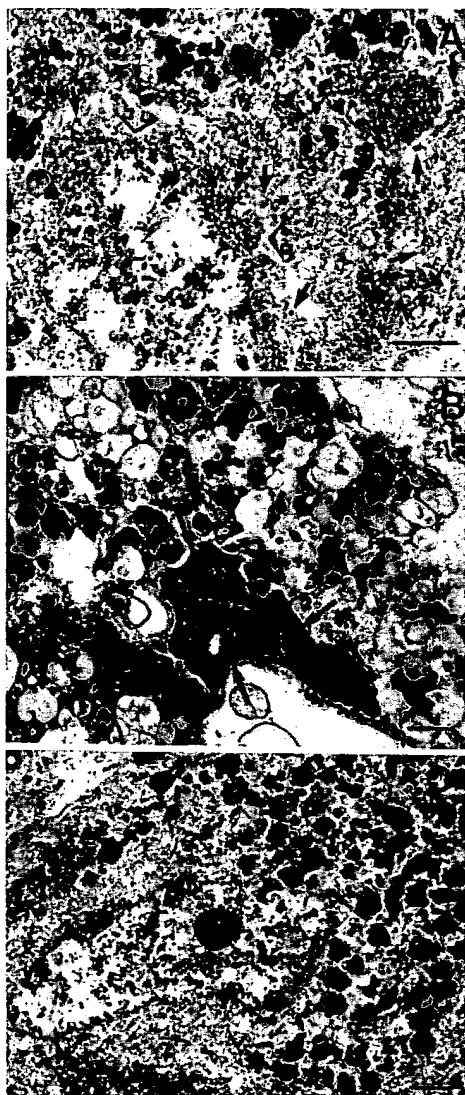


Fig. 4. Electron microscopy photomicrograph of PD SNpc showing melanized dopaminergic neurons recognizable by their neuromelanin-containing vesicles: with cytosolic precipitates (thin arrows) corresponding to activated caspase-3 staining (CM1 antibody) [A; note the dense perinuclear endoplasmic reticulum (thick arrows)]; with apoptotic morphology including chromatin condensation (arrows) (B; note that no CM1 staining can be detected); and displaying neither morphological features of apoptosis nor CM1 staining (C; note that the endoplasmic reticulum is less dense than in Fig. 5A). (Bars = 1 μ m.)

caspase-7, may substitute for caspase-3 in a subset of DA neurons during the apoptotic process.

The Percentage of Activated Caspase-3-Positive Nigral DA Neurons Is Increased in PD. CM1-positive DA neurons were detected both in PD and in control SNpc. Their absolute number per section was higher in control than in PD mesencephalons. However, if the mean estimated total number of CM1-positive DA neurons per section was corrected for the mean estimated total number of TH-positive neurons, the relative percentage of CM1-positive neurons was about five times higher in the PD group. In both groups, these numbers probably reflect a perimortem phenomenon related to hypoxia secondary to the patients' agonal state. Indeed, *in vitro* data show that hypoxia is a potent stimulator of apoptotic death in neurons (32). The number of activated caspase-3 neurons is in agreement with previous studies showing

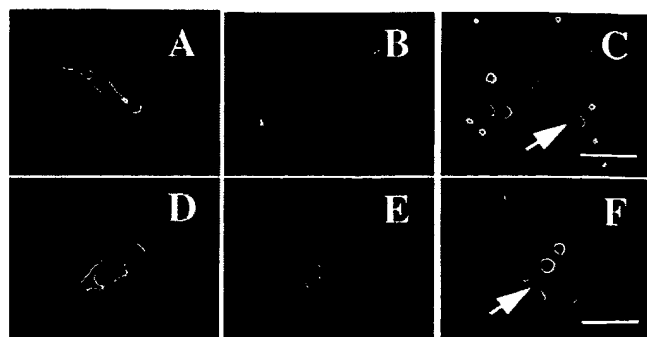


Fig. 5. Immunofluorescent dopaminergic neurons in primary cultures of rat mesencephalic neurons fixed after 12 hr of 1- μ M MPP⁺ treatment stained with a TH monoclonal mouse antibody revealed by FITC (A) and a rabbit polyclonal antibody recognizing activated caspase-3 (CM1) revealed by tetramethylrhodamine B isothiocyanate (B). Hoechst 33258 staining reveals an intact nucleus in this neuron (C, arrow). (Bar = 20 μ m.) In contrast, in a TH-positive neuron (D) with CM1 staining (E), DNA condensation assessed by Hoechst 33258 can be detected after 72 hr of MPP⁺ treatment (F, arrow). Note that a higher magnification was used to show DNA condensation. (Bar = 10 μ m.)

that the number of DA neurons undergoing apoptosis at the time of death is around 1–2% in control and 5–6% in PD brains (1, 2, 33, 34). Given the slow rate of neuronal degeneration in PD, especially at an advanced stage of the disease, as encountered in our sample, it is unlikely that this relatively high percentage reflects a primary disease process. Thus, it is likely that nigral DA neurons in parkinsonian brains already are altered and have a higher vulnerability to apoptosis in response to deleterious stimuli, e.g., hypoxia. In this context, one recent human post-mortem study has shown that in control brains, the number of terminal deoxynucleotidyltransferase-mediated dUTP-biotin 3' end labeling (TUNEL)-positive neurons was correlated with tissue pH, taken as an index of perimortem hypoxia in control subjects (2). Furthermore, it should be noted that if CM1 immunoreactivity reflects caspase-3 activation, the latter does not necessarily correlate with an eventual apoptotic cell death (35).

Caspase-3 Activation Probably Precedes and Does Not Cooccur with Chromatin Condensation During Apoptosis. A key question related to the increased proportion of neurons expressing activated caspase-3 in the parkinsonian SNpc is to know whether caspase-3 activation is associated with cell death or a consequence of it. This issue was addressed by experiments performed on post-mortem material and cell cultures. Using the CM1 antibody, electron microscopy did not reveal any staining in DA neurons exhibiting classic morphological features of apoptosis such as chromatin condensation. In contrast, those DA neurons that were immunoreactive for CM1 typically showed a dense perinuclear ER suggestive of increased protein synthesis. DA neurons negative for CM1 and without apoptotic features did not display dense perinuclear ER aggregation. Because protein synthesis has been shown to be a common although not necessary feature of neuronal apoptosis (36–38), we suggest that caspase-3 activation in these neurons marks the beginning of the effector phase of apoptosis. However, once the program has been completed, activated caspase-3 can no longer be detected, possibly because of degradation of the protease itself.

Low-Dose MPP⁺ Activates Caspase-3, Which Precedes Chromatin Condensation During Apoptosis. The ultrastructural findings in the human postmortem brain are supported by the present *in vitro* data showing that caspase-3 is activated early in the course of DA cell death after treatment with a low concentration of MPP⁺.

Concomitant DNA condensation as assessed by Hoechst 33258 staining can be observed only in late stages of cell demise and probably reflects the transition from caspase activation to cell death. The reason why CM1 staining still can be detected in cells displaying signs of nuclear fragmentation in DA cell cultures compared with the ultrastructural postmortem analysis may be related to the mode of identification of DA neurons: in culture, TH positivity is required for phenotypical identification, which implies at least basic cell viability and, thus, overall enzymatic activity, whereas human DA neurons are identified by their neuromelanin content, the presence of which is not related to cell viability. DA neurons positive for CM1 in the control condition constitute, independently of the time of analysis, around 10% of all DA neurons. This caspase-3 activation probably reflects spontaneous cell death related to astrocytic factors, which results in the death of about 80% of all DA neurons within the first 10 days of culture, representing a mean loss of 8% of cells per day (39) and, therefore, is in agreement with the present data on CM1 immunoreactivity. The finding that caspase-3 activation precedes DNA condensation suggests that it is not a consequence of cell death but associated with this process. Thus, caspase-3 activation after MPP⁺ intoxication strengthens the changes observed postmortem in a PD model open to experimental manipulation. This also appears important because caspase-3 activation in experimental PD models so far has relied on inhibitor studies, which are unable to demonstrate

unambiguously specific caspase-3 activation (14, 16). The caspase inhibitor most widely used to block caspase-3, zDEVD-CHO, also inhibits caspase-7 potently (40).

In conclusion, although activation of several distinct upstream pathways may lead to degeneration of nigral DA neurons, caspase-3 may represent a common integration point and, thus, may constitute an attractive target for antiapoptotic therapy in PD. In this context, it is interesting to note that caspase-3 activation precedes chromatin condensation and the final breakdown of the cell, a stage at which neuroprotective strategies are likely to fail. However, at present, potential side effects induced by the use of caspase inhibitors, such as neoplasia formation and the induction of autoimmune disorders, must be taken into consideration unless cell-specific drug targeting can be achieved. Furthermore, the long-term viability and functionality of DA neurons potentially rescued by caspase inhibitors remain to be determined.

This study was supported by Institut National de la Santé et de la Recherche Médicale and the National Parkinson Foundation, Inc., Miami. A.H. is a postdoctoral fellow of the Deutsche Forschungsgemeinschaft. S.H. is a fellow of the Fondation pour la Recherche Médicale. P.P.M. is supported by Pierre Fabre Laboratories, Paris. B.A.F. is supported by the Association Claude Bernard pour la Recherche Biologique et Médicale dans les Hôpitaux de l'Assistance Publique à Paris.

- Anglade, P., Vyas, S., Javoy-Agid, F., Herrero, M. T., Michel, P. P., Marquez, J., Mouatt-Prigent, A., Ruberg, M., Hirsch, E. C. & Agid, Y. (1997) *Histol. Histopathol.* **12**, 25–31.
- Kingsbury, A. E., Mardsen, C. D. & Foster, O. J. (1998) *Mov. Disord.* **13**, 877–884.
- Tatton, N. A., Malleau-Fraser, A., Tatton, W. G., Perl, D. P. & Olanow, C. W. (1998) *Ann. Neurol.* **44**, Suppl. 1, 142–148.
- Spooren, W. P. J. M., Gentsch, C. & Wiessner, C. (1998) *Neuroscience* **85**, 649–651.
- Tatton, N. A. & Kish, S. (1997) *Neuroscience* **77**, 1037–1048.
- Burke, R. E. & Kholodilov, N. C. (1998) *Ann. Neurol.* **44**, Suppl. 1, 126–133.
- Cohen, G. M. (1997) *Biochem. J.* **326**, 1–16.
- Nicholson, D. W., Ali, A., Thornberry, N. A., Vaillancourt, J. P., King, C. K., Gallant, M., Gareau, Y., Griffin, P. R., Labelle, M., Lazebnik, Y. A., et al. (1995) *Nature (London)* **376**, 37–43.
- Tewari, M., Quan, L. T., O'Rourke, K., Desnoyers, S., Zeng, Z., Beidler, D. R., Poirier, G. G., Salvesen, G. S. & Dixit, V. M. (1995) *Cell* **81**, 801–809.
- Kuida, K., Zheng, T. S., Na, S., Kuan, C., Yang, D., Karasuyama, H., Rakic, P. & Flavell, R. A. (1996) *Nature (London)* **384**, 368–372.
- Bergeron, L. & Yuan, J. (1998) *Curr. Opin. Neurobiol.* **8**, 55–63.
- Pettmann, B. & Henderson, C. E. (1998) *Neuron* **20**, 633–647.
- Schulz, J. B., Weller, M. & Moskowitz, M. A. (1999) *Ann. Neurol.* **45**, 421–429.
- Dodel, R. C., Du, Y., Bales, K. R., Ling, Z. D., Carvey, P. M. & Paul, S. M. (1998) *Neuroscience* **86**, 701–707.
- Dodel, R. C., Du, Y., Bales, K. R., Ling, Z., Carvey, P. M. & Paul, S. M. (1999) *Brain Res. Mol. Brain Res.* **64**, 141–148.
- Lotharius, J., Dugan, L. L. & O'Malley, K. L. (1999) *J. Neurosci.* **19**, 1284–1293.
- Hirsch, E. C., Graybiel, A. M. & Agid, Y. (1988) *Nature (London)* **334**, 345–348.
- Srinivasan, A., Roth, K. A., Sayers, R. O., Shindler, K. S., Wong, A. M., Fritz, L. C. & Tomaselli, K. J. (1998) *Cell Death Differ.* **5**, 1004–1016.
- Hunot, S., Brugg, B., Ricard, D., Michel, P. P., Muriel, M. P., Ruberg, M., Faucheux, B. A. & Hirsch, E. C. (1997) *Proc. Natl. Acad. Sci. USA* **94**, 7531–7536.
- Michel, P. P. & Agid, Y. (1996) *J. Neurochem.* **67**, 1633–1642.
- Krajewska, M., Wang, H. G., Krajewski, S., Zapata, J., Shabaik, A., Gascoyne, R. & Reed, J. C. (1997) *Cancer Res.* **57**, 1605–1613.
- Mouatt-Prigent, A., Karlsson, J. O., Agid, Y. & Hirsch, E. C. (1996) *Neuroscience* **73**, 979–987.
- Hunot, S., Dugas, N., Faucheux, B., Hartmann, A., Tardieu, M., Debre, P., Agid, Y., Dugas, B. & Hirsch, E. C. (1999) *J. Neurosci.* **19**, 3440–3447.
- Anglade, P., Mouatt-Prigent, A., Agid, Y. & Hirsch, E. C. (1996) *Neurodegeneration* **5**, 121–128.
- Fearnley, J. M. & Lees, A. J. (1991) *Brain* **114**, 2283–2301.
- Du, Y., Bales, K. R., Dodel, R. C., Hamilton-Byrd, E., Horn, J. W., Czilli, D. L., Simmons, L. K., Ni, B. & Paul, S. M. (1997) *Proc. Natl. Acad. Sci. USA* **94**, 11657–11662.
- Jeon, B. S., Kholodilov, N. G., Oo, T. F., Kim, S. Y., Tomaselli, K. J., Srinivasan, A., Stefanis, L. & Burke, R. E. (1999) *J. Neurochem.* **73**, 322–333.
- Yamada, T., McGeer, P. L., Baimbridge, K. G. & McGeer, E. G. (1990) *Brain Res.* **526**, 303–307.
- Damier, P., Hirsch, E. C., Agid, Y. & Graybiel, A. M. (1999) *Brain* **122**, 1437–1448.
- Lang, A. E. & Lozano, A. M. (1998) *N. Engl. J. Med.* **339**, 1044–1053.
- Jenner, P. & Olanow, C. W. (1998) *Ann. Neurol.* **44**, Suppl. 1, 72–84.
- Nath, R., Probert, A., Jr., McGinnis, K. M. & Wang, K. K. W. (1998) *J. Neurochem.* **71**, 186–195.
- Anglade, P., Vyas, S., Hirsch, E. C. & Agid, Y. (1997) *Histol. Histopathol.* **12**, 603–610.
- Tompkins, M. M., Basgal, E. J., Zamrini, E. & Hill, W. D. (1997) *Am. J. Pathol.* **150**, 119–131.
- Cosulich, S. C., Savory, P. J. & Clarke, P. R. (1999) *Curr. Biol.* **9**, 147–150.
- Schulz, J. B., Weller, M. & Klockgether, T. (1996) *J. Neurosci.* **15**, 4696–4706.
- Armstrong, R. C., Aja, T. J., Hoang, K. D., Gaur, S., Bai, X., Alnemri, E. S., Litwack, G., Karanewsky, D. S., Fritz, L. C. & Tomaselli, K. J. (1997) *J. Neurosci.* **17**, 553–562.
- Du, Y., Dodel, R. C., Bales, K. R., Hamilton-Byrd, E. & Paul, S. M. (1997) *J. Neurochem.* **69**, 1382–1388.
- Michel, P. P., Marien, M., Ruberg, M., Colpaert, F. & Agid, Y. (1999) *J. Neurochem.* **72**, 2074–2082.
- Garcia-Calvo, M., Peterson, E. P., Leiting, B., Ruel, R., Nicholson, D. W. & Thornberry, N. (1998) *J. Biol. Chem.* **273**, 32608–32613.

BASIC RESEARCH STUDIES

Differential proteolytic activity and induction of apoptosis in fibrous versus atheromatous plaques in carotid atherosclerotic disease

Theresa Jacob, PhD,^a Enrico Ascher, MD,^a Anil Hingorani, MD,^a Yevgeniy Khandros,^a Boris Tsemekhin, MD,^a Linda Zeien, MD,^b and Yilmaz Gunduz, MD,^a Brooklyn, NY

Purpose: Atherosclerotic plaque instability may be a contributing factor to plaque complications, such as rupture, thrombosis, and embolization. Of the two types of plaques, atheromatous and fibrous, the atheromatous type has been reported to be vulnerable and unstable. This instability may be related to changes in the cell cycle and extracellular matrix degradation. Apoptosis may weaken the plaque structurally. In addition, alteration of the cellular component may lead to imbalances in associated proteolytic activity. Our study was designed to compare the two types of plaques in terms of apoptosis, apoptosis-inducing factors, namely Fas/CD95/APO-1 and CPP-32/YAMA/caspase-3, and proteolytic activity.

Methods: Carotid artery plaques were obtained from patients undergoing endarterectomy and were classified as either atheromatous or fibrous on the basis of established criteria. Histologic study included hematoxylin and eosin staining, Verhoeff's van Gieson elastin staining, and trichrome staining. Detection of apoptosis was performed with the TUNEL assay. Immunohistochemical studies were performed to localize the expression of CPP-32/YAMA and Fas/CD95. Gelatin gel zymography was used to compare proteolytic activity levels in the two types of plaque.

Results: Apoptosis was significantly higher ($P < .001$) in atheromatous plaques ($4.90\% \pm 1.27\%$ [SEM]) as compared with fibrous plaques ($0.86\% \pm 0.46\%$ [SEM]). Zymography demonstrated elevated levels of proteinases in atheromatous plaques. Immunohistochemistry revealed significant increases in the expression of Fas/CD95 ($P < .04$) and CPP-32/YAMA ($P < .001$) in atheromatous plaques as compared with that in fibrous plaques.

Conclusions: This is the first study comparing molecular factors that render atheromatous plaques more susceptible to rupture than fibrous plaques. The higher number of apoptotic cells seen in atheromatous plaques as compared with fibrous plaques could contribute to their greater instability. Immunoreactivity to cytoplasmic death domain, Fas/CD95 and CPP-32/YAMA, a prominent mediator of apoptosis, was consistent with the numbers of apoptotic cells detected. The increased levels of proteolytic activity in atheromatous plaques may make these plaques more prone to rupture. These data identifying some of the molecular events and biochemical pathways associated with plaque vulnerability may help in the development of new strategies to prevent plaque rupture. (J Vasc Surg 2001;33:614-20.)

In carotid atherosclerotic disease, fibrous and atheromatous plaques have exhibited different levels of stability.¹⁻³ Fibrous plaque is made up of more than 70% collagen-rich tissue that is thought to stabilize and prevent rupture,⁴ whereas atheromatous plaques, characterized by having high lipid content, thin fibrous cap, and abundant macrophages, are known for their instability.⁵ Although data support the clinical differences between these two

types of plaques, few studies have investigated the different types of plaques by use of modern biochemical and molecular biological techniques.

Previous studies by us, as well as by others,^{6,7} have demonstrated increased levels of apoptosis and signaling molecules of the apoptotic cascade in atherosclerotic plaques as compared with normal arterial tissue. Specifically, changes in the expression of the members of the Bcl-2 family, p53, MDM2, CPP-32, and cyclin D1 have been reported.⁶⁻⁹ It has been proposed that apoptosis, especially of the smooth muscle cells (SMCs) in the fibrous cap and the underlying media, weakens the plaque structurally to the point of rupture whereas death of macrophages and that of other cells contribute to the formation of soft plaque cores and therefore make them vulnerable.¹⁰⁻¹² However, the magnitude of apoptosis and the signaling molecules involved in apoptosis in fibrous versus atheromatous plaques have not been examined.

Plaque rupture may also be affected by the stability of extracellular matrix (ECM). Remodeling of the arterial

From the Division of Vascular Surgery^a and the Department of Pathology,^b Maimonides Medical Center.

Competition of interest: nil.

Supported by a grant from Maimonides Research and Development Foundation.

Presented at the Annual Meeting of Society for Clinical Vascular Society, Rancho Mirage, Calif, March 18, 2000.

Reprint requests: Enrico Ascher, MD, Division of Vascular Surgery, Maimonides Medical Center, 4802 10th Ave, Brooklyn, NY 11219.

Copyright © 2001 by The Society for Vascular Surgery and The American Association for Vascular Surgery

0741-5214/2001/\$35.00 + 0 24/6/111802

doi:10.1067/mva.2001.111802

ECM¹³ occurs during all phases of human atherosclerosis and is a process regulated at the levels of both synthesis and degradation of matrix components. The macrophages and T-cells associated with chronic inflammation are known to secrete cytokines that can stimulate the production of metalloproteinases in the neighboring SMCs and endothelial cells. Elevated levels of proteolytic activity can cause an increase in ECM degradation and affect plaque stability.¹⁴⁻²⁰ However, there is no report comparing proteolytic activity in vulnerable atheromatous plaques and stable fibrous plaques.

This study was performed to determine potential factors that may predispose atheromatous and fibrous plaques to rupture. Degree of apoptosis, along with the levels of known inducers of apoptosis, Fas/CD95/APO-1 and CPP-32/YAMA/caspase-3, were compared between the two types of plaque. Proteolytic activity was examined in fibrous and atheromatous plaques with the goal of observing differences that may explain varying plaque stability between fibrous and atheromatous plaques.

MATERIALS AND METHODS

Patients. Two hundred consecutive patients, admitted for primary carotid endarterectomy to the vascular surgery division of Maimonides Medical Center between April 1998 and February 1999 were considered for this study. Institutional Review Board approval was obtained for procurement of specimens, and all patients gave informed written consent for the study. These carotid endarterectomy specimens were stained by hematoxylin and eosin and screened for type of plaque by an anatomic pathologist (L.Z.) blinded to the clinical symptoms and identity of each patient. Only five of the specimens were found to be fibrous, whereas the rest were atheromatous by standard criteria.^{17,20} The definition of fibrous plaque was a complete lack of histologically identifiable atheroma (macrophages and cholesterol). These plaques were made up of only fibrous tissue. The five fibrous plaques and eight randomly selected atheromatous plaques were chosen for the study.

Preoperative imaging. All patients underwent preoperative carotid artery duplex ultrasound scanning. Carotid artery duplex scanning was performed by registered vascular technologists at a laboratory accredited by the Intersocietal Commission for the Accreditation of Vascular Laboratories, as part of the preoperative evaluation of these patients. The common carotid, internal carotid, and external carotid arteries were scanned bilaterally for the presence of occlusion or stenosis.²¹⁻²³ The arteries were scanned in transverse and longitudinal sections with B-mode and color-flow imaging. Local percent stenosis was estimated as a 10% interval, that is, 60% to 70%. This interval reading accounted for measurement error and variability.²⁴ Velocity criteria were used to confirm these data. The University of Washington criterion was used to corroborate stenosis > 50% with a peak systolic velocity more than 125 cm/s.²¹ An end-diastolic velocity of 100 cm/s^{25,26} was used to corroborate severe stenosis > 70%. All patients who underwent carotid

endarterectomy had > 60% stenosis. None of the lesions were identified as ulcerated or inhomogeneous by duplex scanning.

Tissue specimens. Carotid artery plaques were obtained immediately after endarterectomy. All operations were performed with standard surgical techniques and minimal manipulation of the specimen. One half of each specimen was fixed in paraformaldehyde and embedded in paraffin, whereas the remainder was snap-frozen immediately in liquid nitrogen and stored at -70°C until extraction.

Histologic study. Paraffin-embedded tissues were sectioned transversely at 5- μ m thickness and mounted on 3-aminopropyltriethoxysilane-coated slides. Five random sections from each specimen were used for analysis. In addition to routine hematoxylin and eosin staining used to select specimens for the study, Gomori's one-step trichrome staining was performed to differentiate between collagen and smooth muscle fibers, and Verhoeff's van Gieson elastic tissue staining was performed to observe the elastin network in the specimens.

DNA in situ end-labeling. Detection of apoptosis in the carotid artery plaques was performed with terminal deoxynucleotidyl transferase (TdT)-mediated digoxigenin-deoxyuridinetriphosphate (dUTP) nick end-labeling of free 3' OH DNA termini of fragmented DNA present in the apoptotic cells (TUNEL), with the ApopTag kit (Intergen, Purchase, NY) as previously described.²⁹ The tissue sections were deparaffinized, rehydrated, and incubated in 3% citric acid to remove calcium vesicles. Nuclei were stripped of proteins by incubation with 20 μ g/mL proteinase K (Oncor, Gaithersburg, Md) for 15 minutes at 45°C. After equilibration in buffer for 5 minutes, sections were covered with reaction buffer containing TdT enzyme and digoxigenin-dUTP and incubated in humidifying chambers for 1 hour at 37°C. One negative control slide (per batch) was incubated in the absence of TdT enzyme. Positive control used was tumor tissue. After end-labeling, the slides were immersed in stop-wash buffer for 20 minutes at 37°C. Blocking solution containing anti-digoxigenin antibody (sheep polyclonal) conjugated to fluorescein was applied on tissue and incubated for 30 minutes at 37°C in humidifying chambers. The antibody solution was washed away with three changes of phosphate-buffered saline solution for 5 minutes each. End-labeling was visualized after counterstaining with propidium iodide and observing the fluorescence under a Zeiss Axiophot fluorescence microscope (Carl Zeiss, Inc, Thornwood, NY).

Immunohistochemistry. The primary antibodies used in this study were mouse monoclonal antibodies for CPP-32 and Fas (DAKO, Carpinteria, Calif). Formalin-fixed paraffin-embedded tissue sections were deparaffinized and rehydrated. Antigen retrieval was performed by heat treatment at 95°C with 0.01 mol/L citrate buffer, pH 6.0. After the endogenous peroxidase activity was quenched with 0.3% hydrogen peroxide, the tissue sections were incubated with primary antibodies CPP-32 at 1:200 dilution and Fas at a dilution of 1:200 for 1 hour at room temperature. Sections were incubated with biotinylated

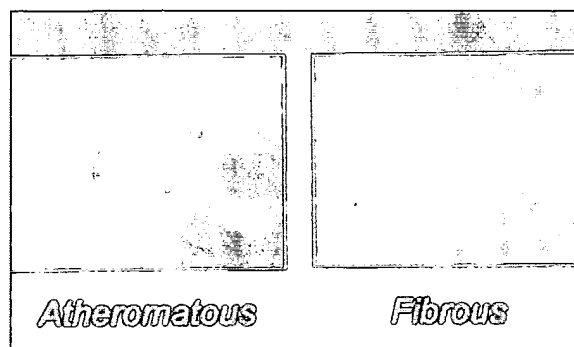


Fig 1. Apoptosis in fibrous and atheromatous plaque. Yellow-green fluorescence represents TUNEL-positive apoptotic bodies against red background of propidium iodide counterstained nuclei of nonapoptotic cells. (Original magnification $\times 1000$.)

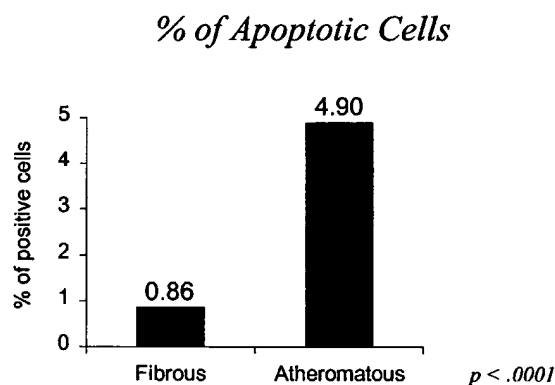


Fig 2. Apoptosis in fibrous and atheromatous plaque. Differences in incidence of apoptosis between fibrous and atheromatous plaque. Cumulative data of all atheromatous and fibrous plaques were obtained. Number of apoptotic cells per thousand cells were counted manually at high-power magnification (original magnification $\times 1000$) for each specimen (random fields were selected).

secondary antibody for 30 minutes at room temperature. The bound primary antibodies were detected with the LSAB2-HorseRadishPeroxidase detection system (DAKO). The peroxidase reaction was developed with diaminobenzidine tetrachloride to produce a brown color at sites of immunoreactivity. Subsequently, the slides were counterstained with Mayers' hematoxylin for 1.5 minutes. Tumor tissue was used as a positive control. The primary antibody was omitted and substituted with an unrelated antibody at the same dilution to check the specificity of the immunohistochemical reactions.

Quantification. Cells only positively stained by TUNEL and containing apoptotic bodies were referred to as "apoptotic cells." Thus, multiple criteria were used to identify apoptotic cells: TUNEL staining and morphologic markings including chromatin condensation. Cells

with these features have been confirmed to be apoptotic with electron microscopic analysis in previous studies by us²⁸ and by others.²⁹ The number of apoptotic cells per thousand cells were counted manually at high-power magnification ($\times 1000$) for each specimen (random fields were selected). The apoptotic index was calculated as the number of apoptotic cells divided by the total number of cells times 100. Cells positive for Fas and CPP-32 were counted manually at original magnification $\times 400$. Cells with no nuclear staining, positive nuclear staining, and cytoplasmic staining were quantified in six random fields per section. Five sections per specimen were analyzed. The number of positive cells is presented as a percentage of the total.

Protein extraction and estimation. Tissue samples were minced and homogenized in salt buffer (50 mmol/L Tris HCl pH 7.5; 2 mol/L NaCl; 0.02% Na Azide). After centrifugation, the supernatants were dialyzed against 0.05 mol/L Tris HCl pH 7.9 overnight at 4°C. Total protein in the dialysate was determined by use of the Pierce protein microassay kit (Pierce Chemical Co, Rockford, Ill) as per the manufacturer's instructions.

Zymography. Proteolytic activity in the extracts was identified by use of substrate gels containing gelatin. Extracts with equalized amounts of protein were mixed in sample buffer in 1:2 ratio and 30 μ L loaded on 10% polyacrylamide gels impregnated with gelatin (1 mg/mL) (BioRad, Hercules, Calif). Electrophoresis was performed under nonreducing conditions and at a constant voltage of 100 V. The gels were renatured for 30 minutes at room temperature and developed overnight in a 37°C water bath. The zymograms were stained in 0.5% (wt/vol) Coomassie blue for 20 minutes. Destaining was performed in 40% methanol and 10% acetic acid in distilled water until gelatinolytic activity was seen as clear bands against a background of stained gelatin. Polyacrylamide gel electrophoresis under reducing conditions was used to evaluate protein content.

Statistical analysis. The clinical data, risk factors, and histologic and immunohistochemical findings were analyzed with the Student *t* test and χ^2 . The Fisher exact test was used to compare the results obtained in the different groups. Statistical analyses were performed with Winks 4.21 program (Texasoft, Cedar Hill, Tex) and Instat 2.05a programs (Graphad, San Diego, Calif).

RESULTS

Patient demographics

There were seven men and six women with ages ranging from 63 to 85 years (mean, 73.6 ± 1.9 years). Eight of the patients had symptoms (history of stroke, transient ischemic attack, or amaurosis fugax), whereas five were symptom free. Patient demographics, risk factors, and clinical symptoms are given in Table I. None of the women were receiving hormone replacement therapy.

Histologic study

Fibrous plaques were observed to contain more smooth

Table I. Clinical risk factors

| | Atheromatous (n = 8) | | Fibrous (n = 5) | | P value |
|---------------------------|----------------------|---------------------|----------------------|---------------------|---------|
| | Asymptomatic (n = 3) | Symptomatic (n = 5) | Asymptomatic (n = 3) | Symptomatic (n = 2) | |
| Age \pm SEM (y) | 72.7 \pm 2.9 | 73.2 \pm 3.6 | 69.7 \pm 3.2 | 82 \pm 2 | NS |
| Male/female (7:6) | 2:1 | 3:2 | 1:2 | 2:0 | 0.67 |
| Diabetes mellitus (n = 4) | 0 | 2 | 2 | 0 | 0.56 |
| Hypertension (n = 5) | 1 | 3 | 0 | 1 | 0.44 |
| Tobacco (n = 7) | 0 | 4 | 1 | 2 | 0.6 |

P values compare atheromatous with fibrous plaque.

Table II. Histopathologic findings

| | Atheromatous (n = 8) | | Fibrous (n = 5) | |
|------------------------|----------------------|---------------------|----------------------|---------------------|
| | Asymptomatic (n = 3) | Symptomatic (n = 5) | Asymptomatic (n = 3) | Symptomatic (n = 2) |
| Plaque rupture | 1 | 2 | — | — |
| Cap thinning | 2 | 2 | — | — |
| Plaque necrosis | 1 | 2 | — | — |
| Cap foam cells | 2 | 1 | — | — |
| Macrophages | 2 | 4 | — | — |
| Intraplaque fibrin | — | 1 | — | — |
| Intraplaque hemorrhage | 3 | 3 | 1 | — |

muscle cells (identified with anti-alpha actin staining and morphologic study) than atheromatous plaques. Verhoeff's elastin staining and trichrome staining also showed a more developed extracellular matrix in atheromatous plaques than in fibrous plaques. The histopathologic findings in the patient groups are summarized in Table II.

Apoptosis detection

We observed that most of TUNEL-positive cells occur within the inflammatory regions of atheromatous plaques, composed mostly of macrophages, smaller number of T lymphocytes, and few B lymphocytes (data not shown). The atheromatous plaques contained $4.9\% \pm 1.27\%$ TUNEL-positive apoptotic cells as compared with $0.86\% \pm 0.46\%$ cells in the fibrous plaques ($P < .001$). In the atheromatous plaques, TUNEL-positive cells were most predominant in the lipid core, followed by the fibrous cap and the plaque shoulder region. There were fewer apoptotic cells in the medial layers. On the other hand, fibrous plaque demonstrated an even or scattered distribution of the less than 1% TUNEL-positive cells (Figs 1 and 2). The apoptotic index in the symptomatic group was 3.26, and that in the asymptomatic group was 3.45 ($P = .47$). There was no correlation of apoptosis with the degree of stenosis.

Immunohistochemical localization of the expression of mediators of apoptosis

CPP-32/YAMA. Cells expressing CPP-32 were preferentially located in areas of atheromatous plaques that had increased evidence of apoptosis, namely lipid core, fibrous cap, and shoulder region. In the atheroma-

tous plaque, $20.3\% \pm 1.78\%$ of the cells were CPP-32 positive, whereas in the fibrous plaque, significantly fewer cells were positive (11.7% ; $P < .001$) (Fig 3).

Fas. There were $17.5\% \pm 2.35\%$ of positive cells in the atheromatous plaques and no reactivity in the fibrous plaques ($P < .04$). This correlated with the apoptotic cell death observed in serial sections of these specimens (Fig 3). We could quantify the immunoreactivity to this inducer of apoptosis, although the specimens demonstrated weakly positive staining results.

Zymography. Zymograms with extracts used from carotid artery plaque specimens demonstrated proteolytic activity. However, there was increased gelatinolytic activity in the atheromatous plaques as compared with the fibrous samples. The activities ranged from 68-94 kDa (Fig 4); however, the band intensities were not quantified.

Clinicopathologic correlation

With the risk factors analyzed, diabetes mellitus, hypertension, and smoking (Table I), no correlation could be established between plaque type and clinical symptoms. Patients who had quit smoking were considered as positive for tobacco use.

DISCUSSION

The data from this study suggest significant differences in the apoptotic cascade in between atheromatous and fibrous carotid artery plaques. We have observed greater numbers of apoptotic cells in atheromatous plaques as compared with fibrous plaques. Programmed cell death in the atheromatous plaques was mainly found

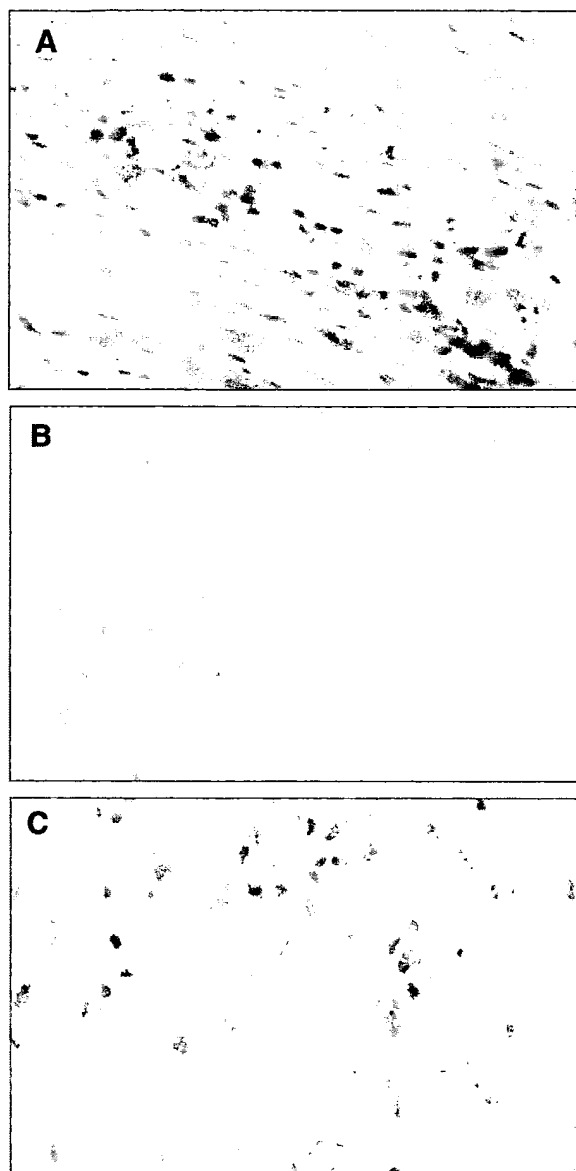


Fig 3. A, Immunohistochemical localization of CPP-32 in atheromatous plaques. Note positive staining (brown) for CPP-32. (Original magnification $\times 400$.) B, Immunohistochemical localization of Fas in atheromatous plaques. Note positive staining result (brown) for Fas. (Original magnification $\times 400$.) C, Negative control. (Original magnification $\times 400$.)

within regions of inflammatory cell infiltration. In contrast, apoptotic cells in fibrous plaques were distributed throughout the whole plaque. Therefore, they may not be able to undermine or compromise plaque stability.^{6,7} In addition, programmed cell death of SMCs may lead to imbalances in secretion of proteases associated with them,²⁹ whereas cell debris of dead macrophages and

other cells may contribute to gruel formation. It has been suggested that the death of SMCs can be detrimental for plaque stability because most of the interstitial collagen fibers that are important for the tensile strength of the fibrous cap are produced by SMCs.³⁰ Because SMCs and macrophages have been characterized as the key cell types involved with matrix turnover, a high degree of apoptosis in atheromatous plaques may account for their relative instability when compared with fibrous plaques.

The apoptosis observed by TUNEL assay identifies DNA fragmentation that occurs at the final phase of the apoptotic cascade. Kockx and Herman³⁰ found that during TUNEL assay if aspecific labeling is avoided, as in this study, the percentage of apoptosis was low in atheromatous plaques. The half-life of apoptotic cells is only a few hours. Even a low incidence of apoptosis has great cell kinetic significance because the short duration of the apoptotic process makes it histologically inconspicuous. Previous reports have emphasized that a small proportion of apoptotic cells visualized in tissue sections can represent a considerable magnitude of cell loss.^{7,11,31}

Cysteine protease CPP-32/YAMA is an inducer for mammalian programmed cell death and is an early marker of apoptosis.³² Our data demonstrate decreased immunopositivity for CPP-32 in fibrous plaques. The fact that cells expressing CPP-32 are preferentially present in the lipid core, fibrous cap, and shoulder regions lends credence to the finding of a significant number of apoptotic cells in these regions. CPP-32 has been shown to lead to apoptosis by cleaving and deactivating poly (ADP-ribose) polymerase, an enzyme required for DNA repair and genome integrity.³² Recent studies have demonstrated the expression of CPP-32 in apoptotic cells of carotid artery plaques.⁹ Our data not only corroborate these findings but also show differential expression of CPP-32 in the two types of plaques studied.

Fas is a cellular death domain protein that is activated by Fas ligand in the apoptotic pathway.^{33,34} The positive expression of Fas/CD95 in atheromatous plaques, as compared with its negative immunoreactivity in fibrous plaques, was consistent with the greater numbers of apoptotic cells observed in these plaques. Because fibrous plaques demonstrated no detectable immunopositivity for Fas, even after repeated immunohistochemical staining, it is possible that cells in the fibrous plaques do not go through the same apoptotic pathway as those in atheromatous plaques. In the atheromatous plaques, Fas seemed to colocalize with inflammatory cells in the necrotic core. Scant expression of Fas may be expected because these cells are either absent or present in small numbers in fibrous plaques.

Atherosclerotic plaque stability also may depend on the structural integrity of its extracellular matrix skeleton. We observed increased proteolytic activity in atheromatous plaque as compared with fibrous plaques. Reduction of ECM, compromising plaque stability, may result from either decreased synthesis of ECM by SMCs or its

increased breakdown by proteolytic enzymes produced by macrophages and other cells in the arterial wall. The loss of SMCs could lead to imbalances in the secretion of metalloproteinases and possibly other associated proteases. Matrix metalloproteinases have been shown to destabilize the atherosclerotic plaques through proteolytic activity, leading to degradation of the ECM.^{13-17,20,35} Evidence exists that proinflammatory molecules stimulate the secretion of metalloproteinases.^{17,19,35} Plaques with reduced tensile strength have been shown to have greater density of metalloproteinase-producing macrophages. This directly correlates with reduced collagen and elastin content.¹⁹ In view of the fact that atheromatous plaques have large amounts of macrophages present in the lipid core as compared with fibrous plaques, it was hypothesized and confirmed by our data that atheromatous plaques have increased levels of proteolytic activity. Zymography demonstrated elevated proteolytic activity in the atheromatous plaques, and the activities were in the 68- to 94-kDa range. This observation is comparable to that of several previous studies identifying these activities to correspond to those of metalloproteinase (MMP)-2 and -9 active and latent forms. Because the numbers in this study are small, we have not attempted to correlate our data with instability such as cap thinning, plaque necrosis, and hemorrhage.

The presence of tissue inhibitors of metalloproteinases (TIMPs) in the specimens was not examined. Fabunmi et al¹⁸ reported that plaques contained abundant amounts of TIMP-1, TIMP-2, and TIMP-3 and that macrophages and SMCs express these factors. Inflammatory molecules augment the levels of TIMP-1 and TIMP-3 but not of TIMP-2, suggesting that TIMPs in the plaques and in the arterial wall counteract MMP activity to influence plaque stability. Thus the role of TIMPs may be a confounding factor that deserves consideration.

The screening of 200 carotid endarterectomy specimens demonstrated that most of the plaques were of the rupture-prone atheromatous type. Conversely, it must be noted that there was no significant difference in programmed cell death between asymptomatic and symptomatic plaques. This may be due to the small numbers of patients. However, this finding is in accordance with those reported previously, which indicated that no correlation could be established between clinical symptoms and specific histologic and biochemical characteristics of the plaque. Other investigators have found no differences between asymptomatic and symptomatic groups with respect to plaque hemorrhage, the presence of a necrotic core, smooth muscle infiltration, and plaque type (fibrous, calcified, or necrotic).^{1,3} Recently, another group found significantly elevated levels of MMP 9 but not MMPs 1, 2, or 3 in carotid artery specimens, but only in the patients with symptoms within 1 month of surgery.¹⁴ This suggests that although plaque composition and structure may determine whether a plaque would be symptomatic, other factors such as heterogeneity, changes in physical

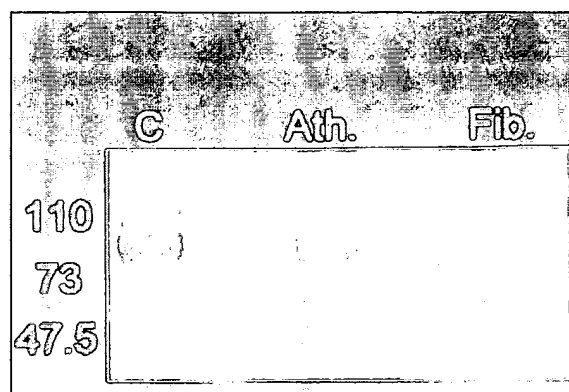


Fig 4. Gelatin zymography of atheromatous and fibrous plaque extracts. (Representative zymogram with one atheromatous specimen extract and one fibrous specimen extract. A total of five atheromatous plaques and five fibrous plaques were analyzed.) Note prominent bands of gelatinolytic activity in atheromatous plaque. Molecular weights are shown on the left. C, Positive control; Ath, atheromatous; Fib, fibrous. Activities ranged from 68 to 94 kDa.

characteristics of the plaque in response to hemodynamic forces, or a combination of factors may play a significant role.

The pathogenesis of intraplaque events in atherosclerotic carotid artery plaques remains a matter of debate. Our data indicate that plaque instability may be caused by programmed cell death of SMCs and inflammatory cells along with ECM degradation. The clear differences in the degree of apoptosis, level of expression of mediators of apoptosis and proteolytic activity between the two groups may be correlated with plaque vulnerability. The challenge remains to further elucidate molecular events and the mechanisms involved to develop future modalities for prevention of plaque rupture.

REFERENCES

1. Carr S, Farb A, Pearce WH, Virmani R, Yao JST. Atherosclerotic plaque rupture in symptomatic carotid artery stenosis. *J Vasc Surg* 1996;23:755-66.
2. Ross R. The pathogenesis of atherosclerosis: a perspective for the 1990s. *Nature* 1993;362:801-9.
3. Feeley TM, Leen EJ, Colgan MP, Moore DJ, Hourihane DO, Shanik GD. Histologic characteristics of carotid artery plaque. *J Vasc Surg* 1991;13:719-24.
4. Falk E, Shah PK, Fuster V. Coronary plaque disruption. *Circulation* 1995;92:657-71.
5. Milei J, Parodi JC, Alonso GF, Barone A, Grana D, Matturfi L. Carotid rupture and intraplaque hemorrhage: immunophenotype and role of cells involved. *Am Heart J* 1998;136:1096-105.
6. Kockx MM, De Meyer GR, Muhring J, Jacob W, Bult H, Herman AG. Apoptosis and related proteins in different stages of human atherosclerotic plaques. *Circulation* 1998;97:2307-15.
7. Konstadoulakis MM, Kymionis GD, Karagiani M, Katergianakis V, Doundoulakis N, Pararas V, et al. Evidence of apoptosis in human carotid atheroma. *J Vasc Surg* 1998;27:733-9.
8. Ihling C, Haendeler J, Menzel G, Hess RD, Fraedrich G, Schaefer

- HE, et al. Co-expression of p53 and MDM2 in human atherosclerosis: implications for the regulation of cellularity of atherosclerotic lesions. *J Pathol* 1998;185:303-12.
9. Mallat Z, Ohan J, Leseche G, Tedgui A. Colocalization of CPP-32 with apoptotic cells in human atherosclerotic plaques. *Circulation* 1997;96:424-8.
10. Björkerud S, Björkerud B. Apoptosis is abundant in human atherosclerotic lesions, especially in inflammatory cells (macrophages and T cells), and may contribute to the accumulation of gruel and plaques instability. *Am J Pathol* 1996;149:367-80.
11. Isner JM, Keamey M, Bortman S, Passeri J. Apoptosis in human atherosclerosis and restenosis. *Circulation* 1995;91:2703-11.
12. Bennet M, Evan GI, Schwartz SM. Apoptosis of human vascular smooth muscle cells derived from normal vessels and coronary atherosclerotic plaques. *J Clin Invest* 1995;95:2266-74.
13. Galis ZS, Sukhova GK, Lark MW, Libby P. Increased expression of matrix metalloproteinases and matrix degrading activity in vulnerable regions of human atherosclerotic plaques. *J Clin Invest* 1994;94:2493-503.
14. Loftus IM, Naylor AR, Goodall S, Crowther M, Jones L, Bell PR, et al. Increased matrix metalloproteinase-9 activity in unstable carotid plaques. *Stroke* 2000;31:40-7.
15. Nikkari ST, O'Brien KD, Ferguson M, Hatsukami T, Welgus HG, Alpers CE, et al. Interstitial collagenase (MMP-1) expression in human carotid atherosclerosis. *Circulation* 1995;92:1393-8.
16. Henney AM, Wakeley PR, Davies MJ, Foster K, Hembry R, Murphy G, et al. Localization of stromelysin gene expression in atherosclerotic plaques by in situ hybridization. *Proc Natl Acad Sci U S A* 1991;88:8154-8.
17. Moreno PR, Falk E, Palacios IF, Newell JB, Fuster V, Fallon JT. Macrophage infiltration in acute coronary syndromes—implications for plaque rupture. *Circulation* 1994;90:775-8.
18. Fabunmi RP, Sukhova GK, Sugiyama S, Libby P. Expression of tissue inhibitor of metalloproteinase-3 in human atheroma and regulation in lesion-associated cells. *Circ Res* 1998;83:270-8.
19. Shah PK, Falk E, Badimon JJ, Fernandez Ortiz A, Mailhac A, Villareal Levy G, et al. Human monocyte-derived macrophages induce collagen breakdown in fibrous caps of atherosclerotic plaques. *Circulation* 1995;92:1565-9.
20. Sukhova GK, Schonbeck U, Rabkin E, Schoen FJ, Poole AR, Billingham RC, et al. Evidence for increased collagenolysis by interstitial collagenases-1 and -3 in vulnerable human atheromatous plaques. *Circulation* 1999;99:2503-9.
21. Strandness DE Jr. Duplex scanning in vascular disorders. New York: Raven Press; 1993.
22. Salles-Cunha S, Andros G. Atlas of duplex ultrasonography. Pasadena: Appleton Davies, Inc; 1988, p.3-48.
23. Beebe HG, Salles Cunha SX, Scissons RP, Dosick SM, Whalen RC, Gale SS, et al. Carotid arterial ultrasound scan imaging: a direct approach to stenosis measurement. *J Vasc Surg* 1999;29:838-44.
24. Salles-Cunha S. Internal carotid artery ultrasonography: a technical perspective. *Vascular Ultrasound Today, Lesson 4, Volume 4, 1999, 5.*
25. Hood DB, Mattos MA, Mansour A, Ramsey DE, Hodgson KJ, Barkmeier LD, et al. Prospective evaluation of new duplex criteria to identify 70% internal carotid artery stenosis. *J Vasc Surg* 1996;23:254-61.
26. AbuRahma AF, Robinson PA, Strickler DL, Alberts S, Young L. Proposed new duplex classification for threshold stenoses used in various symptomatic and asymptomatic carotid endarterectomy trials. *Ann Vasc Surg* 1998;12:349-58.
27. Scheinman M, Ascher E, Kallakuri S, Hingorani A, Gade P, Sherman M, et al. P53 gene transfer to the injured rat carotid artery promotes apoptosis. *Surgery* 1999;126:863-8.
28. Li Y, Sharov VG, Jiang N, Zaloga C, Sabbah HN, Chopp M. Ultrastructural and microscopic evidence of apoptosis after middle cerebral occlusion in the rat. *Am J Pathol* 1995;146:1045-51.
29. Henderson EL, Geng YJ, Sukhova GK, Whittemore AD, Knox J, Libby P. Death of smooth muscle cells and expression of mediators of apoptosis by T lymphocytes in human abdominal aortic aneurysms. *Circulation* 1999;99:96-104.
30. Kockx MM, Herman AG. Apoptosis in atherosclerosis: beneficial or detrimental? *Cardiovasc Res* 2000;45:736-46.
31. Arends MJ, McGregor AH, Wyllie AH. Apoptosis is inversely related to necrosis and determines net growth in tumors bearing constitutively expressed myc, ras, and HPV oncogenes. *Am J Pathol* 1994;144:1045-57.
32. Tewari M, Quan LT, O'Rourke K, Desnoyers S, Zeng Z, Beidler DR, et al. Yama/CPP32 β , a mammalian homolog of CED-3, is a CrmA-inhibitable protease that cleaves the death substrate poly(ADP-ribose) polymerase. *Cell* 1995;81:801-9.
33. Sata M, Walsh K. Oxidized LDL activates Fas-mediated endothelial cell apoptosis. *J Clin Invest* 1998;102:1682-9.
34. Itoh N, Yonehara S, Ishii A, Yonehara M, Mizushima S, Sameshima M, et al. The polypeptide encoded by the cDNA for human cell surface antigen Fas can mediate apoptosis. *Cell* 1991;66:233-41.
35. Rajavashisth TB, Xu XP, Jovinge S, Meisel S, Xu XO, Chai NN, et al. Membrane type 1 matrix metalloproteinase expression in human atherosclerotic plaques: evidence for activation by proinflammatory mediators. *Circulation* 1999;99:3101-9.

Submitted Mar 27, 2000; accepted Sep 15, 2000.



Expression of apoptosis-related proteins and structural features of cell death in explanted aortocoronary saphenous vein bypass grafts

A.Y. Wang*, Y.V. Bobryshev*, S.M. Cherian*, H. Liang*, D. Tran*, S.J. Inder*, R.S.A. Lord*, K.W.S. Ashwell† and A.E. Farnsworth‡

*Surgical Professorial Unit, St Vincent's Hospital, Victoria Street, Darlinghurst, Sydney, NSW 2010, Australia and †School of Anatomy, The University of New South Wales, Sydney, NSW 2052, Australia and ‡Department of Cardiothoracic Surgery, St Vincent's Hospital, Sydney, NSW 2010, Australia

This study aimed to investigate the features of cell death occurring in aortocoronary saphenous vein bypass grafts. Human aortocoronary saphenous vein bypass grafts with angiographic luminal stenosis of >75% were explanted from 14 patients at redo coronary artery bypass grafting. Proteins associated with apoptotic pathways were identified immunohistochemically using antibodies to Bcl-2, Fas, BAX, p53 and CPP32. Cells undergoing DNA fragmentation were identified by terminal deoxynucleotidyl transferase-mediated dUTP nick end labeling (TUNEL). DNA synthesis was investigated using the antibody to proliferating cell nuclear antigen (PCNA). Ultrastructural features of cell death were examined by electron microscopy. Anti-apoptotic (Bcl-2) and pro-apoptotic (Bax, p53, CPP32 and Fas) proteins were expressed throughout the graft wall, but marked differences in the characteristics of cell death were noted between atherosclerotic and non-atherosclerotic areas of the intima. In atherosclerotic areas, pro-apoptotic proteins were widely expressed, but ultrastructural analysis failed to identify cells showing typical features of apoptosis. In these areas, necrotic cells were frequently observed, with negative correlation of Bcl-2 expression with TUNEL. Pro-apoptotic proteins showed no correlation with TUNEL. In contrast, in non-atherosclerotic areas of vein grafts, the expression of both anti-apoptotic (Bcl-2) and pro-apoptotic proteins (p53, Bax and CPP32) correlated with TUNEL. In atherosclerotic areas, non-atherosclerotic intimal areas, and in the underlying media, the numbers of TUNEL+ cells correlated with PCNA positivity. Ultrastructurally, apoptotic bodies and features of necrosis were observed in non-atherosclerotic areas of grafts. The present observations indicate that in atherosclerotic areas, cell death occurs mainly by necrosis, while in non-atherosclerotic areas, cell death occurs by both necrosis and apoptosis. An imbalance between DNA fragmentation and DNA synthesis may contribute to graft instability and failure. © 2001 The International Society for Cardiovascular Surgery. Published by Elsevier Science Ltd. All rights reserved

Keywords: apoptosis, atherosclerosis, cell death, coronary artery disease, necrosis, saphenous vein bypass grafts

Introduction

The long-term usefulness of aortocoronary saphenous vein bypass grafts (ASVBGs) used as conduits in coronary artery bypass grafting (CABG) is limited by a disease complex [1–4] comprised of intimal hyperplasia and atherosclerosis [5,6], with both processes related to cell death.

Cell death is a significant event in graft preservation [7, 8] and rejection [9–15], being recognized as a contributing factor to the failure of various grafts, including cardiac [16–18], neuronal [15], hepatic [14], renal [19] and pancreatic [20] transplants. Cell death has also been noted in vascular diseases [13, 21–25]. Specifically, apoptosis (programmed cell death) has been observed in transplant rejection [9–14] and has recently been reported as an important contributor to the formation of primary atheromas, restenotic lesions [26–29], and in experimental atherosclerotic models [30–34].

The present study aimed to investigate the structural features of cell death in ASVBGs using immunohistochemical markers and electron microscopy.

Materials and methods

This study was approved by the Institutional Review Board of the St Vincent's Hospital, Sydney, Australia. Informed consent was obtained from all patients prior to collection of specimens and the materials collected in accordance with the principles outlined in the Declaration of Helsinki [35].

Specimen collection and clinical data

Human aortocoronary saphenous vein bypass grafts with luminal stenosis of >75% as demonstrated by angiography, were explanted from 14 patients at redo coronary artery bypass graft operation at the St Vincent's Hospital, Sydney. The patients (11 male and 3 female) were aged between 51 and 75 yr (mean age 66.6 yr) with the graft implant time ranging from 8 to 22 yr (mean 12.9 yr). The clinical details of patients are summarized in *Table 1*. Some of the grafts have been examined previously for the presence of dendritic cells [36]. However, in this study, different segments of the grafts were used and were processed separately. Ten segments of normal long saphenous veins were harvested from patients undergoing femoro-popliteal bypass graft operation that served as a control to compare the degree of histological alteration occurring in stenotic saphenous vein bypass grafts.

Tissue preparation

Areas of macroscopic luminal stenosis affecting explanted vein grafts were identified and divided into two segments: one to undertake immunohistochemi-

stry, and the other for electron microscopy. Normal veins were similarly divided into two segments. For immunohistochemical analysis, the segments were fixed in 10% neutral buffered formalin and embedded in paraffin. Consecutive parallel sections of 5 μ m thickness were cut and air-dried. Sections were stained with haematoxylin and eosin for routine histological examination. For transmission electron microscopic analysis, adjacent segments were fixed in 2.5% glutaraldehyde in 0.1 M phosphate buffered saline (pH 7.4).

Histology and selection of graft areas for further quantitative analysis

Routine microscopic examination of vein grafts demonstrated two distinct forms of graft occlusion: four out of the 14 grafts (29%) resulted from an organized fibrotic thrombus, while the remaining (71%) were due to the development of atherosclerotic lesions associated with mural thrombosis. For quantitative analysis, six specific areas within each graft were identified and analyzed. These included areas of hyperplastic intima affected by atherosclerosis evidenced by the presence of foam cells. The non-atherosclerotic intima was classified into two, namely, the cellular and acellular areas. Acellular areas were those that consisted primarily of extracellular connective tissue matrix that contained less than 35 cells per microscopic field of 200 \times 200 μ m² examined at \times 400 magnification. Cellular areas were those that contained larger numbers of intimal cells in comparison to acellular areas, with lower extracellular matrix content. Cellular and acellular areas of the media were similarly selected. Areas of neovascularization in the media were also analyzed.

Immunohistochemical examination for the expression of apoptosis-related proteins

Apoptosis-related proteins, including anti-apoptotic (Bcl-2) and pro-apoptotic (Fas, p53, BAX and caspase-3) proteins were detected using monoclonal antibodies to Bcl-2, Fas, p53, and BAX, and polyclonal antibody to CPP32 (that labels caspase-3). The working concentrations of the antibodies are detailed in *Table 2*.

Immunohistochemical analysis was carried out using the standard avidin–biotin complex (ABC) immunoperoxidase technique [37]. Deparaffinized sections were treated by boiling in citrate buffer (pH 6.0) to retrieve antigenicity. All sections were blocked with 3% hydrogen peroxide (peroxidase blocking) prior to staining. Sections to be stained with the antibody to CPP32 were additionally blocked with 1% normal goat serum (protein blocking). After washing in Tris-buffered saline (TBS, pH 7.6), sections were incubated in the primary antibody for 60 min, followed by incubation

Table 1 Clinical characteristics of aortocoronary saphenous vein bypass grafts^a

| Patient | Sex | Age | 1st surgery | 2nd surgery | Mean graft implant time (years) | Hypercholesterolaemia |
|---------|-----|-----|-------------|-------------|---------------------------------|-----------------------|
| 1 | M | 73 | 1989 | 1999 | 10 | — |
| 2 | F | 71 | 1989 | 1999 | 10 | + |
| 3 | M | 74 | 1988 | 1999 | 11 | + |
| 4 | M | 74 | 1978 | 1999 | 21 | + |
| 5 | F | 71 | 1991 | 1999 | 8 | — |
| 6 | M | 75 | 1983 | 1999 | 16 | — |
| 7 | M | 69 | 1986 | 1998 | 12 | — |
| 8 | M | 64 | 1985 | 1998 | 13 | + |
| 9 | F | 55 | 1988 | 1998 | 10 | — |
| 10 | M | 51 | 1987 | 1998 | 11 | + |
| 11 | M | 52 | 1990 | 1998 | 8 | + |
| 12 | M | 64 | 1982 | 1998 | 16 | + |
| 13 | M | 70 | 1985 | 1998 | 13 | + |
| 14 | M | 69 | 1977 | 1999 | 22 | + |

^aHypercholesterolaemia: +indicates serum cholesterol level >5.5 mmol/l; —indicates serum cholesterol level <5.5 mmol/l

Table 2 Antibodies used in the study

| Designation | Type ^a | Clone | Specificity | Source | Working dilution |
|-------------|-------------------|----------|---|------------|------------------|
| PCNA | M | PC10 | Proliferating cell nuclear antigen | DAKO | 1:50 |
| sma | M | ASM-1 | Smooth muscle α -actin (smooth muscle cells) | Novocastra | 1:25 |
| CD68 | M | PG-M1 | CD68 (macrophages/monocytes) | DAKO | 1:50 |
| CD3 | P | — | CD3 (T cells) | DAKO | 1:500 |
| Fas | M | FAS9 | FAS receptor | Zymed | 1:100 |
| p53 | M | DO-1 | Transcription factor p53 | Immunotech | 1:50 |
| BAX | M | 2D2 | Human BAX protein | Zymed | 1:50 |
| Bcl-2 | M | Bcl2-100 | Bcl-2 oncogene | Zymed | 1:50 |
| CPP-32 | P | — | Caspase-3 | DAKO | 1:50 |

^aM - monoclonal antibody; P - polyclonal antibody

in the appropriate secondary antibody (horse anti-mouse, Vector BA-2000 or goat anti-rabbit, Vector BA-1000) for 20 min, and finally with ABC (Elite Vector PK-6100) for 30 min. The immunological reaction was visualized by treating in 3,3'-diaminobenzidine (DAB) solution for 2 min, which gave a brown colouration. Sections were counterstained with Mayer's haematoxylin. For negative control, the primary antibody was omitted or the sections treated with an immunoglobulin fraction of suitable non-immune serum as a substitute for the primary antibody. No positive staining was observed in any of the negative control sections. Sections were examined under an Olympus microscope at $\times 100$ and $\times 400$ magnifications.

In situ analysis of DNA fragmentation

In situ detection of DNA fragments using TUNEL is commonly used to investigate apoptosis [38, 39]. During apoptosis, cleavage of genomic DNA yields double-stranded, low molecular weight DNA frag-

ments along with single strand breaks ('nicks') of high molecular weight DNA. TUNEL labels these DNA strand breaks with modified nucleotides [38, 39]. However, TUNEL may not only label the early stage of orderly DNA fragmentation in apoptosis, but also the nuclear breakdown during the later stages of necrosis [38, 40]. Hence, although the demonstration of DNA fragmentation in atherosclerotic plaques may provide direct evidence for the presence of degenerating cells, it does not completely discriminate between apoptotic and necrotic cell degeneration [38, 40]. To overcome this uncertainty, in the present study we employed TUNEL labelling to localize and quantify cells dying both by apoptosis and necrosis with an in situ death detection kit (1684817, Boehringer Mannheim), and the differentiation carried out by electron microscopy. Deparaffinized sections were rehydrated, following which they were incubated with proteinase K (20 μ g/ml in 10m M Tris/HCl, pH 7.4) for 15 min and washed with TBS. DNA fragments were labelled

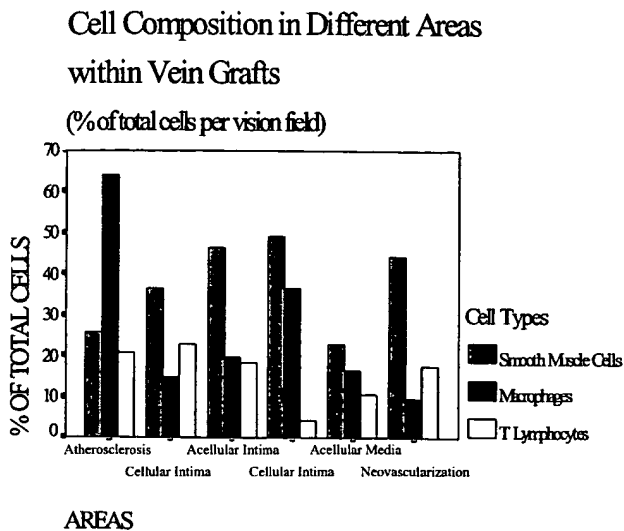


Figure 1 Cell composition in different areas of aortocoronary saphenous vein bypass grafts

with fluorescein-dUTP. The terminal transferase and the labelled DNA fragments were detected with alkaline phosphatase (AP)-conjugated antibody against fluorescein. Fast red was used as the substrate solution, rendering a pink colour to labelled nuclei.

Immunohistochemical analysis of DNA synthesis

DNA synthesis was identified using the monoclonal antibody to proliferating cell nuclear antigen (anti-PCNA), employing the ABC immunoperoxidase technique [37] as described earlier.

Identification of different cell types

Cell type specific antibodies, including anti-CD68 (to identify macrophages), anti-CD3 (T-lymphocytes) and anti- α -SMA (smooth muscle actin to identify smooth muscle cells), were used. The working concentrations of the antibodies are detailed in Table 2.

Quantification and statistics

In every specimen, the expression of apoptosis-related proteins, the numbers of TUNEL+ cells, PCNA+ cells, and the cellular composition were evaluated on consecutive sections in each of the six areas, namely (1) atherosclerotic areas, (2) cellular and (3) acellular non-atherosclerotic hyperplastic intima, (4) cellular and (5) acellular areas of the media, and (6) areas of neovascularization in the media. In each area, the total cell number and the number of cells stained by peroxidase/AP (brown/pink staining) were counted at a high magnification ($\times 400$) in five randomly chosen fields from each section. The average cell counts of the cellular

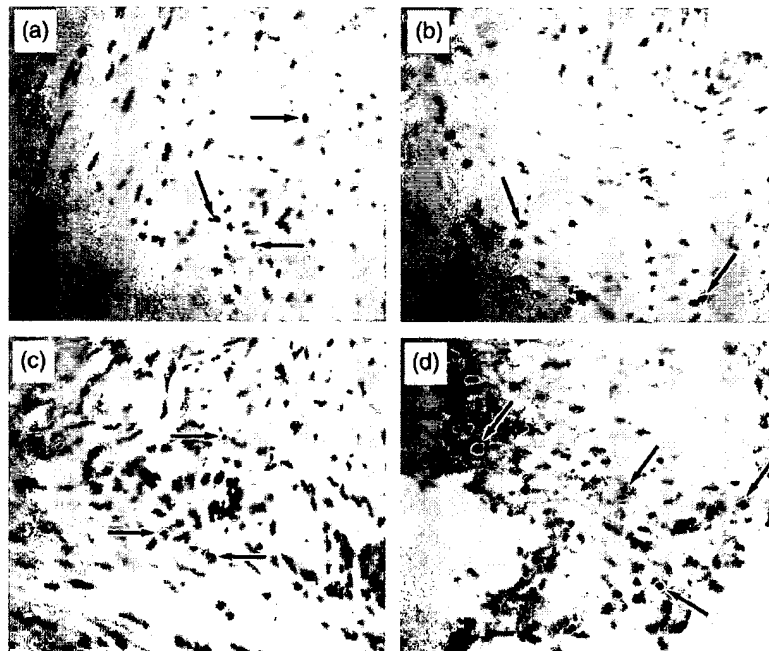


Figure 2 Apoptosis-related protein (p53, Bax) expressions in non-atherosclerotic intima (A,C) and atherosclerotic areas (B,D) of aortocoronary saphenous vein bypass grafts. ABC immunoperoxidase technique, counterstained with Mayer's haematoxylin. (A,B,C,D) $\times 100$

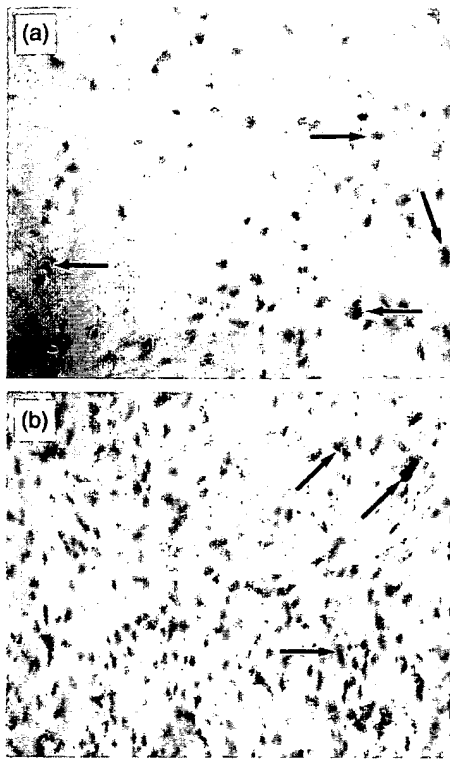


Figure 3 DNA fragmentation (A) and DNA synthesis (B) in aortocoronary saphenous vein bypass grafts. Numerous TUNEL+ (A) and PCNA+ (B) cells are evident in the cellular intima. (A): TUNEL immunoreactivity in the non-atherosclerotic cellular intima. (B): PCNA positivity around inflammatory infiltrates at the base of the non-atherosclerotic cellular intima. TUNEL — In Situ Death Detection Kit, AP; PCNA — ABC immunoperoxidase technique. Counterstaining with Mayer's haematoxylin. (A,B) $\times 100$

and acellular intima in each specimen were taken to be the count of the intima for that specimen for each variable. Similarly, the average values of the cellular and acellular media were taken to be the count of the media for that specimen for each variable. All variables were presented as a percentage of the total number of cells in that area.

Differences in mean were determined by the Student's *t*-test. A value of $P < 0.05$ was considered significant. Correlation between groups was determined by Pearson's rank correlation coefficient. SPSS program (version 7.0, Educational Edition) was used to obtain statistical calculations.

Electron microscopy

For ultrastructural analysis, the specimens were cut transversely into small pieces of 2–3 mm through all the layers of the vessel (tunica intima, media and adventitia), and postfixed in 1% osmium tetroxide. Specimens were dehydrated in graded ethanol before embedding in Araldite resin. Semithin sections were stained with Toluidine blue, and analysed for selecting areas for ultrathin sectioning. Ultrathin sec-

tions stained with uranyl acetate and lead citrate were examined with the aid of a Hitachi H7000 electron microscope at an accelerating voltage of 75 kV.

Results

Cellular density

In general, the cellular density was higher in the intima than in the media. In atherosclerotic plaques, cells of macrophage origin (CD68+) were the major cell type (mean $63.89 \pm 4.95\%$, range 33.3–87.0%; *Figure 1*) with most exhibiting a foam cell appearance. The percentages of T-lymphocytes and smooth muscle cells in plaques varied from 0 to 45.8% (mean $20.73 \pm 3.24\%$), and from 0 to 65.4% (mean $25.51 \pm 5.66\%$) respectively (*Figure 1*). In non-atherosclerotic intimal areas, smooth muscle cells were the predominant cell type (mean $41.23 \pm 3.00\%$, range 19.7–68.9%; *Figure 1*). Similarly, in the media, smooth muscle cells were the major cell type (mean $39.82 \pm 4.57\%$, range 1.0–68.1%; *Figure 1*).

Expression of apoptosis-related proteins

Anti-apoptotic (Bcl-2) and pro-apoptotic (p53, Fas, Bax and CPP-32) proteins were expressed in all areas of grafts. A high level of Bcl-2 positivity was found in atherosclerotic plaques (mean $35.32 \pm 9.00\%$, range 0–90.5%), approximately 6.1 times higher than in the adjacent intima (mean $5.68 \pm 2.1\%$; range 0–20.0%) and media (mean $5.8 \pm 1.38\%$, range 0–14.8%). p53 expression was localized in cellular areas of the intima [mean $22.64 \pm 3.95\%$, range 2.2–44.0%; *Figure 2(A)*]. High levels of p53 immunostaining were also observed in the atherosclerotic areas [mean $19.06 \pm 5.48\%$, range 0–42.2%; *Figure 2(B)*] and were four times higher than that in the media (mean $4.64 \pm 1.45\%$, range 0–13.5%). Bax immunoreactivity was most prominent in the non-atherosclerotic cellular intima [mean $52.17 \pm 7.19\%$, range 0.7–91.8%; *Figure 2(C)*]. In atherosclerotic areas, its expression was $40.36 \pm 4.10\%$ [range 24.5–70.4%; *Figure 2(D)*], while in the media, only $11.05 \pm 2.8\%$ of cells expressed Bax (range 0.3–26.1%). CPP32+ cells were mostly located in the cellular intima (mean $32.18 \pm 5.13\%$, range 8.1–61.0%). In atherosclerotic areas, $28.85 \pm 2.41\%$ of cells showed positivity (range 11.4–38.7%), while the least expression of CPP32 was observed in the media (mean $8.42 \pm 2.61\%$, range 0–23.0%). In all areas of grafts, Fas expression was lower when compared to all other pro-apoptotic proteins, being $5.57 \pm 2.94\%$ (range 0–33%) in atherosclerotic areas, $3.81 \pm 1.87\%$ (range 0–17.5%) in the non-atherosclerotic intima, and $< 0.01\%$ in the media.

In control veins, the expression of all apoptosis-related proteins that were studied was either absent or very low ($< 0.5\%$).

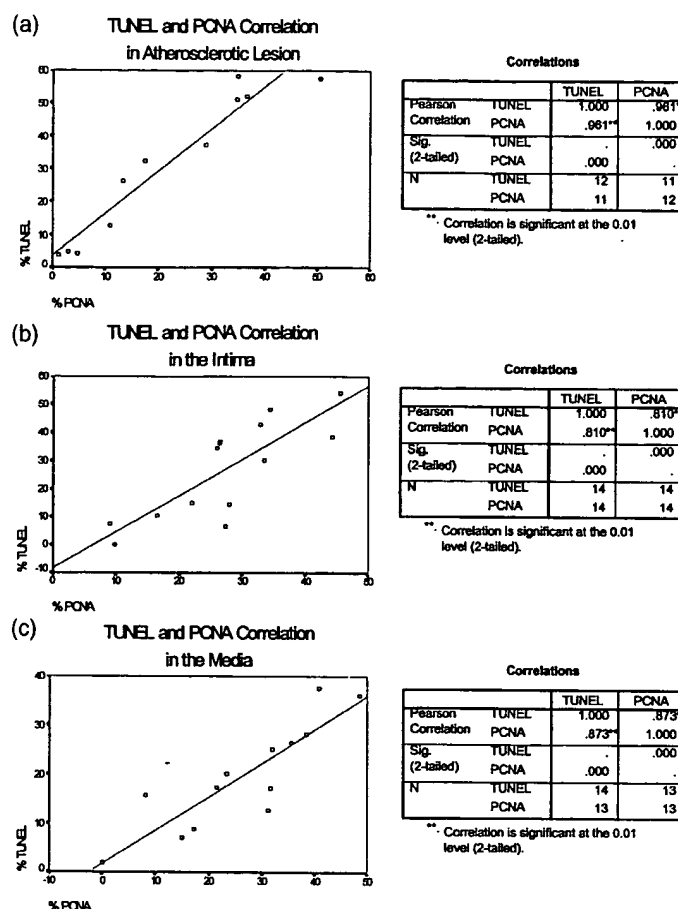


Figure 4 Correlations between TUNEL+ and PCNA+ cells in atherosclerotic areas (A), the intima (B) and the media (C) of aortocoronary saphenous vein bypass grafts, using Pearson correlation coefficient and Student's *t*-test. *P* values <0.05 were taken as being significant.

TUNEL+ cells and PCNA+ cells

TUNEL+ cells were distributed unevenly throughout the graft wall. $28.67 \pm 6.56\%$ of cells stained positive for TUNEL in atherosclerotic areas (range 1.0–58.4%). Aggregates of TUNEL+ cells were mostly present around the necrotic core and these aggregates were usually localized only at one pole rather than being evenly distributed around the necrotic core. There were approximately 1.6 times higher numbers of TUNEL+ cells in the non-atherosclerotic intima [mean $27.01 \pm 4.63\%$, range 3.0–54.3%; *Figure 3(A)*] than in the media (mean $18.73 \pm 2.94\%$, range 2.0–37.7%). In control veins, very scarce or no TUNEL-labelled nuclei were detected (<0.01%).

DNA synthesis as demonstrated by PCNA expression in control veins was either absent or very rare (<0.01%), while in the vein grafts, a large number of cells were PCNA+ [*Figure 3(B)*]. In atherosclerotic areas, the number of PCNA+ cells ranged from 0 to 69.5% (mean $25.55 \pm 6.04\%$). The non-

atherosclerotic intima had a slightly greater proportion of PCNA+ cells than the media ($27.26 \pm 2.56\%$ in the intima vs $24.41 \pm 3.75\%$ in the media). Most PCNA+ cells were located in areas of neovascularization in the media (mean $53.00 \pm 7.18\%$, range 6.3–77.9%) where the percentage of PCNA+ cells was approximately twice as high as that in the intima and media.

Correlation between TUNEL+ cells, PCNA+ cells and apoptosis-related protein expression

The number of TUNEL+ cells strongly correlated to the number of PCNA+ cells in atherosclerotic areas [$r = 0.961$, $P < 0.001$; *Figure 4(A)*] and in the non-atherosclerotic intima [$r = 0.810$, $P < 0.001$; *Figure 4(B)*]. Similarly, there was positive correlation between TUNEL and PCNA immunoreactivities in the media [$r = 0.873$, $P < 0.001$; *Figure 4(C)*]. However, no correlation was noted between the number of TUNEL+ and PCNA+ cells in areas of neovascularization. In these areas, DNA synthesis was notably

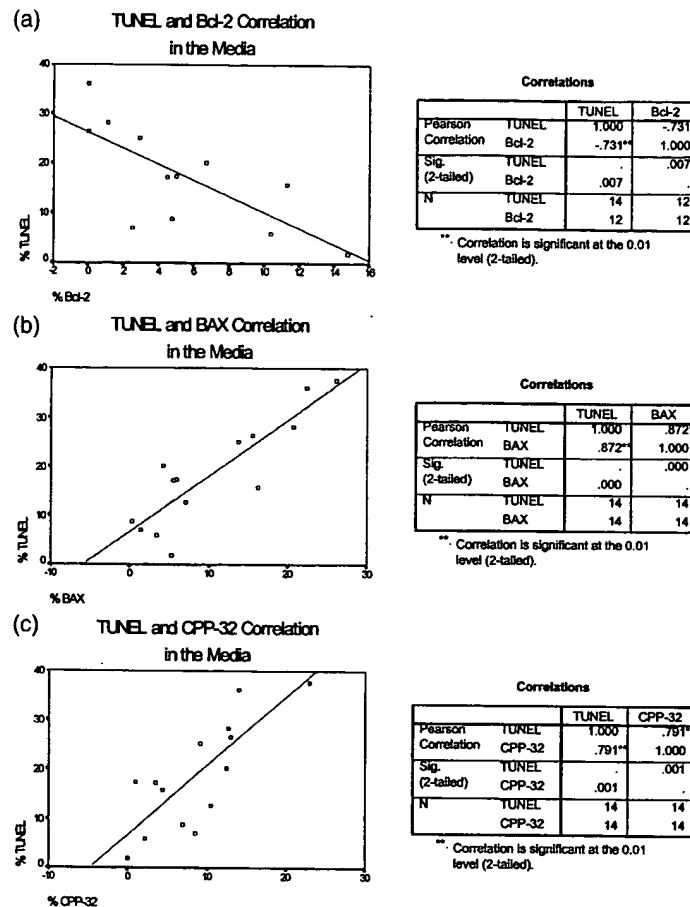


Figure 5 Correlations between TUNEL+ cells and apoptosis-related protein expressions in different areas within aortocoronary saphenous vein bypass grafts. Negative correlations between TUNEL and Bcl-2 positivities were observed in the media (A). In contrast, TUNEL correlated directly with Bax (B) and CPP-32 (C) in the media. P values <0.05 were taken as being statistically significant

higher in comparison to all other areas, but only few cells undergoing DNA fragmentation were observed.

Strong negative correlation was observed between Bcl-2+ cells and TUNEL+ cells in atherosclerotic areas ($r = -0.671$, $P < 0.05$). A strong positive correlation was observed between the numbers of TUNEL+ cells and p53+ cells in cellular areas of the intima ($r = 0.736$, $P < 0.005$). In the media, there was negative correlation between TUNEL+ cells and Bcl-2+ cells [$r = -0.731$, $P < 0.007$; Figure 5(A)], while TUNEL+ cells correlated positively with both Bax+ cells [$r = 0.872$, $P < 0.001$; Figure 5(B)] and CPP32+ cells [$r = 0.791$, $P < 0.001$; Figure 5(C)].

Electron microscopic analysis

Ultrastructural analysis of atherosclerotic and non-atherosclerotic intima of grafts demonstrated large number of cells showing signs of cellular destruction that included features of perinuclear membrane rupture, plasmalemmal degeneration, and oedema of

the cytoplasm [Figure 6(A,B)]. In non-atherosclerotic areas within the hyperplastic intima as well as in the underlying media, some cells contained condensed and fragmented chromatin within the intact cytoplasm [Figure 7(A)]. In other cells, the entire cytoplasm including the chromatin was fragmented [Figure 7(B)]. In these cells, the cytoplasmic fragments were surrounded by an intact membrane and contained intact mitochondria [Figure 7(B)]. Accumulation of these nuclear remnants and cytoplasmic fragments within macrophages was observed in the hyperplastic non-atherosclerotic intima [Figure 8(A,B)]. In contrast, no chromatin fragmentation and no formation of apoptotic bodies were observed in atherosclerotic areas.

Discussion

The present immunohistochemical observations demonstrated that pro-apoptotic proteins were

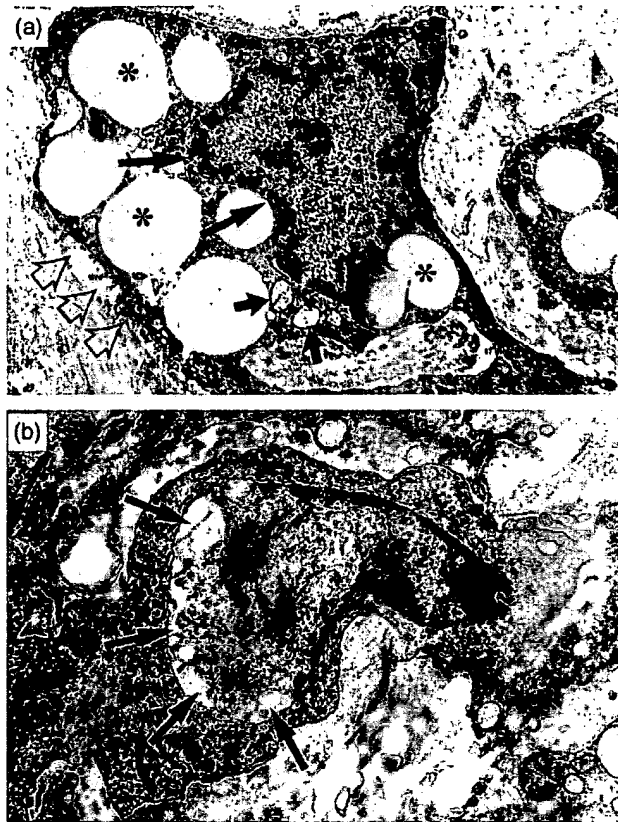


Figure 6 Necrotic alteration in cells located in atherosclerotic areas of aortocoronary saphenous vein bypass grafts. (A): Destructive changes in the nuclear membrane (large solid arrows) and their plasmalemma (open arrows) in a foam cell. Small solid arrows show swollen mitochondria containing destroyed cristae. 'Lipid droplets' are marked by asterisks. (B): Destruction of the nuclear membrane and distortion of the chromatin within a cell which is characterized by the presence of intact cytoplasm. Electron micrographs. Magnifications $\times 7100$; $\times 9600$

widely expressed in stenotic saphenous vein bypass grafts and corresponded to DNA fragmentation as assessed by the TUNEL method. Statistical analysis showed a positive correlation between cell death and DNA synthesis ($P < 0.001$). In primary atherosclerosis, the degree of cell death relates to the disease state [41, 42] with the percentage of TUNEL+ cells ranging from 2 to 40% [41, 42]. In the present analysis, 10 of 14 grafts (71%) failed due to long-term atherosclerotic degeneration complicated by thrombosis. In these grafts, TUNEL-positivity in atherosclerotic areas was relatively high.

The percentage of PCNA+ cells in vein grafts was higher when compared to that of primary atheromas [43]. The high numbers of TUNEL+ cells and PCNA+ cells observed in our study suggests an increased cell turnover in vein grafts. This increase in cell turnover may contribute towards the accelerated atherosclerotic changes, leading to eventual graft failure. The incidence of cell death was noted to be

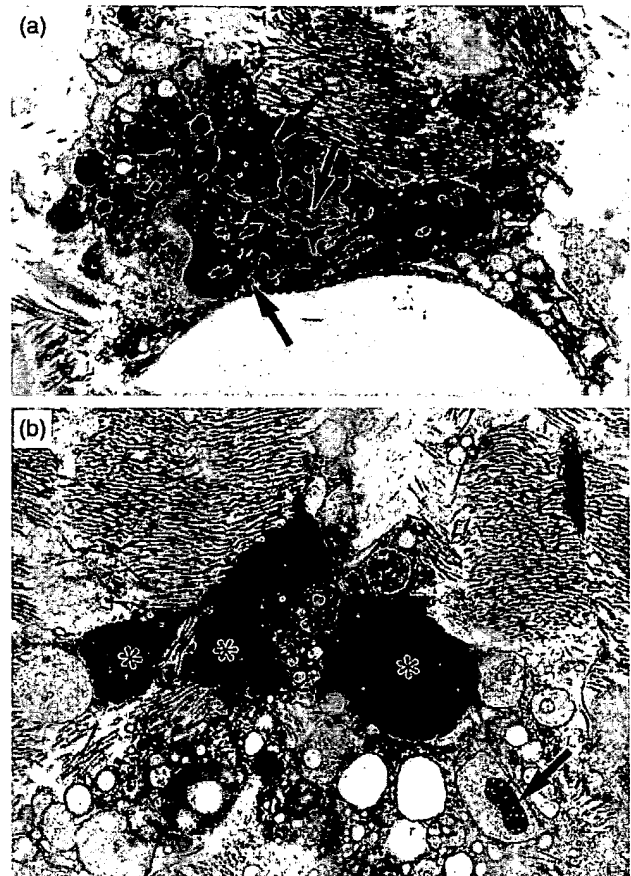


Figure 7 Apoptotic alterations of cells located in the deep portion of the hyperplastic intima of aortocoronary saphenous vein bypass grafts. (A): Condensation and fragmentation of chromatin (arrows) in a cell which is characterized by intact cytoplasm. (B): Fragmentation of condensed chromatin (asterisks) and fragmentation of the cytoplasm. Note that cytoplasmic fragments are surrounded by an intact membrane and are located in the extracellular intimal matrix. An intact mitochondrion in a cytoplasmic fragment is shown by arrow. Electron micrographs. Magnifications: $\times 7100$; $\times 9600$

higher in atherosclerotic areas when compared to the non-atherosclerotic intima, implying that cell death may contribute to graft instability due to the formation and enlargement of acellular necrotic cores.

The micro-environmental factors that initiate cell death in atherosclerosis are unclear. Our study clearly demonstrated that large numbers of TUNEL+ cells were located near the necrotic core of atherosclerotic lesions. Ultrastructural observation of typical necrotic (hypoxic) features suggests that oxidative stress, responsible for the generation of oxidized lipids and free radicals in the plaque, may be involved in the initiation of cell death in the graft wall. PCNA+ cells exceeded the number of TUNEL+ cells by two-fold and was markedly higher than in the primary atheroma. This is probably associated with vein graft arterialization and DNA syn-

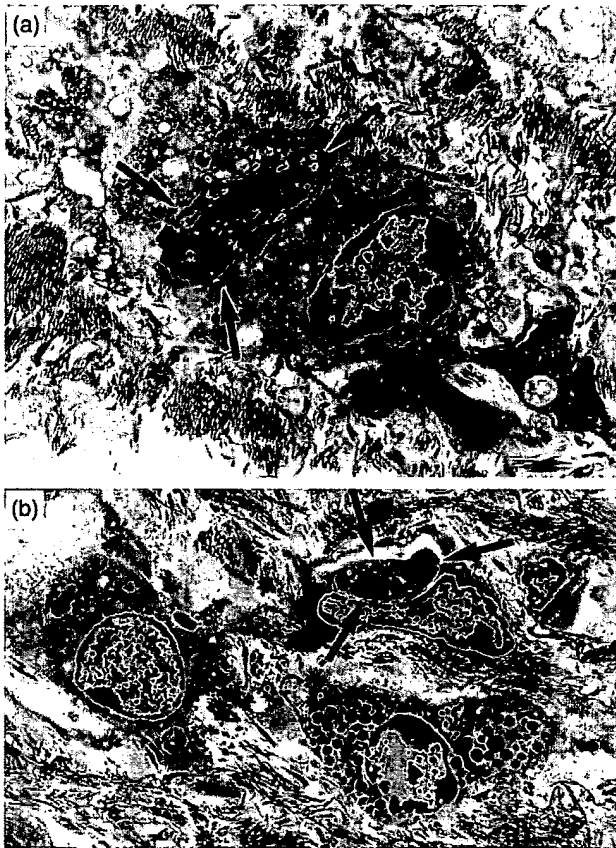


Figure 8 Cell remnants (apoptotic bodies) (arrows) within macrophages in the deep portion of the hyperplastic intima in aortocoronary saphenous vein bypass grafts (A,B). Electron micrographs $\times 7100$; $\times 4200$

thesis in the medial smooth muscle cells, further contributing to graft instability and enhancing failure.

In the media, typical ultrastructural features of both apoptosis and necrosis were evident. Both Bax+ and CPP32+ cells strongly correlated with TUNEL+ cells. However, the extent of these pro-apoptotic protein expressions was generally lower than the TUNEL-positivity. Anti-apoptotic protein (Bcl-2) expression correlated inversely with TUNEL+ cells, while p53 expression, although present, showed no correlation with TUNEL+ cells, suggesting that there exists a complex interaction between pro- and anti-apoptotic proteins that may regulate apoptotic pathways in the vein graft.

Conclusion

The aetiology of long-term ASVBG failure is probably multifactorial and is yet to be fully determined [6]. Our observations indicate that DNA fragmentation and synthesis in both atherosclerotic and non-atherosclerotic areas of vein grafts are higher when compared to normal saphenous veins. In atherosclerotic areas of

stenotic saphenous vein bypass grafts, cell death occurs mostly by necrosis despite a high expression of pro-apoptotic proteins. In non-atherosclerotic areas of the grafts, including the hyperplastic intima and the media, cell death occurs by apoptosis and necrosis.

Acknowledgements

The research was supported by the St Vincent's Clinic Foundation, Sydney, Australia

References

1. Flemma, R. J., Mullen, D. C. and Lepley, D., Aortocoronary vein bypass grafting. In *Vascular Grafts*, eds P. N. Sawyer and M. J. Kaplitt. Appleton Century Crofts, New York 1978.
2. Szilagyi, D. E., Atherogenesis in venous bypass grafts. In *Vascular Grafts*, eds P. N. Sawyer and M. J. Kaplitt. Appleton Century Crofts, New York 1978.
3. Kirklin, J. K. and Barrat-Boyes, B. G., Ischaemic heart disease. In *Cardiac Surgery*, Vol. 1 Churchill Livingstone, Edinburgh, 1993.
4. Cambria, R. P. and Abbott, W. M., Translocated autogenous vein grafts. In., *Vascular Surgery*, Vol. 1 W. B. Saunders Company, Sydney 1989.
5. Nielsen, T. G., Laursen, H., Gronholdt, M. L. et al, Histopathological features of in situ vein bypass stenoses. *European Journal of Vascular and Endovascular Surgery*, 1997, 14 492-498.
6. Motwani, J. G. and Topol, E. J., Aortocoronary saphenous vein graft disease: pathogenesis, predisposition, and prevention. *Circulation*, 1998, 97 916-931.
7. Meyer, D., Baumgardt, S., Lofeler, S. et al, Apoptosis in combined liver/small bowel transplantation. *Transplantation Proceedings*, 1998, 30 2588.
8. Schierle, G. S., Hansson, O., Leist, M. et al, Caspase inhibition reduces apoptosis and increases survival of nigral transplants. *Nature Medicine*, 1999, 5 97-100.
9. Cagiannos, C., Zhong, R., Zang, Z. et al, Effect of major histocompatibility complex expression on murine intestinal graft survival. *Transplantation*, 1998, 66 1369-1374.
10. Hayakawa, K., Sato, H., Aoyagi, T. et al, Apoptosis in acute cellular rejection in murine renal allotransplantation. *Transplantation Proceedings*, 1998, 30 2944-2946.
11. Hayashi, M., Martinez, O. M., Krams, S. M. et al, Characterization of allograft rejection in an experimental model of small intestinal transplantation. *Journal of Gastrointestinal Surgery*, 1998, 2 325-332.
12. Kageyama, Y., Li, X. K., Suzuki, S. et al, Apoptosis is involved in acute cardiac allograft rejection in rats. *Annals of Thoracic Surgery*, 1998, 65 1604-1609.
13. Kirsch, G. M., Kearsey, J., Buttr, T. et al, Medial smooth muscle cell loss in arterial allografts occurs by cytolytic cell induced apoptosis. *European Journal of Cardiothoracic Surgery*, 1998, 14 89-96.
14. Krams, S. M. and Martinez, O. M., Apoptosis as a mechanism of tissue injury in liver allograft rejection. *Seminars in Liver Disease*, 1998, 18 153-167.
15. Boonman, Z. and Isacson, O., Apoptosis in neuronal development and transplantation: role of caspases and trophic factors. *Experimental Neurology*, 1999, 156 1-15.
16. Vriens, P. W., Blankenberg, F. G., Stoot, J. H. et al, The use of technetium Tc 99m annexin V for in vivo imaging of apoptosis during cardiac allograft rejection. *Journal of Thoracic and Cardiovascular Surgery*, 1998, 116 844-853.
17. Fandrich, F., Dresske, B., Lin, X. et al, Alloptide-mediated expression of endothelial Fas-ligand (CD95L) in long-term tolerated heterotopic rat heart grafts. *Transplantation Proceedings*, 1999, 31 1558-1559.

18. Koglin, J., Granville, D. J., Glysine-Jensen, T. *et al*, Attenuated acute cardiac rejection in NOS2 $-/-$ recipients correlates with reduced apoptosis. *Circulation*, 1999, **99** 836–842.
19. August, C., Schmid, K. W., Dietl, K. H. *et al*, Prognostic value of lymphocyte apoptosis in acute rejection of renal allografts. *Transplantation*, 1999, **67** 581–585.
20. Rabinovitch, A., Suarez-Pinzon, W., Trynaska, K. *et al*, Transfection of human pancreatic islets with an anti-apoptotic gene (Bcl-2) protects beta-cells from cytokine-induced destruction. *Diabetes*, 1999, **48** 1223–1229.
21. Johnson, T. M., Epstein, S. E. and Finkel, T., Apoptosis in vascular disease: opportunities for genetic therapeutic intervention. *Seminars in Interventional Cardiology*, 1996, **1** 195–202.
22. Bennett, M. R., Apoptosis in vascular disease. *Transplantation Immunology*, 1997, **5** 184–188.
23. MacLouf, J., Folco, G. and Patrono, C., Eicosanoids and iso-eicosanoids: constitutive, inducible and transcellular biosynthesis in vascular disease. *Thrombosis and Haemostasis*, 1998, **79** 691–705.
24. Murakami, K., Kawase, M., Kondo, T. *et al*, Cellular accumulation of extravasated serum protein and DNA fragmentation following vasogenic edema. *Journal of Neurotrauma*, 1998, **15** 825–835.
25. Pollman, M. J., Hall, J. L., Mann, M. J. *et al*, Inhibition of neointimal cell bcl-x expression induces apoptosis and regression of vascular disease. *Nature Medicine*, 1998, **4** 222–227.
26. Isner, J. M., Kearney, M., Bortman, S. *et al*, Apoptosis in human atherosclerosis and restenosis. *Circulation*, 1995, **91** 2703–2711.
27. Crisby, M., Kallin, B., Thyberg, J. *et al*, Cell death in human atherosclerotic plaques involves both oncosis and apoptosis. *Atherosclerosis*, 1997, **130** 17–27.
28. Lutgens, E., de Muinck, E. D., Kitslaar, P. J. *et al*, Biphasic pattern of cell turnover characterizes the progression from fatty streaks to ruptured human atherosclerotic plaques. *Cardiovascular Research*, 1999, **41** 473–479.
29. Kearney, M., Pieczek, A., Haley, L. *et al*, Histopathology of instant restenosis in patients with peripheral artery disease. *Circulation*, 1997, **95** 1998–2002.
30. Kockx, M. M., de Meyer, G. Y., Bult, H. *et al*, Distribution of cell replication and apoptosis in atherosclerotic plaques of cholesterol-fed rabbits. *Atherosclerosis*, 1996, **120** 115–124.
31. Harada, K., Chen, Z., Ishibashi, S. *et al*, Apoptotic cell death in atherosclerotic plaques of hyperlipidemic knockout mice. *Atherosclerosis*, 1997, **135** 235–239.
32. Kockx, M. M., de Meyer, G. R., Buysse, N. *et al*, Cell composition, replication, and apoptosis in atherosclerotic plaques after 6 months of cholesterol withdrawal. *Circulation Research*, 1998, **83** 378–387.
33. Lutgens, E., Daemen, M., Kockx, M. M. *et al*, Atherosclerosis in APOE*3-Leiden transgenic mice: from proliferative to atheromatous stage. *Circulation*, 1999, **99** 276–283.
34. Shindo, J., Ishibashi, T., Yokoyama, K. *et al*, Granulocyte-macrophage colony-stimulating factor prevents the progression of atherosclerosis via changes in the cellular and extracellular composition of atherosclerotic lesions in watanabe heritable rabbits. *Circulation*, 1999, **99** 2150–2156.
35. World Medical Association Inc World Medical Association Declaration of Helsinki. Recommendations guiding physicians in biomedical research involving human subjects. *Cardiovascular Research*, 1997, **35** 2–3.
36. Cherian, S. M., Bobryshev, Y. V., Inder, S. J. *et al*, Involvement of dendritic cells in long-term aortocoronary saphenous vein bypass graft failure. *Cardiovascular Surgery*, 1999, **7** 508–518.
37. Hsu, S. M., Raine, L. and Fanger, H., Use of avidin-biotin-peroxidase complex (ABC) in immunoperoxidase techniques: a comparison between ABC and unlabelled antibody (PAP) procedures. *Journal of Histochemistry and Cytochemistry*, 1981, **29** 577–580.
38. Kressel, M. and Groscurth, P., Distinction of apoptotic and necrotic cell death by in situ labeling of fragmented DNA. *Cell Tissue Research*, 1994, **278** 549–556.
39. Gavrieli, Y., Sherman, Y. and Ben-Sasson, S. A., Identification of programmed cell death in situ via specific labeling of nuclear DNA fragmentation. *Journal of Cell Biology*, 1992, **119** 493–501.
40. Kimura, K., Sasano, H., Shimosegawa, T. *et al*, Ultrastructural and confocal laser scanning microscopic examination of TUNEL-positive cells. *Journal of Pathology*, 1997, **181** 235–242.
41. Kockx, M. M., Apoptosis in the atherosclerotic plaque: quantitative and qualitative aspects. *Arteriosclerosis Thrombosis and Vascular Biology*, 1998, **18** 1519–1522.
42. Kockx, M. M. and Herman, A. G., Apoptosis in atherogenesis: implications for plaque destabilization. *European Heart Journal*, 1998, **19** (Suppl G) G23–G28.
43. Rekhter, M. D. and Gordon, D., Active proliferation of different cell types, including lymphocytes, in human atherosclerotic plaques. *American Journal of Pathology*, 1995, **147** 668–677.

Paper accepted 18 September 2000

Inhibition of Caspase-3 Improves Contractile Recovery of Stunned Myocardium, Independent of Apoptosis-Inhibitory Effects

Hartmut Ruetten, MD, PhD,* Cornel Badorff, MD,† Christian Ihling, MD,‡ Andreas M. Zeiher, MD,† Stefanie Dimmeler, PhD†

Frankfurt and Freiburg, Germany

| | |
|--------------------|---|
| OBJECTIVES | The aim of this study was to investigate whether the caspase-3 inhibitor Ac-DEVD-CHO functionally improves stunned myocardium. |
| BACKGROUND | Degradation of troponin I contributes to the pathogenesis of myocardial stunning, whereas the role of apoptosis is unknown. Caspase-3 is an essential apoptotic protease that is specifically inhibited by Ac-DEVD-CHO. |
| METHODS | Isolated working hearts of rats were exposed to 30 min of low-flow ischemia, followed by 30 min of reperfusion. Ac-DEVD-CHO (0.1 to 1 μ mol/l) was added 15 min before ischemia/reperfusion or 5 min before reperfusion. Cardiac output, external heart power, left ventricular (LV) developing pressure and contractility (dp/dt_{max}) were measured. Apoptosis was assessed by TUNEL staining and internucleosomal deoxyribonucleic acid fragmentation. Caspase-3 processing and troponin I cleavage were determined by immunoblotting. Caspase-3 activity was measured using a fluorogenic substrate. |
| RESULTS | The addition of Ac-DEVD-CHO before ischemia/reperfusion or before reperfusion dose-dependently and significantly ($p < 0.05$) improved post-ischemic recovery of cardiac output, external heart power, LV developing pressure and dp/dt_{max} , compared with the vehicle (0.01% dimethyl sulfoxide). Ac-DEVD-CHO was similarly effective when given before reperfusion. Ac-DEVD-CHO blocked ischemia/reperfusion-induced caspase-3 activation, but cardiomyocyte apoptosis was unaffected. Troponin I cleavage was not inhibited by Ac-DEVD-CHO. |
| CONCLUSIONS | Caspase-3 is activated in stunned myocardium. Inhibition of caspase-3 by Ac-DEVD-CHO significantly improves post-ischemic contractile recovery of stunned myocardium, even when given after the onset of ischemia. The mechanism(s) of protection by Ac-DEVD-CHO appear to be independent of apoptosis. Inhibition of caspase-3 is a novel therapeutic strategy to improve functional recovery of stunned myocardium. (J Am Coll Cardiol 2001;38:2063-70) © 2001 by the American College of Cardiology |

A significant reduction of coronary blood flow causes myocardial ischemia and contractile dysfunction. The cardiac dysfunction often persists for days, even after coronary artery perfusion has been re-established. This scenario of reversible post-ischemic contractile dysfunction is known as myocardial stunning (1). Depressed contractility, with reduced maximal force generation, is a hallmark of stunning (2-5).

Apoptosis is an evolutionary conserved process of programmed cell death in response to diverse stimuli, such as cardiac development or hypoxia (6). Increased cardiomyocyte apoptosis has been reported in patients with heart failure and experimental myocardial infarction (MI) (7-10). The caspase family of cellular proteases initiates and executes apoptotic cell death (11). Caspase-3, a pivotal effector caspase, is an essential protease of the apoptotic machinery. Caspase-3 proteolytically cleaves a number of death sub-

strates and activates endonucleases, leading to internucleosomal deoxyribonucleic acid (DNA) fragmentation, a hallmark of apoptosis (12). Individual caspases differ in their substrate recognition sequences, which has allowed generation of inhibitors like Ac-DEVD-CHO that specifically inhibit caspase-3 (3). Ac-DEVD-CHO is a tetrapeptide (Asp-Glu-Val-Asp) based on the caspase-3 substrate recognition motif, with an acetylate group coupled to its N-terminal (for enhanced chemical stability) and an aldehyde group conjugated to its C-terminal (for irreversible inactivation of the caspase-3 catalytic cysteine residue) (13,14).

In a rabbit and rat model of MI, administration of a broad-spectrum caspase inhibitor before infarction significantly reduced the infarct size and rate of apoptotic cells in the area at risk (9,10). However, it is unknown whether caspase inhibitors functionally improve stunned myocardium and whether they are effective when given after the onset of myocardial ischemia. The latter would be more relevant to the clinical situation.

Therefore, we investigated the effects of the caspase-3 inhibitor Ac-DEVD-CHO in an isolated working-heart rat model of myocardial stunning. Our data suggest that inhibition of caspase-3 reduces myocardial stunning when

From the *Aventis Pharmaceuticals, Frankfurt, Germany; †Molecular Cardiology, Department of Medicine IV, Goethe-University, Frankfurt, Germany; and ‡Department of Pathology, University of Freiburg, Freiburg, Germany. This study was supported by grants from the Deutsche Forschungsgemeinschaft, Bonn, Germany (Sonderforschungsbereich 533-C2 and Ba-1668/3-1).

Manuscript received November 7, 2000; revised manuscript received August 10, 2001, accepted August 29, 2001.

Abbreviations and Acronyms

| | |
|------|-----------------------------|
| DMSO | = dimethyl sulfoxide |
| DNA | = deoxyribonucleic acid |
| LV | = left ventricular |
| LVP | = left ventricular pressure |
| MI | = myocardial infarction |

initiated after the onset of ischemia (I), but before reperfusion (R). Thus, caspase-3 inhibition represents a novel therapeutic strategy to improve contractile functional recovery of stunned myocardium.

METHODS

Isolated working-heart rat model. Male, 4- to 6-week-old Sprague Dawley rats were anesthetized with pentobarbital (60 mg/kg intraperitoneally [IP]), heparinized (500 IU/100 g body weight IP). The hearts were removed, and the aorta was mounted onto a 1.4-mm cannula and attached to a perfusion apparatus (Hugo Sachs Electronic). The hearts were perfused with oxygenated (95% oxygen, 5% carbon dioxide), noncirculating Tyrode's solution (in mmol/l): 124.6 NaCl; 4.0 KCl; 2.2 CaCl₂; 1.1 MgCl₂; 24.9 NaHCO₃; 0.3 NaH₂PO₄; and 11.1 glucose (pH 7.4) at a perfusion pressure of 51 mm Hg. After equilibration for 15 min, the perfusion was switched to the anterograde working-heart mode, with a preload of 11 mm Hg and an afterload of 51 mm Hg. Aortic pressure was measured through a pressure transducer (Hugo Sachs Electronic). Left ventricular pressure (LVP) was measured by using a microtipped catheter (SPR 407, 2F, Millar Instruments). The maximal rise in LVP was obtained with an electronic differentiation system (PLUGSYS, Hugo Sachs Electronic). Aortic and coronary flow rates were measured by transonic flow probes (Transonic Systems). Heart rate was monitored by electrography (Hugo Sachs Electronic), and the hearts were paced at 5 Hz.

Experimental groups and protocols. In 8 to 10 animals in each experimental group, global low-flow ischemia was induced by reducing the coronary flow to 10%, resulting in a reduction of aortic pressure from 51 to 11 mm Hg. Low-flow ischemia was maintained for 30 min, followed by 30 min of reperfusion. External heart power (EHP) per gram of left ventricular (LV) wet weight was calculated: $EHP_{LV} \text{ (mJ/g per min)} = \text{pressure} - \text{volume work/heart rate}$. Dimethyl sulfoxide (DMSO; 0.01%; Sigma) as vehicle or Ac-DEVD-CHO in 0.01% DMSO final (0.1 to 1 $\mu\text{mol/l}$; Alexis) was started 15 min before ischemia or 5 min before reperfusion and given throughout the reperfusion period.

Immunoblotting. Tissue was homogenized in lysis buffer (10 mmol/l Tris-HCl, pH 8.0; 1% Triton X-100; 0.32 mol/l sucrose; 5 mmol/l EDTA; and 1 mmol/l phenylmethylsulfonylfluoride), and proteins were separated by sodium dodecyl sulfate/polyacrylamide gel electrophoresis (SDS/

PAGE), transferred to PVDF membranes and immunoblotted, as described (15), with the following primary antibodies: anti-troponin I (clone C5), anti-mouse actin (both Chemicon) or anti-caspase-3 (p17 subunit, Santa Cruz Biotechnology). Bound antibodies were studied by chemiluminescence (Amersham).

Caspase-3 and calpain enzymatic assays. Myocardial tissue was homogenized as described previously, and 200 μg of protein was used in 700 μl of caspase-assay buffer (100 mmol/liter HEPES, pH 7.5; 0.32 mol/l sucrose; 100 mmol/l NaCl; 0.1% CHAPS; 2 mmol/l dithiothreitol; 10 $\mu\text{g/ml}$ aprotinin; 10 $\mu\text{g/ml}$ leupeptin; and 10 $\mu\text{g/ml}$ pepstatin A), with 0.24 mmol/l of DEVD-AFC as the fluorogenic caspase-3 substrate, as described (16). For measuring calpain-like activity, 200 μg of protein was used in 600 μl of calpain-assay buffer (60 mmol/l imidazol, pH 7.5; 5 mmol/l L-cysteine; 0.2% Triton X-100; 5 mmol/l CaCl₂; 5 mmol/l dithiothreitol; 10 $\mu\text{g/ml}$ aprotinin; 10 $\mu\text{g/ml}$ leupeptin; and 10 $\mu\text{g/ml}$ pepstatin A), with 0.24 mmol/l of fluorogenic calpain substrate I (Calbiochem). Purified calpain I (5 U; Calbiochem) was used as indicated, and after 60 to 100 s, calpain inhibitor I (Roche) or Ac-DEVD-CHO was added to the reaction mixture, while the increase in fluorescence was still linear.

Detection of apoptosis. The DNA strand breaks were analyzed in situ using 5- μm sections with terminal deoxynucleotidyl transferase (TdT)-mediated dUTP-biotin nick end-labeling (TUNEL), as described (15). Internucleosomal DNA fragmentation ("DNA laddering") was detected by incubation of phenol-chloroform extracted DNA with 5 U of Klenow polymerase and 0.5 μCi of (α -³²P)-dCTP, followed by gel electrophoresis, as described (16).

Statistical analysis. All data are presented as the mean value \pm SEM. Comparisons were performed by analysis of variance for comparison of multiple measurements or by the paired or unpaired Student *t* test. A Bonferroni correction for multiple comparisons was used to determine the level of significance. A *p* value <0.05 was considered statistically significant.

RESULTS

Ac-DEVD-CHO improves post-ischemic contractile recovery in a model of myocardial stunning of isolated working hearts of rats. As an experimental model of myocardial stunning, we used isolated working hearts of rats (17). Figure 1A illustrates the experimental protocol: after initial stabilization for 15 min, the hearts were treated with Ac-DEVD-CHO (0.1 to 1 $\mu\text{mol/l}$) or vehicle (0.01% DMSO) for 15 min before ischemia (8 to 10 hearts per experimental group). After 30 min of low-flow ischemia, reperfusion was established for 30 min. For the first 15 min of reperfusion, the hearts were perfused in the Langendorff mode to allow for recovery. Then, perfusion was switched back to the working-heart mode. Under these conditions,

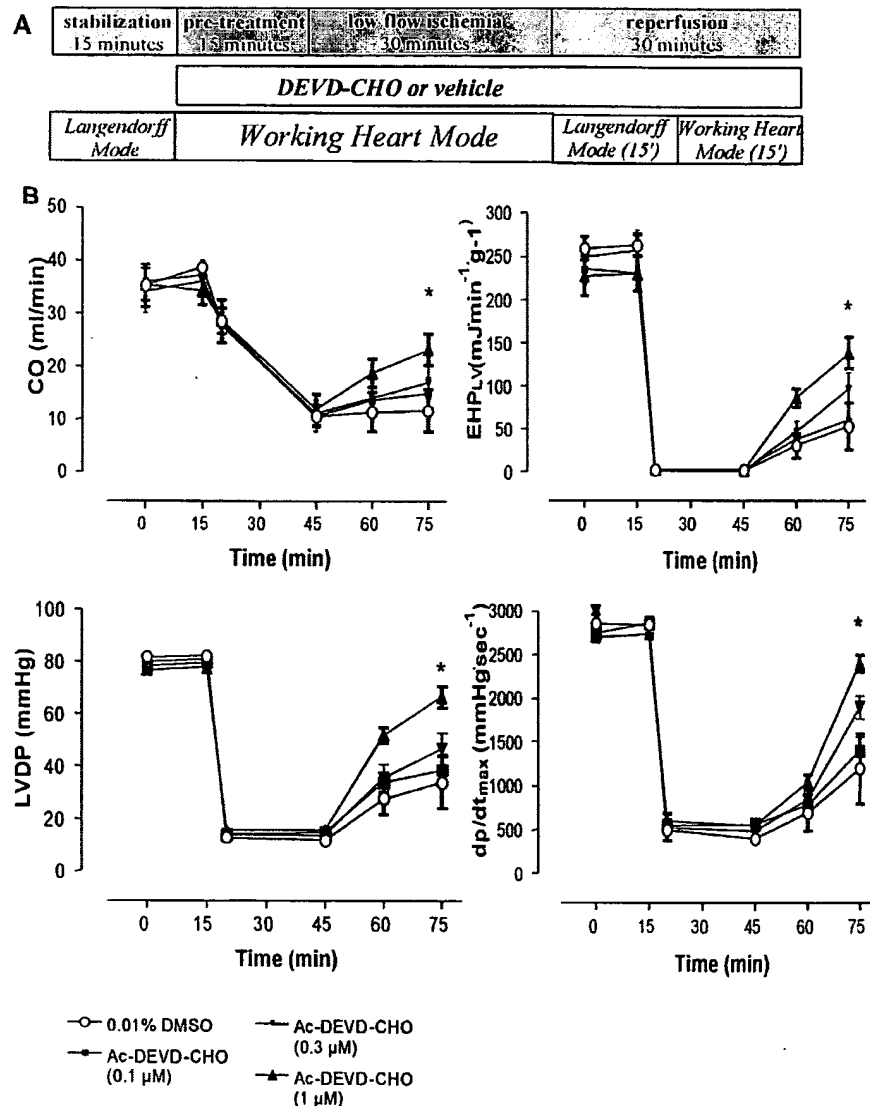


Figure 1. The caspase-3 inhibitor Ac-DEVD-CHO improves contractile recovery of isolated working hearts of rats exposed to ischemia and reperfusion. (A) Schematic diagram of the experimental set-up. (B) Effects of the caspase-3 inhibitor Ac-DEVD-CHO (0.1 to 1 μ mol/liter) or vehicle (0.01% DMSO) on cardiac output (CO), external heart power per gram of LV wet weight (EHP_{LV}), left ventricular developing pressure (LVDP) and contractility (dp/dt_{max}). Data are presented as the mean value \pm SEM; there are 8 to 10 animals per group. *p < 0.05 versus vehicle-treated group.

the residual 10% coronary flow during ischemia largely prevented MI (17).

In the control group, cardiac output, external heart power, (LV) developing pressure, myocardial contractility and aortic and coronary flow (data not shown) severely decreased during the ischemic period and remained depressed during reperfusion (Fig. 1B). Treatment of isolated hearts with 0.1 to 1 μ mol/l of Ac-DEVD-CHO (starting 15 min before ischemia) did not affect cardiac performance at baseline or during ischemia. However, Ac-DEVD-CHO dose-dependently and significantly (p < 0.05 for 1 μ mol/l) improved the contractile recovery of post-ischemic myocardium. Just 1 μ mol/l of Ac-DEVD-CHO significantly enhanced cardiac output, external heart power, LV developing pressure, myocardial contractility (Fig. 1B) and aortic and coronary flow (data not shown).

Figure 2 shows that only 20% to 45% (calculated values relative to pre-ischemic baseline value) of post-ischemic recovery of the various variables was observed in the vehicle-treated group. This indicates severe cardiac dysfunction, even after restoration of perfusion. Treatment with 1 μ mol/l of Ac-DEVD-CHO increased the relative recovery of all variables to 60% to 85% of the pre-ischemic values (Fig. 2). **Ac-DEVD-CHO is equally effective when administered before reperfusion.** To investigate whether Ac-DEVD-CHO protects the myocardium from stunning when administered after the onset of ischemia, Ac-DEVD-CHO (1 μ mol/l) was started 5 min before reperfusion. This scenario more closely resembles the common clinical situation of patients presenting with acute coronary syndromes.

As shown in Figure 2, the group treated with 1 μ mol/liter of Ac-DEVD-CHO, started 5 min before reperfusion, led

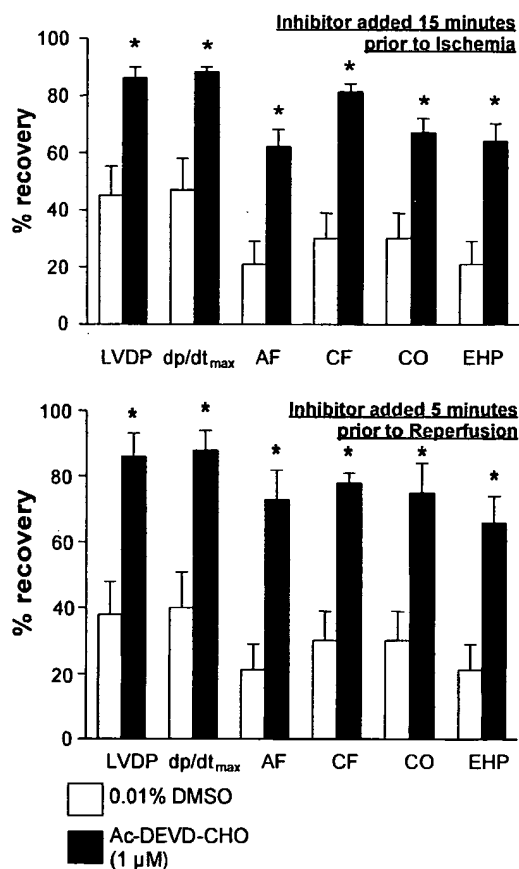


Figure 2. Ac-DEVD-CHO is effective when given 5 min before reperfusion. The effect of Ac-DEVD-CHO on contractile recovery is shown, calculated as percent recovery compared with baseline (pre-ischemic) values of left ventricular developing pressure (LVDP), contractility (dp/dt_{max}), aortic flow (AF), coronary flow (CF), cardiac output (CO) and external heart power (EHP). Data are presented as the mean value \pm SEM; there are 8 to 10 animals in each group. Ac-DEVD-CHO was started 15 min before ischemia (top) or 5 min before reperfusion (bottom). Note the similar beneficial effect of Ac-DEVD-CHO on the relative recovery. * $p < 0.05$ versus vehicle-treated group. Open bars = 0.01% DMSO; solid bars = 1 μ mol/l of Ac-DEVD-CHO.

to a significantly ($p < 0.05$) improved post-ischemic recovery of cardiac performance, compared with the vehicle-treated group. Specifically, Ac-DEVD-CHO started 5 min before reperfusion improved cardiac output, external heart power, LV developing pressure, myocardial contractility and aortic and coronary flow to a similar degree, compared with Ac-DEVD-CHO started 15 min before ischemia (Fig. 2). **Ac-DEVD-CHO blocks ischemia/reperfusion-induced activation of caspase-3.** Next, we investigated the effects of ischemia/reperfusion and Ac-DEVD-CHO on the activation of caspase-3. Caspase-3 exists as an inactive zymogen of 32 kD and is activated by proteolytic processing into p17 and p12 subunits (11,12).

Immunoblotting of rat heart extracts for the p17 subunit of caspase-3 (Fig. 3A, left) detected only the inactive 32-kD zymogen in nonischemic hearts. Ischemia/reperfusion caused caspase-3 activation, with the appearance of the processed p17 subunit in the vehicle group. Treatment with Ac-DEVD-CHO before reperfusion almost completely

blocked activation of caspase-3 induced by ischemia/reperfusion.

To determine catalytic activity of caspase-3 in rat heart extracts, we used a fluorogenic caspase-3 substrate (Fig. 3A, right). When compared with the control group, caspase-3-like activity was more than fivefold increased by ischemia/reperfusion in the vehicle-treated group ($p < 0.05$). Treatment with Ac-DEVD-CHO from 5 min before reperfusion abolished activation of caspase-3, with proteolytic activity remaining close to baseline levels ($p < 0.05$ vs. vehicle-treated group).

These results demonstrate that Ac-DEVD-CHO is able to block the ischemia/reperfusion-induced activation of caspase-3.

Effects of Ac-DEVD-CHO on apoptosis. Increased apoptosis has been implicated in MI (9,10). Because Ac-DEVD-CHO can block apoptosis in various cell types (12), we determined the rate of apoptotic cells by TUNEL staining and internucleosomal DNA fragmentation.

As shown in Figure 3B, we detected single TUNEL-positive cells in the nonischemic myocardium, as well as in the vehicle-treated and Ac-DEVD-CHO-treated myocardium subjected to ischemia/reperfusion. The TUNEL-positive cells appeared to be mostly cardiomyocytes. Quantitative analysis (5 sectors of ~ 500 cells/sector; $n = 4$ hearts in each group) revealed a significant ($p < 0.05$) increase in the number of TUNEL-positive cells in both the vehicle-treated ($0.38 \pm 0.18\%$) and Ac-DEVD-CHO-treated ($0.42 \pm 0.31\%$) groups, compared with nonischemic control group ($0.05 \pm 0.03\%$).

This increase in the rate of myocardial apoptosis during ischemia/reperfusion was confirmed by the internucleosomal DNA fragmentation assay. Compared with the nonischemic control group, ischemia/reperfusion caused an increase in DNA strand breaks, with the typical "ladder" pattern (Fig. 3B, right). The ischemia/reperfusion-induced increase in apoptosis was similar in the vehicle-treated and Ac-DEVD-CHO-treated groups.

Effects of Ac-DEVD-CHO on troponin I degradation and calpain activity. Because the beneficial effect of Ac-DEVD-CHO on contractile recovery was largely independent of apoptosis, we investigated whether Ac-DEVD-CHO may inhibit other cysteine proteases, such as calpain. Because calpain-mediated cleavage of the thin-filament regulatory protein troponin I has been suggested as a molecular mechanism of stunning (1), we investigated the effects of Ac-DEVD-CHO on troponin I degradation and calpain activity.

Immunoblotting with an anti-troponin I antibody showed increased appearance of the characteristic troponin I fragment in vehicle-treated and Ac-DEVD-CHO-treated hearts subjected to ischemia/reperfusion (Fig. 4A). However, Ac-DEVD-CHO started 5 min before reperfusion did not quantitatively alter the troponin I degradation.

Using a fluorogenic calpain substrate, we were unable to

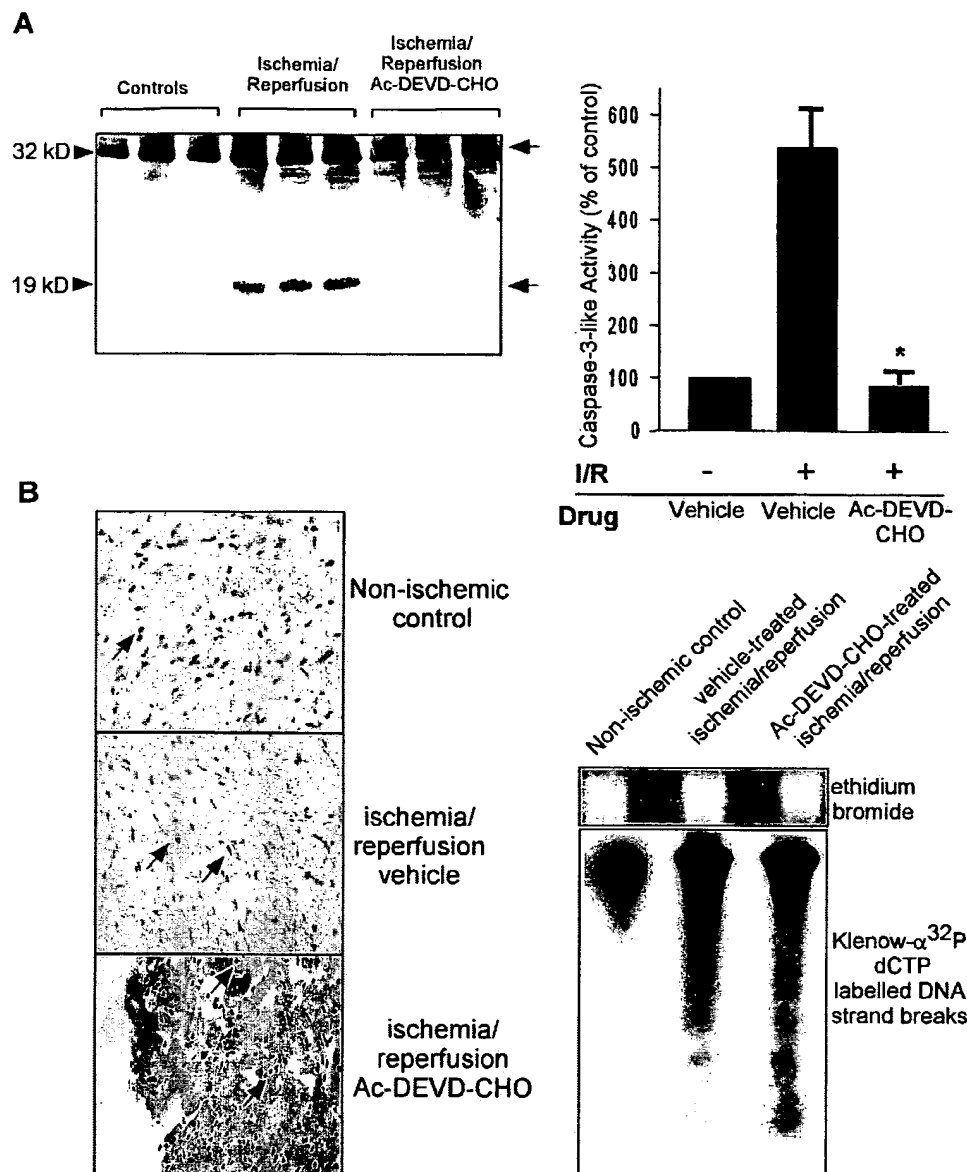


Figure 3. Ac-DEVD-CHO blocks ischemia/reperfusion (I/R)-induced caspase-3 activation but not apoptosis. (A, left), Immunoblotting of rat hearts with an antibody against the p17 subunit of caspase-3; three independent experiments are shown. Arrowheads indicate the molecular weight of the inactive zymogen (32 kD) and the processed, active subunit (17 kD). (A, right), Caspase-3-like proteolytic activity of rat hearts (percent increase relative to the proteolytic activity in control hearts), as measured with a fluorogenic substrate of caspase-3. * $p < 0.05$. (B, left), Representative photomicrographs of myocardial sections stained with the TUNEL technique to detect apoptotic cells in situ in a nonischemic control heart (top), a vehicle-treated heart subjected to ischemia/reperfusion (middle) or an Ac-DEVD-CHO-treated heart subjected to ischemia/reperfusion (bottom). Arrows indicate TUNEL-positive cells. Magnification 200X. (B, right) Autoradiogram of radioactively labeled DNA strand breaks, followed by agarose gel electrophoresis; results from four independent samples in each group. Equal loading was verified by ethidium bromide staining. Note the internucleosomal DNA fragmentation ("ladder pattern") induced by ischemia/reperfusion.

reproducibly detect measurable calpain-like proteolytic activity in any of the rat hearts (data not shown). To address a potential nonspecific effect of Ac-DEVD-CHO on calpain, we determined the effects of Ac-DEVD-CHO on purified calpain I *in vitro*. The addition of calpain to its substrate caused a linear increase in fluorescence (Fig. 4B). While the increase was still linear, calpain inhibitor I or Ac-DEVD-CHO was added. Although 100 nmol/l of calpain inhibitor I almost completely inhibited calpain I, the same concentration of Ac-DEVD-CHO had little inhibi-

tory effect. Quantitative evaluation of the remaining catalytic activity after addition of the inhibitor (Fig. 4C) showed that the cysteine protease calpain could be principally inhibited by the aldehyde Ac-DEVD-CHO at higher concentrations ($\geq 1 \mu\text{mol/l}$). However, 10-fold higher concentrations of Ac-DEVD-CHO were needed to achieve an equal inhibition of calpain, compared with calpain inhibitor I. Taken together, these results indicate that, *in vivo*, Ac-DEVD-CHO does not act primarily through calpain inhibition.

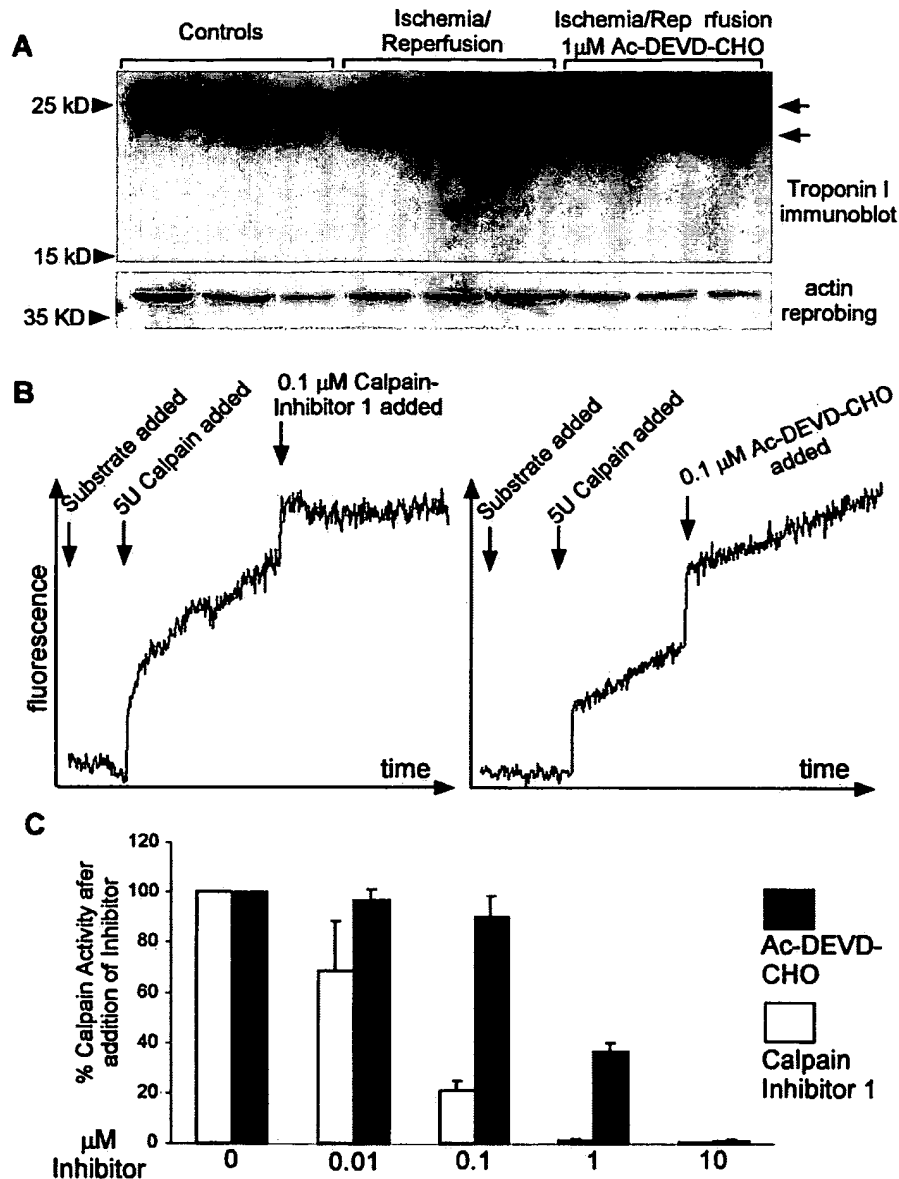


Figure 4. Effects of DEVD-CHO on troponin I degradation and calpain activity. (A) Immunoblots of rat hearts with an antibody against troponin I (upper blots) or actin (lower blots). Arrowheads indicate the molecular weight. The top right arrow indicates full-length troponin I; the lower arrow indicates the major degradation product. (B) Effects of 0.1 μ mol/l of calpain inhibitor I (left) or Ac-DEVD-CHO (right) on the catalytic activity of 5 U of calpain I, as measured in vitro with a fluorogenic calpain I substrate. (C) Quantitative evaluation of the percent activity after addition of the inhibitor, compared with the activity measured before addition of the inhibitor. Data are presented as the mean value \pm SEM from three independent measurements for each data point.

DISCUSSION

The caspase-3 inhibitor Ac-DEVD-CHO significantly improves post-ischemic contractile recovery of isolated working hearts of rats. Interestingly, Ac-DEVD-CHO was effective even when given after the onset of low-flow ischemia. The effects of caspase-3 inhibition appeared to be largely independent of cardiomyocyte apoptosis.

Myocardial stunning and caspase-3 activation. The role of apoptosis in the pathogenesis of myocardial stunning is unknown. Because caspase-3 is a key protease that executes

apoptosis, we investigated whether caspase-3 inhibition reduces myocardial stunning in an isolated working-heart rat model. This model is well established and allows study of myocardial contractility in the intact heart, independent of compounding factors, such as sympathetic activity and activation of an immune response (17). Indeed, caspase-3 was activated in our model of myocardial stunning. Thus, our data confirm and extend two recently published studies demonstrating activation of caspase-3 in a rat and rabbit model of MI (9,10). As hypothesized, Ac-DEVD-CHO was able to block the

ischemia/reperfusion-induced activation of caspase-3 in our experimental model.

Ac-DEVD-CHO functionally improves stunned myocardium. In contrast to the vehicle, the caspase-3 inhibitor Ac-DEVD-CHO dose-dependently and significantly improved post-ischemic contractile recovery. Just 1 $\mu\text{mol/l}$ led to almost a doubling of all contractile variables to 60% to 85% of the pre-ischemic values. These good recovery rates principally achievable with an appropriate pharmacologic intervention also demonstrate that low-flow ischemia/reperfusion in our model causes mainly myocardial stunning but little if any MI. Importantly, Ac-DEVD-CHO was equally potent in reducing myocardial stunning when given 5 min before reperfusion, instead of before the induction of ischemia. This scenario being given resembles the clinical situation.

Myocardial stunning and apoptosis. Although the beneficial effect of caspase inhibitors in experimental MI has been attributed to a reduced rate of apoptosis (7,10), our data do not support a role for the inhibition of apoptosis as the mechanism by which Ac-DEVD-CHO acts on the contractile recovery of stunned myocardium. Ac-DEVD-CHO neither reduced the number of TUNEL-positive cells, nor the amount of internucleosomal DNA fragmentation. Although ischemia/reperfusion-induced caspase-3-activation was associated with a minor increase in the number of apoptotic cells and fragmented DNA, there was no significant effect of DEVD-CHO on the degree of apoptosis. Thus, apoptosis of cardiac myocytes in this experimental setting seems to be mediated by a caspase-independent pathway. Indeed, a recent study suggests that other signalling pathways can induce apoptosis independent of the caspase cascade (18). Moreover, it remains to be clarified whether an increase of apoptosis of $\sim 0.3\%$ has any significant outcome with regard to the early functional integrity of the heart. Therefore, the profound improvement in post-ischemic contractile recovery by the caspase-3 inhibitor Ac-DEVD-CHO appears to be independent of apoptosis in the experimental setting used. These findings indicate that the integrity of the contractile apparatus may be adversely affected by caspase-3 activation in the myocardium during stunning.

Degradation of contractile proteins during myocardial stunning. Selective troponin I degradation has been reported in some (1-5,19), but not all (20), models of myocardial stunning. Transgenic overexpression of the major proteolytic troponin I product in the heart is sufficient to recapitulate many aspects of myocardial stunning (21). Subsequent studies suggested calpain-mediated cleavage of troponin I as an underlying mechanism (2-5,19), and calpain inhibitor I is able to reduce infarct size (22) and improve myocardial stunning (23). Because Ac-DEVD-CHO may inhibit other cysteine proteases, such as calpain, we investigated whether Ac-DEVD-CHO may inhibit troponin I degradation. Consistent with published reports (2-5,19), ischemia/reperfusion in isolated working hearts of

rats resulted in partial troponin I degradation, which was not quantitatively affected by Ac-DEVD-CHO. In vitro, purified calpain could be inhibited by Ac-DEVD-CHO. However, 1 $\mu\text{mol/l}$ of Ac-DEVD-CHO achieved only partial calpain inhibition, indicating that it acts in vivo, primarily through pathway(s) other than calpain inhibition. However, we cannot exclude that Ac-DEVD-CHO exerts some of its beneficial effects by partial calpain inhibition. Calpain or other proteinase(s) may play a pathogenic role in our model, because we achieved only incomplete recovery with Ac-DEVD-CHO.

Alternatively, Ac-DEVD-CHO may inhibit cleavage of other contractile proteins. Through a data bank search with caspase cleavage motifs, we identified a putative caspase cleavage site (DEVD⁶³) in cardiac troponin C (12). However, immunoblots of rat hearts with troponin C antibodies did not show any troponin C degradation during ischemia-reperfusion (data not shown). Further experiments will be required to identify the molecular target(s) of caspase activation during stunning.

Conclusions. Taken together, in an isolated working-heart rat model of myocardial stunning, inhibition of ischemia/reperfusion-induced caspase-3 activation by Ac-DEVD-CHO results in a substantial improvement of post-ischemic contractile recovery. The observed effects appear to be independent of suppression of apoptosis, but most likely involve both caspase and calpain inhibition. Regardless of the underlying mechanism(s), the use of a caspase-3 inhibitor represents a potentially clinically relevant, novel therapeutic strategy to reduce myocardial stunning.

Acknowledgments

We thank Meike Stahmer and Doris Gehring for their excellent technical assistance.

Reprint requests and correspondence: Dr. Stefanie Dimmeler, Molecular Cardiology Unit, Department of Medicine IV, University of Frankfurt, Theodor-Stern-Kai 7, 60590 Frankfurt/Main, Germany. E-mail: Dimmeler@em.uni-frankfurt.de.

REFERENCES

1. Bolli R, Marban E. Molecular and cellular mechanisms of myocardial stunning. *Physiol Rev* 1999;79:609-34.
2. Gao WD, Atar D, Backx PH, Marban E. Relationship between intracellular calcium and contractile force in stunned myocardium: direct evidence for decreased myofilament Ca^{2+} responsiveness and altered diastolic function in intact ventricular muscle. *Circ Res* 1995;76:1036-48.
3. Gao WD, Liu Y, Mellgren R, Marban E. Intrinsic myofilament alterations underlying the decreased contractility of stunned myocardium: a consequence of Ca^{2+} -dependent proteolysis? *Circ Res* 1996;78:455-65.
4. McDonald KS, Moss RL, Miller WP. Incorporation of the troponin regulatory complex of post-ischemic stunned porcine myocardium reduces myofilament calcium sensitivity in rabbit psoas skeletal muscle fibers. *J Mol Cell Cardiol* 1998;30:285-96.
5. Van Eyk JE, Powers F, Law W, Larue C, Hodges RS, Solaro RJ. Breakdown and release of myofilament proteins during ischemia and ischemia/reperfusion in rat hearts: identification of degradation products and effects on the pCa-force relation. *Circ Res* 1998;82:261-71.

6. van den Hoff MJB, van den Eijnde SM, Viragh S, Moorman AFM. Programmed cell death in the developing heart. *Cardiovasc Res* 2000;45:603-20.
7. Gottlieb RA, Engler RL. Apoptosis in myocardial ischemia-reperfusion. *Ann N Y Acad Sci* 1999;874:412-26.
8. Narula J, Haider N, Virmani R. Apoptosis in myocytes in end-stage heart failure. *N Engl J Med* 1996;335:1182-9.
9. Yaoyita H, Ogawa K, Machara K, Maruyama Y. Attenuation of ischemia/reperfusion injury in rats by a caspase inhibitor. *Circulation* 1998;97:276-81.
10. Holly TA, Drincic A, Byun Y, et al. Caspase inhibition reduces myocyte cell death induced by myocardial ischemia and reperfusion in vivo. *J Mol Cell Cardiol* 1999;31:1709-15.
11. Thornberry NA, Lazebnik Y. Caspases: enemies within. *Science* 1998;281:1312-6.
12. Nicholson DW. Caspase structure, proteolytic substrates, and function during apoptotic cell death. *Cell Death Differ* 1999;6:1028-42.
13. Thornberry NA, Rano TA, Peterson EP, et al. A combinatorial approach defines specificities of members of the caspase family and granzyme B: functional relationships established for key mediators of apoptosis. *J Biol Chem* 1997;272:17907-11.
14. Nicholson DW, Ali A, Thornberry NA, et al. Identification and inhibition of the ICE/CED-3 protease necessary for mammalian apoptosis. *Nature* 1995;376:37-43.
15. Weiland U, Haendeler J, Ihling C, et al. Inhibition of endogenous nitric oxide synthase potentiates ischemia/reperfusion-induced myocardial apoptosis via a caspase-3 dependent pathway. *Cardiovasc Res* 2000;4:671-8.
16. Dimmeler S, Haendeler J, Nehls M, Zeiher AM. Suppression of apoptosis by nitric oxide via inhibition of interleukin-1-converting enzyme (ICE)-like and cysteine protease protein (CPP)-32-like proteases. *J Exp Med* 1997;185:601-8.
17. Merin RG. Myocardial "stunning" and substrate metabolism. *J Card Surg* 1994;9:479-81.
18. Susin SA, Daugas E, Ravagnan L, et al. Two distinct pathways leading to nuclear apoptosis. *J Exp Med* 2000;192:571-80.
19. Gao WD, Atar D, Liu Y, Perez NG, Murphy AM, Marban E. Role of troponin I proteolysis in the pathogenesis of stunned myocardium. *Circ Res* 1997;80:393-9.
20. Thomas SA, Fallavollita JA, Lee TC, Feng J, Canty JM, Jr. Absence of troponin I degradation or altered sarcoplasmic reticulum uptake protein expression after reversible ischemia in swine. *Circ Res* 1999;85:446-56.
21. Murphy AM, Kogler H, Georgakopoulos D, et al. Transgenic mouse model of stunned myocardium. *Science* 2000;287:488-91.
22. Iwamoto H, Miura T, Okamura T, et al. Calpain inhibitor-1 reduces infarct size and DNA fragmentation of myocardium in ischemic/reperfused rat heart. *J Cardiovasc Pharmacol* 1999;33:580-6.
23. Yoshida K, Inui M, Harada K, et al. Reperfusion of rat heart after brief ischemia induces proteolysis of caldesmon (nonerythroid spectrin or fodrin) by calpain. *Circ Res* 1995;77:603-10.

EVIDENCE OF APOPTOSIS IN ARRHYTHMOGENIC RIGHT VENTRICULAR DYSPLASIA

ZIAD MALLAT, M.D., ALAIN TEDGUI, PH.D., FABRICE FONTALIRAN, M.D., ROBERT FRANK, M.D., MICHEL DURIGON, M.D., AND GUY FONTAINE, M.D., PH.D.

ABSTRACT

Background Arrhythmogenic right ventricular dysplasia, a disorder that may lead to severe ventricular arrhythmias and sudden death, is characterized by the progressive replacement of myocardial cells by fat and fibrous tissue. We examined whether the loss of myocardial cells in this disease could result from cell death by apoptosis (programmed cell death).

Methods Specimens obtained at autopsy from the right ventricular myocardium of eight patients with arrhythmogenic right ventricular dysplasia and four age-matched normal subjects were analyzed. To identify individual cells undergoing apoptosis, we performed in situ end-labeling of fragmented DNA on paraffin sections using biotinylated deoxyuridine triphosphate and the enzyme terminal deoxynucleotidyl transferase. We also examined the level of expression of CPP-32, a cysteine protease required for apoptotic cell death in mammalian cells, using immunohistochemical techniques.

Results Apoptosis was detected in the right ventricular myocardium of six of the eight patients with arrhythmogenic right ventricular dysplasia and was absent in the controls. High levels of expression of CPP-32 were associated with positive in situ end-labeling of fragmented DNA.

Conclusions These results indicate that apoptotic myocardial cell death occurs in arrhythmogenic right ventricular dysplasia and may contribute to the loss of myocardial cells in this disorder. (N Engl J Med 1996;335:1190-6.)

©1996, Massachusetts Medical Society.

APOPTOSIS, or programmed cell death, is a highly regulated and active process that contributes to the control of cell number during development and to the maintenance of many adult tissues.¹⁻³ It is triggered by the activation of an internally encoded suicide program as a result of either extrinsic or intrinsic signals.⁴ Apoptosis differs morphologically from necrosis: it is characterized by blebbing of the cell membrane, a reduction in cell volume, condensation of nuclear chromatin, and endonucleolytic degradation of DNA at nucleosomal intervals.² Apoptotic bodies are digested or phagocytosed by adjacent cells or macrophages without inducing an inflammatory response.

The crucial role of apoptosis in pathologic conditions is increasingly being recognized.^{5,6} Recently, apoptosis was reported as a possible mechanism for

the loss of myocardial cells in an infant with Uhl's anomaly.⁷ Arrhythmogenic right ventricular dysplasia, a form of right ventricular cardiomyopathy that commonly leads to severe ventricular arrhythmias and sudden death,^{8,9} is characterized by noninflammatory loss of myocardial cells and their progressive replacement by fat and fibrous tissue.⁸⁻¹¹ We hypothesized that this loss of myocardial cells in arrhythmogenic right ventricular dysplasia may result from cell death by apoptosis.⁶

METHODS

Cardiac Specimens

Sections from the right ventricle of eight patients (five men and three women; mean [\pm SD] age, 47 ± 15 years) who died of arrhythmogenic right ventricular dysplasia were examined. Five of the patients had documented ventricular arrhythmias. The final diagnosis of right ventricular dysplasia was based on the following established criteria⁹⁻¹²: massive infiltration of the right ventricular wall by fat tissue, with surviving strands of cardiomyocytes embedded in or bordered by fibrous tissue (Fig. 1), a finding typically distinct from the patchy replacement of myocardium by fat and fibrous tissue that may result from chronic myocarditis and also distinct from the strands of cardiomyocytes found in fatty tissue without fibrosis, which could be a normal variant¹⁰; sparing of subendocardial myocardium which may show trabecular hypertrophy or disarrangement (Fig. 1); substantial sparing of the left ventricular myocardium; and the absence of other cardiac diseases. These criteria were present in all the patients studied. Extensive mononuclear infiltrates and diffuse interstitial fibrosis superimposed on the typical pattern of arrhythmogenic right ventricular dysplasia were observed on histologic analysis in only one patient.

Sections from the right ventricle of four normal subjects (three men and one woman; mean age, 41 ± 16 years) who died of other, noncardiac causes served as controls. None of these control subjects met any of the histologic criteria for right ventricular dysplasia. Although the interval between death and autopsy did not affect the detection of apoptosis, only cases in which this interval was 24 hours or less were included. Tissues were fixed in 10 percent buffered formalin and embedded in paraffin. Four to six sections (6 μ m thick) from each paraffin block were analyzed for the presence of apoptosis.¹³

In Situ Detection of Apoptotic Cells

Sections were deparaffinized, transferred to xylene, and rehydrated in descending concentrations of alcohol (100 percent,

From the Centre de Rythmologie et de Stimulation Cardiaque, Hôpital Jean Rostand, Ivry-sur-Seine (Z.M., F.F., R.F., G.F.); INSERM Unité 141, Hôpital Lariboisière, Paris (Z.M., A.T.); and the Service d'Anatomie et de Cytologie Pathologiques, Hôpital Raymond Poincaré, Garches (M.D.) — all in France. Address reprint requests to Dr. Mallat at the Centre de Rythmologie et de Stimulation Cardiaque, Hôpital Jean Rostand, 39, rue Jean-le-Galleu, 94200 Ivry-sur-Seine, France.

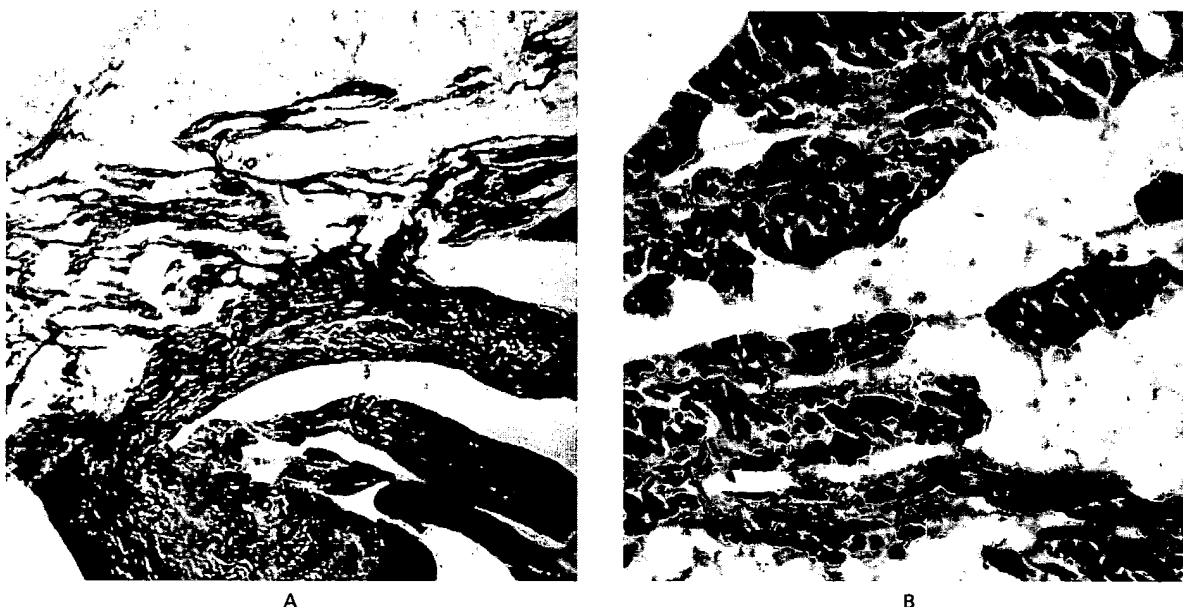


Figure 1. Free Wall of the Right Ventricle of a Patient with Right Ventricular Dysplasia.

In Panel A, there is a large amount of adipose tissue occupying the mediomural and subepicardial layers (hematoxylin-phloxin-safran staining, $\times 10$). In Panel B, high magnification reveals surviving strands of myocardium bordered by or embedded in fibrous tissue. The presence of fibrous tissue is necessary for the diagnosis of right ventricular dysplasia¹⁰ (hematoxylin-phloxin-safran staining, $\times 100$).

95 percent, 70 percent, 50 percent, and 0 percent). After rehydration, the slides were incubated with 20 μ g of proteinase K per milliliter in phosphate-buffered saline. Endogenous peroxidase was inactivated by 3 percent hydrogen peroxide. Tissue sections were stained with an ApopDETEK system (Enzo Diagnostics, Farmingdale, N.Y.) that identifies cells with internucleosomal fragmentation of DNA (apoptosis). The procedure was performed according to the manufacturer's instructions. The method is based on the preferential binding of terminal deoxynucleotidyl transferase (TdT) to the 3'-hydroxyl ends of DNA.¹³ Briefly, residues of biotinylated deoxyuridine triphosphate (dUTP) were catalytically added to the ends of DNA fragments with the enzyme TdT. For negative controls, deionized water was used instead of TdT. After end-labeling, the sections were incubated with avidin-horseradish peroxidase and stained with diaminobenzidine to detect the biotin-labeled nuclei. Apoptotic bodies stained brown. Positive controls consisted of rat mammary glands obtained on the fourth day after weaning (Oncor, Gaithersburg, Md.). Four to six sections from each specimen were examined. Sections were first examined under light microscopy at low magnification ($\times 100$), allowing estimation of the percentage of surface area occupied by apoptotic cells. Then, 10 random fields per section from the regions with apoptotic cells were examined at a higher magnification ($\times 400$) to calculate the percentage of myocardial nuclei with DNA fragmentation. Cardiomyocytes, which were well-shaped, elongated, and striated cells, were easily distinguished morphologically from other rare nonmyocytes under a light microscope at high magnification. In addition to the in situ end-labeling technique, adjacent sections stained with hematoxylin and eosin were examined for signs of apoptosis.¹⁴ The pathologist analyzing the specimens was unaware of the diagnosis in 9 of the 12 cases examined.

Immunohistochemical Detection of Protease CPP-32

CPP-32 is a cysteine protease required for the initiation of apoptotic cell death.¹⁵ It is related to interleukin-1 β -converting en-

zyme (ICE) and CED-3, the product of a gene required for programmed cell death in the nematode *Caenorhabditis elegans*. CPP-32 is the specific ICE/CED-3-like mammalian cysteine protease that cleaves and inactivates poly(adenosine diphosphate ribose) polymerase, an enzyme involved in DNA repair and genome integrity, and thus may be the human equivalent of CED-3.¹⁵ Therefore, to provide further evidence of the occurrence of apoptosis in arrhythmogenic right ventricular dysplasia, we analyzed the level of expression of CPP-32 in the right ventricles of the patients and controls using immunohistochemical techniques.

After deparaffinization and rehydration, the sections were incubated with 1:10 normal horse serum for 30 minutes at room temperature, washed once in phosphate-buffered saline, and stained with a mouse monoclonal anti-CPP-32 antibody (Transduction Laboratories, Lexington, Ky.) at a dilution of 1:1000. The slides were washed in phosphate-buffered saline and then incubated with biotinylated horse antimouse IgG (Vector Laboratories, Burlingame, Calif.) at a dilution of 1:200. Stains were visualized with an avidin-alkaline phosphatase-substrate system (Vectastain ABC Kit and Vector Red, Vector Laboratories, Burlingame, Calif.). As a negative control, serial sections were stained without the primary antibody against CPP-32.

RESULTS

Evidence of Apoptosis

In situ end-labeling of fragmented DNA with TdT and biotinylated dUTP did not reveal apoptosis in sections of right ventricular myocardium from the four normal adult subjects (Fig. 2A). In contrast, sections of right ventricular myocardium from six of the eight patients with arrhythmogenic right ventricular dysplasia showed numerous cells with genomic DNA fragments in their nuclei (Fig. 2B, 2C,

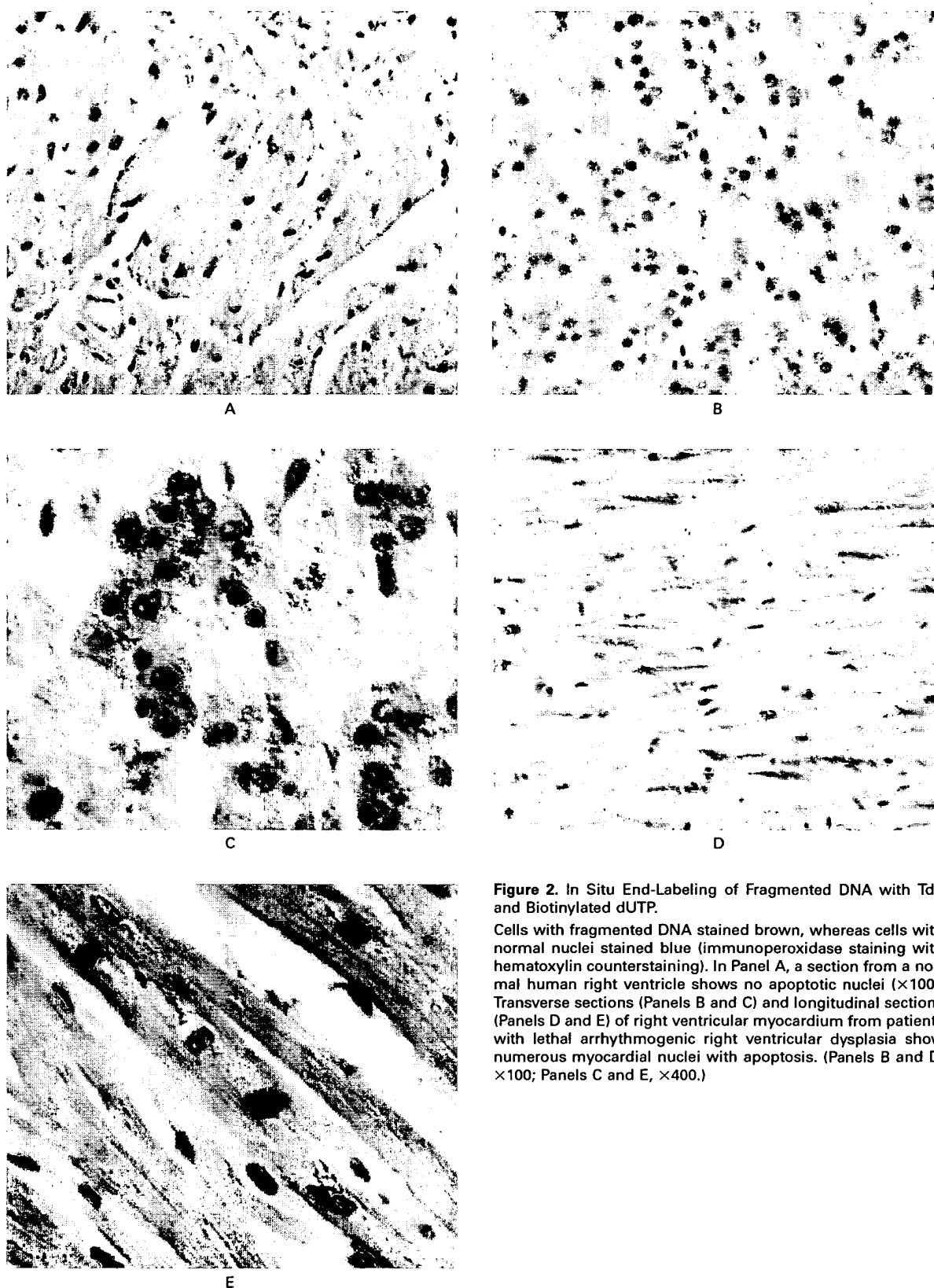


Figure 2. In Situ End-Labeling of Fragmented DNA with TdT and Biotinylated dUTP.

Cells with fragmented DNA stained brown, whereas cells with normal nuclei stained blue (immunoperoxidase staining with hematoxylin counterstaining). In Panel A, a section from a normal human right ventricle shows no apoptotic nuclei ($\times 100$). Transverse sections (Panels B and C) and longitudinal sections (Panels D and E) of right ventricular myocardium from patients with lethal arrhythmogenic right ventricular dysplasia show numerous myocardial nuclei with apoptosis. (Panels B and D, $\times 100$; Panels C and E, $\times 400$.)

2D, and 2E). The majority of these cells were easily recognized as myocardial cells under a light microscope at high magnification, since they were well shaped, elongated, and striated (Fig. 2C and 2E). The apoptotic myocardial cells were frequently in regions of myocardium not already invaded by adipocytes and fibrosis. They were less frequently in regions replaced by fat and fibrous tissue, where rare, nonapoptotic cardiomyocytes were still present. Both the extent of regions with apoptotic cells and the percentage of apoptotic myocardial cells in these regions varied among the patients (Table 1). An inflammatory reaction was detected in sections from one of the eight patients (Patient 1). This patient had the highest percentage of apoptotic myocardial cells, and some inflammatory cells were also apoptotic (Table 1 and Fig. 3).

The detection of apoptotic cells by in situ end-labeling of fragmented DNA was supported by the fact that pathological criteria for apoptosis were also met. In adjacent sections stained with hematoxylin and eosin, nuclei of numerous myocardial cells showed marginated masses of chromatin along with discrete, well-preserved apoptotic bodies (Fig. 4), typical pathological features of apoptosis.¹⁴ No sign of apoptosis was seen in adjacent sections stained with hematoxylin and eosin from the four normal subjects (data not shown).

Expression of CPP-32 in Right Ventricular Myocardium from Patients with Arrhythmogenic Right Ventricular Dysplasia

Protease CPP-32 is important for the induction of apoptotic cell death in mammalian cells.¹⁵ It was undetectable or barely detectable in the right ventricles of the four normal subjects (Fig. 5A), as well as in the two patients with no evidence of apoptosis. However, cardiomyocytes from the right ventricles of the six patients with apoptosis showed high levels of immunoreactive CPP-32 (Fig. 5B). No staining was detected after omission of the primary anti-CPP-32 antibody.

DISCUSSION

We report the occurrence of apoptotic myocardial cell death in right ventricular dysplasia. James⁶ has previously suggested that apoptosis may be a mechanism of cell death in arrhythmogenic right ventricular dysplasia.

In the present study, apoptosis was identified by in situ end-labeling of fragmented DNA with TdT and biotinylated dUTP, a commonly accepted method for the detection of the apoptotic process.¹⁶ There has been concern about the ability of such in situ labeling methods to distinguish between cell necrosis and apoptosis. However, in this study the detection of a positive reaction with in situ end-labeling was correlated with the presence of typical

TABLE 1. EXTENT OF AREAS OF APOPTOSIS AND THE PERCENTAGE OF APOPTOTIC MYOCARDIAL NUCLEI IN THESE AREAS IN SECTIONS OF RIGHT VENTRICULAR MYOCARDIUM FROM PATIENTS WITH LETHAL ARRHYTHMOGENIC RIGHT VENTRICULAR DYSPLASIA.*

| PATIENT NO. | EXTENT OF AREAS WITH APOPTOTIC NUCLEI | PROPORTION OF APOPTOTIC NUCLEI IN POSITIVE AREAS |
|-------------|---------------------------------------|--|
| | % of section | % |
| 1 | 50 | 28 |
| 2 | 20 | 15 |
| 3 | 10 | 18 |
| 4 | 20 | 20 |
| 5 | 0 | 0† |
| 6 | 15 | 22 |
| 7 | 15 | 14 |
| 8 | 0 | 0† |

*Four to six sections from each specimen were examined. After in situ end-labeling of fragmented DNA, sections were examined under light microscopy at low magnification ($\times 100$), allowing an estimation of the surface area occupied by apoptotic cells. Then, 10 random fields per section from these positive areas were examined at high magnification ($\times 400$) to calculate the percentage of myocardial nuclei with DNA fragmentation.

†Only one apoptotic cell per section was found.

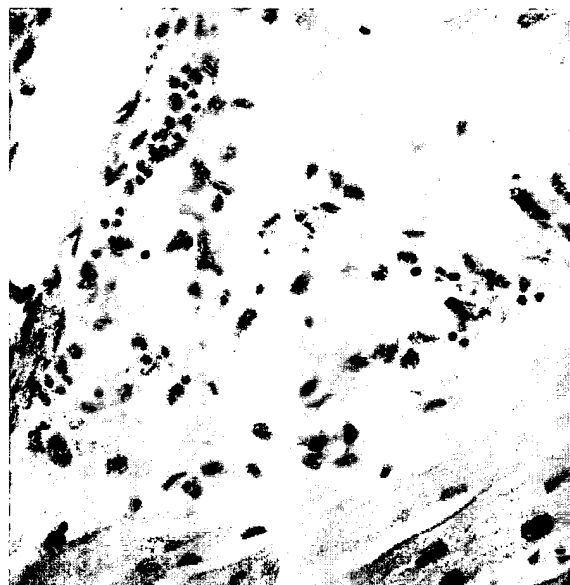


Figure 3. Apoptotic Nuclei in Nonmyocytes in an Inflammatory Reaction in One Patient (Immunoperoxidase Staining with Hematoxylin Counterstaining, $\times 250$).

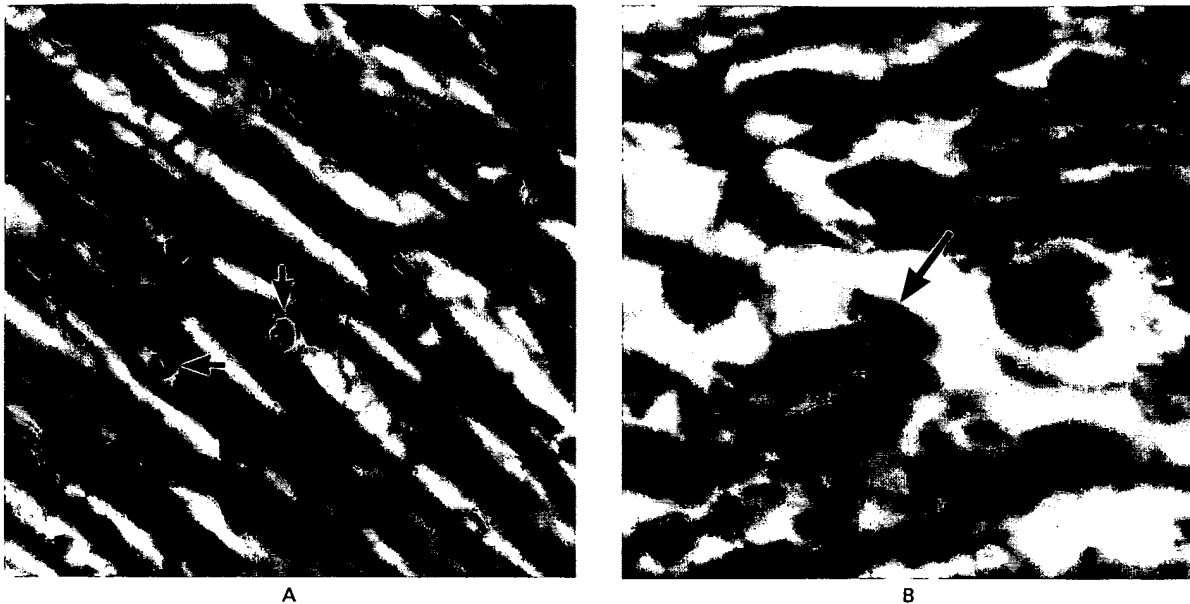


Figure 4. Sections of Right Ventricular Myocardium from Patients with Lethal Arrhythmogenic Right Ventricular Dysplasia (Hematoxylin and Eosin).

In Panel A, there are margined masses of chromatin within myocardial nuclei in a longitudinal section (arrows) ($\times 250$). In Panel B there are multiple round, hyperdense nuclear fragments, whose appearance is consistent with that of apoptotic bodies, in a transverse section (arrow) ($\times 400$).

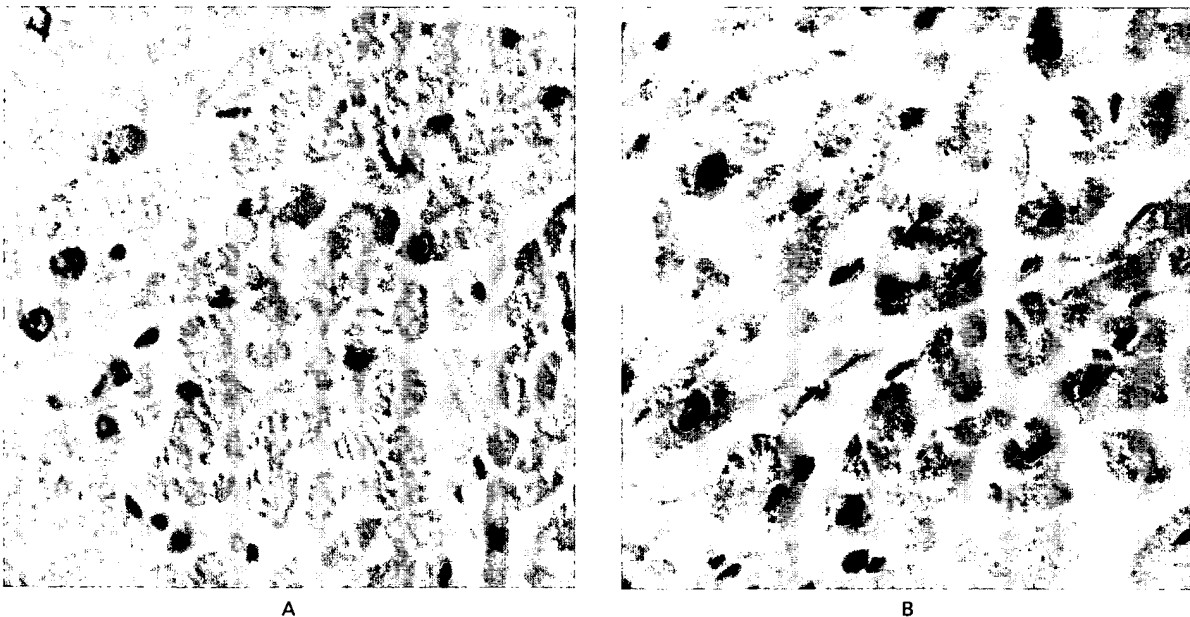


Figure 5. Immunohistochemical Detection of CPP-32.

In Panel A, normal right ventricular myocardium does not stain for CPP-32 ($\times 400$). In Panel B, right ventricular myocardium from a patient with right ventricular dysplasia stains intensely for CPP-32 ($\times 400$). The antibody against CPP-32 was detected with anti-mouse IgG conjugated with biotin and an avidin-alkaline phosphatase-substrate system in which positive cells stain red.

signs of apoptosis (marginated masses of chromatin and well-preserved apoptotic bodies) in sections stained with hematoxylin and eosin.¹⁴ Moreover, the absence of an inflammatory reaction in most of our patients argues against necrosis and for apoptosis. Furthermore, no positive staining was detected in cardiomyocytes from age-matched normal subjects whose hearts were processed in the same manner as those of our patients, and the *in situ* end-labeling of fragmented DNA was not detected when the enzyme TdT was omitted.

To gain further evidence of apoptosis in arrhythmogenic right ventricular dysplasia and extend our findings, we examined the level of expression of protease CPP-32, whose activation is specifically required for apoptotic cell death in mammalian cells.¹⁵ Our finding that high levels of CPP-32 expression were associated with positive *in situ* end-labeling of fragmented DNA provides strong evidence of apoptotic cell death in arrhythmogenic right ventricular dysplasia.

We found that numerous cells in the right ventricle of patients with arrhythmogenic right ventricular dysplasia underwent apoptosis. The majority of these cells were morphologically identified as myocardial cells under high-power magnification. The affected areas had few or no apoptotic cells, whereas apoptotic nuclei were frequently seen in areas with little involvement. This finding suggests that the loss of myocardial cells through apoptosis is, at least in part, a primary process that precedes the filling of acellular space by fat and fibrous tissue in the absence of an inflammatory reaction.

The extent and the percentage of apoptotic myocardial cells varied among the patients. The absence of apoptosis (only one apoptotic cell per section) in two of our patients is intriguing. These patients' clinical and histologic features were similar to those of the other patients. Apoptosis may therefore not have been involved in the pathogenesis of arrhythmogenic right ventricular dysplasia in these patients. However, the possibility that most of the apoptotic cells had already been cleared by the time the heart sections were obtained cannot be ruled out. Studies of the clearance kinetics of apoptotic myocardial cells should clarify this issue.

The triggering factors for apoptotic myocardial cell death in arrhythmogenic right ventricular dysplasia remain to be elucidated. Some evidence from *in vitro* and *in vivo* studies in animals suggests that hypoxia as well as reperfusion injury are possible triggers for apoptosis in cardiomyocytes.^{17,18} These factors may also contribute to the induction of apoptosis in myocardial cells of the failing canine heart.¹⁹ Repeated ventricular arrhythmias may have produced an ischemia-reperfusion injury and contributed to the apoptotic process in our patients. The presence of myocarditis (and its related production of inflammatory cytokines) could also have had a role in the

induction or aggravation of the apoptotic process. However, myocarditis is not a consistent or prominent feature of arrhythmogenic right ventricular dysplasia, and only one of our patients had associated myocarditis. Abnormal levels of resting tension, which could result from the architectural rearrangement of the myocyte compartment in the diseased right ventricle, could also have contributed to the activation of the suicide program in these cells.²⁰ Finally, primary abnormal control of genes involved in the regulation of programmed cell death — for instance, CPP-32 — remains plausible.

In conclusion, we found that numerous myocardial cells from the right ventricles of a majority of patients with lethal arrhythmogenic right ventricular dysplasia actively undergo programmed cell death. This finding could account, at least in part, for the progressive loss of myocardial cells observed in this disease and may shed new light on its pathogenesis.

Supported by the Association pour l'Etude des Cardiomyopathies and by an award from Assistance Publique, Hôpitaux de Paris (to Dr. Mallat).

We are indebted to Dr. Jane-Lyse Samuel for helpful discussion of the manuscript.

REFERENCES

1. Kerr JFR, Wyllie AH, Currie AR. Apoptosis: a basic biological phenomenon with wide-ranging implications in tissue kinetics. *Br J Cancer* 1972; 26:239-57.
2. Wyllie AH, Kerr JFR, Currie AR. Cell death: the significance of apoptosis. *Int Rev Cytol* 1980;68:251-306.
3. Walker NI, Harmon BV, Gobé GC, Kerr JFR. Patterns of cell death. *Methods Achiev Exp Pathol* 1988;13:18-54.
4. Williams GT, Smith CA. Molecular regulation of apoptosis: genetic controls on cell death. *Cell* 1993;74:777-9.
5. Carson DA, Ribeiro JM. Apoptosis and disease. *Lancet* 1993;341:1251-4.
6. James TN. Normal and abnormal consequences of apoptosis in the human heart: from postnatal morphogenesis to paroxysmal arrhythmias. *Circulation* 1994;90:556-73.
7. James TN, Nichols MM, Sapire DW, DiPatre PL, Lopez SM. Complete heart block and fatal right ventricular failure in an infant. *Circulation* 1996; 93:1588-600.
8. Marcus FI, Fontaine GH, Guiraudon G, et al. Right ventricular dysplasia: a report of 24 adult cases. *Circulation* 1982;65:384-98.
9. Thiene G, Nava A, Corrado D, Rossi L, Pennelli N. Right ventricular cardiomyopathy and sudden death in young people. *N Engl J Med* 1988; 318:129-33.
10. Fontaliran F, Fontaine G, Fillette F, Aouate P, Chomette G, Grosgeat Y. Frontières nosologiques de la dysplasie arythmogène: variations quantitatives du tissu adipeux ventriculaire droit normal. *Arch Mal Coeur* 1991; 84:33-8.
11. McKenna WJ, Thiene G, Nava A, et al. Diagnosis of arrhythmogenic right ventricular dysplasia/cardiomyopathy: Task Force of the Working Group Myocardial and Pericardial Disease of the European Society of Cardiology and of the Scientific Council on Cardiomyopathies of the International Society and Federation of Cardiology. *Br Heart J* 1994;71: 215-8.
12. Fontaine G, Fontaliran F, Andrade FR, et al. The arrhythmogenic right ventricle: dysplasia versus cardiomyopathy. *Heart Vessels* 1995;10: 227-35.
13. Gavrieli Y, Sherman Y, Ben-Sasson SA. Identification of programmed cell death *in situ* via specific labeling of nuclear DNA fragmentation. *J Cell Biol* 1992;119:493-501.
14. Kerr JFR, Winterford CM, Harmon BV. Morphological criteria for identifying apoptosis. In: Celis JE, ed. *Cell biology: a laboratory handbook*. Vol. 1. San Diego: Academic Press, 1994:319-29.
15. Nicholson DW, Ali A, Thornberry NA, et al. Identification and inhi-

bition of the ICE/CED-3 protease necessary for mammalian apoptosis. *Nature* 1995;376:37-43.

16. Gold R, Schmied M, Giegerich G, et al. Differentiation between cellular apoptosis and necrosis by the combined use of in situ tailing and nick translation techniques. *Lab Invest* 1994;71:219-25.

17. Gottlieb RA, Bursleson KO, Kloner RA, Babior BM, Engler RL. Reperfusion injury induces apoptosis in rabbit cardiomyocytes. *J Clin Invest* 1994;94:1621-8.

18. Gottlieb RA, Gruol DL, Zhu JY, Engler RL. Preconditioning rabbit cardiomyocytes: role of pH, vacuolar proton ATPase, and apoptosis. *J Clin Invest* 1996;97:2391-8.

19. Sharov VG, Sabbah HN, Shimoyama H, Goussev AV, Lesch M, Goldstein S. Evidence of cardiocyte apoptosis in myocardium of dogs with chronic heart failure. *Am J Pathol* 1996;148:141-9.

20. Cheng W, Li B, Kajstura J, et al. Stretch-induced programmed myocyte cell death. *J Clin Invest* 1995;96:2247-59.

IMAGES IN CLINICAL MEDICINE

Images in Clinical Medicine, a weekly *Journal* feature, presents clinically important visual images, emphasizing those a doctor might encounter in an average day at the office, the emergency department, or the hospital. If you have an original unpublished, high-quality color or black-and-white photograph representing such a typical image that you would like considered for publication, send it with a descriptive legend to Karen Pedersen, *New England Journal of Medicine*, 10 Shattuck St., Boston, MA 02115. For details about the size and labeling of the photographs, the requirements for the legend, and authorship, please contact Karen Pedersen at 617-734-9800 (phone) or 617-739-9864 (fax), or the *New England Journal of Medicine* at images@edit.nejm.org (e-mail).

Quantitative Myocardial Cytokine Expression and Activation of the Apoptotic Pathway in Patients Who Require Left Ventricular Assist Devices

Emma J. Birks, MRCP; Najma Latif, PhD; Virginia Owen, PhD; Christopher Bowles, PhD; Leanne E. Felkin, BS; Anthony J. Mullen, BS; Asghar Khaghani, FRCS; Paul J.R. Barton, PhD; Julia M. Polak, DSc; John R. Pepper, FRCS; Nicholas R. Banner, FRCP; Magdi H. Yacoub, FRS, DSc

Background—Molecular mechanisms underlying the deterioration of patients undergoing LV assist device (LVAD) implantation remain poorly understood. We studied the cytokines tumor necrosis factor (TNF)- α and interleukin (IL)-1 β and IL-6 and the terminal stage of the apoptotic pathway in patients with decompensating heart failure who required LVAD support and compared them with patients with less severe heart failure undergoing elective heart transplantation.

Methods and Results—Myocardial and serum samples from 23 patients undergoing LVAD implantation were compared with those from 36 patients undergoing elective heart transplantation. Myocardial TNF- α mRNA (1.71-fold; $P < 0.05$) and protein (3.43 ± 0.19 versus 2.95 ± 0.10 pg/mg protein; $P < 0.05$) were elevated in the LVAD patients. Immunocytochemistry demonstrated TNF expression in the myocytes. Serum TNF- α was also elevated (12.5 ± 1.9 versus 4.0 ± 0.4 pg/mL; $P < 0.0001$) in the LVAD patients. IL-6 mRNA (2.57-fold higher; $P < 0.005$) and protein (27.83 ± 9.35 versus 4.26 ± 1.24 pg/mg protein; $P < 0.001$) were higher in the LVAD candidates, as was serum IL-6 (79.3 ± 23.6 versus 7.1 ± 1.6 pg/mL; $P < 0.0001$). Interleukin-1 β mRNA expression was 9.78-fold higher in the LVAD patients ($P < 0.001$). iNOS mRNA expression was similar to that in advanced heart failure patients and was not further elevated in the LVAD patients. Levels of procaspase-9 (8.02 ± 0.91 versus 6.16 ± 0.43 oligodeoxynucleotide [OD] units; $P < 0.01$), cleaved caspase-9 (10.02 ± 1.0 versus 7.34 ± 0.40 OD units; $P < 0.05$), intact and spliced DFF-45 (4.58 ± 0.75 versus 2.84 ± 0.23 OD units; $P < 0.05$) were raised in LVAD patients, but caspase-3 and human nuclease CPAN were not.

Conclusions—Elevated TNF- α , IL-1 β , and IL-6 and alterations in the apoptotic pathway were found in the myocardium and elevated TNF- α and IL-6 in serum of deteriorating patients who required LVAD support. These occurrences may have therapeutic implications and influence the timing of LVAD insertion. (*Circulation*. 2001;104[suppl I]:I-233-I-240.)

Key Words: heart-assist device ■ interleukins ■ heart failure ■ nitric oxide synthase

Left ventricular assist devices (LVADs) have become an established treatment for patients with severe heart failure. Molecular mechanisms underlying the decompensation of heart failure remain poorly understood. Understanding the mechanisms involved may help with decisions about timing of LVAD implantation and identifying new therapeutic targets in advanced heart failure.

Expression of the proinflammatory cytokine tumor necrosis factor (TNF)- α has been described in patients with chronic heart failure both in serum and myocardium,¹⁻⁵ and serum levels have been found to correlate with functional status.² TNF- α has been shown to produce myocardial depression both in vitro and in vivo models.^{2,3,6} Interleukin (IL)-6 also is elevated in myocardium and serum of patients with heart failure, and levels correlate with poor functional status.^{1,3,7,8}

IL-1 β is known to cause myocardial depression in vivo^{9,10} and acts synergistically with TNF- α ,¹⁰ but its role in heart failure is unclear.

TNF- α and IL-1 β can activate inducible nitric oxide synthase (iNOS), and their negative inotropic effect can be mediated through iNOS induction.¹¹ iNOS expression has been described in patients with heart failure.⁴ iNOS is a potent producer of nitric oxide, which can have a negative inotropic effect. TNF- α and IL-1 β also can induce apoptosis of cardiac myocytes,^{12,13} whereas IL-6 has antiapoptotic effects.^{14,15}

Apoptosis is tightly regulated by the caspases, which initially are translated as inactive proenzymes and are subsequently cleaved to become active. In the end stage of the apoptotic pathway, release of cytochrome c from the mito-

From the National Heart and Lung Institute at Imperial College School of Medicine (E.J.B., V.O., C.B., L.E.F., A.J.M., A.K., P.J.R.B., J.R.P., N.R.B., M.H.Y.), Royal Brompton and Harefield Hospital, Harefield, Middlesex; and Royal Postgraduate Medical School at Imperial College School of Medicine (J.M.P.), Hammersmith Hospital, London, UK.

Correspondence to Magdi Yacoub, FRS, Professor of Cardiothoracic Surgery, Heart Science Centre, Royal Brompton and Harefield Hospital, Harefield, Middlesex UB96JH, United Kingdom. E-mail emmabirks@hotmail.com

© 2001 American Heart Association, Inc.

Circulation is available at <http://www.circulationaha.org>

chondrion activates procaspase-9 to caspase-9, which, in turn, activates procaspase-3 to caspase-3. Caspase-3 activates DNA fragmentation factor, a heterodimer¹⁶ that consists of the active caspase-activated nuclease (CPAN)/DFF-40 complex, a 40-kDa nuclease, and DFF-45, its 45-kDa inhibitor. Caspase-3 cleaves DFF-45 from the CPAN/DFF-40–DFF-45 complex^{16,17} and generates the functionally active CPAN nuclease, which induces chromatin condensation and DNA fragmentation.¹⁸ Poly(ADP-ribose) polymerase (PARP), a DNA repair enzyme, is inactivated by caspase-3, which contributes to the demise of the cell. Our group and others have previously demonstrated evidence of activation of the apoptotic pathway in advanced heart failure.^{19,20}

These mechanisms all could contribute to decompensation of patients with advanced heart failure, who then require LVAD support. To investigate this hypothesis, we have quantified myocardial TNF- α , IL-1 β , and IL-6 expression; circulating TNF- α , its receptors, and IL-6; and myocardial expression of iNOS and of caspases in the terminal stage of the apoptotic pathway in patients who require insertion of an LVAD and compared them with patients with stable advanced heart failure awaiting heart transplantation. Our aim was to characterize better patients for which the findings could have implications for their management and to help to understand factors that could influence progression of heart failure.

Methods

Patients

Protocol for the present study was approved by the Royal Brompton and Harefield Research Ethics Committee. Informed consent was obtained from each patient.

LVAD Patients

The present study included 23 consecutive patients who required LVAD implantation because of deteriorating clinical status with evidence of secondary organ dysfunction in the context of low cardiac output (cardiac index <1.8), despite having been given appropriate medical treatment (including inotropes and intra-aortic balloon pump).

Serum markers were studied in all 23 patients (male, $n=20$; female, $n=3$; age range, 14 to 58 years; mean age 37 ± 3.1 years). Patients were diagnosed as having dilated cardiomyopathy ($n=17$), ischemic heart disease (IHD; $n=2$), IHD with postinfarct ventriculoseptal defect rupture ($n=2$), postpartum cardiomyopathy ($n=1$), or congenital heart disease ($n=1$). All were patients in New York Heart Association (NYHA) class IV and had deteriorated over a period of 3.2 ± 0.6 days. Mean pulmonary capillary wedge pressure (PCWP) was 26.0 ± 2.1 mm Hg. Mean LV end diastolic diameter (LVEDD) was 73.8 ± 6.0 mm, and LV end-systolic diameter (LVESD) was 68.6 ± 6.3 mm. Blood was collected from each patient immediately before insertion of the device.

Myocardial markers were studied in the first 13 of 23 patients (male, $n=10$; female, $n=3$; age range, 14 to 58 years; mean age, 35.5 ± 4.1 years). These patients were diagnosed as having dilated cardiomyopathy ($n=11$), ischemic heart disease with postinfarct ventriculoseptal defect rupture ($n=1$), or postpartum cardiomyopathy ($n=1$). All were in NYHA class IV with a history of deterioration over a period of 2.3 ± 0.6 days. Mean PCWP was 27.3 ± 2.5 mm Hg. Mean LVEDD was 75.5 ± 7.9 mm, and LVESD was 64.8 ± 9.8 mm. A core of myocardium from the apex of the LV was taken at the time of LVAD insertion, instantly frozen in liquid nitrogen, and stored at -80°C for subsequent analysis.

Heart Failure Patients

Patients with less-severe heart failure who were undergoing heart transplantation and did not meet our criteria for LVAD implantation acted as controls. Serum markers were studied in 17 patients (men, $n=14$; women, $n=3$; age range, 22 to 64 years; mean age, 46.1 ± 3.3 years). NYHA class was III in 13 and IV in 4. Patients were diagnosed as having dilated cardiomyopathy ($n=9$), ischemic heart disease ($n=7$), or postpartum cardiomyopathy ($n=1$). Mean PCWP was 25.4 ± 2.2 mm Hg, mean LVEDD was 70 ± 2 mm, and mean LVESD was 61.2 ± 3 mm.

Myocardial markers were studied in 36 patients (male, $n=30$; female, $n=6$; mean age, 46 ± 3.4 years). NYHA class was III in 31 and IV in 5. Patients were diagnosed as having dilated cardiomyopathy ($n=18$), ischemic heart disease ($n=15$), postpartum cardiomyopathy ($n=2$), or myocarditis ($n=1$). Mean PCWP was 21.9 ± 1.5 mm Hg, mean LVEDD was 71.4 ± 2.6 mm, and mean LVESD was 62.6 ± 2.5 mm. A sample of LV near the apex was taken at the time of transplantation, instantly frozen in liquid nitrogen, and stored at -80°C for subsequent analysis.

For all LVAD and heart failure patients, blood was spun within 4 hours of collection at 2500 rpm for 10 minutes, and serum supernatant was stored at -40°C for analysis.

Methods

Cytokines

Real-Time Quantitative Reverse Transcription-Polymerase Chain Reaction

TNF α , IL-1 β , IL-6, and iNOS mRNA were detected²¹ by polymerase chain reaction (PCR) amplification, quantified by 5' nuclease assay with fluorescence-labeled TaqMan probes and analyzed by use of real-time quantitative PCR as follows. Total RNA was extracted by use of Qiagen Inc RNeasy minicolumns and eluted in diethylpyrocarbonate-treated dH_2O . RNA quality and quantity was assessed by EtBr-agarose gel electrophoresis and by relative absorbance at 260 versus 280 nm. cDNA was synthesized from 150 ng of total RNA by use of the PE Biosystems reverse-transcriptase kit with random hexamer primers. Reactions were diluted to 100 μL . Primers and TaqMan probes for human IL-6 and iNOS were designed. Primer Express software (PE Biosystems) was used to design the IL-6 probe from a published mRNA sequence (EMBL/GenBank accession No. M54894), which gave an amplicon size of 96 bp with the TaqMan probe straddling the exon-exon junction (forward primer [Tm= 58°C], 5'-TGACAAACAAATTCGGTACATCCT-3'; reverse primer [Tm= 60°C], 5'-AGTGCCTCTTGTGCTTTCAC-3'; TaqMan probe [Tm= 68°C] 5'-TTACTCTTGTTACATGCTCTCCTTTCACGGGCTG-3'). The iNOS probe designed was 5'-CACCATAAGGCCAAAGGGATTTTAACTTGCAG-3' (Tm= 70°C), the forward primer was 5'-AGCGGGATGACTTTCCAAGA-3' (Tm= 58°C), and the reverse primer was 5'-TAATGGACCCAGGCAAGATT-3' (Tm= 59°C).

Perkin-Elmer primers and TaqMan probes for TNF- α and IL- β were used. PCR reactions were performed by use of an ABI-prism 7700 sequence detector. PCR amplifications were performed in a 25-mL volume that contained a 2.5-mL cDNA template in 2 \times PCR Master Mix (PE Biosystems) at 50°C for 2 minutes and 95°C for 10 minutes followed by 40 cycles of 95°C for 15 s and 60°C for 1 minute. Results were analyzed by use of Sequence Detection Software (PE Biosystems), and the level of expression of TNF- α , IL-1 β , IL-6, and iNOS mRNA was normalized to 18S rRNA as outlined in User Bulletin No. 2 provided by Perkin-Elmer.

Myocardial Immunoassay

Protein was extracted from myocardial tissue. Protein preparations were made by homogenizing myocardial biopsies in 20 mmol/L of HEPES and 1.5 mmol/L of EDTA solution that contained protease inhibitors aprotinin, leupeptin, DTT, and phenylmethylsulfonyl fluoride. Concentrations of TNF- α and IL-6 were determined by use of commercially available immunoassay kits (Quantikine HS, R&D Systems).

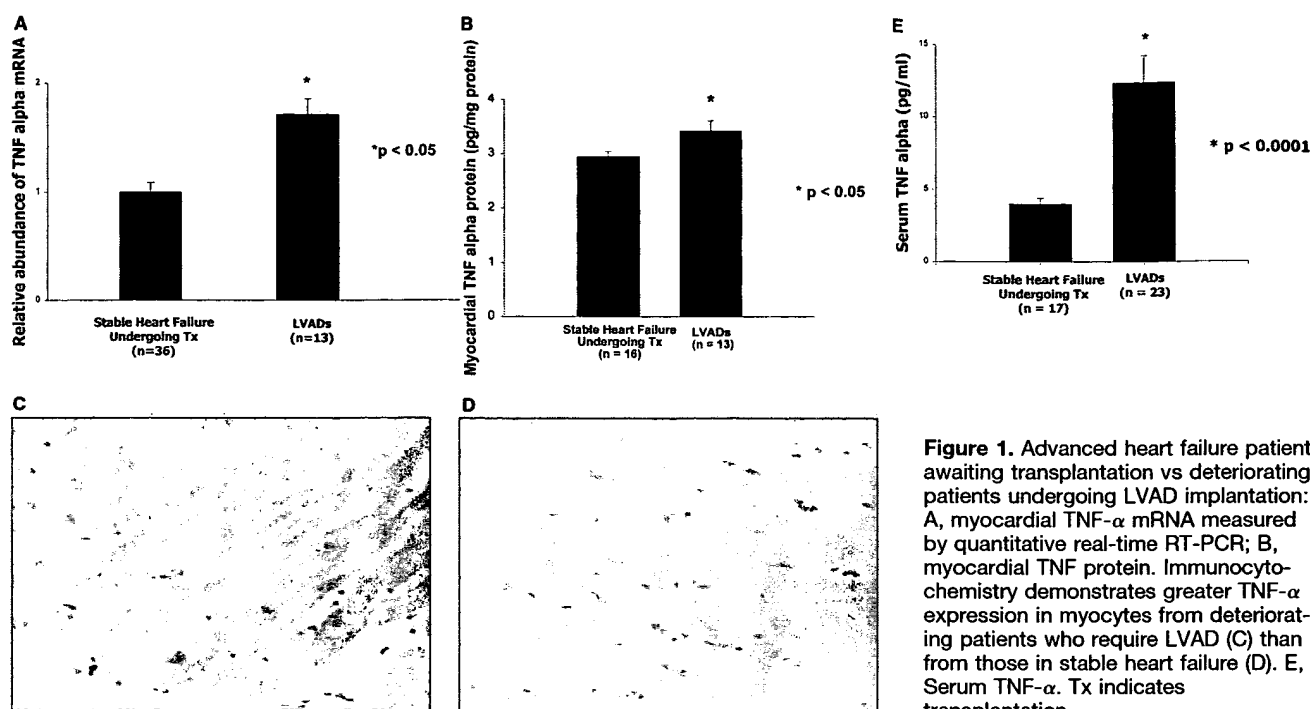


Figure 1. Advanced heart failure patients awaiting transplantation vs deteriorating patients undergoing LVAD implantation: A, myocardial TNF- α mRNA measured by quantitative real-time RT-PCR; B, myocardial TNF protein. Immunocytochemistry demonstrates greater TNF- α expression in myocytes from deteriorating patients who require LVAD (C) than from those in stable heart failure (D). E, Serum TNF- α . Tx indicates transplantation.

Immunocytochemistry

Immunocytochemistry was performed on formalin-fixed paraffin-embedded sections to localize TNF- α and iNOS expression. Avidin-biotin-peroxidase complex method was used. Endogenous peroxidase was blocked with a solution of 0.03% vol/vol hydrogen peroxide in methanol for 20 minutes. After incubation with normal goat serum (1:30 for 30 minutes), sections were incubated overnight at 4°C with primary rabbit antibodies to TNF- α (Antigenex America Inc) diluted 1:100 and incubated overnight with primary rabbit antibodies to iNOS (Transduction Labs) diluted 1:400. Immunoreaction sites were visualized by use of appropriate biotinylated secondary antibodies and the avidin-biotin-peroxidase complex procedure (Vector Labs). Peroxidase activity was revealed with a solution of diaminobenzidine as chromogen with 0.2% vol/vol hydrogen peroxide in PBS to produce a brown reaction product and sections counterstained with Harris' hematoxylin. Controls consisted of replacement of primary antibodies with nonimmune rabbit serum. Staining was graded 0 to 3 by two blinded independent observers.

Serum Immunoassay

Measurements of TNF- α , its receptors TNF-R1 and TNF-R2 and IL-6 were performed by use of commercially available immunoassay kits (Quantikine HS, R&D Systems).

Apoptotic Pathway

SDS-PAGE and Western Blotting

Myocardial tissue was homogenized in 1% SDS, 40 mmol/L phenylmethylsulfonyl fluoride, and total protein homogenates (30 μ g) separated on 12%-T SDS-PAGE gels with a 3%-T stacking gel. Gels were equilibrated for 30 minutes in transfer buffer (20 mmol/L Tris base and 150 mmol/L glycine) and electrophoretically transferred to supported nitrocellulose (Hybond C Super) at 500 mA for 1 hour.

Detection of Cellular Proteins

Nitrocellulose membranes were blocked with 3% non-fat dried milk in PBS that contained 0.05% Tween 20 for 1 hour and then probed with primary antibodies against caspase-9, caspase-3, and substrates (PARP and DFF; Santa-Cruz Biotechnology). After they were washed, blots were incubated for another 1 hour in horseradish peroxidase-conjugated secondary antibodies (Dako). Protein bands

were visualized by use of the Supersignal Ultra chemiluminescence substrate (Pierce).

Stripping Membranes

To stain tubulin after probing, blots were incubated in stripping solution (100 mmol/L 2-mercaptoethanol, 2% vol/vol SDS, and 62.5 mmol/L Tris-chloride; pH 6.7) for 30 minutes at 56°C. Membranes were washed and probed by use of tubulin with secondary horseradish peroxidase-conjugated antibodies. Reactive bands were detected as before.

Densitometry

Levels of expression of the procaspases, active caspases, and their substrates as assessed by immunoreactivity on ECL films was quantitated by laser densitometry and standardized to tubulin reactivity in each respective lane. Densitometric analysis was performed with Quant One software on a SunSparc station.

Cell Culture

Human U-937 myeloid leukemic cell line, treated separately with TNF- α at 4 mg/mL or staurosporine 1 μ mol/L for 4 hours, and Jurkat T lymphoblastoid cell line, treated with 1 μ mol/L of staurosporine for 6 hours, were used as positive controls.

Statistical Analysis

Variables are expressed as mean \pm SEM. Significance was assessed on grouped data with either Student's *t* test or nonparametric Mann-Whitney *U* test. A *P* value < 0.05 was considered significant.

Results

Cytokines

Myocardium

Tumor Necrosis Factor- α

TNF- α mRNA expression in myocardium of LVAD patients at time of implantation was 1.71-fold higher than in stable advanced heart failure patients ($P < 0.05$, Figure 1A). TNF- α

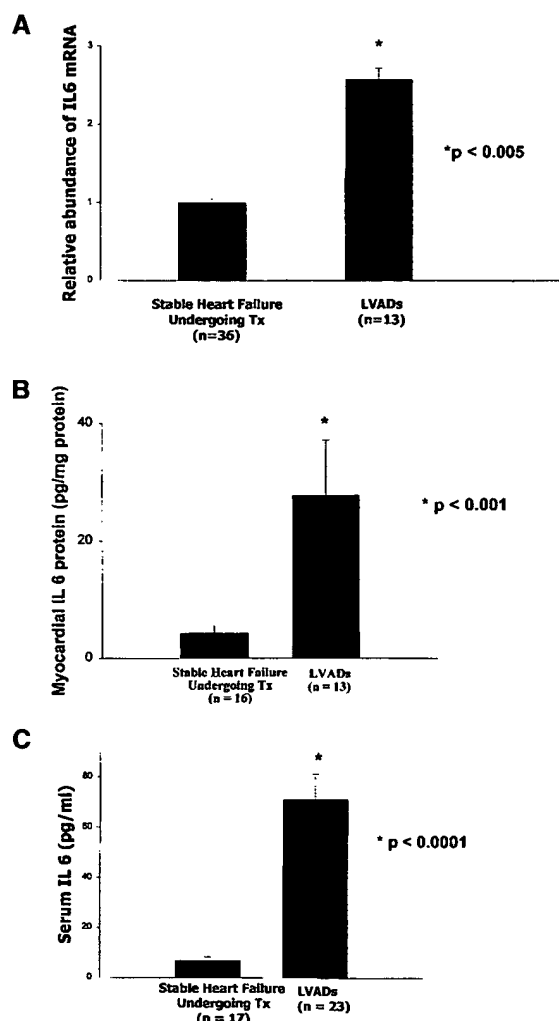


Figure 2. Advanced heart failure patients awaiting transplantation vs deteriorating patients undergoing LVAD implantation: A, myocardial IL-6 mRNA measured by quantitative real-time RT-PCR; B, myocardial IL-6 protein content; C, serum IL-6.

protein content in myocardium of LVAD candidates (3.43 ± 0.19 pg/mg protein) was also higher than in advanced heart failure (2.95 ± 0.10 pg/mg protein; $P < 0.05$, Figure 1B). Myocardial TNF- α protein was slightly higher in those who died after LVAD implantation (3.57 ± 0.2 pg/mg protein) compared with those who survived >1 year (3.1 ± 0.2 pg/mg protein), although this did not reach statistical significance ($P = \text{NS}$).

TNF- α Immunocytochemistry

TNF- α expression was immunolocalized predominantly to cardiac myocytes, although expression also was seen in endothelial cells and vascular smooth muscle cells of blood vessels. Myocyte expression of TNF- α in the LVAD candidates was significantly greater (mean score, 1.75 ± 0.20) than in advanced heart failure patients (mean score, 1.1 ± 0.16 ; $P < 0.05$, Figures 1C and 1D).

Interleukin-6

IL-6 mRNA expression in myocardium at time of LVAD implantation was 2.57-fold higher than in stable advanced

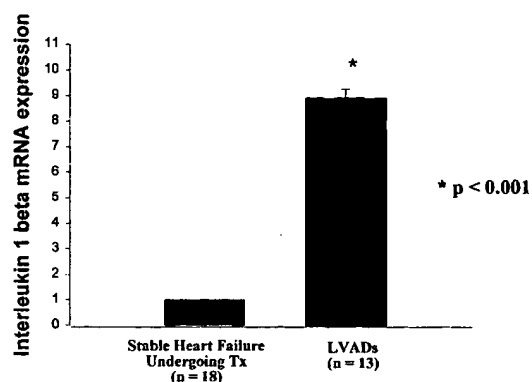


Figure 3. Myocardial IL-1 β mRNA levels in advanced heart failure patients awaiting transplantation vs deteriorating patients undergoing LVAD implantation.

heart failure patients ($P < 0.005$, Figure 2A). Myocardial IL-6 protein content also was significantly higher in LVAD candidates (27.83 ± 9.35 pg/mg protein) compared with advanced heart failure patients (4.26 ± 1.24 pg/mg protein; $P < 0.001$, Figure 2B). Myocardial IL-6 protein was significantly higher in those who died after LVAD implantation (38.94 ± 12.34 pg/mg protein) compared with those who survived >1 year (5.60 ± 1.64 pg/mg protein; $P < 0.005$). These deaths occurred in patients who were on the device; no transplant-related deaths occurred).

Interleukin-1 β

IL-1 β mRNA expression was 9.78-fold higher in LVAD candidates than in stable advanced heart failure patients (9.78 ± 0.36 versus 1 ± 0.23 ; $P < 0.001$, Figure 3). IL-1 β was 1.4-fold higher in those who died after LVAD implantation than in those that survived, but this did not reach statistical significance.

Inducible Nitric Oxide Synthase

iNOS mRNA expression in LVAD candidates (0.81 ± 0.19) was elevated to a level similar to that seen in advanced heart failure (1 ± 0.27), but iNOS mRNA was no higher in deteriorating patients compared with heart failure patients (Figure 4A).

iNOS Immunocytochemistry

Significantly more iNOS expression was seen in blood vessels of the LVAD candidates (vascular smooth muscle staining, 1.75 ± 0.19 versus 0.75 ± 0.17 ; $P < 0.005$, Figures 4B and 4C), and slightly more iNOS staining was seen in myocytes of LVAD candidates (2.35 ± 0.15 versus 1.93 ± 0.13 ; which only just reached statistical significance; $P < 0.05$).

Serum

Serum TNF- α

Serum TNF- α was significantly higher in LVAD candidates (12.5 ± 1.9 pg/mL, $n = 23$) compared with stable advanced heart failure patients (4.0 ± 0.4 pg/mL, $n = 17$; $P < 0.0001$, Figure 1E).

Serum TNF-R1 and TNF-R2

No significant difference was seen between serum TNF-R1 levels in LVAD candidates (2.9 ± 0.6 ng/mL, $n = 23$) and

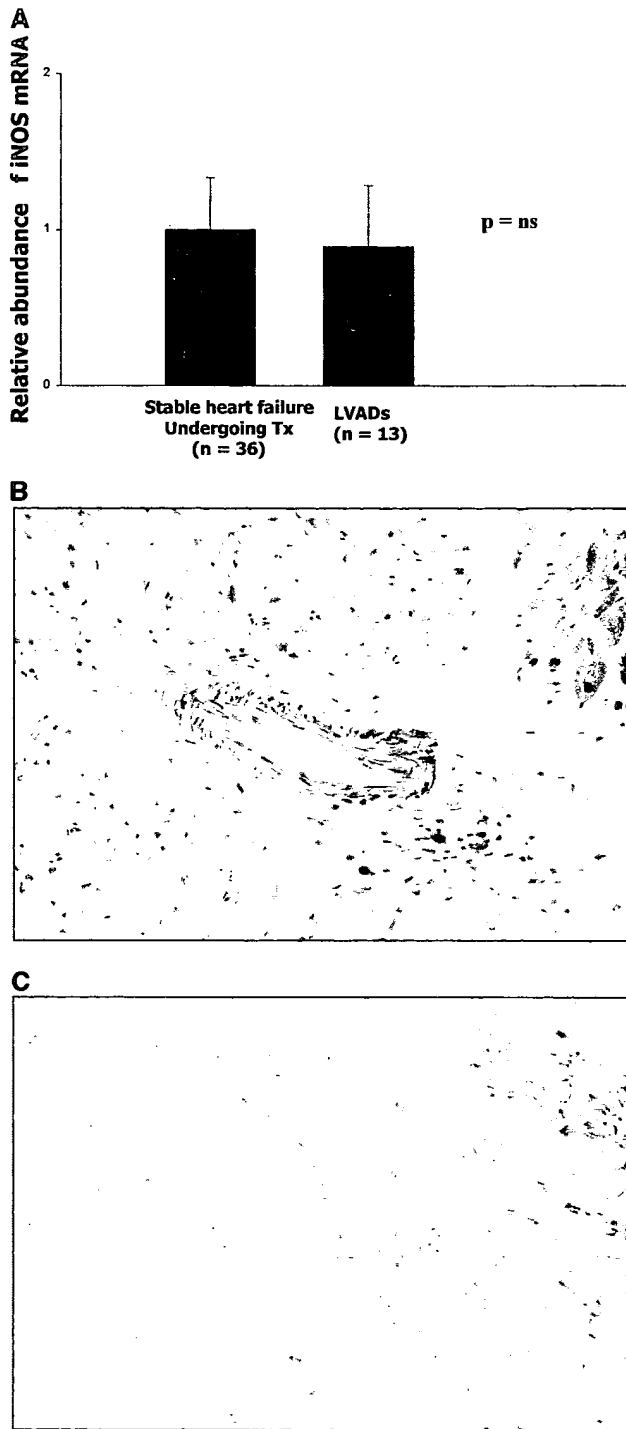


Figure 4. A, Myocardial iNOS mRNA levels in deteriorating patients undergoing LVAD implantation are no higher than in stable advanced heart failure patients awaiting transplantation. B, Immunocytochemistry showing strong iNOS expression in blood vessels of many of the LVAD patients with slightly greater myocyte expression than in (C) advanced heart failure patients.

stable advanced heart failure patients (2.8 ± 0.3 ng/mL, $n=17$; $P=NS$). Serum TNF-R2 levels also were no higher in LVAD candidates (6.9 ± 1.1 ng/mL, $n=23$) than in advanced heart failure patients (9.0 ± 0.8 ng/mL, $n=17$; $P=NS$).

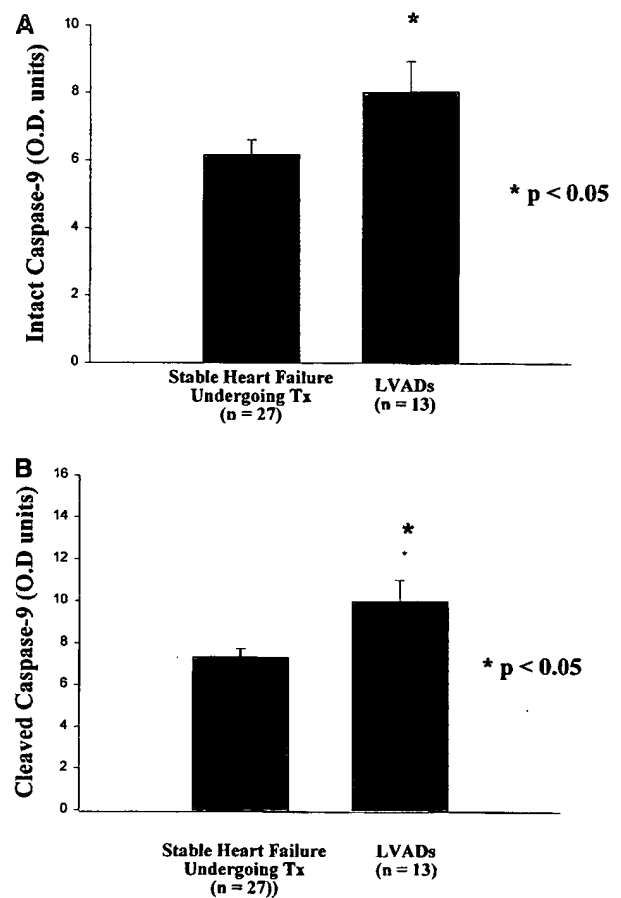


Figure 5. Expression of procaspase-9 and cleaved caspase-9 in stable advanced heart failure patients awaiting transplantation vs deteriorating patients undergoing LVAD implantation.

Serum IL-6

Serum IL-6 was higher in LVAD candidates (79.3 ± 23.6 pg/mL, $n=23$) than in advanced heart failure patients (7.1 ± 1.6 pg/mL, $n=17$; $P<0.0001$; Figure 2C).

Apoptosis

Caspase-9

Caspase-9 antibody recognizes the intact 46- to 48-kDa protein and the cleaved 37-kDa subunit. Levels of 46-kDa procaspase-9 were higher in LVAD candidates (8.02 ± 0.91 oligodeoxynucleotide [OD] units) than in advanced heart failure patients (6.16 ± 0.43 OD units; $P<0.01$, Figure 5A). Expression of 37-kDa cleaved caspase-9 was significantly higher in LVAD candidates (10.02 ± 1.0 OD units) than in stable heart failure patients (7.34 ± 0.40 OD units; $P<0.05$, Figure 5B).

Caspase-3

Caspase-3 antibody recognizes the intact 32-kDa protein and the 2 cleaved subunits of 11 and 20 kDa. Levels of procaspase-3 were not higher in LVAD patients (9.62 ± 0.5 OD units) than in advanced heart failure patients (9.78 ± 0.5 OD units; $P=NS$).

Poly(ADP-Ribose) Polymerase

PARP antibody recognizes both full-length 116-kDa protein and the cleaved 85-kDa fragment. Levels of intact PARP

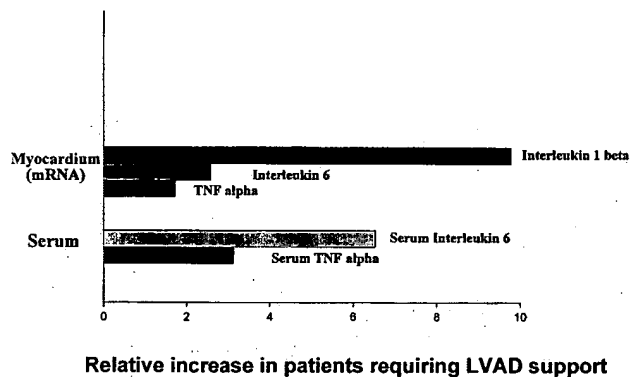


Figure 6. Pattern of increased cytokine expression in myocardium and serum of deteriorating patients requiring LVAD implantation.

were not significantly higher in LVAD candidates (0.37 ± 0.08 OD units) than in stable advanced heart failure patients (0.27 ± 0.05 OD units).

DFF-45

DFF-45 antibody (K-17) recognizes the intact 45-kDa inhibitor, the spliced 35-kDa product, and the cleaved 12-kDa product. Levels of intact DFF-45 were significantly higher in LVAD patients (10.86 ± 0.91 OD units) than in advanced heart failure patients (8.91 ± 0.38 OD units; $P < 0.05$). The spliced 35-kDa product also was significantly higher in LVAD candidates (4.58 ± 0.75 OD units) than in advanced heart failure patients (2.84 ± 0.23 OD units; $P < 0.05$).

CPAN

Levels of CPAN were not significantly higher in the LVAD candidates (2.04 ± 0.5 OD units) than in advanced heart failure patients (2.57 ± 0.23 OD units; $P = \text{NS}$).

Discussion

The present study has shown, for the first time, the specific pattern of increased expression of cytokines (Figure 6) together with alterations in the apoptotic pathway of the myocardium and serum of deteriorating patients who require implantation of an LVAD. We have shown elevated levels of myocardial TNF- α , IL-1 β , and IL-6 (Figure 6) in these patients compared with patients who have less severe heart failure, are undergoing transplantation, and have elevated levels of circulating TNF- α and IL-6. Elevated myocardial expression of caspase-9 and DFF-45, but not caspase-3 and CPAN, in the final stage of the apoptotic pathway also was demonstrated.

An estimated 5 million people in the United States and 600 000 in the United Kingdom have heart failure. Mortality level for NYHA class III and IV heart failure is $\approx 40\%$. The situation is currently worsened by the decreasing supply of donor organs. When heart failure patients deteriorate, insertion of an LVAD can be lifesaving. Early implantation of the device is beneficial to outcome; hence, finding clinical and molecular markers is important for the identification of patients at high risk of deterioration so that corrective action can be taken earlier.

We used real-time PCR to measure myocardial cytokine levels because it is a new, quantitative, highly reliable method. We chose to compare deteriorating patients to those in a stable heart failure group without using a donor control group as we have previously shown increased cytokine expression after brain death in donor hearts.²¹ The 13 patients in whom myocardial markers were measured had clinical parameters that showed them to be representative of the total group of patients. Limitation of tissue did not allow measurement of myocardial markers in all 23 patients.

In the present study, we found elevated levels of TNF- α mRNA and protein in the myocardium of deteriorating patients who required LVAD insertion. TNF- α is known to be elevated in heart failure,¹⁻⁵ and levels are known to correlate with NYHA functional class.² Infusion of TNF- α into rats at levels similar to levels present in end-stage heart failure results in depression of LV function, myocyte shortening, and LV dilatation.⁶ A recent study has shown increased myocardial TNF- α with the progression of heart failure.⁵ Therefore, TNF- α may be a useful marker of deterioration in these patients and also may be involved pathologically in the cause of the deterioration. In our present study, immunocytochemistry demonstrated TNF- α expression in cardiac myocytes, and cardiac myocytes are known to be able to produce large amounts of TNF- α .²² TNF- α acts on 2 cell-surface receptors, TNF-R1 and TNF-R2, which are thought to mediate and regulate most of the effects of TNF- α .²³ These receptors are shed as soluble forms that are thought to act as buffers to neutralize the cytotoxic activity of TNF- α .²⁴ The elevation of serum TNF- α in the LVAD patients in our present study was not accompanied by a rise in TNF receptors. This suggests that the increased TNF- α might not be neutralized by its receptors and, thus, may be able to act pathologically.

We have found elevated IL-6 mRNA and protein in the myocardium and elevated IL-6 in the serum of deteriorating patients who required LVAD insertion in the present study. IL-6 is known to be elevated in patients with heart failure, and raised levels correlate with decreased functional class, low ejection fraction, and poor prognosis.^{1,3,7,8} A recent study has shown increased myocardial IL-6 expression with progression of heart failure.⁵ Although IL-6 is known to increase with norepinephrine levels,⁷ none of the patients in the present study were on norepinephrine at the time of LVAD insertion. Thus, use of norepinephrine is unlikely to be the cause of elevated IL-6 in the present study. IL-6 can be negatively inotropic, and transgenic mice overexpressing the IL-6 gene develop ventricular hypertrophy and increased heart size.²⁵ Of the deteriorating patients who underwent LVAD insertion in our present study, myocardial IL-6 protein expression was higher in those who died after the LVAD was implanted. Hence, IL-6 may be a good marker of deterioration and may be involved pathologically in deterioration (although elevation of IL-6 in the patients who died could imply irreversibility).

IL-1 β negatively affects myocardial function^{9,10} and was 9-fold higher in the myocardium of deteriorating compared with stable patients (Figure 6). To our knowledge, this is the first time IL-1 β has been shown to be elevated in the myocardium of patients with heart failure and to be quanti-

tatively increased in deteriorating patients. IL-1 β may be a useful marker of deterioration and may be involved in its pathogenesis.

Both TNF- α and IL-1 β induce iNOS expression, and both together act synergistically.^{10,11} Therefore, we investigated iNOS expression in these patients and found that although iNOS was elevated to a level similar to that seen in advanced heart failure patients, iNOS mRNA expression was not higher in deteriorating compared with stable patients. This suggests that iNOS is not the mechanism through which these 2 cytokines act in these patients. Immunocytochemistry showed elevated iNOS protein expression in myocytes, which suggests a possible increase at the translational level. However, this barely reached statistical significance. Given that immunocytochemistry alone is not a reliable quantitative method, we feel that these results should be interpreted with caution. Immunocytochemistry demonstrated strong iNOS staining in the vascular smooth muscle cells of intracardiac blood vessels of many LVAD candidates, which suggests that increased nitric oxide release occurs in blood vessels of deteriorating patients, which could contribute to their hypotensive state.

Both TNF- α and IL-1 β can induce apoptosis,^{12,13} whereas IL-6 tends to inhibit it.^{14,15} We examined expression of caspases in the terminal stage of the apoptotic pathway to see whether they were elevated in deteriorating patients. Levels of procaspase-9 and activated, cleaved caspase-9 were elevated in these patients, but caspase-3 levels were not, which suggests a negative feedback mechanism at the level of caspase-3. Furthermore, levels of intact DFF-45 (inhibitor of DFF-45/CPAN) also were elevated, as was the cleaved 35-kDa product, but levels of the nuclease CPAN were not. Again, this occurrence suggests a negative feedback mechanism. IL-6 can increase BclxL and signal transducer and activator of transcription-3 (STAT-3).^{14,15} Thus, IL-6 tends to be antiapoptotic. Given that we have demonstrated it to be elevated in these patients, IL-6 may be part of the negative feedback mechanism. However, it is likely that several molecules are involved in both positive and negative feedback in the apoptotic pathway in these patients. Further investigation is required. For example, nuclear factor- κ B expression is induced by TNF- α and IL-1 β , is known to inhibit apoptosis, and is likely to be a potentially important mechanism. Lack of significant elevation in all of the terminal markers of apoptosis is difficult to explain and could be due to a negative feedback mechanism. Alternatively, our methods may have failed to detect a rise in these markers, or it may be that activation of the apoptotic pathway is not an important contributing mechanism to deterioration in these patients.

In conclusion, the present study has shown a specific pattern of cytokine elevation (Figure 6), alterations to caspases in the final stage of the apoptotic pathway of myocardium, and elevated levels of circulating cytokines in deteriorating patients who require LVAD insertion. Quantitative real-time RT-PCR demonstrated a 9-fold increase in IL-1 β mRNA expression, elevated myocardial TNF- α and IL-6 mRNA and protein, and raised serum TNF- α and IL-6 in deteriorating patients. iNOS was elevated to levels similar to those of heart failure, but no further elevation occurred in the

deteriorating patients, which suggests that iNOS is unlikely to be the pathway through which TNF- α and IL-1 β act in these patients. Increased iNOS vascular smooth muscle expression was seen in blood vessels, which may contribute to the hypotension observed in these patients. Elevations were seen in procaspase-9, cleaved caspase-9, and intact and cleaved DFF-45 of the final part of the apoptotic pathway but not in caspase-3 and CPAN, which suggests that some negative feedback mechanisms are occurring in these patients that need further investigation.

These cytokines might be useful markers for the earlier detection of patients likely to need LVAD implantation. Serial serum cytokine measurements, supplemented if necessary by myocardial biopsy, could augment hemodynamic data and detect decompensation at an earlier stage.

Furthermore, blocking cytokine production may have the potential to prevent disease progression. Pentoxifylline is a xanthine derivative that suppresses or reduces production of TNF- α and is thought to act at the mRNA level. Our study suggests that administration of pentoxifylline to patients with end-stage heart failure potentially could prevent or reverse their deterioration. Etanercept is a p75 TNF-R fusion protein that binds to TNF- α , functionally inactivating it, which also may be effective for prevention of decompensation of such patients. Both of these drugs previously have been shown to produce clinical improvement in patients with less severe heart failure. Our present study suggests that IL-6 antagonists also potentially may prevent disease progression, as might IL-1 antagonists and specific caspase inhibitors, such as caspase-9 inhibitors. These approaches need to be investigated.

Acknowledgments

We thank the British Heart Foundation for their support. Emma J. Birks was supported by the British Heart Foundation (project grant No. 96152), Dr Barton by a British Heart Foundation Senior Research Fellowship, and Dr Yacoub as a British Heart Foundation Professor of Cardiothoracic Surgery. We thank Mahrok Nohadani for her help.

References

1. Birks EJ, Yacoub MH. The role of nitric oxide and cytokines in heart failure. *Coronary Artery Dis.* 1997;8:389–402.
2. Torre-Amione G, Kapiada S, Benedict C, et al. Proinflammatory cytokine levels in patients with depressed left ventricular ejection fraction: a report from the Studies Of Left Ventricular Dysfunction (SOLVD). *J Am Coll Cardiol.* 1996;27:1201–1206.
3. Lommi J, Pulkki P, Koskinen P, et al. Haemodynamic, neuroendocrine and metabolic correlates of circulating cytokine concentrations in congestive heart failure. *Eur Heart J.* 1997;18:1620–1625.
4. Habib FM, Springall DR, Davies GJ, et al. Tumour necrosis factor and inducible nitric oxide synthase in dilated cardiomyopathy. *Lancet.* 1996; 347:1151–1155.
5. Kubota T, Miyagishima M, Alvarez et al. Expression of proinflammatory cytokines in the failing human heart: comparison of recent-onset and end-stage congestive heart failure. *J Heart Lung Transplant.* 2000;19: 819–824.
6. Bozkurt B, Kribbs SB, Clubb FJ, et al. Pathophysiologically relevant concentrations of tumor necrosis factor- α promote left ventricular dysfunction and remodeling in rats. *Circulation.* 1998;97:1382–1391.
7. Tsutamoto T, Hisanaga T, Wada A, et al. Interleukin-6 spillover in the peripheral circulation increases with the severity of heart failure, and the high plasma level of interleukin-6 is an important prognostic predictor in patients with congestive heart failure. *J Am Coll Cardiol.* 1998;31:391–398.

8. Plenz G, Song ZF, Reichenberg S, et al. Left-ventricular expression of interleukin-6 messenger-RNA higher in dilated than in ischemic cardiomyopathy. *Thorac Cardiovasc Surg*. 1998;46:213–216.
9. Hosenpud JD, Campbell SM, Mendelson DJ. Interleukin-1-induced myocardial depression in an isolated beating heart preparation. *J Heart Transplant*. 1989;8:460–464.
10. Cain BS, Meldrum DR, Dinarello CA, et al. Tumour necrosis factor- α and interleukin-1 β synergistically depress human myocardial function. *Crit Care Med*. 1999;27:1309–1318.
11. Schulz R, Panas DL, Catena R, et al. The role of nitric oxide in cardiac depression induced by interleukin-1 beta and tumour necrosis factor-alpha. *Br J Pharmacol*. 1995;114:27–34.
12. Ing DJ, Zang J, Dzau VJ, et al. Modulation of cytokine-induced cardiac myocyte apoptosis by nitric oxide, Bak, and Bcl-x. *Circ Res*. 1999;84:21–33.
13. Krown KA, Page MT, Nguyen C, et al. Tumour necrosis factor alpha-induced apoptosis in cardiac myocytes: involvement of the sphingolipid signaling cascade in cardiac cell death. *J Clin Invest*. 1996;98:2854–2865.
14. Schwarze MM, Hawley RG. Prevention of myeloma cell apoptosis by ectopic bcl-2 expression or interleukin 6-mediated up-regulation of bcl-xL. *Cancer Res*. 1995;55:2262–2265.
15. Fukada T, Hibi M, Yamanaka Y, et al. Two signals are necessary for cell proliferation induced by a cytokine receptor gp130: involvement of STAT3 in anti-apoptosis. *Immunity*. 1996;5:449–460.
16. Liu X, Zou H, Slaughter C, et al. DFF, a heterodimeric protein that functions downstream of caspase-3 to trigger DNA fragmentation during apoptosis. *Cell*. 1997;89:175–184.
17. Tang D, Kidd VJ. Cleavage of DFF-45/ICAD by multiple caspases is essential for its function during apoptosis. *J Biol Chem*. 1998;273:28549–28552.
18. Halenbeck R, MacDonald H, Roulston A, et al. CPAN, a human nuclease regulated by the caspase-sensitive inhibitor DFF45. *Curr Biol*. 1998;8:537–540.
19. Narula J, Pandey P, Arbustani E, et al. Apoptosis in heart failure: release of cytochrome c from mitochondria and activation of caspase-3 in human cardiomyopathy. *Proc Natl Acad Sci, U S A*. 1999;96:8144–8149.
20. Latif N, Khan M, Birks E, et al. Upregulation of the bcl-2 family of proteins in end stage heart failure. *J Am Coll Cardiol*. 2000;35:1769–1777.
21. Birks EJ, Burton PB, Owen V, et al. Elevated tumor necrosis factor-alpha and interleukin-6 in myocardium and serum of malfunctioning donor hearts. *Circulation*. 2000;102(suppl 3):III-352–III-358.
22. Kapadia S, Lee J, Torre-Amione G, et al. Tumor necrosis factor- α gene and protein expression in adult feline myocardium after endotoxin administration. *J Clin Invest*. 1995;96:1042–1052.
23. Torre-Amione G, Kapadia S, Lee J, et al. Expression and functional significance of tumor necrosis factor receptors in human myocardium. *Circulation*. 1995;92:1487–1493.
24. Kapadia S, Torre-Amione G, Yokoyama T, et al. Soluble tumor necrosis factor binding proteins modulate the negative inotropic effects of TNF- α in vitro. *Am J Physiol*. 1995;37:H517–H525.
25. Hirota H, Yoshida K, Kishimoto T, et al. Continuous activation of gp130, a signal-transducing receptor component for interleukin 6-related cytokines, causes myocardial hypertrophy in mice. *Proc Natl Acad Sci U S A*. 1995;92:4862–4866.

Blocking Caspase-Activated Apoptosis Improves Contractility in Failing Myocardium

KARL-LUDWIG LAUGWITZ,^{1*} ALESSANDRA MORETTI,^{1*} HANS-JÖRG WEIG,^{1*}
ANGELIKA GILLITZER,¹ KAI PINKERNELL,¹ THOMAS OTT,¹ INGO PRAGST,²
CHRISTIAN STÄDELE,² MELCHIOR SEYFARTH,¹ ALBERT SCHÖMIG,¹ and MARTIN UNGERER³

ABSTRACT

Cardiac myocyte apoptosis has been demonstrated in end-stage failing human hearts. The therapeutic utility of blocking apoptosis in congestive heart failure (CHF) has not been elucidated. This study investigated the role of caspase activation in cardiac contractility and sarcomere organization in the development of CHF. In a rabbit model of heart failure obtained by rapid ventricular pacing, we demonstrate, using *in vivo* transcatheter adenovirus-mediated gene delivery of the potent caspase inhibitor p35, that caspase activation is associated with a reduction in contractile force of failing myocytes by destroying sarcomeric structure. In this animal model gene transfer of p35 prevented the rise in caspase 3 activity and DNA-histone formation. Genetically manipulated hearts expressing p35 had a significant improvement in left ventricular pressure rise ($+dp/dt$), decreased end-diastolic chamber pressure (LVEDP), and the development of heart failure was delayed. To better understand this benefit, we examined the effects of caspase 3 on cardiomyocyte dysfunction *in vitro*. Microinjection of activated caspase 3 into the cytoplasm of intact myocytes induced sarcomeric disorganization and reduced contractility of the cells. These results demonstrate a direct impact of caspases on cardiac function and may lead to novel therapeutic strategies via antiapoptotic regimens.

OVERVIEW SUMMARY

In human ischemic and dilated cardiomyopathy, activation of the caspase cascade has been documented. This study investigated the role of caspase activation in cardiac contractility and sarcomere organization in the development of CHF. In a rabbit model of heart failure adenovirus-mediated gene delivery of the potent caspase inhibitor p35 improved ventricular function assessed by echocardiographic and hemodynamic measurements. Failing cardiomyocytes isolated from genetically manipulated hearts expressing p35 showed preserved sarcomeric structure and reconstituted contractile performance. Microinjection of caspase 3 into healthy myocytes induced a concentration-dependent destruction of the sarcomeric units and reduced contractility of the cells. These data provide evidence that caspase activation contributes to the progression of CHF and its prevention leads to partial restoration of cardiac function.

INTRODUCTION

DESPITE PROGRESS in the treatment of heart failure, the 5-year mortality of symptomatic patients still exceeds 50% (Braunwald and Bristow, 2000). Histochemical evidence of apoptosis has been identified in several cardiovascular disorders leading to congestive heart failure, including ischemic heart disease, myocarditis, and dilated cardiomyopathy (Haunstetter and Izumo, 2000; MacLellan, 2000). In cardiomyocytes, programmed cell death may be an important component of the transition from adaptive hypertrophy to heart failure (Hirota *et al.*, 1999; Hunter and Chien, 1999). Prolonged growth stimulation of adult cardiomyocytes, which differentiate and withdraw from the cell cycle during the neonatal period, may activate the apoptotic program and lead to cell dysfunction in congestive heart failure (CHF).

Myocardial apoptosis involves highly complex, regulated cell suicide machinery, in which two main signaling pathways lead to activation of the caspase family of cysteine proteases

¹Medizinische Klinik und Deutsches Herzzentrum München, 81675 Munich, Germany.

²Institut für Experimentelle Onkologie und Therapieforschung, Technische Universität München, 81675 Munich, Germany.

³ProCorde GmbH, 82152 Martinsried-Munich, Germany.

*Karl-Ludwig Laugwitz, Alessandra Moretti, and Hans-Jörg Weig contributed equally to this work.

(Reed and Paternostro, 1999; Hengartner, 2000): (1) death receptor signaling (e.g., Fas, tumor necrosis factor [TNF], and DR3-DR5 receptors) (Ashkenazi and Dixit, 1998) and (2) release of cytochrome *c* from mitochondria and subsequent trans-activation of procaspase 9 by apoptosis protease-activating factor (Apaf) (Green and Reed, 1998). Caspases regulate the execution of the mammalian cell death program (Hengartner, 2000). Caspase 3 represents the key effector enzyme and cleaves downstream targets involved in the expression of the apoptotic phenotype, including gelsolin, p21-activated kinase 2 (PAK2), nuclear lamins, and the inhibitory subunit of DNA fragmentation factor (inhibitor of caspase-activated DNase, ICAD) (Rudel and Bokoch, 1997; Enari *et al.*, 1998). In human ischemic and dilated cardiomyopathy, cytochrome *c* release and activation of the caspase 3 cascade have been documented (Narula *et al.*, 1999). Critical questions remain unclear: to what extent do caspases contribute to functional deterioration of cardiomyocytes in failing myocardium and can we develop effective new therapies based on the blockade of apoptotic pathways in the myocardium? As cytoskeletal proteins (e.g., gelsolin, actin, and fodrin) are important targets for activated caspase 3 (Hengartner, 2000), abnormal cytoskeletal structure or loss of sarcomere organization through caspases could lead to abnormalities in myocyte function and decreased force transmission.

The goal of this study was to investigate the role of caspase activation in cardiac contractility and sarcomere organization in the development of heart failure. We tested whether expression of p35, which potentially inhibits members of the caspase family of cysteine proteases (Bump *et al.*, 1995), can improve ventricular function in an animal model of heart failure. In failing myocardium, we analyzed caspase 3, caspase-activated deoxyribonuclease (CAD) activities, and DNA fragmentation over the time course of heart failure development. Two days after pacemaker implantation, rabbits were randomized to receive either a bicistronic adenovirus carrying p35 and green fluorescent protein genes (CHF+Ad-p35) or GFP alone (CHF+Ad-GFP) by using a transcortary gene delivery technique. After 0, 7, and 15 days of rapid pacing, echocardiographic and hemodynamic profiles of the animals were analyzed. To address specifically the molecular mechanism that mediates the caspase-induced deterioration of cardiac performance, we studied the effects of microinjected caspase 3, as principal enzyme of the caspase cascade, on sarcomeric structure and contractile force in isolated ventricular cardiomyocytes.

MATERIALS AND METHODS

Construction and purification of recombinant adenovirus

Recombinant (E1- and E3-deficient) adenovirus (serotype 5) carrying the baculovirus apoptotic suppressor p35 was generated as described (He *et al.*, 1998). The coding sequence of p35 was tagged with the FLAG epitope and inserted into the polylinker sequence of the GFP-expressing pAdTrack vector, between a non-tissue-specific cytomegalovirus (CMV) promoter and a simian virus 40 (SV40) polyadenylation signal. Recombinant adenoviruses were prepared at large scale as described (Laugwitz *et al.*, 1999). Adenoviral titers were determined by plaque titration on HEK 293 cells.

Experimental protocol

The project was approved by the institutional ethics review board. Sixty-three adult male New Zealand White rabbits (2.8 ± 0.5 kg) were initially randomized in two groups: one group of 40 animals with implantation of pacemakers and rapid ventricular pacing and a second group of 23 sham-operated animals with implantation of pacing wires but no pacing. All animals survived the initial operation. In the first group, 18 rabbits received an intracoronary infusion of Krebs-Ringer solution, and were paced for 7 ($n = 7$) or 15 ($n = 11$) days. These animals served as failing rabbits (CHF) for hemodynamic evaluation and apoptotic biochemistry for caspase 3 activity, CAD activity, TUNEL (TdT [terminal deoxynucleotidyl-transferase]-mediated dUTP nick end labeling) staining, and DNA-histone formation. In the other 22 animals of this group, transcortary delivery of recombinant adenoviruses encoding either p35 and GFP (CHF+Ad-p35; $n = 10$) or GFP alone (CHF+Ad-GFP; $n = 12$) was performed, and the rabbits were paced for 15 days. The second group of 23 sham-operated animals received intracoronary Krebs-Ringer solution (sham; $n = 11$), Ad-p35 (sham+Ad-p35; $n = 4$), and Ad-GFP (sham+Ad-GFP; $n = 8$). These animals were used to examine the expression levels of p35 and GFP 0, 4, 7, and 15 days after infection and for apoptotic biochemistry, TUNEL staining, single-cell shortening, confocal laser scanning microscopy, and microinjection experiments.

In vivo transcortary gene delivery

Of the 22 rabbits with ventricular pacing and adenoviral gene transfer, 2 animals in the CHF+Ad-p35 group and 4 in the CHF+Ad-GFP group died during the gene delivery procedure (in each group 8 animals survived). Rabbits were anesthetized intramuscularly with medetomidin ($100 \mu\text{g/kg}$), propofol ($5 \mu\text{g/kg}$ per hr), and a bolus of fentanyl ($10 \mu\text{g/kg}$) intravenously. They were intubated, ventilated, and monitored for electrocardiogram (ECG), echocardiography, and pressure throughout the experiment. Transcortary gene delivery into the rabbit myocardium was performed at the time ventricular pacing was initiated, 2 days after pacemaker implantation. All animals enrolled in the study received a 2-min intracoronary infusion of serotonin ($10 \mu\text{M}$) and low calcium (1.25 mM) into the left coronary ostium, followed by a total dose of 5×10^{10} PFU of adenovirus (Weig *et al.*, 2000). In eight animals of the CHF+Ad-p35 and CHF+Ad-GFP groups hemodynamic and echocardiographic experiments were performed. All animals were killed 15 days after gene delivery and hearts were collected for biochemical studies, single-cell shortening experiments, and phalloidin staining.

Pacemaker implantation

The pacemaker lead (2F; Medtronic, Unterschleißheim, Germany) was placed through the jugular vein into the right ventricular apex. Customized pacemakers (Vitatron, Cologne, Germany) were placed beneath the left epigastrium and connected to the lead. Sham-operated animals had the same intervention with implantation of pacing wires but never underwent initiation of ventricular pacing. Two days after surgery, ventricular pacing was initiated at a rate of 340 beats/min.

In vivo hemodynamic and echocardiographic measurements

Left ventricular (LV) contractility was examined before and 7 and 15 days after adenoviral gene transfer and initiation of pacing. Rabbits were anesthetized as described previously. Transthoracic M-mode and two-dimensional echocardiography was performed with a 5-MHz probe of a Hewlett-Packard (Palo Alto, CA) Sonos 5500 imaging system, as described in previous studies (Gardin *et al.*, 1995), and analyzed by two blinded observers. After preparation of the right carotid artery, a Millar 2.5F tip catheter connected to a differentiating device (Hugo Sachs, Freiburg, Germany) was placed in the left ventricle. After definition of basal contractility and LV pressure (with the pacemaker turned off), 200 μ l of 0.9% NaCl was injected as a negative control. After a sufficient equilibration period, epinephrine was injected in concentrations ranging from 0.1 to 0.8 μ g/kg per min.

Preparation and culture of rat and rabbit adult ventricular cardiomyocytes

Single ventricular myocytes were isolated from male Wistar rats (250–300 g) or from sham-operated and failing male New Zealand White rabbits (2.8 ± 0.5 kg), as described (Laugwitz *et al.*, 1999). Cardiomyocytes were cultured in M199 culture medium (supplemented with minimal essential medium [MEM] vitamins, MEM nonessential amino acids, 25 mM HEPES, insulin [10 μ g/ml], penicillin [100 IU/ml], streptomycin [100 μ g/ml], and gentamicin [100 μ g/ml]) on laminin-precoated dishes (5 μ g/cm²; density of 10^5 cells/cm²) in a humidified atmosphere (5% CO₂) at 37°C. Infection of rat myocytes with adenoviruses was performed *in vitro* at a multiplicity of infection (MOI) of 100 PFU/cell 6–8 hr after plating in M199 medium. Rat cells were used for biochemistry 48 hr after infection. Rabbit cardiomyocytes were infected *in vivo* and isolated 4, 7, or 15 days after gene transfer.

Western blot analysis

Immunodetection was performed in crude extracts of sham-operated and failing myocardium. Extracts were obtained by homogenization in 10 mM HEPES buffer, pH 7.0, containing a mixture of protease inhibitors at 4°C. Protein concentrations were detected by Bradford assay (Bio-Rad Laboratories, Munich, Germany). Equal amounts of protein (150 μ g) were size fractionated on a 12% sodium dodecyl sulfate (SDS)-polyacrylamide gel and electrophoretically transferred to nitrocellulose membrane (Bio-Rad Laboratories). Blots were stained with Ponceau red, in order to monitor the amount of transferred protein in each lane and to detect protein degradation. Native ICAD cleavage products in lysates of sham-operated and failing myocardium were detected with a goat polyclonal antibody directed against the N terminus of the mouse ICAD (1:1000 dilution; Santa Cruz Biotechnology, Santa Cruz, CA). Extracts from sham-operated hearts were also incubated for 30 min at 37°C with recombinant human active caspase 3 (1 ng/ μ l; Becton Dickinson, Heidelberg, Germany), in the presence or absence of the tetrapeptide caspase 3 inhibitor DEVD-FMK (Asp-Glu-Val-Asp-O-methyl-fluoromethylketone, 100 μ M). Immunodetection of p35 and α -sarcomeric actin in extracts of

transcoronary-infected sham+Ad-p35 myocardium was performed with mouse anti-FLAG M2 monoclonal antibody (1:1000 dilution; Stratagene, La Jolla, CA) and mouse anti- α -sarcomeric actin monoclonal antibody (1:5000 dilution; Sigma, Munich, Germany). Antigen-antibody complexes were visualized by chemiluminescence (enhanced chemiluminescence [ECL] detection kit; Amersham Pharmacia Biotech Europe, Freiburg, Germany) and obtained chemiluminograms were evaluated by laser scanning densitometry.

Immunofluorescence staining

To determine transgene expression in transcoronary Ad-p35-infected rabbit hearts 4 days after gene delivery, frozen slices (thickness, 3 μ m) were fixed in 4% paraformaldehyde and permeabilized with 0.1% saponin. p35 was detected with anti-FLAG M2 antibody (10 μ g/ml) and anti-mouse IgG-Texas Red conjugate (4 μ g/ml).

Polymerized actin fibers were visualized in isolated cardiomyocytes by Texas Red-phalloidin (Molecular Probes, Eugene, OR), according to the manufacturer instructions.

α -Sarcomeric actin immunodetection was performed in TUNEL-stained heart sections, using anti- α -sarcomeric actin monoclonal antibody (1:250 dilution; Sigma) and anti-mouse IgG-Texas Red conjugate (4 μ g/ml).

Flow cytometry studies

Fluorescence-activated cell sorting (FACS) analysis was performed on a FACSCalibur with CellQuest software (Becton Dickinson). Cardiomyocytes freshly isolated 0, 4, 7, and 15 days after transcoronary gene delivery of Ad-GFP in sham-operated rabbits were resuspended in phosphate-buffered saline (PBS) and analyzed by flow cytometry at 520 nm (GFP fluorescence). In each measurement 2×10^4 cells were analyzed and myocytes presenting a fluorescence intensity higher than 10^1 were considered GFP positive (GFP fluorescence cutoff [M1]).

Detection of apoptosis

The activity of caspase 3 was determined with a colorimetric CPP32 assay kit by the detection of chromophore *p*-nitroanilide after cleavage of the labeled substrate DEVD-*p*-nitroanilide (Clontech, Heidelberg, Germany). A total of 2×10^6 isolated rat cardiomyocytes in culture or 50 slices from the anterolateral wall of rabbit LV myocardium (7 μ m) were lysed and equal amounts of protein were reacted with 50 μ M DEVD-*p*-nitroanilide at 37°C for 1 hr. The activity was determined photometrically at 405 nm, and the results were calibrated with known concentrations of *p*-nitroanilide. The units of protease activity were defined as the amount of caspase 3 required to produce 1 pmol of *p*-nitroanilide at 25°C.

CAD activity was determined by DNA fragmentation assay, using rat liver nuclei (Enari *et al.*, 1998). Briefly, 100 μ g of protein from crude lysate of sham-operated or failing rabbit heart tissue was incubated with 10^6 liver nuclei in a reaction buffer consisting of 10 mM HEPES (pH 7.0), 40 mM β -glycerophosphate, 50 mM NaCl, 2 mM MgCl₂, 5 mM EGTA, 1 mM dithiothreitol (DTT), 2 mM ATP, 10 mM creatine phosphate, creatine kinase (50 μ g/ml), and a mixture of protease inhibi-

tors. After 90 min of incubation at 37°C nuclei were lysed in 100 mM Tris-HCl (pH 8.5), 5 mM EDTA, 0.2 M NaCl, 0.2% SDS, and proteinase K (1 mg/ml) for 10 min at 56°C. DNA was precipitated by adding an equal volume of isopropanol, dissolved in 20 μ l of Tris-HCl, pH 8.5, containing 1 mM EDTA and RNase A (1 mg/ml) and incubated at 37°C for 30 min. DNA was analyzed by gel electrophoresis.

TUNEL staining was performed with an *in situ* cell death detection kit (Roche Diagnostics, Mannheim, Germany) according to the manufacturer instructions, and combined with Hoechst 33258 (0.5 μ g/ml; Sigma) nuclear counterstaining. Total and TUNEL-positive nuclei were counted in 10 microscopic fields from 7- μ m ventricular sections for each heart. The mean number of nuclei per millimeter squared was multiplied by the section area to calculate the number of total and TUNEL-positive nuclei for each section. More than 1000 nuclei were counted for each section.

Histone-associated DNA fragments in rat ventricular cardiomyocytes and rabbit heart slices were determined with a commercially available quantitative nucleosome enzyme-linked immunosorbent assay (ELISA), according to the manufacturer instructions (Roche). The amount of nucleosomes in the lysate of 2×10^3 cells or 5 slices from the anterolateral wall of the LV (7 μ m) was photometrically determined at 405 nm. The DNA fragmentation enhancement factor was calculated for each group of experiments as $OD_{\text{treatment}}/OD_{\text{control}}$, after subtraction of background OD_{405} .

Cell shortening experiments in vitro

Fractional shortening was measured in rabbit adult cardiomyocytes isolated from the LV of sham-operated or failing hearts 15 days after transcortary adenovirus application and maintained for 1 day in culture. Experiments were performed in a temperature-controlled cuvette (37°C), at constant medium flow and constant electrical field, using an electro-optical monitoring system (Scientific Instruments, Heidelberg, Germany), as described (Laugwitz *et al.*, 1999). As medium, a 1.8 mM Ca^{2+} -Tyrode's solution was used. Infected cells were selected by GFP fluorescence.

Microinjection

Microinjection experiments were performed with freshly isolated myocytes from sham-operated rabbits, using a Femto-Jet microinjector (Eppendorf, Hamburg, Germany). Fluorescein isothiocyanate (FITC)-conjugated dextran (6 mg/ml) alone or plus human recombinant active caspase 3 (4 and 20 ng/ μ l) in 5 mM potassium phosphate buffer (pH 7.4, 100 mM KCl) was injected ($P_i = 1000$ hPa, $t_i = 0.1$ sec, $P_c = 30$ hPa) into the cytoplasm of cells in culture medium supplemented with 200 μ M 2,3-butanedione 2-monoxime (BDM), 10 μ M verapamil, and optionally with 100 μ M DEVD-FMK. After 2 hr of incubation, cells were used for contractility measurements or phalloidin staining. Injected cells were selected by FITC fluorescence.

Assessment of inflammation and necrosis

Hematoxylin-eosin staining was used to detect inflammatory cell infiltrates and necrosis in samples from LV myocardium of animals that had received adenoviral gene transfer (CHF+Ad-p35, $n = 3$; CHF+Ad-GFP, $n = 3$) after 15 days of pacing. Three CHF animals served as controls.

Statistical analysis

Data represent means \pm SEM and were analyzed by one-way analysis of variance (ANOVA) followed by Scheffé post-hoc analysis. Statistical significance was accepted at the level of $p < 0.05$.

RESULTS

Effects of chronic tachycardia in rabbits

The present study investigates a model of low-output CHF that resembles human alterations at the hemodynamic and biochemical levels (Masaki *et al.*, 1993; Akhter *et al.*, 1997). Fifteen days of ventricular pacing at rates of 340 beats/min resulted in gross clinical evidence of systemic heart failure in the animals, including biventricular dilatation, pleural effusions, and abdominal ascites. Echocardiographic studies showed an

TABLE 1. ECHOCARDIOGRAPHIC AND HEMODYNAMIC MEASUREMENTS IN RABBITS AFTER 15 DAYS OF VENTRICULAR PACING AND TRANSCORONARY GENE DELIVERY OF Ad-GFP^a

| | Krebs-Ringer ($n = 8$) | | | Ad-GFP ($n = 8$) | | |
|---------------------|--------------------------|----------------|---------|--------------------|----------------|---------|
| | Prepacing | Postpacing | p Value | Prepacing | Postpacing | p Value |
| HR, bpm | 182 \pm 6.0 | 189 \pm 7.0 | NS | 180 \pm 7.0 | 190 \pm 10.0 | NS |
| Body weight, kg | 2.8 \pm 0.5 | 2.75 \pm 0.8 | NS | 2.85 \pm 0.4 | 2.8 \pm 0.3 | NS |
| LVEDD, mm | 13.2 \pm 0.5 | 17.1 \pm 0.7 | <0.05 | 13.7 \pm 0.4 | 16.5 \pm 0.3 | <0.05 |
| LVESD, mm | 7.9 \pm 0.4 | 14.4 \pm 0.6 | <0.01 | 8.4 \pm 0.3 | 14.0 \pm 0.5 | <0.01 |
| FS, % | 39.7 \pm 1.6 | 15.3 \pm 1 | <0.001 | 38.0 \pm 1.6 | 15.0 \pm 1.5 | <0.001 |
| LVEDP, mmHg | 3.5 \pm 0.4 | 14.3 \pm 1.2 | <0.001 | 2.9 \pm 0.3 | 14.0 \pm 1.0 | <0.001 |
| LVSP, mmHg | 90.0 \pm 7.0 | 67.0 \pm 8.0 | <0.01 | 82.0 \pm 9.0 | 68.0 \pm 6.0 | <0.01 |
| LV +dp/dt, mmHg/sec | 1557 \pm 104 | 896 \pm 68 | <0.005 | 1502 \pm 101 | 883 \pm 150 | <0.005 |

^aValues represent means \pm SEM. HR, heart rate (beats/min [bpm]); LVEDD, left ventricular (LV) end-diastolic dimension; LVESD, LV end-systolic dimension; FS, fractional shortening calculated as % FS = [(EDD - ESD)/EDD] \times 100; LVEDP, LV end-diastolic pressure; LVSP, LV end-systolic pressure; dp/dt_{max}, maximum rate of LV pressure development.

increase in left ventricular (LV) end-diastolic dimension and a reduction of fractional shortening (FS) in the CHF rabbits (Table 1). *In vivo* hemodynamic measurements demonstrated higher left ventricular end-diastolic pressure and lower LV contractility (assessed by LV $+dp/dt$) in the paced animals. LV dimensions, calculated FS, basal hemodynamics, and LV $+dp/dt$ were unaffected by adenoviral gene transfer (Table 1).

Apoptotic parameters in failing myocardium

To assess biochemical hallmarks of apoptosis in the hearts of paced rabbits, a series of molecular analyses was performed. In cytosolic cell extracts prepared from failing and sham-operated LV myocardium, a significant (~ 6 -fold) increase in caspase 3 activity was documented in the CHF tissue after 15 days of pacing (84 ± 5.3 vs. 15.8 ± 3.1 active units; sham, $n = 6$; CHF 7 days, $n = 4$; CHF 15 days, $n = 8$; Fig. 1A). To examine the ability of cell lysates of failing myocardium to cause DNA degradation *in vitro*, liver nuclei were incubated with extracts of CHF heart tissue and DNA was analyzed by agarose gel electrophoresis (Enari *et al.*, 1995). DNA fragmentation activity, producing the typical DNA ladder showing multiples of 180 bp, was already present after 7 days of pacing in failing myocardium but not in tissue of sham-operated animals ($n = 4$ in each group; Fig. 1B). The nuclease responsible for DNA degradation in the caspase 3 apoptotic pathway is CAD, which is produced as a complex with its inhibitor ICAD (Enari *et al.*, 1998). We used immunoblotting of cytosolic fractions from failing myocytes to assess the evidence of ICAD cleavage. The ICAD subunit of ~ 45 kDa was relatively stable in sham-operated control myocardium. In contrast, a main 12-kDa cleavage product was present in failing tissue and in lysates of healthy myocardium after incubation with recombinant caspase 3. This cleavage of ICAD was blocked in the presence of the caspase 3 inhibitor DEVD-FMK ($n = 6$ in each group; Fig. 1C).

In end-stage heart failure, apoptosis is accompanied by DNA degradation (Olivetti *et al.*, 1997). The number of apoptotic nuclei was evaluated in sham-operated and failing myocardium by terminal deoxynucleotidyltransferase (TdT)-mediated dUTP nick end labeling (TUNEL) staining ($n = 3$ in each group; Fig. 2A). Simultaneous α -sarcomeric actin staining confirmed that apoptotic nuclei were predominantly in cardiomyocytes. The increase in TUNEL-positive myocytes assessed by semiquantitative scoring correlated with DNA-histone formation in failing myocardium (Fig. 2B and C). As shown in Fig. 2C, whole cell extracts from myocardium after 15 days of pacing had an almost 6-fold increase in histone-associated DNA fragments compared with extracts from sham-operated controls (sham, $n = 6$; CHF 7 days, $n = 4$; CHF 15 days, $n = 8$). The apoptotic changes regarding caspase 3 and CAD activities, TUNEL-positive nuclei, and nuclear DNA fragmentation consistently increased with the duration of pacing in this animal model (Fig. 1A and B; Fig. 2B and C).

Transcoronary gene delivery and time course of transgene expression

To manipulate caspase 3-activated apoptosis, an adenoviral construct for p35 as a potent caspase inhibitor was generated. Adenovirus was structured to encode transgene and GFP as reporter gene. In addition, the transgene was epitope tagged for immunostaining. We have previously demonstrated robust ex-

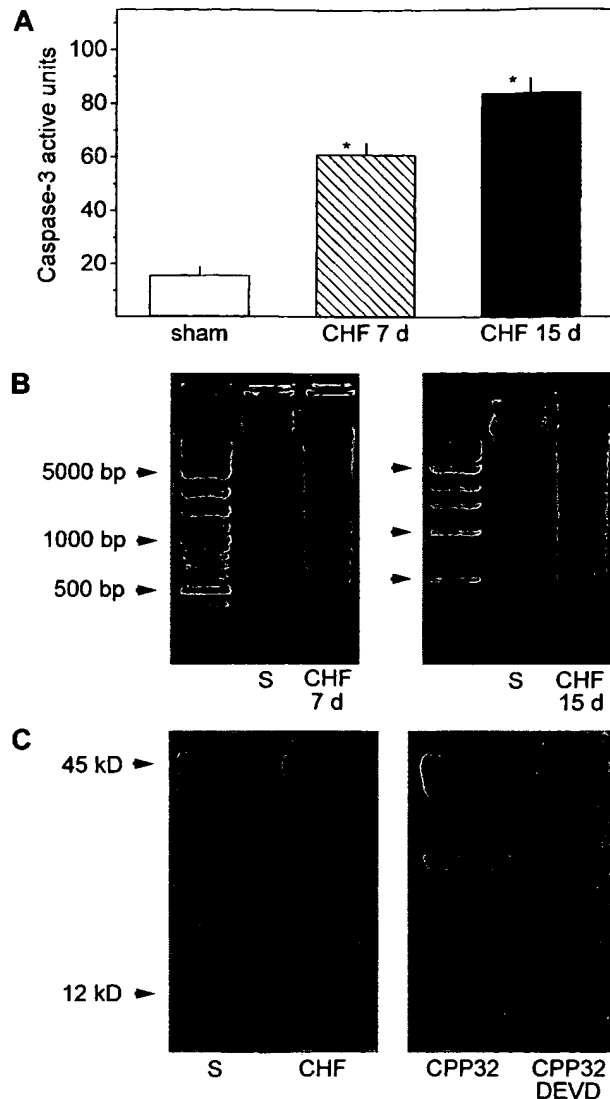


FIG. 1. Induction of caspase 3-mediated CAD activation in myocardium of sham-operated (sham) or paced (CHF) animals. (A) Caspase 3 enzyme activity levels measured in cytosolic fractions of anterolateral LV tissue. Data are expressed as means \pm SEM. Sham, $n = 6$; CHF 7 days, $n = 4$; CHF 15 days, $n = 8$. * $p < 0.005$ in comparison with sham. (B) Fragmentation of genomic DNA purified from isolated rat liver nuclei incubated with cytosolic extracts of sham-operated (S) and failing heart after 7 days (CHF 7 d) and 15 days (CHF 15 d) of pacing. Shown are representative data from one of four animals in each group. (C) Immunoblot analysis of native ICAD cleavage in lysates of myocardium from sham-operated (S) and failing rabbits (CHF). Tissue samples from sham-operated controls were incubated with recombinant human caspase 3 (CPP32) and its tetrapeptide inhibitor DEVD-FMK (CPP32 DEVD). Shown are representative results from one of six animals in each group.

pression of adenoviral transgenes in rabbit myocardium by *in vivo* transcoronary delivery in the left coronary system after serotonin and low calcium pretreatment (Weig *et al.*, 2000).

Fluorescence imaging of microscopic sections of sham-operated heart infected with bicistronic Ad-p35 revealed high levels of GFP expression throughout the manipulated myocardium.

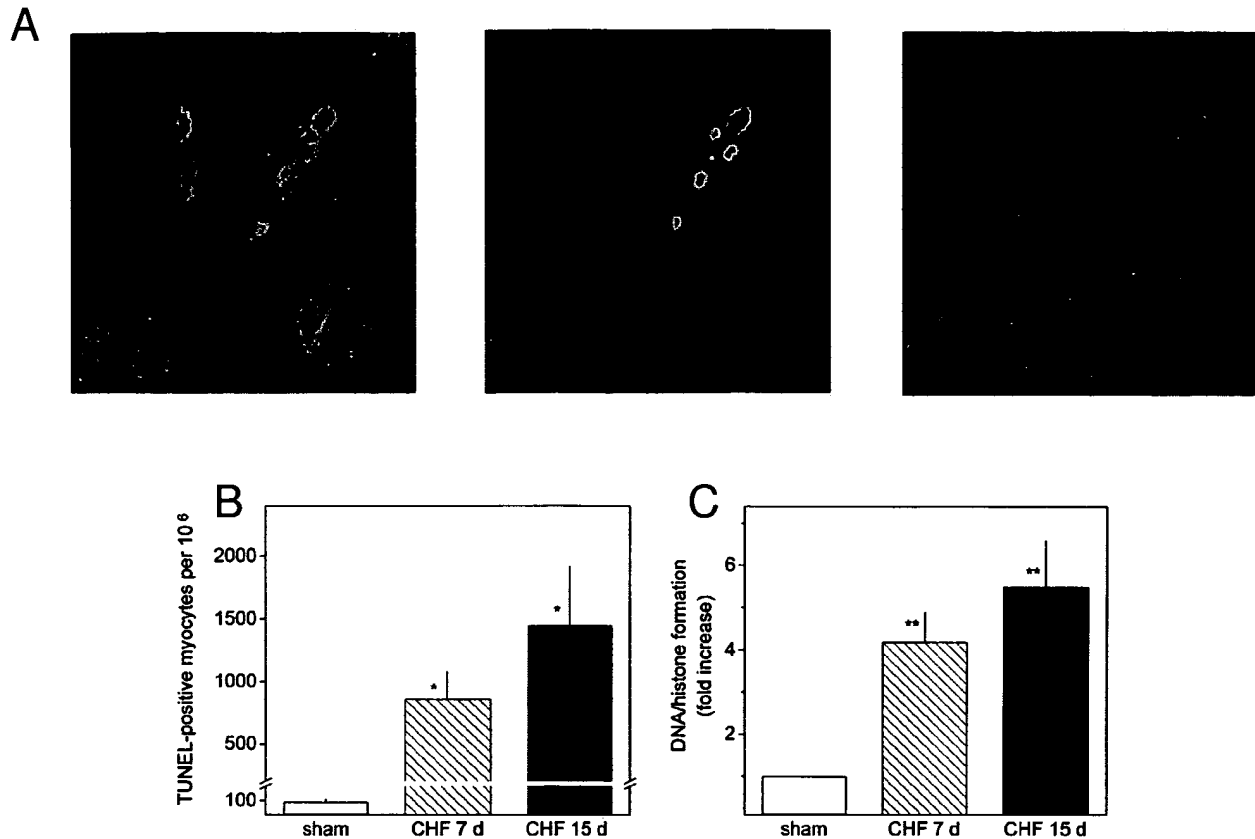


FIG. 2. Nuclear apoptosis in paced myocardium. (A) Fluorescence imaging of heart sections (7 μ m) after 15 days of rapid ventricular pacing. Blue fluorescence (420 nm) illustrates nuclei by Hoechst 33258 and green fluorescence (520 nm) shows apoptotic nuclei identified by TUNEL staining. Immunostaining for α -sarcomeric actin reflects myocytes (red fluorescence, 615 nm). Original magnification: $\times 630$. Shown are representative sections from one of three hearts. (B) Semiquantitative analysis of myocyte apoptosis detected by TUNEL staining in sham-operated (sham) and failing hearts after 7 days (CHF 7 d) and 15 days (CHF 15 d) ventricular pacing. Data are expressed as means \pm SEM; $n = 3$ animals in each group. * $p < 0.01$ in comparison with sham. (C) DNA-histone complex formation measured in cytosolic fractions of anterolateral LV tissue. Data are expressed as means \pm SEM. Sham, $n = 6$; CHF 7 days, $n = 4$; CHF 15 days, $n = 8$. ** $p < 0.005$ in comparison with sham.

Immunostaining for the epitope-tagged transgene showed signals in the same area restricted to the anterolateral wall, corresponding to the perfusion bed of the circumflex artery, the dominant left coronary artery in rabbits (Fig. 3A). To quantify gene expression after transcatheter delivery, we isolated single cardiomyocytes from LV myocardium of sham-operated and GFP-infected rabbits and performed flow cytometry studies for GFP fluorescence 0, 4, 7, and 15 days after infection. In comparison with background fluorescence on day 0, GFP expression clearly increased at 4 days (44%) and 7 days (37%), but gradually declined after 15 days (26%) (Fig. 3B). These data are in accordance with other first-generation adenoviral gene transfer studies (Donahue *et al.*, 2000). We did not observe any GFP expression differences between failing or nonfailing tissue.

No evidence of cell necrosis was present in samples from LV myocardium of 15-day paced animals that had received gene transfer of Ad-p35 and Ad-GFP ($n = 6$). Fifteen days after gene delivery, we observed a mild inflammatory infiltration, mainly of mononuclear cells, both in Ad-p35- and Ad-GFP-infected myocardial tissue.

p35 expression blocks caspase 3 activity and DNA fragmentation in vitro and in failing myocardium in vivo

Before determining the functional consequences of adenoviral infection in failing myocardium, we examined the expression and function of p35 in TNF- α -stimulated apoptotic ventricular myocytes in culture (Fig. 4A and B). TNF- α is an autocrine contributor to myocardial dysfunction and an inducer of programmed cell death in several cardiac diseases (Krown *et al.*, 1996). Because rabbit TNF- α is not available, we performed *in vitro* experiments in adult cardiomyocytes isolated from rat hearts. Forty-eight hours after Ad-p35 infection *in vitro*, extracts from rat myocytes expressed significant levels of recombinant protein, as determined by immunoblotting (data not shown). In TNF- α -treated cells, caspase 3 activity and nucleosome formation were significantly increased. Adenoviral expression of p35 efficiently suppressed TNF- α -stimulated caspase 3 activity to basal levels ($n = 4$ animals; Fig. 4A and B).

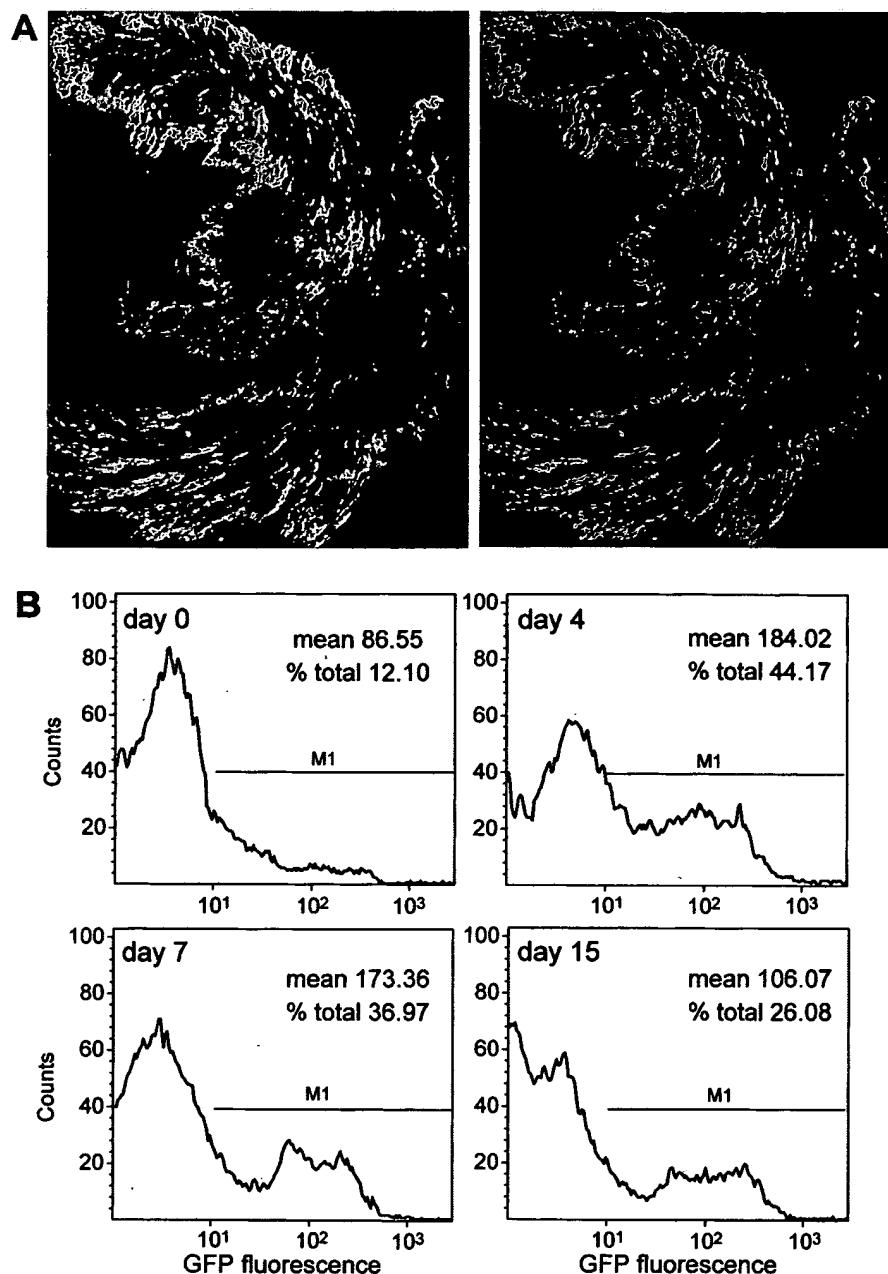


FIG. 3. Transgene expression in LV myocardium after *in vivo* transcortary adenovirus application. (A) Microscopic slices (3 μ m) of sham-operated rabbit heart 4 days after infection with bicortary adenovirus coding for GFP and p35 (5×10^{10} PFU). Direct p35 expression was documented by immunostaining with a monoclonal anti-FLAG M2 antibody directed against the artificial epitope. The samples were visualized by phase-contrast fluorescence microscopy at 520 nm for GFP (*left*) and at 615 nm (Texas Red fluorescence) for p35 (*right*). Original magnification: $\times 25$. (B) Time course of GFP expression was analyzed by flow cytometry experiments in freshly isolated cardiomyocytes from sham-operated rabbit myocardium after Ad-GFP gene delivery. M1 indicates the GFP fluorescence cutoff; 2×10^4 cells were analyzed in each sample. Shown are cumulative data from four animals (one animal each day).

Next, we serially examined *in vivo* expression of p35 4, 7, and 15 days after adenoviral gene transfer in sham-operated animals by immunoblotting. p35 expression showed a maximum after 4–7 days and gradually decreased at day 15 (Fig. 4C). Cell extracts prepared from failing myocardium after 15 days of pacing documented a significant increase in caspase 3 activity, and a 5.5-fold caspase 3-mediated induction of

DNA fragmentation compared with sham-operated controls (Fig. 4D and E). Gene delivery of Ad-p35 to failing hearts efficiently blocked caspase 3 stimulation (28 ± 11 vs. 84 ± 5.3 active units) and clearly reduced DNA–histone formation in comparison with CHF (2.7- vs. 5.5-fold increase; sham, $n = 6$; CHF, $n = 8$; CHF+Ad-p35, $n = 4$; CHF+Ad-GFP, $n = 4$; Fig. 4D and E).

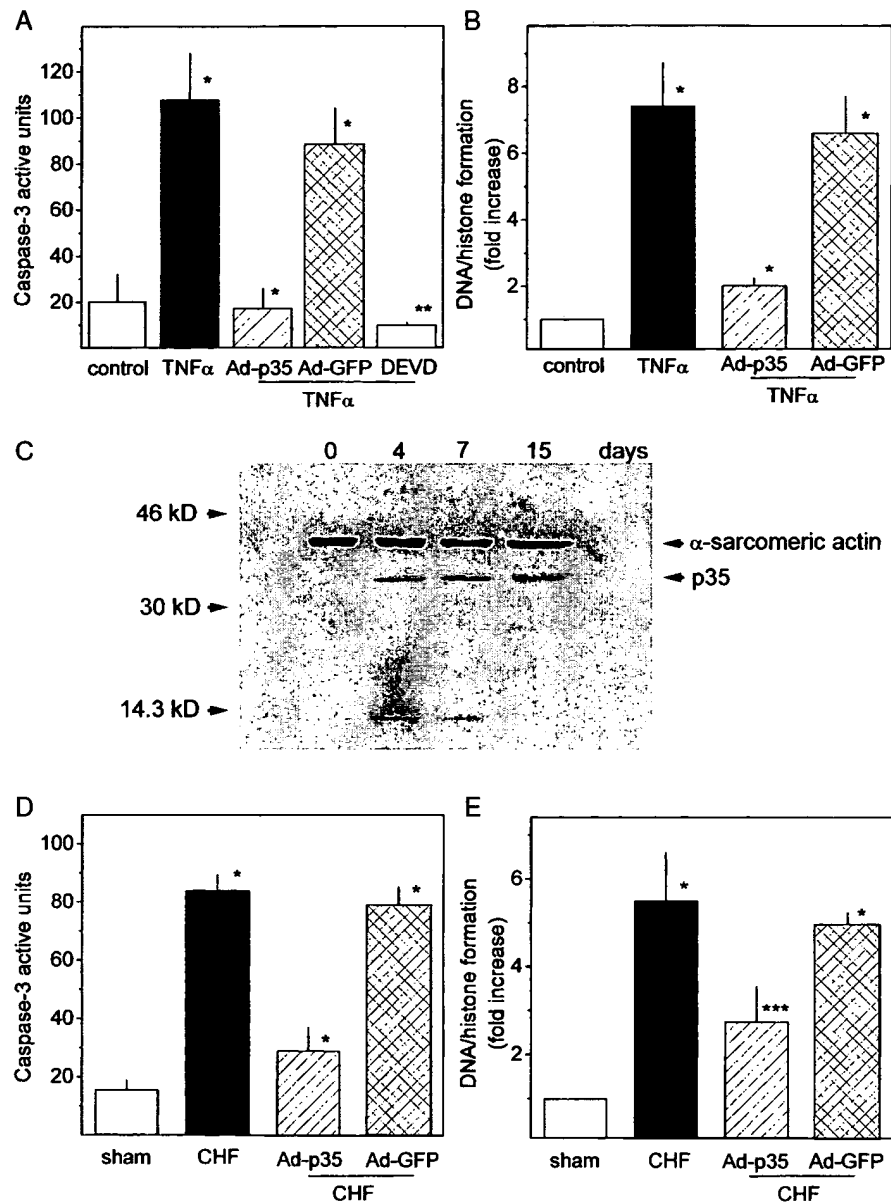


FIG. 4. Blockade of caspase 3 activity and nucleosome formation by adenoviral overexpression of p35 *in vitro* and *in vivo*. (A) Caspase 3 activity and (B) DNA–histone formation determined in lysates of isolated rat cardiomyocytes infected *in vitro* with Ad-p35 and Ad-GFP (MOI of 100 PFU/cell). Apoptosis was induced in the infected cells by incubation with rat TNF- α (3500 IU/ml) for 18 hr. The tetrapeptide inhibitor of caspase 3 (DEVD-FMK) was applied in a concentration of 5 μ M. Data in (A) and (B) are expressed as means \pm SEM; $n = 4$ per each group. (C) Immunoblot analysis of extracts from anterolateral wall of Ad-p35-infected rabbit myocardium 0, 4, 7, and 15 days after gene transfer. Immunostaining was performed with two monoclonal antibodies, anti-FLAG M2 and anti- α -sarcomeric actin, to document in parallel p35 and actin expression. Shown are cumulative data from four animals (one animal each day). (D) Caspase 3 enzyme activity levels and (E) DNA–histone formation assessed in ventricular tissue from sham-operated (sham) and failing hearts (CHF). Rabbits were paced for 15 days and received an intracoronary application of Krebs-Ringer, Ad-p35, or Ad-GFP. Data in (D) and (E) are expressed as means \pm SEM. Sham, $n = 6$; CHF, $n = 8$; CHF+Ad-p35, $n = 4$; CHF+Ad-GFP, $n = 4$. * $p < 0.005$, ** $p < 0.001$, and *** $p < 0.01$ in comparison with control/sham or TNF- α -stimulated/CHF cardiomyocytes.

Blocking caspase 3 activation improves contractile force in vivo

To assess the functional effects of p35 in preventing the progression of heart failure as cytosolic modulator of myocardial

programmed cell death, we measured echocardiographic and hemodynamic parameters after adenovirus-mediated gene delivery. FS was measured after 7 and 15 days of pacing in CHF rabbits and failing animals that received Ad-p35 or Ad-GFP (Fig. 5A and B). FS was significantly elevated at day 15 after

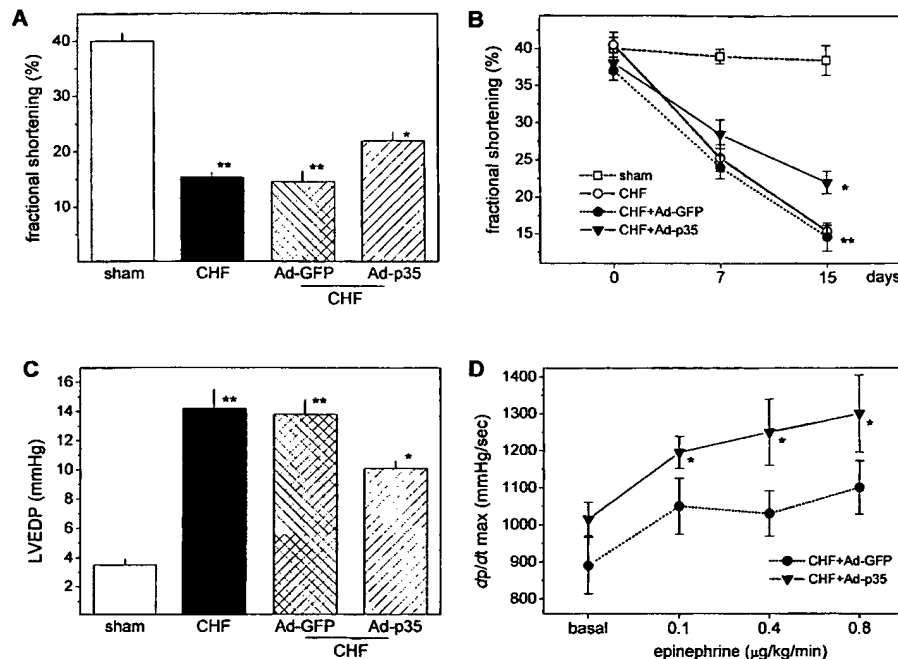


FIG. 5. Echocardiographic and hemodynamic measurements in genetically manipulated hearts infected with Ad-p35. (A) FS and (C) LVEDP were assessed in sham-operated (sham) and failing hearts (CHF) after 15 days of pacing and transcoronary application of Krebs-Ringer, Ad-GFP, or Ad-p35. (B) Time course of fractional shortening after 7 and 15 days of pacing. (D) dp/dt_{\max} recordings after administration of increasing doses of epinephrine. Data are shown as means \pm SEM, $n = 8$ per each group. * $p < 0.05$, ** $p < 0.001$ in comparison with sham and CHF+Ad-GFP hearts.

rapid ventricular pacing in CHF+Ad-p35 animals, whereas no effect was seen in CHF+Ad-GFP rabbits (22 ± 1 vs. $15.0 \pm 1.5\%$, $n = 8$ in each group, $p < 0.05$).

Left ventricular end-diastolic pressure (LVEDP) and dp/dt as characteristics of global ventricular contractility were determined to complement the echocardiographic information. LVEDP in CHF+Ad-p35 animals was reduced compared with the CHF+Ad-GFP group (10.4 ± 0.8 vs. 14.0 ± 1 mmHg, $n = 8$ in each group, $p < 0.05$; Fig. 5C). When cytosolic caspase activity was blocked by overexpression of p35 up to 15 days over the pacing period, cardiac contractility in rabbits, as measured by LV dp/dt , was significantly enhanced in response to epinephrine compared with Ad-GFP-treated failing hearts (Fig. 5D).

The failing hearts in this model had no significant increase in LV mass when normalized to either tibial length or body weight. Overexpression of p35 in the paced hearts did not have

any significant effect on LV mass, normalized to tibial length or body mass (Table 2).

Functional reconstitution of contractile force by overexpression of p35 by reducing sarcomeric disarray

To investigate the effect of p35 expression on contractile function of single ventricular cardiomyocytes 15 days after *in vivo* gene delivery, cells from the target area of sham+Ad-GFP, CHF+Ad-GFP, and CHF+Ad-p35 myocardium were isolated. Transgene-expressing cells were selected by GFP fluorescence. Figure 6A–C show confocal laser scanning microscopy of isolated myocytes after phalloidin staining to visualize polymeric actin. Interestingly, failing cardiomyocytes expressing p35 showed a better organized sarcomeric structure compared with

TABLE 2. MORPHOMETRIC ANALYSES^a

| Group ($n = 4$) | Body weight (g) | LV weight (g) | LV/BW ($\times 10^3$) | LV/TL ($\times 10^3$) (g/cm) |
|----------------------|--------------------|------------------|-------------------------|-----------------------------------|
| Sham + Ad-GFP | 2900 \pm 305 | 9.7 \pm 0.6 | 3.28 \pm 0.8 | 950 \pm 59 |
| CHF + Ad-GFP | 2800 \pm 346 | 9.4 \pm 0.8 | 3.32 \pm 0.4 | 921 \pm 37 |
| Sham + Ad-p35 | 2950 \pm 423 | 9.5 \pm 0.4 | 3.20 \pm 0.9 | 931 \pm 45 |
| CHF + Ad-p35 | 2740 \pm 502 | 9.8 \pm 0.9 | 3.51 \pm 0.7 | 960 \pm 74 |

Abbreviations: LV, left ventricle; BW, body weight; TL, tibial length.

^aFor all groups no significant values were reached.

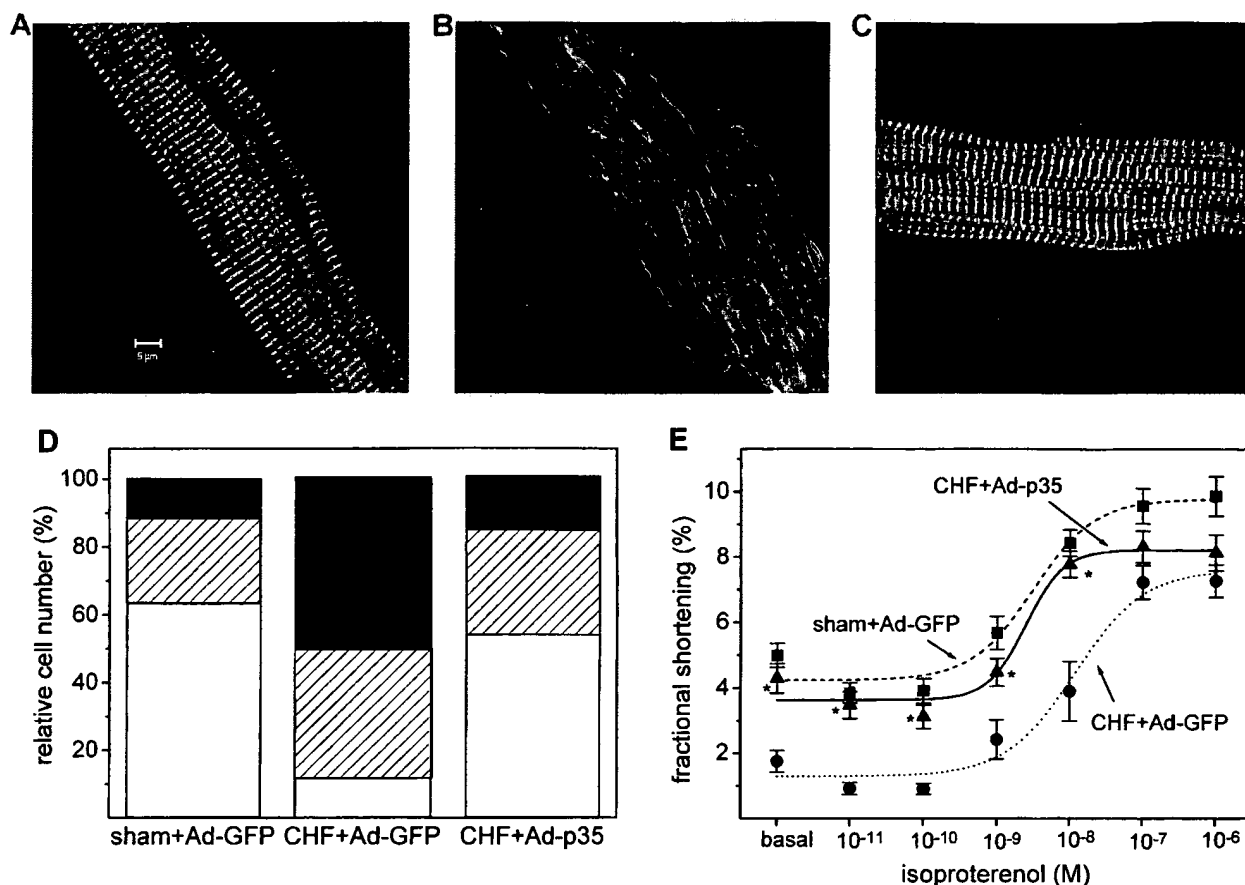


FIG. 6. Effect of p35 expression on sarcomere organization and contractile performance of myocytes from paced hearts. Ventricular rabbit cardiomyocytes were isolated from the anterolateral wall of sham-operated Ad-GFP-infected (A), failing Ad-GFP-infected (B), and failing Ad-p35-infected myocardium (C) and visualized by laser scanning fluorescence microscopy after phalloidin staining. Scale bar corresponds to 5 μ m. (D) Morphology of phalloidin-stained myofibrils was semiquantitatively scored on the basis of the area occupied by organized sarcomere in total cell area: poor, less than one-third (black pattern); moderate, less than two-thirds (striped pattern); good, more than two-thirds (white pattern). Eight hundred cells isolated from 4 animals were counted for each group. (E) Contraction amplitude in isolated cardiomyocytes after *in vivo* gene delivery of Ad-p35 and Ad-GFP in sham-operated or paced rabbits. Data in (E) are expressed as means \pm SEM, $n = 60$ cells from four rabbits in each group. * $p < 0.001$ in comparison with CHF+Ad-GFP.

Ad-GFP-infected failing cells with destroyed sarcomeric units. The degree of sarcomere organization assessed by semiquantitative scoring of rod-shaped cells is presented in Fig. 6D. The ratio of myocytes with well-organized sarcomeres (more than two-thirds of cell area) was $64 \pm 1\%$ in sham+Ad-GFP, $13 \pm 3\%$ in CHF+Ad-GFP, and $52 \pm 4\%$ in CHF+Ad-p35 cardiomyocytes (800 rod-shaped cells, expressing the transgene, and isolated from four animals were analyzed in each group). The percentage of round, dead cells was $28 \pm 4\%$, $39 \pm 8\%$, and $20 \pm 6\%$, respectively (2000 cells isolated from 4 animals were randomly selected and counted in each group).

Shortening amplitude was measured in failing and nonfailing cells from myocardium infected *in vivo* with Ad-p35 or Ad-GFP, electrically stimulated at a rate of ~ 70 contractions per minute. Experiments were performed in myocytes with moderate or good sarcomeric structure. Adenoviral infection did not alter shortening characteristics. As shown in Fig. 6E, failing cardiomyocytes expressing p35 presented a significantly increased basal shortening amplitude compared with equivalent

myocytes infected with Ad-GFP (4.3 ± 0.4 vs. $1.8 \pm 0.2\%$, $n = 60$ in each group, $p < 0.001$). This enhancement of contractile force was also seen after isoproterenol stimulation and the EC₅₀ of the dose-response curve was shifted to higher values, similar to those of nonfailing cells treated with Ad-GFP (Fig. 6E). These results indicate that p35 restores sarcomeric organization and thereby reconstitutes contractile performance of failing myocytes.

Microinjection of activated caspase 3 in isolated ventricular cardiomyocytes

To examine whether activation of caspase 3 is sufficient for induction of sarcomeric disarray, we microinjected activated enzyme into the cytoplasm of rabbit ventricular healthy cardiomyocytes. Positive cells (~ 10 – 20%) were identified by FITC fluorescence. Morphological characteristics of cardiomyocytes 2 hr after microinjection of activated caspase 3 (4 and 20 ng/ μ l) compared with control-injected cells are presented in

Fig. 7A and B. Treatment of myocytes with caspase 3 caused a rapid, concentration-dependent destruction of the straight and striated bundles of the sarcomeric units (Fig. 7B, left and right). Single-cell shortening experiments in microinjected cardiomyocytes showed a caspase 3-mediated reduction in basal and isoproterenol-stimulated contraction (4.3 vs. 9.8% [10^{-8} M isoproterenol], $n = 45$ in each group, $p < 0.005$). These effects were blocked by preincubation of the myocytes with DEVD-FMK (Fig. 7C).

DISCUSSION

In the present study, we report the novel finding that caspase activation influences cardiac performance of failing ventricular myocytes by destroying sarcomeric structure. Caspase 3 activation, present in failing myocardium, can be corrected via adenovirus-mediated gene delivery of p35 with a positive impact on contractility.

In at least four different models of ischemia-reperfusion injury (cardiac, renal, cerebral, and liver), caspase inhibition has resulted in decreased infarct volumes and partially improved organ function (Nicholson, 2000). However, no information was previously available as to whether caspase activation contributes to disease progression in heart failure and whether cardiomyocytes rescued from apoptosis under such conditions preserve their contractile function. Caspases have multiple intracellular targets involved in chromatin condensation, DNA fragmentation, and cytoskeletal destruction (Hengartner, 2000). In cardiac myocytes, the cytoskeleton is a highly specialized structure, whose components can be classified into three groups: (1) the force-generating contractile sarcomeric unit (e.g., actin-myosin filaments, troponin-tropomyosin complex), (2) the intrasarcomeric cytoskeleton regulating the contraction cycle (e.g., titin, α -actinin, and myosin-binding protein C), and (3) the extrasarcomeric cytoskeleton (e.g., desmin, lamins, and dystrophin) (Chen and Chien, 1999). The impact of abnormalities in the cytoskeleton-sarcomeric network on cardiac function has been demonstrated in hereditary forms of hypertrophic and dilated cardiomyopathy (Towbin, 1998; Kamisago *et al.*, 2000). In addition, cleavage of dystrophin by enteroviral protease 2A has been suggested as a molecular mechanism for acquired forms of dilated cardiomyopathy (Badorff *et al.*, 1999). These findings indicate that defective transmission of force through loss of sarcomere integrity or cytoskeletal structures leads to myocyte dysfunction.

In a rabbit model of CHF, we investigated whether activation of caspases contributes to disease progression and influences contractility by sarcomere disorganization. Pacing-induced heart failure has served as a useful experimental model for the study of dilated cardiomyopathy, which is associated with enhanced expression of *bax*, a gene that stimulates apoptosis (Leri *et al.*, 1998). To manipulate caspase activation in failing myocardium, we used the baculoviral cell survival protein p35, which blocks apoptosis induced by TNF, Fas, glucocorticoids, radiation, and DNA-damaging agents by inhibiting caspases 1, 2, 3, 4, 6, 7, 8, and 10 (Villa *et al.*, 1997).

Four lines of evidence support the notion that caspases play a role in the development of CHF. First, the activities of caspase 3 and CAD, two key molecules in the process of myocar-

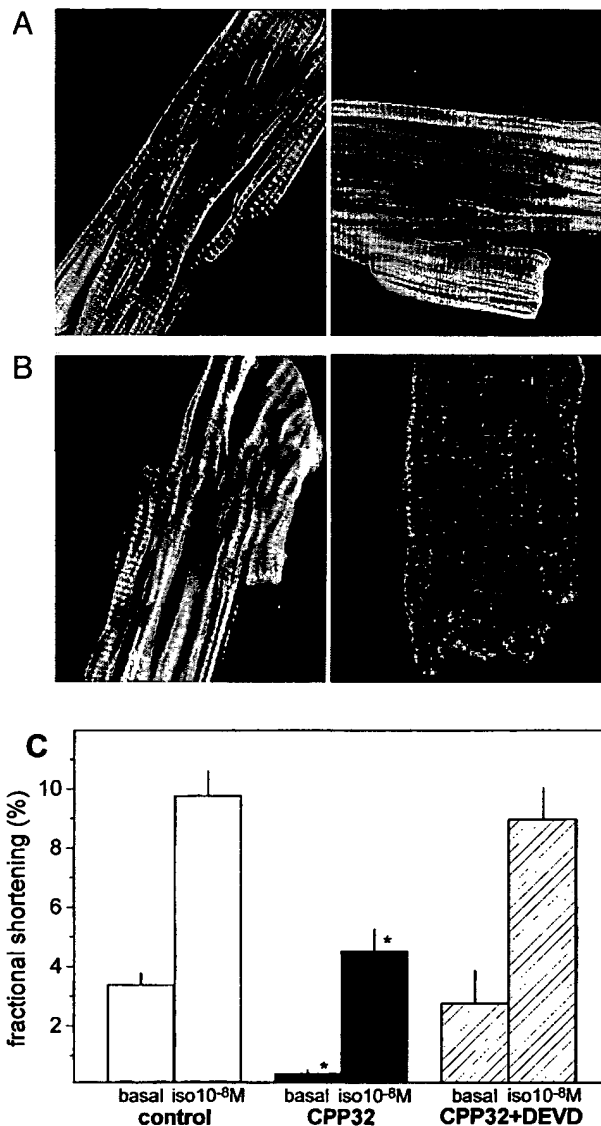


FIG. 7. Microinjection of activated caspase 3 into the cytoplasm of healthy ventricular cardiomyocytes. (A) Myocytes were microinjected with FITC-conjugated dextran alone or (B) plus human recombinant active caspase 3 (4 ng/ μ l, left; 20 ng/ μ l, right). The morphology of actin fibers was visualized by laser scanning fluorescence microscopy after phalloidin staining. Original magnification: $\times 630$. (C) Contraction amplitude under basal conditions and isoproterenol stimulation (10^{-8} M) was determined in cells 2 hr after microinjection of FITC-conjugated dextran (open columns) or caspase 3 at 4 ng/ μ l (CPP32) (solid columns). Preincubation of DEVD-FMK was performed (hatched columns). Data are shown as means \pm SEM, $n = 45$ cells from two animals in each group. * $p < 0.005$ in comparison with control injected cells (basal; isoproterenol 10^{-8} M).

dial apoptosis, are increased in this CHF model (Fig. 1). Similar findings for caspase 3 in biopsies of human cardiomyopathic hearts confirm our results (Narula *et al.*, 1999). Second, somatic gene delivery of p35 into failing myocardium significantly reduced caspase 3 activity and nucleosome formation *in vivo* (Fig. 4). Echocardiographic and hemodynamic function of the p35-expressing hearts was partially restored (Fig. 5).

These results are in accordance with previously published data about reconstitution of visual function in a retinitis pigmentosa model in *Drosophila* by caspase 3 inhibition (Davidson and Steller, 1998). Third, isolated cardiomyocytes of failing hearts treated with Ad-p35 showed significantly increased basal and isoproterenol-stimulated fractional shortening and better organized sarcomeric structure (Fig. 6). Because p35 expression had no positive inotropic effect in healthy cardiomyocytes *in vitro* (data not shown), one might speculate that its preservation of contractile force is due to irreversible caspase inhibition. Fourth, cytoplasmic microinjection of activated caspase 3 in healthy cells induced a concentration-dependent destruction of the sarcomeric units, as demonstrated by phalloidin staining of polymerized actin, and correlated with reduced contractile performance (Fig. 7).

Several mechanisms may cause caspase-mediated sarcomere disorganization in failing cardiomyocytes. Caspase 3-mediated activation of gelsolin and a consecutive shift of polymerized actin to monomeric actin in the sarcomeric unit can be discussed as one molecular mechanism (Sun *et al.*, 1999). Another possibility for caspase-induced sarcomere destruction is the direct cleavage of actin by caspase 3, because cytoskeletal actin is a substrate of caspases (Mashima *et al.*, 1999). Further studies should investigate the interaction of caspase 3 with other sarcomere proteins, because putative cleavage sites are located in the ATP-binding domain of the myosin heavy chain, in troponin T and I, tropomyosin, and tropomodulin. Another important issue to be elucidated is whether myocytes with poor organized sarcomere show caspase 3 activation without nuclear DNA damage in order to examine whether caspases play a role in the deterioration of cell function in the absence of triggering the full death program.

Cardiac-specific deletion of the signaling receptor subunit, gp130, leads to massive cardiac apoptosis and accelerated dilated cardiomyopathy after aortic banding (Hirota *et al.*, 1999). Further investigations should determine the existence of an intersection between the proapoptotic caspase 3 pathway and the antiapoptotic gp130 survival pathway in CHF.

Limitations of this study are (1) transcatheter gene delivery, which affects only a limited area of LV myocardium, and (2) the use of first-generation adenoviral vectors, which induce an inflammatory response and result in transient gene expression. In rabbits, the left coronary system is dominant and the circumflex artery is by far the largest coronary vessel. The gene delivery protocol via the left coronary system used in this study affected ~30% of the whole LV myocardium 4 days after *in vivo* infection (Fig. 3). Hajjar *et al.* established a catheter-based technique that allows for generalized cardiac gene transfer *in vivo* (Hajjar *et al.*, 1998). However, our group and Lai *et al.* reported functional modulation of cardiac performance *in vivo* by using intracoronary adenovirus delivery after modification of the endothelial barrier (Lai *et al.*, 2000; Weig *et al.*, 2000). Infection of rabbit myocardium with recombinant adenoviruses did not affect myocyte apoptosis, as had already been observed *in vitro* (Matsui *et al.*, 1999). Histologic slices showed a mild inflammatory infiltrate 15 days after gene transfer, equally in the Ad-p35- and Ad-GFP-treated group. Therefore, we believe the immunological response did not confound our results.

Fifteen days after gene transfer, ~14% of the cardiomyocytes from whole LV myocardium showed GFP fluorescence. By using a bicistronic vector to control transgene expression

and by studying functionally isolated myocytes from the target area, we were able to verify that the observed increase in contractility *in vivo* was directly mediated by caspase inhibition in cardiomyocytes.

Because the molecular mechanism of p35 is not a direct cAMP- or Ca^{2+} -regulated positive inotropism, but a protection from sarcomere disorganization via irreversible caspase inhibition, protein synthesis is necessary to counteract its effect (Bump *et al.*, 1995). Although p35 expression and caspase 3 activity were inversely correlated over the time course of heart failure development, transgene levels documented in the first week of pacing should be sufficient to block tachycardia-induced caspase activation, and thereby delay heart failure in this animal model.

In summary, we have ameliorated systolic function in failing myocardium by blocking caspases through gene transfer of recombinant adenovirus expressing p35. Improved contractile function and reduced LV end-diastolic pressures were associated with reduction in caspase 3 activity, DNA fragmentation, and sarcomere disorganization. This study provides evidence that caspase activation contributes to the progression of heart failure and that its prevention leads to partial restoration of cardiac hemodynamics.

NOTE ADDED IN PROOF

During the review process of the present article, myocyte apoptosis assessed by caspase 3 and CAD activities and TUNEL staining has been reported in a similar model of rapid ventricular pacing in dogs by Cesselli *et al.* (Circ. Res. 2001;89:279–286).

ACKNOWLEDGMENTS

We thank Dr. S. Nagata (Department of Genetics, Osaka University Medical School, Japan) and Dr. H. Steller (Howard Hughes Medical Research Institute, MIT) for helpful discussions and for providing us with the p35 cDNA.

These studies were supported by the Deutsche Forschungsgemeinschaft and Bayerische Forschungsmittel der Technischen Universität München.

REFERENCES

- AKHTER, S., SKAER, C., KYPSON, A.P., McDONALD, P.H., PEPPEL, K., GLOWER, D., LEFKOWITZ, R.J., and KOCH, W.J. (1997). Restoration of β -adrenergic signaling in failing cardiac ventricular myocytes via adenoviral-mediated gene transfer. *Proc. Natl. Acad. Sci. U.S.A.* **94**, 12100–12105.
- ASHKENAZI, A., and DIXIT, V.M. (1998). Death receptors: Signaling and modulation. *Science* **281**, 1305–1308.
- BADORFF, C., LEE, G.H., LAMPHEAR, B.J., MARTONE, M.E., CAMPBELL, K.P., RHOADS, R.E., and KNOWLTON, K.U. (1999). Enteroviral protease 2A cleaves dystrophin: Evidence of cytoskeletal disruption in an acquired cardiomyopathy. *Nat. Med.* **5**, 320–326.
- BRAUNWALD, E., and BRISTOW, M.R. (2000). Congestive heart failure: Fifty years of progress. *Circulation* **102**, IV14–IV23.
- BUMP, N.J., HACKETT, M., HUGUNIN, M., SOMASEKAR, S., BRADY, K., CHEN, P., FERENZ, C., FRANKLIN, S., GHAYUR, T., LI, P., LICARI, P., MANKOVICH, J., SHI, L., GREENBERG,

- A.H., MILLER, L.K., and WONG, W.W. (1995). Inhibition of ICE family proteases by baculovirus antiapoptotic protein p35. *Science* **269**, 1885–1888.
- CHEN, J., and CHIEN, K.R. (1999). Complexity and simplicity: Monogenic disorders and complex cardiomyopathies. *J. Clin. Invest.* **103**, 1483–1485.
- DAVIDSON, F.F., and STELLER, H. (1998). Blocking apoptosis prevents blindness in *Drosophila* retinal degeneration mutants. *Nature* **391**, 587–591.
- DONAHUE, J.K., HELDMAN, A.W., FRASER, H., McDONALD, A.D., MILLER, J.M., RADE, J.J., ESCHENHAGEN, T., and MARBAN, E. (2000). Focal modification of electrical conduction in the heart by viral gene transfer. *Nat. Med.* **6**, 1395–1398.
- ENARI, M., HASE, A., and NAGATA, S. (1995). Apoptosis by a cytosolic extract from Fas-activated cells. *EMBO J.* **14**, 5201–5208.
- ENARI, M., SAKAHIRA, H., YOKOYAMA, H., OKAWA, K., IWAMATSU, A., and NAGATA, S.A. (1998). Caspase-activated DNase that degrades DNA during apoptosis, and its inhibitor ICAD. *Nature* **391**, 43–50.
- GARDIN, J.M., SIRI, F.M., KITSIS, R.N., EDWARDS, J., and LEINWAND, L.A. (1995). Echocardiographic assessment of left ventricular mass and systolic function in mice. *Circ. Res.* **76**, 907–914.
- GREEN, D.R., and REED, J.C. (1998). Mitochondria and apoptosis. *Science* **281**, 1309–1312.
- HAJJAR, R.J., SCHMIDT, U., MATSUI, T., GUERRERO, L., LEE, K.H., GWATHMEY, J., DEC, W., SEMIGRAN, M.J., and ROSENZWEIG, A. (1998). Modulation of ventricular function through gene transfer *in vivo*. *Proc. Natl. Acad. Sci. U.S.A.* **95**, 5251–5256.
- HAUNSTETTER, A., and IZUMO, S. (2000). Toward antiapoptosis as a new treatment modality. *Circ. Res.* **86**, 371–376.
- HE, T.C., ZHOU, S., DA COSTA, L.T., YU, J., KINZLER, K.W., and VOGELSTEIN, B. (1998). A simplified system for generating recombinant adenoviruses. *Proc. Natl. Acad. Sci. U.S.A.* **95**, 2509–2514.
- HENGARTNER, M.O. (2000). The biochemistry of apoptosis. *Nature* **407**, 770–776.
- HIROTA, H., CHEN, J., BETZ, U.A., RAJEWSKY, K., GU, Y., ROSS, J., MULLER, W., and CHIEN, K.R. (1999). Loss of a gp130 cardiac muscle cell survival pathway is a critical event in the onset of heart failure during biomechanical stress. *Cell* **97**, 189–198.
- HUNTER, J.J., and CHIEN, K.R. (1999). Mechanisms of disease: Signaling pathways for cardiac hypertrophy and failure. *N. Engl. J. Med.* **341**, 1276–1283.
- KAMISAGO, M., SHARMA, S.D., DE PALMA, S.R., SOLOMON, S., SHARMA, P., McDONOUGH, B., SMOOT, L., MULLEN, M., WOOLF, P.K., WIGLE, E., SEIDMAN, J.G., and SEIDMAN, C.E. (2000). Mutations in sarcomeric protein genes as a cause of dilated cardiomyopathy. *N. Engl. J. Med.* **343**, 1688–1696.
- KROWN, K.A., PAGE, M.T., NGUYEN, C., ZECHNER, D., GUTIERREZ, V., COMSTOCK, K.L., GLEMBOTSKI, C.C., QUINTANA, P.J., and SABBADINI, R.A. (1996). Tumor necrosis factor α -induced apoptosis in cardiac myocytes. *J. Clin. Invest.* **98**, 2854–2865.
- LAI, N.C., ROTH, D.M., GAO, M.H., FINE, S., HEAD, B.P., ZHU, J., McKIRNAN, M.D., KWONG, C., DALTON, N., URASAWA, K., ROTH, D.A., and HAMMOND, H.K. (2000). Intracoronary delivery of adenovirus encoding adenylyl cyclase VI increases left ventricular function and cAMP-generating capacity. *Circulation* **102**, 2396–2401.
- LAUGWITZ, K.L., UNGERER, M., SCHÖNEBERG, T., WEIG, H.J., KRONSEIN, K., MORETTI, A., HOFFMANN, K., SEYFARTH, M., SCHULTZ, G., and SCHÖMIG, A. (1999). Adenoviral gene transfer of the human V2 vasopressin receptor improves contractile force of rat cardiomyocytes. *Circulation* **99**, 925–933.
- LERI, A., LIU, J., MALHOTRA, A., LI, Q., STIEGLER, P., CLAUDIO, P., GIORDANO, A., KAJSTURA, J., HINTZE, T., and ANVERSA, P. (1998). Pacing-induced heart failure in dogs enhances the expression of p53 and p53-dependent genes in ventricular myocytes. *Circulation* **97**, 194–203.
- MACLELLAN, W.R. (2000). Advances in the molecular mechanisms of heart failure. *Curr. Opin. Cardiol.* **15**, 128–135.
- MASAKI, H., IMAIZUMI, T., ANDO, S., HIROOKA, Y., HARADA, S., MOMOHARA, M., NAGANO, M., and TAKESHITA, A. (1993). Production of chronic congestive heart failure by rapid ventricular pacing in the rabbit. *Cardiovasc. Res.* **27**, 828–831.
- MASHIMA, T., NAITO, M., and TSURUO, T. (1999). Caspase-mediated cleavage of cytoskeletal actin plays a positive role in the process of morphological apoptosis. *Oncogene* **18**, 2423–2430.
- MATSUI, T., LING, L., DEL MONTE, F., FUKUI, Y., FRANKE, T.H., HAJJAR, R.J., and ROSENZWEIG, A. (1999). Adenoviral gene transfer of activated phosphatidylinositol 3'-kinase and Akt inhibits apoptosis of hypoxic cardiomyocytes *in vitro*. *Circulation* **100**, 2373–2385.
- NARULA, J., PANDEY, P., ARBUSTINI, E., HAIDER, N., NARULA, N., KOLODIE, F.D., DAL BELLO, B., SEMIGRAN, M.J., BIELSA-MASDEU, A., DEC, G.W., ISRAELS, S., BALLESTER M., VIRMANI, R., SAXENA, S., and KHARBANDA, S. (1999). Apoptosis in heart failure: Release of cytochrome *c* from mitochondria and activation of caspase-3 in human cardiomyopathy. *Proc. Natl. Acad. Sci. U.S.A.* **96**, 8144–8149.
- NICHOLSON, D.W. (2000). From bench to clinic with apoptosis-based therapeutic agents. *Nature* **407**, 810–816.
- OLIVETTI, G., ABBI, R., QUAINI, F., KAJSTURA, J., CHENG, W., NITAHARA, J.A., QUAINI, E., DE LORETTO, C., BELTRAMI, C.A., KRAJEWSKI, S., REED, T.C., and ANVERSA, P. (1997). Apoptosis in the failing human heart. *N. Engl. J. Med.* **336**, 1131–1141.
- REED, J.C., and PATERNOSTRO, G. (1999). Postmitochondrial regulation of apoptosis during heart failure. *Proc. Natl. Acad. Sci. U.S.A.* **96**, 7614–7616.
- RUDEL, T., and BOKOCH, G.M. (1997). Membrane and morphological changes in apoptotic cells regulated by caspase-mediated activation of PAK2. *Science* **276**, 1571–1574.
- SUN, H.Q., YAMAMOTO, M., MEJILLANO, M., and YIN, H.L. (1999). Gelsolin, a multifunctional actin regulatory protein. *J. Biol. Chem.* **274**, 33179–33182.
- TOWBIN, J.A. (1998). The role of cytoskeletal proteins in cardiomyopathies. *Curr. Opin. Cell. Biol.* **10**, 131–139.
- VILLA, P., KAUFMANN, S.H., and EARNSHAW, W.C. (1997). Caspases and caspase inhibitors. *Trends Biochem. Sci.* **22**, 388–393.
- WEIG, H.J., LAUGWITZ, K.L., MORETTI, A., KRONSEIN, K., STÄDELE, C., BRÜNING, S., SEYFARTH, M., BRILL, T., SCHÖMIG, A., and UNGERER, M. (2000). Enhanced cardiac contractility after gene transfer of V2 vasopressin receptors *in vivo* by ultrasound-guided injection or transcatheter delivery. *Circulation* **101**, 1578–1585.

Address reprint requests to:
 Dr. Karl-Ludwig Laugwitz
 I. Medizinische Klinik
 Klinikum Rechts der Isar
 Ismaninger Straße 22
 D-81675 Munich, Germany

E-mail: laugwitz@med1.med.tu-muenchen.de

Received for publication May 9, 2001; accepted after revision October 11, 2001.

Published online: November 2, 2001.

Attenuation of Ischemia/Reperfusion Injury in Rats by a Caspase Inhibitor

Hiroyuki Yaoita, MD; Kazuei Ogawa, MD; Kazuhira Maehara, MD; Yukio Maruyama, MD

Background—Z-Val-Ala-Asp(OMe)-CH₂F (ZVAD-fmk), a tripeptide inhibitor of the caspase interleukin-1 β -converting enzyme family of cysteine proteases, may reduce myocardial reperfusion injury in vivo by attenuating cardiomyocyte apoptosis within the ischemic area at risk.

Methods and Results—Sprague-Dawley rats were subjected to a 30-minute coronary occlusion followed by a 24-hour reperfusion. An inert vehicle (dimethylsulfoxide; group 1, n=8) or ZVAD-fmk, at a total dose of 3.3 mg/kg (group 2, n=8), was administered intravenously every 6 hours starting at 30 minutes before coronary occlusion until 24 hours of reperfusion. At this 24-hour point, hemodynamics were assessed by means of cardiac catheterization; then, the rats were killed, and the left ventricle was excised and sliced. The myocardial infarct size/ischemic area at risk and the count of presumed apoptotic cardiomyocytes (terminal deoxynucleotidyl transferase-mediated dUTP-biotin nick end labeling [TUNEL]-positive cells) within the ischemic area at risk were assessed through triphenyltetrazolium chloride staining and TUNEL methods, respectively. Peak positive left ventricular dP/dt was higher ($P=.02$) and left ventricular end-diastolic pressure was lower ($P=.04$) in group 2 than in group 1. The infarct size/ischemic area at risk of group 2 ($52.4\pm4.0\%$) was smaller ($P=.02$) than that of group 1 ($66.6\pm3.7\%$), and TUNEL-positive cells were fewer ($P=.0002$) (group 2, $3.1\pm0.9\%$; group 1, $11.1\pm1.0\%$). Agarose gel electrophoresis revealed DNA laddering in the border zone myocardium of group 1, but DNA ladder formation was attenuated in group 2.

Conclusions—ZVAD-fmk was effective in reducing myocardial reperfusion injury, which could at least be partially attributed to the attenuation of cardiomyocyte apoptosis. (*Circulation*. 1998;97:276-281.)

Key Words: myocardium ■ reperfusion ■ apoptosis ■ caspase

Attempts to reduce the extent of myocardial reperfusion injury have included lowering the risk posed by certain injurious factors and potentiating various aspects of cardioprotection relating to ischemic duration,¹ oxygen free radicals,^{2,3} proinflammatory cytokines,^{4,5} and preconditioning.⁶⁻¹⁰ It has been reported that apoptosis is a significant contributor to myocardial cell death as a result of reperfusion injury.¹ Therefore, it might be hypothesized that this type of injury could be attenuated if a portion of the injured myocardial cells could be rescued from an apoptotic death.

See p 227

The caspase inhibitors, that is, ICE-like protease inhibitors,¹¹ interfere with apoptosis at a point subsequent to the initiation of the proapoptotic process in cells that have already received apoptosis-promoting signals. As opposed to reducing the exposure of cardiomyocytes to injurious stimuli, apoptosis of these cells is attenuated through modulation of the caspase-related proapoptotic process, and this may allow ischemic myocardium to survive even after receiving significant injury. ZVAD-fmk (fluoro-methylketone), a tripeptide inhibitor of the caspase, is reported to attenuate cardiomyocyte apoptosis in

vitro.⁶ In the present study, we investigated whether ZVAD-fmk lowers the extent of experimental myocardial reperfusion injury in vivo by attenuating cardiomyocyte apoptosis. In a rat model for myocardial reperfusion injury, infarct size and the appearance of presumed apoptotic cardiomyocytes were assessed in two groups that were or were not administered this protease inhibitor.

Methods

This study was carried out under the supervision of the Animal Research Committee in accordance with the Guideline on Animal Experiments of Fukushima Medical College and Japanese Government Animal Protection and Management Law (No. 105).

Animal Model

Twenty-six of 36 adult male (290 to 310 g body weight) Sprague-Dawley rats were anesthetized through intraperitoneal administration of 30 mg/kg sodium pentobarbital. Under artificial ventilation with a rodent ventilator, a left thoracotomy was performed. The proximal portion of the left coronary artery was surgically occluded for 30 minutes through ligation with a suture (size 6.0) followed by coronary reperfusion through release of the tie. Coronary occlusion was confirmed through elevation of the ST segment on the ECG obtained from a limb lead. Transient ventricular arrhythmias were evoked in all

Received July 21, 1997; revision received October 2, 1997; accepted October 2, 1997.

From the First Department of Internal Medicine, Fukushima Medical College, Hikarigaoka 1, Fukushima 960-12, Japan.

Correspondence to Yukio Maruyama, MD, Professor and Chairman, First Department of Internal Medicine, Fukushima Medical College, Hikarigaoka 1, Fukushima, 960-12, Japan.

E-mail yaoita@cc.fmu.ac.jp

© 1998 American Heart Association, Inc.

Selected Abbreviations and Acronyms

| | |
|--------------------|---|
| DMSO | = dimethylsulfoxide |
| ICE | = interleukin-1 β -converting enzyme |
| I/R | = infarct size/ischemic area at risk |
| (\pm)-LV dp/dt | = peak positive (+) and negative (–) first derivatives of left ventricular pressure |
| LVEDP | = left ventricular end-diastolic pressure |
| LVSP | = left ventricular peak systolic pressure |
| PMN | = polymorphonuclear leukocyte |
| TdT | = terminal deoxynucleotidyl transferase |
| TTC | = triphenyltetrazolium chloride |
| TUNEL | = terminal deoxynucleotidyl transferase-mediated dUTP-biotin nick end labeling |
| ZVAD-fmk | = Z-Val-Ala-Asp(OMe)-CH ₂ F |

rats \approx 5 minutes after coronary occlusion, but these usually disappeared after 10 minutes of occlusion. After coronary reperfusion, the tie was left loose on the surface of the heart, the chest was closed, and the intratracheal tube and ECG electrodes were removed. The rats were returned to their cages, where they awakened, and they were allowed free access to food and water until they were killed 24 hours later.

One milligram of ZVAD-fmk (Enzyme Systems Products) was dissolved in 107 μ L of DMSO (Wako Pure Chemicals). In group 2 animals ($n=8$), ZVAD-fmk, at one fourth of a total dose of 3.3 mg/kg body weight, was administered as a bolus into the tail vein four times during the study (first 30 minutes before coronary occlusion and then three times every 6 hours after reperfusion). The same amount of an inert vehicle (DMSO) was administered in the same manner to rats of group 1 ($n=8$).

To assess whether the amount of DMSO used as a vehicle would have a toxic effect in vivo, one fourth of a total DMSO volume of 353 μ L/kg body weight ($n=5$) or the same volume of saline ($n=5$) was administered four times to sham-operated rats in the same manner as to groups 1 and 2.

Leukocytes are known to be involved in the formation of myocardial reperfusion injury.¹² As a positive control for this model of coronary reperfusion injury, 4 rats were administered absorbed polyclonal rabbit anti-rat PMN antisera at a dose of 3 mL/kg (Inter-Cell Technologies) 36 hours before coronary occlusion. Each was subjected to the 30-minute coronary occlusion and 24-hour reperfusion protocol, and 0.5 mL of blood was taken before occlusion and just before death.

Hemodynamic Assessment

Twenty-four hours after coronary reperfusion, rats were anesthetized again through intraperitoneal administration of 30 mg/kg sodium pentobarbital. ECG readings were monitored, and a polyethylene tube (PE 50; Becton-Dickinson) was inserted into the left ventricular cavity via the right carotid artery. LVSP, LVEDP, and (\pm)-LV dp/dt were measured using a polygraph system (AP601G; Nihon Koden).

Assessment of Infarcted Area and Detection of TUNEL-Positive Cardiomyocytes

After hemodynamics were assessed at 24 hours of coronary reperfusion, 0.5 mL of blood was obtained from the catheter for measurement of blood cells. Then, an intratracheal tube was inserted, and the chest was reopened under artificial ventilation. The coronary artery was again briefly occluded through ligation of the tie that remained at the site of the previous occlusion. Immediately after the ligation, 1% Evans blue solution was infused through the catheter into the beating left ventricular cavity to delineate the ischemic area at risk (underperfused and then reperfused area) of the left ventricle. After administration of an excessive dose of sodium pentobarbital into the left ventricular cavity, the heart was excised and cross-sectioned from the apex to the atrioventricular groove into five specimens of \approx 2 mm in thickness with the use of a stereoscope. Because there may be some anatomic

differences in the left coronary artery of each rat, the three middle slices were prepared for morphometry to determine the ischemic area at risk. These slices were incubated with a 4% TTC¹³ solution for 30 minutes at 37°C in a dark room. Then, ischemic but viable (TTC-stained) and infarcted (TTC-unstained) zones within the underperfused and then reperfused area (Evans blue-unstained) and the nonischemic area (Evans blue-stained) were stereoscopically measured using the point-counting method of Weibel¹⁴ with an eyepiece equipped with a 25-square grid (Integration No. 1; Zeiss) under 100 \times magnification, and I/R was calculated. These slices were then fixed in 10% neutral-buffered formalin. Using paraffin sections that were 4 μ m thick, TUNEL was performed as described previously¹⁵ with minor modifications. Briefly, nuclei of tissue sections were stripped of proteins through incubation with 20 μ g/mL proteinase K (Sigma Chemical) for 15 minutes at room temperature. The slides were incubated with 2% H₂O₂ for 5 minutes to allow inactivation of endogenous peroxidase and then incubated for 60 minutes at 37°C with 0.3 EU/ μ L TdT (Takara Shuzo Co) and 0.04 nmol/ μ L biotinylated dUTP (Boehringer-Mannheim Biochemica) in TdT buffer containing 30 mmol/L Tris-HCl, pH 7.2, 140 mmol/L sodium cacodylate, and 1 mmol/L cobalt chloride. The reaction was terminated with buffer containing 300 mmol/L NaCl and 30 mmol/L sodium citrate. The slides were coated with avidin-conjugated peroxidase (Medical and Biological Laboratories) diluted 1:3000 in PBS and visualized with the use of chromogen 3,3'-diaminobenzidine (Dojindo) and H₂O₂. Counterstaining was performed with 2% methyl green. Using this method, each cardiomyocyte could be defined, and TdT-positive or -negative nuclei were stained dark brown or light green, respectively, under light microscopy. When the TUNEL method was performed, positive controls were always included. For DNase treatment in situ,¹⁵ sections were processed with proteinase K, and peroxidase inactivation was carried out as described above. Next, the sections were pretreated with DN buffer (30 mmol/L Tris-HCl, pH 7.2, 140 mmol/L K cacodylate, 4 mmol/L MgCl₂, and 0.1 mmol/L dithiothreitol); then, DNase I (Sigma) at 100 ng/mL was dissolved in this buffer and used to cover each section. After a 15-minute incubation at room temperature, the slides were washed extensively with double-distilled water, and DNA nick end labeling was carried out.

Using an eyepiece for the point-counting method (Integration No. 1, Zeiss), which was performed under a light microscope at a magnification of 400 \times , we determined the count ratio of the area of cardiomyocytes with TdT-stained nuclei with that of total cardiomyocytes (TUNEL-positive cardiomyocytes) within the ischemic area at risk. The entire area was searched through an orderly shifting of the visual field using the outer grids of the eyepiece for orientation. TUNEL-positive cardiomyocytes were carefully distinguished from TUNEL-positive noncardiomyocytes, such as macrophages.

To assess the distribution of the infarcted area and TUNEL-positive cardiomyocytes in the left ventricular wall, we subdivided the ischemic area at risk into three transmural stratified layers of equal thickness (epicardial, middle, and endocardial) in each slice mentioned above (Fig 1). We also divided the ischemic area at risk into five radial segments, and then these five radial segments were rearranged as (Fig 1) a right lateral border segment adjacent to the interventricular septum; a total of three central segments; and a left lateral border segment adjacent to the left ventricular posterior wall. For each of the segments or layers, I/R and TUNEL-positive cardiomyocytes were calculated, as well as for the entire ischemic area at risk.

Using some of the paraffin sections of groups 1 and 2, hematoxylin and eosin staining was also performed for confirmation of myocardial reperfusion injury, such as myocardial cell coagulation, contraction bands, bleeding, and inflammatory cell infiltration.

Genomic DNA Extraction and Agarose Gel Electrophoresis

Rats subjected to the same occlusion and reperfusion protocol as groups 1 and 2, respectively ($n=3$ each group), had their hearts excised at 24 hours after reperfusion, and underperfused myocardium was delineated using Evans blue. The excised heart was sliced immediately as described above. Because TUNEL-positive cardio-

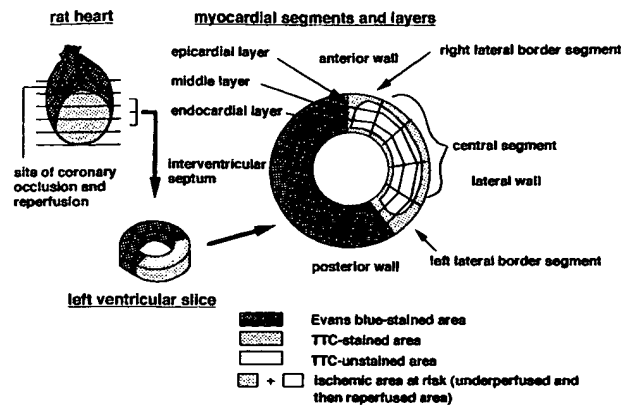


Figure 1. Myocardial segments and layers for assessment of distribution of the infarcted area and TUNEL-positive cardiomyocytes. The three middle slices of the five left ventricular slices of each heart were analyzed for measurements of the infarcted area and TUNEL-positive cardiomyocytes. The entire ischemic area at risk was first divided into five radial segments and then classified into three segments (right lateral border, central three radial segments, and left lateral border segment). The ischemic area at risk (R) was also divided into three myocardial layers (endocardial, middle, and epicardial layers). The measurements of I/R and TUNEL-positive cardiomyocytes were done in the entire ischemic area at risk, as well as in each ischemic portion.

myocytes were found mainly in the lateral border zones and the endocardial side of the ischemic area at risk (as noted in "Results"), we isolated fresh myocardial specimens from these zones and from the core of infarcted zones (mainly corresponding to the zone of the central segment, including middle and epicardial layers in Fig 1) for DNA extraction. Each myocardial specimen weighed ≈ 0.2 mg and was minced in homogenization buffer (10 mmol/L Tris-HCl, 150 mmol/L NaCl, and 10 mmol/L EDTA, pH 8.0) at 0°C and homogenized for 15 seconds at 10 000 rpm using a Polytron homogenizer (Kinematica AG). The homogenate was then treated with 100 μ g/mL proteinase K and 0.1% SDS for 90 minutes at 50°C. The DNA was extracted with phenol and chloroform followed by ethanol precipitation. The pellet was resuspended in TE buffer (10 mmol/L Tris-HCl, pH 8.0, and 1 mmol/L EDTA) and treated with DNase-free RNase (Boehringer-Mannheim) for 2 hours at 37°C. The concentration of DNA was measured through spectrophotometry, and 10 μ g of each DNA sample was then electrophoretically fractionated on a 1.5% agarose gel containing ethidium bromide at a concentration of 0.4 μ g/mL. DNA was visualized with a UV (302 nm) transilluminator, and the gel was photographed with the use of a Polaroid camera.

Statistical Analysis

Data are expressed as mean \pm SEM. To compare group 1 (control ischemia/reperfusion) with group 2 or to compare the two groups of sham-operated rats, an unpaired *t* test was performed. For comparisons

between the positive anti-PMN control and the other groups, one-way ANOVA followed by Fisher's posthoc comparison was carried out. For comparisons in I/R and TUNEL-positive cardiomyocytes among different myocardial portions, two-way ANOVA followed by Fisher's posthoc comparison was carried out. A value of $P < .05$ was considered statistically significant.

Results

Hemograms

White blood cell counts just before death revealed no difference between group 1 ($9502 \pm 351/\mu\text{L}$) and group 2 ($9350 \pm 435/\mu\text{L}$). In anti-PMN-treated rats, white blood cell counts were $956 \pm 132/\mu\text{L}$ ($P < .0001$ versus group 1 and group 2) before coronary occlusion and $1081 \pm 156/\mu\text{L}$ ($P < .0001$ versus group 1 and group 2) just before death. In this positive control group, lymphocytes made up most of the white blood cells ($>99\%$).

Positive Control for the Rat Model of Reperfusion Injury

The ischemic area at risk was $53.0 \pm 2.5\%$ (NS versus group 1 and group 2), and the I/R was $51.0 \pm 1.7\%$ ($P < .05$ versus group 1, NS versus group 2).

Hemodynamics

Although the LVSP did not differ between groups 1 and 2, the LVEDP of group 2 was lower ($P = .04$) than that of group 1 (Table). The positive LV dP/dt of group 2 was greater ($P = .02$) than that of group 1, but the heart rates of the two groups did not differ.

For the sham-operated rats, administration of DMSO or saline resulted in no differences in LVSP/EDP or LV dP/dt value or in the heart rate.

Myocardial Infarct Size and TUNEL-Positive Cardiomyocytes

The ischemic areas at risk of groups 1 and 2 were similar ($53.9 \pm 2.9\%$ in group 1 and $55.4 \pm 3.0\%$ in group 2, NS). In the entire ischemic area at risk, the I/R of group 2 ($52.4 \pm 4.0\%$) was significantly ($P = .02$) smaller than that of group 1 ($66.6 \pm 3.7\%$) (Fig 2, left). The I/Rs of left and right lateral border segments or endocardial and epicardial layers were smaller ($P < .05$, $< .05$, or $P < .05$, $< .01$, respectively) than that of the central segment or that of the middle layer in group 1 (Fig 3). In group 2, the I/Rs of all of three myocardial segments and all of three layers were smaller ($P < .05$, each) than those of group 1.

We confirmed that all nuclei of cardiomyocytes on sections subjected to DNase treatment (as a positive control for the TUNEL

Hemodynamics Before Death

| Group | LVSP/LVEDP, mm Hg | LV dP/dt, mm Hg/s | Heart Rate, bpm |
|----------------------------------|-----------------------------|---|-----------------|
| 1 | $133 \pm 5/9 \pm 1$ | $+4296 \pm 204/-4385 \pm 337$ | 428 ± 18 |
| 2 | $136 \pm 8/5 \pm 1^*$ | $+4907 \pm 129^*/-4715 \pm 227$ | 409 ± 14 |
| PMN-depleted (positive controls) | $126 \pm 1/6 \pm 1$ | $+4716 \pm 143/-4684 \pm 130$ | 410 ± 10 |
| Sham with DMSO | $139 \pm 5/2 \pm 1^\dagger$ | $+5545 \pm 205^\dagger/-5468 \pm 131^\dagger$ | 390 ± 10 |
| Sham with saline | $137 \pm 2/2 \pm 1^\dagger$ | $+5440 \pm 147^\dagger/-5088 \pm 316$ | 398 ± 14 |

* $P < .05$, $^\dagger P < .01$ vs group 1.

In group 2, LVEDP was lower and +LV dP/dt was higher than in group 1.

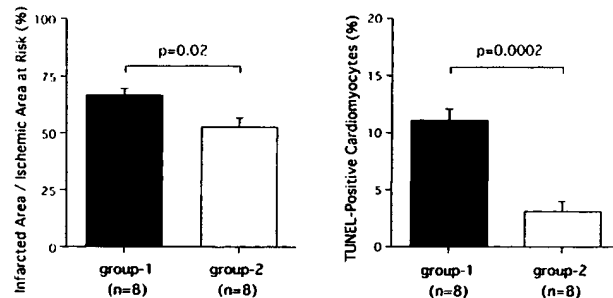


Figure 2. Infarct size and TUNEL-positive cardiomyocytes in the entire underperfused and then reperfused area. Left, I/R. Right, TUNEL-positive cardiomyocytes in the ischemic area at risk. The column representing the infarcted area was lower ($P=0.02$) for group 2 than for group 1. The counts of TUNEL-positive cardiomyocytes in group 2 were lower ($P=.0002$) than in group 1. Group 1, infarcted rats ($n=8$) administered vehicle; group 2, infarcted rats ($n=8$) treated with ZVAD-fmk at a total dose of 3.3 mg/kg.

method) were stained dark brown each time the TUNEL method was performed. The concentration of the TUNEL-positive cardiomyocytes of group 2 ($3.1 \pm 0.9\%$) was significantly ($P=.0002$) less than that of group 1 ($11.1 \pm 1.0\%$) (Fig 2, right). In group 1, TUNEL-positive cardiomyocytes were greater in left and right lateral segments ($P<.05$, $<.01$, respectively) than in the central segment and greater in the endocardial layer ($P<.01$) but smaller in the epicardial layer ($P<.01$) than in the middle layer (Fig 4). In group 2, TUNEL-positive cardiomyocytes of all of three segments ($P<.01$, each) and of endocardial, middle, and epicardial layers ($P<.01$, $<.01$, $<.05$, respectively) were smaller than those of group 1 (Figs 4 and 5). Therefore, there were no significant differences of TUNEL-positive cardiomyocytes in group 2 among the three myocardial segments or three myocardial layers (Fig 4).

Neither TTC-negative zones nor TUNEL-positive cardiomyocytes were detected in the sham-operated rats administered DMSO or saline.

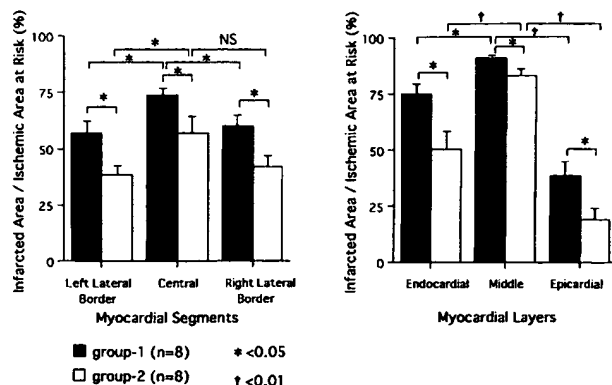


Figure 3. The I/R in myocardial segments or myocardial layers. In group 1, the I/R was smaller in left and right lateral border segments ($P<.05$, respectively) than the central segment (left). Furthermore, in this group, the I/R was smaller in endocardial and epicardial layers ($P<.05$, $<.01$, respectively) than the middle layer (right). In group 2, the I/R of three myocardial segments (left) and of three myocardial layers (right) was smaller than that of the corresponding segments or layers of group 1 ($P<.05$, respectively).

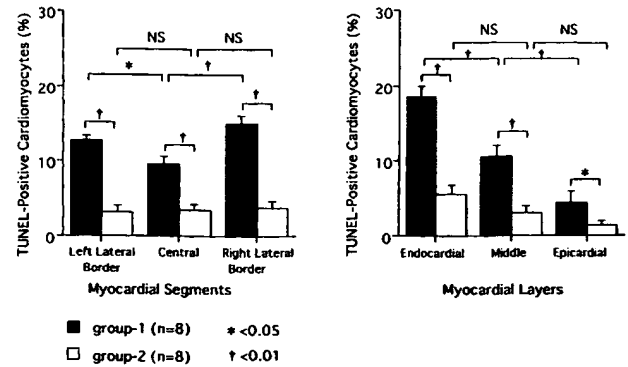


Figure 4. The TUNEL-positive cardiomyocytes in myocardial segments or myocardial layers within the ischemic area at risk. In group 1, TUNEL-positive cardiomyocytes of left and right lateral border segments (left) were greater than that of the central segment ($P<.05$, $<.01$, respectively). In this group, TUNEL-positive cardiomyocytes of the endocardial layer or those of the epicardial layer were greater ($P<.01$) or smaller ($P<.01$) than those of the middle layer, respectively (right). In group 2, TUNEL-positive cardiomyocytes were smaller than those of group 1 in all of three myocardial segments and three myocardial layers ($P<.05$ or $<.01$).

Agarose Gel Electrophoresis

DNA laddering indicative of fragmented DNA was clearly demonstrated in myocardial specimens sampled from the lateral border zones and the endocardial side of the ischemic area at risk in group 1 (lane 4) but was attenuated in group 2 (lane 3), as shown in Fig 6. DNA laddering in the core of infarction was attenuated in group 1 (lane 2) and was absent in group 2 (lane 1).

Discussion

The present study revealed that administration of ZVAD-fmk reduced both the size of the myocardial infarct, as assessed through TTC staining, and the number of TUNEL-positive cardiomyocytes, with significant hemodynamic improvement in vivo in rats that underwent the 30-minute coronary occlusion and 24-hour reperfusion procedure. TUNEL-positive cardiomyocytes appeared to be apoptotic in this study because well-defined (group 1) or attenuated (group 2) DNA laddering on electrophoresis was consistent with a higher or lower value of TUNEL-positive cardiomyocytes, respectively, in the ischemic area at risk of the two groups. In a preliminary study using frozen sections, we confirmed that none of the TUNEL-positive cardiomyocytes were stained with TTC. Therefore, a reduction in their number appeared to contribute to a reduction in the myocardial infarct size. These results suggested that ZVAD-fmk was effective in reducing myocardial reperfusion injury, which could be at least partially attributed to the attenuation of cardiomyocyte apoptosis.

ZVAD-fmk achieved $\approx 21\%$ decrease in the I/R and $\approx 72\%$ decrease in TUNEL-positive cardiomyocytes, as ratios compared with the control ischemia/reperfusion. However, the absolute value for decrease in TTC unstained area ($\approx 14\%$) appeared somewhat greater than that of TUNEL-positive cardiomyocytes ($\approx 8\%$) (Fig 2); we must be careful to simply compare the absolute values of TUNEL-positive cardiomyocytes with the I/R because the methodology for quantification

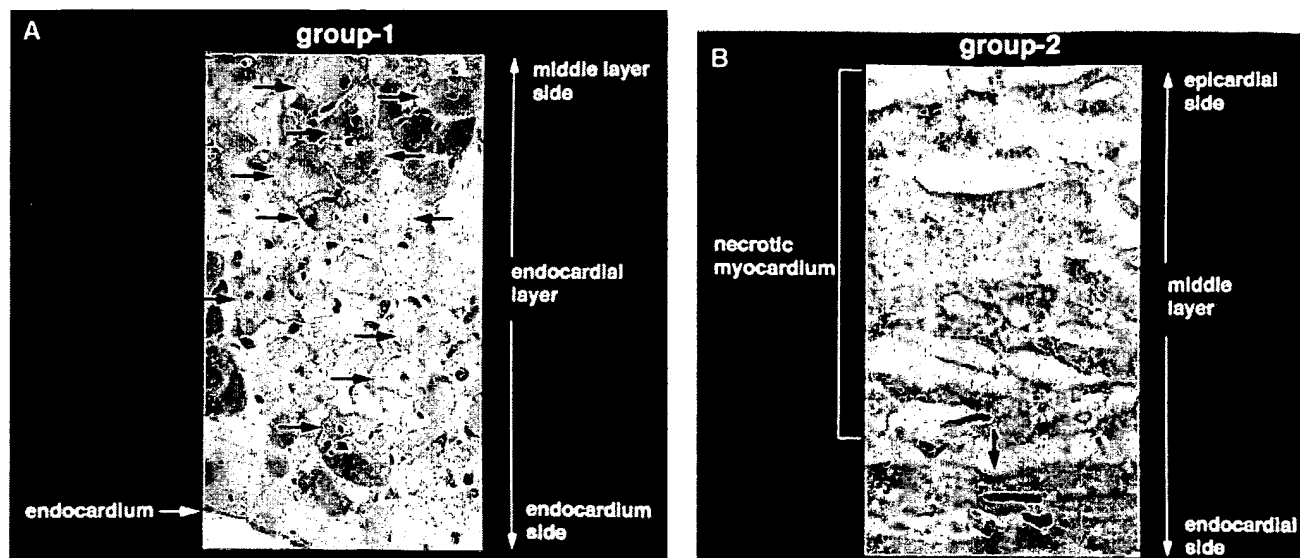


Figure 5. Light microscopic findings on the distribution of TUNEL-positive cardiomyocytes at 24 hours after reperfusion. A, TUNEL-positive cardiomyocytes (arrows) in the endocardial layer of ischemic area at risk on the section from group 1 at a high magnification. B, Possibly necrotic cardiomyocytes (top to middle) and a TUNEL-positive cardiomyocyte (bottom) in the middle layer on the section from group 2. TUNEL-positive cardiomyocytes were frequently detected in the endocardial layer in group 1 (control ischemia/reperfusion) (A). In this group, TUNEL-positive cardiomyocytes were widely spread close to endocardium. In contrast, only a few TUNEL-positive cardiomyocytes were detected mainly in the endocardial side close to the core of infarction in group 2 (ischemia/reperfusion with administration of ZVAD-fmk). The core of infarction consisted of possibly necrotic cardiomyocytes with appearance of disappeared nuclei and degenerated cytoplasm (B). TUNEL-positive cardiomyocytes did not coexist with the mass of these degenerated cardiomyocytes but were present in the surrounding area within central segments or middle layers.

was not the same between TTC staining (histochemical area measurement on myocardial slices) and the TUNEL method (histological cell counting on paraffin sections). Furthermore, we cannot exclude the possibility that ZVAD-fmk interferes

with myocardial necrotic process as well as the apoptotic process.¹⁶⁻¹⁸ Tsujimoto and colleagues^{17,18} recently revealed that ICE inhibitors retarded necrotic cell death as well as apoptotic cell death in their *in vitro* system of chemical hypoxia. The authors speculated that there was possible involvement of common mediators in apoptotic and necrotic signal transductions, although their detailed mechanisms remain to be determined. In the present study, we might have observed effects of ZVAD-fmk on these possible but undetermined common mediators. However, our examination in an *in vivo* system is not suited for approach to signal transductions of these two forms of cell death. The third possibility is the difference in time from initiation of cellular change until elimination between apoptosis and other types of cell death, both forming the infarction. Apoptotic cells are eliminated through phagocytosis in a few minutes in an *in vitro* condition¹⁹ and in a few hours in an *in vivo* condition.²⁰ In contrast, necrotic cardiomyocytes are eliminated much slowly by infiltrating inflammatory cells. Although a turnover of apoptotic cardiomyocytes *in vivo* has not been clarified so far, it may be speculated that the amount of TUNEL-positive cells quantified at a death stage may not equal the total amount of apoptotic cardiomyocytes that appear during a 24-hour reperfusion period.

To date, nothing is known about the fate of cardiomyocytes that have been exposed to ZVAD-fmk but have not undergone a proapoptotic process, such as initiation of apoptotic signal transduction via TNF receptor. These cardiomyocytes may continue to survive or may undergo an early death because of injury already sustained. Myocardial infarct size was assessed only at 24 hours after reperfusion in the present study. Future studies will be needed to evaluate the viability of cardiomyocytes that escape apoptosis through assessment of infarct extension in the later phase of reperfusion.

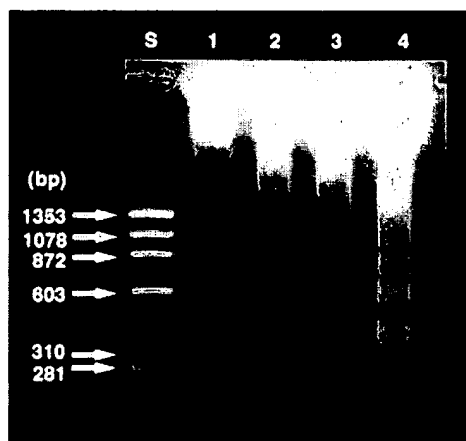


Figure 6. Agarose gel electrophoresis. S indicates size marker (bp). Lane 1, sampled from the core of infarction in myocardium with the same experimental protocol as group 2; lane 2, sampled from the core of infarction in myocardium with the same experimental protocol as group 1; lane 3, sampled from endocardial and lateral border zones of the ischemic area at risk in myocardium with the same experimental protocol as group 2; and lane 4, sampled from endocardial and lateral border zones of the ischemic area at risk in myocardium with the same experimental protocol as group 1. DNA laddering was well defined in the sample from peripheral zone of the ischemic area at risk in control ischemia/reperfusion (lane 4), but DNA ladder formation was attenuated in peripheral zone of the ischemic area at risk in the ZVAD-fmk-treated ischemia/reperfusion (lane 3) or in the core of infarction in control ischemia/reperfusion (lane 2). DNA ladder was not detected in the core of infarction in ZVAD-fmk-treated ischemia/reperfusion (lane 1).

References

1. Fliss H, Gattinger D. Apoptosis in ischemic and reperfused rat myocardium. *Circ Res*. 1996;79:949-956.
2. Ambrosio G, Flaherty JT, Duilio C, Tritto I, Santoro G, Elia PP, Condorelli M, Chiariello M. Oxygen radicals generated at reflow induce peroxidation of membrane lipids in reperfused hearts. *J Clin Invest*. 1991;87:2056-2066.
3. Bolli R, Zughaib M, Li XY, Tang XL, Sun JZ, Triana JF, McCay PB. Recurrent ischemia in the canine heart causes recurrent bursts of free radical production that have a cumulative effect on contractile function: a pathophysiological basis for chronic myocardial 'stunning.' *J Clin Invest*. 1995;96:1066-1084.
4. Kukielka GL, Smith CW, Manning AM, Youker KA, Michael LH, Entman ML. Induction of interleukin-6 synthesis in the myocardium: potential role in postreperfusion inflammatory injury. *Circulation*. 1995;92:1866-1875.
5. Krown KA, Page MT, Nguyen C, Zechner D, Gutierrez V, Comstock KL, Glembotski CC, Quintana PJ, Sabbadini RA. Tumor necrosis factor alpha-induced apoptosis in cardiac myocytes: involvement of the sphingolipid signaling cascade in cardiac cell death. *J Clin Invest*. 1996;98:2854-2865.
6. Gottlieb RA, Gruol DL, Zhu JY, Engler RL. Preconditioning rabbit cardiomyocytes: role of pH, vacuolar proton ATPase, and apoptosis. *J Clin Invest*. 1996;97:2391-2398.
7. Przyklenk K, Zhao L, Kloner RA, Elliott GT. Cardioprotection with ischemic preconditioning and MLA: role of adenosine-regulating enzymes? *Am J Physiol*. 1996;271:H1004-1014.
8. Wolfson RG, Patel VC, Neild GH, Yellon DM. Inhibition of nitric oxide synthesis reduces infarct size by an adenosine-dependent mechanism. *Circulation*. 1995;91:1545-1551.
9. Yao Z, Gross GJ. A comparison of adenosine-induced cardioprotection and ischemic preconditioning in dogs: efficacy, time course, and role of KATP channels. *Circulation*. 1994;89:1229-1236.
10. Homeister JW, Hoff PT, Fletcher DD, Lucchesi BR. Combined adenosine and lidocaine administration limits myocardial reperfusion injury. *Circulation*. 1990;82:595-608.
11. Tatsuta T, Cheng J, Mountz JD. Intracellular IL-1 beta is an inhibitor of Fas-mediated apoptosis. *J Immunol*. 1996;157:3949-3957.
12. Romson JL, Hook BG, Kunkel SL, Abrams GD, Schork MA, Lucchesi BR. Reduction of the extent of ischemic myocardial injury by neutrophil depletion in the dog. *Circulation*. 1983;67:1016-1023.
13. Vivaldi MT, Kloner RA, Schoen FJ. Triphenyltetrazolium staining of irreversible ischemic injury following coronary occlusion in rats. *Am J Pathol*. 1985;121:522-530.
14. Weibel ER. Principles and methods for the morphometric study of the lung and other organs. *Lab Invest*. 1963;12:131-155.
15. Gavrieli Y, Sherman Y, Ben-Sasson SA. Identification of programmed cell death in situ via specific labeling of nuclear DNA fragmentation. *J Cell Biol*. 1992;119:493-501.
16. Shimizu S, Eguchi Y, Kamiike W, Waguri S, Uchiyama Y, Matsuda H, Tsujimoto Y. Bcl-2 expression prevents activation of the ICE protease cascade. *Oncogene*. 1996;12:2251-2257.
17. Shimizu S, Eguchi Y, Kamiike W, Waguri S, Uchiyama Y, Matsuda H, Tsujimoto Y. Retardation of chemical hypoxia-induced necrotic cell death by Bcl-2 and ICE inhibitors: possible involvement of common mediators in apoptotic and necrotic signal transductions. *Oncogene*. 1996;12:2045-2050.
18. Shimizu S, Eguchi Y, Kamiike W, Waguri S, Uchiyama Y, Matsuda H, Tsujimoto Y. Bcl-2 blocks loss of mitochondrial membrane potential while ICE inhibitors act at a different step during inhibition of death induced by respiratory chain inhibitors. *Oncogene*. 1996;13:21-29.
19. Russell SW, Rosenau W, Lee JC. Cytolysis induced by human lymphotoxin. *Am J Pathol*. 1972;69:103-111.
20. Perlman H, Maillard L, Krasinski K, Walsh K. Evidence for the rapid onset of apoptosis in medial smooth muscle cells after balloon injury. *Circulation*. 1997;95:981-987.



J Mol Cell Cardiol 34, 165–174 (2002)

doi:10.1006/jmcc.2001.1498, available online at <http://www.idealibrary.com> on IDEAL®

Apoptosis and Post-infarction Left Ventricular Remodeling

Alfonso Baldi^{1*}, Antonio Abbate^{2*}, Rossana Bussani³, Giuseppe Patti², Rosetta Melfi², Anna Angelini¹, Aldo Dobrina², Raffaele Rossiello¹, Furio Silvestri³, Feliciano Baldi¹ and Germano Di Sciascio²

¹Department of Biochemistry and Biophysics, "E. Cedrangolo", Section of Pathologic Anatomy, Second University of Naples, Naples, Italy, ²Department of Cardiovascular Sciences, University Campus Bio-Medico, Rome, Italy and ³Department of Pathologic Anatomy, University of Trieste, Trieste, Italy

(Received 7 August 2001, accepted for publication 31 October 2001)

A. BALDI, A. ABBATE, R. BUSSANI, G. PATTI, R. MELFI, A. ANGELINI, A. DOBRINA, R. ROSSIELLO, F. SILVESTRI, F. BALDI AND G. DI SCIASCIO. Apoptosis and Post-infarction Left Ventricular Remodeling. *Journal of Molecular and Cellular Cardiology* (2002) 34, 165–174. Apoptosis is a common pathological feature in acute myocardial infarction (AMI), however, its role in the later phases (>10 days) of AMI and in post-infarction left ventricular remodeling has not been characterized. The aim of the study was to identify signs of ongoing cell apoptosis late post AMI. Sixteen hearts were collected at autopsy from subjects 12 to 62 days after the onset of AMI. *In situ* end-labeling of DNA fragmentation (TUNEL) and co-staining with caspase-3 were performed. Double-positive cells were defined as apoptotic and the apoptotic rate was calculated. Values are expressed as median and interquartile range. Co-stainings with muscle-actin, splicing factor (SC35), PCNA, *bax* and *bcl-2* were also performed. Apoptotic rates at site of infarction [25.4% (17.0–28.4%)] were significantly higher v those at remote regions [0.7% (0.5–0.8%); $P < 0.001$] and significantly correlated to left ventricular longitudinal and transverse diameters [$r = +0.70$ ($P = 0.016$) and $r = +0.63$ ($P = 0.004$) respectively]. Moreover, in subjects with persistently occluded infarct-related artery (14 cases) there was a significantly higher apoptotic rate at the site of infarction compared to those (2 cases) with patent artery [26.0% (21.9–28.5%) v 4.5% (0.6% and 8.4%); $P = 0.033$]. A significantly greater *bax* immuno-reactivity close to the infarction v remote areas was found ($P < 0.001$). High grade apoptosis is present at sites of infarction in the later phases post AMI. This is more evident if the infarct-related artery is persistently occluded and signs of ventricular remodeling are present. These data may provide an explanation of progressive late left ventricular dysfunction.

© 2002 Elsevier Science Ltd.

KEY WORDS: Apoptosis; Myocardial infarction; Remodeling; Caspase-3; *bax*; *bcl2*.

Introduction

Apoptosis, or programmed cell death, is an energy-requiring and highly regulated process involved in development, homeostasis and senescence. Apoptosis is triggered by the activation of intracellular signalling pathways associated with the condensation of chromatin into crescentic caps of nuclear DNA at the periphery. Apoptotic cells then undergo extracellular degeneration or phagocytosis

by macrophages without eliciting an inflammatory reaction.¹ It is acknowledged that apoptosis contributes both to homeostasis and human diseases. As such, it has been recognized as a key process in the adaptations of the cardiovascular system to its continuously changing demands.^{2,3} Recently, it has been implicated as a fundamental pathogenetic mechanism in a variety of diseases including acute myocardial infarction (AMI), and post-ischemic and idiopathic dilated cardiopathy.^{4–10} New techniques,

*The first two authors contributed equally to the realization of this manuscript.

Please address all correspondence to: Dr Alfonso Baldi, Via G. Orsi, 25, 80128 Naples, Italy. Fax: +39-081-5569693. E-mail: alfonsobaldi@tiscali.net

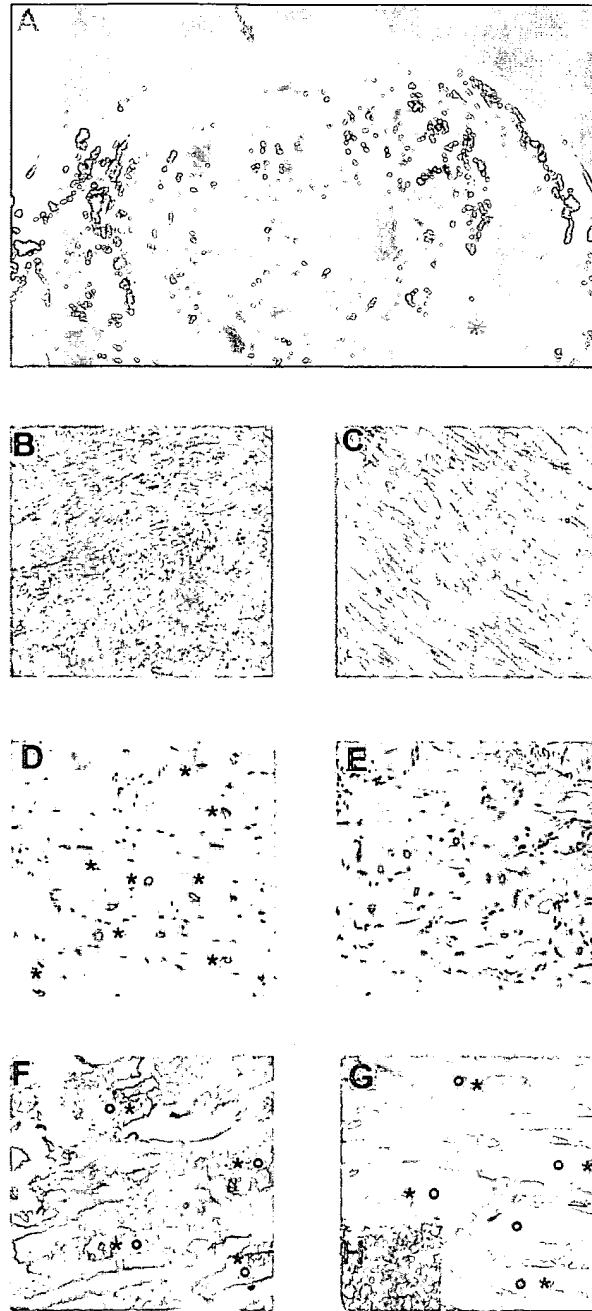


Figure 1 (A) Sampling of the different specimens, at a site of recent infarction (arrow) and at sites remote from it (*), in an examined heart collected from a 82-year old subject with a history of anterior and septal AMI (15 days earlier). AMI, Acute myocardial infarction. (B) Hematoxylin/Van Gieson. Site of recent infarction: reparative fibrosis, newly sprouted vessels and granulation tissue (original magnification $\times 500$). (C) Hematoxylin/Van Gieson. Region remote from the infarcted area (original magnification $\times 500$). (D) TUNEL staining. Region of the left ventricle at the site of infarction: several TUNEL-positive cells are shown (*) (original magnification $\times 500$; lightly counterstained with hematoxylin). (E) TUNEL staining. Region of the left ventricle remote from the infarcted area: no TUNEL-positive cells are detected (original magnification $\times 500$; lightly counterstained with hematoxylin). (F) Double staining: nuclear staining for TUNEL (*) and cytoplasmic staining for muscle-actin (O). TUNEL-positive cells co-express muscle-actin (original magnification $\times 600$; AEC, lightly counterstained with hematoxylin). (G) Double staining: nuclear staining for TUNEL (*) and cytoplasmic staining for Caspase-3 (O). Great majority of TUNEL-positive cells co-express caspase-

especially the *in situ* end-labeling of DNA fragmentation (TUNEL), have enabled an easy qualitative and quantitative evaluation of apoptosis in tissues and proposed a re-interpretation of previously acquired concepts.⁴⁻¹¹ In particular, in AMI a greater incidence of apoptosis v necrosis has been reported in experimental models⁵ and confirmed in humans,^{6,10} with a particular localization at the borders of infarction. However, the incidence of apoptosis in the later phase post AMI (up to 60 days) in humans and its role in determining post-infarction left ventricular (LV) remodeling have not been characterized to date. The primary goal of our study was to evaluate ongoing myocardiocyte apoptosis in these phases and the secondary objective was to investigate its correlation with signs of LV remodeling and infarct-related artery (IRA) patency. To this aim, pathological examination of human hearts late post AMI was performed using TUNEL combined with additional stainings for muscle actin and for markers of cell death mediators (caspase-3, *bax* and *bcl-2*), DNA synthesis (PCNA) and transcription activity (RNA splicing factor SC-35).

Materials and Methods

Selection of the samples

Sixteen hearts were collected at autopsy (University of Trieste and Second University of Naples, Italy) from subjects who died 12 to 62 days after the onset of MI, median interval 23 days. All subjects were hospitalized before death, and none of them suffered from a re-infarction, as indicated by clinical data and serial CK and CK-MB determination. The cause of death was trauma in 4 cases while congestive heart failure and comorbidities were present in the rest. Features of cardiogenic shock or prolonged i.v. inotropic support were not described in the clinical charts. Clinical and demographic characteristics of the subjects are shown in Table 1.

Pathological examination

Autopsy was performed within 30 hours after death in all cases. Gross examination of the hearts was

Table 1 Clinical and demographic characteristics

| | |
|------------------------------|----------|
| Number of subjects | 16 |
| Median age (years) | 73 |
| Range | (60-96) |
| Male sex | 12 (75%) |
| Recent AMI | 16 |
| (≤ 2 months) | (100%) |
| Median time post AMI (days) | 23 |
| Range | (12-62) |
| Previous old AMI | 8 |
| (>6 months) | (50%) |
| Left ventricular dysfunction | 13 |
| (LVEF <45%) | (81%) |

AMI, acute myocardial infarction; LVEF, Left ventricular ejection fraction.

performed to measure LV parameters and to define the infarcted area and the IRA. LV transverse and longitudinal diameters were measured at the atrio-ventricular section. The LV free wall thickness was measured at the median third of the posterior wall. Tissue specimens (125-1000 mm³) were obtained at sites of myocardial infarction and in regions of the left ventricle remote from the infarcted area supplied by a patent coronary artery [Figure 1(A)]. Specimens were fixed in 10% paraformaldehyde in 0.1 M buffer. Different sections were processed for each specimen. Morphologic analysis of tissue structure, cellular and nuclear integrity and inflammatory infiltrates was performed by light-microscopy after dehydration, embedding in paraffin and staining.

TUNEL assay

TUNEL reaction was performed using the peroxidase-based Apoptag kit (Oncor, Gaithersburg, MD, USA). TUNEL positive cells were detected with diaminobenzidine and H₂O₂ according to the supplier's instructions. Moreover, in order to optimize the procedure, we applied the modifications to the protocol suggested by Saraste.¹² The experiment was repeated on different sections for each specimen (two to four). One hundred random fields ($\times 250$) per section were analyzed (12.5 mm²).

Immunocytochemistry

Several series of TUNEL-stained sections, as well as consecutive deparaffinized and dried sections were

3. (original magnification $\times 600$; AEC, lightly counterstained with hematoxylin). (H) Caspase-3 immunohistochemical staining of human lymph nodes as a positive control. Strong immunoreactivity for activated caspase-3 in the apoptotic-prone germinal center B-lymphocytes of a lymph node is clearly visible (original magnification $\times 500$; AEC, lightly counterstained with hematoxylin).

subsequently stained for different markers. All the sections were heated in a microwave oven twice for 5 min at 700 W in citrate buffer (pH 6), then incubated with antibodies against muscle actin (mouse monoclonal anti-human actin HHH35 from DAKO, CA, USA; dilution 1:50), caspase-3 (rabbit polyclonal anti-human caspase-3 from Upstate Biotechnology, NY, USA; dilution 1:100), PCNA (mouse monoclonal anti-human PCNA PC10 from DAKO; dilution 1:100) and splicing factor (mouse monoclonal anti-splicing factor SC-35 from Sigma, Milan, Italy; dilution 1:200), and visualized by the streptavidin-biotin system (DAKO), using either 3-amino-9-ethylcarbazide (AEC) or diaminobenzidine (DAB) as the final chromogen. The optimal working dilutions were defined on the basis of titration experiments. Negative controls for each tissue section were prepared by leaving out the primary antibodies, which resulted in a complete disappearance of the nuclear staining for the antibodies used, indicating the non-interference of TUNEL with the secondary antibodies. Immunoreactivity (positive/negative) for each staining coincided between pairs of identical nuclei of myocytes on mirror sections. Positive controls were run with each set of slides. Immunocytochemistry for *bax* protein and *bcl-2* were also performed using specific antibodies (mouse monoclonal anti-human *bax* sc-7480 and mouse monoclonal anti-human *bcl-2* sc-7382 from Santa Cruz, CA, USA; at a dilution 1:100). Immunoreactivity for these two antigens was quantitated as percentage of positive cells per field ($\times 250$).

Apoptotic rate

Myocardiocytes were defined as apoptotic if colocalization of markers of DNA fragmentation (TUNEL) and cell death effectors (caspase-3) was evident. The apoptotic rate (AR), expressed as a ratio of number of myocardiocytes co-expressing TUNEL and caspase-3 positivity on nucleated cells per field ($\times 250$) at light microscopy, was calculated and compared in different specimens by two separate observers (A.B. and A.A.) in a double blind fashion. Consensus on the percentage of TUNEL positive cells was reached in all cases.

Statistical analysis

For statistical analysis, the software SPSS 10.0 for Windows (SPSS, Chicago, IL, USA) was used.

Table 2 Gross pathology characteristics

| | |
|--|-------------|
| Weight (g) median | 540 |
| Interquartile range | (480–565) |
| Transverse diameter (mm) median | 128 |
| Interquartile range | (124–139) |
| Longitudinal diameter (mm) median | 104 |
| Interquartile range | (102–110) |
| LV posterior wall thickness (mm) median | 15 |
| Interquartile range | (12–16) |
| Previous old AMI (>6 months) | 8 (50%) |
| Significant multivessel coronary disease | 8 (50%) |
| Persistently occluded IRA | 14 (88%) |

AMI, acute myocardial infarction; IRA, infarct-related artery; LV, left ventricle.

Quantitative results were expressed as median and interquartile range. Non-parametric tests were used to compare AR among different regions of each subject (Wilcoxon test for paired data) and among different subjects (*U* Mann–Whitney for non-paired data). Correlation between variables was determined by Spearman rank test, *r* values represent correlation coefficients. *P* values ≤ 0.05 were considered significant.

Results

Gross pathology and light-microscopy examination

Table 2 summarizes the gross pathology characteristics of the hearts. Median transverse and vertical diameters were 128 mm and 104 mm respectively. Posterior wall thickness was 15 mm. In six cases of posterior AMI those values were not included for further analysis. In fourteen cases (88%) an occluded IRA was found, while in the remaining two cases (12%) the IRA was found to be patent.

Areas of scarring consistent with previous necrotic cell death were demonstrable in the infarcted area. At light-microscopy signs suggestive of ongoing necrosis (i.e. nuclear or cytoplasmic abnormalities, evidence of cell rupture) were absent in all examined sections while reparative fibrosis and newly sprouted capillaries were present, and typical post-infarction granulation tissue was evident [Fig. 1(B)]. Muscle damage was not present in specimens derived from the same subjects at areas remote from the infarction [Fig. 1(C)]. These areas

Table 3 Correlation between TUNEL staining and Caspase-3, SC-35 and PCNA. (Median value and interquartile range)

| | |
|----------------------------|-------------------|
| TUNEL+ cells (%) | 30 (20–34) |
| Caspase-3+ (%) | 85 (83–88) |
| SC35+ (%) | 10 (4–12) |
| PCNA+ (%) | 0.7 (0.01–1.1) |
| Caspase-, SC35-, PCNA- (%) | 5 (2–12) |

appeared normal at gross anatomy and light-microscopy and a patent related coronary was identified.

TUNEL assay and immunocytochemistry for caspase-3, PCNA and SC-35

TUNEL assay in myocardial specimens collected at the site of infarction showed a high rate of positive cells in all examined fields [Fig. 1(D)], while in regions remote from the infarcted area TUNEL positive cells were rare [Fig. 1(E)]. Light-microscopy examination of consecutive sections from the specimens with immunocytochemistry was performed for muscle actin. The great majority of TUNEL positive cells co-stained was for muscle actin, thus showing to be myocardiocytes [Fig. 1(F)]. Interstitial and inflammatory cells were not included in the cell count.

Table 3 summarizes data showing correlation between TUNEL staining and immunocytochemistry for caspase-3, PCNA and SC-35. A high percentage of the TUNEL positive cells [median 85% (83–88%)] were overexpressing caspase-3 [Fig. 1(G)]. About 5% of caspase-3 expressing cells did not show positivity at TUNEL, and were not considered apoptotic. Non-apoptotic myocardiocytes at the site of infarction, as well as in regions remote from the infarction, were mostly negative for caspase-3 or contained only weak immunoreactivity. Staining of a lymph node is shown as a control for the specificity of the immunohistochemical reaction for the activated caspase-3. The typical strong immunoreactivity for activated caspase-3 in the apoptosis-prone germinal center B-lymphocytes is clearly visible [Fig. 1(H)].

TUNEL-positive myocardiocytes were mostly negative for PCNA and SC-35 immunocytochemistry [Figures 2(A) and 2(B); Table 3]. None of the myocardiocytes (0%) which expressed co-localization of TUNEL and caspase-3 were positive for PCNA or SC-35.

Apoptotic rate

The rate of apoptotic myocardiocytes was significantly higher at sites of infarction [25.4% (17.0–28.4%)] v remote regions [0.7% (0.5–0.8%), $P < 0.001$] [Fig. 3(A)]. In two hearts of subjects with patent IRA the AR was significantly lower (0.6% and 8.4%) compared to those with a persistently occluded IRA [26.0% (21.9–28.5%), $P = 0.033$] [Fig. 3(B)]. Moreover, the AR at the site of infarction was found to be positively correlated to signs of LV remodeling, LV longitudinal ($r = +0.70$, $P = 0.016$) [Fig. 3(C)] and transverse diameter ($r = +0.63$, $P = 0.004$) [Fig. 3(D)]. Not considering data from six subjects who had posterior wall infarctions, AR remote from infarction showed a mild correlation with the LV posterior wall thickness ($r = -0.64$, $P = 0.06$) [Fig. 3(E)].

AR in hearts of subjects with a traumatic death (four cases, 25%; AR 27.2%) was similar to the AR in the others (12 cases, 75%; AR 25.2%; $P = 0.8$). No statistically significant difference was found comparing AR in those patients who died within 23 days after AMI (median value) v the others (27.3% v 25.4%; $P = 0.85$).

Immunocytochemistry for *bax* and *bcl-2*

Bax protein expression within the myocardium showed a similar localization of TUNEL with a significantly higher number of myocardiocytes expressing intense *bax* immunoreactivity in the cytoplasm at site of infarction [52.2% (34.3–58.0%)] v remote area [2.5% (0.7–3.4%), $P < 0.001$] [Fig. 2(C)]. In Figure 2(D) a control for *bax* immunoreactivity on a lymph node is shown. Most cells within the germinal center of the lymph node were positive for *bax* expression, while the majority of cells within the interfollicular zone were negative.

Compared to *bax* expression *bcl-2* appeared only slightly overexpressed in the infarcted site [2.1% (1.4–4%)] v the remote site [0.5% (0.2–1.0%), $P = 0.16$] [Fig. 2(E)].

Discussion

To the best of our knowledge, this is the first report in humans of persisting myocardiocyte death due to apoptosis late post AMI. Necrosis is known to cause an important loss of myocardiocytes, with attendant ventricular dysfunction and heart failure post AMI. Previous studies indicate that myocardial

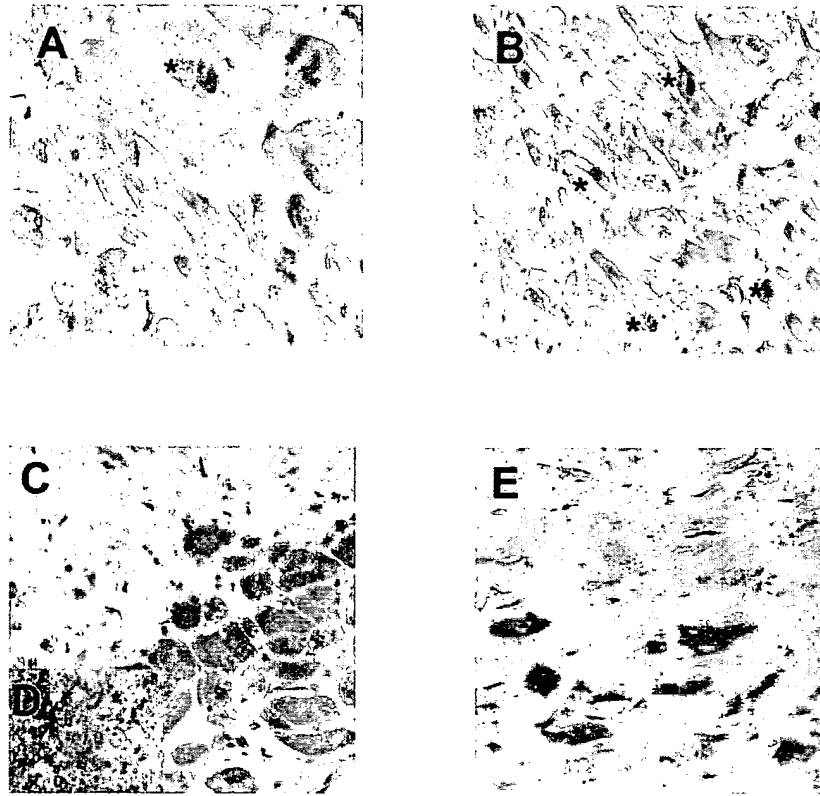


Figure 2 (A) Double staining for TUNEL and PCNA. Rare TUNEL-positive cells express PCNA. A double-positive cell is shown (*) (original magnification $\times 500$; AEC, lightly counterstained with hematoxylin). (B) Double staining for TUNEL and SC-35. A small portion of TUNEL-positive cells express SC-35. Double-positive cells are shown (*) (original magnification $\times 500$; AEC, lightly counterstained with hematoxylin). (C) Dark-brown positive *Bax* immunoreactivity is evident in the cytoplasm of myocardiocytes close to the infarcted area (original magnification $\times 500$; DAB, lightly counterstained with hematoxylin). (D) Positive control for *bax* immunostaining in the germinal center of a lymph node (original magnification $\times 500$; DAB, lightly counterstained with hematoxylin). (E) A case of *bcl-2* immunohistochemical staining of salvaged tissues surrounding the infarcted areas. Few *bcl-2* positive myocardiocytes close to the infarcted area are detected (original magnification $\times 500$; DAB, lightly counterstained with hematoxylin).

apoptosis may be as important as necrosis in determining myocardiocyte loss in the early phases of AMI.^{5,6,10} In particular, an apoptosis/necrosis ratio close to 30:1 was described in experimental AMI models in rats.⁵ These data were confirmed in humans^{6,10} by the examination of hearts of patients who died within 10 days post AMI, with a preferential localization of apoptotic myocytes at the borders of the infarcted site. A reduction of the apoptotic rate post AMI was described, but no direct observation after the tenth day was reported. In our study a persistent myocardiocyte loss due to apoptosis late post AMI is suggested by the presence of an elevated rate of myocardiocytes positive for TUNEL and caspase-3 immunocytochemistry. Apoptosis appears highly selective for myocardiocytes and localized to the infarcted area. The persistence of viable cells next to apoptotic ones shows the

gradual incidence of the event compared to the abrupt onset observed with necrosis. The absence of ongoing necrosis enhances the specificity of TUNEL examination. However, current opinions regarding the association between apoptosis and necrosis support a possible common feature of cell death beginning as apoptosis and ending as secondary necrosis.^{1,4,13,14}

Apoptosis and post-infarction left ventricular remodeling

The presence of apoptosis late post AMI suggests a possible relation with the progression of LV dysfunction sometimes observed in the later phases post AMI. In fact, an increased AR up to 232-fold in the hearts of patients with end-stage heart failure^{7,8} has been described. Saraste *et al.*⁹ reported

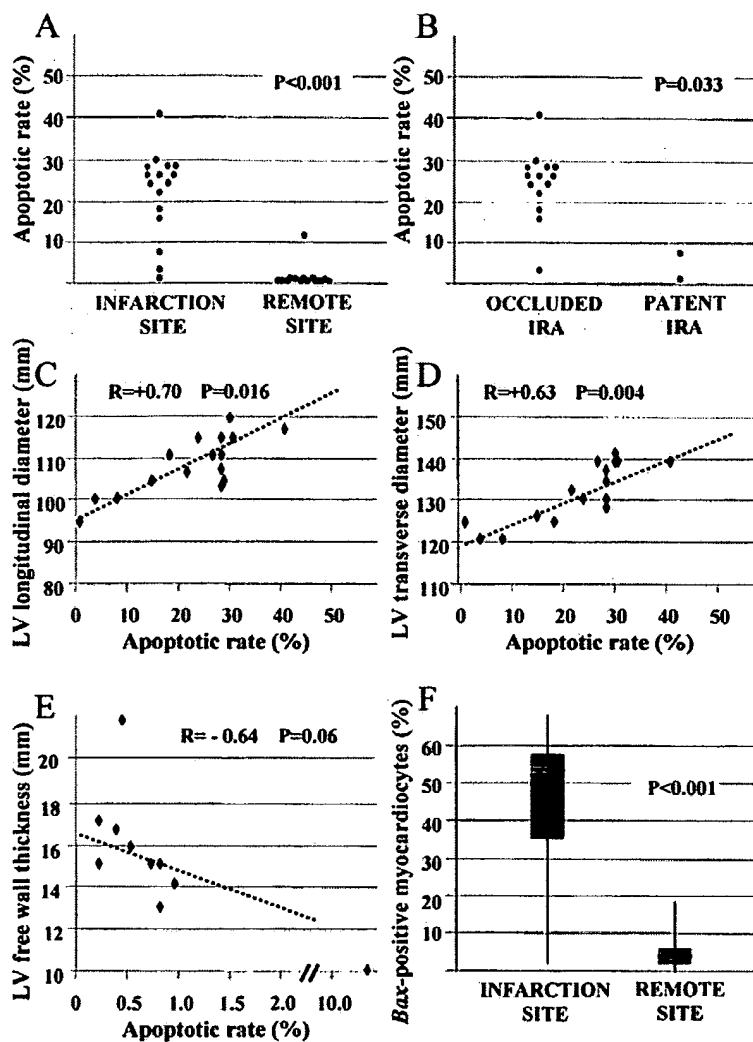


Figure 3 (A) Apoptotic rate at the site of the infarction and at regions remote from it. (B) Significantly lower AR at the site of infarction in two hearts with patent IRA (infarct-related artery) v those hearts with persistently occluded IRA. (C) Correlation between AR at the site of infarction and left ventricular (LV) longitudinal diameter. (D) Correlation between AR at the site of infarction and left ventricular (LV) transverse diameter. (E) Correlation between AR at site remote from the infarction (LV posterior wall) and LV wall thickness. (F) Significantly greater *bax* immuno-reactivity in the cytoplasm of myocardiocytes close to the infarction v remote area. AR, apoptotic rate; IRA, infarct-related artery; LV, left ventricular.

a significantly higher AR vs controls in explanted failing human heart, with a significant correlation between the AR and the severity of clinical manifestations and the rapidity of progression of heart failure in patients with ischemic heart disease. Their data also confirmed a higher AR in proximity of infarcted sites, and the highest value observed (14%) was in a subject with an AMI within the preceding year.⁹ Most of the subjects in our series showed some degree of LV dysfunction before death,

and AR correlated with macroscopic signs of post-infarction LV remodeling (LV dilatation and LV free wall thinning). Similar data were recently described in rats.¹⁵ In regions remote from the infarction an AR of 0.7% was observed, although significantly lower than the AR at the site of AMI, it appears to be substantially greater than the rate described among control samples by others.^{9,10} These data may support a role for apoptosis in regions remote from acute ischemic insult to promote LV re-

modeling in response to increased mechanical stress.¹⁵⁻¹⁷

Moreover, "the open-artery hypothesis", improved LV function in the long term post AMI deriving from a patent IRA¹⁸ – was already formulated in the early 1990s, but the underlying mechanisms were not clear. In our specimens, a patent IRA was associated with a lower AR at the site of infarction. Therefore, the benefit observed with late coronary revascularization could be due to inhibition of apoptosis and prevention of LV remodeling, even if a cause-effect link between persistent IRA occlusion and apoptosis late post AMI cannot be supported by these data. However studies of delayed coronary revascularization have already shown their clinical efficacy, predicting full recovery at site of infarction and overall survival benefits.^{19,20}

Demonstration of apoptosis

Some authors have suggested a lack of specificity of TUNEL on human hearts^{13,21,22} whereas others have strongly supported its accuracy.^{11,12} Kanoh *et al.* described TUNEL-positive myocytes in hearts with dilated cardiomyopathy as living cells with increasing activity of DNA repair rather than apoptotic cells.²¹ While a strict relation between PCNA and TUNEL was present in their data, in our cases most of the TUNEL-positive myocytes were PCNA-negative and therefore could not be considered cells with intense DNA synthesis. On the other hand, while it has been suggested that RNA synthesis and splicing interferes with TUNEL detecting apoptosis,²² TUNEL-positive cells were mostly negative for SC35 in our data. The association of TUNEL and high expression of caspase-3 in over 80% of TUNEL-positive myocytes further supports the definition of apoptosis. As a central mediator of apoptosis in mammalian cells, caspase-3 induces caspase-activated DNase activation which leads to DNA fragmentation and also cleaves cytoskeletal proteins, leading to significant alteration of the cytoskeleton and cell death, even in the absence of DNA fragmentation.^{23,24} The apoptotic activity of caspase depends mostly on post-transcriptional events, however, increases in the mRNA levels have been associated with apoptosis.²⁵ It has been shown that high immunohistochemical expression of caspase-3 is present in cells undergoing apoptosis,²⁶ co-localization of caspase-3 and TUNEL staining has been detected in neurons and myocytes undergoing apoptosis^{23,27} and even

if the antibody used for caspase-3 in our study recognized both the precursor and the p20 subunit, it was recently demonstrated that high caspase-3 immunostaining with this antibody corresponded mostly to increased expression of the activated form of caspase-3.²³ Moreover, *bax* expression appeared substantially higher in infarcted v remote areas, with a high *bax/bcl-2* ratio. *Bax*'s pro-apoptotic activity depends on its ability to form heterodimers with the inhibitor of apoptosis *bcl-2*. The ratio of *bcl-2* to *bax* expression determines survival or death after an apoptotic stimulus^{28,29} and different site-dependent expression of *bcl-2* and *bax* within the heart has been described.³⁰

The AR may appear overestimated. It has been suggested that even a much lower apoptotic rate (<1%) in the hearts of subjects with heart failure would lead to a loss of more than 25% of myocytes during the first year.³¹ Notably, the time required for the *in vivo* formation of apoptotic bodies and their removal has not been determined in the heart, and is currently unknown whether apoptosis persists chronically or if its incidence decreases during the healing process. In our specimens, AR was calculated on a small quantity of myocardium, localized in regions of recent infarction in a definite time frame. In fact, the rate tended to decrease, reaching normal levels (<1%) as the samples were taken further away from the infarcted area and subjects with previous (>6 months) AMI had a much lower apoptotic rate at the infarcted site (A. Baldi and A. Abbate, unpublished data, 2000). Further studies on the dynamics of myocyte apoptosis are necessary to define the impact of calculated AR on effective myocyte loss over time.

Conclusions

Myocardial apoptosis is present late post AMI and may be related to progressive ventricular dysfunction by a cause-effect link. It may therefore be considered part of the cellular and topographic rearrangements (i.e. cell hypertrophy, elongation, side-to-side slippage) in LV remodeling. These data deserve further investigation, discussion and confirmation in appropriate studies targeted to analyze this interesting cause-effect relation. Recent studies raised the possibility of the regeneration of myocytes at the site of infarction in hearts with AMI³² and suggested that the balance between cell death and regeneration may determine whether LV remodeling occurs after AMI. PCNA-positive

myocardiocytes in our samples may indicate regenerating myocardiocytes, with active DNA synthesis, as described by Beltrami *et al.*³² *In vivo* diagnosis of apoptosis appears a promising feature³³ and interestingly, in experimental models, anti-apoptotic therapy (i.e. treatment with ZVAD-fmk,³⁴ a broad caspase inhibitor) reduced infarct size, enzyme leakage and remodeling, thus opening new avenues in the diagnosis and treatment of ischemic heart disease.

Acknowledgements

The authors thank Dr G. Condorelli (Thomas Jefferson University, Philadelphia), Dr S. Miccicci (Regina Elena Cancer Institute, Rome) and Dr L. M. Biasucci (Catholic University of Rome) for their suggestions and critical review of the manuscript, and Mr T. Battista for his skilful technical assistance.

References

- SEARLE J, KERR JFR, BISHOP CH. Necrosis and apoptosis: distinct modes of cell death with fundamentally different significance. *Pathol Annu* 1982; 17: 229–259.
- WATANABE M, CHOUDHRY A, BERLAN M, SINGAL A, SIWIK E, MOHR S, FISHER SA. Developmental remodeling and shortening of the cardiac outflow tract involves myocyte programmed cell death. *Development* 1998; 125: 3809–3820.
- CHENG W, LI B, KAJSTURA J, LI P, WOLIN MS, SONNENBLICK E, HINTZE TH, OLIVETTI G, ANVERSA P. Stretch-induced programmed myocyte cell death. *J Clin Invest* 1995; 96: 2247–2259.
- HAUNSTETTER A, IZUMO S. Apoptosis. Basic mechanisms and implications for cardiovascular disease. *Circ Res* 1998; 82: 1111–1129.
- KAJSTURA J, CHENG W, REISS K, CLARK WA, SONNENBLICK EH, KRAJEWSKI S, REED JC, OLIVETTI G, ANVERSA P. Apoptotic and necrotic myocyte cell deaths are independent contributing variables of infarct size in rats. *Lab Invest* 1996; 74: 86–107.
- VEINOT JP, GATTINGER DA, FLISS H. Early apoptosis in human myocardial infarcts. *Hum Pathol* 1997; 28: 485–492.
- NARULA J, HAIDER N, VIRMANI R, DiSALVO TG, KOLODIE FD, HAJJAR RJ, SCHMIDT U, SEMIGRAN MJ, DEE GW, KHAW BA. Apoptosis in myocytes in end-stage heart failure. *N Engl J Med* 1996; 335: 1182–1189.
- OLIVETTI G, ABBI R, QUAINI F, KAJSTURA J, CHENG W, NITAHARA JA, QUAINI E, Di LORETO C, BELTRAMI CA, KRAJEWSKI S, REED JC, ANVERSA P. Apoptosis in the failing human heart. *N Engl J Med* 1997; 336: 1131–1141.
- SARASTE A, PULKKI K, KALLAJOKI M, HEIKKILA P, LAINE P, MATTILA S, NEIMINEN NS, PARVINEN M, VOIPIO-PULKKI LM. Cardiomyocyte apoptosis and progression of heart failure to transplantation. *Eur J Clin Invest* 1999; 29: 380–386.
- OLIVETTI G, QUAINI F, SALA R, LAGRASTA C, CORRADI D, BONACINA E, GAMBERT SR, CIGOLA E, ANVERSA P. Acute myocardial infarction in humans is associated with activation of programmed myocyte cell death in the surviving portion of the heart. *J Mol Cell Cardiol* 1996; 28: 2005–2016.
- JAMES TN. Homage to James B Herrick: a contemporary look at myocardial infarction and sickle-cell heart disease, the 32nd Annual Herrick lecture of the council of Clinical Cardiology of the American heart Association. *Circulation* 2000; 101: 1874–1887.
- SARASTE A. Morphologic criteria and detection of apoptosis. *Herz* 1999; 24: 189–195.
- OHNO M, TAKEMURA G, OHNO A, MISAO J, HAYAKAWA Y, MINATOGUCHI S, FUJIWARA T, FUJIWARA H. "Apoptotic" myocytes in infarct area in rabbit hearts may be oncotic myocytes with DNA fragmentation. *Circulation* 1998; 98: 1422–1430.
- BUJA LM, ENTMAN M. Modes of myocardial cell injury and cell death in ischemic heart disease. *Circulation* 1998; 98: 1355–1357.
- PALJOJOKI E, SARASTE A, ERIKSSON A, PULKKI K, KALLAJOKI M, VOIPIO-PULKKI LM, TIKKANEN I. Cardiomyocyte apoptosis and ventricular remodeling after myocardial infarction in rats. *Am J Physiol – Heart Circ Physiol* 2001; 280: H2726–H2730.
- SAM F, SAWYER DB, CHANG DL, EBERLI FR, NGOY S, JAIN M, AMIN J, APSTEIN CS, COLUCCI WS. Progressive left ventricular remodeling and apoptosis late after myocardial infarction in mouse heart. *Am J Physiol – Heart Circ Physiol* 2000; 279: H422–H428.
- CONDORELLI G, MORISCO C, STASSI G, NOTTE A, FARINA F, SGARAMELLA G, DE RIENZO A, RONCARATI R, TRIMARCO B, LEMBO G. Increased cardiomyocyte apoptosis and changes in proapoptotic and antiapoptotic genes bax and bcl-2 during left ventricular adaptations to chronic pressure overload in the rat. *Circulation* 1999; 99: 3071–3078.
- KIM CB, BRAUNWALD E. Potential benefits of late reperfusion of infarcted myocardium: the open artery hypothesis. *Circulation* 1993; 88: 2426–2436.
- PIZZETTI G, BELOTTI G, MARGONATO A, CAPPELLETTI A, CHIERCHIA SL. Coronary recanalization by elective angioplasty prevents ventricular dilation after anterior myocardial infarction. *J Am Coll Cardiol* 1996; 28: 837–845.
- LANCELLOTTI P, ALBERT A, BERTHE C, PIERARD LA. Full recovery of contraction late after acute myocardial infarction: determinants and early predictors. *Heart* 2001; 85: 521–526.
- KANOH M, TAKEMURA G, MISAO J, HAYAKAWA Y, AOYAMA T, NISHIGAKY K, NODA T, FUJIWARA T, FUKUDA K, MINATOGUCHI S, FUJIWARA H. Significance of myocytes with positive DNA *in situ* nick end-labeling (TUNEL) in hearts with dilated cardiomyopathy. No apoptosis but DNA repair. *Circulation* 1999; 99: 2757–2764.
- KOCKX MM, MUHRING J, KNAAPEN MW, DE MEYER G. RNA synthesis and splicing interferes with DNA *in situ* end labeling techniques used to detect apoptosis. *Am J Pathol* 1998; 152: 885–888.

23. NAKAJIMA W, ISHIDA A, LANGE MS, GABRIELSON KL, WILSON MA, MARTIN LJ, BLUE ME, JOHNSTON MV. Apoptosis has a prolonged role in the neurodegeneration after hypoxic ischemia in the newborn rat. *J Neurosci* 2000; 20: 7994–8004.
24. SAKAHIRA H, ENARI M, NAGATA S. Cleavage of CAD inhibitor in CAD activation and DNA degradation during apoptosis. *Nature* 1998; 391: 96–99.
25. KONDO S, BARNA BP, MORIMURA T, TAKEUCHI J, YUAN J, AKBASAK A, BARNETT GH. Interleukin-1 β -converting enzyme mediates cisplatin-induced apoptosis in malignant glioma cells. *Cancer Res* 1995; 55: 6166–6171.
26. KRAJEWSKA M, WANG HG, KRAJEWSKI S, ZAPATA JM, SHABAIK A, GASCOYNE R, REED JC. Immunohistochemical analysis of *in vivo* patterns of expression of CPP32 (caspase-3), a cell death protease. *Cancer Res* 1997; 57: 1605–1613.
27. BLACK SC, HUANG JQ, REZAIEFAR P, RADINOVIC S, EBERHART A, NICHOLSON DW, RODGER IW. Co-localization of the cysteine protease caspase-3 with apoptotic myocytes after *in vivo* myocardial ischemia and reperfusion in the rat. *J Mol Cell Cardiol* 1998; 30: 733–742.
28. OLTVAI ZN, MILLIMAN CL, KORSMEYER SJ. Bcl-2 heterodimerizes *in vivo* with a conserved homolog, bax, that accelerates programmed cell death. *Cell* 1993; 74: 609–619.
29. HANADA M, AIME-SEMPE C, SATO T, REED JC. Structure–function analysis of bcl-2 protein: identification of conserved domains important for homodimerization with bcl-2 and heterodimerization with bax. *J Biol Chem* 1995; 270: 11962–11969.
30. MISAO J, HAYAKAWA Y, OHNO M, KATO S, FUJIWARA T, FUJIWARA H. Expression of bcl-2 protein, an inhibitor of apoptosis, and bax, an accelerator of apoptosis, in ventricular myocytes of human hearts with myocardial infarction. *Circulation* 1996; 94: 1506–1512.
31. FEUERSTEIN G, RUFFOLO RR, YUE T. Apoptosis and congestive heart failure. *Trends Cardiovas Med* 1997; 7: 249–255.
32. BELTRAMI AP, URBANEK K, KAJSTURA J, YAN SM, FINATO N, BUSSANI R, NADAL-GINARD B, SILVESTRI E, LERI A, BELTRAMI CA, ANVERSA P. Evidence that human cardiac myocytes divide after myocardial infarction. *N Engl J Med* 2001; 344: 1750–1757.
33. HOFSTRA L, LIEM IH, DUMONT EA, BOERSMA HH, VAN HEERDE WL, DOEVENDANS PA, DE MUINCK E, WELLENS HJ, KEMERINK GJ, REUTELINGSPERGER CP, HEIDENDAL GA. Visualisation of cell death *in vivo* in patients with acute myocardial infarction. *Lancet* 2000; 356: 209–212.
34. YAIOTA H, OGAWA K, MACHARA K, MARUYAMA Y. Attenuation of ischemia/reperfusion injury in rats by a caspase inhibitor. *Circulation* 1998; 97: 276–281.

Role of Interleukin-1 in the Pathogenesis of Experimental Shigellosis

Philippe J. Sansonetti,* Josett Arondel,* Jean-Marc Cavaillon,[†] and Michel Huerre[‡]

*Unité de Pathogénie Microbienne Moléculaire, Unité 389 Institut National de la Santé et de la Recherche Médicale

[†]Unité d'Immuno-Allergie, [‡]Unité d'Histopathologie, Institut Pasteur, F-75724 Paris Cédex 15, France

EXHIBIT

48

Abstract

The effect of human recombinant interleukin-1 receptor antagonist on intestinal inflammation, tissue destruction, and bacterial invasion during experimental shigellosis caused by *Shigella flexneri* was studied in the rabbit-ligated loop infection model. Intravenous infusion of the inhibitor at a dose of 2 mg/kg per h, was initiated 30 min before intestinal loops were ligated and infected, and continued during the 8-h period of infection. The animals treated with IL-1 receptor antagonist showed a striking decrease in inflammation, destruction, and bacterial invasion of their tissues, both at the level of the villous intestine and Peyer's patches. This is conclusive evidence that interleukin-1 plays a critical role in the pathogenesis of shigellosis. This proinflammatory cytokine is here proposed as a major trigger of the inflammatory reaction which is characteristic of this invasive disease of the intestine, due to the particular interaction existing between *S. flexneri* and macrophages. (*J. Clin. Invest.* 1995; 96:884-892.) Key words: shigellosis • invasion • inflammation • interleukin-1 • interleukin-1 receptor antagonist

Introduction

Shigellosis is an invasive disease of the human colon, caused by *Shigella*, a gram-negative bacillus of the family enterobacteriaceae. Children in developing areas are the principal victims of this disease which is largely caused, in its endemic form, by *Shigella flexneri*.

The clinical symptoms of shigellosis range from diarrhea to dysentery, characterized by fever, severe intestinal cramps, and emission of stools containing blood, pus, and mucus.

The disease is caused by penetration of invasive shigellae into the colonic and rectal mucosa. Intestinal cells are generally considered the primary target for the pathogen (1). As recently reviewed, in vitro experiments demonstrate that *Shigella* has the capacity to establish efficient intracellular colonization of an epithelial layer by hijacking components of the host cell cytoskeleton both for entry and for cell to cell spread (2).

Address correspondence to Philippe J. Sansonetti, Unité de Pathogénie Microbienne Moléculaire, Institut National de la Santé et de la Recherche Médicale U389, Institut Pasteur, 28 rue du Dr. Roux, F-75724 Paris Cédex 15, France. Phone: 33-1-45-68-83-42; FAX: 33-1-45-68-89-53; E-mail: psanson@pasteur.fr.

Received for publication 22 February 1995 and accepted in revised form 17 April 1995.

J. Clin. Invest.

© The American Society for Clinical Investigation, Inc.

0021-9738/95/08/0884/09 \$2.00

Volume 96, August 1995, 884-892

Mutants unable to enter cells are avirulent in vivo, and those impaired in cell to cell spread express attenuated virulence in a model of dysentery in macaque monkeys (3).

However, several observations indicate that shigellosis is not exclusively characterized by invasion of colonic and rectal epithelial cells. Acute inflammation occurring early after infection (4) by a small bacterial inoculum (5) may not only account for final mucosal destruction, but also, at an early stage, for disruption of the epithelial barrier, thus facilitating bacterial invasion through the basolateral pole of epithelial cells, which appears to be the essential site of entry (6). This has recently been confirmed in vitro, by showing that invasive shigellae inoculated on the apical side of a differentiated monolayer of human colonic T84 cells are unable to invade these cells. On the other hand, they can promote strong transmigration of PMN deposited on the basal side, thus allowing invasion by opening of the paracellular pathway to the bacteria (7). In a model of mucosal invasion in rabbit ligated intestinal loops, pretreatment of animals by infusion of an anti-CD18 monoclonal antibody which blocks immigration of PMN leukocytes into the mucosa, decreases bacterial invasion and prevents tissue destruction (8). Shigellosis therefore resembles an acute inflammatory bowel disease, sharing significant clinical and histopathological similarities with ulcerative colitis.

Based on these data, we have recently started to investigate the pathogenesis of this acute inflammatory process. The macrophage appears to be a key player. In vitro, infected macrophages undergo apoptosis when infected with an invasive isolate of *S. flexneri* (9). IpaB, a 62-kD invasin of this species accounts for induction of programmed cell death (10). The period preceding macrophage apoptosis is characterized by the release of large quantities of IL-1 α precursor and mature IL-1 β (11). A scheme emerges in which bacteria invade the intestinal barrier, essentially through M cells of the dome epithelium covering the lymphoid follicles of the mucosa (8, 12). They are then rapidly translocated to local macrophages, trigger their apoptosis, thus achieving release of significant quantities of IL-1, and triggering a cascade of proinflammatory cytokines. This early inflammatory response is expected to spread from these areas and to destabilize the epithelium, thus facilitating bacterial invasion.

We therefore hypothesized that if IL-1 played a major role at early stages of shigellosis, antagonizing its biological function should have an effect on the development of the disease. This work demonstrates, in a model of mucosal infection of ligated intestinal loops in rabbits, that intravenous infusion of IL-1 receptor antagonist (IL-1ra)¹ starting 30 min before infection and continuing for the duration of the experiment, causes considerable attenuation of the disease symptoms, encompassing alterations in volume and composition of fluid exudate, tissue

1. Abbreviations used in this paper: IBD, inflammatory bowel disease; IL-1ra, IL-1 receptor antagonist; L/W, length/width.

architecture, and bacterial invasion. In as much as this animal model reflects the exact pathogenesis of shigellosis, this work demonstrates that IL-1 is a key player mediating invasion and inflammation of the intestinal mucosa in the course of this disease.

Methods

Bacterial strains and growth conditions. *S. flexneri* strain M90T, a serotype 5 invasive isolate (13), was used throughout these experiments. Bacteria were routinely grown in Tryptic Soy broth (TSB; Difco Laboratories Inc., Detroit, MI). For animal infections, a confluent culture was obtained on TSB medium after overnight growth at 37°C. From these plates, a bacterial suspension was established in saline at a concentration of 10^{10} bacteria/ml.

Rabbit intestinal loop assay. A total of 12 New Zealand White rabbits, weighing 2.5–3.0 kg (Charles River Laboratories, St. Aubin les Elbert, France), was used in these studies. Animals were fasted 24 h before infection and all manipulations were performed under general anaesthesia obtained by intravenous injection of 6% sodium pentobarbital (0.5 ml/kg).

Perfusion of IL-1ra was initiated 30 min before intestinal loop ligation. Briefly, local surgery allowed for exposure of the femoral vein. A catheter was inserted, and IL-1ra (Synergen, Boulder, CO) diluted in hospital-grade saline was perfused at constant flow, with an electric pump, at a concentration of 2 mg/kg per h, for a total of 8 h and 30 min. Control animals were perfused under similar conditions with saline.

Intestinal segments of 10 cm in length were ligated, some of which contained a Peyer's patch. The blood supply was carefully preserved while ligation was performed. In each loop, 0.5 ml of a bacterial suspension containing 10^{10} bacteria/ml was injected. The abdominal cavity was then closed and animals were killed 8 h later. Ligated intestinal loops were dissected. The volume of fluid exudate was aspirated and measured. 1 ml of fluid was immediately frozen for dosage of TNF activity.

Depending on the next step, loops were either filled with 5 ml of a gentamicin solution (50 µg/ml in 0.1 M PBS) for counting of invasive intracellular bacteria, or opened and dissected for histopathological analysis.

In each rabbit, eight loops were ligated, four corresponding to villous intestine and four to Peyer's patches. Therefore a total of 48 blocks of villous intestine and 48 blocks of Peyer's patches were submitted to histopathological analysis.

Bacterial counts in tissue samples. These experiments were performed as recently described (8). As mentioned above, loops used for counting invasive bacteria were treated with a solution of gentamicin. This antibiotic, which penetrates poorly into cells, was used twice to eliminate as many extracellular bacteria as possible. First by replacing the fluid accumulated in the loop, and second by soaking the biopsy samples from these loops into gentamicin solution. Intestinal tissue samples were obtained by punching a disk of 8 mm diameter with a skin biopsy apparatus (Biopsy Punch; Stiefel, Nanterre, France). Extensive washing was performed with 0.1 M PBS to eliminate residual gentamicin, and ice-cold PBS was added to prevent further bacterial growth. Tissue samples were then ground in an Ultra-turrax apparatus (Janke & Kunkel GmbH, Staufen, Germany) in ice-cold PBS. A $\frac{1}{10}$ solution was obtained in TSB and incubated for 30 min at 37°C. Serial dilutions of these suspensions were then plated onto Tryptic Soy agar plates. CFUs were counted and the number of bacteria was calculated for an area of 1 cm² of intestinal mucosa.

Tissue sampling for histopathological analysis, observation, and recording of the results. All tissue samples were immediately fixed in 10% paraformalin, dehydrated, and embedded in historesin (Leica Instruments, Heidelberg, Germany). Sequential sections were taken at different levels of the sample. Thin cuts of 1–2 µm were made and stained with hematoxylin and eosin. Histopathological observations

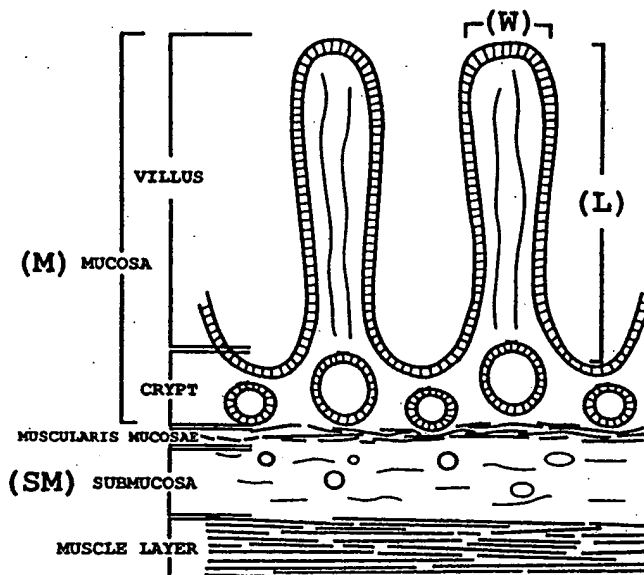


Figure 1. Schematic representation of a histopathological section of rabbit intestinal tissue. The criteria used to establish parameters of mucosal damage are shown.

were carried out as follows. For each sample, either from villous intestine or from Peyer's patches, four thin sections were observed, belonging to different areas of the block. The parameters selected to establish the criteria of villous tissue modification are shown on Fig. 1.

Four criteria were considered: (a) length/width ratio (L/W) of the villi: 40 villi were measured on each thin section, their length and width were recorded, and the ratio calculated; since four thin sections were observed on each block, the mean value was therefore computed on a total of 160 villi; (b) percentage of villi with an ulceration; (c) ratio between thickness of the submucosa and thickness of the submucosa + mucosa (SM/SM + M) of villi, this ratio was calculated, based on measures taken in 10 different areas of each thin section observed. The mean was therefore calculated on 40 ratios for each block; (d) number of PMN leukocytes invading tissues. On each of the 40 intestinal villi examined on thin sections, PMN were counted at two levels as shown on Fig. 1: in the crypt area and in the villus area. Again, the mean was calculated from a total of 160 observations for each block.

For Peyer's patches, only typical histopathological description is given.

IL-1ra bioassay. Serum levels of perfused human IL-1ra were measured at 2 and 8 h after initiation of the perfusion, using the Quantikine IL-1ra Immunoassay kit (Research & Diagnostics Systems, Minneapolis, MN). Similar measures were performed in control animals. In brief, the assay used a quantitative sandwich ELISA in which a monoclonal antibody specific for human IL-1ra was coated onto a microtiter plate. After addition of serum samples, enzyme-linked polyclonal antibody specific for human IL-1ra was added, followed by washing and addition of the substrate. The enzymatic reaction was then stopped and the optical density read on a spectrophotometer. A standard curve was prepared to determine the actual concentration of IL-1ra present in each sample.

TNF bioassay. Fluid aspirated from infected loops were stored frozen for subsequent TNF bioassay. WEHI 164 (clone 13) cells were seeded (3×10^4 cells/well) in 96-well plates and incubated for 24 h at 37°C in 5% CO₂. Supernatants, in six different dilutions, were added to the assay wells, RPMI-1640 was added to negative control wells, and TNF to positive control wells. Incubation was resumed for 20 h at 37°C in 5% CO₂. 125 µg of MTT (3-(4,5-dimethyl-thiazolyl-2-yl)-2,5-diphenyltetrazoliumbromide) in PBS was added to the wells and after 2 h of incubation at 37°C, the test was stopped with 100 µl of extraction

buffer (20% SDS, 50% dimethylformamide in H₂O, 2.5% HCl 1 N, 2.5% of a 80% solution of acetic acid, pH 7.4). After overnight incubation at 37°C, the absorbance was measured at 540 nm, using an automated microELISA autoreader (Dynatech MR4000; Dynatech, Guernsey, United Kingdom). One unit of TNF α activity was defined as the amount required to lyse 50% of WEHI 164 (clone 13) target cells (14).

Results

Control of the titers of serum IL-1ra during the course of infection, with or without perfusion of the antagonist. These controls were carried out at 2 and 8 h of perfusion of 2 mg/kg per h of human recombinant IL-1ra. As expected, very high serum titers of 23,282 \pm 5,649 pg/ml, and 27,757 \pm 1,163 pg/ml were, respectively, observed. Control animals infected with M90T and perfused with saline showed titers \sim 1,000 pg/ml, similar to those of noninfected animals. As the assay is not designed to dosing rabbit IL-1ra, no conclusion can be drawn from these latter values.

Effect of IL-1ra treatment on intestinal inflammation caused by *S. flexneri*. Three major criteria were used to assess the decrease of intestinal inflammation caused by continuous intravenous administration of IL-1ra during mucosal invasion by shigellae.

The volume of mucopurulent and often bloody exudate that constitutes the fluid produced in infected loops, correlates well with intensity of the inflammatory process, as already demonstrated (8). As shown in Fig. 2 A, the average volume of exudate pooled from the eight ligated loops in each rabbit was three times higher in control animals (57.3 \pm 36.4 ml) than in animals treated with IL-1ra (18.0 \pm 9.5 ml).

The amount of TNF present in the mucosal exudate has also been shown to correlate with the intensity of intestinal inflammation caused by *Shigella* invasion (8). As shown in Fig. 2 B, the average quantity of TNF present in the pooled fluid of the eight loops in each control rabbit was 176.408 \times 10³ \pm 16.394 \times 10³ U, as compared to 45.402 \times 10³ \pm 4.043 \times 10³ U in animals treated with IL-1ra, a fourfold difference.

Infiltration of the lamina propria with PMN. Upon observation of histopathological sections of intestinal tissues in control animals, we noticed that PMN were migrating into the connective tissue of the lamina propria and then on to the epithelial layer, by following two routes. One corresponded to PMN extravasating from the small vessels of the submucosa, crossing the muscularis mucosae, infiltrating the lamina propria between the crypts, transmigrating to the crypt lumen, thus causing cryptitis, and also migrating higher in the axis of the villus. Another route consisted in PMN extravasating from the blood capillaries present in the villus axis, directly invading the lamina propria of the villus, and proceeding to the basal side of the epithelial layer before transmigrating to the intestinal lumen, or destroying the basement membrane, thus causing detachment of the epithelium from the villus.

Based on this observation, PMN were counted in these two "compartments," crypt and villus axis. Results are shown in Fig. 3 A as the average number of PMN per one villus. Numeration of PMN in the tissue of control animals was underevaluated because, in some cases, infiltrates were so dense that the actual number could not be counted. In the lamina propria of the crypts, an average number of 14.8 \pm 6.7 PMN was observed in the control animals, whereas only 1.8 \pm 0.68 PMN were ob-

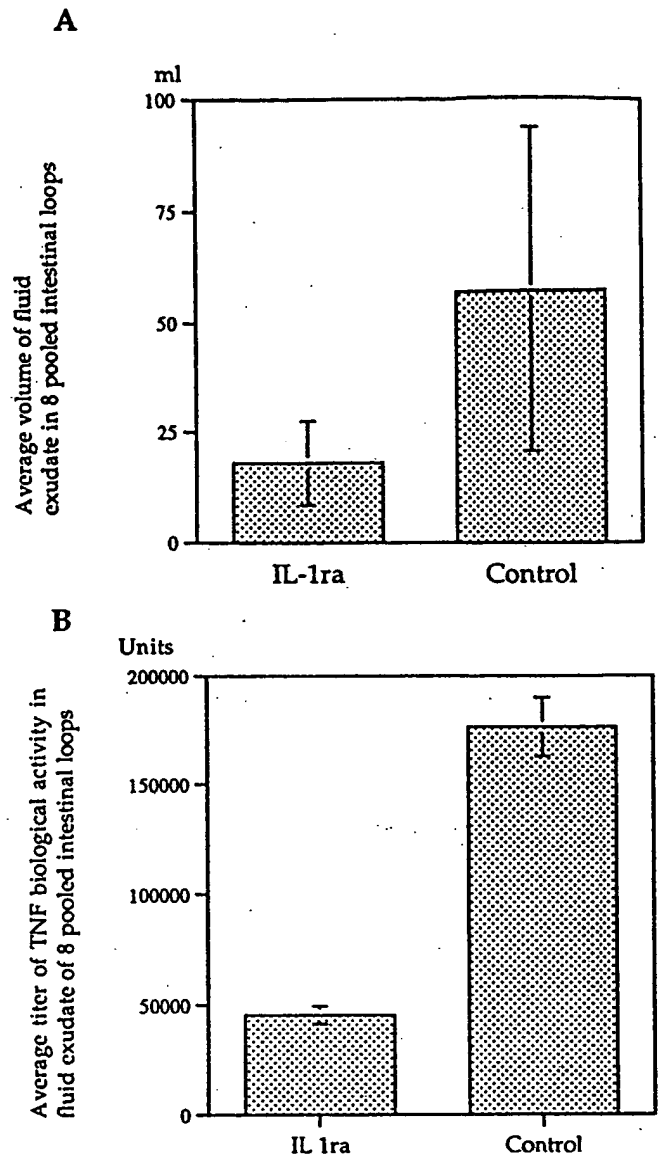


Figure 2. Characteristics of fluid exudate in infected loops of IL-1ra-treated and control rabbits. Average volume (A) and average TNF content (B) of the pooled exudate fluid collected from the eight intestinal loops infected in each animal.

served in animals treated with IL-1ra, close to the number of PMN observed in uninfected tissues (data not shown). In the lamina propria of the villus axis, 15.2 \pm 6.6 PMN were counted in control animals whereas 5.7 \pm 2.5 PMN leukocytes were counted in animals treated with IL-1ra.

These results clearly demonstrated that perfusion of IL-1ra achieved very efficient control of the inflammatory reaction, primarily by preventing extravasation of PMN and their immigration into the lamina propria. It must be emphasized, however, that IL-1ra achieved better control of the PMN infiltrate in the crypt area than in the villus axis.

Evaluation of the degree of tissue modification and destruction. An obvious criteria of tissue alteration was the frequency of ulcerated villi. Any disruption of the continuity of the villus epithelium associated with significant inflammatory infiltrate

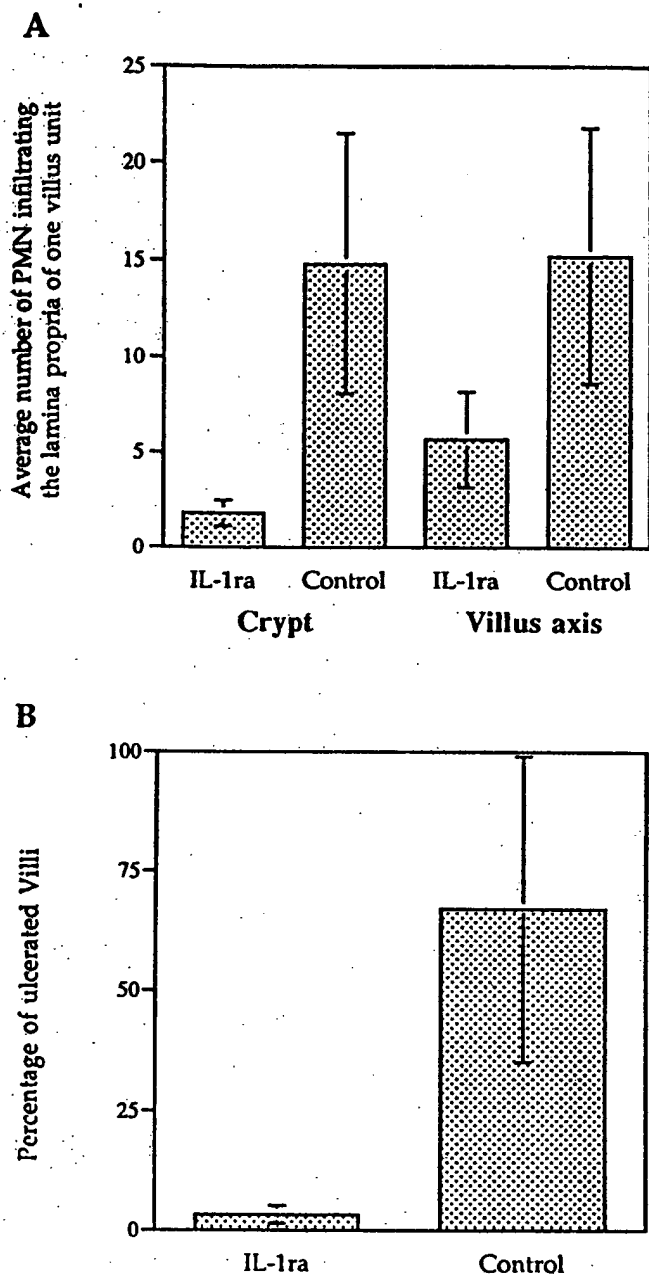


Figure 3. Tissue inflammation and destruction in IL-1ra-treated and control rabbits. (A) Average number of PMN leukocytes infiltrating the lamina propria of one crypt and one villus axis. (B) Average percentage of ulcerated villi in the eight intestinal loops of each animal.

was considered as an ulceration. According to these criteria, as shown in Fig. 3 B, $67 \pm 3\%$ of the villi presented ulcerations in control animals, whereas only $3.3 \pm 1.9\%$ of the villi were ulcerated in animals treated with IL-1ra. Lesions ranged from limited ulcers to purulent necrosis of the entire villus. Severity of the ulcerations has not been recorded here. It must be emphasized that purulent necrosis of the entire villus was only observed in control animals, whereas animals treated with IL-1ra presented only limited ulcerations of the tip of their villi.

For more global evaluation of tissue alterations, we considered two criteria. The reduction in the length/width ratio of

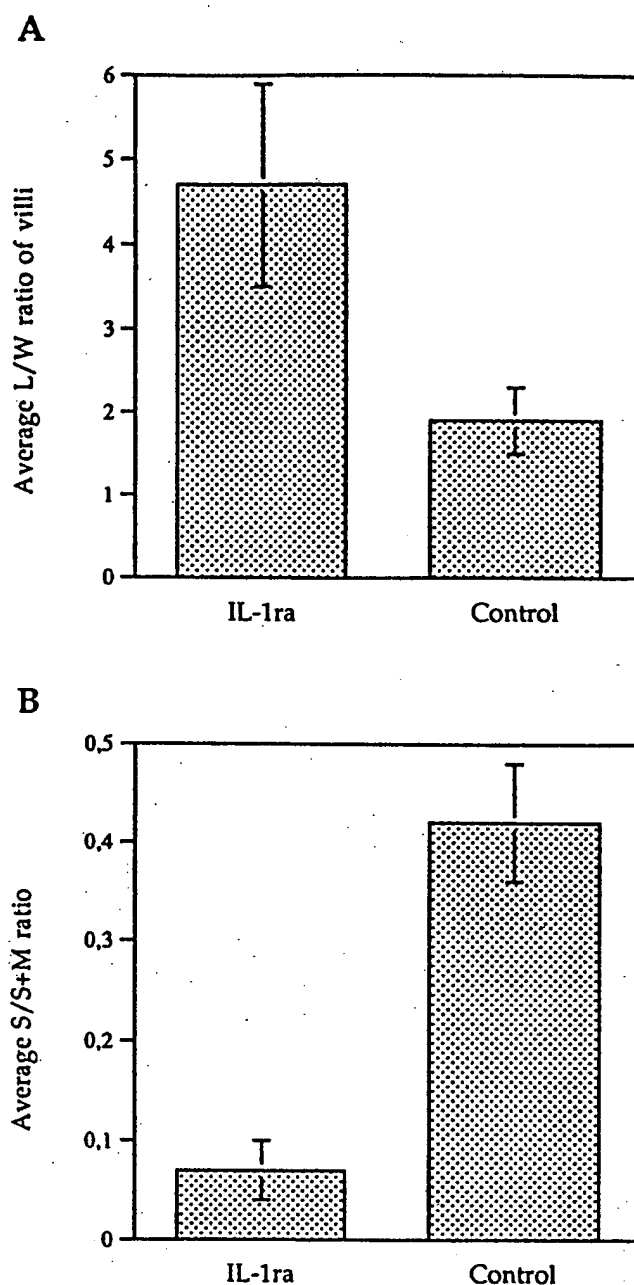


Figure 4. Villus atrophy and submucosal inflammation in IL-1ra-treated and control rabbits. (A) Average L/W ratio reflecting villus atrophy. (B) Average submucosa/submucosa + mucosa ratio reflecting intensity of the submucosal edema, a characteristic of experimental shigellosis in rabbit-ligated loops.

villi, which is among the first symptoms of dysfunction in intestinal tissues (i.e., mucosal atrophy). The ratio between thickness of the submucosa and thickness of the entire mucosal plus submucosal layer, as it appeared that severe inflammation was reflected by major submucosal edema (see Fig. 5 A).

Length/Width (L/W) ratio of intestinal villi is shown in Fig. 4 A. Control animals showed striking flattening of their intestinal villi with a L/W ratio of 1.9 ± 0.4 characteristic of severe villus atrophy. The actual ratio was even lower since a large number of villi were destroyed. However, only nonulcer-

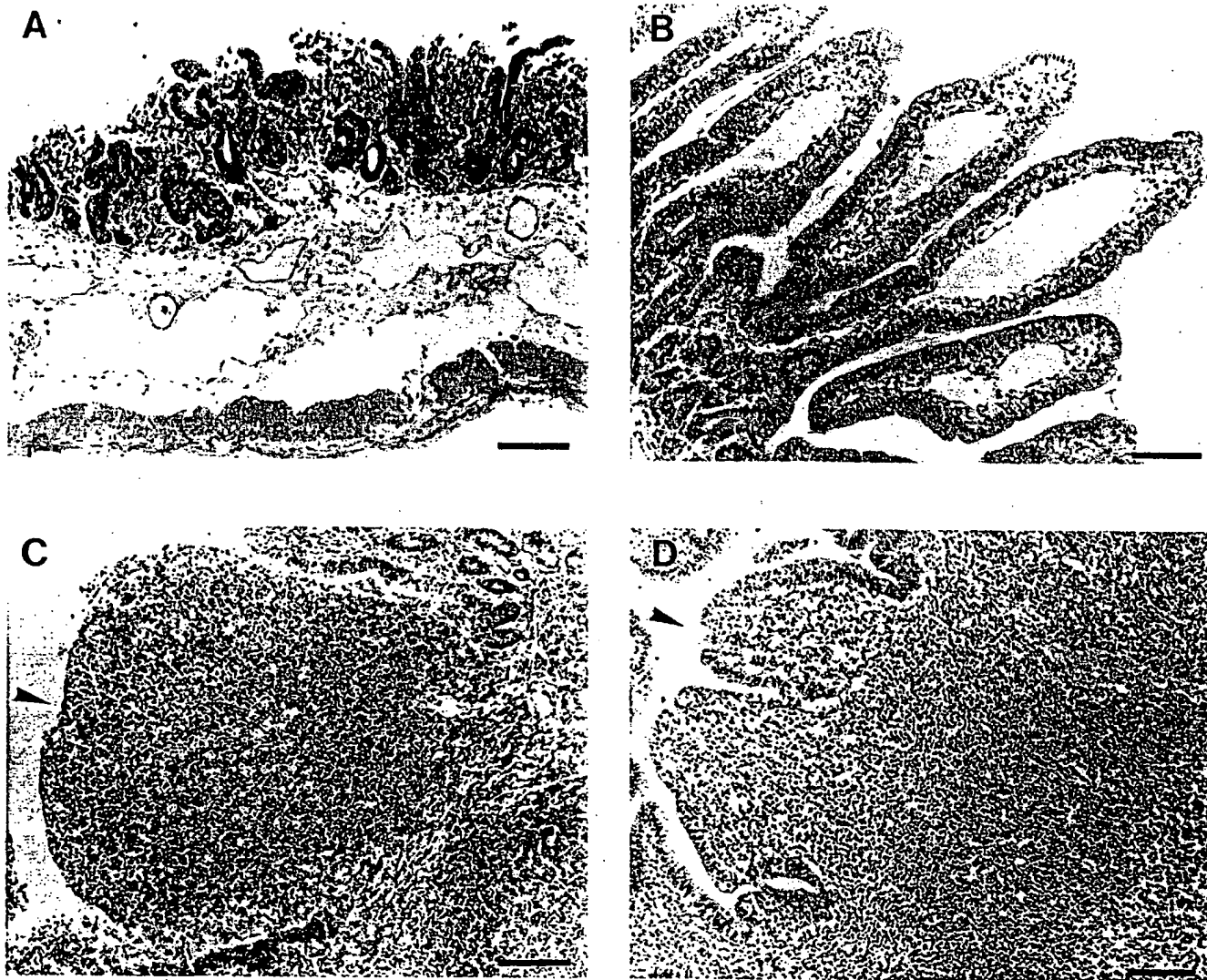


Figure 5. Characteristic aspect of villi and Peyer's patch tissue in animals infected by M90T. Bar = 30 μ m. (A) Villous intestine in control animals. (B) Villous intestine in animals treated by IL-1ra. (C) Peyer's patch in control animals. Arrowhead points to the destroyed dome that leaves the lymphoid nodule exposed to the lumen. (D) Peyer's patch in animals treated by IL-1ra. Arrowhead points to preserved epithelium of the dome in spite of a significant edema in the subepithelial zone.

ated villi or villi presenting limited tip ulcers were taken into account here. In comparison, the L/W ratio was 4.7 ± 1.2 in animals treated with IL-1ra, indicating reasonable preservation of the villi structures, since the average ratio in non infected loops in this model was 6 (data not shown).

Submucosa/submucosa + mucosa ratio. These results are shown in Fig. 4 B. Control animals showed a high ratio of 0.42, reflecting the enormous edema that often characterized the submucosal layer of these animals. Conversely, the ratio of 0.07 observed in animals treated with IL-1ra was extremely low and equivalent to the ratio observed in noninfected loops (data not shown).

Fine histopathological analysis of the lesions. Histopathological analysis was carried out both on sections of the villous intestine and on Peyer's patches.

Examination of villous intestinal tissues revealed significant differences between samples taken from control animals and animals treated with IL-1ra. As shown in Fig. 5 A, and already

suggested in Figs. 3 and 4, the villi of control animals were either reduced in length, or destroyed by a purulent necrotic process leaving vast areas of the crypt choriion infiltrated with PMN, and dissected by large hemorrhagic foci. Complete detachment of the epithelial layer was seen in many places. The subepithelial layer was characterized by enormous edema and infiltration of inflammatory cells, primarily PMN. Numerous PMN were seen immigrating from the vessels localized in the submucosa into the lamina propria surrounding the crypts, often leading to disruption of the muscularis mucosae.

In animals treated by IL-1ra, the histopathological aspect was strikingly different. Villi were consistently altered in length and shape, but never destroyed. As shown in Fig. 5 B, they often showed a "club-like" aspect, the tip of the villus being inflated by edema, whereas the basal half of the villus and the crypt area appeared normal. As suggested in Fig. 3 A, two compartments of PMN infiltration were constituted. One corresponding to the crypt region which is colonized by PMN immi-

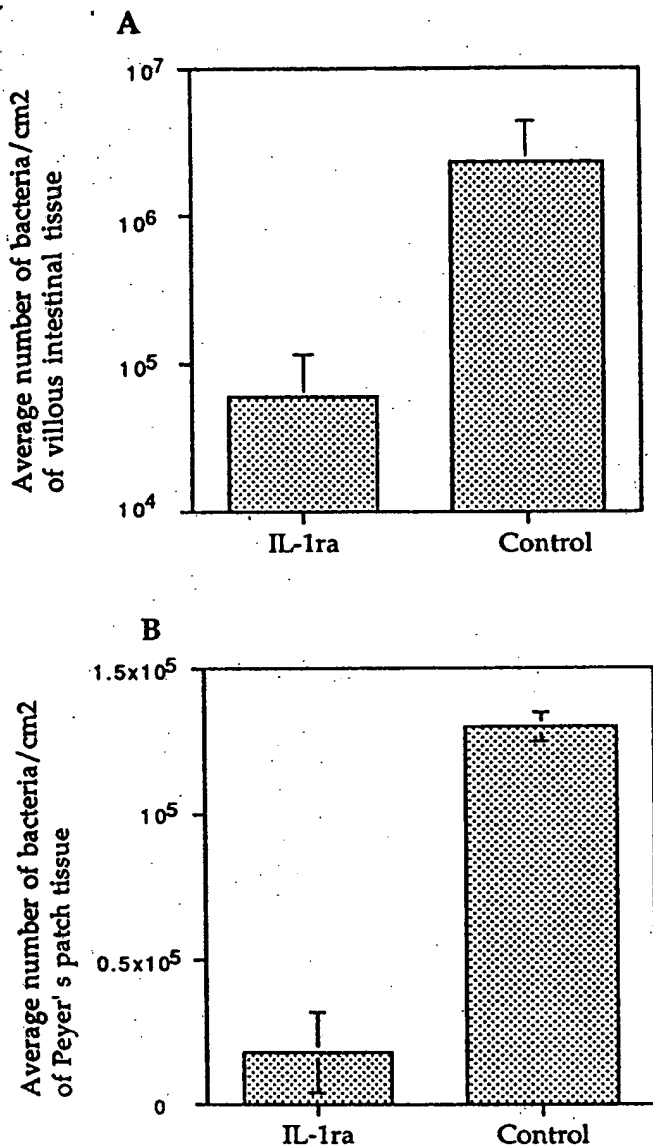


Figure 6. Tissue invasion by M90T in IL-1ra-treated and control animals. (A) Average number of bacteria/cm² of villous intestinal tissue. (B) Average number of bacteria/cm² of Peyer's patch tissue.

grating from the small and medium-size vessels of the submucosa, the other corresponding to the villus axis in which PMN seem to immigrate from local capillaries. This observation suggests that IL-1ra is mainly preventing the inflammatory process elicited at the crypt level, at a distance from the bacteria, whereas it is more difficult for IL-1ra to control inflammation elicited in areas of the villus that are in close contact with the offending microorganism.

Histopathological examination of Peyer's patches also showed striking differences between control and IL-1ra-treated animals. In control animals, extensive destruction of the dome was consistently observed with intense edema and infiltration by PMN. In contrast, in IL-1ra-treated animals, in spite of significant edematous reaction and infiltration by PMN, the dome was preserved or presented only few superficial ulcers of

the epithelial layer. These results are summarized in Fig. 5, C and D.

Bacterial invasion of mucosal tissues. As shown in Fig. 6, control of the inflammatory process by IL-1ra caused significant decrease in the capacity of shigellae to invade the mucosa. The average number of bacteria per cm² of mucosal tissue was $2.3 \times 10^6 \pm 2.1 \times 10^6$ in control animals and $6 \times 10^4 \pm 5 \times 10^4$ in animals treated with the inhibitor. The average number of bacteria per cm² of Peyer's patch tissue was $1.3 \times 10^5 \pm 0.5 \times 10^5$ in control animals and $1.8 \times 10^4 \pm 1.4 \times 10^4$ in animals treated with the inhibitor. Bacterial invasion of the villus mucosa was therefore reduced by a factor of ~ 40 in the presence of IL-1ra, whereas it was reduced only by a factor of 7 in Peyer's patches tissue. This probably indicated that the physiological capacity of the epithelial dome of Peyer's patches to internalize bacteria reduced the need for an inflammatory infiltrate to destabilize the epithelial structure and facilitate invasion.

In conclusion, based on all the criteria considered, treatment of animals with IL-1ra caused significant protection against both *Shigella* invasion and intestinal tissue destruction.

Discussion

There is now evidence that IL-1 is involved in the pathogenesis of inflammatory bowel diseases (IBDs). On the other hand, there has been no investigation addressing the role of this proinflammatory cytokine in the pathogenesis of an invasive infection of the gut such as shigellosis.

Clinical and histopathological observations (15), and recent experiments on the pathogenesis of shigellosis (8), suggest that a pattern of acute inflammation is initiated at the early stage of intestinal invasion by *S. flexneri*, particularly in the lymphoid follicles associated with the mucosa. In addition to ultimately causing tissue destruction, inflammation is essential to disorganizing the epithelial barrier and facilitating bacterial invasion (8). Macrophages present in the dome of lymphoid structures become infected by invasive shigellae, and some of them are rapidly killed. In vitro experiments have demonstrated that virulent *S. flexneri* causes apoptosis of infected macrophages (9). Initiation of the cell death program in macrophages preactivated with LPS induces their release of large amounts of IL-1 α precursor and mature IL-1 β (11). These data suggest that releasing IL-1 may be a characteristic of resident macrophages present in the follicular dome of mucosal lymphoid structures when they phagocytose the invading pathogen. This population of macrophages, due to its permanent contact with bacterial products, particularly LPS, is probably more reactive to a pathogen like *S. flexneri*. In addition, M cells themselves have the capacity to produce IL-1 after stimulation with LPS (16). Inflammation elicited in these areas may spread beyond lymphoid structures to the villous epithelium. In patients at the acute stage of shigellosis, immunohistochemical analysis of rectal biopsies, has shown a predominance of IL-1-producing cells, particularly in tissue samples showing signs of severe inflammation. Mononuclear cells, but also PMN and endothelial cells were the predominant IL-1-producing cell populations (17). These experiments therefore point to IL-1 as a likely key player in the cascade causing the inflammatory process of shigellosis.

Similarly, current evidence indicates that IL-1 plays a crucial role in colonic lesions in IBDs. This is suggested by clinical and experimental studies. Clinical studies show that IL-1 is

transcribed and expressed at a significantly higher level by mononuclear cells purified from intestinal tissues of patients at the acute phase of IBD (16–23). In mice, recombinant IL-1 alone has been shown to be able to induce intestinal pathology, particularly villus atrophy, crypt hyperplasia, and increase in number of intraepithelial lymphocytes (24, 25). In the various animal models of ulcerative colitis, clear demonstration of the proinflammatory role of IL-1 has been provided by demonstrating the antiinflammatory effect of IL-1ra. Intravenous administration of this molecule before and during the development of rabbit immune complex colitis, significantly reduced all the parameters of intestinal inflammation and injury (26). These data were further confirmed in a series of experiments showing that in a similar animal model, IL-1ra did not alter the level of IL-1 α present in intestinal tissues, but induced a decrease in levels of proinflammatory molecules such as PGE₂ and leukotriene B₄ (27). IL-1ra was also effective in reducing bowel inflammation in a model of rat colitis induced by local instillation of acetic acid (28). In addition, in various experimental models, the receptor blocking activity of IL-1ra has significantly reduced the severity of diseases such as septic shock, lethal sepsis, and experimental arthritis (29). The role of other inflammatory cytokines is less clear, although TNF α , IFN γ , and IL-8 are good candidates to induce further inflammation and tissue destruction. Moreover, the chronic enterocolitis and ulcerative colitis patterns observed in interleukin-2 and interleukin-10-deficient mice harboring an intestinal flora (30, 31) suggest that these two cytokines, particularly IL-10, a potent suppressor of macrophage activation in vitro (32), may be important negative regulators to consider in vivo in IBD as well as in shigellosis.

A major limitation to experimental approaches of shigellosis, however, is the lack of a reliable intestinal model of invasion. The guinea pig keratoconjunctivitis test is reliable to assess *Shigella* invasiveness but is irrelevant in this case. Mice do not develop rapid and consistent intestinal invasion by *Shigella* even in ligated loops. Alternatively, the rabbit-ligated loop assay appears sufficiently reliable to use it as a model of tissue invasion and inflammation. This allows us to consider using antagonists of proinflammatory molecules such as IL-1ra. This inhibitor binds to both IL-1 receptors, but particularly relevant is its competitive binding to IL-1 receptor 1 which blocks signal transduction induced by IL-1 α and IL-1 β . It has no agonist effect and is produced by the same cells which produce IL-1 with a delay of a few hours (33). Rabbit IL-1ra exhibits 77% amino acid sequence homology to the human molecule (34). This high degree of conservation accounts for the capacity of human recombinant IL-1ra to antagonize rabbit IL-1. These characteristics made IL-1ra the best candidate molecule to assess the role of IL-1 in shigellosis.

The present experiments have demonstrated that IL-1ra could significantly reduce the severity of intestinal lesions observed in rabbit experimental shigellosis as well as mucosal invasion by *Shigella*. The amount of circulating IL-1ra obtained by perfusion of 2 mg/kg per h in rabbits reached values of 25,000 pg/ml similar to those obtained in human volunteers by perfusion of 10 mg/kg over a period of 3 h (i.e., 29,000 pg/ml) (35). The general structure of the intestinal epithelium was preserved in animals treated by the inhibitor, whereas massive destruction was observed in control animals. The amount of luminal exudate was reduced, as well as its content in TNF, an

established parameter of the inflammatory process of experimental, but also natural shigellosis (8, 36). In the complete pathogenic scheme, it is important to understand whether TNF α or IL-1 is the primary initiator. We are currently conducting experiments with TNF inhibitors to address this point. We would also like to evaluate how much of the epithelial destruction observed in shigellosis is due to the high titer of TNF α produced and secreted intraluminally. These experiments also confirm our recent observation that the severity of mucosal inflammation accounts for the extent of mucosal invasion by the bacteria (7, 8). It seems as if the initial interaction of the bacteria with cellular components of the intestinal barrier triggers an early inflammatory response which causes serious destabilization of epithelial cohesiveness thus facilitating further bacterial invasion.

An unexpected observation was made here concerning the traffic of extravasating PMN. IL-1ra appeared more efficient at attenuating (eliminating in many animals) immigration of PMN from submucosal vessels into the crypt lamina propria than at attenuating immigration of PMN from villi capillaries into the lamina propria occupying the upper half of intestinal villi. This caused the characteristic club-like morphology of the villi (see Fig. 5, B and E), with localized edema. The reason for this "compartmentalization" of the inflammatory response remains unclear. However, it is possible that long range triggering of PMN extravasation requires a full cascade of inflammatory cytokines. IL-1 playing a major role in this process. On the other hand, elicitation of short range extravasation of PMN from villi capillaries may somewhat bypass the need for IL-1. It has recently been shown in vitro that infected epithelial cells or epithelial cells exposed to LPS are able to produce inflammatory cytokines, including the potent chemokine IL-8 (37, 38). Recent work indicates that *Shigella dysenteriae*, upon invasion of human colon epithelial cells, induces expression of IL-8, MCP-1, GM-CSF, and TNF α (39). A similar situation in vivo may lead to direct inflammation through the epithelium by invading microorganisms. However, based on the present experiments, it appears obvious that IL-1-mediated long range inflammatory response is much more deleterious for tissues.

These observations validate the hypothesis that IL-1 plays a significant physiopathological role in shigellosis and that the macrophage, which is a major producer of IL-1 (40), is a key player in the pathogenesis of this disease, particularly in the lymphoid structures associated with the intestinal mucosa. In the current experimental system, after 8 h of intestinal infection in ligated loops, it is difficult to demonstrate a different reactivity of the lymphoid structures of Peyer's patches and of the villous intestine. Ligation of the intestine and high bacterial inoculum artificially facilitate invasion of the intestinal barrier. A closer model to human shigellosis is intragastric infection of macaque monkeys, followed by endoscopic observation of the colo-rectal mucosa as the disease develops (3). However, these experiments are almost impossible to achieve, particularly if constant infusion of IL-1ra needs to be maintained. The rabbit model, within well-defined limits, allows to draw conclusions on the role of IL-1 which would need definitive confirmation in a human trial as also suggested for IBD.

We believe that based on these observations, there is now solid ground to draw a parallel between shigellosis and some acute forms of IBD, particularly ulcerative colitis. In support of this idea, it is worth noting that the deleterious effect of

IL-1 in experimental shigellosis appears rather specific of the causing pathogen *Shigella*. Indeed, in many other models of infection, such as *Pseudomonas aeruginosa* and *Klebsiella pneumoniae* (41), *Listeria monocytogenes* (42), *Salmonella typhimurium* (43), *Escherichia coli* (44, 45), and *Mycobacterium avium* (46), IL-1 was shown to play a protective role, and IL-1 blockade was reported to exacerbate the infectious process (47, 48). This indicates that, as in IBDs, destructive inflammation is the predominant feature of shigellosis. Whether colonic destruction is the price to pay to eradicate *Shigella* from tissues, or whether these bacteria, even at low inoculum, can generate massive uncontrolled inflammation, remains to be analyzed.

Finally, it is not at all clear how shigellosis resolves. It has been shown that healthy human volunteers receiving *E. coli* endotoxin showed plasma levels of IL-1 β peaking at 79 pg/ml, whereas their levels of IL-1ra, 1–3 h later were ~100-fold higher (49). This excess amount of IL-1ra may be sufficient to antagonize the biological effect of IL-1 β . Moreover, in acutely ill surgical patients, very high levels of IL-1ra (i.e., 54,300 pg/ml) have been observed (50). This indicates that serious conditions (with or without sepsis) may cause circulating levels of IL-1ra equivalent to those obtained by perfusion, ranging between 1 and 10 mg/kg per h. We can therefore speculate that a physiological increase of IL-1ra to high titers may be observed in the course of severe sepsis such as shigellosis. IL-1ra titers produced locally by intestinal mononuclear cells and possibly other cell populations may account for efficient antagonism of IL-1 β , thus leading to healing.

Acknowledgments

We are extremely indebted to Synergen, especially, Dr. James L. Van-nice for his generous provision of recombinant IL-1ra. It is obvious that without their help, this work would not have been possible. We also wish to thank Catherine Fitting for cytokine measurement, Nicole Wuscher for her expertise in histopathological studies, and Colette Jac-querin for the editing of this manuscript.

This work was in part funded by the European Union (EEC grant No. BI02 - CT 92-0134).

References

1. LaBrec, E. H., H. Schneider, T. J. Magnani, and S. B. Formal. 1964. Epithelial cell penetration as an essential step in the pathogenesis of bacillary dysentery. *J. Bacteriol.* 88:1503–1518.
2. Goldberg, M. B., and P. J. Sansonetti. 1993. *Shigella* subversion of the cellular cytoskeleton: a strategy for epithelial colonization. *Infect. Immun.* 61:4941–4946.
3. Sansonetti, P. J., J. Arondel, A. Fontaine, H. d'Hauteville, and M. L. Bernardini. 1991. OmpB (osmo-regulation) and icsA (cell to cell spread) mutants of *Shigella flexneri*. Evaluation as vaccine candidates. Probes to study the pathogenesis of shigellosis. *Vaccine* 9:416–422.
4. Mathan, M. M., and V. I. Mathan. 1986. Ultrastructural pathology of the rectal mucosa in *Shigella* dysentery. *Am. J. Pathol.* 123:25–38.
5. DuPont, H. L., M. M. Levine, R. B. Hornick, and S. B. Formal. 1989. Inoculum size in shigellosis and implications for expected mode of transmission. *J. Infect. Dis.* 159:1226–1228.
6. Mounier J., T. Vasselon, R. Hellio, M. Lesourd, and P. J. Sansonetti. 1992. *Shigella flexneri* enters human colonic Caco-2 epithelial cells through their basolateral pole. *Infect. Immun.* 60:237–248.
7. Perdomo, J. J., P. Gounon, and P. J. Sansonetti. 1994. Polymorphonuclear leukocyte (PMN) transmigration promotes invasion of colonic epithelial monolayer by *Shigella flexneri*. *J. Clin. Invest.* 93:633–643.
8. Perdomo, J. J., J. M. Cavaillon, M. Huerre, H. Ohayon, P. Gounon, and P. J. Sansonetti. 1994. Acute inflammation causes epithelial invasion and mucosal destruction in experimental shigellosis. *J. Exp. Med.* 180:1307–1319.
9. Zychlinsky, A., M. C. Prevost, and P. J. Sansonetti. 1992. *Shigella flexneri* induces apoptosis in infected macrophages. *Nature (Lond.)* 358:167–168.
10. Zychlinsky, A., B. Kenny, R. Ménard, M. C. Prevost, I. B. Holland, and P. J. Sansonetti. 1994. IpaB mediates macrophage apoptosis induced by *Shigella flexneri*. *Mol. Microbiol.* 11:619–627.
11. Zychlinsky, A., C. Fitting, J. M. Cavaillon, and P. J. Sansonetti. 1994. Interleukin-1 is released by macrophages during apoptosis induced by *Shigella flexneri*. *J. Clin. Invest.* 94:1328–1332.
12. Wassef, J., D. F. Keren, and J. L. Mailloux. 1989. Role of M cells in initial bacterial uptake and in ulcer formation in the rabbit intestinal loop model in shigellosis. *Infect. Immun.* 57:858–863.
13. Sansonetti, P. J., D. J. Kopecko, and S. B. Formal. 1982. Involvement of a plasmid in the invasive ability of *Shigella flexneri*. *Infect. Immun.* 35:852–860.
14. Cavaillon, J. M., C. Fitting, N. Haennfner-Cavaillon, S. T. Kirsch, and H. S. Warren. 1990. Cytokine response by monocytes and macrophages to free and lipoprotein bound lipopolysaccharide. *Infect. Immun.* 58:2375–2382.
15. Mathan, M. M., and V. I. Mathan. 1991. Morphology of rectal mucosa of patients with shigellosis. *Rev. Infect. Dis.* 13 (Suppl. 4):S314–S318.
16. Pappo, J., and R. T. Mahlman. 1993. Follicle epithelial M cells are a source of interleukin-1 in Peyer's patches. *Immunology* 78:505–507.
17. Raquib, R., A. A. Lindberg, B. Wretling, P. K. Bardhan, U. Andersson, and J. Andersson. 1995. Persistence of local cytokine production in shigellosis in acute and convalescent stages. *Infect. Immun.* 63:289–296.
18. Sartor, R. B. 1991. Pathogenic and clinical relevance of cytokines in inflammatory bowel disease. *Immunol. Res.* 10:465–471.
19. Mahida, Y. R., K. Wu, and D. P. Jewell. 1989. Enhanced production of interleukin-1 β by mononuclear cells isolated from mucosa with active ulcerative colitis or Crohn's disease. *Gut* 30:835–838.
20. Isaacs, K. L., R. B. Sartor, and S. Haskill. 1992. Cytokine messenger RNA profiles in inflammatory bowel disease mucosa detected by polymerase chain reaction amplification. *Gastroenterology* 103:1587–1595.
21. Youngman, K. R., P. L. Simon, G. A. West, F. Cominelli, D. Rachmilewitz, J. S. Klein, and C. Focchi. 1993. Localization of intestinal interleukin-1 activity and protein and gene expression to lamina propria cells. *Gastroenterology* 104:749–758.
22. Ligumsky, M., P. L. Simon, F. Karmeli, D. Rachmilewitz. 1990. Role of interleukin-1 in inflammatory bowel disease-enhanced production during active disease. *Gut* 31:686–689.
23. Satsangi, J., R. A. Wolstencroft, J. Cason, C. C. Ainley, D. C. Dumona, and R. P. Thompson. 1989. Interleukin-1 in Crohn's disease. *Clin. Exp. Immunol.* 67:594–604.
24. Mowat, A. M., A. K. Hutton, P. Garside, and M. Steel. 1993. A role for Interleukin-1 α in immunologically mediated intestinal pathology. *Immunology* 80:110–115.
25. Brynskov, J., N. Tvede, C. B. Andersen, and M. Vilien. 1992. Increased concentrations of interleukin-1 β , interleukin-2, and soluble interleukin-2 receptors in endoscopic mucosal biopsy specimens with active inflammatory bowel disease. *Gut* 33:55–58.
26. Cominelli, F., C. C. Nast, B. D. Clark, R. Schindler, R. Llerena, V. E. Eysselein, R. C. Thompson, and C. A. Dinarello. 1990. Interleukin 1 (IL-1) gene expression, synthesis, and effect of specific IL-1 receptor blockade in rabbit immune complex colitis. *J. Clin. Invest.* 86:972–980.
27. Cominelli, F., C. C. Nast, A. Duchini, and M. Lee. 1992. Recombinant Interleukin-1 receptor antagonist blocks the pro-inflammatory activity of endogenous Interleukin-1 in rabbit immune colitis. *Gastroenterology* 103:65–71.
28. Thomas, T. K., P. C. Will, A. Srivastava, C. L. Wilson, M. Harbison, J. Little, R. S. Chesonis, M. Pignatello, D. Schmolze, J. Symington, et al. 1991. Evaluation of an interleukin-1 receptor antagonist in the rat acetic acid-induced colitis model. *Agents Actions* 34:187–192.
29. Dinarello, C. A. 1992. The role of interleukin-1 in host responses to infectious diseases. *Infect. Agents Dis.* 1:227–236.
30. Sadlack, B., H. Merz, H. Schorle, A. Schimpl, A. C. Feller, and I. Horak. 1993. Ulcerative colitis-like disease in mice with a disrupted interleukin-2 gene. *Cell* 75:253–261.
31. Kühn, R., J. Löhler, D. Rennick, K. Rajewsky, and W. Müller. 1993. Interleukin-10-deficient mice develop chronic enterocolitis. *Cell* 75:263–274.
32. Fiorentino, D. F., A. Zlotnik, T. R. Mosmann, M. Howard, and A. O'Garra. 1991. IL-10 inhibits cytokine production by activated macrophages. *J. Immunol.* 147:3815–3822.
33. Arend, W. P. 1993. Interleukin-1 receptor antagonist. *Adv. Immunol.* 54:167–227.
34. Goto, F., K. Goto, T. Miyata, S. Ohkawara, T. Takao, T. Mori, S. Furukawa, T. Maeda, S. Iwanaga, Y. Shimouishi, and M. Yoshinaga. 1992. Interleukin-1 receptor antagonist in inflammatory exudate cells of rabbits. Production, purification and determination of primary structure. *Immunology* 77:235–244.
35. Granowitz, E. V., R. Porat, J. V. Mier, J. P. Pribble, D. M. Stiles, D. C. Bloedow, M. A. Catalano, S. M. Wolff, and C. A. Dinarello. 1992. Pharmacokinetic

- ics, safety and immunomodulatory effects of human recombinant interleukin-1 receptor antagonist in healthy humans. *Cytokine*. 4:353-360.
36. Nicholls, S., S. Stephens, C. P. Braegger, J. A. Walker-Smith, and T. T. MacDonald. 1993. Cytokines in stools of children with inflammatory bowel disease or infective diarrhoea. *J. Clin. Pathol.* 46:757-760.
 37. Eckmann, L., M. F. Kagnoff, and J. Fierer. 1993. Epithelial cells secrete the chemokine Interleukin-8 in response to bacterial entry. *Infect. Immun.* 61:4569-4574.
 38. Schueker-Maly, C. C., L. Eckmann, M. F. Kagnoff, M. T. Falco, and F. E. Maly. 1994. Colonic epithelial cell lines as a source of interleukin-8: stimulation by inflammatory cytokines and bacterial lipopolysaccharide. *Immunology*. 81:85-91.
 39. Jung, H. C., L. Eckmann, S.-K. Yang, P. Asit, J. Fierer, E. Morzycka-Wroblewska, and M. Kagnoff. 1995. A distinct array of proinflammatory cytokines is expressed in human colon epithelial cells in response to bacterial invasion. *J. Clin. Invest.* 95:55-65.
 40. Dinarello, C. A. 1991. Interleukin-1 and interleukin-1 antagonism. *Blood*. 77:1627-1652.
 41. Ozaki, Y., T. Ohashi, A. Minami, and S. I. Nakamura. 1987. Enhanced resistance of mice to bacterial infection induced by recombinant interleukin-1 α . *Infect. Immun.* 55:1436-1440.
 42. Czuprynski, C. J., and J. F. Brown. 1987. Recombinant murine interleukin-1 α enhancement of non-specific antibacterial resistance. *Infect. Immun.* 55:2061-2065.
 43. Morrissey, P., and J. Charrier. 1991. Interleukin-1 administration to C3H/HeJ mice after but not prior to infection increases resistance to *Salmonella typhimurium*. *Infect. Immun.* 59:4729-4731.
 44. Pelkonen, S., and G. Pluschke. 1989. Recombinant interleukin-1 stimulates clearance of *Escherichia coli* K1 bacteraemia. *Microb. Pathog.* 6:415-424.
 45. Cross, A. S., J. C. Sadoff, N. Kelly, E. Bernton, and P. Genski. 1989. Pretreatment with recombinant murine tumor necrosis factor- α and murine interleukin-1 α protect mice from lethal bacterial infection. *J. Exp. Med.* 169:2021-2027.
 46. Denis, M., and E. Gharirian. 1994. Interleukin-1 is involved in mouse resistance to *Mycobacterium avium*. *Infect. Immun.* 62:457-461.
 47. Mancilla, J., P. Garcia, and C. A. Dinarello. 1993. The interleukin-1 receptor antagonist can either reduce or enhance the lethality of *Klebsiella pneumoniae* sepsis in newborn rats. *Infect. Immun.* 61:926-932.
 48. Havell, E. A., L. L. Moldawer, D. Helfgott, P. L. Kilian, and P. B. Sehgal. 1992. Type I IL-1 receptor blockade exacerbates murine listeriosis. *J. Immunol.* 148:1486-1492.
 49. Granowitz, E. V., A. A. Santos, D. D. Poutsika, J. G. Cannon, D. W. Wilmore, S. M. Wolff, and C. A. Dinarello. 1991. Production of interleukin-1-receptor antagonist during experimental endotoxaemia. *Lancet*. 338:1423-1424.
 50. Fischer, E., K. J. Van Zee, M. A. Marano, C. S. Rock, J. S. Kenney, D. D. Poutsika, C. A. Dinarello, S. F. Lowry, and L. L. Moldawer. 1992. Interleukin-1 receptor antagonist circulates in experimental inflammation and in human disease. *Blood*. 79:2196-2200.

Caspase-1 Activation of IL-1 β and IL-18 Are Essential for *Shigella flexneri*-Induced Inflammation

Philippe J. Sansonetti,* Armelle Phalipon,*

Josette Arondel,* Kavitha Thirumalai,†

Subhashis Banerjee,‡ Shizuo Akira,§

Kiyoshi Takeda,§ and Arturo Zychlinsky^{||}

*Unité de Pathogénie Microbienne Moléculaire
INSERM U389

Institut Pasteur

75724 Paris Cedex 15

France

†Skirball Institute

Department of Microbiology and

Kaplan Cancer Center

New York University School of Medicine

New York, New York 10016

‡BASF Bioresearch Corporation

Worcester, Massachusetts 01605

§Department of Host Defense

Research Institute for Microbial Diseases

Osaka University

Osaka 565-0871

Japan

Summary

Caspases are intracellular proteases that mediate mammalian cell apoptosis. Caspase-1 (Casp-1) is a unique caspase because it activates the proinflammatory cytokines interleukin (IL)-1 β and IL-18. *Shigella flexneri*, the etiological agent of bacillary dysentery, induces macrophage apoptosis, which requires Casp-1 and results in the release of mature IL-1 β and IL-18. Here we show that *casp-1*^{-/-} mice infected with *S. flexneri* do not develop the acute inflammation characteristic of shigellosis and are unable to resolve the bacterial infection. Using *casp-1*^{-/-} mice supplemented with recombinant cytokines and experiments with IL-1 β ^{-/-} and IL-18^{-/-} mice, we show that IL-1 β and IL-18 are both required to mediate inflammation in *S. flexneri* infections. Together, these data demonstrate the importance of Casp-1 in acute inflammation and show the different roles of its substrates, IL-1 β and IL-18, in this response.

Introduction

Caspase-1 (Casp-1), like all caspases, is a cysteine protease that induces apoptosis when overexpressed in cultured cells (Miura et al., 1993). However, unlike mice with targeted deletions in most other caspase genes, *casp-1*^{-/-} mice do not have any developmental defects, and cells isolated from these animals respond normally to "classical" apoptotic stimuli (Kuida et al., 1995; Li et al., 1995), suggesting that Casp-1 causes apoptosis only on dysregulated activation. In addition, the cleavage

products of Casp-1, IL-1 β , and IL-18 are proinflammatory cytokines (Dinarello, 1998), although apoptosis is often immunologically silent and does not cause inflammation (Savill, 1997).

Bacillary dysentery is a severe bloody diarrhea caused by the gram-negative bacteria *Shigellae*. *Shigella flexneri* accounts for the worldwide endemic form of the disease, which is particularly prevalent in young children living in developing areas in which poor hygiene facilitates transmission (Kotloff et al., 1999). After ingestion, *S. flexneri* invades and remains localized to the colonic and rectal mucosa, where it causes an acute inflammation characterized by a massive influx of polymorphonuclear cells (PMN) (Mathan and Mathan, 1991). Inflammation in classical shigellosis is of striking severity, resembling the acute phase of inflammatory bowel diseases (IBD), such as ulcerative colitis (MacDermott, 1994; Sartor, 1995). The inflammatory response causes significant tissue destruction and facilitates further tissue invasion by the bacteria (Perdomo et al., 1994). Eventually, however, the inflammation eradicates *Shigella* (Maurelli and Sansonetti, 1988; Hale, 1991; Lindberg and Pál, 1993).

Shigella invades host cells by macropinocytosis (Adam et al., 1995) and quickly escapes from phagosomes into the cytoplasm (Sansonetti et al., 1986). In contrast to epithelial cells, which allow *Shigella* to multiply in their cytoplasm, macrophages undergo apoptosis after bacterial uptake (Zychlinsky et al., 1992). The upregulation of apoptosis was demonstrated in animal models of *Shigella* infection (Zychlinsky et al., 1996) and in intestinal biopsies from dysenteric patients (Islam et al., 1997). The invasion plasmid antigen (Ipa) B is a protein encoded in the *Shigella* virulence plasmid that is secreted from bacteria through a type III secretion apparatus. IpaB alone is sufficient to induce apoptosis (Chen et al., 1996). IpaB binds to Casp-1 in the macrophage cytosol and activates an apoptotic cascade (Chen et al., 1996; Thirumalai et al., 1997). Interestingly, macrophages isolated from mice with a targeted deletion in *casp-1* but not from *casp-3* or *casp-11* null mice are resistant to *Shigella*-induced apoptosis (Hilbi et al., 1998). Thus, unlike most other apoptotic stimuli, *Shigella*-induced apoptosis in macrophages requires Casp-1.

Here we demonstrate that Casp-1 is essential for the inflammation provoked by *Shigella*. *Shigella* causes an inflammatory response of the lung tissue of mice that parallels the acute inflammation in the intestinal mucosa of dysenteric patients, when administered intranasally (Voino-Yasenetsky and Voino-Yasenetska, 1961; Phalipon et al., 1995). We use this model of infection because *Shigella* cannot infect mice orally. Wild-type mice develop a severe inflammatory response within 6 hr of infection. The bacterial load diminishes over time and the inflammation starts to resolve 48 hr later. In contrast, *casp-1*^{-/-} mice do not generate an inflammation in response to a *Shigella* infection until much later. Moreover, the inflammation that eventually develops in *casp-1*^{-/-} mice is more severe than the acute inflammation in wild-type mice. Even after extended periods of infection,

^{||}To whom correspondence should be addressed (e-mail: zychlinsky@saturn.med.nyu.edu).

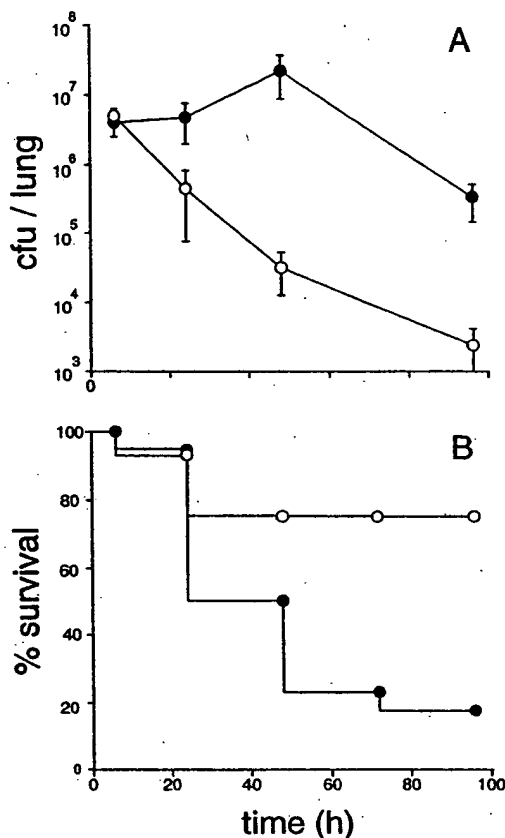


Figure 1. *casp-1*^{-/-} Mice Cannot Control *Shigella* Infections

(A) The number of bacteria in the lungs of wild-type (open circles) and *casp-1*^{-/-} (closed circles) mice are presented as the mean and standard error of the number of colony-forming units. Six hours after infection, there were similar numbers of bacteria in wild-type and *casp-1*^{-/-} mice. The number of bacteria significantly decreased in wild-type animals starting as early as 24 hr and continuing up to 96 hr. In *casp-1*^{-/-} mice, the bacterial load increased slightly by 24 hr and remained unresolved even at 96 hr postinfection. (B) Wild-type (open circles) and *casp-1*^{-/-} (closed circles) mice were infected with *Shigella* and their survival recorded for 96 hr. In contrast to wild-type mice, *casp-1*^{-/-} null mice were susceptible to *Shigella* especially 48 hr after infection.

casp-1^{-/-} mice are unable to control the infection and the inflammation continues to worsen. We demonstrate that IL-1 β is the Casp-1 substrate responsible for the intensity of the acute inflammation observed in *Shigella* infections, while the other substrate, IL-18, is important in eliciting an effective anti-bacterial response. Therefore, in vivo activation of Casp-1 by *Shigella* is proinflammatory.

R suits

Bacterial Load and Mortality in *Shigella* Infections of *casp-1*^{-/-} and Wild-Type Mice

To evaluate the in vivo role of Casp-1 in *Shigella* infections, we infected *casp-1*^{-/-} and wild-type mice with a sublethal dose of bacteria intranasally. The number of bacteria in the lungs of infected wild-type and *casp-1*^{-/-} mice after 6 hr of infection was not statistically different ($p = 0.59$) (Figure 1). However, a difference was manifest

at later time points. In wild-type mice, there was a significant drop in the number of bacteria recovered 24 hr ($p = 0.0039$) after infection, and by 96 hr bacterial recovery was reduced by three orders of magnitude. In contrast, 24 and 48 hr after infection, *casp-1*^{-/-} mouse lungs had 10- and 670-fold more bacteria than wild-type mice, respectively ($p = 0.0011$). *casp-1*^{-/-} mice still harbored a large number of bacteria even at 96 hr postinfection.

Mice with a targeted deletion in *casp-1* succumbed to the *Shigella* infection. As shown in Figure 1B, there were a few wild-type mice that died early on after infection. In contrast, the mortality of *casp-1*^{-/-} mice increased during the experiment. Together, these data show that wild-type but not *casp-1* null mice are able to efficiently control the microbial infection.

Shigella Does Not Upregulate Apoptosis in *casp-1*^{-/-} Mice

To determine whether *Shigella* induces apoptosis in this infection model, we labeled sections of infected lung tissue by the terminal d-transferase dUTP nick end labeling (TUNEL) technique. In histopathological sections taken at 6 hr after infection, we observed apoptotic cells that had a macrophage morphology in wild-type (Figures 2A–2C), but we did not see apoptosis in *casp-1*^{-/-} mice (Figures 2D–2F).

Reconstruction of complete sections of lungs from wild-type (Figures 2I and 2J) and *casp-1*^{-/-} (Figures 2G and 2H) mice demonstrated a striking difference in the number of TUNEL-positive cells. Many apoptotic cells were present in the middle portion of the wild-type lung with greatest density around the bronchi, mirroring the distribution of bacteria. Very few apoptotic cells were detected in the lungs of *casp-1*^{-/-} mice. These apoptotic cells localized to the periphery of the tissue. A similar distribution of apoptotic cells was observed in uninfected lungs or lungs infected with *S. flexneri* strain with a targeted deletion in *ipaB* ($\Delta ipaB$, data not shown), suggesting that this was a phenomenon unrelated to shigellosis. Thus, in vivo, *Shigella* requires Casp-1 to induce apoptosis.

Inflammation in *Shigella* Infections of *casp-1*^{-/-} Mice

To determine the role of Casp-1 in inducing an inflammatory response, we evaluated the extent of tissue inflammation in *casp-1*^{-/-} mice by histopathological analysis. A qualitative analysis of a selection of typical histopathological aspects is shown in Figure 3. In wild-type mice, extensive inflammation is observed at 6 hr in the peribronchial/bronchiolar area and in the pulmonary tissue, causing acute diffuse alveolitis (Figure 3A). At 24 hr, inflammation is less extensive; alveolar walls remain thickened but the alveolitis is already resolving (Figures 3B and 3C). By 48 hr, the overall alveolar structure has almost returned to normal, with a few remaining macrophages and PMN (Figure 3D). Although a persistent edema still thickens the alveolar walls, the tissue has almost recovered. The disappearance of inflammatory cells at 96 hr (Figure 3E) shows the complete regression of the inflammation.

The pathology is strikingly different in *casp-1*^{-/-} animals. Very few inflammatory foci are observed at 6 hr

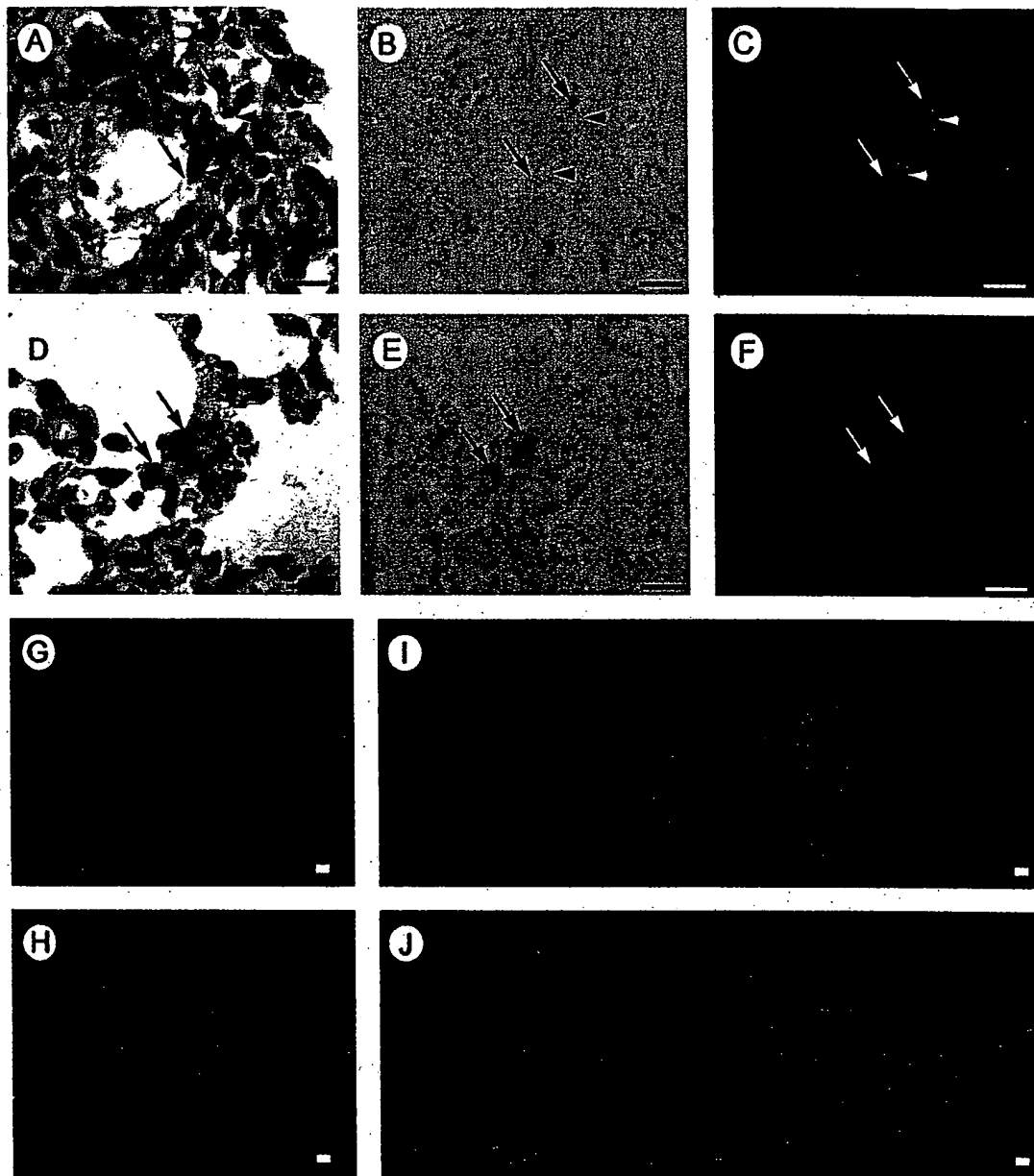


Figure 2. *Shigella* Induces Macrophage Apoptosis in Wild-Type but Not in *casp-1*^{-/-} Infected Mice

- (A) Two cells with macrophage morphology (arrowheads) were identified in wild-type mice in a section stained with hematoxylin and eosin (H&E) stain.
- (B) The same cells were labeled with an anti-LPS antiserum (arrows) indicating that they are infected with *S. flexneri*.
- (C) The same two cells were positively stained by fluorescent TUNEL (arrows). Thus, we were able to identify infected macrophages undergoing apoptosis in these animals.
- (D and E) H&E-stained macrophages (arrowheads) of *casp-1* null mice were also labeled with anti-LPS serum (E), indicating that they were infected.
- (F) These same cells were not stained by TUNEL, showing that in vivo *casp-1*^{-/-} macrophages do not undergo apoptosis with *Shigella*.
- (G) Reconstruction of a section from a lung from a *casp-1*^{-/-} mouse infected with *S. flexneri* and stained with fluorescent TUNEL. Few cells toward the edge of the lung were labeled, serving as a positive control.
- (H) Reconstruction of the same section shown in (G) stained with the DNA stain propidium iodide that allows the visualization of the complete lung section.
- (I) Reconstruction of a lung from a wild-type mouse infected with *S. flexneri* and stained with fluorescent TUNEL. Large numbers of TUNEL-positive cells are evident in the middle portion of the lung, with a greater concentration in close proximity to bronchi, a distribution similar to that of bacteria.
- (J) Reconstruction of the same section shown in (I) and stained with propidium iodide. Scale bars in (A–F) are 10 μ m. Scale bars in (G–J) are 1 mm.

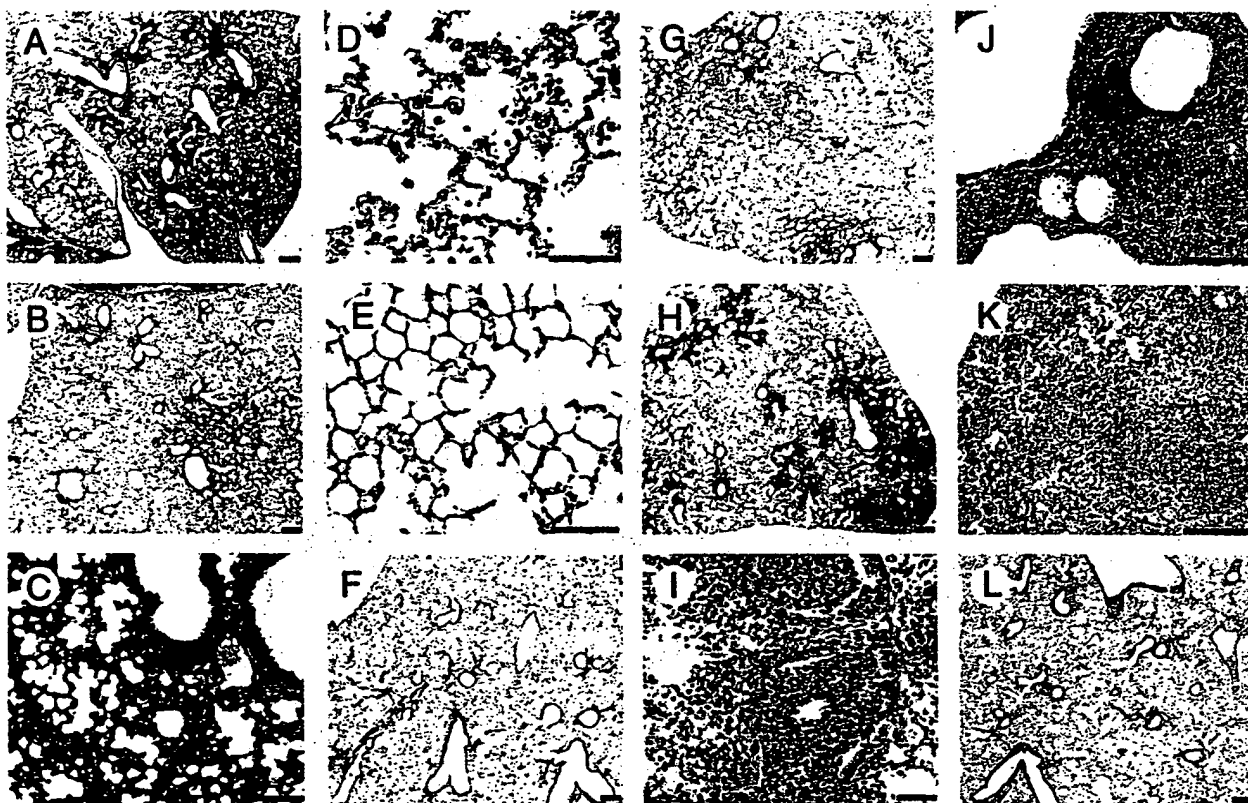


Figure 3. Inflammation in the Lungs of Wild-Type and *casp-1*^{-/-} Mice Infected with *S. flexneri*

Lungs of infected mice were processed for histopathological analysis and stained with H&E.

- (A) Wild-type mice 6 hr after infection show extensive inflammation, starting in the peribronchial region and spreading through the lung, causing acute diffuse alveolitis.
 (B) In wild-type mice 24 hr after infection, the inflammation is starting to resolve.
 (C) High magnification of (B) showing some thickened alveolar walls.
 (D) Forty-eight hr after infection some mononuclear cells are still observed in thickened alveoli in wild-type mice.
 (E) Ninety-six hours postinfection the lung has almost normal morphology.
 (F) Wild-type mice 24 hr after infection with ΔpaB do not show any signs of inflammation.
 (G) *casp-1*^{-/-} mice 6 hr after infection present very few inflammatory sites concentrated in the peribronchial and bronchiolar areas, without significant acute condensing alveolitis.
 (H) At 24 hr postinfection there is a strong diffuse inflammation with formation of multiple foci of acute condensing alveolitis.
 (I) Higher magnification of (H) showing intense inflammation and many bronchi and bronchioli occluded by inflammatory exudates in *casp-1* null mice.
 (J) Forty-eight hours after infection *casp-1*^{-/-} mice still show condensing inflammation with edema and emphysema.
 (K) The inflammation, edema, and emphysema are unabated 96 hr postinfection. Strong hemorrhagic necrosis is also evident at this late time point.
 (L) *casp-1* null mice 24 hr after infection with ΔpaB without any sign of inflammation. Scale bars, 30 μ m.

(Figure 3G). However, 24 hr after infection, there is a strong diffuse inflammation with extensive areas of alveolitis. Many bronchi and bronchioli are occluded by a massive inflammatory exudate (Figure 3H and 3I). By 48 hr postinfection (Figure 3J), the tissue damage worsens as condensing lesions predominate with tissue necrosis and hemorrhages. Ninety six hours after inoculation (Figure 3K), the histopathology remains the same: large areas of condensing inflammation, often centering around vessels occluded with mononuclear cells, and areas with hemorrhages and necrotic tissue. The inflammation in *casp-1*^{-/-} mice was richer in macrophages than in wild-type mice.

There were no lesions observed in either wild type or *casp-1*^{-/-} mice infected with ΔpaB either at 6 hr (data not shown) or 24 hr (Figures 3F and 3L).

In order to quantify the severity of inflammation, lung sections stained by hematoxylin and eosin (H&E) were

scanned at high resolution onto a computer. Using image analysis, we measured the area of the tissue sections which had a high color density and granularity. Because of its structure, a healthy lung has very few areas with high color density, while an inflamed lung, where the alveoli are infiltrated with inflammatory cells, has large areas with high color density. The ratio of the high color density surface to the entire surface of the tissue section, excluding the anatomic "holes" (i.e., the lumen of large blood vessels and bronchi) yields an "inflammatory index" (IF). This measure underestimates the inflammation, since it is biased toward well-delineated and condensed foci, omitting diffuse noncondensing processes. The analysis showed that by 6 hr, wild-type mice developed an IF of 15.0, whereas the *casp-1*^{-/-} mice had an IF of 0.80, indicating a lack of an inflammatory response in the latter. The inflammation decreased in wild-type animals at 24 and 48 hr and reached an IF of

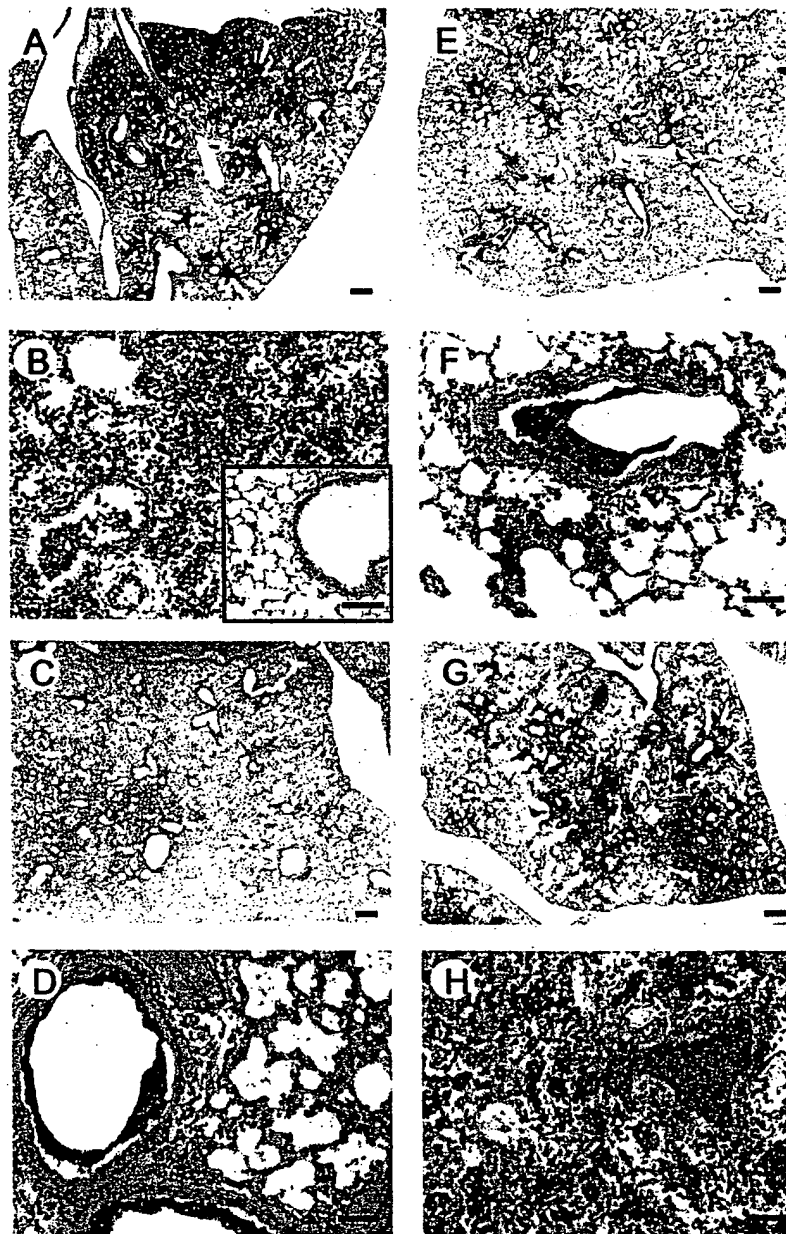


Figure 4. Distribution of LPS in Lungs of Wild-Type and *casp-1*^{-/-} Mice Infected with Virulent *S. flexneri*

Lungs of infected mice were processed for histopathological analysis using standard techniques and immunostained with an anti-*S. flexneri* serotype 5 LPS-specific antiserum. (A and B) Wild-type mice 6 hr after infection present large amounts of LPS throughout the lung, particularly in association with areas of acute alveolitis. Inset shows a section stained with an isotype control mAb (B) and demonstrates the specificity of the immunostaining. (C and D) Wild-type mice 24 hr after infection display diffuse localization of LPS, which is more abundant in bronchial/bronchiolar walls. (E and F) In *casp-1*^{-/-} mouse 6 hr after infection LPS is diffusely distributed in the lung and is more prominent in the lumen and walls of bronchi and bronchioli. (G and H) *casp-1* null mice 24 hr after infection show massive amounts of LPS that fill luminal spaces and are associated with inflammatory cells. Scale bars, 300 μ m.

only 3.6 by 96 hr. In contrast, *casp-1*^{-/-} mice experienced a striking increase in the intensity of their lesions by 24 hr when they achieved an IF of 12.5, which continued to increase to almost 40 by 48 hr and 96 hr. The inflammation seen in the wild-type lungs was significantly different from *casp-1*^{-/-} at each time point ($p < 0.001$).

We used a serotype-specific anti-LPS monoclonal antibody to determine the distribution of bacteria in the infected tissue. As shown in Figure 4, *Shigella* were present throughout the middle portion of the lung section 6 hr postinfection. The LPS immunostaining was specific, since a control with an isotype-matched monoclonal did not stain the tissue (Figure 4B, inset). The bacteria were found in more defined foci at 24 hr in the lungs of wild-type mice. Although there was almost no inflammation in the lungs of *casp-1*^{-/-} mice at 6 hr postinfection, there were areas in the lungs that were occupied by bacteria. The distribution and amount of bacteria

in *casp-1*^{-/-} mice 24 hr after infection were unchanged from 6 hr. These results are in agreement with the data on the number of colony-forming units in the lungs of wild-type and *casp-1*^{-/-} mice presented in Figure 1.

Recombinant IL-1 β Exacerbates the Infection While IL-18 Restores the Wild-Type Phenotype in *casp-1* Null Mice

Casp-1 activates the proinflammatory cytokines IL-1 β and IL-18 (Dinarello, 1998). To test the roles of IL-1 β and IL-18 individually in inflammation during *Shigella* infection, we injected *casp-1*^{-/-} mice intraperitoneally with either recombinant IL-1 β or IL-18 and sacrificed the mice 48 hr postinfection. *Shigella*-infected *casp-1*^{-/-} mice presented the previously described phenotype of condensing inflammation with defined areas of infection (Figures 5A and 5B). Treatment with recombinant IL-1 β resulted in a more diffuse and severe inflammatory response and a more dispersed distribution of bacteria

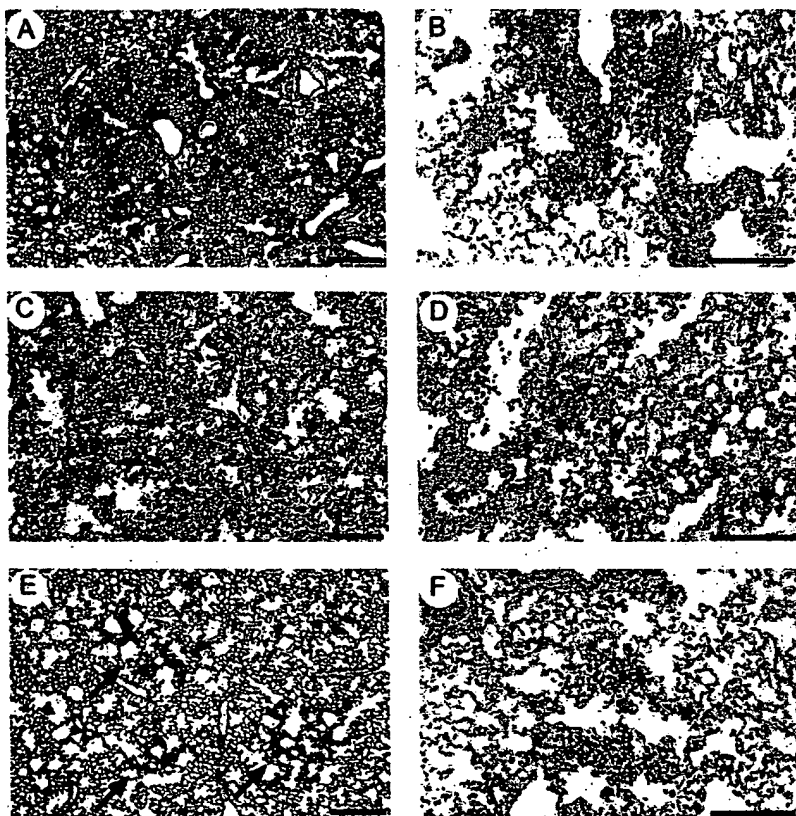


Figure 5. Recombinant IL-1 β and IL-18 Have Different Functions in *Shigella* Infections

casp-1 null mice were either mock treated or treated with recombinant IL-1 β or IL-18 as described in Experimental Procedures and infected with *Shigella* for 24 hr. The tissue was processed either for H&E staining or immunostaining with an anti-*Shigella* serotype 5 mAb.

(A and B) Control *casp-1* null mice show a strong diffuse inflammation with formation of multiple foci of acute condensing alveolitis and (B) large amounts of LPS.

(C and D) *casp-1*^{-/-} mice treated with IL-1 β show a similar, if slightly increased, inflammation and (D) abundant LPS staining.

(E and F) In contrast, *casp-1* null mice injected with recombinant IL-18 show a decreased nondiffuse inflammation (arrows) (F) and the corresponding localization of LPS.

in the lungs of these mice (Figures 5C and 5D). In contrast, treating *casp-1*^{-/-} mice with recombinant IL-18 decreased the inflammation and restricted the distribution of the bacteria to a similar degree to that observed in wild-type mice (Figures 5E and 5F).

The enumeration of bacteria in the lungs of these mice corroborated the histological observations. At 48 hr wild-type mice were resolving the infection ($7.2 \times 10^3 \pm 4.5$ SD cfu/lung) while *casp-1* null mice were still heavily infected ($110 \times 10^3 \pm 4.5$ SD, $p = 0.01$), as observed earlier. Surprisingly, at the same time point, *casp-1* null mice injected with recombinant IL-1 β presented an even higher number of bacteria ($966 \times 10^3 \pm 526$), that was significantly greater ($p = 0.01$) than seen in untreated *casp-1*^{-/-} mice. In contrast, administration of recombinant IL-18 resulted in a bacterial load ($18 \times 10^3 \pm 16.3$) that was not different from wild-type mice ($p = 0.7$).

Infection of IL-1 β and IL-18 Null Mice

Macrophages from both IL-1 β null and IL-18 null mice are susceptible to *Shigella*-induced apoptosis (data not shown). Thus, neither of these cytokines is necessary in the Casp-1-dependent apoptotic pathway. To determine downstream effectors of Casp-1-mediated inflammation in response to *Shigella*, we infected IL-1 β ^{-/-} and IL-18^{-/-} mice with these bacteria. The number of bacteria in wild-type and IL-1 β ^{-/-} mice was not significantly different at 6, 24, or 48 hr postinfection (Figure 6A). In contrast, although the level of infection was similar at 6 hr between IL-18 null and wild-type mice, IL-18 null mice did not control the infection at later time points (Figure 6B). Twenty four and 48 hr after infection, the lungs of IL-18^{-/-} mice had 61 ($p = 0.02$) and 1150 ($p =$

0.04) fold more bacteria than wild-type mice, respectively. Thus, similar to *casp-1*^{-/-} mice, IL-18^{-/-} mice could not control the *Shigella* infection.

Figure 7 shows the LPS immunostaining of wild-type, IL-1 β null, and IL-18 null mice at 24 and 48 hr postinfection. Lungs from wild-type mice showed a restricted

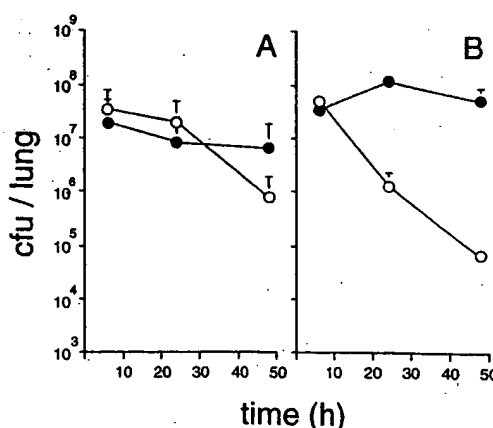


Figure 6. IL-18 but Not IL-1 β Is Required to Control *Shigella* Infection

The number of bacteria in the lungs of wild-type (open circles) and IL-1 β ^{-/-} (A) or IL-18^{-/-} (B) (closed circles) mice are presented as the mean and standard error of the number of colony-forming units. Six hours after infection, there were similar numbers of bacteria in wild-type and either IL-1 β null or IL-18 null mice infected with *Shigella*. The number of bacteria was similar in wild-type and IL-1 β ^{-/-} mice at later times after infection. In contrast, the bacterial load increased slightly by 24 hr and was higher than wild type by 48 hr in IL-18 null mice.

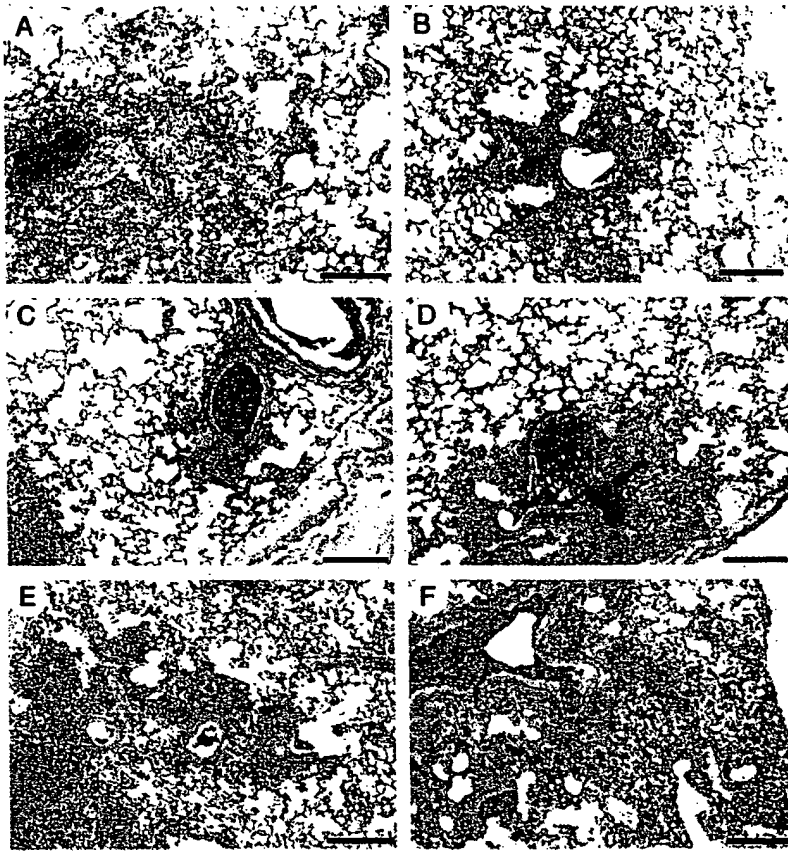


Figure 7. IL-1 β and IL-18 Have Distinct Roles in the Acute Inflammation Characteristic of Shigellosis

The distribution of LPS and inflammation in lungs of wild-type, IL-1 β null, and IL-18 null mice infected with virulent *S. flexneri* is visualized using standard histopathological techniques and immunostaining with an anti-*S. flexneri* serotype 5 LPS-specific mAb.

(A) In wild-type mice 24 hr after infection, the inflammation is starting to resolve and there is a diffuse localization of LPS, which is more abundant in bronchial/bronchiolar walls.

(B) Forty-eight hours after infection, wild-type mice show a clear resolution of the inflammation and a decrease in LPS staining.

(C) Mice with a targeted deletion in IL-1 β show a diffuse inflammation at 24 hr.

(D) This inflammatory response increases and LPS is abundant at 48 hr.

(E) In contrast, IL-18 null mice show a very intense inflammation with abundant LPS staining at 24 hr.

(F) Forty eight hours after infection, the IL-18 $^{-/-}$ mice show an unabated inflammation rich in LPS staining, reminiscent of the phenotype of *casp-1* null mice.

bacterial distribution with occlusion of a few bronchi at 24 hr postinfection and a diminution in both inflammation and the amount and distribution of LPS. This progression was similar to the one already described in Figures 3 and 4. Mice with a targeted deletion in IL-1 β showed a more localized inflammation than wild-type mice at 24 hr. This inflammatory response did not appear to progress toward resolution at 48 hr. Consistent with the results obtained from infection of *casp-1* null mice treated with recombinant IL-18, mice with a targeted deletion in IL-18 showed a very intense inflammation at 24 hr, with diffuse LPS staining, reflecting the spread of *Shigella*. At 48 hr postinfection, the inflammation was more severe, with several bronchi occluded and a continued diffuse distribution of LPS. Thus, the patterns of infection and inflammation in *casp-1* and IL-18 null mice were similar.

Discussion

Severe intestinal inflammation is a hallmark of bacillary dysentery. Therefore, to understand the pathogenesis of dysentery, it is crucial to determine how the bacteria activate this inflammatory response. In vivo, *Shigella* induces apoptosis in a rabbit ileal loop model (Zychlinsky et al., 1996), in dysenteric patients (Islam et al., 1997), and in the murine lung infection model (Figure 2). *Shigella*-induced apoptosis appears to initiate a unique cell death pathway, since, in contrast to other apoptotic stimuli (Li et al., 1995), *Shigella* does not induce apoptosis in macrophages from *casp-1* $^{-/-}$ mice (Hilbi et al.,

1998). These data probably reflect the fact that IpaB binds to Casp-1 and not to other caspases (Hilbi et al., 1998). The requirement for Casp-1 in *Shigella*-induced apoptosis allowed us to study the proinflammatory functions of this caspase in *Shigella* infection.

Shigella is an invasive bacteria that triggers an acute inflammation that eliminates the infection in humans. The murine lung model of infection mimics the invasive and proinflammatory properties of *S. flexneri* in the human intestinal mucosa. When mice are inoculated intranasally, shigellae invade the tracheobronchial and alveolar epithelia. An acute tracheobronchitis and alveolitis characterized by a massive influx of PMN results from the infection (Voino-Yasenetsky and Voino-Yasentska, 1961; Phalipon et al., 1995). Furthermore, mice, like humans, are able to control the *Shigella* infection. Noninvasive mutants of *Shigella* such as the Δ IpaB strain, used as a control in this study, do not cause pulmonary pathology (Phalipon et al., 1995), confirming the validity of the model.

Mice with a targeted deletion in *casp-1* were unable to generate an early inflammation (6 hr) or resolve the infection (Figures 1A and 4) and eventually succumbed to the infection significantly more frequently (Figure 1B) than wild-type mice. Interestingly, at later time points, the lungs of *casp-1* $^{-/-}$ mice develop more severe inflammation than that in wild-type mice. Monocytes, rather than PMN, dominated the inflammatory response in *casp-1* $^{-/-}$ mice. In order to test the induction of a proinflammatory cytokine not dependent in Casp-1 activation, we tested the concentration of IL-6 in the serum

of infected animals. At 6 hr postinfection, the levels of IL-6 were similar in *casp-1*^{-/-} and wild-type mice (data not shown), indicating that Casp-1-independent proinflammatory mechanisms were active in *casp-1* null mice. Furthermore, the distribution of *Shigella* seems to be more restricted in *casp-1*^{-/-} than in wild-type mice (Figure 4). *Shigella* is a nonmotile organism that uses the host cell cytoskeleton to move from cell to cell (Bernardini et al., 1989). Therefore, it is possible that in wild-type mice, but not in *casp-1*^{-/-} nulls, *Shigella* spreads more efficiently after tissue disruption by the inflammatory response. *casp-1*^{-/-} mice could not eradicate the *Shigella* infection (Figures 1 and 4), suggesting that only Casp-1-mediated inflammation could effectively clear the bacteria. Interestingly, there were 2-fold higher levels of serum IL-6 in *casp-1*^{-/-} than in wild-type mice, probably reflecting the persistence of the infection (data not shown). These data indicate that the host requires Casp-1 to mount the inflammatory response characteristic of shigellosis. Future investigation will determine whether the timing or the type of cell recruited in the inflammation is important for the eradication of *Shigella*.

Both IL-1 β and IL-18 are synthesized as inactive precursors that lack a secretion signal sequence and are proteolytically activated by Casp-1 (Thornberry et al., 1992; Ghayur et al., 1997; Gu et al., 1997). We used two independent approaches to test the roles of IL-1 β and IL-18 in *Shigella* infections; *casp-1*^{-/-} mice reconstituted with recombinant IL-1 β or IL-18 as well as IL-1 β null and IL-18 null mice. Recombinant IL-1 β enhanced both the inflammatory response and, more importantly, the bacterial infection load in *casp-1* null mice challenged with *Shigella* (Figure 5). Consistent with this notion, infection of IL-1 β ^{-/-} mice resulted in an inflammatory process that was more localized than in wild-type mice and that restricted the distribution of bacteria to the sites of entry more effectively than wild-type mice (Figure 7). These mice, however, progressed toward the resolution of the infection (Figure 6). It has been proposed that the destruction of the tissue by the initial inflammation in response to *Shigella* allows further bacterial infection (Perdomo et al., 1994). These data would be consistent with the hypothesis that IL-1 β is involved in the initial inflammatory response to *Shigella* and invasion into the lungs, and that in the absence of this cytokine, the infectious foci are more restricted than in wild-type mice. Indeed, IL-1 β is induced and activated very early after *Shigella* infection (Arondel et al., 1999) and blocking IL-1 with IL-1 receptor antagonist (IL-1ra) decreases the inflammation in the rabbit ileal loop model (Sansone et al., 1995).

Recombinant IL-18 reconstituted a wild type inflammatory response in *casp-1*^{-/-} mice (Figure 5). The role of IL-18 in *Shigella* infections was corroborated by the IL-18^{-/-} mice infected with *Shigella*, which did not regulate the inflammation nor control the bacterial growth (Figures 6 and 7), a phenotype similar to that observed in *casp-1* null mice. Taken together, these data show that IL-18 is required to generate an inflammatory response capable of eradicating *Shigella* effectively. IL-18 induces IFN γ and activates a Th1 response (reviewed in Dinarello, 1998). Interestingly, Way et al. showed that IFN γ -deficient mice were significantly more susceptible to *Shigella* infection at later time points (Way et al., 1998).

Given the rapid inflammatory response to *Shigella*, it would be surprising if IL-18 was acting solely as an IFN γ -inducing factor. In fact, IL-18 seems to have IFN γ -independent proinflammatory functions (Kohka et al., 1998; Shapiro et al., 1998). More detailed studies on the early events of infection using IFN γ null mice will further delineate the functions of IL-18 in *Shigella* infections.

IL-1 β is essential in the innate immune response to many different microbial pathogens (Dinarello, 1998), and recently IL-18 was also shown to be crucial in the immune response to *Mycobacterium tuberculosis* (Sugawara et al., 1999), *Salmonella typhimurium* (Mastroeni et al., 1999), *Yersinia enterocolitica* (Bohn et al., 1998), *Leishmania major*, and in sequelae to *Staphylococcus aureus* (Wei et al., 1999). The mechanisms of IL-1 β and IL-18 activation in these infections, except in *Salmonella*, are not yet clear. *Salmonella* encodes SipB, a homolog of IpaB that activates Casp-1 (Hersh et al., 1999). Recently Casp-1 was shown to be essential for the progression of salmonellosis in vivo (Monack et al., unpublished data). It remains to be determined whether Casp-1-mediated inflammation through IL-1 β and IL-18 is a common pathway in other microbial infections.

The data presented here directly link the bacterial virulence factor IpaB with the initiation of inflammation through Casp-1. We propose that Casp-1 is a component of the innate immune response. Invasion of macrophages by *Shigella* directly activates Casp-1, which triggers an acute inflammation by proteolytically activating IL-1 β and IL-18. It remains to be determined whether induction of apoptosis is necessary to allow the rapid release of these two cytokines. Thus, Casp-1 might have coevolved with the virulence factors of acute pathogens such as *Shigella*. In this model, Casp-1 emerges as a protease that coordinates the use of an apoptotic pathway to release mature cytokines.

Experimental Procedures

Bacteria and Growth Conditions

M90T, an invasive isolate of *S. flexneri* serotype 5, was our virulent strain of reference (Sansone et al., 1981). An IpaB deletion mutant of M90T referred to as Δ IpaB was used as a negative control (Ménard et al., 1993). Bacteria were routinely grown in Luria Broth at 37°C with aeration. The bacteria were washed and resuspended in RPMI for macrophage infection and in PBS for mouse infections.

Mice

casp-1^{-/-} mice were obtained from the Animal Resource Facility at BASF BioResearch Corporation (Li et al., 1995). IL-1 β ^{-/-} mice were obtained from Merck (Zheng et al., 1995), and IL-18^{-/-} mice (Takeda et al., 1998) were obtained from Dr. Kiyoshi Takeda at Osaka University. Animals were housed at the Institut Pasteur or NYU Medical Center animal facility. *casp-1* and IL-18 null mice are C57BL/6, and IL-1 β ^{-/-} mice are in the 129 Sv background. All three null strains were backcrossed at least eight times and were controlled with the appropriate isogenic mice. The course of the *Shigella* infection is indistinguishable in mice with different genetic background (P. J. S. et al., unpublished data). Control mice were obtained from the Unité de Génétique Murine and Central Animal Facility at the Institut Pasteur.

Treatment with Recombinant Cytokines

Mice were injected intraperitoneally with 0.5 μ g/mouse mature murine recombinant IL-1 β (Cirulli et al., 1998; Neveu et al., 1998) and 10 μ g/mouse IL-18 (both cytokines from Biosource International, CA) at the infection time and every 24 hr thereafter. These protocols

have been shown to be effective in other systems (Kawakami et al., 1997; Cirulli et al., 1998; Neveu et al., 1998).

Mice Infection and Bacterial Counts

Mice were inoculated intranasally with 2×10^8 bacteria in 20 μ l as described (Phalipon et al., 1995). For bacterial enumeration, the mice were sacrificed at the indicated time points and the lungs were rapidly removed "en bloc" and ground in 10 ml sterile PBS (Ultra Turax T25 apparatus, Janke and Kunkel IKA Labortechnik GmbH, Staufen, Germany). Dilutions were then plated on Trypticase Soy Broth plates for cfu enumeration. Each data point is the mean of at least 10 (range 10–12) infected mice per group from two independent experiments. Susceptibility to *Shigella* infections was done in groups of at least 16 animals.

TUNEL

Terminal d-transferase dUTP nick end labeling (TUNEL) was done using the Apoptosis Detection System, Fluorescein kit (Promega, Madison, WI). For double-labeling experiments, the sections were first labeled with anti-LPS antiserum as described (Sansone et al., 1996), then labeled with TUNEL and mounted in 50% glycerol in PBS. After photographing the LPS label by light microscopy and the TUNEL label with epifluorescence, the sections were washed, stained with H&E, dehydrated, and mounted in Permount. The same field that was photographed for LPS and TUNEL labeling was localized and photographed again. To reconstitute the TUNEL and propidium iodide label in a whole section, each field was scanned with a confocal microscope (Molecular Dynamics, Sunnyvale, CA) in both channels. The sections were reconstructed using Adobe Photoshop.

Histopathological Studies

At the indicated time points, the mice were anesthetized, their trachea catheterized, and 4% formalin injected in order to fill the bronchoalveolar space. Lungs were then removed and fixed in 4% formalin before being processed for histopathological studies. Ten-micrometer paraffin sections were stained with H&E, and observed with a BX50 Olympus microscope (Olympus Optical, Europa, GmbH, Hamburg, Germany). To quantify the inflammatory response, the microscopic images were scanned into a computer and analyzed with NIH image software. The ratio of the surface of these areas to the entire surface of the tissue section minus the anatomic "holes", i.e., the lumen of large blood vessels and bronchi, was computed as the "inflammatory index." The resulting inflammatory index was the median of at least 17 mice (range 17–24) in each group.

Statistics

All two-way comparisons were done using the Mann Whitney non-parametric test.

Acknowledgments

This work was supported by a collaborative NATO grant (CLG.976285) shared by the P. J. S. and A. Z. laboratories, by a grant from the Biotechnology Program of the French Ministère de l'Éducation Nationale de la Recherche et la Technologie to P. J. S. and by a National Institutes of Health grant (AI37720) to A. Z. We wish to thank Michel Huerre and his group (laboratoire d'histopathologie, Institut Pasteur) for excellent assistance in histopathology and Lionel Lafitte (Service Photographie, Institut Pasteur) for assistance in image analysis.

Received December 21, 1999; revised April 18, 2000.

References

Adam, T., Arpin, M., Prevost, M.C., Gounon, P., and Sansone et al., P.J. (1995). Cytoskeletal rearrangements and the functional role of T-plastin during entry of *Shigella flexneri* into HeLa cells. *J. Cell Biol.* 129, 367–381.

Arondel, J., Singer, M., Matsukawa, A., Zychlinsky, A., and Sansone et al., P.J. (1999). Increased interleukin-1 (IL-1) and imbalance between IL-1 and IL-1 receptor antagonist during acute inflammation in experimental Shigellosis. *Infect. Immun.* 67, 6056–6066.

Bernardini, M.L., Mounier, J., d'Hauteville, H., Coquis-Rondon, M., and Sansone et al., P. J. (1989). Identification of *icsA*, a plasmid locus of *Shigella flexneri* that governs bacterial intra- and intercellular spread through interaction with F-actin. *Proc. Natl. Acad. Sci. USA* 86, 3867–3871.

Bohn, E., Sing, A., Zumbihl, R., Bielfeldt, C., Okamura, H., Kurimoto, M., Heesemann, J., and Autenrieth, I.B. (1998). IL-18 (IFN-gamma-inducing factor) regulates early cytokine production in, and promotes resolution of, bacterial infection in mice. *J. Immunol.* 160, 299–307.

Chen, Y., Smith, M.R., Thirumalai, K., and Zychlinsky, A. (1996). A bacterial invasin induces macrophage apoptosis by binding directly to ICE. *EMBO J.* 15, 3853–3860.

Cirulli, F., De Acetis, L., and Alleve, E. (1998). Behavioral effects of peripheral interleukin-1 administration in adult CD-1 mice: specific inhibition of the offensive components of intermale agonistic behavior. *Brain Res.* 27, 308–312.

Dinarello, C. (1998). Interleukin-18, Interleukin-18, and the Interleukin-1 beta converting enzyme. *Ann. N.Y. Acad. Sci.* 856, 1–11.

Ghayur, T., Banerjee, S., Hugunin, M., Butler, D., Herzog, L., Carter, A., Quintal, L., Sekut, L., Talanian, R., Paskind, M., et al. (1997). Caspase-1 processes IFN-gamma-inducing factor and regulates LPS-induced IFN-gamma production. *Nature* 386, 619–623.

Gu, Y., Kuida, K., Tsutsui, H., Ku, G., Hsiao, K., Okamura, H., Nakaniishi, K., Kurimoto, M., Tanimoto, T., Flavell, R.A., et al. (1997) Activation of interferon- γ inducing factor mediated by interleukin-18 converting enzyme. *Science* 275, 206–209.

Hale, T.L. (1991). Genetic basis of virulence in *Shigella* species. *Microbiol. Rev.* 55, 206–224.

Hersh, D., Monack, D., Smith, M., Ghori, N., Falkow, S., and Zychlinsky, A. (1999). The *Salmonella* invasin SipB induces macrophage apoptosis by binding to Caspase-1. *Proc. Natl. Acad. Sci. USA* 96, 2396–2401.

Hilbi, H., Moss, J.E., Hersh, D., Chen, Y., Arondel, J., Banerjee, S., Flavell, R.A., Yuan, J., Sansone et al., P.J., and Zychlinsky, A. (1998). *Shigella*-induced apoptosis is dependent on caspase-1 which binds to IpaB. *J. Biol. Chem.* 273, 32895–32900.

Islam, D., Veress, B., Bardhan, P.K., Lindberg, A.A., and Christensson, B. (1997). In situ characterization of inflammatory responses in the rectal mucosae of patients with Shigellosis. *Infect. Immunol.* 65, 739–749.

Kawakami, K., Qureshi, M.H., Zhang, T., Okamura, H., Kurimoto, M., Saito, A. (1997). IL-18 protects mice against pulmonary and disseminated infection with *Cryptococcus neoformans* by inducing IFN-gamma production. *J. Immunol.* 159, 5528–5534.

Kohka, H., Yoshino, T., Iwagaki, H., Sakuma, I., Tanimoto, T., Matsuo, Y., Kurimoto, M., Orita, K., Akagi, T., and Tanaka, N. (1998). Interleukin-18/interferon-gamma-inducing factor, a novel cytokine, up-regulates ICAM-1 (CD54) expression in KG-1 cells. *J. Leukoc. Biol.* 64, 519–527.

Kotloff, K.L., Winickoff, J.P., Ivanoff, B., Clemens, J.D., Swerdlow, D.L., Sansone et al., P.J., Adak, G.K., and Levine, M.M. (1999). Global burden of *Shigella* infections: implications for vaccine development and implementation of control strategies. *Bull. World Health Organ.* 77, 651–666.

Kuida, K., Lippke, J.A., Ku, G., Harding, M.W., Livingston, D.J., Su, M.S.-S., and Flavell, R.A. (1995). Altered cytokine export and apoptosis in mice deficient in interleukin-1 β converting enzyme. *Science* 267, 2000–2003.

Li, P., Allen, H., Banerjee, S., Franklin, S., Herzog, L., Johnston, C., McDowell, J., Paskind, M., Rodman, L., Salfeld, J., et al. (1995). Mice deficient in IL-1 β -converting enzyme are defective in production of mature IL-1 β and resistant to endotoxic shock. *Cell* 80, 401–411.

Lindberg, A.A., and Pál, T. (1993). Strategies for development of potential candidate *Shigella* vaccines. *Vaccine* 11, 168–179.

MacDermott, R.P. (1994). Alterations in the mucosal immune system in ulcerative colitis and Crohn's disease. *Med. Clin. North Am.* 78, 1207–1231.

Mastroeni, P., Clare, S., Khan, S., Harrison, J.A., Hommaeche, C.E.,

- Okamura, H., Kurimoto, M., and Dougan, G. (1999). Interleukin 18 contributes to host resistance and gamma interferon production in mice infected with virulent *Salmonella typhimurium*. *Infect. Immun.* 67, 478-483.
- Mathan, M.M., and Mathan, V.I. (1991). Morphology of rectal mucosa of patients with shigellosis. *Rev. Infect. Dis.* 13, suppl.4, S314-318.
- Maurelli, A.T., and Sansonetti, P.J. (1988). Genetic determinants of *Shigella* pathogenicity. *Ann. Rev. Microbiol.* 42, 127-150.
- Ménard, R., Sansonetti, P.J., and Parsot, C. (1993). Nonpolar mutagenesis of the *ipa* genes defines IpaB, IpaC, and IpaD as effectors of *Shigella flexneri* entry into epithelial cells. *J. Bacteriol.* 175, 5899-5906.
- Miura, M., Zhu, H., Rotello, R., Hartwig, E.A., and Yuan, J. (1993). Induction of apoptosis in fibroblasts by IL-1 β converting enzyme, a mammalian homologue of the *C. elegans* cell death gene *ced-3*. *Cell* 75, 653-660.
- Neveu, P.J., Bluthé, R.M., Liege, S., Moya, S., Michaud, B., and Dantzer, R. (1998). Interleukin-1-induced sickness behavior depends on behavioral lateralization in mice. *Physiol. Behav.* 15, 587-590.
- Perdomo, O.J., Cavaillon, J.M., Huerre, M., Ohayon, H., Gounon, P., and Sansonetti, P.J. (1994). Acute inflammation causes epithelial invasion and mucosal destruction in experimental shigellosis. *J. Exp. Med.* 180, 1307-1319.
- Phalipon, A., Kaufmann, M., Michetti, P., Cavaillon, J.M., Huerre, M., Sansonetti, P.J., and Kraehenbuhl, J.P. (1995). Monoclonal immunoglobulin A antibody directed against serotype-specific epitope of *Shigella flexneri* lipopolysaccharide protects against murine experimental shigellosis. *J. Exp. Med.* 182, 769-778.
- Sansonetti, P.J., Kopecko, D.J., and Formal, S.B. (1981). *Shigella sonnei* plasmids: evidence that a large plasmid is necessary for virulence. *Infect. Immun.* 34, 75-83.
- Sansonetti, P.J., Ryter, A., Clerc, P., Maurelli, A.T., and Mounier, J. (1986). Multiplication of *Shigella flexneri* within HeLa cells: lysis of the phagocytic vacuole and plasmid-mediated contact hemolysis. *Infect. Immun.* 51, 461-469.
- Sansonetti, P.J., Arondel, J., Cavaillon, J.-M., and Huerre, M. (1995). Role of IL-1 in the pathogenesis of experimental shigellosis. *J. Clin. Inv.* 96, 884-892.
- Sansonetti, P.J., Arondel, J., Cantey, R., Prevost, M.C., and Huerre, M. (1996). Infection of rabbit Peyer's patches by *Shigella flexneri*: effect of adhesive or invasive bacterial phenotypes on follicle-associated epithelium. *Infect. Immun.* 64, 2752-2764.
- Sartor, R.B. (1995). Current concepts in the etiology and pathogenesis of ulcerative colitis and Crohn's disease. *Gastroenterol* 24, 475-508.
- Savill, J. (1997). Apoptosis in resolution of inflammation. *J. Leuk. Biol.* 61, 375-380.
- Shapiro, L., Puren, A.J., Barton, H.A., Novick, D., Peskind, R.L., Shenkar, R., Gu, Y., Su, M.S., and Dinarello, C.A. (1998). Interleukin 18 stimulates HIV type 1 in monocytic cells. *Proc. Natl. Acad. Sci. USA* 95, 12550-12555.
- Sugawara, I., Yamada, H., Kaneko, H., Mizuno, S., Takeda, K., and Akira, S. (1999). Role of interleukin-18 (IL-18) in mycobacterial infection in IL-18-gene-disrupted mice. *Infect. Immun.* 67, 2585-2589.
- Takeda, K., Tsutsui, H., Yoshimoto, T., Adachi, O., Yoshida, N., Kishimoto, T., Okamura, H., Nakanishi, K., and Akira, S. (1998). Defective NK cell activity and Th1 response in IL-18-deficient mice. *Immunity* 8, 383-390.
- Thirumalai, K., Kim, K., and Zychlinsky, A. (1997). IpaB, a *Shigella flexneri* invasin, colocalizes with Interleukin-1 β converting enzyme (ICE) in the cytoplasm of macrophages. *Infect. Immun.* 65, 787-793.
- Thornberry, N.A., Bull, H.G., Calaycay, J.R., Chapman, K.T., Howard, A.D., Kostura, M.J., Miller, D.K., Molineaux, S.M., Weidner, J.R., Aunins, J., et al. (1992). A novel heterodimeric cysteine protease is required for interleukin-1 β processing in monocytes. *Nature* 356, 768-774.
- Voyno-Yasenetsky, M.V., and Voyno-Yasenetska, M.K. (1961). Experimental pneumonia caused by bacteria of the *Shigella* group. *Act. Morphol.* X, 440-454.
- Way, S.S., Borczuk, A.C., Borczuk, A.C., Dominitz, R., and Goldberg, M.B. (1998). An essential role for gamma interferon in innate resistance to *Shigella flexneri* infection. *Infect. Immun.* 66, 1342-1348.
- Wei, X.Q., Leung, B.P., Niedbala, W., Piedrafita, D., Feng, G.J., Sweet, M., Dobbie, L., Smith, A.J., and Liew, F.Y. (1999). Altered immune responses and susceptibility to *Leishmania major* and *Staphylococcus aureus* infection in IL-18-deficient mice. *J. Immunol.* 163, 2821-2828.
- Zheng, H., Fletcher, D., Kozak, W., Jiang, M., Hofmann, K.J., Conn, C.A., Soszynski, D., Grabiec, C., Trumbauer, M.E., and Shaw, A. (1995). Resistance to fever induction and impaired acute-phase response in interleukin-1 beta-deficient mice. *Immunity* 3, 9-19.
- Zychlinsky, A., Prevost, M.C., and Sansonetti, P.J. (1992). *Shigella flexneri* induces apoptosis in infected macrophages. *Nature* 358, 167-168.
- Zychlinsky, A., Thirumalai, K., Arondel, J., Cantey, J. R., Aliprantis, A., and Sansonetti, P.J. (1996). In vivo apoptosis in *Shigella flexneri* infections. *Infect. Immun.* 64, 5357-5365.

Expression of Interleukin-18 in the Lung after Endotoxemia or Hemorrhage-Induced Acute Lung Injury

Patrick G. Arndt, Giamilla Fantuzzi, and Edward Abraham

Divisions of Pulmonary and Critical Care Medicine, and Infectious Diseases, University of Colorado Health Sciences Center, Denver, Colorado

Hemorrhage and endotoxemia are important risk factors for the development of acute lung injury. Interleukin (IL)-18 is a recently described cytokine released in its mature, active form after pro-IL-18 is cleaved by the IL-1 converting enzyme (ICE). IL-18 has multiple immunomodulating properties, including induction of interferon- γ (IFN- γ), IL-1 β , tumor necrosis factor- α , and intercellular adhesion molecule-1. To examine the possible involvement of IL-18 in acute lung injury, we examined its expression, as well as that of IFN- γ , IL-12, and ICE, using murine hemorrhage or endotoxemia models. The amounts of IL-18 messenger RNA (mRNA) increased in the lung after hemorrhage or endotoxemia. However, only endotoxemia was associated with elevations in lung and plasma concentrations of IL-18 protein. ICE expression was increased in the lungs after endotoxemia but not after hemorrhage. Although IFN- γ expression increased in the lungs after hemorrhage or endotoxemia, elevations in lung IL-12 mRNA levels were found only after endotoxemia. These results indicate that hemorrhage and endotoxemia induce different patterns of immunomodulatory cytokine expression in the lungs. In particular, differences in the expression of ICE after hemorrhage or endotoxemia may affect generation of the active forms of downstream cytokines, including IL-18. IFN- γ expression in the lungs after hemorrhage appears to occur through a pathway independent of IL-12 and IL-18. IL-18 may play a role in modulating the development of acute lung injury after endotoxemia but not after hemorrhage.

Acute lung injury (ALI) and its most severe form, acute respiratory distress syndrome (ARDS), are important clinical entities affecting approximately 150,000 patients in the United States per year (1, 2). Infection and blood loss are two major, well-described etiologies predisposing to the development of ALI (1, 2). Endotoxemia or hemorrhage induces increases in the expression of proinflammatory cytokines, including tumor necrosis factor (TNF)- α , interleukin (IL)-1 β , IL-1 α , interferon (IFN)- γ , and macrophage inflammatory peptide-2 in murine lung cells (3–8), and increased levels of TNF- α and IFN- γ are present in bronchoalveolar lavage fluid (BALF) after hemorrhage (8).

(Received in original form June 15, 1999 and in revised form January 6, 2000)

Address correspondence to: Edward Abraham, M.D., Division of Pulmonary and Critical Care Medicine, University of Colorado Health Sciences Center, 4200 East Ninth Avenue, Box C-272, Denver, CO 80262. E-mail: Edward.Abraham@UCHSC.edu

Abbreviations: acute lung injury, ALI; acute respiratory distress syndrome, ARDS; bronchoalveolar lavage fluid, BALF; electrochemiluminescence, ECL; glyceraldehyde-3-phosphate dehydrogenase, G3PDH; hypoxanthine phospho-ribosyl transferase, HPRT; interleukin-1 converting enzyme, ICE; interferon, IFN; interleukin, IL; lipopolysaccharide, LPS; messenger RNA, mRNA; phosphate-buffered saline, PBS; reverse transcriptase/polymerase chain reaction, RT-PCR; standard error of the mean, SEM; tumor necrosis factor, TNF.

Am. J. Respir. Cell Mol. Biol. Vol. 22, pp. 708–713, 2000
Internet address: www.atsjournals.org

These experimental findings correlate with those from clinical studies where elevated levels of immunoregulatory cytokines, including IL-1 β , IL-8, TNF- α , and IL-6, are present in the plasma and BALF of patients with ARDS compared with control patients receiving mechanical ventilation (9–12). Recently, the proinflammatory activity of BALF was shown to be significantly greater than that of plasma in patients with ARDS, suggesting that the lung is an active, local site of inflammation in this setting (13, 14).

IL-18, also called interferon gamma inducing factor, is a recently described cytokine initially isolated from hepatic Kupffer cells (15–18). IL-18 is constitutively expressed in lung, skin, skeletal muscle, kidney, and pancreas (18, 19). In *in vitro* studies, IL-18 increases IL-1 β , TNF- α , IL-8, IL-2, and granulocyte macrophage colony-stimulating factor (GM-CSF) release (20–22), decreases IL-10 release (20), up-regulates intercellular adhesion molecule-1 expression (23), enhances T-cell proliferation (20, 24), increases natural killer cell activity through Fas ligand-mediated pathways (25–27), and can decrease angiogenesis in tumor models (28).

Similar to pro-IL-1 β , pro-IL-18 lacks a signal sequence and requires cleavage to its mature and active form, which is then secreted (29, 30). The interleukin-1 converting enzyme (ICE) is the predominant enzyme responsible for the cleavage of pro-IL-18 to mature IL-18 (29–31).

The importance of IL-18 in the underlying pathophysiologic response to endotoxemia, an important risk factor for the development of ALI, was recently illustrated in IL-18 receptor knockout mice that were resistant to the effects of endotoxemia compared with wild-type control mice (27). However, little is known concerning the kinetics of expression of IL-18 in the lungs after endotoxemia or other inflammatory insults, such as blood loss, that are associated with the development of ALI. We therefore investigated the effects of endotoxemia and hemorrhage on IL-18 and ICE expression in the lungs. Because IL-12 and IL-18 have overlapping properties of inducing IFN- γ expression (32–36), we also examined the ability of endotoxemia or hemorrhage to modulate pulmonary expression of IL-12 and IFN- γ .

Materials and Methods

Animals

Male BALB/c mice, ages 8 to 12 wk, were obtained from Harlan Sprague Dawley (Indianapolis, IN) and housed in the University of Colorado Health Sciences Center animal care facility. Mice were kept on a 12-h light/dark cycle with free access to food and water.

Endotoxemia or Hemorrhage Models

The endotoxemia and hemorrhage models used in these experiments have been described previously by our laboratory (3, 4, 6–

8). Both are associated with onset of ALI within 72 h as evidenced by pulmonary neutrophil infiltration, interstitial pulmonary edema, and proteinaceous alveolar exudate (3, 7, 37, 38).

For endotoxemia, mice were injected intraperitoneally with lipopolysaccharide (*Escherichia coli* 0111:B4; Sigma, St. Louis, MO) at the dose of 25 mg/kg in 0.2 ml phosphate-buffered saline (PBS). Control mice received 0.2 ml PBS intraperitoneally. Hemorrhage was performed by removal of 30% of the calculated total blood volume (0.55 ml for a 20-g mouse) by cardiac puncture over 60 s under methoxyflurane anesthesia. With this method, overall mortality is < 12%, with no evidence of bleeding into the pericardial space, hemothorax, or lung or cardiac contusion (3, 4, 6–8). Control animals underwent cardiac puncture under methoxyflurane anesthesia without blood removal.

Lung Isolation and BALF Collection

At predetermined time points, mice were exsanguinated by cardiac puncture under methoxyflurane anesthesia. The blood was drawn into a heparinized syringe (5 U heparin), then centrifuged at 2,500 rpm for 10 min for plasma collection. After death, the chest cavity was opened, the right ventricle flushed with 3 to 5 ml of PBS at 4°C, and the lungs removed with avoidance of the peritracheal lymph nodes (3, 5, 8). The lungs were then snap-frozen in liquid nitrogen with the right lung used for RNA extraction and the left lung used for protein analysis.

Semiquantitative Reverse Transcriptase/Polymerase Chain Reaction

The techniques used for semiquantitative reverse transcriptase/polymerase chain reaction (RT-PCR) have been previously described by our laboratory (3–8). Total RNA was isolated from the right lung by phenol-chloroform extraction after homogenization in 2 ml of 4 M guanidine thiocyanate/5 mM sodium citrate/0.5% sarcosyl and 0.1 M 2-mercaptoethanol. Complementary DNA (cDNA) was then synthesized from 1 µg total RNA using Moloney murine leukemia virus reverse transcriptase and random hexamer oligonucleotides as previously described by our laboratory (3, 4, 6–8).

Semiquantitative PCR for IL-18, IFN- γ , IL-12, and ICE was performed using 5 µl of the cDNA mixture under the following cycle conditions (except for ICE): initial 2 min 94°C denaturation step followed by 30 to 38 cycles of 60 s, 94°C denaturation; 60 s, 55 to 65°C annealing (depending on cytokine primers); and 60 s, 72°C extension. A final 4-min extension at 72°C was then performed. For ICE, the cycle conditions were an initial 1 min 95°C denaturation step followed by 38 to 40 cycles of 30 s, 94°C denaturation; 30 s, 54°C annealing; and 60 s, 72°C extension. This was followed by a 5-min 72°C final extension step. PCR products were visualized by electrophoresis on 1.6% agarose gels with ethidium bromide staining. Cycle number was adjusted so that the PCR products were between barely visible and below saturation. The housekeeping genes glyceraldehyde-3-phosphate dehydrogenase (G3PDH) and hypoxanthine phospho-ribosyl transferase (HPRT) were used as controls. Analysis of the gel was done by densitometry (ImageStore 5000; UVP, San Gabriel, CA) with relative absorbance determined by comparison of the density of the PCR product of the cytokine of interest to the housekeeping gene.

Measurement of IL-18 Protein

For assessment of IL-18 protein levels, an electrochemiluminescence (ECL) assay was used. The techniques used for the ECL assay have been described previously (22). Briefly, the left lung was homogenized in lysis buffer containing *N*-2-hydroxyethylpiperazine-*N'*-ethane sulfonic acid 10 mM, NaCl 150 mM, Igepal 1% vol/vol, ethylenediaminetetraacetic acid 1 mM, leupeptin 1 µg/ml,

phenylmethylsulfonyl fluoride 100 µg/ml, aprotinin 1 µg/ml, pepstatin 1 µg/ml, and soybean trypsin inhibitor 1 µg/ml; centrifuged at 2,500 rpm for 10 min; and the supernatant was then removed, aliquoted, and kept at –80°C until analyzed for IL-18 levels. Antibodies used were an affinity-purified, antimurine IL-18 polyclonal antibody (R&D Systems, Minneapolis, MN) that was labeled with biotin (Igen Inc., Gaithersburg, MD) as per manufacturer's protocol, and a monoclonal, antimurine IL-18 antibody (R&D Systems) labeled with ruthenium (II) trisbipyride chelate (Igen) as per the manufacturer's instructions. The biotinylated antibody was diluted to a final concentration of 0.5 µg/ml in PBS (pH 7.4) containing 0.25% bovine serum albumin, 0.5% Tween-20, and 0.01% azide (ECL buffer). In each assay tube, 25 µl of the above biotinylated anti-IL-18 antibody was incubated at room temperature with 25 µl of a 1-mg/ml solution of streptavidin-coated paramagnetic beads (Dynal Corp., Lake Success, NY), diluted in ECL buffer for 30 min with mixing by vigorous shaking. To each assay tube, 25 µl of sample or standard concentrations of recombinant murine IL-18 (Pepro-Tech Inc., Rocky Hill, NJ) were added, followed by 25 µl of the ruthenylated antibody (final concentration 1 mg/ml, diluted in ECL buffer), and incubated overnight at room temperature with shaking. The reaction was quenched with 200 µl of PBS per tube and the amount of chemiluminescence was determined using an Origen 1.5 analyzer (Igen Inc.). A standard curve was constructed using recombinant IL-18 (Pepro-Tech, Inc.). The IL-18 ECL detects both pro- and mature IL-18 with a sensitivity of 20 pg/ml.

Statistical Analysis

Groups of 5 to 8 mice were used for each time point. For each experimental condition, groups of control, unmanipulated animals were included. Data are presented as mean normalized to controls \pm standard error of the mean (SEM) for each experimental group. Groups were compared using one-way analysis of variance and the Tukey-Kramer multiple comparison tests for differences between groups. A *P* value < 0.05 was considered to be statistically significant.

Results

IL-18 Expression Is Increased in the Lung after Endotoxemia or Hemorrhage

As reported previously (18, 19), we found that IL-18 messenger RNA (mRNA) is constitutively expressed in the lung (Figure 1). As early as 1 h after endotoxemia, there was increased expression of IL-18 mRNA in the lungs, followed by a decrease to below baseline levels of expression 4 h after endotoxin administration. No detectable IL-18 mRNA, even with 40 cycles of PCR, could be found 8 h after endotoxemia (Figures 1A and 1B).

Amounts of IL-18 mRNA were increased in the lung after hemorrhage. As shown in Figure 1, IL-18 expression in the lungs increased more slowly after hemorrhage than after endotoxemia, with peak in IL-18 mRNA levels being present 4 h after hemorrhage with return to below baseline levels 4 h later.

IL-18 Protein Levels Are Increased in the Lung and Plasma after Endotoxemia but Not after Hemorrhage

Because alteration in IL-18 mRNA levels may not necessarily correlate with changes in protein, we investigated IL-18 protein in the lung and plasma of mice either given endotoxin or hemorrhaged. Significant increases in IL-18 protein were present in the lungs 1 h after endotoxemia (Figure

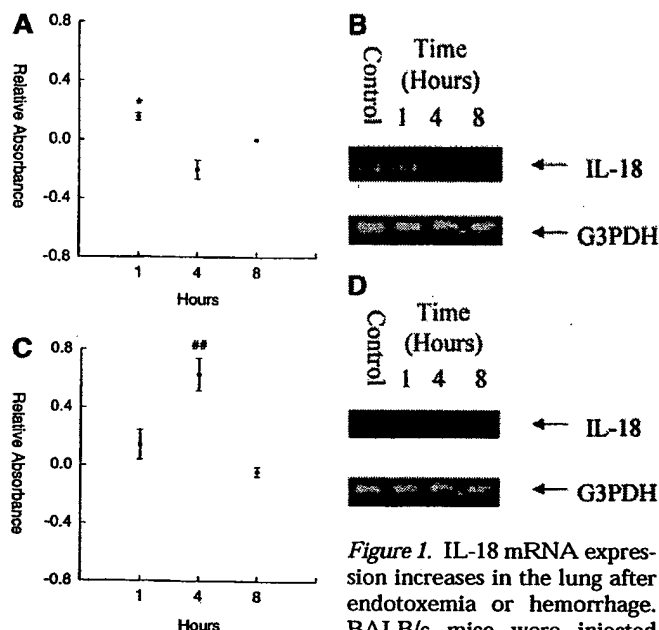


Figure 1. IL-18 mRNA expression increases in the lung after endotoxemia or hemorrhage. BALB/c mice were injected

with LPS or PBS as control (A and B) or were hemorrhaged 30% of their blood volume (C and D). At the indicated time points, RT-PCR for IL-18 was performed. No IL-18 PCR product was visualized 8 h after endotoxemia, even after 40 cycles. Results are normalized to G3PDH and are expressed as relative absorbance normalized to controls \pm SEM. * $P < 0.05$, ** $P < 0.001$. Representative gels for IL-18 mRNA expression after LPS (B) or hemorrhage (D) are shown.

2A). Pulmonary IL-18 levels remained significantly elevated, compared with those present in unmanipulated mice, 4 h after endotoxemia, and then returned to baseline levels 8 h after endotoxin administration. In contrast to the increased levels of IL-18 present in the lung after endotoxemia, we did not find any significant alterations in IL-18 protein in the lung during the 8-h period after hemorrhage. In bronchoalveolar lavage, IL-18 was undetectable in control, unmanipulated mice and at all time points after endotoxemia or hemorrhage (data not shown).

In plasma, low levels of IL-18 were found at baseline. Increases in plasma IL-18 occurred as early as 1 h after endotoxin administration, reached statistical significance 4 h after endotoxemia, and then returned to baseline 4 h later

(Figure 2B). In contrast to endotoxemia, hemorrhage did not produce any statistically significant changes in plasma IL-18 levels (data not shown).

IFN- γ Expression Is Increased in the Lung after Endotoxemia or Hemorrhage

IFN- γ mRNA levels rose after endotoxin injection, with significant increases, compared with baseline, being present 4 and 8 h after endotoxin administration (Figure 3A). The expression of IFN- γ mRNA in the lung also increased after hemorrhage, but with kinetics different from those seen after endotoxin administration. The peak in expression of IFN- γ mRNA occurred 4 h after hemorrhage and was of short duration, with a return to below baseline 8 h after blood loss (Figure 3B).

Expression of IL-12 mRNA Is Increased in the Lung after Endotoxemia but Not after Hemorrhage

IL-12 induces IFN- γ expression both alone and in synergy with IL-18, in part by upregulating IL-18 receptors (32–36). In the present experiments, there was a rapid, but transient, increase in the expression of IL-12 mRNA in the lung after endotoxin administration (Figure 4). IL-12 mRNA levels were significantly greater than those present in the lungs of control, unmanipulated mice 1 h after endotoxin administration. By 4 h after endotoxin administration, IL-12 expression was similar to baseline. After hemorrhage, the only significant alteration in IL-12 expression was a decrease 8 h after blood loss.

ICE mRNA Expression Is Increased in the Lung after Endotoxemia but Not after Hemorrhage

Because ICE is important in cleaving pro-IL-18 to mature IL-18 (29–31), we investigated its expression in the lung after endotoxemia or hemorrhage. ICE mRNA was constitutively present in the lung (Figure 5), and then increased 4 h after endotoxemia, before returning to baseline levels 8 h after endotoxin administration (Figure 5). After hemorrhage, there was no alteration in the expression of ICE mRNA in the lung at any of the time points investigated.

Discussion

In these experiments, we found that endotoxemia and hemorrhage produce rapid increases in the expression of IL-18 mRNA in the lung, present between 1 and 4 h, re-

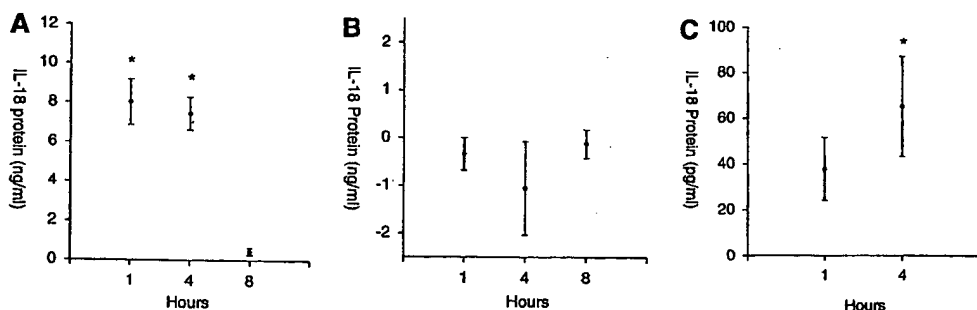


Figure 2. (A and B) IL-18 protein levels are increased in the lung after endotoxemia, but not after hemorrhage. BALB/c mice were injected with LPS or PBS as control (A) or were hemorrhaged 30% of their total blood volume (B). At the indicated time points, whole lung IL-18 protein was determined. Results are normalized to controls and are expressed as mean \pm SEM. * $P < 0.001$. (C) IL-18 protein levels

are increased in plasma after endotoxemia, but not after hemorrhage. BALB/c mice were injected with LPS or PBS as control. At the indicated time points, plasma was collected and IL-18 levels determined. Results are normalized to controls and are expressed as mean \pm SEM. * $P < 0.05$.

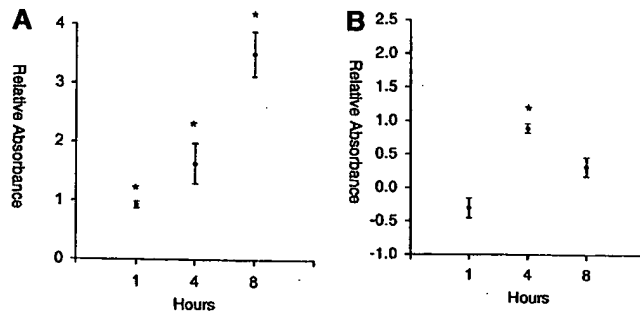


Figure 3. IFN- γ mRNA expression increases in the lung after endotoxemia or hemorrhage. BALB/c mice were injected with LPS or PBS as control (A) or were hemorrhaged 30% of their total blood volume (B). At the indicated time points, RT-PCR for IFN- γ was performed. Results are normalized to G3PDH and are expressed as relative absorbance normalized to controls \pm SEM. * $P < 0.001$.

spectively, after each of these conditions. The kinetics of IL-18 mRNA expression in the lung after endotoxemia or hemorrhage are consistent with those reported in previous *in vitro* studies (39, 40). In keratinocytes exposed to contact allergens, IL-18 mRNA levels increased between 4 and 6 h (39). When human peripheral blood mononuclear cells are exposed to endotoxin, IL-18 mRNA levels peak between 2 and 6 h (40). In the only other *in vivo* study investigating IL-18 after endotoxemia, an increase in IL-18 mRNA levels in murine splenocytes was found within 2 h after endotoxin administration (41). In that study, pulmonary expression of IL-18 was not examined (41).

In addition to inducing increases in IL-18 mRNA expression, we found that endotoxin administration was followed by increased IL-18 protein in the lung and plasma. The elevations in lung and plasma IL-18 protein levels were of short duration, occurring between 1 and 4 h after endotoxemia, and suggest that IL-18 may be active in the lung early in the proinflammatory response. Our findings of increased IL-18 plasma levels after endotoxemia are similar to the kinetics of IL-18 protein levels seen in an

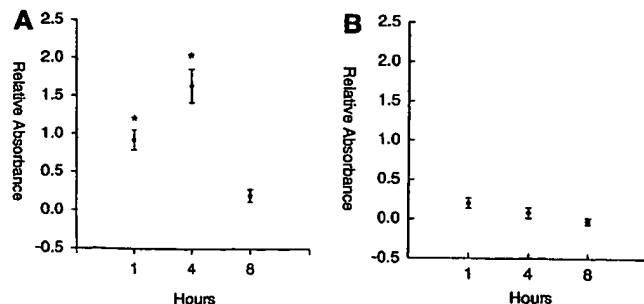


Figure 4. IL-12 mRNA expression is increased in the lung after endotoxemia, but not after hemorrhage. BALB/c mice were injected with LPS or PBS as control (A) or were hemorrhaged 30% of their total blood volume (B). At the indicated time points, RT-PCR for IL-12 was performed on excised lungs. Results are normalized to HPRT and are expressed as relative absorbance normalized to controls \pm SEM. * $P < 0.001$.

earlier *in vivo* study (15) where IL-18 serum levels peaked 2 h after endotoxemia, with a gradual return to baseline over the next 4 h.

We did not find an increase in IL-18 protein levels in the lung or plasma after hemorrhage, suggesting that there are differences in the post-transcriptional regulation and therefore probable importance of IL-18 in these two models of ALI. The explanation for the lack of an increase in IL-18 levels after hemorrhage, in the face of elevated IL-18 mRNA expression, may be related to differences in ICE activity after endotoxemia or hemorrhage. We found that ICE expression in the lung was increased after endotoxemia, but not after hemorrhage. Unlike pro-IL-1 β where proteases other than ICE are able to generate mature IL-1 β , ICE is currently the only known protease able to cleave pro-IL-1 β into its mature and active form (29-31).

Endotoxin-associated increases in IFN- γ mRNA levels occurred after the peak in IL-18 mRNA expression and simultaneously with the peak in IL-18 plasma levels. This suggests that IL-18 may be responsible for the enhanced expression of IFN- γ in the lung after endotoxemia. Previous studies showed that IL-18 occupies an important role in inducing IFN- γ expression after endotoxemia (15, 16, 27, 31). In particular, IFN- γ expression was markedly reduced both in ICE and in IL-18 knockout mice compared with wild-type control mice after endotoxin administration (27, 31).

Because IL-18 protein levels do not increase in the lungs after hemorrhage, other factors would appear to be responsible for inducing IFN- γ expression in this setting. The importance of IL-18 in inducing IFN- γ expression af-

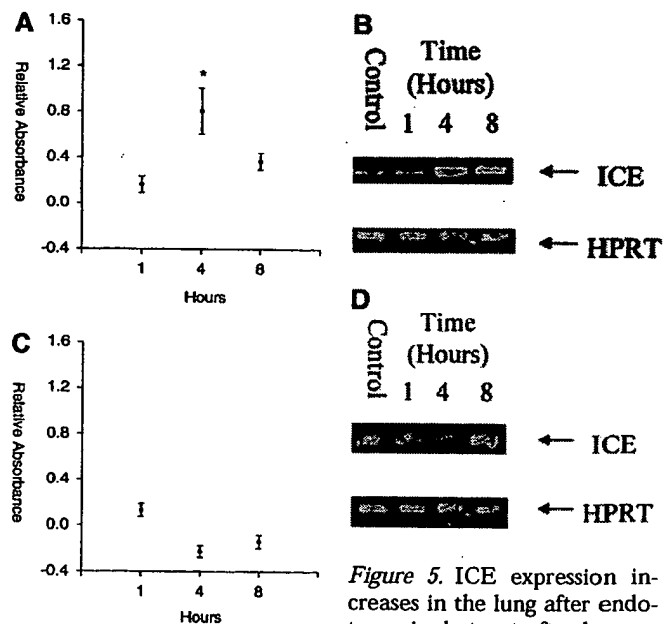


Figure 5. ICE expression increases in the lung after endotoxemia, but not after hemorrhage. BALB/c mice were injected with LPS or PBS as control (A and B) or were hemorrhaged 30% of their total blood volume (C and D). At the indicated time points, RT-PCR for ICE was performed. Results are normalized to HPRT and are expressed as relative absorbance normalized to controls \pm SEM. * $P < 0.001$. Representative gels for ICE mRNA expression after LPS (B) or hemorrhage (D) are shown.

ter inflammatory insults other than endotoxemia has not been well characterized. A recent study showed that IL-18 is important for IFN- γ expression after zymosan exposure (31). However, there are no previous studies that have investigated interrelationships between IL-18 and IFN- γ after hemorrhage.

IL-2, TNF- α , and IL-12 can increase IFN- γ expression (15, 33–36, 42). IL-12, although considered a weaker inducer of IFN- γ than IL-18, increases IFN- γ expression, both primarily and in synergy with IL-18 (32–36). In our study, we failed to find an increase in IL-12 mRNA levels in the lung after hemorrhage, indicating that IL-12 was unlikely to have been responsible for the observed effects on IFN- γ . In previous studies (4), we found that hemorrhage resulted in upregulation of TNF- α , but not of IL-2, in the lungs, suggesting that TNF- α , but not IL-2, may play a role in modulating IFN- γ expression after blood loss. Additionally, signaling through the p38 mitogen-activated protein (MAP) kinase pathway has previously been shown to upregulate IFN- γ expression *in vitro* (43). This suggests that other mediators, such as IL-1 β , IL-3, and GM-CSF, which use the p38 MAP kinase signaling pathway, may be involved in the induction of IFN- γ expression in the lung after hemorrhage (43).

Acknowledgments: This study was supported in part by National Institutes of Health grant HL 50284 (E.A.) and Glaxo Wellcome Pulmonary Fellowship Award (P.G.A.).

References

- Hudson, L., J. Milberg, D. Anardi, and R. Maunder. 1995. Clinical risk for development of acute respiratory distress syndrome. *Am. J. Respir. Crit. Care Med.* 151:293–301.
- Garber, B., P. Hebert, J. D. Yelle, R. Hodder, and J. McGowan. 1996. Adult respiratory distress syndrome: a systemic overview of incidence and risk factors. *Crit. Care Med.* 24:687–695.
- Shenkar, R., W. Coulson, and E. Abraham. 1994. Hemorrhage and resuscitation induce alterations in cytokine expression and the development of acute lung injury. *Am. J. Respir. Cell Mol. Biol.* 10:290–297.
- Shenkar, R., and E. Abraham. 1993. Effects of hemorrhage on cytokine gene transcription. *Lymphokine Cytokine Res.* 12:237–247.
- Abraham, E., D. Kaneko, and R. Shenkar. 1999. Effects of endogenous and exogenous catecholamine on LPS-induced neutrophil trafficking and activation. *Am. J. Physiol.* 276:L1–L8.
- Tulzo, Y., R. Shenkar, D. Kaneko, P. Mione, G. Fantuzzi, C. Dinarello, and E. Abraham. 1997. Hemorrhage increases cytokine expression in lung mononuclear cells in mice. *J. Clin. Invest.* 99:1516–1524.
- Abraham, E., S. Bursten, R. Shenkar, J. Albee, R. Tudor, P. Woodson, D. Guidot, C. Rice, J. Singer, and J. Repine. 1995. Phosphatidic acid signaling mediates lung cytokine expression and lung inflammatory injury after hemorrhage in mice. *J. Exp. Med.* 181:569–575.
- Abraham, E., W. F. Coulson, M. D. Schwartz, and J. Albee. 1994. Effects of therapy with soluble tumor necrosis factor receptor fusion protein on pulmonary cytokine expression and lung injury following hemorrhage and resuscitation. *Clin. Exp. Immunol.* 98:29–34.
- Millar, A. B., M. Singer, A. Meager, N. M. Foley, N. Johnson, and G. A. W. Rook. 1989. Tumour necrosis factor in bronchopulmonary secretions of patients with adult respiratory distress syndrome. *Lancet* 2:712–713.
- Chollet-Martin, S., P. Montravers, C. Gibert, C. Elbim, J. M. Desmonts, J. Y. Fagon, and M. A. Gougerot-Pocidalo. 1993. High levels of interleukin-8 in the blood and alveolar spaces of patients with pneumonia and adult respiratory distress syndrome. *Infect. Immun.* 61:4553–4559.
- Miller, E. J., A. B. Cohen, S. Nagao, D. Griffith, R. J. Maunder, T. R. Martin, J. P. Weiner-Kronish, M. Sticherling, E. Christophers, and M. A. Matthay. 1992. Elevated levels of NAP-1/interleukin-8 are present in the air-spaces of patients with the adult respiratory distress syndrome and are associated with increased mortality. *Am. Rev. Respir. Dis.* 146:427–432.
- Chollet-Martin, S., B. Jourdain, C. Gibert, C. Elbim, J. Chastre, and M. A. Gougerot-Pocidalo. 1996. Interactions between neutrophils and cytokines in blood and alveolar spaces during ARDS. *Am. J. Respir. Crit. Care Med.* 153:594–601.
- Pugin, J., B. Ricou, K. Steinberg, P. Suter, and T. Martin. 1996. Proinflammatory activity in bronchoalveolar lavage fluids from patients with ARDS, a prominent role for interleukin-1. *Am. J. Respir. Crit. Care Med.* 153:1850–1856.
- Pugin, J., G. Verhese, M. C. Widmer, and M. Matthay. 1999. The alveolar space is the site of intense inflammatory and profibrotic reactions in the early phase of acute respiratory distress syndrome. *Crit. Care Med.* 27:304–312.
- Nakamura, K., H. Okamura, M. Wada, K. Nagata, and T. Tamura. 1989. Endotoxin-induced serum factor that stimulates gamma interferon production. *Infect. Immun.* 57:590–595.
- Nakamura, K., H. Okamura, K. Nagata, T. Komatsu, and T. Tamura. 1993. Purification of a factor which provides a costimulatory signal for gamma interferon production. *Infect. Immun.* 61:64–70.
- Okamura, H., K. Nagata, T. Komatsu, T. Tanimoto, Y. Nukuta, F. Tanabe, K. Akita, K. Torigoe, T. Okura, S. Fukuda, and M. Kurimoto. 1995. A novel costimulatory factor for gamma interferon induction found in the livers of mice causes endotoxic shock. *Infect. Immun.* 63:3966–3972.
- Ushio, S., M. Namba, T. Okura, K. Hattori, Y. Nukuda, K. Akita, F. Tanabe, K. Konishi, M. Micallef, M. Fujii, K. Torigoe, T. Tanimoto, S. Fukuda, M. Ikeda, H. Okamura, and M. Kurimoto. 1996. Cloning of the cDNA for human IFN- γ -inducing factor, expression in *Escherichia coli*, and studies on the biologic activities of the protein. *J. Immunol.* 156:4274–4279.
- Tone, M., S. Thompson, Y. Tone, P. Fairchild, and H. Waldman. 1997. Regulation of IL-18 (IFN- γ -inducing factor) gene expression. *J. Immunol.* 159:6156–6163.
- Micallef, M., T. Ohtsuki, K. Kohno, F. Tanabe, S. Ushio, M. Namba, T. Tanimoto, K. Torigoe, M. Fujii, M. Ikeda, S. Fukuda, and M. Kurimoto. 1996. Interferon- γ -inducing factor enhances T helper 1 cytokine production by stimulated human T cells: synergism with interleukin-12 for interferon- γ production. *Eur. J. Immunol.* 26:1647–1651.
- Horwood, N. J., N. Udagawa, J. Elliott, D. Grahl, H. Okumura, M. Kurimoto, A. R. Dunn, T. Martin, and M. T. Gillespie. 1998. Interleukin 18 inhibits osteoclast formation via T cell production of granulocyte macrophage colony-stimulating factor. *J. Clin. Invest.* 101:595–603.
- Puren, A., G. Fantuzzi, Y. Gu, M. Su, and C. Dinarello. 1998. Interleukin-18 (IFN- γ -inducing factor) induces IL-8 and IL-1 β via TNF- α production from non-CD14 $^{+}$ human blood mononuclear cells. *J. Clin. Invest.* 101:711–721.
- Kohka, H., T. Yoshino, H. Iwagaki, I. Sakuma, T. Tanimoto, Y. Matsuo, M. Kurimoto, K. Orita, T. Akagi, and N. Tanaka. 1998. Interleukin-18/interferon- γ -inducing factor, a novel cytokine, upregulates ICAM-1 (CD45) expression in KG-1 cells. *J. Leukoc. Biol.* 64:519–527.
- Xu, D., W. Chan, B. Leung, D. Hunter, K. Schulz, R. Carter, I. McInnes, J. Robinson, and F. Liew. 1998. Selective expression and functions of interleukin 18 receptor on T helper (Th) type 1 but not Th2 cells. *J. Exp. Med.* 188:1485–1492.
- Tsutsui, H., K. Nakanishi, K. Matsui, K. Higashino, H. Okamura, Y. Miyazawa, and K. Kaneda. 1996. IFN- γ -inducing factor upregulates Fas ligand-mediated cytotoxic activity of murine natural killer cell clones. *J. Immunol.* 157:3967–3973.
- Micallef, M., T. Tanimoto, K. Kohno, M. Ikeda, and M. Kurimoto. 1997. Interleukin 18 induces the sequential activation of natural killer cells and cytotoxic T lymphocytes to protect syngeneic mice from transplantation with Meth A sarcoma. *Cancer Res.* 57:4557–4563.
- Takeda, K., H. Tsutsui, T. Yoshimoto, O. Adachi, N. Yoshida, T. Kishimoto, H. Okumura, K. Nakanishi, and S. Akira. 1998. Defective NK cell activity and TH1 response in IL-18 deficient mice. *Immunity* 8:383–390.
- Coughlin, C., K. Salhany, M. Wysocka, E. Aruga, H. Kurzawa, A. Chang, C. Hunter, J. Fox, G. Trinchieri, and W. Lee. 1998. Interleukin-12 and interleukin-18 synergistically induce murine tumor regression which involves inhibition of angiogenesis. *J. Clin. Invest.* 101:1441–1452.
- Gu, Y., K. Kuida, H. Tsutsui, G. Ku, K. Hsiao, M. Fleming, N. Hayashi, K. Higashino, H. Okamura, K. Nakanishi, M. Kurimoto, T. Tanimoto, R. Flavell, V. Sato, M. Harding, D. Livingston, and M. Su. 1997. Activation of interferon- γ -inducing factor mediated by interleukin-1 β converting enzyme. *Science* 275:206–209.
- Ghayur, T., S. Banarjee, M. Hugunin, D. Butler, L. Herzog, A. Carter, L. Quintal, L. Sekut, R. Talanian, M. Paskind, W. Wong, R. Kamen, D. Tracey, and H. Allen. 1997. Caspase-1 processes IFN- γ -inducing factor and regulates LPS-induced IFN- γ production. *Nature* 386:619–623.
- Fantuzzi, G., A. Puren, M. Harding, D. Livingston, and C. Dinarello. 1998. Interleukin-18 regulation of interferon γ production and cell proliferation as shown in interleukin-1 β -converting enzyme (caspase-1) deficient mice. *Blood* 91:2118–2125.
- Kobayashi, M., L. Fitz, M. Ryan, R. Hewick, S. Clark, S. Chan, R. Loudon, F. Sherman, B. Perussia, and G. Trinchieri. 1989. Identification and purification of natural killer cell stimulatory factor (NKSF), a cytokine with multiple biologic effects on human lymphocytes. *J. Exp. Med.* 170:827–845.
- Heinzel, F., R. Rerko, P. Ling, J. Hakimi, and D. Schoenhaut. 1994. Interleukin 12 is produced *in vivo* during endotoxemia and stimulates synthesis of gamma interferon. *Infect. Immun.* 62:4244–4249.
- Wysocka, M., M. Kubin, I. Viera, L. Ozmen, G. Garotta, P. Scott, and G. Trinchieri. 1995. Interleukin-12 is required for interferon γ production and

- lethality in lipopolysaccharide-induced shock in mice. *Eur. J. Immunol.* 25:672-676.
35. Ahn, H. J., S. Maruo, M. Tomura, J. Mu, T. Hamaoka, K. Nakanishi, S. Clark, M. Kurimoto, H. Pkamura, and H. Fujiwara. 1997. A mechanism underlying synergy between IL-12 and IFN- γ -inducing factor in enhanced production of IFN- γ . *J. Immunol.* 159:2125-2131.
36. Munder, M., M. Mallo, K. Eichmann, and M. Modolell. 1998. Murine macrophages secrete interferon γ upon combined stimulation with interleukin (IL)-12 and IL-18: a novel pathway of autocrine macrophage activation. *J. Exp. Med.* 187:2103-2108.
37. Nathans, A., R. Bitar, C. Davreux, M. Bujard, J. Marshall, A. Dackiw, R. Watson, and O. Rotstein. 1997. Pyrrolidine dithiocarbamate attenuates endotoxin-induced acute lung injury. *Am. J. Respir. Cell Mol. Biol.* 17:608-616.
38. Kelley, D., A. Lichtenstein, J. Wang, A. Taylor, and S. Dubinett. 1994. Corticotropin-releasing factor reduces lipopolysaccharide-induced pulmonary vascular leak. *Immunopharmacol. Immunotoxicol.* 16:139-148.
39. Stoll, S., G. Muller, M. Kurimoto, J. Saloga, T. Tanimoto, H. Yamauchi, H. Okamura, J. Knop, and A. Enk. 1997. Production of IL-18 (IFN- γ -inducing factor) messenger RNA and functional protein by murine keratinocytes. *J. Immunol.* 159:298-302.
40. Marshall, J., M. Adte-Amezaga, S. Chehimi, M. Murphy, H. Olsen, and G. Trinchieri. 1999. Regulation of human IL-18 mRNA expression. *Clin. Immunol.* 90:15-21.
41. Puren, A., G. Fantuzzi, and C. Dinarello. 1999. Gene expression, synthesis, and secretion of interleukin 18 and interleukin 1 β are differently regulated in human blood mononuclear cells and mouse spleen cells. *Proc. Natl. Acad. Sci. USA* 96:2256-2261.
42. Tripp, C., S. Wolf, and E. Unanue. 1993. Interleukin 12 and tumor necrosis factor α are costimulators of interferon γ production by natural killer cells in severe combined immunodeficiency mice with listeriosis, and interleukin 10 is a physiologic antagonist. *Proc. Natl. Acad. Sci. USA* 90:3725-3729.
43. Rincon, M., H. Ensleer, J. Raingeaud, M. Recht, T. Zapton, M. Su, L. Penix, R. Davis, and R. Flavell. 1998. Interferon- γ expression by Th1 effector cells mediated by the p38 MAP kinase signaling pathway. *EMBO J.* 17:2817-2829.

FILE COPY

EXHIBIT

51

The critical role of interleukin-6, interleukin-1B and macrophage colony-stimulating factor in the pathogenesis of bone lesions in multiple myeloma

Régis Bataille¹, Daniel Chappard², and Bernard Klein¹

¹ Immunorhumatologie and INSERM U 291, Centre Gui de Chauliac, Hôpital Saint-Eloi, F-34059 Montpellier, France

² LBTO Faculté de Médecine, Saint-Etienne, F-42023 Cedex 2, France

Summary. Lytic bone lesions and hypercalcemia are common features of multiple myeloma. In contrast, they are exceptional in other B-cell malignancies. Myeloma bone involvement is related to an uncoupling process associating increased osteoclastic resorption with decreased bone formation. Several osteoclast-activating factors, such as interleukin-1, macrophage colony-stimulating factor, and interleukin-6, are involved in this process. However, interleukin-6, the major myeloma cell growth factor, plays a critical role in myeloma-induced bone resorption.

Key words: Multiple myeloma – Bone resorption – Osteoclast-activating factors – Interleukin-6

Introduction

Lytic bone lesions and hypercalcemia are common features in patients with multiple myeloma (MM) [33]. Few patients with MM fail to develop lytic bone lesions; exceptionally, some patients present with osteosclerotic lesions [32]. Mixed and sclerotic bone lesions are more frequently observed in patients with either solitary myeloma or POEMS syndrome [32]. In contrast to MM, other B-cell malignancies (except for hairy-cell leukemia) are not associated with bone involvement despite bone marrow invasion [41]. It is thus critical to clarify the mechanisms leading to bone lesions in MM (and those leading to bone protection observed in a minority of MM patients), and to understand why bone involvement is restricted to MM. This is important for understanding the pathogenesis of both MM and B-cell malignancies. Furthermore, this could improve the management of myeloma-induced bone changes, or even prevent these changes independently of standard anti-myeloma treatments. Bone healing is only observed in 30% of chemotherapy-induced remissions [39].

Excessive osteoclastic resorption induced by myeloma cells

Increased bone resorption is a characteristic feature of patients with MM. This excessive bone resorption is easily evaluated by quantitative bone biopsy and is observed in all patients with active disease (diagnosis, relapse), regardless of the presence (or not) of lytic bone lesions on radiography, provided that myeloma cells are present in the bone sample. In contrast, a normal bone resorption is observed in non-invaded biopsies and/or in biopsies from patients in remission. The increased bone resorption is generally observed in the close vicinity of myeloma cells. However, some patients with active disease do not present any increased bone resorption (Table 1) and these patients lack myeloma cells in the bone biopsy. These patients correspond to exceptional osteoblastic MM (lacking bone lesions on radiography) or to osteosclerotic MM.

Since the first investigation by Mundy et al. [33], several studies (including ours) have confirmed an excessive bone resorption in the bone marrow of patients with MM [1, 22, 48]. This excessive bone resorption is related to an increase in trabecular osteoclast number [5, 22, 26]. However, the increase in osteoclast number is only observed in 75% of patients [11]. Until now, no evaluation of cortical

Table 1. Histomorphometric features of patients with osteoblastic-osteosclerotic myeloma

| Patient no. Source | Trabecular bone volume (%) | Eroded surfaces (%) | Osteoid volumes (%) | Osteoid surfaces (%) | Mineral apposition rates (µm/day) |
|--------------------|----------------------------|---------------------|---------------------|----------------------|-----------------------------------|
| 1 [16] | 41.5↑ | 6.3↑ | 3.2 | 33.7↑ | ND |
| 2 [16] | 29↑ | 12↑ | 3.5 | 39.5↑ | ND |
| 3 [30] | 45↑ | 2.3 | ND | 19.8↑ | 0.80↑ |
| 4* | 32.4↑ | 7.7↑ | 8.3↑ | 51.2↑ | 1.40↑ |
| 5 [9] | 9.9 | 12.2↑ | 4.6↑ | 26.7↑ | ND |
| 6 [9] | 15 | 15.5↑ | 7.6↑ | 37.5↑ | ND |

ND, Not determined; ↑, increased values

* L. Heraud, unpublished data

osteoclasts has been performed in MM. Our morphometric studies have shown that these osteoclasts have only one or few nuclei and are of normal length, in contrast to the large multinucleated osteoclasts encountered in primary hyperparathyroidism and Paget's disease of bone [15]. In contrast, an increase in abnormal osteoclasts, i.e., small mononuclear osteoclasts (micro-osteoclasts), was observed in most patients with B-cell malignancies other than MM, including chronic lymphocytic leukemia, non-Hodgkin's lymphoma, Waldenström's disease, and mainly hairy-cell leukemia [31, 42]. Our morphometric data suggested that the increased osteoclastic resorption in MM was associated with a normal maturation of osteoclasts, which was not observed in other B-cell malignancies. In these latter cases, mainly in hairy-cell leukemia, tumor induced an increase in early and late osteoclastic precursors, without complete maturation. This suggests a biology completely different from that of MM.

The increased osteoclastic resorption in MM explains the high sensitivity of myeloma patients to the acute effects of calcitonin a potent anti-osteoclastic agent [3, 4], supports the potentially beneficial effects of bisphosphonates in the treatment of myeloma-induced bone changes as illustrated by preliminary published results [1, 17, 36, 44], and is in agreement with previous mouse studies [38]. When quantitative bone biopsies were performed in individuals with early (i.e., subclinical) MM, an excessive bone resorption was also observed, as marked as that in patients with overt MM [11]. In contrast, this abnormal remodelling was not found in individuals with either benign monoclonal gammopathy [11] or smouldering MM (R. Bataille, D. Chappard, unpublished data). These critical data have shown that excessive osteoclastic resorption is an early phenomenon in MM which can be observed several years before the first clinical symptoms of the disease and is thus a useful parameter for discriminating benign monoclonal gammopathy or smouldering MM from early active MM [11].

Mechanisms of lytic bone lesions in MM

The observation that increased osteoclastic resorption occurred in almost all patients with MM suggested that lytic bone lesions could not be simply explained by an increased bone resorption [7]. When we compared at the time of diagnosis the histomorphometric features of patients with lytic bone lesions with those of patients lacking such lesions, it was evident that the two groups had an opposite bone profile. An uncoupling bone process (i.e., increased bone resorption with decreased bone formation) was a characteristic feature of patients with lytic bone lesions. Such uncoupling was not observed in patients lacking lytic bone lesions [7]. Thus, these data have shown that the inhibition of bone formation was as critical for the development of lytic bone lesions as excessive bone resorption [7]. This concept was further supported by studies in patients who never developed lytic bone lesions or who presented with sclerotic MM (L. Heraud, unpublished data) [9, 16, 30]. As shown in Table 1, five of

these patients had increased parameters of both bone resorption and bone formation, whereas one had a selective increase in parameters of bone formation. Serial biopsies (performed in the same patient) have confirmed the existence of an uncoupling process during bone destruction, and conversely the maintenance of a coupling process in patients lacking lytic bone lesions despite active disease (R. Bataille, D. Chappard, unpublished data). Osteoblastic and osteosclerotic MM were restricted to the O⁻M_{cg}⁻ λ isotype for unknown reasons (R. Bataille, unpublished data obtained with antibodies kindly supplied by R. Jefferis).

The critical role of bone formation in the occurrence of lytic bone lesions in patients with MM was further supported by our studies with the bone gla protein (BGP) [6, 10]. A good correlation was found between BGP serum levels and bone formation rates (evaluated on bone biopsies) in patients with either early or overt MM. Extensive studies of serum BGP in MM have shown an inverse correlation between BGP serum levels and the lytic potential of the tumor [6, 10]. Patients lacking lytic bone lesions had significantly higher BGP serum levels than those with lytic bone lesions. We have previously shown that the lytic potential of the tumor is directly correlated with the *in vivo* instantaneous rate of bone resorption in the body evaluated by a standard calcitonin-induced hypocalcemia test [3, 4]. In contrast to the excessive osteoclastic resorption, which was found to be an early phenomenon in the pathogenesis of MM, the inhibition of bone formation was progressively observed during disease progression. We have recently shown that bone formation is normal or rather increased in early MM [11]. As previously emphasized, serial biopsies in the same patient have shown that the uncoupling is a secondary process. Thus, the early myeloma-induced abnormal bone remodelling was generally characterized by stimulation of both bone resorption and bone formation [11]. These data suggest that osteoblasts able to produce many growth and osteoclast-activating factors could play a critical role in the early part of the disease (see next section).

Pathogenesis of myeloma-induced bone changes

As outlined in the previous section, the generation of new osteoclasts with increased osteoclastic resorption in the close vicinity of myeloma cells is an early and characteristic feature of myeloma bone marrow [11]. With advanced disease bone formation is suppressed, whereas in early disease osteoblastic activity is maintained or rather stimulated [11]. Another critical observation is the strong natural killer (NK)-cell activity which has been found in the bone marrow of patients with MM and not in that of patients with B-cell malignancies other than MM [46]. Thus, accelerated maturation of both osteoclasts and NK-cells are the most specific features of MM compared with other B-cell malignancies and could have a similar (common) origin. We, and others, have demonstrated that interleukin-6 (IL-6) is the major myeloma cell growth factor *in vitro* and *in vivo* [24, 26, 54]. IL-6 is

overproduced in the bone marrow of patients with MM and circulates in the peripheral blood [8]. We and others, have shown that other factors are involved in myeloma cell growth, as co-factors of IL-6; these include IL-1, tumor necrosis factor (TNF), IL-3, and granulocyte-macrophage and granulocyte colony-stimulating factor [55] (B. Klein, R. Bataille, unpublished data). As IL-6, some of these factors are present in the bone marrow of patients with MM in vitro and even in vivo. Importantly, almost all these factors are able to stimulate the generation of new osteoclasts and osteoclastic activity, and to inhibit bone formation [14]. Among these bone factors, IL-6 appears to play a critical role as an osteoclast-activating factor mediating the bone effects of both IL-1 and TNF [2].

Since the first study of Mundy et al. [34], several studies have confirmed the presence of a strong bone-resorbing activity in the bone marrow of patients with MM [8–21, 23, 25, 40, 43, 52]. Furthermore, in three of these studies, IL-1 β was shown to be the cytokine supporting the bone-resorbing activity [21, 25, 52]. The recent demonstrations of: (1) the bone-resorbing activity of IL-6 in vitro and in vivo (in mouse), (2) the induction of IL-6 by IL-1 β , (3) the synergy between IL-1 β and IL-6 in vitro in terms of bone-resorbing activity, and (4) the IL-6 mediation of IL-1 β bone-resorbing activity shown that IL-6 rather than IL-1 β , which is overproduced in MM, is certainly one of the most critical and final products involved in myeloma-induced bone changes [2]. The hypocalcemic effects of an anti-IL-6 murine monoclonal antibody, able to inhibit myeloma cell proliferation in vivo, support this concept [27]. Recently, IL-6 has been shown to increase NK-cell activity [28, 45]. Thus, IL-6 is probably involved in both the excessive osteoclastic and NK-cell activities found in the bone marrow of patients with MM. We have shown that IL-6 is a paracrine rather than autocrine growth factor in MM [26, 37]. In agreement with a recently reported model [53], myeloma-induced bone changes as myeloma cell growth could be IL-6-mediated paraneoplastic syndromes.

Intensive research has to be devoted to the nature of known and unknown factors produced by myeloma cells and able to both stimulate the production of IL-6 by the tumoral microenvironment and synergize with IL-6 to increase bone resorption as myeloma cell growth. Several recent reports suggest that IL-1 β could be one of these factors [21, 25, 52]. Others suggest that macrophage colony-stimulating factor (MCSF) could be another critical factor in this process. Indeed, MCSF is overproduced in vivo in MM in relation to disease severity [50] (B. Klein, R. Bataille, unpublished data). Myeloma cell lines produce MCSF in vitro [35]. MCSF is documented as an inducer of several cytokines and could be a putative inducer of IL-6, as is IL-1 β [49]. Its synergy with IL-6 as a hematopoietic growth factor is well known [12]. The role of MCSF in bone resorption is probably essential, since, in mouse, osteopetrosis (characterized by a lack of bone resorption) is related to a total and selective absence of MCSF [51]. MCSF stimulates the generation of osteoclasts in vitro [29]. Taken together, these data suggest that MCSF, which is overproduced in vivo, maybe by the

myeloma cells themselves, could be critical in the pathogenesis of myeloma-induced bone changes. Recent additional data support this concept [13, 47]. In the mouse, osteoclasts can be generated from peripheral blood monocytes in the presence of osteotropic hormones and stromal cells producing MCSF (and probably some other critical factors) [47]. The same observation (i.e., generation of new osteoclasts from peripheral blood precursors in the presence of stromal cells) was recently made in MM by Caligaris-Cappio et al. [13]. IL-3 and IL-6, were mainly involved in this culture system, but MCSF was not investigated. Finally, the same culture system allowed not only the generation of osteoclasts but also myeloma cells from unidentified precursors, showing that both phenomena are closely related and dependent on the same microenvironment and stromal growth factors. It is clear that unknown factors released by such stromal cells are also involved. New cytokines able to stimulate bone resorption (OPF) or NK-cell activity (NKCSF) deserve special attention in MM.

Conclusions

Bone involvement, mainly bone destruction, is a characteristic and usual feature of MM. In contrast, it is exceptional in B-cell malignancies other than MM. Bone destruction is the consequence of an uncoupling process associating an increased osteoclastic resorption with an inhibition of bone formation. Conversely, patients lacking lytic bone lesions or those with sclerotic MM have an increased bone resorption and maintain a normal or have an increased bone formation (coupling process). This excessive osteoclastic resorption is an early phenomenon, as opposed to the inhibition of bone formation. It is observed several months or years before the occurrence of the first clinical symptoms of the disease. Thus, it is an early criterion of malignancy, useful for discriminating benign monoclonal gammopathy and smouldering MM from early active MM. Several osteoclast-activating factors, produced either by the myeloma cells themselves or the hematopoietic microenvironment, are probably involved in the pathogenesis of such bone lesions. At present, IL-6 (the major myeloma cell growth factor) and IL-1 β appear to be the most critical factors. Indirect arguments suggest that other hematopoietic growth factors (mainly MCSF) play a role. Taken together, these data demonstrate a close relationship between myeloma cell growth factors and osteoclast-activating factors.

Acknowledgements. We thank L. Bataille-Zagury for editing the English text and M. Frei for typing the manuscript. This work was supported by grants from l'Association pour la Recherche sur le Cancer and la Ligue Nationale contre le Cancer, Paris, France.

References

1. Ascari E, Attardo-Parrinello G, Merlini G, Treatment of painful bone lesions and hypercalcemia. *Eur J Haematol* 43:135, 1989

2. Bataille R, Klein B, The bone resorbing activity of interleukin-6. *J Bone Miner Res* 1991 (in press)
3. Bataille R, Sany J, Clinical evaluation of myeloma osteoclastic bone lesions. II. Induced hypocalcemia test using salmon calcitonin. *Metab Bone Dis Relat Res* 4:39, 1982
4. Bataille R, Legendre O, Sany J, Acute effects of salmon calcitonin in multiple myeloma: a valuable method for serial evaluation of osteoclastic lesions and disease activity. A prospective study of 125 patients. *J Clin Oncol* 3:229, 1985
5. Bataille R, Chappard D, Alexandre C, Sany J, Importance of quantitative histology of bone changes in monoclonal gammopathy. *Br J Cancer* 53:805, 1986
6. Bataille R, Delmas P, Sany J, Serum bone gla-protein (osteocalcin) in multiple myeloma. *Cancer* 59:329, 1987
7. Bataille R, Chappard D, Marcelli C, Dessauw P, Sany J, Baldet P, Alexandre C, Mechanism of bone destruction in multiple myeloma. The importance of an unbalanced process in determining the severity of lytic bone disease. *J Clin Oncol* 7:1909, 1989
8. Bataille R, Jourdan M, Zhang XG, Klein B, Serum levels of interleukin-6, a potent myeloma cell growth factor, as a reflection of disease severity in plasma cell dyscrasias. *J Clin Invest* 84:2008, 1989
9. Bataille R, Chappard D, Marcelli C, Rossi JF, Dessauw P, Baldet P, Sany J, Alexandre C, Osteoblast stimulation in multiple myeloma lacking lytic bone lesions. *Br J Haematol* 76:484, 1990
10. Bataille R, Delmas PD, Chappard D, Sany J, Abnormal serum bone gla protein levels in multiple myeloma: crucial role of bone formation and prognostic implications. *Cancer* 66:167, 1990
11. Bataille R, Chappard D, Marcelli C, Dessauw P, Baldet P, Sany J, Alexandre C, The recruitment of new osteoblasts and osteoclasts is the earliest critical event in the pathogenesis of human multiple myeloma. *J Clin Invest* 88:62, 1991
12. Bot FJ, Eijk L van, Broeders L, Aarden LA, Lowenberg B, Interleukin-6 synergizes with M-CSF in the formation of macrophage colonies from purified human marrow progenitor cells. *Blood* 73:435, 1989
13. Caligaris-Cappio F, Bergui L, Gregoret MG, Gaidano G, Gaboli M, Schena M, Zamboni-Zallone A, Marchisio PC, Role of bone marrow stromal cells in the growth of human multiple myeloma. *Blood* 77:2688, 1991
14. Canalis E, McCarthy T, Centrella M, Growth factors and the regulation of bone remodelling. *J Clin Invest* 81:277, 1988
15. Chappard D, Rossi JF, Bataille R, Alexandre C, Cyto-morphometry of osteoclasts demonstrates an abnormal population in B-cell malignancies but not in multiple myeloma. *Calcif Tissue Int* 48:13, 1991
16. Charhon S, Le myélome multiple à forme ostéocondensante - à propos de deux observations personnelles et revue de la littérature. Thèse de médecine, Lyon, France 1979
17. Delmas PD, Charmon S, Chapuy MC, Vignon E, Briancon D, Edouard C, Meunier PJ, Long-term effects of dichloromethylene diphosphonate (Cl₂MDP) on skeletal lesions in multiple myeloma. *Metab Bone Dis Rel Res* 4:163, 1982
18. Durie BGM, Salmon SE, Mundy GR, Relation of osteoclast activating factor production to extent of bone disease in multiple myeloma. *Br J Haematol* 47:21, 1981
19. Gailani S, McLimans WF, Mundy GR, Nussbaum A, Roholt O, Zeigel R, Controlled environment culture of bone marrow explants from human myeloma. *Cancer Res* 36:1299, 1976
20. Garrett IR, Durie BGM, Nedwin GE, Gillespie A, Bringman T, Sabatini M, Bertolini DR, Mundy GR, Production of lymphotoxin, a bone resorbing cytokine, by cultured human myeloma cells. *N Engl J Med* 317:526, 1987
21. Gozzolino F, Torcia M, Aldinucci D, Rubartelli A, Miliani A, Shaw R, Lansdorp AR, Di Guglielmo R, Production of interleukin-1 by bone marrow myeloma cells. *Blood* 74:380, 1989
22. Grauer JL, Blanc D, Zagala A, Sotto JJ, Duplan B, Drevet JG, Phelip X, L'histomorphométrie osseuse dans les dysglobulinémies monoclonales. *Rev Rhum Mal Osteoartic* 53:517, 1986
23. Josse RG, Murray TM, Mundy GR, Jez D, Heersche JNM, Observation of the mechanism of bone resorption induced by multiple myeloma marrow culture fluids and partially purified osteoclast-activating factor. *J Clin Invest* 67:1472, 1981
24. Kawano M, Hirano T, Matsuda T, Taga T, Horii Y, Iwato K, Asaoku H, Tang B, Tanabe O, Tanaka H, Kuramoto A, Kishimoto T, Autocrine generation and essential requirement of BSF/2 IL-6 for human multiple myeloma. *Nature* 322:73, 1988
25. Kawano M, Yamamoto I, Iwato K, Tanaka H, Asaoku H, Tanabe O, Ishikawa H, Nobuyoshi M, Ohmoto Y, Hirai Y, Kuramoto A, Interleukin-1 beta rather than lymphotoxin as the major bone resorbing activity in human multiple myeloma. *Blood* 73:1646, 1989
26. Klein B, Zhang XG, Jourdan M, Content J, Houssiau F, Aarden L, Piechaczyk M, Bataille R, Paracrine rather than autocrine regulation of myeloma cell growth and differentiation by Interleukin-6. *Blood* 73:517, 1989
27. Klein B, Widjenes J, Zhang XG, Jourdan M, Boiron JM, Brochier J, Liautard J, Merlin M, Clément C, Morel-Fournier B, Lu ZY, Mannoni P, Sany J, Bataille R, Murine, anti-Interleukin-6 monoclonal antibody therapy for a patient with plasma cell leukemia. *Blood* 1991 (in press)
28. Luger TA, Kruttman J, Kirnbauer R, Urbanski A, Schwarz T, Klappacher G, Köck A, Micksche M, Malejczyk J, Schauer E, May LT, Sengal PB, IFN β /IL-6 augments the activity of human natural killer cells. *J Immunol* 143:1206, 1989
29. MacDonald BR, Mundy GR, Clark S, Wang EA, Kuehl TJ, Stanley ER, Roodman GD, Effects of human recombinant CSF-6 and highly purified CSF-1 on the formation of multinucleated cells with osteoclast characteristics in long-term bone marrow cultures. *J Bone Miner Res* 1:227, 1986
30. Macro M, Troussard X, Galateau F, Renan O, Leporrier M, Loyau G, Myélome ostéocondensant diffus avec localisation thyroïdienne. *Rev Rhum Mol Osteoartic* 56:613, 1989
31. Marcelli C, Chappard D, Rossi JF, Jaubert J, Alexandre C, Dessauw P, Baldet P, Bataille R, Histologic evidence of an abnormal bone remodeling in B-cell malignancies other than multiple myeloma. *Cancer* 62:1163, 1988
32. Meszaros WT, The many facets of multiple myeloma. *Semin Roentgenol* IX:219, 1974
33. Mundy GR, Bertolini DR, Bone destruction and hypercalcemia in plasma cell myeloma. *Semin Oncol* 13:291, 1986
34. Mundy GR, Raisz LG, Cooper RA, Schechter GP, Salmon SE, Evidence for the secretion of an osteoclast stimulating factor in myeloma. *N Engl J Med* 291:1041, 1974
35. Nakamura M, Merchav S, Carter A, Ernst TJ, Demetri GD, Furukawa Y, Anderson K, Expression of a novel 3-5-kb macrophage colony-stimulating factor transcript in human myeloma cells. *J Immunol* 143:3543, 1989
36. Paterson AD, Kanis JA, Cameron EC, Douglas DL, Beard DJ, Preston FE, Russell RGG, The use of dichloromethylene diphosphonate for the management of hypercalcemia in multiple myeloma. *Br J Haematol* 54:121, 1983
37. Portier M, Rajzbaum G, Zhang XG, Attal M, Rusalén C, Maraninchi D, Widjenes J, Manonni P, Piechaczyk M, Bataille R, Klein B, In vivo paracrine but not autocrine interleukin-6 gene expression in multiple myeloma. *Eur J Immunol* 21:1759, 1991
38. Radl J, Croese JW, Zurcher C, Enden-Vieveen MHM van den, Brondijk RJ, Kazil M, Haaijman JJ, Reitsma PH, Bijvoet OLM, Influence of treatment with APD-biphosphonates on the bone lesions in the mouse 5T2 multiple myeloma. *Cancer* 55:1030, 1985
39. Rodriguez LH, Finkelstein JB, Shullenberger CC, Alexanian R, Bone healing in multiple myeloma with melphalan chemotherapy. *Ann Intern Med* 76:551, 1972
40. Rossi JF, Bataille R, In vitro osteolytic activity of human myeloma plasma cells and the clinical evaluation of myeloma osteoclastic bone lesions. *Br J Cancer* 50:119, 1984
41. Rossi JF, Bataille R, Chappard D, Alexandre C, Janbon C, Unusual B cell malignancies presenting unusual bone involve-

- ment and mimicking multiple myeloma. A personal study of 9 cases. *Am J Med* 83:10, 1987
42. Rossi JF, Chappard D, Marcelli C, Baldet P, Alexandre C, Janbon C, Jourdan J, Bataille R, Micro-osteoclastic resorption as a characteristic feature of B-cell malignancies other than multiple myeloma. *Br J Haematol* 76:469, 1990
43. Schechter GP, Wahl LM, Horton JE, In vitro bone resorption by human myeloma cells. In: Potter M (ed) *Progress in myeloma. Biology of myeloma*. pp 67-77, 1980
44. Siris ES, Sherman WH, Baquiran DC, Schlatterer JP, Osserman EF, Canfield RF, Effects of chloromethylene diphosphate on skeletal mobilization of calcium in multiple myeloma. *N Engl J Med* 302:310, 1980
45. Smyth MJ, Ortaldo JR, Comparison of the effect of IL-2 and IL-6 on the lytic activity of purified human peripheral blood large granular lymphocytes. *J Immunol* 146:1380, 1991
46. Uchida A, Yagital M, Sugiyama H, Hoshino T, Moore M, Strong natural killer (NK) cell activity in bone marrow of myeloma patients: accelerated maturation of bone marrow NK cells and their interaction with other bone marrow cells. *Int J Cancer* 34:375, 1984
47. Udagawa N, Takahashi N, Akatsu T, Tanaka H, Sasaki T, Nishihara T, Koga T, Martin TJ, Suda T, Origin of osteoclasts: mature monocytes and macrophages are capable of differentiating into osteoclasts under a suitable microenvironment prepared by bone-marrow derived stromal cells. *Proc Natl Acad Sci USA* 87:7260, 1990
48. Valentin-Opran A, Charmon SA, Meunier PJ, Edouard CM, Arlot ME, Quantitative histology of myeloma-induced bone changes. *Br J Haematol* 52:601, 1982
49. Warren MK, Ralph P, Macrophage growth factor CSF-I stimulates human monocyte production of interferon, tumor necrosis factor and colony-stimulating activity. *J Immunol* 137:2281, 1986
50. Wiczorek AJ, Belch AR, Jacobs A, Bowen D, Padua RA, Paietta E, Stanley ER, Increased circulating colony-stimulating factor-1 in patients with pre-leukemia, leukemia and lymphoid malignancies. *Blood* 77:1796, 1991
51. Wiktor-Jedrzejczak W, Bartocci A, Ferrante AW, Ansari AA, Sell KW, Stanley ER, Total absence of colony-stimulating factor-1 in the macrophage deficient osteopetrotic (op/op) mouse. *Proc Natl Acad Sci USA* 87:4828, 1990
52. Yamamoto I, Kawano M, Sone T, et al., Production of interleukin-1 β , a potent bone resorbing cytokine, by cultured myeloma cells. *Cancer Res* 49:4242, 1989
53. Yoneda T, Alsina MA, Chavez JB, Bonewald L, Nishimura R, Mundy GR, Evidence that tumor necrosis factor plays a pathogenetic role in the paraneoplastic syndromes of cachexia, hypercalcemia and leukocytosis in a human tumor in male mice. *J Clin Invest* 87:977, 1991
54. Zhang XG, Klein B, Bataille R, Interleukin-6 is a potent myeloma-cell growth factor in patients with aggressive multiple myeloma. *Blood* 74:11, 1989
55. Zhang XG, Bataille R, Jourdan M, Saeland S, Banchereau J, Mannoni P, Klein B, Granulocyte-macrophage colony-stimulating factor synergizes with interleukin-6 in supporting the proliferation of human multiple myeloma cells. *Blood* 76:2599, 1990

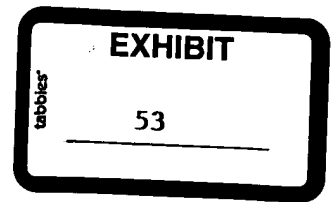
Alcohol 2002 May;27(1):63-8

Ethanol, oxidative stress, and cytokine-induced liver cell injury.

Hoek JB, Pastorino JG.

Alcohol Research Center, Department of Pathology, Anatomy and Cell Biology,
Thomas Jefferson University, JAH Room 269, 1020 Locust Street, Philadelphia, PA
19107, USA. Jan.Hoek@mil.tju.edu

Both clinical findings and results of experiments with animal models of alcoholic hepatitis have shown the importance of cytokine-mediated cell-cell interactions in the onset of ethanol-induced liver damage. Proinflammatory cytokines, such as tumor necrosis factor-alpha (TNF-alpha), **interleukin (IL)-1 beta (IL-1 beta)**, and interleukin-6, are released from Kupffer cells or infiltrating neutrophils and macrophages and elicit defensive responses in parenchymal cells, including activation of apoptosis. Reactive oxygen species (ROS) and reactive nitrogen species (RNS), generated in response to cytokine-induced stress signals in parenchymal cells and also by activation of Kupffer cells and inflammatory cells, further mobilize cellular defense mechanisms. When these defensive responses are overwhelmed cells may die by necrosis, further stimulating inflammatory responses and infiltration of neutrophils. Chronic ethanol intake (i.e., many years of heavy alcohol use in human patients, several weeks or months in experimental animals) enhances the damaging consequences of these events through a variety of mechanisms. The formation of cytokines in the liver is stimulated by increasing circulating levels of endotoxin and by enhancing the responsiveness of Kupffer cells to such stimuli. In addition, ethanol promotes oxidative stress, both by increased formation of ROS and by depletion of oxidative defenses in the cell. Furthermore, liver cells from ethanol-treated animals are more susceptible to the cytotoxic effects of TNF-alpha and other cytokines than cells from control animals. Mitochondria play a critical role in the **apoptotic** response, and alterations in mitochondrial function after chronic ethanol treatment may contribute to enhanced cell death by apoptosis or necrosis. How the shift in the balance of cytokine-induced defensive and damage responses in hepatocytes contributes to the liver injury that occurs in alcoholic hepatitis remains poorly characterized and should be a rewarding area for future studies.



Curr Opin Rheumatol 1998 Jul;10(4):314-8 Related Articles, Links

Acute anterior uveitis and spondyloarthropathies.

Feltkamp TE, Ringrose JH.

Arthron, Amsterdam, The Netherlands.

Acute anterior uveitis (AAU) is characterized by sudden-onset, mostly unilateral exacerbations of an inflammation of the iris and ciliary body. The duration of illness is short if the patient is treated with corticosteroids. Half of all patients with any type of anterior uveitis are HLA-B27-positive, and more than half of the B27-positive patients have spondyloarthropathy. Ophthalmologists should therefore refer all patients with AAU who are HLA-B27-positive to a rheumatologist. Because attacks of AAU are extremely painful and frightening, most spondyloarthropathy patients with AAU will seek out an ophthalmologist on their own. The anterior chamber of the eye and the joints are mesenchymal cavities that are cleaned by macrophages. Anterior chamber-associated immune deviation is the mechanism by which specific regulatory T cells normally produce sufficient transforming growth factor-beta to impair inflammatory reactions that might hamper vision. Another mechanism of immune privilege is **Fas-ligand induced apoptosis**. Because the cells of the anterior eye **express Fas-ligand, infiltrating cells are apoptotically killed**. Comparable mechanisms may occur at a lower level in joints. The cause of AAU and spondyloarthropathy is unknown. B27 is probably only responsible for one quarter of the pathogenesis, other non-B27 genetic factors for another quarter, and unknown exogenous factors for the remaining half. It is possible that Gram-negative bacteria such as Klebsiella or Yersinia are involved in the pathogenesis in a yet unknown way.

Dig Dis Sci 2001 Aug;46(8):1668-76 Related Articles, Links

Expression of proinflammatory cytokines and their inhibitors during the course of spontaneous bacterial peritonitis.

Rodriguez-Ramos C, Galan F, Diaz F, Elvira J, Martin-Herrera L, Giron-Gonzalez JA.

Digestive Diseases, Hospital Universitario Puerta del Mar, Cadiz, Spain.

The aim of this work was the evaluation, in cirrhotic patients with noninfected ascites and with spontaneous bacterial peritonitis (SBP), of serum and ascitic fluid levels of proinflammatory cytokines [interleukin (IL) 1-beta, tumor necrosis factor alpha (TNF-alpha), and IL6] and antiinflammatory compounds [IL10, soluble IL-1 receptor antagonist (sIL-1Ra), soluble receptors of TNF p55 and p75 (sTNFR55 and sTNFR75), and soluble receptor of IL6 (sIL6R)], as well as their relationship with the outcome of the infection in those with SBP. These molecules were assayed by ELISA in noninfected cirrhotic controls (n = 15), patients with SBP (n = 32), and healthy controls (n = 20). Serum levels of IL6 and of the majority of antiinflammatory mediators, sIL1Ra, sTNFR75, and sIL6R, were higher in control cirrhotic patients compared to healthy subjects. **SBP was associated with significantly elevated ascitic fluid levels of every one of the proinflammatory cytokines** compared to those in cirrhotic controls. Also, serum levels of IL10 and both TNF receptors and ascitic fluid levels of sIL1Ra and sTNFR55 were higher in patients with SBP compared to cirrhotic controls. Ascitic fluid levels of proinflammatory cytokines decreased rapidly after resolution of the infection; however, nonsignificant changes were detected in ascitic fluid concentrations of antiinflammatory molecules. Thus, elevated levels of antiinflammatory compounds both in noninfected cirrhotic patients and in patients with SBP suggest a regulatory control of the inflammatory process by these molecules in liver cirrhosis patients.

Inflammation 1998 Dec;22(6):619-29 Related Articles, Links

Mediators of microvascular injury in dermal burn wounds.

Ravage ZB, Gomez HF, Czermak BJ, Watkins SA, Till GO.

University of Michigan Medical School, Ann Arbor 48109-0602, USA.

In previous studies we have demonstrated that second-degree thermal injury of skin in rats leads to secondary effects, such as systemic complement activation, C5a-mediated activation of blood neutrophils, their adhesion-molecule-guided accumulation in lung capillaries and the development of acute pulmonary injury, largely caused by neutrophil-derived toxic oxygen metabolites. In the dermal burn wound, however, pathophysiologic events are less well understood. The injury is fully developed at four hours post-burn. To further elucidate the pathogenesis of the "late phase" dermal vascular damage, rats were depleted of neutrophils or complement by pretreatment with rabbit antibody against rat neutrophils or with cobra venom factor, respectively. In other experiments, rats were treated with **blocking antibodies to IL-6, IL-1**, and TNF alpha immediately following thermal burning or were pretreated with hydroxyl radical scavengers (dimethyl sulfoxide, dimethyl thiourea). Extravasation of 125I-labeled bovine serum albumin into the burned skin was studied, as well as, skin myeloperoxidase levels. The studies revealed that, like in secondary lung injury, neutrophils and toxic oxygen metabolites, are required for full development of microvascular injury. In contrast, however, development of dermal vascular damage in thermally injured rats was not affected by complement depletion. Our data suggest that the **development of microvascular injury in the dermal burn wound is complement-independent, involves the pro-inflammatory cytokines IL-1**, TNF alpha and IL-6, and may result from reactive oxygen metabolites generated by neutrophils accumulating in the burn wound.

Pathol Oncol Res 2000;6(2):130-5 Related Articles, Links

[Click here to read](#)

Apoptosis-related proteins, BCL-2, BAX, FAS, FAS-L and PCNA in liver biopsies of patients with chronic hepatitis B virus infection.

Ehrmann J Jr, Galuszkova D, Ehrmann J, Krc I, Jezdinska V, Vojtesek B, Murray PG, Kolao Z.

Faculty of Medicine, PalackyUniversity, Institute of Pathology & Centre of Molecular Biology and Medicine Hnivotinska 3, Olomouc, Czech Republik. erman@tunw.upol.cz.

While the elimination of hepatitis B virus (HBV) is a common phenomenon at the end of the acute phase of disease, the persistence of HBV is characteristic for chronic hepatitis (CHB). Recent evidence indicates that the elimination of HBV is achieved by FAS/FAS-L induced apoptosis of infected hepatocytes. The aim of this study was to test the hypothesis that HBV persistence in the hepatocytes of CHB patients is due to the delayed onset of apoptosis caused by altered FAS/FAS-L interactions between lymphocytes and hepatocytes. The expression of FAS, FAS-L, BAX, BCL-2, ICE and PCNA in the liver biopsies of 55 patients (14 HBsAg positive, 20 patients with alcoholic hepatopathy, 21 patients with other hepatopathies) was tested by immunohistochemistry. Apoptosis of hepatocytes was evaluated by morphological as well as by TUNEL method. The results were correlated with a grading/staging score and analysed statistically using a one way analysis of variance and the Duncan test. Significantly highernumbers of BAX positive hepatocytes were observed in HBsAg positive patients when compared to control groups. Similarly, both BAX and FAS positive lymphocytes were more frequent in HBsAg positive patients. FAS-L positive lymphocytes and hepatocytes were numerous in all patient groups. Increased numbers of BAX positive hepatocytes in CHB may reflect the increased readiness of these cells to undergo apoptosis. However, the increased numbers of both BAX and FAS positive lymphocytes in CHB suggest that these cells may be particularly sensitive to FAS-L mediated apoptosis potentially resulting in lowered viability of these lymphocytes. This may explain, at least in part, the defective removal of virus-infected cells in chronic hepatitis. However, we cannot rule out the possibility that survival of hepatocytes during CHB may be due to other mechanisms such as defects in apoptosis activation triggered by CD40, defects involving DNase and/or other caspases downstream in the apoptotic cascade within these cells, or to defects in CTL function.

Hepatology 2001 Oct;34(4 Pt 1):758-67 Related Articles, Links

[Click here to read](#)

Caspase activation correlates with the degree of inflammatory liver injury in chronic hepatitis C virus infection.

Bantel H, Luger A, Poremba C, Luger N, Held J, Domschke W, Schulze-Osthoff K.

Department of Immunology and Cell Biology, University of Munster, Munster, Germany.

Hepatitis C virus (HCV) infection is a major cause of liver disease characterized by inflammation, cell damage, and fibrotic reactions of hepatocytes. Apoptosis has been implicated in the pathogenesis, although it is unclear whether proteases of the caspase family as the central executioners of apoptosis are involved and how caspase activation contributes to liver injury. In the present study, we measured the activation of effector caspases in liver biopsy specimens of patients with chronic HCV infection. The activation of caspase-3, caspase-7, and cleavage of poly(ADP-ribose)polymerase (PARP), a specific caspase substrate, were measured by immunohistochemistry and Western blot analysis by using antibodies that selectively detect the active truncated, but not the inactive precursor forms of the caspases and PARP. We found that caspase activation was considerably elevated in liver lobules of HCV patients in comparison to normal controls. Interestingly, the immunoreactive cells did yet not reveal an overt apoptotic morphology. **The extent of caspase activation correlated significantly with the disease grade, i.e.,** necroinflammatory activity. In contrast, no correlation was observed with other surrogate markers such as serum transaminases and viral load. In biopsy specimens with low activity (grade 0) 7.7% of the hepatocytes revealed caspase-3 activation, whereas 20.9% of the cells stained positively in grade 3. Thus, our results suggest that caspase activation is involved in HCV-associated liver injury. Moreover, measurement of caspase activity may represent a reliable marker for the early detection of liver damage, which may open up new diagnostic and therapeutic strategies in HCV infection.

Proc Natl Acad Sci U S A 2002 Aug 20;99(17):11340-5 Related Articles, Links
Click here to read

IL-18 contributes to the spontaneous development of atopic dermatitis-like inflammatory skin lesion independently of IgE/stat6 under specific pathogen-free conditions.

Konishi H, Tsutsui H, Murakami T, Yumikura-Futatsugi S, Yamanaka K, Tanaka M, Iwakura Y, Suzuki N, Takeda K, Akira S, Nakanishi K, Mizutani H.

Department of Dermatology, Mie University School of Medicine, Tsu 514-8507, Japan.

Atopic dermatitis (AD) is a pruritic inflammatory skin disease. Because IL-18 directly stimulates T cells and mast cells to release AD-associated molecules, Th2 cytokines, and histamine, we investigated the capacity of IL-18 to induce AD-like inflammatory skin disease by analyzing KIL-18Tg and KCASP1Tg, which skin-specifically overexpress IL-18 and **caspase-1**, respectively. They spontaneously developed relapsing dermatitis with mastocytosis and Th2 cytokine accumulation accompanied by systemic elevation of IgE and histamine. Stat6-deficient KCASP1Tg displayed undetectable levels of IgE but manifested the same degree of cutaneous changes, whereas IL-18-deficient KCASP1Tg evaded the dermatitis, suggesting that IL-18 causes the skin changes in the absence of IgE/stat6. KIL-18Tg and IL-1-deficient KCASP1Tg took longer to display the lesion than KCASP1Tg. **Thus, AD-like inflammation is initiated by overrelease of IL-18 and accelerated by IL-1.** Our present study might provide insight into understanding the pathogenesis of and establishing therapeutics for chronic inflammatory skin diseases including AD.

Lab Invest 2000 Mar;80(3):345-57 Related Articles, Links

[Click here to read](#)

Enhanced expression of caspase-3 in hypertrophic scars and keloid: induction of caspase-3 and apoptosis in keloid fibroblasts in vitro.

Akasaka Y, Ishikawa Y, Ono I, Fujita K, Masuda T, Asuwa N, Inuzuka K, Kiguchi H, Ishii T.

Second Department of Pathology, School of Medicine, Toho University, Tokyo, Japan.
akasakay@med.toho-u.ac.jp

Recent studies have suggested that the regulation of apoptosis during wound healing is important in scar establishment and development of pathological scarring. To examine the phenomenon of apoptosis and its involvement in the process of pathological scarring, we immunohistochemically quantified differential levels of expression of caspase-3 and -2, which are activated during apoptosis in vitro, in surgical resected scar tissues. We divided 33 cases of normally healed flat scars and 18 cases of pathological scars (15 cases of hypertrophic scars and 3 cases of keloid) into three groups (S1 = <10 months' duration; S2 = 10 to 40 months' duration; and S3 = >40 months' duration) according to the duration of scar. In all three groups examined, the semiquantitative scores for caspase-3 staining were significantly higher for the combination of hypertrophic scars and keloid as a group compared with normally healed flat scars, suggesting reduced cell survival and increased apoptotic cell death in hypertrophic scars and keloid. Apoptosis and caspase proteolytic activities were examined in vitro using two flat scar-derived fibroblast lines (FSFB-1 and -2) and two keloid-derived fibroblast lines (KFB-1 and -2). After 24 hours of serum deprivation, apoptotic cells were significantly increased in both KFB lines, whereas serum deprivation of FSFB-1 cells did not result in a significant increase in apoptotic cell number. After serum deprivation, significant increases in caspase-3 proteolytic activities were detected in both KFB lines compared with both FSFB lines. In contrast, no significant differences with caspase-8 activity were observed between similarly treated KFB and FSFB lines. Furthermore, serum deprivation-induced apoptosis of KFB-2 cells was significantly inhibited by the caspase-3 inhibitor Ac-Asp-Glu-Val-Asp-fluoromethyl ketone (DEVD-FMK), indicating that caspase-3 is important for serum deprivation-induced apoptosis in KFB-2 cells. Considering the role of caspase-3 as a key effector molecule in the execution of apoptotic stimuli, our results suggested that enhanced expression of caspase-3 in hypertrophic scars and keloid induces apoptosis of fibroblasts, which may play a role in the process of pathological scarring.

Leukemia 2000 Dec;14(12):2045-51 Related Articles, Links

Comment in:

* Leukemia. 2000 Dec;14(12):2017-8.

Expression and activity of caspases 1 and 3 in myelodysplastic syndromes.

Boudard D, Sordet O, Vasselon C, Revol V, Bertheas MF, Freyssenet D, Viallet A, Piselli S, Guyotat D, Campos L.

Equipe Mort Cellulaire et Neoplasie, Faculte de Medicine, Saint-Etienne, France.

Myelodysplastic syndromes (MDS) are characterized by abnormal growth of committed progenitors in clonogenic assay, with reduced number of colonies and decreased colony/cluster ratio. It has been suggested that excessive apoptosis is the cause of marrow failure in MDS. We studied the expression of caspase-1 (interleukin-1beta-converting enzyme, ICE) and caspase-3 (CPP32/apopain) in marrow mononuclear cells, and the growth pattern of committed progenitors in a series of 83 MDS cases. The percentage of apoptotic cells as detected by TUNEL technique, and the percentage of caspase-3-positive cells were significantly higher in refractory anemia (RA) and RA with ringed sideroblasts (RAS) than in chronic myelomonocytic leukemia (CMML), refractory anemia with excess of blasts (RAEB) and RAEB in transformation (RAEB-T). Spontaneous growth of CFU-GM was associated with a higher percentage of blasts, and with a lower expression of caspase-3 and caspase-1. The yield of CFU-E, BFU-E, and CFU-GM (in the presence of growth factors) was decreased by comparison to normal marrow, but large individual differences were observed in all cytological categories. Inhibition of caspase-1 and caspase-3 activities by specific inhibitors resulted in a significant increase of the production of all types of colonies (up to 50-fold of control). In the presence of caspase-3 inhibitor, the number of BFU-E and CFU-E was in the range of normal values in most cases of RA and RAS. In addition, caspase-1 and -3 protease activities were detectable by fluorogenic assay in all cases studied. Western blot analysis confirmed the expression of caspase-3, including the cleaved (activated)-p17 form in most cases of RA/RAS analyzed. It is concluded that caspase-3 is implicated in the increased apoptosis observed in MDS and that inhibition of its activity can restore at least partially the growth of committed progenitors.

Am J Physiol Heart Circ Physiol 2002 Oct;283(4):H1634-44 Related Articles, Links

[Click here to read](#)

Pyruvate improves redox status and decreases indicators of hepatic apoptosis during hemorrhagic shock in swine.

Mongan PD, Capacchione J, West S, Karaian J, Dubois D, Keneally R, Sharma P.

Department of Anesthesiology, Uniformed Services University of the Health Sciences, Bethesda, Maryland 20814, USA. pmongan@usuhs.mil

Previous studies have shown that the liver is the first organ to display signs of injury during hemorrhagic shock. We examined the mechanism by which pyruvate can prevent liver damage during hemorrhagic shock in swine anesthetized with halothane. Thirty minutes after the induction of a 240-min controlled arterial hemorrhage targeted at 40 mmHg, hypertonic sodium pyruvate (0.5 g. kg⁻¹. h⁻¹) was infused to achieve an arterial concentration of 5 mM. The volume and osmolality effects of pyruvate were matched with 10% saline (HTS) and 0.9% saline (NS). Although the peak hemorrhage volume increased significantly in both the pyruvate and HTS group, only the pyruvate treatment was effective in delaying cardiovascular decompensation. In addition, pyruvate effectively maintained the NADH/NAD redox state, as evidenced by increased microdialysate pyruvate levels and a significantly lower lactate-to-pyruvate ratio. Pyruvate also prevented the loss of intracellular antioxidants (GSH) and a reduction in the GSH-to-GSSG ratio. These beneficial effects on the redox environment decreased hepatic cellular death by apoptosis. Pyruvate significantly increased the ratio of Bcl-X1 (antiapoptotic molecule)/Bax (proapoptotic molecule), **prevented the release of cytochrome c from mitochondria, and decreased the fragmentation of caspase 3** and poly(ADP ribose) polymerase (DNA repair enzyme). These beneficial findings indicate that pyruvate infused 30 min after the onset of severe hemorrhagic shock is effective in maintaining the redox environment, preventing the loss of the key antioxidant GSH, and decreasing early apoptosis indicators.

J Neuroimmunol 2001 Apr 2;115(1-2):182-91 Related Articles, Links

[Click here to read](#)

Expression of inducible nitric oxide synthase, interleukin-1 and caspase-1 in HIV-1 encephalitis.

Zhao ML, Kim MO, Morgello S, Lee SC.

Department of Pathology (Neuropathology), F-717, Albert Einstein College of Medicine, 1300 Morris Park Avenue, Bronx, NY 10461, USA.

Inflammatory cytokines and enzymes such as IL-1 and inducible nitric oxide synthase (iNOS) may play an important role in the pathogenesis of AIDS dementia, a condition associated with infection of the CNS cells by the HIV-1. In this report, we investigated the expression of iNOS, IL-1, and caspase-1 (interleukin-1 converting enzyme) in HIV-1 encephalitis (HIVE) by immunocytochemistry and analyzed their expression with respect to HIV-1 infection and glial activation. In HIVE, all three molecules were expressed at high levels in areas of HIV-1 infection (microglial nodules with HIV-1 p24 immunoreactivity) and in areas of diffuse white matter gliosis. Expression was cell-type specific, with IL-1 and caspase-1 being expressed in macrophages and microglia, and iNOS in activated astrocytes. Multinucleated giant cells, a hallmark of virally infected cells, showed intense staining for both IL-1 and caspase-1, suggesting induction of these molecules by HIV-1. Double immunocytochemistry demonstrated a regional co-localization of astrocyte iNOS and microglial IL-1 and caspase-1. These results support the notion that autocrine and paracrine interactions between HIV-1 infected macrophages and microglia, activated microglia, and astrocytes lead to expression of proinflammatory and neurotoxic molecules. iNOS and caspase-1 may provide additional therapeutic targets for HIVE.

Neuropathol Appl Neurobiol 1999 Oct;25(5):380-6 Related Articles, Links

[Click here to read](#)

Expression of caspase-3 in brains from paediatric patients with HIV-1 encephalitis.

James HJ, Sharer LR, Zhang Q, Wang HG, Epstein LG, Reed JC, Gelbard HA.

Department of Neurology (Child Neurology Division), The University of Rochester Medical Center, NY 14642, USA.

Apoptosis of neurones, macrophages, and microglia occurs in the brains of paediatric patients with human immunodeficiency virus (HIV) type 1 encephalitis, which is often associated with pre-mortem neurological disease (progressive encephalopathy). We have previously reported that TUNEL-positive neurones in brain tissue from paediatric patients with HIV type 1 encephalitis and progressive encephalopathy are strikingly devoid of the pro-apoptotic gene product Bax, in marked contrast to brain-resident macrophages and microglia. Using immunocytochemical methods, the present study demonstrate that neurones in patients with HIV type 1 encephalitis and progressive encephalopathy, as well as macrophages and microglia, but not astrocytes, overexpress caspase-3, a pro-apoptotic enzyme that is proteolytically activated downstream of Bax-Bcl-2 dysregulation. Co-localization of neuronal cytoplasmic caspase-3 and nuclear TUNEL staining, a marker for fragmented DNA, was also infrequently observed in brain tissue from patients with HIV type 1 encephalitis and progressive encephalopathy. These findings suggest that vulnerable neurones in brain tissue from patients with HIV virus type 1 encephalitis and progressive encephalopathy undergo apoptosis by a mechanism that involves upregulation of caspase-3 in a pathway that is independent of Bax-Bcl-2 dysregulation. Furthermore, caspase-3 upregulation in apoptotic neurones likely occurs prior to DNA fragmentation.

Exp Gerontol 2002 Jun;37(6):777-89 Related Articles, Links

[Click here to read](#)

Age-associated increases in the activity of multiple caspases in Fisher 344 rat organs.

Zhang Y, Chong E, Herman B.

Department of Cellular and Structural Biology, Centre at San Antonio, The University of Texas Health Science, Mail Code 7762, San Antonio, TX 78229-3900, USA.

As organisms age, an increase in the number of terminal deoxynucleotidyltransferase-mediated dUTP nick end labeling positive cells has been observed in a variety of tissues and cell types. However, whether this represents the increase of apoptosis has not been validated on molecular level. In this study we examined the endogenous activity of caspases that are known to be responsible for the execution of caspase-dependent apoptosis as a function of age in rat liver, lung, and spleen. We demonstrate that the extent of apoptosis in rat liver increases late during the aging process (i.e. 23-27 month) as indicated by the activation of executioner caspases-3, -6, and -7. We also found that the activity of caspase-3, -6, and -7 increased drastically in rat lung and spleen at late stages of aging. Despite reports that the level of Fas mRNA increases with age in rat liver and that Fas system regulates liver homeostasis, we did not detect activation of caspase-8, a key mediator of Fas-induced apoptosis, in aged liver. We also observed increased activities of two caspases, caspase-2 and caspase-9, which are involved in mitochondrion-mediated apoptosis in livers isolated from old rats, and found that hepatocytes isolated from old animals (>23 month) are more sensitive to oxidative stress that targets the mitochondria compared to those isolated from young (6 month) animals. Lastly, we demonstrate that the level of cytochrome c is lower in liver from old animals, probably as a result of expeditious degradation following its release into cytosol. Collectively, our results demonstrate that aging is associated with an increase in the activity of multiple caspases, suggesting that the extent of apoptosis increases as organs age. In the case of rat liver, this increase in caspase activation is more likely associated with the mitochondrial (i.e. intrinsic) pathway rather than the Fas-mediated caspase-8 (extrinsic) pathway of apoptosis.

PMID: 12175478 [PubMed - indexed for MEDLINE]

Eur J Pharmacol 2001 Dec 14;433(1):37-45 Related Articles, Links

[Click here to read](#)

Inhibitory effect of M50054, a novel inhibitor of apoptosis, on anti-Fas-antibody-induced hepatitis and chemotherapy-induced alopecia.

Tsuda T, Ohmori Y, Muramatsu H, Hosaka Y, Takiguchi K, Saitoh F, Kato K, Nakayama K, Nakamura N, Nagata S, Mochizuki H.

Research Center, Mochida Pharmaceutical Co., Ltd., 722 Jimba-aza-Uenohara, Gotemba, Shizuoka 412-8524, Japan. toshi-t@mochida.co.jp

M50054, 2,2'-methylenebis (1,3-cyclohexanedione), was identified as a novel inhibitor of apoptosis (programmed cell death) using an in vitro cell death assay system induced in human Fas-expressing WC8 cells by soluble human Fas ligand. Furthermore, M50054 inhibited the apoptotic cell death of U937, a human monocytic leukemic cell line, induced by anticancer agents such as etoposide; it was also confirmed that M50054 inhibited apoptotic features such as DNA fragmentation and phosphatidylserine exposure in these cells. These anti-apoptotic effects were attributable to inhibition of caspase-3 activation. Additionally, M50054 significantly inhibited anti-Fas-antibody-induced elevation of plasma alanine aminotransferase and aspartate aminotransferase. Alopecia (hair loss) symptoms were also significantly improved with topical treatment with M50054. In conclusion, M50054 inhibits apoptosis induced by a variety of stimuli via inhibition of caspase-3 activation, and may thus be effective for hepatitis and chemotherapy-induced alopecia.



J Cutan Med Surg 2002 Jan-Feb;6(1):1-9 Related Articles, Links

Effects of finasteride on apoptosis and regulation of the human hair cycle.

Sawaya ME, Blume-Peytavi U, Mullins DL, Nusbaum BP, Whiting D, Nicholson DW, Lotocki G, Keane RW.

ARATEC Research, Ocala, Florida 34478, USA. ARATEC@worldnet.att.net

BACKGROUND: A number of studies have provided evidence that apoptosis is a central element in the regulation of hair follicle regression. In androgenetic alopecia (AGA), the exact location and control of key players in the apoptotic pathways remains obscure. **OBJECTIVE:** In the present study, we used a panel of antibodies and investigated the spatial and cellular pattern of expression of caspases and inhibitors of apoptosis (IAPs), such as XIAP and FLIP, in men with normal scalp and in men with AGA before and after 6 months of treatment with 1 mg oral finasteride treatment. **METHODS AND RESULTS:** Constitutive expression of caspases-1, -3, -8, and -9 and XIAP was detected predominantly within the isthmic and infundibular hair follicle area, basilar layer of the epidermis, and eccrine and sebaceous glands. AGA-affected tissues showed an increase in caspase (-1, -3, -6, -9) immunoreactivity with a concomitant decrease in XIAP staining. After 6 months of finasteride treatment, both caspases and XIAP were similar to levels exhibited by normal subjects. Immunoblot analysis was performed to determine antibody specificity and cellular expression of caspases. Purified populations of keratinocytes, melanocytes, dermal papilla, and dermal fibroblasts derived from human hair follicles were cultured in vitro and treated with 0.5 mM staurosporin. Time-course experiments revealed that processing of caspase-3 is a principal event during apoptosis of these hair cell types. **CONCLUSION:** These data suggest that alterations in levels of caspases and IAPs regulate hair follicle homeostasis. Moreover, finasteride appears to influence caspase and XIAP expression in hair follicle cells thus signaling anagen, active growth in the hair cycle.

Wien Klin Wochenschr 2002 Aug 30;114(15-16):671-7 Related Articles, Links

Tubular apoptosis in the pathophysiology of renal disease.

Hauser P, Oberbauer R.

Abteilung für Nephrologie, Universitätsklinik für Innere Medizin, Universität Wien, Vienna, Austria.

Apoptosis of renal tubular epithelial cells plays a major role in acute renal failure. Several external and internal signals can induce apoptosis, which is then effectuated via several pathways. These pathways are either the FAS/FAS-L pathway and downstream MAPK (mitogen-activated protein kinases) and JNK (c-Jun N-terminal kinase) signal transduction, or the RANK/RANK-L (receptor activator of NFkB) pathway **via activation of the caspase cascade**. Other pathways, especially for apoptosis induction by toxins, include the mitochondrial permeability transition pore activation and Bcl-2 superfamily member differential regulation. An important final, irreversible branch of these pathways is the release of cytochrome c from the mitochondria, leading to nuclear fragmentation. Therapeutic interventions of acute tubular injury focus on the prevention of apoptosis by either modulation of the balance of the bcl-2 family or by selectively blocking angiotensin receptors. It is not clear yet, which receptor blockade or combination of receptor blockers are most effective in apoptosis prevention. In chronic renal failure, tubular apoptosis has been found in biopsies from polycystic kidneys, but not in a quantitatively meaningful amount in other chronic human renal diseases. On the other hand, given the short half-life of apoptotic cells of few hours, even low numbers over time might turn out to be important modulators of chronic kidney disease, which are characterized by tubular cell loss. Potential therapeutic interventions to prevent tubular apoptosis in chronic renal disease include angiotensin system inhibition, whereby the angiotensin II AT2 receptor blockade seems more promising in apoptosis inhibition than the inhibition of other receptor subtypes.

1: Kidney Int 2001 Nov;60(5):1765-76 Related Articles, Links
Click here to read
Caspase-3 and apoptosis in experimental chronic renal scarring.

Yang B, El Nahas AM, Thomas GL, Haylor JL, Watson PF, Wagner B, Johnson TS.

Sheffield Kidney Institute, Northern General Hospital Trust, Sheffield University,
Sheffield S5 7AU, England, UK. Bin.Yang@Sheffield.ac.uk

BACKGROUND: Caspase-3 is a member of the caspase enzyme family, having a central role in the execution of apoptosis. However, the significance of Caspase-3 in the inappropriate and excessive apoptosis that contributes to the progression of non-immune-mediated renal scarring has not been established. **METHODS:** Kidneys from sham-operated and subtotal nephrectomized (SNx) rats were harvested on days 7, 15, 30, 60, 90 and 120 post-surgery. These were analyzed for apoptosis (in situ end labeling of DNA, light and electron microscopy), Caspase-3 activity (fluorometric substrate cleavage assay), protein and mRNA (Western and Northern blotting), as well as distribution (immunohistochemistry), inflammation (ED-1 immunohistochemistry) and fibrosis (Masson's Trichrome staining). **RESULTS:** Apoptosis, inflammation and fibrosis gradually increased in glomeruli, tubules and interstitium of SNx rats. Caspase-3 was mainly located in damaged tubules, but also was found in some glomerular and interstitial cells. Little or no staining was noted in sham-operated kidneys. In SNx kidneys, Caspase-3 activity was significantly increased from day 30 and peaked on day 120 (2.5-fold). This resulted from increases in the 17 and 24 kD active protein subunits. The 32 kD precursor was increased at all time points (1861% on day 120, $P < 0.01$). Caspase-3 changes were transcription-dependent with the 2.7 kb caspase-3 mRNA significantly increased at all time points (287% on day 120). Caspase-3 activity was a better predictor of apoptosis (Std beta coefficient = 0.347, $P < 0.05$) than Caspase-3 proteins or mRNA; however, Caspase-3 at all levels correlated with apoptosis, inflammation and fibrosis (all $P < 0.01$). **CONCLUSIONS:** Up-regulation of apoptosis in remnant kidneys is likely to be Caspase-3-dependent as it is associated with increases in Caspase-3 at the activity, protein and mRNA levels. Therefore, Caspase-3 is a potential therapeutic target for the modification of renal cell apoptosis and subsequently renal fibrosis.

1: Microbes Infect 2002 Jun;4(7):713-22 Related Articles, Links

[Click here to read](#)

In vivo and in vitro activation of caspase-8 and -3 associated with *Helicobacter pylori* infection.

Ashktorab H, Neapolitano M, Bomma C, Allen C, Ahmed A, Dubois A, Naab T, Smoot DT.

Cancer Center and Gastroenterology Division, Department of Medicine, Howard University College of Medicine, University Hospital, 2041 Georgia Avenue N.W., Washington, DC 20060, USA. hashktorab@howard.edu

In vivo and in vitro studies have shown an increase in apoptosis in gastric epithelial cells in persons infected with *Helicobacter pylori*. *H. pylori*-induced activation of caspase-8 and -3 was evaluated using a human gastric adenocarcinoma cell line (AGS) and gastric tissue from humans and monkeys colonized with *H. pylori*. The enzymatic activity of caspase-8 was detected only in AGS cells exposed to *H. pylori* up to 24 h. The active form of caspase-8 was present by Western blot after exposure to *H. pylori* for 3 h and persisted through 24 h. Caspase-3 activity was present in AGS cells exposed to *H. pylori* for 3 h, reaching a maximum after 24 h (a sevenfold increase in activity). Caspase-8-mediated cleavage of procaspase-3 generated a 20-kDa band (indicative of the presence of active caspase-3) present only in AGS cells exposed to *H. pylori*. Active caspase-3 staining was markedly increased in gastric mucosa from infected persons and animals, compared to uninfected controls by immunohistochemistry. Stimulation of downstream events leading to apoptosis, such as the cleavage of PARP (poly adenosine-diphosphate-ribose polymerase) and DFF45 (DNA fragmentation factor 45) as a result of activation of caspase-3, was evaluated. PARP was cleaved, resulting in the presence of both an 89- and a 24-kDa band along with DFF45, resulting in the presence of 10- and 12-kDa bands only in gastric cells exposed to *H. pylori*. Our data show that *H. pylori* stimulates the activation of caspases and downstream mediators of caspase-induced apoptosis. This suggests that *H. pylori*-induced apoptosis is mediated through caspase pathways, which include the activation of caspase-8 and subsequent cleavage and activation of caspase-3. This is consistent with caspase-3 activation that was found in the gastric mucosa of humans and monkeys infected with *H. pylori*.

PMID: 12067831 [PubMed - indexed for MEDLINE]

1: J Immunol 2002 Jun 15;168(12):6358-65 Related Articles, Links
[Click here to read](#)

Mycobacterium tuberculosis promotes apoptosis in human neutrophils by activating caspase-3 and altering expression of Bax/Bcl-xL via an oxygen-dependent pathway.

Perskvist N, Long M, Stendahl O, Zheng L.

Division of Medical Microbiology, Faculty of Health Sciences, Linköping University, Linköping, Sweden.

In addition to direct bactericidal activities, such as phagocytosis and generation of reactive oxygen species (ROS), neutrophils can regulate the inflammatory response by undergoing apoptosis. We found that infection of human neutrophils with *Mycobacterium tuberculosis* (Mtb) induced rapid cell death displaying the characteristic features of apoptosis such as morphologic changes, phosphatidylserine exposure, and DNA fragmentation. Both a virulent (H37Rv) and an attenuated (H37Ra) strain of Mtb were equally effective in inducing apoptosis. Pretreatment of neutrophils with antioxidants or an inhibitor of NADPH oxidase markedly blocked Mtb-induced apoptosis but did not affect spontaneous apoptosis. Activation of caspase-3 was evident in neutrophils undergoing spontaneous apoptosis, but it was markedly augmented and accelerated during Mtb-induced apoptosis. The Mtb-induced apoptosis was associated with a speedy and transient increase in expression of Bax protein, a proapoptotic member of the Bcl-2 family, and a more prominent reduction in expression of the antiapoptotic protein Bcl-x(L). Pretreatment with an inhibitor of NADPH oxidase distinctly suppressed the Mtb-stimulated activation of caspase-3 and alteration of Bax/Bcl-x(L) expression in neutrophils. These results indicate that infection with Mtb causes ROS-dependent alteration of Bax/Bcl-x(L) expression and activation of caspase-3, and thereby induces apoptosis in human neutrophils. Moreover, we found that phagocytosis of Mtb-induced apoptotic neutrophils markedly increased the production of proinflammatory cytokine TNF-alpha by human macrophages. Therefore, the ROS-dependent apoptosis in Mtb-stimulated neutrophils may represent an important host defense mechanism aimed at selective removal of infected cells at the inflamed site, which in turn aids the functional activities of local macrophages.

PMID: 12055253 [PubMed - indexed for MEDLINE]

1: Ann Neurol 2002 Mar;51(3):319-29 Related Articles, Links

[Click here to read](#)

Role of Caspase-1 in experimental pneumococcal meningitis: Evidence from pharmacologic Caspase inhibition and Caspase-1-deficient mice.

Koedel U, Winkler F, Angele B, Fontana A, Flavell RA, Pfister HW.

Department of Neurology, Klinikum Grosshadern, Ludwig Maximilians-University, Munich, Germany.

Caspase 1 plays a pivotal role in generating mature cytokine interleukin-1beta. Interleukin-1beta is implicated as a mediator of pneumococcal meningitis, both in experimental models and in humans. We demonstrated here that (1) Caspase 1 mRNA and protein expression is upregulated in the brain during experimental pneumococcal meningitis, and (2) Caspase 1 levels are elevated in the cerebrospinal fluid of patients with acute bacterial meningitis. The upregulation/activation of Caspase 1 was associated with increased levels of interleukin-1beta. Depletion of the Caspase 1 gene and pharmacologic blockade of Caspase 1 significantly attenuated the meningitis-induced increase in interleukin-1beta. This was paralleled by a significantly diminished inflammatory host response to pneumococci. The antiinflammatory effect of Caspase 1 depletion or blockade was associated with a marked reduction of meningitis-induced intracranial complications, thus leading to an improved clinical status. In humans, cerebrospinal fluid Caspase 1 levels correlated with the clinical outcome. Thus, pharmacologic inhibition may provide an efficient adjuvant therapeutic strategy in this disease.

1: Nat Med 1999 Mar;5(3):298-302 Related Articles, Links

[Click here to read](#)

Neuroprotection by a caspase inhibitor in acute bacterial meningitis.

Braun JS, Novak R, Herzog KH, Bodner SM, Cleveland JL, Tuomanen EI.

Department of Infectious Diseases, St. Jude Children's Research Hospital, Memphis, Tennessee 38105, USA.

Half of the survivors of bacterial meningitis experience motor deficits, seizures, hearing loss or cognitive impairment, despite adequate bacterial killing by antibiotics. We demonstrate that the broad-spectrum caspase inhibitor N-benzyloxycarbonyl-Val-Ala-Asp-fluoromethyl-ketone (z-VAD-fmk) prevented hippocampal neuronal cell death and white blood cell influx into the cerebrospinal fluid compartment in experimental pneumococcal meningitis. Hippocampal neuronal death was due to apoptosis derived from the inflammatory response in the cerebrospinal fluid. Apoptosis was induced in vitro in human neurons by inflamed cerebrospinal fluid and was blocked by z-VAD-fmk. As apoptosis drives neuronal loss in pneumococcal meningitis, caspase inhibitors might provide a new therapeutic option directed specifically at reducing brain damage.